Environmental Impact Statement

–Joint Test of Deep-sea Miner and Buffer Station in Beijing Pioneer Polymetallic Nodule Contract Area, Western Pacific

Beijing Pioneer High-tech Development Co., Ltd.

October, 2024

Contents

List of Figures

List of Tables

EXECUTIVE SUMMARY

Introduction

According to the contract signed in 2019 between Beijing Pioneer High-tech Development Co., Ltd. (hereinafter referred to as "Beijing Pioneer Company (BPC)") and the International Seabed Authority (hereinafter referred to as "ISA") for the exploration of polymetallic nodules in the Northwest Pacific, BPC is required to complete contract area verification test and environmental monitoring of key mining technologies during the first five-year period of the exploration stage, and assess the environmental impact based on the test and environmental monitoring data.

Since the signing of the contract, BPC has gradually advanced the research of deep-sea mining technology based on the GERIS (Green, Economy, Reliability and Robustness, Intelligence, and Safe) mining concept. By developing the "Manta" series of polymetallic nodule sampling test machines and collection test prototypes, it has eventually evolved into a green deep-sea mining system suitable for commercial use.

According to the concept of "research-oriented exploitation", this project plans to conduct a polymetallic nodule deep-sea collection and buffer station joint test to verify the reliability of the suspended collection method and the buffer station joint, while carrying out long-term environmental impact monitoring and assessment. Based on the environmental baseline data collected previously and the environmental monitoring data collected before, during, and after the test, the environmental impact assessment of the test is carried out. At the same time, research will be conducted on scientific issues related to the potential impacts of deep-sea mining, in order to develop environmental impact mitigation measures for future deep-sea commercial mining plans and provide design basis for the development of deep-sea green mining technologies.

BPC plans to conduct a 1:5 scale polymetallic nodule deep-sea collection and buffer station joint test in a 500 m × 500 m area in the southern foothills of Magoshichi-no-Hoshi Seamount in Block M2 of the Northwest Pacific polymetallic nodule contract area in the second half of 2025. According to the *Recommendations for the Guidance of Contractors for the Assessment of the Possible Environmental Impacts arising from Exploration for Marine Mineral in the Area* (ISBA/25/LTC/6/Rev.3), activities such as testing of mining components (mineral collection machine, transport hose, buffer station) require environmental impact

assessment. The Environmental Impact Statement (EIS) must be submitted to the Secretary-General of ISA no later than one year before the start of the activity.

This report is prepared in accordance with the *Environmental Impact Statement Template for Reporting an Environmental Impact Assessment Undertaken During Exploration*, as detailed in Annex III of the ISA document (ISBA/25/LTC/6/Rev.3).

Environmental Management

According to the *Draft Standards and Guidelines for the Development and Application of Environmental Management Systems* (ISBA/27/C/7), BPC has established the BPC Environmental Management System. The project management is incorporated into the company's environmental management system (for the "Pioneer Company Environmental Management System Concept, Objectives, and Policies", please see Appendix I). The company's environmental management system aims to carry out environmental work under the guidance of company leadership and policies, identify and utilize resources, knowledge, and capabilities that can provide support, communication, and documentation around core processes. Core processes include planning, operation management, and improvement, and provide supporting services at all levels.

Based on the project situation, an organizational management framework at the project level is established. The Chinese government is the guarantor of the BPC's exploration contract of polymetallic nodules in the Northwest Pacific, and the China Ocean Affairs Administration is the competent department for China's "Area" affairs. BPC's activities in the contract area are managed according to the relevant regulations, standards, guidelines, and recommendations of the ISA, and are supervised by the China Ocean Affairs Administration in accordance with Chinese laws such as the *Deep Seabed Area Resource Exploration and Exploitation Law of the People's Republic of China.*

Environmental Objectives and Strategies

Environmental Objectives

Long-term objective: With the objective of protecting and preserving the environment and biodiversity of the deep-sea polymetallic nodule area, promote the rational utilization of the common heritage of mankind for the benefit of social development. To establish a strategy of "research-oriented exploitation", incorporate deep-sea scientific research throughout the entire process of deep-sea activities, continuously improve knowledge of deep-sea

ecosystems, and develop environmental monitoring and restoration technologies by applying precautionary approaches in a timely manner. Apply the highest environmental management standards, conduct environmental impact assessments in advance and adopt the best environmental management measures and tools. With green standards, develop technical and equipment systems for deep-sea mining and achieve sustainable utilization of deep-sea mineral resources.

Medium-term objective: Formulate the main standards for deep-sea environmental protection and preservation; initially construct the company's environmental protection and preservation standard system for deep-sea mining activities. Enrich and increase the collection of data related to deep-sea mining environmental assessments; establish an environmental baseline data index system and standardization system. Establish an environmental impact assessment model; determine the preservation reference zone and impact reference zone; and comprehensively monitor the biological communities potentially affected by mining activities in the contract area. Formulate and implement a complete set of internal environmental control systems to manage and reduce the impact of the company's activities on the environment.

Short-term objective: Establish a company environmental management system to provide a systematic and structured operational mechanism for the company's environmental management. Through the implementation of the environmental management system, strengthen the environmental management of the mining area and the company's operations; make more effective use of energy and resources; reduce energy consumption; save operating costs; and continuously improve the company's environmental performance, achieving minimal impact on the environment from the activities conducted by the company. Establish a mining area environmental management system; clarify the research and development tasks of green key technology and equipment; and propose technical requirements for green mining equipment.

Strategies

- Establish the concept of "research-oriented exploitation"; strengthen cooperation with domestic and international scientific communities; continuously improve the understanding of deep-sea ecosystems; and provide scientific basis for the development of green mining processes and technologies, commercial development scale determination, regional environmental management plan establishment, cumulative impact model and environmental threshold research, and the formulation of

environmental impact mitigation measures.

● Adhere to the implementation of sustainable development and responsible environmental management strategies. Prioritize responsible and sustainable management of the environment in all company operations, incorporating it into every aspect of business and exploration and development activities. Persist in using an integrated approach to optimize production and operational energy efficiency; establish company environmental performance objectives; and regularly review these goals to achieve optimal environmental management.

● Explore responsible deep-sea mining operations that are considerate of the environment. Undertake technological and equipment innovation, improve work methods; enhance the efficiency of natural resources, equipment, and energy usage, and develop green deep-sea mining systems. Advance comprehensive digital ocean technologies that enhance human understanding, deep-sea clean energy technologies, and environmental protection planning and ecological restoration technologies for deep-sea spaces.

● Implement environmental risk management strategies and preventive measures. Conduct environmental risk management to identify risks and potential consequences; establish a corporate ethic of environmental responsibility, and develop and implement environmental education and training programs. Ensure that company employees, contractors, and suppliers of equipment, materials, and services understand and comply with the company's environmental policies and specific requirements. Develop strategies for stakeholder participation and environmental public welfare promotion to maintain and enhance the company's reputation.

Research activities

Environmental baseline survey

Since BPC conducted the first cruise survey in 2021, four cruises have been completed till November 2023 (see Table 0-1). The environmental baseline data obtained are detailed in Table 0-2.

Table 0-1 Environmental and resource survey cruise information statistics from 2021 to 2023.

Year	Cruise	Surveyed Area	Investigation Time	Acquired data, samples, and video materials, among other results.
2021	DY69	Blocks M1 and M2 of the BPC's contract area in the Northwest Pacific	2021.10–11 (34 Days)	Underwater video materials, ADCP and CTD data, seawater chemistry and chlorophyll *a* data, sediment samples collected by box corer and multicorer, plankton samples, benthic and scavenger organism samples, geotechnical data, seabird observation data, etc.
2022	DY75	Blocks M1 and M2 of the BPC's contract area in the Northwest Pacific	2022.8–11 (112 Days)	Multibeam sonar survey data, underwater video materials, ADCP and CTD data, seawater chemistry and chlorophyll *a* data, sediment samples collected by box corer and multicorer, plankton and nodule organism samples, benthic and scavenger organism samples, geotechnical data, and seabird observation data, etc.
2022	DY76	Block M2 of the BPC's contract area in the Northwest Pacific	2022.11–12 (18 Days)	Three sets of subsurface buoy data and sediment trap samples, sediment samples collected by box corer and multicorer, benthic and scavenger organism samples.
2023	DY81	Blocks M1 and M2 of the BPC's contract area in the Northwest Pacific	2023.8–11 (80 Days)	Subsurface buoy data and sediment trap samples, AUV underwater video, hydrophone data, CTD data, seawater chemistry and chlorophyll *a* data, sediment samples, plankton samples, benthic and scavenger organism samples, and seabird observation data, etc.

Chapters 4 to 5 of this report primarily rely on the baseline data and samples obtained from the environmental and resource surveys conducted during four cruises from 2021 to 2023 in Blocks M1 and M2 (referred to as "Block M") of the contract areas. Additionally, during the execution of the cobalt-rich crust exploration contract by the China Ocean Mineral Resources Research and Development Association (COMRA), environmental surveys were also carried out in Block M2 of the BPC polymetallic nodule contract area and the adjacent sea areas, the results of which are also referenced in this report. According to the ISA guidelines, the environmental baseline includes 8 major categories with 93 parameters. To date, a total of 73 environmental parameters have been obtained. 1 parameter is under analysis. There are plans to collect 13 parameters before the collection tests of collector components in 2024 or 2025, and 6 parameters that can only be monitored during the collection tests (Table 0-2).

Table 0-2 Statistics on types and parameters of environmental baseline data acquired between 2021 and 2023

Environmental baseline data types	Number of parameters required by ISA (items)	Number of parameters obtained (items)	Number of parameters (items) planned to be collected prior to the 2024 or 2025 test	Number of parameters that can be monitored only during collection tests (items)
Physical oceanography	13	12	1 (optical properties)	0
Chemical oceanography	22	19	2 (trace elements and total organic carbon, etc.)	1 (what additional chemicals may be released in the discharge plume)
Sediment characteristics	15	11	4	0
Geological feature	2	1	0	1 (Information on heavy metals and trace elements that may be released during the test and their concentrations)
Ecological community	34	28	6 (genetic connectivity of key species, trophic levels of megafauna, etc.)	0
Ecosystem functioning - Food web	1	0	1	0
Ecotoxicology - Heavy metals in dominant species - (trace metals and potentially toxic elements in muscle and target organs of benthic fish and invertebrates)	1	0	0	1
bioturbation	1	1	0	0
Sedimentation flux - flux of material from the upper water column into the deep ocean	1	1	0	0
Parameters collected during the collection test				
Dose effects of sediment-covered benthic organisms	1	0	0	1

Environmental baseline data types	Number of parameters required by ISA (items)	Number of parameters obtained (items)	Number of parameters (items) planned to be collected prior to the 2024 or 2025 test	Number of parameters that can be monitored only during collection tests (items)
Chronic disturbance test	1	0	0	1
Ecosystem resilience	1	0	0	1
Total	93	73	14	6

BPC will continue to conduct environmental baseline surveys in 2024 (survey items and workloads are shown in Table 9-5), and the analysis results of the 2024 cruise and the results of the current meters and sediment trap subsurface buoys deployed in the 2023 cruise will be supplemented in the report.

Selection of the Test Area (IRZ/PRZ)

Based on the characteristics of the project's test equipment and environmental baseline features, The Collector Test Area (CTA), Preservation Reference Zone (PRZ), and Impact Reference Zone (IRZ) have been designated.

The IRZ includes CTA and the plume diffusion impact area (Figures 3-2 and 3-3), located in the southern foothills of Magoshichi-no-Hoshi Seamount. According to the plume simulation results, the sediment plume from CTA has a maximum diffusion distance of 5.43 km (see Chapter 6). Therefore, this monitoring plan aims to center on the CTA and expand 5.5 km to the west, east, north, and south, which constitutes the plume impact area. The total area of the IRZ is approximately 11.5 km × 11.5 km, with a water depth range of 5550 to 5600 meters.

A PRZ has been established, located in the southern foothill of Matsuzaki Guyot in Block M1 (Figure 3-4), with an area of about 21 km × 16 km and a water depth range of 5250 to 5650 meters, approximately 78 km away from CTA. The PRZ will monitor the physical, chemical, and biological disturbances at a distance from the test site and will play a significant role in determining the natural variations of the environmental baseline, and will be used to assess the impact of the collector test.

Mineral Collection Machine Test Components

Based on the mining philosophy of green, economical, reliable, intelligent, and safe extraction, BPC has designed the overall technical architecture of the mineral collection system, forming a complete system technical plan from the surface mother ship, underwater

riser, near-bottom buffer station, horizontal transport hose, to the underwater mineral collection machine. According to the technical design, BPC has developed a polymetallic nodule sampling test machine with a sampling head width of 0.5 meters—"Manta I," and conducted sampling tests in the contract area in 2022.

The "Manta II" underwater mineral collection test system, planned to be tested in 2025, consists of three parts: the Manta II main body, the horizontal transport hose, and the buffer station. The basic carrier of Manta II is a gantry-type electric ROV, with a hollow abdomen and clear front and back passages. The nodule collection and transportation device are installed inside the abdominal frame.

The mineral collection test machine "Manta II" inherits the "Manta I" suspended collection travel method and the throat channel flow acceleration direct suction hydraulic mineral collection technology. During the design process, it follows the pursuit of high collection efficiency, low operational energy consumption, low sediment disturbance, and reliable work. The equipment is planned to be completed and tested in 2024 and will conduct the contract area mineral collection test in 2025.

Mineral Collection Machine Test Procedure

The support ship for the mineral collection machine system is "Da Yang Yi Hao", which deploys the machine. The support mother ship for the buffer station is "Da Yang Hao", which also deploys and recovers the horizontal transport hose. The specific deployment and connection sequence is as follows: first, deploy the horizontal transport hose, then deploy the mineral collection machine, and finally deploy the buffer station; first use the mineral collection machine to dock with the inlet end of the horizontal transport hose and adjust the hose position, then use the buffer station to dock with the outlet end of the horizontal transport hose. After the three components complete the connection and construction on the seabed of the mining area, the hose connects the mineral collection machine and the buffer station, forming an arch shape in the seawater, and the umbilical cables of the mineral collection machine and buffer station form an S-shaped bend at the base, extending upward to their respective support mother ships.

The CTA is 500 m × 500 m in size, and the planned path of the mineral collection test is S-shaped. The length of the S-shape is 50 m and the reciprocating interval is 4.2 m, with the total width being 500 m. The collection trajectory length is less than 31.5 km. The total duration of the mineral collection test in the exploration contract area is 20 days, including

100.5 hours of underwater mineral collection test, collecting less than 7500 tons of wet nodules with disturbing about 6-cm surface sediment, and disturbing less than 29400 tons of sediment (disturbed sediment = area×disturbance depth×sediment density×collection head width / turnback spacing = 500m×500m×0.06m×1400kg/m^3×4.2 / 3 = 29400 t). This test will be conducted to joint test of the collector and buffer station without lifting the nodules to the deck of the ship, the way in which the nodules pile up on the seafloor is shown in Figure 3-20.

Physical and Chemical Environmental Baseline Features

The Block M is located in the intermountain basins of the Magellan Seamount Chain in the western Pacific Ocean, where the upper water layer is primarily influenced by the North Equatorial Current (NEC) and the North Equatorial Counter Current (NECC), while the bottom current field is mainly affected by the large-scale thermohaline circulation. A permanent and thick thermocline is a major characteristic of the water body in this area, which separates the nutrient-rich deep water from the euphotic zone (with an average annual thickness of about 100 m) and preventing the upward transport of nutrients from the deep, resulting in extremely low nutrient concentrations in the euphotic zone and minimal horizontal gradients in temperature, salinity, and nutrient elements.

Meteorological Features

Block M belongs to the subtropical monsoon climate, mainly influenced by the subtropical high-pressure system and the equatorial convergence zone, with prevailing easterly winds. From August to December, the sea surface wind direction in Block M is predominantly easterly. Between late August and early October, the area is mainly affected by tropical cyclones, subtropical high pressure, and cold air, with strong weather processes being relatively rare. Block M is generally less affected by typhoons, with wave heights mainly ranging from 2.0 to 3.5 meters. The wind scale is primarily between levels 4 and 5, and the sea conditions are relatively good.

Marine Geological Features

The eastern part of Block M1 is affected by the landslide on the southern side of Matsuaki Guyot, and the northwest part of Block M2 is affected by the landslide on the southern side of Magoshichi-no-Hoshi Seamount. The seamount landslides have formed unique morphologies, such as steep cliffs, gullies and channels, and wavy terrains.

Water Depth. The vast majority of the water depth in Block M is between 4000 and 6000 meters, accounting for 91.23% of the total area; areas deeper than 6000 meters account for 1.67%, and areas shallower than 4000 meters account for 7.10%. The shallow water areas with water depths less than 5000 meters are mainly distributed in the northern boundary of the block, affected by the seamount landslide, and in the southwestern hilly area of Block M1. The deep-sea plain area has a water depth mainly between 5000 and 6000 meters.

Slope. The slope of the terrain in Block M ranges from 0 to 80 degrees, mainly concentrated between 0 and 5 degrees, accounting for about 92% of the area. This indicates that the terrain changes are stable and have small undulations within the area. In the landslide area, there are blocks of varying sizes, with slopes reaching over 20 degrees where the blocks are distributed.

Echo Intensity. The echo intensity of Block M is mainly concentrated between –25 and –40 dB, accounting for about 82%. The high-intensity areas with echo intensities greater than –25 dB are mainly distributed in the southwestern hilly area of Block M1, the eastern part of Block M1 affected by the Matsuzaki Guyot landslide, and the northwestern part of Block M2 affected by the Magoshichi-no-Hoshi Seamount landslide, accounting for 30% of the block area. The deep-sea plain area has an echo intensity range mainly between –30 and –40 dB, accounting for 62% of the block area.

Nodule Abundance and Coverage. The average abundance of nodules in Block M2, where CTA is located, is 26.16 ± 11.11 kg/m². The average coverage of nodules is 61.31 ± 20.80%.

Nodule Type Characteristics. Based on the size of the nodule particles, there are four types of nodules in Block M2: giant (>=7 cm), large (5–7 cm), medium (3–5 cm), and small (<3 cm). The test area is mainly dominated by large nodules, with the mass of large nodules accounting for over 70%.

Sediment Type. The surface sediment types in the slope and plain areas of Block M are both deep-sea clays, with siliciclastic debris (including clay minerals and fine silt-sized terrigenous detritus) as the main component (75% – 98%), containing small amounts of siliciclastic biological detritus (mainly radiolarians, sponge spicules) and volcanic detritus, with the volcanic detritus content in the slope area slightly higher than in the plain area.

Sediment Mineral Characteristics. The clay minerals in the surface sediments of Block M are mainly illite (content ranging from 58.81% to 76.58%, with an average value of

70.35%), followed by chlorite, montmorillonite, and kaolinite. The content of montmorillonite in the slope area sediments is relatively high, while the content of illite in the plain area sediments is relatively high.

Sediment Elemental Composition. The main elemental analysis results of the surface sediments in Block M show that the range of SiO_2/Al_2O_3 is 2.94 – 3.75, with an average value of 3.20, Fe_2O_3/Al_2O_3 ranges from 0.47 to 0.60, with an average value of 0.51, and TiO_2/Al_2O_3 ranges from 0.05 to 0.06, with an average value of 0.05. This indicates that the surface sediments in the working area are mainly terrigenous deep-sea clays and are influenced by volcanic materials and biogenic material inputs. The content of rare earth elements ($\sum REY$) ranges from 52.95×10^{-6} to 599.39×10^{-6}, with an average value of 332.23×10^{-6}. All station surface sediments show negative anomalies of Ce and positive anomalies of Eu.

Sediment pH and Eh. The pH data of the surface sediments in Block M show a main range of 5.67 to 9.60, with about 78% of the station surface sediment pH values between 7.00 and 9.60, indicating that the pH of the surface sediments (pore water) in the area is neutral to slightly alkaline. The Eh value of the surface sediments ranges from 166 mv to 343 mv, with 84% of the station surface sediment Eh values ranging from 180 mv to 280 mv, indicating that the surface sediments (pore water) in the area have a high degree of oxidizing properties.

Geotechnical Mechanics. The geotechnical test results of Block M show that the geotechnical properties of the surface sediments in this area are influenced by the underwater topography. Considering the complexity of the sediment sources in the slope area, the geotechnical properties do not show obvious changes with depth, while the sediment sources in the deep-sea plain are stable, and their geotechnical properties show regular changes with depth. In the area affected by the underwater fan, the geotechnical properties of the sediments are influenced by the wavy terrain.

Interstitial Water Metal Elements. The main metal element contents in the interstitial water of the sediments in Block M do not show a obvious pattern vertically, but the variation range is large, with the order of variation being Cu (108.0%) > Mn (80.6%) > Pb (73.9%) > Zn (69.2%) > Fe (63.1%) > Co (60.6%) > Cd (46.9%).

Physical Oceanographic Features

Temperature and Salinity. The results of 16 full-depth CTD profiles in the three-year period show that the sea surface temperature in the region is varied between 29.06 and 29.67 °C, and the depths of the mixed layer are relatively shallow, between 26 and 76 m. The

thermocline of each station is located between the bottom of the mixed layer and the depth of about 400 m, and the temperature at the bottom of the thermocline is about 10 – 11 °C. The temperature of the seawater at the depth of 400 m decreases with the increase of the water depth, and the temperature of the bottom layer is about 1.51 °C. The salinity of the sea surface is 34.46 – 34.82, and the salinity profile shows an "Inverse S-shaped" double halocline pattern, with the maximum salinity layer located at approximately 93–150 m, and the maximum salinity ranging from 35.04 to 35.21. The minimum salinity layer is located at about 500–560 m, with a minimum value of 34.10 – 34.17. There is a strong halocline from the bottom of the mixed layer to the maximum salinity layer, as well as between the maximum and minimum salinity layer, with dramatic changes in salinity. At depths deeper than the depth with minimum value, the salinity gradually increases with depth, and basically stabilizes at 34.5 – 34.7 at depths deeper than 1000 m.

Currents. Observations of the currents in the subsurface buoy in Block M show the following: (1) The surface currents are characterized as follows: current speed in the upper layer of the area (shallow than 250 m) is very large, with a maximum value exceeding 50 cm/s, and the current speed decreases with water depth. From the change of current direction, it can be seen that this area is affected by the large-scale circulation, and there are obvious interannual and seasonal variations. In the IRZ, strong and stable westward current occurs around May, and the strong current at 100 m depth mainly occurs in March (northward current), the end of April and the beginning of May (southwester current), and June (westward current). In the PRZ, there is a stable westward current from January to April, and the current direction is reversed to an eastward current from May to June, and the strong currents at 100 m depth mainly occur in March (northward current), late April and early May (southwestward current), June (southward current) and November (southward current). (2) the mid-level currents are characterized as follows: The mid-level current field was mainly influenced by tides. The maximum current velocity of the mid-level (1990 m) current field in the IRZ is 15.83 cm/s, the mean current velocity of the east and north component is –0.28 cm/s and – 0.02 cm/s respectively, and the mean current direction is southwestward. The maximum current velocity of the mid-level (2000 m) current field in the PRZ is 18.57 cm/s, the mean current velocity of the east and north components is –0.47 cm/s and –0.04 cm/s respectively, and the mean current direction is southwestward. The mid-level current field in the end of September to November of 2022 may be affected by the mesoscale process, and

the current velocity is large. (3) The near-bottom current is influenced by tides. The observed result shows that: the maximum current velocity in the 5324 m layer in the IRZ is 17.26 cm/s, the mean current velocity of the east and north component is –0.81 cm/s and 0.05 cm/s respectively, and the mean current direction is northwest; the maximum current velocity in the 5534 m layer current field is 18.40 cm/s, and the mean current direction is northwest. The mean current velocity of the east and north component is –1.20 cm/s and –0.06 cm/s respectively, the mean current direction is southwest, and the mean current magnitude is larger than that in the 5324 m layer. The near-bottom current field in the PRZ has stable strong southwest current during June–July and October–November in 2022.The maximum current velocity in the 5322 m layer is 15.65 cm/s, the mean current velocity of the east and north component is –2.81 cm/s and –2.17 cm/s, respectively. The maximum current velocity in the 5532 m layer is 16.85 cm/s, the mean current velocity of the east and north component mean current velocity is –0.06 cm/s, and the mean current velocity is larger than that in the 5324 m layer. The maximum current velocity in layer 5532 m was 16.85 cm/s, the mean current velocity of the east and north component was –3.15 cm/s and –2.48 cm/s, and the mean current velocity was bigger than that in layer 5322 m.

Mesoscale Eddies. Based on the META dataset, statistical analyzing was carried out to the mesoscale eddies in the rectangular block of 18–20 °N and 150–156 °E. Totally 324 cyclonic eddies and 314 anticyclonic eddies characterized by an active period of more than 10 days within the block from 1993 to 2021 were analyzed. Obvious monthly variations of mesoscale eddies are found. Most cyclonic eddies (76 totally) appear in this rectangular in March, the second highest in April (73), and the least in October (42). Anticyclonic eddies were highest in January (70); next highest in March and May (66); and lowest in June (36).

Turbidity. The turbidity monitoring results in the near-bottom layer of Block M show that the turbidity is less than 0.1 NTU from September 2021 to May 2022, and increases to 0.2 NTU from May 2022, and high turbidity phenomenon occurs in July, September, and November 2022, and comparing with the near-bottom current field of this station, it is found that the current velocity is obviously enhanced during this period of time, and it is initially judged that the high turbidity in the near-bottom layer is positively correlated with the large current velocity. A positive correlation exists between high near-bottom turbidity and high current velocities.

Tides and Currents. Based on the results of the TPXO global tidal model, it is found that irregular semidiurnal tides dominate on the east side of 153 °E in Block M2, while irregular full-day tides dominate on the west side of 153 °E in the Block M2 and in Block M1. The maximum tide at each station is the M2 tide, followed by the S2 tide. According to the formula for determining the tidal type, the near-bottom tidal currents at each station are mixed tidal currents.

Chemical Characteristics of Seawater

Nutrients. Overall, the nutricline in Block M is between 200 m and 800 m. Within the euphotic zone of Block M, nutrient concentrations are as low as nanomoles per liter, increasing gradually with depth. Beyond the nutricline, the nutrient concentrations remain relatively stable with increasing depth, though slight variations are noted in near-bottom water nutrient levels. The primary nitrite maximum (PNM) can be found from the vertical distribution of nitrite with relatively high nitrite concentration around 100 m to 150 m.

pH. The pH in Block M ranges from 7.53 to 8.27. Surface to 200 m depth shows relatively high pH levels, gradually decreasing with depth to a minimum at about 800 m, with subsequent slight and stable increases with further depth.

Dissolved Oxygen (DO). The range of DO concentration is from 112.1 μmol/L to 479.2 μmol/L (as O). DO exhibits high concentrations in the mixed layer, decreasing with depth and reaching a minimum around 800 m, followed by a gradual increase thereafter.

Total Alkalinity (TA). In the upper water, TA slowly increases with depth from the surface water to the chlorophyll maximum layer, then slowly decreases down to 500 m. Overall, the concentration of TA increases with depth. This is attributed to the dissolution of $CaCO_3$ shells or skeletons of calcium-bearing organisms after their death in the deep water. This dissolution increases the concentration of bicarbonate in the water, leading to higher TA in deep water.

Dissolved Inorganic Carbon (DIC). The concentration range of DIC in this region is from 1991 μmol/L to 2531 μmol/L. Generally, DIC concentration increases rapidly with depth from the surface to 800 m, with little variation thereafter.

Suspended Solid (SS). The concentration of SS in most stations ranges from 0.1 mg/L to 3.2 mg/L. From the overall distribution of SS in Block M, the concentration of SS is low and does not change obviously, with no obvious pattern of change.

Sinking flux: Analysis of sediment trap samples deployed in the subsurface buoy showed an overall obvious seasonal trend in the total mass of sinking particulate matter (SPM) in the region, with the total mass of settled SPM obviously higher in the summer than in the winter. The least amount of particulate matter, 26.8 mg, was obtained from November 1–16, 2021; the most amount of particulate matter, 159.1 mg, was obtained from July 16, 2022–August 1, 2022, and the average value of the mass of sedimentary particulate matter for the entire monitoring period was 83.7 mg. During this time series period, the compositional percentage of sedimentary SPM, total carbon (TC), ranged from 15.32 –30.47%, with a mean value of 20.38%, and total nitrogen (TN) ranged from 0.84 – 4.64%, with a mean value of 2.09%. Seasonal variations of TC and TN were not obvious, but the percentage of TC was obviously higher than that of TN in all cases.

Sound Pressure Level of Noise

The highest root mean square sound pressure level of environmental noise is close to 120 dB re 1μPa, but the overall sound pressure level in the survey area varies within the range of 92–115 dB, with an amplitude difference of about 23 dB and a median sound pressure level of about 101.4 dB.

Characteristics of Biological Communities

The benthic ecosystems of the seamounts and intermountain basins in the northwest Pacific Ocean are characterized by the following features: Firstly, the benthic communities form obvious zonal distribution along a huge depth gradient from the summit of deep-sea seamounts to deep-sea basins below the foothills; Secondly, due to the low primary productivity of the upper ocean, the benthic communities in this region show low biomass and abundance. Thirdly, due to the obvious influence of topography and geomorphology on near-bottom currents, they also have a obvious impact on the distribution characteristics of benthic organisms (for example, there are obvious differences in the benthic communities on the eastern and western slopes of seamounts). In terms of biogeographical characteristics, the benthic community in this area belongs to the north central Pacific biogeographical region.

Chlorophyll *a*. The contract area belongs to the global low biomass and low productivity zone. The mean values of chlorophyll *a* in the water column from 2021 to 2023 were 35.23 ± 4.91 mg/m^2, 35.45 ± 3.80 mg/m^2, and 40.97 ± 9.06 mg/m^2, respectively, with little annual variation. The vertical distribution of chlorophyll *a* at all stations showed a clear

single-peak structure, with the maximum concentration of chlorophyll *a* at most stations located between 120 and 150 m depth.

Primary Productivity. Primary productivity was low in Block M. The average values of primary productivity from 2021 to 2023 were 25.03±10.43 mgC/(m^2·h), 20.95±9.09 mgC/(m^2·h), and 25.80± 5.51 mgC/(m^2·h), respectively, with little annual variation. The maximum values all occurred at depth of 50% surface light intensity. The main reason for low primary productivity in autumn is due to the high water temperature in the subtropical circulation zone of the north Pacific Ocean in fall, which increases the difference between the water density of the upper and the lower ocean, impeding the upward transport of nutrients, and inhibiting the growth of the net primary productivity of the ocean.

Microorganisms. (1) Microorganisms in the water column of Block M. The dominant bacterial phyla were Proteobacteria, Actinobacteria, Planctomycetes, Bacteroidetes, Cyanobacteria, Firmicutes, Candidatus, Saccharibacteria, Acidobacteria, Verrucomicrobia, Chloroflexi. Planctomycetes is highly abundant in almost all water layers. They can maintain metabolism through nitrification and denitrification in oxygen-deficient conditions, thus may play an important role in the process of nitrogen cycling in the water body of Block M. (2) Sediment microorganisms in Block M. The results of β-diversity analysis showed that there was no obvious difference in the structure of microbial communities in Blocks M1 and M2. The top 10 genera in terms of abundance included *Nitrosopumilus* from Crenarchaeota, *Sphingomonas*, *Woeseia* and *Ralstonia* from Pseudomonadota, and six uncultured genus-level taxa (Subgroup_21, JTB23, BD2-11_terrestrial_group, bacteriap25, S085, NB1-j).

Picoplankton. The abundance of picoplankton, *prochlorococcus*, *synechococcus* and eukaryotic algae in Block M was relatively stable in autumn, with unobvious annual changes. Chromatographic analysis showed that the abundance of *prochlorococcus* was the highest in this area, followed by *synechococcus* and dinophyceae, and the abundance of diatoms, dinoflagellates and Prasinophyceae were very low; picoplankton abundance in the DCM layer varied obviously among the survey stations, but the differences in community structure were not obvious.

Nanoplankton and Microplankton. (1) Nanoplankton (from CTD samples); A total of 65 species belonging to 37 genera and 4 phyla of nanoplankton were identified. Among them, diatoms are the most dominant group, including 26 genera and 44 species, accounting for 67.69% of the total species; Dinoflagellates come second, including 9 genera and 19 species,

accounting for 29.23% of the total species; (2) Microplankton: A total of 155 species, belonging to 56 genera and 6 phyla, were identified in Block M over a period of 3 years. Among them, diatoms are the most dominant group, including 38 genera and 88 species, accounting for 56.77% of the total species; Dinoflagellates come second, including 14 genera and 62 species, accounting for 40.00% of the total species.

Zooplankton. (1) Species composition and abundance: A total of 406 species (including unidentified spp.) of zooplankton in 6 phyla and 13 major categories were recorded in the upper layer of Block M, with 3-year average abundances of 79.02 ind/m^3, 46.37 ind/m^3, and 88.35 ind/m^3, respectively. The zooplankton community was generally characterized by low abundance and high biodiversity. Vertical distribution showed that although the abundance of zooplankton showed a decreasing trend with the increase of water depth, the diversity still maintained a very high level. Copepods were the only dominant taxon in the zooplankton community, accounting for over 90% of the total abundance of zooplankton in all water layer. As the water depth increases, the percentage of copepods in the total abundance gradually increased, and at depths below 200 m, copepods accounted for over 98% of the total abundance. Therefore, copepods play a dominant role in planktonic animal communities. (2) Diurnal Vertical Migration**.** Zooplankton in this area showed a diurnal vertical migration phenomenon. Zooplankton collected at night in Block M was higher in diversity and abundance than those collected during the daytime. Copepods as the main group dominated the vertical migration behavior of the zooplankton community, while ostracods and pteropods did not show vertical migration in the euphotic layer.

Mesozoan meiofauna. A total of 15 groups of meiofauna were found in Block M, among which nematodes were the dominant group. Meiofauna was mainly found in the surface sediments of 0–2 cm, with the size of 63–125 μm being dominant. The meiofaunal abundance in the contract area ranged from 4.94 to 64.33 ind./10 cm^2, with a mean value of 26.21 ind./10 cm^2 and 22.86 ind./10 cm^2 in 2022 and 2023, respectively. The mean abundance of meiofauna in the IRZ and PRZ was 23.2 ± 10.3 ind./10 cm^2 and 35.7 ± 16.4 ind./10 cm^2, respectively. For nematodes diversity, a total of 37 genera belonged to 19 families was found in this area.

Macrofauna. A total of 46 species of macrofauna were found in Block M. Crustaceans were the most abundant in terms of species composition, followed by polychaetes. The average abundance of macrofauna in 2022 and 2023 showed obvious changes, with 13.44±15.69 ind/m^2 and 18.0±2.8 ind/m^2, respectively. Macrofauna abundance in this area is obviously lower than that of the eastern Pacific nodule area. The macrofauna mainly distributed in 0–3 cm surface sediments. The species richness of macrofauna in this region was predicted to be about 193 using the chao1 index.

Megafauna. Based on the preliminary analysis of the seabed photographs of Block M, there were 35 morphological species belonging to 10 megafauna taxa, including the phyla of Porifauna, Cnidaria, Annelida, Arthropoda, Mollusca, Echinodermata, Hemichordata, Chordata, Urochordata and Bryozoa. Among them, echinoderms had the highest number of species and the highest abundance, followed by sponge. There was a great difference in the community structure of the megafauna between the transect near Magoshichi Guyot and the two transect in the basin area, with high abundance of annelids and hemipterans in the near seamount area and relatively high abundance of sponges, arthropods, echinoderms, and chordates in the basin area. Similar species compositions were found in the IRZ and PRZ, with 20 common species and a co-dominant species *Peniagone* sp., *Hyalonema* sp., *Caulophacus* sp., *Cerataspis monstrosus*, *Coryphaenoides* sp., *Synallactes* sp., *Benthodytes sanguinolenta.*

Scavengers and Demersal Fishes. Lander system was used to obtain four species of benthic scavengers and fishes, including *Eurythenes gryllus*, *Paralicella tenuipes*, *Hirondellea dubia*, and Macrouridae sp. Video analysis also revealed five groups of organisms, including two species of fish (*Coryphaenoides* sp. and Ophidiidae), and three species of arthropods (Pycnogonida, Gammaridea and *Glyphocrangons* sp.).

Marine Mammals, Seabirds and Sea Turtles. Using observations from cruises and public data, a total of 4 species of mammals belonging to 4 genera, 3 families, and 1 order were recorded in Block M and adjacent sea areas, as well as 3 species of sea turtles belonging to 3 genera, 2 families, and 1 order, and 24 species of seabirds belonging to 18 genera, 11 families, and 3 orders. Among them, there is one species of global endangered species: *Numenius madagascariensis*, six vulnerable species: *Lepidochelys olivacea*, *Caretta Liposcelis*, *Dermochelys coriacea*, *Physeter macrocephalus*, *Calidris acuminata*, and *Oceanodroma leucorhoa*, and one near-threatened species: *Calonectris leucomelas*. Six species of baleen whales, including *Megaptera novaeangliae*, *Balaenoptera physalus*, *Balaenoptera acutorostrata*, *Balaenoptera musculus*, *Balaenoptera borealis*, *Balaenoptera brydei* have been documented in the BPC contract area by hydrophones from October 2021 to October 2023, they occurred seasonally (Table 7-3), but they were not recorded from July to August.

Eukaryotic Molecular Biology Characteristics. Using DNA high-throughput sequencing technology, the molecular diversity of eukaryotic organisms in the sediments of

the contract area was investigated, and a total of 379,431 valid sequences were obtained, which could be classified into 10,944 OTUs at a similarity of 98.65%. A total of 652 species (excluding unannotated species) were assigned in 30 phyla, 82 orders, and 272 families. The taxon with the highest number of OTUs was nematodes.

Assessment of Physicochemical Environmental Impacts and Proposed Mitigation Measures

Physicochemical Environmental Impact Assessment

Categories of potential impacts on the physicochemical environment. Noise, light pollution, and discharge of tailings and domestic sewage from surface support vessels, mining systems during ore collection have potential impacts on the environment and organisms, etc. Potential environmental impacts of deep-sea mining include the following three depth zones: (1) potential impacts on the deep seafloor environment; (2) potential impacts on the environment of the mid-water column (below the euphotic layer to the 100 m layer above the bottom); (3) potential impacts on the upper environment (euphotic layer).

For the proposed polymetallic nodule collector test activity by BPC, the nodules are discharged directly in the CTA and are not lifted to the ship through risers, while the tail water is also discharged near the bottom (4 m above the bottom), and therefore the environmental and biological impacts of this activity will occur mainly in two depth zones, the seabed environment near the collector mining track, and the sea-surface area influenced by the ship's activities. The potential impact on the mid-water column environment and organisms is only from noise.

Plume Modeling and Impact Prediction. In order to better assess and predict the diffusion range and impacts of the plume generated by the collector component test, the project adopts a high-resolution regional ocean model (FVCOM) to simulate the diffusion of the deep-sea near-bottom sediment plumes during the collector test based on previous field observation data, and analyzes the horizontal and vertical distribution characteristics of plumes and the distribution characteristics of redeposition thickness, providing a scientific basis for the formulation of plume monitoring plans during the collector test.

Based on the near-bottom suspended sediment concentration obtained from the baseline survey, 0.1 mg/l was selected as the boundary value for the plume dispersion impact. Ten typical conditions were selected, corresponding to weak northeastward current (July 5th), strong westward current (August 5th), weak southwestward current (August 9th), strong

eastward current (September 26th) and strong southwestward current (October 12th), to carry out the simulation of the test plume at a discharge height of 4 m above the bottom. The results show that: (1) In the average case, the maximum dispersal distance of the deep-sea mining plume is 5.42 km with an area of 8.12 km^2, and the mining plume disappeared 3–4 days after the end of the test; in the extreme case, the maximum dispersal distance of the deep-sea mining plume is 27.86 km with an area of 69.75 km^2, and the mining plume disappeared 7–9 days after the end of the test. (2) In the average case, the maximum vertical influence of the Plume is 231 m, and the high suspended sand concentration (>10 mg/l) is mainly located within 60 m from the bottom; in the extreme case, the maximum vertical influence of the Plume is 346 m, and the high suspended sand concentration (>10 mg/l) is mainly located within 110 m from the bottom. (3) In the average case, the maximum thickness of redeposition is 2.60 cm, and the area with the thickness of redeposition more than 1 cm is 0.28–0.31 km^2, which is slightly larger than the area of the CTA (0.25 km^2), i.e., the 1 cm thick redeposition thickness is basically limited to the vicinity of the CTA. In the extreme case, the maximum redeposition thickness was 1.48 cm, and the area with redeposition thickness greater than 1 cm ranged from 0.0–0.16 km^2. (4) The horizontal diffusion direction of the plume depends on the bottom current direction, and the extent of horizontal diffusion depends on the bottom current velocity (see Section 6.2.3 for details).

Shipping Routes. The closest route to the BPC's contract area is the Far East–Australia route, starting from Tokyo to Sydney via the Solomon Islands. The nearest distance between the CTA and this route is approximately 400 km, so the impact of the collection test activities and merchant shipping on each other can be neglected.

Air Quality. The vessels used in this project strictly comply with the obligations and standards of the International Maritime Organization on marine environmental practices, including *International Convention for the Prevention of Pollution from Ships, 1973, as modified by the Protocol of 1978* (MARPOL73/78), and the *1997 MARPOL Protocol on the Prevention of Air Pollution from Ships*. Carbon emissions from the test are measured in accordance with the formula for calculating the carbon emission factor for marine diesel fuel in accordance with the 2019 Refinement to the 2006 IPCC Guidelines for National Greenhouse Gas Inventories. The greenhouse gas emission equivalent is 2783.3 tons.

Transboundary Impact. According to the results of the plume simulation, the maximum influence distance of the sediment plume diffusing outward from the CTA is

3.57km, and the plume influence range does not exceed the boundary of the BPC's contract area, so there will be no transboundary impact. During the test period, the range of light exposure is limited, and there will be no transboundary impacts. Noise is unavoidable during the test period and may have a transboundary impact. However, there are fewer studies on the environmental impacts of noise, and an impact assessment of noise impacts is provided in Section 7.2.4. The submarine test duration of this project is 100.5 hours, and the collector is in 1:5 scale, so the potential noise impact range is relatively small. The likelihood of transboundary social or economic impacts is also extremely low, with the vast majority of polymetallic nodules remaining on the seafloor and only a very small amount being recovered with the collector to the ship for smelting studies, which will not affect any of the existing metal producers.

Proposed Mitigation Measures:

International conventions such as the *International Convention for the Prevention of Pollution from Ships* (MARPOL 73/78) will be strictly enforced by the test vessel and the environmental monitoring vessel during the test, and the following mitigation measures will be taken:

(1) The "Manta" suspended collector is adopted in the design of this project, which can greatly reduce the milling and stirring of the seabed by the collector. The collection test shows that the depth of the collector track is only 4–6 cm, which obviously reduces the disturbance to the seabed compared to the tracked collector;

(2) Instead of collecting nodules by hydraulic mining, the "Manta" uses a pumping device to draw in polymetallic nodules, which will reduce the disturbance to the seafloor sediments;

(3) Discharge of mining tail water near the bottom (4 m above the bottom) will reduce the diffusion range of the tailings plume;

(4) The vast majority of polymetallic nodules collected will be retained on the seafloor, without mineral lifting system and discharge of surface or intermediate tailings.

Assessment of Impacts on the Biological Community and Proposed Mitigation Measures

Impact Assessment on the Biological Community:

Removal of Nodules and Its Impact on Benthos. The test activity will remove most of the nodules from the collecting track, which will obviously destroy almost all of the sessile

megafauna attached to the nodules, such as sponges, anemones, sea lilies, etc., and will turn the original benthic community, which was a mixture of soft-sediment and hard-substrate, into a purely soft-sediment benthic community, thus decreasing the benthic biodiversity of the CTA.

Removal of Sediment and Its Impact on Benthos. After the sediment around the nodule being extracted by the collector, the organisms in the sediment will inevitably be caught up in the collector, and then drifted away with the current or re-settled. This process may lead to sudden death of some of the benthos, thus decreasing the abundance of benthos in the CTA.

Compaction of Sediments and Its Effects on Benthos. Disturbance and compaction of the surface sediments will also reduce the abundance of macrofauna and meiofauna, but microbial abundance may increase. The project uses suspended collector, and the area of this collection test is very small (about 0.25 km²). Although it will locally reduce the abundance of benthos, it is not expected to affect the community structure, gene flow or species connectivity of the benthos and benthic ecosystem function in the contract area.

Plumes and Their Effects on Organisms. Burial or smothering effects may occur for zoobenthos, such as sponges and corals, which are sessile or less motile near the source of disturbance. High concentrations of SS may impair respiration and feeding by clogging gills or other filtering organs. Olfaction may be the primary mechanism for attracting and guiding benthic scavengers to prey on food. Sediment plumes generated by test activities can interfere with odors released by food and reduce the probability of finding food, leading to a general reduction in food availability for scavengers. Enhanced turbidity in sediment plumes can reduce light transmission, and therefore may obviously reduce bioluminescent visibility, thereby reducing the likelihood of finding mates and leading to reduced rates of reproduction of organisms.

Light Impacts. Artificial light sources that are much stronger than bioluminescence may alter vertical migration of zooplankton, trigger aggregations of fish that lead to increased predation, and attract seabirds to collide with brightly lit vessels. However, there is currently no scientific evidence to confirm that anthropogenic light pollution in deep-sea environments will causes direct adverse effects at the community or ecosystem level. Due to the short duration and small scale of this experiment, the effects of light on organisms are only temporary and limited to the vicinity of the CTA.

Noise Impacts. (1) Impacts on Birds: Since the 2021 cruise, according to our on-site surveys and observations on the shipping route from the East China Sea to BPC's contract area, we have observed a relatively small number of seabird species and individuals, especially in the contract area where there are only sporadic records. BPC's contract area is far away from the main shipping routes for commercial transportation and there are very few passby vessels, so it is expected that project-related activities will not obviously interfere with seabird mating or foraging behavior. (2) Impacts to Cetaceans and Sea Turtles: Six species of baleen whales, including *Megaptera novaeangliae*, *Balaenoptera physalus*, *Balaenoptera acutorostrata*, *Balaenoptera musculus*, *Balaenoptera borealis*, *Balaenoptera brydei* have been documented in the BPC's contract area by hydrophones from October 2021 to October 2023. They appear seasonally in the contract area (Table 7-3), but were absent in July and August. While this test is scheduled to be conducted in July to August, it is expected that there will be no obvious impacts on large cetaceans such as *Balaenoptera physalus*. Small and medium-sized cetaceans toothed whales have been recorded in some amount each season, with sperm whales being one of the cetacean species with a high frequency of occurrence in the contract area, but the contract area is not a major distribution area for sperm whales, nor is it located in their main migratory paths, thus the chances of occurrence are very low (Figure 7-13). Therefore, no obvious impacts on small and medium-sized cetaceans are expected. The Sea Turtle website (2024) indicates that sea turtles are primarily distributed along the coast and in the EEZs of the SILs, with a migratory route in the vicinity of BPC's contract area (Figure 7-14), and no turtles were documented by BPC's surveys. (3) Noise from seafloor collector: The operation of seafloor collector trucks inevitably generates a large amount of noise, which also has a potential impact on deep-sea benthos and aquatic organisms. However, there is currently few research in this area, so it is not yet possible to assess how much noise is generated by the collector test and the extent of its impact. BPC will deploy multiple hydrophones for monitoring during the collector test. Given the short duration of the collector test, it is expected that it will not cause permanent harm to aquatic organisms.

Toxicity of Potentially Released Heavy Metals. The obvious shortcomings of the current toxicity tests for heavy metals are mainly in the following 2 aspects: (a) most of the tests have used single metal rather than combinations of metals; and (b) the tests have been based mainly on shallow-water species. Therefore, more research work is needed to

determine heavy metal concentration thresholds in the current toxicological risk assessment of potential polymetallic nodule mining.

Warming Effects. There are no reports of warming caused by polymetallic nodule mining. In the case of the present test, any thermal stresses generated by the plume during the test activity of the collector were negligible due to its small size. The shifting location of the discharge, and the tail water is mixed and diluted with the surrounding seawater, which is not expected to cause local temperature rise.

Hypoxia Effect. The CTA of this project is located in the oligotrophic area of the Northwest Pacific Ocean, the organic carbon content of surface sediments is extremely low, and a large amount of total organic carbon in deep-sea sediments is inert organic carbon (Arndt et al., 2013). Considering the small scale of the total disturbance and the mobility of the bottom seawater of the CTA, we anticipate that the alteration of the bottom dissolved oxygen will be very slight, and the ecological effect caused by the test is not obvious.

Biological Resilience. The recovery potential of deep-sea species following disturbance also varies according to the extent of their habitat destruction, and although there is some potential for recovery, the environmental impacts of polymetallic nodule mining are likely to be long-term. In the case of the present collector test, owing to the short duration and small area of disturbance, no widespread long-term impacts are expected.

Impacts on Fishery Resources. The BPC's contract area is not a major fishing ground in the Pacific Ocean (Figure 5-114). The main type of fishery operation in the waters of the contract area is longlining, but according to the BPC survey period from 2021 to 2023, no fishing vessels have been observed in the area. Therefore, no adverse effects on fishing operations and fishery resources are expected during this test period.

Cumulative Impacts. Since this test is only a single activity, it is not expected that cumulative impacts from multiple operations will occur. Cumulative impacts from different pressures from a single activity can be expected, but at this stage, there is limited publicly available information on the cause-effect activity-pressure-effect relationships for the target ecosystems and their components (i.e., populations and communities, habitats, and ecosystem functions) and the cumulative pressures that mining activities may exert on ecosystems and their components (Tamis et al., 2016). In particular in the abyssal Northwest Pacific, more data are needed to quantify the impacts of mining activities and to identify specific pressures and their cumulative impacts on ecosystem vulnerability and resilience. Figure 7-18

illustrates the potential relationships between activities and pressures on different ecosystem components.

Proposed Mitigation Measures

BPC will conduct this test activity with reference to the principles of protection and preservation set out in the relevant environmental standards being prepared by the International Seabed Authority, taking a precautionary approach, utilizing best available techniques and good environmental practices to avoid and mitigate the impacts of this test activity, and will take the following measures:

- During the operation of surface support vessels, specialized personnel will be assigned to monitor the activities of sea turtles and large mammals (such as whales) around the vessels, and to take proactive collision avoidance measures to avoid causing damage to these organisms.

- During night operations, reduce ship lighting as much as possible under the premise of safeguarding operational safety, and avoid upward exposure to light to reduce the impact on bird activities.

- BPC will take avoidance/prevention measures in strict accordance with the Regulations on the Prevention and Control of Marine Pollution from Ships (MARPOL) and the guidelines of the International Maritime Organization (IMO) in order to guarantee the legal disposal of pollutants such as garbage, domestic sewage, oily sewage, sewage containing poisonous and hazardous substances, and exhaust gases from ships during the event.

- During the collector test, BPC will monitor environmental parameters in real time through the monitoring equipment carried by the collector itself, AUVs, and monitoring master stations and monitoring base stations deployed around the CTA. Based on the results of tracking monitoring and follow-up evaluation, activities with actual impacts greater than the predicted impacts will be immediately stopped on-site and reported to the competent authorities.

Risk and Contingency Plans

Based on the analysis of this collector test and associated activities, it was assessed that these activities were routine in nature (e.g., operation of surface vessels) and that the scale of the collector test was relatively small, and therefore none of the activities were assessed as presenting a high level of risk. Activities with medium-level risks include vessel collisions, fires, and hazardous chemical spills. Low-level risks include unexpected weather hazards

such as typhoons, and dislodging of umbilical cables from the ore collector. Contingency plans will be developed during project implementation to minimize the likelihood of these low and medium level risks, including the following measures.

Ships used in this project strictly comply with the obligations and standards of the International Maritime Organization on maritime safety and environmental practices, including the *International Convention for the Prevention of Pollution from Ships, 1973, as modified by the Protocol of 1978* (MARPOL73/78). At the same time, the ships will formulate emergency response plans for meteorological protection and severe weather, emergency response plans for ship fire safety, emergency response plans for ship collision accidents, etc., and carry out regular training for relevant personnel to minimize the risks arising from ship failures and severe weather.

To prevent spills of chemicals or fuels due to equipment leaks, accidental failures or extreme accidents. Spills may have harmful effects on water quality and adversely affect marine ecosystems. Taking into account the results of the spill risk assessment, the project will develop a shipboard marine pollution contingency plan and review and revise mitigation measures and operating procedures as needed. Proactive and reactive measures will be implemented to minimize the risk of fuel and other hazardous materials and their potential impacts. Proactive measures may include: appropriate material selection and corrosion control for equipment and tanks; monitoring of piping/hose pressures for early detection of any leaks or spills; establishment of equipment maintenance and monitoring programs to ensure equipment integrity and detect loss of containment; system setup of emergency stop and containment systems; acquire and maintain spill response and containment equipment appropriate to the level and type of risk to be deployed in all potential spill areas; implement personnel training and field drills in spill prevention, containment, and response.

Environmental Monitoring Program

In conjunction with the collector component test in the polymetallic nodule area of the western Pacific Ocean, a deep-sea mining environmental impact monitoring system will be deployed in the IRZ and the PRZ to collect environmental impact monitoring data during and after the test, in order to compensate for the lack of existing deep-sea mining knowledge and to enhance the scientific rigor of environmental impact assessments for such activities. At the same time, scientific research related to the potential impacts of deep-sea mining will be carried out to develop preventive measures for potential future deep-sea mining plans, and to provide design basis for the development of deep-sea green mining technology.

Monitoring Areas:

The monitoring area includes an IRZ (including the CTA and the plume dispersion impact area) and a PRZ. The IRZ is located in the northeastern part of the Block M2 at the southern foothills of the Magoshichi Guyot, with a total area of approximately 11.5 km × 11.5 km (see Figure 3-3). The PRZ, located in Block M1, at the southern foothills of the Matsuzaki Guyot (Figure 3-4), covers an area of approximately 21 km × 16 km and is approximately 78 km away from the CTA. In addition, according to the concept of "research-oriented exploitation" and the precautionary principle, a seamount monitoring area is proposed to be established at the southern foothill and slope of the Magoshichi Guyot (Figure 9-3).

Monitoring Phases:

The environmental monitoring work is divided into 4 phases. Phase I: the environmental baseline survey before the test is divided into 2 subphases. Subphase I-1: to carry out environmental baseline survey in 2024 in the CTA, the plume impact area and the PRZ, respectively. Subphase I-2: in 2025 before the collector test, to deploy short-term subsurface buoys in the CTA and the plume impact area in order to obtain the bottom current data, which will provide a basis for determining or adjusting the environmental monitoring program. Samples such as sediment will also be collected from these 2 areas using multicorer and box corer. Phase II: environmental monitoring during the test in the second half of 2025. Phase III includes two subphases. Subphase III-1: after the test completed and the environmental monitoring equipment recovered in 2025, AUVs will be used to conduct optical and acoustic surveys of the CTA and the plume impact area and sediment samples from the three areas will be collected using multicorer and box corer, and one set of long-term observation Lander

system will be deployed at the CTA. Subphase III-2: the above 3 areas will be revisited in 2026 (i.e. 1 year after the test) for post-test environmental monitoring. Phase IV: long-term environmental monitoring in the 3rd, 5th, and 7th year after the test, respectively (see Figure 9-6). Meanwhile, one set of subsurface buoys will be deployed at in the southern foothills and slope of Magoshichi-no-Hoshi Seamount before the 2025 test to monitor the potential risk of upward transport of SS from the seabed along the slopes of the seamount.

Monitoring Index System:

The monitoring index system includes nearly 90 parameters in four categories: physical oceanography, chemical oceanography, biological communities, and physical properties of sediments.

Monitoring Techniques and Equipment:

These include operational platforms such as ROV, HOV and AUV, observation equipment such as CTD, ADCP, subsurface buoys (current meters, ADCP, turbidimeters, sediment traps, hydrophones), lander system, sediment profiling cameras, deep-sea particle observation cameras, and sampling equipment such as box corer, multicorer and sediment porewater corer.

Spatial Layout of Monitoring Equipment:

Upstream of the CTA: A portable turbidity meter, a current meter node and a set of observation nodes will be deployed 200 m from the edge of the CTA, and a subsurface buoy will be deployed 300 m away.

Both sides and downstream of the CTA: A portable turbidity meter, a current meter and an ADCP node will be deployed 50 m from the border of the CTA. Most of the other equipment will be mainly placed in the plume dispersal area downstream of the CTA, with three observation nodes placed at 100, 300 and 600 m downstream of the CTA. Two sampling nodes will be placed at 100 and 300 m. The six subsurface buoys downstream will be arranged in a fan shape, with the first one 200 m downstream of the CTA, the second and third 500 m downstream of the CTA, and the fourth to sixth 800 m downstream of the CTA. The main communication station will be located 1 km downstream of the CTA (Figure 9-23 and Figure 9-24). An AUV survey line will be designed for the area 1000 m downstream of the CTA, cruising at different heights from the bottom to obtain turbidity data (Figure 9-8).

PRZ: 1 set of subsurface buoys and 1 set of observation nodes will be deployed respectively.

Southern foothills and slopes of Magoshichi Guyot: 1 set of subsurface buoys will be deployed respectively (Figure 9-3).

On the collector: turbidity, hydrophone and water sampler will be installed.

Three-Dimensional Monitoring of the Test Process Plume:

AUV-based multi-parameter detection technology was used to obtain turbidity, dissolved oxygen, Eh, temperature and salinity data in seawater at different heights of 5 m, 10 m, 25 m and 50 m around the collector during the test process, to identify the test plume anomalies and to define the three-dimensional spatial distribution range of the plume.

Post-Test Monitoring:

After the test is completed and the environmental monitoring equipment is recovered (Phase III-1 in Figure 9-6), an AUV will be used to navigate at a fixed altitude of 5 m above the bottom to obtain sediment thickness data for redeposition and seafloor video and photographs (Figure 9-23). Sediment samples will also be collected using multicorer and box corer, and near-bottom water samples will be collected by CTD.

In 2026 (Phase III-2 in Figure 9-6), a one-year post-test environmental monitoring will be conducted in the CTA, the plume impact area and the PRZ.

Long-Term Monitoring:

Long-term environmental impact monitoring will start in 2027, with impact monitoring at least at the 3rd, 5th and 7th years after the tests.

Monitoring Parameters and Methods:

The CTA, plume impact area and PRZ require monitoring parameters and methods at different phases as detailed in Section 9.2.5.5.2.

In Situ Experiments and Monitoring Programs:

(1) Sediment Coverage Experiment: Use "Jiaolong" HOV or ROV to carry out the sediment coverage (dose response) experiment; (2) Heavy Metal Exposure Experiment: Heavy metal-treated food bait will be deployed by lander system to trap demersal scavengers. Through the genome analysis of the trapped animals, the molecular level response of the demersal scavenger to the exposure to heavy metals will be investigated.

Post Impact Assessment:
- To establish high-resolution bottom plume model to reveal the bottom plume diffusion mechanism;

- To conduct in situ sediment coverage experiments to study the relationship between sediment plume resedimentation thickness and benthic mortality;

- To evaluate the effects of plumes and redeposition on benthic organisms and investigate the kinetic mechanisms of upward transport of SS along the slope of seamount;

The following studies will be conducted based on pre-test baseline surveys, monitoring data and samples during and after the test:
- To study benthic community changes before and after the collector component test and to assess the rate of recovery of the benthic community;

- To study the noise of collector and organisms' behavioral response to the noise;

- To study the impacts of the collector component test on marine ecosystem functions, including the bottom food chain, and to assess the resilience and recovery of benthic ecosystems;

- To assess the potential environmental impacts of suspended collector and provide a scientific basis for the development of green mining technologies.

Reporting

Incident Report:

In accordance with regulation 33 of ISBA/19/C/17, the contractor shall promptly report in writing to the Secretary-General by the most effective means any incident arising out of the activities that has caused, is causing or is likely to cause serious harm to the marine environment.

Incident reports to the International Seabed Authority will include the following:
- Details of incident;

- Incident -cause analysis;

- Actions taken at the incident site to avoid or mitigate any adverse environmental impacts;

- Any corrective measures taken or likely to be taken;

- Next steps to prevent the recurrence of similar incidents.

Corrective Measures:

To eliminate further impacts from environmental hazards, personnel injury/illness, or other system failures as a result of an environmental incident that has occurred, BPC will take appropriate corrective action by reevaluating the test effort, identifying the causes of the impacts, developing steps to correct specific measures, implementing response measures, and

verifying the effectiveness of the new initiatives to avoid a recurrence of a similar environmental incident.

Supervision

To implement the relevant regulatory requirements, BPC will invite observers from the sponsoring State (China) and the ISA to board the experimental vessel to conduct supervisory activities.

Transparency

BPC has consulted with the ISA observer, the China Biodiversity Conservation and Green Development Foundation (CBCGDF), and invited it to participate in relevant environmental monitoring and assessment activities. The company will also regularly disclose the progress of the experimental mining activities and related data to the public through its website or other media.

Stakeholder consultations

During the stakeholder consultation period from May 1 to June 6, 2024, a total of 308 comments were received from 10 international organizations/governments via email. Among these, 12 comments expressed approval or appreciation. Additionally, there were 270 comments that offered clear and relevant feedback, covering 16 specific topics (see Chapter 10 for details).

Conclusion

According to the simulation results of the numerical model for this test, with 0.1 mg/l SS as the background value,, the maximum dispersal distance of the deep-sea mining plume was 5.43 km and the area was 8.12 km^2 in average, and the mining plume disappeared 3–4 days after the end of the test; the maximum influence range of the plume in the vertical direction at the distance of 100 m from the boundary was 231 m, and the high concentration of SS (more than 10 mg/l) was mainly located within 60 m from the bottom; the maximum redeposition thickness was 2.60 cm, and the area with redeposition thickness greater than 1 cm was 0.28–0.31 km^2, which was slightly larger than the test area (0.25 cm^2) was mainly located within 60 m from the bottom; the maximum redeposition thickness was 2.60 cm, and the area with redeposition thickness greater than 1 cm was 0.28–0.31 km^2, slightly larger than that of the CTA (0.25 km^2), i.e., the redeposition thickness of 1 cm was basically confined to the vicinity of the CTA. In the extreme case, the maximum spreading distance of the deep-sea mining Plume was 27.86 km, with an area of 69.75 km^2 (25 m layer), and the mining

plume disappeared 7–9 days after the end of the test; 100 m from the boundary, the maximum influence area of the plume was 346 m, and the high concentration of SS (more than 10 mg/l) was mainly located within 110 m from the bottom; the maximum thickness of redeposition was 1.48 cm. The area with redeposition thickness greater than 1 cm is 0.0–0.16 km^2.

Considering the facts that (a) the project will adopt a suspended collector; (b) an environmental monitoring plan and proposed mitigation measures will be implemented, and (c) rigorous reporting and regulatory procedures will be followed during the testing process, the impacts of the small-scale testing of collector on the physicochemical environment and biological community could be reduced to a non-significant level. In the absence of significant events, the risk of "serious harm" to the marine environment on a regional scale from the testing of the collector is low.

1 INTRODUCTION

1.1 Goal

Based on the GERIS (Green, Economy, Reliability and Robustness, Intelligence, and Safe) mining concept, Beijing Pioneer High-tech Development Co., Ltd. (hereinafter referred to as "Beijing Pioneer Company (BPC)") has gradually promoted research of the deep-sea mining technology, and through the research and development of the of polymetallic nodule sampling test machine ("Manta") and mining test prototype, it will eventually be developed into a commercially available green deep-sea mining system.

Out of prudence to advance, this project will only test and technically validate the collector, and at the same time carry out long-term environmental impact monitoring. Based on the environmental baseline information and environmental monitoring information, it will carry out the environmental impact assessment of the collector test, and provide a scientific basis for developing green mining technology.

1.2 Background

The BPC signed a fifteen-year polymetallic nodule exploration contract with the International Seabed Authority (hereinafter referred to as the "ISA") in 2019. The contract area is located in the western Pacific and consists of four blocks totaling 74,052 km^2, and it is divided into four blocks, C1 (26,112 km^2), C2 (11,370 km^2), M1 (12,903 km^2) and M2 (23,667 km^2). Blocks C1 and C2 are located in the northern part of the Marcus-Wake Seamounts, and Blocks M1 and M2 are located in the southern part of the Magellanic Seamounts (Figure 1-1).
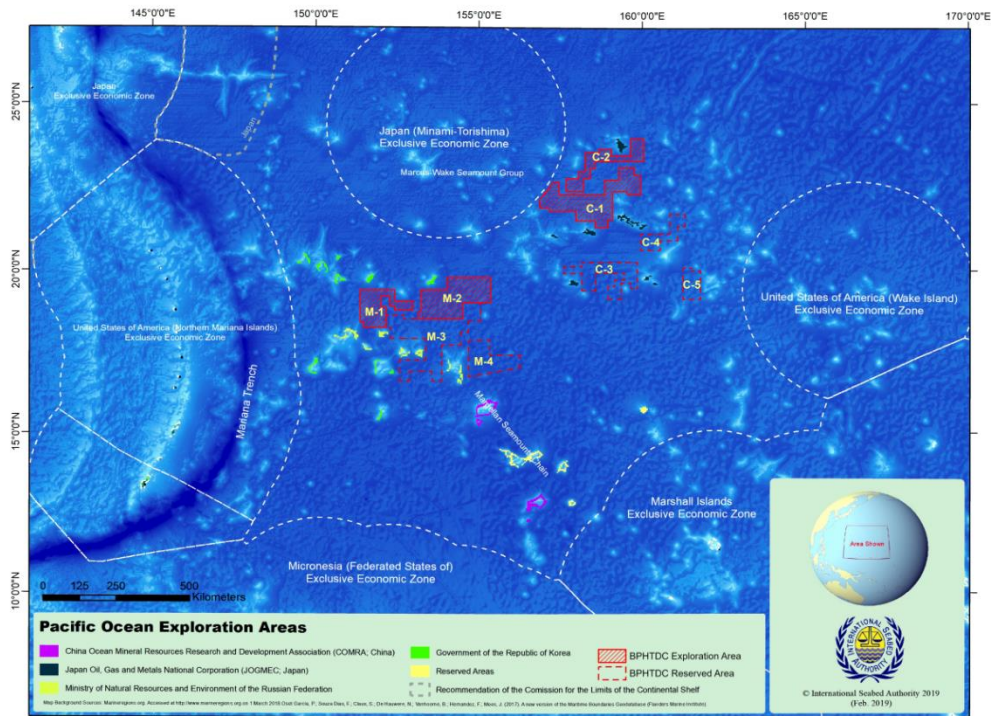
Figure 1-1 Location of the polymetallic nodule contract area of the BPC

The BPC has carried out four cruises about resource and environmental surveys in blocks M1 and M2 since 2021, and combined with the environmental baseline data applying for exploration mining area, the 3-year environmental baseline data requirement is fulfilled. The BPC's offshore baseline surveys are still ongoing and laboratory studies are in progress. As the offshore survey and laboratory research progresses, the environmental baseline data will continue to be added to this project. The environmental baseline survey was mainly concentrated on the northwestern part of Block M2 and the southeastern area of Block M1, which meets the needs of environmental baseline establishment for this project.

Based on the GERIS (Green, Economy, Reliability and Robustness, Intelligence, and Safe) mining concept, the BPC, together with a number of Chinese scientific research institutions, designed the overall technical architecture of the nodule collecting system and made a whole system technical plan from the surface mother ship, underwater riser, near-bottom buffer station, horizontal transportation hose to the underwater collector, and subsequently designed and developed the nodule sampling test machine "Manta I". In 2022, the BPC completed the development of the nodule sampling test machine "Manta I" and its offshore trials. The "Manta I" nodule sampling test vehicle utilizes an ROV-based suspension travel scheme and is designed to collect nodule samples with a width of only 50 cm.

The proposed "Manta II" is a full-featured collector system with a collector capacity ratio greater than 1:5. The "Manta II" inherits the suspended travel method and the accelerated throat flow direct water hydraulic mining technology from the "Manta I". The design phase was initiated in 2023, with plans to complete the equipment construction and factory testing in 2024, followed by the commencement of at-sea mining trials in 2025.

1.3 Project Feasibility

(1) The project is the subject of the exploration contract

According to the exploration contract between BPC and the ISA in 2019, the BPC is required to carry out collector collection tests and environmental monitoring in fifth year, and evaluate the effectiveness of mining on the basis of the data from the test and environmental monitoring.

(2) Baseline data for the scope of the project is available

The BPC has carried out resource and environmental surveys in the mining area after signing the exploration contract, and has collected 3-year environmental baseline data for the preparation of the EIA, which is sufficient to the baseline establishment for this project. In addition to the cruise survey, satellite remote sensing data and public data are also cited in this report, which are complementary to the observation data of the cruise.

(3) Equipment development is progressing steadily and is expected to be completed by 2025

The BPC, based on the suspended mining scheme, has completed the overall design of the collection head equipment. The research and development work are currently progressing steadily and is expected to be completed by 2025.

1.4 Project History

BPC signed a fifteen-year exploration contract in October 2019 with the ISA. Prior to the signing of the exploration contract, a number of cruises, including DY36 cruise, DY41B cruise, DY48 cruise, DY61 cruise and DY66 cruise, carried out resource and environmental surveys in the mining area and its adjacent areas. After the signing of the exploration contract, four cruises of resource and environmental surveys (Figure 1-2) have been carried out in Blocks M1 and M2 of the contract area since 2021, namely, BPC Cruise 1 (i.e., DY69 Cruise),

BPC Cruise 2 (i.e., DY75 Cruise), BPC Cruise 3 (i.e., DY76 Cruise) and BPC Cruise 4 (i.e., DY81 Cruise). The data from the cruises meet the requirements for baseline establishment.

The project continues to utilize the suspended travel mode of the "Manta I" nodule sampling test machine, the development and offshore trials of which have been completed by BPC in 2022. Traditional collector traveling mostly adopts the tracked locomotion, which cannot avoid exerting strong compression and shear forces on the seafloor sediments, leading to obvious sediment disturbance and strong environmental impacts. In terms of hydraulic mining techniques, the widely used Coanda effect and its derived solutions both present issues with the disturbance of seafloor sediments due to water jet impingement. The BPC, based on the environmentally friendly concept, has made two major innovations and breakthroughs in the overall technical approach: 1) The collector carrier adopts a suspended travel scheme based on the ROV; 2) The nodule collector employs a direct water hydraulic mining technology that uses accelerated water flow in the throat to dislodge nodules.
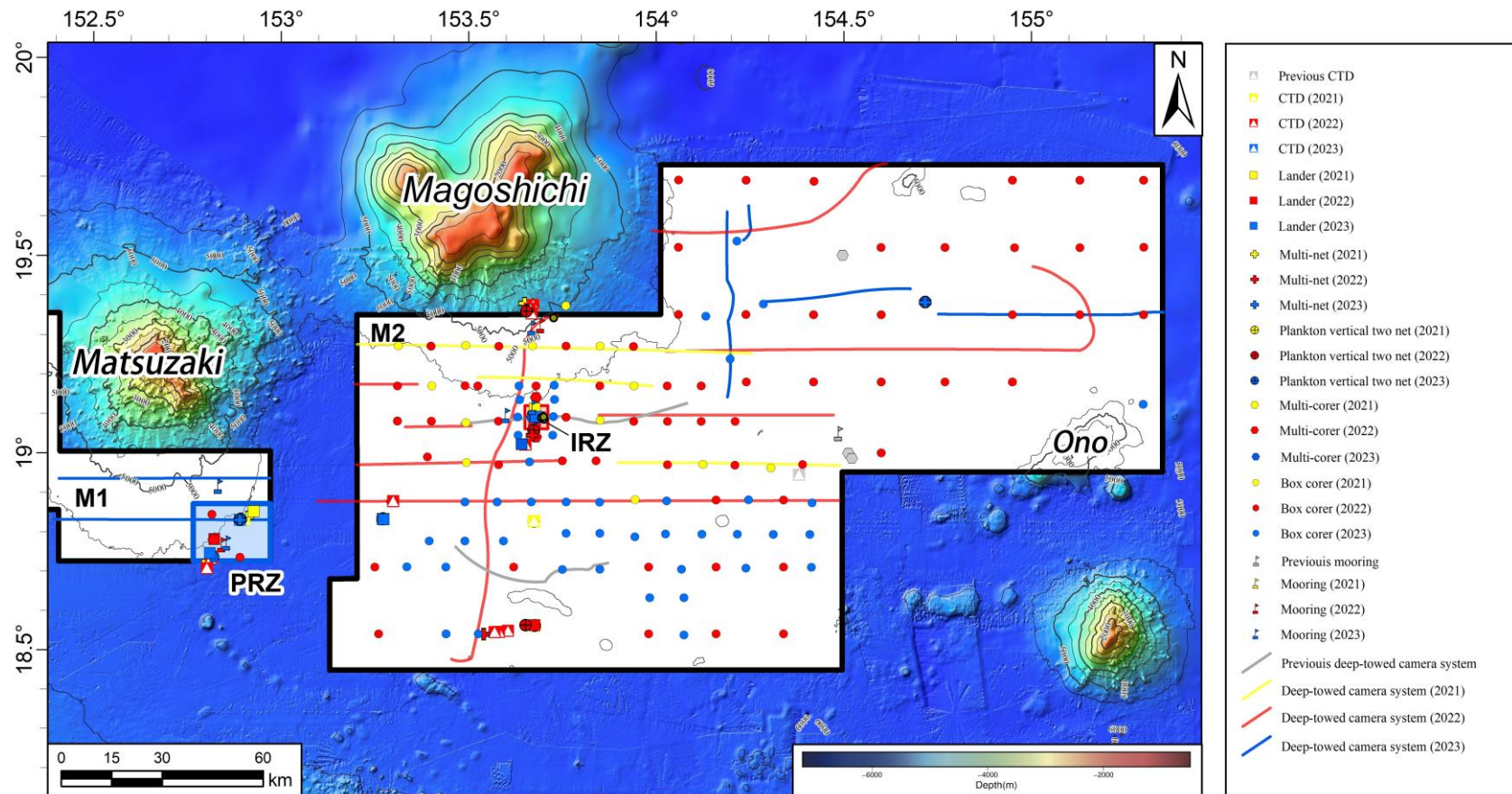
Figure 1-2 Map for Environmental Baseline Survey of the Project Area

1.5 Project Organization Structure

The project is sponsored by the BPC. and the sponsoring State of the exploration contract is China. According to the *1982 United Nations Convention on the Law of the Sea*, all rights in the resources of the Area are vested in mankind as a whole, on whole behalf the ISA shall act. In 2019, BPC signed a fifteen-year exploration contract for a polymetallic nodule mining area in the Western Pacific with the ISA. Activities within the contract area are in compliance with the contractual stipulations and the relevant regulations established by the ISA. Activities in the Area comply with the contractual agreements and the relevant regulations of the ISA. The China Ocean Mineral Resources Research and Development Association (COMRA) is the competent authority for matters in the Area for China, the Government of China is the sponsoring State of the BPC's polymetallic nodule mining area in the Western Pacific, and the activities of BPC in this polymetallic nodule contract area are under the supervision of COMRA (Figures 1-3). This project is overseen by the Project Commander, who is fully responsible for the entire process and is guided by the Overall Expert Group. The positions of Chief Technical Engineer and Chief Environmental Scientist have been established, who are accountable for the project's technical and environmental aspects. The execution of the project is managed by the General Manager of the Project. The project operations consist of the Offshore Execution Department and the Onshore Command Center. The Onshore Command Center includes the Security Management, the Operation Support, and the Emergency Coordination. The Offshore Execution Department, comprising the Captain, the Chief Scientist, and the Offshore Project Manager, coordinates the maritime implementation of the project. The Offshore Execution Department also establishes Contingency Planning, and designates roles for Data Managers, Sample Managers, and Key Equipment Managers.

Figure 1-3 Project Organization Chart

1.6 Present Report

1.6.1 Scope

In accordance with the *Recommendations for the guidance of contractors for the assessment of the possible environmental impacts arising from exploration for marine minerals in the Area* (ISBA/25/LTC/6/Rev.3), during exploration (a) the use of sediment disturbance systems to create artificial disturbances and plumes on the sea floor; (b) the testing of mining components; (c) test-mining; (d) testing of discharge systems and equipment; (e) drilling activities using on-board drilling rigs; (f) sampling with epibenthic sled, dredges or trawls, or similar technique, in nodule fields, that exceeds 10,000 m²; (g) taking of large samples to test land base processes.

The aim of this project is to develop and test the "Manta II" sampling test machine Based on the GERIS (Green, Economy, Reliability and Robustness, Intelligence, and Safe) mining concept. Potential environmental impacts will be assessed, monitored at different phases and the environmental impacts of the header test will be verified after the test.

Therefore, this report introduces the overall project, selection of preservation reference zones (PRZ) and impact reference zones (IRZ), estimation of mineral resources in the CTA, equipment to be used, physicochemical environment in the CTA, biological

environments, possible impacts on the physicochemical and biological environments, plume modeling, environmental monitoring plan, environmental management, and stakeholder consultation.

1.6.2 Report Structure

This report follows the "Environmental impact statement template for reporting an environmental impact assessment undertaken during exploration", as contained in Annex III to the *Recommendations for the guidance of contractors for the assessment of the possible environmental impacts arising from exploration for marine minerals in the Area* (ISBA/25/LTC/6/Rev.3).

2 POLICY, LEGAL AND ADMINISTRATIVE BACKGROUND

2.1 Applicable Mining and Environmental Legislation, Policies and Agreements

2.1.1 International Legislation, Policies, Procedures and Codes

2.1.1.1 Relevant Provisions of the United Nations Convention on the Law of the Sea (UNCLOS)

The 1982 UNCLOS is an international framework convention for regulating maritime activities. Article 1 of the UNCLOS defines "activities in the Area" as all activities of exploration for, and exploitation of, the resources of the Area; Article 133 defines "resources" as all solid, liquid or gaseous mineral resources in situ in the Area at or beneath the seabed, including polymetallic nodules; Article 209 provides the obligations of States to adopt laws and regulations to prevent, reduce and control pollution of the marine environment from activities in the Area. China became a party to the UNCLOS on May 15, 1996. The nodule exploration activities involved in this EIS will be conducted in the Area defined in Article 1 of the UNCLOS, that is, at or beneath the seabed and ocean bottom and its subsoil beyond the limits of national jurisdiction (Article 1 (1) (1) of the UNCLOS). Therefore, this Project will be governed by the UNCLOS and the 1994 Agreement relating to *the Implementation of Part XI of the United Nations Convention on the Law of the Sea of December 10, 1982* (the "Implementation Agreement"), and comply with the requirements of international law related to the implementation of activities and the environment.

2.1.1.2 Relevant Regulations, Recommendations and Standardized Guidelines Developed by the ISA

As an autonomous international organization established according to the UNCLOS, the ISA is responsible for organizing, regulating and controlling activities in the Area. According to the relevant provisions of Part XI of the UNCLOS and its Implementation Agreement (1994), the ISA has the duty to adopt appropriate rules, regulations and procedures to ensure the effective protection of the marine environment from the possible

harmful effects of related activities (Article 145 of the UNCLOS). The ISA is composed of the European Union and 169 member states. China is one of the member states with permanent missions and a member of the ISA Council from 1996. It became a member of the ISA Council A Team in 2004 and has continued to this day.

2.1.1.3 The ISA Mining Code

The ISA Mining Code consists of a series of rules, regulations and procedures issued within the general legal framework established by the UNCLOS (e.g. Part XI) and the 1994 Implementation Agreement to regulate the prospecting, exploration and exploitation of marine resources in the Area.

2.1.1.3.1 Regulations on Nodule Exploration

Up to now, the ISA has issued three Exploration Regulations, including the "*Regulations on Prospecting and Exploration for Polymetallic Nodules in the Area*" (ISBA/19/C/17, Annex) adopted in 2000 and revised in 2013. The most relevant contents for this Project include:

The Part V (Protection and preservation of the marine environment) involves:

(1) Applying a precautionary approach and best environmental practices, and take necessary measures to prevent, reduce and control pollution and other hazards to the marine environment arising from activities in the Area as far as reasonably possible (Regulation 31);

(2) Proposal on the establishment of the IRZs and PRZs (Regulation 31);

(3) Gathering environment baseline data and establishing baseline (Regulation 32);

(4) Formulation of EMP and monitoring requirements for the environmental impact of activities (Regulation 32);

(5) Reporting any incident arising from activities which have caused, are causing or pose a threat of serious harm to the marine environment, and take necessary measures to prevent, contain and minimize serious harm or the threat of serious harm to the marine environment arising out of activities in the Area (Regulation 33);

(6) Taking all measures necessary to ensure that the activities are conducted so as not to cause serious harm to the marine environment under the jurisdiction or sovereignty of coastal States (Regulation 34);

(7) Reporting and protecting any human remains and objects and sites of an archaeological or historical nature (Regulation 35).

The above-mentioned requirements cover the Contractors obligations to the ISA in respect of exploration activities in the Area stipulated in the Contract. The preparation of this EIS and other specified documents related to the test of this Project meets the above-mentioned requirements. At the same time, the Contractor can provide with a guarantee of

its financial and technical capabilities to comply with emergency orders to assure that the council can take such emergency measures (Regulation 33 (8)).

Sections 5 to 7 of Annex IV to the Regulations (Standard Clauses for Exploration Contracts) explain in detail the above matters involved in Part V, and specifically stipulate that:

5.2 Prior to the commencement of exploration activities, the Contractor shall submit to the ISA:

(a) An impact assessment of the potential impacts on the marine environment of the proposed activities;

(b) A proposal for an EMP to determine the potential impact on the marine environment of the proposed activities; and

(c) Data that could be used to establish an environment baseline against which to assess the impact of proposed activities.

The data obtained from this test will provide information for establishment of environment baselines, EIA and mining equipment design, and will be helpful for the design of the EMP and the final preparation of the EIS.

2.1.1.3.2 Draft Mining Regulations, Standards and Guidelines

The "*Draft regulations on exploitation of mineral resources in the Area*" and the drafts of relevant environmental standards and guidelines are in the process of consultation and revision. The proposals and related discussions in the draft regulations and codes on the contents of the environmental impact report prepared for the exploitation stage, the determination of environment baseline data, and the preparation of EMMPs provide the Contractor with useful information related to the obligations that may need to be fulfilled in the subsequent exploitation stage. Bearing in mind the relationship between the test-mining activities in the exploration stage and the subsequent commercial mining activities, this EIS referred as appropriate the contents of draft Exploitation Regulation and related codes that are in line with the requirements of the Exploration Regulation and have guiding significance in the preparation stage of this EIS. In this way, we will more effectively fulfill the relevant requirements stipulated in the Exploration Contract during the implementation of this Project. We believe that a comprehensive understanding of the latest legislative background will also be conducive to improving the design and implementation of test-mining activities in the exploration stage as well as to more effectively carrying out studies, monitoring, assessment and management related to the status quo of and impact on the existing environment.

2.1.1.3.3 Recommendations on EIA

In 2002, the LTC issued the "*Recommendations for the guidance of the Contractors for the assessment of the possible environmental impacts arising from exploration for polymetallic nodules in the Area*" (ISBA/7/LTC/1/Rev.1), which was revised in 2010 (contained in ISBA/16/LTC/7). In March 2013, the LTC issued a set of consolidated environmental guidelines "*Recommendations for the guidance of contractors for the assessment of the possible environmental impacts arising from exploration for marine minerals in the Area*"(ISBA/19/LTC/8), and then three revisions in March and June 2020 (ISBA/25/LTC/6/Rev.1 and ISBA/25/LTC/6/Rev.1/Corr.1), July 2022 (ISBA/25/LTC/6/Rev.2) and August 2023 (ISBA/25/LTC/6/Rev.3). The Recommendations determines the exploration activities that need prior EIA, the form and content of the EIA, and provides relevant guidelines on baseline studies, monitoring and reporting.

The most relevant contents in the Recommendations (ISBA/25/LTC/6/Rev.3) are as follows:

(1) Activities requiring EIA during exploration

Section VI (B)(33) states: The following activities require prior EIA, as well as an EMP to be conducted during and after the specific activity, in accordance with the recommendations contained in paragraphs 33 and 38. It is important to note that these baselines, monitoring and impact assessment studies are likely to be the primary inputs to the EIA for commercial mining. The activities include:

(a) Use of sediment disturbance systems that create artificial disturbances and plumes on the sea floor;

(b) Testing of mining components;

(c) Test-mining;

(d) Testing of discharge systems and equipment;

(e) Drilling activities using on-board drilling rigs;

(f) Sampling with epibenthic sled, dredge or trawl, or similar technique, in nodule fields, that exceeds 10,000 m^2;

(g) Taking of large samples to test land base processes.

Therefore, this test needs an EIA and an EMMP as the main basis for the EIA for subsequent commercial mining activities.

(2) Related procedure steps

Section VI (B)(34) states: The EIS and data mentioned in Paragraph 38 of the Recommendations shall be submitted by the Contractor to the Secretary-General not later than one year before the start of the activity.

Section VI (E) outlines the process for reviewing the EIS on the testing of mining components.

Accordingly, this EIS will be submitted with relevant documents and materials in accordance with the above-mentioned timetable and procedural steps.

(3) Relevant requirements for environment baseline data

Sections III and IV of the Recommendations specify in detail the requirements for environment baseline studies, baseline data collection, data collection and analysis, reporting and archiving procedures. The explanatory commentary in Annex I also provides additional information on baseline data requirements.

Sections VI (C) and VI (D) respectively define the information and measurement to be provided by contractors performing an activity that requires EIA during exploration, and the observations and measurements to be made after undertaking an activity that requires an EIA during exploration.

Baseline data are essential in monitoring variations resulting from these activities and predicting the impacts of commercial mining activities. Since 2021, we have formulated the sampling strategy of environment baseline survey through the design and planning of geographic information system, conducted long-term data collection, obtained and recorded sufficient information on the natural conditions of the collector before testing from the exploration zone, and collected other data related to sea surface, middle ocean layer, near-bottom layer and seabed communities, so as to establish baseline data for EIA. Therefore, this EIS meets the relevant requirements of the above-mentioned recommendations.

(4) EIS template

Annex III of the Recommendations provides a template for the EIS. It is also noted that a more detailed template for preparing the EIS is contained in the Annex IV of the "*Draft regulations for exploitation of mineral resources in the Area*" (ISBA/25/C/WP.1). Therefore, this EIS is mainly arranged according to the contents of the Recommendations, and seeks to obtain some more specific operational guidelines from Annex IV (Environmental Impact Statement) of the draft Exploitation Regulations for the contents that are consistent with the Exploration Regulations, recommendations and the basic requirements related to this Project.

(5) Relevant progress of stakeholder consultation

Article VI. (E)(41)(a) of the Recommendations clearly states that "In its submission, the contractor is to include information on the stakeholder consultation conducted, as reflected in annex I to the present recommendations", and Annex I provides methodological guidance for implementing the relevant recommendations of the consultation process, including the consultation time, methods and progress, and the handling of relevant concerns of stakeholders. The above-mentioned guiding recommendations were fully taken into account in the stakeholder consultation process for the activities in this EIS (see

Chapter 10 of this EIS). The output of stakeholder consultation is helpful to the compilation of the final EIS and has a positive effect on the Contractors better perform of environmental obligations.

2.1.1.4 Relevant Environmental Management Policies of the ISA

The Regional Environmental Management Plan (REMP) is a precautionary measure adopted in accordance with Article 145 of the UNCLOS, which calls for the "effective protection for the marine environment from harmful effects which may arise from activities in the Area". REMPs guide the design of environmental management objectives and measures for activities in the Area. Contractors have emphasized and considered REMP-related objectives in the design of the test.
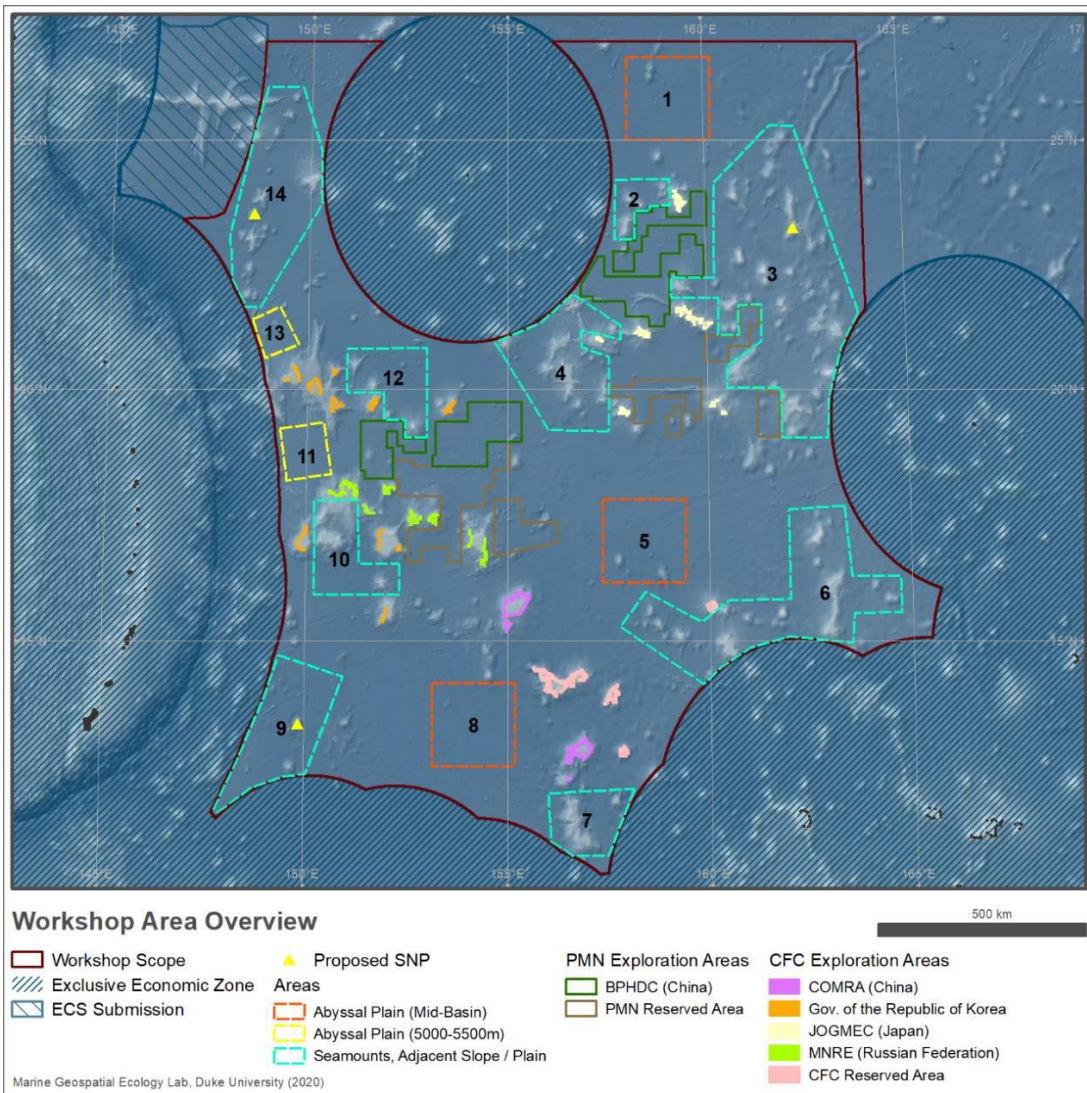
Figure 2-1 Areas described as potential AINPs from REMP Regional Workshop 2020

2.1.2 Other International Conventions and Agreements Relevant to Deep-sea Activities

In addition to the provisions on seabed mining in Part XI, Part XII of the UNCLOS stipulates the general obligations for the protection and preservation of the marine environment and the requirements for measures to prevent, reduce and control the pollution of the marine environment, which are applicable to "pollution from installations and devices used in exploration or exploitation of the natural resources of the seabed and subsoil" (Article 194 (3)(c). Article 143 of the UNCLOS stipulates the promotion of marine scientific research and the publication and dissemination of research and analysis results in the Area. The research work and related data output of this Project are in line with these provisions.

Table 2-1 provides other international conventions and agreements related to this test on the aspects of maritime affairs, environment and maritime safety. Among which: The conventions of the IMO on environmental protection and maritime safety are applicable to the operation activities of the ships in this Project. Each ship used for activities in the Area holds valid certificates issued in accordance with these international rules and standards (in accordance with standard clause 15.1 of the Contract in Annex IV of the Exploration Regulations), which meets the requirements of environmental rules and measures of relevant instruments.

Table 2-1 Relevant international conventions and agreements

Conventions and agreements	Notes to relevant contents
Maritime navigation	
International Convention for the Prevention of Pollution from Ships (MARPOL 73/78) and its annexes	The Convention stipulates the environmental rules and measures applicable to ships, aiming at preventing ships from polluting the marine environment by discharging harmful substances or waste liquid containing such substances.
International Convention for the Control and Management of Ships' Ballast Water and Sediments, 2004 (BWM Convention)	The BWM Convention puts forward specific technical requirements for the discharge control of ballast water and sediments from ships, so as to prevent, reduce and finally eliminate the harm of ballast water discharge to the marine environment and public safety.
International Convention on the Control of Harmful Anti-fouling Systems on Ships (AFS), 2001	The AFS stipulates the control measures of the anti-fouling bottom system of ships to reduce or eliminate the adverse effects of the anti-fouling bottom system on the marine environment and human health.
Convention on the Prevention of Marine Pollution by Dumping of Wastes and Other Matter, 1972, and its 1996 Protocol	The Convention and Protocol stipulate the marine dumping permit system, aiming at protecting the marine environment from dumping activities. Article 1(4)(3) provides that: The provisions of this Protocol do not include the disposal or storage of wastes or

	other substances directly produced by or related to the exploration, development and related at-sea processing of seabed mineral resources.
Maritime safety	
International Convention for the Safety of Life at Sea (SOLAS), 1974	The Convention makes detailed provisions on ship construction, number of passengers and safety facilities, so as to improve the safety of life at sea.
Labour	
Maritime Labour Convention (MLC), 2006, International Labour Organization	The MLC specifies the minimum requirements for seafarers' employment, employment conditions, standards of living facilities on board, occupational health and safety protection, etc., and defines the rights of seafarers and the obligations of member states.
	The current requirements of the International Labour Organization, such as crew training and protection of labour rights and interests, are applicable to seafarers at sea.
Biodiversity	
Convention on Biological Diversity (CBD), 1992	Articles 3 and 4 of the CBD clarify that all countries have the responsibility to ensure that activities and processes under their jurisdiction or control do not cause damage to the environment in areas beyond national jurisdiction. Article 14 sets out the requirements for the notification obligation in the case of impact assessment and minimization of adverse effects, as well as in the case of serious danger or damage. The related objectives of marine biodiversity protection in the "Kunming-Montreal Global Biodiversity Framework" reached in 2022 and the description of EBSAs-related work under the framework of the Convention have global scientific reference significance.
	On March 2023, under the CBD, the draft agreement of the Conservation and Sustainable Use of Marine Biodiversity Beyond Areas of National Jurisdiction (BBNJ) was adopted. Although not yet formally in effect, the test has taken into full consideration the significant concerns of the agreement. The test activities will take into account the protection and use of biodiversity in the test area, based on the actual circumstances of the activity.
Climate	
1992 United Nations Framework Convention on Climate Change (UNFCCC) and its Kyoto Protocol and Paris Agreement	The UNFCCC system provides measures to control greenhouse gas (GHG) emissions and provides guidelines and framework for solving global climate change problems.
Vienna Convention for the Protection of the Ozone Layer (1985) and Montreal Protocol (1987)	The Convention defines the principle of international cooperation in protecting the ozone layer, and the Protocol defines the framework of global international cooperation in protecting the ozone layer. It provides guidelines for global ozone-depleting substance management and ozone layer protection.

2.2 National Laws, standards and codes

2.2.1 National Laws, Standards and Codes Related to Seabed Mining

In February 2016, China promulgated the "*Law of the People's Republic of China on the Exploration for and Exploitation of Resources in the Deep Seabed Area*" (hereinafter referred to as the "Deep Seabed Law"). The purpose of this law is to "standardize the exploration and exploitation activities of resources in the deep seabed area, promote deep-sea scientific and technological research and resource survey, protect the marine environment, promote the sustainable utilization of resources in the deep seabed area and safeguard the common interests of mankind" (Article 1), which is applicable to "citizens, legal persons or other organizations in People's Republic of China that are engaged in resource exploration, exploitation and related environmental protection, scientific and technological research and resource survey activities in the deep seabed area" (Article 2). According to Article 5, the State Oceanic Administration (currently the Ministry of Natural Resources) is responsible for the supervision and management of exploration and exploitation of resources, as well as survey activities in the deep seabed area, and other relevant departments of the State Council are responsible for related management according to the functions prescribed by the State Council. The State Oceanic Administration of China, which is directly under the Ministry of Natural Resources of the People's Republic of China, is responsible for approving matters related to the exploration and exploitation of resources in deep seabed regions.

2.2.1.1 System for Administration of Exploration Activities

The "Deep Seabed Law" defines exploration as: Use and testing of collecting systems and equipment, processing facilities and transportation systems and the conducting of studies of the environmental, technical, economic, commercial and other appropriate factors that must be taken into account in exploitation (Article 27 (1)).

This Project belongs to the exploration activities to which this law applies, and this law clearly stipulates the legal obligations directly related to the contractors exploration operations:

—The obligations under the exploration and exploitation contracts shall be fulfilled, the personal safety of the personnel engaged in exploration and exploitation operations shall be guaranteed, and the marine environment shall be protected (Article 9).

—Cultural relics and laying in the exploration and exploitation areas shall be protected (Article 9).

—The exploration and exploitation operations shall also abide by the laws and administrative regulations of the People's Republic of China concerning safety in production and labor protection (Article 9).

—Emergency response plans shall be initiated and measures shall be taken when accidents with serious harm to the marine environment occur or may occur (Article 11).

Therefore, the Contractor will fulfill the Contract obligations in strict accordance with the law, abide by the applicable operation-related requirements mentioned above, under the supervision of the competent national authorities.

2.2.1.2 Environmental Protection System

Chapter III of the "Deep Seabed Law" specifically stipulates the environmental obligations of prospectors to prevent, reduce and control pollution and other hazards caused by activities to the marine environment, and to take necessary measures to protect and preserve rare or fragile ecosystems. The following specific requirements are directly related:

—In accordance with the requirements of the Contract, survey and study the marine conditions in the exploration and exploitation areas, determine the environment baselines, and assess the possible impact of the activities on the marine environment;

—Formulate and implement an EMP, monitor the impact of activities on the marine environment in the project area, ensure the normal operation of monitoring equipment, and keep original monitoring records so as to provide a basis for inspection.

The above-mentioned requirements are consistent with the requirements of the ISA related rules, regulations and procedures, and the activities conducted and planned in this Project will strictly comply with the relevant regulations.

2.2.1.3 Scientific Sesearch and Data Management

The Chapter IV of the "Deep Seabed Law" makes special provisions on scientific and technology Research, resource investigation and capacity building, and clarifies the relevant contents of strengthening the collection and sharing of deep-sea scientific and technological research data, which is related to the relevant activities of this Project. Among them, Article 18 provides requirements for the submission, registration, storage and utilization of relevant data and physical samples obtained by the Contractor through exploration and exploitation activities. In 2017, the former State Oceanic Administration issued normative documents—"Interim Measures for Administration of Samples in Exploration and Exploitation of Resources in Deep Seabed Areas" and "Interim Measures for Administration of Materials in Exploration and Exploitation of Resources in Deep Seabed Areas" (in the process of studying and revising to meet the variations required by the new ISA regulations), which provided specific guidance for the reporting and

management of samples and data obtained from related activities of this Project. The international exchange of deep-sea data obtained from this Project will be conducted under the unified management of the national competent authorities and in accordance with the relevant requirements and procedures of the ISA.

2.2.1.4 Relevant National Standards and Guidelines

In addition to complying with the obligations and management procedures of the relevant laws and supporting normative documents of the "Deep Seabed Law", a series of relevant standards and guidelines will also be applied or considered during the implementation of this Project.

Table 2-2 below lists the national standards and guidelines that provide technical methods and work codes for this Project.

Table 2-2 Relevant standards and guidelines

Standards and guidelines	Notes to relevant contents
"Specification for oceanic polymetallic nodules exploration" (GB/T 35571-2017)	Provision of normative guidance for resource exploration.
"Classification code of ocean sample management" (GB/T 42330-2023)	Provision of reference for the information and standardized management standards of the obtained ocean samples.
"Terminology for oceanic resources survey" (GB/T 34908-2017)	Provision of normative guidance for the standard terminology of resource survey.
"The technology specification for the pre-treatment of deep-sea microorganism samples" (GB/T 30744-2014)	Provision of technical guidance for deep-sea microbial sample treatment.
"Chemical analysis methods for marine polymetallic nodules" (GB/T 20259-2006)	Provision of guidelines for nodule-related chemical analysis methods.
"Specifications for oceanographic survey"（GB/T 12763.1 - GB/T 12763.11） Parts 1-11	Provision of guidelines for on marine hydrology, meteorology, chemistry, sound and light, ecology, geology and geophysics, biology, seabed topography and geomorphology, marine engineering geological survey, and survey data exchange.
"Code of practice for international seabed area and high seas environmental survey—Part 1: General" (GB/T 42629.1-2023)	Provision of methods and guidelines for environmental survey and assessment in the high seas and international seabed areas.

"Code of practice for international seabed area and high seas environmental survey—Part 2: Marine chemical survey" (GB/T 42629.2-2023)	Provision of methods and guidelines for chemical oceanography survey and assessment in the high seas and international seabed areas.
"Code of practice for international seabed area and high seas environmental survey—Part 3: Marine biological survey" (GB/T 42629.3-2023)	Provision of methods and guidelines for the survey and assessment of marine organisms in the high seas and international seabed areas
"Code of practice for international seabed area and high seas environmental survey—Part 4: Physical features survey of marine sediments" （GB/T 42629.4-2023 ）	Provision of methods and guidelines for conducting physical characterization surveys of marine sediments in the high seas and international seabed area

2.2.2 Other Relevant National Legislation, Policies and Regulations

In addition to the above-mentioned national laws, procedures and technical codes related to seabed mining activities and their environmental protection, other national laws and policies related to maritime navigation, pollution prevention and control of vessels and operational activities, marine traffic safety, safety in production and labor protection also provide the Contractor with normative guidance on related work, and the relevant legal provisions mainly observed or referred to include:

The "Marine Environmental Protection Law of the People's Republic of China" (2023 Revision, 2024 in effect) is the "basic law" on the protection of marine ecology and environment, which is applicable to the sea areas under the jurisdiction of China. Although the "Marine Environmental Protection Law of the People's Republic of China" is applicable to the waters under the jurisdiction of China, it is the basic law of marine environmental protection in China after all, and the concepts, systems and methods of marine protected areas can provide reference in carrying out related work in international waters. Article 9 stipulates that all entities and individuals have the obligation to protect the marine environment. Article 124 provides that: if the international treaties related to marine environmental protection concluded or acceded to by People's Republic of China have different provisions from this Law, the provisions of the international treaties shall prevail, except the provisions on which the People's Republic of China has made reservation. Therefore, the Contractor of this Project will follow the relevant legal guidance of this Law and the provisions of environment-associated international treaties during the implementation of the related activities involved in this EIS, so as to ensure that the implementation of related activities in the high seas and the Area will not cause pollution

or potential risks to the sea areas under national jurisdiction, and will be supervised by relevant state departments and institutions.

The "Regulation on the Prevention and Control of Vessel-induced Pollution to the Marine Environment" (2018, Revision) is a regulation formulated according to the "Marine Environmental Protection Law", and Article 10 thereof stipulates: "The structure, equipment and instruments of a vessel shall conform to the relevant technical requirements of the state for preventing and controlling the vessel-induced pollution to the marine environment and the requirements of the international treaties concluded or acceded to by the People's Republic of China. The vessels shall, in accordance with the laws, administrative regulations, provisions of the transport administrative department under the State Council and the requirements of the international treaties concluded or acceded to by the People's Republic of China, obtain and carry on board corresponding certificates and documents relating to the prevention and control of vessel-induced pollution to the marine environment." Article 73 provides that: "If the international treaties concluded or acceded to by the People's Republic of China have provided for the prevention and control of the pollution caused by vessels and the relevant operations to the marine environment, such provisions shall prevail, except the provisions on which the People's Republic of China has made reservation." Therefore, the vessels and related equipment used in the exploration and follow-up activities of this Project meet the relevant national qualification requirements, and we will conduct relevant operation activities in a manner consistent with the above provisions and relevant international treaties as appropriate as possible.

The "Maritime Traffic Safety Law of the People's Republic of China" (Revised in 2021) is applicable to navigation, berthing, operation and other activities related to marine traffic safety in the waters under the jurisdiction of China. This law stipulates the requirements of relevant national laws, administrative regulations, standards and technical specifications that China-registered vessels and other important marine equipment, components and materials must abide by, including ship inspection, safety management, maritime labor qualification licensing, early warning of overseas emergencies and emergency response. As stipulated in Article 86, "If a vessel of Chinese nationality has a marine traffic accident outside the sea areas under the jurisdiction of the People's Republic of China, the accident shall be promptly reported to the maritime administrative agency and investigated." Therefore, the qualification of operating vessels, maritime labor certificate, maritime safety management and guarantee in this Project "conform to relevant national laws and regulations, mandatory standards and applicable international treaties."

In addition, China has promulgated a series of laws, regulations, codes and standards to prevent and control pollution caused by vessels, including the "Prevention and Cure of Pollution Damage of Marine Environment by Seashore Construction Project", "Oil Spill

Contingency Plan for Marine Ships in China", "Regulations of the People's Republic of China on Inspection of Ships and Shipborne Installations", "Regulations of the People's Republic of China on the Management of Marine Dumping Measures for Implementation", "HJ 1300-2023 Technical Specification for Assessment of Sea Water, Marine Sediment and Marine Biological Quality".

2.3 Stakeholder Consultation

BPC plans to conduct a 1:5 scale polymetallic nodule joint test of deep-sea miner and buffer station in the southern piedmont of Magoshichi Guyot within the Block M2 of the contract area in the latter half of 2025. The aim is to verify the reliability of the suspended collection method and the buffer station joint test. Based on the environmental baseline data collected in advance and the environmental monitoring data during and after the test, an environmental impact assessment of the test activities will be carried out. Moreover, following the concept of "Research-oriented exploitation", this test will be utilized as a significant opportunity to enhance understanding of the deep-sea and ecosystems. It will facilitate open research on relevant scientific issues in the deep-sea domain, providing a basis for the formulation of regulations for future deep-sea mining activities and the development of green mining technologies.

BPC has prepared an environmental impact statement in accordance with the recommendations of the ISA - *Recommendations for the Guidance of Contractors for the Assessment of the Possible Environmental Impacts arising from Exploration for Marine Mineral in the Area* (ISBA/25/LTC/6/Rev.3). From May 1, 2024, to June 6, 2024, the *Environmental Impact Statement-Joint Test of Deep-sea Miner and Buffer Station in Beijing Pioneer Polymetallic Nodule Contract Area, Western Pacific* has been simultaneously released to the public on the ISA website and BPC's official website to solicit feedback from all relevant stakeholders (Figure 2-2).
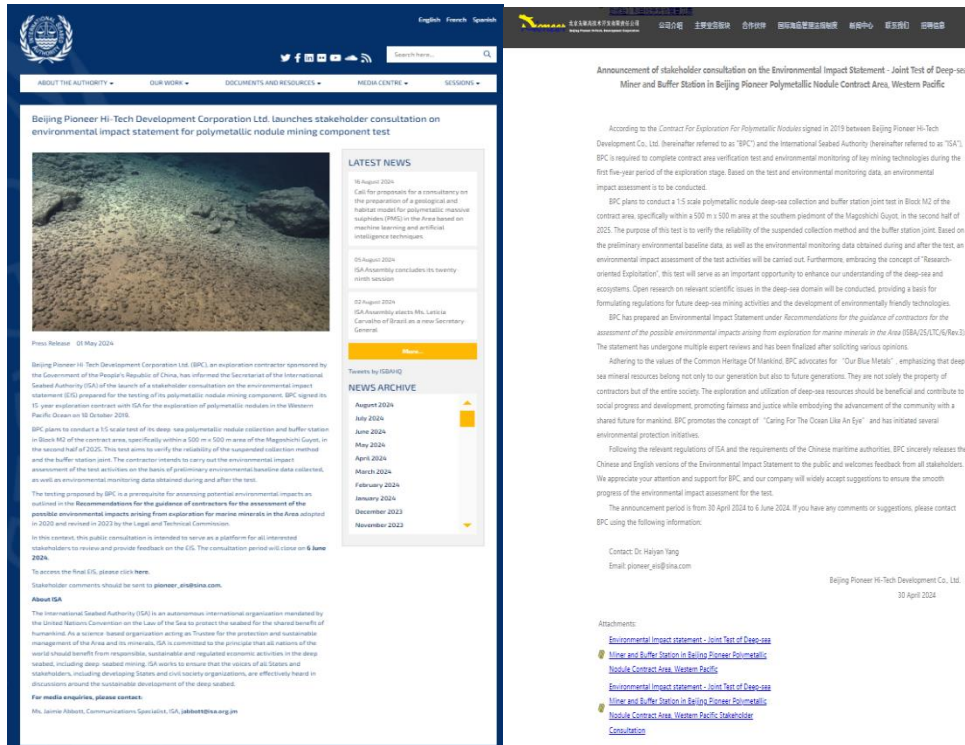
Figure 2-2 Public Stakeholder Consultation Statement (Left: News on the Official Website of the ISA; Right: News on the Official Website of the BPC)

During the stakeholder consultation period, a total of 10 emails were received from international organizations/national governments including the UK government, Canada government, U.S. Observer Delegation to the International Seabed Authority, Deep Sea Conservation Coalition, etc. See Table 2-3 for the list of submitters.

Table 2-3 Submitter of Stakeholder Consultation

NO.	Government/Organization
1	China Biodiversity Conservation and Green Development Foundation
2	Deep Sea Conservation Coalition
3	World Wildlife Fund
4	UK government
5	Pew Charitable Trusts
6	Ocean Foundation
7	Deep-Ocean Stewardship Initiative
8	Oceans North
9	Canada government
10	U.S. Observer Delegation to the International Seabed Authority

BPC received a total of 308 comments, of which 12 were positive or appreciative comments. For example, the UK government mentioned that "The fully suspended nature of the Manta II sampling equipment reduces the impact on the seabed when compared to equipment that would be affixed to or deposited onto the seabed…This constitutes good practice, in our view, to reduce environmental impacts as far as possible", "It's valuable that, beyond monitoring of natural variability and impacts, in situ experiments are being developed to explore specific knowledge gaps concerning the effects of identified impacts", "The inclusion of a summarizing table of which environmental parameters have been collected, and whether they cover spatial, temporal, and depth variability, is highly valued and provides welcome transparency for parameters which were difficult to obtain".

There were 270 specific and relevant comments, covering the following 16 topics (see Figure 2-3 for the number distribution):

1）Baseline data

2）Collector test

3）Cumulative impacts

4）Ecotoxicology

5）Ecosystem function

6）Light impacts

7）Mitigation measures

8）Monitoring plan

9）Noise impacts

10）Plume

11）Reasonable identification of PRZ/IRZ

12）Policy and law

13）Stakeholder engagement

14）EIS text/figure update

15）Survey methods

16）Flocculation experiment
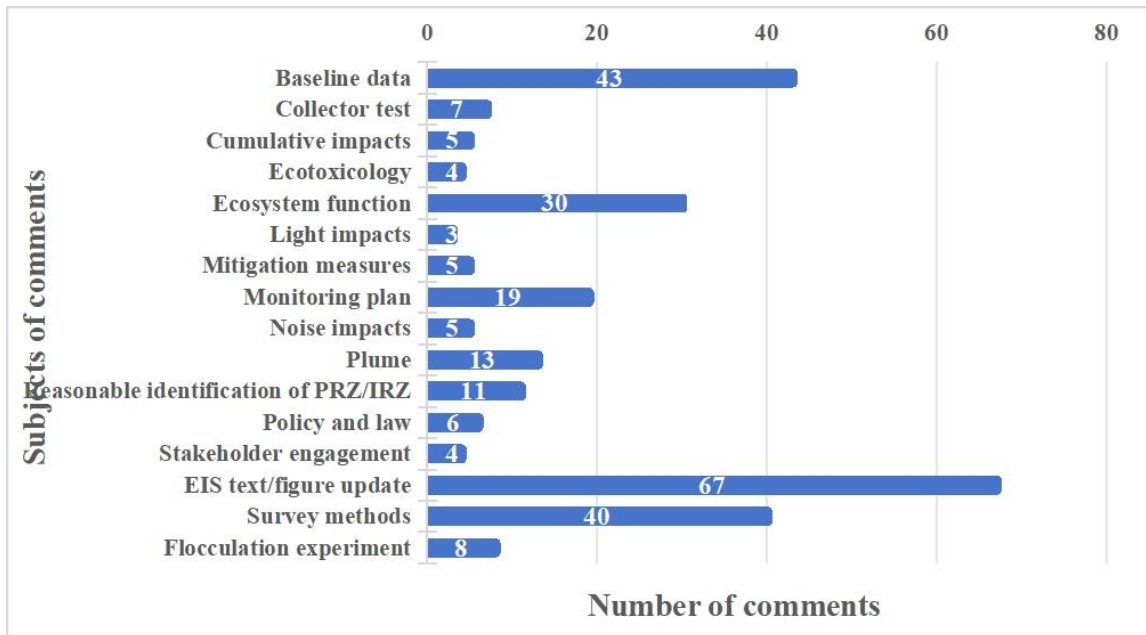
Figure 2-3 Number of the stakeholder consultation comments

2.4 BPC Environmental Management System

2.4.1 Environmental Objective

Long-term objective: With the objective of protecting and preserving the environment and biodiversity of the deep-sea polymetallic nodule area, promote the rational utilization of the common heritage of mankind for the benefit of social development. To establish a strategy of "research-oriented exploitation", incorporate deep-sea scientific research throughout the entire process of deep-sea activities, continuously improve knowledge of deep-sea ecosystems, and develop environmental monitoring and restoration technologies by applying precautionary approaches in a timely manner. Apply the highest environmental management standards, conduct environmental impact assessments in advance and adopt the best environmental management measures and tools.

With green standards, develop technical and equipment systems for deep-sea mining and achieve sustainable utilization of deep-sea mineral resources.

Medium-term objective: Formulate the main standards for deep-sea environmental protection and preservation; initially construct the company's environmental protection and preservation standard system for deep-sea mining activities. Enrich and increase the collection of data related to deep-sea mining environmental assessments; establish an environmental baseline data index system and standardization system. Establish an environmental impact assessment model; determine the PRZ and IRZ; and comprehensively monitor the biological communities potentially affected by mining activities in the contract area. Formulate and implement a complete set of internal environmental control systems to manage and reduce the impact of the company's activities on the environment.

Short-term objective: Establish a company environmental management system to provide a systematic and structured operational mechanism for the company's environmental management. Through the implementation of the environmental management system, strengthen the environmental management of the mining area and the company's operations; make more effective use of energy and resources; reduce energy consumption; save operating costs; and continuously improve the company's environmental performance, achieving minimal impact on the environment from the activities conducted by the company. Establish a mining area environmental management system; clarify the research and development tasks of green key technology and equipment; and propose technical requirements for green mining equipment.

2.4.2 Environmental Strategy

● Establish the concept of "research-oriented exploitation", strengthen cooperation with domestic and international scientific communities; continuously improve the understanding of deep-sea ecosystems; and provide scientific basis for the development of green mining processes and technologies, commercial development scale determination, regional environmental management plan establishment, cumulative impact model and environmental threshold research, and the formulation of environmental impact mitigation measures.

● Adhere to the implementation of sustainable development and responsible environmental management strategies. Prioritize responsible and sustainable management of the environment in all company operations, incorporating it into every aspect of business and exploration and development activities. Persist in using an integrated approach to optimize production and operational energy efficiency;

establish company environmental performance objectives; and regularly review these goals to achieve optimal environmental management.

- Explore responsible deep-sea mining operations that are considerate of the environment. Undertake technological and equipment innovation, improve work methods; enhance the efficiency of natural resources, equipment, and energy usage, and develop green deep-sea mining systems. Advance comprehensive digital ocean technologies that enhance human understanding, deep-sea clean energy technologies, and environmental protection planning and ecological restoration technologies for deep-sea spaces.

- Implement environmental risk management strategies and preventive measures. Conduct environmental risk management to identify risks and potential consequences; establish a corporate ethic of environmental responsibility, and develop and implement environmental education and training programs. Ensure that company employees, contractors, and suppliers of equipment, materials, and services understand and comply with the company's environmental policies and specific requirements. Develop strategies for stakeholder participation and environmental public welfare promotion to maintain and enhance the company's reputation.

2.4.3 Environmental Policy

BPC is a promoter of deep-sea environmental protection, insisting on the development concept of green and low carbon, the business principle of "Exploration, Innovation, Cooperation and Sharing", exploring sustainable ways of deep-sea mineral exploitation, implementing environmentally sustainable development policies. The company will enhance the value of its sustainable development by integrating good environmental practices into all aspects of its business, develop the resources of the international seabed area for the benefit of all mankind, and support the realization of the United Nations Sustainable Development Goals (SDGs). The Company's environmental policy contains the following aspects.

●In compliance with all applicable laws, regulations, and environmental protection guidelines for deep-sea resource exploration, development, and conservation, the company is committed to developing and refining its internal environmental policy framework. The Company undertakes to effectively comply with the *Deep Seabed Area Resource Exploration and Exploitation Law of the People's Republic of China*, the *United Nations Convention on the Law of the Sea* , and the *Regulations on Prospecting and Exploration for Polymetallic Nodules in the Area* established by the

ISA. Operating in accordance with the company's environmental regulations, the company will establish a baseline environmental monitoring system for the mining area, an environmental impact assessment system, and environmental management and monitoring protocols. It will also develop and regularly update contingency plans and closure plans.

●To explore sustainable approaches to deep-sea mineral development and to integrate environmental protection requirements and awareness throughout the mining process. The Company is committed to considering environmental impacts and implementing a precautionary approach at all phases of a mining project. The Company adopts best industry practices to protect the environment and resources in the exploration and development activities. It will utilize available advanced technology and take the necessary measures to prevent, reduce and control pollution and other hazards to the marine environment caused by deep-sea exploration and development activities. Efforts are made to protect and preserve rare or fragile ecosystems, as well as the living environment of depleted, threatened or endangered species and other marine organisms, conserve marine biodiversity, and safeguard the sustainable use of marine resources.

●In the company's strategic planning, procurement, and operational decision-making, environmental impacts are taken into account to minimize the effects on the environment and the consumption of resources. The Company is committed to considering reducing environmental impact and operational carbon emissions in all phases of deep-sea exploration and development, as well as in its daily business. By advancing resource conservation, energy efficiency, waste reduction, and recycling initiatives, the company is actively committed to the sustainable reuse of resources and strives to preserve biodiversity and the environment. The company educates, trains, and encourages employees to carry out their daily tasks with an environmentally friendly way, and support our suppliers and subcontractors to work together to protect the environment.

●Establish reasonable and appropriate long-term environmental objectives and specific environmental targets, and regularly review these goals. Promote continuous improvement in environmental performance by regularly reviewing the company's operations and service processes to make sure that reasonable environmental objectives are established and their implementation is monitored to help the company evaluate and continually improve its environmental performance. Collaborate with stakeholders and take their opinions and suggestions into account when developing environmental objectives and improving environmental actions.

2.4.4 Organizational Structure

2.4.4.1 Regulatory Framework

Under the guidance of the company's leadership and policies, environmental work is conducted around core processes, identifying and leveraging supportive resources, knowledge and capabilities, communications, and documentation. The core processes include planning, operations management, and improvement, with each level providing support services in turn. (Figure 2-4).
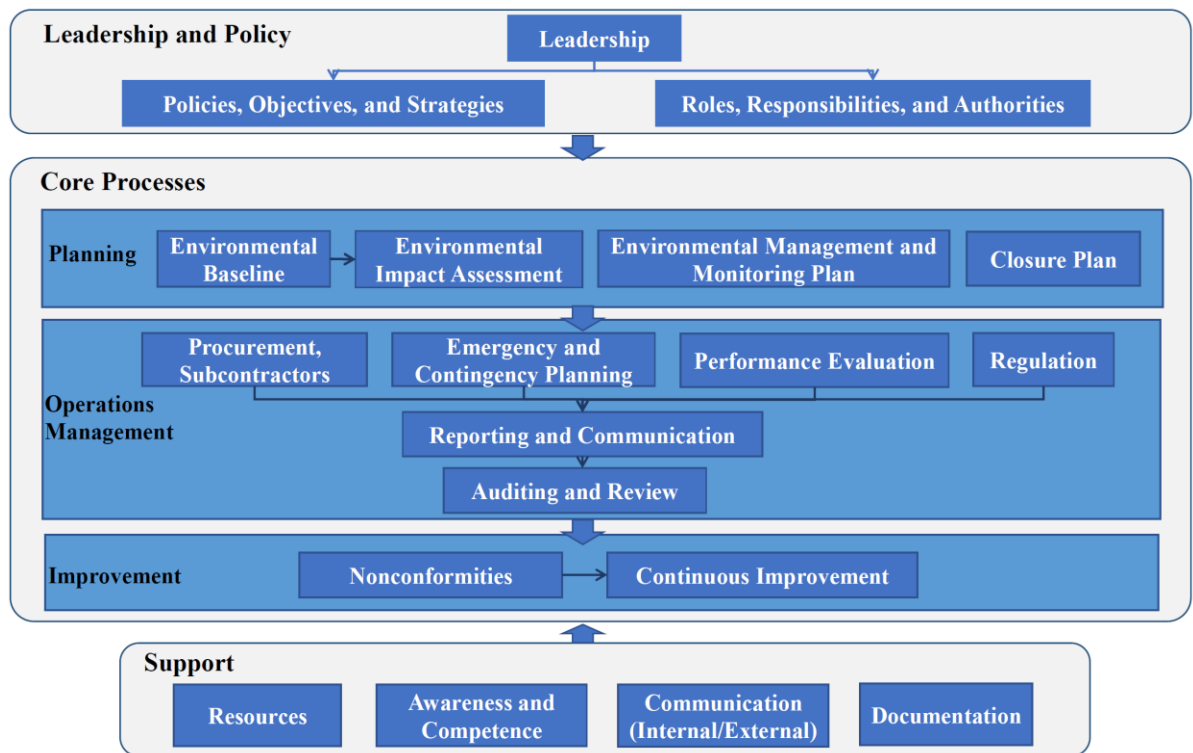
Figure 2-4 Organizational chart of environmental measures

●Leadership and policy: The leadership role of the company in ensuring that the EMS is established and operated.

(1) Leadership: Positions, deployments and commitments made by the company in the EMS.

(2) Policies, Objectives and Strategies: The policies followed by the company's EMS, the objectives set, and the strategies for achieving these objectives.

(3) Roles, Responsibilities, and Authorities: the responsibilities and authorities of the relevant roles in the EMS, and the work done to establish and implement it.

●Core Processes: Under the leadership of the company, operate the core processes of the environmental management system, including planning, operations management, and

improvement.

(1) Planning: Clarify the environmental work requirements in the company's business activities, and carry out environmental work that is appropriate for different business stages.

a. Environmental Baseline: Collect environmental baseline data during the exploration phase, establish an environmental baseline, and provide baseline data for environmental impact assessments.

b. Environmental Impact Assessment (EIA): An EIA is conducted prior to testing mining components, test mining and development applications to control potential environmental impacts within thresholds.

c. Environmental Management and Monitoring: Based on the scale and equipment of the activities (testing of mining components, test mining, or application development), as well as the results of the environmental impact assessment, develop an environmental management and monitoring plan.

d. Closure plan: Develop a closure plan based on the results of the EIA and the plan of work.

(2) Operational Management: Operational management is carried out during the execution of planned operations, including management of procurement, subcontractors, emergency and contingency plans, performance evaluation, supervision, reporting and notification, and auditing and review.

a. Procurement, Subcontractors: Procurement includes purchase of equipment and other physical assets as well as services. Subcontracting refers to the company assigning a part of its business activities to subcontractors.

b. Emergency and Contingency Plan: Aims to establish, implement, maintain, and improve the processes required to prepare for and respond to potential emergencies.

c. Performance Evaluation: Evaluate the performance of the requirements of the EMS through established standards, methods, and frequencies, including environmental performance evaluation.

d. Supervision: Define the positions, responsibilities and authorities for supervision.

e. Reporting and Notification: Report and notify as required by domestic management agencies and the ISA.

f. Audit and Review: Audit and review the planning, operation, inspection and improvement of the EMS.

●Improvement: Identify nonconformities through implementation and propose improvement measures.

a. Nonconformities: Items that do not meet the requirements.

b. Continuous Improvement: Continuously improve the suitability, adequacy and effectiveness of the EMS.

●Support: Resources, awareness and competence, communication and documentation that support the establishment and implementation of the EMS.

a. Resources: Resources used in the EMS, including personnel, equipment, funds and time with relevant capabilities.

b. Awareness and Competence: Knowledge and capabilities for scientific understanding of the deep sea, environmental management, protection and conservation of the deep-sea environment.

c. Communication (Internal and External): Internal and external communication on the concept, establishment and implementation of the EMS.

d. Documentation: Documents in the process of establishing and implementing the EMS.

2.4.4.2 Organizational Structure

The personnel organizational structure is shown in Figure 2-5.
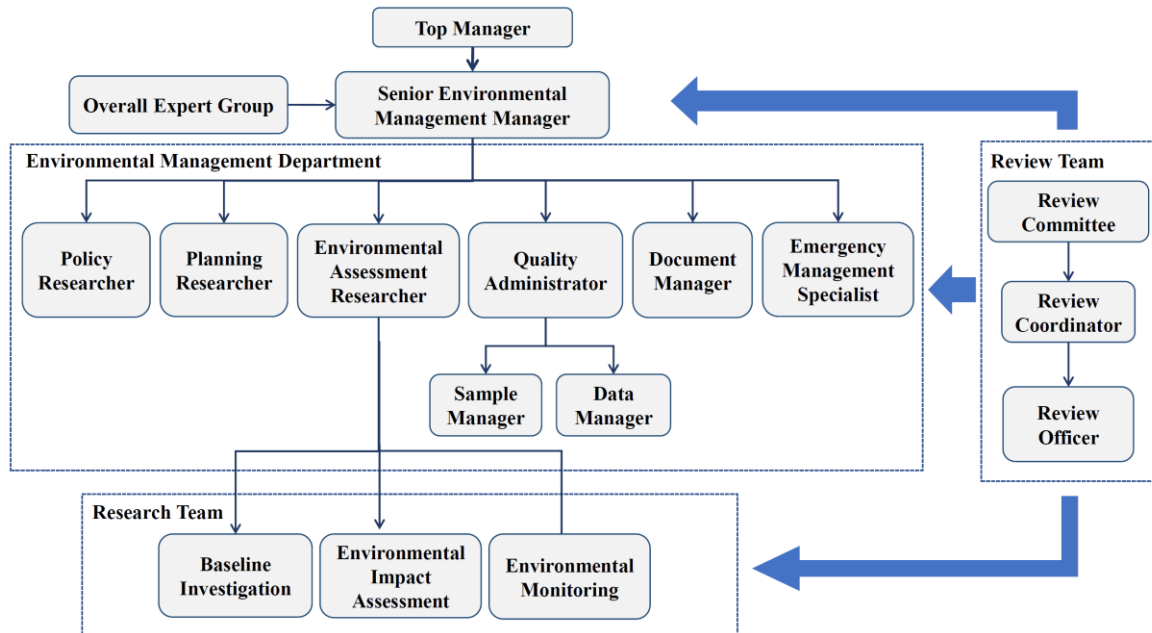
Figure 2-5 Personnel organization chart

Top management

●Top Manager: The top manager of the company, responsible for the overall planning and top leadership of the EMS.

●Overall Expert Group: Responsible for providing expert advice and guidance on the establishment and implementation of the EMS.

●Senior Environmental Management Manager: Responsible for leading the establishment and implementation of the EMS.

Ministry of Environmental Management

●Policy Researcher: Responsible for conducting research on domestic and international environmental policies, including international law, relevant requirements of the International Seabed Authority, domestic deep-sea law, environmental law, etc., and formulating policies and environmental systems that are in line with the development objectives of the company's EMS.

●Planning Researcher: Responsible for the planning of environmental work in the EMS, including planning of environmental baseline surveys, planning of environmental impact assessment work, environmental management and monitoring plans, closure plans, and other related operations.

●Environmental Assessment Researcher: Responsible for environmental assessment, including baseline assessment, environmental impact assessment, and monitoring.

●Quality Administrator: Responsible for the overall quality of samples and data obtained in the company's environmental operations.

●Sample Manager: Responsible for the management of samples obtained in the company's environmental business, including the collection, warehousing, and use of samples.

●Data Manager: Responsible for the management of data acquired in the company's environmental business, including the collection, entry, and use of data.

●Documentation Manager: Responsible for organizing and compiling documents in the EMS.

Research Team

●Baseline Survey: Responsible for environmental baseline survey and analysis.

●EIA: Responsible for assisting environmental assessment researchers with environmental impact assessments, etc.

●Environmental Monitoring: Responsible for assisting the Environmental Assessment Fellow with environmental monitoring.

Review Team

●Review Committee: The EMS Audit Committee is elected by the company's management to supervise and manage the audit work, and to elect an audit coordinator before each audit.

●Review Coordinator: Responsible for conducting regular internal audits of the EMS, and is elected by the Audit Committee before each audit.

●Review Officer: Responsible for assisting the Audit Coordinator in conducting internal audits of the EMS. Audit Officers are temporarily assigned from various departments, and in principle, there should be no fewer than three Audit Officers.

2.5 Relevant domestic procedures for the administration of exploration activities

This EIS is one of the materials that should be submitted to the national competent authorities for review, as required by the relevant domestic procedures for the management of exploration under Deep Seabed Law in the sponsoring State mentioned in 2.2.1. Therefore, the Contractor made the EIS, the EMMP, and other materials public under relevant regulations on May 1, 2024, and started the consultation process with stakeholders. The contractor further modified/supplemented the report according to the consultation opinions, and then prepared a report and submitted it to the State Oceanic Administration of China. The administration put forward modification/supplement suggestions after the standard review procedure of the third party (CCSOA). The contractor further modified/supplemented the report according to these view opinions, prepared a report, and submitted it to the State Oceanic Administration of Chin for filing.

3 PROJECT DESCRIPTION

3.1 Location of Proposed Activities

3.1.1 Overview of the Contract Area

The mining area of the BPC is located in the intermountain basins between the Magellan and Marcus-Wake seamounts in the northwest Pacific Ocean. The contract area consists of four blocks, C1, C2, M1, and M2 (Figure 3-1). Block C1 and C2 are located in the Marcus-Wake seamount area, while Block M1 and M2 are located in the Magellan seamount area with a total area of 74,052 km^2.
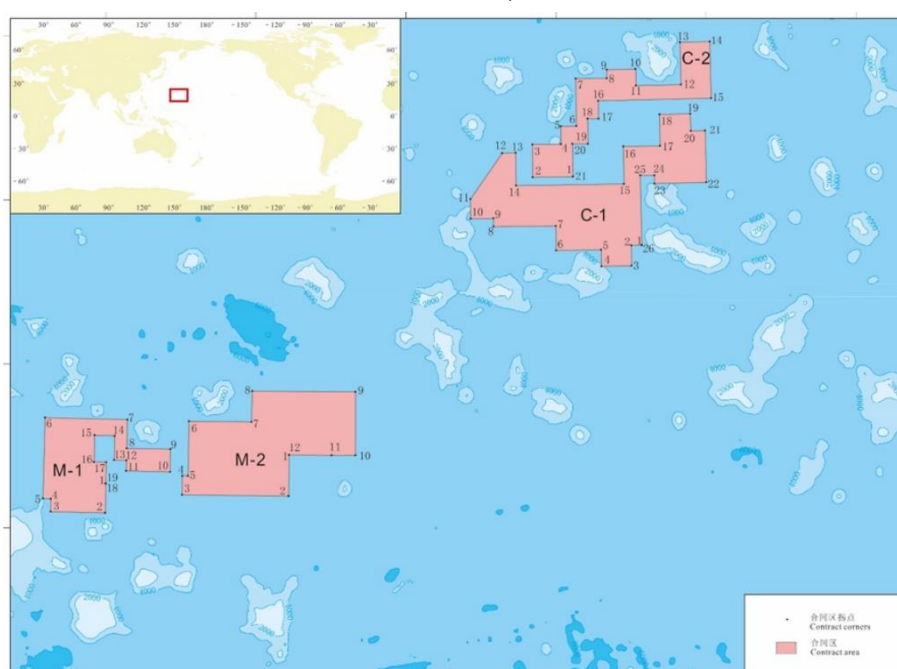
Figure 3-1 Location of the contract area of the BPC

Geological background: The age of the oceanic crust in the contract area ranges from 172 Ma to 150 Ma. The ancient basement provides a suitable growth environment for the development of cobalt-rich crusts and nodules in seamounts and deep-sea basins. The western Pacific seamount region has the greatest potential for cobalt-rich crust resources, and cobalt-rich nodules in deep-sea basins, which are newly discovered solid mineral resource with economic potential on the seabed. The multiple periods of tectono-magmatic activity during the Mesozoic in the region have created a complex geographical pattern in the Northwest Pacific, with alternating distribution of seamount chains and intermountain basins formed in different eras, mainly including the three seamount chains—Marcus-Wake, Magellan, and Marshall, as well as deep-sea basins such as the Najelda, the Kardagrave, the Pikaffeta, the Eastern Mariana and Nauru.

Climate: The surveyed area belongs to a subtropical monsoon climate, mainly influenced by subtropical high pressure and equatorial convergence zone in summer, with prevailing easterly winds and weak winds. The northeast monsoon prevails in winter, with strong winds and poor sea conditions. The Northwest Pacific is the region with the most frequent tropical cyclone activity in the world. The origin of tropical cyclones is located between 5 and 22°N, and the surveyed area is located in this zone. The formation period of Northwest Pacific cyclones is mainly concentrated from July to September, accounting for about half of the year, with the weakest activity in February.

Current: Overall, the contract area is under the control of the North Equatorial Current (NEC) and the North Equatorial Counter Current (NECC). The upper ocean is mainly affected by these two currents, while the lower part is mainly affected by the oceanic thermohaline circulation. The Antarctic bottom water (AABW) flows from south to north in this area.

Nutrients and primary productivity: The results of large-scale analysis indicate that the entire region is characterized by oligotrophic characteristics, with obvious stratification of regional chemical elements (pH, DO, nitrate, phosphate, and silicate). The depth of water layers with high DO values increases from south to north, while salinity increases obviously from 0 to 200 meters north of 19°N. There are certain latitudinal differences in the water profile environment. Satellite data shows that there is a certain north-south difference in the concentration of surface POC and *chlorophyll-a*, with the northern part being lower than the central part, and the depth of the maximum *chlorophyll-a* layer gradually becoming shallower from south to north; However, at the scale of the contract area, there is not much difference in the levels of surface *chlorophyll-a* and primary productivity; There are long-term cold and warm eddies in the surface area of the anomalous data of geostrophic flow and sea surface height. The vortices will affect the upper environment of the region, and are affected by the edge and center effects of the vortices. Within the range of vortex influence, nutrients will increase to a certain extent, leading to increased productivity and biomass, which may affect the sedimentation flux in small areas and affect the energy supply of bottom organisms.

3.1.2 Test Area, Impact Reference Zone, and Preservation Reference Zone

3.1.2.1 The Basis of Delineation

According to Regulation 31 (6) of the *Regulations on Prospecting and Exploration for Polymetallic Nodules in the Area* (ISBA/19/C/WP.1), contractors, sponsoring countries, and other relevant countries or entities shall cooperate with the ISA to

develop and implement plans for monitoring and evaluating the impact of deep-sea mining on the marine environment. If requested by the Commission, such a plan should include proposals to designate areas specifically for use as IRZ and PRZ. The basis also includes *Recommendations for the Guidance of Contractors for the Assessment of the Possible Environmental Impacts arising from Exploration for Marine Mineral in the Area* (ISBA/25/LTC/6/Rev.3) and *Deep Seabed Area Resource Exploration and Exploitation Law of the People's Republic of China*.

3.1.2.2 The Principles of Delineation

The experiment area should comply with the following principles:

Located within the IRZ;

According to the type and scale of activities to be tested, delineation should be carried out that the CTA of mining components such as collectors should not exceed 1 km×1 km.

The IRA should comply with the following principles:

(1) Select areas that can represent the environmental characteristics, for instance, the benthic species composition and community structure to be similar to other areas in the contract area;

(2) The IRZ needs to include the experiment area;

(3) The size of the reference area should be determined by the impact scope of the plume based on the diffusion model.

The PRZ should comply with the following principles:

(1) Similar habitats to the impact reference area;

(2) The composition of benthic organisms has both comparability and specificity with the impact reference area;

(3) Located at the upstream of the plume, ensuring that the preservation reference area is not affected by the plume;

(4) The PRZ for testing mining components such as collectors shall not be less than 10 km × 10 km;

(5) The distance between the PRZ and the IRZ is at least 30 km (based on plume simulations, the finest grain size sediment dispersal distance is about 20 km, see Chapter 6).

3.1.2.3 The Methods of Delineation

Based on parameters such as water depth, topography, nodule abundance, nodule coverage, bottom currents, total organic carbon, and similarity in benthic species composition, we select PRZ that is similar to the environmental background of the experiment area.

3.1.2.4 The Result of Delineation

The IRZ (including the experiment area and the plume diffusion influence area) is located in the northeast of the Block M2. In order to protect and preserve the marine environment, we established a PRZ, which is located in the Block M1, and the IRZ is located in the foothills, about 78 km away from the CTA. The PRZ is mainly used to monitor the natural environmental changes of the foothills, and to compare the various environmental impacts that may be caused by the trial activities, and to offer a basis for assessing potential impacts of the test on the environment (Figure 3-2).

The IRZ and PRZ were selected on the basis of the principle of similarity, in which the geologic environments of the two zones are similar. The PRZ is located in the southwest of the Matsuzaki Guyot, with the center 50 km away from the hilltop, and the IRZ is located in the south of the Magoshichi Guyot, with the center about 50 km away from the foothill. The two zones are characterized by similar geological environments, similar nodule types and distributions (Yao et al., 2024), and are located in the foothill-type nodule deposits.

The southern sector of the Matsuzaki Guyot covers an area of about 2900 km^2 with a slope of about 3°, a backscatter intensity of about –30 dB, Eh values varying from 285–301 mv (n=4), and the development of an undulating topography with symmetrical cross-sections and curved to rectilinear wave crests (Wang et al., 2024). The nodule types in the area are dominated by large and medium-sized ellipsoidal and spherical nodules. The southern sector of Magoshichi Guyot covers an area of about 2800 km^2, with a slope of about 3°, a backscatter intensity of about –26 dB, Eh varying from 197–343 mv (n=20), and the development of an undulating topography with irregular cross-sections and curved wave crests (Wang et al., 2024). The nodule types in the area are dominated by medium- to large-sized ellipsoidal and spherical nodules. The two seamounts are located next to each other, and the geological and sedimentary processes, substrate types and the range of sediment Eh variations in the foothill area are similar in parameters.
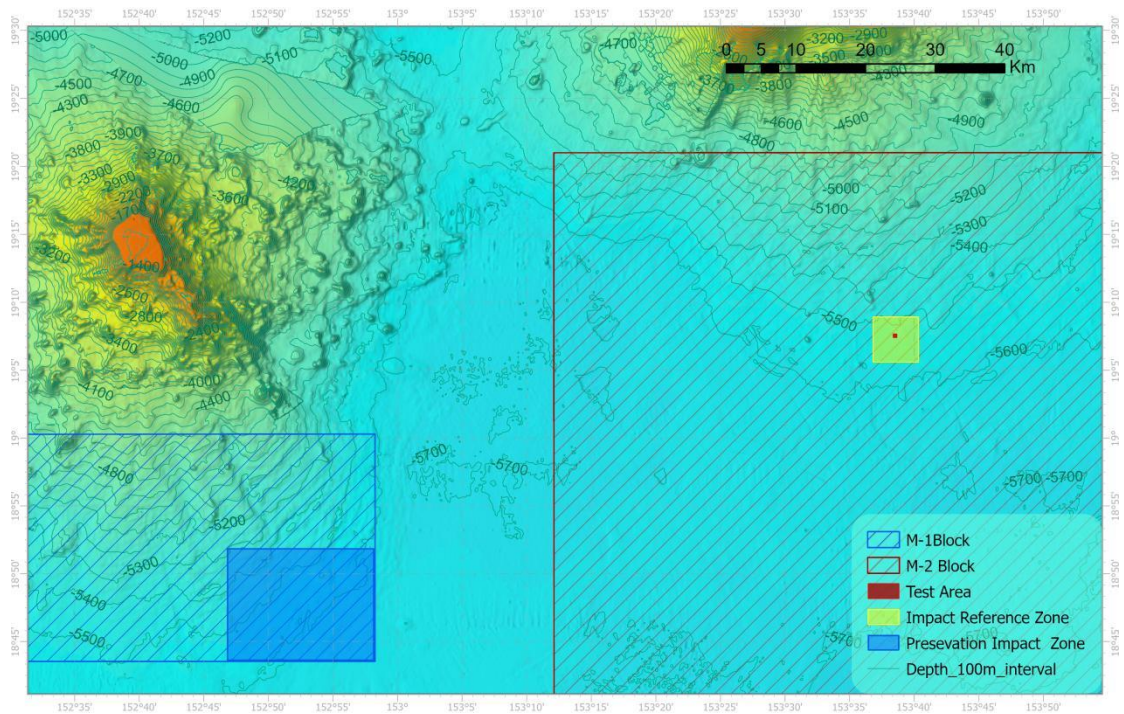
Figure 3-2 Location of the CTA, PRZ and IRZ

3.1.2.5 Collector Test Area Location, Resource and Environmental

Characteristics

The collector test area (CTA) is located in the center of the IRZ in the southern foothills of the Magoshichi Guyot (Figure 3-3), covering an area of 500 m × 500 m, with an average water depth of 5550–5600 m. The sediment type is deep-sea clay, with siliceous detritus as the dominant material component (88%–98%, with a mean value of 92%, n=13), and the siliceous bioclasts content ranging from 1% to 4%, with a mean value of 1% (n=13), volcanic detritus content ranged from 1% to 8% with a mean value of 5% (n=13), nodule cover was 64.7%, the maximum bottom flow velocity was 18.40 cm/s, the mean flow velocity of the eastern component was –1.20 cm/s, the mean flow velocity of the northern component was –0.06 cm/s, and the mean direction of the flow was south–west. Meiofauna mean abundance was 15.43–16.77 ind./10cm^2 (Table 3-1).

Table 3-1 Comparison of environmental parameters between the IRZ and PRZ

Environmental baseline	IRZ (including CTA)	PRZ
Geographic location and type	Northeastern part of Block M2 in the contract area, southern foothills of Magoshichi Guyot, with core area of 11.5 km × 11.5 km, and a water depth range of 5,550 to 5,600 m	Western part of Block M1 of the contract area, the southern foothills of the Matsuzaki Guyot, covers an area of approximately 21 km x 16 km, with a water depth range of 5,250 to 5,650 m.
Sediment type	Deep-sea clay, material composition dominated by siliceous detritus (88% to 98%, mean 92%, n=13), siliceous bioclastic content varied between 1% and 4%, mean 1% (n=13), volcanic detritus content ranged from 1% to 8%, mean 5% (n=13)	Deep-sea clay, material composition dominated by siliceous detritus (75% to 95%, mean value 89%, n=7), siliceous bioclastic content varied between 1% and 15%, mean value 3% (n=7), volcanic detritus content ranged from 3% to 10%, mean value 5% (n=7)
Sediment chemistry	Eh: 198 mv – 321 mv with a mean value of 246.86 mv (n=8);	Eh: 186 mv –245 mv with a mean value of 209.14 mv (n=7);
Sediment Pore water	The mean value of Cd was 0.510 mg/L Co mean value of 0.836 mg/L The mean Cu value was 4.025 mg/L The mean Fe value was 17.208 mg/L. The mean value of Mn was 16.166 mg/L The mean value of Pb was 2.001 mg/L The mean value of Zn was 144.121 mg/L	The mean value of Cd was 0.496 mg/L Co mean value of 0.709 mg/L The mean Cu value was 2.193 mg/L. The mean Fe value was 10.112 mg/L. The mean value of Mn was 14.773 mg/L The mean value of Pb was 1.479 mg/L The mean value of Zn was 134.609 mg/L
Total mass flux of settled particulate matter	1.69 mg m^{-2} d^{-1} −24.37 mg m^{-2} d^{-1} , with an average value of 12.94 mg m^{-2} d^{-1}	2.18 mg m^{-2} d^{-1} −41.53 mg m^{-2} d^{-1}, with an average value of 12.35 mg m^{-2} d^{-1}
Nodule abundance and coverage	The mean abundance value was 34.51 kg/m^2 The average coverage was 64.7%	The mean abundance was 14.6 kg/m^2 The average coverage was 25.3%
Deep current	The maximum flow velocity was 18.40 cm/s, the mean flow velocity of the eastern component was –1.20 cm/s, the mean flow velocity of the northern component was –0.06 cm/s, and the mean flow direction was southwesterly.	The maximum flow velocity was 16.85 cm/s, the mean flow velocity of the eastern component was –3.15 cm/s, the mean flow velocity of the northern component was –2.48 cm/s, the
Chlorophyll *a*	38.27 ± 8.29 mg/m^3	35.93 ± 8.13 mg/m^3
Primary productivity	16.59 ± 9.92 mgC/(m^2·h)	26.80 ± 10.24 mgC/(m^2·h)
Abundance of picoplankton	(56.34 ± 7.14) × 10^3 cells/mL	(44.84 ± 3.18) × 10^3 cells/mL

Environmental baseline	IRZ (including CTA)	PRZ
Abundance and diversity of nanoplankton	The surface abundance was 1.08×10^3 cells/L, diversity index (H') was 1.73, the richness (D) was 0.44, and the evenness (J) was 0.76.	The surface abundance was 0.38×10^3 cells/L, diversity index (H') is 1.71, the richness (D) was 0.35, and the evenness (J) was 0.87.
Abundance and diversity of microplankton	Abundance was 3.93×10^3 cells/m³, diversity index (H') was 3.73, richness (D) was 2.76, evenness (J) was 0.77	Abundance was 3.08×10^3 cells/ m³, diversity index (H') was 3.12, richness (D) was 2.26, evenness (J) was 0.68
Zooplankton abundance and diversity	Abundance was 72.63 ind/m³, diversity index (H') was 4.90, richness (D) was 20.39, evenness (J) was 0.73	Abundance was 57.19 ind/m³, diversity index (H') was 4.83, richness (D) was 19.90, evenness (J) was 0.73
Similarity of species composition of meiofauna	Meiofauna were all dominated by nematodes, which accounted for more than 85% of the total. The dominant genera are *Halalaimus* and *Desmoscolex,* followed by harpacticoides.	Meiofauna were all dominated by nematodes, which accounted for more than 90% of the total. The dominant genera are *Halalaimus* and *Desmoscolex,* followed by harpacticoides.
Meiofaunal abundance	Mean abundance 23.2 ± 10.3 ind./10cm²	Mean abundance 35.7 ± 16.4 ind./10cm²
Similarity of species composition of macrofauna	Average species richness of 10 ± 12 species/m² The main taxa are crustaceans and polychaetes, the dominant species is Spionidae sp.2	Mean species richness was 12 ± 6.9 species/m² The main taxa are crustaceans and polychaetes, the dominant species is Spionidae sp.2
Macrofauna abundance	Average abundance of 18 ± 4.9 ind/m²	Average abundance of 22.0 ± 2.8 ind/m²
Megafauna	Abundance was 18.7 ind./km; Species composition: 29 morphotypes, 20 species shared by the two regions, dominant species: *Peniagone* sp., *Caulophacus* sp., *Hyalonema* sp., *Ophiacantha* sp., Mopseidae gen. indet., *Cerataspis monstrosus*, *Benthodytes sanguinolenta*, *Coryphaenoides* sp., *Synallactes* sp. Etc.	Abundance* was: ; Species composition: 29 morphotypes, 20 species shared by the two regions, dominant species: *Peniagone* sp., *Hyalonema* sp., *Caulophacus* sp., *Cerataspis monstrosus*, *Coryphaenoides* sp., *Synallactes* sp., *Benthodytes sanguinolenta*
Microbial diversity of sediment	Shannon- Wiener's diversity index was 6.85 ± 0.47 on average.	Shannon- Wiener's diversity index was 6.95 ± 0.13 on average.

* The Megafauna data for PRZ is under analysis and will be submitted to ISA in the Annual Report 2024 by the end of March 2025, together with the results and data of the 2024 baseline survey.

3.1.2.5.1 IRZ Location, Resource and Environmental Characteristics

The IRZ includes the experiment area and the plume diffusion influence area (Figure 3-3), located at the southern foothills of Magoshichi Guyot. According to the modelling results of the plume diffusion in Chapter 6, the extreme distance affected by the sediment plume spreading outward from the test position is 3.48 km. Therefore, this monitoring program plans to expand the plume influence area by 3.5 km from the test

position to the west, east, and north and south, respectively. The total area of the IRZ is approximately 11.5 km × 11.5 km.

The resources and environmental characteristics in the CTA are basically consistent with the reference zone.
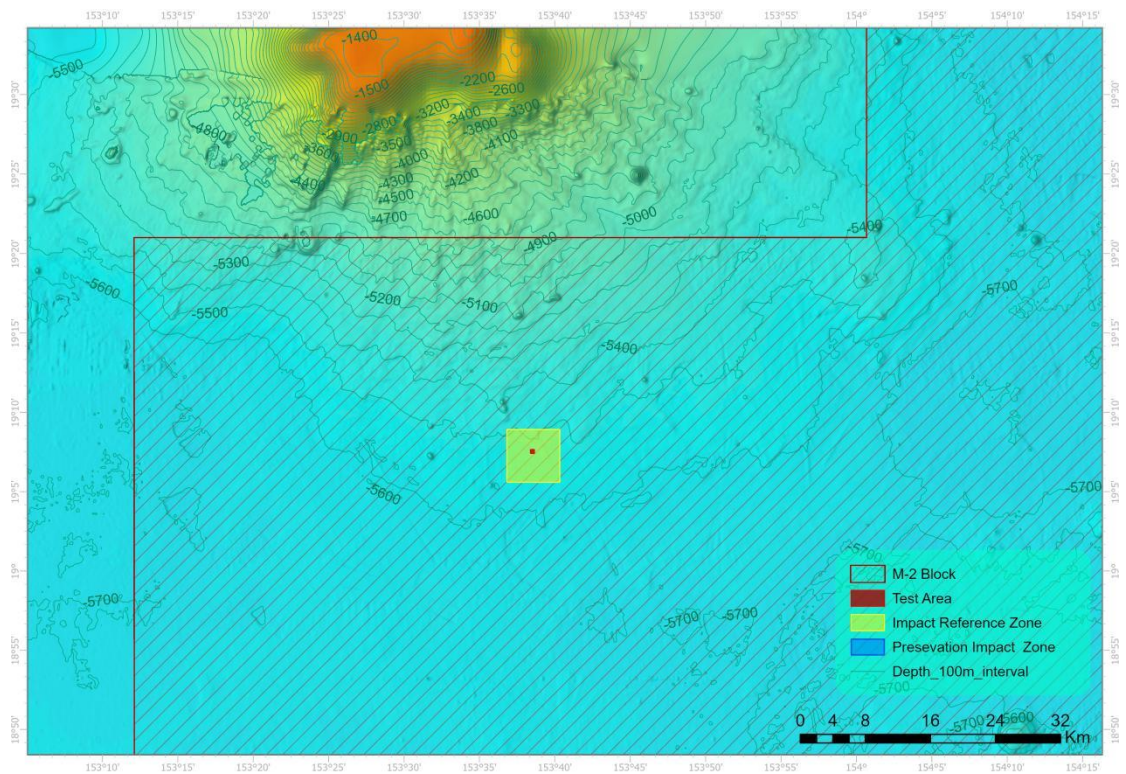
Figure 3-3 Bathymetric map of the CTA and the IRZ

3.1.2.5.2 PRZ Location, Resources, Environmental Characteristics

The PRZ is located at the southern foothills of Matsuzaki Guyot (Figure 3-4), with an area of approximately 21 km×16 km and a water depth range from 5250 – 5650 m. The sediment type is deep-sea clay, with siliceous debris (range from 75% – 95%, mean value = 89%, n=7) as the main component. The content of siliceous bioclastic varies between 1%–15% (mean value = 3%, n=7), and the content of volcanic debris ranges from 3% to 10% (mean value = 5%, n=7). The mean nodule coverage is 25.3%, with a maximum current velocity of 16.85 cm/s in the bottom. The average velocity in the east component is –3.15 cm/s, and the average velocity in the north component is –2.48 cm/s. The average abundance of meiofauna is 28.15 – 38.64 ind./10cm^2.
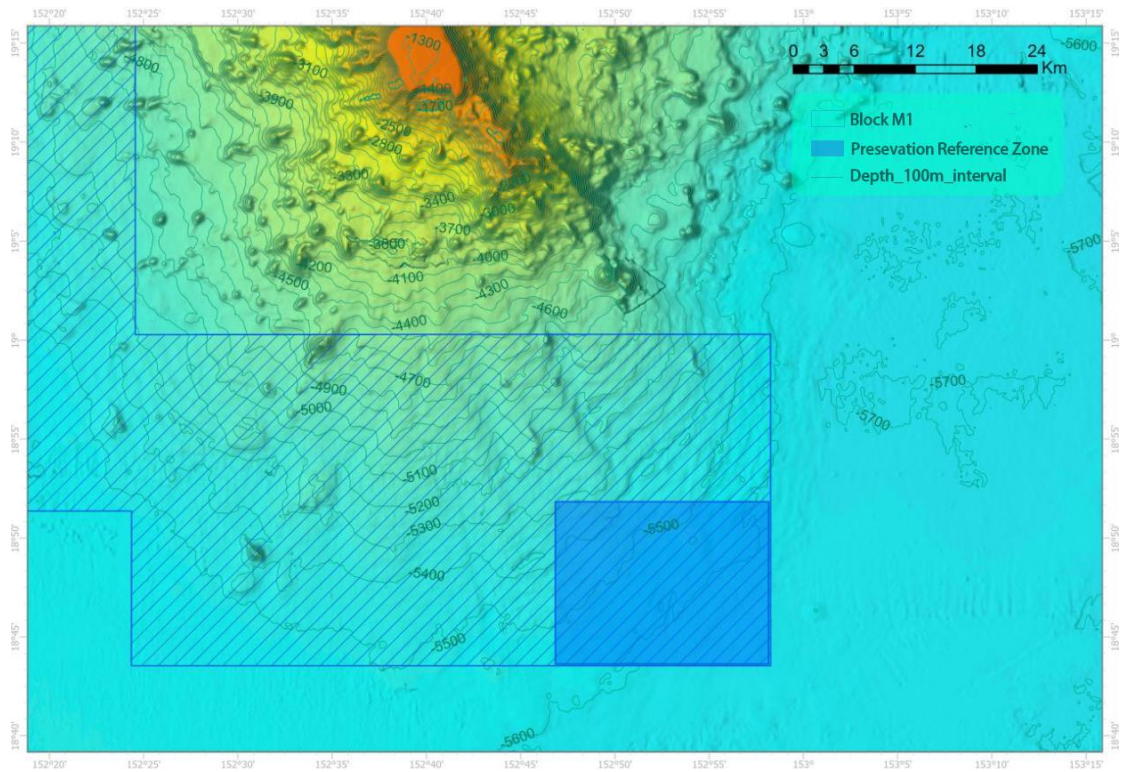
Figure 3-4 Bathymetric map of the PRZ

3.1.2.5.3 Comparison of Benthic Organisms Between the PRZ and the IRZ
（1）Macrofauna

Table 3-2 Station and species information on macrofauna biodiversity between the PRZ and the IRZ by comparison

Area	Station	Number of specimens / stations	Species richness/ stations	Species
IRZ	DY75-BC77	1	1	Crustaceans (Isopoda)
	DY75-BC78	1	1	Crustaceans (Protopoda)
	DY81-BC55	10	7	Crustaceans（Epipoda, Isopoda, Copepoda)
PRZ	DY81-BC43	7	4	Polychaetes
	DY81-BC44	9	4	Polychaetes & Crustaceans
	DY75-BC74	1	1	Crustaceans (Isopoda)

The average abundance of macrofauna in the IRZ and the PRZ is 16.0 ± 20.8 ind./m^2 and 22.7 ± 16.6 ind./m^2, respectively, and the species richness is 10 ± 12 spices/m^2 and 12 ± 6.9 spices/m^2, respectively. There is an obvious variation in the abundance and species richness among different stations within the IRZ. The difference in abundance between them is not obvious ($p = 0.30$, Wilcoxon difference test), and the difference in species richness is not obvious ($p = 0.69$, Wilcoxon difference test). The IRZ and PRZ share similarities in species richness and average abundance.

The PRZ includes 6 species and the IRZ includes 9 species. Among them, 3 species are shared (Table 3-3 and Table 3-4).

Table 3-3 Results of identification and analysis of macrofauna in the IRZ

Station	Burial depth/ (cm)	Order	Family	Genus	Species
DY75-I-M2-BC77	0–3	Crustacea	Isopoda	-	Isopoda sp. indet.1
DY75-I-M2-BC78	0–3	Crustacea	Tanaidacea	-	Tanaidacea sp. indet.1
DY81-BC55	0–3	Decapoda	Amphipoda	-	Amphipoda sp.
DY81-BC55	0–3	Crustacea	Isopoda	-	Isopoda sp.4
DY81-BC55	0–3	Crustacea	Harpacticoida	-	Harpacticoida sp.
DY81-BC55	0–3	Polychaeta	-	Spionidae	Spionidae sp.2
DY81-BC55	0–3	Polychaeta	-	Polynoidae	Polynoidae sp.
DY81-BC55	0–3	Polychaeta	-	Flabelligerida	Flabelligerida sp.
DY81-BC55	0–3	Other unknown	-	-	-
DY81II-M2-ES03-BC56*	0–3	Polychaeta	Terebellida	Cirratulidae	Cirratulidae sp.

Table 3-4 Results of identification and analysis of macrofauna in the PRZ

Station	Burial depth/ (cm)	Order	Family	Genus	Species
DY81II-M1-ES08-BC43	0–3	Crustacea	Harpacticoida	-	Harpacticoida sp.
DY81II-M1-ES08-BC43	0–3	Polychaeta	Terebellida	Cirratulidae	Cirratulidae sp.3
DY81II-M1-ES08-BC43	3–5	Polychaeta	-	-	Polychaeta sp.
DY81II-M1-ES08-BC43	5–10	Polychaeta	-	-	Polychaeta sp.
DY81II-M1-ES08-BC43	5–10	Crustacea	Tanaidacea	-	Tanaidacea sp.8
DY81II-M1-ES08-BC44	0–3	Polychaeta	-	-	Polychaeta sp.
DY81II-M1-ES08-BC44	0–3	Crustacea	Harpacticoida	-	Harpacticoida sp.
DY81II-M1-ES08-BC44	3–5	Crustacea	Harpacticoida	-	Harpacticoida sp.
DY81II-M1-ES08-BC44	3–5	Crustacea	Tanaidacea	-	Tanaidacea sp.8
DY81II-M1-ES08-BC44	3–5	Polychaeta	-	-	Polychaeta sp.
DY81II-M1-ES08-BC44	5–10	Polychaeta	-	Spionidae?	Spionidae sp.2
DY75-I-M1-BC74	0–3	Crustacea	Isopoda	-	Isopoda sp.12

(2) Meiofauna

The results of the 2022 and 2023 surveys showed that the mean abundance of meiofauna in the IRZ and the PRZ was 23.2 ± 10.3 ind/m^2 and 35.7 ± 16.4 ind/m^2, respectively. According to the statistical results of the one-way analysis of variance, there is a large difference in meiofauna abundance between the two areas.

Table 3-5 Composition of meiofaunal abundance in IRZ and PRZ in 2022 and 2023

Area	Year of survey	Investigation station	Abundance range (ind./10cm²)	Average abundance (ind./10cm²)	Major group
IRZ	2022	6	5.9–36.7	20.20±11.10	Nematodes accounted for 85.8% of the total and Harpacticoides for 5.5% of the total
	2023	2	15.1–38.7	26.1±9.3	Nematodes accounted for 83.9% of the total and Harpacticoides for 9.4% of the total
PRZ	2022	6	22.0–64.3	39.0±18.0	91.8% nNematodes, 4.1% Harpacticoides
	2023	6	24.3–27.9	26.1±2.6	Nematodes 85.9%, Harpacticoides 6.3%

Table 3-6 Results of ANOVA analysis of meiofaunal abundance composition in IRZ and PRZ

		Sum of squares	Degrees of freedom	Mean square	F	Significance
Nematoda	Intergroup	718.998	1	718.998	4.753	0.043
Harpacticoida	Intergroup	0.121	1	0.121	0.126	0.727
Kinorhyncha	Intergroup	0.017	1	0.017	0.621	0.441
Polychaeta	Intergroup	0.098	1	0.098	1.921	0.183
Sipuncula	Intergroup	0.003	1	0.003	1.440	0.246
Tardigrada	Intergroup	0.011	1	0.011	0.993	0.332
Ostracoda	Intergroup	0.001	1	0.001	0.032	0.861
Gastrotricha	Intergroup	0.028	1	0.028	1.872	0.188
Nauplius	Intergroup	0.020	1	0.020	0.039	0.847
Other Copepda	Intergroup	0.017	1	0.017	1.690	0.210
Amphipoda	Intergroup	0.017	1	0.017	0.655	0.429
Acari	Intergroup	0.000	1	0.000	0.003	0.957
Bivalvia	Intergroup	0.000	1	0.000	0.084	0.776
Loricifera	Intergroup	0.081	1	0.081	3.488	0.078
Isopoda	Intergroup	0.001	1	0.001	0.655	0.429
Other	Intergroup	0.001	1	0.001	0.119	0.735
Total	Intergroup	760.219	1	760.219	4.503	0.048

Comparing the composition of meiofaunal taxa in the two regions, nematodes were the absolute dominant taxa, accounting for more than 65% of the total. However, the difference in nematode abundance between the two regions was obvious (p=0.043), while the abundance of other taxa did not have an obvious difference.

3.2 Nodule Characteristics

3.2.1 Nodule Abundance and Coverage

The distribution of nodule abundance in Block M2, where CTA is located, ranges from 0 kg/m^2 to 52.8 kg/m^2 , with a mean value of 26.16 kg/m^2 (n=109), a standard deviation of 11.11 kg/m^2, and a coefficient of variation of 42.47% (Figure 3-5), with a median value of 28.4 kg/m^2 being higher than the mean, and with peaks in the range of 30 kg/m^2 to 35 kg/m^2 , and the nodule abundance is mainly distributed in 10 kg/m^2 to 45 kg/m^2.
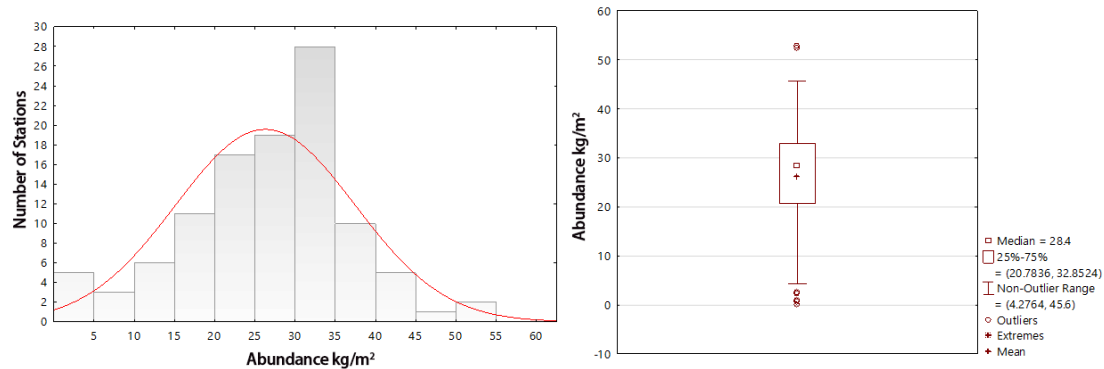
Figure 3-5 Histogram (left) and box (right) plot of polymetallic nodule abundance in Block M2 of the working area (N=109)

The distribution of nodule coverage in Block M2 ranges from 0% to 90%, with a mean value of 61.31% (n=109), a standard deviation of 20.80%, a coefficient of variation of 33.93%, a median of 69% above the mean, and peaks between 70 and 80%, with coverage mainly distributed between 50 and 80% (Figures 3-6).
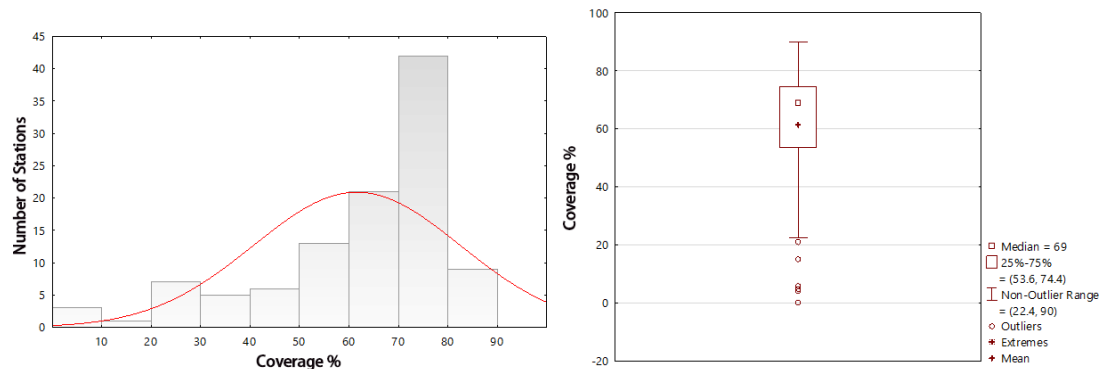
Figure 3-6 Histogram (left) and box (right) plot of polymetallic nodule coverage in Block M2 (N=109)

The correlation analysis of the data on abundance and coverage of polymetallic nodules from 109 stations in the Block M2 shows that the abundance of polymetallic nodules is positively correlated with the coverage, with a correlation coefficient of 0.8786. The linear equation of them is expressed as y = –2.6096 + 0.4694*x (r = 0.8786, p = 0.0000; r^2 = 0.7720, n=109) (Figure 3-7).
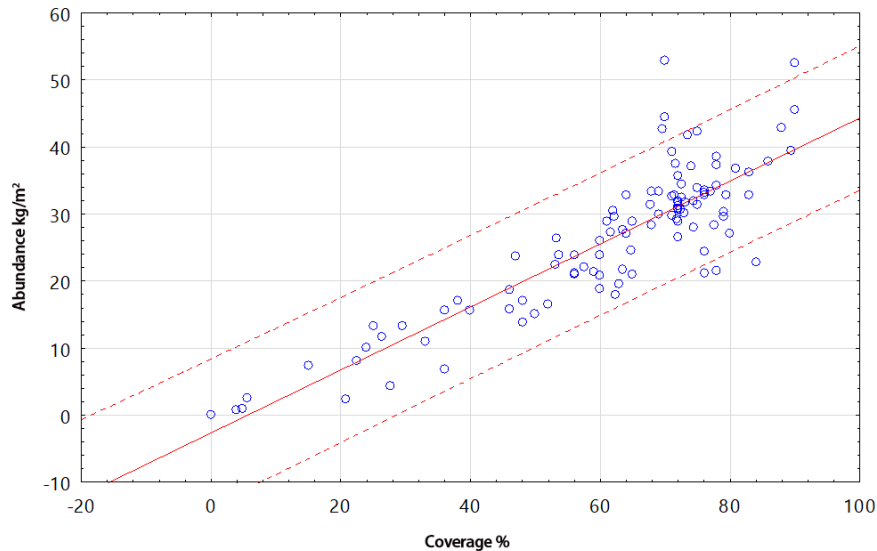
Figure 3-7 Correlation between polymetallic nodule abundance and coverage in the Block M2
(N=109)

3.2.2 Characterization of Nodule Types

Polymetallic nodule samples collected from 78 stations in the Block M2 were subjected to the determination of parameters such as mass, grain size and morphology of various types of nodules (except detrital nodules), and the polymetallic nodules obtained were categorized on the basis of grain size, morphology and surface characteristics. The distribution of the shape and grain size (four types of nodules, namely, giant (≥7 cm), large (5–7 cm), medium (3–5 cm) and small (<3 cm)), were characterized.

The Nodule Test Area nodules shapes are mainly dominated by ellipsoidal nodules, spherical and conidial nodules show a tendency of aggregated distribution, and mushroom, discoidal nodules show the characteristics of scattered distribution; the quantity of nodule is also dominated by large nodules, with more than 40 samples within the 0.25 m^2 area and more than 70% of large nodules in mass, followed by medium-sized with more than 20 samples, small nodules with <20 samples, and giant nodule with less than 10 samples (Figure 3-8).

Figure 3-8 Representive photographs of nodules collected from the CTA

3.2.3 Test Area Resources

The foregoing characteristics of nodule abundance, coverage and distribution of nodule types show that the CTA has high nodule abundance (> 30 kg/m^2). The nodule coverage is continuous and stable. The area of the CTA is 500 m×500 m and the estimated inferred wet nodule resource is 0.95 million tons.

3.3 Technical Objectives and Equipment for This Test

3.3.1 Background

3.3.1.1 Overall Technical Blueprint of BPC Polymetallic Nodule

Collection System

Based on the principles of green, environmental protection, economy, safety and reliability, BPC collaborated with several domestic scientific research institutions in China to design the comprehensive technical framework for the mineral collection system. This framework encompasses the entire system, from the surface mother ship, underwater riser, near-bottom buffer station, horizontal conveying hose to underwater miner (Figure 3-9).

The miner serves as the initial stages of the entire mining process. After collecting nodules, they are conveyed to the buffer station through the horizontal conveying hose, and subsequently transported to the sea surface by the riser. Following deliberation and planning, BPC has formed the following R & D plan of the whole mining system:

Step 1: Overall technical planning, specifying the system architecture and operational parameters;

Step 2: Development and testing of the 'Manta' suspended sampling testing machine;

Step 3: Development and testing of the 1: 5 scale suspended ore collector test machine;

Step 4: Implementation of the development and testing of the 1: 1 polymetallic nodule collecting testing machine, the development of buffer station, horizontal conveying hose and vertical lifting riser system, followed by comprehensive system testing.

Step 5: Technical refinement and optimization of the polymetallic nodule collection test system, conducting small-scale continuous mining tests for over a year, with a focus on verifying the economic viability of the mining system and its long-term environmental sustainability.

Step 6: Optimization of the continuous test system developed in the previous phase, scaling up production capacity for commercial mining, and initiating commercial mining of polymetallic nodules.

This experiment is part of the implementation of the third phase of the work plan.
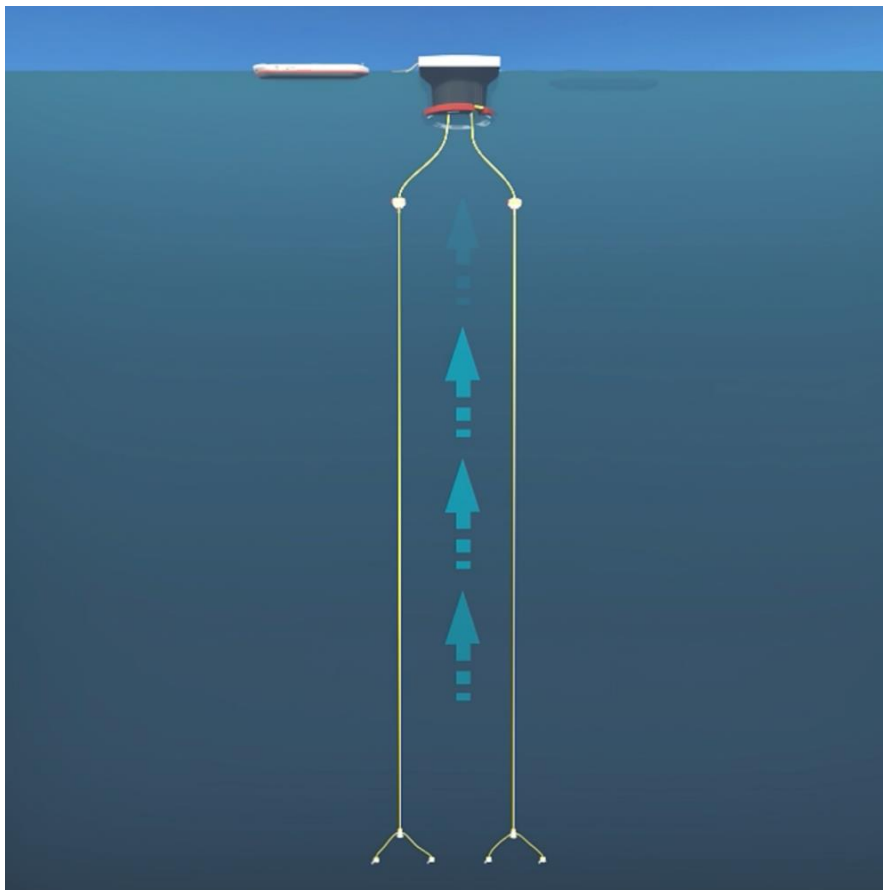
Figure 3-9 Composition diagram of the whole mining system

3.3.1.2 Development and Testing of Nodules Sampling Test Machine

("Manta I")

    The development and testing of the polymetallic nodule sampling test machine which is named "Manta I" (Figure 3-10) marked the second phase in BPC's comprehensive mining system development plan. It commenced its design and construction in March 2022 and completed the factory test in October 2022. The "Manta I" sampling test machine employs a suspended Remotely Operated Vehicle (ROV) as its basic carrier, equipped with a sampling head designed for minimal contact with the seabed while mining, with a width of 0.5 meters.
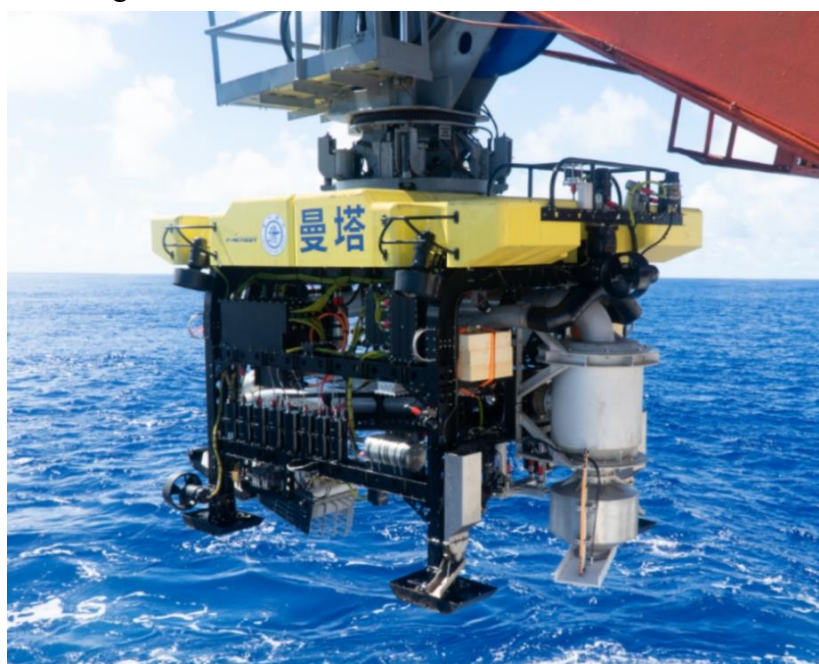
Figure 3-10 "Manta I" nodules sampling tester

    In 2022, the 2nd voyage of China Ocean successfully deployed "Manta I" sampling test machine in Block M2 of the BPC's contracted area for seabed sampling tests and delivering satisfactory results. During sampling operations, the ROV carrier remained suspended in the water column away from the seabed, while the sampling head smoothly glided along the seabed for sampling (Figure 3-11).; After sampling completion, the ROV carrier could retract the sampling head, and the "Manta I" adopted a contactless suspension mode to inspect the sampling effects.
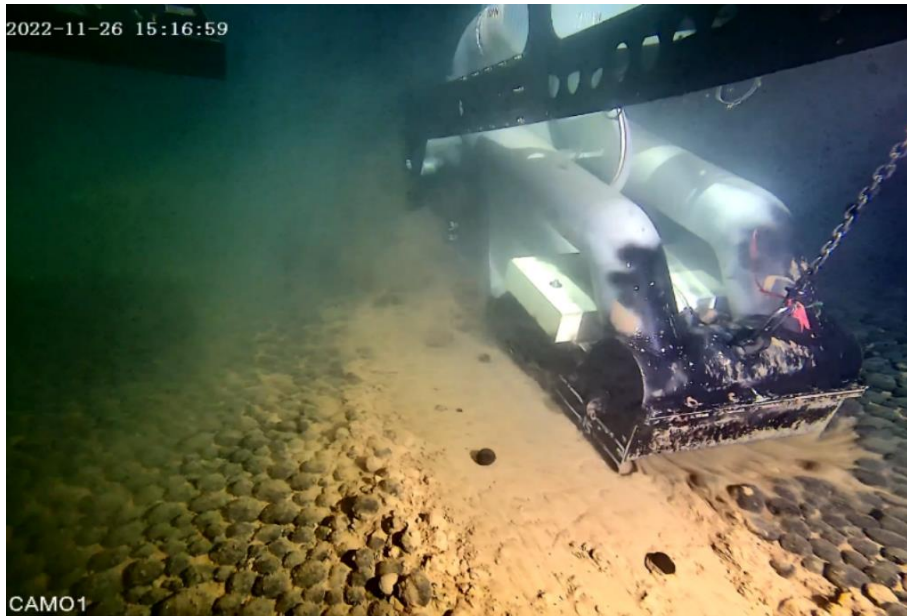
Figure 3-11 In-situ video screenshots of "Manta I" sampling on the seabed

Several on-site sampling tests conducted by the "Manta I" in the contracted area led to the following conclusions:

1) The suspended mining approach is feasible and offers obvious advantages.

2) The hydraulic mining technology of direct suction with accelerated water flow through the throat is viable.

The fundamental characteristic of the suspended mining approach is that the carrier exerts minimal pressure on the seabed, resulting in minimal disturbance. Additionally, the suspended mode demonstrates good adaptability to terrain and seabed conditions, requiring no specific sediment load-bearing capacity or shear strength, and imposing no constraints on terrain slope or topography. It is an exceptionally suitable mode of operation for seabed mining. During actual mining operations, the collector can rotate in place, simplifying the complexity of mining path planning.

The combination of a suspended carrier with an articulated collection head achieves the technical effect of stable, low-contact seabed gliding based on the weight of the collection head itself. The sampling device used by the Manta I is mounted on a sled, equipped with hydraulic cylinders to adjust the height of the mining head from the seabed. This measure quantifies the height of the mining head above the seabed. In practical tests, the nodule sample collection rate consistently exceeds 90%.

The achievements of the Manta I sampling tests lay a solid foundation for the subsequent expansion and extension of the Manta series mining system. The experiences and lessons learned from the Manta I will be incorporated into the design of later-stage mining systems.

3.3.2 Introduction of Technical Design of Nodule Collection Test

3.3.2.1 Overview of Suspended Miner Test Technology

BPC's planned development, the "Manta II", is a fully functional suspended polymetallic nodule collector test machine system with a collection capacity ratio of 1:5. BPC plans to conduct sea trials of the Manta II polymetallic nodule collector test machine in 2025, with the trial objectives including:

1) On-site testing of the nodule collector machine's performance in the mining area, with specific goals to:

a. Verify the mining capacity parameters of the miner.

b. Access the adaptability of multiple collection units to terrain bottom and seabed conditions.

c. Test flexible pipe butt joint technology of miner.

d. Test the technical parameters of nodule transport through the hoses.

e. Assess the disturbance stability of the nodule collector machine's motion via the hoses.

The sea trials of the nodule collector test machine will last approximately 20 days and will be conducted within a 0.25 km^2 (0.5 km × 0.5 km) area for nodule collection testing, with environmental monitoring equipment positioned in the periphery of the CTA to assess plume impact zones (see Chapter 9).

The development and testing of the Polymetallic Nodule Collector Test Machine ("Manta II") mark the third phase in the comprehensive mining system development plan of BPC. It commenced design work in 2023, with plans to complete equipment construction and factory testing in 2024 and to conduct mining trials in the contracted area in 2025.

The "Manta II" polymetallic nodule collector test machine inherits the suspended nodule collection approach and throat flow acceleration hydraulic nodule collection technology from "Manta I". During the design process, Pioneer Company engineers followed requirements for high collection efficiency, low operational energy consumption, minimal sediment disturbance, and reliable operation. They utilized computational fluid dynamics (CFD) for parameter design and laboratory testing for parameter validation.

3.3.2.2 Purposes of This Trial Test

The purposes of this trial test:

1) Validate the operational capability and collection efficiency of the 1:5 scale collector.

2) Verify the pumping capacity of the simulated buffer station per unit time.

3) Validate the collaborative operational capability of the collector, simulated buffer station, and hoses.

3.3.2.3 Composition of the Trial Test Equipment

The trial test equipment consists of three main components: the "Manta II" body, horizontal conveying hoses, and buffer stations, as shown in Figure 3-12.
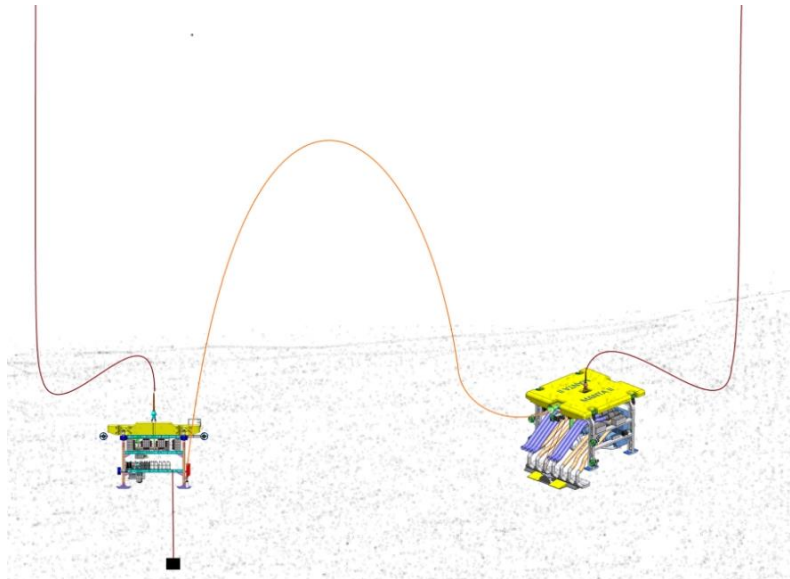
Figure 3-12 Near-bottom system composition of "Manta II"

3.3.2.4 Description of Test Equipment

Body configuration of miner

1) "Manta II" suspended ore collector body

2) Water surface monitoring power station

3) Supporting armored cable and winch system

4) The test ship is equipped with A-type gantry and stopper for hoisting.

The three-dimensional model and parameters of the collector body are shown in Figure 3-13 and Table 3-7.
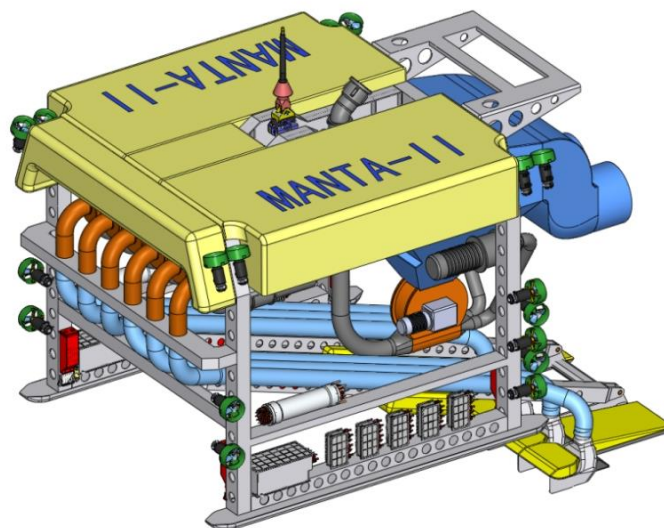
Figure 3-13 Three-dimensional model of "Manta II" miner

Table 3-7 The general characteristics of "Manta II"

Index	Parameter	Unit	Remarks
The Maximum Depth	6000	m	
Working Sea State	Level 4		
Underwater Power	180	KW	
Body Size	L7×B5.6×H3.8	m	
Weight in the Air	⩽12	ton	
Weight in the Water	0	ton	
Surface Speed	Forward 2.5, lateral 1.5, Vertical 1.5 knots	phase	
Power Supply	4200VAC/3phase		
Surface Monitoring Power	20 feet standard high box		

3.3.2.5 Parameter Configuration of the Prototype Buffer Station

The prototype buffer station configuration is as follows:

1) Buffer station body

2) Surface monitoring power station

3) Supporting armored cable and winch system

4) The test vessel is equipped with A-type gantry and stopper for lifting operations.

The three-dimensional model is shown in Figure 3-14.
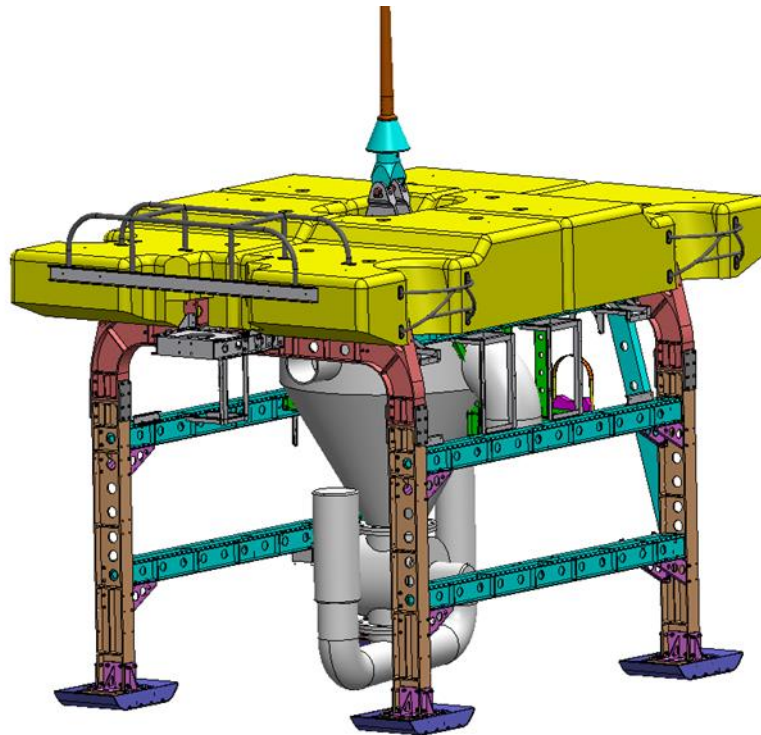
Figure 3-14 The three-dimensional model of buffer station

The prototype buffer station parameters are shown in Table 3-8.

Table 3-8 General characteristics of "Prototype Buffer Station"

Index	Parameter	Unit	Remarks
The Maximum Depth	6000	m	
Working Sea State	Level 4		
Underwater Power	55	KW	
Body Size	L5×B2.8×H2.6	m	
Weight in the Air	About 4.2	ton	
Weight in the Water	0	ton	
Power Supply	4200VAC/3phase		
Surface Monitoring Power	20 feet standard high box		

In the trial test system, the purpose of setting up the prototype buffer station is to:

(1) Coordinate with the horizontal conveying hose to simulate the transportation of nodules from the collector to the prototype buffer station.

(2) Control the discharge and backfilling of collected polymetallic nodules to the seabed.

(3) Regulate the discharge volume of minerals per unit time.

The prototype buffer station mainly features the following functions:

1) Basic functions of the ROV.

2) Installation and removal of horizontal hoses.

3) Control of connection points at the end of horizontal hoses.

4) Comprehensive precise positioning integrated with the long baseline system.

5) Synchronized maneuvering with the nodule collector machine.

6) Loading and unloading functions for ballast.

7) External transportation of mineral pumping functions.

3.3.2.6 Flexible Pipe

The flexible pipe section is composed of two different types of pipes. A steel wire composite hose is used in 12 m (1 piece) of the side of the miner, and the rubber flexible pipe was used in the remaining 84 m (12 m × 7 pieces).

Figure 3-15 Flexible pipe

In order to meet the special application conditions of the mining, the flexible pipe composition system must be configured with the following measures:

1) A flexible pipe with a length of 100 m and an inner diameter of 0.2 m is used to transport the minerals of the miner to the buffer station.

2) Several buoyancy materials are installed on the outer layer of the flexible pipe to balance the buoyancy.

3) The flexible pipe inlet end is provided with a pair of joints, which can be docked with the miner, and has a certain water weight for the joint.

4) The outlet end of the flexible pipe can be captured and connected by the buffer station, and two sets of pressure irons are set for diving and floating.

5) The flexible pipe is directly laid by the surface mother ship.

6) The deck retracting device is used for the placement and recovery of flexible pipe.

7) Deck configuration side guide.

3.3.3 Related Parameters of Environmental Disturbance in Collection Test

3.3.3.1 Overall Description

The collector utilizes the mining head to suction seawater, sediment, and nodules, forming a mixture of these three components.

After passing through the separation chamber, nodules meeting size standards are intercepted and transferred by the transfer device to the mixing conveyor, where they are pumped with clean seawater. The mixture is then transferred through the horizontal hose to the prototype buffer station. Sediment, seawater, and small nodules are discharged directly from the tail discharge pipe of the collector on-site.

Nodules and seawater mixture are directly discharged from the prototype buffer station, with the discharge port of the prototype buffer station located 5 meters above the seabed, downward discharge

3.3.3.2 Configuration of Test Parameters for "Manta II"

"Manta II" Collector Head Width: 0.7 m / piece × 6 = 4.2 m

Test speed: 0.25 m / s

Depth of Mining Trace: 5 cm

3.3.3.3 Calculation of Related Parameters

Hydraulic Suction Flow Rate: 1692 m^3 / h (0.47 m^3 / s)

Sediment Collection: 140 m 3 / h (0.039 m^3 / s).

Tuberculosis Collection: 29.43 kg / s (70 t / h, 35 m^3 / h).

Conveyor pump flow: 350 m^3 / h

Miner Discharge: 1692 m^3 / h sea water + 120 m^3 / h sediment mixture

Prototype Buffer station Discharge: 315 m^3/h seawater + 35 m^3/h polymetallic nodule mixture.

3.4 Nodule Collection Trial Test Plan

3.4.1 Trial Test Design

3.4.1.1 Flexible Pipe Test

(1) Spatial design of flexible pipe laying down to the seabed (Figure 3-16)
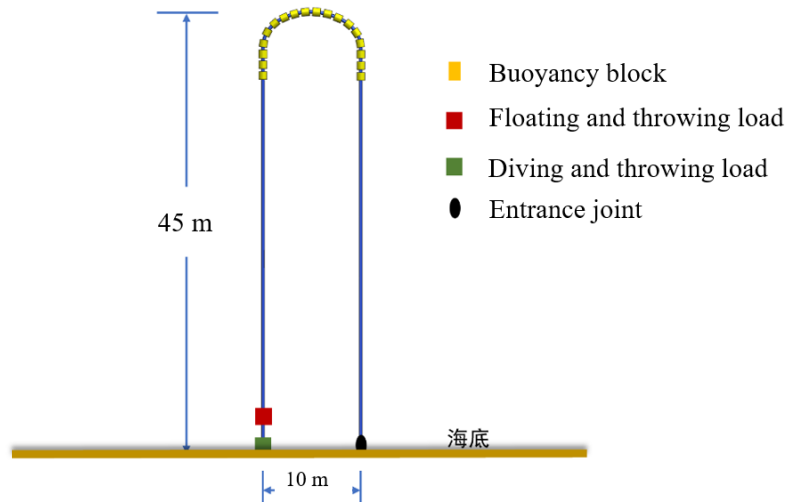
Figure 3-16 Spatial configuration diagram of flexible pipe laying down to the seabed

(2) Spatial design of flexible pipe in nodule collection operation status (Figure 3-17)
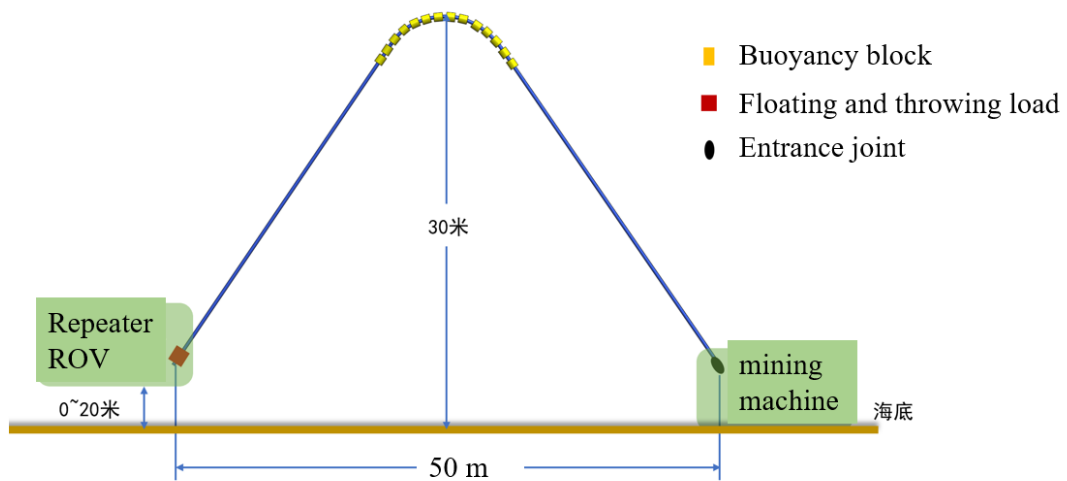
Figure 3-17 Spatial configuration diagram of flexible pipe in nodule collection operation status

(3) Spatial design of flexible pipe floating on sea surface (Figure 3-18)
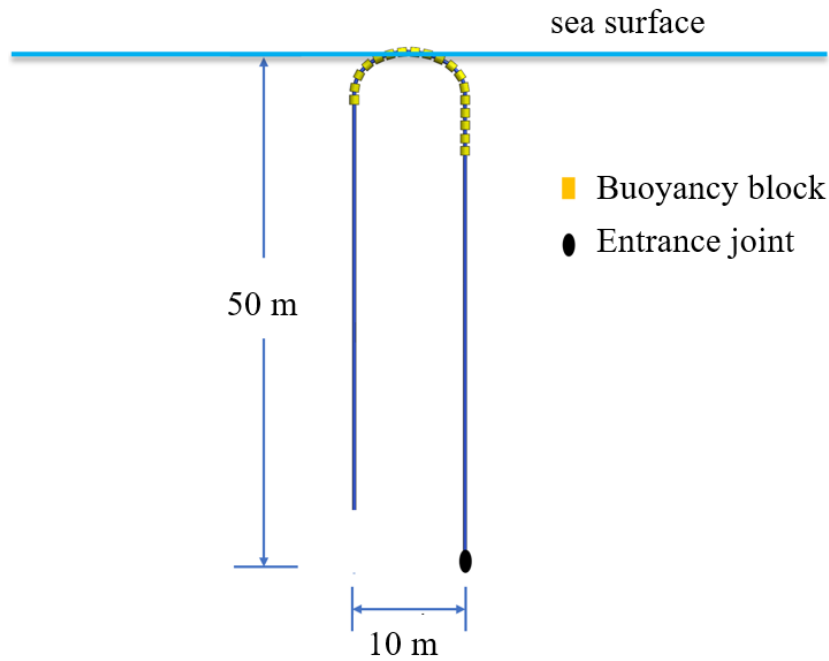
Figure 3-18 Spatial configuration diagram of flexible pipe floating on sea surface

(4) Deployment of prototype buffer station

The deployment is performed by surface vessel following with large ROV operation procedures.

3.4.1.2 Test Area and Operation Path Design

The collection test was carried out in the center of the declared area within the range of 500m × 500m. In the 2023 sea trial, "Manta I" has marked the 500m × 500m CTA.

The environmental monitoring equipment has arranged outside the boundary of the declared planning operation area.
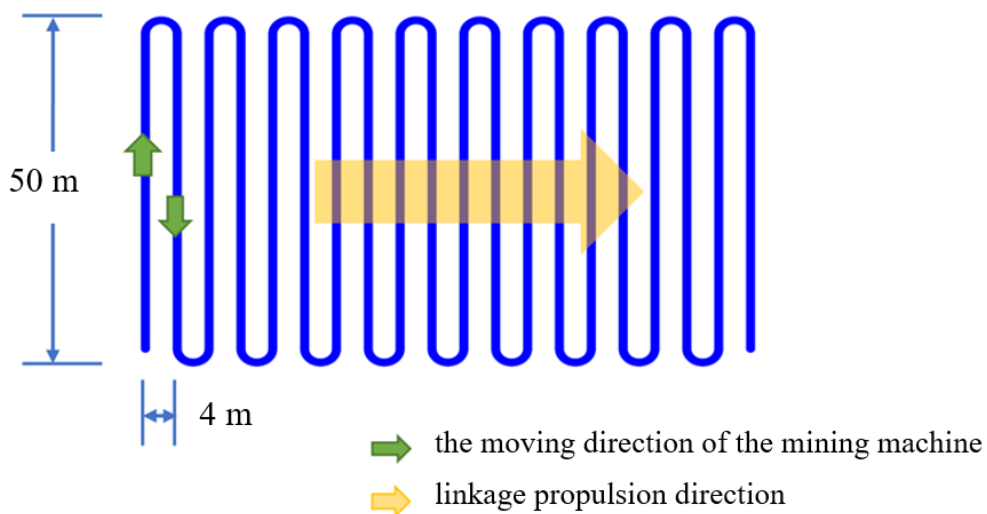
Figure 3-19 Path design of the collection test
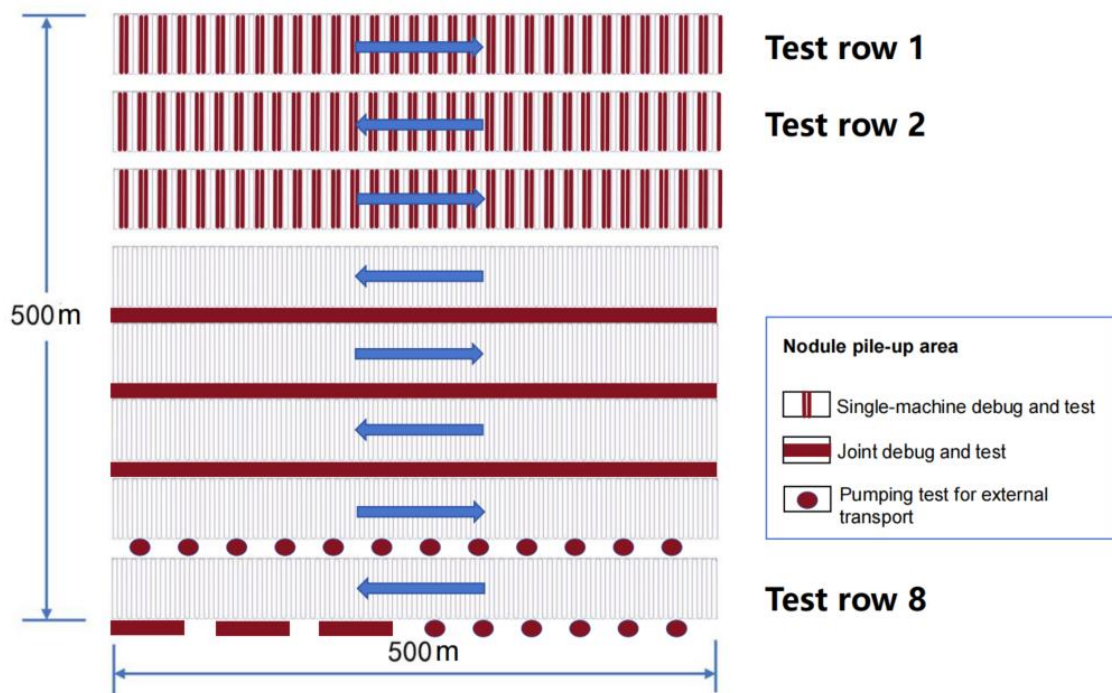
Figure 3-20 Test area and path plan

Trial test planning, risk control, time-saving and efficiency, and functional coverage are the key factors to be considered in the design of the test. In the design of test paths, a total of 8 test rows were planned (Figure 3-20). The test row is 50 m width, and the distance between each two test rows is 15 m. The specific tests are as follows:

The 1st row is used for miner equipment test;

The 2nd to 3rd rows are used for the miner unit extreme ore collection capacity test;

The 4th row is used for the commission test of the joint system;

The 5th to 6th row is used for joint system ore collection test;

The 7th row is used for ore pumping and transportation test through the prototype buffer station;

The 8th row is used for unscheduled testing arrangements.
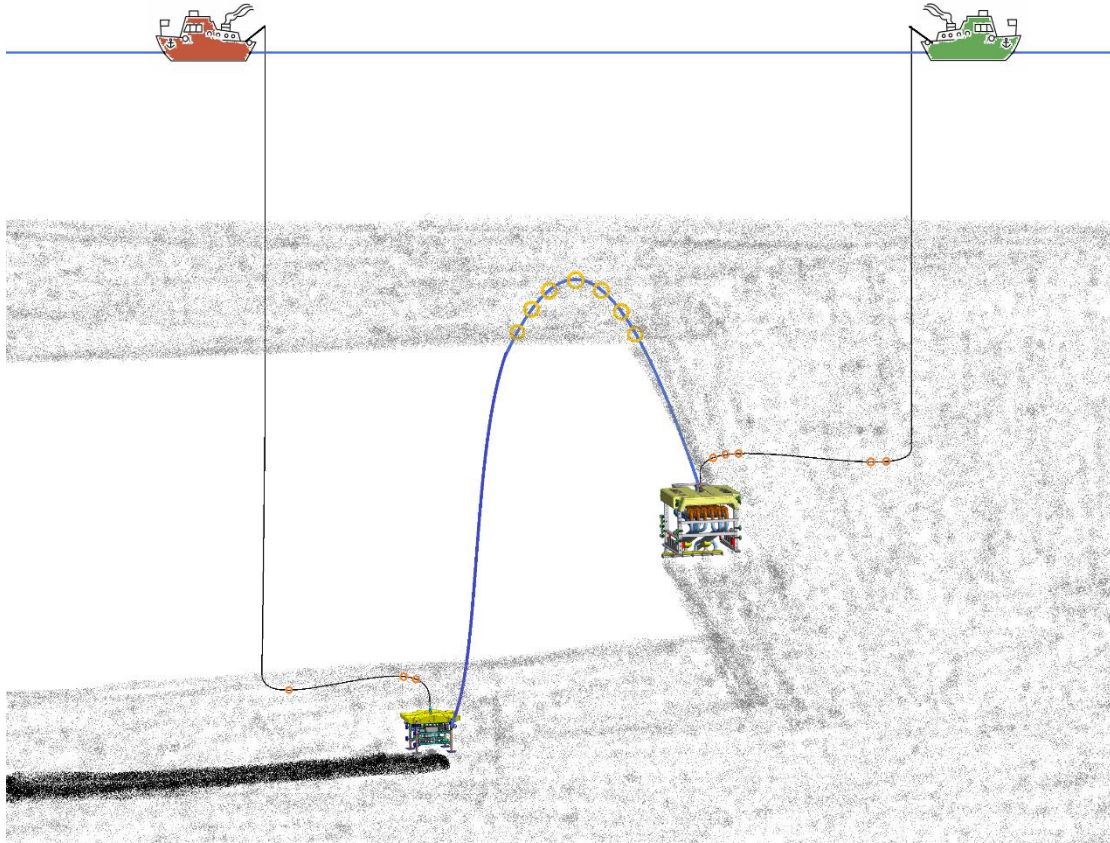
Figure 3-21 Front view of joint system test

3.4.2 Test Plan

3.4.2.1 Overall Schedule

The overall schedule is shown in Table 3-9.

The duration of the collection test in the exploration contract area is 20 days, which involves 100 hours of seabed ore collection test.

Table 3-9 The overall schedule of the test plan

Activities	Description	Aug 1st, 2024- Aug 1st, 2025	Aug 1st - Aug 10th	Aug 10th - Aug 15th	Aug 15th - Aug 17th	Aug 17th - Aug 19th	Aug 20th	Aug 21st	Aug 22nd - Aug 23rd	Aug 24th	Aug 25th	Aug 26th	Aug 27th	Aug 28th	Aug 29th	Aug 30th	Aug 30th - Sep 20th	2027	2028/2030/2032
Monitoring phase I-1	Baseline survey before trail test.	■																	
Transportation Manta I miner and prototype buffer station and sea trial personnel to test area	Transportation Manta I miner and prototype buffer station and staffs to test area.		■																
Monitoring phase I-2	Short-term subsurface buoy deployment, box-core, multi-core.			■															
Offshore inspection and test preparation	Arrive at test area, check if the ship dynamic positioning function is good, select the appropriate operation window period according to the weather forecast.				■														
	Da Yang Yi Hao deploys "Manta II" miner to carry out seabed inspection.					■													
	Da Yang Hao deploys prototype buffer station to carry out seabed inspection.					■													
	Recovery "Manta II" and prototype buffer station to the deck, then buffer station will carry with LBL and dive to seabed to deployment the LBL at planned location.						■												
	Da Yang Yi Hao cooperated LBL array for positioning calibration test.						■												
	Launch "Manta II" miner and prototype buffer station, test the positioning effect of LBL system.							■											
Monitoring phase I	Launch monitoring equipments during the test period.								■										
Deployment of ore collection testing system	Da Yang Hao deploys flexible pipe.									■									
	Da Yang Yi Hao deploys "Manta II" miner.									■									
	Miner unit collection test.									■									
	Da Yang Hao deploys the prototype buffer station.									■									
	Connect "Manta II" miner and flexible pipe. "Manta II" dives to the working area, then searching flexible pipe through acoustic positioning system and sonar detection system. Use pipe capture clamp on "Manta II" to grab the joint of flexible pipe, and connect flexible pipe to "Manta II" pipe connector.										■								
	Connect prototype buffer station and flexible pipe. The buffer station dives to the working area, then searching flexible pipe and "Manta II" miner through the acoustic positioning system and sonar detection system. Use pipe capture clamp on buffer station to grab the joint of flexible pipe.										■								
System testing	The prototype buffer station is dynamically positioned at a predetermined position, maintaining a horizontal position and keep a height of 5 meters from seabed.											■							
	Open the miner's nodule collection system in situ, test the functions of pumps, each executive components and sensors.											■							
	Operate miner performing ore collection at a speed of 0.15 m/s, in a distance of 50 m.												■						
	Turn miner around, operate miner performing ore collection at a speed of 0.25 m/s, in a distance of 50 m.													■					
	Keep the driving speed at 0.25 m/s, follow the 50m turning back path plan, continue the miner ore collection test.														■				
	Ore tranportation test for prototype buffer station.															■			
Monitoring phase I	The monitoring equipment was partially recovered during the test.															■			
Monitoring phase III-1	Using an AUV to perform optical and acoustic measurements in mining test areas and plume-affected areas. Investigations were carried out in three regions using equipment such as multi-tube and box samplers. Sampling of sediments etc.																■		
Monitoring phase III-2	Monitoring within 1 year after the test.																	■	
Monitoring phase III-3	Long-term monitoring in 3 / 5 / 7 years after the test.																		■

3.4.2.2 Test Work Plan Before Trial Test in the Area

The development of the "Manta II" ore collection test machine is carried out according to the relevant guidelines and standards of ocean engineering. The R & D team and partners of BPC have rich experience in the development of ultra-deepwater equipment. According to the standard procedure, testing systems will carry out a series of functional and performance testing work (Table 3-10).

Table 3-10 System functional test plan

Serial Number	Test Content	Date	Location	Duration	Purpose
1	Nodules transport test	Aug 1st, 2024	Shanghai China	5 days	Test the nodule conveyor function.
2	Main structure load capacity test	Sept 1st, 2024	Shanghai China	3 days	Test the strength of the main structure of "Manta II", and check if it meets the launch and recovery specification in sea state 4.
3	Launch and recovery system test	Oct 15th, 2024	Qingdao China	10 days	Umbilical cable, winch, A-frame and snubber test, strength test of cable carrier head.
4	Flexible pipe approval test	Nov 10th, 2024	Shanghai China	1 day	Quality inspection and approval test of flexible pipe.
5	Miner pool test	Nov 10th, 2024	Shanghai China	20 days	Test the basic function of the miner, including the functional test of sensors, actuators, software, and control system.
6	Pumping function laboratory test of prototype buffer station	Mar 1st, 2025	Shanghai China	20 days	Test the ore transportation capacity of the pumping device on the prototype buffer station per unit time.

3.4.2.3 Trial Test Plan in the Area

The shallow water test will be carried out before the trial test, which purpose is to expose the problems and defects of the system in advance of the trial test performed in the contract area in 2025. Focus on the problems found in the shallow water test, improvements will be made in early 2025 to ensure "Manta II" completes the sea trial test preparation in June 2025. The sea trial test will be carried out in July 2025.

The trial test in the contract area will be divided into the following test works:

1) Transportation of "Manta II" miner, prototype buffer station, and staffs to the CTA

2) Marine inspection and test preparation

3) Launch and deployment of flexible pipe

4) Launch and deployment of miner

5) Miner unit collection test

6) Launch and deployment of prototype buffer station

7) Connect miner and prototype buffer station with flexible pipe

8) System functional test and joint system motion performance test

9) Miner recovery

10) Prototype buffer station recovery

11) Flexible pipe recovery

12) Deployment of prototype buffer station after installing pumping device

13) Pumping functional test of prototype buffer station on the seabed

14) Prototype buffer station recovery

The engineering team of the BPC has designed a variety of test scenarios to ensure the working ability of the miner, prototype buffer station and underwater joint system is fully tested and verified.

3.4.2.4 Transportation of "Manta II", Prototype Buffer Station and staffs to the Test Area

The "Manta II" miner will be carried with "Da Yang Yi Hao" scientific research vessel from Qingdao, China, which will take about 8 days to arrive at the trial CTA. Technical staff of "Manta II" and trial test headquarters will be on board of "Da Yang Yi Hao" at the same time.

Prototype buffer station and flexible pipe will be carried with "Da Yang Hao" scientific research ship from Zhoushan, China, which will take about 7 days to arrive at the trial CTA. Technical staff of buffer station will be on board of "Da Yang Hao" scientific research vessel.

3.4.2.5 Offshore Inspection and Test Preparation

"Manta II" miner and prototype buffer station are both underwater floating submersibles, which are both special ROVs. Therefore, no extra ROV is prepared for the trial test. After arriving at the CTA, "Manta II" miner and prototype buffer station will both dive to the seabed

to carry out on-site inspections to ascertain the seabed conditions of the CTA. The work includes:

1) Arrive at CTA, check if the ship dynamic positioning function is good, select the appropriate operation window period according to the weather forecast.

2) "Da Yang Yi Hao" deploys "Manta II" miner to carry out seabed inspection.

3) "Da Yang Hao" deploys prototype buffer station to carry out seabed inspection.

4) Recovery "Manta II" and prototype buffer station to the deck, then buffer station will carry with LBL and dive to seabed to deployment the LBL at planned location.

5) "Da Yang Yi Hao" cooperated LBL array for positioning calibration test.

6) Launch "Manta II" miner and prototype buffer station, test the positioning effect of LBL system.

7) The entire offshore inspection and test preparation will be completed within 5 days.

3.4.3 Deployment of Nodule Collection Test System

1) "Da Yang Hao" deploys flexible pipe.

2) "Da Yang Yi Hao" deploys "Manta II" miner.

3) "Da Yang Hao" deploys prototype buffer station.

4) Connect "Manta II" miner and flexible pipe. "Manta II" dives to the working area, then searching flexible pipe through acoustic positioning system and sonar detection system. Use pipe capture clamp on "Manta II" to grab the joint of flexible pipe, and connect flexible pipe to "Manta II" pipe connector.

5) Connect prototype buffer station and flexible pipe. The buffer station dives to the working area, then searching flexible pipe and "Manta II" miner through the acoustic positioning system and sonar detection system. Use pipe capture clamp on buffer station to grab the joint of flexible pipe.

6) The deployment of test system is planned to be completed within 2 days.

3.4.4 Miner Unit Collection Test

When the miner deployment is completed, the miner unit collection test will be started.

1) Open the miner's nodule collection system in situ, test the functions of pumps, each executive components and sensors.

2) Operate miner performing ore collection at a speed of 0.15 m/s, in a distance of 50 m.

3) Turn miner around, operate miner performing ore collection at a speed of 0.25 m/s, in a distance of 50 m.

4) In the ore collection test, adjust the control parameters to keep the current ore collection path adjacent to the last ore collection path, but the overlapping area should be as small as possible.

5) Keep the driving speed at 0.25 m/s, follow the 50m turning back path plan, continue the miner ore collection test.

3.4.5 System Function and Joint System Performance Test

1) The prototype buffer station is dynamically positioned at a predetermined position, maintaining a horizontal position and keeping a height of 5 meters from seabed.

2) Miner, prototype buffer station and flexible pipe are joint together, test the joint system at a moving speed of 0.15 m/s, at a distance of 50 m.

3) Turn back the miner, and test the joint system at a moving speed of 0.25 m/s.

3.4.6 Prototype Buffer Station Test

The prototype buffer station is equipped with pumping device to test the ore transport function per unit time.

3.5 Other Supporting Equipment

3.5.1 Vessel

（1）Collection mechanism surface support vessel

In this test, the surface support vessel for collection mechanism is "Da Yang Yi Hao" (Figure 3-22). The total tonnage of the vessel is 4412 tons, the designed displacement is 5600 tons, the ship's endurance is 15000 nautical miles, the self-sustainability is 60 days and nights, and the designed economic speed is 12 knots, with stable dynamic positioning capability (DP1). There are eight laboratories, including Multi-beam and Shallow Profiling Laboratory,

Gravity and ADCP Laboratory, Deep Towing and Underwater Positioning Laboratory (ROV-AUV Laboratory), Seismic Laboratory, Hydrological Laboratory, Network Laboratory, Physical Oceanography Laboratory, X-ray Fluorescence Analysis Laboratory. There are one sample room and one Data & Information Center. The total area of laboratories is 340 square meters. The parameters and specifications of the vessel are shown in Table 3-11.

Figure 3-22 "Da Yang Yi Hao" vessel

Table 3-11 Main parameters of "Da Yang Yi Hao" vessel

Serial Number	Name	Data
1	Builder/Year	Russia/84.2
2	Call sign/Port of registry	BNTM/Qingdao
3	Ship radio identification code	412923000
4	Total tons/Net tons	4412/1323
5	Displacement	5600 tons
6	IMO No.	8226961
7	Nationality Certificate No.	050003000001
8	Total length/Height	104.50/35.0M
9	Width/Depth	16.00/7.40M
10	Endurance	15000 nautical miles
11	Draught/Speed	5.86M/14.5 knots
12	Design of economic speed	12 knots
13	Requirement of a minimum safe water depth when approaching and departing the port	8.8m
14	The length of the left and right anchor chain	Left, right 275M
15	Fuel reserves	1100.00 tons
16	Freshwater reserves	500.00 tons
17	Authorized Occupants / Crews	75 personnel /30 personnel
18	Lifeboat/（number）	44 crews/boat（2）
19	Life raft/（number）	20 crews/raft（2）
20	endurance / self-sustaining / wind resistance	15000 n miles/60 days/level 12
21	propeller/（number）	Variable pitch propeller/（1）
22	Approval / Registration navigation area	A1+A2+A3/Unlimited navigation area
23	Main engine model/unit / Power / Speed	6PC2-6L/2/2970kW/(500r/min)
24	Generator/unit / Power / Voltage	3units/400kW/400V
25	Prime motor model/unit / Power	VOLVO D16 MG/3units/450kW
26	Shaft generator / Power / Voltage	2/1800kW/400
27	Main navigation device	GPS、Radar, compass, dynamic positioning

（2）Buffer station surface support vessel

The "Da Yang Hao" is a modernized oceanic comprehensive resource survey vessel that integrates multidisciplinary, multifunctional and multitechnological means to meet the needs of oceanic multi-resource and environmental surveys, as well as research in deep-sea related fields (Figure 3-23). The main technical parameters are shown in Table 3-12. During this test period, it was used as a prototype buffer station surface support vessel, as well as environmental monitoring.

Figure 3-23 "Da Yang Hao" vessel

Table 3-12 "Da Yang Hao" vessel principal technical parameters

Total length	98 m
Width	17 m
Design of draught	5.4 m
Design of displacement	4780 tons
Personnel	60 personnel (including 22crew members)
Endurance	14000 nautical miles/12kn
Self-sustainability	60 days
Maximum speed	16 kn
Propulsion mode	All-electric propulsion
Noise standard	Reference DNV Silent-R
Total area of the laboratory	More than 360m^2
Working area of the rear deck	More than 400m^2
Classification symbols	CSA SPS/Research Ship, PSPC, Ice Class B3, COMF (NOISE) 3, COMF (VIB) 3 CSM AUT-0, OMBO, DP-1, Loading Computer (I, D), Lifting Appliance, Clean, FTP, BWMP, BWMS, GPR

"Da Yang Hao" on board survey equipment is shown in Table 3-13。

Table 3-13 "Da Yang Hao" main survey equipment

Equipment Name	Model
Multi-beam system	Kongsberg EM124
Medium-shallow water multi-beam	Kongsberg EM712
Sub bottom Profiler	PARASOUND P70
Single beam system	EA640（12/38/200 kHz）
Multi-frequency sonar	EK80（18/38/70/120/200/333 kHz）
Ultra-short baseline system	IXSEA Posidonia II
Rowing ADCP	TRDI, OS38/OS150 kHz

Onboard operation support equipment and the main technical parameters of "Da Yang Hao" are shown in Table 3-14。

Table 3-14 "Da Yang Hao" on board operation support equipment and main technical parameters

Equipment Name	Model	Technical Parameters
The stern A-frame	Triplex TR-SAF-170	Static load 25T， dynamic load 12T Dynamic amplification system 1.8， net height 8.5 m Internal static width 5.5 m
Main crane	Palfinger PFM4500E	20T@ 12.5 m,10T@20 m
Launch and recovery system for survey operation on stern starboard (port) side	Palfinger PF150002ME	4T@16 m
Launch and recovery system for CTD special on midship starboard side	Triplex-16986	3T
Launch and recovery system for geological special on midship starboard side	Triplex TR-SCTB	25T@1.5 m, 10T@3.5 m
CTD sampling system	10000/6000 m	RAPP RWLEV-2320EBS
Geological sampling system	8000 m	RAPP RW2300E-GEO
Visual sampling system	coaxial 8000 m	RAPP RW2300E-EM
Towing detection control system	8400 m	RAPP RW2300E-EOM

4 PHYSICAL AND CHEMICAL ENVIRONMENT

4.1 Overview of the Environmental Baseline Survey in Block M of the BPC Contract Area

4.1.1 Baseline Survey Cruises in the Block M

BPC has carried out four cruises for resource exploration and environmental investigation in the contract area M1 and M2 blocks (referred to as Block M) since 2021, namely BPC Cruise 1 (i.e., DY69 Cruise), BPC Cruise 2 (i.e., DY75 Cruise), BPC Cruise 3 (i.e., DY76 Cruise) and BPC Cruise 4 (i.e., DY81 Cruise) (see Table 4-1 for details). In addition, on board the China Ocean Mineral Resources Research and Development Association (COMRA) cruise for exploration of cobalt-rich crusts (DY61 & DY66 Cruise), environmental survey was also carried out in Block M2 and the adjacent area. Results of the environmental survey from these cruises are also included in the present report. Specific survey items are shown in Table 4-2 and Figure 4-1.

Table 4-1 Information on exploration cruises carried out by BPC

Cruise number	Time	Investigation days
Cruise 1	October – November, 2021	34 days
Cruise 2	August – December, 2022	112 days
Cruise 3	November – December, 2022	18 days
Cruise 4	August – November, 2023	80 days

The number of survey projects and stations currently carried out in the area include 34 CTD stations, 8 Lander stations, 19 plankton vertical tow net stations, 18 Multinet stations, 31 multicorer stations, 16 survey lines totaling more than 1,000 km of deep-towed camera system surveys, 10 subsurface buoys, and 158 box-corer stations with shared resources and environment. The environmental baseline survey work in the contract area is mainly focused on the northwestern part of Block M2 and the southeastern part of Block M1.

Table 4-2 Environmental Baseline Survey Items

Methods	Historical position		2021 Station (DY66 & DY69)		2022 Station (DY75 & DY76)		2023 Station (DY81)		Total
	M1	M2	M1	M2	M1	M2	M1	M2	
CTD	0	1	3	10	3	11	2	4	34
Lander	0	0	1	1	1	2	1	2	8
Plankton vertical tow net	0	0	2	5	2	5	1	4	19
Multi-net	0	0	2	5	1	3	2	5	18
Multicorer	0	3	0	2	6	8	2	10	31
Deep-towed camera system	0	0	0	3	0	7	2	4	16
Subsurface buoy	0	1	1	3	1	2	1	1	10
Box-corer	8	15	3	20	20	78	4	10	158
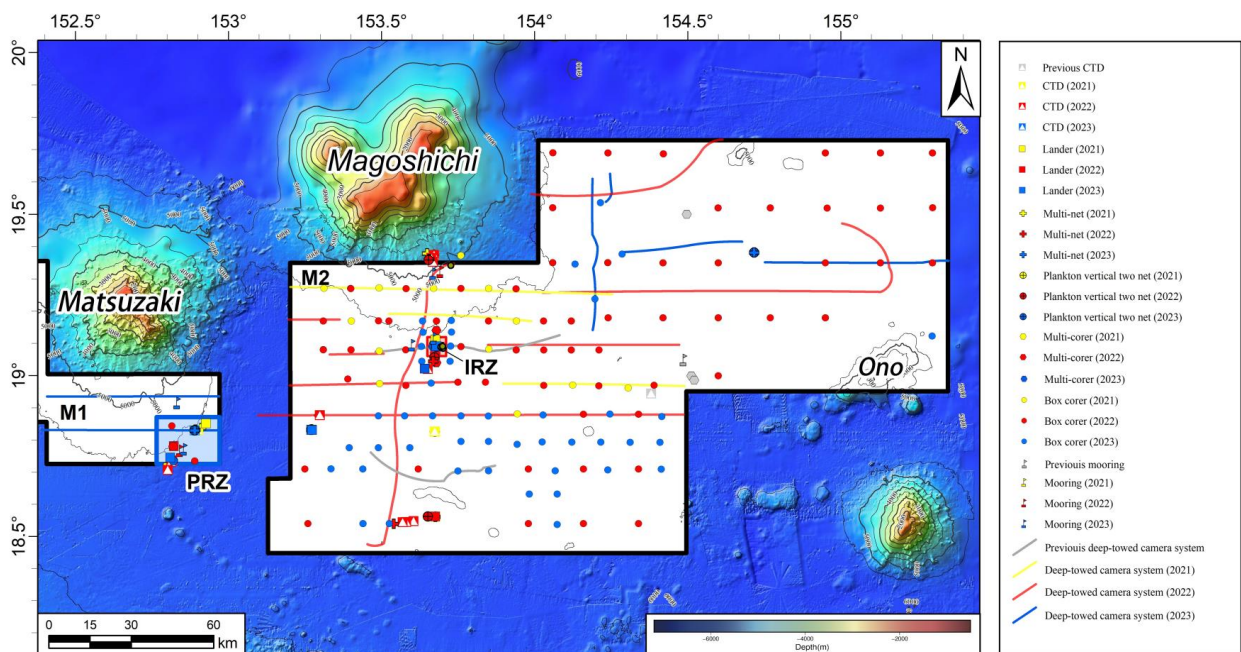
Figure 4-1 Sampling stations and survey lines for Environmental Baseline Survey

4.1.2 Laboratory analysis

Under the environmental guidelines issued by the ISA (ISBA/25/LTC/6/Rev.3), the contractor is required to carry out a systematic environmental baseline survey to collect a total of approximately 93 environmental parameters in different areas, including physical oceanography, chemical oceanography, sediment characteristics, geological properties and

biological communities. Upon comparison (Table 4-3), BPC has collected 73 environmental parameters in the contract area, representing 78% of all parameters.

20 environmental baseline parameters have not yet been collected, 1 is under analysis, 5 have been scheduled to be collected on the 2024 cruise and 8 on the 2025 cruise before the test; 6 parameters related to mining technology tests will be conducted in conjunction with the current proposed mining test.

Table 4-3 Comparison of Environmental Baseline Data and Environmental Guidelines Requirements for the BPC's contract area

Environmental baseline parameters	Acquired	Quantity type (S: Spatial variation; D: Depth profiles; (T: Temporal variation)	note
Physical Oceanography			
Pressure	√	SDT	
Temperature	√	SDT	
Salinity	√	SDT	
Turbulence-Turbidity	√	T	
Currents	√	SDT	
Tides and waves	√	ST	
Optical properties	N.A.	/	Planned for 2025
Background noise (from the sea surface to the seabed)	√	ST	
Concentration of SPM in water	√	SDT	
Sea surface large-scale phenomena	√	TS	Mesoscale eddy
Oceanographic three-dimensional hydrodynamic model	√	TS	Plume model
Satellite data (SST)	√	TS	
Satellite data (Productivity)	√	TS	
Chemical Oceanography			
Heavy metal	√	D	
Trace element	N.A.	/	Planned for 2024
Determine what additional chemicals may be released from the discharged plume during test mining	N.A.	/	Parameters related to the mining test, to be monitored during the test.
DO	√	SDT	
pH	√	SDT	
Total alkalinity	√	SDT	
Suspended Solid	√	SDT	
Nitrate	√	SDT	

Environmental baseline parameters	Acquired	Quantity type (S: Spatial variation; D: Depth profiles; (T: Temporal variation)	note
Nitrite	√	SDT	
Phosphates	√	SDT	
Silicate	√	SDT	
Ammonium	√	SDT	
Vertical profile:			
Total organic carbon	N.A..	/	Planned for 2024
Chlorophyll *a*	√	SDT	
Phosphates	√	SDT	
Nitrate	√	SDT	
Nitrite	√	SDT	
Silicate	√	SDT	
Salinity	√	SDT	
DO	√	SDT	
Particulate and dissolved matter	√	SD	
Total alkalinity/carbonate system	√	SD	
Sediment Characteristics			
Specific gravity	√	SD	
Bulk density	√	SD	
Shear strength	√	SD	
Grain size	√	SD	
Sediment depth of change from oxic to suboxic	N.A.	/	Planned for 2025
Organic carbon	√	SD	
Inorganic carbon	N.A.	/	Planned for 2025
Nutrient:			
Phosphates	√	SD	
Nitrate	√	SD	
Nitrite	√	SD	
Ammonium	√	SD	
Silicate	√	SD	
Carbonate (alkalinity)	N.A.	/	Planned for 2025
Redox systems in pore water	N.A.	/	Planned for 2025
Geochemistry of pore water sediments down to 20 cm	√	SD	
Geological Feature			
Produce Geographic Information System regional maps with high-resolution bathymetry and sea floor bottom type showing major geological and geomorphological features to reflect the heterogeneity of the environment.	√	S	

Environmental baseline parameters	Acquired	Quantity type (S: Spatial variation; D: Depth profiles; (T: Temporal variation)	note
These maps should be produced at a scale appropriate to the resource and habitat variability			
Collect information on the heavy metals and trace elements that may be released during test mining and their concentrations.	N.A.	/	Parameters related to the mining test, to be monitored during the test.
Biological Community			
Record sightings of marine mammals, other near-surface large animals (such as turtles and fish schools) and bird aggregations	√	ST	
Establishment of at least one station to evaluate temporal changes; at least one monitoring station within each habitat type or region, as appropriate, to evaluate temporal changes in the water column and benthic communities.	√	T	Stations ES03 and ES06 are long-term stations with 2 years of observations completed
Assessment of the regional distribution of species	√	S	
Genetic connectivity of key representative species	N.A.	/	Planned for 2025
Gather time series data on the sinking flux and composition of materials (including particulate organic matter) from the upper water column to the seabed	√	SDT	
Habitat GIS maps	N.A.	S	Under analysis
Megafauna			
Abundance	√	S	
Biodiversity	√	S	
Trophic level	N.A.	/	Planned for 2025
Biomass	√	S	
Macrofauna (>250 μm)			
Abundance	√	SDT	
Vertical distribution	√	SDT	
Biodiversity	√	SDT	
Community structure	√	SDT	
Biomass	√	SDT	

Environmental baseline parameters	Acquired	Quantity type (S: Spatial variation; D: Depth profiles; (T: Temporal variation)	note
Meiofauna (>32 μm)			
Abundance	√	SDT	
vertical distribution	√	SDT	
Biodiversity	√	SDT	
community structure	√	SDT	
biomass	√	SDT	
Microbiota			
Microbial metabolic activity	N.A.	/	Planned for 2025
Microeukaryotes (especially foraminifera)	√	SD	
Nodule fauna			
Abundance	√	/	Occurrence is fortuitous and it is difficult to count abundance.
Community structure	√	S	
Assessment of pelagic biological communities			
Phytoplankton composition	√	SDT	
Phytoplankton biomass	√	SDT	
Phytoplankton productivity	√	SDT	
Community composition	√	SDT	
Zooplankton abundance	√	SDT	
Nekton	√	SD	acoustical survey
Vertical migration	√	SDT	
Bacterioplankton	√	SD	
Bacterial biomass	N.A.	/	Planned for 2024
Bacterial productivity	N.A.	/	Planned for 2024
Ecosystem function—Food web	N.A.	/	Planned for 2024
Ecotoxicology - Trace metals found in dominant species. (Trace metals and potentially toxic elements in muscle and target organs of demersal fish and invertebrate species)	N.A.	/	Parameters related to the mining test, to be monitored during the test.
Bioturbation	√	D	
Fluxes to the sediment			
Flux of material from the upper water column into the deep sea	√	SDT	
Data Collection during Test Mining			
Dose effects of sediment-covered benthic organisms	N.A.	/	Parameters related to Test Mining, to

Environmental baseline parameters	Acquired	Quantity type (S: Spatial variation; D: Depth profiles; (T: Temporal variation)	note
Chronic disturbance test	N.A.	/	be collected during the test Parameters related to Test Mining, to be collected during the test
Ecosystem resilience	N.A.	/	Parameters related to Test Mining, which need to be Carried out during the test

4.2 Characterization of the Regional Physicochemical Environment

The regional physicochemical environmental characteristics are primarily based on published papers and materials.

4.2.1 Regional Geological Features

The Beijing pioneer polymetallic nodule contract area is located in the North−West Pacific Basin (Figure 4-2). The Northwest Pacific basin is characterized by the development of seamount chains, including the Magellan Seamount Chain, the Wake–Marcus Seamount Chain, the Caroline Seamount Complex, the Marshall Seamount Chain, etc., which divide the Northwest Pacific basin into numerous sub-basins and intermontane basins. The Marcus–Wake Seamount Chain is located north of the Pigafetta Basin, to the north of the Magellan Seamount Chain, and west of the Central Pacific Seamount Group, which is an intermittent submarine volcanic chain formed by the intraplate volcanic hotspot, with only Minamitorishima Island exposed to the sea surface. The Marcus–Wake Seamount Chain spreads in the NW direction with an extension of nearly 1,200 km. The depths of the intermountain basin of the Marcus–Wake Seamount Chain range from 5,000 to 6,500 m. The Magellan Seamount Chain is located in the northeast of the Eastern Marianas Basin. The

Magellan Seamount Chain is located in the northeastern edge of the East Marianas Basin and belongs to the intermittent extension of the submarine volcanic chain formed by the volcanic hotspot within the plate. The seamount chain extends in the direction of NNW, with a prolongation of nearly 1,200 km, and is mainly composed of relatively independent flat-topped seamounts, and the water depth of the neighboring deep-sea basins is 5,000–6,500 m.
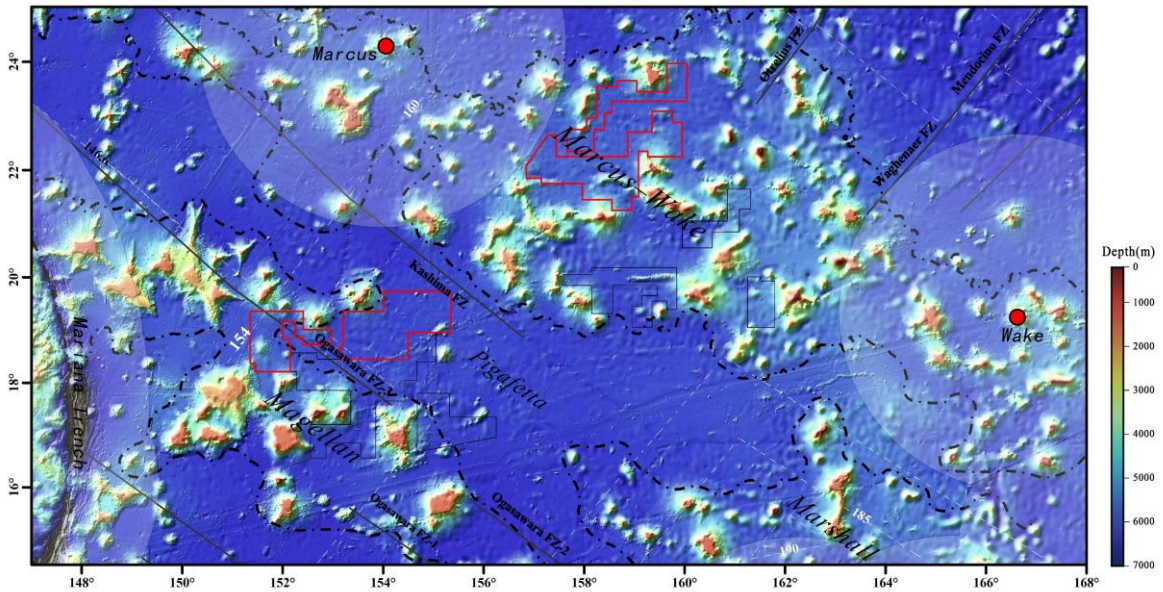
Figure 4-2 Geologic Map of the Northwest Pacific basin

The BPC contract area consists of four blocks, two in Block M (M1, M2) and two in Block C (C1, C2). Blocks M and C are located in the inter-mountain basins of the Magellan Seamount Chain and the Marcus–Wake Seamount Chain, respectively. The basement rocks of the Seamounts in the Magellan Seamounts Chain are mainly basalts, with some seamount tops also exhibiting volcanic breccia, limestone, and phosphorite (Zhu, 2002). The basement rocks of the Marcus–Wake Seamounts Chain are mainly Early Cretaceous basalt and alkaline olivine basalt. The thickness of seamount sediment is notably lower than that of the Magellan Seamounts Chain, with some seamounts of the Marcus–Wake Seamounts Chain even lacking sediment layers, particularly lacking shallow marine carbonate sediment (Winterer et al., 1993). Controlled by regional geological structures, surface sediments in the Northwest Pacific basin mainly comprise deep-sea clay (pelagic/semi-pelagic clay), calcareous ooze, and siliceous ooze (Figure 4-3). Deep-sea clay is distributed within deep-sea basins, calcareous ooze is found on the summits of seamounts, and siliceous ooze is sporadically

distributed around calcareous ooze. The sedimentation rate of the BPC contract area is between 1–5 mm/kyr.
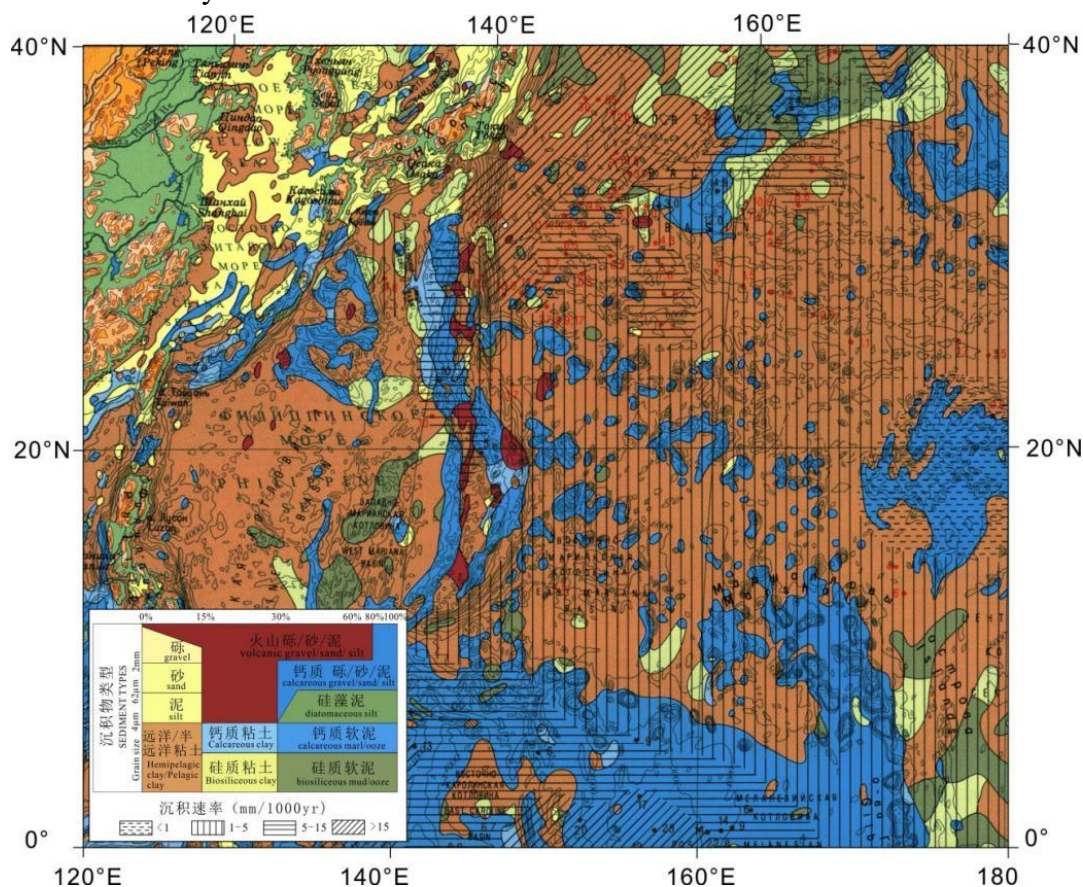
Figure 4-3 Distribution of seafloor surface sediment types in the Northwest Pacific

(Source： International Geological-Geophysical Atlas of the Pacific Ocean, 2003)

4.2.2 Regional Physical Oceanographic Features

The BPC polymetallic nodule contract area is situated in the subtropical waters of the Northwest Pacific Ocean, in the control zone of the North Equatorial Current (NEC) and the North Equatorial Counter Current (NECC). The upper layer ocean dynamics in this region are predominantly influenced by these two currents (Figure 4-4). Conversely, the deep layer circulation is primarily impacted by the thermohaline circulation, with the Antarctic bottom water flowing from south to north in this region (Figure 4-5). According to the theory of ventilated subduction of water masses, water masses located at different depths are generated at mid- and high-latitude sources and converge through the action of ocean currents, resulting

in a very complex structure of water masses in the area. This includes the North Pacific tropical water, the North Pacific Intermediate Water and subtropical mode water, among others. (Figure 4-6).
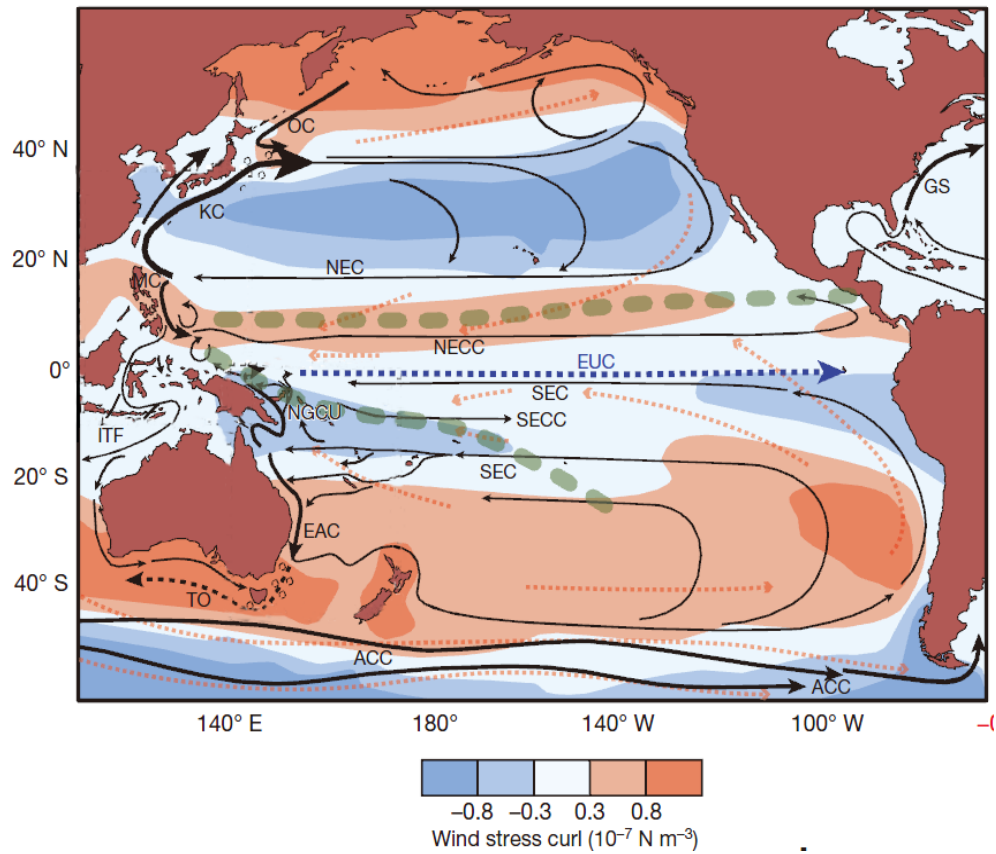
Figure 4-4 Schematic of Major current in the Pacific Ocean (Hu et al. 2015)
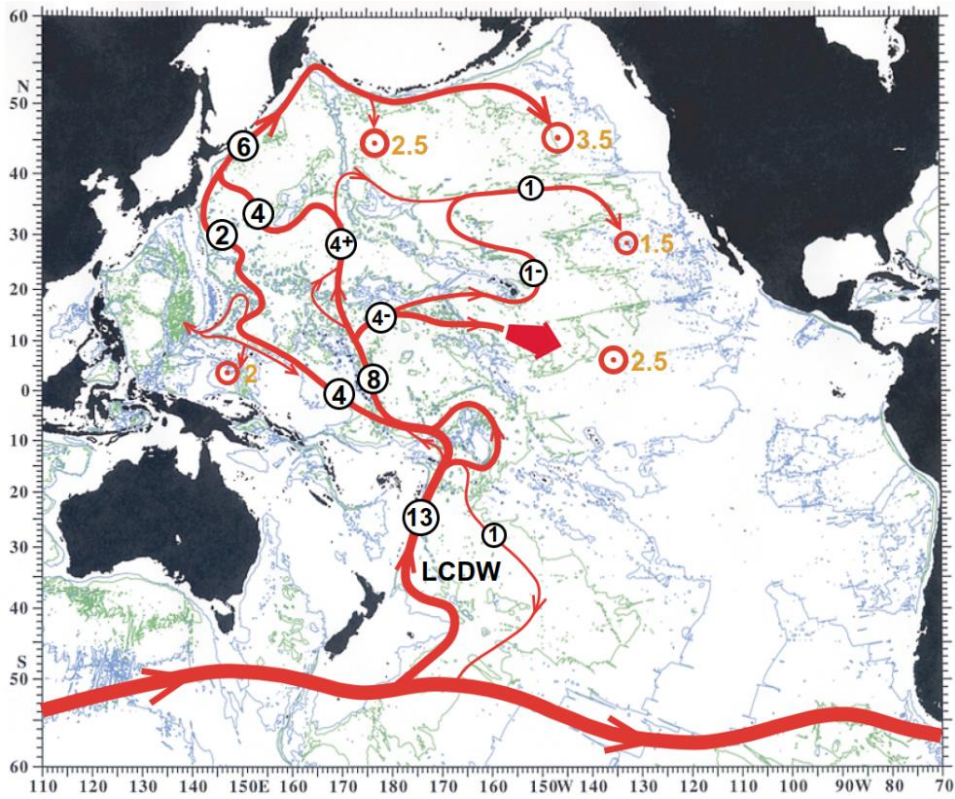
Figure 4-5 Schematics of the deep circulation in the lower deep layer in the western Pacific (Kato & Kawabe, 2010)
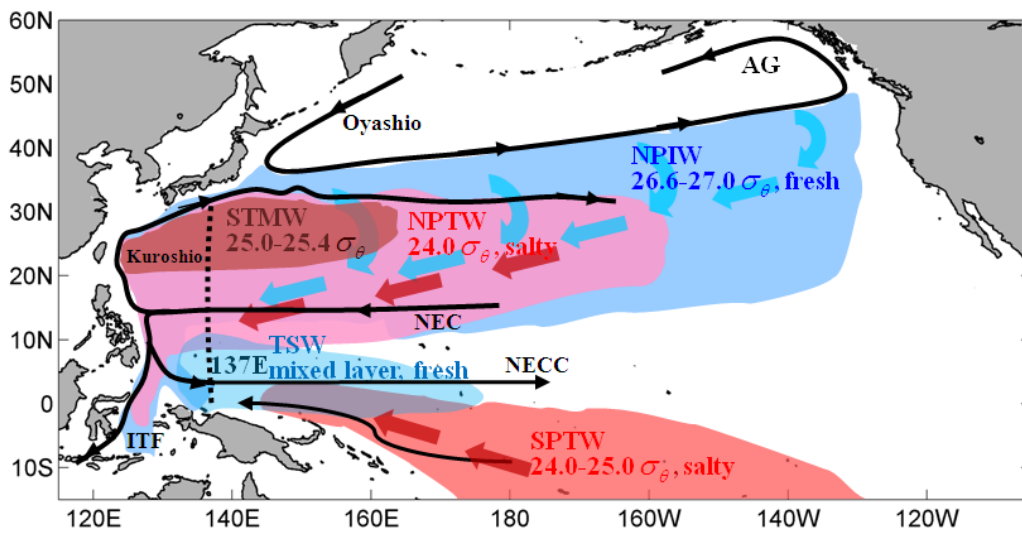
Figure 4-6 Schematic distribution of water masses in the western Pacific Ocean (Ma, 2015)

4.2.3 Regional Chemical Characteristics

The contract area is located in the subtropical waters of the western Pacific Ocean. In terms of oceanic biogeochemical environmental zoning, this region falls within the North Pacific Subtropical Gyre (NPSG) (Wu et al., 2007). The NPSG is surrounded by the Kuroshio, North Pacific Warm Current, California Current, and North Equatorial Warm Current, with anticyclonic circulation encircling its perimeter. This configuration isolates the upper water column of the NPSG from surrounding waters, creating a relatively autonomous ecosystem. A permanent, thick thermohaline is a major feature of the water column in this area, effectively separating nutrient-rich deep waters from the euphotic zone. Additionally, the presence of anticyclonic circulation leads to subsidence at its periphery, further impeding upward nutrient transport and resulting in extremely low nutrient concentrations in the euphotic zone of this region. Spatial distributions of temperature, salinity, dissolved oxygen, and dissolved oxygen saturation in the surface waters of the Northwest Pacific are illustrated in Figure 4-7 (WOA, 2023). Deep waters in the NPSG region primarily originate from the Antarctic Circumpolar Current, characterized by low temperature, high salinity, nutrient richness, and high dissolved oxygen (Figure 4-8).
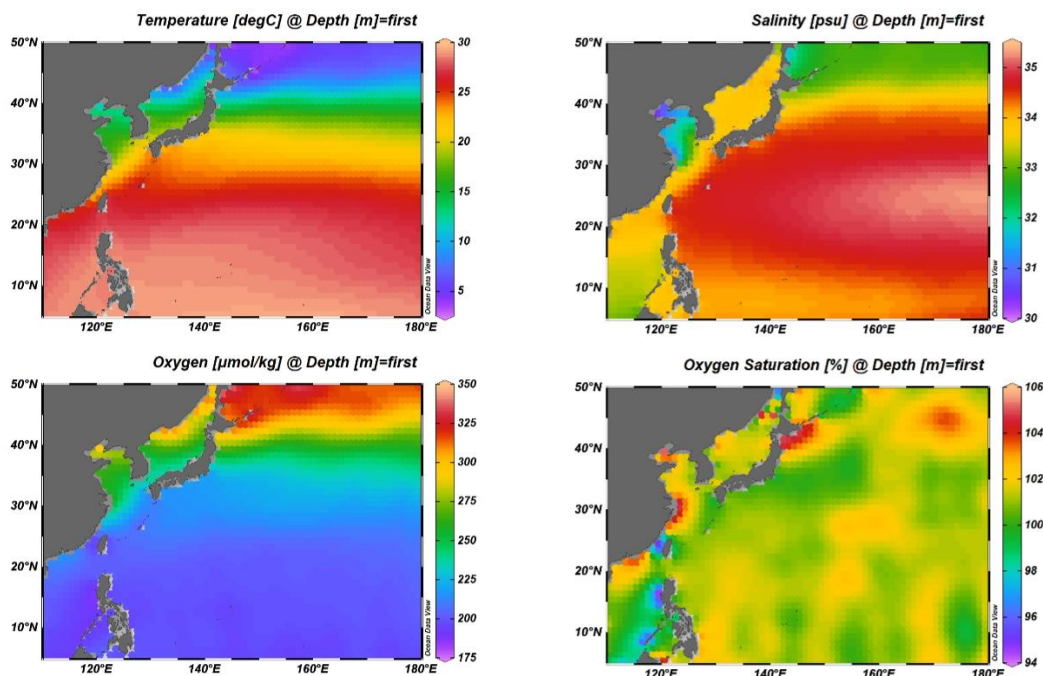
Figure 4-7 Spatial distribution of temperature, salinity, dissolved oxygen and dissolved oxygen saturation in the surface water of the Northwest Pacific (data source: WOA 2023)
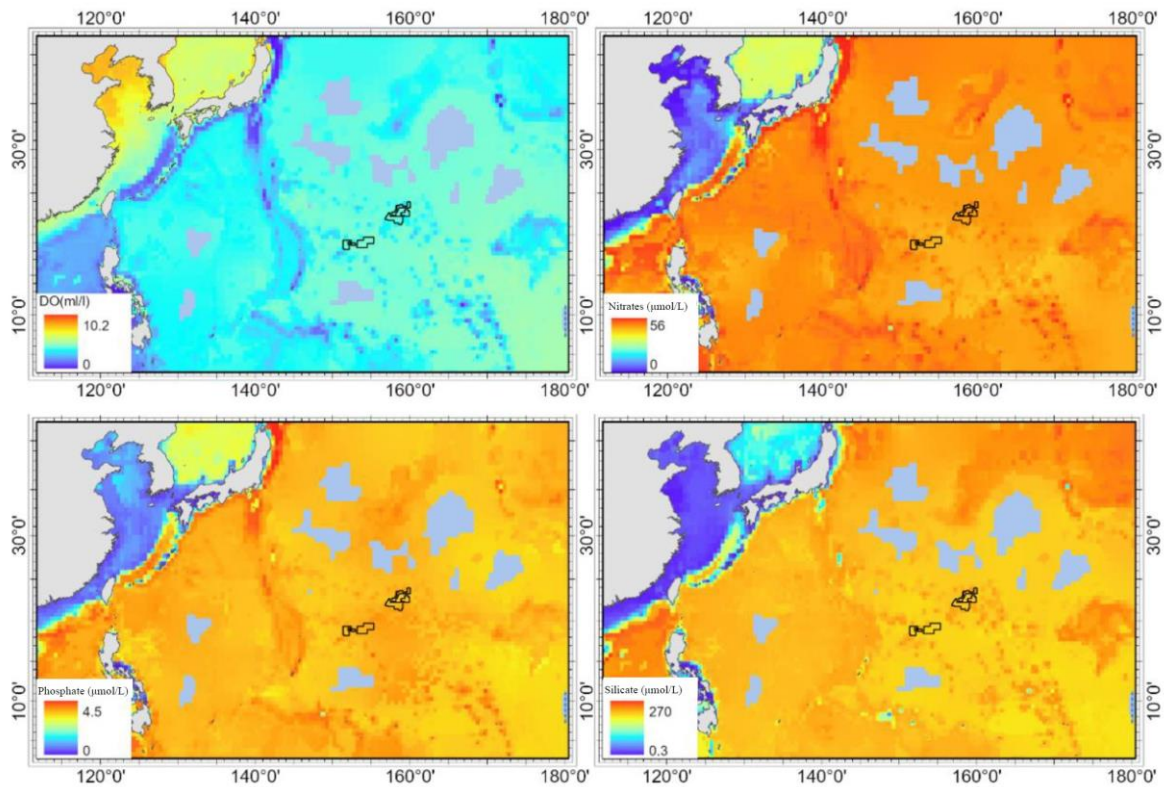
Figure 4-8 Spatial distribution of dissolved oxygen, nitrate, phosphate, and silicate in the bottom waters of the Northwest Pacific (Data source: GEMD)

The vertical distribution characteristics of seawater chemical components across the Block M2 at 155°E transect in the contract area are shown in Figure 4-9. The vertical distribution of seawater pH in this area is shown in Figure 4-9f. The pH of the surface water exceeds 8.10, primarily due to biological photosynthesis utilizing CO_2 from water, resulting in pH elevation. With increasing depth, pH decreases, reaching a minimum of about 7.4 at approximately 1000 m depth. The decrease in pH is mainly attributed to the oxidation and decomposition of organic debris, which increases CO_2 levels in the water, thus causing pH to reach its minimum. Below this minimum layer, the pH value increases slightly and remains at about 7.50 to 7.60.

The vertical distribution of dissolved oxygen in seawater in this region is illustrated in Figure 4-9g. The maximum dissolved oxygen concentration exceeds 210 μmol/kg in surface waters, with a minimum appearing around 1000 m depth. This minimum is due to the oxidation and decomposition of organic matter and the respiration of marine organisms, causing dissolved oxygen levels to decrease with increasing depth. Below the minimum layer,

DO content gradually increases. In the deeper layers, characterized by the presence of Lower Circumpolar Water replenished by oxygen-rich water sinking from high latitudes, temperatures are low, and dissolved oxygen and salinity levels are high.
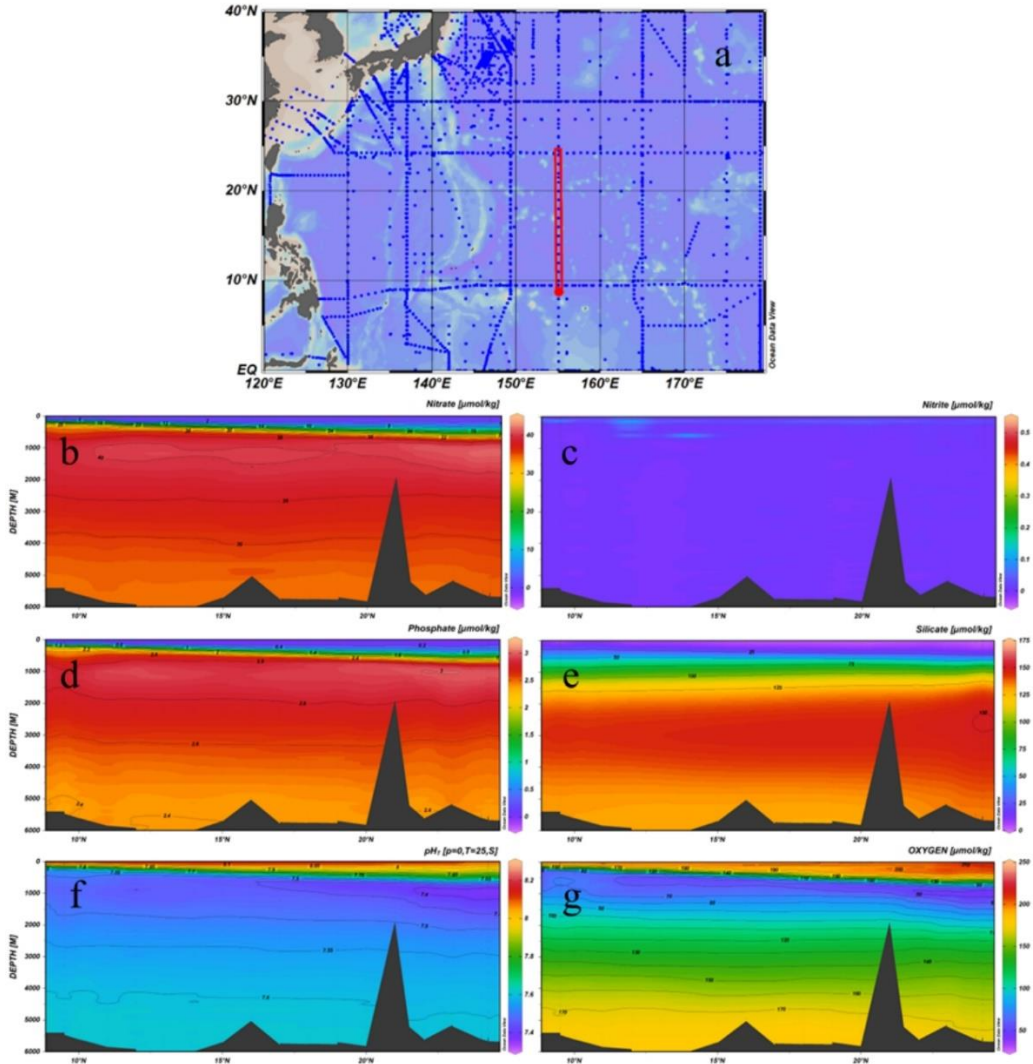
Figure 4-9 the vertical distribution characteristics of seawater chemical constituent along the 155 °E transect in the Northwest Pacific Ocean. (Data source: CCHDO)

The seasonal variation characteristics of nitrate within the mixed layer of the NPSG region are shown in Figure 4-10. Research by Yang et al. (2018) indicates minimal vertical variations in nitrate concentration within the mixed layer of the subtropical ocean where the contract area is located, suggesting unobvious seasonal changes in nitrate concentration within this region's mixed layer.
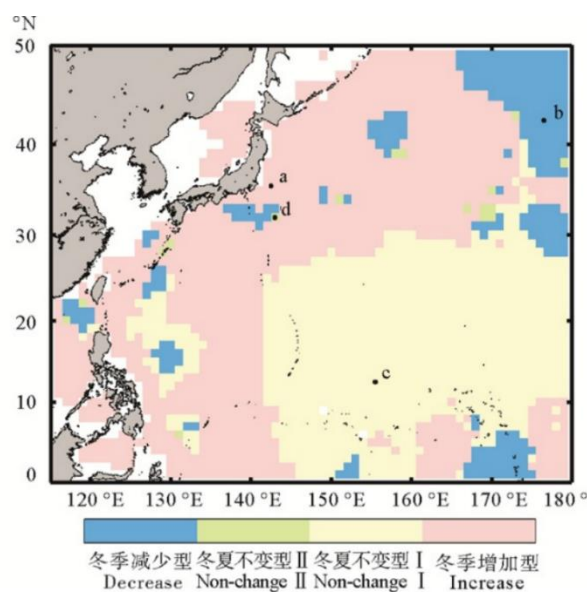
Figure 4-10 Types of seasonal variations of nitrate within the mixed layer of the NPSG region (Yang et al., 2018)

4.3 Characterization of the Physicochemical Environment of Block M

4.3.1 Meteorological Feature

Meteorological data of Block M were obtained through the XZC6 ship automatic meteorological measurement system during the survey of the BPC Cruise 2 (DY75) in 2022, and the meteorological and sea state characteristics within Block M were analyzed.

4.3.1.1 Meteorology

Block M is characterized by a subtropical monsoon climate, predominantly influenced by the subtropical ridge and the equatorial convergence zone, with prevailing easterly winds. From August to December, the sea surface wind direction over Block M is primarily easterly (Figure 4-11).

From late August to early October, the main weather systems affecting Block M include tropical cyclones, the subtropical high, and cold air masses. There are relatively few instances of severe weather events; although tropical cyclones may occasionally form in the southwestern part, their tracks are generally far from the surveyed area, resulting in minimal

impact. Sea conditions are generally favorable. The diurnal temperature range and its variation are relatively stable, remaining between 28 to 31°C. Atmospheric pressure values primarily fluctuate between 1005 and 1017 hPa. The average humidity is 78.91%.

From late October to mid-December, the principal weather systems influencing the area are temperate cyclones and cold air masses. The diurnal temperature range and its variation are minimal, generally maintaining between 27 to 30°C. Atmospheric pressure values are mainly within the range of 1010 to 1016 hPa. The average humidity is 77.2%.
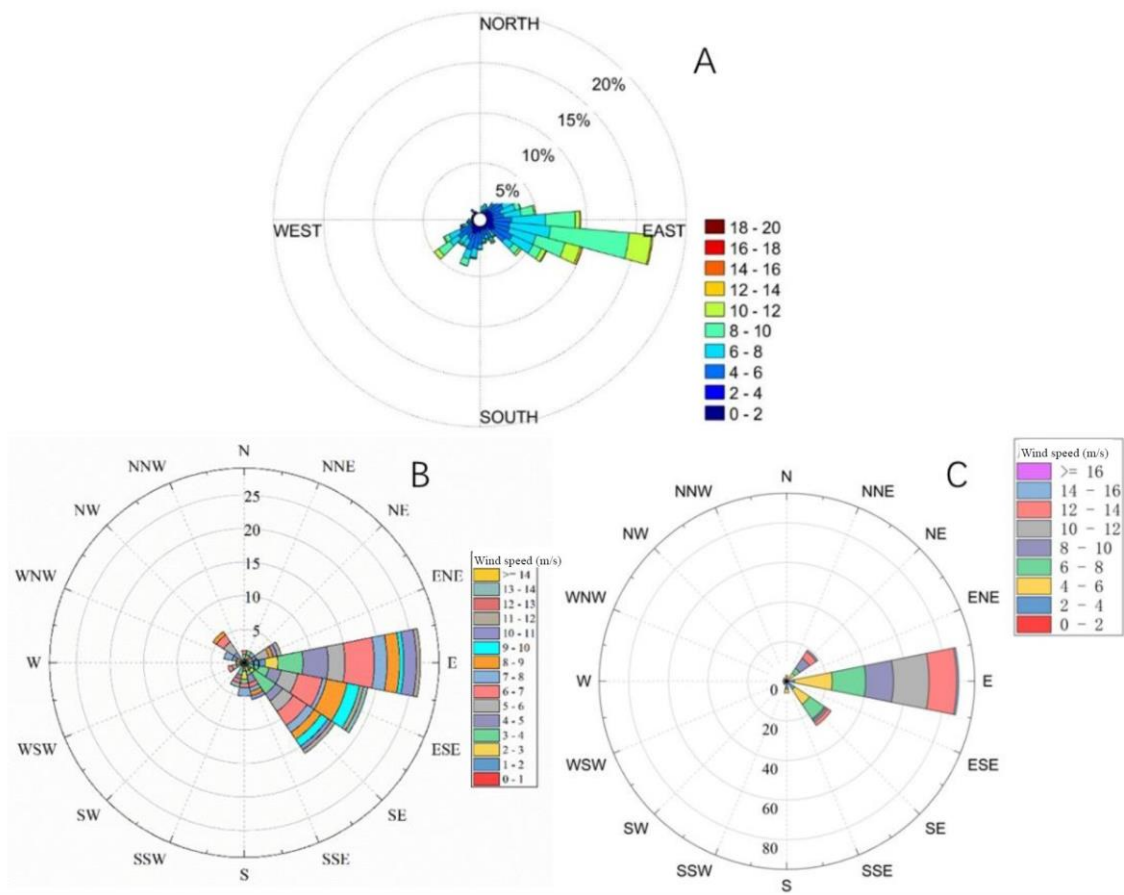
Figure 4-11 Distribution of measured sea surface winds in Block M from August to December

A. October 2021 (cruise 1) B. August to December 2022 (cruise 2) C. November to December 2022 (cruise 3)

4.3.1.2 Sea Conditions

In Block M, wave heights ranging from 2.0 to 3.5 m prevail between late August and early October. Winds were mainly force 4–5 (Beaufort wind force scale), primarily easterly and southeasterly, with an average wind speed of 5.61 m/s and a maximum of 13.0 m/s.

During November, the average wave height was between 2.0 and 2.5 meters, while in December, it ranged from 2.5 to 3.0 meters. The wind was mainly force 4–5, primarily easterly and with a small portion of northeasterly and southeasterly, with an average wind speed of 7.64 m/s and a maximum of 16.2 m/s. The average wave height was between 2.0 to3.5 m in November and a minimum of 3.0 m in December, and the average wave height was 1.0–3.0 m in November.

4.3.1.3 Tides

4.3.1.3.1 Tides

Based on the results of the TPXO global tidal model, the co-amplitude and co-phase lines of the K_1, O_1, M_2, and S_2 tidal constituent in the area and its adjacent region are shown in Figure 4-12 to Figure 4-15. These Figures indicate a pattern where the amplitude of the diurnal tide increases from the western to the eastern regions, while the semidiurnal tide amplitude decreases in the same direction. Specifically, the amplitudes of the K_1 constituent range from 12 to 14 cm in Blocks M1 and M2, the amplitudes of the O_1 constituent exhibit amplitudes of 8–9 cm, the M_2 constituent ranges from 3 to 12 cm, and the S_2 constituent ranges from 4 to 8 cm
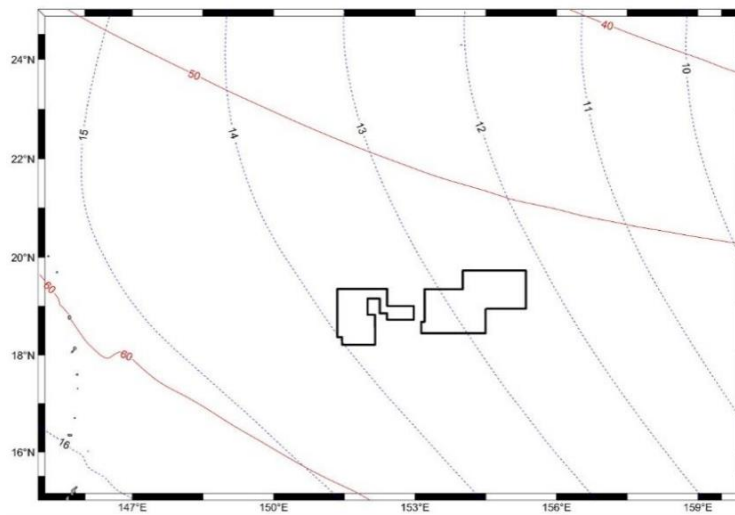
Figure 4-12 K_1 tidal constituent co-amplitude lines (in blue, unit: cm) and the co-phase lines (in red, the black lines represent the boundary lines of the M_2 and M_1 blocks, same below)
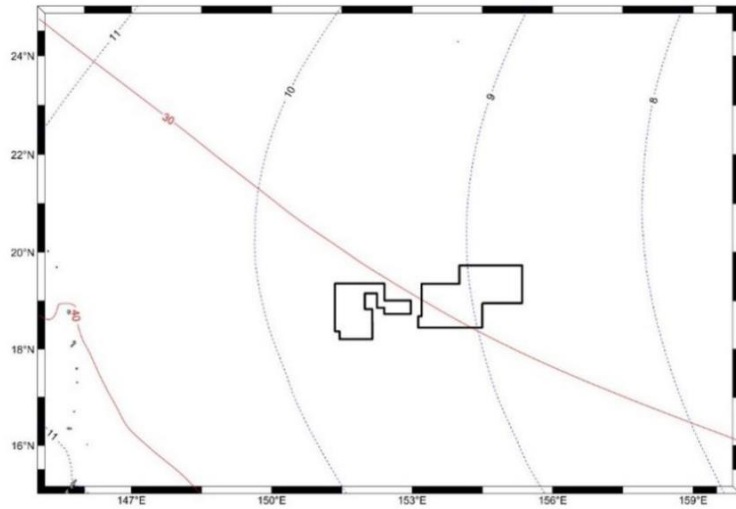
Figure 4-13 O_1 tidal constituent co-amplitude lines (in blue, unit: cm) and the co-phase lines (in red, unit:°)
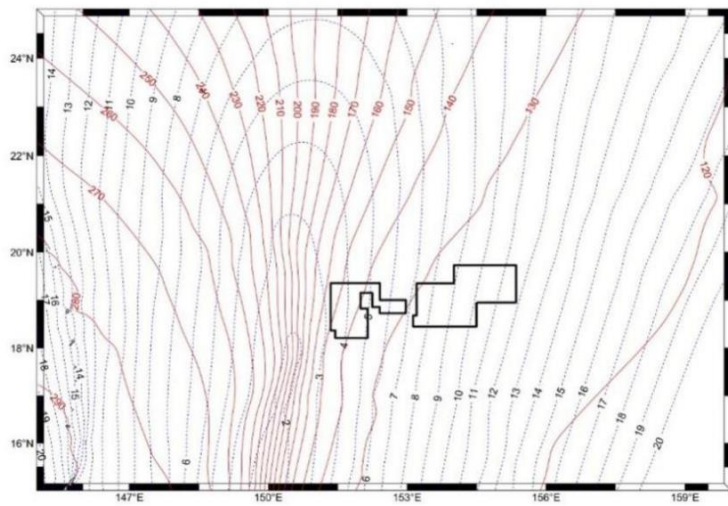
Figure 4-14 M_2 tidal constituent co-amplitude lines (in blue, unit: cm) and the co-tidal lines (in red, unit:°)

Figure 4-15 S_2 tidal constituent co-amplitude contour lines (in blue, unit: cm) and the co-phase lines (in red, unit:°)

Based on the tidal type determination formula by Lee and Chang (2019), the tidal types of the mining area and its adjacent region were calculated, with the results shown in Figure 4-16. The findings illustrate that Block M2 situated east of 153°E exhibits predominantly irregular semi-diurnal tides, whereas the regions west of 153°E within the Blocks M2 and M1 region are primarily dominated by irregular diurnal tides.
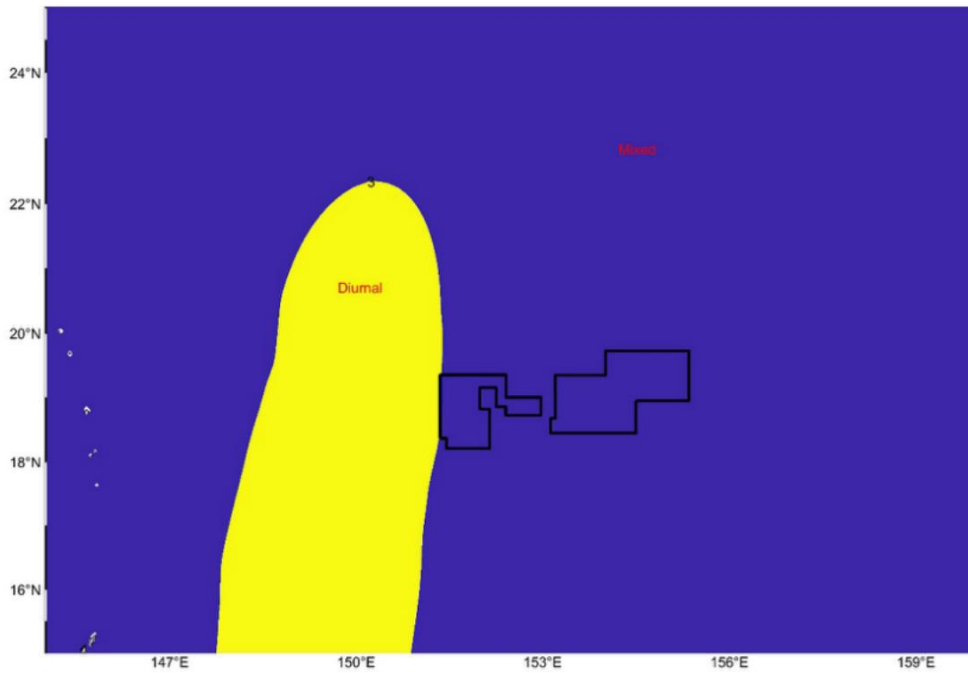
Figure 4-16 Distribution of tidal types in the Mining Area

4.3.1.3.2 Tidal Current

Harmonic analysis was carried out to investigate the near-bottom tidal elliptical characteristics at subsurface buoys DY66-M2-MX2101, DY69-ES04-MX01, DY69-ES03-MX02, and DY69-ES06-MX03, as detailed in Table 4-4 The negative values of the minor axis in the table indicate clockwise rotation, while positive values indicate counterclockwise rotation. The predominant near-bottom tidal current component at each station was found to be the M2 tidal constituent, with the S2 constituent following closely. Through the application of the tidal current type determination formula, it was determined that the near-bottom tidal current at each station exhibits characteristics of a mixed tidal current.

Table 4-4 The ellipse elements of near-bottom tidal currents for the four major constituents of four stations.

Station	Tidal constituent	Frequency (cph)	Major Axis (cm/s)	Minor Axis (cm/s)	Inclination (°)	Phase (°)
DY66-M2-MX2101	O1	0.0387307	0.359	0.085	49.62	197.91
	K1	0.0417807	0.459	0.232	93.79	252.70
	M2	0.0805114	1.532	−0.241	151.39	178.17
	S2	0.0833333	0.715	−0.232	151.24	214.53
DY69-ES04-MX01	O1	0.0387307	0.631	0.074	32.23	196.79
	K1	0.0417807	0.438	0.348	71.48	244.30
	M2	0.0805114	2.156	0.361	162.40	193.87
	S2	0.0833333	0.766	0.125	128.65	194.22
DY69-ES03-MX02	O1	0.0387307	0.506	0.069	37.22	209.15
	K1	0.0417807	0.647	0.058	109.06	277.06
	M2	0.0805114	1.351	−0.797	161.24	235.98
	S2	0.0833333	0.795	−0.134	163.04	235.03
DY69-ES06-MX03	O1	0.0387307	0.615	−0.021	174.38	355.31
	K1	0.0417807	0.551	0.066	39.19	207.96
	M2	0.0805114	1.736	−1.350	154.22	218.67
	S2	0.0833333	0.901	−0.333	152.06	229.96

4.3.2 Topography and Landforms

According to the *Regulations on Prospecting and Exploration for Polymetallic Nodules in the Area* (ISBA/19/C/17) and exploration contracts, contractors are required to collect baseline environmental geological data, including geological and geomorphological features, basic properties of sediments, etc. They record baseline data on the natural conditions before testing or collector component tests, which are used to evaluate the potential impact of their

exploration work plans on the marine environment and to develop monitoring and reporting plans. These parameters can reflect the characteristics of the environment that may be affected by exploration and potential testing or mining component testing activities, making it crucial to monitor the changes brought by these activities and predict the impact of commercial mining activities.

The topographical data and backscatter intensity data in the contract area mainly come from the surveyed data of eight cruises by the Chinese vessels "Hai Yang Di Zhi Liu Hao", "Xiangyanghong 10", "Da Yang Yi Hao", and " Xiangyanghong 03" from 2014 to 2018 and 2021 to 2022. The multi-beam data accuracy is about 50 meters. The multibeam systems used in the cruises include the EM122 multibeam system and the SeaBeam 3012 deep-water multibeam system.

4.3.2.1 Landform Types and Features

Block M is located in the Magellan Seamount Chain in the Northwest Pacific Ocean, which preserves the oldest oceanic crust on Earth and has developed numerous seamounts of different forms. These seamounts were mainly formed by the intense activity of mantle hotspots ranging from 140 to 120 Ma, followed by multiple episodes of magma activity. The fracture zones in the northwest Pacific Ocean are mainly oriented in NW–SE and NE–SW directions, predating later intraplate volcanic activity. These seamounts are all flat-topped seamounts, with summit depths of about 1500 m and ages ranging from 100 to 80 Ma. Around the seamounts, aprons formed by gravitational flank failure are commonly developed.

The acquired multibeam bathymetric data and backscatter intensity data of Blocks M1 and M2 serve as the basis for delineating the geomorphological units of Block M. The results of the geological unit delineation are shown in Figure 4-24.

The characteristics of each geomorphological unit are as follows:

1) Gullies and channels: Gullies and channels are erosional features left by gravity flows on seamount slopes. Gullies are located close to scarps at their upper ends and typically have a "V" shape in cross-section, often serving to collect debris and sediment. Channels are distributed on the middle and lower slopes of aprons, with a cross-section typically exhibiting a "U" shape, facilitating the transport of debris, blocks, and sediment (Quartau et al., 2018). The backscatter intensity of gullies and channels is approximately 5–10 dB lower than the surrounding area, and the cross-sectional slopes are generally less than 5°.

2) Sediment waves: the sediment wave geomorphology of the aprons is divided into

two types: small-scale sediment waves caused by turbidity flow erosion and irregularities, and large-scale sediment waves formed at the forefront of aprons due to sediment creep deformation. These features reveal the flow processes of gravity flows (Symons et al., 2016). The backscatter intensity at locations with large-scale sediment waves is relatively high, approximately –10 dB to –25 dB.

3) Aprons: The extent of the apron is delineated based on the distribution of gullies, channels, and sediment waves, as well as the characteristics of backscatter intensity and terrain features.

4.3.2.2 Topographic Features

Block M is mainly affected by the landslides of two seamounts: the eastern part of Block M1 is influenced by landslides on the southern side of the Matsuzaki Guyot, while the northwest part of Block M2 is affected by landslides on the southern side of the Magoshichi Guyot. The landslides of seamounts have formed distinctive features such as steep scarps, gullies, channels, and sediment waves (Figure 4-17 and Figure 4-18). The upper part of the landslide is the area where debris from the scarps converges into gullies, while the middle part is where the debris is transported through gullies and channels, and the lower part is where the landslide material accumulates.

The Magoshichi Guyot deposits in the northwest of Block M2, with a scarp on its southern side featuring an invagination-arc shape. The apron covers an area of approximately 3500 km^2, with scattered blocks within the region, branching gullies and channels diverging downward. Sediment waves develop in the middle and lower parts of the apron, as well as in some gullies. The crescent-shaped sediment waves with symmetrically developed deposits in the middle of the apron indicate erosion by gravity flows. The irregular-shaped sediment waves with a gentle slope at the bottom of the apron may be caused by sediment creep. The cross-section of crescent-shaped sediment waves within gullies is cyclic steps with an upslope asymmetric shape, suggesting formation by erosion from supercritical gravity flows and deposition from subcritical flows. Block M2 is characterized by small hills scattered. A protrusion with a length of approximately 26 km deposits in the southern part of the block, and small seamounts develop in the southeast boundary.
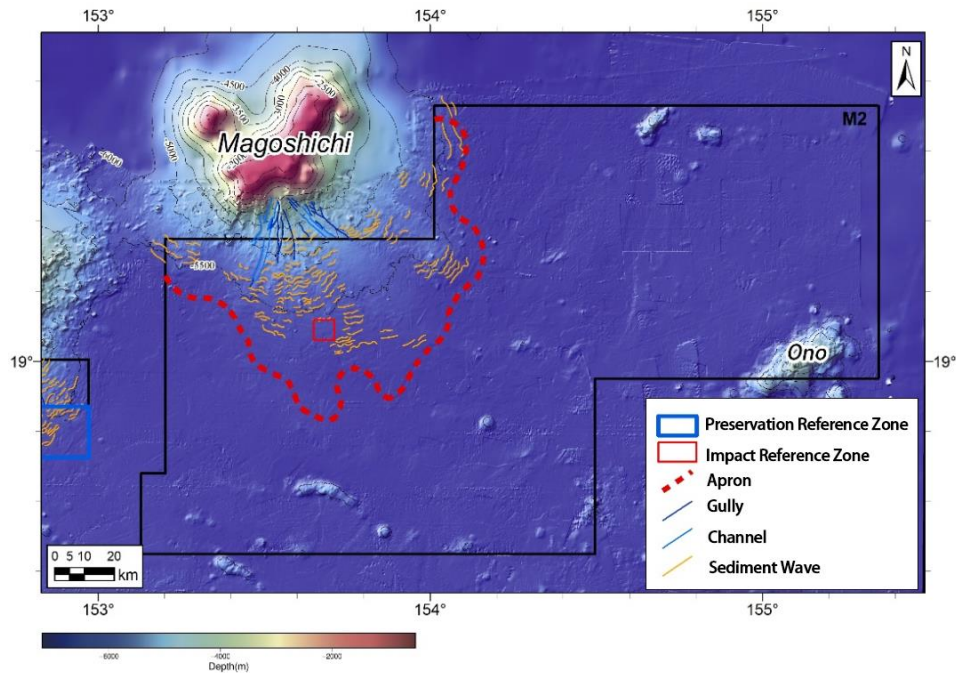
Figure 4-17 Unit Classification of Block M2 Geomorphic

The Matsuzaki Guyot is located on the northeastern side of Block M1, with a scarp on its southern side featuring an invagination-arc shape. The apron covers an area of approximately 2200 km^2, with scattered blocks within the western side and a few gullies and channels. The cross-section of sinuous-shaped sediment waves in the middle of the apron are cyclic steps with symmetric shapes. The cross-section of sediment waves in the bottom of the apron are irregular with a gentle slope. The cross-section of sinuous-shaped sediment waves in the gullies and channels are cyclic steps with an upslope asymmetric shape. Block M1 is characterized by small hills scattered, and a small seamount lies in the southwestern part of the block.
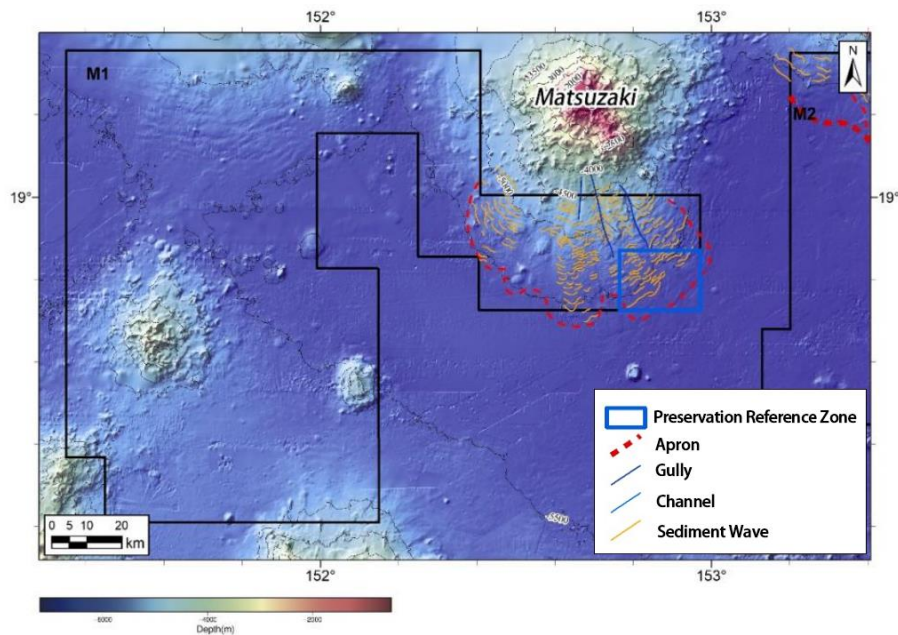
Figure 4-18 Block M1 geomorphic unit delineation

The IRZ is located in the northwest part of Block M2, on the southern apron of the Magoshichi Guyot, and near the abyssal plain. Sediment waves develop in this area, characterized by gentle slopes and irregular-shaped cross-sections, suggesting influenced by sediment creep. The CTA is located within the IRZ.

The PRZ is located in the eastern part of Block M1, on the southern apron of the Matsuzaki Guyot, near the abyssal plain. Sediment waves develop in this area, characterized by gentle slopes and irregular-shaped cross-sections, suggesting influenced by sediment creep.

4.3.2.3 Bathymetric Feature

Using multibeam data, a bathymetric chart of the Block M (Figure 4-19) was created. Depth statistics (Table 4-5 and Figure 4-20) indicate that the depth range of Blocks M1 and M2 primarily falls between 4000–6000 m, covering 91.23% of the area. Depths exceeding 6000 m account for 1.67%, while those below 4000 m constitute 7.09%. Shallow areas with depths less than 5000 m are mainly distributed along the northern boundary of Block M1 affected by seamount landslides. Depths in the abyssal plain are primarily concentrated between 5000–6000 m.
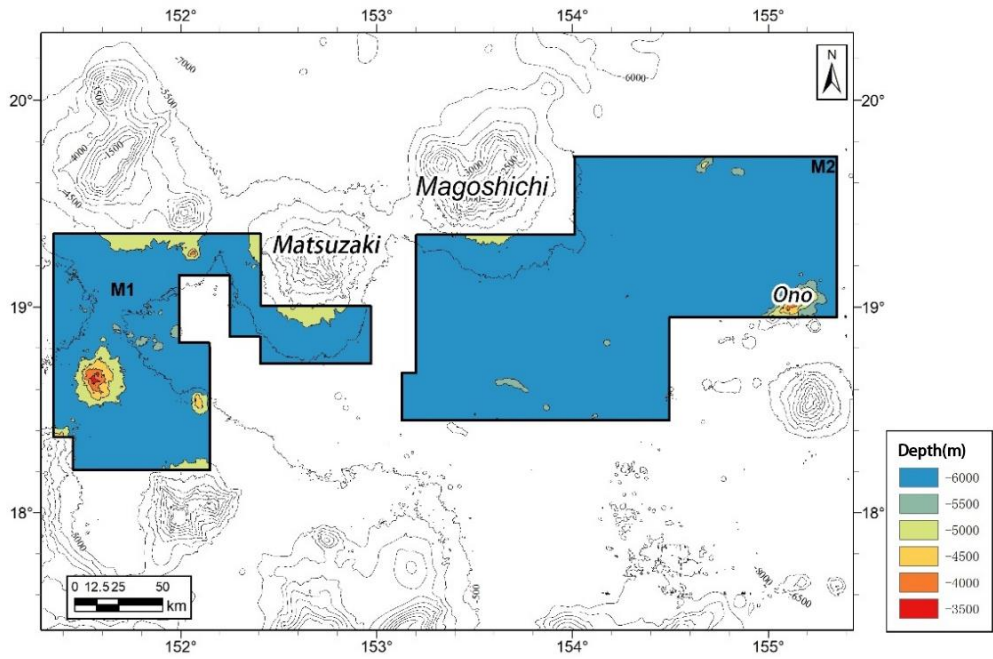
Figure 4-19 Bathymetric contour map of contract area
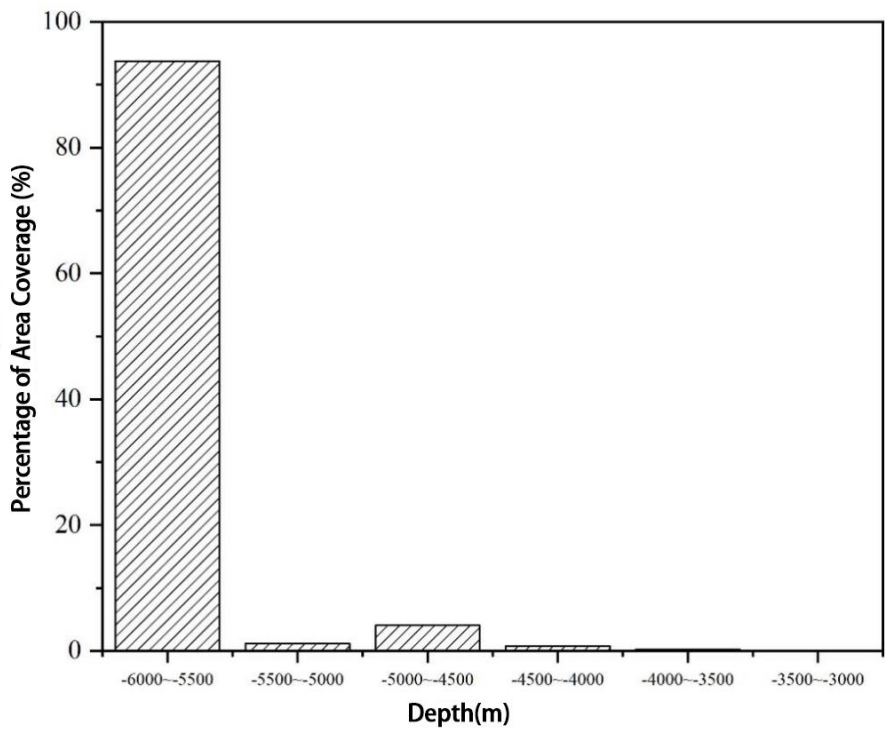
Figure 4-20 Statistical map of water depth values in Block M

Table 4-5 Frequency Distribution Statistics for Bathymetry Values in Block M

Water depth range (m)	Percentage (%)
−6000 to −5500	93.77
−5500 to −5000	1.15
−5000 to −4500	4.03
−4500 to −4000	0.77
−4000 to −3500	0.25
−3500 to −3000	0.03

4.3.2.4 Slope

Using multibeam data, a slope map of the contract area (Figure 4-21) was generated. Slope statistics (Table 4-6 and Figure 4-22) indicate that the slope in Block M ranges from 0–80°, with the majority concentrated between 0–5°, covering approximately 92% of the area. This suggests that the terrain in the region is characterized by smooth changes with small undulations. Within the landslide area, blocks of varying sizes are distributed, with slopes exceeding 20° in some locations.
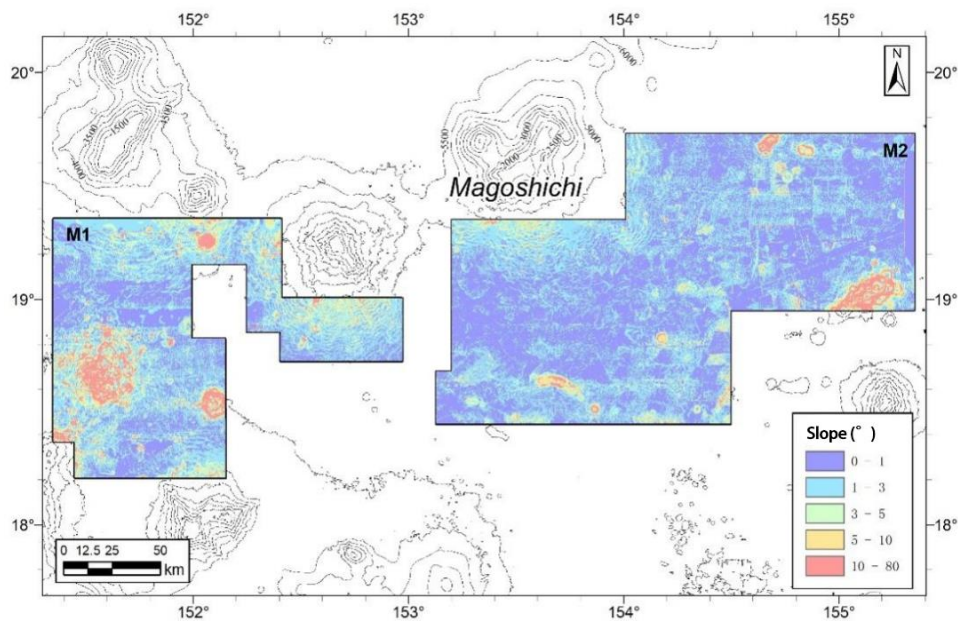
Figure 4-21 Slope contour map of Block M
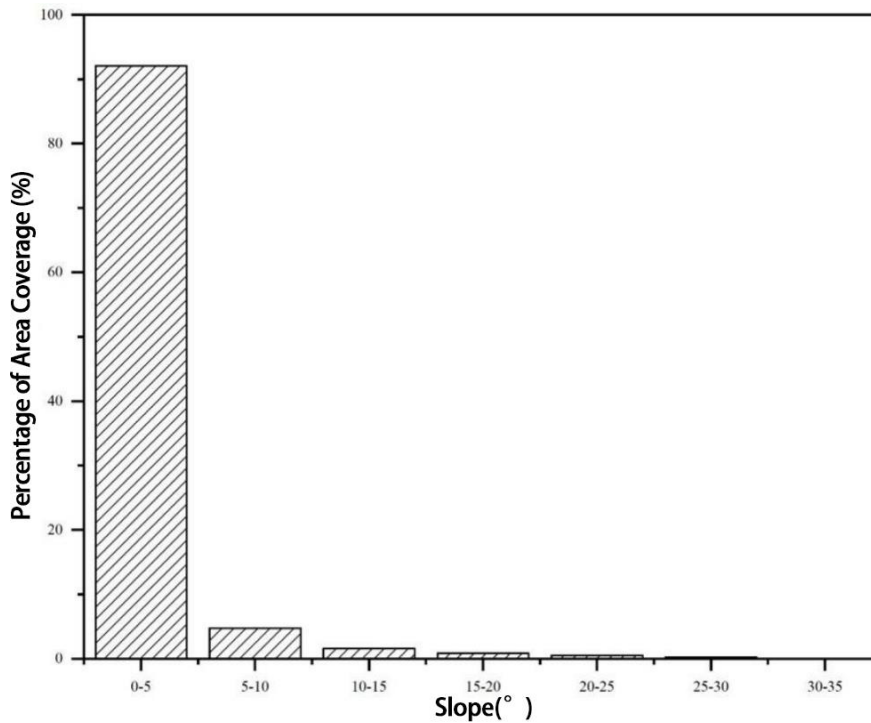
Figure 4-22 Statistical map of slope values in Block M

Table 4-6 Frequency distribution statistics for slope values in Block M

Slope (°)	Percentage (%)
0 to 5	92.03
5 to 10	4.76
10 to 15	1.55
15 to 20	0.83
20 to 25	0.50
25 to 30	0.24
30 to 35	0.06
>35	0.03

4.3.2.5 Backscatter Intensity

The distribution of backscatter intensity in Block M is illustrated in Figure 4-23, with statistical results provided in Table 4-7 and Figure 4-24. It indicates that the backscatter intensity in Block M is concentrated in the range of –25 dB to –40 dB, accounting for approximately 82%. Areas with backscatter intensity greater than –25 dB, indicating high intensity, are mainly distributed in the southwestern hilly region of Block M1, within the influence range of the Matsuzaki Guyot landslide in the eastern part of Block M1, and the influence range of the Magoshichi Guyot landslide in the northwestern part of Block M2,

covering 30% of the Block M. In the deep-sea plain area, the backscatter intensity ranges mainly from –30 dB to –40 dB, covering 42% of Block M.
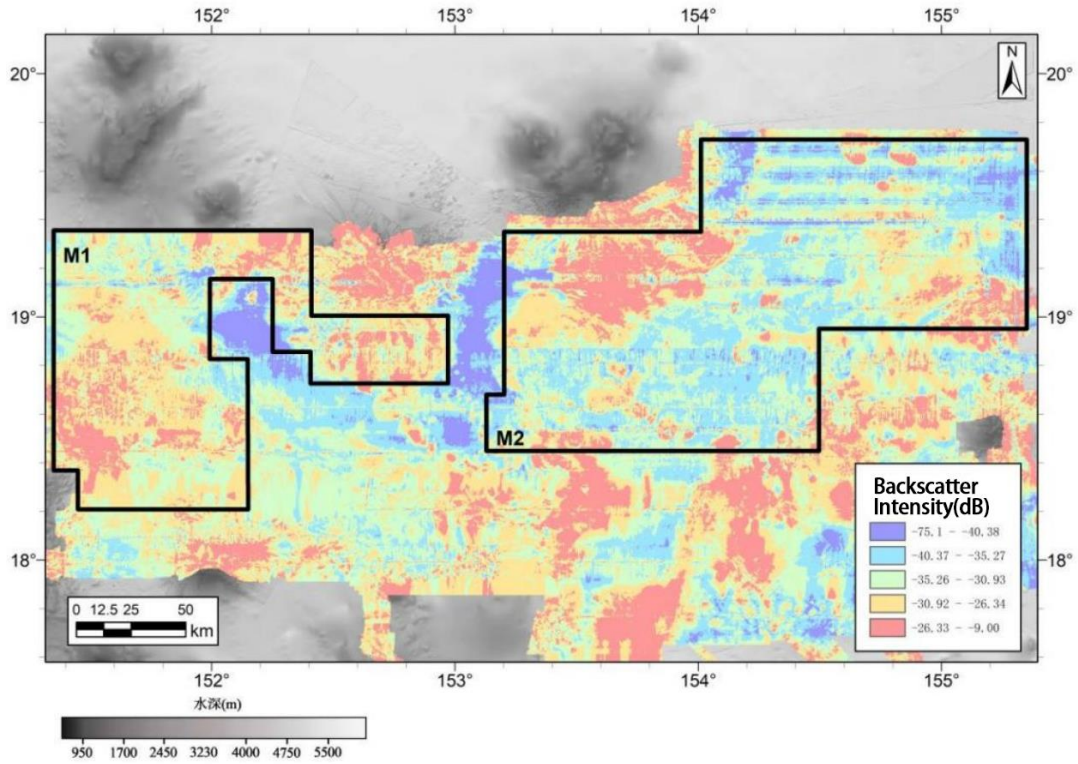
Figure 4-23 Backscatter intensity contour map of Block M
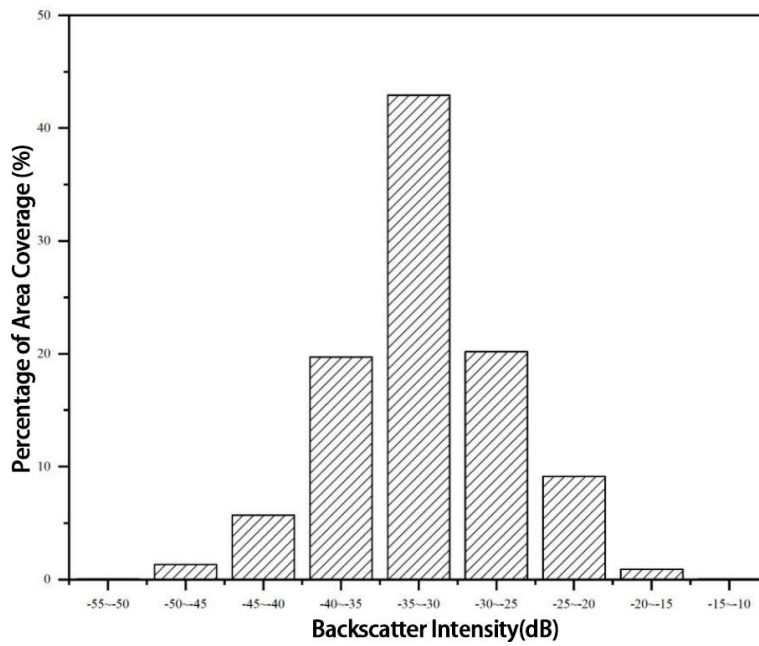
Figure 4-24 Frequency distribution statistics of backscatter intensity in Block M

Table 4-7 Frequency distribution statistics of backscatter intensity values in Block M

Backscatter intensity (dB)	Percentage (%)
<−50	0.05
−50 to −45	1.32
−45 to −40	5.71
−40 to −35	19.71
−35 to −30	42.93
−30 to −25	20.19
−25 to −20	9.13
−20 to −15	0.90
−15 to −10	0.06

4.3.3 Sedimentary Feature

4.3.3.1 Sediment Type

4.3.3.1.1 Surface Sediment Type

Sediment smear analysis (surface 0–3 cm) was carried out on the Surface sediment samples collected from 110 stations in Block M during the DY69 cruise (2021) and DY75 cruise (2022) were subjected to sediment smear slide identification analysis (Table 4-8 and Figure 4-25). The identification results indicate that the surface sediment types in Block M are predominantly deep-sea clay, with material compositions primarily consisting of terrestrial siliceous debris (including clay minerals and fine sand-sized terrigenous clasts) (75%–98%), with a small amount of biogenic silicon debris (dominated by radiolarians and sponge bony needles) (<1% to 20%), and volcanic debris (1%–10%). In addition, the surface sediment of Station DY75I-M2-BC83 was collected from the summit of a seamount outside the block, at a depth of 1287 m above the CCD (Calcite Compensation Depth), is identified as calcareous ooze.

Table 4-8 Surface sediment types in Block M

Stations	Water depth (m)	Volcanic debris (%)	Biogenic siliceous debris (%)	Siliceous debris (%)	Sediment types
DY69-M2B1-PS13-BC01	5702	2	2	96	deep-sea clay
DY69-M2B1-PS01-BC02	5718	1	1	98	deep-sea clay
DY69-M2B1-PS02-BC03	5675	3	2	95	deep-sea clay
DY69-M2B1-PS05-BC04	5434	1	1	98	deep-sea clay
DY69-M2B1-PS04-BC05	5589	10	10	80	deep-sea clay
DY69-M2B1-PS08-BC06	5520	5	1	94	deep-sea clay
DY69-M2B1-PS07-BC07	5576	5	2	93	deep-sea clay
DY69-M2B1-PS11-BC08	5443	1	10	89	deep-sea clay
DY69-M2-ES04-BC09	4842	5	5	90	deep-sea clay
DY69-M2B1-PS10-BC10	5193	1	1	98	deep-sea clay
DY69-M2B1-PS06-BC11	5508	1	20	79	deep-sea clay
DY69-M2B1-PS03-BC12	5621	1	10	89	deep-sea clay
DY69-M2B1-ESO3-BC13	5569	1	4	95	deep-sea clay
DY69-M2B1-PS14-BC14	5632	5	15	80	deep-sea clay
DY69-M2B1-PS15-BC15	5593	1	20	79	deep-sea clay
DY69-M2B1-PS09-BC16	5248	1	20	79	deep-sea clay
DY69-M1-ES06-BC17	5528	10	15	75	deep-sea clay
DY69-M2B1-ES06-BC20	5668	1	8	91	deep-sea clay
DY69-M2B1-ES02-BC22	5650	1	5	94	deep-sea clay
DY69-M2B1-ES01-BC25	5645	3	5	92	deep-sea clay
DY75I-M2-BC03A	5685	4	1	92	deep-sea clay
DY75I-M2-BC04	5651	2	1	95	deep-sea clay
DY75I-M2-BC05	5625	5	1	92	deep-sea clay
DY75I-M2-BC06	5675	3	1	93	deep-sea clay
DY75I-M2-BC07	5716	2	1	96	deep-sea clay
DY75I-M2-BC08	5616	3	1	94	deep-sea clay
DY75I-M2-BC09	5675	3	1	94	deep-sea clay
DY75I-M2-BC11	5658	2	1	95	deep-sea clay
DY75I-M2-BC12	5678	3	1	94	deep-sea clay
DY75I-M2-BC13	5629	3	1	94	deep-sea clay
DY75I-M2-BC14	5671	5	1	92	deep-sea clay
DY75I-M2-BC15	5659	4	1	92	deep-sea clay
DY75I-M2-BC16A	5690	4	1	92	deep-sea clay
DY75I-M2-BC17	5719	3	1	94	deep-sea clay
DY75I-M2-BC19	5704	4	1	92	deep-sea clay
DY75I-M2-BC20	5669	3	1	94	deep-sea clay

Stations	Water depth (m)	Volcanic debris (%)	Biogenic siliceous debris (%)	Siliceous debris (%)	Sediment types
DY75I-M2-BC21	5673	2	1	94	deep-sea clay
DY75I-M2-BC22	5659	3	1	93	deep-sea clay
DY75I-M2-BC23	5737	3	1	93	deep-sea clay
DY75I-M2-BC24	5770	6	1	90	deep-sea clay
DY75I-M2-BC25	5585	4	1	93	deep-sea clay
DY75I-M2-BC26	5636	4	1	92	deep-sea clay
DY75I-M2-BC27	5695	3	1	93	deep-sea clay
DY75I-M2-BC28	5500	3	1	93	deep-sea clay
DY75I-M2-BC29	5664	6	1	89	deep-sea clay
DY75I-M2-BC31	5571	5	1	90	deep-sea clay
DY75I-M2-BC32	5507	6	1	89	deep-sea clay
DY75I-M2-BC33	5148	4	1	92	deep-sea clay
DY75I-M2-BC34	5478	5	1	91	deep-sea clay
DY75I-M2-BC35	5471	4	1	90	deep-sea clay
DY75I-M2-BC36	5539	4	1	93	deep-sea clay
DY75I-M2-BC38A	5302	6	1	90	deep-sea clay
DY75I-M2-BC39A	5428	3	1	93	deep-sea clay
DY75I-M2-BC40	5647	1	5	90	deep-sea clay
DY75I-M2-BC41A	5654	3	1	92	deep-sea clay
DY75I-M2-BC42	5618	3	1	93	deep-sea clay
DY75I-M2-BC43	5655	3	1	94	deep-sea clay
DY75I-M2-BC44	5632	2	1	95	deep-sea clay
DY75I-M2-BC45	5680	4	1	91	deep-sea clay
DY75I-M2-BC46	5673	5	1	92	deep-sea clay
DY75I-M2-BC47	5626	9	1	88	deep-sea clay
DY75I-M2-BC50	5695	3	1	93	deep-sea clay
DY75I-M2-BC53	5660	5	1	92	deep-sea clay
DY75I-M2-BC54	5696	5	1	92	deep-sea clay
DY75I-M2-BC55	5706	7	1	89	deep-sea clay
DY75I-M2-BC56	5657	4	1	94	deep-sea clay
DY75I-M2-BC57	5665	5	1	93	deep-sea clay
DY75I-M2-BC58	5659	7	1	89	deep-sea clay
DY75I-M2-BC59	5654	6	1	91	deep-sea clay
DY75I-M2-BC60A	5667	7	1	89	deep-sea clay
DY75I-M2-BC61	5664	6	1	91	deep-sea clay
DY75I-M2-BC63	5678	6	1	91	deep-sea clay
DY75I-M2-BC64	5731	6	1	92	deep-sea clay

Stations	Water depth (m)	Volcanic debris (%)	Biogenic siliceous debris (%)	Siliceous debris (%)	Sediment types
DY75I-M2-BC65	5706	4	1	93	deep-sea clay
DY75I-M1-BC73	5625	3	1	94	deep-sea clay
DY75I-M2-BC78	5562	7	1	89	deep-sea clay
DY75I-M2-BC79	5611	7	1	90	deep-sea clay
DY75I-M2-BC80	5618	8	1	89	deep-sea clay
DY75I-M2-MC02	5519	8	1	88	deep-sea clay
DY75I-M2-MC05	5619	7	1	90	deep-sea clay
DY75I-M2-MC06	5561	5	1	93	deep-sea clay
DY75I-M2-BC10	5684	3	1	95	deep-sea clay
DY75I-M2-BC30	5587	8	1	89	deep-sea clay
DY75I-M2-BC49	5702	7	1	90	deep-sea clay
DY75I-M2-BC51	5698	6	1	91	deep-sea clay
DY75I-M2-BC52	5692	4	1	94	deep-sea clay
DY75I-M2-BC66	5690	2	1	96	deep-sea clay
DY75I-M1-BC68	5525	4	1	94	deep-sea clay
DY75I-M1-BC69	5529	5	1	89	deep-sea clay
DY75I-M1-BC71	5554	3	1	95	deep-sea clay
DY75I-M1-BC72	5623	5	1	90	deep-sea clay
DY75I-M1-BC74	5393	6	1	88	deep-sea clay
DY75I-M2-BC75	5496	6	1	91	deep-sea clay
DY75I-M2-BC77	5543	3	1	95	deep-sea clay
DY75II-M2-BC81	5681	3	1	94	deep-sea clay
DY75II-M2-BC82	5669	3	1	95	deep-sea clay
DY75II-M1-BC83	1287	0	1	0	calcareous ooze
DY75II-M1-BC84	5483	5	1	93	deep-sea clay
DY75II-M1-BC85	5157	6	1	92	deep-sea clay
DY75II-M1-BC86	4398	3	1	95	deep-sea clay
DY75II-M1-BC87	4526	6	1	91	deep-sea clay
DY75II-M1-BC88	4567	3	1	95	deep-sea clay
DY75II-M1-BC89	4570	3	1	95	deep-sea clay
DY75II-M2-BC90	5490	3	1	95	deep-sea clay
DY75II-M2-BC91	5078	3	1	95	deep-sea clay
DY75II-M2-BC48A	5660	2	1	97	deep-sea clay
DY75II-M2-BC92	5687	3	1	93	deep-sea clay
DY75II-M2-BC93	5656	5	1	93	deep-sea clay
DY75II-M2-BC94	5711	2	1	96	deep-sea clay
DY75II-M2-BC95	5712	3	1	95	deep-sea clay

The material composition of surface sediments in Block M is dominated by siliceous debris, with the siliceous debris content in most stations exceeding 90%. Only a small number of stations have siliceous debris content ranging from 75% to 90%. Therefore, the distribution pattern of the sediment material composition is mainly controlled by the variation of volcanic debris and biogenic silicon debris contents. According to the data on the material composition of surface sediments from 110 stations in the working area, as depicted in the sediment material composition distribution map (Figure 4-25), the high value of volcanic debris content (>3%) in surface sediments of Block M are mainly distributed in the area of landslide of large submarine guyot and small seamounts and foothill of seamounts in inter-mountain basins. The high value areas of biogenic silicon debris (>5%) are more scattered, but there is also a trend of increased content near large seamounts, suggesting a possible relationship with ocean productivity and hydrodynamic conditions (e.g., oceanic eddies).
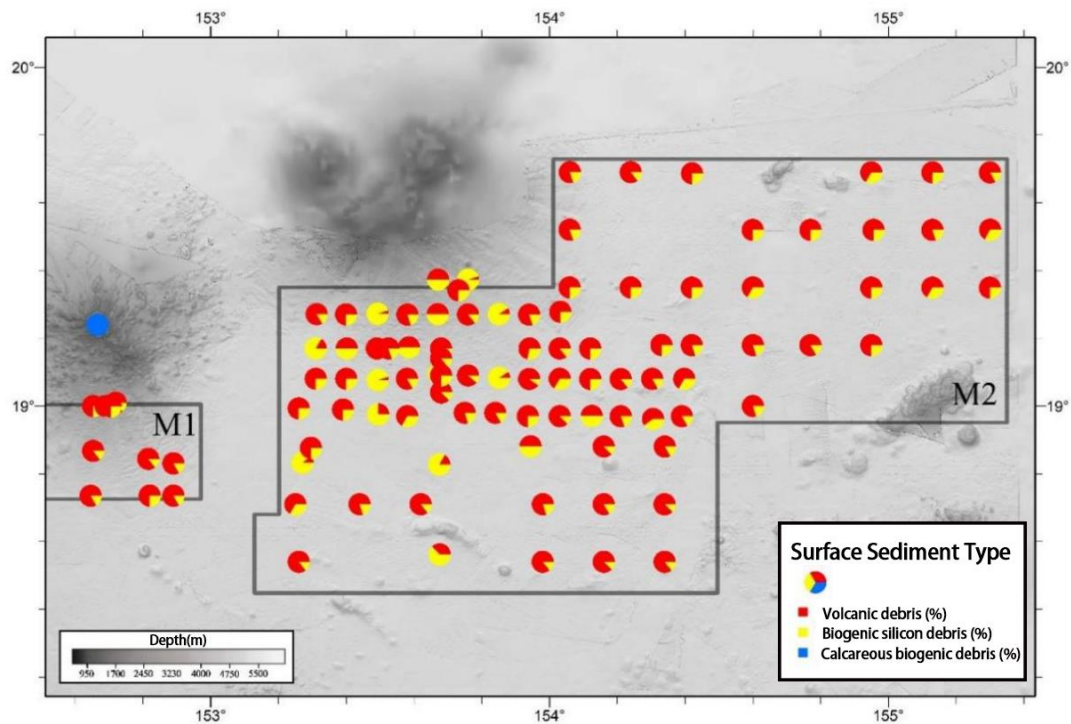
Figure 4-25 Distribution of material composition of surface sediments in Block M

4.3.3.1.2 Sediment Grain Size Characteristics

Surface sediment samples from 20 stations and short piston sediment samples from 5 stations collected during the DY69 (2021) in Block M were subjected to sediment grain size analysis. The results show that the surface sediments of 20 stations contain no gravels (>2000

μm). The contents of sand (63–2000 μm), silt (4–63 μm), and clay (<4 μm) range from 0% to 50.16% (mean 11.51%), 32.15% to 57.60% (mean 48.95%), and 17.69% to 60.26% (mean 39.54%), respectively (Table 4-9).

Table 4-9 Grain size compositions of surface sediments from Block M

Sample name	Depth (m)	Sand (%)	Silt (%)	Clay (%)	Md (φ)	Mz (φ)	σi (φ)	Ski	Kg
DY69-M2B1-PS01-BC02	5718	9.04	53.31	37.65	7.43	7.23	2.12	-0.17	1.18
DY69-M2B1-PS02-BC03	5675	0.99	52.95	46.06	7.83	7.84	1.52	-0.01	1.13
DY69-M2B1-PS03-BC12	5621	14.94	49.57	35.49	7.27	6.83	2.42	-0.24	1.03
DY69-M2B1-PS04-BC05	5589	18.41	45.28	36.30	7.27	6.70	2.64	-0.28	0.97
DY69-M2B1-PS05-BC04	5434	0.00	39.74	60.26	8.24	8.30	1.11	0.11	1.05
DY69-M2B1-PS06-BC11	5508	13.61	48.55	37.85	7.39	6.99	2.40	-0.24	1.10
DY69-M2B1-PS07-BC07	5576	14.79	44.68	40.53	7.53	7.01	2.52	-0.29	1.12
DY69-M2B1-PS08-BC06	5520	13.92	50.60	35.48	7.28	6.88	2.33	-0.22	1.03
DY69-M2B1-PS09-BC16	5248	2.46	52.41	45.13	7.80	7.79	1.59	-0.04	1.17
DY69-M2B1-PS10-BC10	5193	7.45	47.83	44.72	7.76	7.69	2.01	-0.17	1.39
DY69-M2B1-PS11-BC08	5443	2.42	52.25	45.34	7.81	7.81	1.54	-0.02	1.16
DY69-M2B1-PS13-BC01	5702	0.89	50.83	48.28	7.91	7.93	1.46	0.01	1.11
DY69-M2B1-PS14-BC14	5632	7.69	54.37	37.94	7.45	7.33	2.00	-0.13	1.18
DY69-M2B1-PS15-BC15	5593	16.88	46.80	36.32	7.30	6.76	2.54	-0.27	1.04
DY69-M2B1-ES01-BC25	5645	11.15	51.49	37.36	7.37	7.06	2.28	-0.20	1.07
DY69-M2B1-ES02-BC22	5650	5.33	57.60	37.07	7.46	7.34	1.82	-0.11	1.17
DY69-M2B1-ES03-MC02	5576	15.17	48.48	36.36	7.32	6.87	2.46	-0.25	1.11
DY69-M2-ES04-BC09	4842	15.40	47.54	37.06	7.27	6.86	2.49	-0.21	0.93
DY69-M2B1-ES05-BC20	5668	9.49	52.56	37.95	7.43	7.19	2.13	-0.18	1.12
DY69-M1-ES06-BC17	5528	50.16	32.15	17.69	3.96	4.60	2.91	0.32	0.68

The grain size frequency distribution curve (Figure 4-26) reveals that the majority of samples exhibit bimodal or multimodal sediment frequency distribution curves, indicating the presence of at least two or more different grain components with distinct origins and sources in the sediment. Correlation analysis between the material composition and grain size data of surface sediment samples in Block M (Figure 4-27) reveals that the content of volcanic debris in surface sediments is positively correlated with the sand (r=0.70) and positively correlated with the content of coarse particles (total content of sand and silt) (r=0.56). The biogenic silicon debris shows a weak positive correlation with both sand (r=0.32) and coarse particles (total content of sand and silt) (r=0.37). The siliceous debris component is positively correlated with the clay content (r=0.55). From the above results, it can be inferred that the coarse particle component (sand and silt) in sediments from Block M

is mainly composed of volcanic debris, with some influence from biogenic silicon debris, while the fine particle component is primarily composed of siliceous debris.
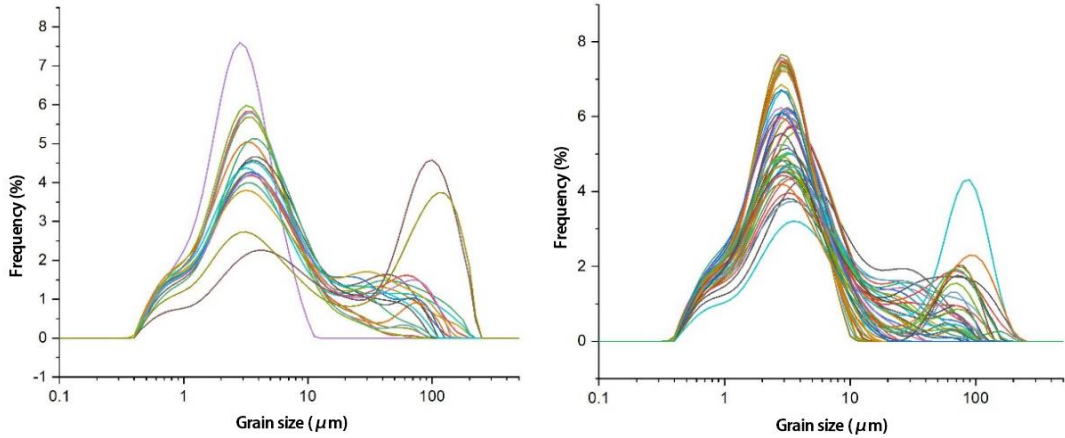
Figure 4-26 Grain size frequency distribution curves for surface sediments (left) and short piston sediments (right)
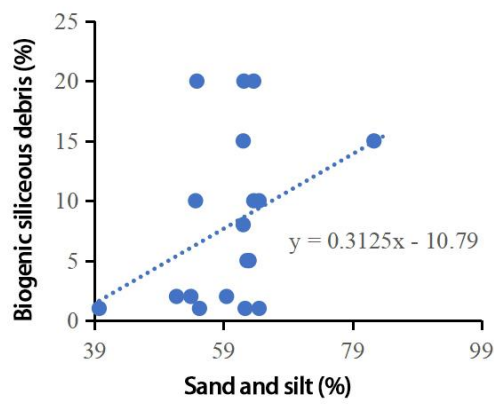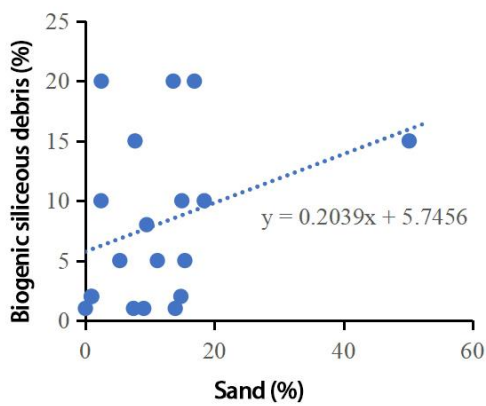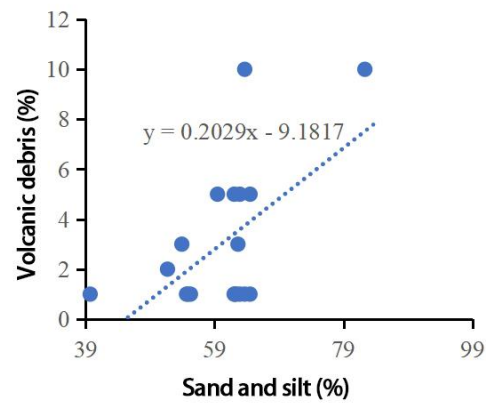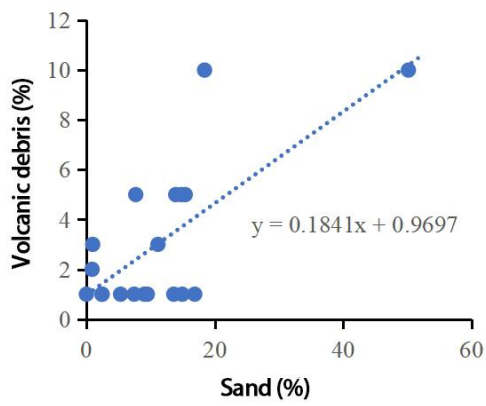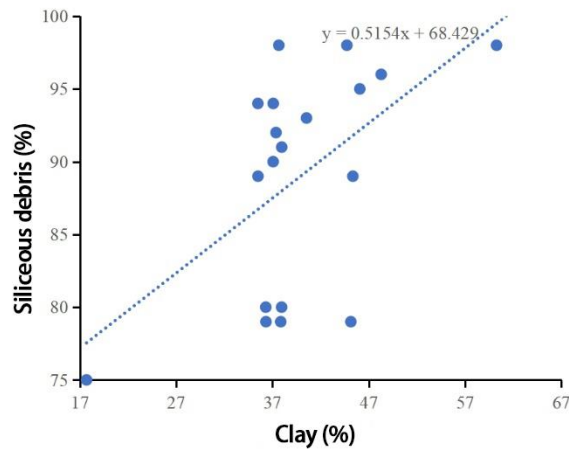
Figure 4-27 Correlation between material composition and grain size composition of surface sediments

Based on the grain size analysis data of surface sediment from 20 stations in Block M, the sediment grain size characteristic distribution map (Figure 4-28) reveals that the high-value areas (>3%) of coarse particle components (sand and silt) in sediments from Block M exhibit similar distribution patterns to the high-value areas of volcanic debris and biogenic silicon debris. Specifically, they are mainly distributed in the areas of landslide of guyot and small seamounts and foothills of seamounts in intermontane basins.
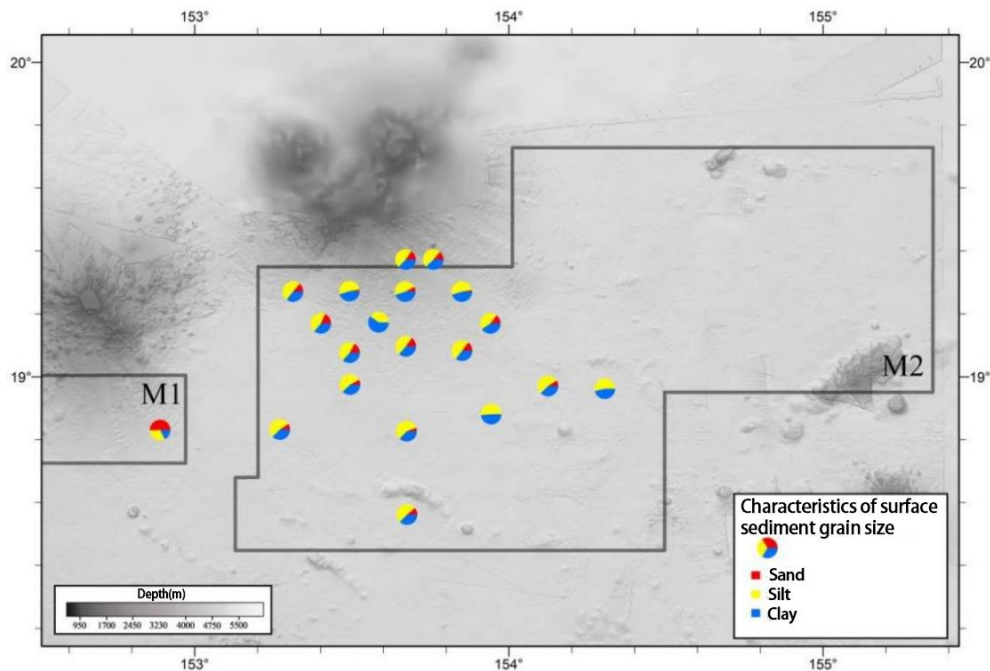
Figure 4-28 Distribution of surface sediment grain size characteristics in Block M

Grain size analysis was conducted on short piston sediment samples collected from 5 stations during the DY69 cruise (2021). Station DY69-M1-ES06-BC17 is located in the southern foothill of the Matsuzaki Guyot in Block M1, while the other four stations are located in the southern part of the Magoshichi Guyot in Block M2, ranging from the southern foothill to the deep-sea basin as follows: DY69-M2-ES04-BC09, DY69-M2B1-ES03-MC02, DY69-M2B1-ES02-BC22, and DY69-M2B1-ES01-BC25 (Figure 4-29).
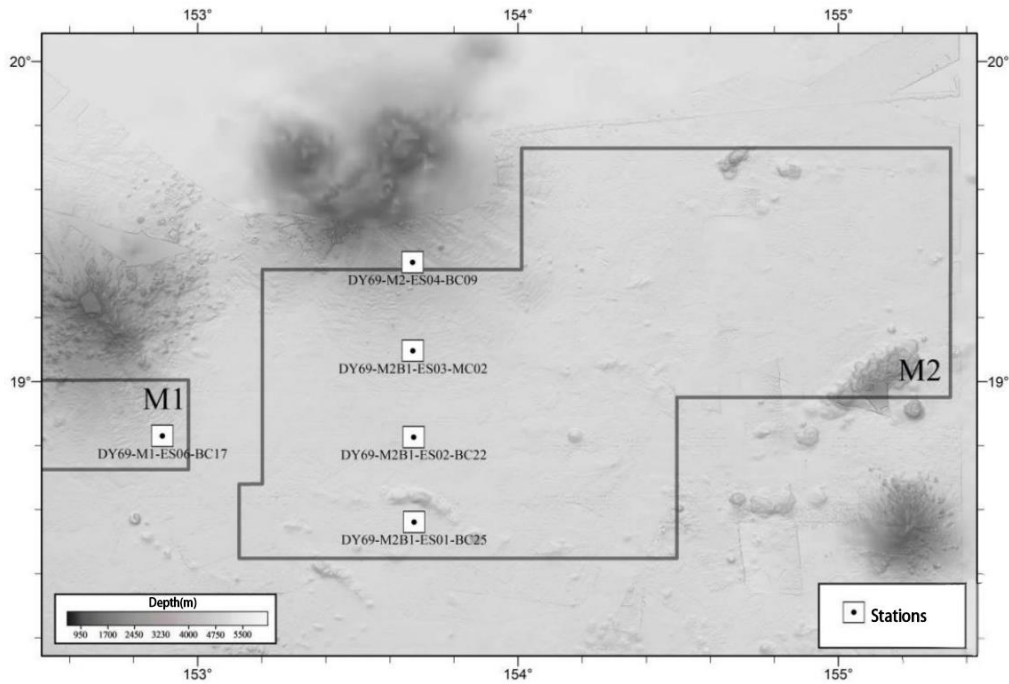
Figure 4-29 Short piston sediment station distribution Map

The vertical variation of sand, silt and clay contents, as well as average grain size, sorting coefficient, bias and peak of 5 short piston sediments are shown in Figure 4-30 to Figure 4-34. Stations DY69-M2-ES04-BC09 and DY69-M2B1-ES03-MC02 are located on the southern foothill of the Magoshichi Guyot. In the upper layers (0-8 cm for DY69-M2-ES04-BC09 and 0-6 cm for DY69-M2B1-ES03-MC02), there is an obvious increasing trend in the content of coarse particles (sand and silt) from bottom to top, with the content stabilizing in the lower part. This suggests a recent supply of material (volcanic debris) from the southern part of the Magoshichi Guyot. Station DY69-M2B1-ES02-BC22 is situated near low hills in the intermontane deep-sea basin, where the content of coarse particles in the upper layers (0–30cm) exhibit cyclic variations, with the content stabilizing in the lower part. Station DY69-M2B1-ES01-BC25 is situated near a small seamount chain in the intermontane

deep-sea basin. There is a noticeable increasing trend in the content of coarse particle components from bottom to top in the upper layers (0 to 25 cm), while the content stabilizes in the lower part. This likely represents a recent supply of material (volcanic debris) from the nearby seamount area. Station DY69-M1-ES06-BC17 is situated on the southern foothill of the Matsuzaki Guyot in Block M1, where the sediment has an obviously higher sand content compared to other stations (Figure 4-34), with a maximum value of 39% in the surface layer. The sand content increases from bottom to top, while the clay content has an opposite trend, suggesting a supply of material (volcanic debris) from the northern Matsuzaki Guyot.
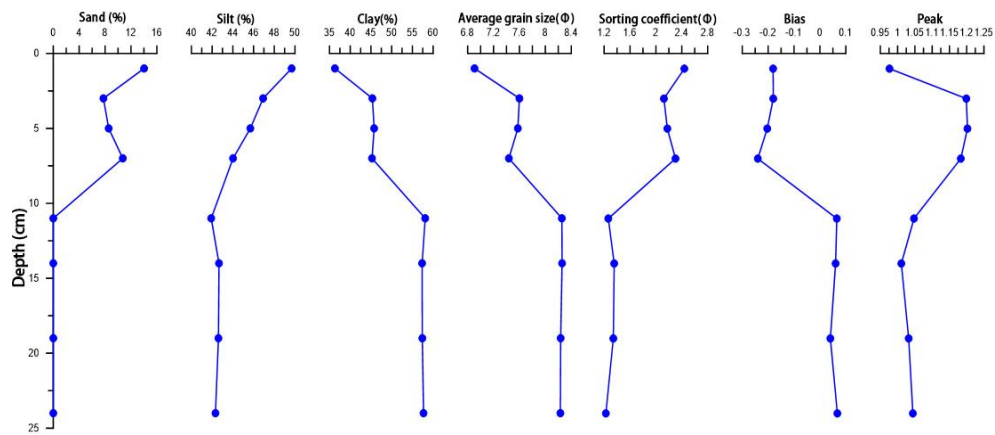
Figure 4-30 Vertical variation of grain size parameters of short piston sediments from Station DY69-M2-ES04-BC09
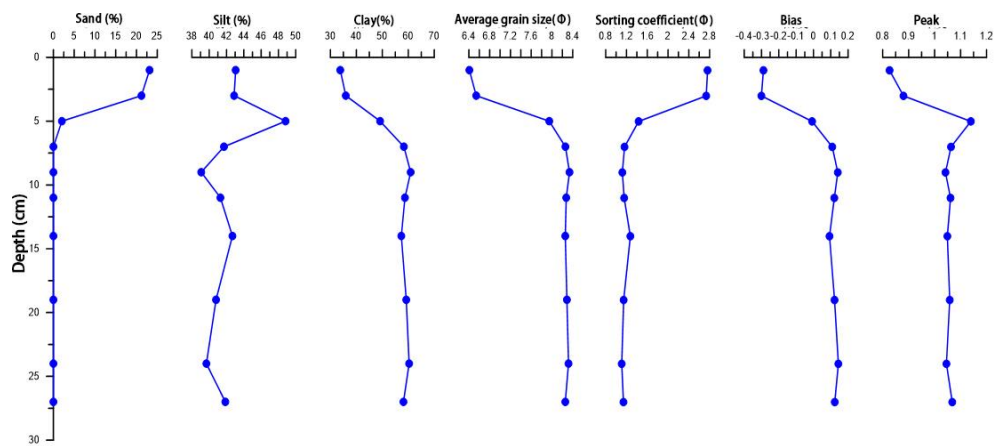
Figure 4-31 Vertical variation of grain size parameters of short piston sediments from Station DY69-M2B1-ES03-MC02
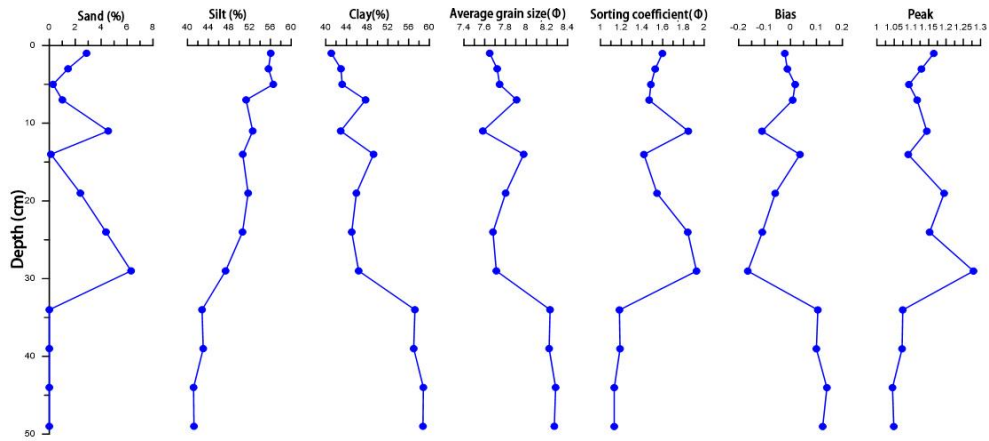
Figure 4-32 Vertical variation of grain size parameters of short piston sediments from Station DY69-M2B1-ES02-BC22
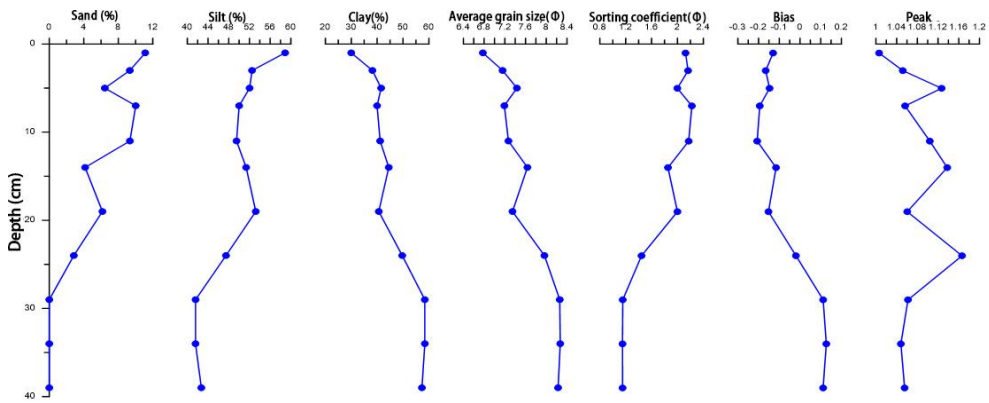
Figure 4-33 Vertical variation of grain size parameters of short piston sediments from Station DY69-M2B1-ES01-BC25
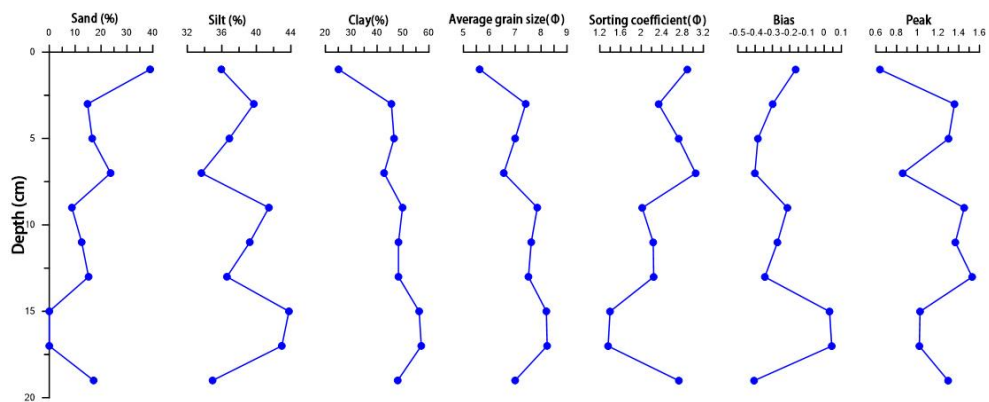
Figure 4-34 Vertical variation in grain size parameters of short piston sediments from Station DY69-M1-ES06-BC17

4.3.3.2 Surface Sediment pH and Eh

The chemical parameters such as Eh, pH of the surface sediments from Block M2 were analyzed during the DY75 cruise (2022).

4.3.3.2.1 pH

The pH of surface sediments from Block M2 ranges from 5.67 to 9.60. After the box-corer is brought back to the deck, the electrode of the "INESA-PHB-J-260 portable tester" is inserted directly into the surface sediment in the corer to measure the pH. The pH of the surface sediment is mainly used to analyze the differences and spatial changes in the seabed sediment environment. Most of the surface sediments have pH of 7.0–8.0 (41 stations) and 8.0–9.6 (32 stations), with only 12 stations having pH values between 6.5 and 7.0 (Figure 4-36), indicating that the surface sediments (pore water) are neutral to weakly alkaline. Figure 4-36 shows that high pH value (>8.3) stations are scattered sporadically within the block, showing no apparent distribution pattern. The low pH value (<7.7) stations are mainly distributed in the central plain of the block and the landslide fan on the northwest side of the seamount.
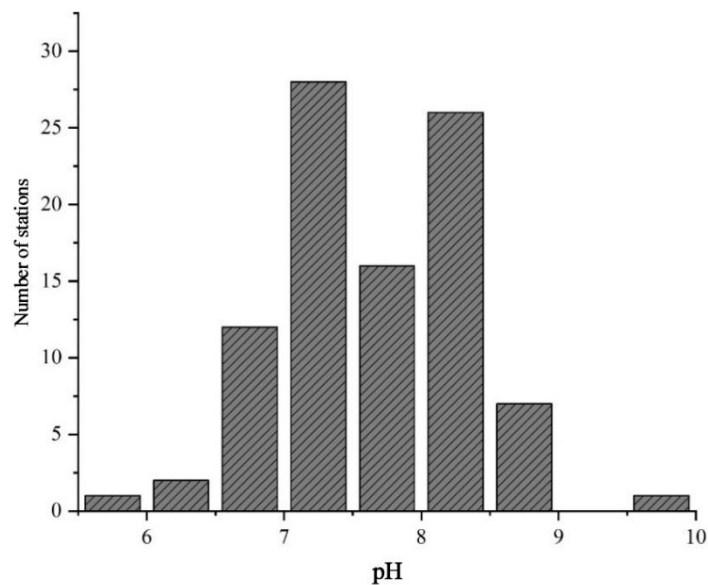
Figure 4-35 Histogram of pH of surface sediments in Block M2
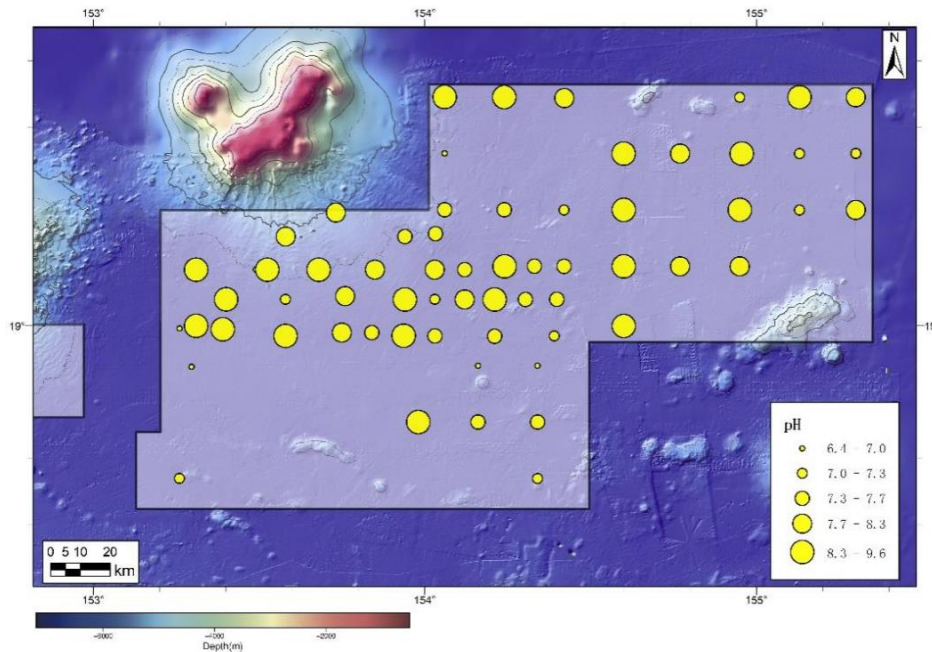
Figure 4-36 Distribution of surface sediments pH in Block M2

4.3.3.2.2 Eh

The Eh of surface sediment from Block M2 ranges from 166 mV to 343 mV. Among these, 84% of stations have Eh ranging from 180 mV to 280 mV, and 34% of stations have Eh ranging from 220 mV to 240 mV (Figure 4-37), indicating that the surface sediments (pore water) in Block M2 exhibit relatively high oxidative conditions, which are favorable for the growth of polymetallic nodules. The high value areas (>245 mV) are mainly distributed within the landslide fan in the northwest, decreasing as the distance from the landslide increases. The medium-value areas (225–245 mV) are distributed in most areas except the eastern part, including the entire western and central plains. The low value areas (<225 mV) are located in the eastern deep-sea plain, occasionally appearing near the western boundary (Figure 4-38).
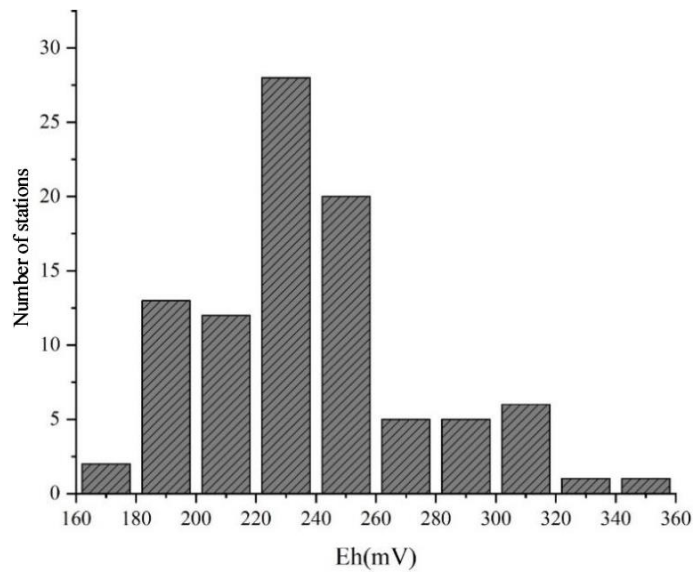
Figure 4-37 Histogram of Eh of surface sediments in Block M2
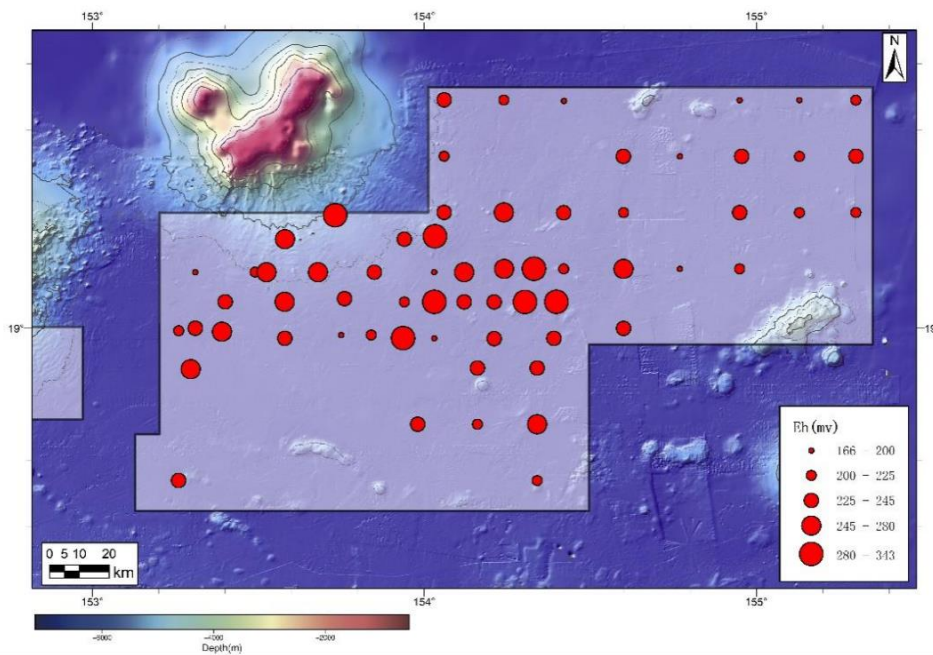
Figure 4-38 Distribution of surface sediment Eh in Block M2

4.3.3.3 Sediment Clay Mineral Composition Characterization

Short piston sediment samples from five stations, identical to those used for sediment grain size analysis, were subjected to clay mineral composition analysis. The positions of the 5 stations are shown in Figure 4-29.

The XRD analysis results of 51 sediment samples from 5 short piston show that the illite, chlorite, kaolinite, and montmorillonite contents ranged from 59% to 77% (mean70.35%), 12% to 30% (mean 17%), 3% to 10% (mean 6%), and 1% to 22% (mean7%), respectively. The montmorillonite/illite (M/I) ratios, illite index, and illite/kaolinite (I/K) ratios ranged from 0.02 to 0.35 (mean 0.10), 0.16 to 0.49 (mean 0.24), and 5.80 to 20.84 (mean 12.13), respectively. The compositions of the clay mineral content of the five piston samples are shown in Table 4-10.

Table 4-10 Clay Mineral content statistics in sediment column samples

	Clay	DY69-M2B1-ES01-BC25	DY69-M2B1-ES02-BC22	DY69-M2B1-ES03-MC02	DY69-M2-ES04-BC09	DY69-M1-ES06-BC17
Illite	Average (%)	71	72	71	74	65
	Maximum value (%)	76	74	73	77	76
	Minimum (%)	66	70	68	71	59
Chlorite	Average (%)	17	18	16	17	16
	Maximum value (%)	22	19	18	19	30
	Minimum (%)	13	15	15	15	12
Kaolinite	Average (%)	6	6	6	6	5
	Maximum value (%)	8	7	7	7	10
	Minimum (%)	4	6	3	5	4
Montmorillonite	Average (%)	6	4	7	3	14
	Maximum value (%)	7	7	11	3	22
	Minimum (%)	4	2	3	2	1
Illite Index	average value	23	26	23	23	23
	maximum values	25	37	28	28	49
	minimum value	19	17	20	18	16
M/I	average value	9	6	10	4	22
	maximum values	10	10	15	5	35
	minimum value	6	3	4	3	2
I/K	average value	11	12	13	12	13
	maximum values	17	13	21	14	20
	minimum value	9	10	10	10	6

The composition and variation of clay minerals in marine sediments record information such as transportation, redeposition, and environmental evolution. They are of great importance for the study of marine sedimentation processes, sedimentary environments, and material sources. The M/I ratio reflects volcanic alteration origin and the relative proportions of authigenic and terrigenous clays. It can be considered as an "authigenic index" of clay minerals. A smaller M/I ratio indicates a higher content of terrigenous clays and a lower

content of volcanic alteration source clays, while a larger M/I ratio indicates the opposite. The average content of montmorillonite in sediments from Block M2 is only 7%, which is obviously lower than that of illite (average content of 70.35%), and the M/I ratio is 0.10, which is obviously lower than those of the North Atlantic (0.29) and South Atlantic (0.55) sediments. Previous studies have indicated that clay minerals in the Atlantic Ocean are mostly terrigenous clays (Chamley, 1989), suggesting that the material source of clay minerals in sediment from Block M is predominantly terrigenous.

Generally, illite is the most stable phase among clay minerals and is a typical weathering product that can form under different climatic conditions and alkaline environments. Studies have shown that illite in the ocean primarily originates from land, with rivers and wind being the main transport ways (Yu et al., 1984). Block M is far away from the continent, with relatively little influence from inland rivers. Additionally, the North Equatorial Current and the mid-depth waters of the North Pacific flow from east to west, coupled with the influence of near-shore currents, island arcs, trenches, and Seamount chains, it is difficult for the sediments from the West Philippine Sea and the Parece Vela Basin to be transported to the study area by ocean currents. Therefore, illite in Block M is likely mainly transported by wind. The surrounding continents of Block M are mainly Asia, Australia, and America, with Asia being the closest. The I/K ratios of sediments from range from Australia, America and Asia range from 0.8 to 1.9 (Gingele et al., 2001), 1.1 to 3.5 in (Leinen et al., 1994), and 1 to 22 in (Arnold et al., 1998), respectively. The I/K ratio of Block M varies from 5.80 to 20.84 (mean 12.13), which is much larger than that of Australia and the Americas sediments and closest to that of Asia sediment. Therefore, it can be inferred that the primary source of illite in sediment from Block M is Asian dust.

By averaging the clay content data of each piston from five stations, a distribution map of clay minerals (average content) of five stations can be drawn (see Figure 4-39): the content of montmorillonite in the foothill area of Block M is slightly higher, while the content of illite in the plain area is slightly higher, indicating that sediment in the foothill area receives more material (montmorillonite) from seamounts.
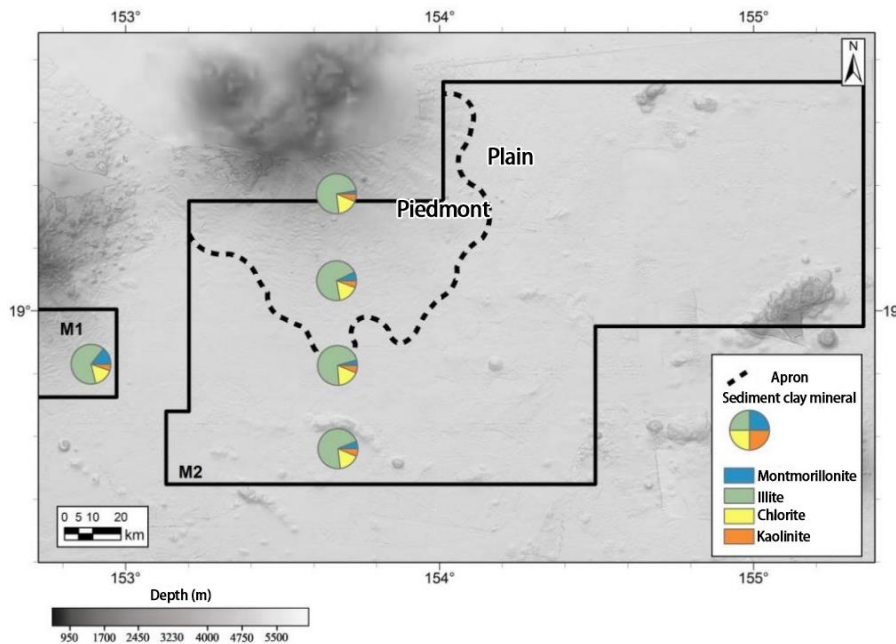
Figure 4-39 Short piston sediment clay mineral (average content) distribution map

The vertical variations of clay mineral contents in the short piston sediment samples of five stations are shown in Figure 4-40–Figure 4-44. The montmorillonite content in the short column samples at Station DY69-M2-ES04-BC09 ranged from 2% to 3% (mean 3%), and the M/I ratios ranged from 0.03 to 0.05 (mean 0.04), which was the lowest value among the five stations. The vertical variation characteristics are also different from the other four stations. Specifically, in the upper sediment layers (0–15 cm), there is an oscillatory increase in montmorillonite content and M/I ratio from bottom to top, while the lower sediment layers show no obvious changes. This difference is likely related to the location of this station, which is the shallowest (4843 m) and closest to the seamount among the five stations. The strong bottom water dynamics at this station are not conducive to the deposition of sediment with high montmorillonite content carried by the Lower Circumpolar Deep Water (LCDW). Therefore, the primary source of montmorillonite at this station is likely volcanic weathering material from the Magoshichi Guyot.

In the Stations DY69-M2B1-ES03-MC02 and DY69-M2B1-ES02-BC22, the variation trends of montmorillonite contents and M/I ratios in the upper sediment layers are similar. They gradually decrease from bottom to top and exhibit two peaks. The lower sediment layers show no obvious changes. However, this variation trend in the sediment from Station DY69-M2B1-ES02-BC22 (0–35 cm) is much thicker than that in Station DY69-M2B1-ES03-MC02

(0-15 cm). This difference is likely related to the water depth of the two stations. Station DY69-M2B1-ES03-MC02 is relatively shallow (5576 m), with stronger bottom water dynamics and lower sedimentation rates, while Station DY69-M2B1-ES02-BC22 is relatively deep (5650 m), with weaker bottom water dynamics and higher sedimentation rates. Although the Station DY69-M2B1-ES01-BC25 is also located in a deep-water basin (5645 m), its vertical variation characteristics of clay mineral content in short piston sediments are obviously different from the Station DY69-M2B1-ES02-BC22. Specifically, in the upper sediment layers (0–6 cm), there is a gradual increase in montmorillonite content and M/I ratio from bottom to top, while the lower sediment layers show no clear trend. This difference is likely related to the development of a small seamount chain in the northern part of this station. The volcanic weathering material from this seamount chain may be one of the main sources of montmorillonite at this station. The Station DY69-M1-ES06-BC17 is located on the southern slope of the Matsuzaki Guyo in Block M1, with a depth of 5528 m, similar to the relative position to the seamount as Station DY69-M2B1-ES02-BC22. The vertical variation of clay mineral content in short piston sediments at this station is also similar to Station DY69-M2B1-ES02-BC22, where montmorillonite content and M/I ratio gradually decrease in the upper sediment layers (0–15 cm), while the lower sediment layers show no obvious changes.
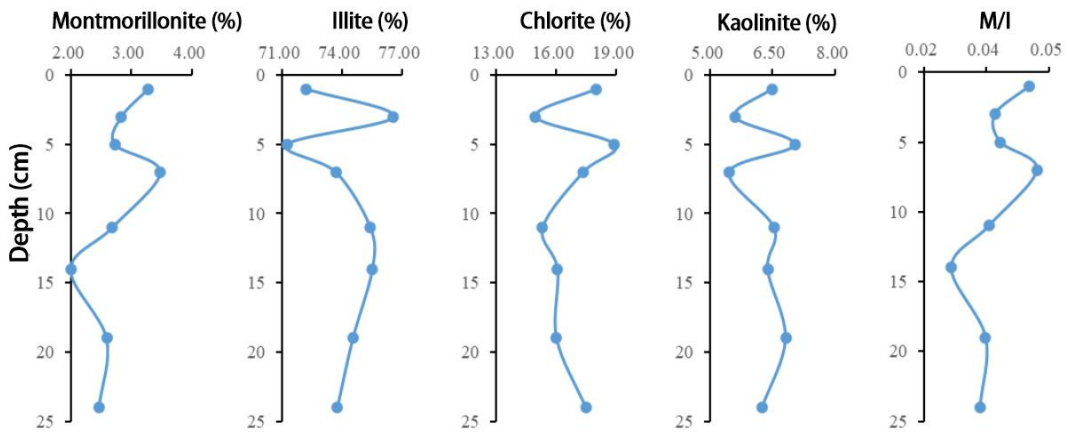
Figure 4-40 Vertical variation of clay mineral contents of short piston samples from Station DY69-M2-ES04-BC09
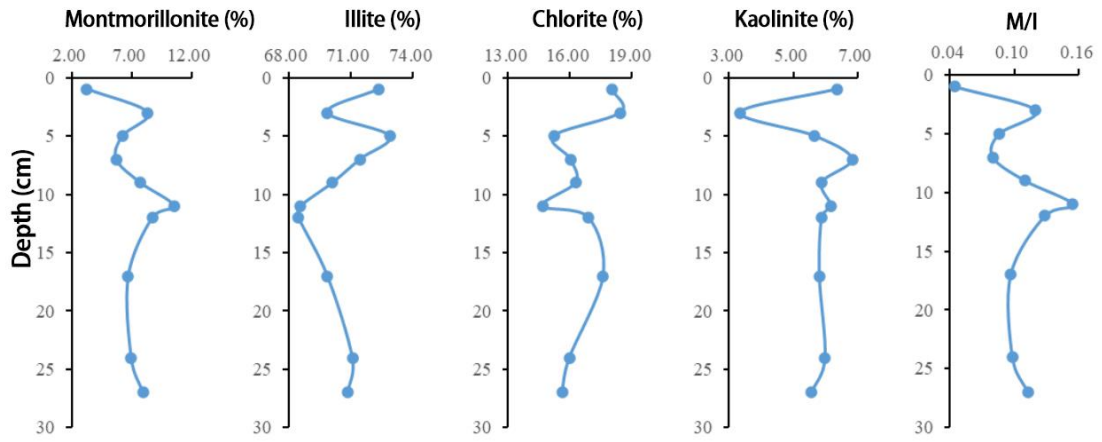
Figure 4-41 Vertical variation of clay mineral contents of short piston samples from Station DY69-M2B1-ES03-MC02
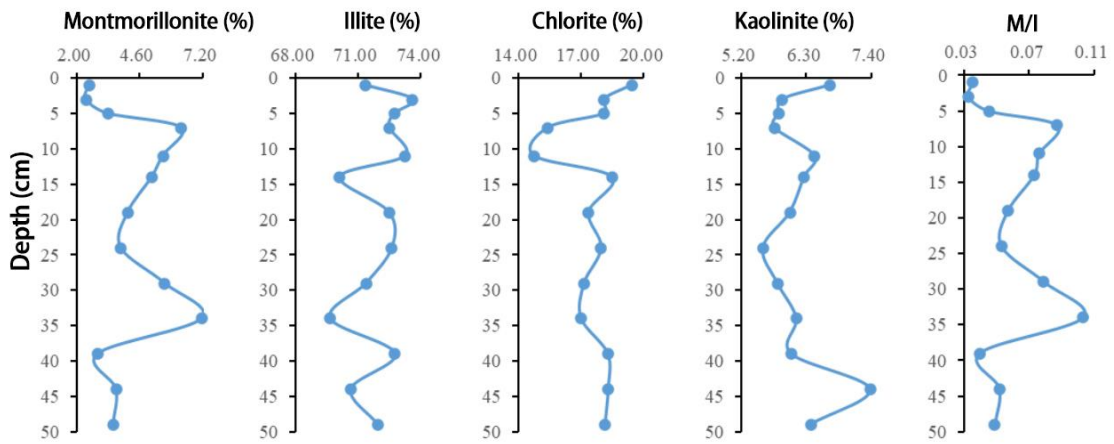
Figure 4-42 Vertical variation of clay mineral contents of short piston samples from Station DY69-M2B1-ES02-BC22
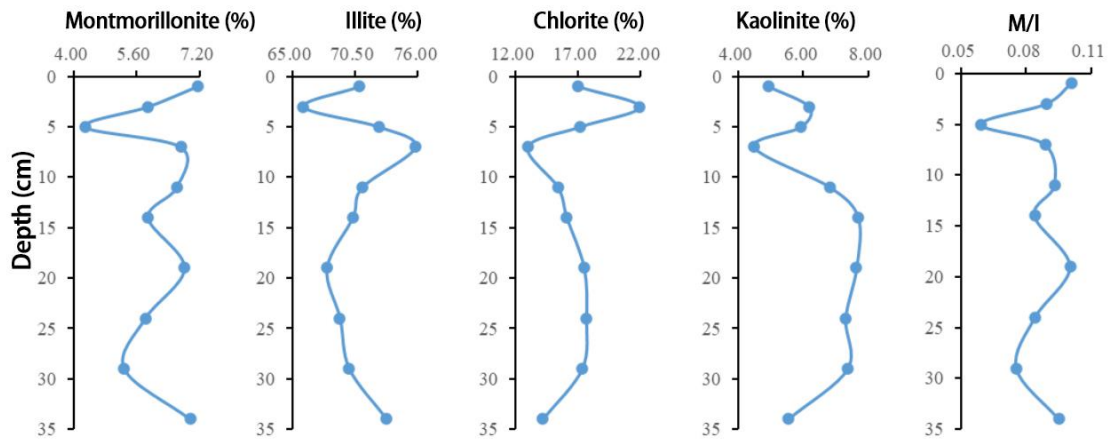
Figure 4-43 Vertical variation of clay mineral contents of short piston samples from Station DY69-M2B1-ES01-BC25
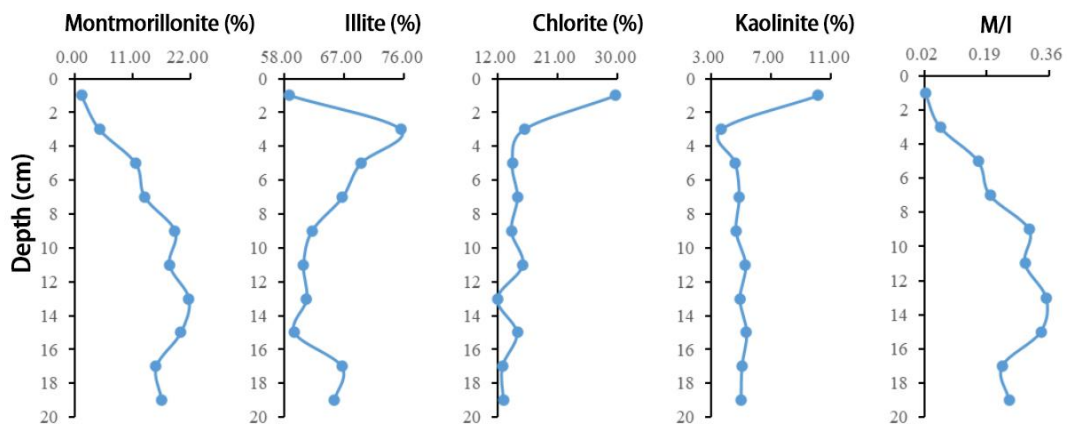
Figure 4-44 Vertical variation of clay mineral contents of short piston samples from Station DY69-M1-ES06-BC17

4.3.3.4 Geochemistry of Sediments

4.3.3.4.1 Major Elements

（1）Surface distribution

There are four main sources of major elements in Pacific pelagic sediments, namely, Pacific deep-sea clays (with complex sources, including continental margins and a small number of volcanic sources), volcanic debris, biologic debris and autochthonous sources. In pelagic sediments, Al_2O_3 plays a "dilution effect" on other elements. therefore, the ratio of other oxides to Al_2O_3 (standard value) can effectively reflect the composition and source

characteristics of sediments. Among them, the Pacific deep-sea clay PPC values (SiO_2/Al_2O_3=3.3, Fe_2O_3/Al_2O_3=0.46, TiO_2/Al_2O_3=0.05) representing terrestrial properties, the Pacific MORB APT values (SiO_2/Al_2O_3=2.97, Fe_2O_3/Al_2O_3=0.55, TiO_2/Al_2O_3=0.09) representing volcanic debris characteristics, and the composition of SS within 400 meters of the bottom (SiO_2/Al_2O_3=7.63, Fe_2O_3/Al_2O_3=1.18, TiO_2/Al_2O_3=0.11) are widely used (Engel, 1965; Bischoff, 1979; Zhang et al. 1994; Han et al. 1997; Yang, 2008).

The surface sediment samples from 110 stations collected during the DY69 and DY75 cruises were analyzed for the major and trace elements contents and calculated the SiO_2/Al_2O_3, Fe_2O_3/Al_2O_3, and TiO_2/Al_2O_3 ratios (Table 4-11 and Figure 4-45). Only two stations in Block M, DY75I-M2-BC40 and DY75II-M1-BC83, were particularly distinctive. At Station DY75I-M2-BC40, the SiO_2/Al_2O_3 ratio exhibited an unusually high value (9.83), Fe_2O_3/Al_2O_3 was 0.53, and TiO_2/Al_2O_3 was 0.06. Combined with smear slide identification results, sediment at this station contained abundant biogenic siliceous debris, with the exceptionally high SiO2 (67.64%) likely influenced by the input of abundant biogenic materials. At DY75II-M1-BC83, the Fe_2O_3/Al_2O_3 ratio exhibited an unusually high value (1.32), SiO_2/Al_2O_3 ratio was unusually low (2.61), and TiO_2/Al_2O_3 was unusually high (0.09). Combined with smear slide identification results, surface sediment at this station was calcareous ooze, with the exceptionally high CaO (51.56%) primarily derived from biogenic calcareous debris. The SiO_2/Al_2O_3, Fe_2O_3/Al_2O_3, and TiO_2/Al_2O_3 ratios of the surface sediment at the rest of stations in Block M are in the range of 2.94–3.75 (mean 3.20), 0.47–0.60 (mean 0.51), and 0.05–0.06 (mean 0.05), indicating that the type of surface sediment in Block M is dominated by deep-sea clays of terrestrial origin nature, and are influenced by inputs of volcanic and biogenic materials.

Table 4-11 Major elements compositions of surface sediments from Block M

	Average (%)	Maximum (%)	Minimum (%)	DY75I-M2-BC40	DY75II-M1-BC83
Al_2O_3	16.46	17.64	14.85	6.88	0.42
CaO	1.88	3.27	1.37	0.90	51.56
Fe_2O_3	8.34	9.62	7.08	3.63	0.55
K_2O	3.10	3.47	2.50	1.67	0.12
MgO	3.43	3.62	2.68	2.11	0.49
MnO	0.77	2.66	0.46	0.26	0.10
Na_2O	4.12	5.32	2.67	6.40	1.70
P_2O_5	0.31	0.71	0.22	0.09	0.05
SiO_2	52.56	56.21	49.52	67.64	1.10
TiO_2	0.88	1.04	0.80	0.39	0.04
SiO_2/Al_2O_3	3.20	3.75	2.94	9.83	2.61
Fe_2O_3/Al_2O_3	0.51	0.60	0.47	0.53	1.32
TiO_2/Al_2O_3	0.05	0.06	0.05	0.06	0.09
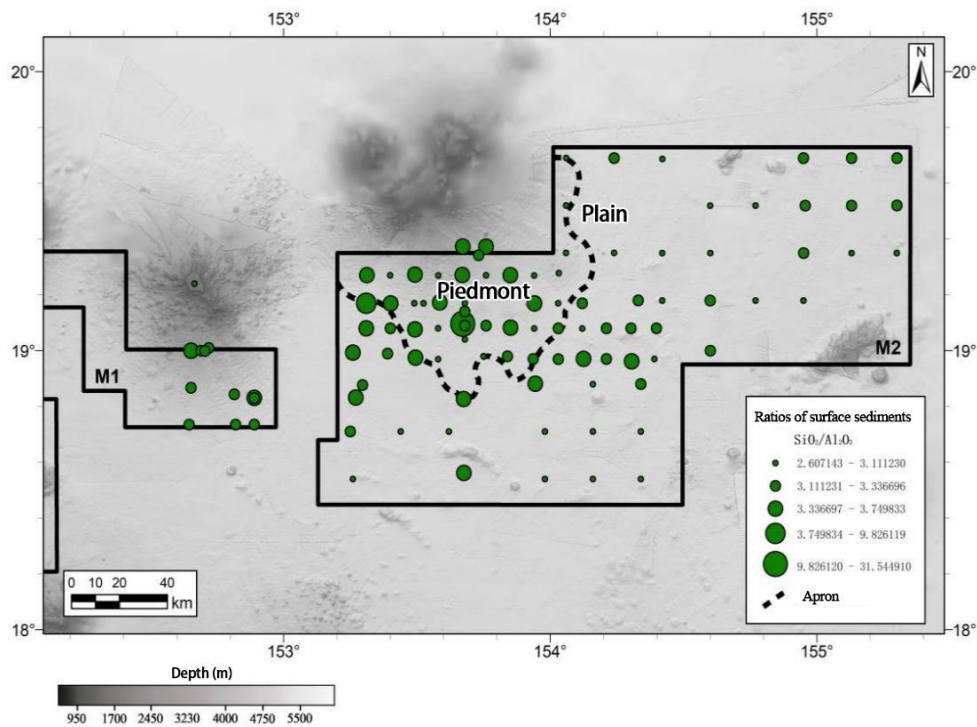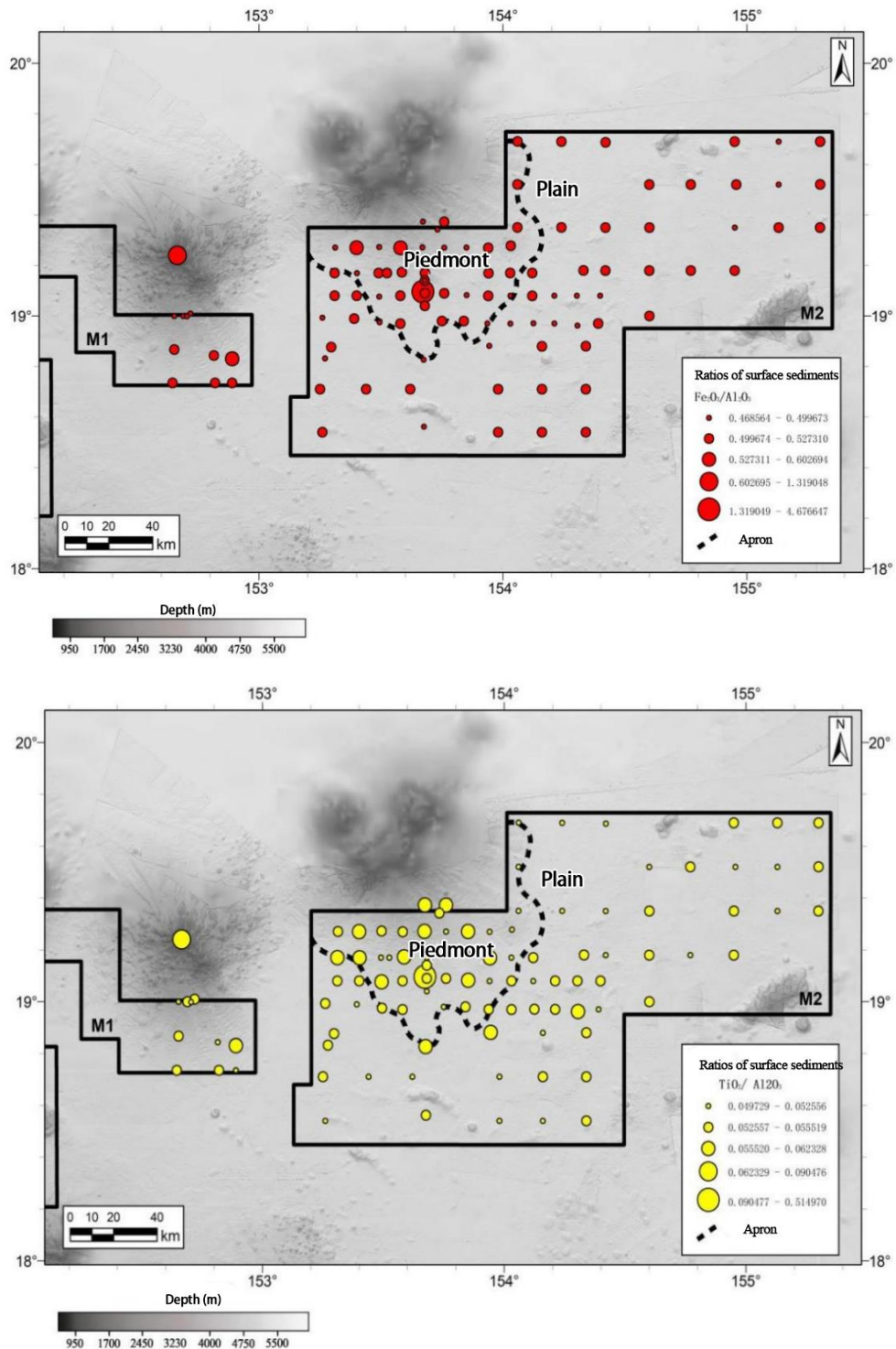
Figure 4-45 Distribution of SiO$_2$ /Al$_2$O$_3$, Fe$_2$O$_3$ /Al$_2$O$_3$, and TiO$_2$ / Al$_2$O$_3$ ratios of surface sediments

Factor analysis (principal component analysis of covariance) of the major elements using Stats software yielded that the variance contributions of the first four factors were

40.0%, 17.2%, 14.8%, and 8.9%, respectively, with a cumulative contribution of 80.9% (Table 4-12). Based on the loadings of each element on the four main factors, factor F1 is correlated with Al_2O_3, Fe_2O_3, Na_2O, MgO, K_2O, SiO_2, and TiO_2, factor F2 is correlated with MnO, Fe_2O_3, and TiO_2, factor F3 is primarily associated with CaO, and P_2O_5, and factor F4 is mainly correlated with changes in SiO_2 content (see Table 4-13). Based on the results of the analysis above, it can be seen that the type of surface sediments in Block M is dominated by deep-sea clays of terrestrial origin, and the main relevant element of main factor F1 is the category of elements related to alumino-silicate rocks, so F1 represents the influence of terrestrial origin material components. The main correlated elements of factor F2 are Mn and Fe, suggesting that it may represent the primary components of micro-nodules in surface sediments, with Ti possibly existing in micro-nodules through adsorption or isomorphic substitution. The main correlated elements of factor F3 are Ca and P, which are the main components of biogenic phosphorite in sediments. Therefore, it is inferred that factor F3 represents biogenic phosphorite. The main correlated element of factor F4 is Si, and according to the analysis above, besides being of continental origin, biogenic Si is also an important source in Block M sediments, thus factor F4 is inferred to represent biogenic siliceous debris.

Table 4-12 Total variance

Composition	Initial Eigenvalues			Extract the sum of squares and load			Rotate the sum of squares to load		
	Total	Variance (%)	Cumulative (%)	Total	Variance (%)	Cumulative (%)	Total	Variance (%)	Cumulative (%)
1	4.005	40.045	40.045	4.005	40.045	40.045	3.407	34.069	34.069
2	1.718	17.178	57.223	1.718	17.178	57.223	1.741	17.409	51.477
3	1.483	14.828	72.051	1.483	14.828	72.051	1.524	15.242	66.720
4	0.889	8.886	80.937	.889	8.886	80.937	1.422	14.217	80.937
5	0.694	6.945	87.882						
6	0.564	5.642	93.524						
7	0.266	2.660	96.184						
8	0.196	1.956	98.139						
9	0.128	1.282	99.421						
10	0.058	0.579	100.000						

Table 4-13 Post-rotation factor loading matrix

	Component			
	F1	**F2**	**F3**	**F4**
Al_2O_3	0.708	−0.136	0.117	−0.033
CaO	0.013	−0.165	0.893	−0.181
Fe_2O_3	0.792	0.425	0.262	0.130
K_2O	0.931	0.093	−0.037	0.082
MgO	0.877	0.073	−0.125	0.095
MnO	0.010	0.900	0.030	0.090
Na_2O	0.945	0.008	0.098	−0.028
P_2O_5	0.087	0.419	0.763	0.068
SiO_2	−0.680	−0.519	−0.189	0.311
TiO_2	0.411	0.496	−0.008	0.221

（2）Vertical distribution

Short piston sediment samples from the same five stations (layers) as in the sediment grain size and clay mineral analysis were selected for major element contents analysis.

There is a trend of increasing SiO_2 /Al_2O_3 ratio from bottom to top in the short piston sediments, representing the dissolution process of biogenic siliceous debris. In Station DY69-M2B1-ES03-MC02, the SiO_2 /Al_2O_3 ratio is obviously different from the other four stations. In the upper sediment layer (0–6 cm), the SiO_2 /Al_2O_3 ratio is less than 3.3 (PPC value), suggesting that the sediment flux of biogenic siliceous debris near this station is relatively smaller than that of other stations. This is consistent with the smear slide identification results of surface sediment at Station DY69-M2B1-ES03-MC02, indicating that the content of biogenic siliceous debris in the surface sediment at this station is lower than that at other stations.
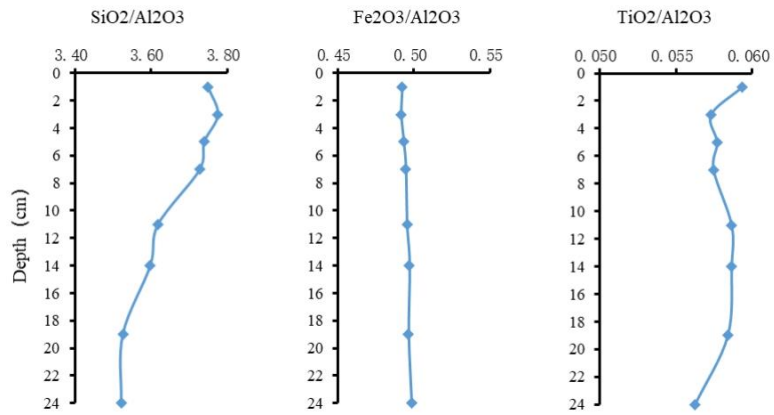
Figure 4-46 Vertical variations of SiO$_2$/Al$_2$O$_3$, Fe$_2$O$_3$/Al$_2$O$_3$ and TiO$_2$/ Al$_2$O$_3$ ratios of sediments from Station DY69-M2-ES04-BC09
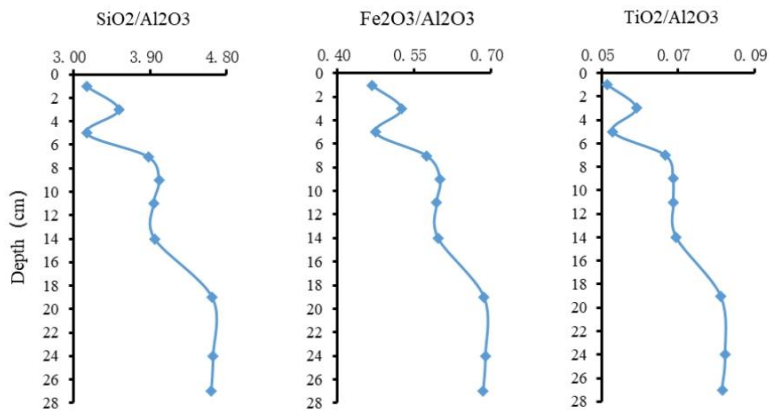
Figure 4-47 Vertical variation of SiO$_2$ /Al$_2$O$_3$, Fe$_2$O$_3$ /Al$_2$O$_3$, TiO$_2$/ Al$_2$O$_3$ ratios of sediments from Station DY69-M2B1-ES03-MC02
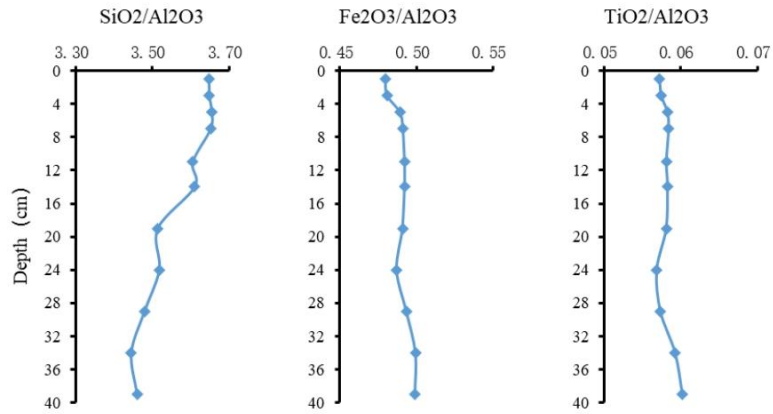
Figure 4-48 Vertical variation of SiO_2/Al_2O_3, Fe_2O_3/Al_2O_3, TiO_2/Al_2O_3 ratios of sediments from Station DY69-M2B1-ES02-BC22
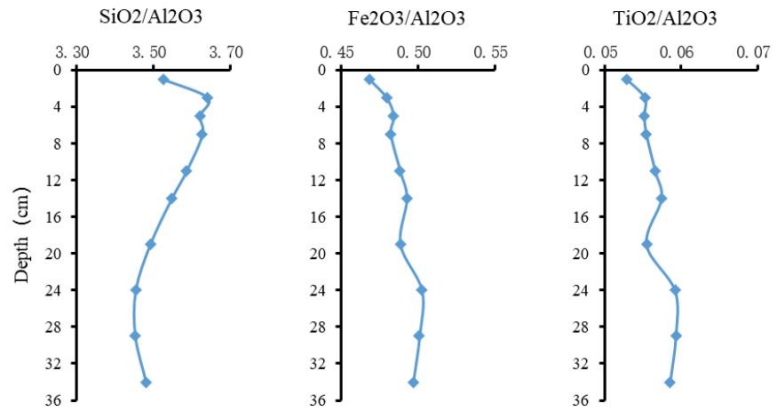
Figure 4-49 Vertical variation of SiO_2/Al_2O_3, Fe_2O_3/Al_2O_3, TiO_2/Al_2O_3 ratios of sediments from Station DY69-M2B1-ES01-BC25
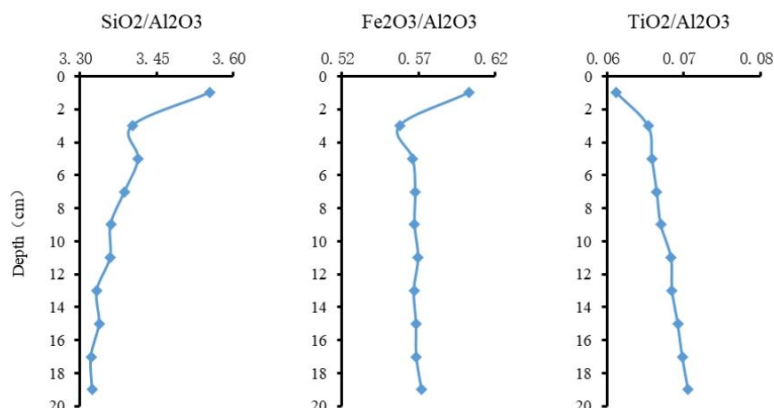
Figure 4-50 Vertical variation of SiO_2 /Al_2O_3, Fe_2O_3 /Al_2O_3, TiO_2 / Al_2O_3 ratios of sediments from Station DY69-M1-ES06-BC17

4.3.3.4.2 Trace Element

The trace element contents and statistical characteristics of 20 stations of surface sediments and 5 stations of short core sediment samples from Block M are shown in Table 4-14.

Apart from Co, Ni, Cu, Zn, and Ba, the differences in the content of other elements between surface sediments and core samples are relatively small. In the core sample DY69-M1-ES06-BC17, the content of Co, Ni, Cu, and Zn is obviously higher than that in surface sediments and the other 4 core samples, while the content of Ba is notably lower than that in surface sediments and the other 4 core samples (Figure 4-51). Elements such as Co, Ni, Cu, and Zn are predominantly found in iron-manganese nodules, while Ba is of biological origin. Since the core sample DY69-M1-ES06-BC17 represents partially consolidated sediment, the sediment characteristics at this station are markedly different from those at other stations, indicating that the sediment at this station formed in a different age compared to other stations. During the formation period of the sediment layer at Station DY69-M1-ES06-BC17, the geological environment of this station caused elements such as Co, Ni, Cu, and Zn to precipitate from seawater into the sediment, and the biomass at this station was relatively low during that period, leading to a lower Ba content compared to current biological production levels.

Table 4-14 Statistics of trace element contents in Block M

Trace element	Minimum (μg/g)	Maximum (μg/g)	Average (μg/g)	Variance (statistics)	Standard deviation	Variation ratio
Li (3)	41	61	54	14	4	0.07
Be (4)	2	3	2	0	0	0.07
Sc (21)	20	26	22	2	1	0.06
V (23)	150	185	164	50	7	0.04
Cr (24)	60	97	85	41	6	0.08
Co (27)	67	140	99	352	19	0.19
Ni (28)	106	406	176	7306	85	0.49
Cu (29)	176	397	246	3637	60	0.25
Zn (30)	130	208	150	243	16	0.10
Ga (31)	16	23	21	1	1	0.05
Ge (32)	1	2	2	0	0	0.06
As (33)	13	24	17	10	3	0.18
Rb (37)	77	130	113	98	10	0.09
Sr (38)	177	227	199	123	11	0.06
Zr (40)	159	198	174	83	9	0.05
Nb (41)	11	25	14	6	2	0.17
Mo (42)	4	18	7	11	3	0.46
Cd (48)	0	0	0	0	0	0.15
In (49)	0	0	0	0	0	0.09
Sb (51)	1	3	2	0	1	0.31
Cs (55)	7	16	11	2	2	0.14
Ba (56)	350	1917	1227	193241	440	0.36
Hf (72)	5	8	6	0	1	0.11
Ta (73)	1	1	1	0	0	0.16
W (74)	3	8	5	1	1	0.24
Hg (80)	0	0	0	0	0	0.61
Tl (81)	1	3	2	0	0	0.14
Pb (82)	25	60	36	36	6	0.17
Bi (83)	0	1	1	0	0	0.16
Th (90)	7	12	9	1	1	0.11
U (92)	2	2	2	0	0	0.06
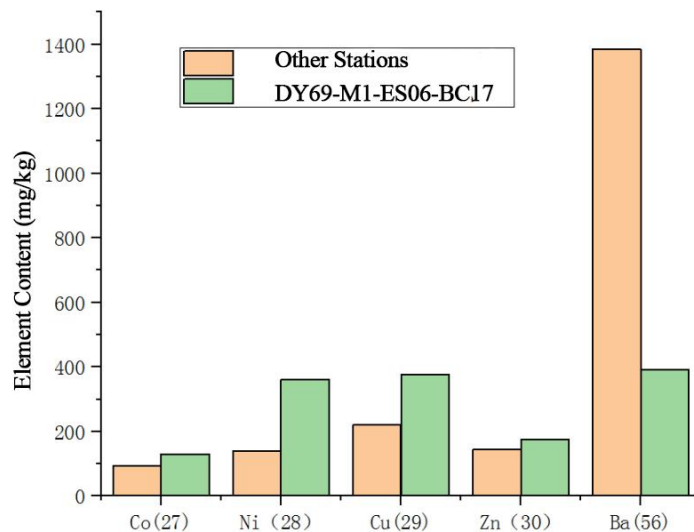
Figure 4-51 Trace element content in the core sample DY69-M1-ES06-BC17 compared with other stations.

4.3.3.4.3 Rare Earth Elements

The total rare earth element and yttrium content ($\sum$REY) in Block M sediments ranged from 53×10^{-6} –599.39×10^{-6}, with a mean value of 332×10^{-6}, which was slightly higher than that of Pacific deep-sea clays ($\sum$REY= 274×10^{-6}). In the average Post-Archaean Australian Sedimentary Rock (PAAS)-normalized REY patterns (Figure 4-52), the surface sediments at all stations in Block M show negative anomalies of Ce and positive anomalies of Eu, which are similar to those of the Central Pacific sediments.
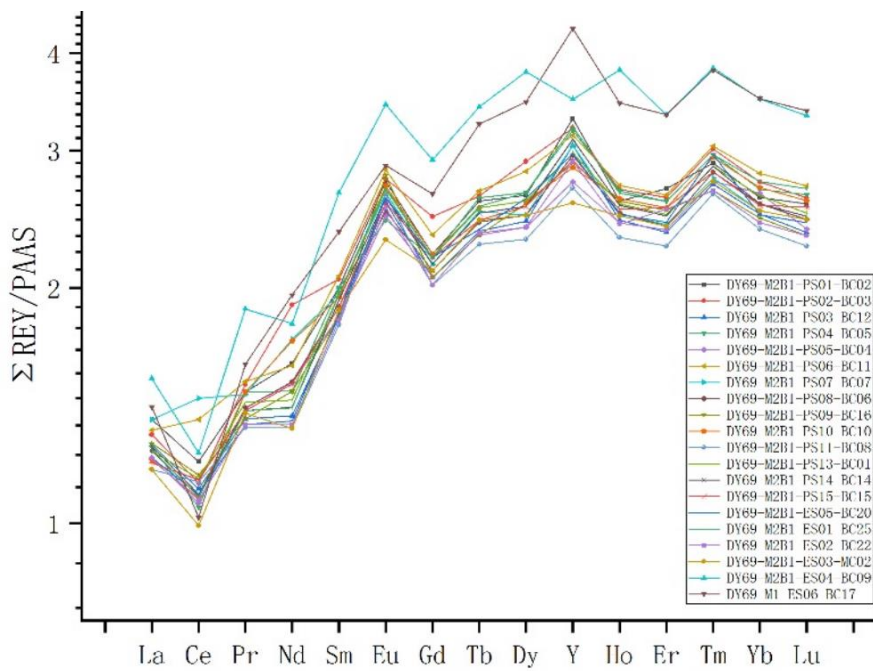
Figure 4-52 PAAS-normalized REY patterns of sediments from Block M

Correlation analysis of the ∑REY and the major elements of the sediments shows that ∑REY has a strong positive correlation with the P (r=0.85), and a positive correlation with the Fe (r=0.70) and Mn (r=0.47) (Figures 4-53–4-55). Therefore, it can be inferred that the REY in the sediments from Block M is primarily associated with biogenic phosphorite and micro-nodules.
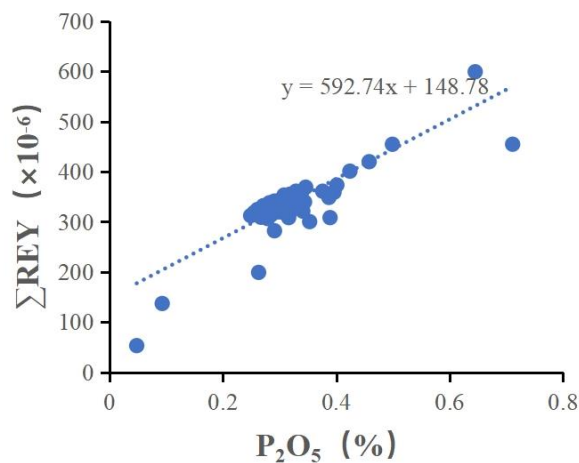
Figure 4-53 Correlation of rare earth element content ($\sum$ REY) with P_2O_5
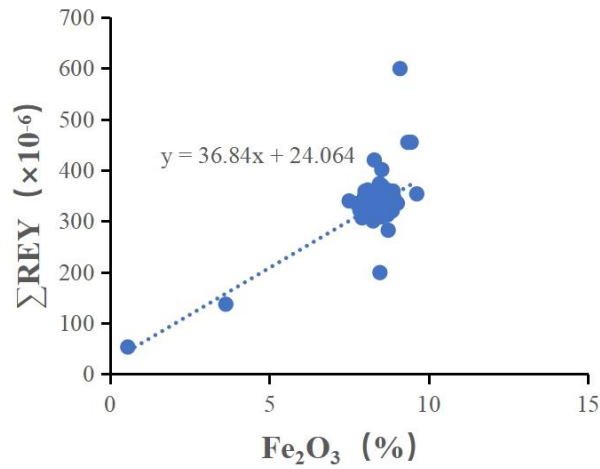
Figure 4-54 Correlation between rare earth element content (Σ REY) and Fe_2O_3
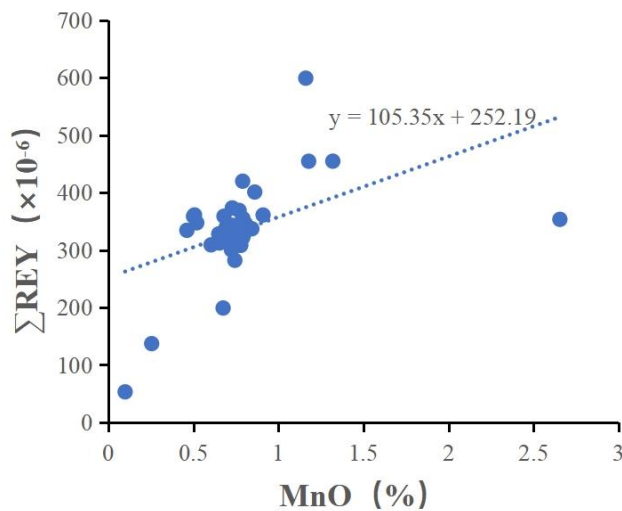
Figure 4-55 Correlation between rare earth element content (Σ REY) and MnO

4.3.3.4.4 Sediment Organic Carbon

The results of organic carbon analysis on short core sediments from six stations during the DY69 cruise show that the organic carbon content in the region ranges from 0.25% to 0.99%, with an average of 0.54%. The average organic carbon content in surface sediments (0–1 cm) is 0.71%, with organic matter content gradually decreasing with depth (Figure 4-56). The average value of organic carbon did not vary much between stations, ranging from 0.40% to 0.66%.
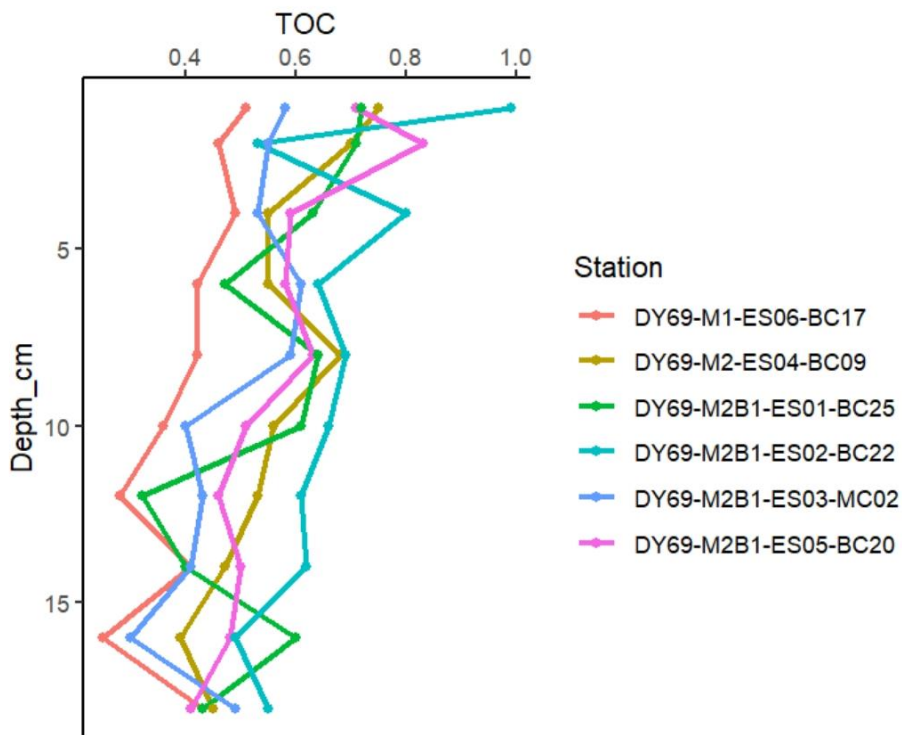
Figure 4-56 Vertical variation in sediment total organic carbon TOC (%) distribution

4.3.3.5 Sediment Pore Water

4.3.3.5.1 Pore Water Metal Contents Analysis

Short core sediments collected from six stations in Block M during the cruise DY69 (2021) were selected for pore water metal contents analysis. After extracting pore water from sediment samples at various layers, main metal contents analysis was conducted. The main metal contents in pore water samples are shown in Table 4-15, and their vertical distribution is depicted in Figure 4-57. The results indicate that there is no clear pattern in the vertical distribution of metal contents in pore water, and the magnitude of variation is obvious. The order of variation magnitude is as follows: Cu (108%) > Mn (80.6%) > Pb (73.9%) > Zn (69.2%) > Fe (63.1%) > Co (60.6%) > Cd (46.9%).

Table 4-15 Major metal contents in pore water samples (Unit: µg/L)

		Cd	Co	Cu	Fe	Mn	Pb	Zn
DY69-M2-ES04-BC09	Minimum	0.496	0.576	0.548	7.16	9.42	1.99	51.2
	Maximum	1.64	1.90	16.7	25.9	67.4	5.08	287
	Average	0.807	1.05	5.25	14.2	23.6	3.26	132
	Relative standard deviation (%)	45.6	42.3	99.7	50.0	90.1	36.7	62.7
DY69-M2B1-ES03-MC02	Minimum	0.411	0.600	0.562	7.92	8.87	1.28	71.4
	Maximum	0.582	1.88	8.16	34.7	27.7	4.27	219
	Average	0.510	0.836	4.03	17.2	16.2	2.00	144
	Relative standard deviation (%)	10.6	44.9	74.8	54.9	35.5	43.8	35.3
DY69-M1-ES06-BC17	Minimum	0.368	0.564	0.593	5.91	7.44	1.14	104
	Maximum	0.602	1.21	4.52	18.6	31.2	1.82	180
	Average	0.496	0.709	2.19	10.1	14.8	1.48	135
	Relative standard deviation (%)	14.7	27.9	66.0	41.1	51.7	14.7	18.2
DY69-M2B1-ES05-BC20	Minimum	0.234	0.253	0.209	1.28	2.43	0.537	0.982
	Maximum	0.368	1.64	6.48	27.4	17.6	1.09	21.2
	Average	0.327	0.483	2.42	11.9	8.56	0.788	12.3
	Relative standard deviation (%)	13.7	88.7	86.4	72.9	52.9	25.3	59.8
DY69-M2B1-ES02-BC22	Minimum	0.294	0.289	0.195	8.05	5.95	0.529	56.0
	Maximum	0.394	0.817	3.24	25.9	17.2	2.49	145
	Average	0.346	0.457	1.11	14.2	9.74	0.971	79.8
	Relative standard deviation (%)	9.5	31.8	89.3	38.0	40.8	64.0	31.7
DY69-M2B1-ES01-BC25	Minimum	0.248	0.246	0.124	2.34	5.01	0.358	24.8
	Maximum	0.419	1.72	3.01	9.60	34.5	0.813	81.5
	Average	0.345	0.518	1.57	4.45	10.8	0.573	51.3
	Relative standard deviation (%)	16.2	88.4	72.9	49.8	93.0	25.7	31.2
All stations	Minimum	0.234	0.246	0.124	1.28	2.43	0.358	0.982
	Maximum	1.64	1.90	16.7	34.7	67.4	5.08	287
	Average	0.466	0.669	2.72	12.0	13.8	1.48	91.7
	Relative standard deviation (%)	46.9	60.6	108	63.1	80.6	73.9	69.2
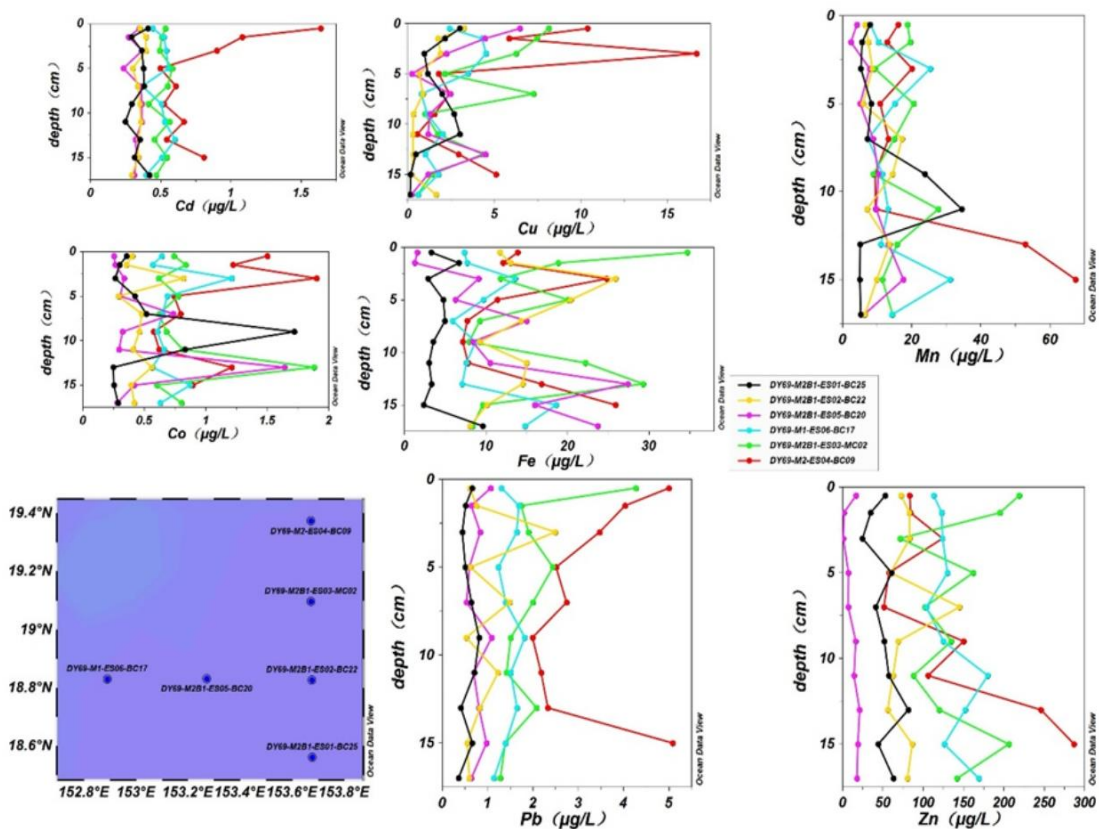
Figure 4-57 Vertical variation of major metal contents in pore water samples

Short core sediments collected from five stations in Block M2 during the DY75 cruise (2022) were selected for pore water metal contents analysis. The main metal contents in pore water are shown in Table 4-16, and their vertical distribution is depicted in Figure 4-58. The results indicate that, among the five stations, pore water from Station DY75I-M2-BC33, located at the foothill, exhibits slightly higher levels of various metal contents compared to the other four stations in the plain area (see Figure 4-58).

Table 4-16 Major metal contents of pore water samples collected in 2022 (Unit: μg/L)

		Cd	Co	Cu	Fe	Mn	Pb	Zn
DY75I-M2-BC20	Minimum	0.26	0.11	0.92	149.3	2.09	1.15	15.53
	Maximum	0.87	0.24	3.25	370.61	5.33	2.85	62.65
	Average	0.46	0.17	1.87	207.39	4.28	1.95	41.58
	Relative standard deviation (%)	46.50	29.40	43.20	35.80	26.50	37.10	46.60
DY75I-M2-BC63	Minimum	0.24	0.08	0.29	150.74	2.4	0.4	6.83
	Maximum	0.41	0.18	4.46	207.72	3.44	1.92	137.56
	Average	0.32	0.12	2.27	183.74	2.92	1.14	46.09
	Relative standard deviation (%)	17.90	24.00	68.30	10.10	11.50	50.30	89.80
DY75I-M2-BC06	Minimum	0.19	0.05	0.53	154.36	1.49	0.06	8.1
	Maximum	0.34	0.27	4.1	319.24	9.42	4.04	45.54
	Average	0.29	0.12	2.03	208.5	4.79	1.34	27.04
	Relative standard deviation (%)	17.40	67.20	61.60	24.50	64.90	89.60	49.20
DY75I-M2-BC33	Minimum	0.24	0.05	0.89	181.58	2.93	1	17.07
	Maximum	0.46	9.44	18.78	355.55	276.57	3.15	122.41
	Average	0.31	1.38	4.61	255.18	43.77	1.51	57.72
	Relative standard deviation (%)	24.20	236.80	131.70	21.50	215.40	46.50	69.90
DY75I-M2-BC44	Minimum	0.17	0.03	0.62	186.49	2.09	0	12.89
	Maximum	0.31	0.38	4.5	444.78	103.88	3.08	34.05
	Average	0.25	0.12	1.81	253	20.54	0.88	24.21
	Relative standard deviation (%)	19.90	89.60	69.20	29.90	182.80	105.20	28.10
All stations	Minimum	0.17	0.03	0.29	149.3	1.49	0	6.83
	Maximum	0.87	9.44	18.78	444.78	276.57	4.04	137.56
	Average	0.32	0.36	2.47	221.86	14.99	1.32	38.18
	Relative standard deviation (%)	36.70	389.60	115.00	27.70	293.30	67.60	75.20
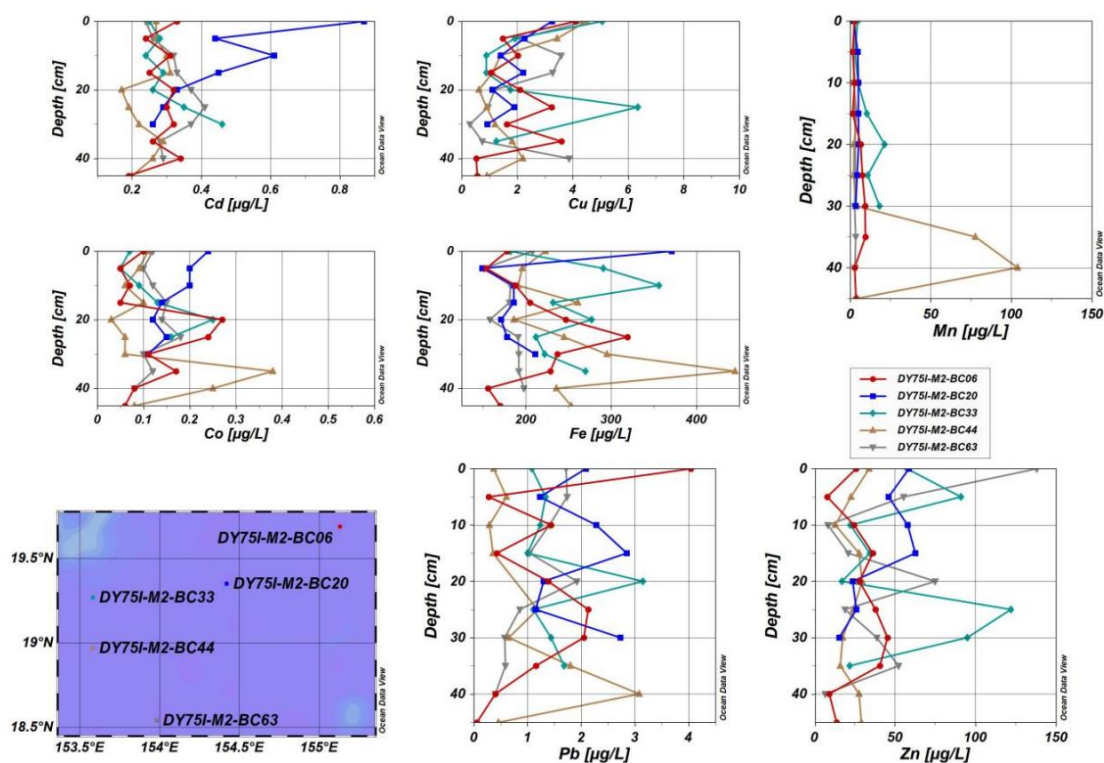
Figure 4-58 Vertical variation of major metal contents in pore water samples collected in 2022

The distribution of metal contents in the pore water of six short core sediments collected during the DY81 cruise (2023) was shown in Figure 4-59. The content of As in the pore water is lower than that of the overlying seawater, Ni and Pb in the pore water are similar to that of the overlying seawater. The content of other metals in the pore waters is always higher than that of the overlying seawater, but most of the samples do not have any order-of-magnitude change from the overlying seawater as well. The content of Co, Zn, Cr, Cd have a tendency to increase with depth, Pb has similar content in all layers, Mn, Fe, Ni, Cu, V, As mostly have an obvious peak in the surface layer, while other layers have very small changes and low content, which indicates that the sediment-seawater interface is the most important interface for the variation of heavy metals. Overall, the thickness of this high value layer of heavy metals is very thin, only ~5 cm for most of the samples, and the absolute values of their contents are still very low.

The content of As in pore water is lower than that in overlying seawater, while the content of Ni and Pb in pore water is similar to that in overlying seawater. The content of other measured metals in pore water tends to be higher than that in overlying seawater, but most samples also do not show orders of magnitude changes compared to overlying seawater.

166

Co, Zn, Cr, and Cd show an increasing trend in content with depth. The content of Pb remains relatively consistent across all depths. Mn, Fe, Ni, Cu, V, and As mostly exhibit a distinct peak in the surface layer, with little variation and lower content in other layers, indicating that the sediment-seawater interface is the primary interface for the variation of heavy metals. However, overall, the thickness of the layer with high values of these heavy metals is very thin, with most samples only around 5 cm thick, and their absolute content values remain low.
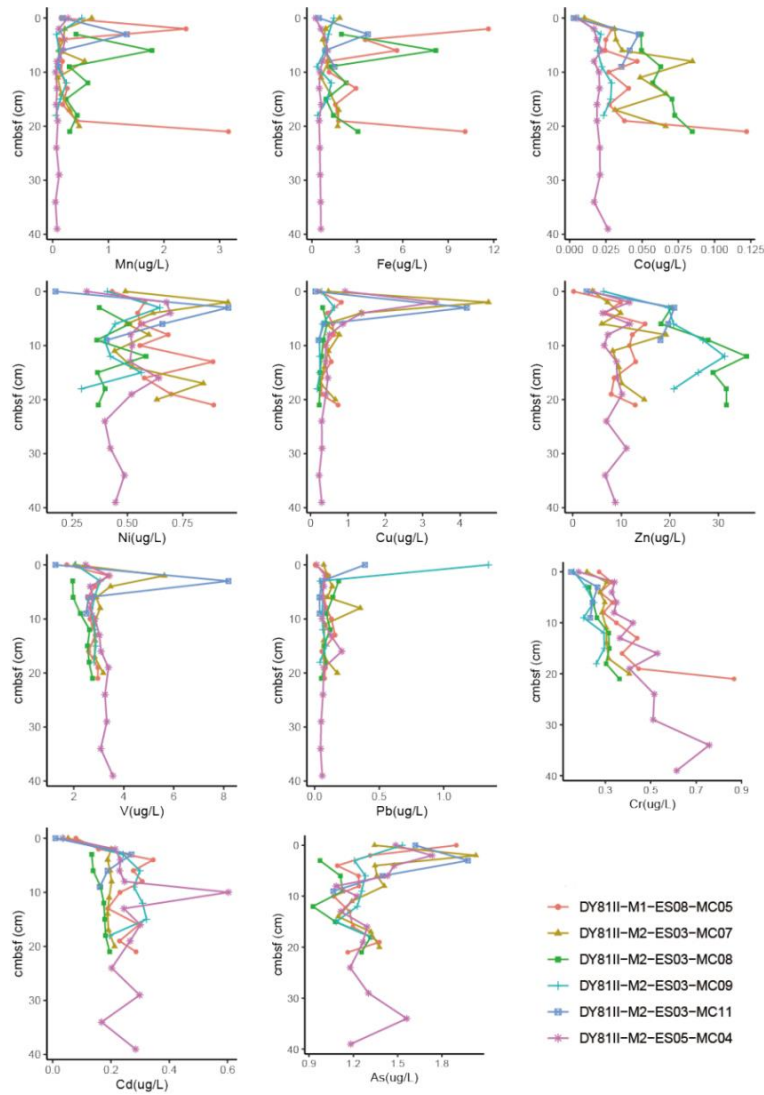
Figure 4-59 Vertical variation of heavy metal contents in pore water samples collected in 2023

(Note: Samples with a depth of 0 are overlying seawater)

4.3.3.5.2 Pore water Nutrient Concentrations

The short cylindrical sediment samples collected from five stations in the working area (Block M2) during the second cruise of the BPC in 2022 (DY75) were used to extract pore water from each sediment layer. Subsequently, testing and analysis of the nutrient components in the pore water were conducted. The concentrations of various nutrients in the pore water are presented in Table 4-17, while their vertical distribution can be observed in Figure 4-60. The analysis results indicate that the overall nutrient concentration in the pore water of the sediment in the working area is relatively low, with no obvious variation in content with depth. This pattern is speculated to be related to the low primary productivity of the overlying seawater in this area.

Table 4-17 Nutrient concentrations in sediment pore water （μmol/L）

		NO_3^-	NH_4^+	NO_2^-	PO_4^{3-}	SiO_2
	Average	0.65	9.91	0.00	4.58	181.62
DY75I-M2-BC33	Minimum	0.53	2.14	0.00	1.90	84.88
	Maximum	0.73	21.42	0.00	8.84	254.65
	Average	0.36	5.93	0.00	6.19	191.07
DY75I-M2-BC44	Minimum	0.32	1.43	0.00	2.74	123.16
	Maximum	0.39	12.85	0.00	10.32	259.64
	Average	0.21	3.67	0.00	5.10	216.61
DY75I-M2-BC20	Minimum	0.10	0.00	0.00	3.16	176.42
	Maximum	0.36	6.43	0.00	6.95	244.66
	Average	0.49	2.86	0.14	7.10	216.37
DY75I-M2-BC63	Minimum	0.11	0.00	0.00	4.63	153.12
	Maximum	0.97	8.57	0.43	10.32	274.62
	Average	0.37	2.86	0.00	5.77	221.03
DY75I-M2-BC06	Minimum	0.29	0.00	0.00	3.37	63.25
	Maximum	0.42	7.14	0.00	8.63	312.90
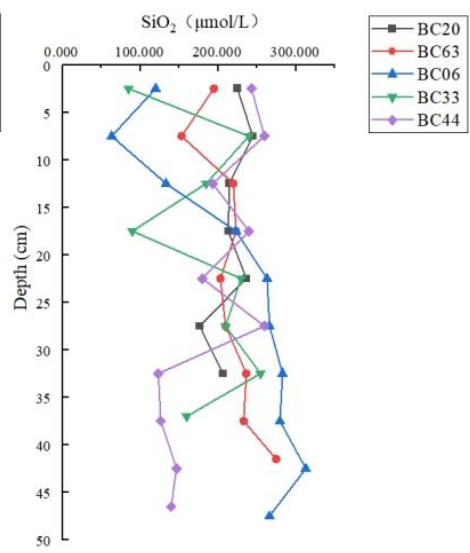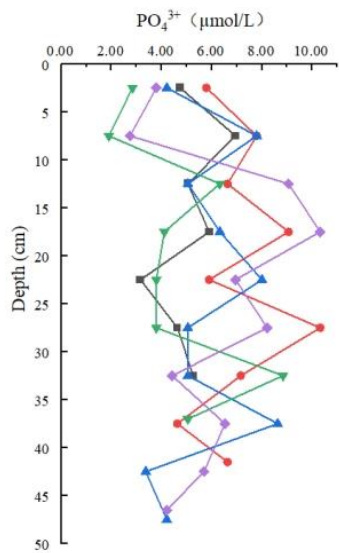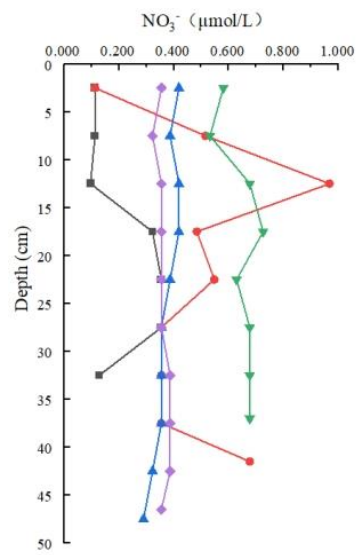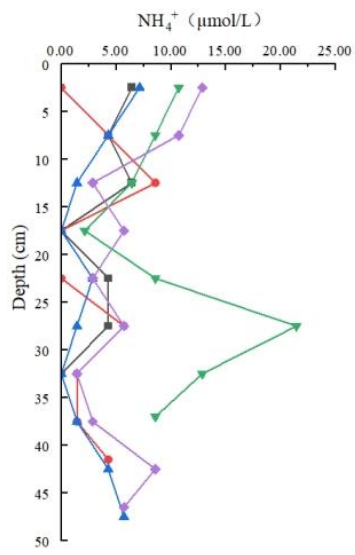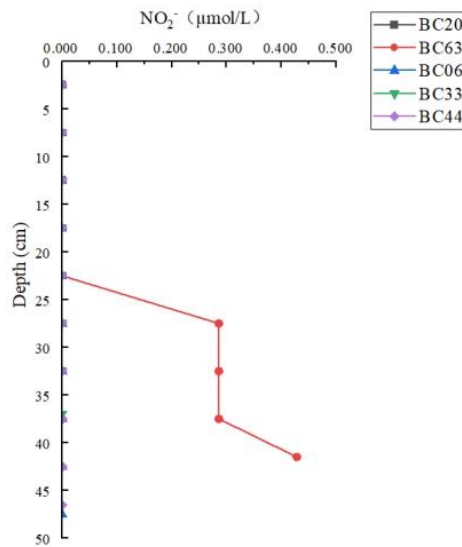
Figure 4-60 Vertical variation diagram of nutrient concentrations in sediment pore water

4.3.3.6 Sediment Geotechnical Mechanics

4.3.3.6.1 Geotechnical Testing of Core Sediments on board

The DY75 cruise (2022) completed the geotechnical testing of 76 stations of box corer and 6 stations of multi-corer sediment samples (0–30 cm) (sediment moisture content, wet density, penetration resistance and shear strength), and the sediment at each station was sampled at a sampling thickness of 5 cm and tested in layers.

Statistical analysis of the penetration strength data for sediments at each station in Block M indicates a similar vertical trend of increasing penetration strength with depth (Figure 4-61).

Similarly, statistical analysis of the shear strength data for sediments at each station in Block M reveals a consistent vertical trend of increasing shear strength with depth (Figure 4-62).
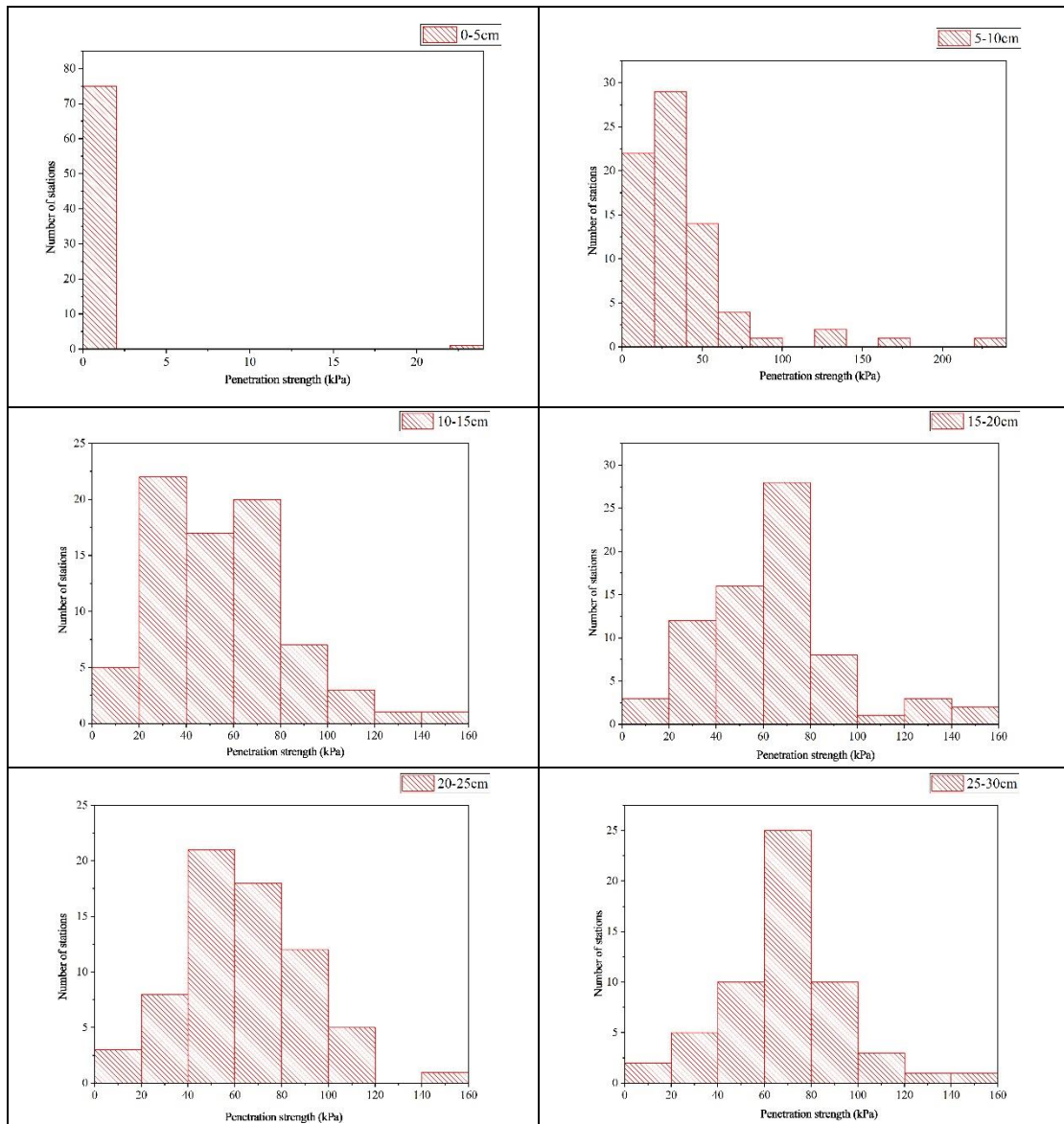
Figure 4-61 Histogram of sediment penetration strength data at each station
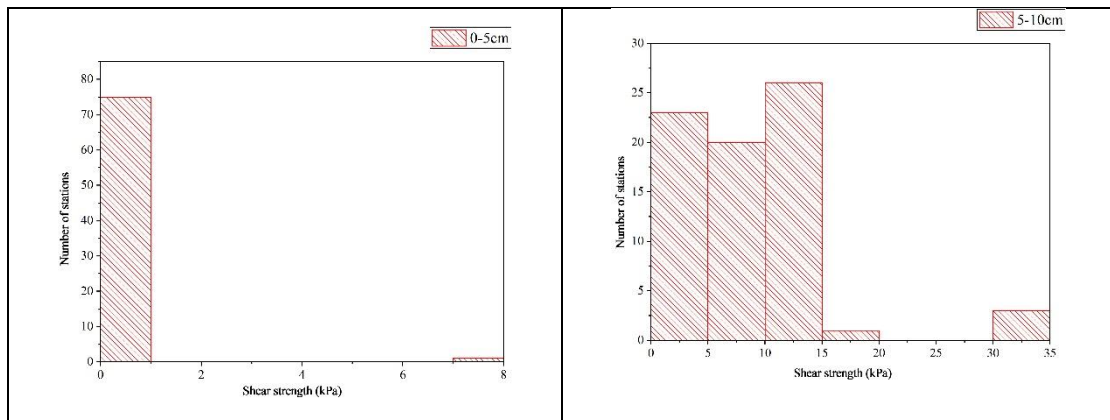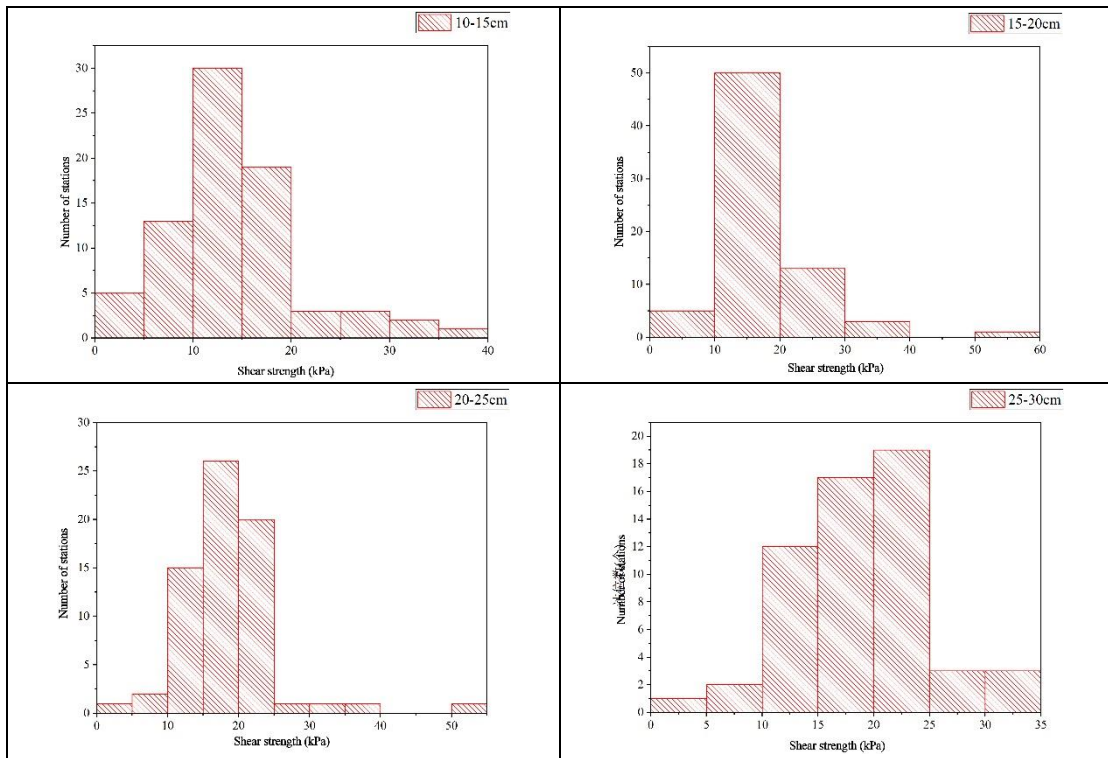
Figure 4-62 Histogram of sediment shear strength data at each station

The vertical distribution of sediment moisture content at each layer in stations across Block M shows a similar trend, namely a decrease in sediment moisture content with increasing depth (Figure 4-63).
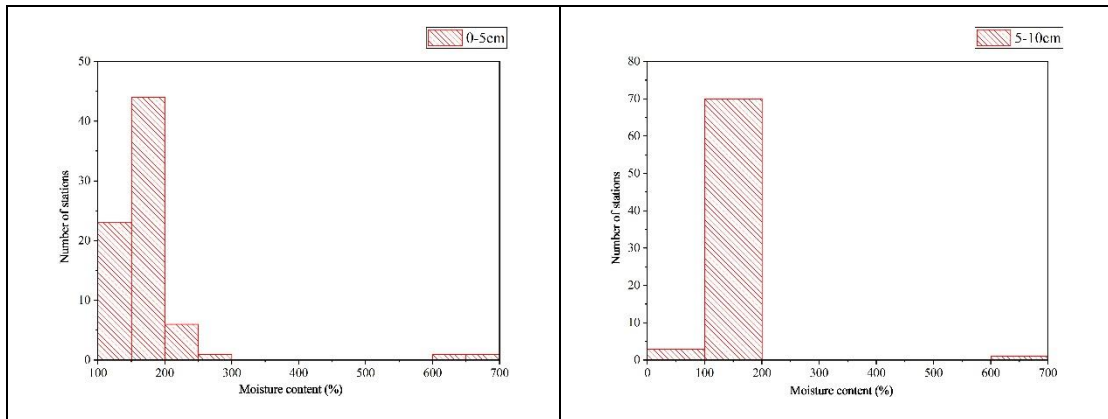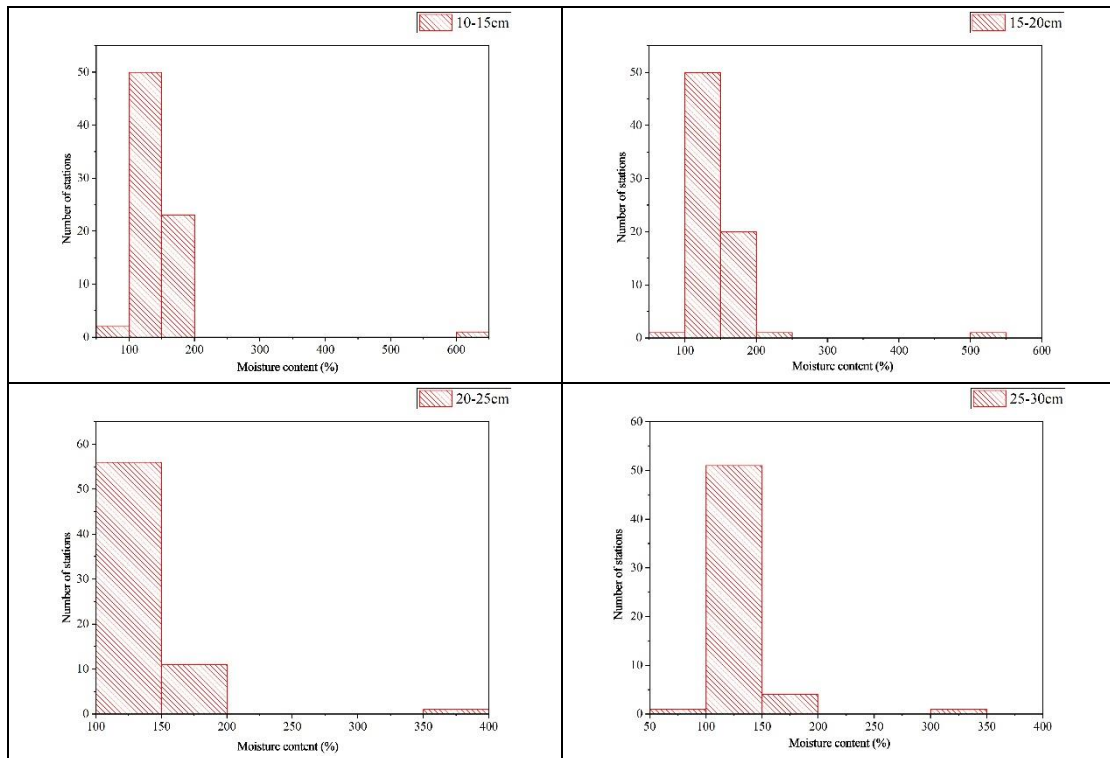
Figure 4-63 Histogram of sediment moisture content data at each station

The vertical distribution of the wet density of sediments at each station in Block M exhibits a similar trend: the wet density of sediments slightly increases with depth, but the mean value remains around 1.4 g/cm³ (Figure 4-64)
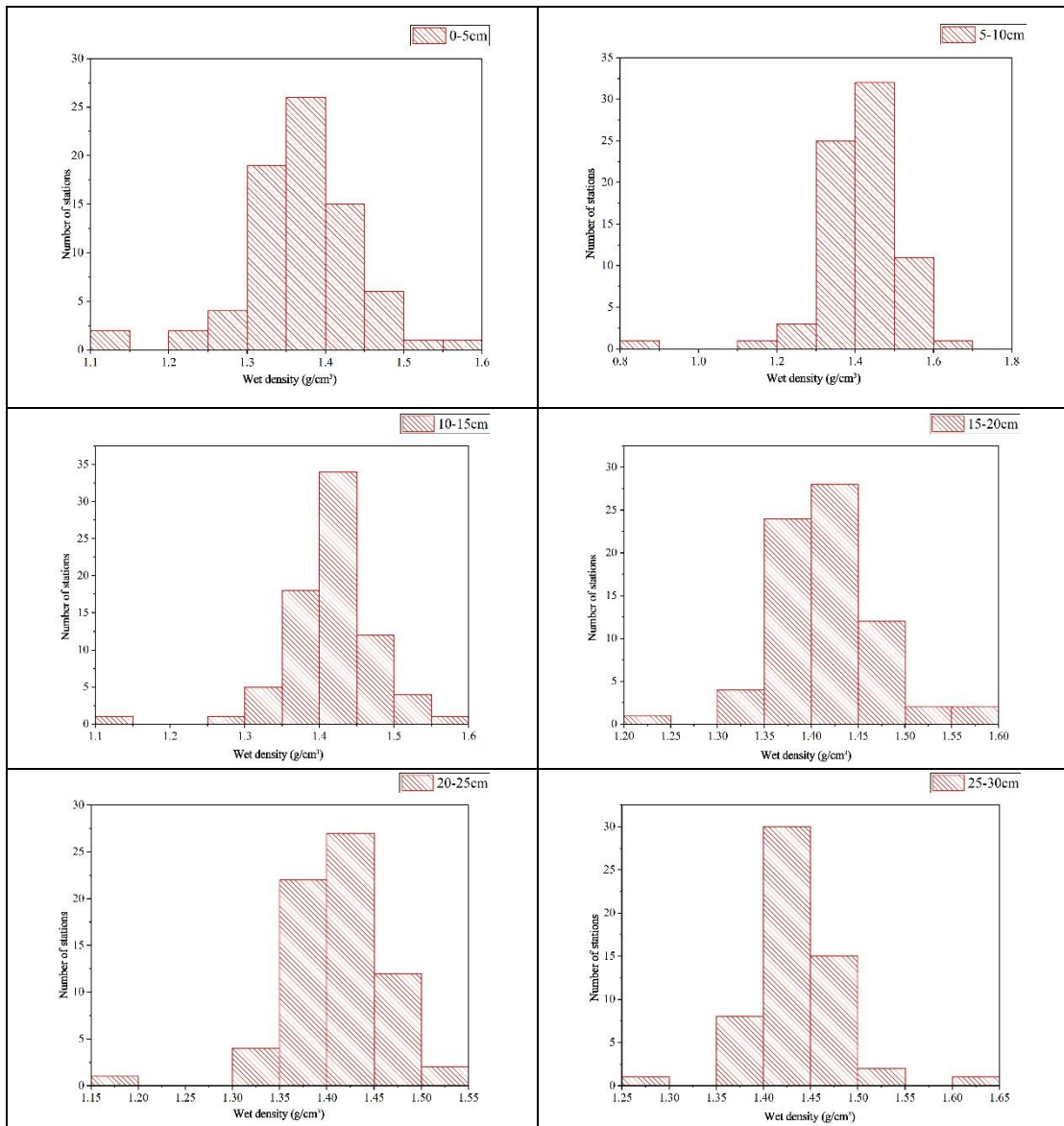
Figure 4-64 Histogram of sediment wet density data at each station

Combined with the topographic and geomorphologic analysis (Figure 4-65 – Figure 4-67), it is evident that in the influence areas of the submarine fan structure on the south side of the Magoshichi Guyot in the Block M2, the chain of southern seamounts, and the small seamounts in the southeast, the penetration strength of sediments is obviously higher than that of sediments in the deep-sea plain areas. This suggests that sediment penetration strength is influenced by terrain, with sediment in the foothill areas exhibiting higher penetration strength than sediments in the deep-sea plain.

In the influence areas of the submarine fan structure on the south side of the Magoshichi Guyot, the chain of southern seamounts, and the small seamounts in the southeast, the penetration strength of sediments is obviously higher than that of sediments in the deep-sea plain areas. This indicates that sediment penetration strength is controlled by terrain, with sediment in the foothill areas exhibiting higher penetration strength than sediments in the deep-sea plain.

In the influence area of the submarine fan structure on the south side of the Magoshichi Guyot, wave-like terrain develops in the central and lower parts of the fan body and some channels. At layers 5–10 cm and 10–15 cm, the high-value areas of penetration strength coincide with the areas where wave-like terrain develops. At layer 15–20 cm, the influence of wave-like terrain on the high values of sediment penetration strength weakens. This indicates that at depths shallower than 15 cm, sediment penetration strength was influenced by the wave-like terrain of the submarine fan on the south side of the Magoshichi Guyot.
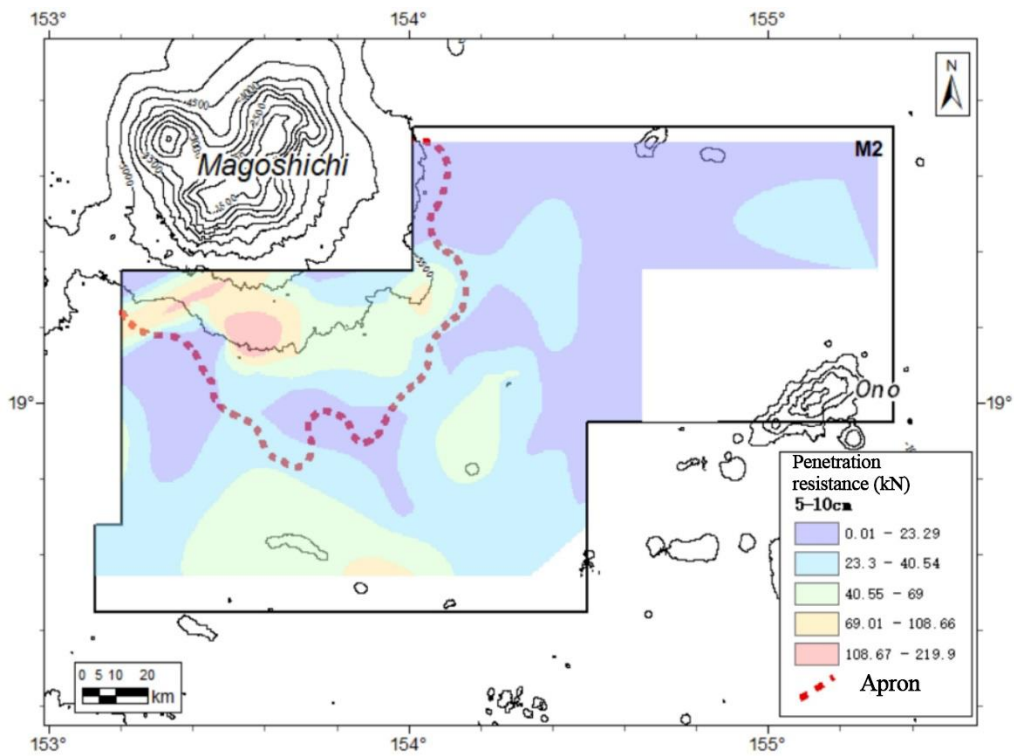
Figure 4-65 Distribution of penetration resistance values of layer 5–10 cm sediment
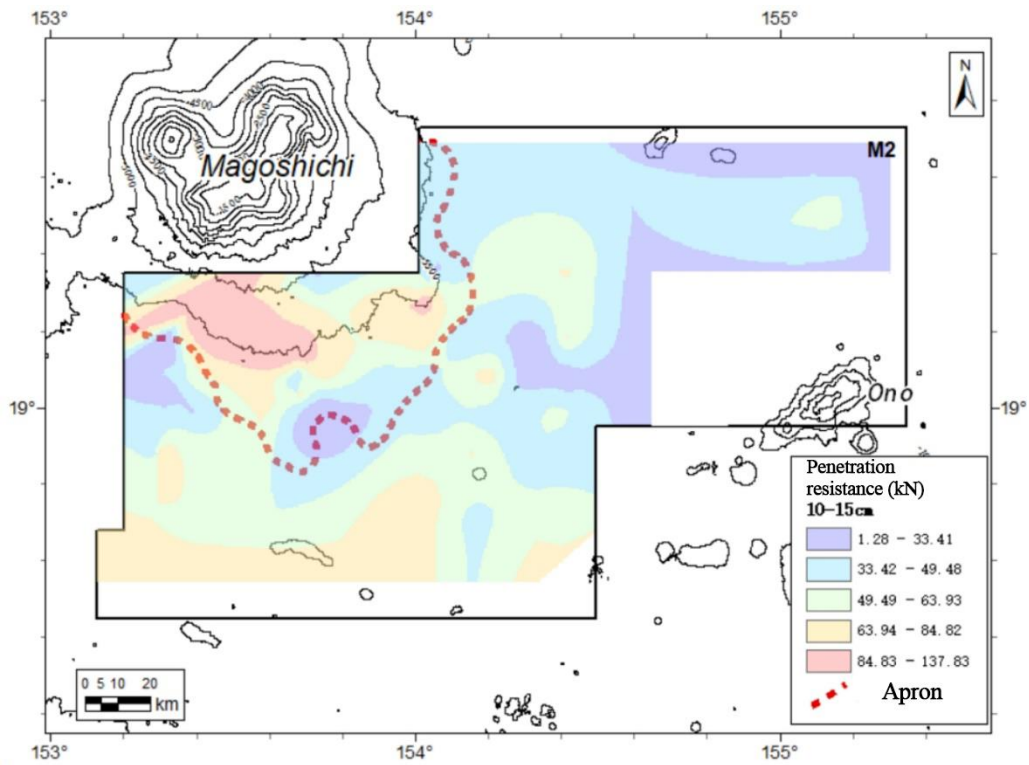
Figure 4-66 Distribution of penetration resistance values of layer10–15 cm sediments
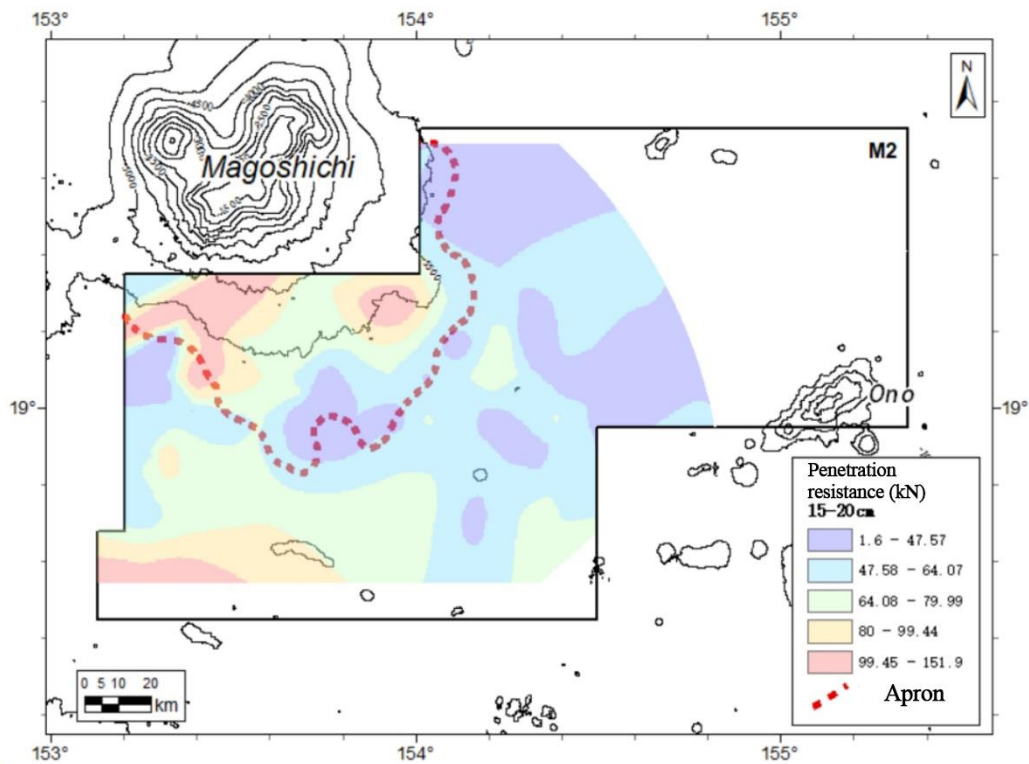
Figure 4-67 Distribution of penetration resistance values of layer 15–20 cm sediments

Figures 4-68 to 4-70 show that in the influence areas of the submarine fan structure on the south side of the Magoshichi Guyot, the chain of southern seamounts, and the small seamounts in the southeast, the shear strength of sediments at each layer is obviously higher than that of sediments in the deep-sea plain areas. This indicates that sediment shear strength was influenced by terrain, with sediments in mountainous regions exhibiting higher shear strength than sediments in the deep-sea plain.
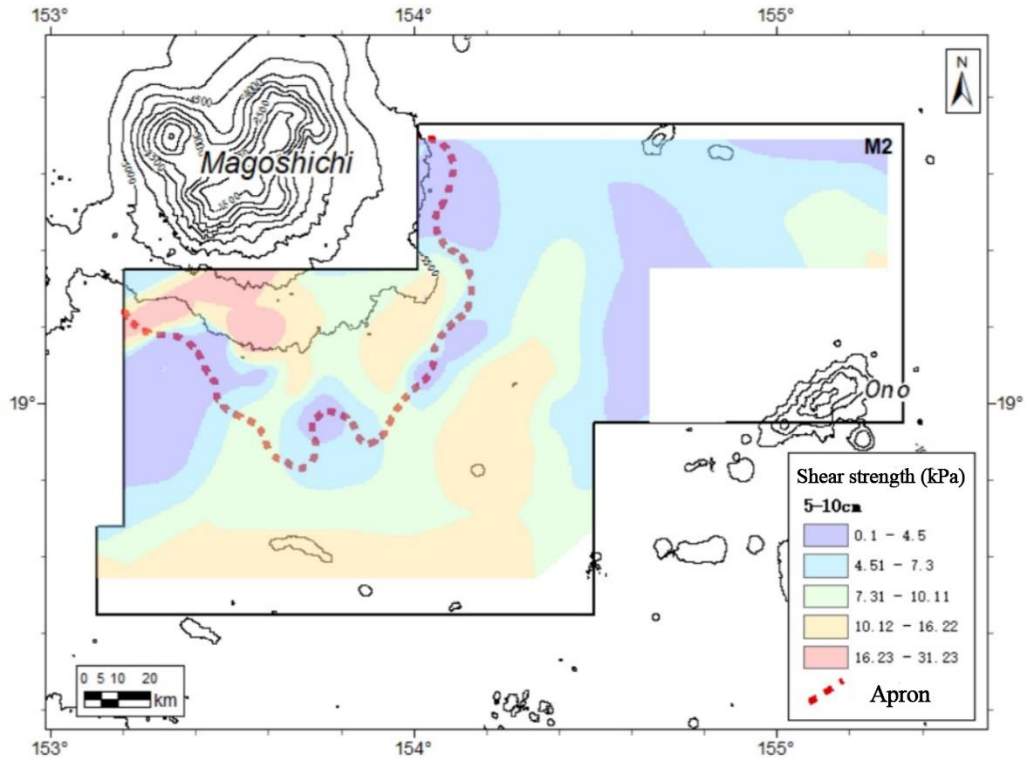
Figure 4-68 Distribution of shear strength values of layer 5–10 cm sediments
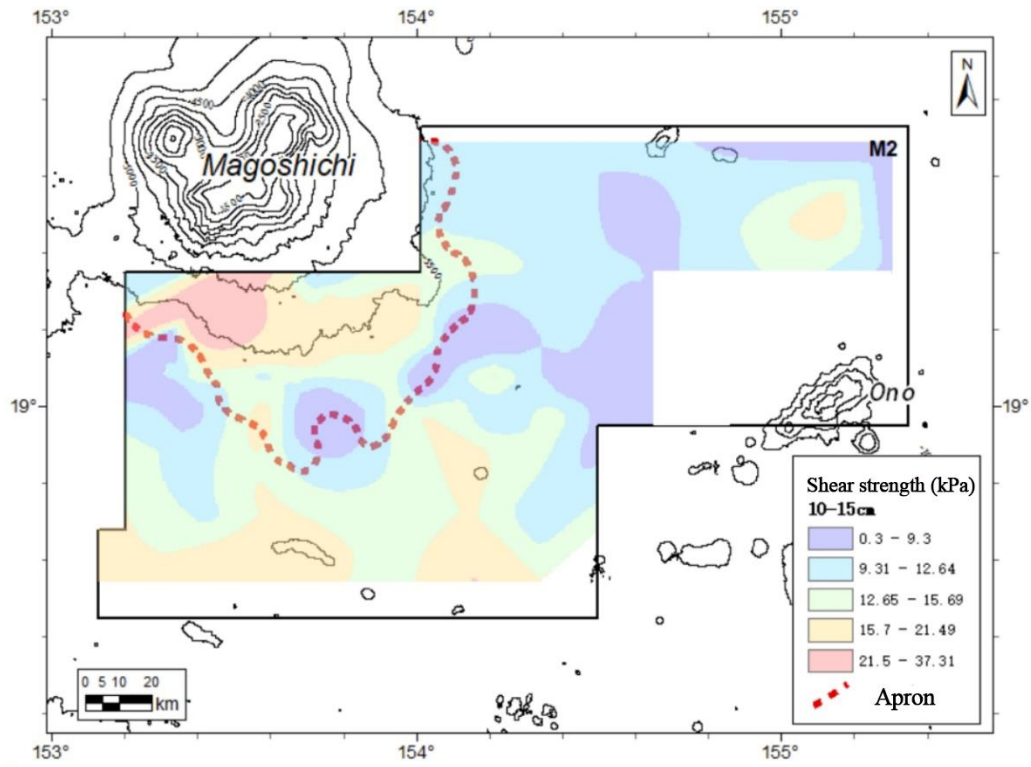
Figure 4-69 Distribution of shear strength values of layer 10–15 cm sediment
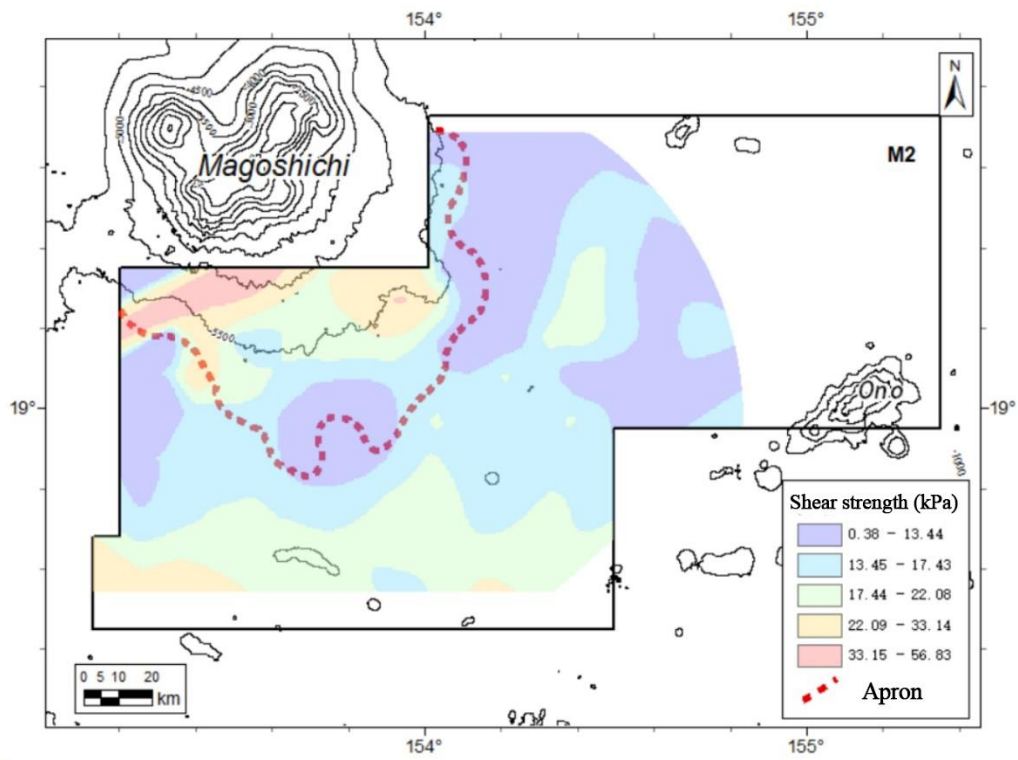
Figure 4-70 Distribution of shear strength values of layer 15–20 cm sediment

In the influence area of the submarine fan structure on the south side of the Magoshichi Guyot, wave-like terrain develops in the central and lower parts of the fan body and some channels. At layer 5–10 cm, the high-value areas of shear strength coincide with the areas where wave-like terrain develops. At layers 10–15 cm and 15–20 cm, the influence of wave-like terrain on the high values of sediment shear strength gradually weakens. This indicates that at depths shallower than 10 cm, sediment shear strength was obviously influenced by the wave-like terrain of the submarine fan on the south side of the Magoshichi Guyot.

4.3.3.6.2 Laboratory Geotechnical Testing of Core Sediments

Laboratory geotechnical testing was conducted on short core sediment samples from 14 box-corer stations in Block M2. The testing included experiments for moisture content, density, specific gravity, consolidation, and shear strength. This yielded engineering physical properties parameters (natural moisture content, specific gravity, natural density, natural porosity ratio, liquid limit, plastic limit, plasticity index, and liquidity index) and mechanical properties parameters (compression coefficient, compression modulus, cohesion, and internal friction coefficient) of deep-sea sediments.

（1）Natural Moisture Content

The natural moisture content of core sediments at 14 stations in Block M2 is relatively high, ranging from 106.7% to 183.0%, with an average value of 149.1%. The natural moisture content exhibits four different patterns of variation with depth.

Group I: As shown in Figure 4-71a, the natural moisture content of sediments in this group initially decreases and then increases with depth. Specifically, at Stations DY75I-M2-BC33, DY75I-M2-BC35, and DY75I-M2-BC31, the moisture content reaches a minimum at the layer 10–15 cm, and the moisture content at layer 20–25 cm is greater than that at layer 0–5 cm. At Stations DY75I-M2-BC11, DY75I-M2-BC06, and DY75I-M2-BC63, the moisture content reaches a minimum at the layer 15–20 cm, with the maximum moisture content at layer 0–5 cm, showing an overall decreasing trend with depth. At Station DY75I-M2-BC20, the moisture content reaches a minimum at layer 5–10 cm, increasing with depth, and the moisture content at layer 20–25 cm is greater than that at layer 0–5 cm.

Group II: As shown in Figure 4-71b, the natural moisture content of sediments in this group decreases with depth.

Group III: As shown in Figure 4-71c, the natural moisture content of sediments in this group initially decreases, then increases, and finally decreases again with depth. The moisture content reaches a maximum at layer 0–5 cm, showing an overall decreasing trend with depth.

Group IV: As shown in Figure 4-71d, the natural moisture content of sediments in this group fluctuates with depth, initially increasing, then decreasing, and increasing again, with no obvious overall trend
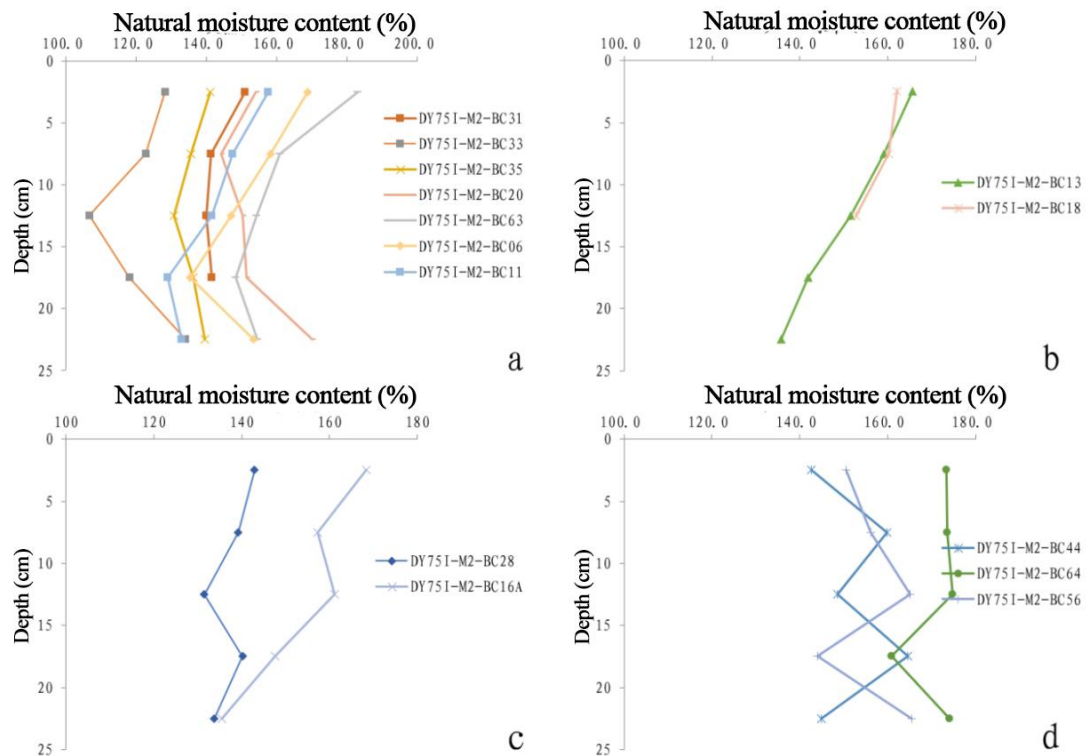
Figure 4-71 Vertical variation of sediment natural moisture content

Combined with the topographic features of Block M2, the natural moisture content of sediments was influenced by the seafloor topography. As shown in Figure 4-72, within the influence area of the seabed fan structure on the south side of the Magoshichi Guyot, the natural moisture content of sediments fluctuates with increasing depth. In the deep-sea plain area, however, the natural moisture content of sediments decreases with depth. It can be inferred that within the influence area of the seabed fan, influenced by submarine landslides, the sediment source in the fan area is complex, leading to obvious fluctuations in the natural moisture content of sediments.
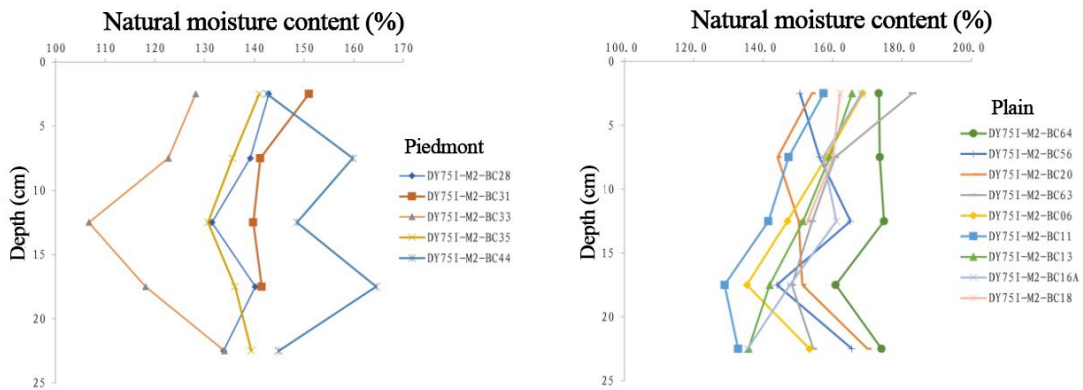
Figure 4-72 Vertical variation of sediment natural moisture content in different topographic regions

（2）Specific Gravity

The specific gravity values of the core sediments from 14 stations in Block M2 were relatively stable, ranging from 2.70 to 2.82, with an average value of 2.75.

Group I: As shown in Figure 4-73a, the specific gravity of sediments in this group fluctuates with depth, showing a pattern of increase followed by decrease and then increase again, with fluctuations within the range of 0.05

Group II: As depicted in Figure 4-73b, the specific gravity of sediments in this group fluctuates with depth, exhibiting a pattern of decrease followed by increase and then decrease again, with fluctuations within the range of 0.10. Notably, sediment specific gravity at the Station DY75I-M2-BC33 fluctuates more obviously compared to other sites.

Group III: As illustrated in Figure 4-73c, the specific gravity of sediments in this group shows no obvious variation with depth and remains relatively stable.

Group IV: As shown in Figure 4-73d, sediment specific gravity at the Station DY75I-M2-BC31 exhibits a linear increase with depth.
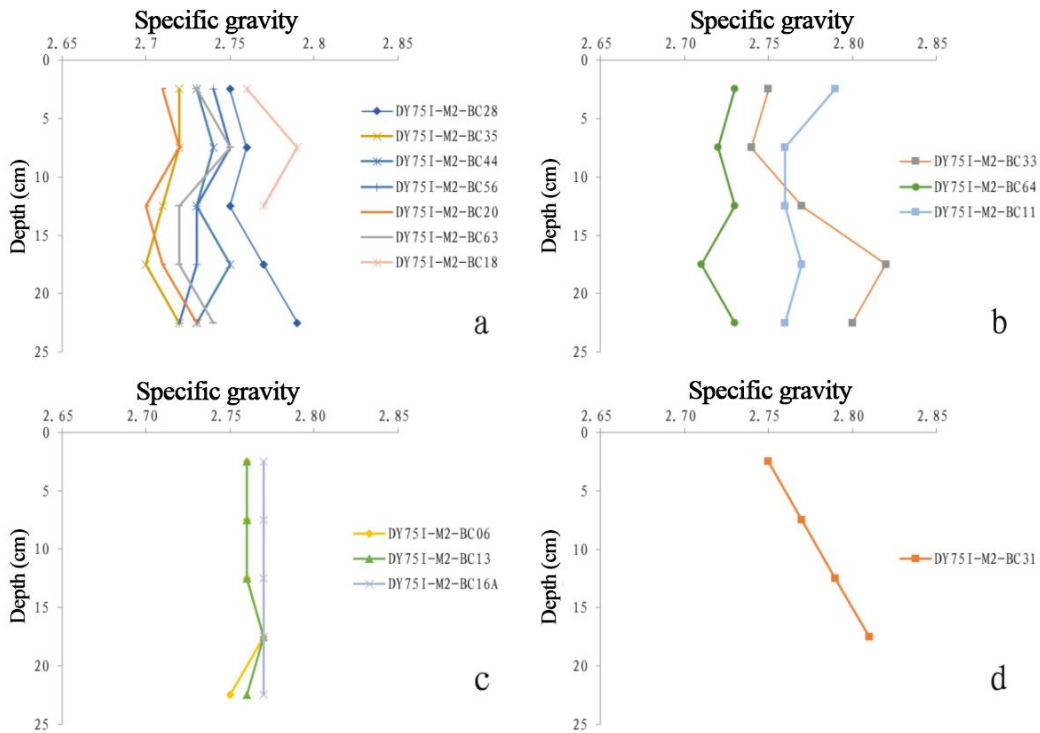
Figure 4-73 Vertical variation of sediment specific gravity

In conjunction with the topographic features of the Block M2, sediment specific gravity is influenced by the seafloor topography. As depicted in Figure 4-74, within the influence area of the seabed fan structure on the southern side of Magoshichi Guyot, sediment specific gravity fluctuates with increasing depth. In contrast, in the deep-sea plain region, the change in sediment specific gravity with increasing depth is minimal, showing relatively stable values. It is inferred from this that within the influence area of the seabed fan, influenced by submarine landslides of Magoshichi Guyot, the sediment sources in the seabed fan region are complex, leading to unstable sediment specific gravity.
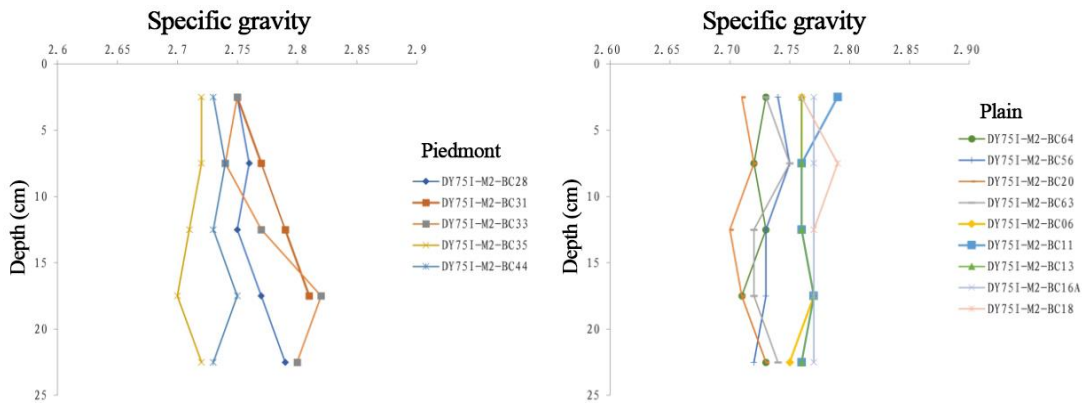
Figure 4-74 Vertical variation of sediment specific gravity in different topographic regions

（3）Natural Density

The natural densities of core sediments at 14 stations in Block M2 ranged from 1.28 g/cm^3 to 1.40 g/cm^3, with an average value of 1.34 g/cm^3. As shown in Figure 4-75, the natural density exhibits four different patterns of change with depth.

Group I: As depicted in Figure 4-75a, the natural density of sediments in this group gradually increases with depth. Specifically, at the Station DY75I-M2-BC13, the natural density stabilizes at 10–20 cm layer. At the Station DY75I-M2-BC18, the density stabilizes between 0-10 cm layer but sharply increases at 10–15 cm layer. Similarly, at the Station DY75I-M2-BC31, the density stabilizes at 5–20 cm layer.

Group II: As shown in Figure 4-75b, the natural density of sediments in this group initially increases and then decreases with depth. For instance, at the Station DY75I-M2-BC64, DY75I-M2-BC06, and DY75I-M2-BC11, the density reaches its maximum value at 15-20 cm layer, showing an overall increasing trend with depth. Conversely, at the Station DY75I-M2-BC33 and DY75I-M2-BC35, the density reaches its maximum value at 5-10 cm layer.

Group III: Illustrated in Figure 4-75c, sediments in this group exhibit fluctuating changes in natural density, initially increasing, then decreasing, and then increasing again with depth, with no obvious overall trend.

Group IV: As shown in Figure 4-75d, sediments in this group demonstrate fluctuating changes in natural density, initially decreasing, then increasing, and then decreasing again with depth, with no obvious overall trend.
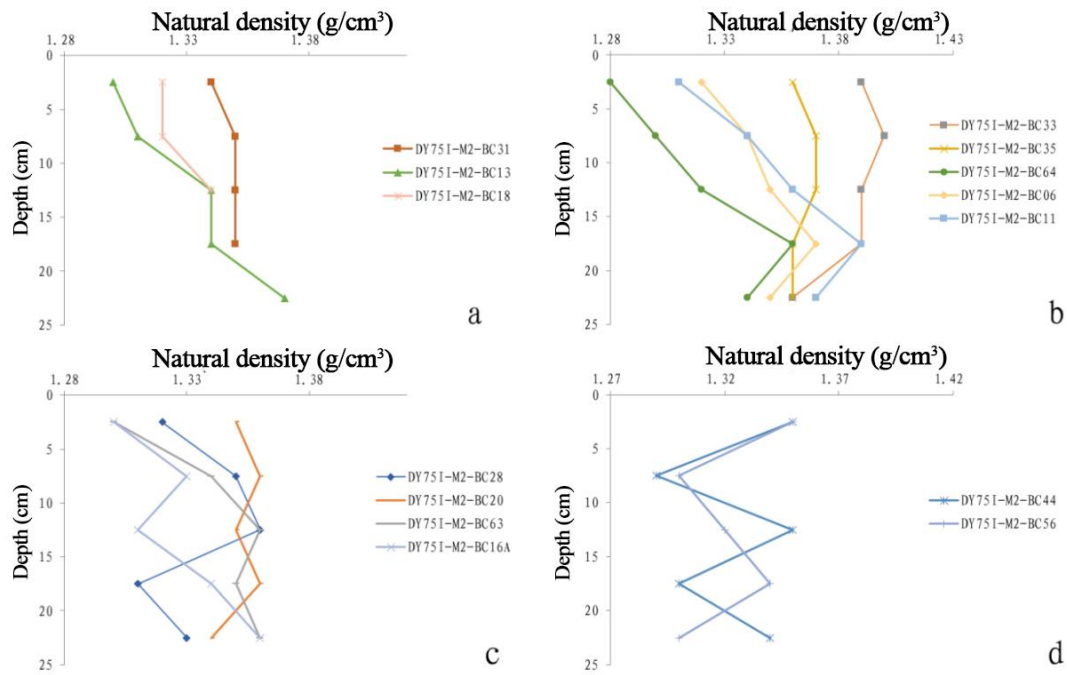
Figure 4-75 Vertical variation of sediment natural density

Taking into account the topographical features of the Block M2, the natural density of sediments is influenced by the seafloor topography. As depicted in Figure 4-76, within the influence area of the seabed fan structure on the south side of the Magoshichi Guyot, the natural density of sediments fluctuates with increasing depth. In contrast, in the deep-sea plain region, the density of sediments gradually increases with depth. From this, it can be inferred that within the influence area of the seabed fan, influenced by submarine landslides, the sediment source is complex, leading to obvious variations in the natural density of sediments.
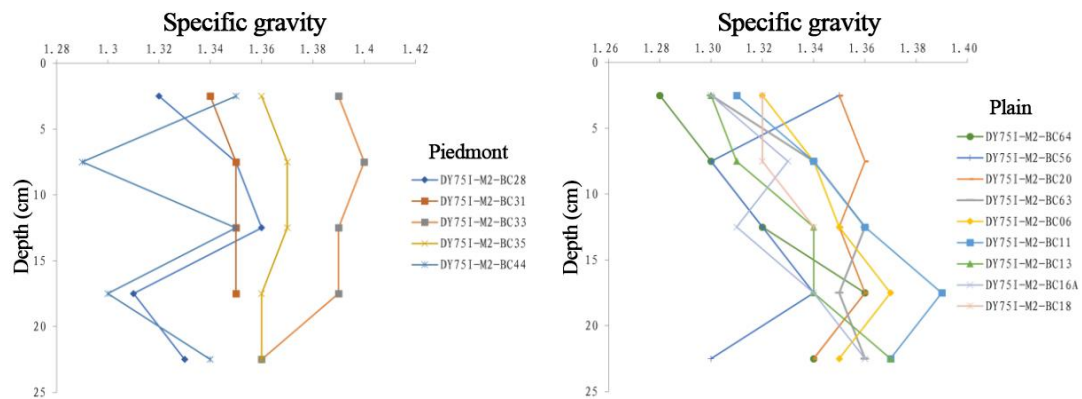
Figure 4-76 Vertical variation of sediment natural density in different topographic regions

（4）Natural Porosit Ratio

The natural porosity ratios of the core sediments at 14 stations in Block M2 ranged from 3.119 to 4.943, with an average value of 4.111. As shown in Figure 4-77, the natural porosity ratio exhibits four different patterns of change with depth.

Group I: As depicted in Figure 4-77a, the natural porosity ratios of sediments in this group decrease initially and then increase with depth. Specifically, at Station DY75I-M2-BC20 and DY75I-M2-BC31, the natural porosity ratios reach a minimum in the 5–10 cm layer; at Station DY75I-M2-BC33 and DY75I-M2-BC35, it reaches a minimum in the 10–15 cm layer; at Station DY75I-M2-BC11, DY75I-M2-BC06, DY75I-M2-BC63, and DY75I-M2-BC64, it reaches a minimum in the 15–20 cm layer. Overall, there is a trend of decreasing porosity with increasing depth, with a sharp decrease before reaching the minimum value.

Group II: As shown in Figure 4-77b, the natural porosity ratios of sediments in this group fluctuate initially, decreasing and then increasing before decreasing again with increasing depth. Overall, there is a trend of decreasing porosity with increasing depth.

Group III: Illustrated in Figure 4-77c, the natural porosity ratios of sediments at the Station DY75I-M2-BC13 exhibit a nearly linear decrease with increasing depth, with the highest porosity in the 0–5 cm layer.

Group IV: As shown in Figure 4-77d, the natural porosity ratios of sediments in this group fluctuate, initially increasing and then decreasing with increasing depth, with no obvious overall trend.
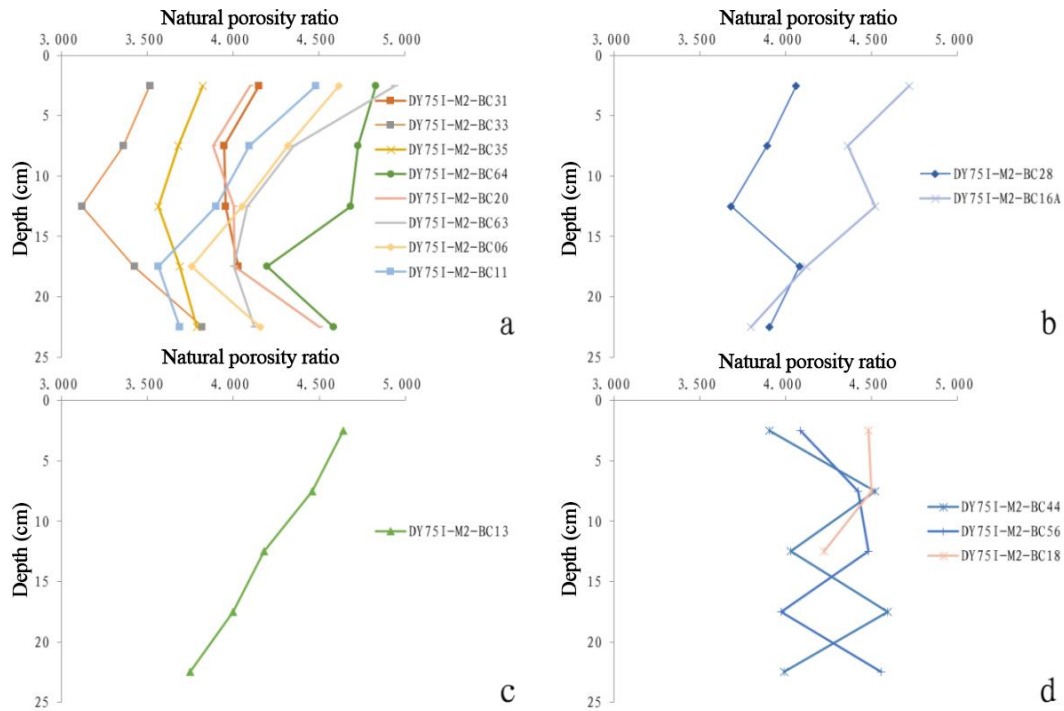
Figure 4-77 Vertical variation of sediment natural porosity ratio

Considering the topographical features of the Block M2, the natural porosity ratio of sediments is influenced by the seafloor topography. As shown in Figure 4-78, within the influence area of the seabed fan structure on the southern side of the Magoshichi Guyot, the natural porosity ratio of sediments fluctuates with increasing depth. In contrast, in the deep-sea plain region, the natural porosity ratio of sediments gradually decreases with depth. This suggests that within the influence area of the seabed fan, influenced by submarine landslides and the complex sediment sources, sediment natural porosity ratio exhibits obvious fluctuations. Conversely, in the deep-sea plain region, sediment compaction increases with depth, resulting in a decrease in natural porosity ratio.
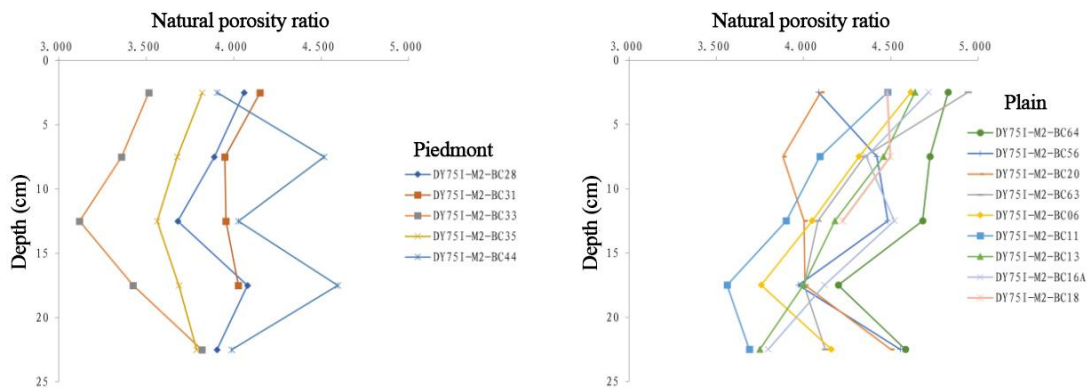
Figure 4-78 Vertical variation of sediment natural porosity ratio in different topographic regions

（5）Plasticity of Soils

The liquid limit, plastic limit, plasticity index and liquidity index of core sediments at 14 stations in Block M2 are relatively high. The liquid limit of core sediments ranges from 77.9% to 106.9%, with an average value of 86.2%. As depicted in Figure 4-79, the liquid limit exhibits four distinct patterns of variation with depth.

Group I: As shown in Figure 4-79a, exhibits a trend where the liquid limit of sediment decreases initially and then increases with depth. Moreover, the sediment at Station DY75I-M2-BC31 and DY75I-M2-BC33 shows the minimum liquid limit values in 5–10 cm and 10–15 cm layers, respectively.

Group II: As depicted in Figure 4-79b, demonstrates a fluctuating pattern of decrease-increase-decrease-increase in the liquid limit with depth, with no obvious overall trend.

Group III: As illustrated in Figure 4-79c, displays a trend where the liquid limit of sediment increases initially and then decreases with depth. Additionally, sediment at Stations DY75I-M2-BC18 and DY75I-M2-BC11 shows the minimum liquid limit values in 5–10 cm and 10–15 cm layers, respectively, with no obvious overall trend.

Group IV: shown in Figure 4-79d, indicates an overall trend where the liquid limit of sediment increases initially, then decreases, and then increases again with depth, showing an overall increase in liquid limit with increasing depth.
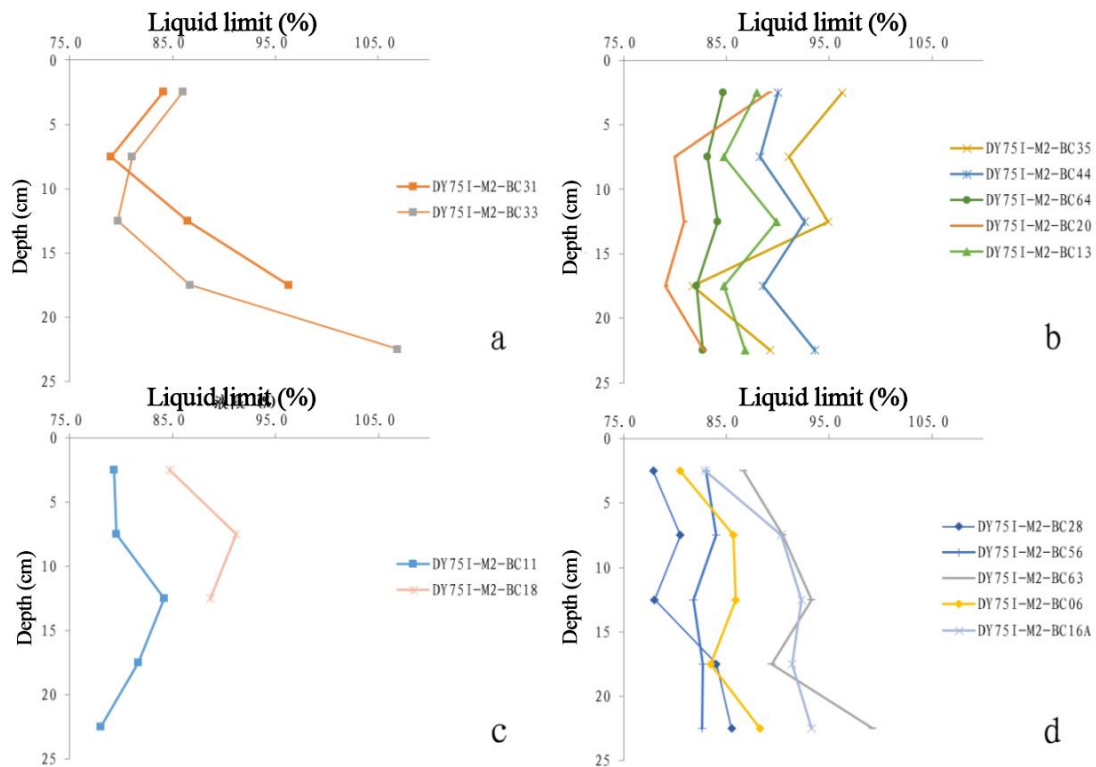
Figure 4-79 Vertical variation of sediment liquid limit

The plastic limit of core sediments ranged from 27.9% to 72.9%, with an average value of 41.3%. As depicted in Figure 4-80, the plastic limit shows four different patterns of variation with depth.

Group I: As shown in Figure 4-80a, the plastic limit of this group of sediment decreases initially and then increases with depth. Specifically, sediment from Station DY75I-M2-BC31 and DY75I-M2-BC16A exhibits a minimum plastic limit in the 5–10 cm layer, with an overall increasing trend as depth increases.

Group II: Illustrated in Figure 4-80b, the plastic limit of this group of sediment initially decreases, then increases, and finally decreases again with depth, although the overall trend is not obvious. Among them, sediment from the Station DY75I-M2-BC56 shows the smallest variation in plastic limit.

Group III: As shown in Figure 4-80c, the plastic limit of this group of sediment generally increases with depth.

Group IV: Presented in Figure 4-80d, the plastic limit of this group of sediment fluctuates initially by increasing and then decreasing with depth. Among them, sediment from the Station DY75I-M2-BC64 exhibits the smallest variation in plastic limit.
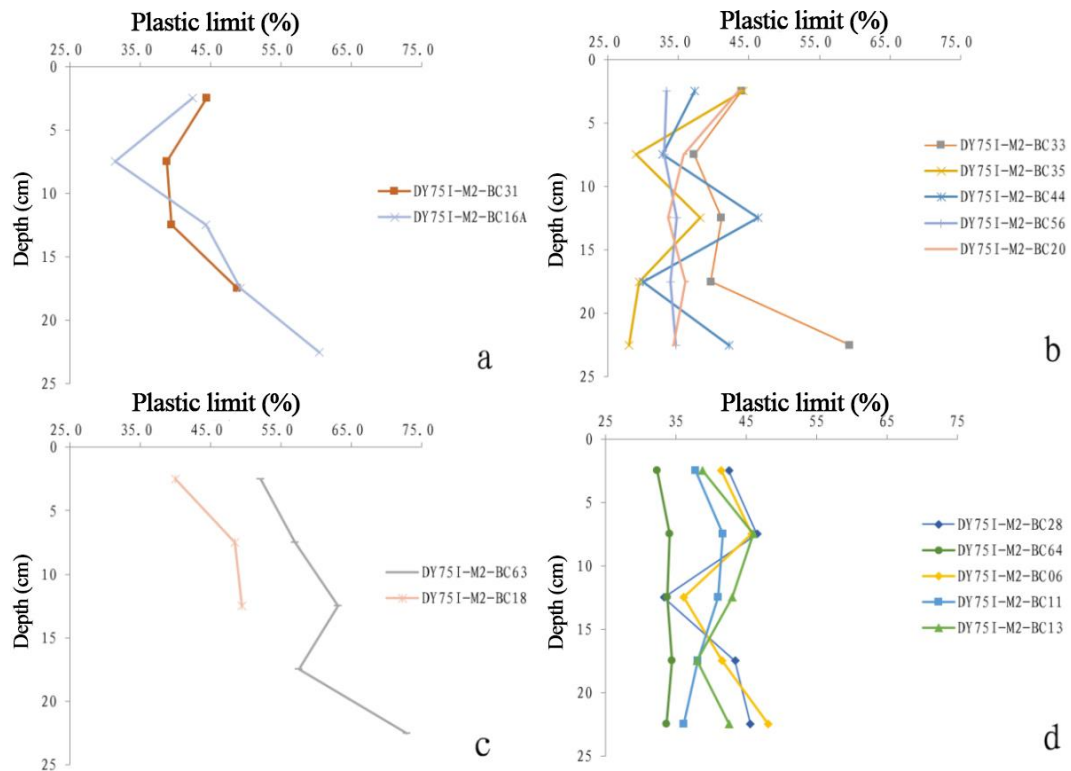
Figure 4-80 Vertical variation of sediment plastic limit

The plasticity index of core sediments ranged from 26.3 to 62.2, with an average value of 44.9. As illustrated in Figure 4-81, the plasticity index shows four different patterns of variation with depth.

Group I: As depicted in Figure 4-81a, the plasticity index of this group of sediment generally decreases with increasing depth.

Group II: As illustrated in Figure 4-81b, the plasticity index of this group of sediment fluctuates initially by decreasing, then increasing, and finally decreasing again with depth, although the overall trend is not obvious.

Group III: As shown in Figure 4-81c, the plasticity index of sediment from Station DY75I-M2-BC31 exhibits a stepwise increase with depth, with a sharp increase observed in the 10–15 cm layer.

Group IV: As presented in Figure 4-81d, the plasticity index of this group of sediment initially increases and then decreases with depth. Specifically, sediment from the Station DY75I-M2-BC33 shows an overall increasing trend in plasticity index with depth, while sediment from Station DY75I-M2-BC56 and DY75I-M2-BC16A shows a decreasing trend.

It can be observed that the sediment in the study area has a relatively high plasticity index, indicating a high plasticity and a high clay content.
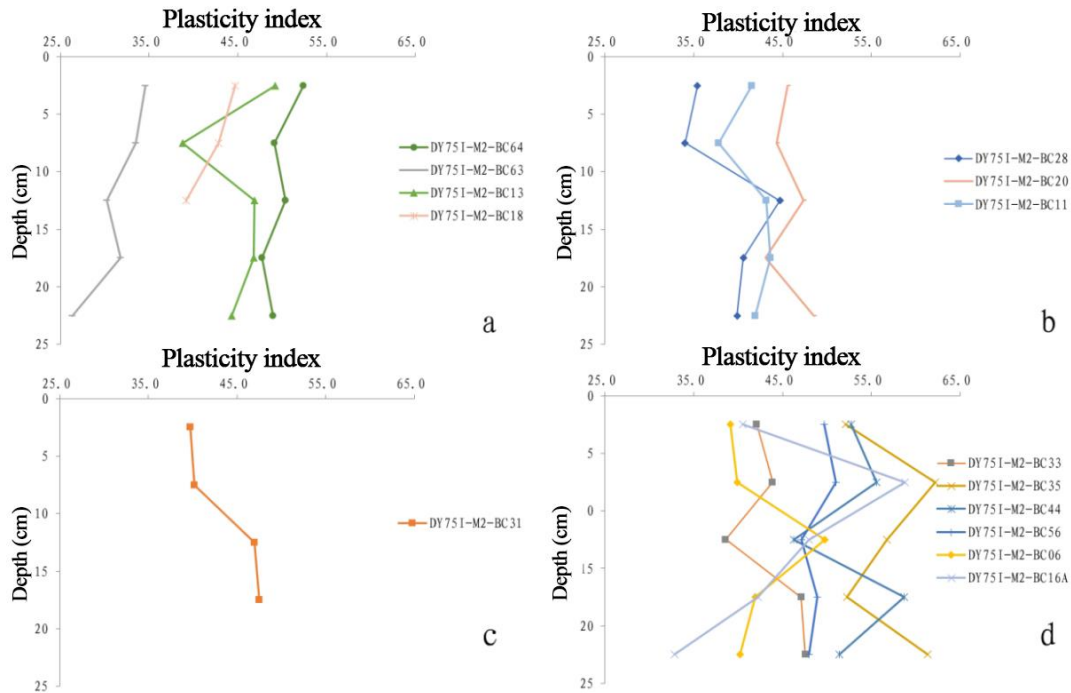
Figure 4-81 Vertical variation of sediment plasticity index

The liquidity index of core sediments ranged from 1.57 to 3.78, with an average value of 2.44. As shown in Figure 4-82, the liquidity index exhibits four different patterns of variation with depth.

Group I: Illustrated in Figure 4-82a, the liquidity index of this group of sediment decreases stepwise with increasing depth. The maximum liquidity index is reached in the 0-5 cm layer.

Group II: As depicted in Figure 4-82b, the liquidity index of this group of sediment initially decreases, then increases, and finally decreases again with depth. The overall trend of this group is a decrease in liquidity index with increasing depth.

Group III: Shown in Figure 4-82c, the liquidity index of sediment from the Station DY75I-M2-BC20 gradually increases with depth, with a sharp increase observed in the 15–20 cm layer.

Group IV: Presented in Figure 4-82d, the liquidity index of this group of sediment initially increases and then decreases with depth. Specifically, sediment from the Station

DY75I-M2-BC13 shows a decreasing trend in liquidity index with depth, while sediment from Station DY75I-M2-BC44, DY75I-M2-BC64, and DY75I-M2-BC56 does not exhibit an obvious trend in liquidity index.

Overall, it can be observed that the liquidity index of sediment in the study area is obviously greater than 1, indicating that the deep-sea surface sediment is in a plastic state.
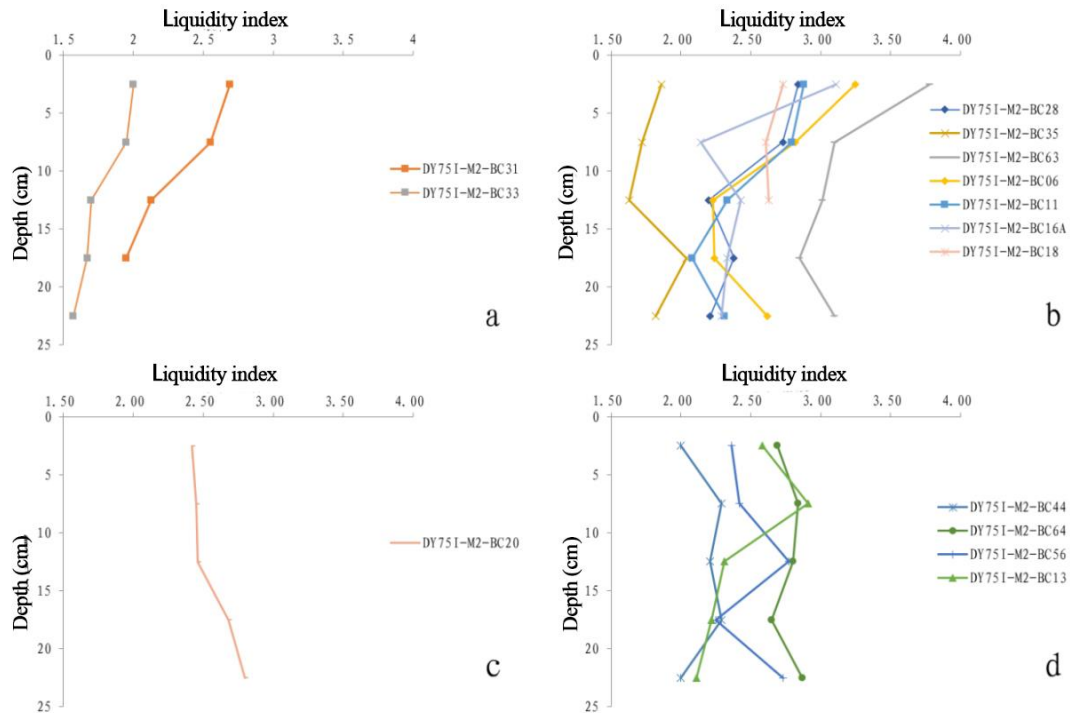
Figure 4-82 Vertical variation of sediment liquidity index

（6）Compressibility of Soil

The core sediment samples from the 14 stations in the Block M2 underwent indoor rapid consolidation tests, and the compression curves are depicted in Figure 4-83, yielding two compression properties: compression coefficient and compression modulus.

The compression coefficient of sediment in this study area ranges from 3.07 MPa^{-1} to 6.95 MPa^{-1}, with an average value of 4.16 MPa^{-1}.
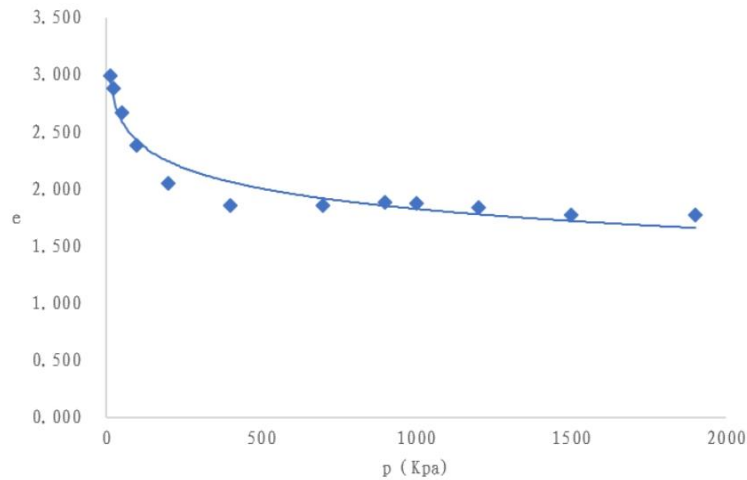
Figure 4-83 Sediment Compression Curve at Station DY75-M2-BC33, 10–15 cm layer

The vertical variation of compression coefficient exhibits four different patterns (Figure 4-84).

Group I: As shown in Figure 4-84a, exhibits a pattern where the compression coefficient of sediment initially increases and then decreases with depth. Specifically, in the 10–15 cm layer, the compression coefficient of sediment at Station DY75I-M2-BC31 and DY75I-M2-BC13 reaches its maximum value. Overall, there is a trend of increasing compression coefficient. At the Station DY75I-M2-BC11, the compression coefficient of sediment reaches its maximum value in the 15–20 cm layer.

Group II: As shown in Figure 4-84b, the compression coefficient of sediment shows fluctuating patterns of increase-increase-decrease-increase with depth. The fluctuation range is small, and the trend is not obvious.

Group III: As shown in Figure 4-84c, the compression coefficient of sediment decreases initially and then increases with depth. At the Station DY75I-M2-BC33, the compression coefficient of sediment reaches its minimum value in the 5–10 cm layer, followed by a nearly linear increase with further depth. The compression coefficient of sediment at Station DY75I-M2-BC56 and DY75I-M2-BC20 reaches its minimum value in the 15–20 cm layer.

Group IV: As shown in Figure 4-84d, the compression coefficient of sediment fluctuates with depth, initially decreasing, then increasing, and finally decreasing again. Overall, there is a decreasing trend in the compression coefficient with increasing depth.
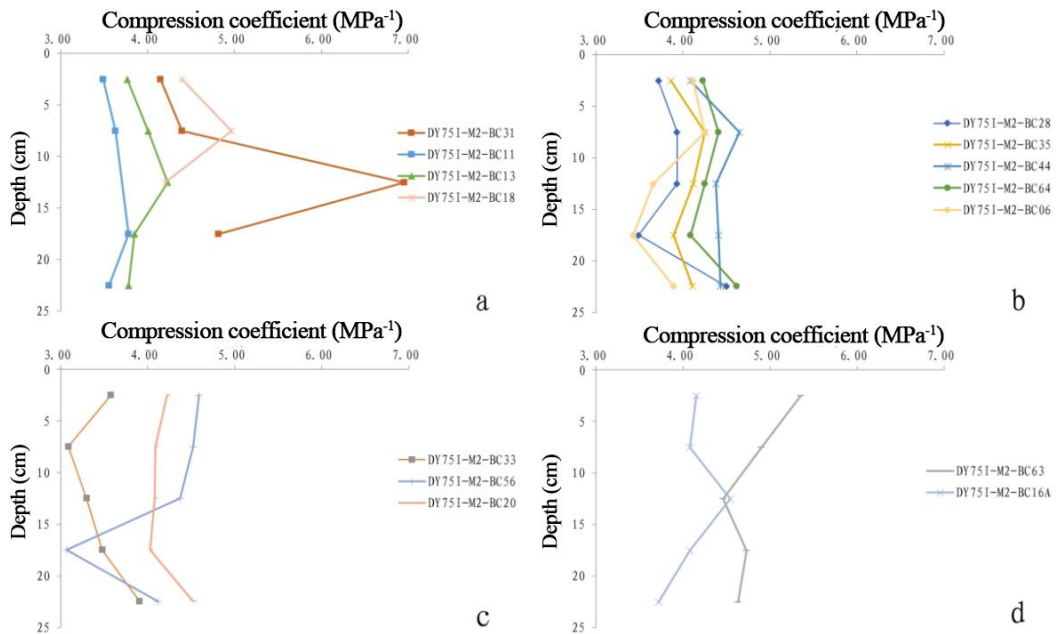
Figure 4-84 Vertical variation of sediment compression coefficient

The compression modulus of core sediments ranged from 0.71 MPa to 1.62 MPa, with an average value of 1.24 MPa. As shown in Figure 4-85, the compression modulus exhibits four different patterns of variation with depth.

Group I: As shown in Figure 4-85a, the compression modulus of the sediment increases initially and then decreases with depth. Specifically, at the Station DY75I-M2-BC56, the compression modulus experiences a sharp increase and reaches its maximum value in the 15–20 cm layer, and overall exhibits an increasing trend. The sediment at the Station DY75I-M2-BC33 shows a dramatic increase in compression modulus, and reaches its maximum value in the 5–10 cm layer.

Group II: Depicted in Figure 4-85b, the compression modulus decreases initially and then increases with depth, exhibiting an overall decreasing trend.

Group III: As shown in Figure 4-85c, demonstrates a pattern where the compression modulus decreases initially, then increases, and finally decreases again with increasing depth. Overall, there is a decreasing trend in compression modulus with depth.

Group IV: As indicated in Figure 4-85d, shows a fluctuating pattern of compression modulus with depth, with no clear overall trend.
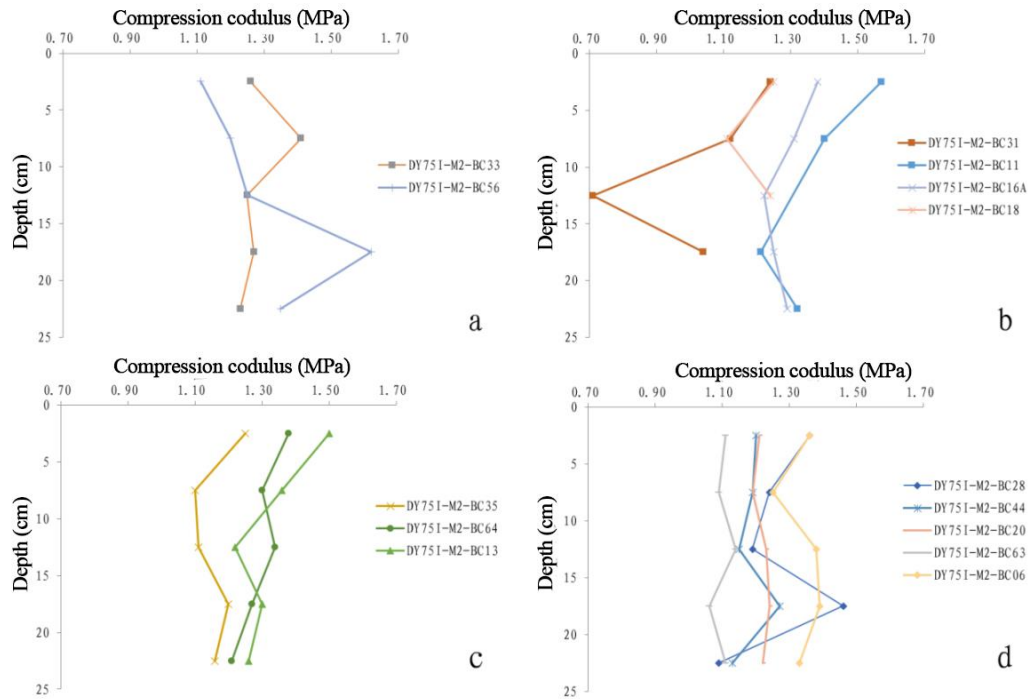
Figure 4-85 Vertical variation of sediment compression modulus

The parameters of compression coefficient and compression modulus indicate that the sediment in the study area belongs to highly compressible soil.

（7）Soil Shear Strength

The cohesion of core sediments at 14 stations in Block M2 ranges from 0.3 kPa to 6.5 kPa, with a mean value of 2.5 kPa. The internal friction angle ranges between 0° and 3.4° degrees, with an average value of 1.6°.

In summary, the sediment in the study area is unconsolidated and soft. Specific characteristics include the following: low specific gravity, low density, high moisture content, high plasticity (natural water content is in a plastic state above the liquid limit), and high compressibility. Under external loading, soft marine sediment can undergo severe deformation.

4.3.3.7 Comparison of Foothills and Plains

The basic topography of Block M can be divided into two types: foothills and plains. The characteristics of sediment from two topography types are as follows:

(1) Sediments from both the foothill area and the plain area of Block M are deep-sea clays, with siliceous debris (including clay minerals and fine sand-sized terrigenous clasts)

as the main component, and a small amount of siliceous biogenic debris (primarily radiolarian and sponge spicules) and volcanic debris. The volcanic clasts content of sediments in foothill areas is slightly higher than that in plain areas.

(2) The dominant clay minerals in the surface sediments of the Block M are illite, followed by chlorite, montmorillonite, and kaolinite. The content of montmorillonite is relatively higher in the mountain foothill area sediments, while the content of illite is relatively higher in the plain area sediments.

(3) The Fe_2O_3/Al_2O_3, TiO_2/Al_2O_3 ratios of the sediments from the foothill area are slightly higher than those of the sediments from the plain area, suggesting that the seamount is one of the main sources of the sediments in Block M.

(4) The geotechnical properties of the surface sediments in Block M2 are influenced by the seafloor topography. Considering the complex sediment sources in the mountain foothill areas, the variation of geotechnical properties with depth is not obvious. In contrast, sediments from deep-sea plains have stable sediment sources, and their geotechnical properties exhibit regular changes with depth. The influence of aprons in the mountain foothill areas affects the geotechnical properties of sediments due to their wave-like terrain.

4.3.4 Physical Oceanographic Environment

The relevant data for the physical oceanographic baseline section of this report includes subsurface buoy data, CTD profile data, shipboard ADCP data, and other publicly available data. Subsurface buoy data were collected from a total of 10 subsurface buoys deployed during five cruises (2020–2023) in the BPC contract area (two of which will be recovered during 2024 cruise); CTD profiles analyzed 16 full-depth stations during four cruises; shipboard ADCP data were collected during two cruises. The survey stations and transects are shown in Figures 4-86 to 4-88.
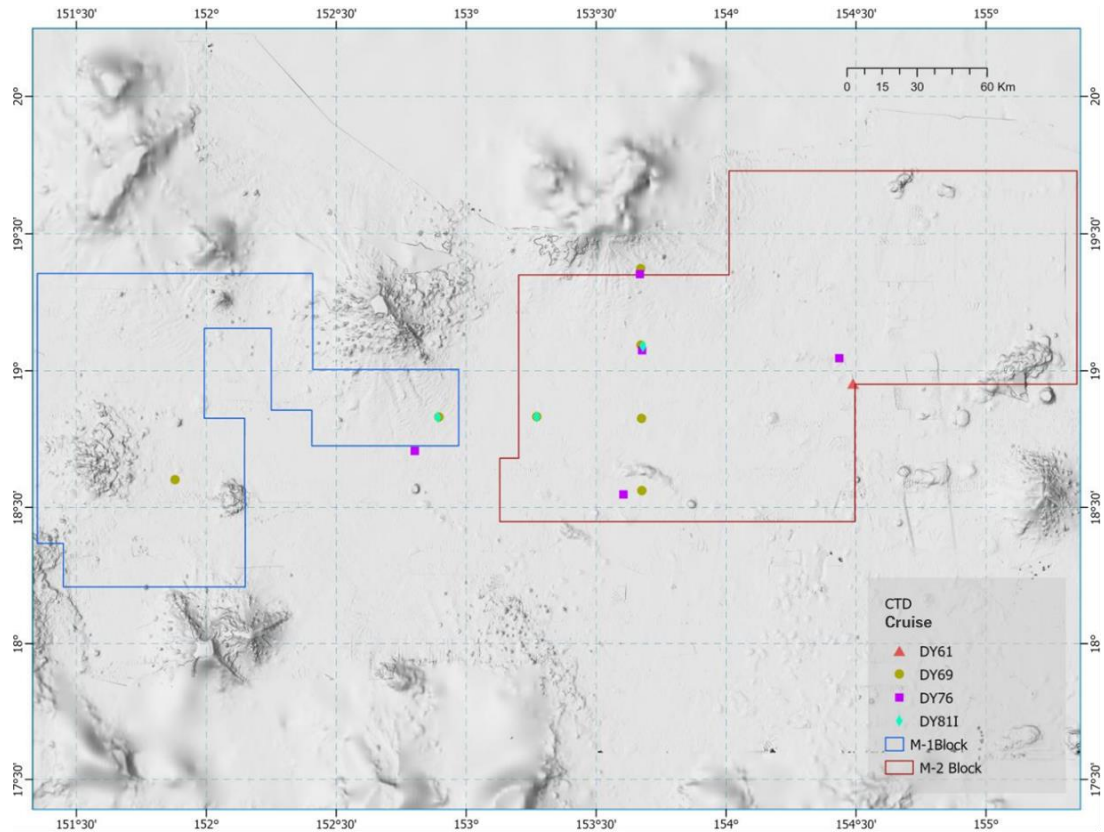
Figure 4-86 Historical CTD profile survey stations in the Blocks M1 and M2 of the BPC contract area
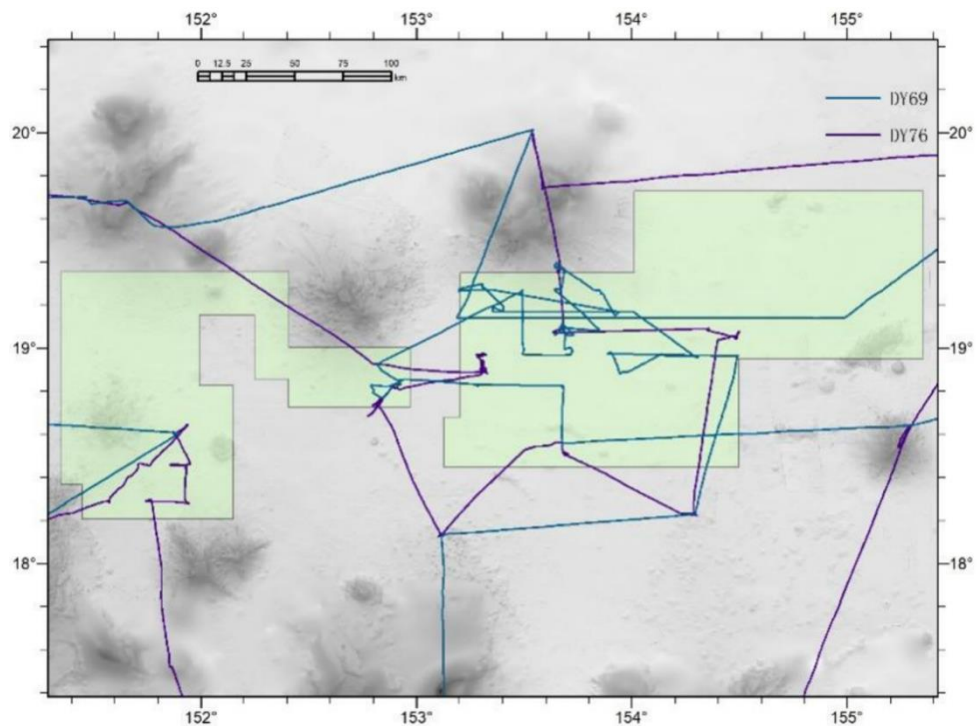
Figure 4-87 Shipboard ADCP track for DY69 and DY76 cruises
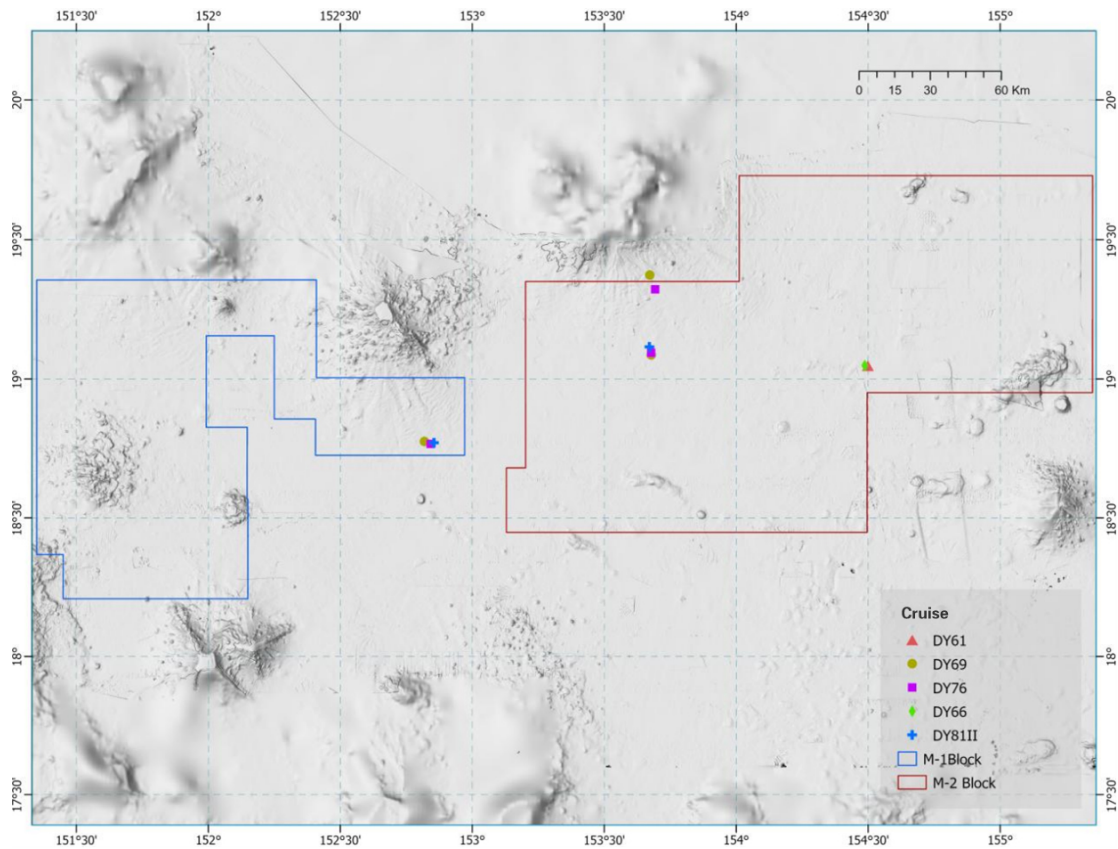
Figure 4-88 Current meter subsurface buoy for the M block of the BPC contract area

Furthermore, public datasets were collected including the WOA23 dataset, sea level anomaly dataset (SLA), and Mesoscale Eddy Trajectory Atlas (META).

4.3.4.1 Temperature-Salinity Structure

4.3.4.1.1 Temperature-Salinity Profiles

Integrating the results of CTD profiles from 16 full-depth stations across four cruises (Figures 4-89 and 4-90), the sea surface temperature ranges from 29.06 to 29.67°C, with a relatively shallow mixed layer depth of approximately 26 to 76 m. The deepest mixed layer among them is 76 m at Station DY76-I-M2-S062CTD14, and the shallowest is 26 m at Station DY81I-M2-ES05-CTD02. The thermocline at each station was identified to be situated between the bottom of the mixed layer and approximately 400 m deep, with a temperature range from 10 to 11°C at the lower boundary of the thermocline. Below 400m, seawater temperature gradually decreases with depth, reaching a bottom layer temperature of approximately 1.51°C (Figure 4-90).

In terms of sea surface salinity, values ranged from 34.46 to 34.82 psu. The salinity profile exhibits an "Inverse S-shaped" three-halocline pattern, with the maximum salinity layer located approximately between 93 to 150 m. The maximum salinity value ranges from 35.04 to 35.21 psu. The minimum salinity layer was situated around 500 to 560 m, with the minimum salinity values ranging between 34.10 and 34.17 psu. A pronounced salinity gradient was observed from the bottom of the mixed layer to the maximum salinity layer, as well as between the maximum and minimum salinity layer, indicating an obvious halocline. Below the minimum salinity layer, salinity gradually increases with depth, stabilizing at around 34.5 to 34.7 psu below 1000 meters (Figure 4-91).

A comparative analysis of temperature and salinity profiles from the years 2020 (DY61), 2021 (DY69), 2022 (DY76), and 2023 (DY81) revealed that the surface temperature was lowest and the surface salinity was highest in 2022. While surface temperature and salinity in 2020, 2021, and 2023 were relatively similar. Notably, in 2020 and 2023, the maximum salinity layer occurred at shallower depths, approximately 50 meters shallower compared to that of 2021 and 2022.
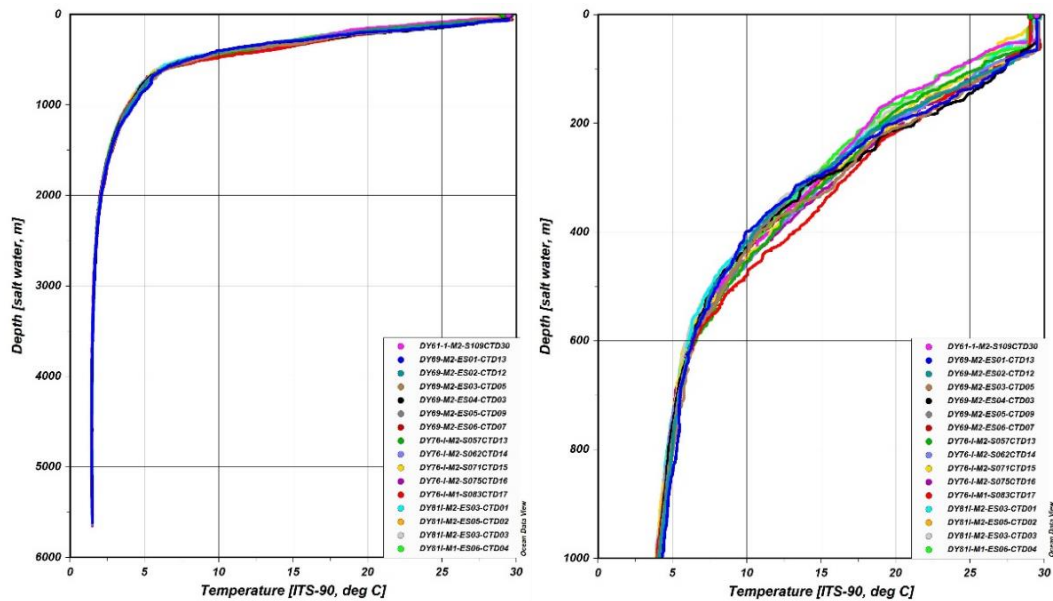
Figure 4-89 Vertical temperature variation characteristics at survey stations
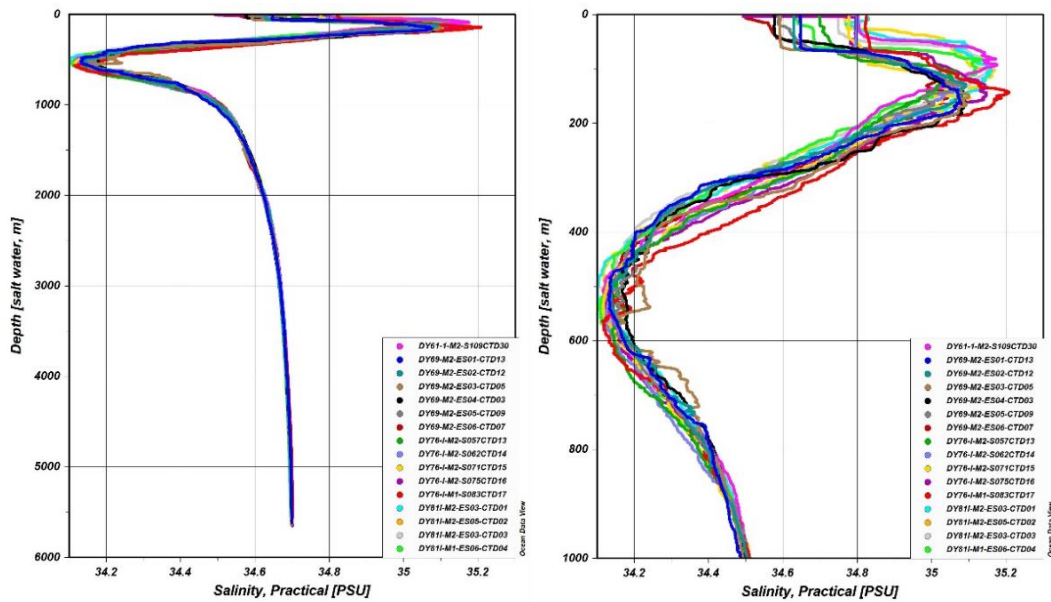
Figure 4-90 Vertical salinity variation characteristics at survey stations

The four stations (DY69-M2-ES04-CTD03, DY69-M2-ES03-CTD05, DY69-M2-ES02-CTD12, and DY69-M2-ES01-CTD13) selected along the north-south cross-section from the M2 foothill area to the plain area, exhibit difference in surface salinity between the plain and foothill areas, with the plain area showing higher surface levels and lower subsurface minimum salinity values compared to the foothill area (Figure 4-91). Similarly, the three stations (DY69-M2-ES06-CTD07, DY69-M2-ES05-CTD09, and DY69-M2-ES02-CTD12) chosen along the east-west cross-section from the M1 foothill area to the plain area, demonstrate higher surface salinity in the plain compared to the foothill area (Figure 4-92). The surface salinity characteristics along north-south cross-section of M2 in 2022 are consistent with the 2021 cruise results, although the subsurface maximum salinity value in the plain area is higher than in the foothill area, and the subsurface minimum salinity value in the plain area is lower than in the foothill area (Figure 4-93). In the east-west cross-section of 2022, the bottom layer temperature and salinity distribution in the M2 foothill area is lower than in the plain area, while the subsurface salinity maximum is also higher in the foothill area than in the plain area (Figure 4-94). The bottom layer potential temperature in the M2 foothill area is higher than in the plain area (Figure 4-95). Furthermore, the bottom layer temperature and salinity in the M1 foothill area are comparable to those in the plain area (Figure 4-96).
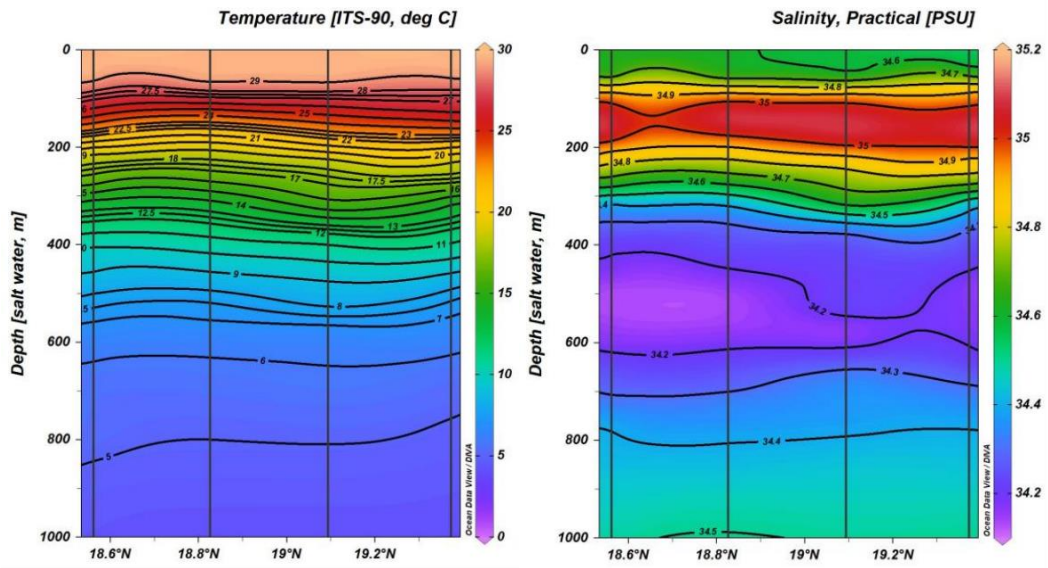
Figure 4-91 Vertical temperature and salinity variation characteristics along the M2 north-south cross-section (2021)
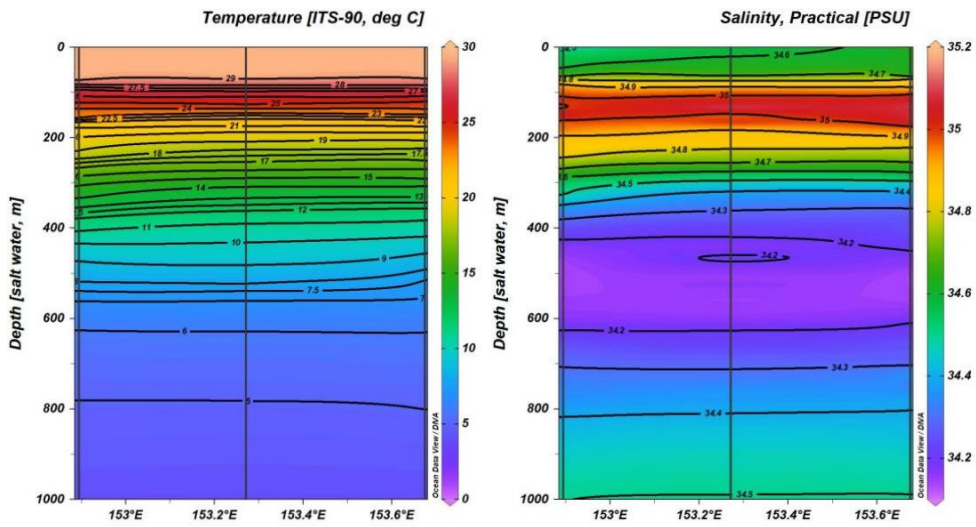
Figure 4-92 Vertical temperature and salinity variation characteristics along the M1 east-west cross-section (2021)
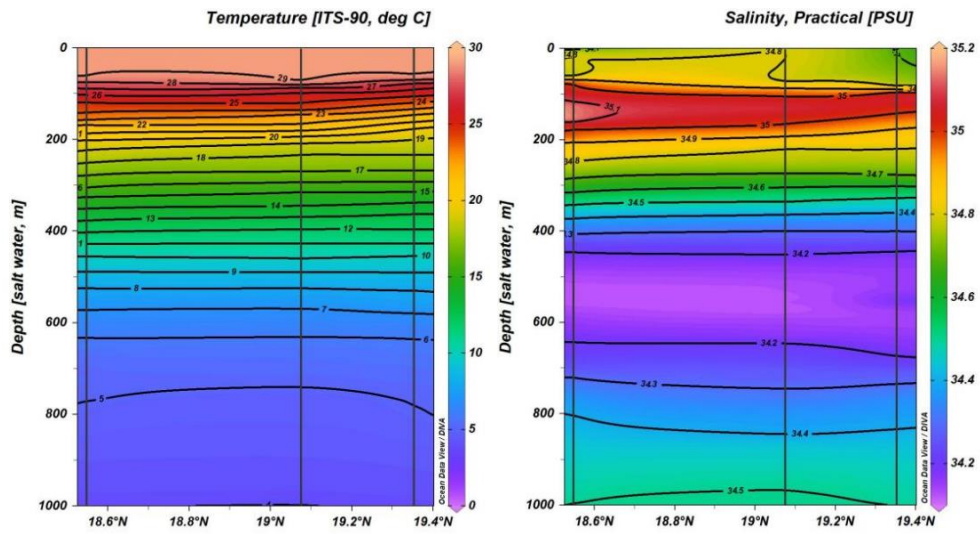
Figure 4-93 Vertical temperature and salinity variation characteristics along the M2 north-south cross-section (2022)
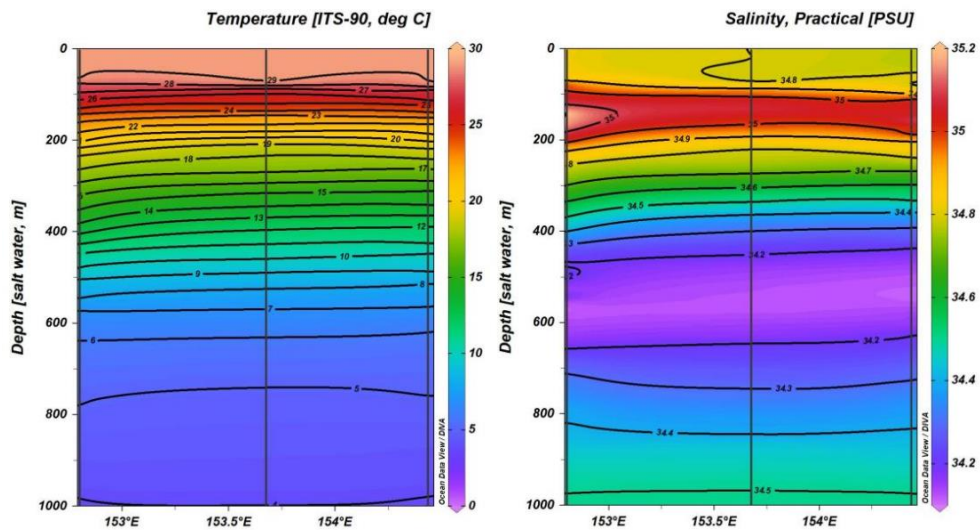
Figure 4-94 Vertical temperature and salinity variation characteristics along the M1 east-west cross-section (2022)
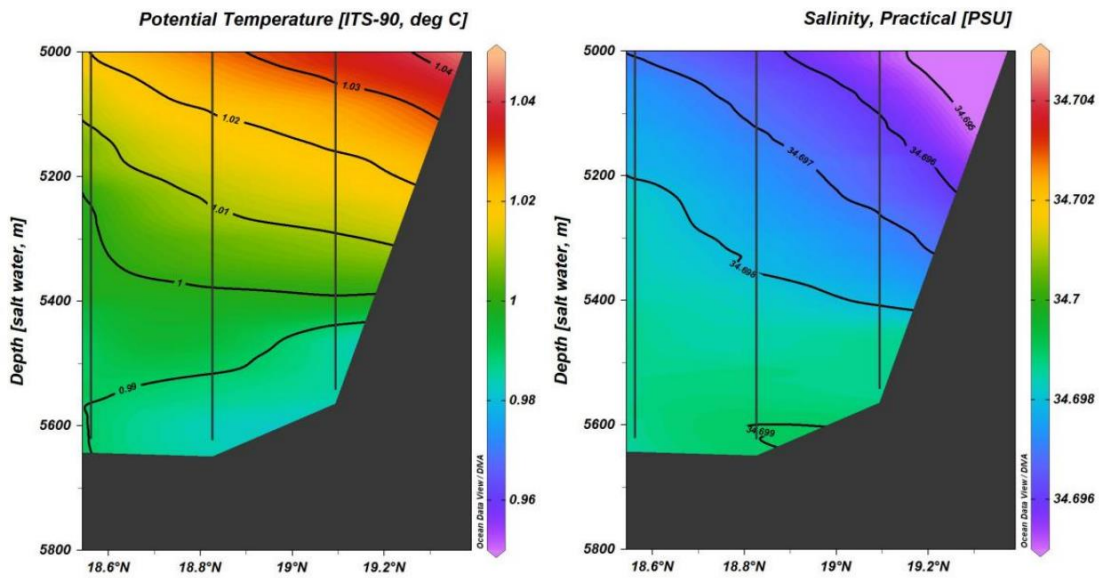
Figure 4-95 Vertical temperature and salinity variation characteristics along the M2 north-south cross-section at the bottom layer (2021)
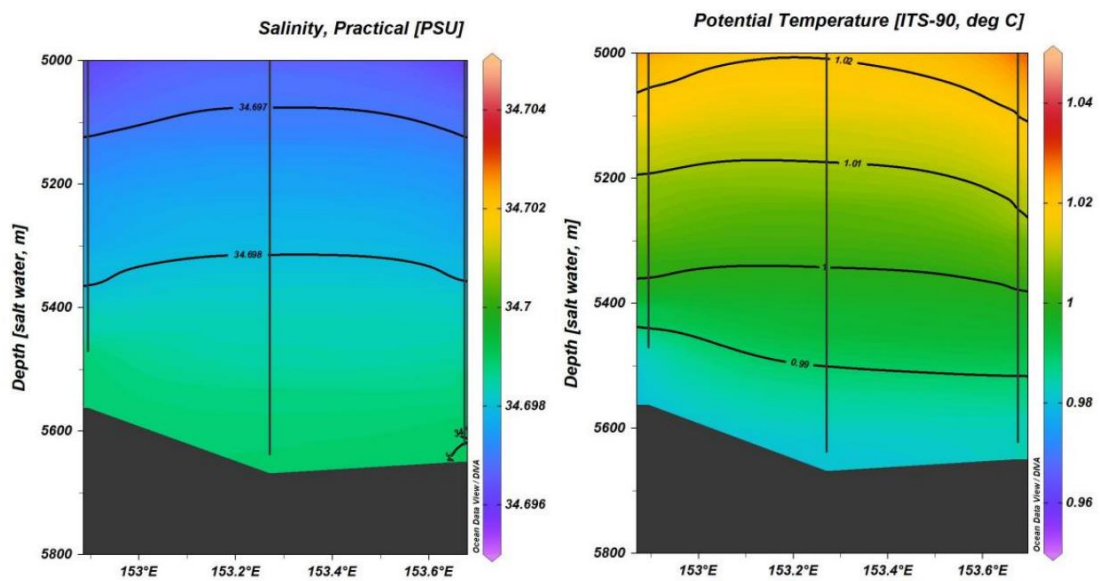
Figure 4-96 Vertical temperature and salinity variation characteristics along the M1 east-west cross-section at the bottom layer (2021)

The analysis of data from the WOA23 dataset (Figures 4-97 to 4-100) reveals a constituent pattern in the distribution of seawater temperature across various depths (100 m, 200 m, 1000 m, and 1500 m) and seasons. The findings indicate that temperatures are generally higher in southern regions and lower in the northern regions for all seasons, except

at 500 m depth where the pattern is reversed, with higher temperatures observed in the north and lower in the south. Additionally, salinity levels exhibit a distinct spatial distribution, with higher values at 0 m and 100 m depths in the north and lower values in the south. Conversely, salinity levels from 200 m to 1500 m depths show an opposite trend, being higher in the south and lower in the north.
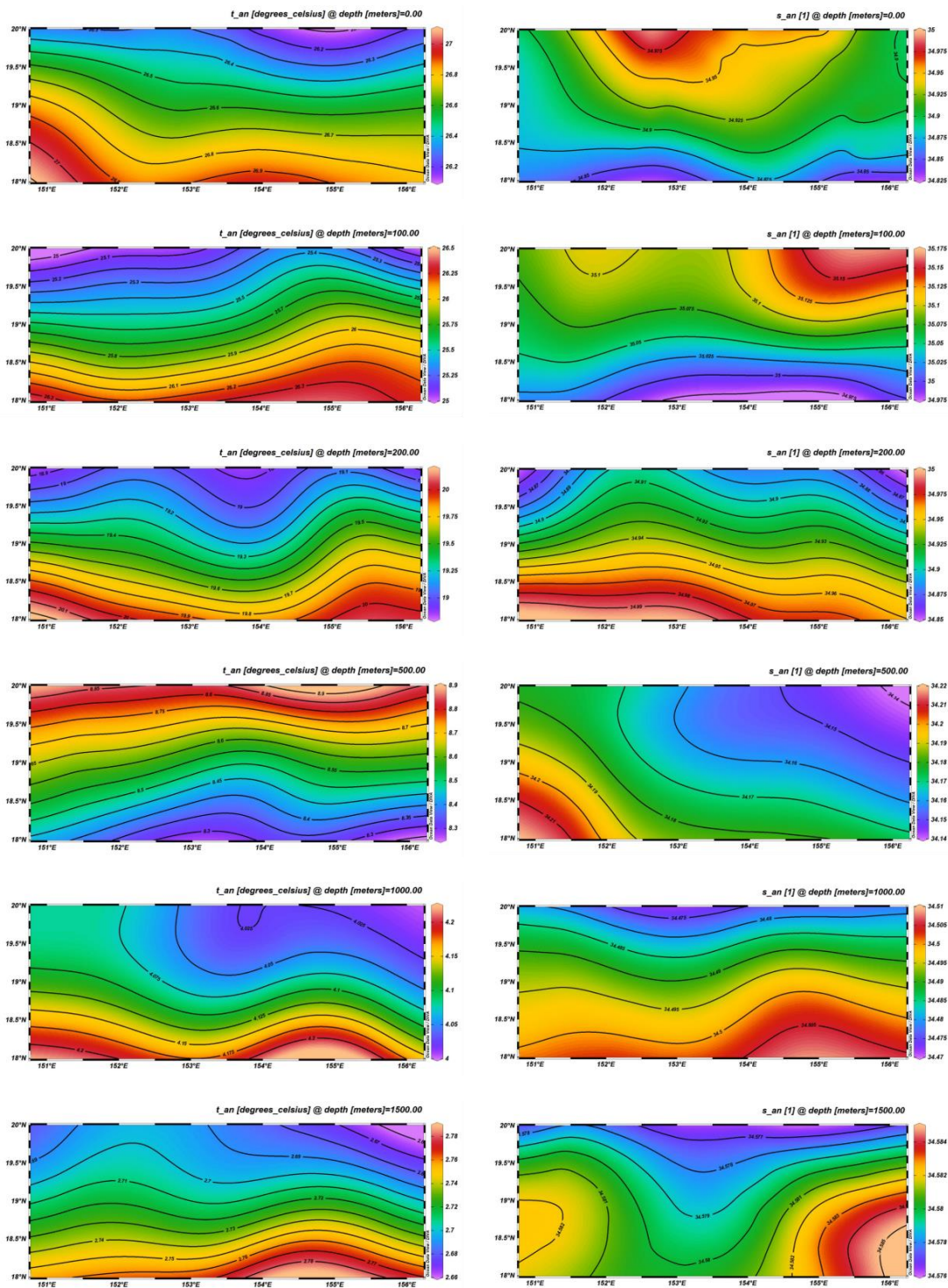
Figure 4-97 Spring season horizontal temperature and salinity variations at different water layers in the Block M (The left figure is for temperature, right figure is for salinity, distributed from top to bottom as 0 m, 100 m, 200 m, 500 m, 1000 m, 1500 m, data source: WOA23, the same below)
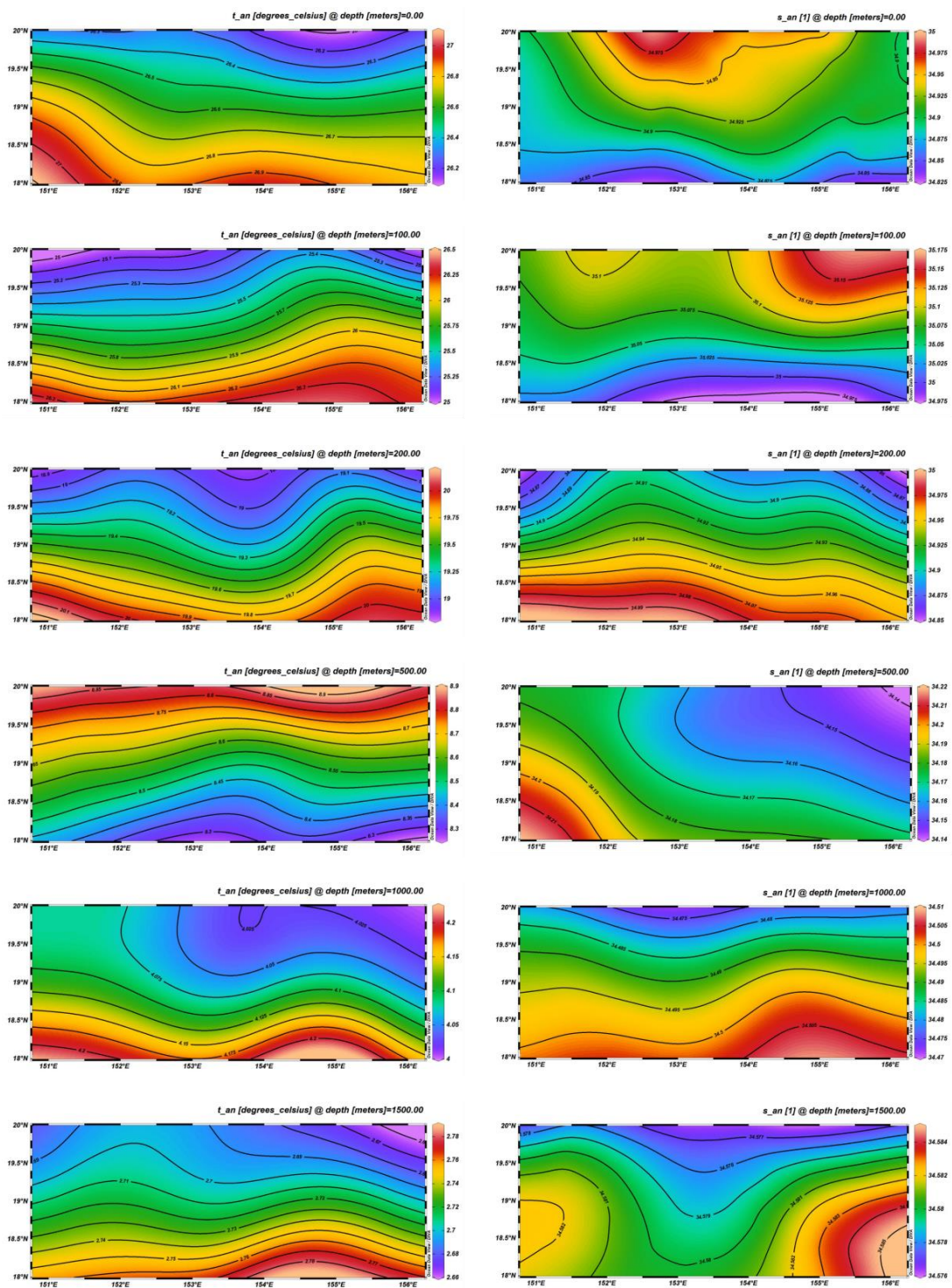
Figure 4-98 Summer season horizontal temperature and salinity variations at different water layers in the block
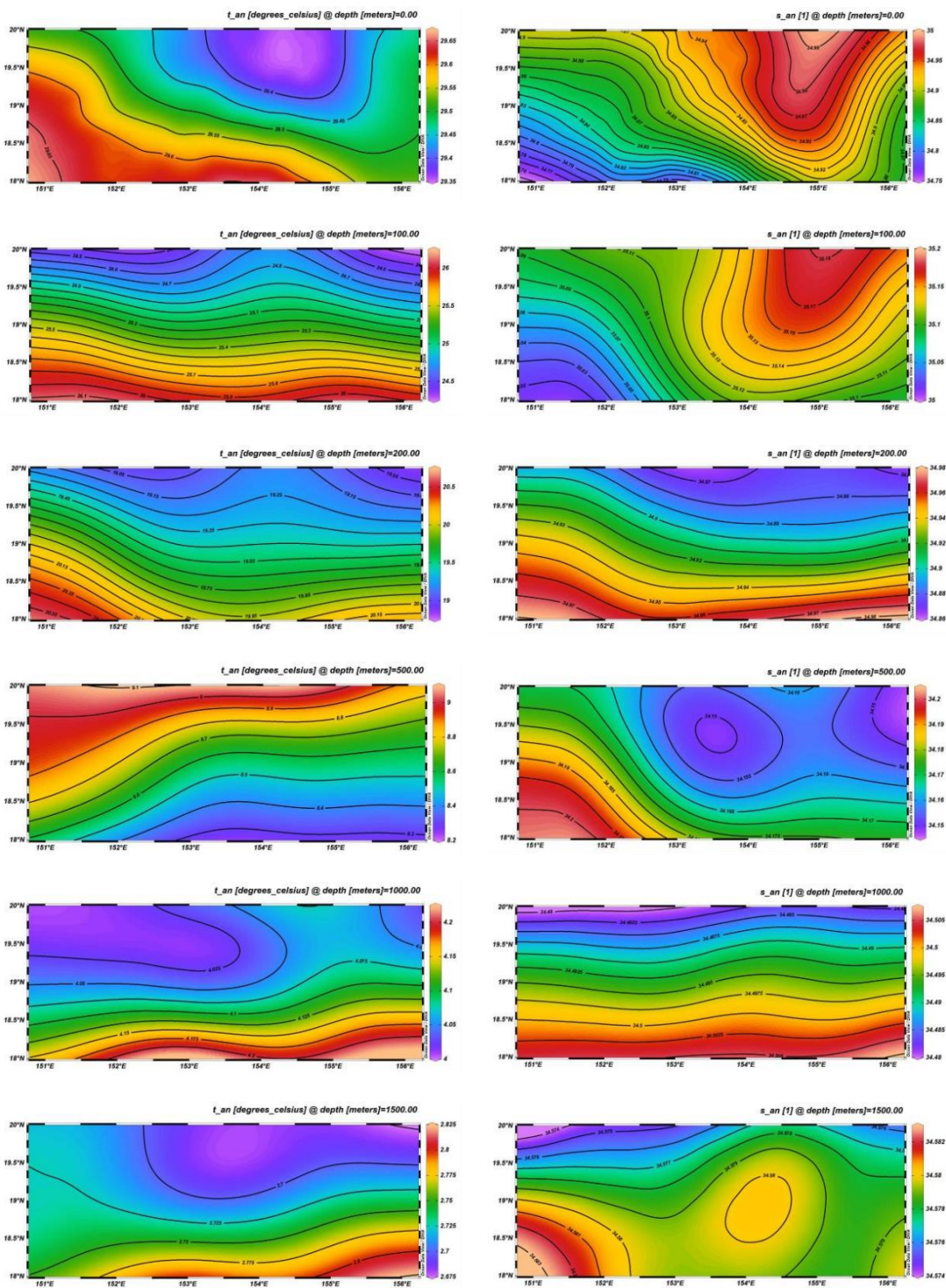
Figure 4-99 Autumn season horizontal temperature and salinity variations at different water layers in the block

206
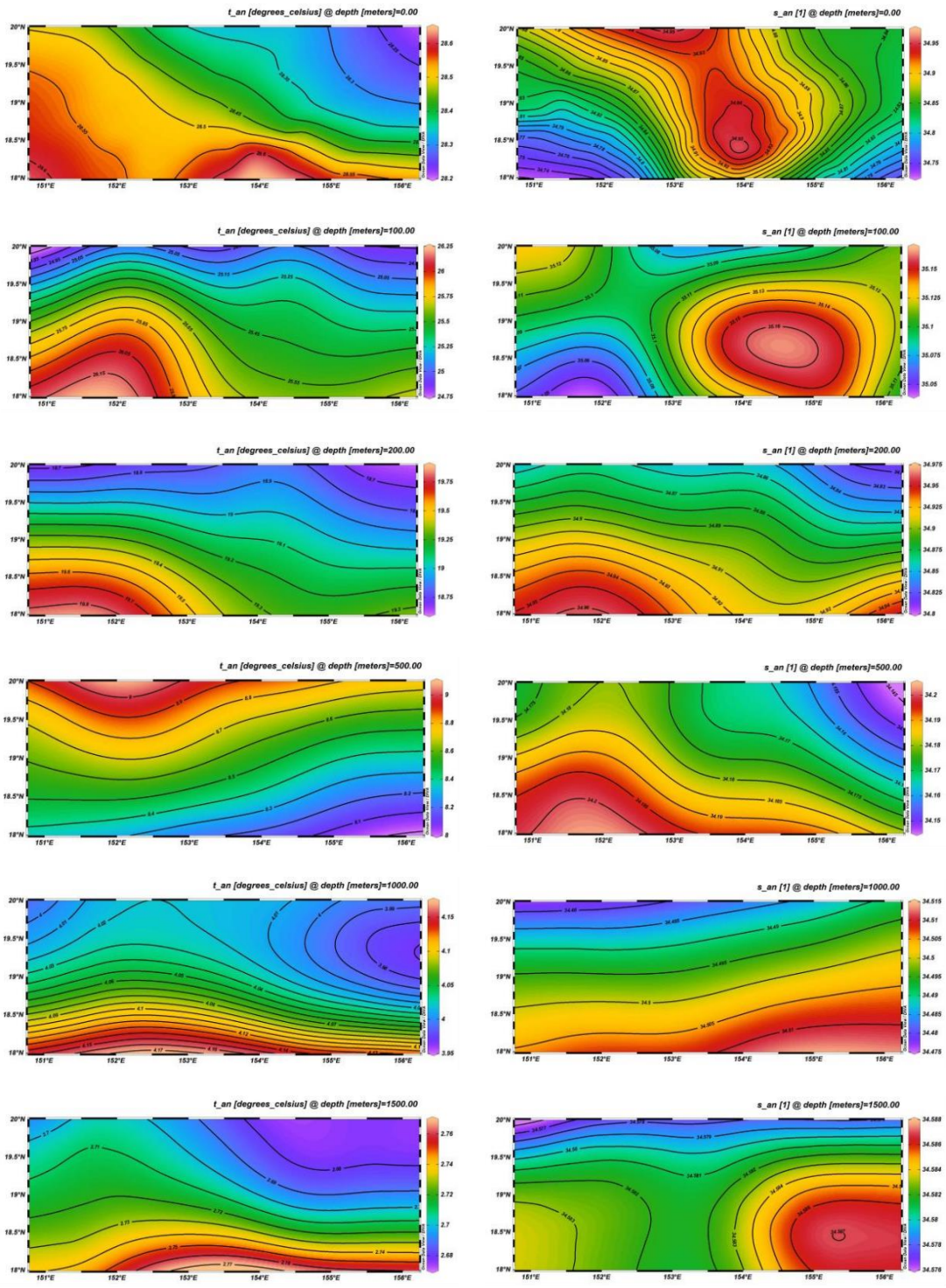
Figure 4-100 Winter season horizontal temperature and salinity variations at different water layers in the block

4.3.4.1.2 Long-term Temperature-Salinity Variation

Based on the long-term temperature and salinity data obtained from CTDs deployed on subsurface buoys during the five cruises (DY61, DY66, DY69, DY76, and DY81), the temperature and salinity variation within the contract area are revealed.

The potential temperature and salinity variation at the near-bottom layer (5646 m) of Station DY61-M2-MX2006 are depicted in Figure 4-101. During the observation period, the potential temperature at 5646 m exhibited a range from a maximum of 0.985°C to a minimum of 0.969°C, with an average of 0.976°C. Salinity ranged from a maximum of 34.6991 psu to a minimum of 34.6978 psu, with an average of 34.6986 psu. Monthly average results (Table 4-18) reveal that the lowest potential temperature occurred in January, and the highest in November, with salinity showing minimal variation.
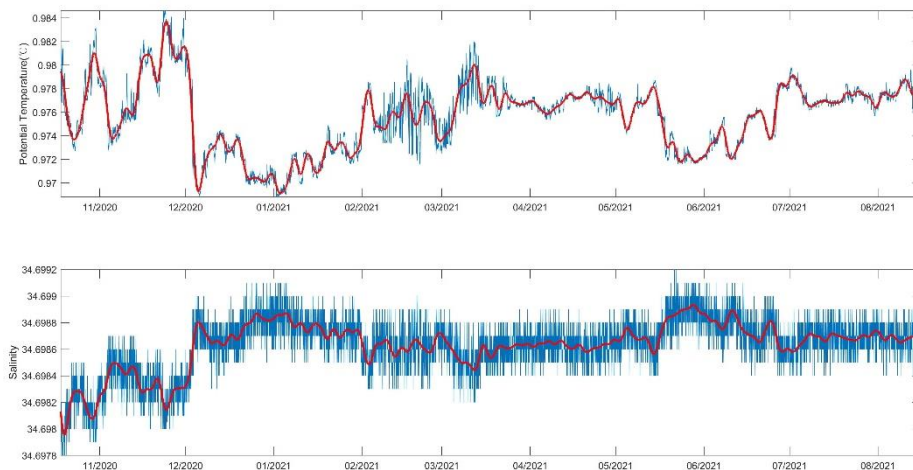
Figure 4-101 Potential temperature and salinity variation at 5646 m water depth of Station DY61-M2-MX2006

(Blue line represents observed values, red line represents values after 48-hour low-pass filtering, the same as below)

Figures 4-102 and 4-103 depict the variability in potential temperature and salinity variation at the upper and middle layers (951 m and 1233 m water depth) of Station DY66-M2-MX2101. The potential temperature at 951 m ranged from a maximum of 4.392°C to a minimum of 3.853°C, with an average of 4.139°C. While salinity ranged from a maximum of 34.5033 psu to a minimum of 34.4338 psu, with an average of 34.4793 psu. At 1233 m, potential temperature ranged from a maximum of 3.341°C to a minimum of 3.002°C, with an average of 3.226°C. Salinity ranged from a maximum of 34.5478 psu to a minimum of

34.5049 psu, with an average of 34.5306 psu. Analysis of the monthly average data (Table 4-18) revealed that the lowest potential temperature at 951 m was recorded in August 2022, with the highest in May 2022. Salinity was lowest in May 2022 and highest in November 2021. Seasonal variations were observed in the potential temperature at 1233 m, with the lowest temperature occurring in June 2022 and the highest in December 2021. Salinity at this depth was lowest in May 2022 and highest in November 2021, with a difference of 0.018 psu between the highest and lowest salinity values.
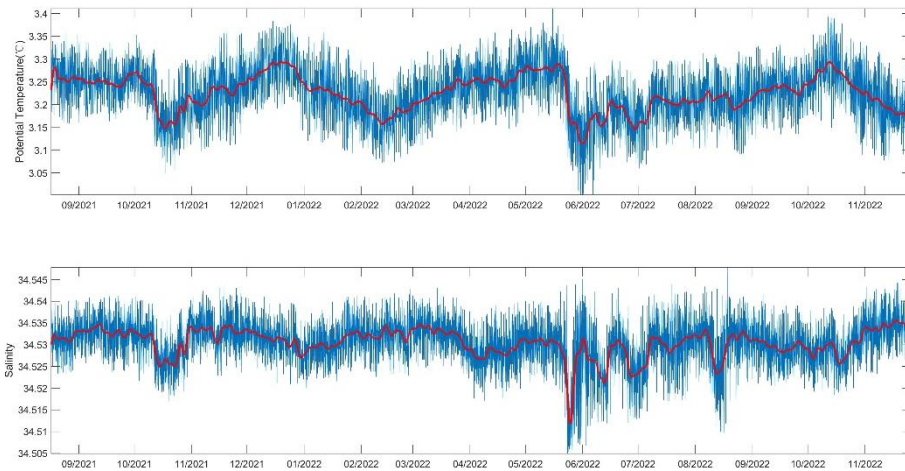
Figure 4-102 Potential temperature and salinity variation at 951 m water depth of Station DY66-I-M2-MX2101
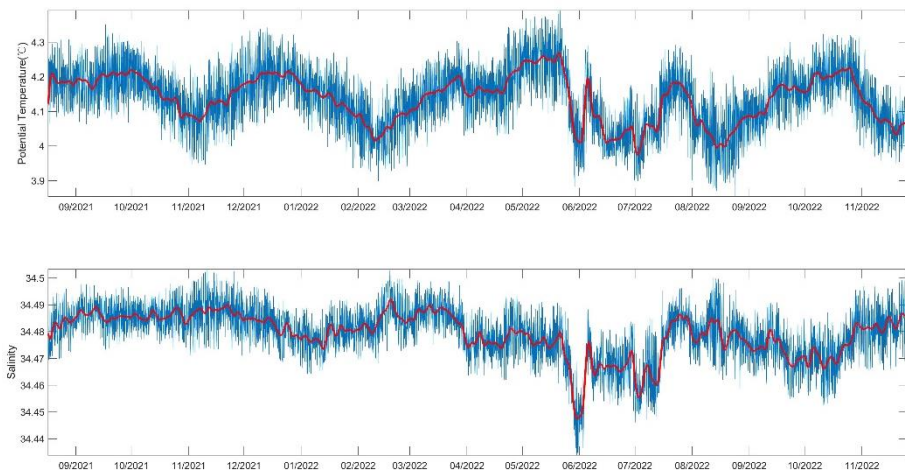
Figure 4-103 Potential temperature and salinity variation at 1233 m water depth of Station DY66-I-M2-MX2101

Figure 4-104 illustrates the variation of potential temperature and salinity at the near-bottom layer (4805 m) of Station DY69-ES04-MX01. The potential temperature ranged from a maximum of 1.057°C to a minimum of 1.033°C, with an average of 1.046°C. While salinity ranged from a maximum of 34.6952 to a minimum of 34.6918, with an average of 34.6935. Analysis of the monthly average data in Table 4-18 indicates that the lowest potential temperature was recorded in July, and the highest in May, with minimal fluctuations in salinity.
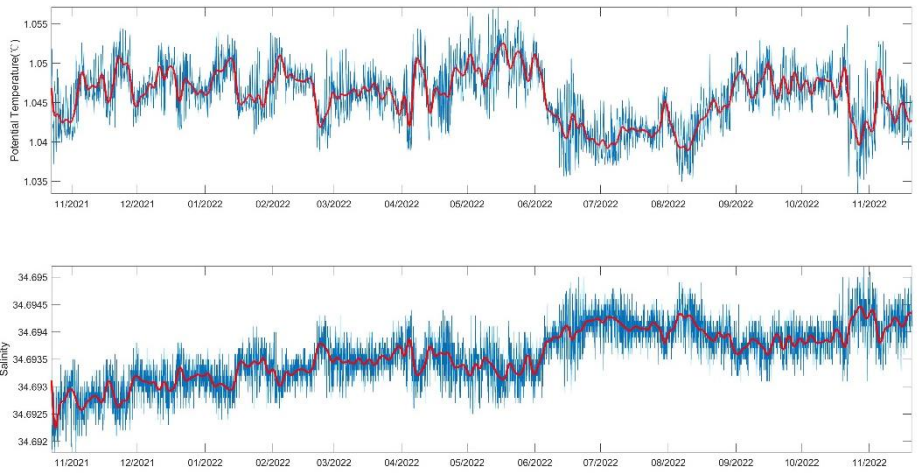
Figure 4-104: Potential temperature and salinity time variation at 4805 m of Station DY69-ES04-MX01

Table 4-18 Statistical table of subsurface buoy temperature-salinity characteristics

Station	Depth（m）	Year	Month	Potential Temperature（℃）			Salinity (PSU)		
				Maximum	Minimum	Average	Maximum	Minimum	Average
DY61-M2-MX2006	5647	2020	10	0.983	0.973	0.977	34.6985	34.6978	34.6982
		2020	11	0.985	0.973	0.979	34.6987	34.6980	34.6983
		2020	12	0.981	0.969	0.972	34.6991	34.6982	34.6987
		2021	1	0.976	0.969	0.972	34.6991	34.6985	34.6988
		2021	2	0.980	0.972	0.976	34.6990	34.6983	34.6986
		2021	3	0.982	0.973	0.977	34.6989	34.6982	34.6986
		2021	4	0.978	0.975	0.977	34.6989	34.6984	34.6986
		2021	5	0.979	0.972	0.975	34.6992	34.6984	34.6988
		2021	6	0.979	0.972	0.975	34.6991	34.6984	34.6987
		2021	7	0.980	0.976	0.977	34.6989	34.6984	34.6987
		2021	8	0.980	0.976	0.978	34.6989	34.6984	34.6987
DY66-M2-MX2101	951	2021	8	4.309	4.065	4.186	34.4960	34.4694	34.4825
		2021	9	4.352	4.063	4.198	34.4977	34.4733	34.4860
		2021	10	4.303	3.982	4.155	34.4978	34.4740	34.4857
		2021	11	4.319	3.947	4.121	34.5033	34.4710	34.4876
		2021	12	4.344	4.057	4.201	34.4967	34.4671	34.4822
		2022	1	4.274	3.936	4.134	34.4918	34.4642	34.4789
		2022	2	4.226	3.898	4.062	34.5028	34.4683	34.4846
		2022	3	4.303	3.998	4.156	34.4991	34.4687	34.4860
		2022	4	4.343	4.031	4.174	34.4932	34.4619	34.4770
		2022	5	4.392	3.883	4.208	34.4911	34.4338	34.4718
		2022	6	4.290	3.901	4.057	34.4883	34.4364	34.4663
		2022	7	4.292	3.899	4.105	34.4963	34.4460	34.4730
		2022	8	4.224	3.853	4.044	34.5001	34.4590	34.4789
		2022	9	4.300	3.992	4.139	34.4909	34.4549	34.4730
		2022	10	4.324	4.002	4.197	34.4955	34.4526	34.4727
	1233	2021	8	3.355	3.158	3.259	34.5403	34.5233	34.5318
		2021	9	3.337	3.163	3.251	34.5413	34.5237	34.5330
		2021	10	3.353	3.049	3.203	34.5410	34.5170	34.5292

Station	Depth（m）	Year	Month	Potential Temperature（℃）			Salinity (PSU)		
				Maximum	Minimum	Average	Maximum	Minimum	Average
		2021	11	3.358	3.098	3.226	34.5432	34.5229	34.5331
		2021	12	3.384	3.144	3.276	34.5410	34.5209	34.5310
		2022	1	3.358	3.093	3.222	34.5412	34.5200	34.5305
		2022	2	3.300	3.072	3.179	34.5429	34.5226	34.5323
		2022	3	3.333	3.109	3.228	34.5431	34.5222	34.5327
		2022	4	3.365	3.147	3.255	34.5396	34.5171	34.5285
		2022	5	3.411	3.002	3.243	34.5451	34.5049	34.5278
		2022	6	3.299	3.002	3.170	34.5430	34.5068	34.5265
		2022	7	3.300	3.060	3.199	34.5438	34.5131	34.5295
		2022	8	3.317	3.091	3.210	34.5478	34.5097	34.5302
		2022	9	3.331	3.125	3.233	34.5415	34.5199	34.5297
		2022	10	3.393	3.090	3.260	34.5402	34.5185	34.5290
		2021	10	1.052	1.037	1.043	34.6934	34.6918	34.6926
		2021	11	1.054	1.040	1.047	34.6938	34.6918	34.6928
		2021	12	1.053	1.042	1.047	34.6938	34.6923	34.6931
		2022	1	1.054	1.041	1.047	34.6941	34.6924	34.6932
		2022	2	1.054	1.039	1.047	34.6943	34.6926	34.6934
		2022	3	1.052	1.041	1.046	34.6943	34.6928	34.6935
DY69-ES04-MX01	4805	2022	4	1.054	1.039	1.047	34.6944	34.6926	34.6935
		2022	5	1.057	1.043	1.050	34.6943	34.6925	34.6933
		2022	6	1.053	1.036	1.043	34.6950	34.6928	34.6939
		2022	7	1.047	1.037	1.041	34.6948	34.6933	34.6941
		2022	8	1.051	1.035	1.043	34.6949	34.6932	34.6940
		2022	9	1.053	1.043	1.048	34.6945	34.6931	34.6938
		2022	10	1.055	1.033	1.046	34.6952	34.6931	34.6940
		2022	11	1.053	1.038	1.044	34.6951	34.6933	34.6942
		2021	10	2.002	1.905	1.956	34.6278	34.6183	34.6230
		2021	11	1.998	1.853	1.929	34.6298	34.6147	34.6226
DY69-ES03-MX02	1992	2021	12	1.999	1.862	1.942	34.6276	34.6128	34.6203
		2022	1	2.011	1.909	1.957	34.6289	34.6127	34.6185
		2022	2	1.998	1.879	1.942	34.6279	34.6135	34.6200

Station	Depth（m）	Year	Month	Potential Temperature（℃）			Salinity (PSU)		
				Maximum	Minimum	Average	Maximum	Minimum	Average
		2022	3	2.017	1.886	1.949	34.6270	34.6147	34.6206
		2022	4	2.016	1.899	1.957	34.6277	34.6152	34.6216
		2022	5	2.022	1.899	1.958	34.6280	34.6154	34.6219
		2022	6	2.025	1.886	1.947	34.6296	34.6155	34.6233
		2022	7	1.983	1.862	1.923	34.6288	34.6175	34.6230
		2022	8	1.979	1.878	1.931	34.6296	34.6187	34.6245
		2022	9	2.035	1.905	1.962	34.6284	34.6156	34.6229
		2022	10	2.026	1.905	1.969	34.6281	34.6146	34.6205
		2022	11	2.013	1.900	1.953	34.6267	34.6140	34.6199
		2021	10	0.990	0.984	0.987	34.6966	34.6957	34.6960
		2021	11	0.990	0.972	0.980	34.6974	34.6956	34.6966
		2021	12	0.990	0.973	0.981	34.6977	34.6958	34.6967
		2022	1	0.984	0.975	0.978	34.6978	34.6961	34.6970
		2022	2	0.987	0.978	0.982	34.6975	34.6962	34.6969
		2022	3	0.991	0.979	0.984	34.6974	34.6963	34.6968
	5540	2022	4	0.991	0.983	0.987	34.6972	34.6963	34.6968
		2022	5	0.992	0.978	0.984	34.6976	34.6965	34.6970
		2022	6	0.984	0.978	0.981	34.6977	34.6967	34.6972
		2022	7	0.991	0.979	0.984	34.6975	34.6965	34.6971
		2022	8	0.989	0.978	0.983	34.6976	34.6966	34.6971
		2022	9	0.991	0.977	0.983	34.6977	34.6965	34.6971
		2022	10	0.994	0.979	0.986	34.6979	34.6963	34.6970
		2022	11	0.998	0.973	0.979	34.6980	34.6963	34.6973
		2021	10	2.037	1.939	1.992	34.6195	34.6110	34.6151
		2021	11	2.037	1.864	1.947	34.6233	34.6082	34.6164
		2021	12	2.023	1.854	1.929	34.6258	34.6105	34.6177
		2022	1	2.052	1.918	1.984	34.6244	34.6120	34.6175
DY69-ES06-MX03	1999	2022	2	2.040	1.913	1.979	34.6233	34.6118	34.6176
		2022	3	2.016	1.904	1.954	34.6228	34.6115	34.6175
		2022	4	2.023	1.905	1.966	34.6241	34.6143	34.6192
		2022	5	2.041	1.888	1.955	34.6250	34.6107	34.6187

Station	Depth (m)	Year	Month	Potential Temperature (℃)			Salinity (PSU)		
				Maximum	Minimum	Average	Maximum	Minimum	Average
		2022	6	2.047	1.892	1.969	34.6233	34.6083	34.6160
		2022	7	2.017	1.903	1.960	34.6234	34.6100	34.6162
		2022	8	1.987	1.856	1.920	34.6273	34.6128	34.6210
		2022	9	2.000	1.835	1.904	34.6278	34.6129	34.6208
		2022	10	2.037	1.845	1.935	34.6301	34.6133	34.6231
		2022	11	2.035	1.874	1.941	34.6274	34.6116	34.6176
		2021	10	1.005	1.000	1.002	34.6957	34.6945	34.6949
		2021	11	1.008	0.989	1.000	34.6964	34.6943	34.6954
		2021	12	1.001	0.985	0.992	34.6970	34.6955	34.6963
		2022	1	1.015	0.987	1.006	34.6970	34.6946	34.6956
		2022	2	1.004	0.995	0.999	34.6966	34.6956	34.6962
		2022	3	1.001	0.990	0.996	34.6969	34.6959	34.6964
	5333	2022	4	1.008	0.991	0.998	34.6969	34.6954	34.6963
		2022	5	1.008	0.998	1.002	34.6966	34.6954	34.6961
		2022	6	1.008	0.992	1.000	34.6970	34.6955	34.6962
		2022	7	1.000	0.987	0.996	34.6972	34.6960	34.6965
		2022	8	1.000	0.993	0.997	34.6970	34.6961	34.6965
		2022	9	1.003	0.992	0.998	34.6970	34.6961	34.6965
		2022	10	1.015	0.990	1.004	34.6971	34.6934	34.6957
		2022	11	1.007	0.993	0.998	34.6969	34.6957	34.6964
		2022	12	10.248	8.337	9.361	34.2607	34.0914	34.1831
		2023	1	10.314	8.145	9.190	34.2448	34.0934	34.1608
		2023	2	10.449	8.243	9.440	34.2432	34.0908	34.1662
		2023	3	10.435	8.584	9.441	34.2435	34.0982	34.1657
		2023	4	10.008	8.507	9.266	34.2168	34.0714	34.1491
DY76-ES04-MX01	468	2023	5	9.934	8.162	8.953	34.2263	34.0472	34.1298
		2023	6	10.380	8.326	9.270	34.2349	34.0612	34.1504
		2023	7	10.368	8.464	9.507	34.2965	34.0780	34.1770
		2023	8	10.174	7.911	8.939	34.2425	34.0700	34.1397
		2023	9	9.669	7.911	8.683	34.2023	34.0750	34.1444
		2023	10	9.854	7.948	9.028	34.2252	34.0862	34.1528

Station	Depth（m）	Year	Month	Potential Temperature（℃）			Salinity (PSU)		
				Maximum	Minimum	Average	Maximum	Minimum	Average
	5024	2022	12	1.032	1.018	1.025	34.6921	34.6910	34.6916
		2023	1	1.032	1.018	1.025	34.6924	34.6911	34.6917
		2023	2	1.032	1.022	1.027	34.6920	34.6911	34.6916
		2023	3	1.028	1.020	1.024	34.6922	34.6913	34.6918
		2023	4	1.032	1.018	1.025	34.6923	34.6912	34.6917
		2023	5	1.028	1.017	1.023	34.6925	34.6915	34.6919
		2023	6	1.031	1.020	1.025	34.6922	34.6912	34.6917
		2023	7	1.031	1.018	1.025	34.6923	34.6913	34.6918
		2023	8	1.035	1.022	1.028	34.6921	34.6909	34.6915
		2023	9	1.033	1.023	1.028	34.6919	34.6910	34.6915
		2023	10	1.035	1.017	1.027	34.6924	34.6908	34.6916
DY76-ES03-MX02	5352	2022	12	1.000	0.992	0.996	34.6945	34.6934	34.6941
		2023	1	1.007	0.987	1.000	34.6948	34.6934	34.6940
		2023	2	1.005	0.992	0.998	34.6947	34.6935	34.6941
		2023	3	1.002	0.988	0.995	34.6947	34.6937	34.6942
		2023	4	1.000	0.991	0.995	34.6946	34.6938	34.6942
		2023	5	1.000	0.994	0.997	34.6946	34.6938	34.6942
		2023	6	1.000	0.989	0.994	34.6948	34.6938	34.6944
		2023	7	1.000	0.989	0.994	34.6948	34.6939	34.6943
		2023	8	1.017	0.990	1.005	34.6948	34.6928	34.6937
		2023	9	1.011	0.996	1.004	34.6945	34.6930	34.6937
		2023	10	1.003	0.987	0.995	34.6949	34.6936	34.6942
DY76-ES06-MX03	5554	2022	12	0.984	0.976	0.979	34.7096	34.7083	34.7092
		2023	1	0.988	0.980	0.984	34.7095	34.7082	34.7088
		2023	2	0.995	0.982	0.987	34.7092	34.7075	34.7087
		2023	3	0.996	0.979	0.986	34.7090	34.7045	34.7065
		2023	4	0.987	0.980	0.983	34.7080	34.7068	34.7074
		2023	5	0.994	0.975	0.984	34.7089	34.7070	34.7079
		2023	6	0.980	0.976	0.978	34.7091	34.7081	34.7085
		2023	7	0.981	0.965	0.971	34.7095	34.7081	34.7089
		2023	8	0.968	0.965	0.966	34.7095	34.7087	34.7091

Station	Depth（m）	Year	Month	Potential Temperature（℃）			Salinity (PSU)		
				Maximum	Minimum	Average	Maximum	Minimum	Average
		2023	9	0.986	0.967	0.974	34.7098	34.7073	34.7087
		2023	10	0.987	0.968	0.974	34.7094	34.7076	34.7086

Figures 4-105 and 4-106 illustrate the variation in potential temperature and salinity at the mid-depth (1992 m) and near-bottom (5540 m) levels of Station DY69-ES03-MX02. During the observation period, the potential temperature at mid-depth ranged from a maximum of 2.035°C to a minimum of 1.853°C, with an average of 1.948°C; while salinity ranged from a maximum of 34.6298 psu to a minimum of 34.6127 psu, with an average of 34.6216 psu. At the near-bottom level, potential temperature ranged from a maximum of 0.998°C to a minimum of 0.972°C, with an average of 0.983°C; while salinity ranged from a maximum of 34.6980 to a minimum of 34.6956, with an average of 34.6969. Analysis of the monthly average data (Table 4-18) reveals that the lowest mid-depth potential temperature occurred in July and highest in October, with salinity being lowest in January and highest in August. For the near-bottom level, the potential temperature was lowest in January and highest in April, with minimal fluctuations in salinity.
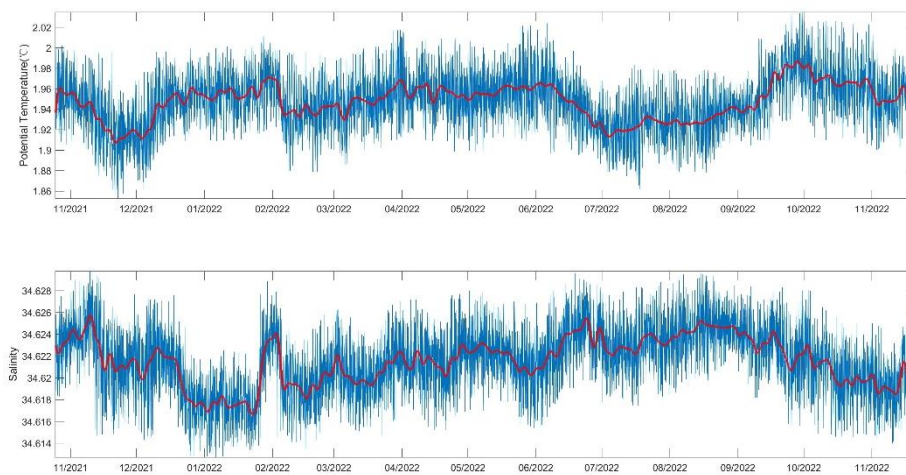
Figure 4-105 Potential temperature and salinity time variation at 1992 m water depth of Station DY69-ES03-MX02
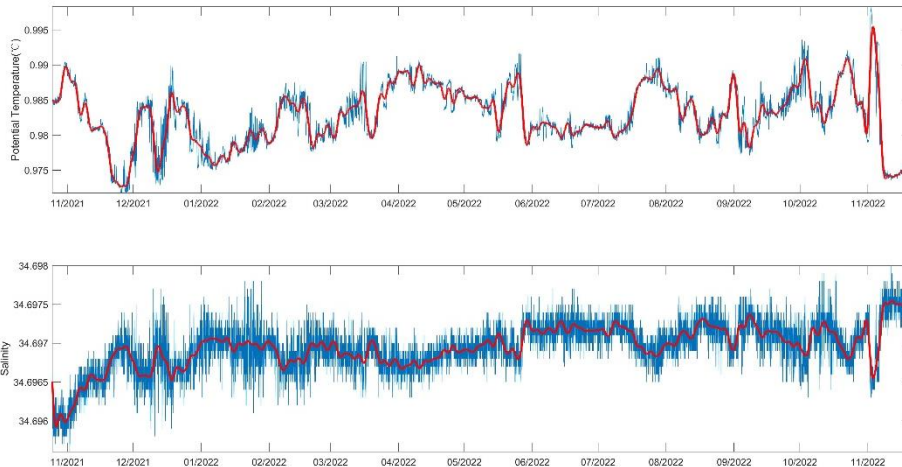
Figure 4-106 Potential temperature and salinity time variation at 5540 m water depth of Station DY69-ES03-MX02

Figures 4-107 and 4-108 illustrate the variation in potential temperature and salinity at the mid-depth (1999 m) and near-bottom (5333 m) levels of Station DY69-ES06-MX03. The mid-depth potential temperature ranged from a maximum of 2.052°C to a minimum of 1.835°C, with an average of 1.952°C; while salinity ranged from a maximum of 34.6301 psu to a minimum of 34.6082 psu, with an average of 34.6182 psu. At the near-bottom, potential temperature ranged from a maximum of 1.015°C to a minimum of 0.985°C, with an average of 0.999°C; while salinity ranged from a maximum of 34.6972 psu to a minimum of 34.6934 psu, with an average of 34.6961 psu. Analysis of the monthly average data in Table 4-18 reveals that the mid-depth potential temperature was at its lowest in September 2022 and highest in October 2021, with salinity reaching its lowest in October 2021 and its highest in October 2022. In contrast, the near-bottom potential temperature was lowest in December 2021 and highest in January 2022, with minimal fluctuations in salinity.
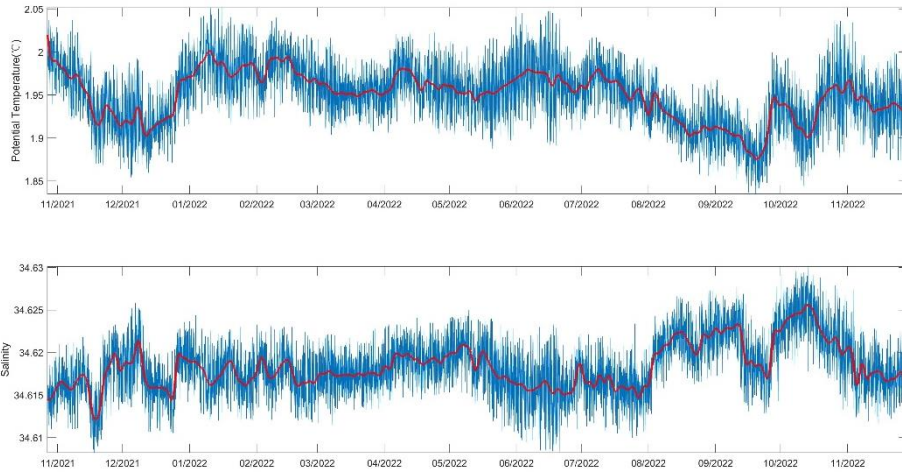
Figure 4-107 Potential temperature and salinity time variation chart at 1999 m water depth in Station
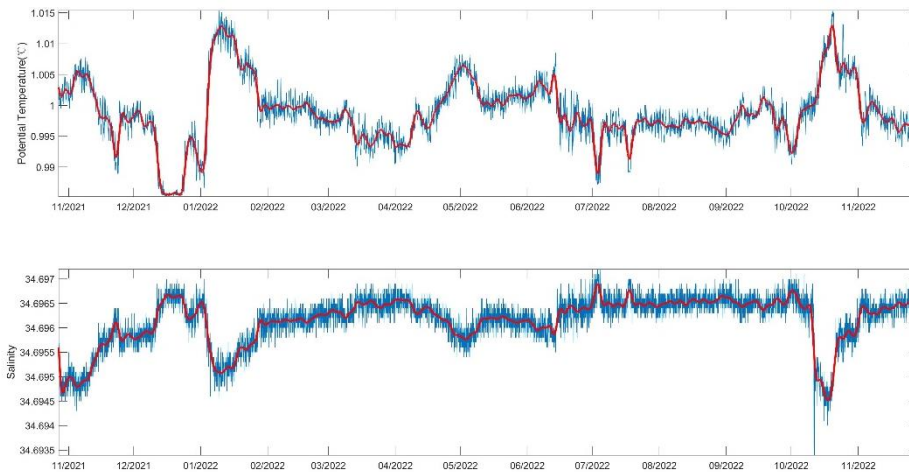
DY69-ES06-MX03

Figure 4-108 Potential temperature and salinity time variation chart at 5333 m water depth in Station

DY69-ES06-MX03

Figures 4-109 and 4-110 illustrate the variation in potential temperature and salinity at the upper (468 m) and near-bottom (5024 m) levels of Station DY76-ES04-MX01. The upper layer potential temperature ranged from a maximum of 10.380°C to a minimum of 7.911°C, with an average of 9.233°C; while salinity ranged from a maximum of 34.2965 psu to a minimum of 34.0472 psu, with an average of 34.1563 psu. At near-bottom, potential temperature ranged from a maximum of 1.035°C to a minimum of 1.017°C, with an average of 1.026°C; while salinity ranged from a maximum of 34.6925 psu to a minimum of 34.6908 psu, with an average of 34.6917 psu. Analysis of the monthly average data in Table 4-18 reveals that the upper layer potential temperature was at its lowest in October 2023 and

highest in July 2023, with salinity reaching its lowest in May 2023 and its highest in December 2022. In contrast, the near-bottom potential temperature was lowest in August-September 2022 and highest in May 2023, with minimal fluctuations in salinity.
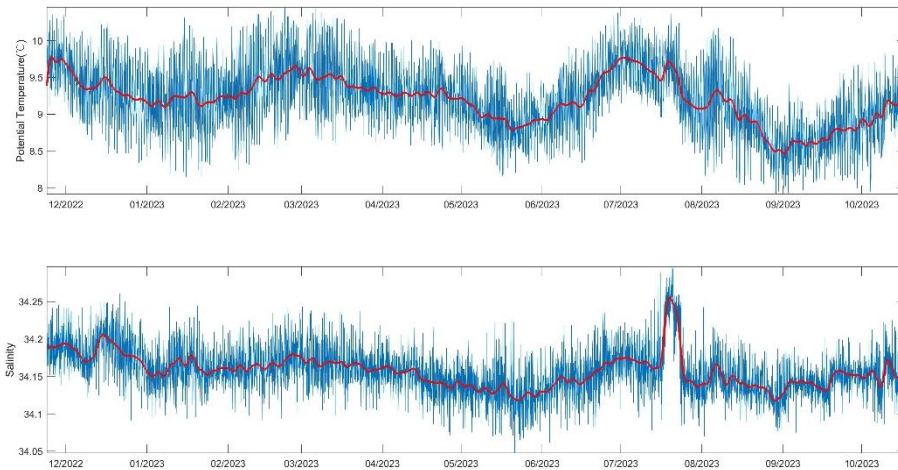
Figure 4-109 Potential temperature and salinity time variation chart at 468 m water depth in Station
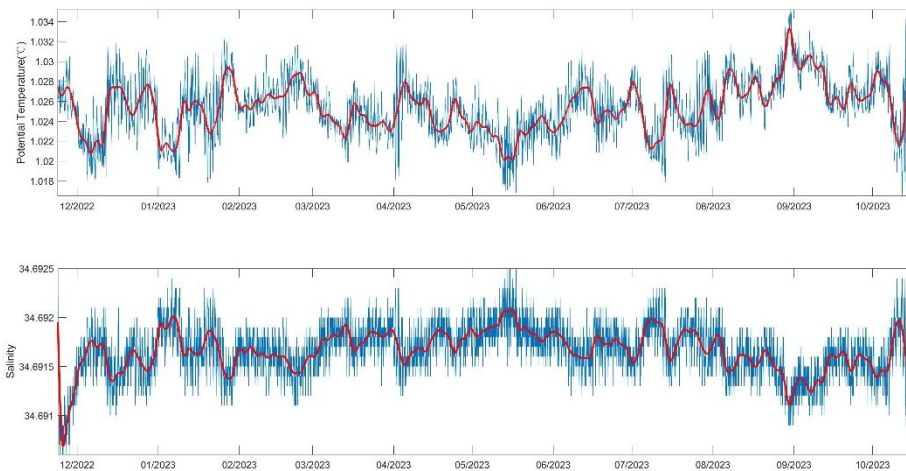
DY76-ES04-MX01

Figure 4-110 Potential temperature and salinity time variation chart at 5024 m water depth in Station

DY76-ES04-MX01

Figure 4-111 illustrates the variation in potential temperature and salinity at the near-bottom (5352 m) level of Station DY76-ES03-MX02. The potential temperature ranged from a maximum of 1.017°C to a minimum of 0.987°C, with an average of 0.998°C; while salinity ranged from a maximum of 34.6949 to a minimum of 34.6928, with an average of 34.6941. Analysis of the monthly average data in Table 4-18 reveals that the potential temperature was

at its lowest in June–July 2023 and highest in August 2023, with minimal fluctuations in salinity.
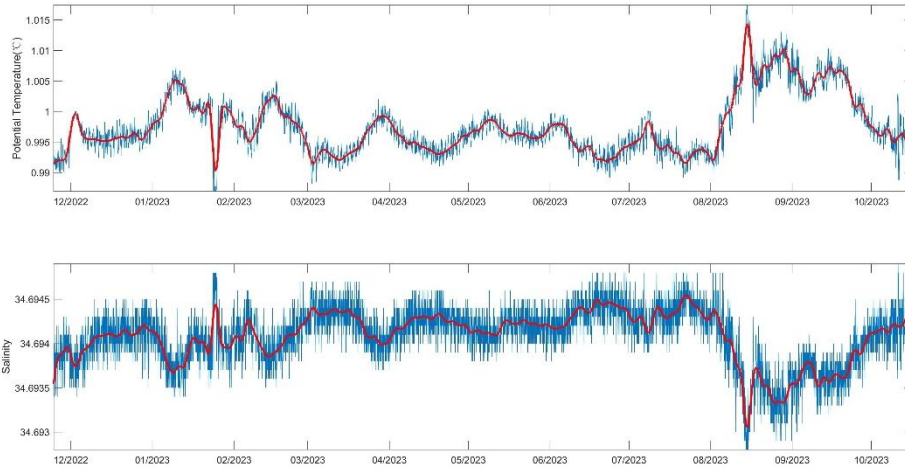
Figure 4-111 Potential temperature and salinity time variation chart at 5352 m water depth in Station DY76-ES03-MX02

Figure 4-112 illustrate the variation of potential temperature and salinity at the near-bottom (5554 m) level of Station DY76-ES06-MX03. The potential temperature ranged from a maximum of 0.996°C to a minimum of 0.965°C, with an average of 0.979°C; while salinity ranged from a maximum of 34.7098 to a minimum of 34.7045, with an average of 34.7084. Analysis of the monthly average data in Table 4-18 reveals that the potential temperature was at its highest in February 2023 and lowest in August 2023. In contrast, salinity exhibited its lowest during March–April 2023, while displaying relatively stable values across the remaining months.
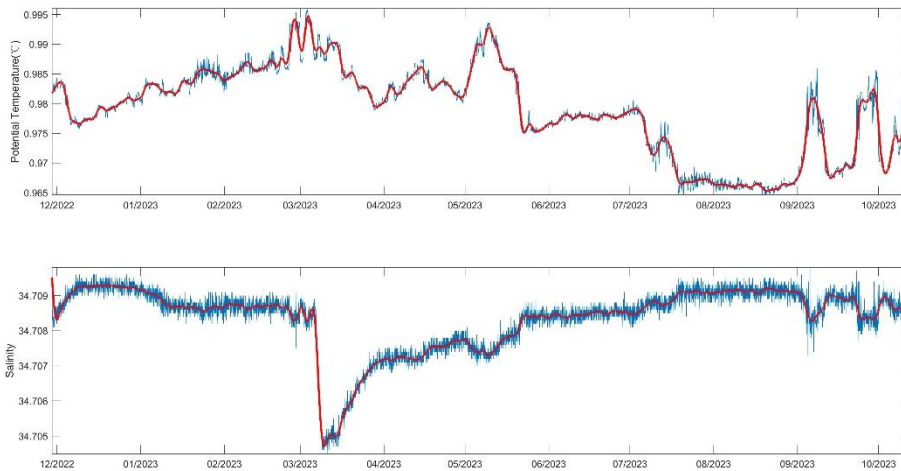
Figure 4-112 Potential temperature and salinity time variation chart at 5554 m water depth in Station

DY76-ES06-MX03

4.3.4.2 Current

The study analyzed the characteristics of current field variations in the upper, middle, and bottom layers of the contract area based on subsurface buoy data collected during four cruises (DY61, DY66, DY69, and DY76) between 2020 and 2023.

4.3.4.2.1 Upper Layer Currents

Figure 4-113 illustrates the distribution of current speed profiles in the upper layer (shallower than 300 m) as recorded by the 75K ADCP of Station DY69-ES04-MX01 situated in the northern region of Block M2. The data indicates a predominant northwestward/southwestward flow direction in the upper layer, with a noticeable decrease in the current speed as depth increases.
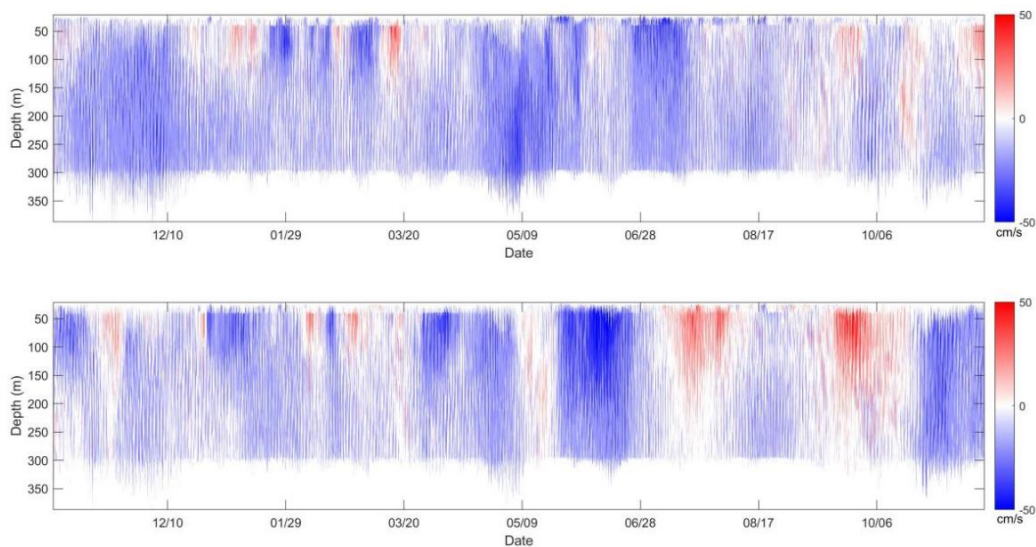
Figure 4-113 Upper layer current speed profile contour map of Station DY69-ES04-MX01 (top figure for east component, bottom figure for north component, same as below)

By choosing the 100 m layer for analysis and plotting its temporal evolution (Figure 4-114), it is evident that peak current velocity was observed at the conclusion of May through the commencement of June (in a southward direction), during July (in a northward direction), and in October (in a northward direction). The highest recorded current speed at the 100 m depth is 60.28 cm/s, accompanied by mean eastward and northward component values of –0.52 cm/s and 0.59 cm/s, respectively.
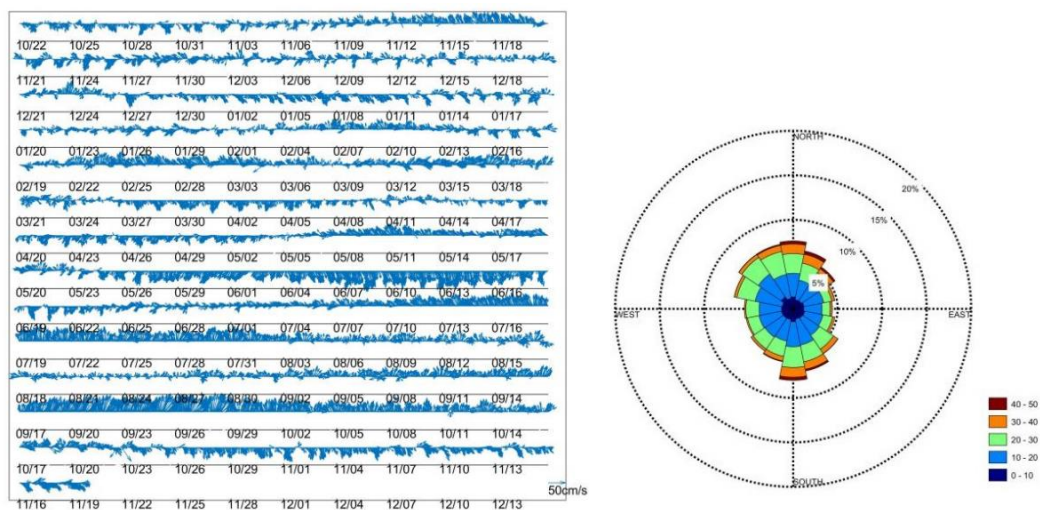
Figure 4-114 Current vector and current rose diagram at the 100 m layer of Station DY69-ES04-MX01

223

Figure 4-115 illustrates the distribution of current speed profiles in the upper layer (shallower than 250 m) as observed by the 75K ADCP of Station DY69-ES03-MX02 in Block M2. It indicates a notable flow velocity in the upper layer at this station, with the highest current speed exceeding 50 cm/s, and a gradual decrease in speed as depth increases. The variation in current direction suggests the influence of large-scale circulation in this area, with a prominent and consistent westward flow observed around May, extending to depths greater than 250 m. By focusing on the 100 m layer and examining its temporal evolution (Figure 4-116), it is evident that peak current speeds occur towards the end of April to early May (in a southwestward direction), March (in a northward direction), and June (in a westward direction). The highest recorded current speed at 100 m is 70.6 cm/s, accompanied by mean eastward and northward component values of 0.2 cm/s and 0.8 cm/s, respectively.
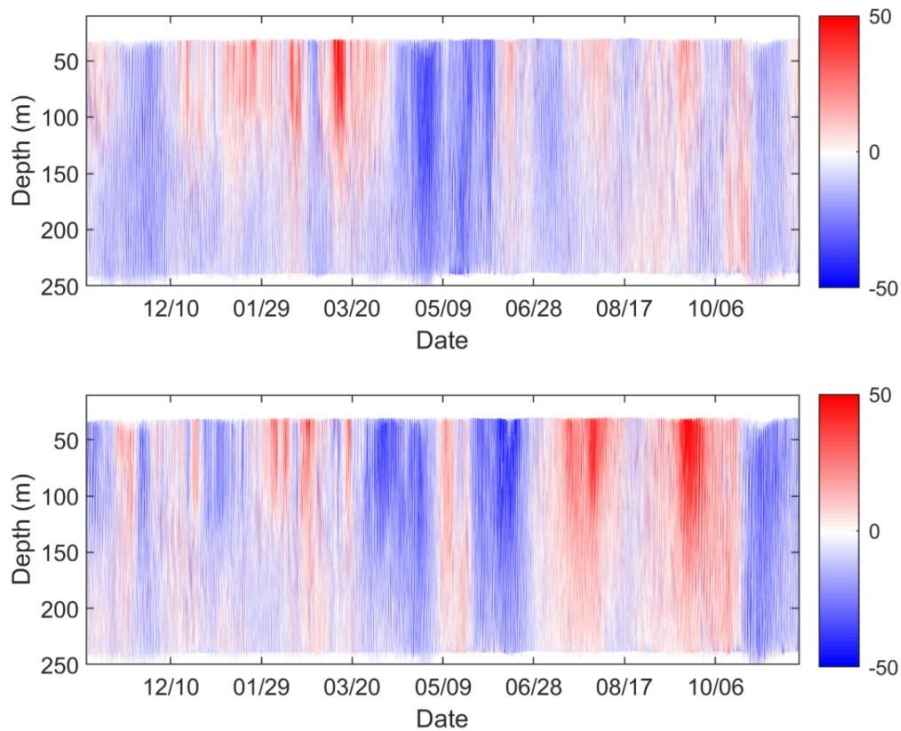
Figure 4-115 Upper layer current speed profile contour map of Station DY69-ES03-MX02
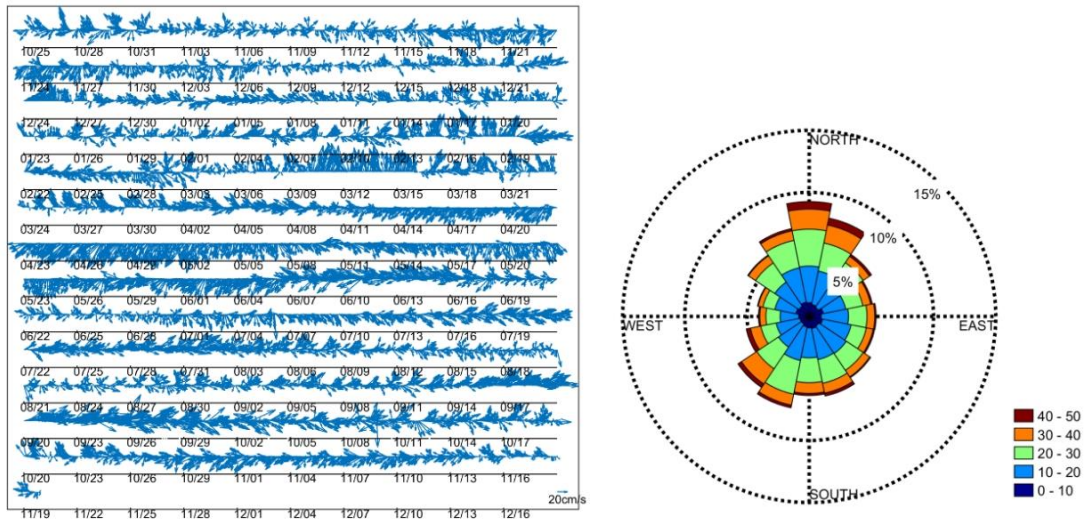
Figure 4-116 Current vector and current rose diagram at the 100 m layer of Station DY69-ES03-MX02

Figure 4-117 illustrates the distribution of current speed profiles in the upper layer (shallower than 300 m) as observed by the 75K ADCP of Station DY69-M1-ES06-MX03 in Block M1. It indicates an obvious flow speed in the upper layer at this statin, with the maximum current speed exceeding 50 cm/s, and a gradual decrease in speed with increasing depth. The observations in the U direction reveal a consistent westward flow from January to April, followed by an eastward flow from May to June, suggesting the influence of large-scale circulation in this area.
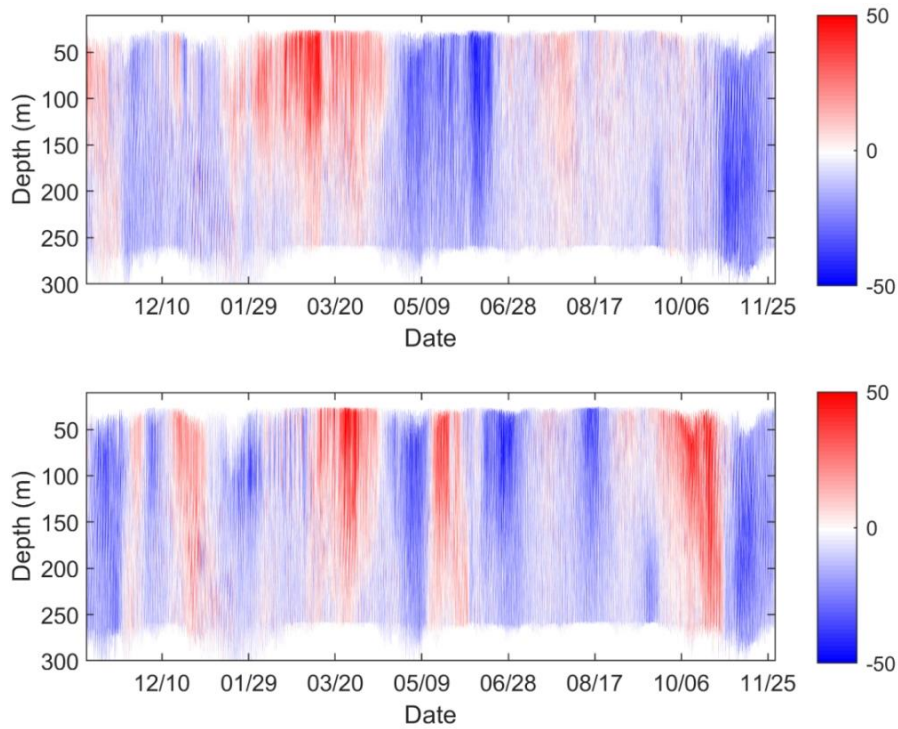
Figure 4-117 Upper layer current speed profile contour map at Station DY69-ES06-MX03

By focusing on the 100 m layer and examining its temporal evolution (Figure 4-118), it is evident that peak current speeds occur towards the end of April to early May (in a southwestward direction), March (in a northward direction), June (in a westward direction), and November (in a southward direction). The highest recorded current speed at 100 m reaches 78.3 cm/s, accompanied by mean eastward and northward component values of 0.8 cm/s and 0.1 cm/s, respectively.
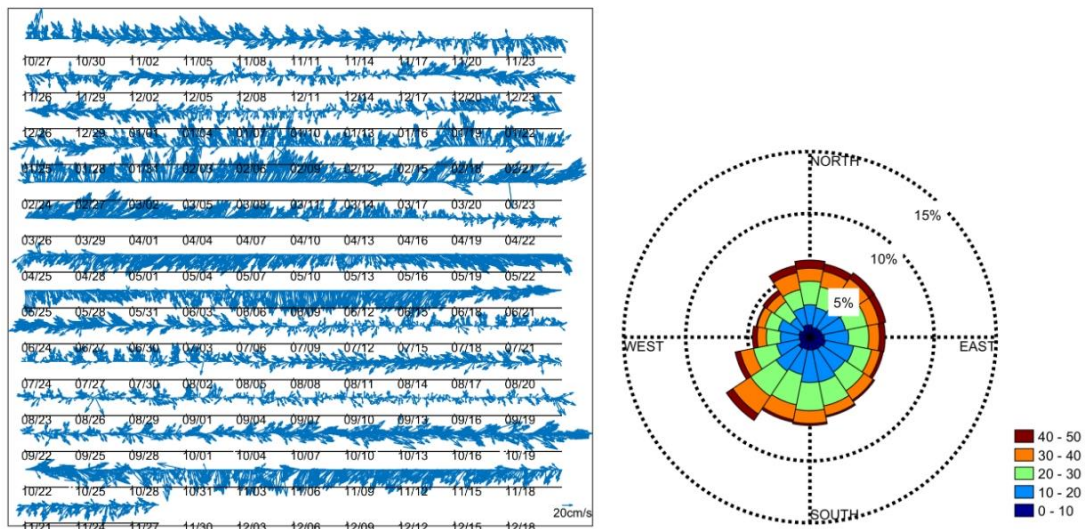
Figure 4-118 Current vector and current rose diagram at the 100 m layer of Station DY69-ES06-MX03

Figure 4-119 illustrates the distribution of current speed profiles in the upper layer (shallower than 1000 m) as observed by the 75K ADCP of Station DY76-ES04-MX01. The figure indicates a notable flow speed in the upper layer at this station, showing a decrease in current speed as water depth increases. Notably, there is a distinct seasonal variation in the current direction, with a northeastward flow observed from November to January, northwestward flow from January to March, southeastward flow from March to June, northeastward flow from June to July, and southwest/northwestward flow from July to October. Analyzing the current speed at the 100 m layer for statistical purposes (Figure 4-120), it is observed that the maximum current speed at this layer is 60.93 cm/s. Additionally, the average east component value is 6.24 cm/s, and the average north component value is 2.87 cm/s.
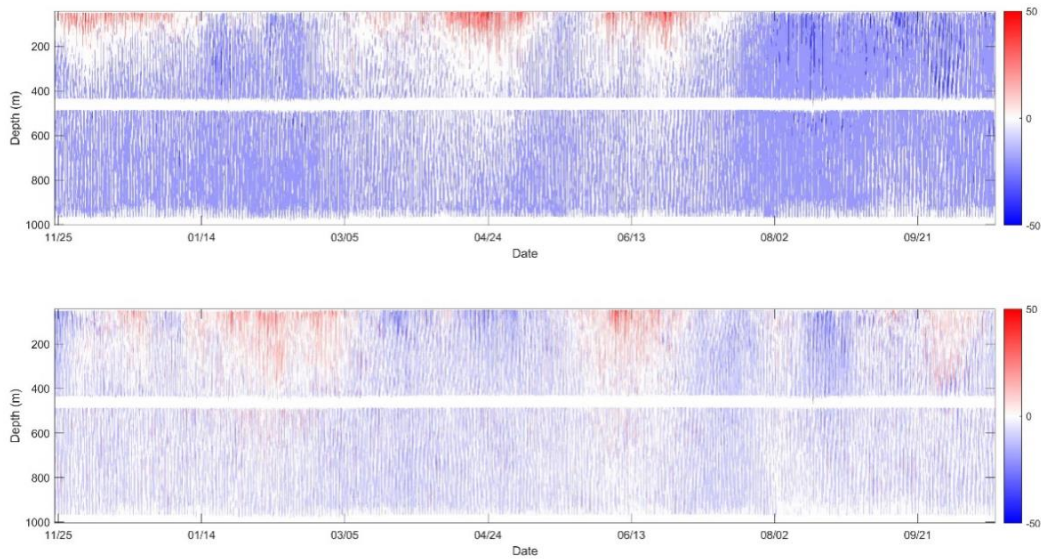
Figure 4-119 Upper layer current speed profile contour map at Station DY76-ES04-MX01
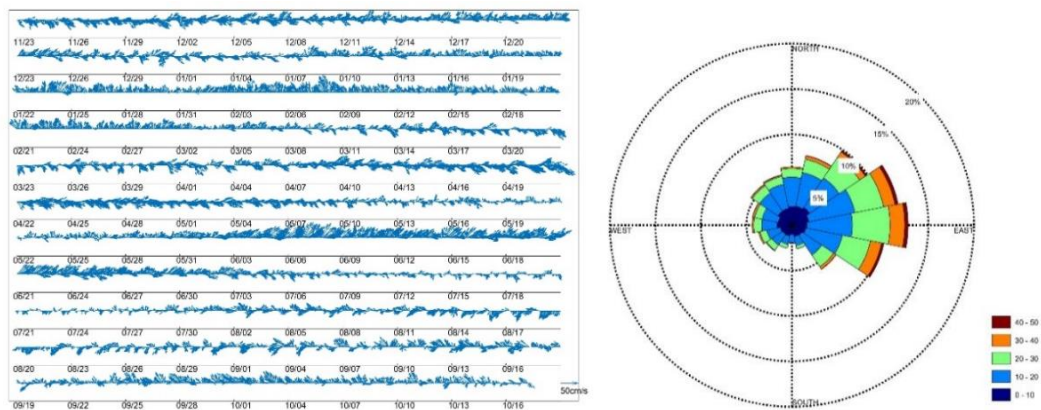
Figure 4-120 Current vector and current rose diagram at the 100 m layer of Station DY76-ES04-MX01

Figure 4-121 illustrates the distribution of current speed profiles in the upper layer (less than 1000 m depth) as observed by the 75K ADCP of Station DY76-ES03-MX02. The figure indicates a notable flow speed in the upper layer at this station, showing a decrease in current speed as water depth increases. By focusing on the current speed at the 100 m layer for analysis (Figure 4-122), it is noted that the maximum current speed at this layer is 66.01 cm/s. Additionally, the average east component value is 11.32 cm/s, while the average north component value is 2.41 cm/s.
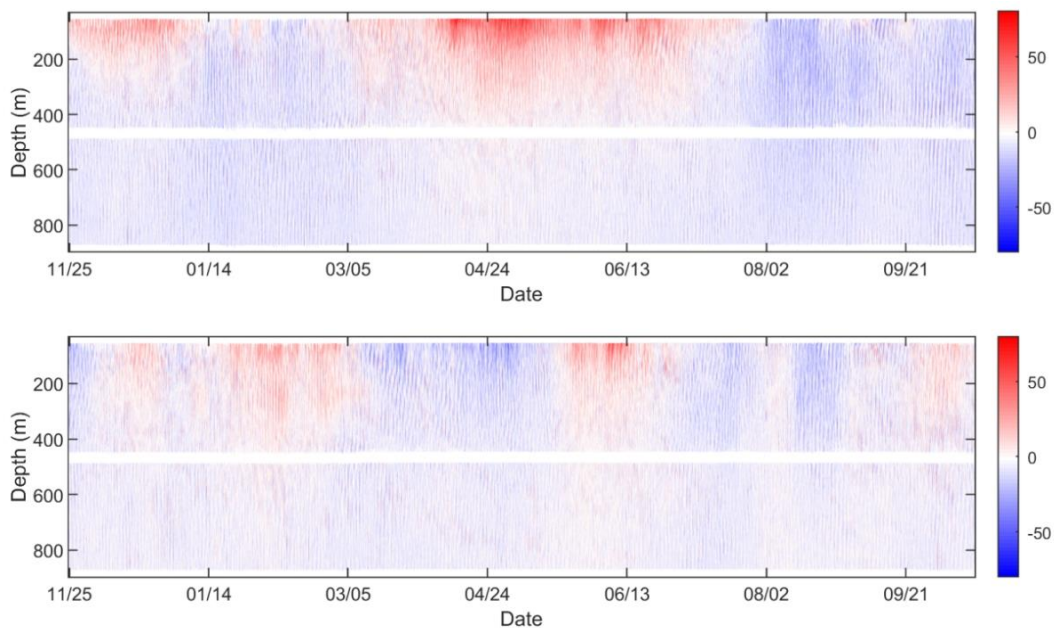
Figure 4-121 Upper layer current speed profile contour map at Station DY76-ES03-MX02
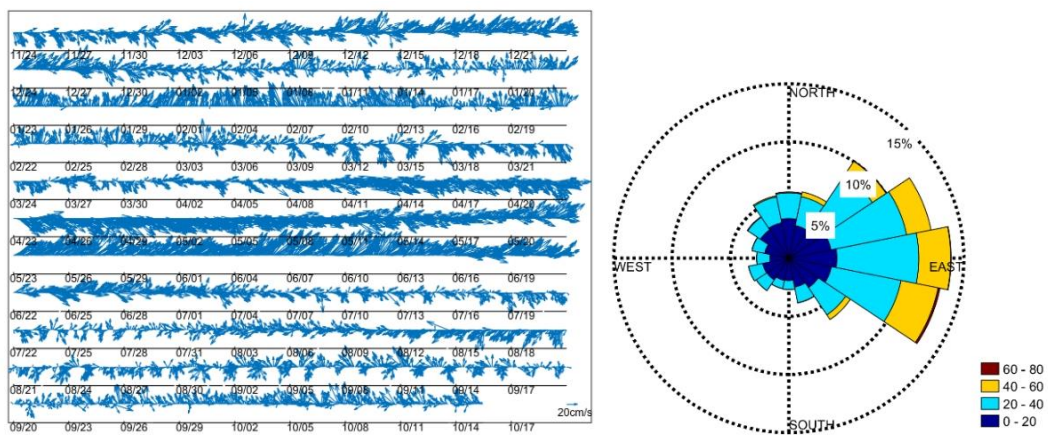
Figure 4-122 Current vector and current rose diagram at the 100 m layer of Station DY76-ES03-MX02

4.3.4.2.2 Mid-depth Currents

Figures 4-123 and 4-124 depict the findings of the single-point current meter deployed at the mid-depth (1090 m and 1350 m) of Station DY61-M2-MX2106. The data presented in the figures illustrate noticeable tidal fluctuations within the current field. At the 1090 m depth, the maximum current velocity is recorded at 29.18 cm/s, with an average eastward flow speed of –0.81 cm/s and an average northward flow speed of 0.07 cm/s, predominantly directed towards the northwest. Conversely, at 1350 m, the maximum current speed is measured at

18.38 cm/s, with an average eastward flow speed of –0.71 cm/s and an average northward flow speed of –0.07 cm/s, predominantly directed towards the southwest. It is observed that the average flow velocity in the mid-depth decreases as the depth increases.
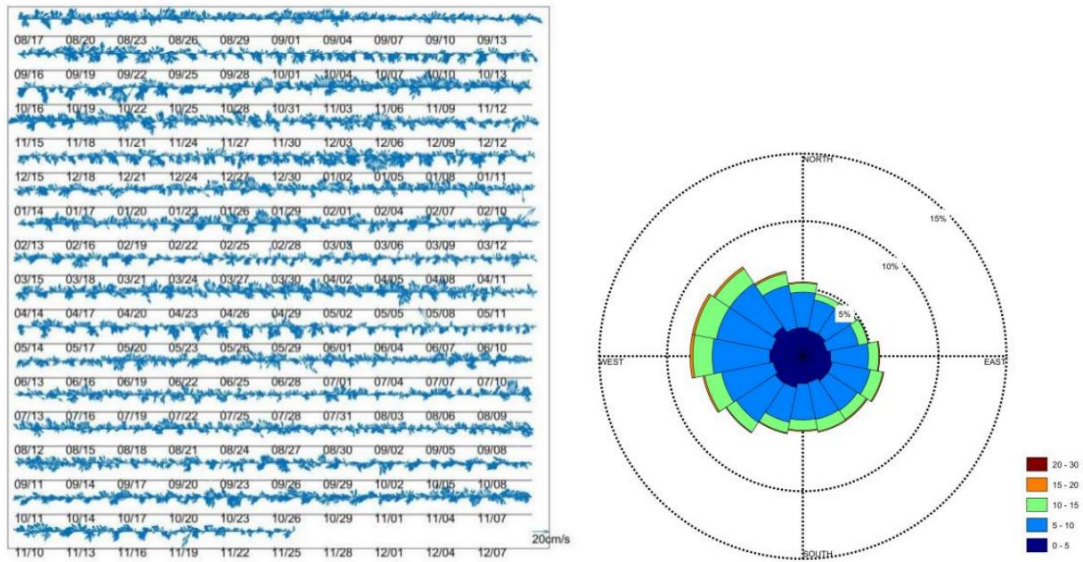
Figure 4-123 Current vector and current rose diagram at the mid-depth (1090 m) of Station DY66-M2-MX2101
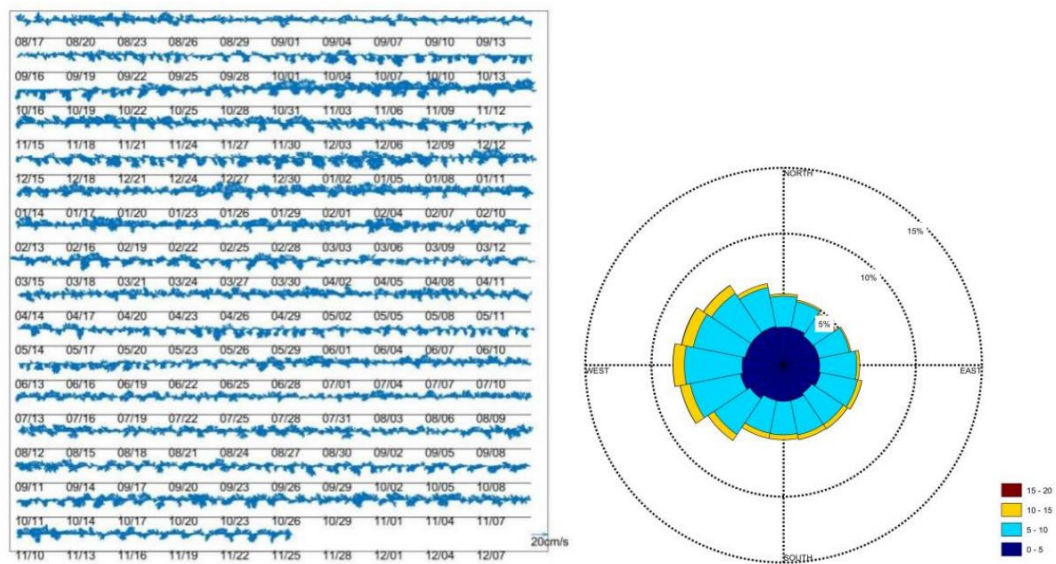
Figure 4-124 Current vector and current rose diagram at the mid-depth (1350 m) of Station DY66-M2-MX2101

Figure 4-125 illustrates the findings of the single-point current meter at the mid-depth (1990 m) of Station DY69-ES03-MX02. The data presented in the figure indicates notable tidal fluctuations within the current field. The highest recorded current velocity reached 15.83 cm/s, with an average eastward flow speed of –0.28 cm/s and an average northward flow speed of –0.02 cm/s, predominantly directed towards the southwest.
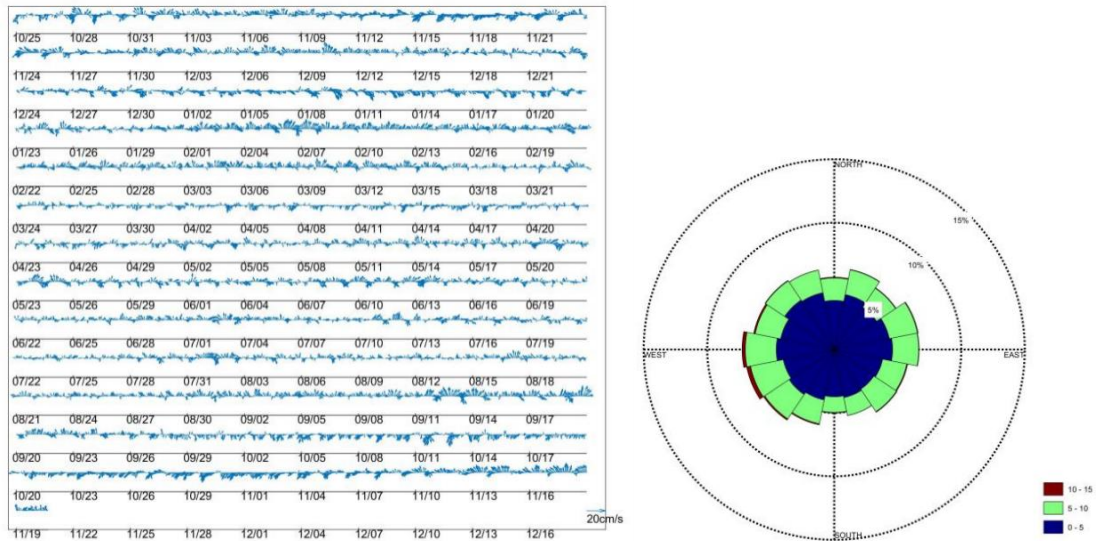
Figure 4-125 Current vector and current rose diagram at the middle layer (1990 m) of Station DY69-ES03-MX02

Figure 4-126 illustrates the findings of the single-point current meter at the mid-depth of Station DY69-ES06-MX03. The data presented in the figure indicates notable tidal fluctuations within the current field. The highest recorded current velocity reached 18.57 cm/s, with an average eastward flow speed of –0.47 cm/s and an average northward flow speed of –0.04 cm/s, predominantly directed towards the southwest. It is noted that the mid-depth current field may be affected by mesoscale processes during the period from late September to November 2022, resulting in relatively high current velocities.
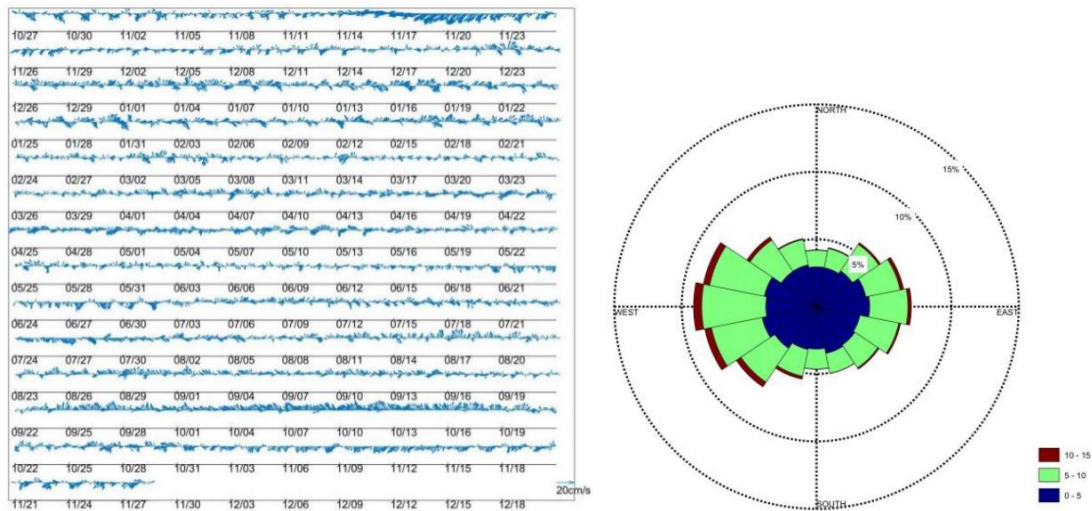
Figure 4-126 Current vector and current rose diagram at the mid-depth (2000 m) of Station DY69-ES06-MX03

Figure 4-127 illustrates the findings of the single-point current meter at the mid-depth (2000 m) of Station DY76-ES04-MX01. The data presented in the figure indicates notable tidal fluctuations within the current field. The highest recorded current velocity reached 14.74 cm/s, with an average eastward flow speed of –0.64 cm/s and an average northward flow speed of –0.17 cm/s, predominantly directed towards the southwest.
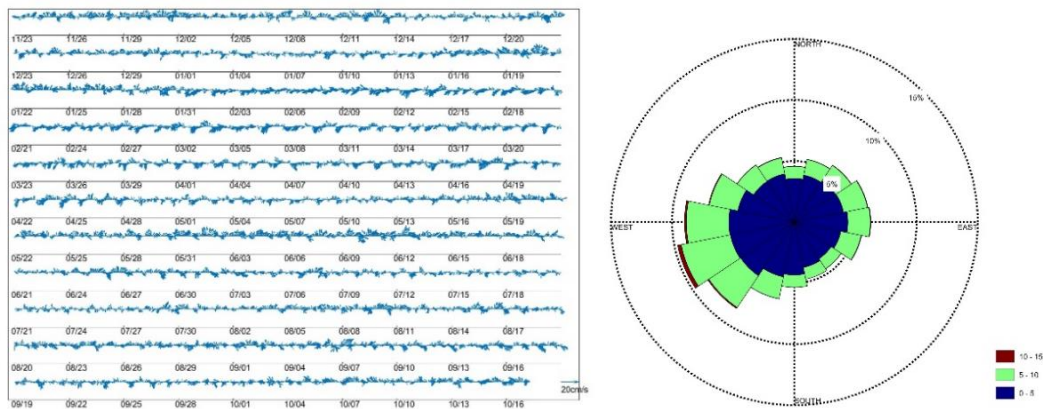
Figure 4-127 Current vector and current rose diagram at the mid-depth (2000 m) of Station DY76-ES04-MX01

Figure 4-128 illustrates the findings of the single-point current meter at the mid-depth (2000 m) of Station DY76-ES03-MX02. The data indicate a predominant westward flow within the mid-depth current field. The highest recorded current velocity reached 11.72 cm/s,

with an average eastward flow speed of –0.97 cm/s and an average northward flow speed of –0.07 cm/s, predominantly directed towards the southwest.
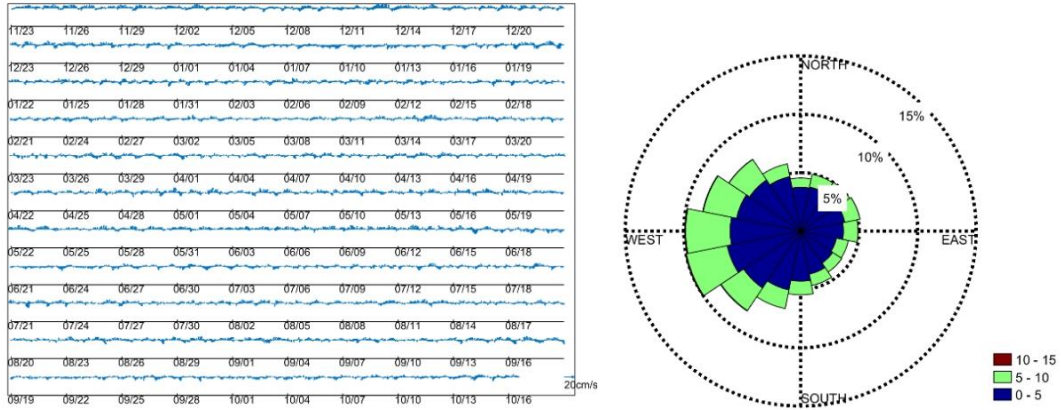
Figure 4-128 Current vector and current rose diagram at the mid-depth (2000 m) of Station DY76-ES03-MX02

Figure 4-129 illustrates the findings of the single-point current meter at the mid-depth (1990 m) of Station DY76-ES06-MX03. The data indicate a predominant westward flow within the mid-depth current field. The highest recorded current velocity reached 14.0 cm/s, with an average eastward flow speed of –2.5 cm/s and an average northward flow speed of –0.12 cm/s, predominantly directed towards the southwest.
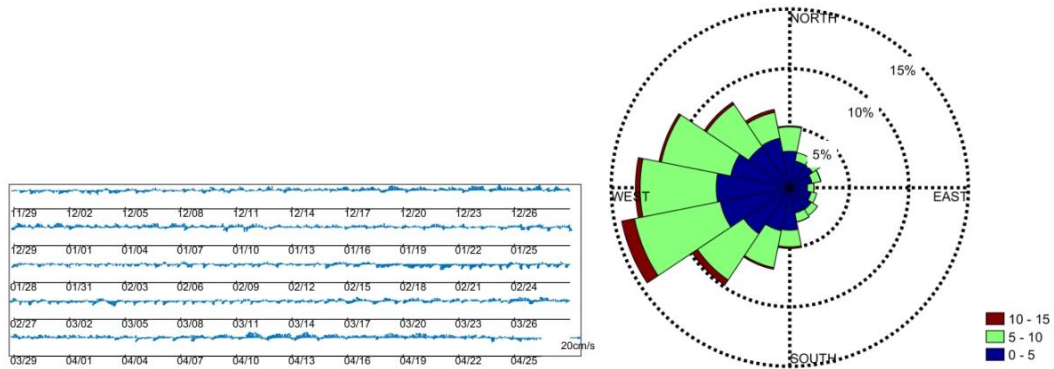
Figure 4-129 Current vector and current rose diagram at the mid-depth（2000 m）of Station DY76−ES06−MX03

4.3.4.2.3 Deep Layer Currents

Figures 4-130 and 4-131 depict the findings of the single-point current meter deployed at the near-bottom (5560 m and 5656 m) which was at a height of 25 m above the seabed at Station DY61-M2-MX2106. The data presented in the figures illustrate noticeable tidal

fluctuations in the near-bottom current patterns. Analysis of the data reveals a consistent strong northeastward current flow during the periods of January to February and April to May 2020. Throughout the observation timeframe, the predominant direction of the near bottom current field remained northeastward. The highest recorded current velocity at 5560 m was 11.48 cm/s, with an average eastward flow speed of 0.13 cm/s and an average northward flow speed of 0.96 cm/s. Similarly, at 5656 m, the maximum current speed is 11.18 cm/s, with an average eastward flow speed of 0.50 cm/s and an average northward flow speed of 1.05 cm/s, which exceeded the values observed at 5560 m.
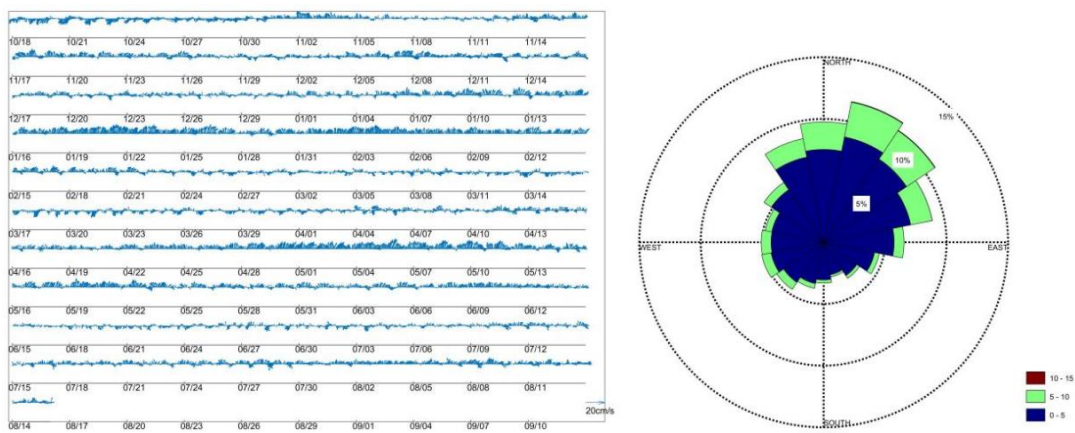
Figure 4-130 Current vector and current rose diagram at the near-bottom (5560 m) of Station DY61-M2-MX2006
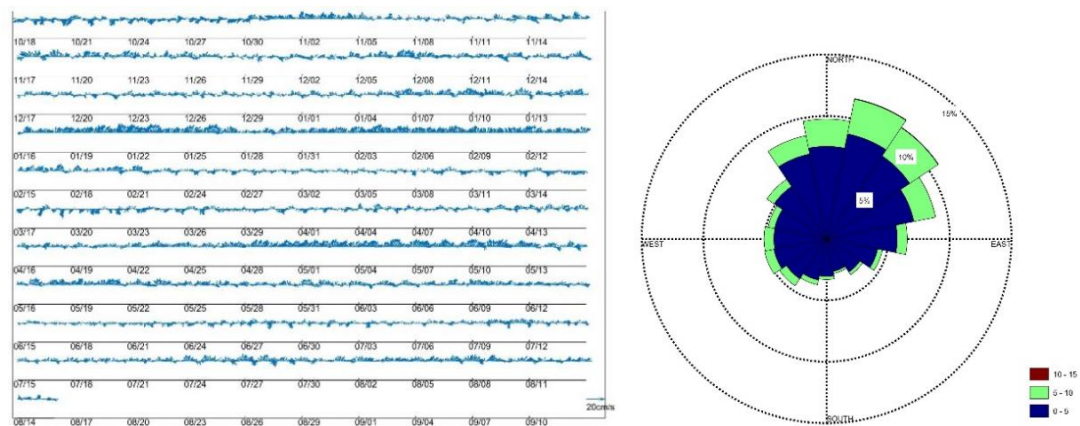
Figure 4-131 Current vector and current rose diagram at the near-bottom (5656 m) of Station DY61-M2-MX2006

Figures 4-132 to 4-134 depict the findings of the single-point current meter deployed at the deep layer (3350 m, 5450 m, and 5660 m) of Station DY61-M2-MX2101. The data presented in the figures illustrate noticeable tidal fluctuations in the near-bottom current patterns. Notably, a consistent strong northeastward current prevailed during specific periods, namely from late September 2021, early January to early March 2022, July to August, and November 2022. Throughout the observation timeframe, the near-bottom current predominantly exhibited a northeastward direction. The highest recorded current velocity at 3350 m was 12.45 cm/s, with an average eastward flow speed of –0.50 cm/s and an average northward flow speed of 0.19 cm/s. Similarly, the 5450m displayed a maximum current speed of 15.71 cm/s, with average eastward a northward flow speeds of 1.16 cm/s and 1.38 cm/s, respectively. At the 5660 m, the maximum current speed reached 17.05 cm/s, with average eastward and northward flow speeds of 1.49 cm/s and 1.70 cm/s, respectively. Notably, the average flow speed across these three layers exhibited an increasing trend corresponding to greater water depths.
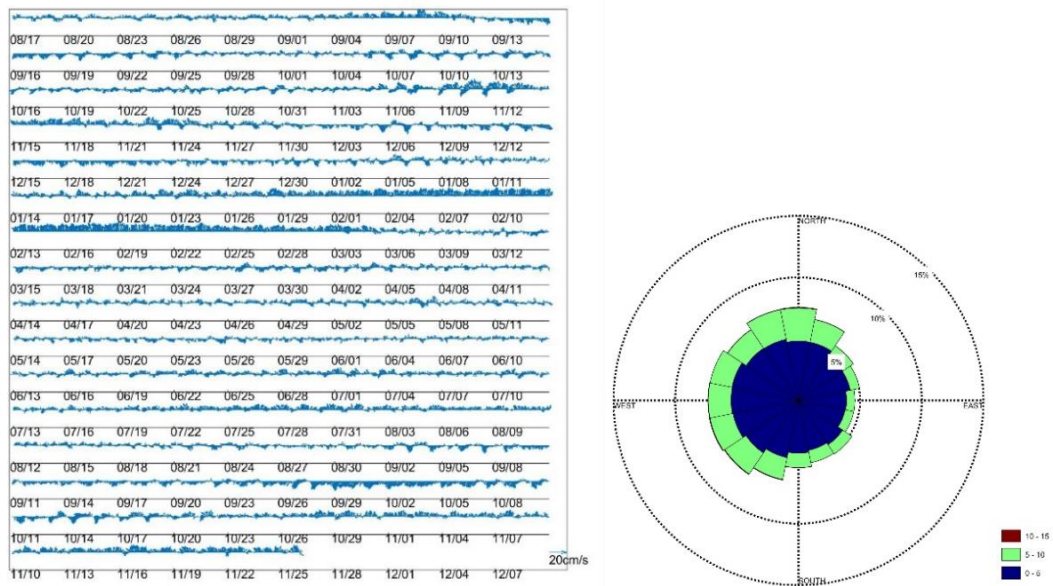
Figure 4-132 Current vector and current rose diagram at the deep layer (3350 m) of Station DY66-M2-MX2101
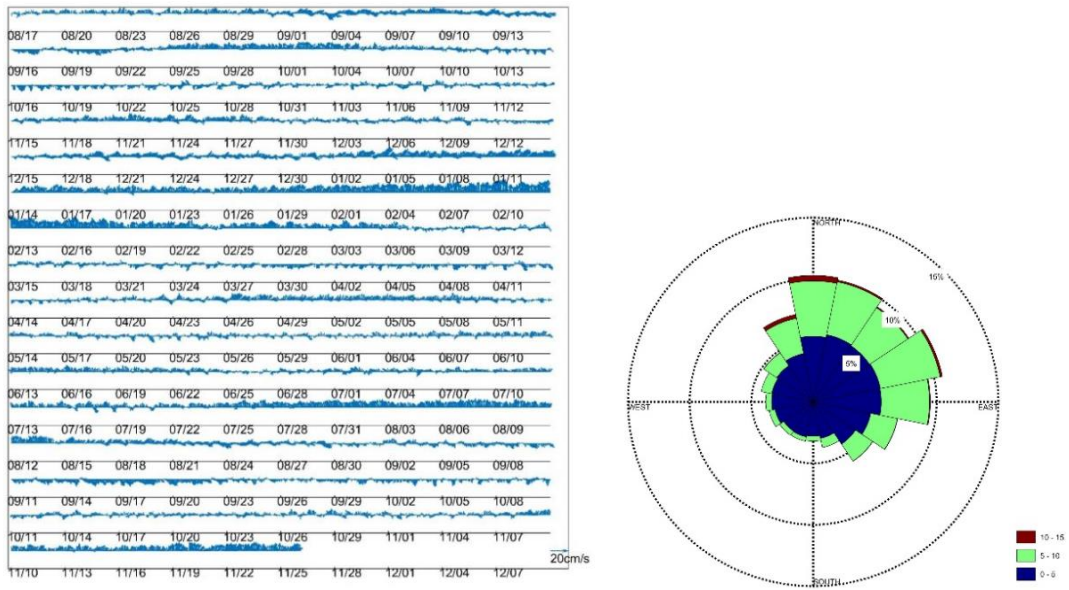
Figure 4-133 Current vector and current rose diagram at the near-bottom (5450 m) of Station DY66-M2-MX2101
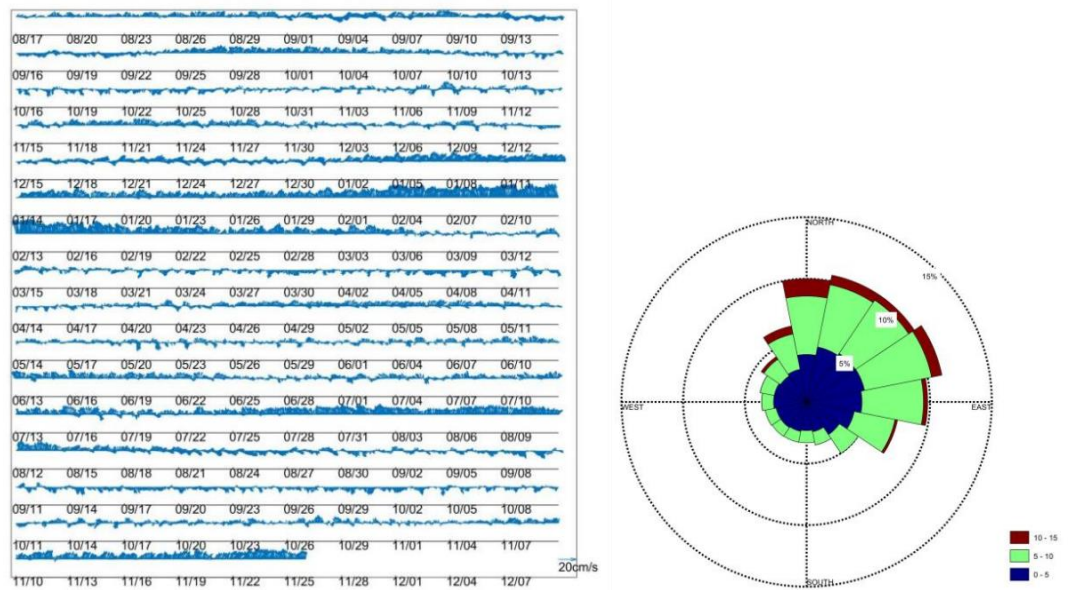
Figure 4-134 Current vector and current rose diagram at the near-bottom (5660 m) of Station DY66-M2-MX2101

Figure 4-135 illustrates the findings of the single-point current meter deployed at the near-bottom (4811 m) of Station DY69-ES04-MX01. The data presented in the figure indicates that the current field near-bottom is predominantly influenced by tidal currents. The highest recorded current velocity in near-bottom is 11.94 cm/s, with an average eastward flow

speed of –0.39 cm/s and an average northward flow speed of –0.14 cm/s, characterized by an average southwest direction.
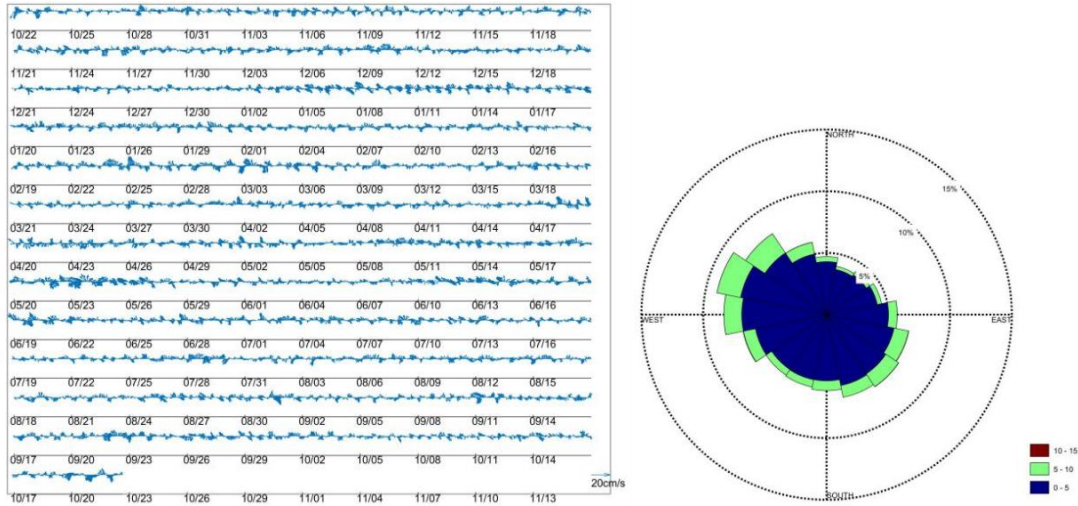
Figure 4-135 Current vector and current rose diagram at the near-bottom (4811 m) of Station DY69-ES04-MX01

Figures 4-136 and 4-137 present the observations obtained from the single-point current meter deployed at the near-bottom (5324 m and 5534 m) of Station DY69-ES03-MX02. These figures reveal the presence of tidal fluctuations in the near-bottom current field. At 5324 m layer, the maximum current speed recorded is 17.26 cm/s, with an average eastward flow speed of –0.81 cm/s and an average northward flow speed of 0.05 cm/s, with a prevailing direction to the northwest. Meanwhile, at 5534 m layer, the maximum current speed is 18.40 cm/s, with an average eastward flow speed of –1.20 cm/s and an average northward flow speed of –0.06 cm/s, with prevailing direction to the southwest. Additionally, the average flow speed at 5534 m layer is larger than that at the 5324 m layer.
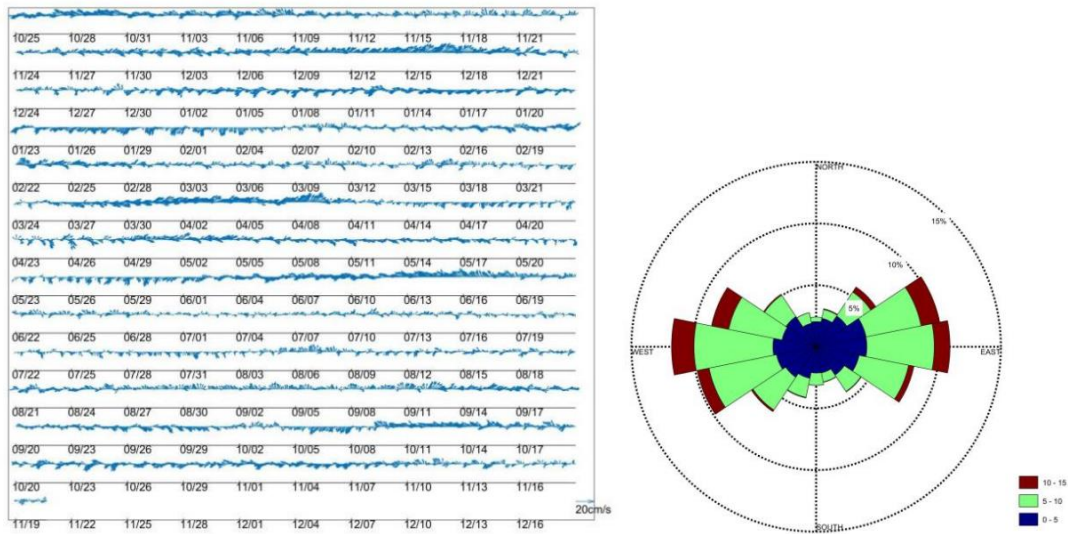
Figure 4-136 Current vector and current rose diagram at the near-bottom (5324 m) of Station DY69-ES03-MX02
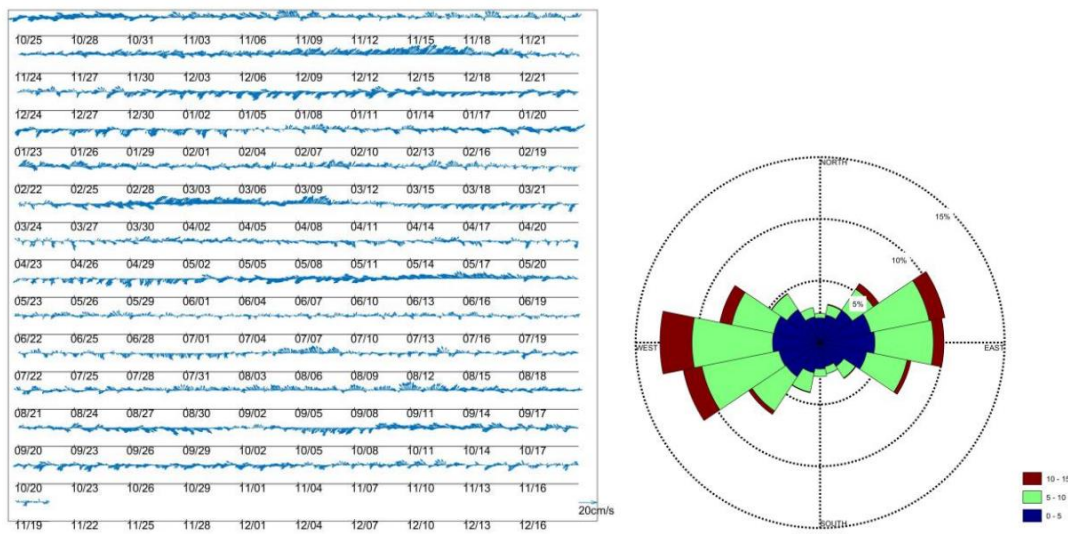
Figure 4-137 Current vector and current rose diagram at the near-bottom (5534 m) of Station DY69-ES03-MX02

Figures 4-138 and 4-139 present the observation results of the single-point current meter deployed at the near-bottom (5322 m and 5532 m) of Station DY69-ES06-MX02.The data illustrates consistent and robust southwestward currents in the near-bottom current field during the periods of June to July 2022 and October to November 2022, with a notable mesoscale process observed in December 2021. Throughout the observation period, the near-

bottom current field predominantly exhibited southwestward flow. At 5332 m, the highest recorded current speed was 15.65 cm/s, with an average eastward flow speed of –2.81 cm/s and an average northward flow speed of –2.17 cm/s. Similarly, in the 5532 m current field, the maximum current speed was 16.85 cm/s, with an average eastward flow speed of –3.15 cm/s and an average northward flow speed of –2.48 cm/s, indicating a higher average flow speed compared to the 5322 m layer.
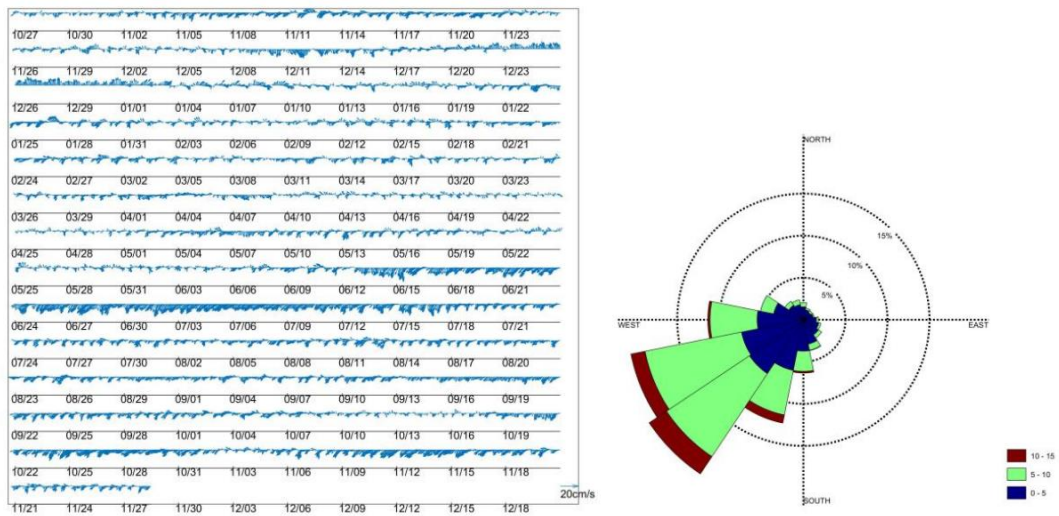
Figure 4-138 Current vector and current rose diagram at the near-bottom (5322 m) of Station DY69-ES06-MX03
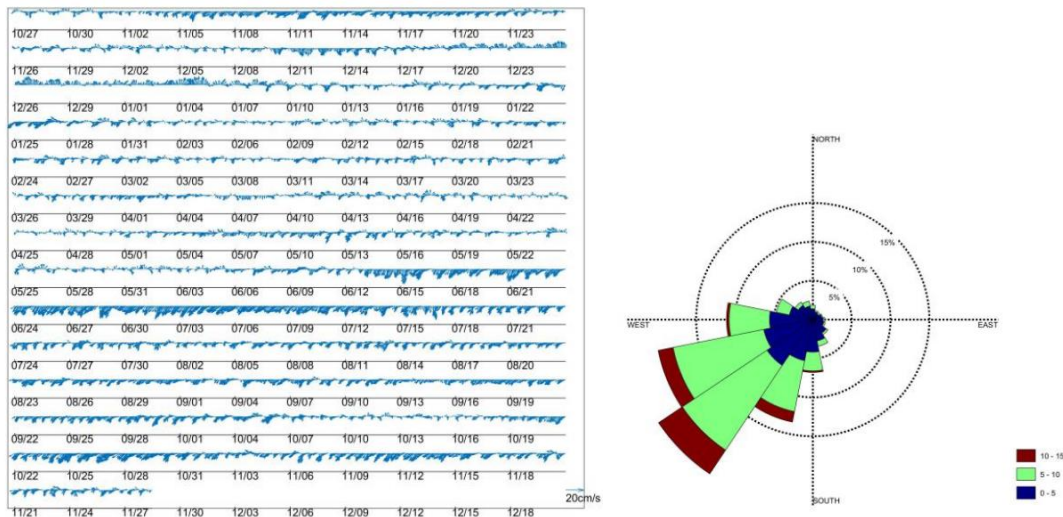
Figure 4-139 Current vector and current rose diagram at the near-bottom (5532 m) of Station DY69-ES06-MX03

Figures 4-140 to 4-142 depict the findings of the single-point current meter deployed at the near-bottom (4859 m, 4964 m, and 5029 m) of Station DY76-ES04-MX01. The data illustrates that the near-bottom current field is predominantly influenced by tidal force, exhibiting a prevailing southwest direction. Notably, the highest recorded current speed at the 4859 m layer is 10.70 cm/s, with an average eastward current speed of –0.56 cm/s and an average northward current speed of –0.31 cm/s, with prevailing direction to the southwest. Similarly, the 4964 m layer showcases a maximum current speed of 11.75 cm/s, with an average eastward current speed of –0.63 cm/s and an average northward current speed of –0.41 cm/s, also directed southwest. At 5534 m, the maximum current speed is recorded at 11.79 cm/s, with average eastward and northward current speeds of –0.62 cm/s and –0.52 cm/s, respectively, maintaining a southwest direction. Analysis of the vertical distribution of the average current speeds indicates a positive correlation between water depth and near-bottom current speed.
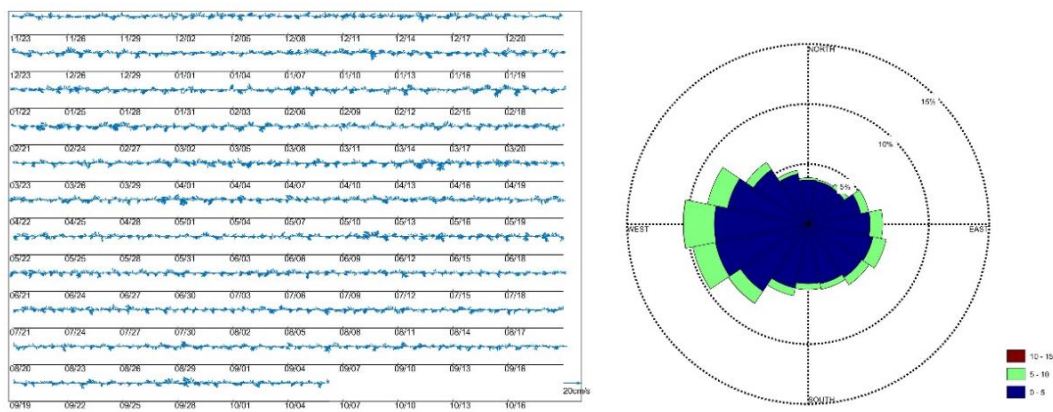
Figure 4-140 Current vector and current rose diagram at the near-bottom (4859 m) of Station DY76-ES04-MX01
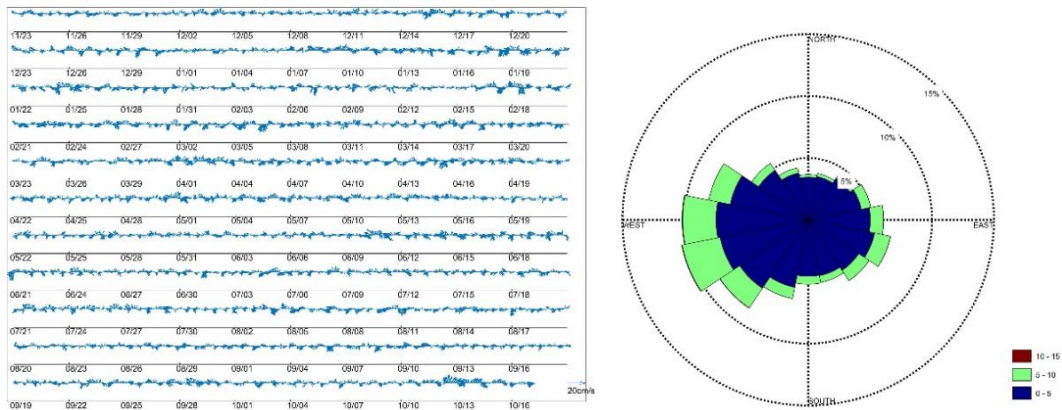
Figure 4-141 Current vector and current rose diagram at the near-bottom (4964 m) of Station DY76-ES04-MX01
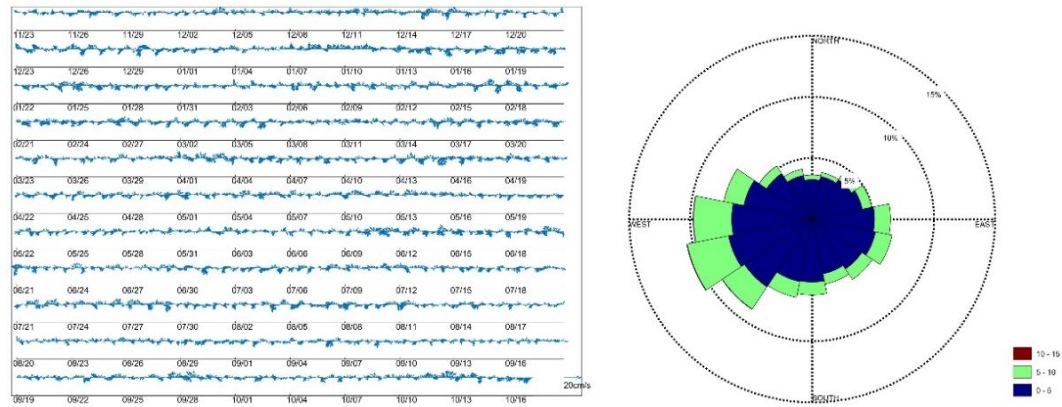
Figure 4-142 Current vector and current rose diagram at the near-bottom (5029 m) of Station DY76-ES04-MX01

Figures 4-143 to 4-144 depict the findings of the single-point current meter deployed near the bottom (5039 m and 5530 m) of Station DY76-ES03-MX02 in IRZ. The observations reveal that the near-bottom current fields exhibit obvious similarity, characterized by distinct tidal fluctuations. Throughout the monitoring period, the current field near the bottom at this location predominantly flowed in an east-west direction, reaching a peak current velocity of 14.3 cm/s at the 5039 m layer. The average eastward current speed was measured at 0.4 cm/s, the average northward current speed at –0.3 cm/s, with an average direction pointing southeast. Similarly, at the 5530 m layer, the maximum current speed recorded was 16.5 cm/s, with average eastward and northward current speeds of 0.6 cm/s and –0.3 cm/s, respectively, and an average direction towards the southeast.
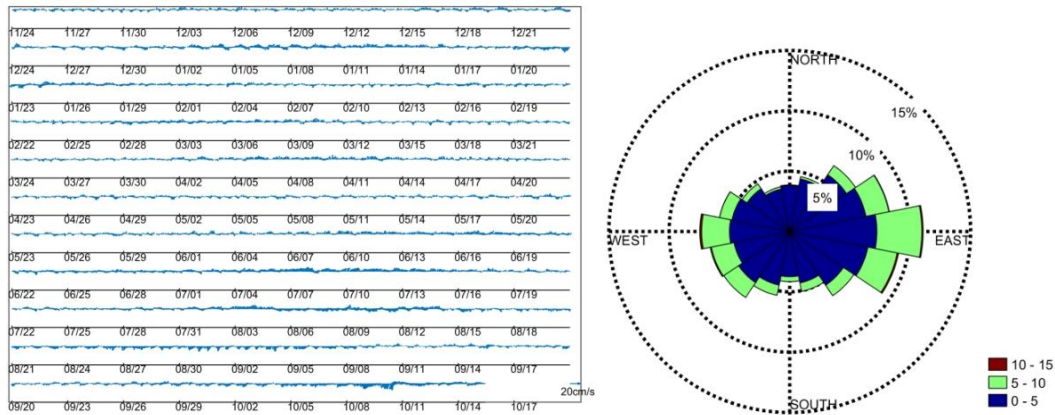
Figure 4-143 Current vector and current rose diagram at the near-bottom (5039 m) of Station DY76-ES03-MX02
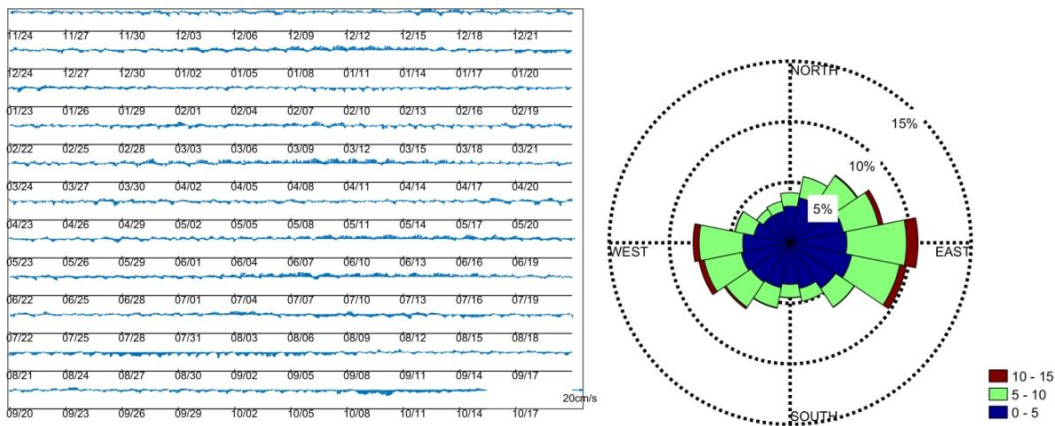
Figure 4-144 Current vector and current rose diagram at the near-bottom (5530 m) of Station DY76-ES03-MX02

Figures 4-145 to 4-146 present the outcomes of the single-point current meter deployed near the bottom (5053 m and 5542 m) of Station DY76-ES06-MX03 in PRZ. The depicted near-bottom current fields at this site exhibit notable similarity, with evident tidal variations in the currents. Throughout the observation period, the near-bottom current fields of this station predominantly flowed southwestward. The maximum current speed at the 5053 m layer was recorded at 13.8 cm/s, with average eastward and northward current speeds of –2.2 cm/s and –1.0 cm/s, respectively, and an average direction pointing southwest. At the 5542 m layer, the maximum current speed measured was 16.2 cm/s, with average eastward and northward current speeds of –2.4 cm/s and –1.6 cm/s, respectively, and an average direction towards the southwest. Statistical analysis indicates that the average flow at the bottom of

this station surpasses that at the mid-depth and obviously exceeds the average flow at the near-bottom of Stations DY76-ES04-MX01 and DY76-ES03-MX02.
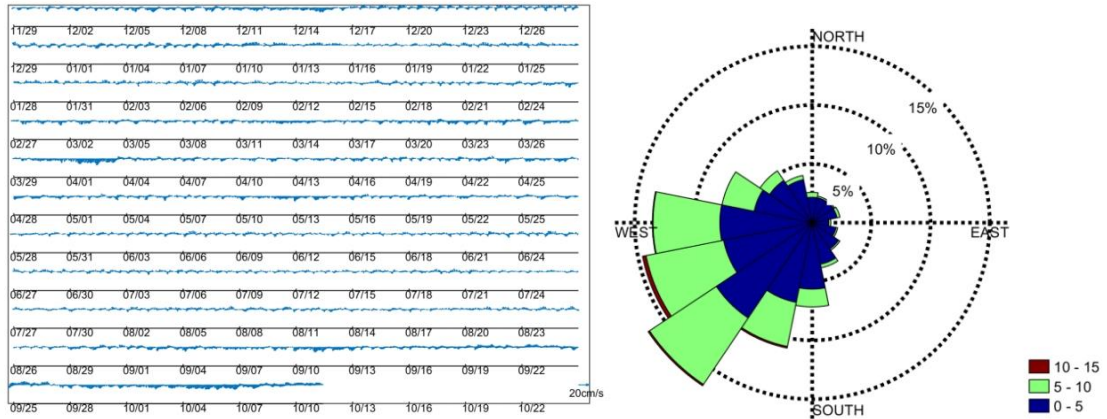
Figure 4-145 Current vector and current rose diagram at the near-bottom (5053 m) of Station DY76-ES06-MX03
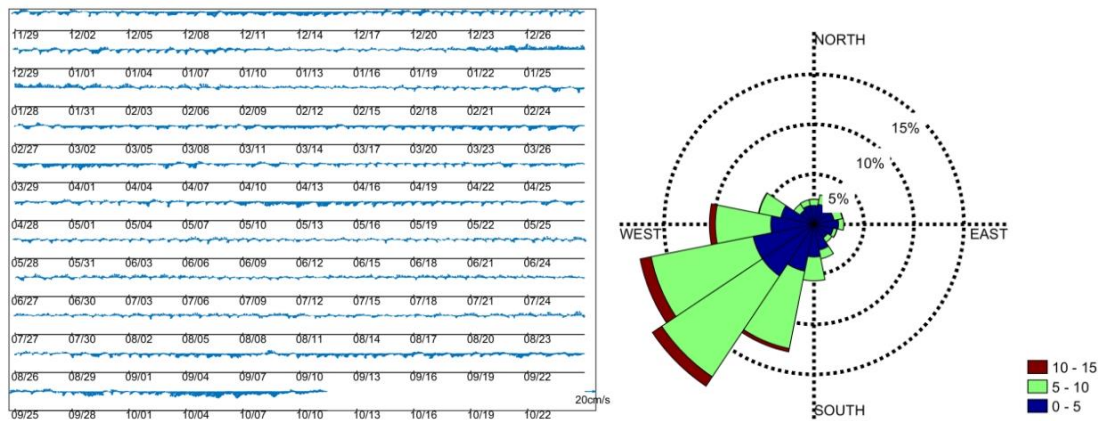
Figure 4-146 Current vector and current rose diagram at the near-bottom (5542 m) of Station DY76-ES06-MX03

The spectrum analysis (confidence interval 95%) of the near bottom layer current at four stations in the mining area is shown in Figure 4-147. The results show that the near bottom layer current field has obvious tidal variation, mainly semi-diurnal and diurnal tides, and the direction of rotation is mainly clockwise. At the same time, the near bottom layer current field also has the near-inertial oscillation in the clockwise direction.
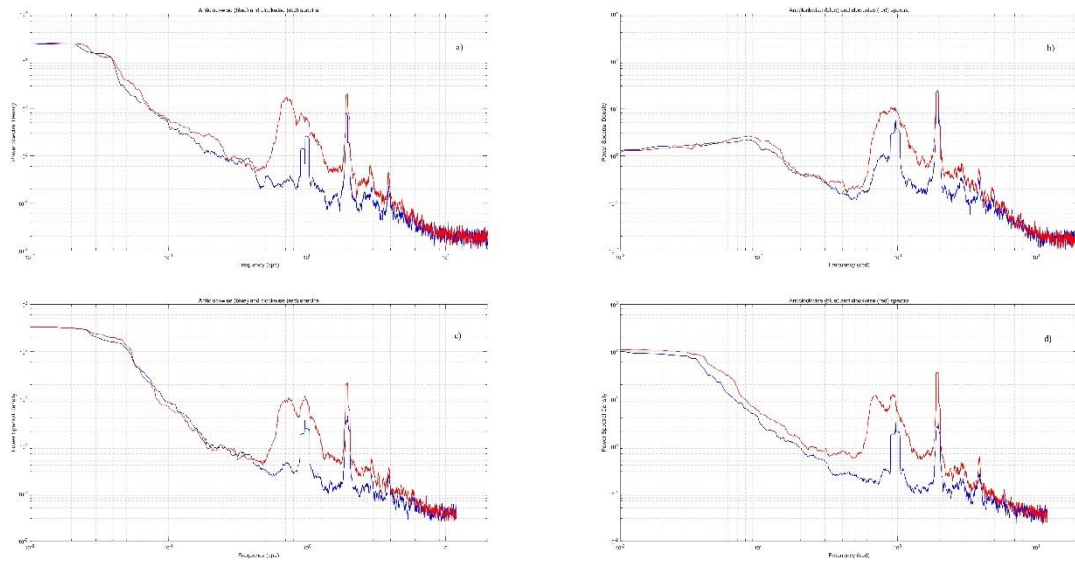
Figure 4-147 Spectral analysis of the current field at each station (red indicates clockwise direction, blue indicates counterclockwise direction；　a is Station DY66-MX2101，b is Station DY69-ES04-MX01，c is Station DY69-ES03-MX02，d is Station DY69-ES06-MX03）

Two-year period of near-bottom current field observations at four designated stations were conducted. Figure 4-148 illustrates the monthly average current vector at the near-bottom of Station DY66-M2-MX2201 situated in the central region of the Block M2. The figure indicates a predominant northeastward flow of the bottom current at this station, exhibiting seasonal and interannual fluctuations. The highest monthly average current velocity recorded over the two-year period was observed in February 2022, peaking at an average of 8.61 cm/s. Conversely, the near-bottom monthly average current speed at Station ES04 remains minimal, measuring less than 1 cm/s, and flows in a southwestward direction (Figure 4-149). At Station ES03, the near-bottom monthly average current predominantly flows in a southwest-northeast direction, displaying noticeable monthly variations (Figure 4-150). Similarly, the near-bottom monthly average current at Station ES06 primarily flows southwestward, also exhibiting distinct monthly variations (Figure 4-151).
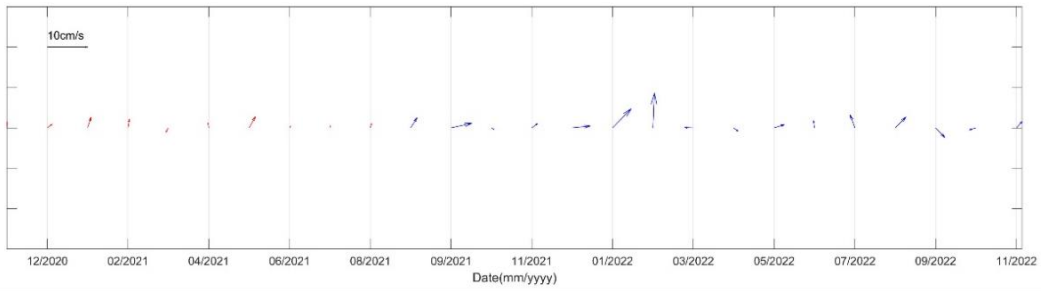
Figure 4-148 Monthly average current vector chart at the near-bottom of Station DY66-M2-MX2201

(red: DY61 cruise, blue: DY66 cruise)
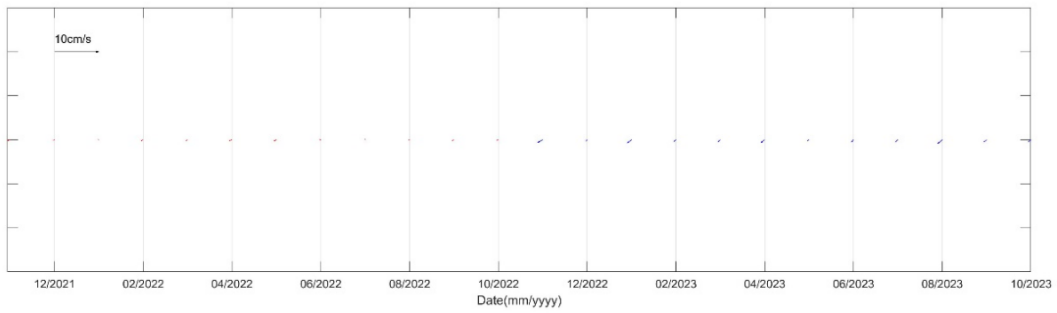
Figure 4-149 Monthly average current vector chart at the near-bottom of Station ES04 (red: DY69

cruise, blue: DY76 cruise, the same below)
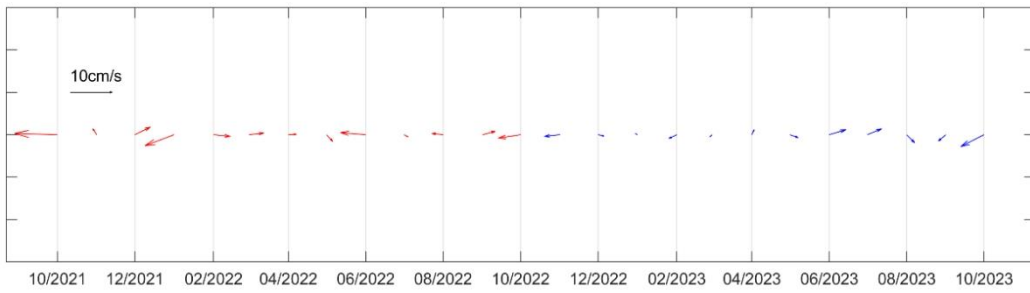
Figure 4-150 Monthly average current vector chart at the near-bottom of Station ES03
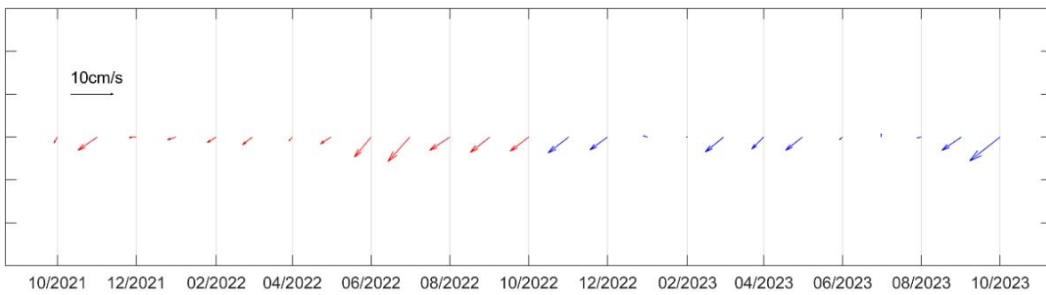
Figure 4-151 Monthly average current vector chart at the near-bottom of Station ES06

The illustration in Figure 4-152 displays the distribution of annual average current speed vectors at near-bottom of the Block M as recorded by a subsurface buoy in 2021. Analysis of the data reveals that the highest average current speed at near-bottom is observed at Station DY69-ES06-MX03, followed by Station DY66-M2-MX2101, while the remaining two stations exhibit lower flow velocities. Notably, the geographical features of the sea mountain influence the flow patterns, with Station DY69-ES04-MX01 situated in the foothill region displaying a cyclonic recirculation pattern. In the flat terrain, the seabed current field is predominantly influenced by the Antarctic bottom current, with distinct branches extending towards the northeast (Station DY66-M2-MX2101 in the Block M2) and southwest (Station DY69-ES06-MX03 in the Block M1) directions.
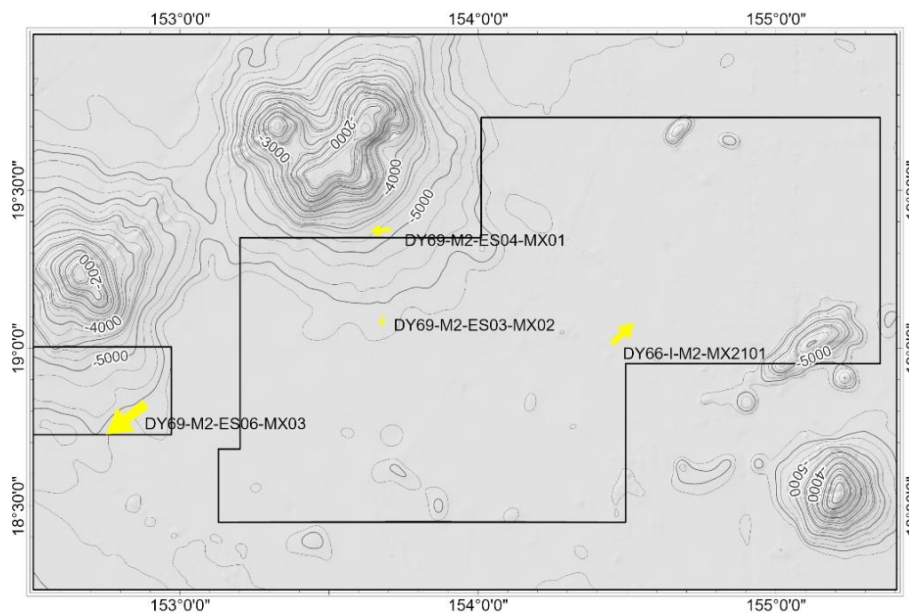
Figure 4-152 Distribution of average current speed vectors at the near-bottom of the Block M in the contract area

4.3.4.2.4 Mesoscale Eddies

Based on the META dataset, the geographical region spanning from 18–20 °N and 150–156 °E has been designated as the area of interest for the statistical examination of the impact zone of mesoscale eddies. An analysis was conducted on the characteristics, including amplitude, radius, and rotational velocity, of 324 cyclonic eddies and 314 anticyclonic eddies that were active for more than 10 days within this specified region from 1993 to 2021 (refer to Table 4-19). Figure 4-153 illustrates that the primary source region for mesoscale eddies

influencing this area lies within the range of 160–170°E. In this region, the average duration of activity for cyclonic and anticyclonic eddies is 35 days and 31 days, respectively, with the longest recorded duration being 160 days for an anticyclonic eddy. The average amplitude of cyclonic eddies is 4.89 cm, exceeding the 3.79 cm average for anticyclonic eddies, while the maximum amplitude for cyclonic eddies is 33.3 cm, higher than the 24.87 cm maximum for anticyclonic eddies. The average velocity of cyclonic eddies is 21.26 cm/s, with a maximum velocity of 57.39 cm/s, both surpassing the corresponding values for anticyclonic eddies at 18.20 cm/s and 48.84 cm/s, respectively. Both types of eddies exhibit similar spatial dimensions, with the average, maximum, and minimum radii of cyclonic eddies measuring 80.47 km, 278.8 km, and 26.2 km, respectively, and those of anticyclonic eddies averaging 78.56 km, with maximum and minimum radii of 254.8 km and 27.1 km, respectively.

Table 4-19 Statistical table of information on mesoscale eddies in the block (influence greater than 10 days)

Parameter	Cyclonic Eddy	Anticyclonic Eddy
Number	324	314
Average influence time (days)	35	31
Maximum influence time (days)	118	160
Minimum influence time (days)	10	10
Average amplitude (cm)	4.89	3.79
Maximum amplitude (cm)	33.3	24.87
Minimum amplitude (cm)	0.004	0.004
Average speed (cm/s)	21.26	18.20
Maximum speed (cm/s)	57.39	48.84
Minimum speed (cm/s)	4.48	4.81
Average radius (km)	80.47	78.56
Maximum radius (km)	278.8	254.8
Minimum radius (km)	26.2	27.1
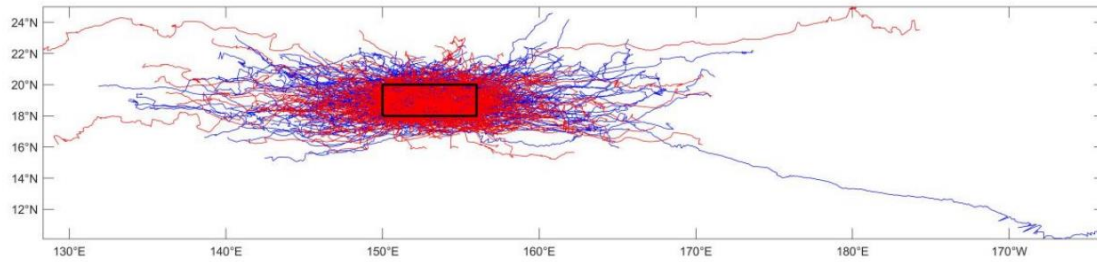
Figure 4-153 Trajectory map of mesoscale eddies affecting the M block (Blue represents cyclonic eddies, red represents anticyclonic eddies, and the black square box represents the statistical area of mesoscale eddy influence)

The monthly variability in the influence of mesoscale eddies within the specified region is statistically examined (refer to Figure 4-154), revealing distinct fluctuations across different months. Notably, March exhibits the highest occurrence of cyclonic eddies, with 76 instances, followed by April with 73 occurrences, and the lowest count observed in October, with only 42 instances. Conversely, the highest number of anticyclonic eddies is recorded in January, totaling 70 occurrences, with March and May each registering 66 occurrences, while June exhibits the lowest count with only 36 instances.
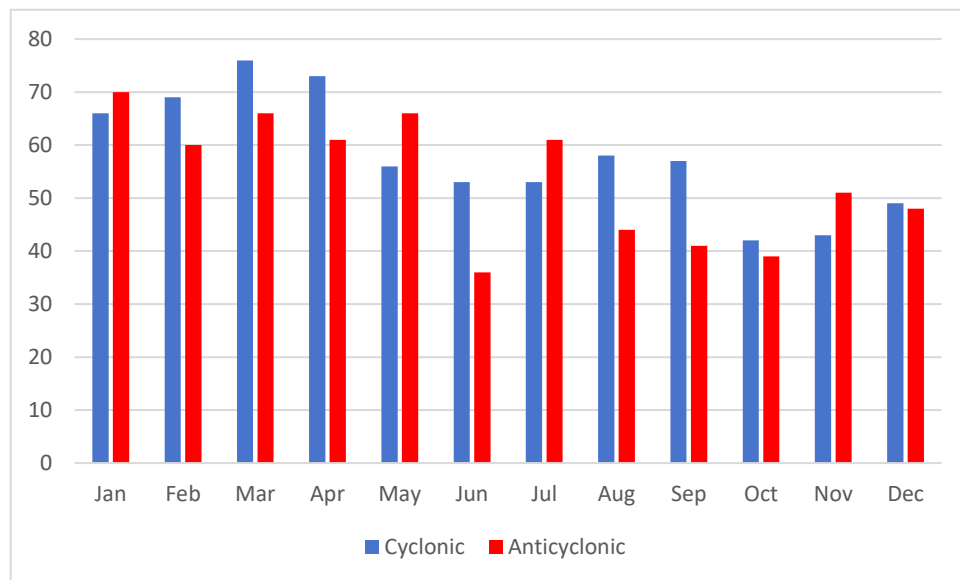
Figure 4-154 Monthly statistics of mesoscale eddy influence

4.3.4.3 Turbidity

Figure 4-155 is a time process chart of turbidity at the near-bottom of Station DY66-M2-MX2101. The turbidity at this station was less than 0.1 NTU from deployment to May 2022. It began to rise to 0.2 NTU in May 2022, and high turbidity phenomena occurred in July, September, and November 2022. Comparing the near-bottom current field of this station, it was found that the current speed was obviously enhanced during this period, and it is preliminarily judged that the high turbidity at the near-bottom is positively correlated with the high current speed.
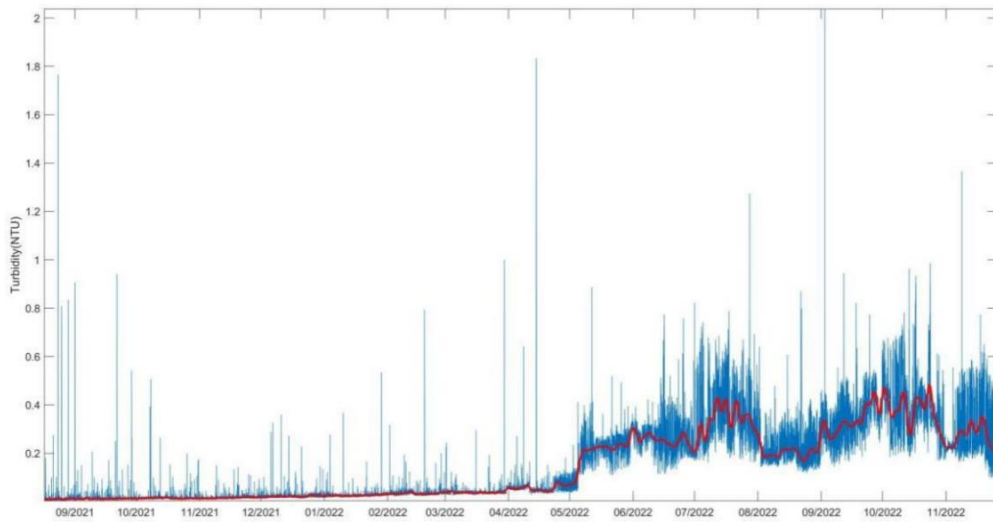
Figure 4-155 Time process chart of turbidity at the near-bottom of Station DY66-M2-MX2101 (Blue is the observed value of the turbidimeter, red is the value after low-pass filtering)

Figures 4-156 and 4-157 show the time variation process charts of turbidity at the near-bottom of Stations DY76-ES03-MX02 and DY76-ES06-MX03. The observation results show that the turbidity value observed during the survey at Station ES03 is low, with a small variation range, and most of the time the turbidity value is lower than the lowest observed value of the turbidimeter. The bottom turbidity value at Station ES06 is also very low, with average values of 5362 m layer and 5553 m layer both below 0.1 NTU.
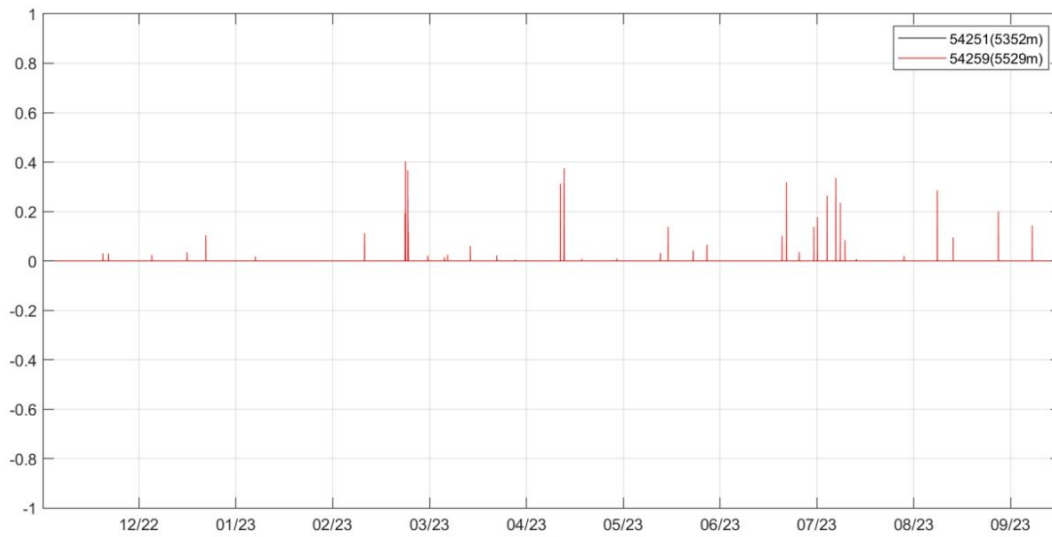
Figure 4-156 Time process chart of turbidity at the near-bottom of Station DY76-ES03-MX02
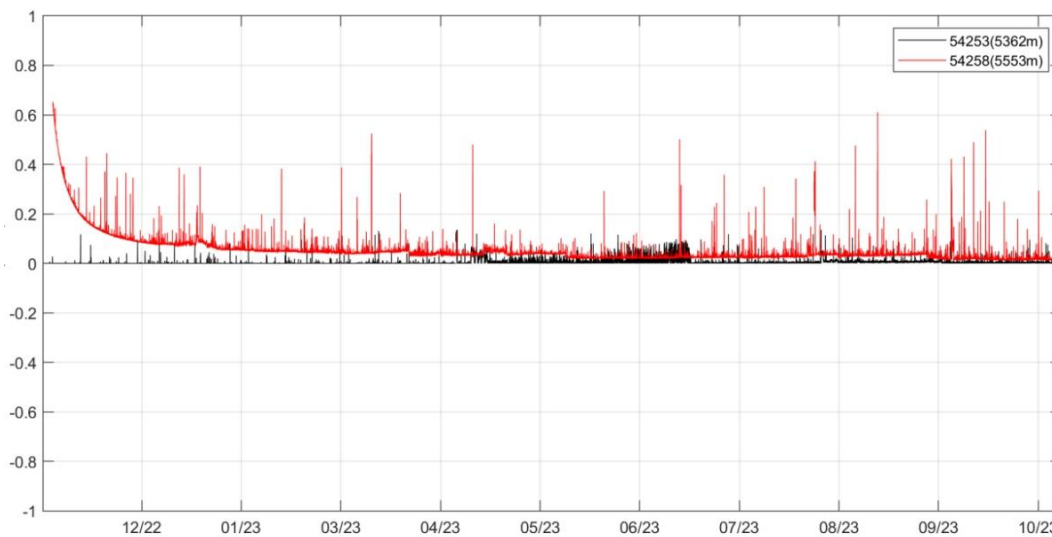
Figure 4-157 Time process chart of turbidity at the near-bottom of Station DY76-ES06-MX03

4.3.5 Chemical Environment

A series of three consecutive research cruises seawater chemical baseline surveys were conducted in the Block M from 2021 to 2023. A total of 15 survey stations were set up, with 6 stations in 2021, 5 stations in 2022, and 4 stations in 2023, As illustrated in Figure 4-158.
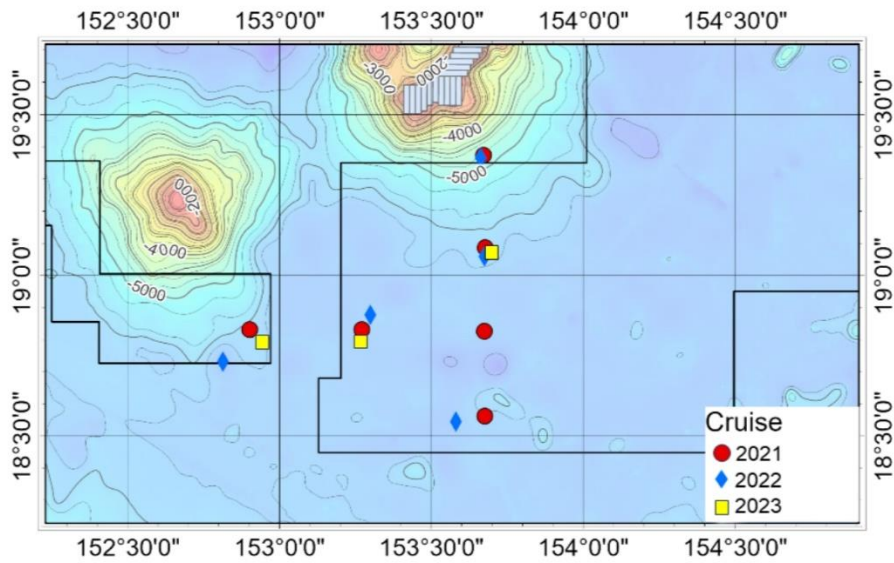
Figure 4-158 Schematic diagram of seawater chemical survey stations in the Block M

Considering the influence of climate change, a moderate La Niña event occurred in the tropical Pacific Ocean at the end of 2020, gradually diminishing in the spring of 2021. From May to June 2021, sea surface temperatures (SST) in the eastern equatorial Pacific approached almost neutral conditions, followed by a negative anomaly of SST from August to September 2021. Subsequently, a secondary La Niña cold event occurred in autumn 2021, persisting until 2022 and gradually diminishing by spring 2023, and El Niño event was observed from summer 2023 (Figure 4-159). it's evident that the working area during these three research cruises was affected to varying degrees by the La Niña event.
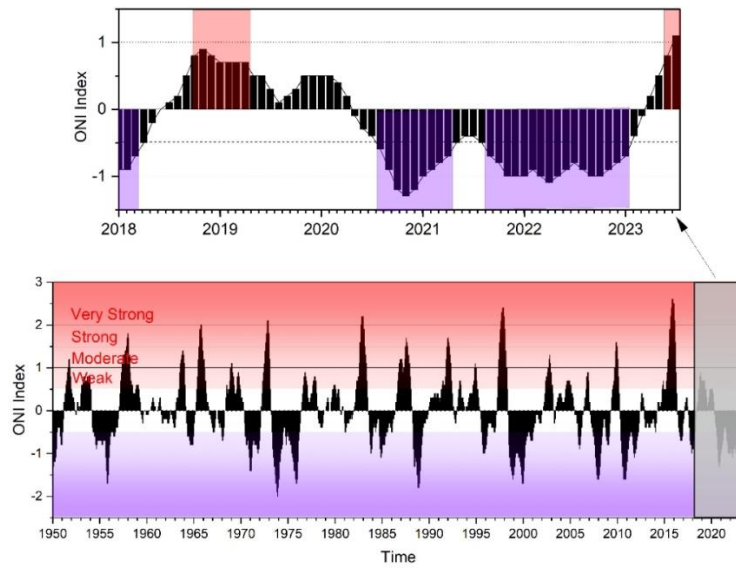
Figure 4-159 the Pacific multivariate El Niño-southern oscillation index (Data source: NOAA)

4.3.5.1 Dissolved Oxygen

The survey results of dissolved oxygen (DO) in the Block M from 2021 to 2023 are shown in Figure 4-160. The range of DO concentration is from 112.1 μmol/L to 479.2 μmol/L (as O). From the distribution of DO in the entire water column, high values of DO appear in the surface layer and bottom layer, with a minimum value around 800 m depth. Generally, DO concentrations are highest in the mixed layer and decrease with depth, reaching a minimum at 800 m. Below this minimum, DO concentration gradually increases with depth.
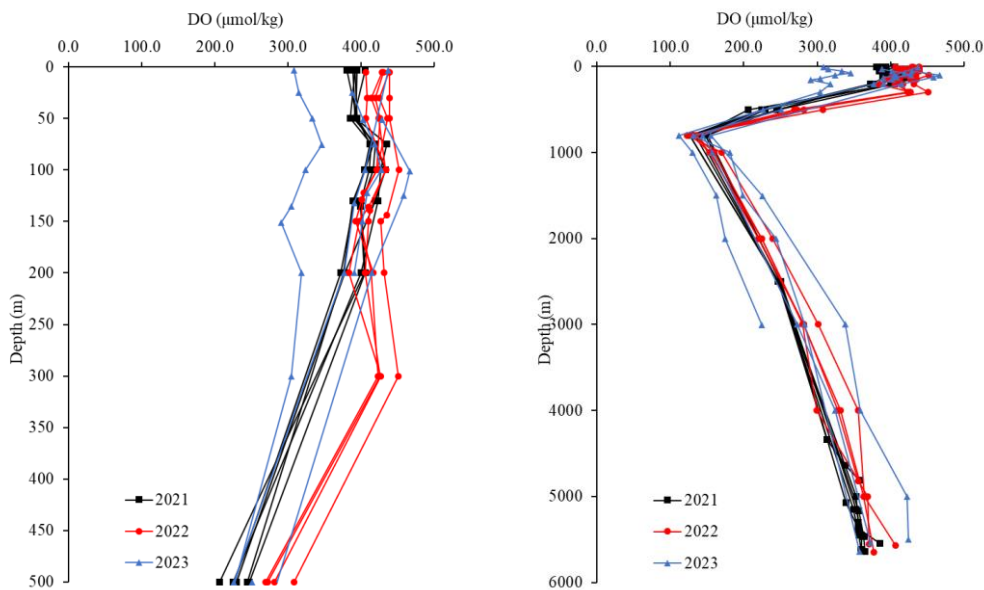
Figure 4-160 Vertical distribution of DO in the Block M from 2021 to 2023

The sources of DO in seawater primarily include two pathways: atmospheric input and photosynthesis by marine organisms. Due to the close contact between the sea surface and the atmosphere, oxygen in the atmosphere can enter the sea surface layer through exchange at the air-sea interface, and then, through the convection and diffusion of water, the surface oxygen-rich water is brought to the deep waters. The typical characteristics of DO in the open ocean can be seen from the vertical distribution in the figure: (1) The concentration of dissolved oxygen in the oceanic mixed layer is relatively high and evenly distributed, depending on the solubility of atmospheric oxygen in seawater; (2) Below the mixed layer, due to the oxidative decomposition of organic matter and the respiration of marine organisms, the DO concentration decreases with depth, reaching a minimum around 800 m; (3) Below 800 m, the concentration of DO gradually increases with depth. This is due to the presence of oxygen-rich Antarctic Bottom Water, which diffuses upward along concentration gradients.

4.3.5.2 pH

The pH measurement is conducted by collecting water samples with CTD and analyzing them in the shipboard laboratory using a pH meter. The results of the seawater pH survey in Block M from 2021 to 2023 are shown in Figure 4-161. Overall, pH in Block M ranged from 7.53 to 8.27. Surface to 200 m showed higher pH values, gradually decreasing with depth,

reaching a minimum around 800 m. Below this depth, pH slowly increased with depth, showing minimal variation.
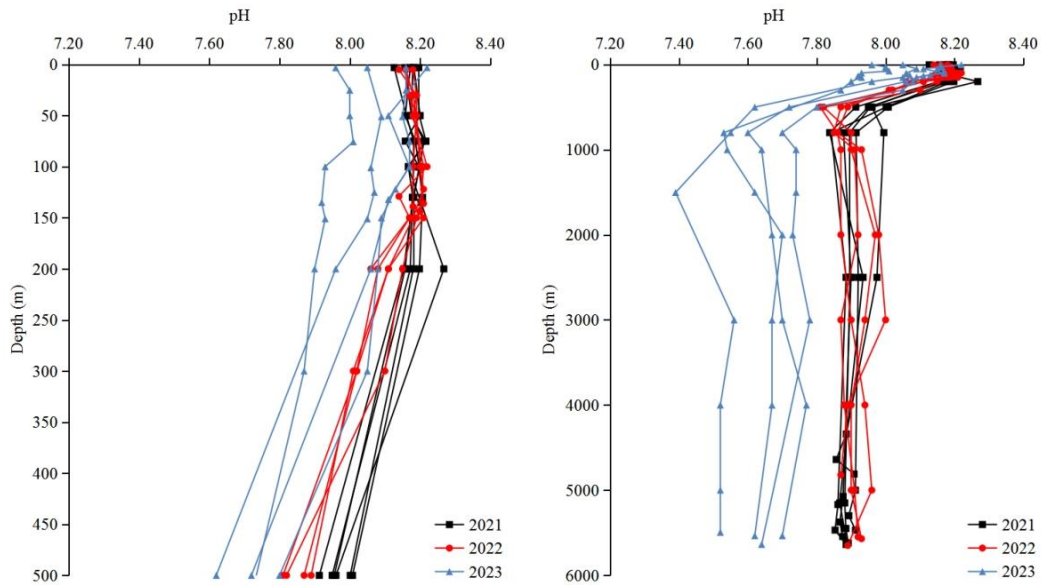
Figure 4-161 Vertical distribution of pH in the Block M from 2021 to 2023

Seawater is a multi-component electrolyte solution, and while the overall pH variation in the Block M is limited, minor fluctuations persist. These fluctuations are mainly influenced by the inorganic carbon system in seawater and marine biological activities, including temperature, salinity, pressure, and the formation and dissolution of $CaCO_3$ and $MgCO_3$ precipitates, which impact the balance of the inorganic carbon system, as well as the effects of photosynthesis and respiration of marine organisms on this balance. From the figure above, surface water exhibits a pH maximum due to photosynthesis of organisms, which leads to the removal of CO_2 from the water, consequently increasing the pH value. As the depth increases, the pH value gradually decreases, reaching a minimum around 800 m, where the pH minimum is at the similar layer as the DO minimum. In 2021 and 2022, pH values are similar but generally higher than those in 2023, which is mainly due to pH measurements using in-situ sensors in previous voyages, where water temperature variations in different water layers influenced the results. Subsequent voyages will standardize pH measurements by collecting water samples with a CTD device and using a pH meter to ensure data quality and comparability.

4.3.5.3 Total Alkalinity

The vertical distribution of total alkalinity (TA) in seawater in the Block M from 2021 to 2022 is illustrated in Figure 4-162. TA in seawater generally exhibits conservative behavior, meaning it does not very with changes in temperature or pressure. In the upper water, TA slowly increases with depth from the surface water to the chlorophyll maximum layer, then slowly decreases down to 500 m. Overall, the concentration of TA in the Block M increases with depth. This is attributed to the dissolution of $CaCO_3$ shells or skeletons of calcium-bearing organisms after their death in the deep water. This dissolution increases the concentration of bicarbonate in the water, leading to higher TA in deep water.
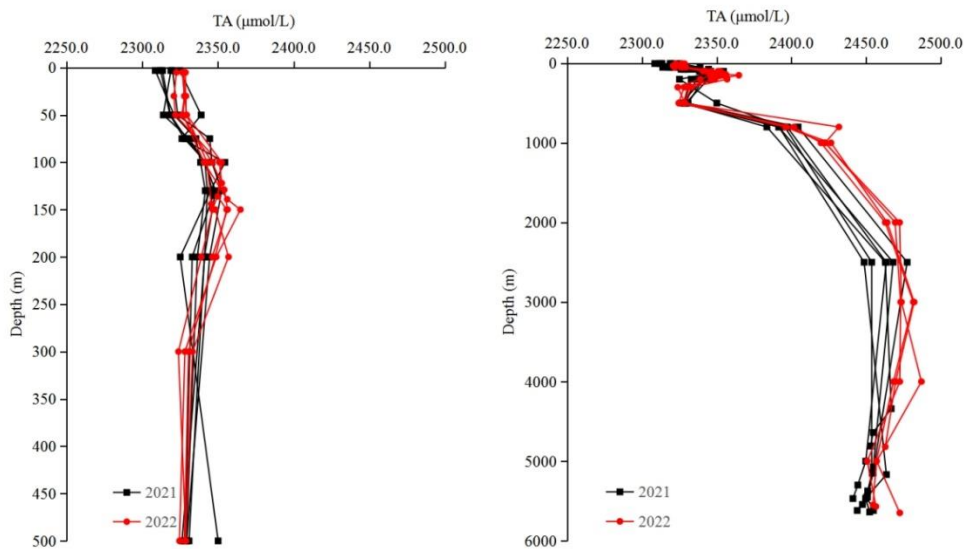
Figure 4-162 Vertical distribution of TA in the Block M from 2021 to 2022

4.3.5.4 Nutrients

During the period from 2021 to 2023, investigations on nutrients were conducted in the Block M. Overall, the concentration of nutrients in the euphotic zone of the Block M is extremely low, the nutricline is between 200 m and 800 m, and minimal variations is observed in deep water. The Primary nitrite maximum (PNM) can be found from the vertical distribution of nitrite with relatively high nitrite content at depths of 100 m to 150 m, consistent with the general pattern of nitrite vertical distribution in the ocean.

The vertical distribution of nitrate in the Block M from 2021 to 2023 is shown in Figure 4-163. It can be seen that within the euphotic zone, nitrate is consumed due to the

photosynthesis of phytoplankton, thus the concentration of nitrate is extremely low. Below the nutricline, the nitrate concentration increases rapidly with depth, reaching maximum at 800 m to 1000 m with the concentration of about 40.0 µmol/L. This is mainly attributed to the degradation of organic matter at this depth. Furthermore, nitrate slightly decreases below 1000 m with increasing depth.
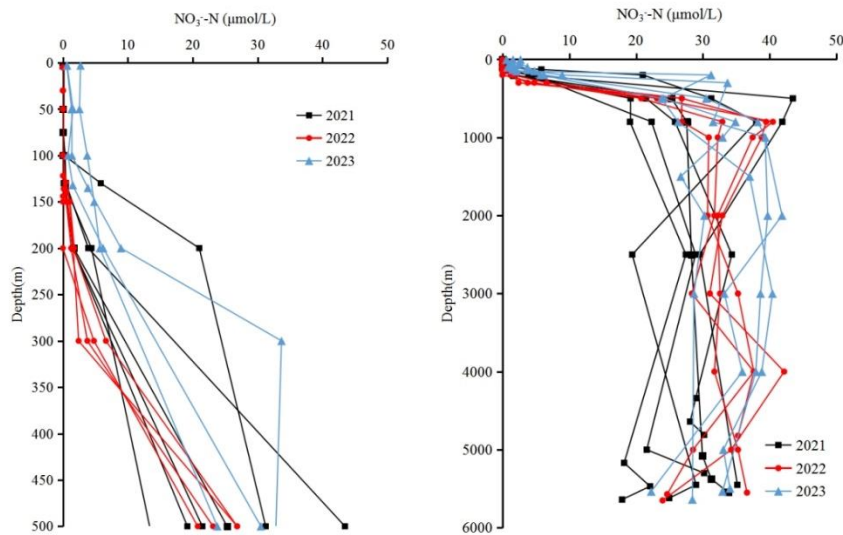
Figure 4-163 Vertical distribution of nitrate in the Block M from 2021 to 2023

The vertical distribution of phosphate in the Block M from 2021 to 2023 is illustrated in Figure 4-164. According to the vertical distribution of phosphate, the phosphate concentration is extremely low within the euphotic zone. An increase of phosphate concentration is evident from 150 m, rising rapidly between 300 m and 500 m, and reaching maximum around 800 m and 1000 m.

These variations are primarily related to the following factors: (1) Phosphorus-bearing particles sink under the influence of gravity to depths of 800 m to 1,000 m in seawater, where they are decomposed and oxidized by bacteria, releasing phosphate back into the seawater; (2) The convection of water masses is weak, leading to relatively small changes in the concentration of phosphate below 1,000 m depth.
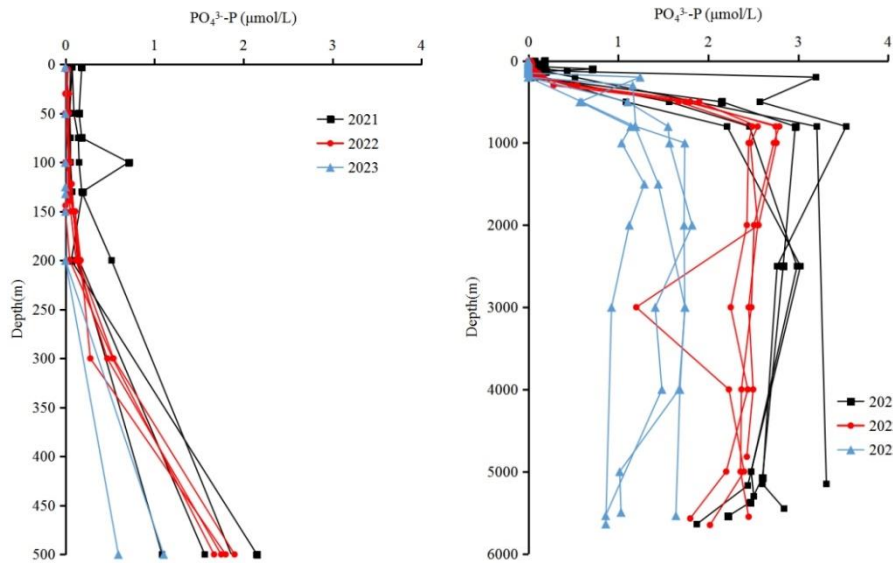
Figure 4-164 Vertical distribution of phosphate in the Block M from 2021 to 2023

Figure 4-165 illustrates the vertical distribution of silicate in the Block M from 2021 to 2023. The silicate concentration is generally below 2 µmol/L within the euphotic zone (<100 m). The concentration gradually increases from 150 m, rising rapidly between 300 m and 800 m, reaching maximum between 2,500 m to 4,000 m. Unlike nitrate and phosphate, the recycling efficiency of silicate is lower, mainly due to the slow dissolution of opal, resulting in deeper silicate regeneration compared to nitrogen and phosphorus. Generally, deep waters of the Pacific and Indian Oceans contain much higher silicate concentrations than those of the Atlantic Ocean. This is due to the accumulation silicate from the dissolution of opal and diffusion from seafloor sediments along the path of global thermohaline circulation.
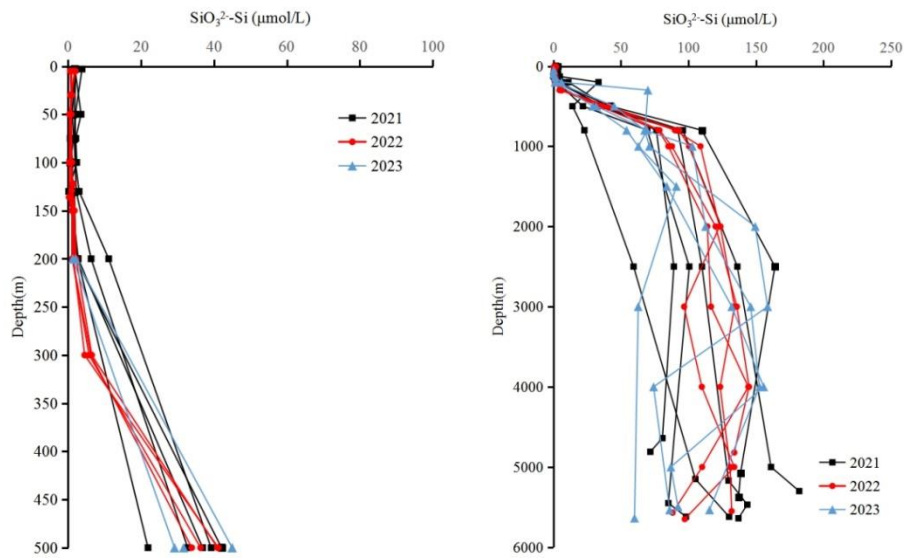
Figure 4-165 Vertical distribution of silicate in the Block M from 2021 to 2023

4.3.5.5 Dissolved Inorganic Carbon

The vertical distribution of dissolved inorganic carbon (DIC) in the Block M from 2021 to 2022 is depicted in Figure 4-166. The concentration range of DIC in the Block M is from 1991 μmol/L to 2531 μmol/L. Generally, DIC concentration increases rapidly with depth from the surface to 800 m, with little variation thereafter.
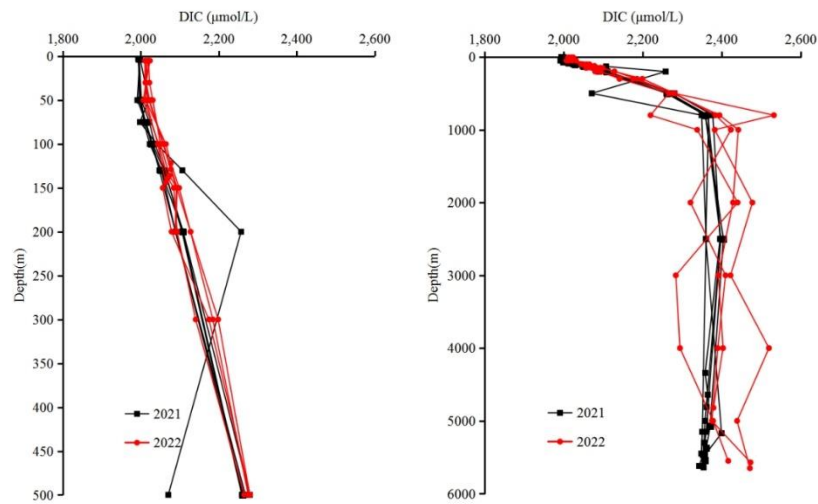
Figure 4-166 Vertical distribution of DIC in the Block M from 2021 to 2022

4.3.5.6 Suspended Solid

The vertical distribution of suspended solid (SS) in Block M during the survey voyages of 2021 and 2023 is shown in Figure 4-167. The concentration of SS in most stations ranges from 0.1 mg/L to 3.2 mg/L. Due to the very low concentration of SS in open ocean, the volume of water sample filtered will affect the data accuracy. From the overall distribution of SS in Block M depicted in the figure, the overall concentration of SS is low and does not change obviously, with no obvious pattern of change.
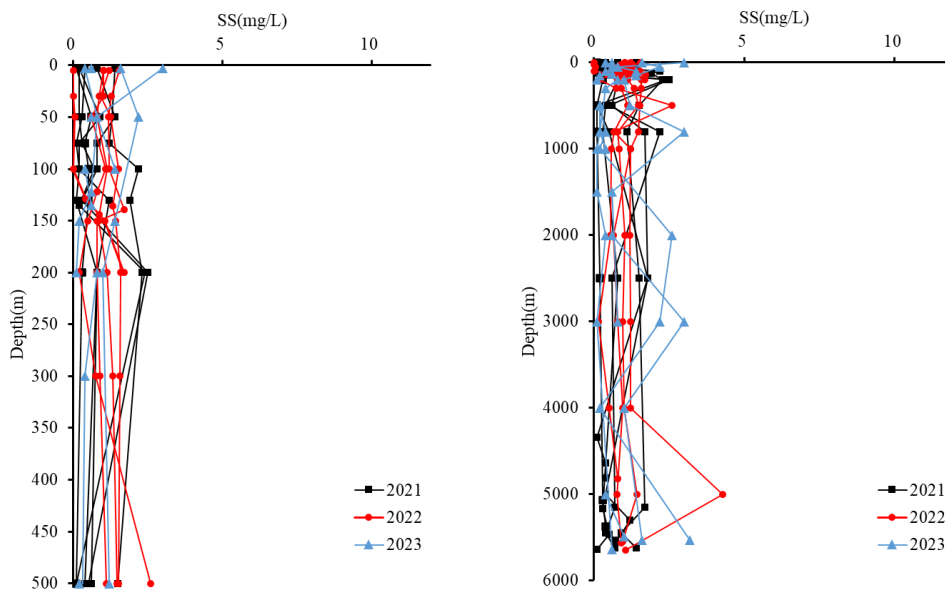
Figure 4-167 Vertical distribution of SS in seawater at survey stations in the Block M from 2021 to 2023

4.3.5.7 Particulate Organic Carbon

The particulate organic carbon (POC) research within the Block M has yet to be conducted by Beijing Pioneer Company. This report is based on the Level-3 product of oceanic annual average POC concentration data from July 2002 to January 2023 provided by MODIS. Figure 4-168 illustrates the distribution of surface seawater POC concentration in the Northwest Pacific. A discernible increase of POC concentration in the surface seawater is observed from low to mid latitudes, with a multi-year average surface POC concentration of 25 mg/m^3 in the Block M2. Ma et al. (2020) reported the vertical distribution of POC in the Kocebu Seamount near the Block M2 in spring, as shown in Figure 4-169. Overall, POC concentration in this region generally decreases with increasing water depth, remaining relatively stable in the water layer deeper than 700 m. The average surface POC concentration

is 23.61 mg/m^3, aligning closely with the aforementioned satellite remote sensing data. The maximum POC concentration is observed in the chlorophyll maximum layer, averaging 24.50 mg/m^3, with mid-layer and bottom-layer average concentrations 14.93 mg/m^3 and 12.02 mg/m^3, respectively.
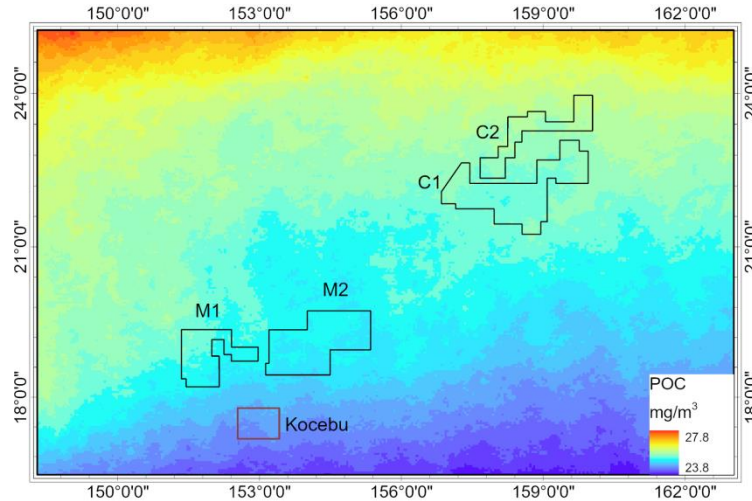
Figure 4-168 Distribution of surface seawater POC concentration in the Northwest Pacific (Data source: MODIS)
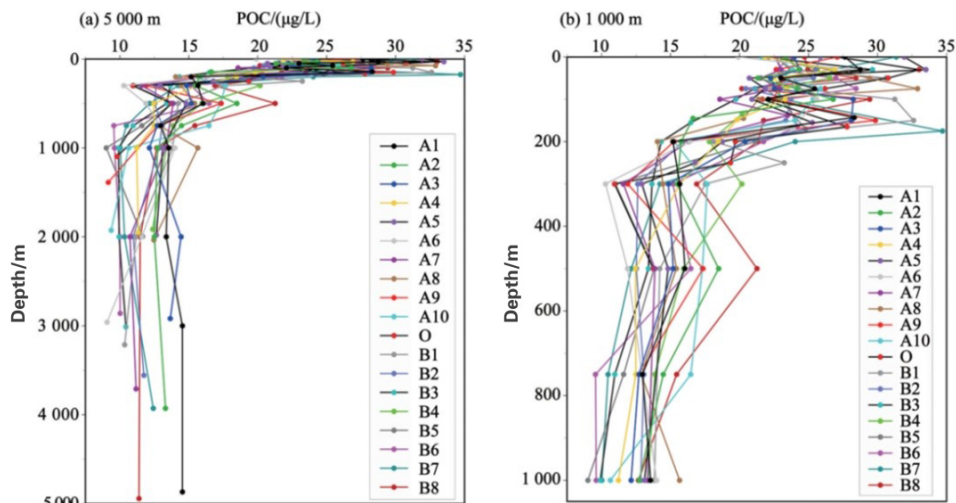
Figure 4-169 Vertical distribution of POC in the Kocebu Seamount of the Northwest Pacific (Ma et al., 2020)

4.3.5.8 Sinking Flux

Building upon the net primary productivity (NPP) data collected from the SeaWiFS.R2014 (January 1998 to December 2002) and MODIS.R2018 (January 2003 to

December 2019), NPP data from 1998 to 2019 were obtained through band operations. Moreover, the global ocean euphotic zone data were calculated using the Global Marine Environment Dataset, while POC output fluxes at a resolution of 9 km were calculated using the model proposed by Lutz et al. (2007). The results reveal that from 1998 to 2019, the POC sinking flux in the Block M2 of the contract area was 0.66 g m^{-2} yr^{-1}, and the POC sinkingflux in the Block M1 was 0.67 g m^{-2} yr^{-1} (Figure 4-170), indicating a gradual increase in spatial distribution from south to north in this region.
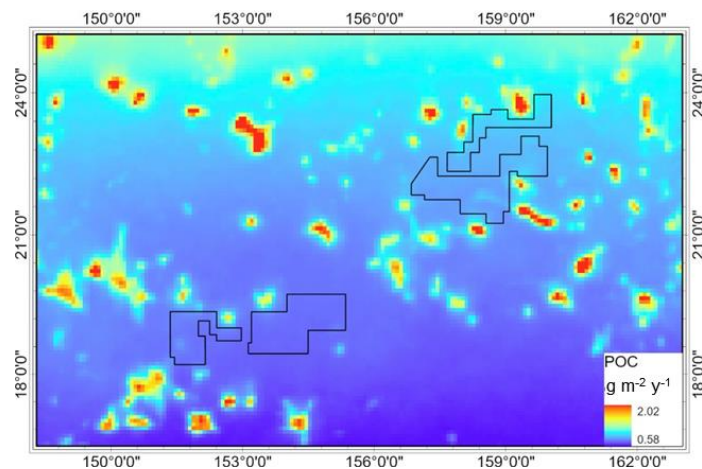
Figure 4-170 POC sinking flux on the seafloor in the Northwest Pacific

During the DY69 cruise (2021), sediment traps were deployed at Stations MX02 and MX03, and were retrieved during the DY76 cruise (2022) and then redeployed. Additionally, a sediment trap was deployed at Station MX2203 near Station MX02, and the traps deployed during the DY76 cruise (2023) were retrieved during the DY81 cruise (2023). The sediment traps deployed in 2021 were the KUM (Germany) and NIGK (Japan) sediment traps, while those deployed in 2022 were NIGK sediment traps (Japan) and McLane sediment traps (American). The sampling intervals for the traps at Stations MX02 and MX03 were 1 month, while for the traps at Station MX2203 was 15/16 days, with four samples collected at monthly intervals. The observation period for Stations MX02 and MX03 spanned from October 2021 to October 2023, totaling about 24 months, while the observation period for Station MX2203 was 11 months.

Sample acquisition details: During the period from 2021 to 2022, there were 14 samples collected from the 2050 m layer at Station MX02, with almost no samples in the first 12 sampling bottles. At Station MX03, 6 samples were obtained, with extremely low sample

contents in the first 3 sampling bottles. The sixth sample represents the total sample collected from March to November 2022, while sample acquisition from other layers was normal. From 2022 to 2023, sample acquisition at all stations and layers was normal. The deployment location, time, and effective sample acquisition of sediment traps are shown in Table 4-20.

Table 4-20 Sample acquisition details of the sediment traps

Station	Longitude (°E)	Latitude (°N)	Depth (m)	Trap model	Deployment time	Recovery time	Number of effective Samples
MX02	153.6792	19.0982	2050	KUM K/MT 234	2021.10.26	2022.11.26	2
			5450	KUM K/MT 234	2021.10.26	2022.11.26	13
MX03	152.7995	18.7382	2050	McLane Mark-78H	2021.10.28	2022.11.29	3
			5400	McLane Mark-78H	2021.10.28	2022.11.29	14
MX02	153.6775	19.09445	2000	KUM K/MT 234	2022.11.27	2023.10.16	11
			5000	KUM K/MT 234	2022.12.01	2023.10.16	11
MX03	152.8424	18.7667	2000	McLane Mark-78H	2022.12.01	2023.10.12	11
			5000	McLane Mark-78H	2022.12.01	2023.10.12	11
MX2203	153.6928	19.32189	2000	McLane Mark-78H	2022.11.23	2023.10.17	18
			4594	McLane Mark-78H	2022.11.23	2023.10.17	18

4.3.5.8.1 Sinking Particulate Matter Fluxes

(1) Sinking Particulate Matter Fluxes at Station MX02

Figure 4-171 shows the total mass flux (TMF) of sinking particulate matter at different levels of the Station MX02. During the period from November 2021 to November 2022, sinking particles at the depth of 2,050 m was only observed in October and November of 2021, with fluxes of 35.19 $\text{mg m}^{-2} \text{d}^{-1}$ and 50.34 $\text{mg m}^{-2} \text{d}^{-1}$, respectively, higher than those observed at 5,450 m during the same period. At the depth of 5,450 m, TMF ranged from 1.69 $\text{mg m}^{-2} \text{d}^{-1}$ to 24.37 $\text{mg m}^{-2} \text{d}^{-1}$, with an average of 12.94 $\text{mg m}^{-2} \text{d}^{-1}$, exhibiting relatively higher values in winter and summer.

From December 2022 to October 2023, at the depth of 2,000 m, TMF ranged from 8.73 $\text{mg m}^{-2} \text{d}^{-1}$ to 34.12 $\text{mg m}^{-2} \text{d}^{-1}$, with an average of 21.27 $\text{mg m}^{-2} \text{d}^{-1}$. During the period from

February to July 2023, TMF was higher. At the depth of 5,000 m, TMF ranged from 3.16 mg m^{-2} d^{-1} to 13.92 mg m^{-2} d^{-1}, with an average of 7.74 mg m^{-2} d^{-1}, showing obvious seasonal differences, with higher values in summer than in other seasons. Compared to the previous observation period, the average TMF at the bottom layer decreased, and high TMF values occurred only in summer.
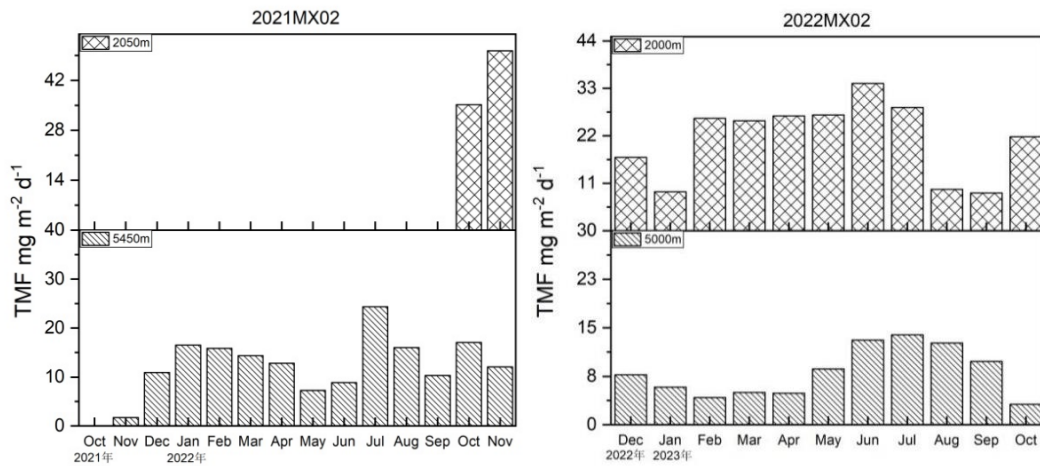
Figure 4-171 The TMF of sinking particulate matter at the Station MX02

(2) Sinking Particulate Matter Fluxes at Station MX03

The TMF of sinking particulate matter at Station MX03 is illustrated in Figure 4-172. From October 2021 to November 2022, at the depth of 2,050 m of Station MX03, sinking particle was observed only in January and February 2022, with TMF of 7.01 mg m^{-2} d^{-1} and 3.78 mg m^{-2} d^{-1}, respectively. At the depth of 5,040 m, TMF ranged from 2.18 mg m^{-2} d^{-1} to 41.53 mg m^{-2} d^{-1}, with an average of 12.35 mg m^{-2} d^{-1}, with high TMF values mainly occurring in October 2021 and November 2022.

From December 2022 to October 2023, at the depth of 2,000 m of the Station MX03, TMF ranged from 2.79 mg m^{-2} d^{-1} to 21.60 mg m^{-2} d^{-1}, with an average of 10.86 mg m^{-2} d^{-1}. At the depth of 5,000 m, TMF ranged from 4.24 mg m^{-2} d^{-1} to 18.35 mg m^{-2} d^{-1}, with an average of 7.73 mg m^{-2} d^{-1}. There are obvious seasonal differences in TMF, with higher values in summer than in other seasons. Compared to the previous observation period, the average TMF at the bottom layer decreased, and the periods of high TMF values also changed obviously, occurring in summer.
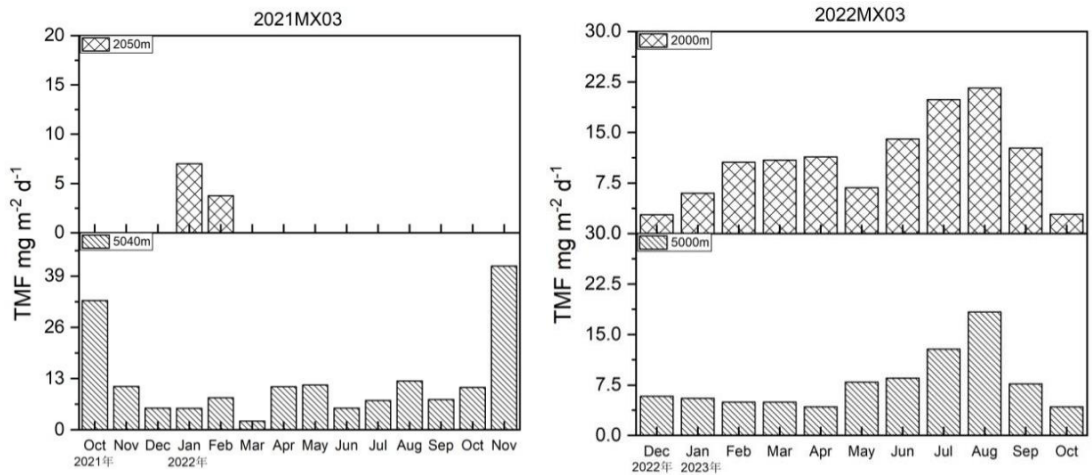
Figure 4-172 The TMF of sinking particulate matter at Station MX03

Figure 4-173 shows the TMF of sinking particle of the Station MX2203. From December 2022 to October 2023, at the depth of 2,000 m, TMF exhibited a gradual increase from winter to summer, with obviously higher values in summer than in winter. The range of TMF was from 6.47 mg m^{-2} d^{-1} to 27.09 mg m^{-2} d^{-1}, with an average of 14.20 mg m^{-2} d^{-1}. At the depth of 4,954 m, the variation trend of TMF was similar to that at 2,000 m, with an average of 9.28 mg m^{-2} d^{-1}, which was much lower than that at 2,000 m.

During the period from December 2022 to October 2023, the average TMF values at Stations MX02, MX03, and MX2203 showed characteristics of lower values in the bottom layer than that at 2,000 m and higher values in summer compared to other seasons.
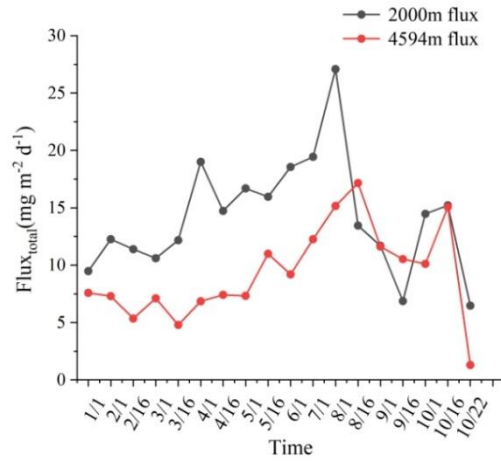
Figure 4-173 The TMF of sinking particulate matter at Station MX2203

The TMF of sinking particle at the depth of 2,000 m from December 2022 to October 2023 is shown in Figure 4-174. The variation of TMF shows a trend of gradual increase from winter to summer, with the flux in summer obviously higher than in winter. During this period, the range of TMF was 6.47 mg m^{-2} d^{-1} to 27.09 mg m^{-2} d^{-1}, with an average of 14.20 mg m^{-2} d^{-1}. At the depth of 4,954 m, the average value of TMF was 9.28 mg m^{-2} d^{-1}. The overall flux was much lower than that at 2,000 m except two time periods: August 1, 2023 to August 16, 2023, and September 1, 2023 to September 16, 2023.
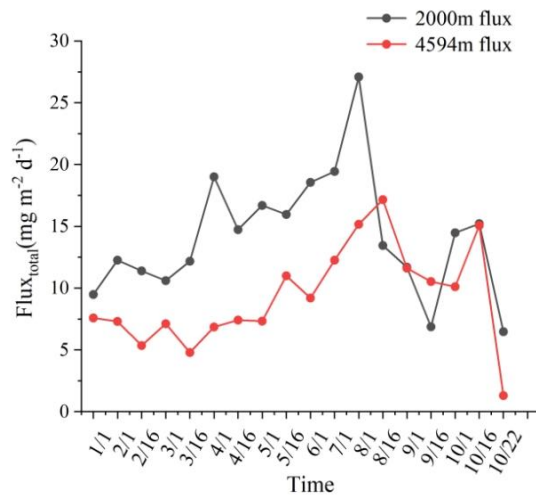
Figure 4-174 The TMF of sinking particulate matter at 2000 m and 4954 m

4.3.5.8.2 Composition of Sinking Particulate Matter

The composition of sinking particulate matter at Station DY69-M2-ES04-MX recovered in 2022 has been analyzed. The content of total carbon and total nitrogen in the sinking particulate matter, the content of particulate organic carbon and calcium carbonate, and the stable isotope values of particulate carbon and particulate nitrogen were determined.

The proportion of total carbon and total nitrogen in the 1000m layer from November 2021 to September 2022 is shown in Figure 4-175. During this time series, the compositional percentage of the sinking particulate matter ranged from 15.32–30.47% for total carbon (TC) with a mean value of 20.38%, and ranged from 0.84–4.64% for total nitrogen (TN) with a mean value of 2.09%. Seasonal variations in TC and TN were not obvious, but the percentage of TC was obviously higher than that of TN in all cases.
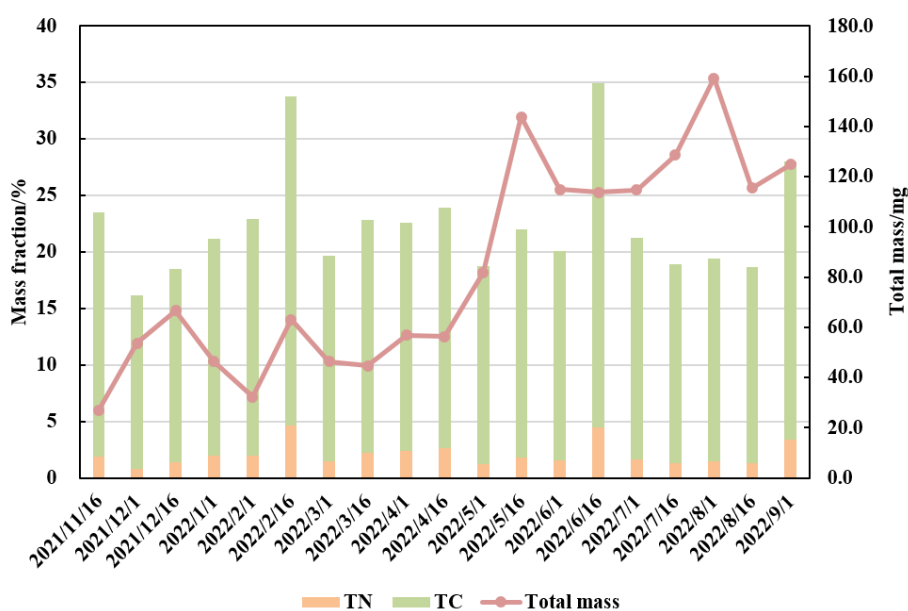
Figure 4-175: Content of total mass, total carbon and total nitrogen of sinking particulate matter

At the 1000 m layer, the fluxes of POC and $CaCO_3$ from November 2021 to September 2022 are shown in Figure 4-176. The fluxes of POC and $CaCO_3$ show similar seasonal changes, with an overall gradual upward trend from winter to summer, and the fluxes in summer are obviously higher than those in winter. There is a clear difference, with TMF>$CaCO_3$>POC. During the sampling period, TMF flux ranged from 3.57 to 19.89 mg m^{-2} d^{-1}, with an average of 10.68 mg m^{-2} d^{-1}; POC flux ranged from 0.32 to 3.99 mg m^{-2} d^{-1},

with an average of 1.36 mg m^{-2} d^{-1}; and the CaCO$_3$ flux varied between 1.55 and 14.56 mg m^{-2} d^{-1}, with an average of 7.29 mg m^{-2} d^{-1}. In addition, four obvious high particle flux peaks (circled in Figure 4-176) were observed during the monitoring period, each lasting for about two sampling periods. During this period, the CaCO$_3$ flux also showed the highest flux, and the CaCO$_3$ flux was obviously correlated with the total mass flux (R=0.91, P<0.01). Compared with CaCO$_3$, the POC flux change was relatively poor in consistency with the change of total mass flux (R=0.67, P<0.05). During the monitoring period, the CaCO$_3$ flux was higher than the POC flux. The average contribution of CaCO$_3$ flux was 65.35%, while the average contribution of POC flux was only 12.54%.
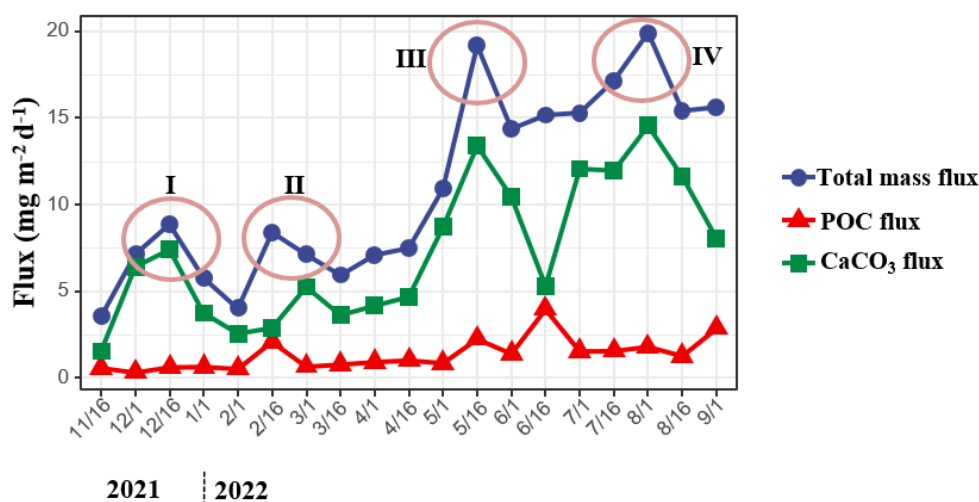
Figure 4-176 Fluxes of TMF, POC and CaCO$_3$

The variation of the stable isotope values of carbon and nitrogen in the particulate matter of the 1000m layer from November 2021 to September 2022 is shown in Figure 4-177. The δ^{13}C values varied from –24.3‰ to –21.5‰, with an average value of –22.7‰; the δ^{15}N values varied from 1.2‰ to 5.8‰, with an average value of 3.3‰. In addition, the fluctuations in δ^{13}C and δ^{15}N values are relatively synchronous, and simultaneously showing an upward or downward trend. They also show seasonal fluctuations, mainly in the form of lower δ^{13}C and δ^{15}N values in summer and higher δ^{13}C and δ^{15}N values in winter. It is worth noting that in the first high-flux event, both δ^{13}C and δ^{15}N values were heavier, while in the third and fourth high-flux events, both δ^{13}C and δ^{15}N values were lighter.
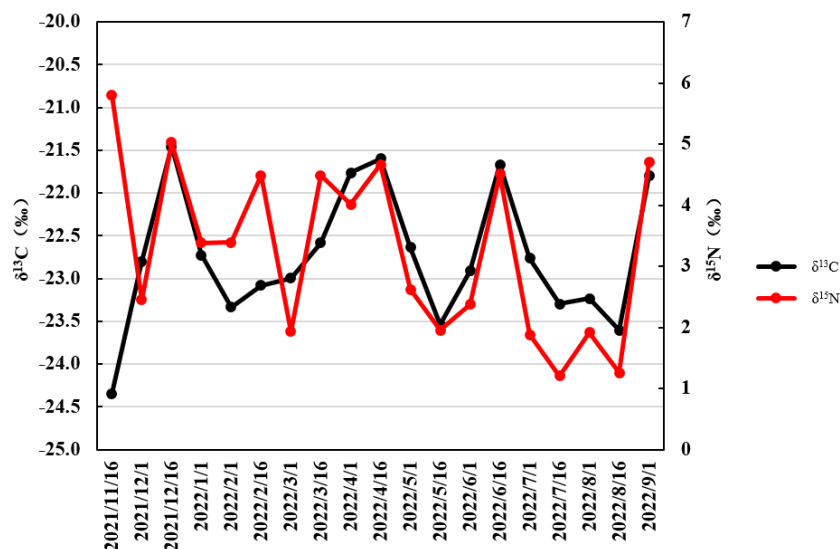
Figure 4-177 Carbon and nitrogen stable isotopes in the sinking particulate matter

At the 4340 m layer, the total mass of sinking particulate matter from October 2021 to November 2022 was 160 mg, and the proportions of total nitrogen and total carbon components were 0.52% and 13.08%, respectively. Flux of total mass of the sinking particulate matter was 0.81 mg m^{-2} d^{-1}, and the POC flux was 0.028 mg m^{-2} d^{-1}, both of which were much lower than the flux at the 1000 m layer. In addition, the stable isotope values of carbon and nitrogen in the sinking particles during this period were measured, with δ^{13}C of –25.0‰ and δ^{15}N of 1.0‰, respectively, both of which were lower than that at the 1000 m layer.

4.3.5.8.3 Horizontal Distribution Characteristics

Based on the topographical features described in Section 4.3.2, the Block M is divided into piedmont and plain areas. The chemical parameters of the near-bottom (within 50 m of the bottom) seawater at each survey site in these areas are statistically analyzed, with the results shown in Table 4-21. The statistical results indicate that there are no obvious differences in the chemical elements of seawater between the piedmont and plain areas within the contract area, suggesting a high level of consistency in the distribution of chemical elements in the bottom seawater of this area.

Table 4-21 Comparison of seawater chemical elements in the piedmont and plain areas

Area	Station	pH	DO (μmol/)	NO$_3^-$ (μmol/L)	NO$_2^-$ (μmol/L)	PO$_4^{3-}$ (μmol/L)	SiO$_3^{2-}$ (μmol/L)	SS (mg/L)	TA (μmol/L)	DIC (μmol/L)	DIN (μmol/L)
Piedmont	DY69-M2B1-ES02-CTD12	7.89	359.8	24.96	0.047	-	130.09	0.70	2444.1	2342.2	25.011
Piedmont	DY69-M2B1-ES03-CTD05	7.88	385.5	33.76	0.146	2.22	-	0.70	2447.6	2356.4	33.908
Piedmont	DY69-M2-ES04-CTD03	7.91	357.2	30.18	0.107	4.21	71.82	0.40	2452.9	2361.3	30.291
Piedmont	DY69-M1-ES06-CTD07	7.91	363.9	-	0.057	-	-	0.90	2441.2	2351.8	-
Piedmont	DY76-I-M2-S062CTD14ES03	7.93	406.5	24.65	0.000	1.80	88.30	-	-	-	24.650
Piedmont	DY76-I-M2-S055CTD13ES04	7.87	355.9	35.25	0.000	2.43	133.93	-	-	-	35.250
Piedmont	Average	7.90	371.5	29.76	0.059	2.66	106.03	0.68	2446.5	2352.93	29.822
Plain	DY61-I-M2-S110CTD31	-	321.1	23.49	0.000	2.35	105.23	-	-	-	23.490
Plain	DY69-M2B1-ES01-CTD13	7.89	360.7	-	0.037	-	98.22	1.40	2454.9	2350.6	-
Plain	DY69-M2B1-ES05-CTD09	7.89	365.0	17.91	0.047	1.87	137.04	0.10	2452.4	2353.6	17.958
Plain	DY76-I-M2-S075CTD16ES01	7.89	376.7	23.97	0.000	2.02	97.28	-	-	-	23.970
Plain	DY76-I-M1-S080CTD17ES10	7.92	370.4	36.60	0.000	2.45	131.99	-	-	-	36.600
Plain	Average	7.90	358.8	25.49	0.017	2.17	113.95	0.75	2453.65	2352.10	25.504

4.3.5.9 Summary

Overall, there are minimal differences of various seawater elements between stations within Block M. The distribution of the major chemical elements largely conforms to the typical patterns of the NPSG, indicating a markedly oligotrophic status throughout the region. Obvious variations are observed in the vertical profiles of each major chemical constituent. DO exhibits high concentrations in the mixed layer, decreasing with depth and reaching a minimum around 800 m, followed by a gradual increase thereafter. Surface to 200 m depth shows relatively high pH levels, gradually decreasing with depth to a minimum at about 800 m, with subsequent slight and stable increases with further depth. Within the euphotic zone of Block M, nutrient concentrations are as low as nanomoles per liter, increasing gradually with depth. Beyond the nutricline, the nutrient concentrations remain relatively stable with increasing depth, though slight variations are noted in near-bottom water nutrient levels.

4.3.6 Ambient Noise

All the sound recordings used in 2021 and 2022 were collected in the CTA. However, one hydrophone was deployed in the PRZ and IRZ respectively last year, and high-quality passive acoustic data are expected to be acquired for comparison.

4.3.6.1 Ambient Noise Monitoring in 2021

In 2021, a self-contained underwater acoustic recorder was deployed on a subsurface buoy to monitor ambient noise in the contract area. The station was positioned near the CTA (153.6724 °E, 19.3739 °N), with the acoustic recorder affixed to the bottom of the buoy at a depth of 4820 meters, approximately 25 meters above the seafloor.

The hydrophone utilized in this study exhibits an end-to-end system sensitivity of −170.3±1 dB re 1V/μPa, accompanied by a flat response across frequencies ranging from 20 Hz to 5 kHz, and boasts a gain exceeding 100 dB, with the frequency band used in calculating SPLs from 20 Hz to 2 kHz. To record a broad spectrum of underwater sounds, a sample rate of 24 kHz was selected. In addition, to ensure prolonged deployment periods, a duty cycle of 5 minutes every three hours was implemented, facilitating continuous recording for over one year. Acoustic data were collected over a span extending from October 2021 to October 2022, encompassing a duration of 362 days.

4.3.6.1.1 Ambient Noise Sound Pressure Level in the Block M

The root mean square sound pressure level (RMS SPL) for the surveyed area is shown in Figure 4-178. Interannually, although the RMS SPL exceeding 105 dB re 1μPa occasionally occurs, the overall SPL is relatively low, ranging from 77 to 97 dB, with a difference of ~20 dB in amplitude. Further analysis reveals that the median SPL within the region is approximately 88.1 dB, lower than the global ambient noise levels in gentle weather conditions (approximately 94 dB re 1μPa). This aligns with the fact that the surveyed area is not on a major shipping route and experiences relatively low human activity. However, it also suggests that noise generated by exploration and deep-sea mining activities in the contract area may increase the noise SPLs, potentially adversely affecting the biodiversity conservation of this environmentally sensitive area.
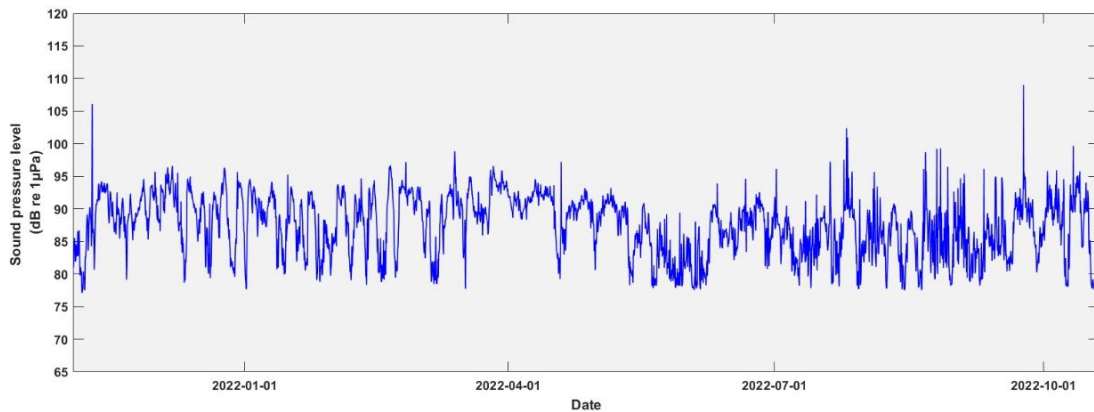
Figure 4-178 Broadband sound pressure levels in 2021

4.3.6.1.2 Noise Power Spectral Density in the Block M

The long-term ambient noise power spectral density (PSD) in 20Hz–10kHz band (Figure 4-179) indicates that the noise power spectrum level in the contract area varies between 30 and 60 dB re 1 μPa^2/Hz. However, the ambient noise energy is primarily concentrated in the low-frequency range of 20 Hz to 2 kHz, with lower amplitude above 5 kHz. Temporally, low-frequency noise exhibits discernible seasonal variations to a certain extent.
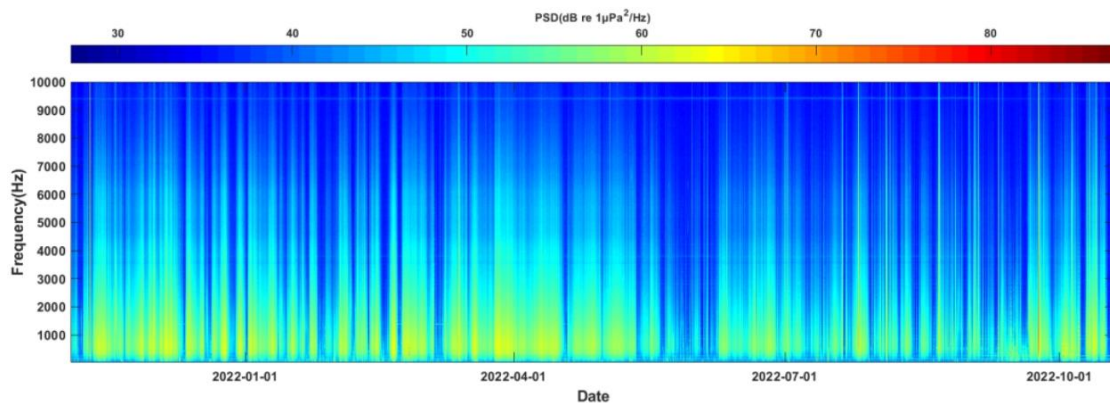
Figure 4-179 Long-term noise power spectral density for 2021

Monthly ambient noise PSDs were obtained by averaging the noise power spectrum level for each month and corresponding sound spectrum levels were shown by season (Figures 4-180 to 4-184).

In general, the monthly average sound pressure spectrum levels within the contract area primarily range from 45 to 57 dB re 1 μPa^2/Hz. The curve exhibits a unimodal shape, with

271

higher values in the middle frequencies and lower values towards both ends. Specifically, there is notable energy concentration between 150 Hz and 3 kHz, while energy diminishes below 150 Hz and above 3 kHz. Energy fluctuations below 150 Hz are minimal; however, sudden increases are observed within the 20 to 30 Hz band during certain months, attributed to noise emissions from large cetaceans such as fin whales. Energy above 3 kHz declines rapidly, yet nearly all months exhibit two obvious peaks and several smaller ones within the 3.5k to 10 kHz band, research indicating these as noises generated by medium-sized to small cetaceans. The spectrum levels between 150 Hz and 3 kHz manifest a complex pattern with multiple minor peaks, attributed to various sources such as weather conditions, marine fauna, and anthropogenic activities including vessel traffic and airgun surveys.

For the inter-month variations, there is relatively minimal disparity in energy levels below 150 Hz and above 3 kHz across the months, particularly in the higher frequency range (approaching 12 kHz), where energy levels are within 2 dB of each other. However, within the 150 Hz to 3 kHz band, there exists a maximum difference of ~7 dB in monthly average sound pressure spectrum levels. During spring (March to May), there is higher energy in the low-frequency spectrum levels in 20 and 30 Hz band compared to other months, attributed to increased activity of large cetaceans. Summer months show considerable variation in monthly average sound pressure spectrum levels, with July registering higher levels and August lower levels. Throughout autumn (September to November), the monthly average sound pressure spectrum levels exhibit minimal variation and remain consistent. In winter (December to February), there is a slight fluctuation in the monthly average sound pressure spectrum levels. Overall, from October 2021 to October 2022, the highest monthly average sound pressure spectrum levels were recorded in July, while the lowest in November, indicating relatively higher ambient noise in the contract area during July and lower noise levels in November during the deployment.
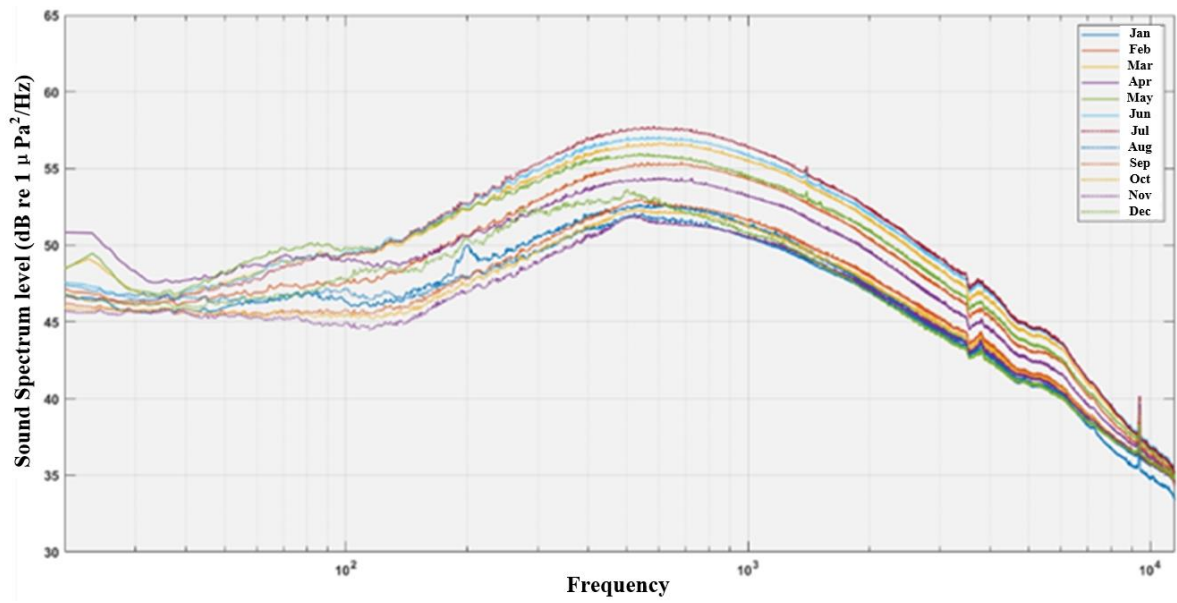
Figure 4-180 Monthly averaged ambient noise sound pressure spectrum levels during the deployment
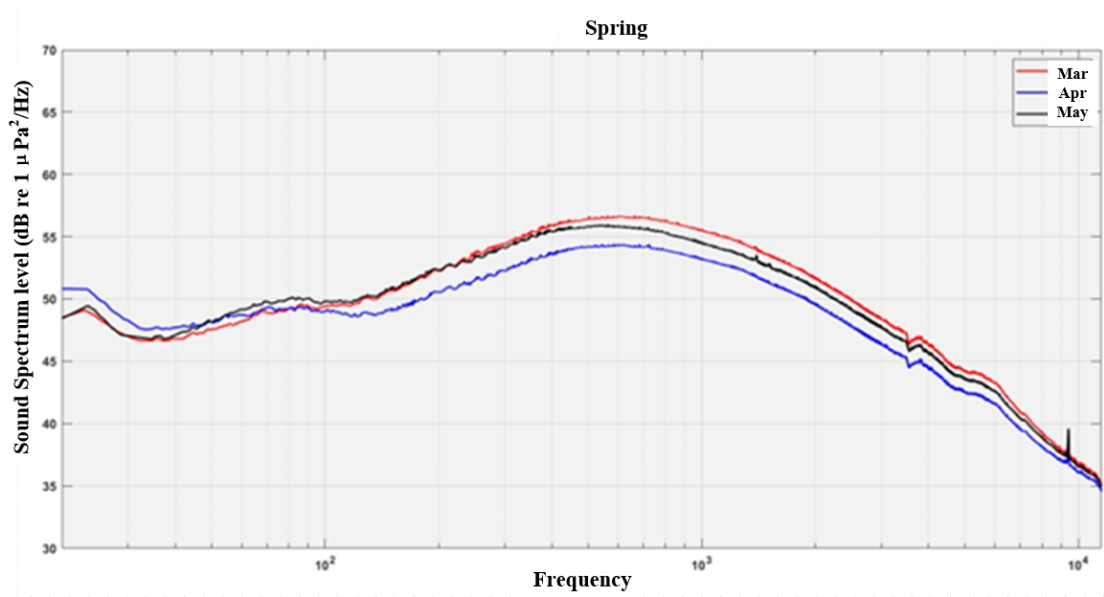
Figure 4-181 Monthly averaged ambient noise sound pressure spectrum levels in spring 2021
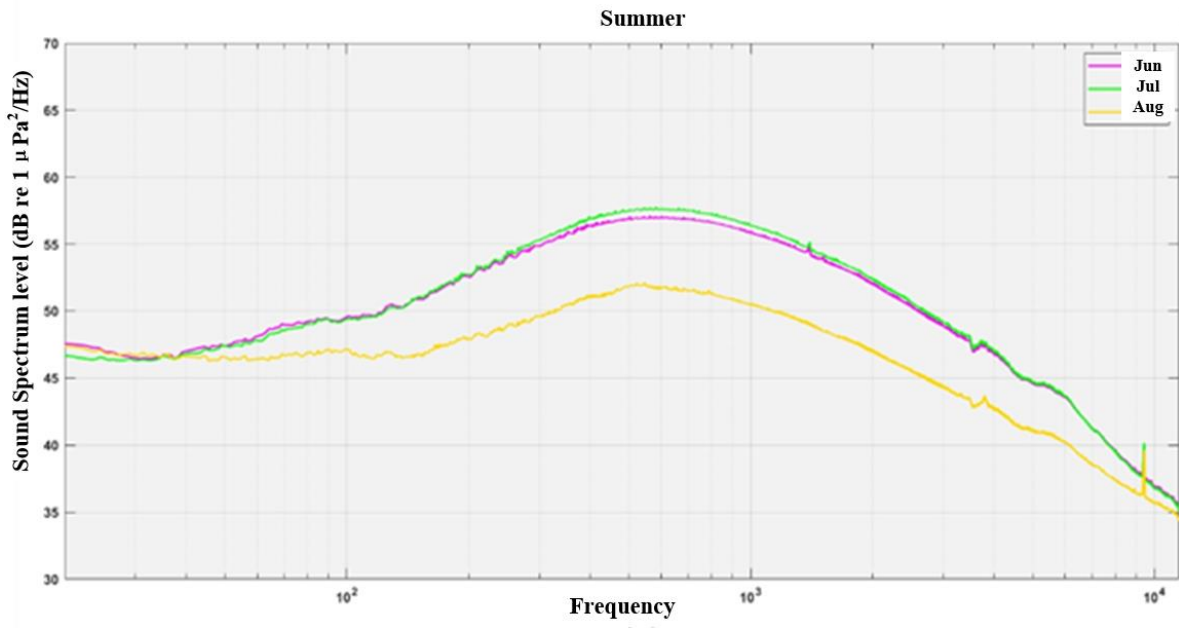
Figure 4-182 Monthly averaged ambient noise sound pressure spectrum levels in summer 2021
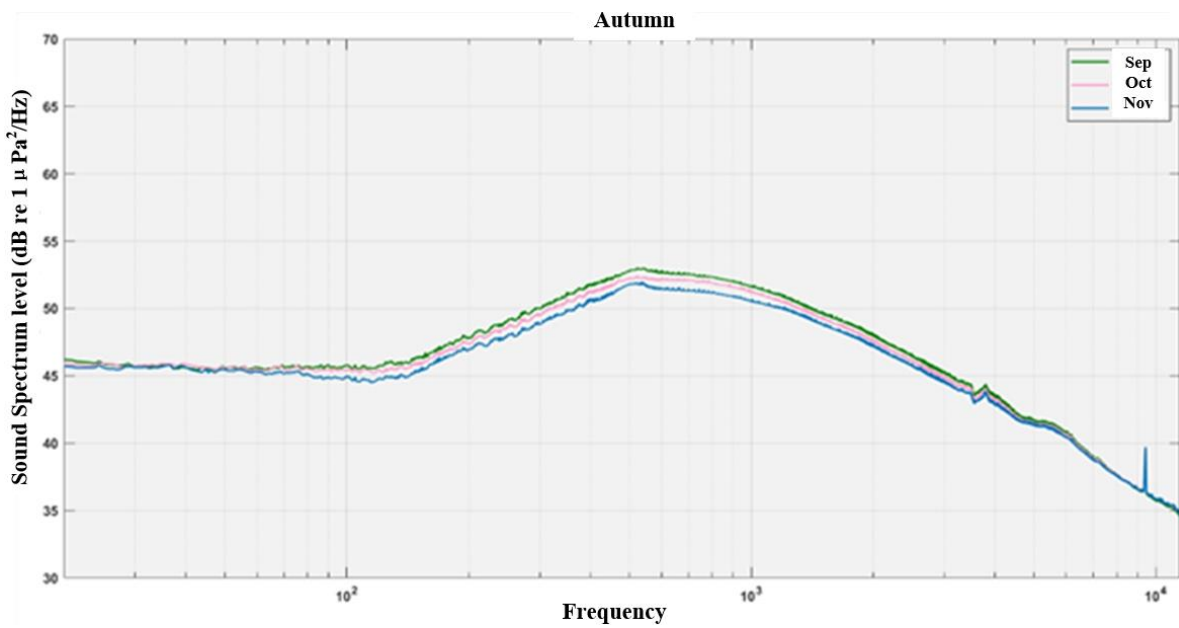
Figure 4-183 Monthly averaged ambient noise sound pressure spectrum levels in autumn 2021
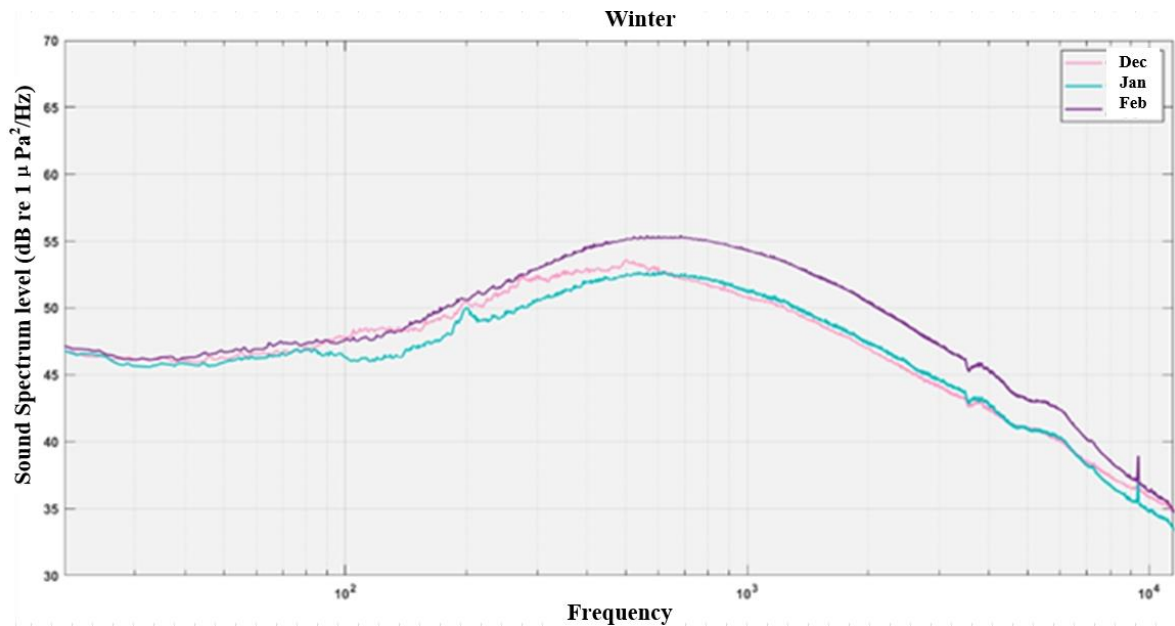
Figure 4-184 Monthly averaged ambient noise sound pressure spectrum levels in winter 2021

4.3.6.2 Noise Monitoring in 2022

In 2022, an autonomous deep-sea acoustic recorder system was deployed on a subsurface buoy for ambient noise monitoring. The buoy was placed near CTA (153.6929 °E, 19.3219 °N), with a water depth of 5094 meters at the station and the receiving depth is approximately 5060m (~30 meters above the seafloor). The acoustic recorder used was the USR-6000 manufactured by the Institute of Acoustics, Chinese Academy of Sciences, with a maximum operating depth of 6000m. The device had a sensitivity of –170.3±1 dB re 1 V/μPa with a flat response in the 20 Hz to 5 kHz frequency band, an analog-to-digital (AD) resolution of 24 bits, and a gain greater than 100 dB, with the frequency band used in calculating SPLs from 20 Hz to 7.5 kHz. The sampling rate was set at 16 kHz. A duty cycle of 5 min each hour was set so the recorders could be deployed for one year at a time. The recording period was from November 23, 2022, to October 18, 2023, with 7885 recorded files and a duration of 330 days.

4.3.6.2.1 Ambient Noise Sound Pressure Levels in the Block M in 2022

The root mean square sound pressure level (rms SPL) of ambient noise in the surveyed area in a wide frequency band (20–7500 Hz) is shown in Figure 4-185. Interannually, the highest rms SPL approached 120 dB re 1μPa, but the overall SPL varied between 92 and 115

dB, with a difference of ~23 dB. Further analysis showed that the median SPL in the broadband was approximately 101.4 dB.
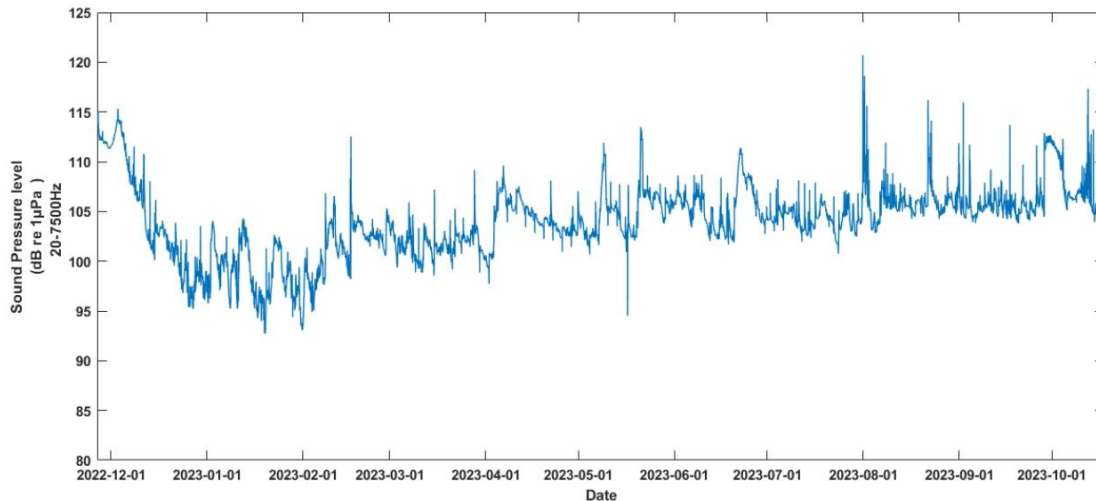
Figure 4-185 Ambient noise sound pressure level in 20-7500 Hz band

The ambient noise SPLs were divided into four frequency bands for analysis: 200−600 Hz, 1000−2000 Hz, 2500−4000 Hz, and 5000−7500 Hz, as depicted in Figures 4-186 to 4-189. Although there was an anthropogenic noise peak caused by the nearby survey operations from late November to mid-December 2022 (up to ~105 dB), the median SPLs for each frequency band throughout the entire survey period were 94.0 dB, 90.68 dB, 86.67 dB, and 83.33 dB, respectively. These values are lower than the global ambient noise levels in gentle weather conditions, which are approximately 94 dB re 1 μPa. The results indicate that although the surveyed area is not on a major shipping route and is less affected by human activities, resource exploration and deep-sea mining activities during the survey period elevated the noise SPL within the region by 6 to 10 dB, which could have negative effects on the biodiversity conservation in this environmentally sensitive area. Furthermore, it underscores the necessity of conducting noise monitoring for seabed mining within the contract area and emphasizes the importance of implementing green mining practices.
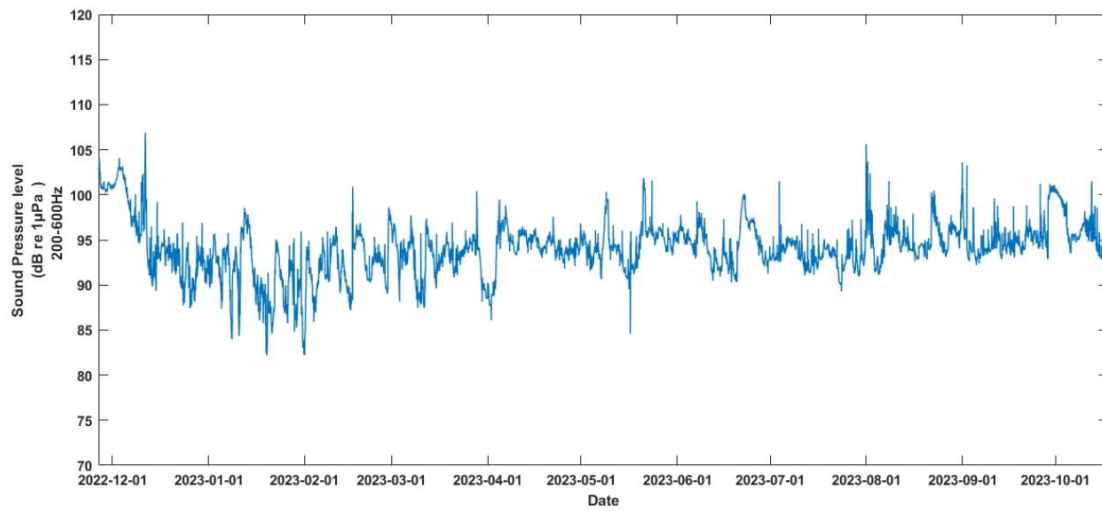
Figure 4-186 Sound pressure level in the 200–600 Hz band
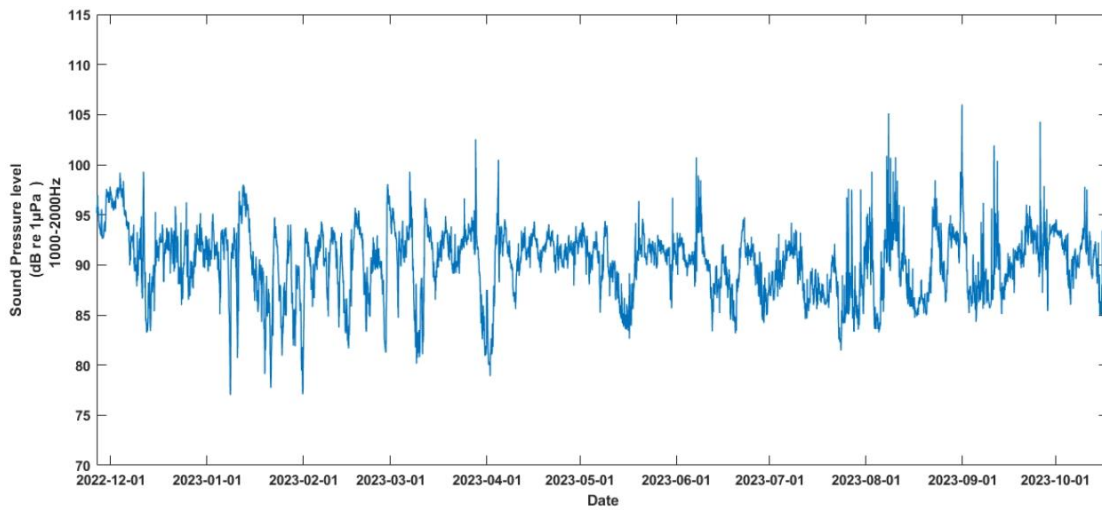
Figure 4-187 Sound pressure level in the 1000–2000 Hz band
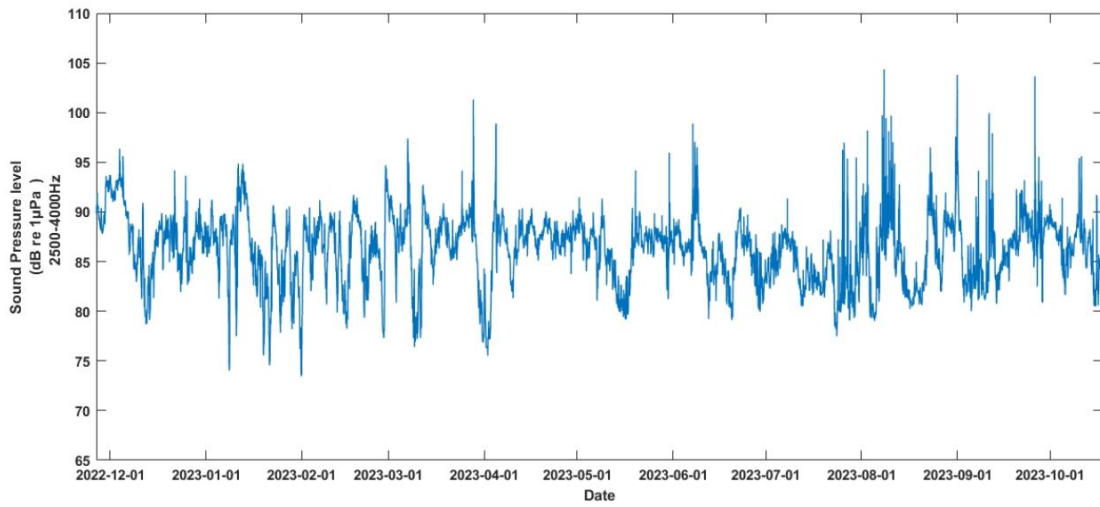
Figure 4-188 Sound pressure level in the 2500–4000 Hz band
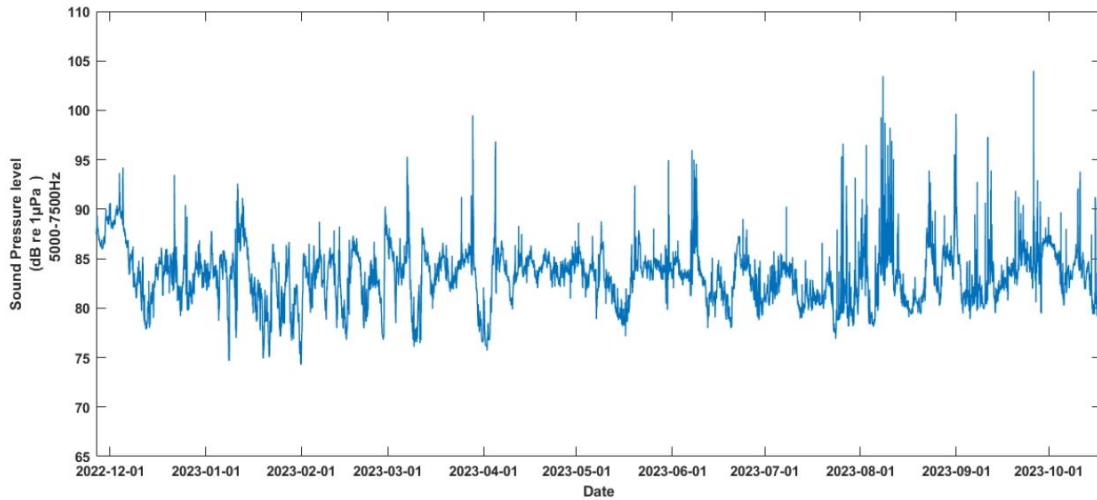
Figure 4-189 Sound pressure level in the 5000–7500 band

4.3.6.2.2 Noise Power Spectral Density in the Block M in 2022

The long-term power spectral density of the ambient noise in broadband 20 Hz to 7.5 kHz (Figure 4-190) shows that the noise power spectrum level in the surveyed area varies between 35 and 70 dB re $1\mu Pa^2$/Hz, with peaks reaching up to 130 dB re 1µPa²/Hz. Overall, these levels are slightly higher than those observed in the 2021–2022 period, possibly due to increased global maritime activity following the end of the COVID-19 pandemic. However, the distribution of noise energy in the current year remains similar to the previous year, with a predominant concentration in the 20 Hz to 2 kHz band, while energy levels above 5 kHz

are relatively weaker. Regarding temporal distribution, the noise exhibits some seasonal variations.
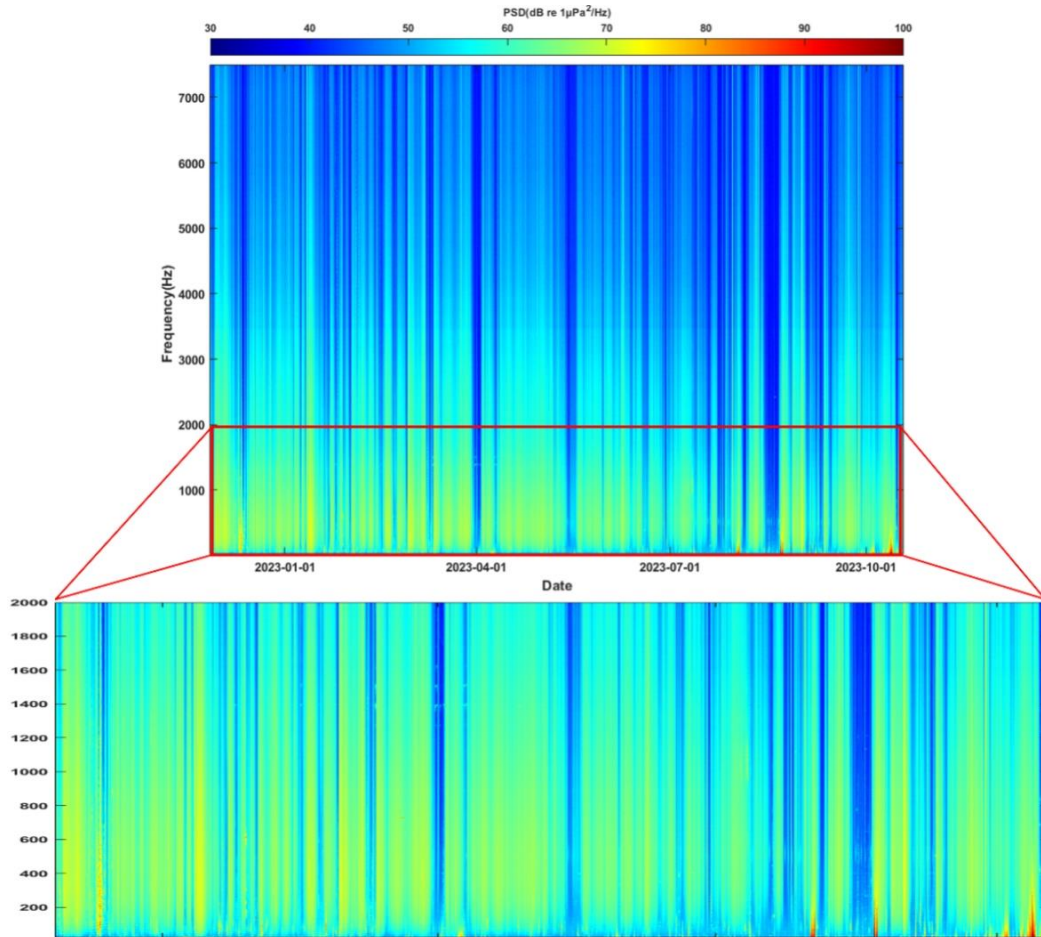
Figure 4-190 Long-term spectrogram of ambient noise

After averaging the noise power spectral levels for each month, the inter-monthly noise power spectral levels were obtained, and corresponding sound pressure spectrum curves were plotted based on seasons (Figures 4-191 to 4-197).

The passive acoustic data collected in 2022 BPC cruise are from November 22, 2022 to October 23, 2023, but the curves of monthly values in Figure 4-191 are from December 2022 to October 2023. The curve of November 2022 was omitted because only 8-day data were acquired in the month and the soundscape is dominated by ship noise and navigation noises which do not reflect the ambient noises. In general, the monthly average sound pressure spectrum levels in the contract area primarily range from 45 to 66 dB re 1μPa²/Hz (Figure 4-191). The curve exhibits an unimodal shape, with higher values in the middle frequencies

and lower values towards both ends. Specifically, there is notable energy concentration in the 100 Hz and 1500 Hz band, with levels exceeding 55 dB, while energy diminishes below 150 Hz and above 1500 Hz. The power spectral levels below 100 Hz demonstrates some variability, with most months showing increasing energy levels with frequency, though certain periods exhibit a decreasing trend with frequency, particularly in the 20 to 35 Hz band. Throughout the entire survey period, power spectral levels below 150 Hz show multiple obvious peaks, notably at 26 Hz, 35 Hz, and 55 Hz, primarily attributed to vocalizations from large cetaceans such as fin whales and blue whales. Energy above 2 kHz generally shows a monotonic decrease with frequency, with several smaller peaks observed, believed to be generated by medium-sized to small cetaceans. The sound pressure spectrum level in 150 Hz and 2 kHz band is complex, with peak energy occurring within the 300 to 600 Hz range, along with multiple smaller peaks associated with natural factors such as weather, earthquakes, marine mammals, fish, as well as anthropogenic sources including vessel traffic (Figure 4-196), airgun survey operations (Figure 4-197), and marine engineering surveys.

During winter (December to February), December exhibits the highest average sound pressure spectrum level of the year, with notable differences compared to January and February, which show nearly identical spectrum levels. In the 100–1000 Hz band, the level in December is 2–3 dB higher than in January and February. However, in the 20–30 Hz band, the spectrum levels in January and February unexpectedly reverse, being 5–6 dB higher than in December. In spring (March to May), the overall shape of the spectrum curves remains consistent across months but shows a gradual decrease in energy of 1–2 dB per month. During summer (June to August), there are relatively obvious variations in monthly average sound pressure spectrum levels, with June recording higher levels compared to July, exhibiting a difference of 5–6 dB. Additionally, in June and July, there are two peaks observed in the low-frequency band (20–40 Hz), indicating increased activity of large cetaceans during these months. In autumn (September to October), the low-frequency noise in October is notably higher than in other months (up to 15 dB), likely due to survey operations. The large deviation in October line at lower frequencies is mainly caused by the anthropogenic noises in polymetallic nodules resources exploration, since the 2023 BPC Cruise was carried out during the period. The low-frequency noises were primarily generated by ship propellers and

the Dynamic Positioning System. However, there are no obvious changes in the spectrum levels above 500 Hz between September and October.

Above all, from November 2022 to October 2023, the highest monthly average sound pressure spectrum level was in December, and the lowest was in July, indicating that the ambient noise in the contract area was greater in December and smaller in July during the deployment.

Overall, from December 2022 to October 2023, December recorded the highest monthly average sound pressure spectrum level, while July recorded the lowest. This indicates that ambient noise levels were higher in December and lower in July in the contract area during the deployment.
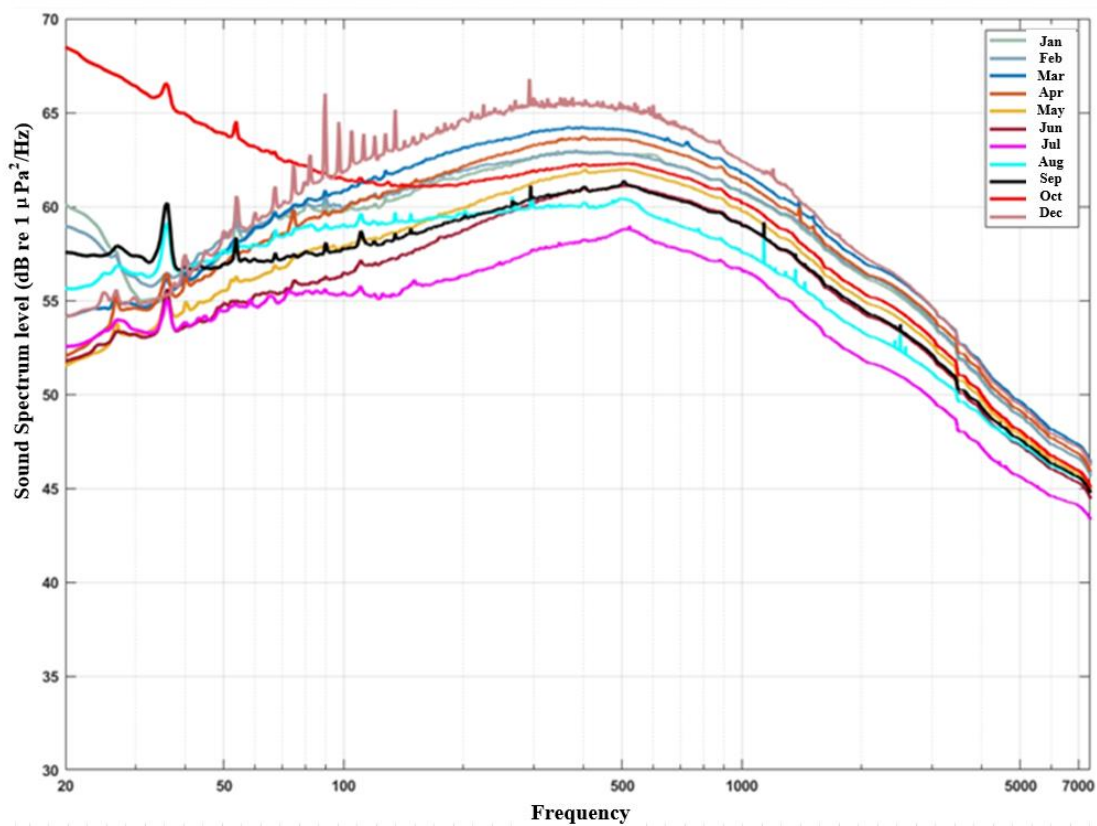
Figure 4-191 Monthly averaged ambient noise sound pressure spectrum level from November 2022 to October 2023
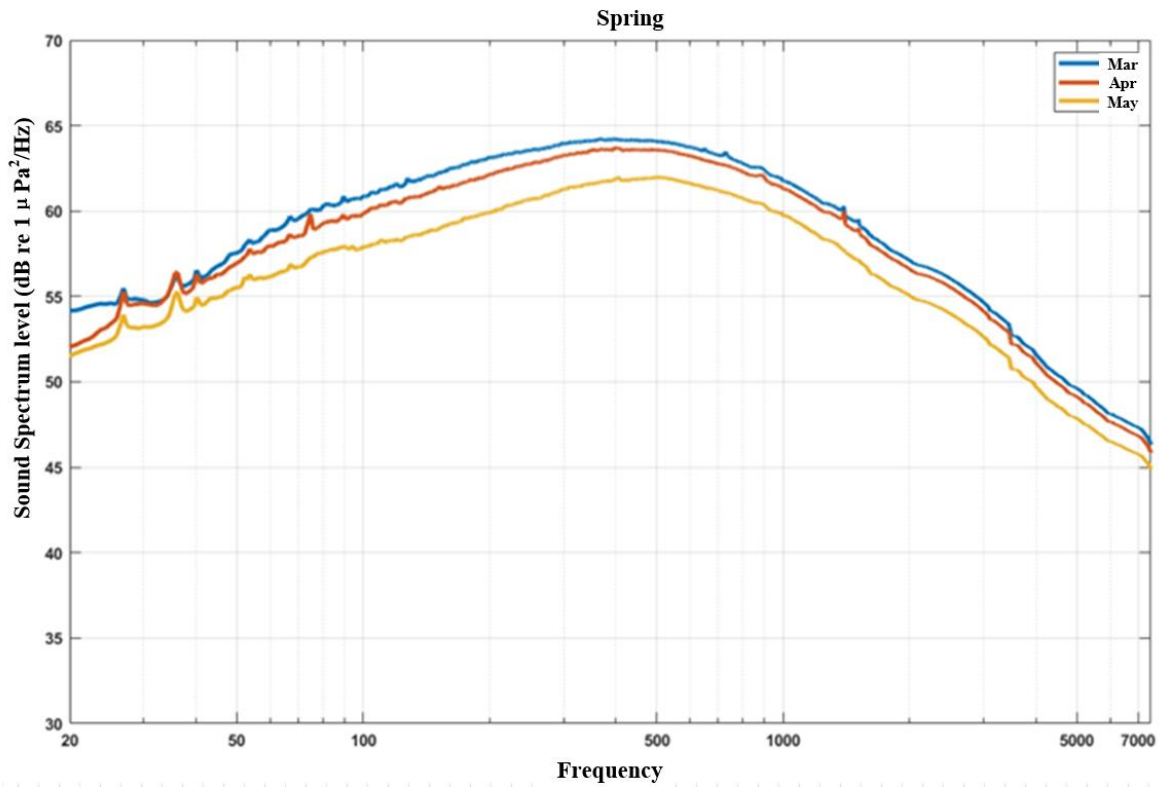
Figure 4-192 Monthly averaged ambient noise sound pressure spectrum level in spring 2022
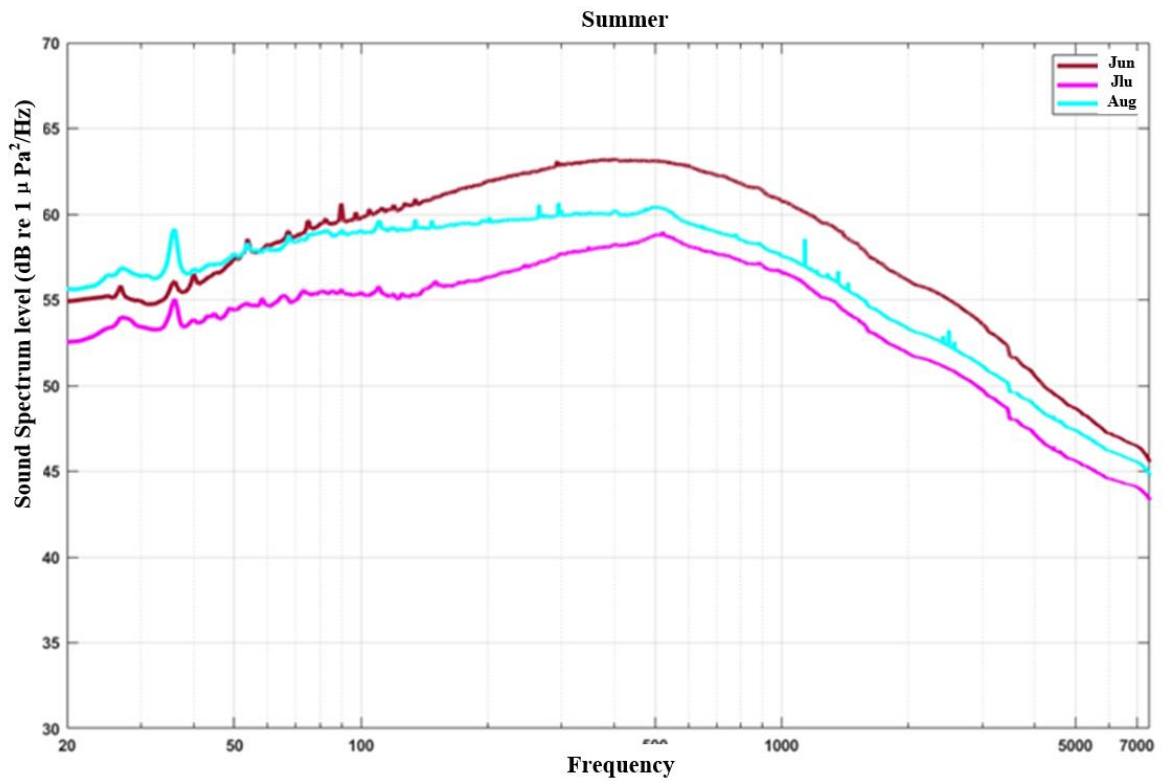
Figure 4-193 Monthly averaged ambient noise sound pressure spectrum level in summer 2022
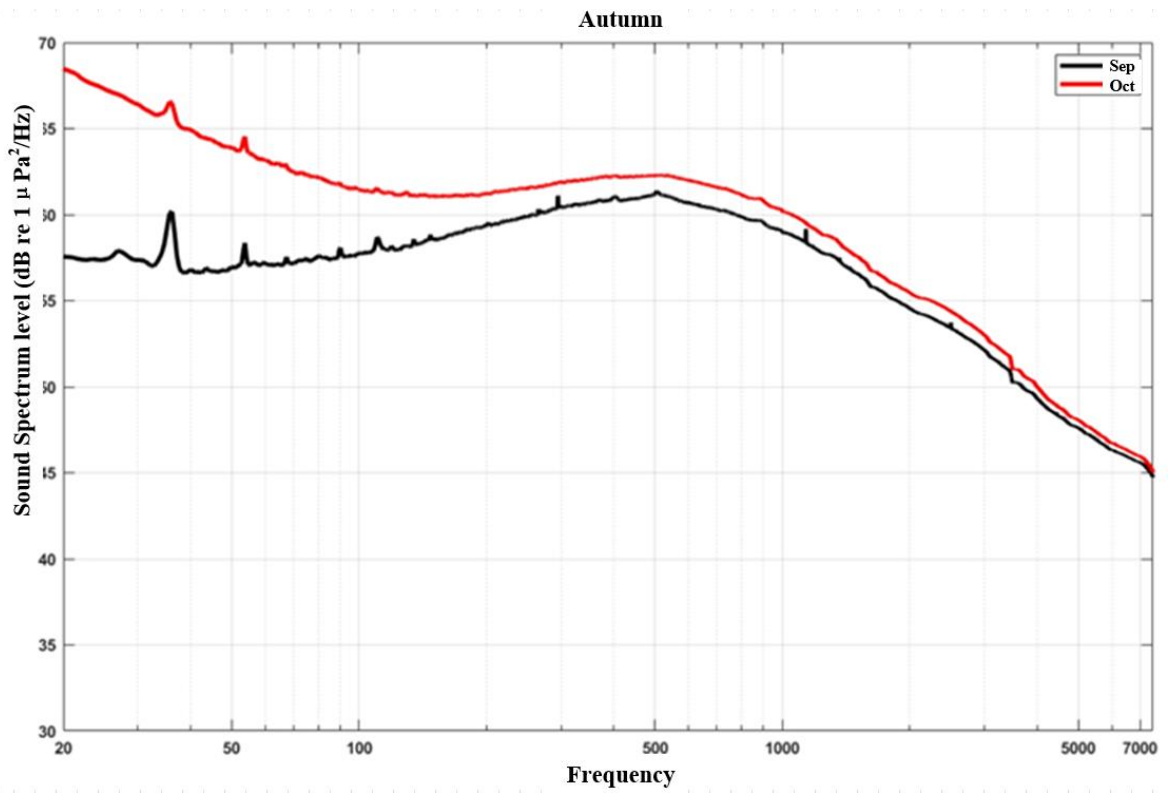
Figure 4-194 Monthly averaged ambient noise sound pressure spectrum level in autumn 2022
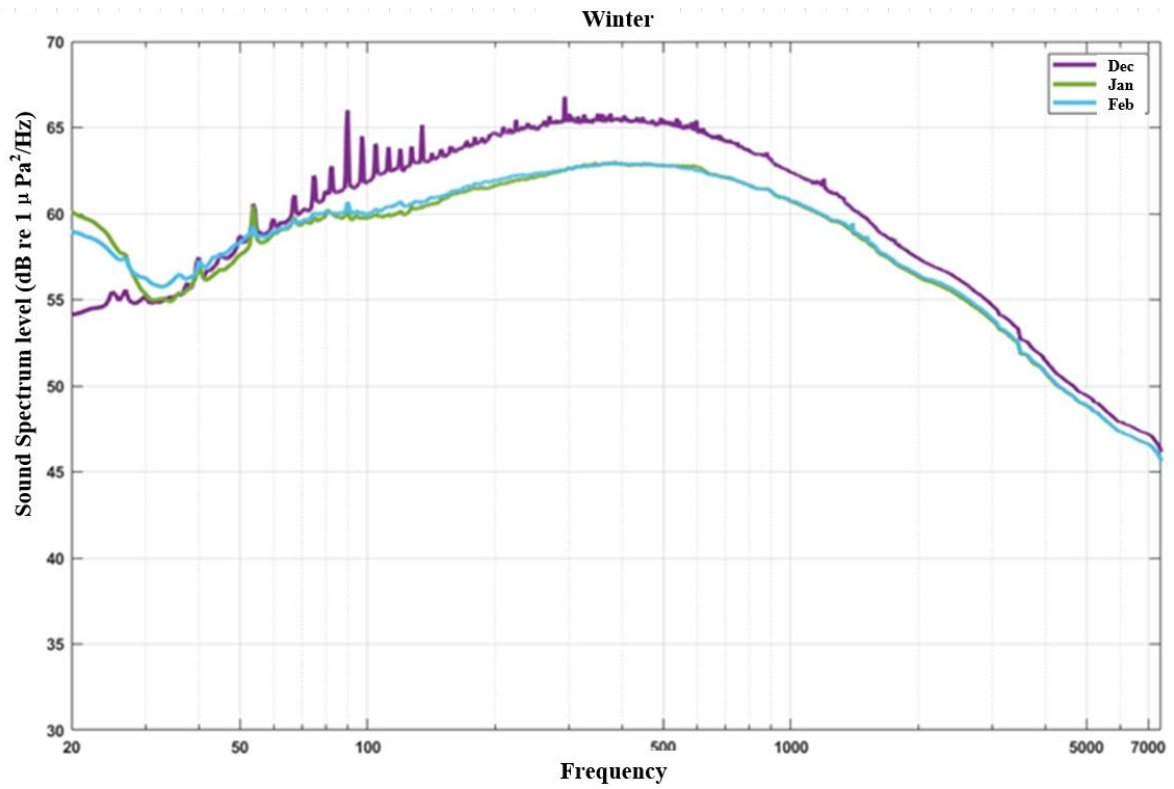
Figure 4-195 Monthly averaged ambient noise sound pressure spectrum level in winter 2022
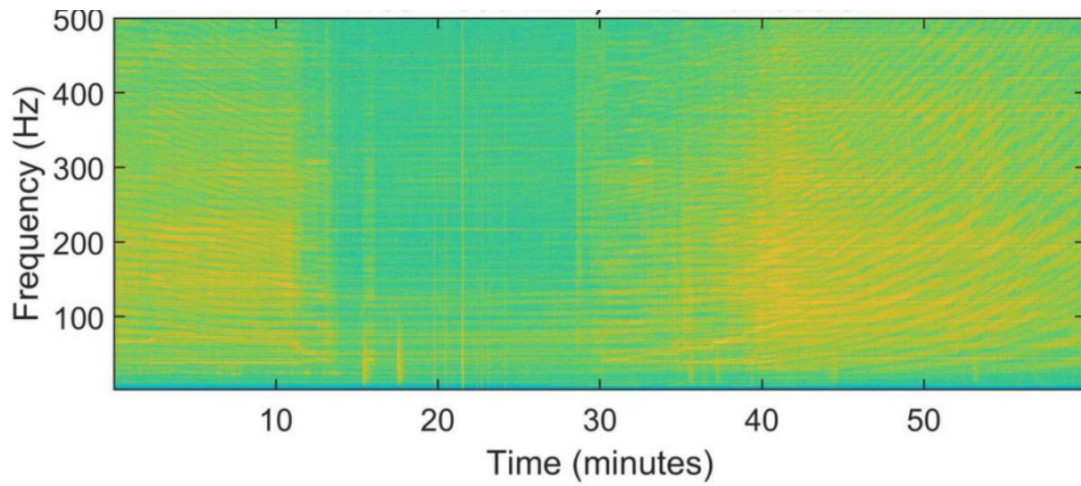
Figure 4-196 Ship Noise
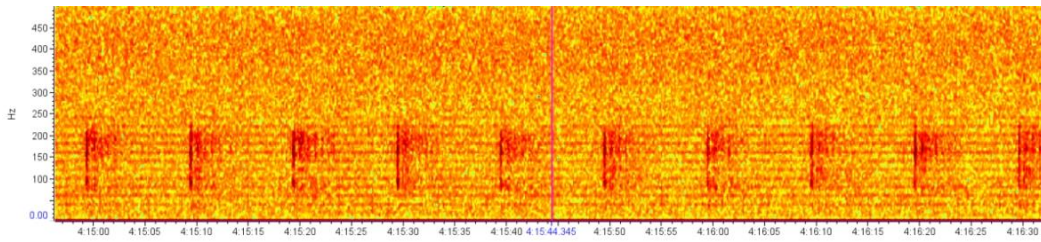
Figure 4-197 Air Gun Noise

4.3.7 Natural Disasters

Potential natural disasters that may affect activities within the area include earthquakes, volcanic eruptions, tsunamis, and tropical storms.

4.3.7.1 Earthquakes

The western side of the circum-Pacific seismic zone is over 600 km away from CTA. Figure 4-198 shows the distribution of earthquakes above magnitude 4 that have historically occurred at the junction of the Pacific Plate and the Philippine Sea. The closest earthquake activity, with a magnitude of 5.5, occurred in March 2023 on the east side of Saipan.
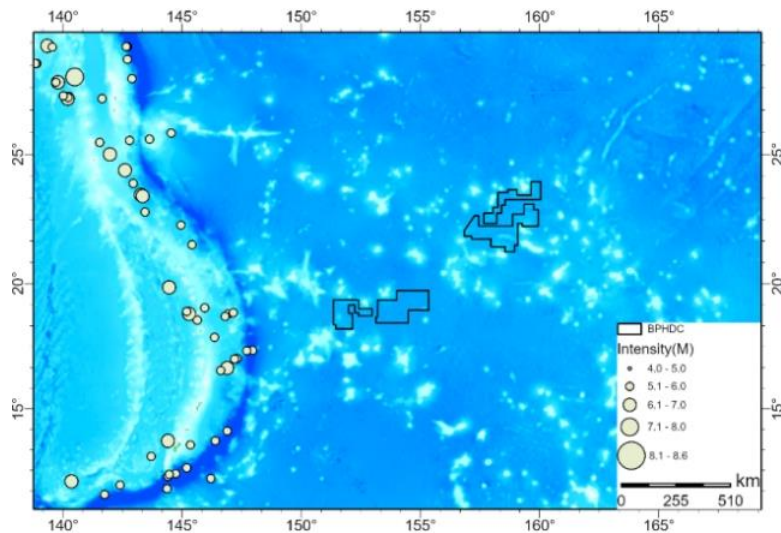
Figure 4-198 Distribution of earthquakes above magnitude 4 in the western circum−Pacific seismic zone since 2012（Data source： China Earthquake Networks Center）

4.3.7.2 Volcanic Eruptions

Figure 4-199 presents information on the distribution of volcanic eruptions in the Northwest Pacific since 1960. The closest active volcano to the BPC Contract Area, Pagan, is over 600 km away. This volcano had its largest eruption in 1981, with the most recent eruption occurring in September 2021. Its emissions of gas and ash can reach up to 5 kilometers in height and extend 600 kilometers to the west.
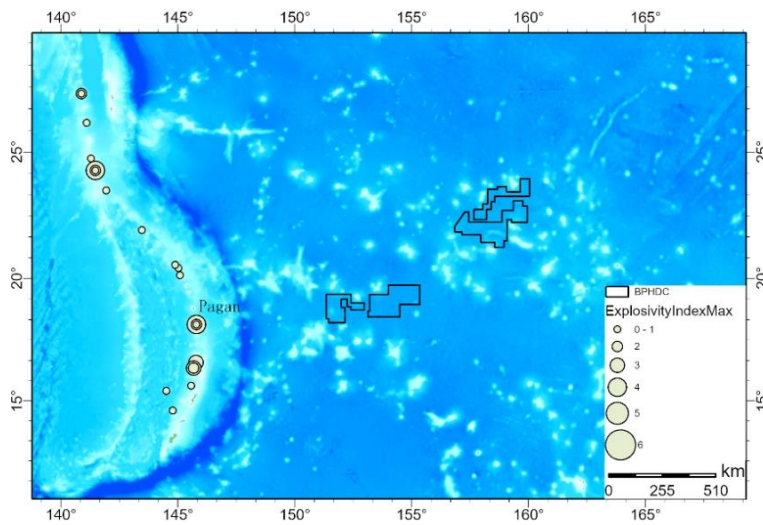
Figure 4-199 Distribution of volcanic eruptions in the northwest Pacific since 1960 (Data source: Smithsonian Institution)

4.3.7.3 Tsunamis

Tsunamis that could potentially affect the area are mainly triggered by surrounding earthquakes or volcanic eruptions. Figure 4-200 shows the location of tsunami observation points in the area. The largest tsunami recorded at Wake Island since records began was no more than 0.5 meters, caused by the 1960 Great Chilean Earthquake. The tsunami triggered by a magnitude 6.3 earthquake in the eastern sea area of Honshu, Japan, in 2011 reached a height of 1.2 meters at Saipan and 0.5 meters at Minamitorishima Island.
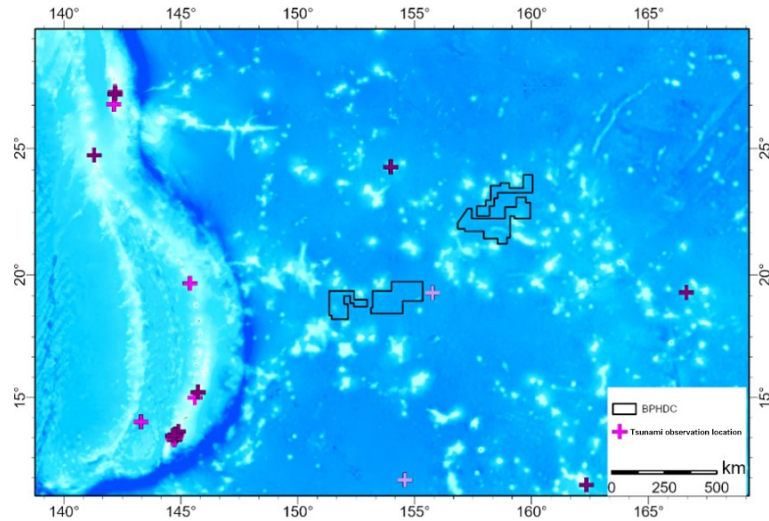
Figure 4-200 Distribution of west Pacific tsunami observation points (Data source: NGDC Natural Hazards)

4.3.7.4 Tropical Cyclones

The Northwest Pacific has more tropical cyclones forming above its waters than any other oceanic region in the world, with an average of about 35 per year. Approximately 80% of these tropical cyclones develop into typhoons. On average, about 30 tropical cyclones each year reach at least the intensity of a tropical storm (Qian et al., 2006). From Figure 4-201, it can be seen that the BPC Contract Area is on the outer edge of the distribution of historical tropical storm paths.
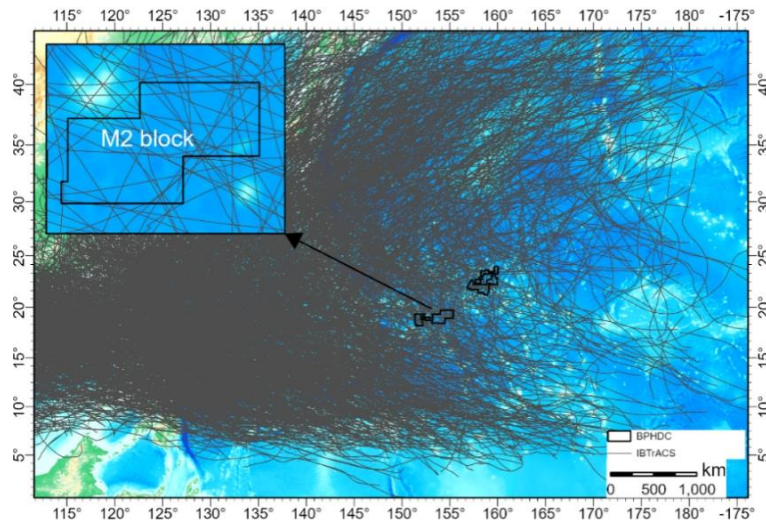
Figure 4-201 Best track map of tropical storms in the northwest Pacific since 1950 (Data source: IBTrACS)

4.3.8 Shipping Routes

The main shipping routes in the Pacific include (1) Far East–West Coast of North America; (2) Far East–West Coast of South America; (3) Far East–Southeast Asia; (4) Far East–Australia, New Zealand; (5) Australia, New Zealand–East and West Coasts of North America.

Ship position monitoring data from the World Maritime Trade Monitoring System from 2015 to 2020 shows that the Block M is not on the aforementioned main shipping routes (Figure 4-202).
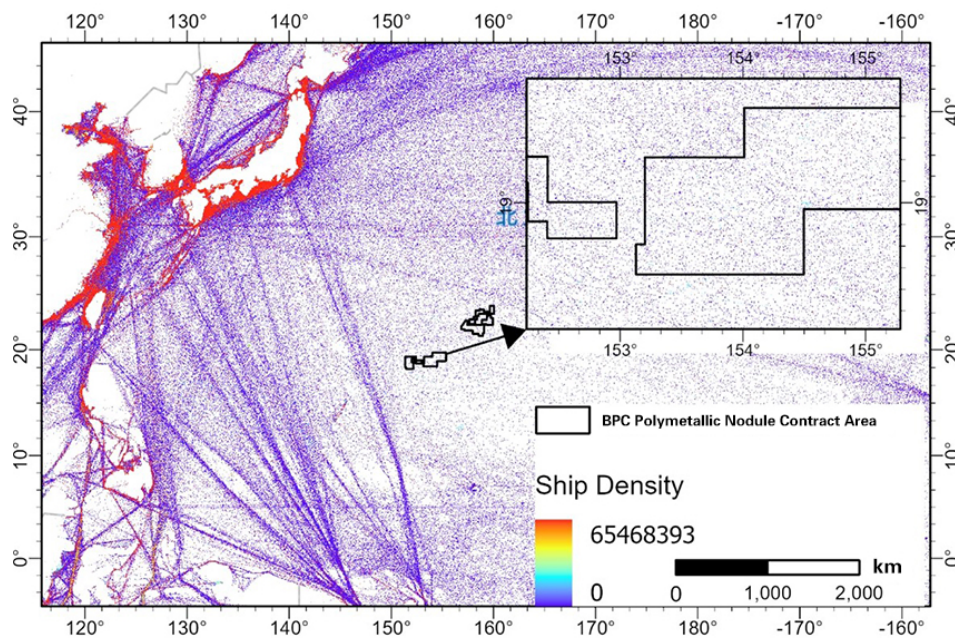
Figure 4-202 West Pacific ship traffic density map

(Data source: Cerdeiro et al., 2020)

5 BIOLOGICAL COMMUNITY

5.1 Regional Biological Community Characterization

The BPC's polymetallic nodule contract area is located in the subtropical oligotrophic northwestern Pacific Ocean. The pelagic biological community in this area is characterized by the following features: the biomass of both phytoplankton and zooplankton is very low, and picoplankton constitute the dominant autotrophs. Due to the spatial differences of regional physical oceanographic characteristics (described in Section 4.2.2), the biological community also have the following spatial differences: in the North Pacific subtropical gyre (NPSG), there are obvious seasonal variations in the depth of the mixed layer and the intensity of stratification in the upper ocean, which is influenced by seasonal change of surface water temperature. Therefore, there is a certain degree of phytoplankton bloom in spring, and a low level of phytoplankton productivity for the rest of the year (Figure 5-1). While in the Western Pacific Warm Pool region in the south, due to hardly vary of upper water mixing, it remains in an oligotrophic state throughout the year.
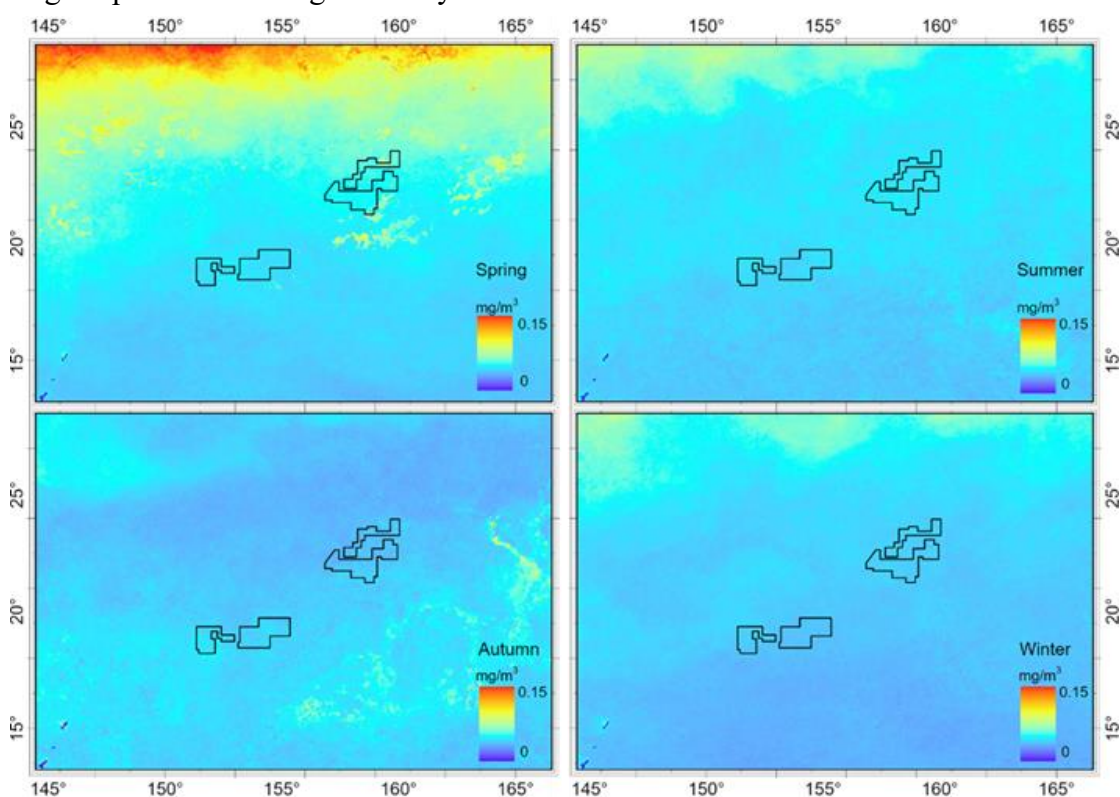
Figure 5-1 Surface chlorophyll *a* concentration of four seasons in the Northwest Pacific (Data source: MODIS)

This region has a long geological history and weak tectonic activity. The complex and diverse seabed topography have formed a huge depth gradient of ecological niches, and these environments have nurtured ancient benthic communities. The benthic ecosystem in this region is mainly characterized by the following features: Firstly, the benthic communities form a remarkable zonal distribution pattern along the huge depth gradient from the summit to the piedmont of seamount and to the deep-sea basins; Secondly, constrained by the low primary productivity of the upper ocean, the benthos generally show low biomass (Figure 5-2) and low abundance characteristics (Table 5-1); Thirdly, seabed topography and current has an obvious impact on the distribution of benthic community. Due to the influence of bottom current and a long evolutionary history, the spatial connectivity of benthic communities may differ from other deep-sea ecosystems, but lack of study. According to Watling et al. (2013), the biological communities in this region belong to the Central North Pacific biogeographical zone (Figure 5-3).
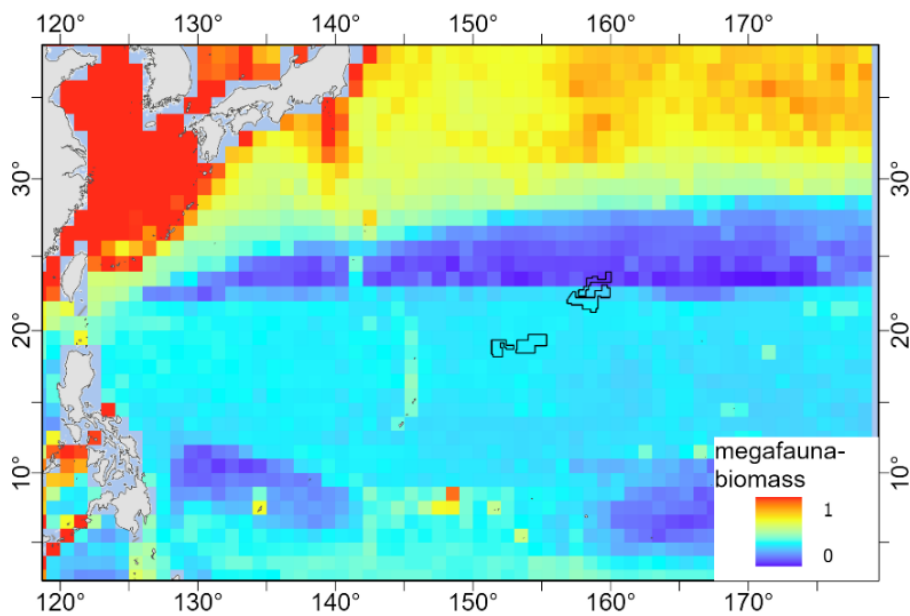
Figure 5-2 Megafauna biomass distribution pattern in the Northwest Pacific

(Data source：Wei, 2010, unit: log mg C m^{-2})

Table 5-1 Comparison of metazoan meiofauna abundance in the polymetallic nodule area in the

North Pacific Ocean

Area		Location	Water Depth (m)	Sampling Time	Abundance (ind./10 cm^2)	Data Source
IOM reference zone in contract area（control sites）		Center coordinates: 11.0667°N, 119.6667°W	4380–4430	1995.07	201.6±124.52	Radzie jewska, 2002
GSR contract area	B6S02	13.85°N, 123.25°W	4524	2015.09	151.1±54.2	Pape et al., 2017
	B4S03	14.11°N, 125.87°W	4490	2015.09	106.6±29.3	
	B4N01	14.796°N, 125.45°W	4504	2015.10	88.1±55.0	
COMRA contract area	East Area	8.3251°–8.3916°N 145.3514°–145.3968°W	5236–5329	2005.07	104.4±20.48	Wang et al., 2013
	West Area	10.0266°–10.0690°N 154.0037°–154.0700°W	5074–5159	2005.07	40.26±25.84	
BPC's contract area in Block M	Impact reference zones	19.0961°–19.1548°N 153.6111°–153.6729°E	5550–5600	2022.08–2022.11	16.77±12.24	BPC survey data
				2023.08–2023.10	26.12±9.33	
	Preservation reference zones	18.8639°–18.7271°N 152.7806°–152.9693°E	5250–5650	2022.08–2022.11	38.64±18.04	
				2023.08–2023.10	26.10±2.59	
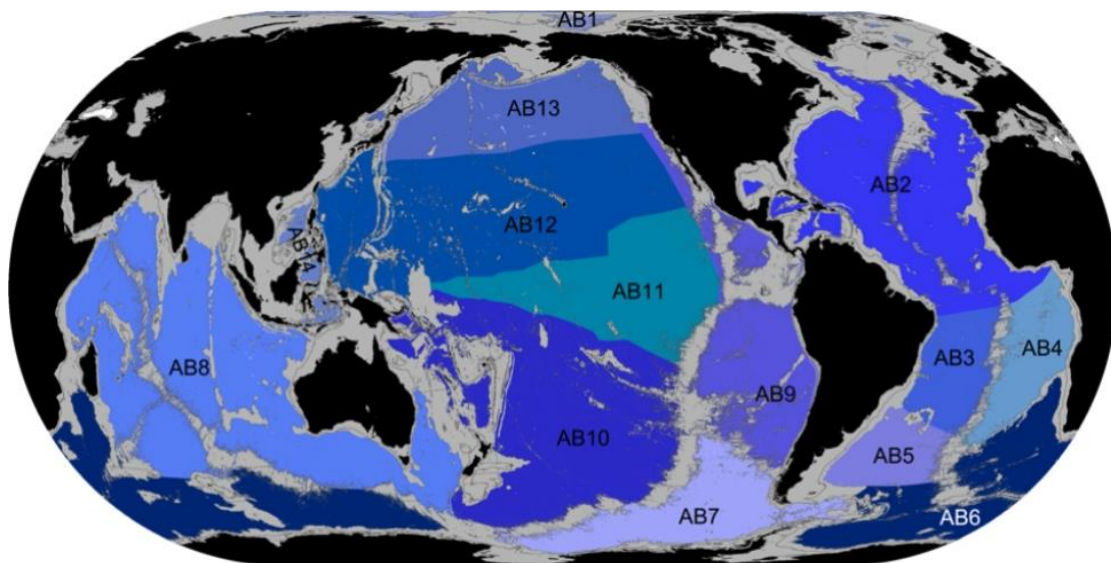
AB1: Arctic Basin AB6: Antarctica East AB11: Equatorial Pacific
AB2: North Atlantic AB7: Antarctica West AB12: North Central Pacific
AB3: Brazil Basin AB8: Indian AB13: North Pacific
AB4: Angola, Guinea, Sierra Leone Basins AB9: Chile, Peru, Guatemala Basins AB14: West Pacific Basins
AB5: Argentine Basin AB10: South Pacific

Figure 5-3 Global abyssal biogeographic zones (Source: Watling et al., 2013)

Biodiversity information from the OBIS database shows little biological surveys have been conducted at water depths greater than 3,000 m (Figure 5-4) in this region,

and there is no public information on benthic surveys within the BPC's contract area before.
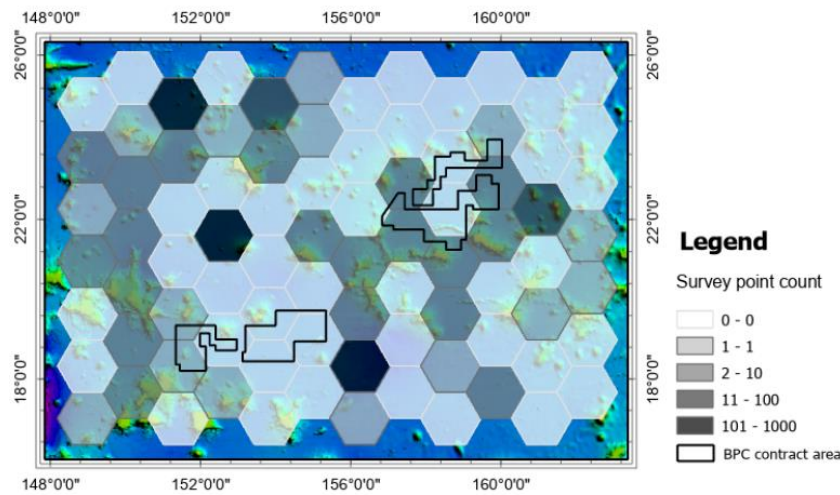
Figure 5-4 Biological survey density in the adjacent areas of the BPC contract area (Data Source: OBIS, only data from stations at water depths greater than 3,000 m were selected)

5.2 Biological Environment Characterization in Block M

5.2.1 Sea-surface Organisms

5.2.1.1 Chlorophyll *a* and Photosynthetic Pigment

5.2.1.1.1 Chlorophyll *a*

（1）Remote Sensing Observations

Based on the data of chlorophyll *a* concentration from five sensors, namely SeaWIFS, Terra-MODIS, Aqua-MODIS, MERIS, and VIIRS, the interannual variations of surface chlorophyll *a* in the Block M2 of the BPC contract area were analyzed from January 1998 to December 2018 (Figure 5-5), which showed that the annual mean chlorophyll *a* concentration at surface in this block was 0.04 mg/m^3 in the 21-year period, with a long-term trend of decreasing.

In addition, monthly surface chlorophyll *a* data from 2018 to 2020 (Figures 5-6) were selected. The orange box above represents the El Niño that occurred during this period, the purple box represents the La Niña, and the blue box below represents the year without El Niño/La Niña. Because El Niño was an important factor that affected the ecosystem in this region, the specific time when the phenomenon occurred was described in this section as background information. We can see that there were obvious

monthly variations in surface chlorophyll *a* concentration during a 12-month period from summer 2019 to summer 2020, when the Pacific ONI index was in a nearly neutral state (i.e., there was no El Niño or La Niña). Surface chlorophyll *a* concentration showed a typical unimodal distribution pattern, with higher value in winter and spring, and lower value in summer.
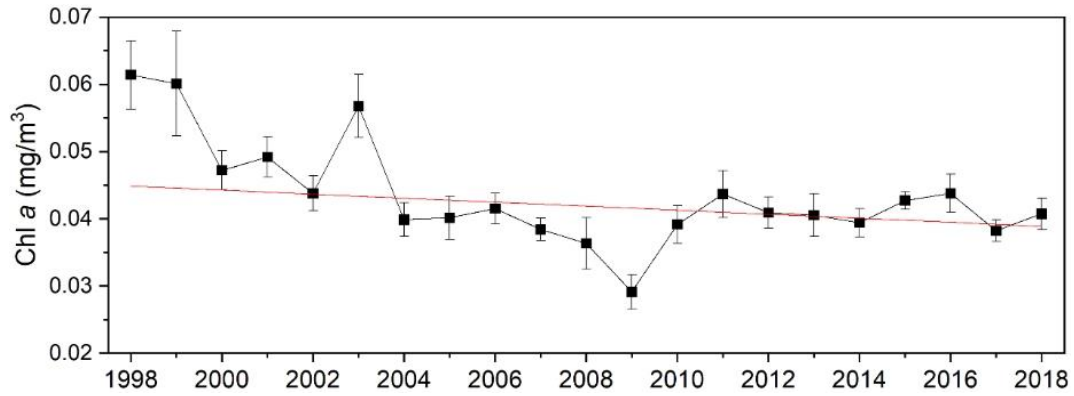
Figure 5-5 Interannual variation of surface chlorophyll *a* concentration in Block M2 of the BPC

contract area (1998−2018)
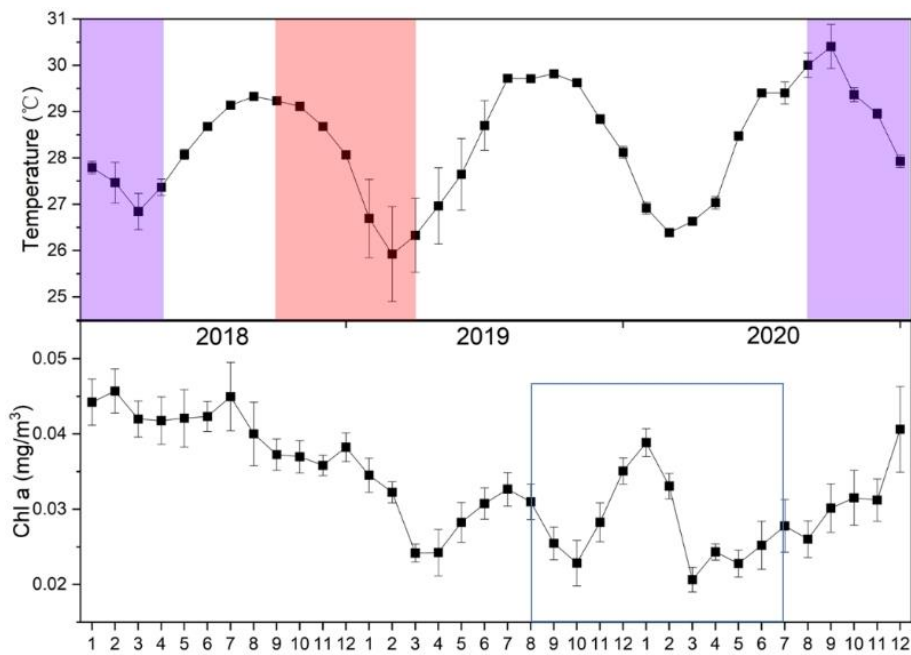
Figure 5-6 Monthly variation of surface chlorophyll *a* concentration in Block M2 of the BPC

contract area

（2）Horizontal Distribution

Chlorophyll *samples* were collected by CTD for eight layers of one station in each area. In autumn of 2021, the chlorophyll *a* content of seawater in Block M was 35.23 ± 4.91 mg/m^2, comparable to that in autumn of 2022 (35.45 ± 3.80 mg/m^2) and slightly

lower than that in autumn of 2023 (40.97 ± 9.06 mg/m^2) (Table 5-2). The horizontal distribution (Figures 5-7 – 5-12) showed that the chlorophyll *a* content in the water column and each layer in 2021 and 2022 decreased from west to east, and varied between high and low from north to south. The chlorophyll *a* content in the water column and each layer in 2023 first increased and then decreased from west to east in longitude, while no obvious distribution trend was found in latitude.
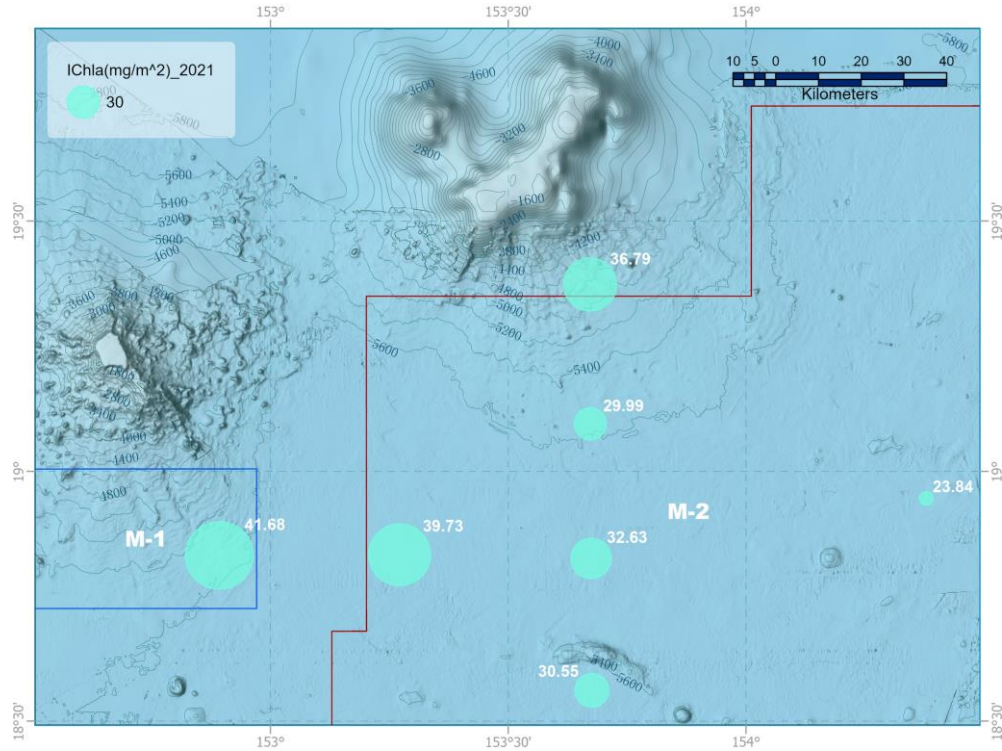
Figure 5-7 Distribution of chlorophyll *a* concentration in the water column of Block M in 2021 (mg/m^2)
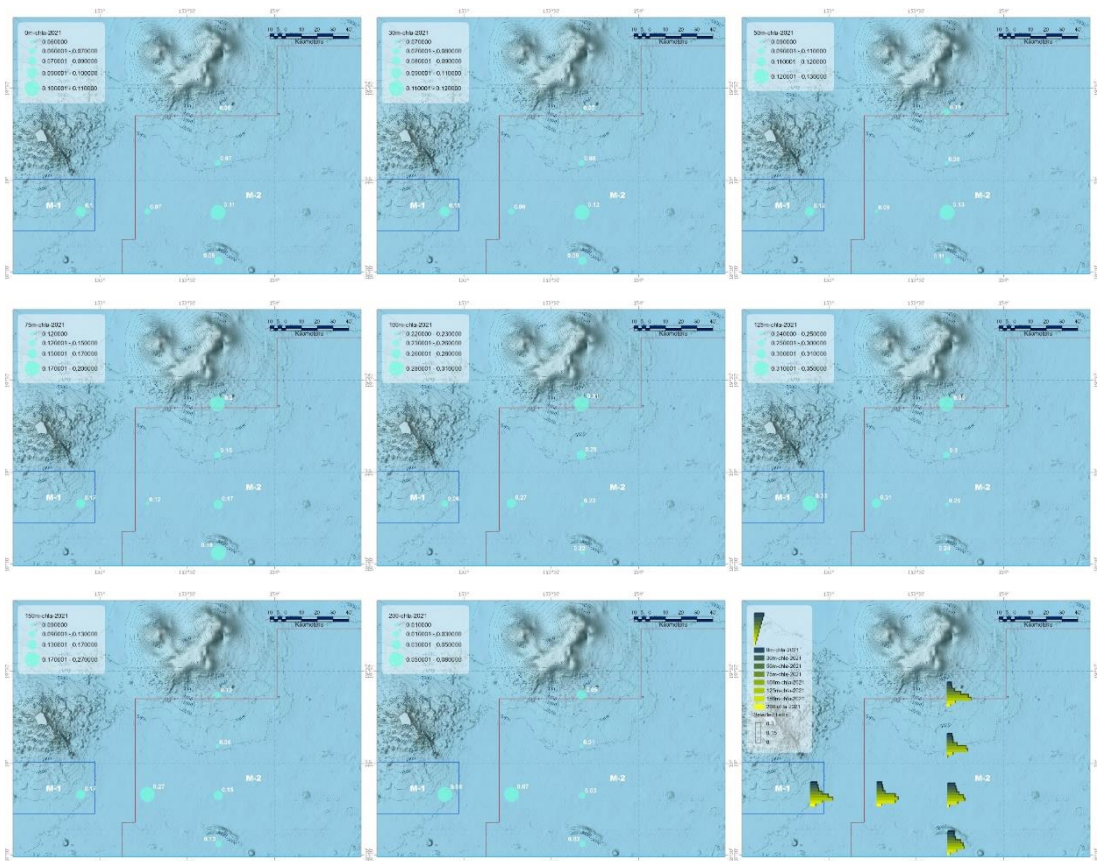
Figure 5-8 Distribution of chlorophyll *a* concentration in each layer of Block M in 2021 (mg/m^3)
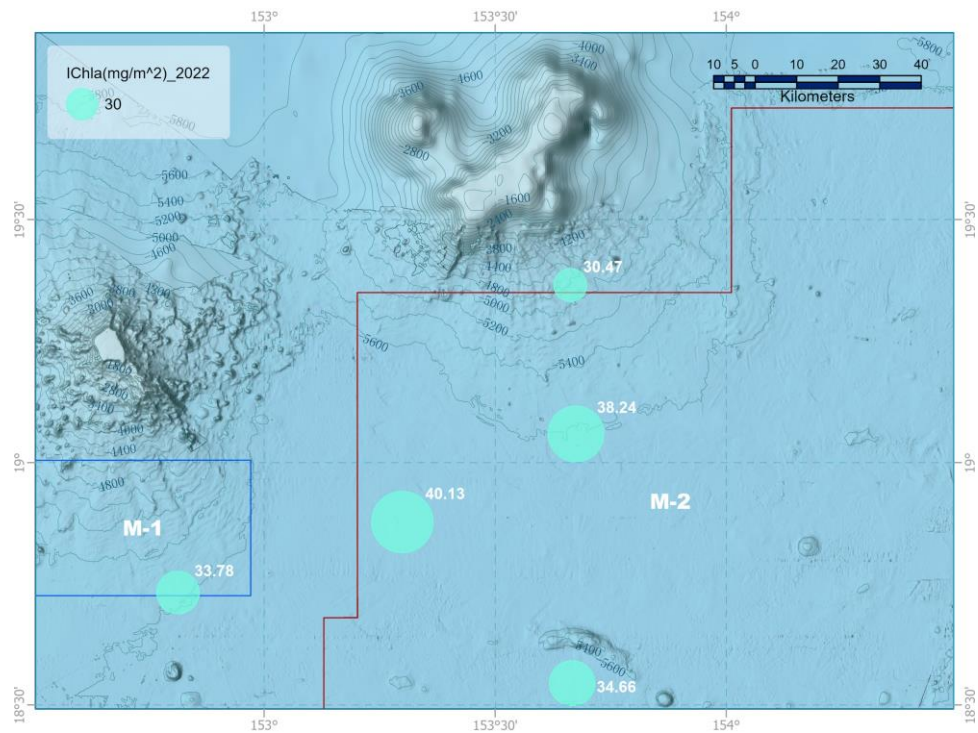
Figure 5-9 Distribution of chlorophyll *a* concentration in the water column of Block M in 2022 (mg/m^2)
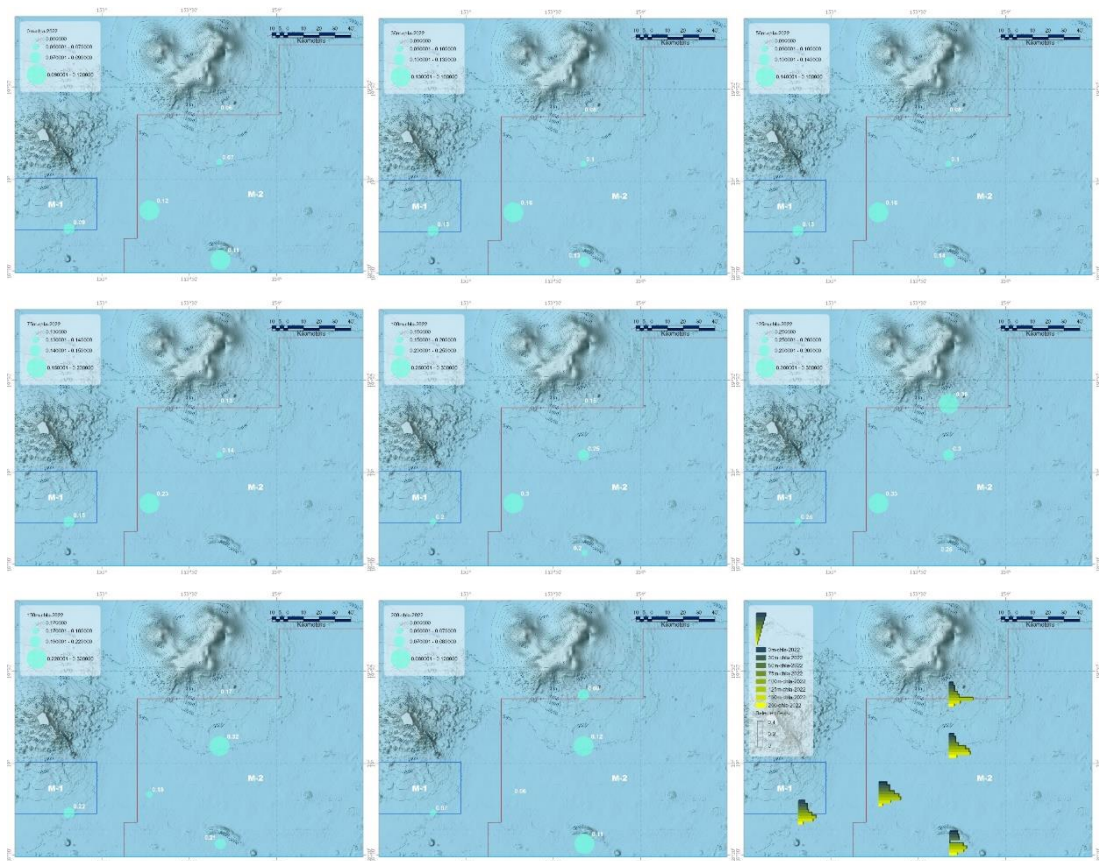
Figure 5-10 Distribution of chlorophyll *a* concentration in each layer of Block M in 2022 (mg/m^3)
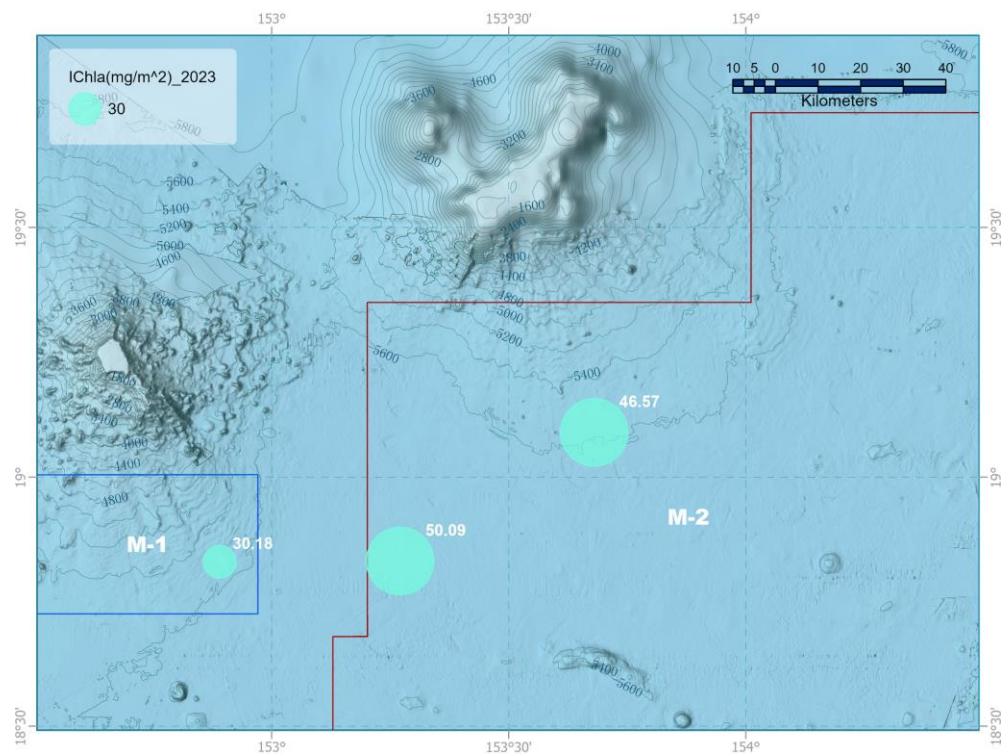
Figure 5-11 Distribution of chlorophyll *a* concentration in the water column of Block M in

Autumn 2023 (mg/m^2)
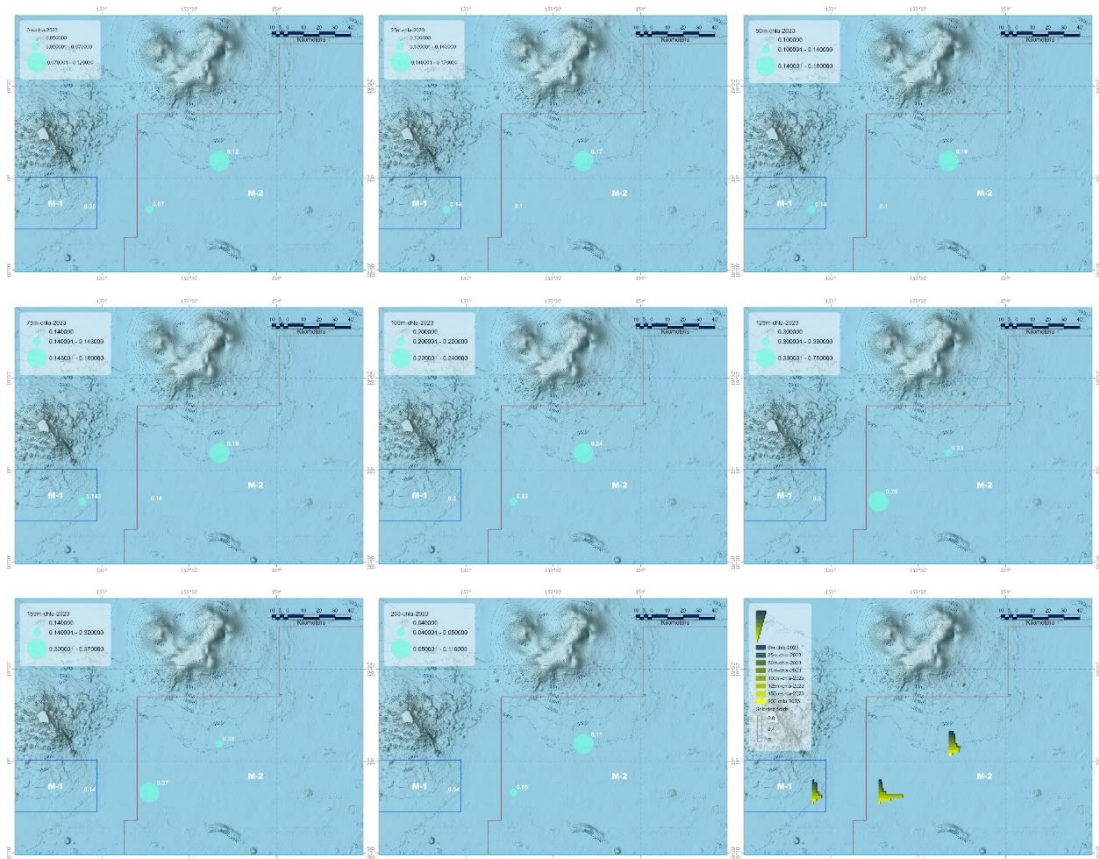
Figure 5-12 Distribution of chlorophyll *a* concentration in each layer of Block M in 2023 (mg/m³)

Table 5-2 Mean value and varying range of chlorophyll *a* content in Block M from 2021 to 2023

Year	Sampling Time	Mean Value (mg/m²)	Varying Range (mg/m²)
2021	2021.10.21–2021.10.29	35.23±4.91	29.99～41.68
2022	2022.11.20–2022.11.29	35.45±3.80	30.47～40.13
2023	2023.08.26–2023.09.13	40.97±9.06	30.18～50.09

（3）Vertical Distribution

From 2021 to 2023, the average chlorophyll *a* content of each layer showed a general trend of first increasing and then decreasing, with a typical unimodal vertical distribution in the ocean. The average depths of the DCM were 132 m, 137 m, and 129 m, with an average content of 0.33 mg/m³, 0.38 mg/m³, and 0.56 mg/m³, respectively (Table 5-3).

Table 5-3 Mean chlorophyll *a* content of each layer in Block M from 2021 to 2023 (mg/m³)

Layer Year	0 m	30 m	50 m	75 m	100 m	125 m	DCM	150 m	200 m
2021	0.08	0.09	0.11	0.17	0.26	0.30	0.33	0.16	0.05
2022	0.09	0.12	0.12	0.16	0.22	0.30	0.38	0.22	0.09
2023	0.09	0.13	0.14	0.15	0.22	0.42	0.56	0.27	0.06

Note: Deep Chlorophyll Maximum (DCM)
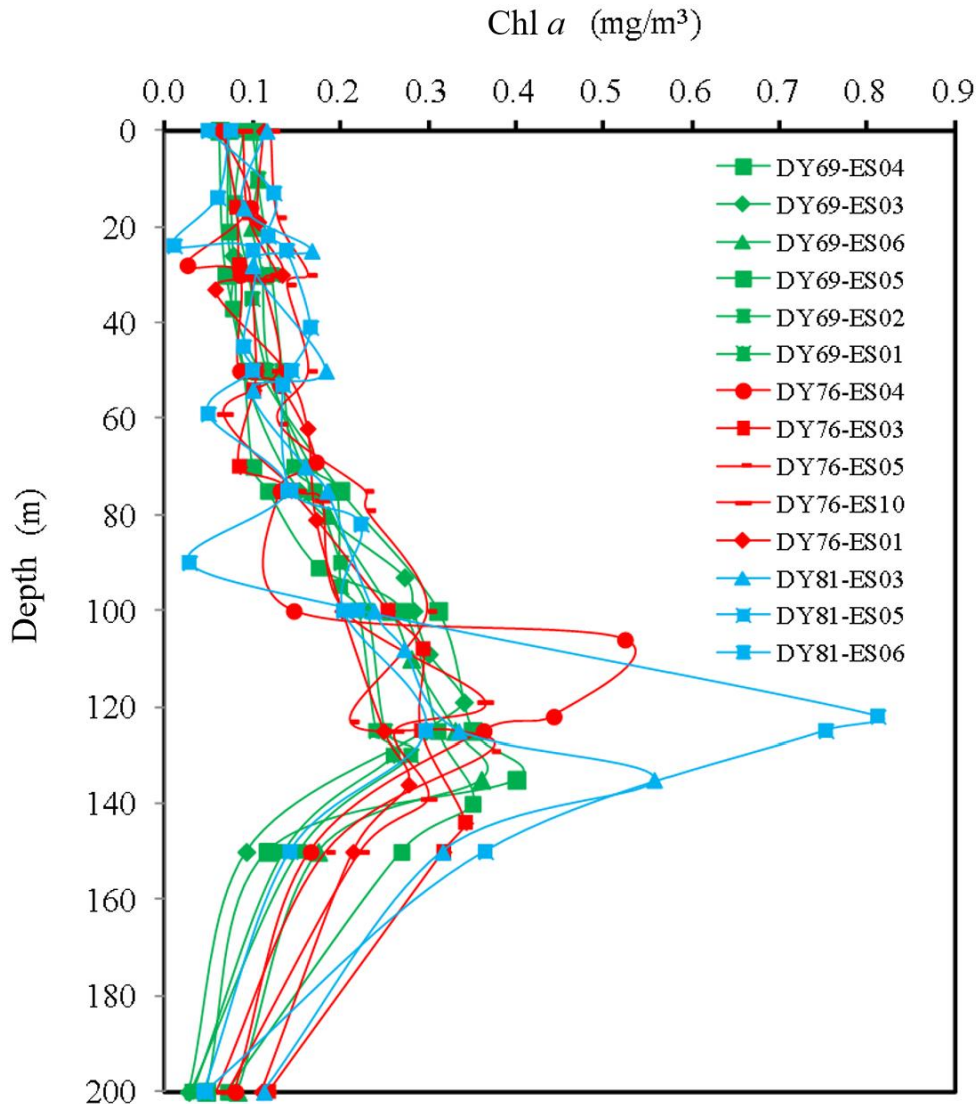
Figure 5-13 Vertical distribution of chlorophyll *a* concentration (mg/m³) in Block M from 2021 to 2023

5.2.1.1.2 Photosynthetic Pigment

The distribution of major pigment concentrations at the surface and DCM layers in Block M was shown in Figure 5-14 and Figure 5-15 (2021 survey results). All pigments were low at the surface layer, but different types of pigments also showed different spatial distribution. At DCM layer, the pigments with highest concentrations

were mainly divinyl Chl *a*, zeaxanthin, and chlorophyll *b*. And followed by the two characteristic pigments of Haptophyta. Fucoxanthi (the characteristic pigment of Bacillatiophyta), and peridinin (the characteristic pigment of Dinophyta), showed very low concentration. This indicated that phytoplankton in this area was mainly dominated by picoplankton, *Prochlorococcus* and *Synechococcus*, with a certain number of Haptophyta, and low biomass of Bacillatiophyta and Dinophyta.

The profiles of major photosynthetic pigment concentrations showed that the DCM layer at each station was mostly located at 100–130 m, with little differences in depth, but the TChl *a* concentration varied greatly, with the maximum value of 373.769 ng/L at 100 m of Station ES05, and the minimum value of 205.657 ng/L at 125 m of Station ES03. Although the TChl *a* concentration was different, the profiles of major pigment concentrations at each station were almost consistent. All of them were composed of divinyl Chl *a* and zeaxanthin, which indicated that the phytoplankton community structure in this area was similar (Figure 5-16).
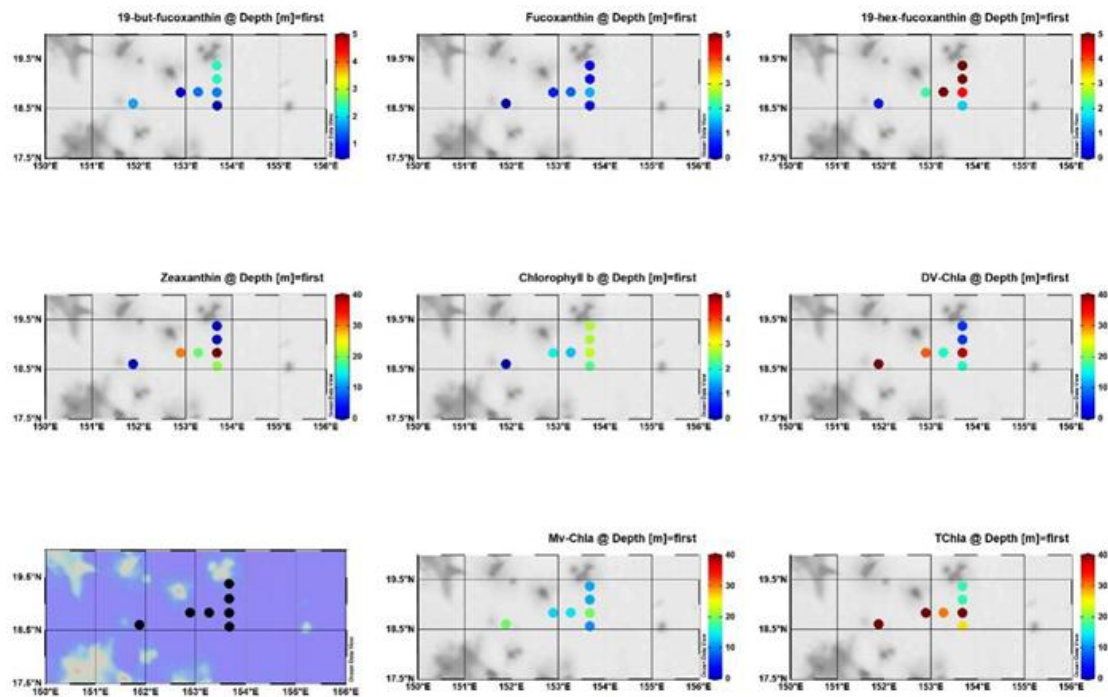
Figure 5-14 Distribution of major photosynthetic pigment concentration at the surface in the contract area in 2021
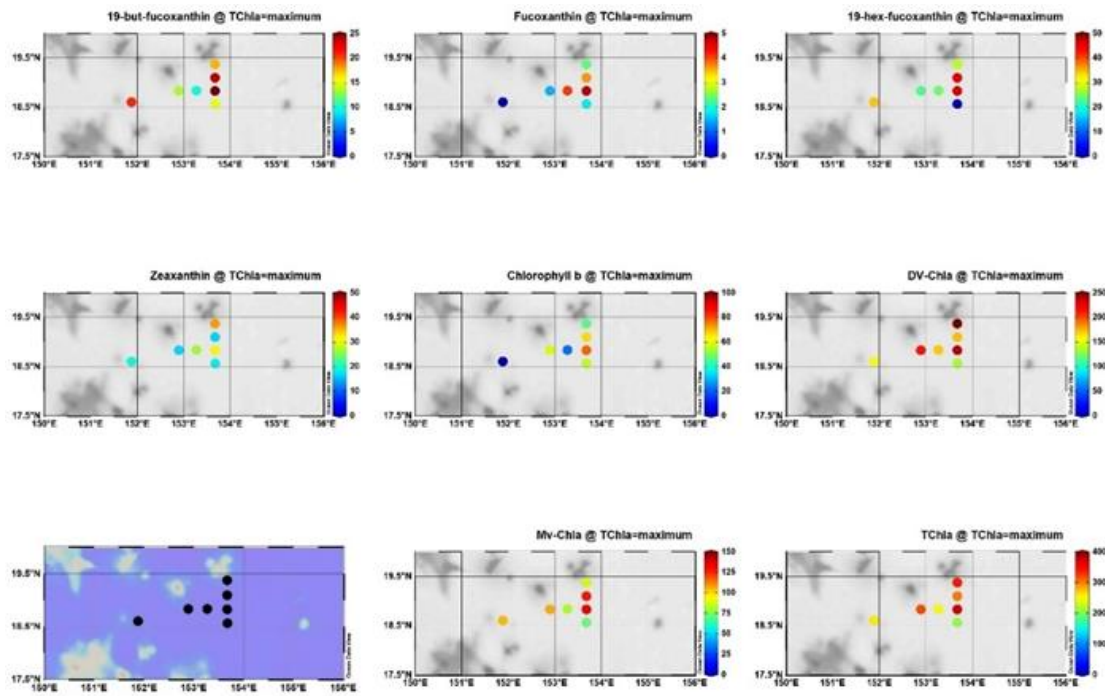
Figure 5-15 Distribution of major photosynthetic pigment concentration at DCM layer in the contract area in 2021
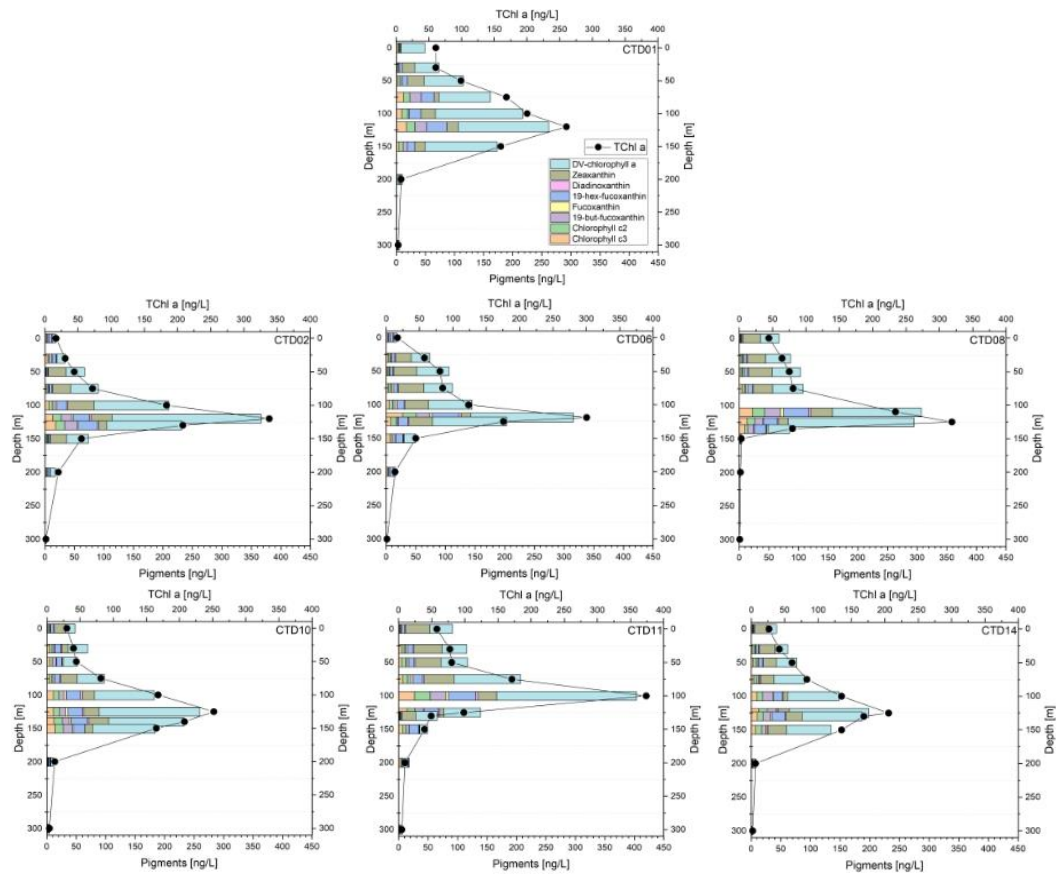
Figure 5-16 Vertical distribution of major photosynthetic pigment concentration in Block M

5.2.1.2 Microbe

Microbial community structure was determined by analyzing 72 layers of samples, which was collected by CTD during DY69 cruise (2021) from 6 stations of Blocks M1 and M2 in the contract area. A total of 738,487 sequences were obtained, with an average sequence length of 1,433.6 bp.

5.2.1.2.1 Alpha Diversity Index Analysis

The number of OTUs varied greatly, ranging from 279 to 4986, and the Shannon diversity index of microbial populations ranged from 6.3 to 12.2 (Table 5-4), which suggested that microbial α-diversity differed greatly in these samples.

Table 5-4 Marine microbial diversity index in Block M (2021)

Sample	Reads	Chao	Richness	Shannon	Simpson	Ace	Evenness	Coverage
ES01_W_3	2230	1260.601	1007	8.7447	0.0147	1427.147	0.8766	0.7834
ES01_W_50	9872	4375	4375	11.5913	0.0032	4375	0.9584	1
ES01_W_75	5500	2497.739	2469	10.7025	0.003	2658.152	0.9497	0.9378
ES01_W_100	1474	2650.452	679	7.4467	0.0585	3001.541	0.7916	0.6357
ES01_W_130	7227	3460.881	3459	11.4836	0.0021	3516.2	0.9768	0.9845
ES01_W_200	794	1989.442	493	8.4114	0.0052	2383.359	0.9403	0.5025
ES01_W_500	8726	4306.699	4306	12.0363	0.0002	4344.635	0.997	0.9912
ES01_W_800	1683	1042.742	960	9.7784	0.0013	1189.776	0.987	0.8105
ES01_W_2500	5680	2573.364	2525	10.8748	0.0011	2765.193	0.9622	0.9241
ES01_W_5146	4080	2055.291	1640	9.8187	0.0035	2438.535	0.9194	0.8203
ES01_W_5446	8740	3939.797	3939	11.579	0.0013	3977.778	0.9695	0.9911
ES01_W_5616	9346	4208.707	4208	11.7714	0.0006	4245.711	0.9778	0.9919
ES02_W_3	9176	3968.728	3968	11.3119	0.0041	4005.246	0.9463	0.9918
ES02_W_50	5635	2377.935	2347	10.1771	0.0107	2537.456	0.909	0.9391
ES02_W_75	3462	2918.431	1063	7.2267	0.07	3311.233	0.7188	0.7822
ES02_W_100	2116	2071.509	729	6.3004	0.1403	2427.12	0.6625	0.7453
ES02_W_130	6509	2936.765	2932	10.8526	0.0087	3014.746	0.9423	0.9753
ES02_W_200	1837	2457.776	846	8.674	0.0084	2961.913	0.892	0.6668
ES02_W_500	8637	4248.398	4248	11.9962	0.0003	4277.117	0.9953	0.9933
ES02_W_800	1045	1873.692	590	8.4667	0.0072	2138.755	0.9198	0.5713
ES02_W_2500	5338	2279.691	2220	10.3618	0.0033	2469.527	0.9321	0.9176
ES02_W_5150	5823	2508.17	2498	10.3493	0.0143	2610.901	0.917	0.9634
ES02_W_5450	7412	3390.59	3385	11.4585	0.0008	3479.62	0.9773	0.9749
ES02_W_5620	6606	2854.072	2842	10.8895	0.0028	2970.166	0.9492	0.9629
ES03_W_3	1904	1474.07	819	8.0074	0.026	1902.342	0.8274	0.7216
ES03_W_50	8423	3566.249	3564	11.082	0.0047	3626.008	0.9392	0.9854
ES03_W_75	2852	2693.795	950	7.7866	0.027	3254.891	0.7872	0.7619
ES03_W_100	1650	2820.76	783	7.8909	0.0251	3445.778	0.8209	0.6206
ES03_W_120	2207	1332.851	925	8.2812	0.0337	1627.397	0.8405	0.7676

Sample	Reads	Chao	Richness	Shannon	Simpson	Ace	Evenness	Coverage
ES03_W_200	3416	2542.163	1209	9.0069	0.006	2906.968	0.8796	0.7813
ES03_W_500	5801	2824.89	2819	11.3235	0.0006	2910.335	0.988	0.9698
ES03_W_800	2448	2849.913	1110	9.2007	0.005	3022.619	0.9095	0.694
ES03_W_2500	4870	3044.605	1453	8.9741	0.0078	3460.78	0.8543	0.8193
ES03_W_5074	3036	1491.5	1219	8.9339	0.0174	1733.895	0.8715	0.8205
ES03_W_5374	816	1143.037	291	6.4877	0.0414	1039.905	0.7926	0.7365
ES03_W_5534	9642	4496	4496	11.9567	0.0005	4496	0.9854	1
ES04_W_3	671	1327.5	279	6.0897	0.066	1660.207	0.7496	0.6513
ES04_W_50	9664	4130.429	4130	11.3292	0.0036	4159.184	0.9432	0.9939
ES04_W_75	4601	2013.655	1974	10.0875	0.0059	2177.934	0.9215	0.9237
ES04_W_100	8988	3967.982	3967	11.4078	0.0025	4010.738	0.9543	0.9903
ES04_W_135	8153	3815.472	3814	11.6025	0.0019	3866.275	0.9752	0.9872
ES04_W_200	2383	1273.085	1193	9.8881	0.002	1421.15	0.9675	0.8527
ES04_W_500	4965	2853.955	1603	9.2664	0.0061	3331.287	0.8704	0.8155
ES04_W_800	4634	2274.533	2262	10.9891	0.0007	2381.574	0.9862	0.9519
ES04_W_2500	8190	3776.021	3776	11.6932	0.0005	3782.386	0.9841	0.9984
ES04_W_4040	2435	1180.444	1179	10.0581	0.0015	1208.491	0.9858	0.9766
ES04_W_4340	9777	4247.05	4247	11.4215	0.0044	4257.38	0.9477	0.9979
ES04_W_4810	8798	3738.11	3737	11.3245	0.0022	3780.74	0.9542	0.9899
ES05_W_3	5934	2560.197	2532	10.4829	0.0068	2717.613	0.9272	0.9424
ES05_W_50	10071	4280.119	4280	11.3784	0.0045	4295.736	0.9432	0.9968
ES05_W_75	8992	3823.286	3821	11.2339	0.0045	3884.358	0.944	0.9858
ES05_W_100	3378	1615.25	1497	9.4439	0.0133	1822.944	0.8953	0.8597
ES05_W_130	8549	3851.666	3849	11.4522	0.0035	3918.892	0.9615	0.9837
ES05_W_200	2812	2870.5	1026	7.7969	0.0621	3141.404	0.7795	0.7461
ES05_W_500	10250	4986.009	4986	12.2394	0.0002	4990.928	0.9964	0.999
ES05_W_800	5350	2612.01	2595	11.1191	0.0011	2743.974	0.9804	0.9484
ES05_W_2500	8749	3782.656	3780	11.4681	0.001	3848.182	0.965	0.9843
ES05_W_5169	9142	4236.431	4236	11.6909	0.0026	4265.866	0.9703	0.9934
ES05_W_5469	6026	2582.907	2566	10.5661	0.0055	2712.447	0.933	0.9547
ES05_W_5639	8425	3840.281	3839	11.6621	0.0006	3887.16	0.9795	0.9885
ES06_W_3	6104	2600.433	2579	10.5566	0.0049	2742.274	0.9315	0.95
ES06_W_50	2725	1249.215	1149	8.9391	0.0138	1413.391	0.8793	0.8613
ES06_W_75	3055	3828.131	1132	8.1112	0.0231	4767.293	0.7996	0.7185
ES06_W_100	3379	3477.893	1171	7.7808	0.0326	3893.531	0.7633	0.7464
ES06_W_130	2209	2680.333	890	7.8533	0.0355	3074.026	0.8016	0.703
ES06_W_200	1752	1950.256	859	8.8488	0.0081	2294.564	0.9079	0.6667
ES06_W_500	817	2064.609	466	7.9123	0.0136	2639.543	0.8926	0.53
ES06_W_800	1247	1811.065	631	8.2621	0.0112	2180.644	0.8883	0.6239
ES06_W_2500	2778	3011.25	1012	8.4058	0.0114	3443.106	0.842	0.7383
ES06_W_5000	2366	2115.218	722	6.3157	0.1318	2661.236	0.6651	0.7756
ES06_W_5300	3969	1708.411	1635	9.7029	0.0069	1886.725	0.9089	0.8972
ES06_W_5470	3328	1442.771	1364	9.5212	0.0052	1606.283	0.9143	0.887

5.2.1.2.2 Beta Diversity Index Analysis

Hierarchical cluster analysis of OTU abundance obtained from high-throughput sequencing showed that the community composition of these samples could be divided into two major branches. The samples below 135 m clustered together and the samples above 135 m clustered into one large branch (Figure 5-17), which indicated that there were obvious differences in the microbial communities' structure between the upper and deeper water bodies of Block M.

In addition, microbes in the DCM (around 130 m) clustering together indicated that the microbial community composition was similar in this layer. Microbes were also clustered together at the 200 m layer (Figure 5-17), and there was no similar distribution for microbial community structure in the other layers.
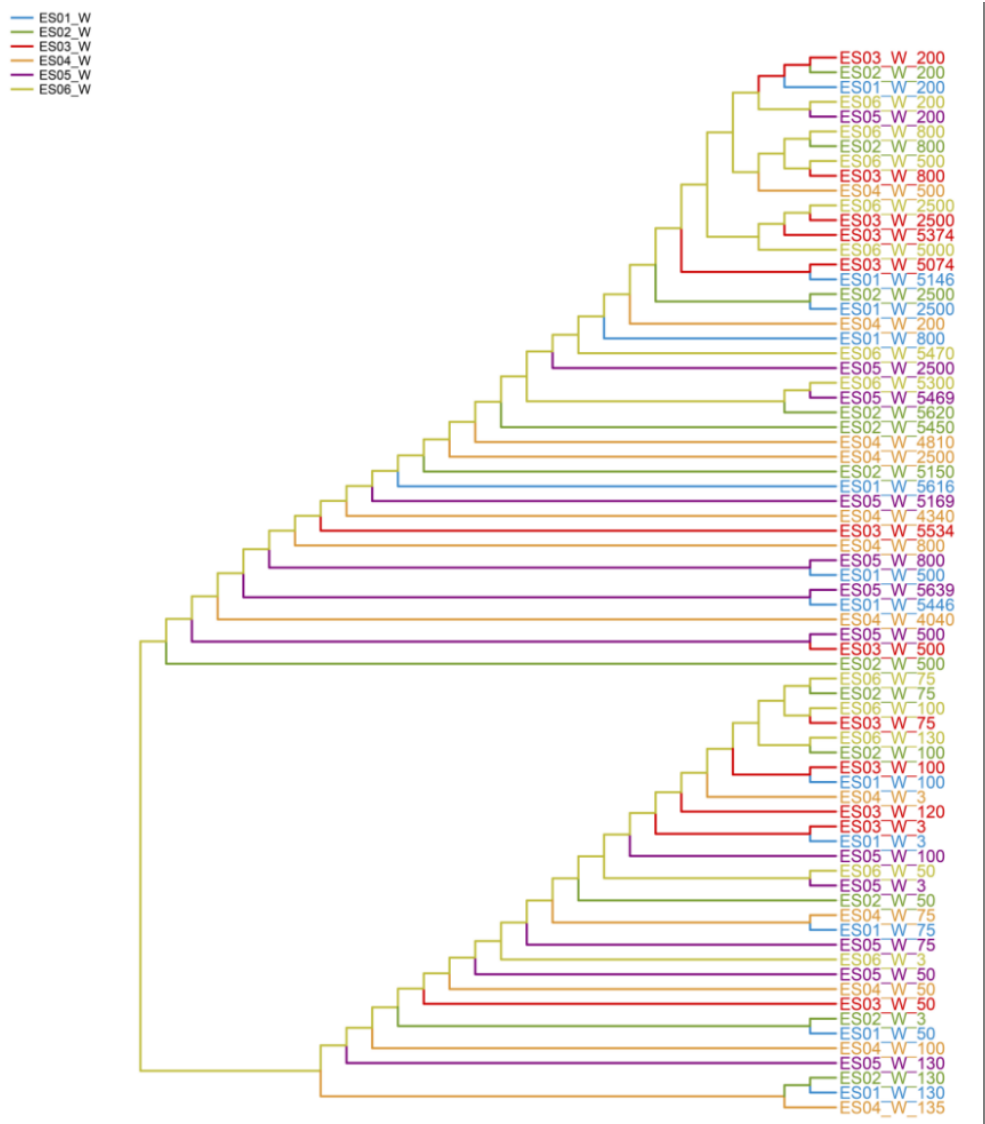
Figure 5-17 Hierarchical clustering tree of marine microbial community OTUs in Block M (2021)

Species composition analysis showed that the dominant pylum of Bacteria in Block M were Proteobacteria, Actinobacteria, Planctomycetes, Bacteroidetes, Cyanobacteria, Firmicutes, Candidatus, Saccharibacteria, Acidobacteria, Verrucomicrobia, and Chloroflexi. The dominant pylum of Archaea were Nitrospinae and the phylum Balneolaeota in the FCB group (Figure 5-18). The community structure composition showed that Planctomycetes was highly abundant in almost all water layers, and this taxon could maintain metabolism through nitrification and denitrification during hypoxia or anaerobic environments. Thus, we hypothesized that this taxon might play an important role in the nitrogen cycling in the Blocks M1 and M2.
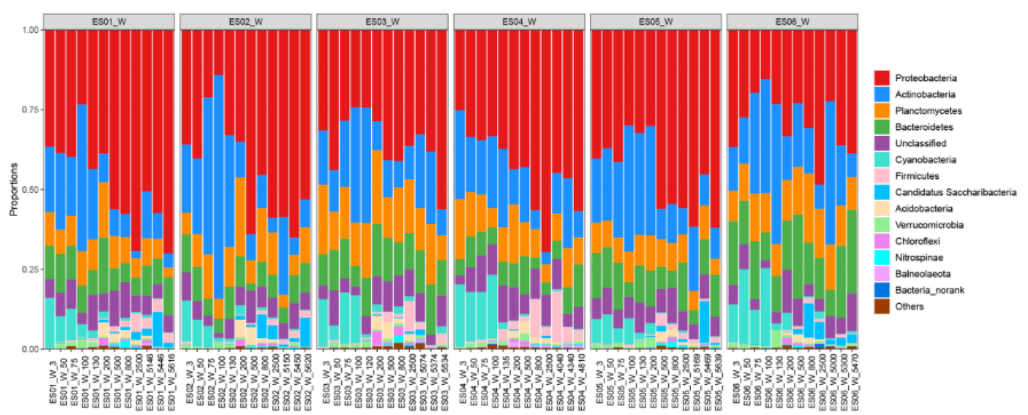
Figure 5-18 Composition of seawater prokaryotic microbe in Block M (2021)

5.2.1.3 Picoplankton

5.2.1.3.1 Horizontal Distribution

The results of DY69 cruise (2021) showed that the mean water column abundance of picoplankton in Block M was $50.38\pm7.31 \times 10^3$ cells/ml, ranging from 41.29 to 59.38 $\times 10^3$ cells/ ml with a relatively small variation, which was similar with the results of 2022 ($48.62\pm3.94 \times 10^3$ cells/ml), and was lower than that of 2023 ($56.21\pm8.05 \times 10^3$ cells/ml) (Table 5-5). Its horizontal distribution from 2021 to 2023 showed more obvious spatial differences, with the high-value area mainly concentrated in Station ES06 located in the west of 153°E, and the low-value area mainly distributed in Station ES03 located in the north and south of 18.8°N. A distribution trend of high in the west, low in the east, and high in the north, low in the south was generally presented (Figure 5-19~Figure 5-21).

Table 5-5 Annual changes in mean abundance of picoplankton (10^3 cells/ ml) in Block M, 2021-2023

Year	Sampling time	Prochlorococcus	Synechococcus	Picoeukaryotes	Picoplankton
2021	2021.10.21–2021.10.29	47.63±6.91	2.14±0.32	0.61±0.13	50.38±7.31
2022	2022.11.20–2022.11.29	45.79±3.88	2.25±0.11	0.59±0.07	48.62±3.94
2023	2023.08.26–2023.09.13	52.58±8.12	2.85±0.24	0.78±0.20	56.21±8.05

In terms of taxonomic groups, the distribution of *Prochlorococcus* and picoeukaryotes was essentially consistent with the distribution of the total picoplankton, especially for picoeukaryotes, which closely resembled the distribution of chlorophyll *a*. *Synechococcus* showed slight differences. In the percentage of the total abundance, there was an order of magnitude difference between the abundance of *Prochlorococcus*, *Synechococcus*, and picoeukaryotes, with *Prochlorococcus* having an absolute advantage.
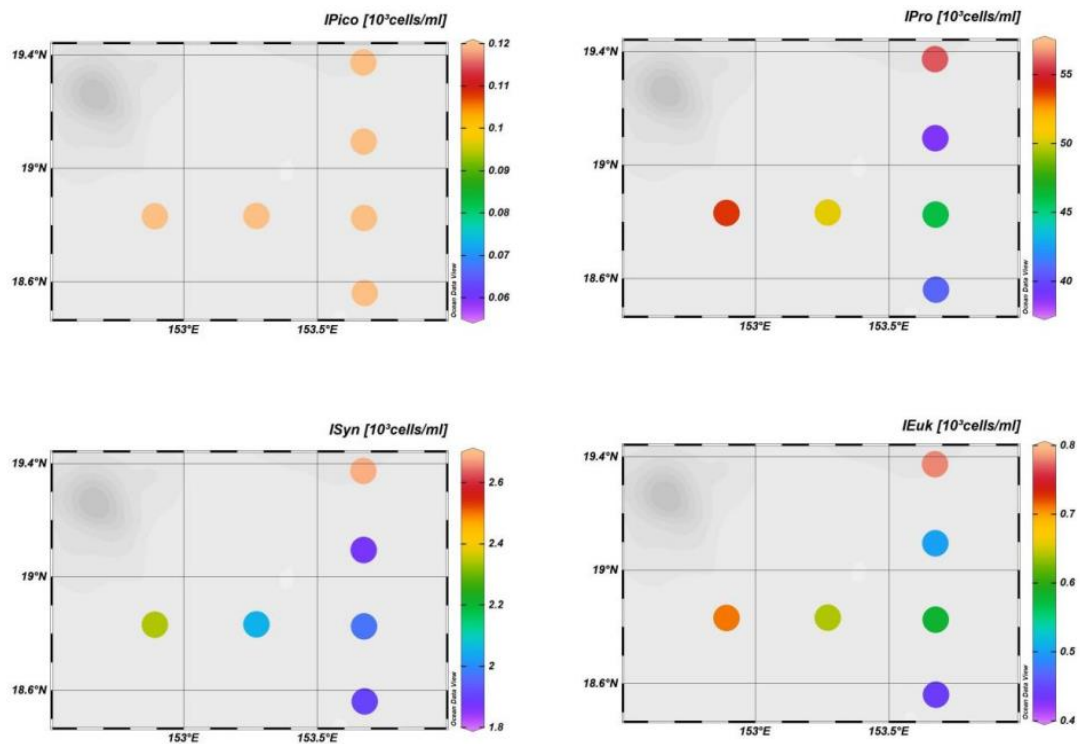
Figure 5-19 Distribution of picoplankton (including all groups) abundance in Block M in 2021
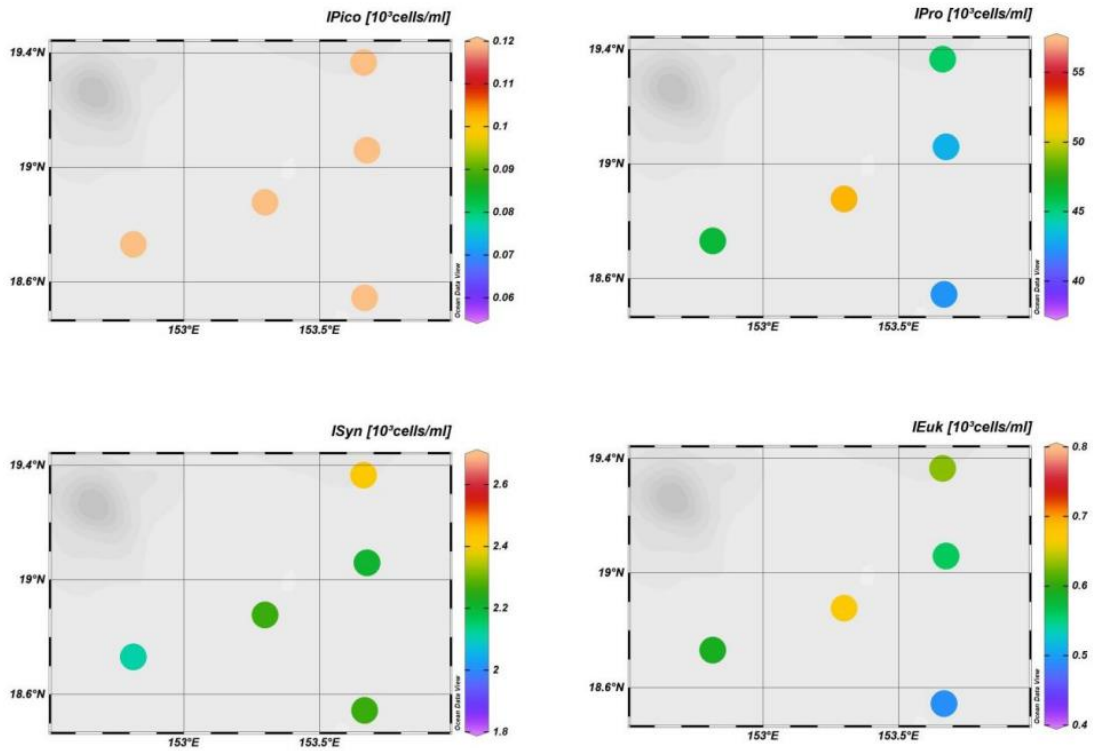
Figure 5-20 Distribution of picoplankton (including all groups) abundance in Block M, 2022
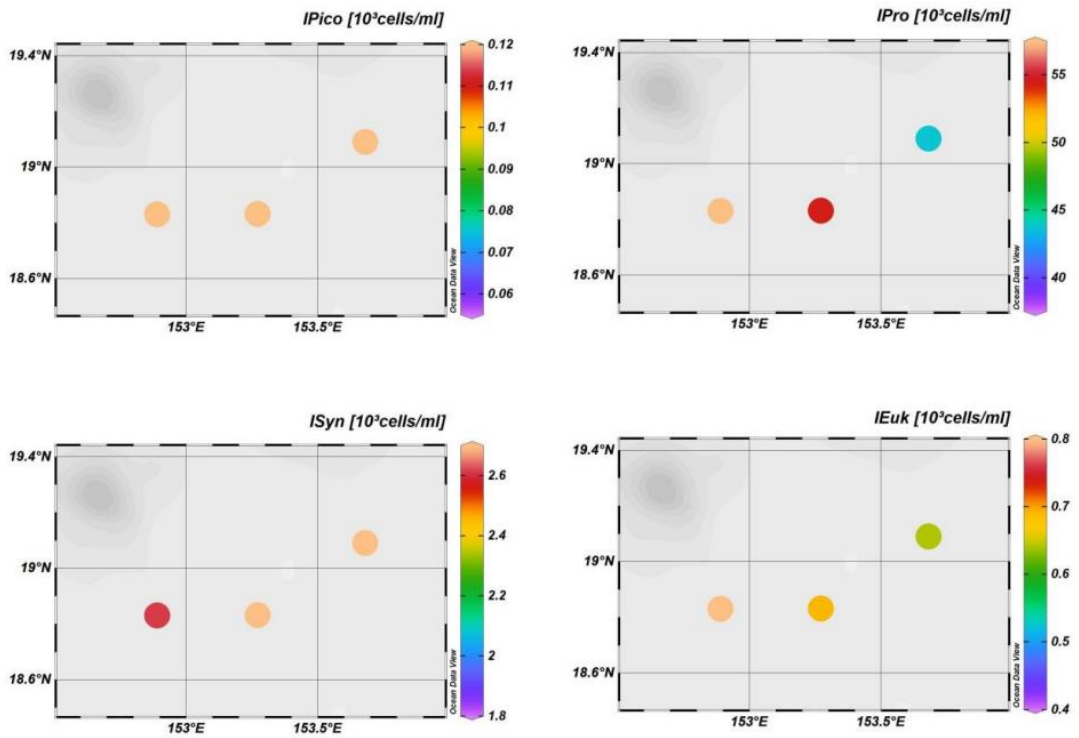
Figure 5-21 Distribution of picoplankton (including all groups) abundance in Block M in 2023

5.2.1.3.2 Vertical Distribution

The vertical distribution of picoplankton in Block M in 2021–2023 showed that the average abundance of *Synechococcus* was at a high level in the mixed layer, with the highest values appearing in the surface or sub-surface layer, while the abundance decreased obviously in the deeper layer of 150 m. The vertical distribution of *Prochlorococcus* and picoeukaryotes showed a single-peak distribution pattern, with the highest values appearing at the bottom of the chlorophyll *a* maximum layer or the euphotic layer, while the abundance decreased obviously in other water layers, especially approaching to zero at 300 m (Figure 5-22).
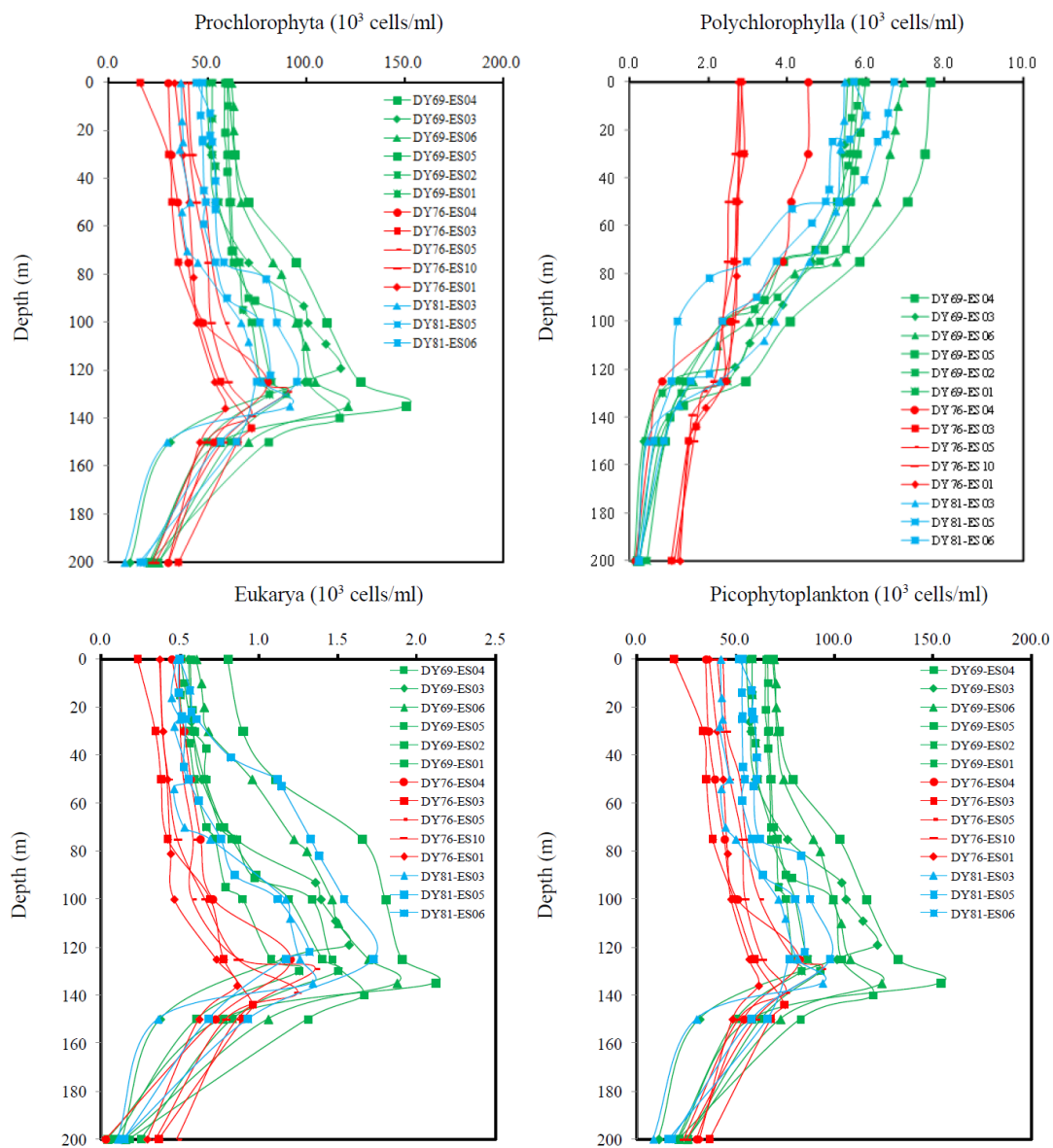
Figure 5-22 Vertical distribution of total picoplankton *Prochlorococcus*, *Synechococcus*, and Picoeukaryotes abundance in Block M, 2021–2023 ($\times 10^3$ cells/ml)

5.2.1.3.3 Transect Distribution

In 2021, sections E and N were selected in the contract area to study the vertical distribution characteristics of picoplankton. Section E started from Station ES06 (152.90 °E, 18.83 °N) in the west to Station ES02 (153.67 °E, 18.83 °N) in the east, with an east-west span of less than 1 °; section N started from Station ES04 (153.67 °E, 19.37 °N) in the north, which was close to seamount, to Station ES01 (153.67 °E, 18.56 °N) in the south, with a north-south span of less than 1°.

The results of the DY69 cruise (2021) showed that the high value areas of *Prochlorococcus* were west of section E and north of section N, while the low values were mainly located at Station ES03 and south of section N. The distribution of the high value area of *Synechococcus* was basically the same as that of *Prochlorococcus*, but the range of its low value area was enlarged. The abundance of the southern areas of section 19.2°N was all lower than 50×10^3 cells/ml. The picoeukaryotes showed obvious differences in both the north-south and east-west directions, with an overall distribution trend of high in the north, low in the south, and high in the west, low in the east (Figure 5-23 and 5-24).

The areas of high total picoplankton abundance in section E of Block M were all concentrated in the water layer around 125 m to 140 m (Figure 5-23). In terms of longitude variation, the total picoplankton abundance showed a distribution trend of decreasing from west to east. Transect distribution of *Prochlorococcus* was almost identical to the distribution trend of total picoplankton abundance, which showed that *Prochlorococcus* was the main contributor to the total picoplankton abundance. The transect distribution of *Synechococcus* was different from that of *Prochlorococcus* and picoplankton. Firstly, the high value area was basically located in the surface or subsurface layer at a depth of 30 m, and secondly, the abundance of *Synechococcus* in the west of the section was slightly higher than that in the east of the section. The distribution of picoeukaryotes was basically the same as that of chlorophyll *a* in the section, with the peaks basically located between 125 m and 140 m, and the abundance of picoeukaryotes in the east-west direction was slightly higher in the west than that in the east of 153.2°E.

The areas of high total picoplankton abundance in section N of Block M were all concentrated in the upper waters around 119 m to 135 m (Figure 5-24). In terms of latitudinal variation, the total picoplankton abundance showed a distribution trend of gradually increasing from south to north, and the abundance in the north was about 2.6 times of that in the south. The transect distribution trend of *Prochlorococcus* was almost

the same as that of picoplankton, except that the value of abundance was slightly lower than that of picoplankton. Although the transect distribution of *Synechococcus* still showed the trend of gradually increasing from south to north, its high value area was obviously concentrated in the surface layer, and the trend of gradually decreasing from the surface to the bottom was shown in the euphotic layer. The abundance of picoeukaryotes gradually increased from low to high latitude, and the abundance in the north was about 2.5 times of that in the south, with most of the peaks centered between 119 m and 135 m. Thereafter, it decreased obviously with the increase of depth, and was close to zero at a depth of 300 m.
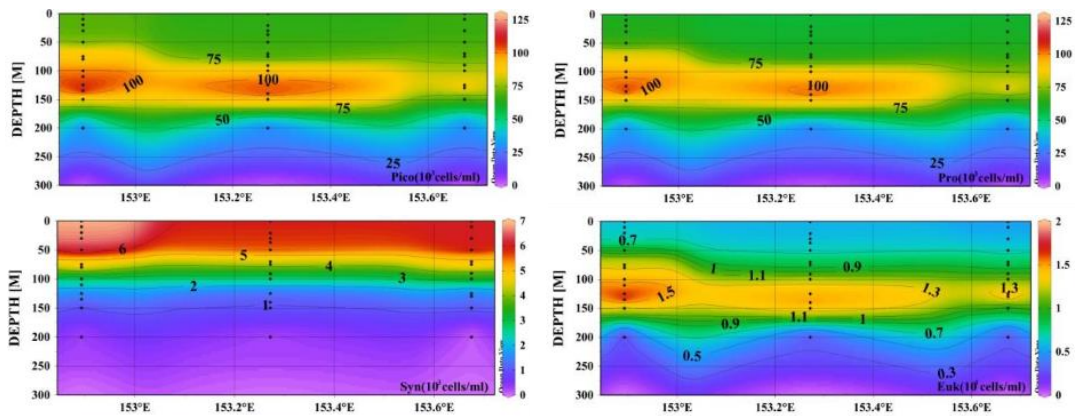
Figure 5-23 Distribution of total picoplankton, *Prochlorococcus*, *Synechococcus* and picoeukaryotes abundance in section E, 2021(×10³ cells/ml)
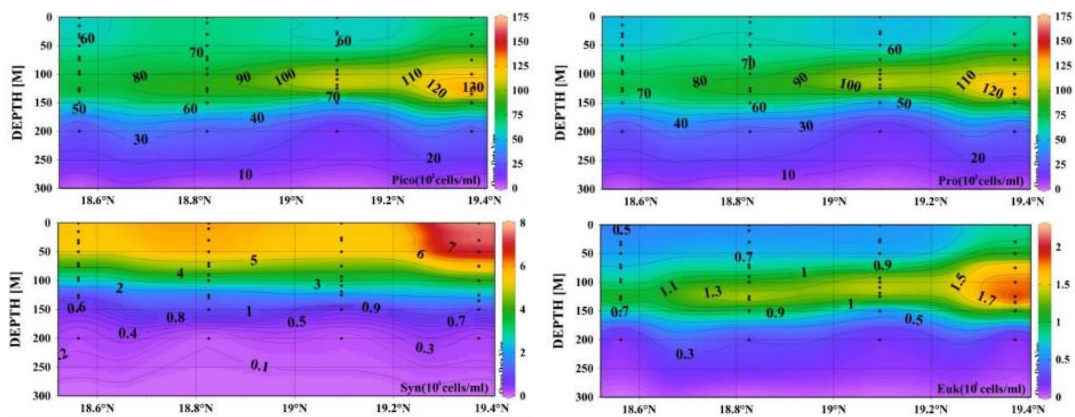
Figure 5-24 Distribution of total picoplankton, *Prochlorococcus*, *Synechococcus* and picoeukaryotes abundance at section N in 2021 (×10³ cells/ml)

Section N was selected to study the vertical distribution of picoplankton in the western Pacific Ocean during the 2022 cruise. Section N extended from Station ES04 (153.67 °E, 19.37 °N) in the north to Station ES01 (153.67 °E, 18.56 °N) in the south, with a span of less than 1°.

The areas of high total picoplankton abundance in section N were all concentrated in the upper waters around 122 m to 144 m (Figure 5-25). In terms of latitudinal

variation, the total picoplankton abundance showed a distribution trend of gradually increasing from south to north. The transect distribution trend of *Prochlorococcus* was almost the same as that of picoplankton except that the abundance was slightly lower than that of picoplankton. Although the transect distribution of Synechococcus still showed the trend of gradually increasing from south to north, its high value area was obviously concentrated in the surface layer, and the trend of gradually decreasing from surface to bottom was shown in the euphotic layer. The abundance of picoeukaryotes showed a gradually increasing from low to high latitudes, with most of the peaks concentrated between 122 m and 144 m, and then decreased with the increase of depth, and was close to zero at the depth of 200 m.
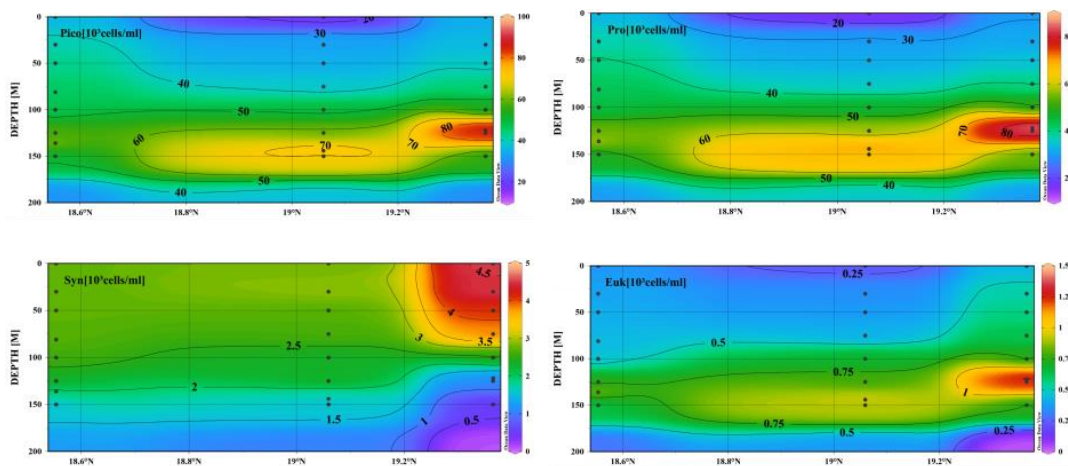
Figure 5-25 Distribution of total picoplankton, *Prochlorococcus*, *Synechococcus* and picoeukaryotes abundance at section N in 2022 ($\times 10^3$ cells/ml)

5.2.1.4 Microplankton and nanoplankton

Samples for nanoplankton analysis were collected using a SBE911plus CTD by collecting 2L of seawater per layer. Microplankton analysis samples were collected using a phytoplankton net.

5.2.1.4.1 Microplankton

(1) Species composition

18 samples from three cruises were totally analyzed in Block M. A total of 155 species of microplankton belonged to 6 phylums and 56 genera were identified in Block M. Among which, Bacillatiophyta were the most dominant group, including 38 genera and 88 species, accounting for 56.77% of the total number of species; Dinophyta were the second dominant group, including 14 genera and 62 species, accounting for 40.00%; in addition, there were one genus and two species of Cyanophyta (1.29%), one genus

and one species of Chrysophyta (0.65%), one genus and one species of Haptophyta (0.65%) and one species of Xanthophyta (0.65%).

The microplankton identified in the 2021 survey in Block M belonged to 3 phylums, 21 genera and 38 species, including 16 genera and 27 species of Bacillatiophyta, 4 genera and 10 species of Dinophyta and 1 genus and 1 species of Cyanophyta. Among the phytoplankton which had been identified to species level at each station, there were 5 dominant species with dominance (Y) ≥ 0.02. The occurrence frequency and dominance of dominant species were shown in Tables 5-6.

Table 5-6 Microplankton dominant species and dominance (Y) in 2021

Species	Occurrence Frequency (%)	Dominance (Y)
Rhizosolenia alata	100	0.379
Rhizosolenia alata f. *indica*	100	0.174
Rhizosolenia styliformis	100	0.094
Rhizosolenia setigera	83	0.047
Trichodesmium thiebautii	83	0.027

A total of 107 species of microplankton belonged to 5 phylums and 43 genera were identified in the surveyed area in 2022, including 30 genera and 52 species of Bacillatiophyta, 10 genera and 51 species of Dinophyta, 1 genus and 2 species of Cyanophyta, 1 genus and 1 species of Chrysophyta, and 1 genus and 1 species of Xanthophyta. There were 9 dominant species in total with dominance (Y) ⩾ 0.02. The occurrence frequency and dominance of dominant species were shown in Tables 5-7.

Table 5-7 Microplankton dominant species and dominance (Y) in 2022

Species	Occurrence Frequency (%)	Dominance (Y)
Pseudosolenia calcar-avis	100	0.174
Nitzschia spp.	100	0.113
Rhizosolenia hebetata f. *semispina*	100	0.058
Skeletonema costatum	86	0.038
Bacillaria paxillifera	71	0.032
Thalassionema nitzschioides	86	0.023
Trichodesmium thiebautii	100	0.022
Thalassionema nitzschioides var. *parva*	71	0.020
Hemiaulus hauckii	100	

A total of 51 species of microplankton in 4 phylums and 28 genera were identified in the surveyed area in 2023, including 21 genera and 34 species of Bacillatiophyta, 5 genera and 15 species of Dinophyta, 1 genus and 1 species of Cyanophyta, and 1 genus and 1 species of Haptophyta. There were 3 dominant species with dominance (Y) ⩾

0.02. The occurrence frequency and dominance of dominant species were shown in Table 5-8.

Table 5-8 Microplankton dominant species and dominance (Y) in 2023

Species	Occurrence Frequency (%)	Dominance (Y)
Rhizosolenia alata	100	0.763
Rhizosolenia styliformis	100	0.099
Trichodesmium thiebautii	100	0.064

(2) Abundance

The results of 2021 survey showed that the average abundance of microplankton in Block M was 24.17×10^2 cells/m^3. The highest value appeared at Station ES06, with an abundance of 44.05×10^2 cells/m^3; the lowest value was 10.48×10^2 cells/m^3, which appeared at Station ES05. The horizontal distribution showed that the abundance of microplankton in Block M was higher in the northwest and lower in the southeast (Figure 5-26), which was consistent with the horizontal distribution trend of photosynthetic pigments as described in the previous section.
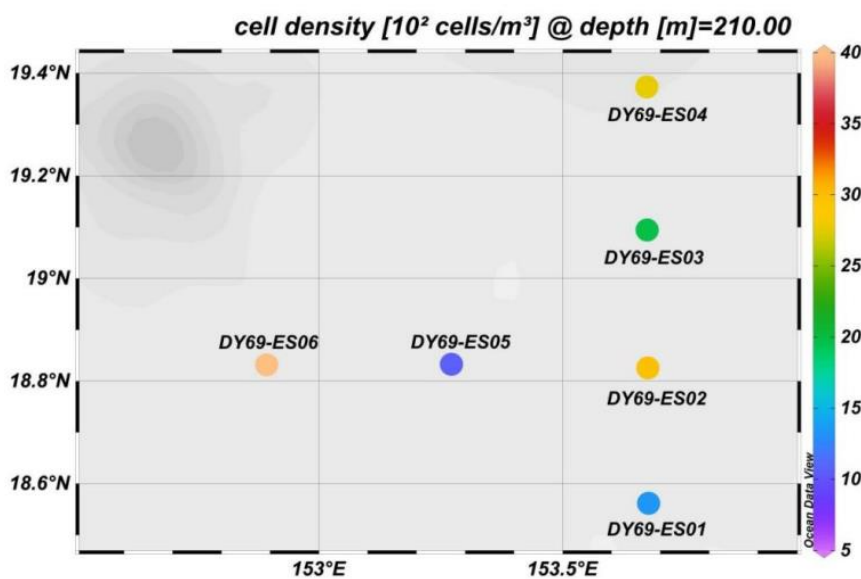
Figure 5-26 Distribution of microplankton cell abundance in 2021

The average abundance of microplankton in the surveyed area in 2022 was 26.64×10^2 cells/m^3. The highest value appeared at Station DY76-I-M2-S059VN13, with an abundance of 43.20×10^2 cells/m^3, and the lowest value was 14.60×10^2 cells/m^3, which appeared at Station DY76-I-M2-S074VN15-1. The horizontal distribution showed that the abundance of microplankton in the surveyed area showed a trend of higher in the north and lower in the south. The horizontal distribution of abundance was shown in Figure 5-27.
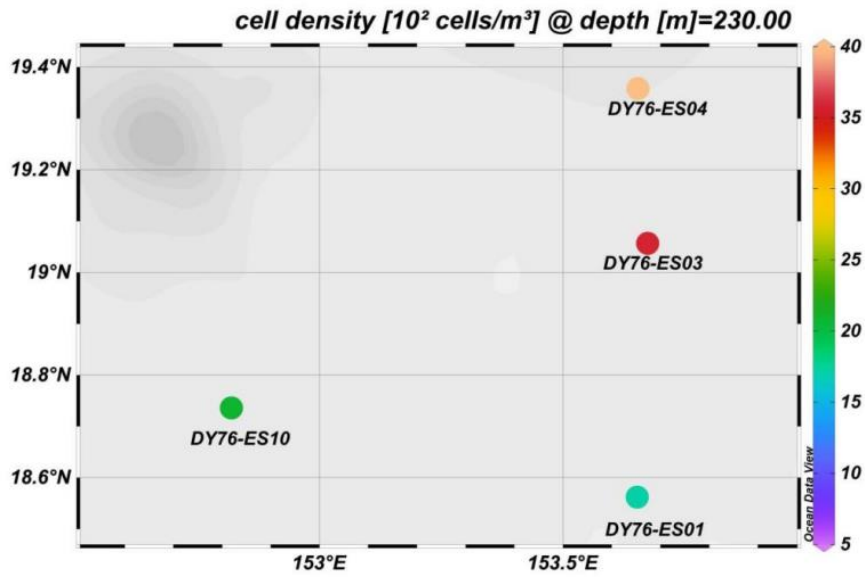
Figure 5-27 2 Distribution of microplankton cell abundance in 2022

The average abundance of microplankton in the surveyed area in 2023 was 26.30×10^2 cells/m^3. The highest value appeared at Station DY81I-M2-DX04, with an abundance of 115.08×10^2 cells/m^3, which was much higher than that of other stations, and the abundance of other stations was closer, and the lowest value was 2.93×10^2 cells/m^3, which appeared at Station DY81I-M2-ES03-DX02. The horizontal distribution of cell abundance was shown in Figure 5-28.
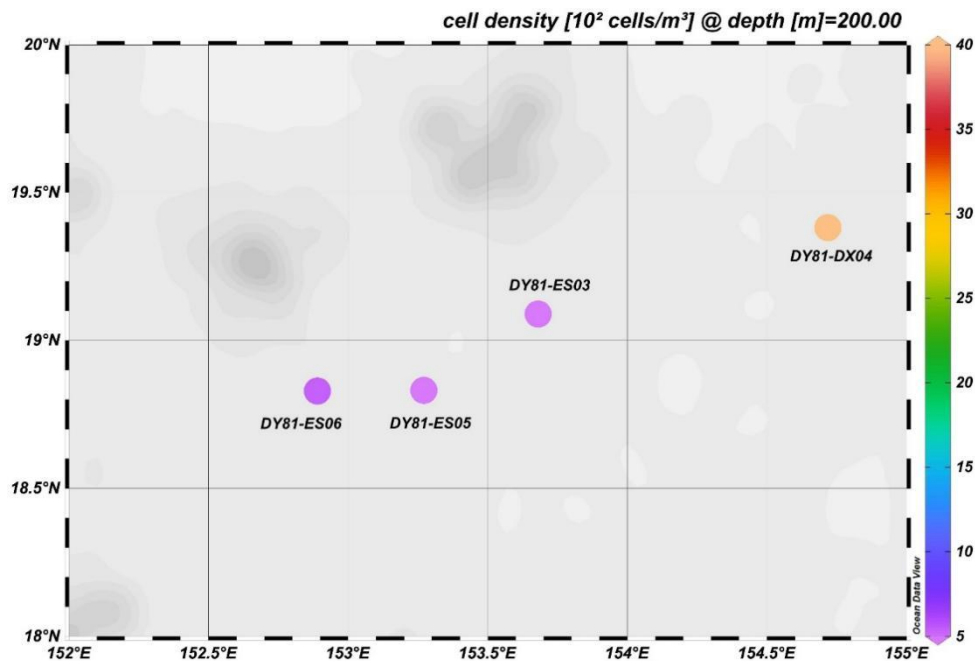
Figure 5-28 Distribution of microplankton cell abundance in 2023

(3) Community Structure

The 2021 analysis results of microplankton species richness (D), evenness (J), and diversity index (H′) in the contract area were shown in Table 5-9;

1) Species richness (D): The range of species richness for microplankton was 1.06 to 1.59. The highest value appeared at Station ES05 and the lowest at Station ES01.

2) Evenness (J): The range of evenness for microplankton was 0.61 to 0.87. The highest value appeared at Station ES05 and the lowest at Station ES01.

3) Diversity index (H′): The diversity index of microplankton ranged from 2.18 to 3.54, with the highest value appearing at Station ES05 and the lowest at Station ES01. The diversity index of microplankton was higher than 2 at all stations in the surveyed area.

Table 5-9 Microplankton biodiversity index for 2021

Stations	D	J	H'
DY69-M2B1-ES01	1.06	0.61	2.18
DY69-M2B1-ES02	1.21	0.63	2.48
DY69-M2B1-ES03	1.37	0.81	3.26
DY69-M2-ES04	1.40	0.73	2.97
DY69-M2B1-ES05	1.59	0.87	3.54
DY69-M1-ES06	1.49	0.71	3.03

Based on the results of microplankton abundance and diversity, 6 stations were clustered and analyzed, and the results were shown in Figure 5-29. Overall, the 6 stations could be clustered into 2 major categories, with three Stations ES01, ES03 and ES05 grouped into one category, and three Stations ES02, ES04 and ES06 grouped into another category.
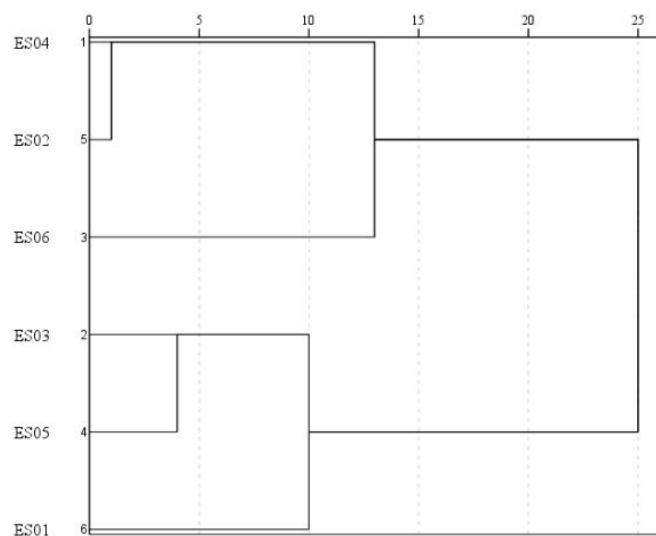
Figure 5-29 Cluster analysis results for microplankton stations in 2021

Species richness (D), evenness (J), and diversity index (H′) for the 2022 surveyed areas were analyzed as follows (Tables 5-10):

1) Species richness (D): The range of species richness for microplankton was 3.64-4.57. The highest value appeared at Station DY76-I-M2-S074VN15-1, and the lowest at Station DY76-I-M2-S059VN13.

2) Evenness (J): The range of evenness for the microplankton was 0.76-0.90. The highest value appeared at Station DY76-I-M2-S074VN15-1, and the lowest at Station DY76-I-M2-S063VN14-2.

3) Diversity index (H′): The diversity index of microplankton ranged from 4.24 to 5.06. The highest value was found at Station DY76-I-M2-S074VN15-1, and the lowest value was at Station DY76-I-M2-S059VN13. Phytoplankton diversity index was higher than 4 at all stations in the surveyed area.

Table 5-10 Microplankton biodiversity index for 2022

Stations	D	J	H'
DY76-I-M2-S059VN13	3.64	0.77	4.24
DY76-I-M2-S063VN14-1	3.67	0.83	4.55
DY76-I-M2-S063VN14-2	4.24	0.76	4.29
DY76-I-M2-S074VN15-1	4.57	0.90	5.06
DY76-I-M2-S074VN15-2	4.56	0.83	4.71
DY76-I-M1-S079VN16-1	4.35	0.83	4.63
DY76-I-M1-S079VN16-2	4.36	0.82	4.59

Species richness (D), evenness (J), and diversity index (H′) for the 2023 surveyed areas were analyzed as follows (Table 5-11):

1) Species richness (D): The range of species richness for microplankton was 1.46-2.48. The highest value appeared at Station DY81I-M2-ES05-DX01, and the lowest value at Station DY81I-M2-ES03-DX02.

2) Evenness (J): The range of evenness for microplankton was 0.24–0.79. The highest value appeared at Station DY81I-M1-ES06-DX05 and the lowest value at Station DY81I-M2-DX04.

3) Diversity index (H′): The diversity index of microplankton ranged from 1.08 to 3.55. The highest value was found at Station DY81I-M1-ES06-DX05, and the lowest value was at Station DY81I-M2-DX04. The phytoplankton diversity index was higher than 1 at all stations in the surveyed area.

Table 5-11 Microplankton biodiversity index for 2023

Stations	D	J	H'
DY81I-M2-ES05-DX01	2.48	0.65	2.92
DY81I-M2-ES03-DX02	1.46	0.40	1.49
DY81I-M2-ES03-DX03	1.47	0.49	1.85
DY81I-M2-DX04	1.56	0.24	1.08
DY81I-M1-ES06-DX05	2.43	0.79	3.55

5.2.1.4.2 Nanoplankton

(1) Species Composition

In 2021, a total of 27 genera and 46 species of nanoplankton belonged to 3 phyla were identified from the seawater samples collected by CTD. Among them, Bacillatiophyta was the most dominant group, including 18 genera and 31 species, which accounted for 67% of the total species number; Dinophyta was the second dominant, including 8 genera and 14 species, which accounted for 31% of the total species number; in addition, there was one genus and one species of Chrysophyta (2%) (Figure 5-30).
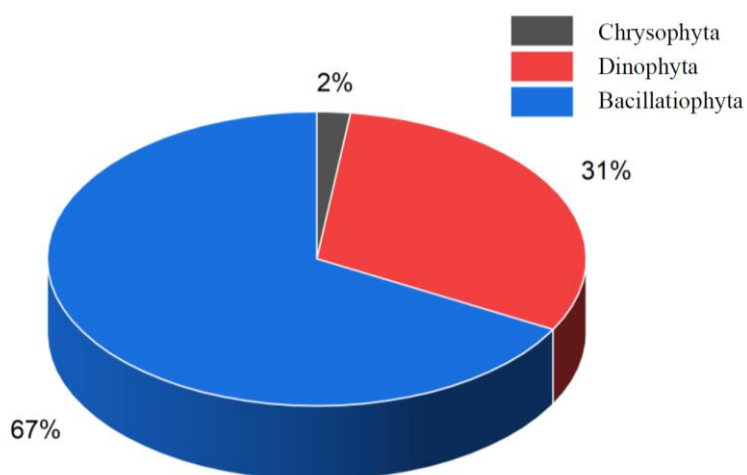
Figure 5-30 Composition of nanoplankton species in Block M in 2021

In 2022 a total of 27 genera and 40 species of nanoplankton belonged to 3 phyla were identified from the seawater samples collected by CTD. Among them, Bacillatiophyta was the most dominant group, including 18 genera and 26 species, which accounted for 65% of the total species number; Dinophyta was the second dominant, including 8 genera and 13 species, which accounted for 32.5% of the total species number; in addition, there was one genus and one species of Cyanophyta (2.5%) (Figure 5-31).

■ Bacillariophyta ■ Dinophyta ■ Cyanophyta

65.00%   32.50%

2.50%
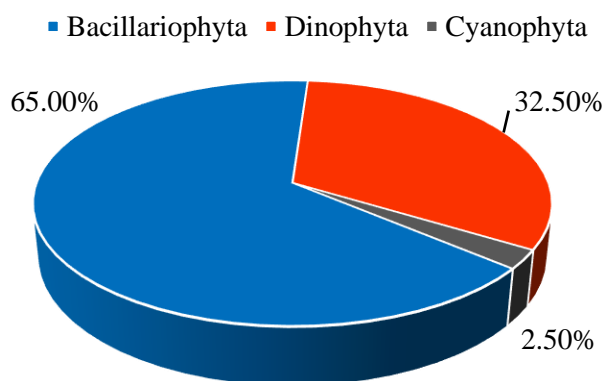
Figure 5-31 Composition of nanoplankton species in Block M in 2022

(2) Abundance

In 2021, the average abundance of nanoplankton in the surface layer of Block M was 0.63×10^3 cells/L, with the highest value of 1.85×10^3 cells/L appearing at Station ES06, and the lowest value was 0.20×10^3 cells/L, which appeared at Station ES01; the average abundance of nanoplankton in the DCM layer was 0.43×10^3 cells/L, with the highest value of 0.65×10^3 cells/L appearing at Station ES06, and the lowest value of 0.20×10^3 cells/L appeared at Station ES04.

The horizontal distribution of nanoplankton abundance in Block M was shown in Figure 5-32. Although the trends presented by the abundance of nanoplankton in each water layer were different, in general, the abundance of nanoplankton in the contract area showed a higher trend in the northwest and a lower trend in the southeast.

Transect distribution of nanoplankton abundance in the contract area was shown in Figure 5-33. The distribution of longitudinal transects showed that the maximum abundance appeared in the surface layer of the water body at the western stations, and the abundance at the central and eastern stations was relatively low; the distribution of latitudinal transects showed that the maximum abundance appeared in the 150 m layer of the southern stations, and the abundance was relatively low at the central stations, while the maximum abundance appeared in the 30 m layer of the northern stations.
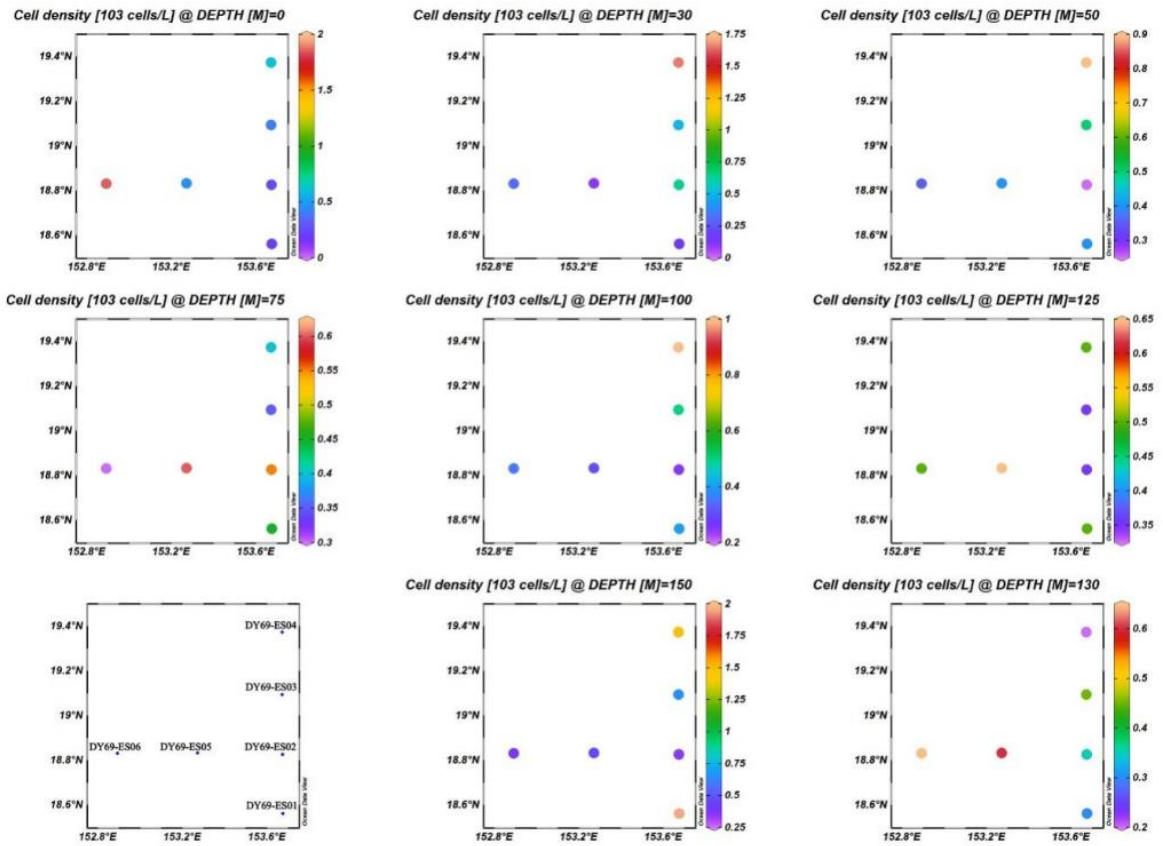
Figure 5-32 Distribution of nanoplankton abundance in 2021
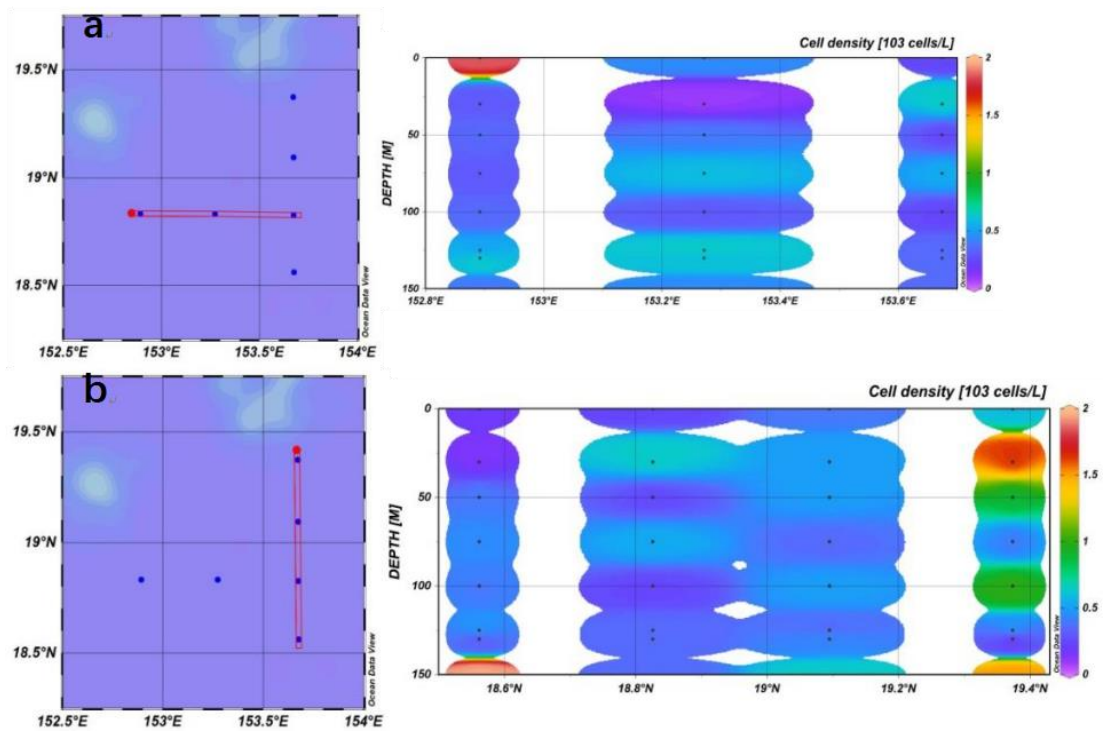
Figure 5-33 Transect distribution of nanoplankton abundance in 2021

In 2022, the average abundance of nanoplankton in the surface layer of Block M was 0.38×10^3 cells/L, with the highest value of 0.75×10^3 cells/L appearing at Station ES01, and the lowest value was 0.20×10^3 cells/L, which appeared at Station ES04; the average abundance of nanoplankton in the DCM layer was 0.21×10^3 cells/L, with the highest value of 0.35×10^3 cells/L appearing at Station ES03, and the lowest value of 0.15×10^3 cells/L appeared at Station ES05.

The horizontal distribution of nanoplankton abundance in Block M was shown in Figure 5-34. Although the trends presented by the abundance of nanoplankton in each water layer were different, in general, the abundance of nanoplankton in the contract area showed a higher trend in the southeast and a lower trend in the northwest.
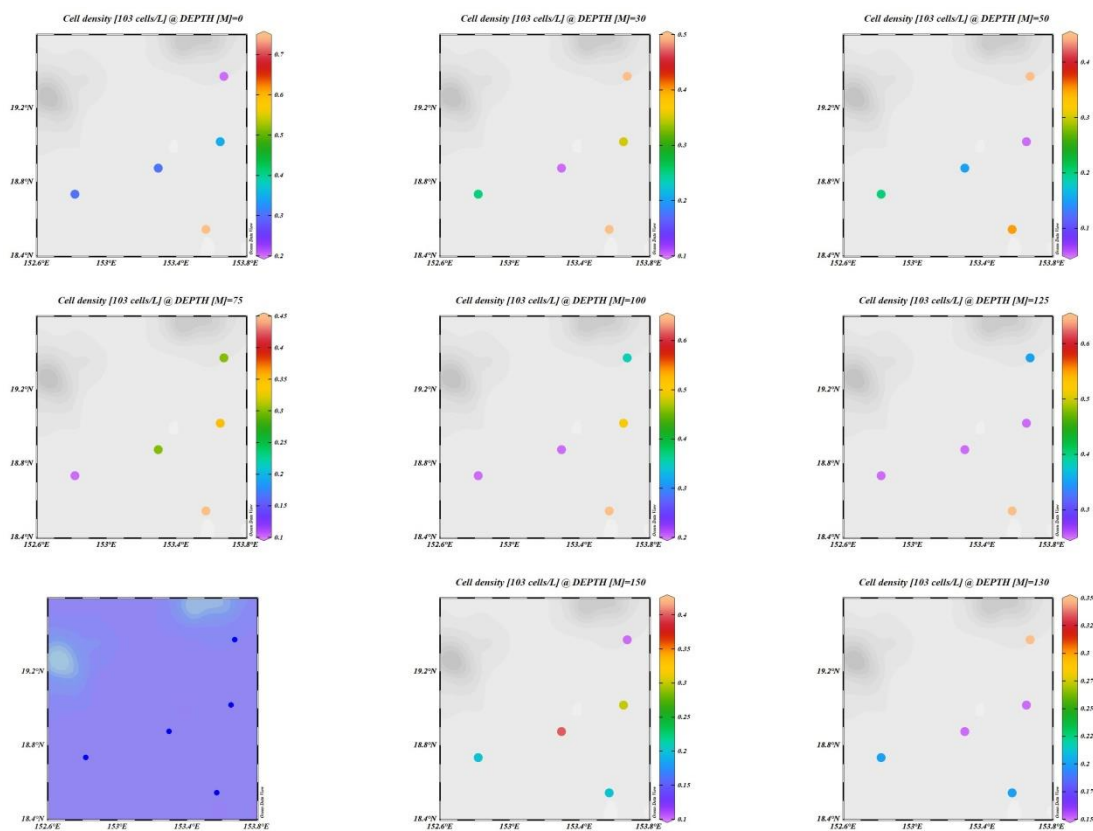
Figure 5-34 Distribution of nanoplankton abundance in 2022

(3) Dominant Species

In 2021, the dominant nanoplankton species (dominance (Y) ≥ 0.02) at each station in Block M were shown in Table 5-12.

The dominant species of nanoplankton varied with the water depth to some extent, but in general, the dominant species in each water layer were relatively similar, with Bacillatiophyta and Dinophyta as the main dominant groups. Among them, *Cyclotella striata* was the common dominant species in each water layer.

Table 5-12 Phytoplankton dominant species in each water layer (2021)

Depth	Dominant species
0 m	*Cyclotella striata, Gyrodinium spirale, Melosira sulcata, Scrippsiella trochoidea*
30 m	*Cyclotella striata, Melosira sulcata, Scrippsiella trochoidea*
50 m	*Cyclotella striata, Scrippsiella trochoidea, Gyrodinium spirale, Karenia mikimotoi*
75 m	*Cyclotella striata，Nitzschia frustulum，Melosira sulcata*
100 m	*Cyclotella striata, Gyrodinium spirale, Nitzschia frustulum, Melosira sulcata*
125 m	*Cyclotella striata, Nitzschia frustulum, Melosira sulcata, Scrippsiella trochoidea*
150 m	*Melosira sulcata, Cyclotella striata, Thalassionema nitzschioides, Gyrodinium spirale*
DCM	*Cyclotella striata, Nitzschia frustulum, Gyrodinium spirale*

In 2022, the dominant nanoplankton species (dominance (Y) ≥ 0.02) at each station in Block M were shown in Table 5-13.

The dominant species of nanoplankton varied with the water depth to some extent, but in general, the dominant species in each water layer were relatively similar, with Bacillatiophyta and Dinophyta as the main dominant groups. Among them, *Cyclotella striata* was the common dominant species in each water layer.

Table 5-13 Phytoplankton dominant species in each water layer (2022)

Depth	Dominant species
0 m	*Cyclotella striata, Coscinodiscus subtilis, Chaetoceros tortissimus, Gyrodinium spirale, Scrippsiella trochoidea*
30 m	*Cyclotella striata, Synedra gaillonii, Scrippsiella trochoidea*
50 m	*Cyclotella striata, Gyrodinium spirale*
75 m	*Cyclotella striata, Gyrodinium spirale, Prorocentrum donghaiense, Trichodesmium thiebautii, Nitzschia frustulum*
100 m	*Cyclotella striata, Scrippsiella trochoidea, Gyrodinium spirale, Trichodesmium thiebautii, Leptocylindrus danicus*
125 m	*Cyclotella striata, Nitzschia frustulum, Prorocentrum sigmoides, Leptocylindrus danicus, Gyrodinium spirale*
150 m	*Cyclotella striata, Trichodesmium thiebautii, Nitzschia frustulum*
DCM	*Cyclotella striata, Gyrodinium spirale*

(4) Community Structure

In 2021, the richness (D), evenness (J) and diversity index (H′) of nanoplankton in Block M were shown in Table 5-14.

1) Species richness (D): The species richness of surface nanoplankton ranged from 0.11 to 0.65. The highest value appeared at Station ES04 and the lowest at Station ES05.

2) Evenness (J): The evenness of surface nanoplankton ranged from 0.74 to 0.95. The highest value appeared at Station ES01 and the lowest at Station ES06.

3) Diversity index (H′): The diversity index of surface nanoplankton ranged from 0.76 to 2.29, with the highest value appearing at Station ES04 and the lowest at Station

ES05. Except for Station ES05, the diversity index of phytoplankton was higher than 1 at all stations in the surveyed area.

Table 5-14 Surface nanoplankton diversity index in Block M (2021)

Stations	D	J	H'
DY69-M2B1-ES01	0.26	0.95	1.50
DY69-M2B1-ES02	0.25	0.86	1.37
DY69-M2B1-ES03	0.23	0.82	1.30
DY69-M2-ES04	0.65	0.82	2.29
DY69-M2B1-ES05	0.11	0.76	0.76
DY69-M1-ES06	0.64	0.74	2.21

In 2022, the richness (D), evenness (J) and diversity index (H′) of nanoplankton in Block M were shown in Table 5-15.

1) Species richness (D): The species richness of surface nanoplankton ranged from 0.24 to 0.49. The highest value appeared at Station ES05 and the lowest at Station ES10.

2) Evenness (J): The evenness of surface nanoplankton ranged from 0.79 to 0.97. The highest value appeared at Station ES05 and the lowest at Station ES10.

3) Diversity index (H′): The diversity index of surface nanoplankton ranged from 1.25 to 2.25, with the highest value appearing at Station ES05 and the lowest at Station ES10. The diversity index of phytoplankton was higher than 1 at all stations in the surveyed area.

Table 5-15 Surface nanoplankton diversity index in Block M (2022)

Stations	D	J	H'
DY76-ES01	0.42	0.83	1.93
DY76-ES03	0.47	0.92	2.13
DY76-ES04	0.26	0.95	1.50
DY76-ES05	0.49	0.97	2.25
DY76-ES10	0.24	0.79	1.25

5.2.1.5 Zooplankton

Macro- and meso-plankton (zooplankton) were collected by vertical plankton net and multi-net. The vertical plankton net was mainly used to collect zooplankton up to 200 m, and the multi-net was used to collect zooplankton in middle and deep layer (The depth of 200-1000 m was the middle layer (disphotic layer), and the deep layer was below the middle layer to the abyssal boundary). The plankton samples were collected in the same stations during summer either in the PRZ or IRZ for each year.

(1) Species Composition

A total of 406 species (including undetermined species) of zooplankton were identified in Block M belonging to 6 phyla and 13 major groups. Among them, 160 species of Copepoda accounted for the largest proportion (39.41%) of the total zooplankton species number. In general, the surveyed area had a high level of species diversity.

A total of 200 species of zooplankton (including undetermined species) belonged to 6 phyla and 11 major groups were recorded in Block M in 2021. Copepoda and Medusae accounted for 31.4% and 16.19% of the total species number, respectively, and the rest were Tunicata, Ostracoda, and Chaetognatha, etc. (Figure 5-35).
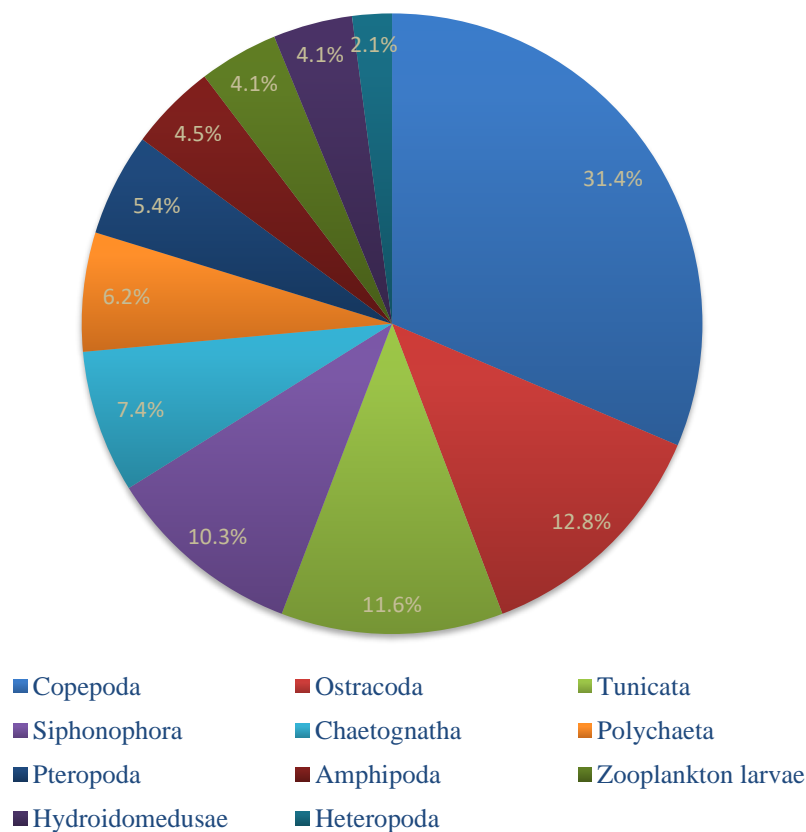
Figure 5-35 Composition of zooplankton species in 2021

A total of 220 species of zooplankton (including undetermined species) belonged to 6 phyla and 12 major groups were recorded in 2022. Copepoda accounted for the largest proportion (42.3%), and the rest were Siphonophora, Pteropoda, and Tunicata, etc. (Figure 5-36).
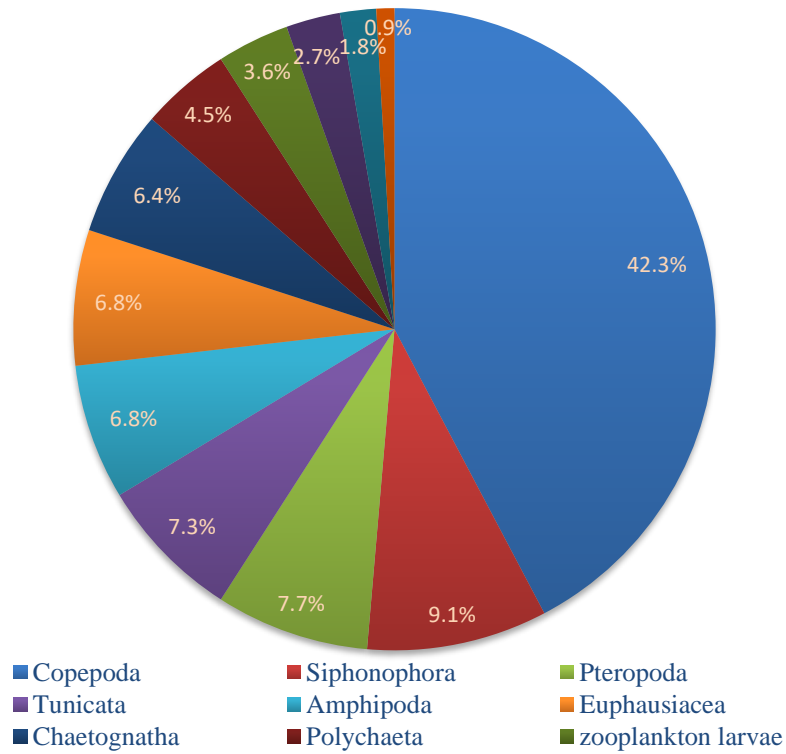
Figure 5-36 Composition of zooplankton species in 2022

A total of 213 species of zooplankton (including undetermined species) belonged to 6 phyla and 13 groups were recorded in 2023. The largest proportion of zooplankton group were Copepoda (50.7%), followed by Siphonophora, Tunicata and Euphausiid, etc. (Figure 5-37).
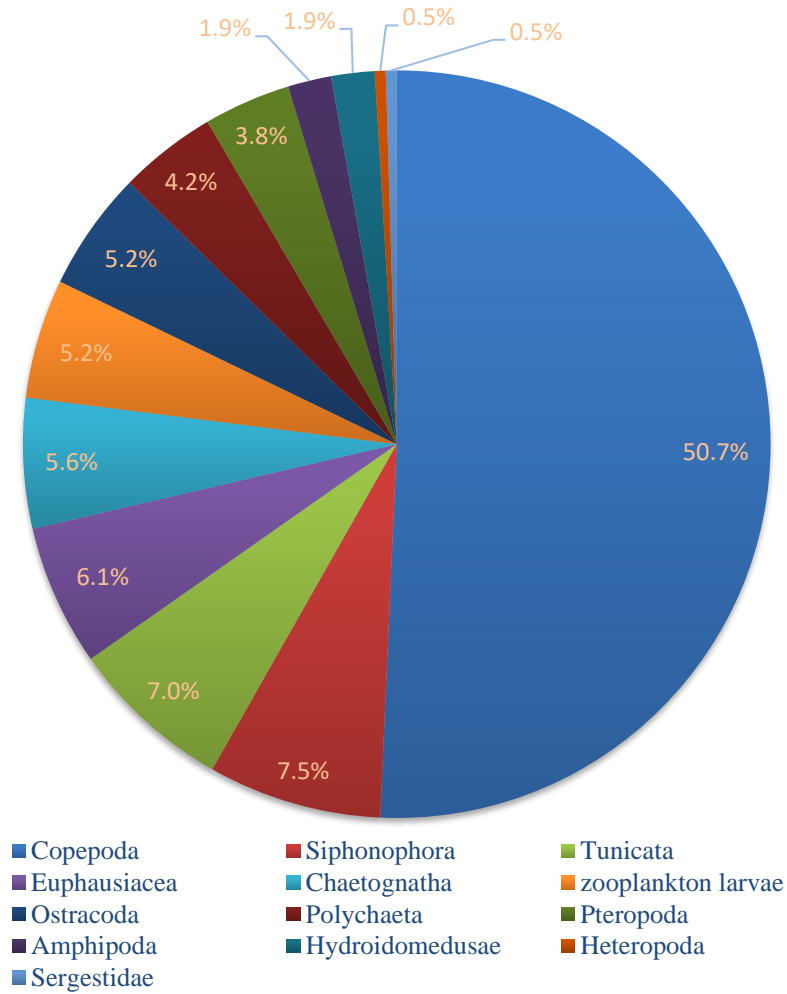
Figure 5-37 Composition of zooplankton species in 2023

(2) Abundance

Copepoda were the most dominant group in Block M in 2021, accounting for 85.17% of the total zooplankton abundance, with the dominant species of *Lucicutia flavicornis*, *Oncaea media*, and *Oithona tenuis*. This was followed by Tunicata (5.45%) and Chaetognatha (4.92%) (Figure 5-38).

Total zooplankton abundance varied from 30.86 to 106.40 ind/m^3, with an average of 79.02 ind/m^3 (Table 5-16). The horizontal distribution showed a trend of high in the south and low in the north (Figure 5-39).
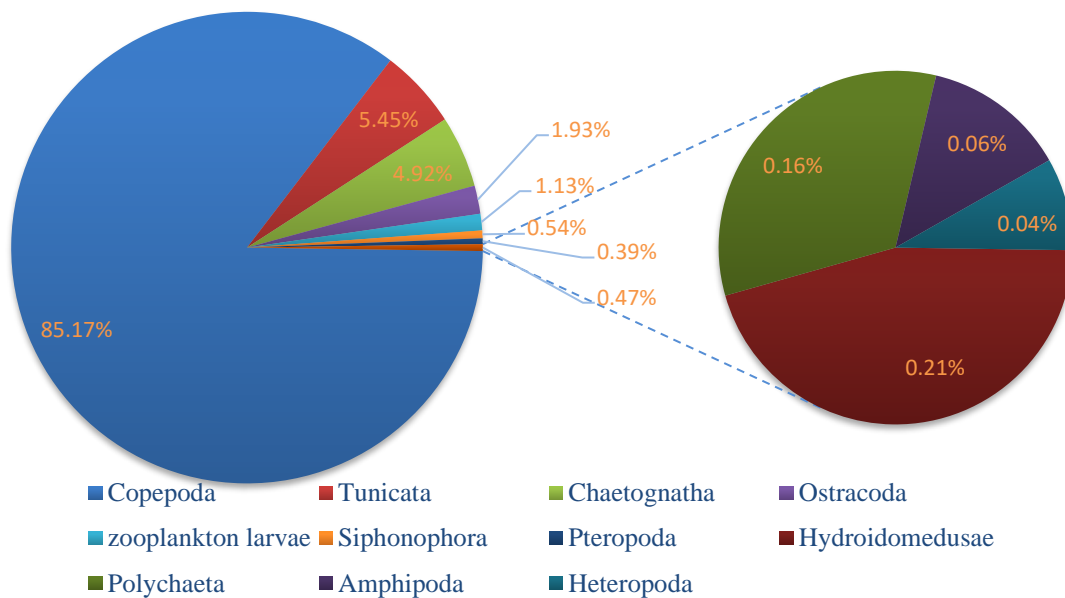
Figure 5-38 Composition of zooplankton abundance in 2021

Table 5-16 Zooplankton species number, abundance and diversity index for each station in 2021

Station	Number of species	Abundance （ind/m³）	Richness d	Evenness J′	Diversity H′(log₂)
DY69-M2B1-ES01	115	103.64	24.56	0.74	5.04
DY69-M2B1-ES02	100	106.40	21.21	0.73	4.83
DY69-M2B1-ES03	117	78.94	26.55	0.68	4.64
DY69-M2-ES04	103	54.96	25.46	0.71	4.77
DY69-M2B1-ES05	107	95.88	23.23	0.74	4.99
DY69-M1-ES06	120	82.44	26.97	0.76	5.24
DY69-M1-ES07	69	30.86	19.83	0.66	4.01
Average	104	79.02	23.97	0.72	4.79
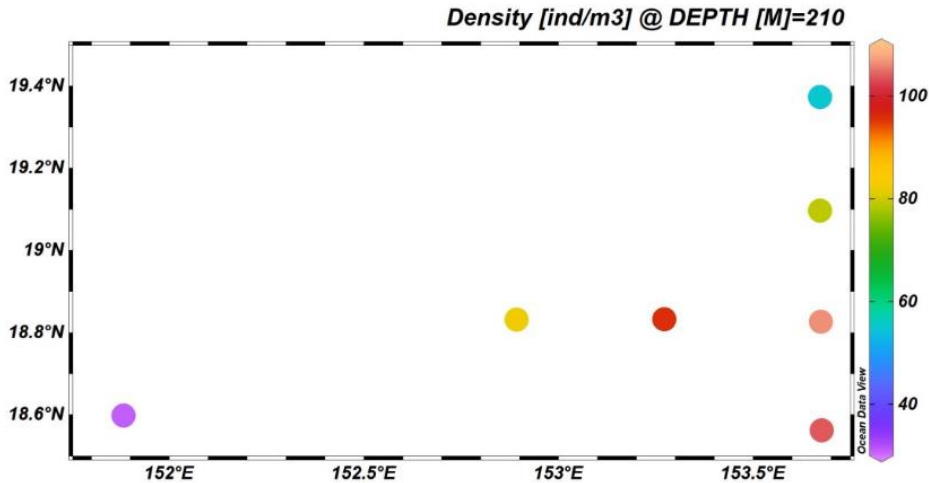
Figure 5-39 Horizontal distribution of zooplankton abundance in 2021

Zooplankton abundance in 2022 was also dominated by Copepoda (approximately 88.01% of the total zooplankton abundance), with the dominant species of Calanoida juveniles, *Oithona setigera*, *Oncaea mediterranea*, and *Acartia negligens*. This was followed by Tunicata (5.96%) and Chaetognatha (2.34%) (Figure 5-40).

Zooplankton abundance varied from 28.68 to 105.62 ind/m^3, with an average of 46.37 ind/m^3 (Table 5-17), and total abundance was lower than that in 2021 and 2023. The horizontal distribution showed a trend of high in the north and low in the south (Figure 5-41).
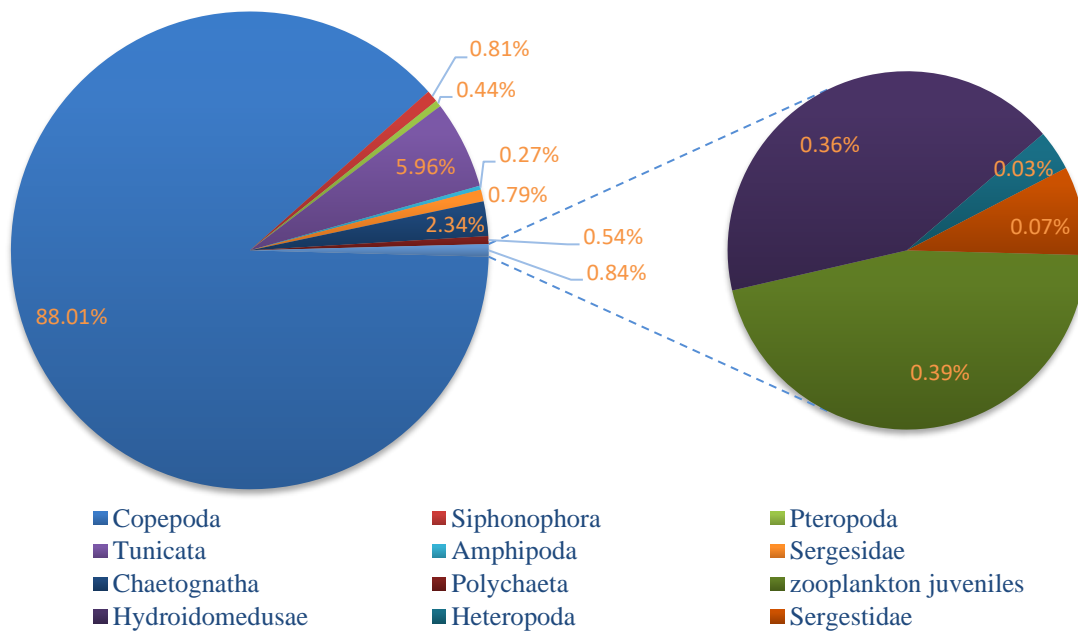
Figure 5-40 Composition of zooplankton abundance in 2022

Table 5-17 Zooplankton species number, abundance and diversity index for each station in 2022

Station	Number of species	Abundance (ind/m³)	Richness d	Evenness J′	Diversity H′(log₂)
DY76-I-M2-S059VN13	122	105.62	18.00	0.70	4.85
DY76-I-M2-S063VN14-1	95	40.12	17.65	0.75	4.95
DY76-I-M2-S063VN14-2	104	52.86	17.99	0.77	5.13
DY76-I-M2-S074VN15-1	93	30.14	18.72	0.71	4.66
DY76-I-M2-S074VN15-2	98	37.27	18.58	0.72	4.77
DY76-I-M1-S079VN16-1	86	29.93	17.33	0.69	4.42
DY76-I-M1-S079VN16-2	87	28.68	17.76	0.76	4.89
Average	97.86	46.37	18.01	0.73	4.81
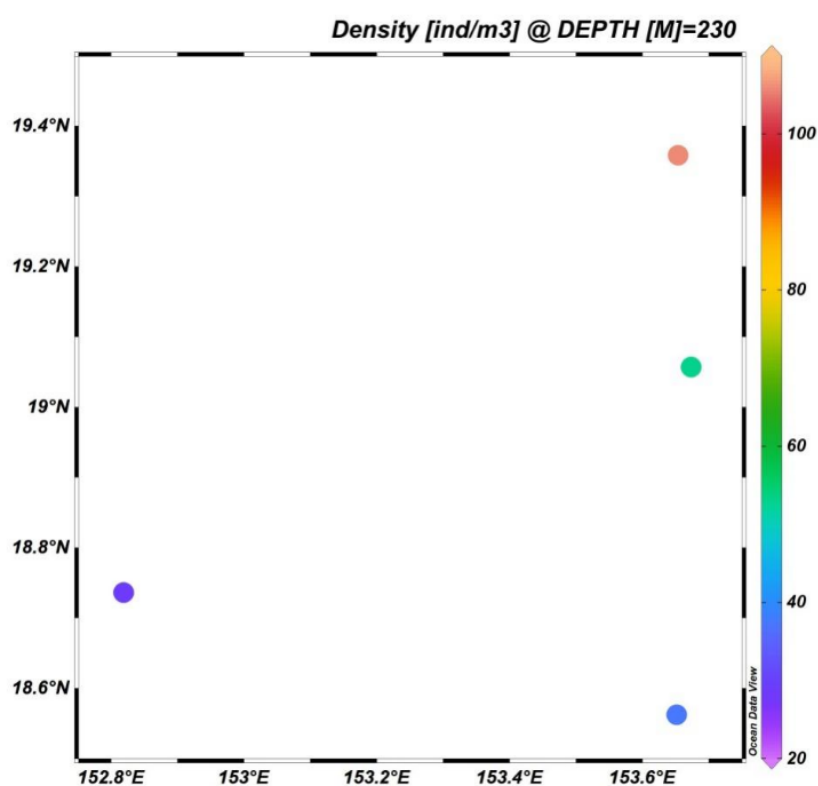
Figure 5-41 Horizontal distribution of zooplankton abundance in 2022

Zooplankton abundance in 2023 was also dominated by Copepoda (about 93.51% of total zooplankton abundance), which were dominated by Calanoida juveniles, *Oncaea venusta*, *Acartia negligens*, and *Oithona plumifera*. This was followed by Chaetognatha (2.71%) and Tunicata (1.15%) (Figure 5-42).
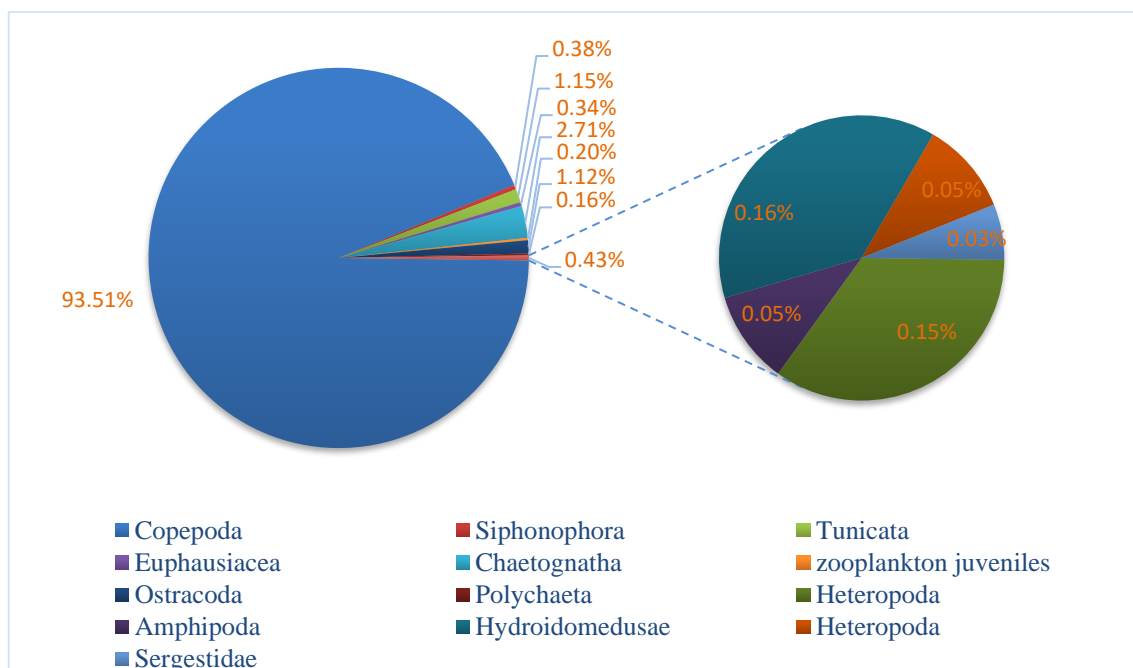
Figure 5-42 Composition of zooplankton abundance in 2023

The interval variation of total zooplankton abundance ranged from 32.20 to 167.42 ind/m^3, with an average of 88.35 ind/m^3 (Table 5-18). The horizontal distribution showed a trend of high in the north and low in the south (Figure 5-43).

Table 5-18 Zooplankton species number, abundance and diversity index for each station in 2023

Station	Number of species	Abundance （ind/m^3）	Richness d	Evenness J'	Diversity $H'(log_2)$
DY81I-M2-ES05-DX01	82	75.94	12.97	0.73	4.61
DY81I-M2-ES03-DX02	90	32.20	17.77	0.75	4.84
DY81I-M2-ES03-DX03	77	60.06	12.86	0.76	4.76
DY81I-M2-DX04	106	167.42	14.21	0.64	4.28
DY81I-M1-ES06-DX05	113	106.14	16.64	0.70	4.79
Average	93.60	88.35	14.89	0.71	4.66
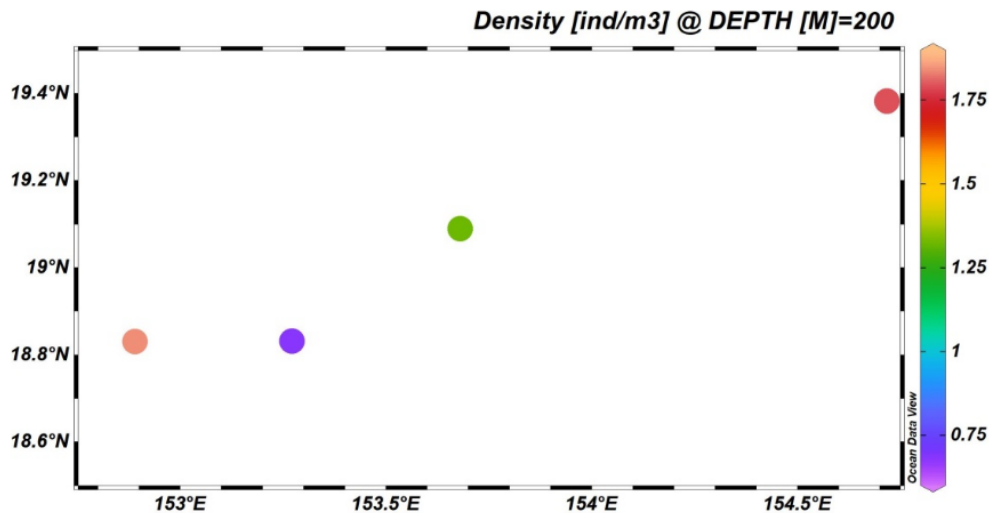
Figure 5-43 Horizontal distribution of zooplankton abundance in 2023

(3) Community Structure

An average of 104 species were detected per station in Block M in 2021, with a richness index of 23.97, reflecting the very high species richness of zooplankton in the contract area, with a diversity index averaging 4.79, and evenness averaging 0.72 (Table 5-16).

In the 2022 surveyed area, an average of 98 species were detected per station with a richness index of 18.01, reflecting the very high species richness in the surveyed area, the diversity index averaged 4.81, and the evenness averaged 0.73 (Table 5-17).

During the DY81 cruise (2023), an average of 94 species were detected per station with a richness index of 14.89, reflecting the high species richness in the surveyed area, the diversity index averaged 4.66, and the evenness averaged 0.71 (Table 5-18).

In general, the Copepoda was characterized by a prominent degree of dominance and a high number of dominant species. The zooplankton community was generally characterized by low abundance and high biodiversity.

(4) Dominant Species

Among the zooplankton identified to species in 2021, species with dominance (*Y*) greater than 0.02 included *Lucicutia flavicornis*, *Oncaea media*, and *Oithona tenuis* (Table 5-19). In addition to the dominant species listed above, there were also *Oithona setigera*, *Flaccisagitta enflata*, *Acartia negligens*, *Nannocalanus minor*, *Oncaea minuta*, *Farranula concinna*, *Pleuromamma robusta*, etc. (Table 5-19). The top ten dominant species in 2021 were all Copepoda except for *Flaccisagitta enflata*.

For the three most dominant species, the detection rate of the other two species was 100%, except for the *Oithona setigera*, which was not detected at Station ES07.

Table 5-19 Zooplankton dominant species in Block M in 2021

Group	Species	Dominance
Copepoda	*Lucicutia flavicornis*	0.028
Copepoda	*Oncaea media*	0.027
Copepoda	*Oithona tenuis*	0.020

Among the zooplankton identified to species in 2022, dominance (*Y*) greater than 0.02 included *Oithona setigera*, *Oncaea mediterranea*, *Thalia democratica*, *Lucicutia flavicornis Nannocalanus minor*, *Temoropia mayumbaensis*, and *Acartia negligens* (Table 5-20). In addition to the above dominant species, relatively dominant species included *Oncaea venusta*, *Oncaea media*, *Neomormonilla minor, Haloptilus longicornis*, *Oithona tenuis*, *Clausocalanus farrani*, *Pleuromamma gracilis*, and *Clausocalanus minor*. The top ten dominant species of the year were all Copepoda, except for *Thalia democratica*.

Table 5-20 Zooplankton dominant species in Block M in 2022

Group	Species	Occurrence frequency (%)	Dominance (*Y*)
Copepoda	*Oithona setigera*	100	0.063
Copepoda	*Oncaea mediterranea*	86	0.029
Tunicata	*Thalia democratica*	100	0.025
Copepoda	*Lucicutia flavicornis*	100	0.023
Copepoda	*Nannocalanus minor*	100	0.023
Copepoda	*Temoropia mayumbaensis*	86	0.023
Copepoda	*Acartia negligens*	71	0.021

Among the identified zooplankton in 2023, species with dominance (*Y*) greater than 0.02 included *Oncaea venusta*, *Acartia negligens*, *Oithona plumifera*, *Calocalanus pavo*, *Oithona setigera*, *Oncaea mediterranea*, and Swordflea *Oithona tenuis* (Table 5-21). The dominant species in this year were all Copepoda, reflecting the dominance of Copepoda in the zooplankton community structure.

Table 5-21 Zooplankton dominant species in Block M in 2023

Group	Species	Occurrence frequency （%）	Dominance （Y）
Copepoda	*Oncaea venusta*	100	0.086
Copepoda	*Acartia negligens*	100	0.057
Copepoda	*Oithona plumifera*	100	0.057
Copepoda	*Calocalanus pavo*	60	0.033
Copepoda	*Oithona setigera*	100	0.025
Copepoda	*Oncaea mediterranea*	80	0.022
Copepoda	*Oithona tenuis*	80	0.020

5.2.2 Mesopelagic and Abyssal Organisms

Mesopelagic and abyssal organisms were collected using a MultiNet with mesh size of 200 μm, and sampling layers of 0–50, 50–100, 100–200, 200–500, 500–1000, 1000–2000, 2000–3000, 3000–4000, 4000–4500 m.

5.2.2.1 Community Structure in 2021

In 2021, there were 397 species of zooplankton belonged to 11 phyla and 15 classes (including undetermined species), of which Copepoda and Medusae were the dominant groups, accounting for 53.90% and 11.95% of the total zooplankton abundance, respectively. The rest were Ostracoda, Tunicata, Chaetognatha and Pteropoda.

(1) Zooplankton Species Composition and Biodiversity at 200~500 m

A total of 183 species of macro- and meso- plankton were recorded from 200 to 500 m, accounting for 41.03% of the total species number, with the dominant groups of Copepoda, Ostracoda and Medusae accounting for 50.82%, 17.49% and 13.66% of the total abundance, respectively.

An average of 62 species were detected per station from 200 to 500 m, with a richness index of 24.78, a diversity index averaging 3.89, and evenness averaging 0.65 (Table 5-22).

Table 5-22 Zooplankton community structure and diversity index in the 200–500 m layer in 2021

Station	Number of species	Abundance(ind/m³)	Richness d	Evenness J'	Diversity H'(log₂)
DY69-M2-ES04-BIO01	78	8.60	35.79	0.76	4.75
DY69-M2B1-ES03-BIO02	50	4.19	34.22	0.74	4.16
DY69-M2B1-ES03-BIO03	63	11.69	25.22	0.74	4.42
DY69-M1-ES06-BIO04	52	23.35	16.19	0.56	3.19
DY69-M1-ES06-BIO05	65	27.85	19.24	0.61	3.66
DY69-M2B1-ES05-BIO06	67	18.52	22.61	0.61	3.69
DY69-M2B1-ES01-BIO07	61	19.61	20.16	0.56	3.34
Average	62	16.26	24.78	0.65	3.89

Among the zooplankton identified to species, species with dominance (Y) greater than 0.02 included Copepoda such as *Neomormonilla minor*, *Oithona setigera,* and *Haloptilus longicornis* (Table 5-23).

Although abundance showed a decreasing trend with increasing depth, diversity remained extremely high.

Table 5-23 Zooplankton dominant species in the 200–500m layer in 2021

Group	Species	Dominance
Copepoda	*Neomormonilla minor*	0.13
Copepoda	*Oithona setigera*	0.05
Copepoda	*Haloptilus longicornis*	0.03

(2) Zooplankton Species Composition and Biodiversity at 500~1000 m

A total of 128 species of macro- and meso-zooplankton were recorded in the 500-1000 m layer, accounting for 28.70% of the total species number, and Copepoda and Ostracoda were the dominant groups in this layer.

An average of 38 species were detected per station in the 500–1000 m layer, with the richness index of 25.12, diversity index averaging 3.06, and evenness averaging 0.58 (Table 5-24).

Table 5-24 Zooplankton community structure and diversity index in the 500~1000m layer in 2021

Station	Number of species	Abundance (ind/m³)	Richness d	Evenness J'	Diversity H'(log₂)
DY69-M2-ES04-BIO01	53	7.12	26.49	0.51	2.93
DY69-M2B1-ES03-BIO02	37	1.91	55.67	0.57	2.99
DY69-M2B1-ES03-BIO03	35	6.73	17.84	0.57	2.92
DY69-M1-ES06-BIO04	33	5.72	18.34	0.68	3.41
DY69-M1-ES06-BIO05	39	5.95	21.30	0.59	3.14
DY69-M2B1-ES05-BIO06	35	6.59	18.03	0.54	2.79
DY69-M2B1-ES01-BIO07	37	7.27	18.15	0.61	3.19
Average	38	5.90	25.12	0.58	3.06

Among the zooplankton identified to species, species with dominance (Y) greater than 0.02 included Copepoda such as *Neomormonilla minor*, *Oncaea gracilis*, and *Oncaea ornate* (Table 5-25).

Although the number and abundance of species declined sharply with water depth, their species richness showed an increasing trend.

Table 5-25 Zooplankton dominant species in the 500–1000m layer in 2021

Group	Species	Dominance
Copepoda	*Neomormonilla minor*	0.30
Copepoda	*Oncaea gracilis*	0.18
Copepoda	*Oncaea ornata*	0.08

(3) Zooplankton Species Composition and Biodiversity at 1000~2000 m

A total of 109 species of macro- and meso-zooplankton were collected and recorded in the 1000~2000 m layer, accounting for 24.44% of the total species number. Consistent with the dominant groups in the 500~1000 m layer, Copepoda and Ostracoda were still the dominant groups, accounting for 75.23% and 11.93% of the total zooplankton abundance in this layer and the proportion of Copepoda in the community structure further increased.

An average of 27 species were detected per station from 1000 to 2000 m. The richness index averaged 201.64, the diversity index averaged 2.75, and the evenness averaged 0.59 (Table 5-26).

Table 5-26 Zooplankton community structure and diversity index in the 1000~2000m layer in 2021

Station	Number of species	Abundance (ind/m³)	Richness d	Evenness J′	Diversity H′(log₂)
DY69-M2-ES04-BIO01	19	0.69	NA	0.59	2.49
DY69-M2B1-ES03-BIO02	17	0.40	NA	0.60	2.45
DY69-M2B1-ES03-BIO03	34	1.08	446.08	0.57	2.89
DY69-M1-ES06-BIO04	34	1.80	56.31	0.55	2.79
DY69-M1-ES06-BIO05	34	1.38	102.54	0.55	2.78
DY69-M2B1-ES05-BIO06	28	0.85	NA	0.63	3.05
DY69-M2B1-ES01-BIO07	20	0.99	NA	0.65	2.82
Average	27	1.03	201.64	0.59	2.75

Among the zooplankton identified to species, species with dominance (Y) greater than 0.02 included Copepoda such as *Neomormonilla minor*, *Oncaea gracilis*, and *Oncaea ornate* (Table 5-27).

Abundance still declined rapidly with water depth, but the decreasing trend of the species number appeared to be moderated, with an increase in their species richness.

Table 5-27 Zooplankton dominant species in the 1000–2000m layer in 2021

Group	Species	Dominance
Copepoda	*Neomormonilla minor*	0.13
Copepoda	*Oncaea gracilis*	0.05
Copepoda	*Oncaea ornata*	0.03

(4) Zooplankton Species Composition and Biodiversity at 2000~3000 m

A total of 75 species of macro- and meso-zooplankton were recorded in the 2000~3000 m layer, accounting for 16.82% of the total recorded species, with Copepoda and Ostracoda still being the main groups, accounting for 82.67% and 12.00% of the total zooplankton abundance in this layer, respectively.

An average of 18 species were detected per station from 2000 to 3000 m. The richness index declined to 0.24, the diversity index averaged 3.04, while the stability of the community structure was constantly changing, and the evenness averaged 0.76, with the dominance of Copepoda being extremely prominent (Table 5-28).

Table 5-28 Zooplankton community structure and diversity index in the 2000~3000m layer in 2021

Station	Number of species	Abundance (ind/m³)	Richness d	Evenness J'	Diversity H'(log₂)
DY69-M2-ES04-BIO01	22	0.11	0.87	3.88	22.00
DY69-M2B1-ES03-BIO02	14	0.13	0.80	3.06	14.00
DY69-M2B1-ES03-BIO03	29	0.34	0.66	3.21	29.00
DY69-M1-ES06-BIO04	24	0.66	0.66	3.04	24.00
DY69-M1-ES06-BIO05	19	0.18	0.78	3.30	19.00
DY69-M2B1-ES05-BIO06	8	0.03	0.88	2.65	8.00
DY69-M2B1-ES01-BIO07	10	0.27	0.65	2.15	10.00
Average	18	0.24	0.76	3.04	18.00

Among the zooplankton identified to species, species with dominance (Y) greater than 0.02 included Copepoda such as *Oncaea ornata*, *Oncaea gracilis*, *Neomormonilla minor*, *Spinocalanus oligospinosus*, and other copepods (Table 5 -27). Abundance and number of species continued to decline with increasing depth.

Table 5-29 Zooplankton dominant species in the 2000–3000m layer in 2021

Group	Species	Dominance
Copepoda	*Oncaea ornata*	0.18
Copepoda	*Oncaea gracilis*	0.17
Copepoda	*Neomormonilla minor*	0.11
Copepoda	*Spinocalanus oligospinosus*	0.02

(5) Zooplankton Species Composition and Biodiversity at 3000~4000 m

A total of 50 species of macro- and meso-zooplankton were recorded from 3000 to 4000 m, accounting for 11.21% of the total species number, and Copepoda was the only dominant group, accounting for 84.00% of the total zooplankton abundance in this layer.

An average of 12 species were detected per station from 3000 to 4000 m, with the richness index of 0.09, and the diversity index averaged 2.83 (Table 5-30).

Among the zooplankton identified to species, species with dominance (Y) greater than 0.02 included Copepoda such as *Oncaea ornata*, *Neomormonilla minor*, and *Oncaea gracilis* (Table 5-31).

Table 5-30 Zooplankton community structure and diversity index in the 3000~4000m layer in 2021

Station	Number of species	Abundance (ind/m³)	Richness d	Evenness J'	Diversity H'(log₂)
DY69-M2-ES04-BIO01	14	0.04	0.81	3.07	14.00
DY69-M2B1-ES03-BIO02	6	0.02	0.84	2.16	6.00
DY69-M2B1-ES03-BIO03	16	0.17	0.71	2.83	16.00
DY69-M1-ES06-BIO04	20	0.12	0.79	3.40	20.00
DY69-M1-ES06-BIO05	10	0.10	0.75	2.48	10.00
DY69-M2B1-ES05-BIO06	13	0.04	0.97	3.58	13.00
DY69-M2B1-ES01-BIO07	7	0.15	0.82	2.29	7.00
Average	12	0.09	0.81	2.83	12.29

Table 5-31 Zooplankton dominant species in the 3000–4000m layer in 2021

Group	Species	Dominance
Copepoda	*Oncaea ornata*	0.20
Copepoda	*Neomormonilla minor*	0.12
Copepoda	*Oncaea gracilis*	0.11

(6) Zooplankton Species Composition and Biodiversity at 4000~4500 m

A total of 64 species of macro- and meso-zooplankton were recorded from 4000 to 4500 m, accounting for 14.35% of the total species number, and Copepoda was the only dominant group, accounting for 90.14% of the total zooplankton abundance in this layer.

An average of 18 species were detected per station from 4000 to 4500 m. The diversity index averaged 2.96, and the evenness averaged 0.83 (Table 5-32).

Oncaea ornata, *Neomormonilla minor* and *Oncaea gracilis* remained the main dominant species.

Table 5-32 Zooplankton community structure and diversity index in the 4000~4500m layer in 2021

Station	Number of species	Abundance (ind/m³)	Evenness J'	Diversity H'(log₂)
DY69-M2-ES04-BIO01	7	0.14	0.98	2.75
DY69-M2B1-ES03-BIO02	20	0.52	0.81	3.50
DY69-M2B1-ES03-BIO03	26	0.42	0.83	3.88
DY69-M1-ES06-BIO04	24	0.37	0.85	3.89
DY69-M1-ES06-BIO05	34	0.39	0.78	3.99
DY69-M2B1-ES05-BIO06	NA	NA	NA	NA
DY69-M2B1-ES01-BIO07	12	0.48	0.75	2.68
Average	18	0.33	0.83	2.96

5.2.2.2 Community Structure in 2022

In 2022, four stations were settled in the surveyed area for stratified sampling, and a total of 317 species of zooplankton (including undetermined species were identified belonged to 6 phyla and 13 groups, with Copepoda accounting for the largest proportion (59.54%) of the total abundance, followed by Euphausia, Siphonophora, Pteropoda, and Chaetognatha (Figure 5-44).
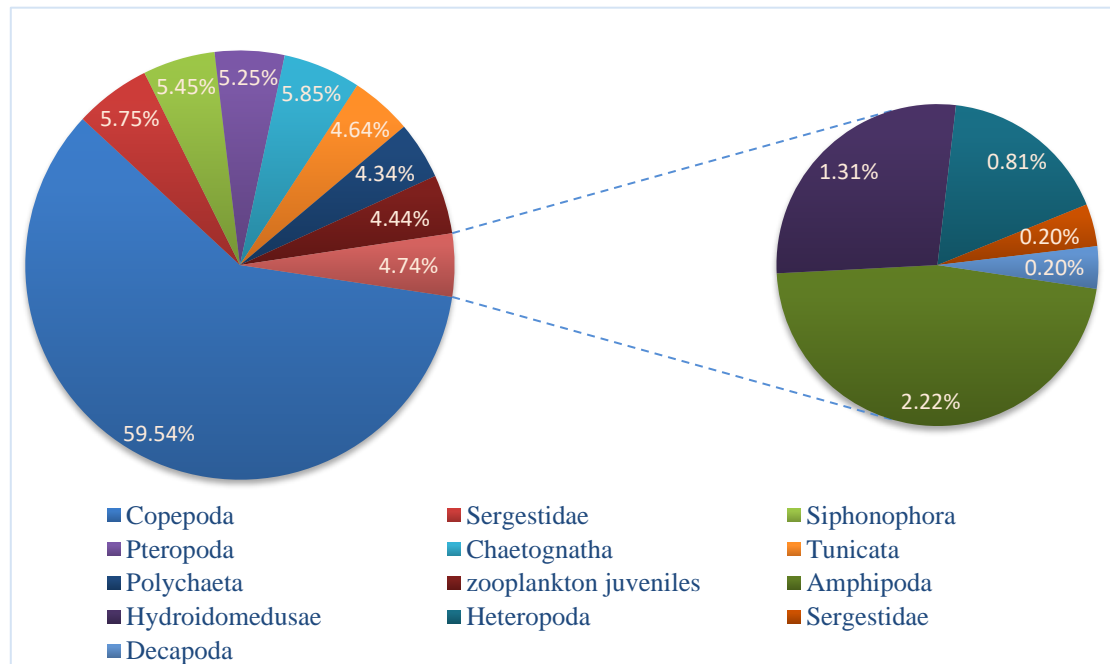
Figure 5-44 Verticalspecies composition of zooplankton in 2022

(1) Zooplankton Species Composition in the surface layer (0~50 m)

The zooplankton species number in the surface layer was small, with a total of 75 species recorded, with Copepoda, Tunicata, Pteropoda, and zooplankton juveniles accounting for 48.00%, 12.00%, 12.00%, and 8.00% of the total species number, respectively. Copepoda accounted for 91.11% of the total zooplankton abundance in this layer.

(2) Zooplankton Species Composition in the subsurface layer (50~100 m)

A total of 138 species of zooplankton were recorded in the subsurface layer, which was higher than the species number in the surface layer. Copepoda, Tunicata, Chaetognatha, Siphonophora, Pteropoda, zooplankton juveniles, and Euphausia accounted for 45.65%, 7.97%, 7.97%, 7.25%, 7.25%, 6.52%, and 5.80% of the total species number, respectively. Copepoda accounted for 94.85% of the total zooplankton abundance in this layer.

(3) Zooplankton Species Composition in the 100~200 m layer

A total of 153 species of zooplankton were recorded in this layer, slightly more than that in the subsurface layer, with Copepoda, Chaetognatha, Siphonophora, Polychaeta, Euphausia, and zooplankton juveniles accounting for 55.56%, 8.50%, 7.19%, 5.88%, 5.88%, and 5.23% of the total species number, respectively. Copepoda accounted for 96.49% of the total zooplankton abundance in this layer.

(4) Zooplankton Species Composition in the 200~500 m layer

A total of 116 species of zooplankton were recorded in this layer. Although the species number decreased slightly with the increase of depth, it was still an important distribution layer of zooplankton, with Copepoda, Euphausia, Chaetognatha, and Siphonophora accounting for 54.31%, 10.34%, 9.48%, 7.76%, and 5.17% of the total species number, respectively. Copepoda accounted for 98.66% of the total zooplankton abundance in this layer.

(5) Zooplankton Species Composition in the 500~1000 m layer

A total of 73 zooplankton species were recorded in this layer, and the species diversity was still high, with Copepoda accounting for 84.93% of the total species number and 99.52% of the total zooplankton abundance, respectively.

(6) Zooplankton Species Composition in the 1000~2000 m layer

A total of 49 zooplankton species were recorded in this layer, and the abundance and diversity showed a sharp decrease with the increase of depth, Copepoda accounted for 87.76% of the total species and 99.52% of the total abundance, respectively.

(7) Zooplankton Species Composition in the 2000~3000 m layer

A total of 21 zooplankton species were recorded in this layer, with an obvious decrease in abundance and diversity. Copepoda accounted for 95.24% of the total species and 99.13% of the total abundance, respectively.

(8) Zooplankton Species Composition in the 3000~4000 m layer

A total of 32 zooplankton species were recorded in this layer, accounting for 10.09% of the total species number recorded in the stratified sampling, with Copepoda dominating (87.50%), and one species was recorded for Tunicata, Polychaeta, Pteropoda, and Pteropoda respectively. Copepoda accounted for 98.28% of the total zooplankton abundance.

(9) Zooplankton Species Composition in the 4000~45000 m layer

A total of 17 species of zooplankton were recorded in this layer, with very low abundance and diversity, which was dominated by Copepoda (94.12%), and one species

was recorded for zooplankton juveniles. Copepoda accounted for 98.10% of the total zooplankton abundance in this layer.

5.2.2.3 Vertical Distribution in 2021

The results in 2021 showed that the abundance of zooplankton was vertically distributed, with a maximum value in the surface layer (0~50 m), followed by the subsurface layer (50~100 m). The species richness of zooplankton was the highest in the mid-water layer (200~1000 m), followed by the subsurface layer and the surface layer. The species number and abundance of zooplankton showed an obvious decreasing trend with the increase of the depth, and the abundance of zooplankton was extremely low in the deeper water layer, but the species number still maintained a high level, showing a very high species diversity. When reaching a certain depth ($\geq$3000 m), its abundance and species diversity showed an increasing trend (Figure 5-45~Figure 5-48). Among them, Copepoda dominated in all water layers, and showed the same characteristics with the overall distribution trend of zooplankton. With the increase of depth, its proportion in the vertical community structure and dominance gradually increased. In the horizontal distribution (Figure 5-48), the distribution of zooplankton in the surface layer was similar to that in the euphotic layer, indicating that the distribution of zooplankton in the euphotic layer was dominated by that of the surface layer. The abundance in deeper water layers was all low. The overall distribution trend was high in the south, low in the north, and high in the west, low in the east.

0–50 m

3.61% 4.22%
9.04%
1.20%
3.61%
1.81%
6.63%
6.63%
8.43%
7.23%
47.59%

200–500 m

3.28% 0.55% 3.83%
0.55%
2.73%
1.64%
10.93%
2.19%
6.01%
17.49%
50.82%

2000–3000 m

1.33% 1.33% 1.33% 1.33%
12.00%
82.67%

50–100 m

5.15% 1.03%
4.64%
6.19%
1.03%
5.67%
1.55%
7.73%
6.70%
7.22%
9.79%
43.30%

500–1000 m

0.78% 0.78%
0.78%
3.91%
1.56%
6.25%
19.53%
62.50%
3.91%

3000–4000 m

2.00% 2.00% 2.00%
2.00%
8.00%
84.00%

100–200 m

3.90% 4.33%
5.19%
0.87%
5.63%
2.60%
8.23%
8.23%
5.19%
11.69%
44.16%

1000–2000 m

0.92% 0.92% 0.92%
2.75%
0.92%
2.75%
11.93%
75.23%
3.67%

4000–4500 m

4.69% 4.69% 1.56%
89.06%

■ Copepoda   ■ Ostracoda   ■ Chaetognatha   ■ Tunicata

■ Siphonophora   ■ Amphipoda   ■ Polychaeta   ■ Heteropoda

■ Pteropoda   ■ Hydroidomedusae   ■ zooplankton juveniles   ■ Scyphomedusae

Figure 5-45 Zooplankton species composition in different water layers in 2021
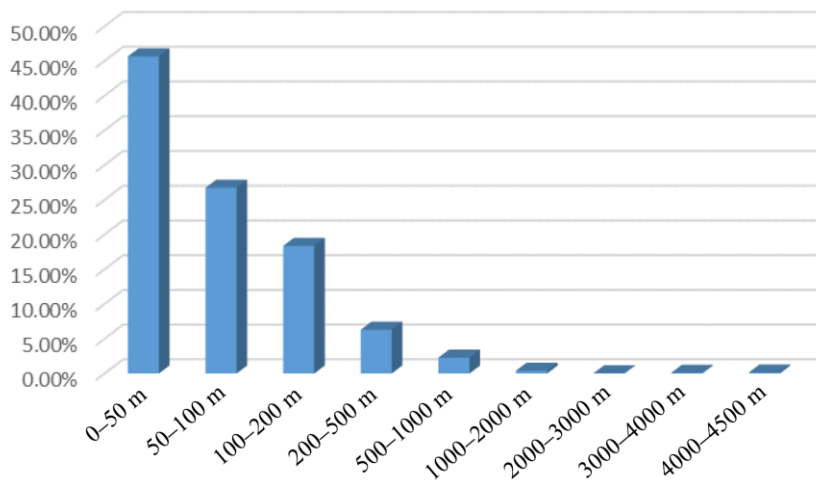
Figure 5-46 Vertical distribution of zooplankton abundance in 2021
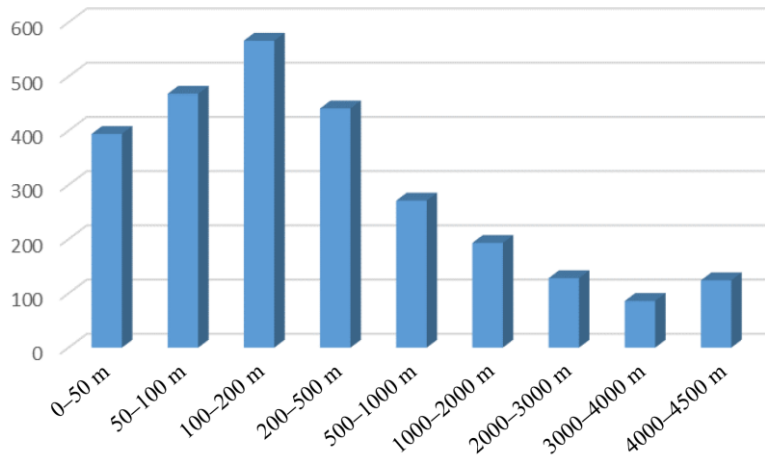
Figure 5-47 Vertical distribution of zooplankton species number in 2021
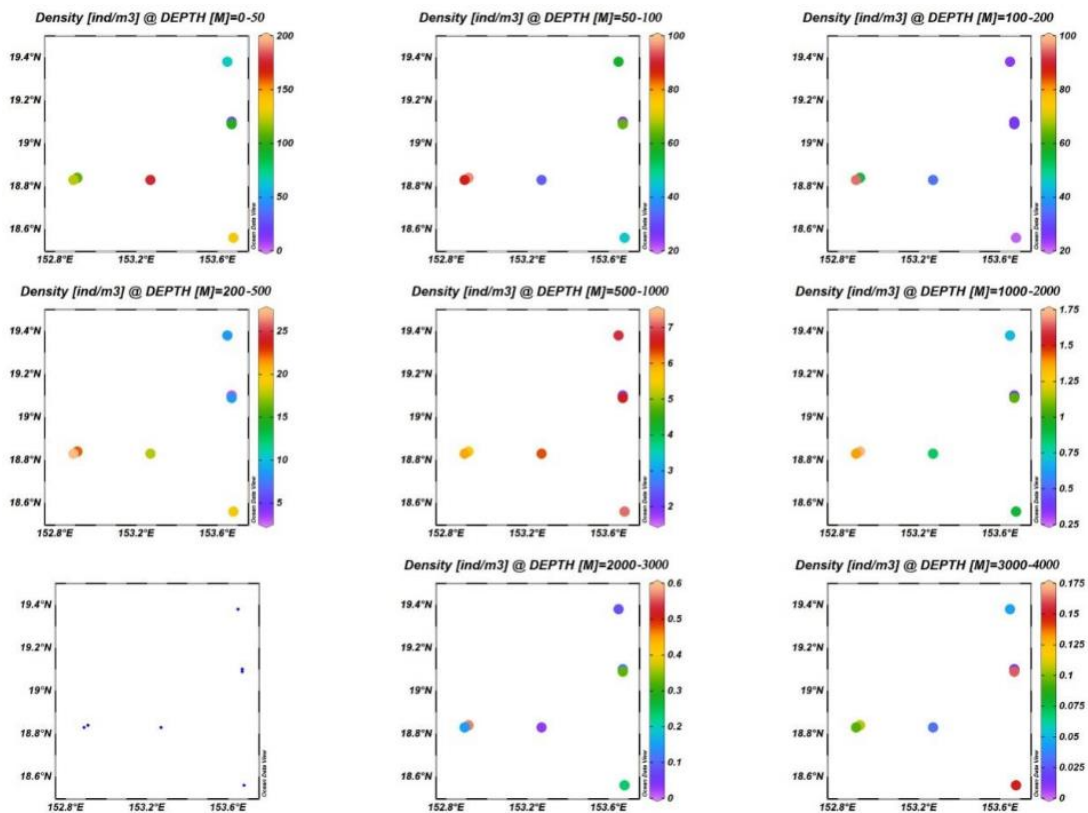
Figure 5-48 Zooplankton abundance in different water layers in 2021

5.2.2.4 Vertical Distribution in 2022

The results in 2022 showed that the vertical distribution of abundance showed a maximum value in the subsurface layer (50–100 m), followed by the 100–200 m layer. With the increase of depth, the species number and abundance of zooplankton showed an obvious decreasing trend, and the abundance of zooplankton was extremely low in deeper water, but the species number still maintained a certain level (Figure 5-49). Among them, Copepoda was dominant in all water layers and showed the same

characteristics with the overall distribution trend of zooplankton, and their proportion in the zooplankton community gradually increased with the increase of depth.
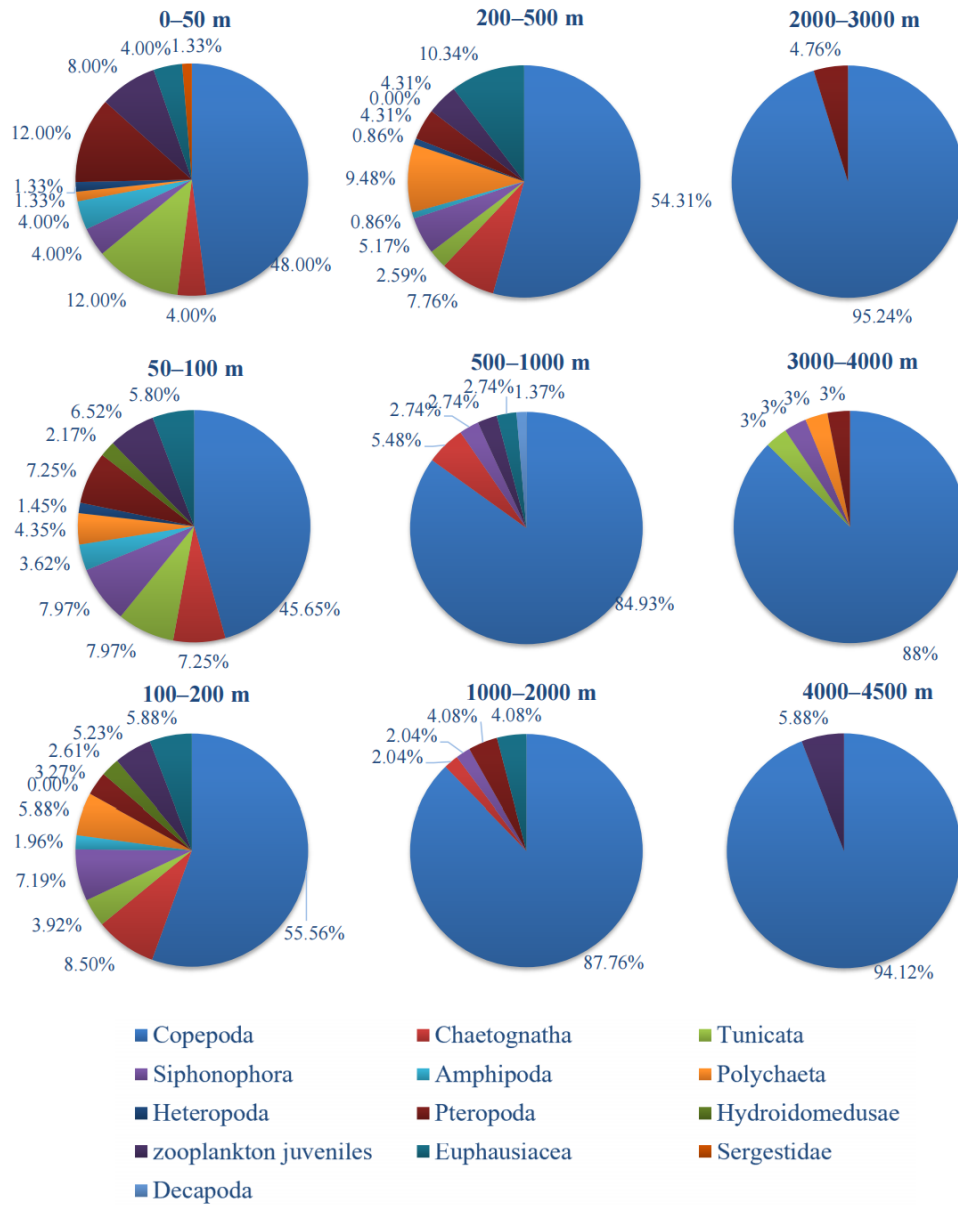
Figure 5-49 Zooplankton species composition in different water layers in 2022
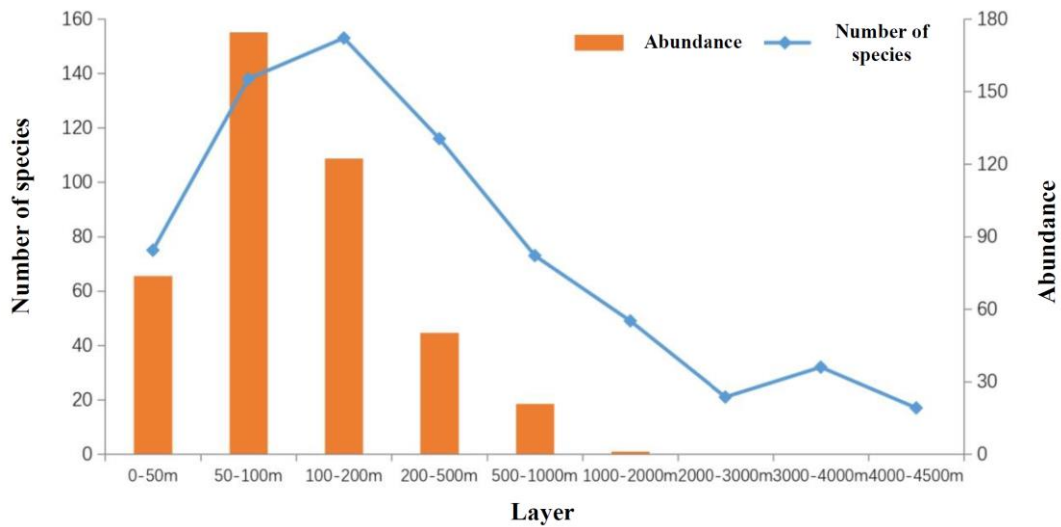
Figure 5-50 Vertical distribution of zooplankton species number and abundance in 2022

5.2.2.5 Diurnal Migration

In 2021, one station was settled to investigate zooplankton vertical stratification diurnally in Block M2, and twice vertical stratification sampling at 12-h intervals were conducted for the study of zooplankton vertical migration in the pelagic layer. In general, the number of species and abundance of zooplankton sampled at night were higher than those sampled at day (Figure 5-51). In the upper 200 m water layer where zooplankton mainly lived, diurnal variation was shown in the surface water. Zooplankton migrated from the deep layer to the surface layer at night. In the middle water layer, the number of species did not change much, but the abundance showed relatively large changes at night. The variation of species number and abundance in the water layer deeper than 200 m indicated that the species in the deep water layer also had diurnal vertical migration behavior.
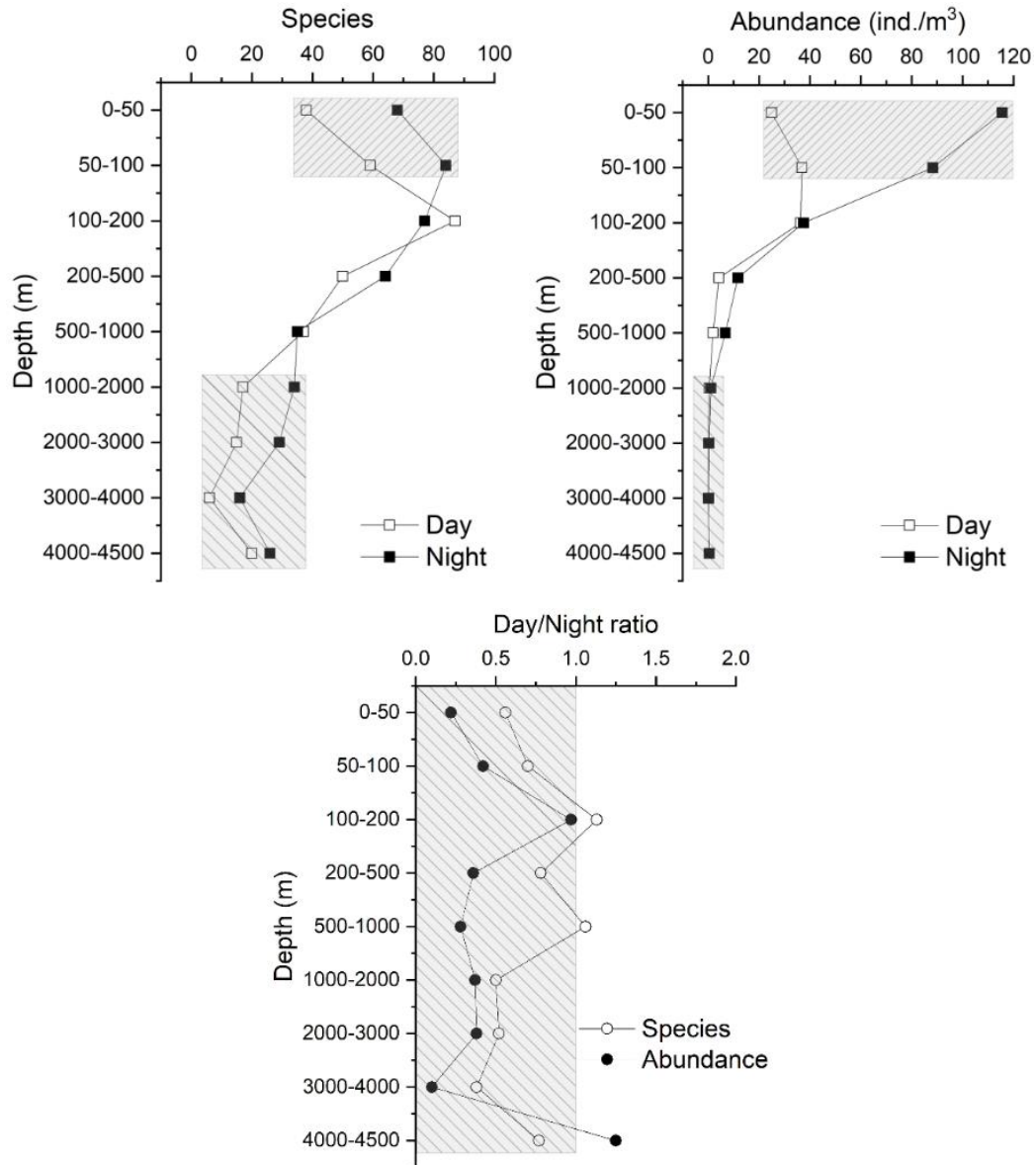
Figure 5-51 Vertical diurnal variation in zooplankton species number and abundance

Among the major zooplankton groups, the vertical diurnal variation of Copepoda was consistent with the overall trend, indicating that Copepoda dominated the migration of the zooplankton community (Table 5-33, Table 5-34); vertical migration of Ostracoda and Pteropoda in the euphotic layer was not obvious.

Table 5-33 Diurnal variation of zooplankton species number in Block M

Layer (m)	Copepoda		Tunicata		Chaetognatha		Ostracoda		Medusae		Larva		Pteropoda	
	D	N	D	N	D	N	D	N	D	N	D	N	D	N
0~50	11	38	3	5	6	6		2	8	6	5	5	5	2
50~100	31	37	1	7	6	9	6	6	9	5	2	4	4	5
100~200	34	34	6	8	6	8	18	13	7	4	6	5	2	3
200~500	23	27	1		4	5	14	18	11		2	3	2	2
500~1000	31	27	1		1	1	3	5			1	2		
1000~2000	15	26				1	1	4			1	3		
2000~3000	13	26	1				1	3						
3000~4000	6	15						1						
4000~4500	17	24			2	1	1	1						
Total	181	254	13	20	25	31	44	53			17	22	13	12

Note: "D" is Daytime; "N" is Night.

Table 5-34 Diurnal variation of zooplankton abundance in Block M (ind/m^3)

Layer (m)	Copepoda		Tunicata		Chaetognatha		Ostracoda		Medusae		Larva		Pteropoda	
	D	N	D	N	D	N	D	N	D	N	D	N	D	N
0~50	20.00	108.15	0.27	0.52	3.23	5.33		0.07	1.24	0.45	0.31	0.33	0.27	0.11
50~100	33.55	79.23	0.03	0.54	2.13	6.77	0.32	0.31	0.33	0.29	0.13	0.35	0.19	0.27
100~200	33.94	33.45	0.20	0.22	0.52	1.55	1.00	1.78	0.20	0.12	0.23	0.17	0.03	0.07
200~500	3.67	10.36	0.01		0.21	0.10	0.24	1.11	0.09		0.01	0.04	0.01	0.01
500~1000	1.88	6.64	0.00		0.01	0.03	0.01	0.04			0.00	0.01		
1000~2000	0.40	1.05				0.00	0.00	0.01			0.00	0.01		
2000~3000	0.12	0.33	0.00				0.00	0.01						
3000~4000	0.02	0.17						0.00						
4000~4500	0.51	0.40			0.01	0.01	0.01	0.01						
Total	94.08	239.78	0.51	1.28	6.10	13.79	1.59	3.35	1.85	0.87	0.68	0.90	0.50	0.46

Note: "D" is Daytime; "N" is Night.

.

5.2.3 Benthos

5.2.3.1 Microbe

5.2.3.1.1 Alpha Diversity

During 2022 cruise, we used multicorer and box-corer to collect sediment samples in Blocks M1 and M2 of the contract area for microbe diversity analysis. We extracted DNA from the sediment samples and specifically amplifying one or two consecutive high-variable regions, and sequencing the sequences of the high-variable regions by using a high-throughput sequencing platform. The sequencing data were processed and analyzed by bioinformatics analysis methods to obtain information on the diversity of microbe communities in this area. The statistical results of microbe diversity indices of all stations are shown in Table 5-35, and the Shannon diversity index ranged from 4.8 to 10.3.

Table 5-35 Statistics of Sediment Microbe Diversity Index in the Contract Area

Station	Feature Count	Chao	Shannon	Observed_features	Faith_pd	Evenness
DY75II-M1-MC09	37052	552	8.8641	552	25.5665	0.9731
DY75II-M1-MC10	31108	511	8.8052	511	24.777	0.979
DY75II-M1-MC11	61121	129	5.2463	129	4.037	0.7489
DY75II-M1-MC12	31197	512	8.805	512	23.5071	0.9791
DY75II-M1-MC13	24190	384	8.404	384	21.4177	-
DY75II-M1-MC14	22380	370	8.3051	370	18.6836	-
DY75II-M2-MC03C	28270	465	8.6646	465	24.564	-
DY75II-M2-MC15	29291	497	8.7613	497	25.0655	0.9785
DY75II-M2-MC16	47226	733	9.3369	733	30.5973	0.9802
DY75I-M1-BC69	81836	1056	9.3165	1056	39.9485	0.926
DY75I-M1-BC70	68782	793	8.917	793	32.7375	0.9244
DY75I-M1-BC71	43519	663	9.1241	663	32.3577	0.9734
DY75I-M1-BC72	115651	196	4.7901	196	9.9086	0.6257
DY75I-M1-BC73	74382	945	9.2436	945	34.0032	0.9341
DY75I-M1-BC74	102804	1251	9.6553	1251	40.9963	0.9369
DY75I-M2-BC03A	102527	1336	9.8644	1336	41.5587	0.9473
DY75I-M2-BC04	110309	1441	10.0323	1441	45.425	0.9532
DY75I-M2-BC05	83691	1256	9.853	1256	40.366	0.9555
DY75I-M2-BC06	41517	670	9.0998	670	28.5449	0.9678
DY75I-M2-BC07	93201	1166	9.3779	1166	39.2628	0.917
DY75I-M2-BC08	107511	1410	10.0387	1410	43.5476	0.9565
DY75I-M2-BC09	108365	1489	10.1172	1489	45.5587	0.9568
DY75I-M2-BC10	108180	1387	9.9711	1387	41.6596	0.9537
DY75I-M2-BC11	91586	1467	10.0279	1466	45.4746	0.9502
DY75I-M2-BC12	114470	1549	10.1619	1549	44.4784	0.9568

Station	Feature Count	Chao	Shannon	Observed_features	Faith_pd	Evenness
DY75I-M2-BC13	111584	1396	9.75	1396	42.8527	0.9305
DY75I-M2-BC14	117550	1644	10.2902	1644	43.2209	0.9602
DY75I-M2-BC15	93475	1366	10.0997	1366	40.9588	0.9673
DY75I-M2-BC16A	79368	1254.25	9.8918	1254	38.2554	0.9593
DY75I-M2-BC17	121513	1629	10.2444	1629	47.7173	0.9564
DY75I-M2-BC18	82750	1135	9.6361	1135	36.4586	0.947
DY75I-M2-BC19	95652	1394	9.9413	1394	43.2818	0.9492
DY75I-M2-BC20	91624	1168	9.5211	1168	38.2516	0.9315
DY75I-M2-BC21	67866	1059	9.6357	1059	35.2821	0.9572
DY75I-M2-BC22	63666	1006	9.6873	1006	36.9955	0.9692
DY75I-M2-BC23	64248	1095	9.7649	1095	37.3474	0.9654
DY75I-M2-BC24	68016	1158	9.84	1158	38.7535	0.9651
DY75I-M2-BC25	100328	1427	10.0571	1427	41.2474	0.9572
DY75I-M2-BC26	90445	1261	9.9522	1261	40.4361	0.9645
DY75I-M2-BC27	59534	958	9.632	958	36.8618	0.9716
DY75I-M2-BC28	91347	1289	9.9542	1289	40.3927	0.9606
DY75I-M2-BC29	29363	487	8.6864	487	24.4658	-
DY75I-M2-BC30	87762	1154	9.5399	1154	38.0804	0.9347
DY75I-M2-BC31	87342	1279	9.9444	1279	41.1426	0.9616
DY75I-M2-BC32	72243	1004	9.4041	1004	32.8795	0.9419
DY75I-M2-BC33	32820	170	6.0824	170	8.7199	0.8176
DY75I-M2-BC34	80564	1217	9.8289	1217	38.5139	0.9551
DY75I-M2-BC35	66032	849	9.0993	849	32.8446	0.934
DY75I-M2-BC36	61695	1065	9.6923	1065	34.7979	0.9625
DY75I-M2-BC37A	119607	1236	9.476	1236	33.0266	0.918
DY75I-M2-BC38A	43473	664	9.094	664	27.1411	0.9687
DY75I-M2-BC39A	56715	864	9.481	864	31.0968	0.9704
DY75I-M2-BC40	123518	398	6.1041	398	19.8509	0.706
DY75I-M2-BC41	121653	1416	9.8513	1416	39.5856	0.9377
DY75I-M2-BC41A	61508	875	9.287	875	32.5985	0.9479
DY75I-M2-BC42	120682	1556	10.0588	1556	47.3975	0.9444
DY75I-M2-BC43	112085	1636	10.244	1636	48.8139	0.956
DY75I-M2-BC44	98011	1245	9.8168	1245	41.2413	0.9531
DY75I-M2-BC45	96485	1493	10.1568	1493	45.6439	0.9599
DY75I-M2-BC47	113985	1409	9.8286	1409	44.0021	0.9355
DY75I-M2-BC48	70817	689	8.335	689	26.0683	0.8813
DY75I-M2-BC49	94836	1120	9.5298	1120	40.6568	0.9378
DY75I-M2-BC50	88262	1177	9.675	1177	38.5587	0.9468
DY75I-M2-BC51	105248	1503	10.1391	1503	45.927	0.9575
DY75I-M2-BC52A	102693	1555	10.2564	1555	41.6176	0.9642
DY75I-M2-BC53	85796	1285.25	9.9551	1285	38.9903	0.9621
DY75I-M2-BC54	123003	1448	9.865	1448	44.9383	0.9376
DY75I-M2-BC55	108850	1287	9.6103	1287	39.6225	0.9285
DY75I-M2-BC56	36153	554	8.7429	554	24.9481	0.9582
DY75I-M2-BC57	36682	634	8.9435	634	27.3625	0.9599
DY75I-M2-BC58	60871	965	9.5583	965	35.4844	0.9625
DY75I-M2-BC59	59210	853	9.349	853	32.5443	0.9594

Station	Feature Count	Chao	Shannon	Observed_features	Faith_pd	Evenness
DY75I-M2-BC60A	46248	767	9.1839	767	29.5309	0.9568
DY75I-M2-BC61	46469	715	9.1355	715	30.2509	0.9619
DY75I-M2-BC62	33226	569	8.8236	569	24.9874	0.963
DY75I-M2-BC63	62158	176	4.821	176	10.2989	0.6393
DY75I-M2-BC64	99848	1184	9.1473	1184	37.0147	0.8945
DY75I-M2-BC66	74374	988	9.5644	988	35.8878	0.9603
DY75I-M2-BC75	75494	980	9.0727	980	38.839	0.9109
DY75I-M2-BC76	49955	739	9.2001	739	28.653	0.9643
DY75I-M2-BC77	56731	849	9.3803	849	32.985	0.9631
DY75I-M2-BC78	50961	731	9.2291	731	27.7833	0.9686
DY75I-M2-BC79	41619	637	8.9813	637	27.0512	0.9634
DY75I-M2-BC80	62947	961	9.5437	961	32.7767	0.9608
DY75I-M2-MC02	60248	903	9.531	903	32.7654	0.9679
DY75I-M2-MC04A	42727	716	9.1982	716	28.6443	0.9693
DY75I-M2-MC05	53207	816	9.3397	816	29.8387	0.9644
DY75I-M2-MC06	62639	929	9.6125	929	35.5889	0.9726
DY75I-M2-MC07A	23936	382	8.3946	382	19.9811	-

The Shannon index statistics for the sediment microbe community in Block M showed that the difference in microbe diversity between the two blocks was not obvious (P=0.102), but overall Block M2 was slightly higher than Block M2 (Figure 5-52).
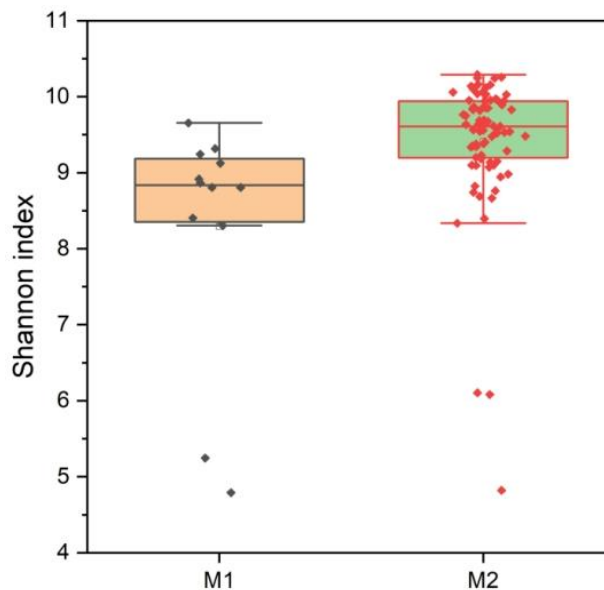
Figure 5-52 Shannon's index for sediment microbe communities in the contract area

5.2.3.1.2 Beta Diversity

The Bray-Curtis distance is a commonly used Beta diversity index to measure similarities and differences in microbe communities between samples.

The results of β diversity analysis showed no obvious difference in the structure of microbe community between Block M1 and Block M2 (Figure 5-53).
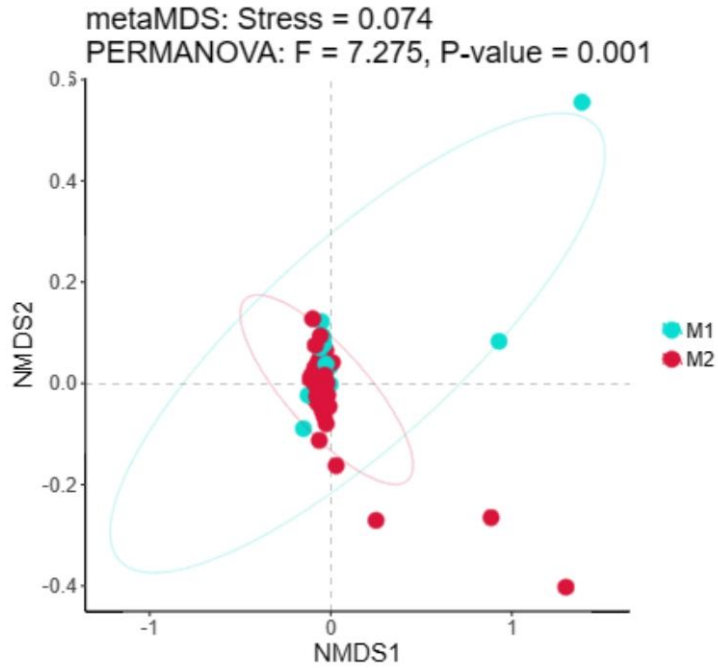
Figure 5-53 Bray-Curtis NMDS analysis of microbe community in BPC's contract area
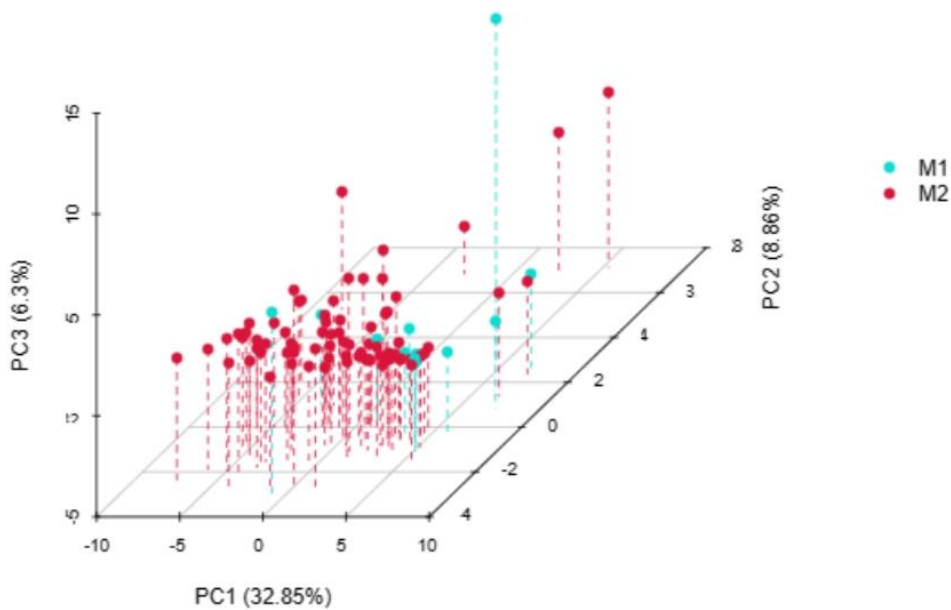
Figure 5-54 PCA Principal Component Analysis (3D) of microbe community in BPC's contract area

5.2.3.1.3 Diversity and Abundance

The genera composition of microbe in sediments of Block M is shown in Figure 5-55. The most abundant 10 genera include *Nitrosopumilus* from Crenarchaeota, *Sphingomonas*, *Woeseia*, and *Ralstonia* from Pseudomonadota, and six uncultured taxa (Subgroup_21, JTB23, BD2-11_terrestrial_group, bacteriap25, S085, NB1-j).
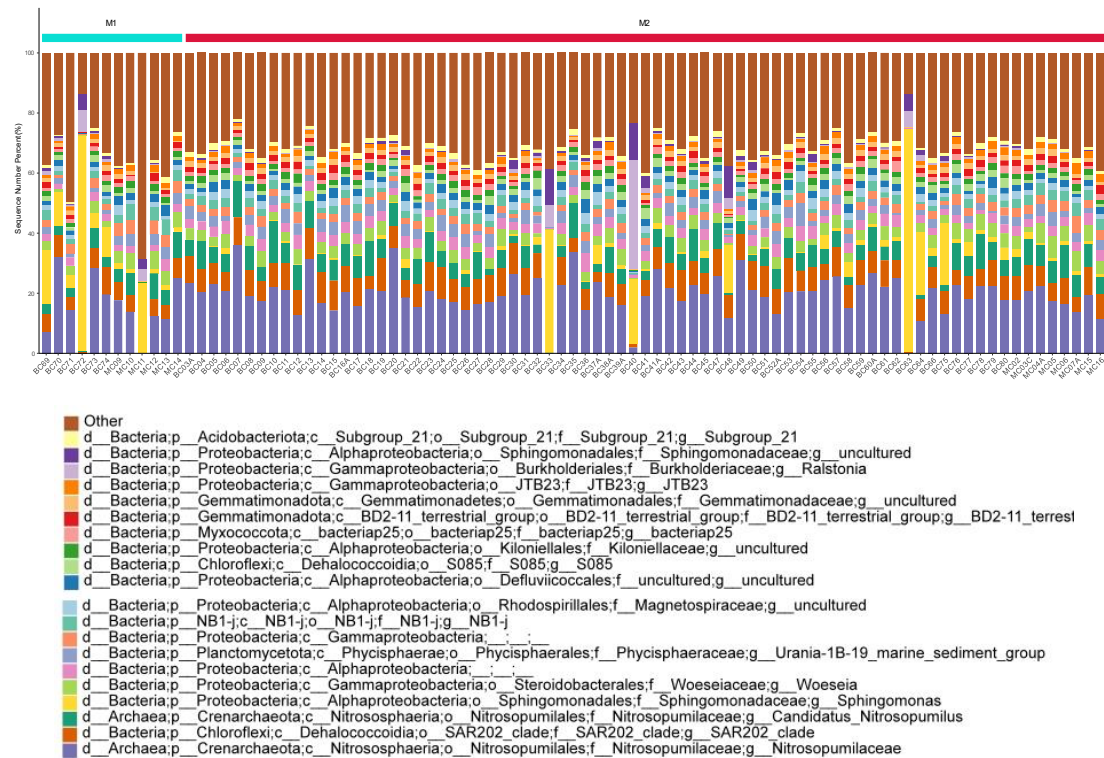
Figure 5-55 Genera composition of microbe in sediments of Block M

Result of cluster analysis at the phylum level are shown in Figure 5-56. It shows that there was no obvious difference in the biodiversity of microbe at the phylum level between Block M1 and Block M2. Microbe such as Nitrospirae, Chloroflexi, Gemmatimonadetes, and Planctomycetes had slightly higher abundance in the northeastern part than the southwestern part of Block M2.
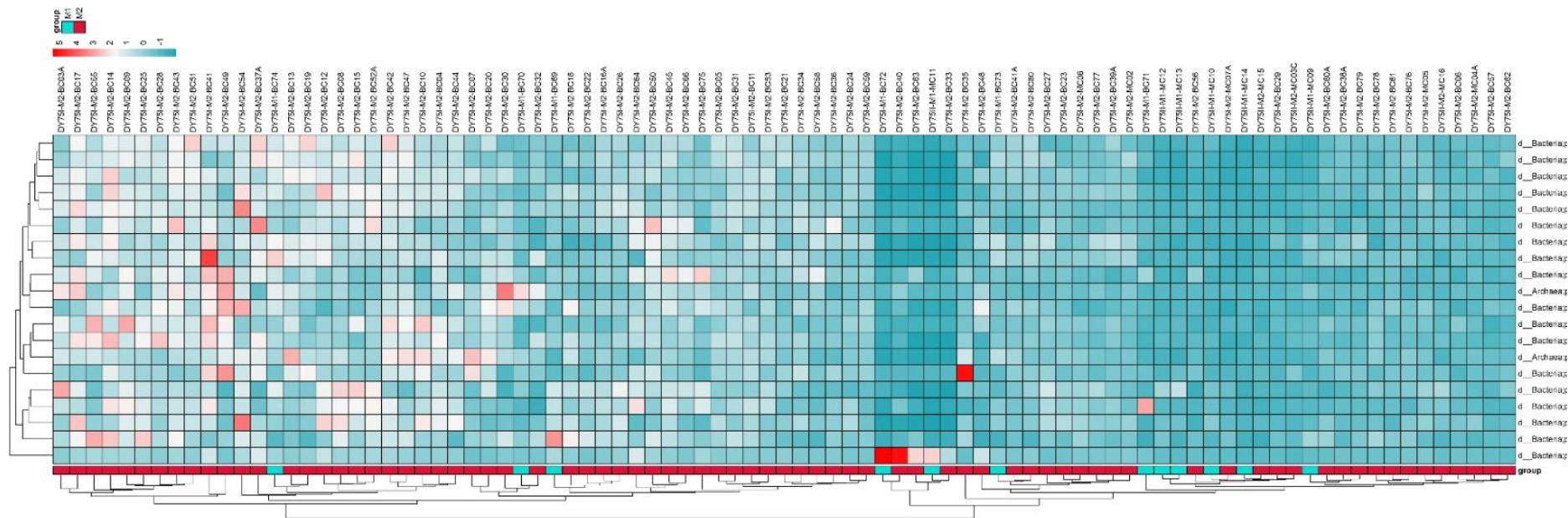
Figure 5-56 Clustered heat map of horizontal groupings of microbe in Block M sediments

5.2.3.2 Eukaryotic Molecular Biology

The molecular diversity of eukaryotic organisms in the sediments of the contract area was investigated using DNA high-throughput sequencing, and a total of 379,431 valid sequences were obtained, which could be classified into 10,944 OTUs at 98.65% similarity. A total of 652 species (excluding unannotated species) were distributed in 30 phyla, 82 orders and 272 families. Specific phylum/higher orders include Annelida, Apicomplexa, Arthropoda, Bacillariophyta, Brachiopoda, Bryozoa, Cercozoa, Chlorophyta, Chordata, Ciliophora, Cnidaria, Discosea (Protozoa), Endomyxa subphylum, Euglenozoa, Evosea, Foraminifera, Gastrotricha, Haptista, Heterolobosea, Imbricatea, Mollusca, Nematoda, Nemertea, Perkinsozoa, Platyhelminthes, Porifera, Rhodophyta, Streptophyta, Tubulinea, and Xenacoelomorpha. The number of species and OTUs for each phylum is shown in Figure 5-57, and the relative proportions of OTUs at different sediment depth are shown in Figure 5-58, within which the highest number of OTUs is the Nematoda, followed by the Euglenozoa and the Ciliophora.
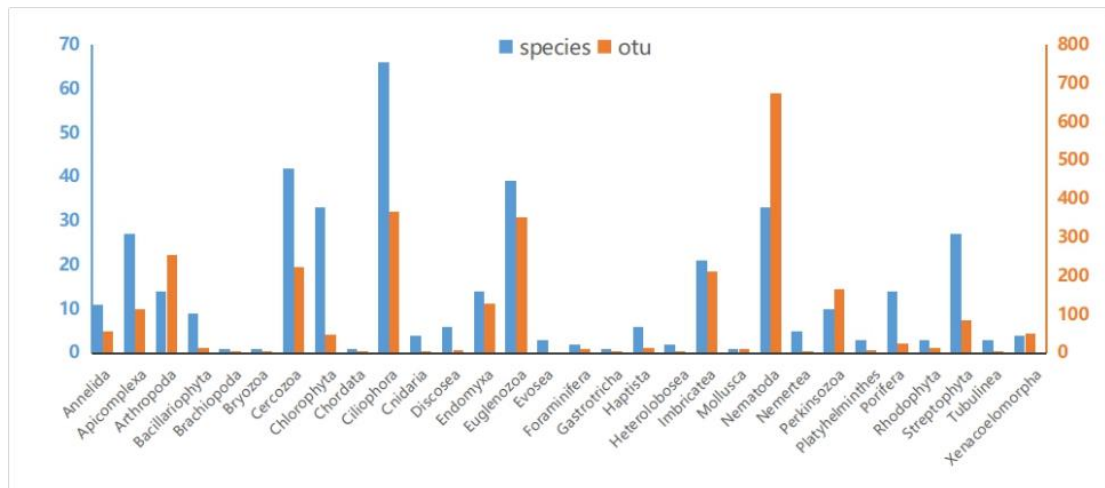
Figure 5-57 Number of OTUs and species of different eukaryotic phylum in Block M
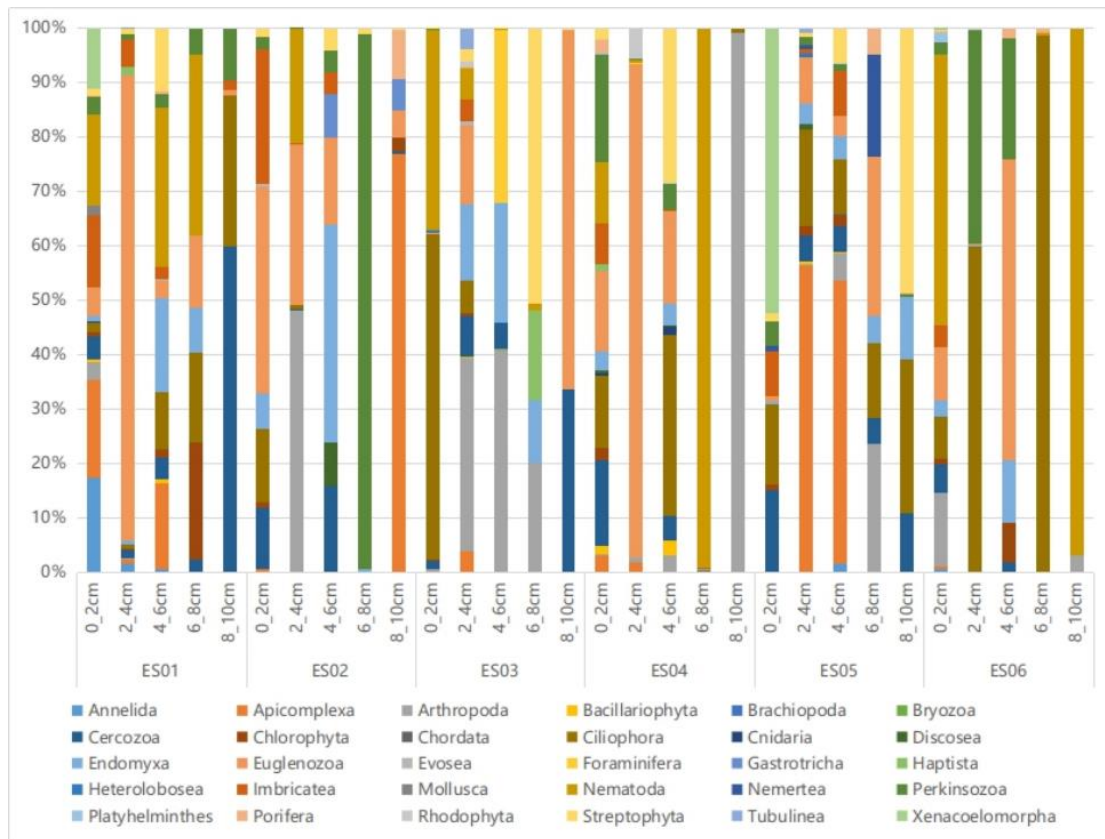
Figure 5-58 Proportion of OTUs for eukaryote at survey stations at different depth in Block M

Based on OUT analysis, it was found that the mean value of regional species richness index (richness) was 691, ranging from 178 to 1432, with the highest values occurring in ES03_2~4, followed by ES04_0~2 and ES01_0~2, and the lowest values occurring in ES05_6~8. The mean values of Chao index and ACE index were 829 and 906, ranging from 213 to 1669 and 249 to 1872, respectively. The mean values of Shannon's biodiversity index, Simpson diversity index and evenness index were 5.160, 0.137 and 0.553, with ranges between 1.973~8.024, 0.019~0.137 and 0.264, respectively. The diversity indices showed a high level of microbe diversity in Block M. The detail information of each index is shown in Figure 5-59.
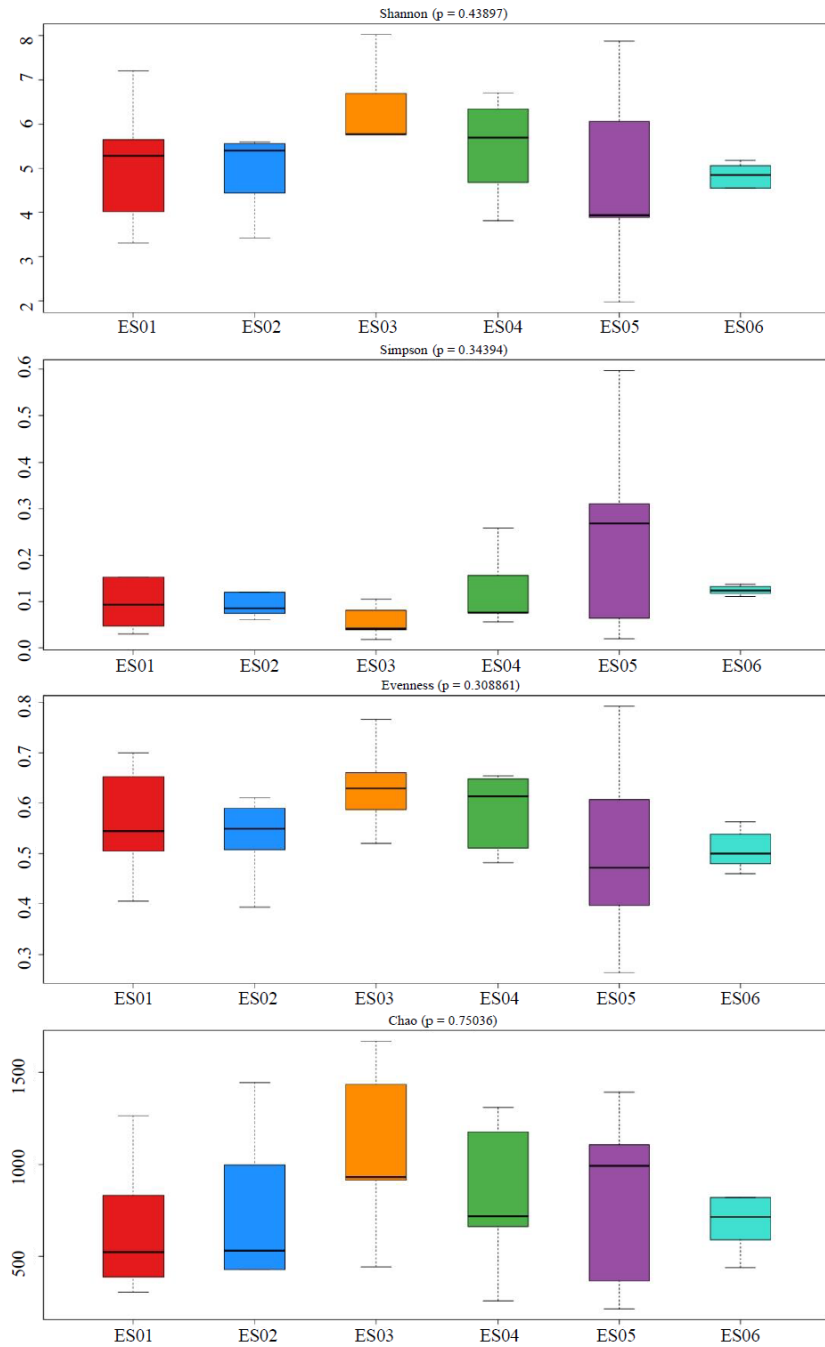
Figure 5-59 Characteristics of the sediment eukaryotic species richness index and biodiversity index in the contract area

As for vertical distribution, number of eukaryotic species showed a decreasing trend from the surface to the bottom, but increased at 8–10 cm depth. Diversity index indicated little difference between each layer (Figure 5-60).
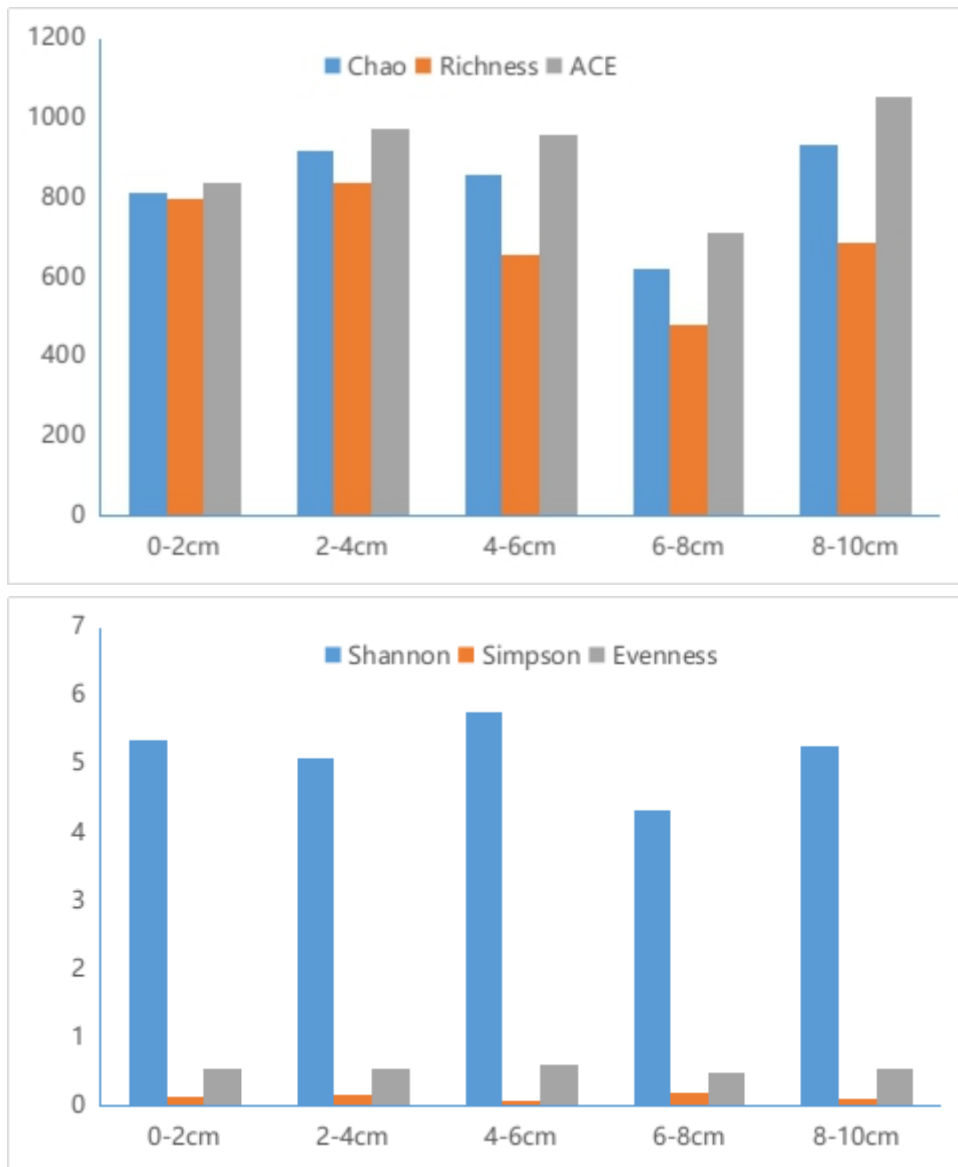
Figure 5-60 Vertical distribution of eukaryotic diversity indices in Block M.

The statistical test of the eukaryotic species diversity index among the six environmental stations revealed that there was no obvious difference among the stations. However, the Venn diagram (Figure 5-61) showed that there were not many shared OTUs, genera and species among the stations, with only 26 shared OTU genera, 12 shared genera and 8 shared species, most of which were unique to each station.
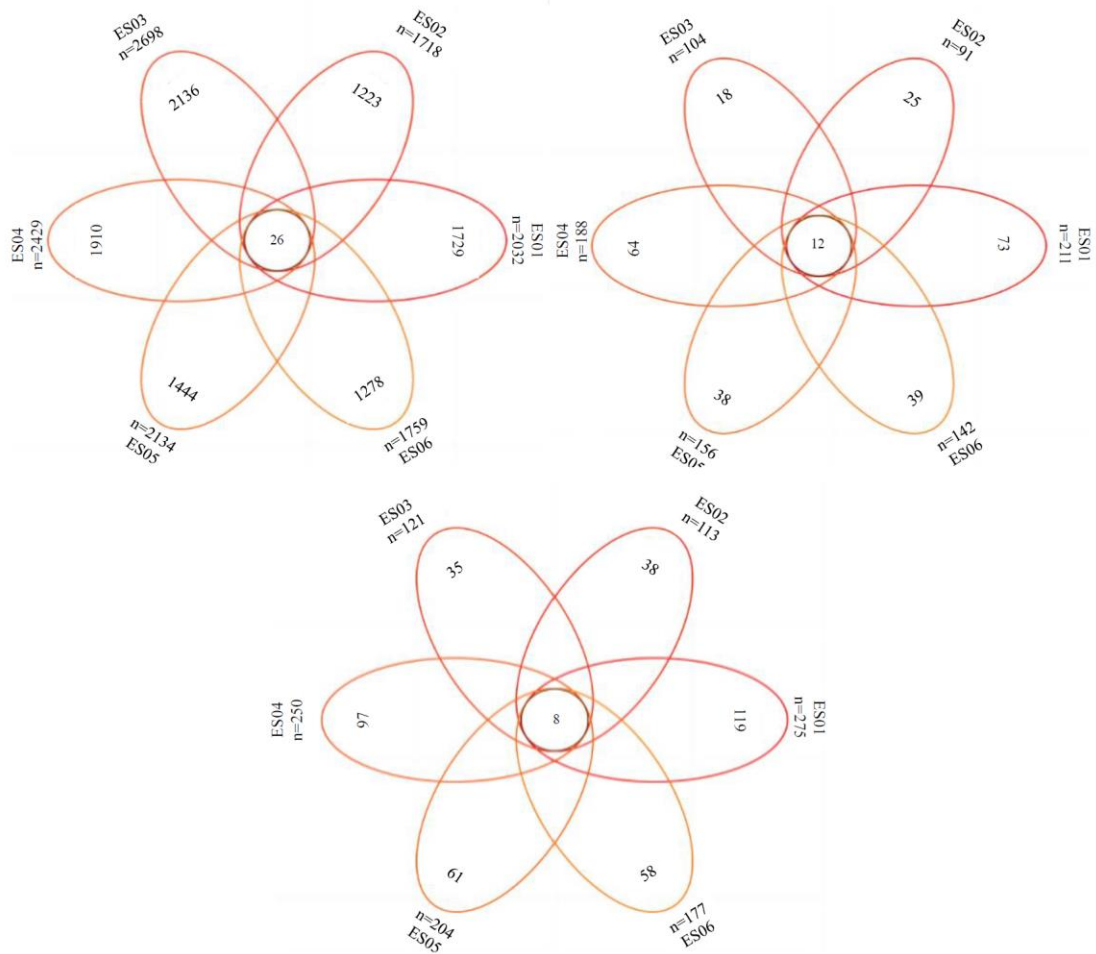
Figure 5-61 Venn analysis of Block M eukaryotic OUT (left), genus (right), and species hierarchy (bottom)

Although most sequencing depth levels basically meet the requirements of diversity analysis (Figure 5-62), the analysis of species accumulation curves showed a sharp increase trend, indicating that the existing level of sampling is not yet able to provide an adequate assessment of eukaryotic diversity in this area, and further additional sampling are needed.
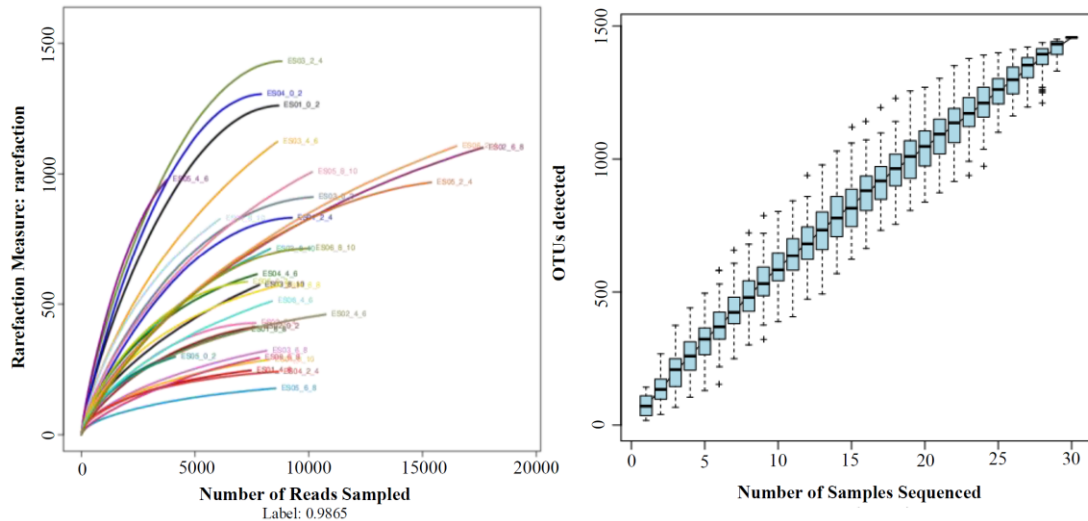
Figure 5-62 OTU-based dilution curves and species accumulation curves

5.2.3.3 Foramanifera

The molecular diversity of benthic eukaryotes at six environmental stations in the contract area was studied using DNA high-throughput sequencing. Based on the 18s comparison results, two genera and two species of foraminifera were found, which are *Syringammina corbicula* in the family Psamminidae, and *Ammonia beccarii var. parkinsoniana* in the family Ammoniidae. among them, *Syringammina corbicula* belong to the Xenophyophore. According to Mullineaux (1987), species of this genus, together with *Semipsammina, Stannoma, Stannophyllum*, etc., are commonly distributed in the nodule regions of the central North Pacific and Equatorial North Pacific area.

5.2.3.4 Metazoan Meiofauna

Multicorer was used to collect sediment samples in Block M for meiofauna analyses in three subareas during the 2022 cruise, and duplicated sampling was carried out at seven sampling sites for a total of 14 stations in accordance with the requirements of the ISA (ISBA/25/LTC6/Rev.3) (Figure 5-63). The seven sampling sites were distributed in three zones: MC02a–MC07a are located in the southeastern piedmonts of the Magoshichi Guyot (Block M2 IRZ, Zone 1), Stations MC09-MC14 are located in the southeastern piedmonts of the Matsuzaki Guyot (PRZ, Zone 2), and MC15–MC16 are located in the basin between the IRZ and the PRZ (Zone 3).
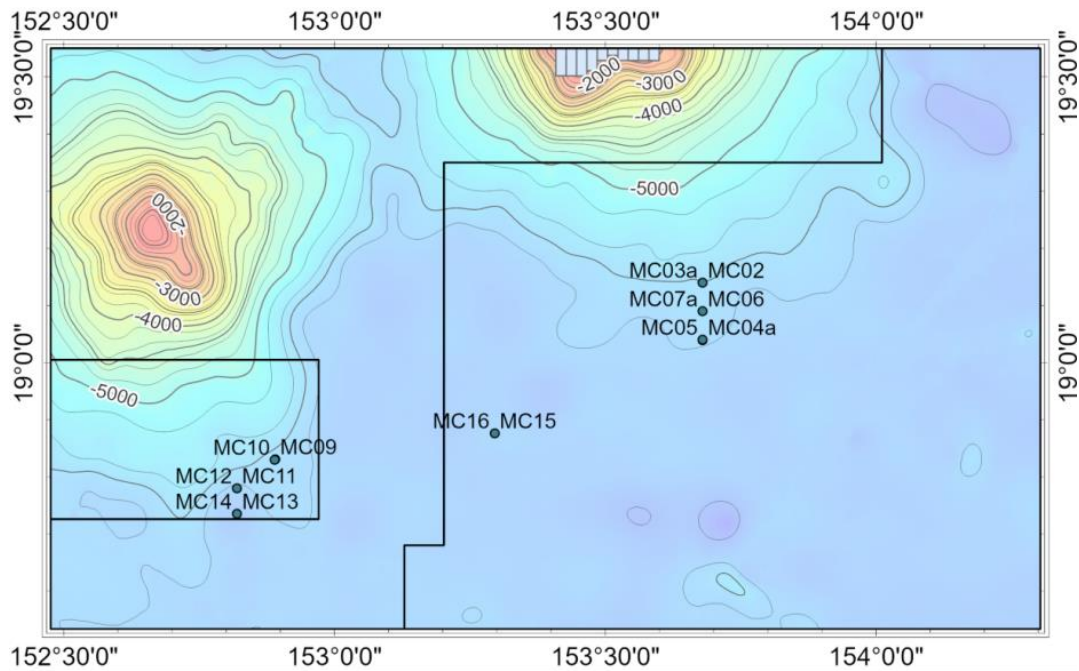
Figure 5-63 Schematic of multicorer sampling stations in the contract area during 2022 cruise

5.2.3.4.1 Metazoan Meiofaunal Community Composition

A total of 15 groups of metazoan meiofauna were found in Block M, including Nematoda, Harpacticoida, Kinorhyncha, Polychaeta, Sipuncula, Tardigrada, Ostracoda, Gastrotricha, Nauplius, other copepoda, Amphipoda, Acari, Bivalvia, Loricifera and other unidentified taxa. Nematodes were the dominant taxa, accounting for 90.65% of the total abundance of metazona Meiofauna, followed by Harpacticoida and Nauplius (Figure 5-64), while the remaining 12 taxa were count less than 5% of the total abundance. There were some differences in the composition of taxa between stations (Figure 5-65), with the lowest proportion of nematode abundance (<70%) and highest harpacticoida contribution occcured at Station MC02. At Stations MC06 and MC16, the proportion of nematodes was only about 80%, while the highest proportion of nematodes occured at Station MC10, which was 94.7%. Among all taxa, nematodes and harpacticoida were found at all stations, while amphipoda were found only at two stations.
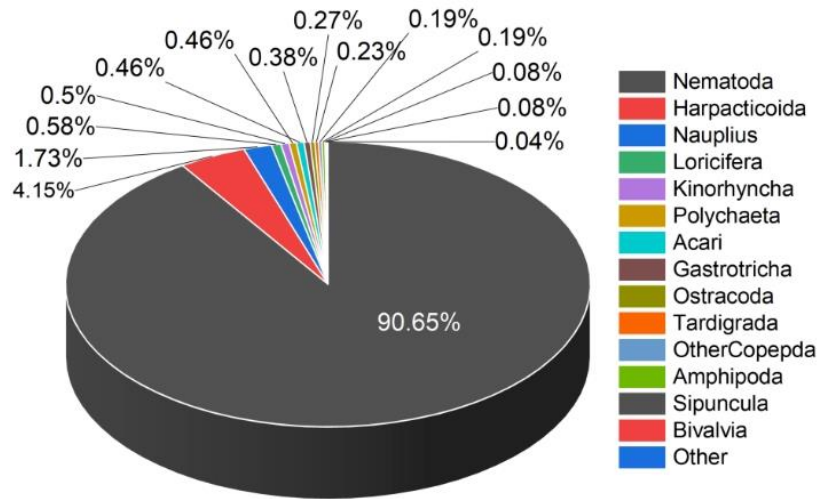
Figure 5-64 Composition of meiofauna group in the contract area
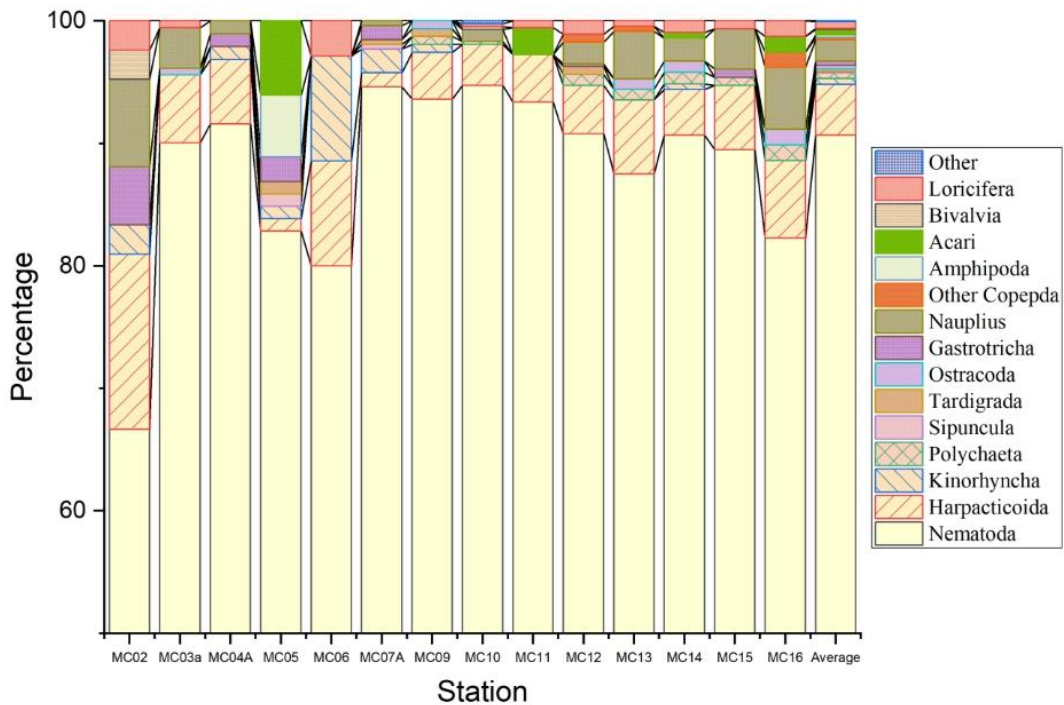
Figure 5-65 Composition of metazoa meiofauna at different stations in the contract area

5.2.3.4.2 Size Composition of Meiofauna

Size composition of meiofauna is shown in Figure 5-66. 63–125 μm size meiofauna fraction accounted for 50% of the total abundance of meiofauna, followed by 125–250 μm fraction, which accounted for 31%; 32–63 μm size accounted for 11%; and taxa larger than 250 μm only accounted for 8%. Generally, meiofauna in PRZ were smaller than in IRZ, with a predominance of size less than 125 μm, while in IRZ it was predominant by fraction larger than 125 μm.
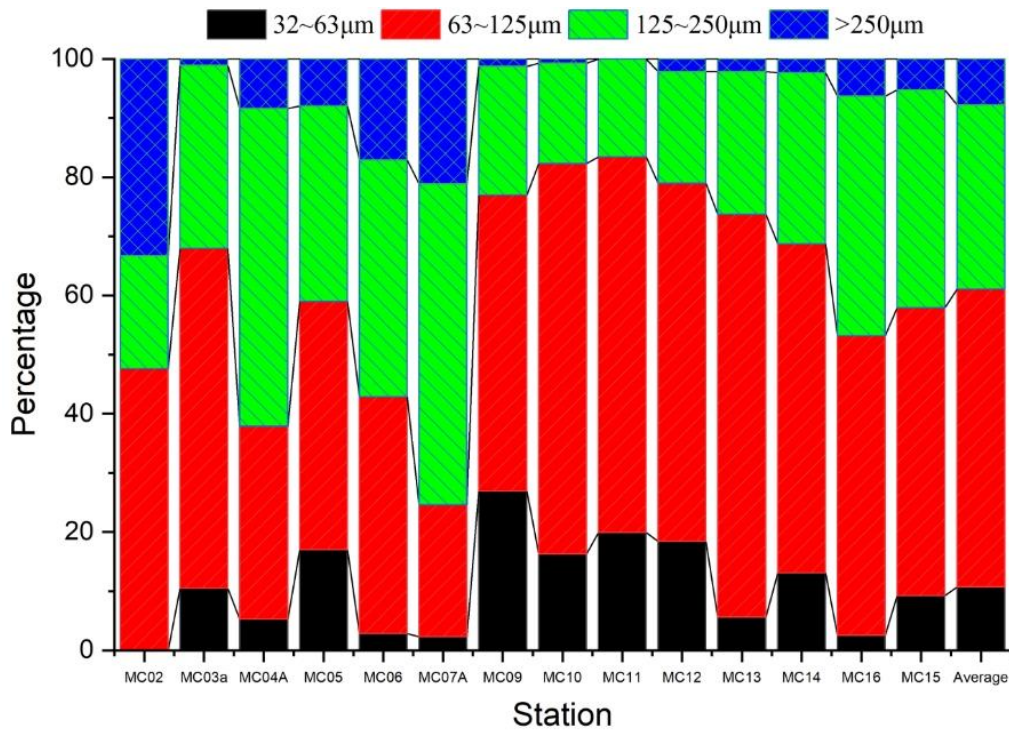
Figure 5-66 Size composition of metazoan meiofauna in Block M

5.2.3.4.3 Abundance of Metazoan Meiofauna

The average abundance of metazoan meiofauna in Block M was 26.21 ind./10 cm^2 in 2022, and varied from 4.94 to 64.33 ind./10 cm^2, with the highest value distributed in the PRZ at Station MC12, and the lowest value located in the IRZ at Station MC06 (Figure 5-67). Meiofauna abundance in the IRZ (zone1, Figure 5-67) was obviously lower than in the PRZ (zone2, Figure 5-67).

Compared with the polymetallic nodule areas in the Northeast Pacific CCZ area, we found a gradual trend of decreasing abundance from the east Pacific nodule area to the west Pacific nodule area. And the abundance of metazoan meiofauna in the BPC contract area is obviously lower than in the CCZ area (Table 5-1).
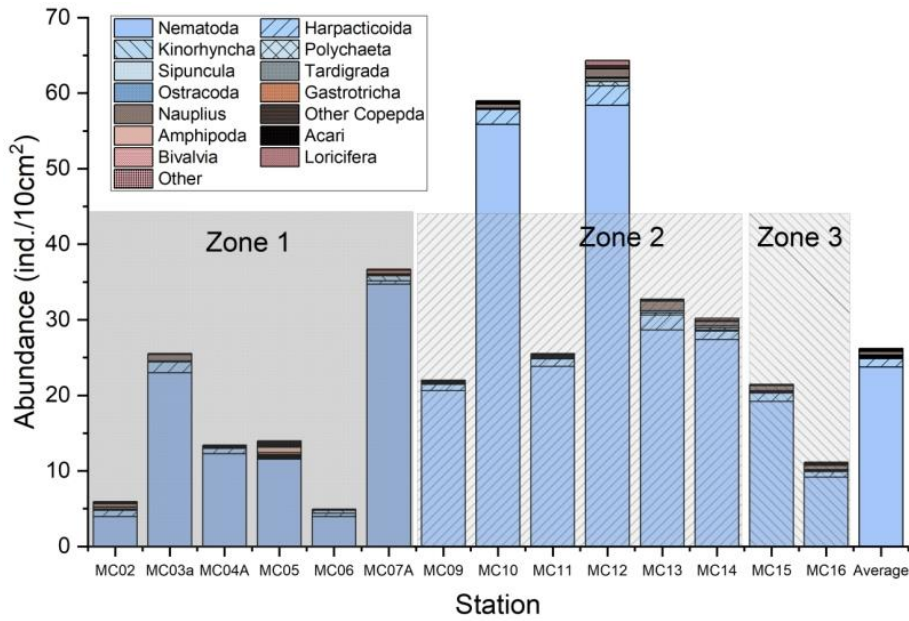
Figure 5-67 Distribution of metazoan meiofaunal abundance in Block M.

5.2.3.4.4 Vertical Distribution of Meiofauna

Analysis of the distribution of meiofaunal abundance in different depth sediments showed that meiofaunal abundance presented a decreasing trend from the surface layer to the deeper layer, with the highest abundance in the 0–1 cm layer, accounting for 73% of the total abundance, and the lowest abundance in the 4–5 cm layer, which accounted for only 2% of the total abundance (Figure 5-68 and Figure 5-69).
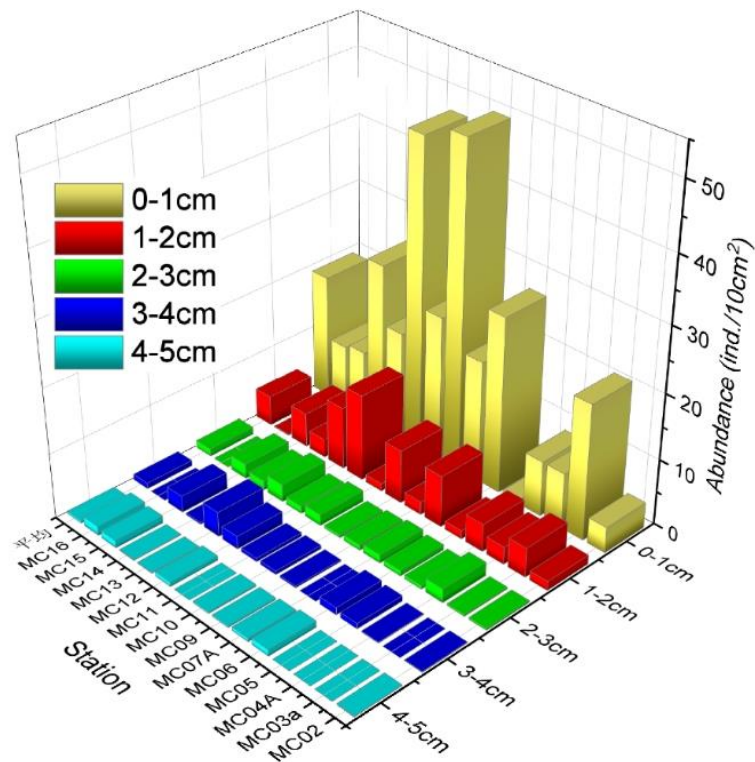
Figure 5-68 Vertical distribution of metazoan meiofaunal abundance in the contract area
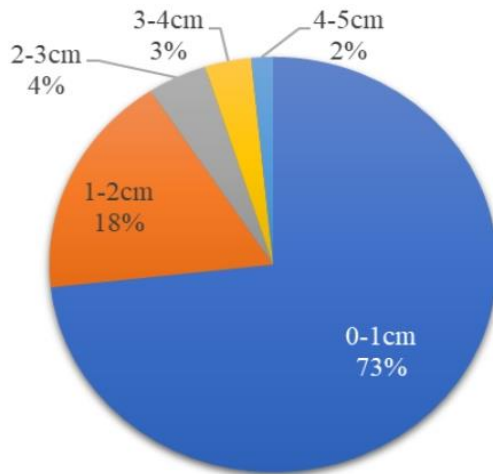
Figure 5-69 Vertical distribution characteristics of meiofaunal abundance in Block M.

5.2.3.4.5 Differences in the Spatial Distribution of Metazoan Meiofauna

Results of cluster analysis among 14 stations in the 2022 cruise meiofauna survey is shown in Figure 5-70, and the heatmap shows that the six stations in Block M1 zone 2 (group1) and the eight stations in Block M1 (group2) are nested combinations of each other, suggesting that the composition of meiofauna is similar in the two blocks.
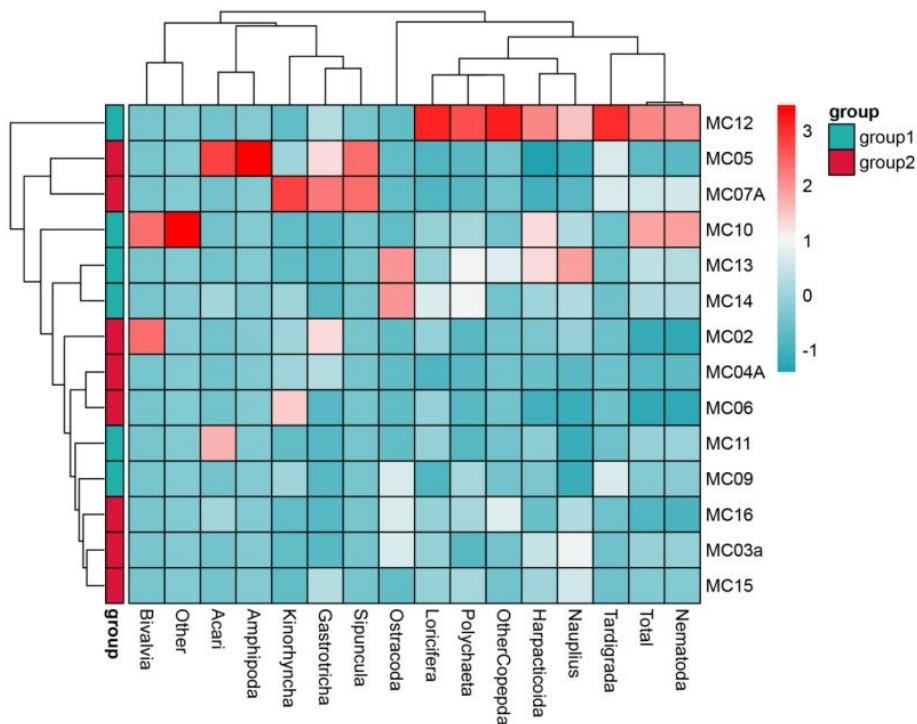
Figure 5-70 Heatmap of meiofauna diversity in Block M

Differences in meiofaunal abundance among the three blocks were compared using a one-way ANOVA. Results indicated that the difference in meiofaunal abundance among these three blocks was not obvious ($p=0.117$), but the abundance of the group Harpacticoida, Kinorhyncha, and Nauplius differed at an obvious level among the 3 blocks (Figure 5-71 and Table 5-36).
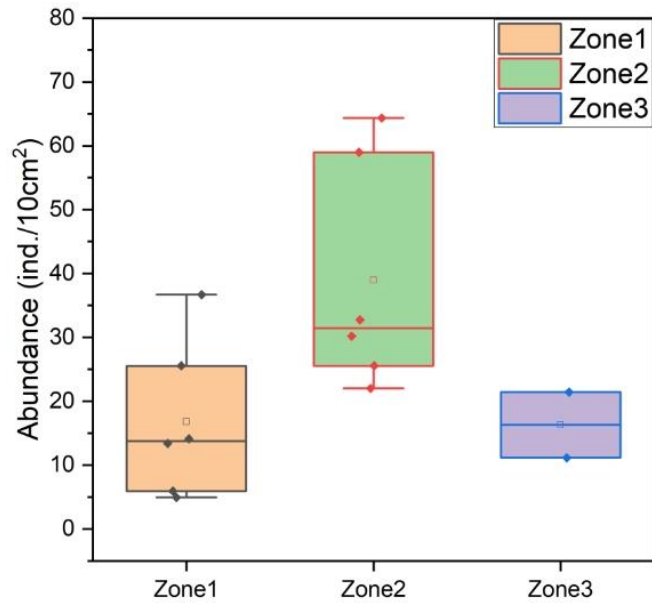
Figure 5-71 Box plot of meiofaunal abundance in three zones of Block M

Table 5-36 ANOVA analysis results of meiofaunal abundance in three zones of Block M

		Square sum	Degrees of freedom	Mean square	F	Significance
Nematoda	Intergroup	1142.742	2	571.371	2.460	0.131
	Within a group	2555.191	11	232.290		
	Total	3697.933	13			
Harpacticoida	Intergroup	3.003	2	1.501	5.531	0.022*
	Within a group	2.986	11	0.271		
	Total	5.988	13			
Kinorhyncha	Intergroup	0.241	2	0.120	4.485	0.038*
	Within a group	0.295	11	0.027		
	Total	0.536	13			
Polychaeta	Intergroup	0.140	2	0.070	3.634	0.061
	Within a group	0.212	11	0.019		
	Total	0.353	13			
Sipuncula	Intergroup	0.008	2	0.004	1.571	0.251
	Within a group	0.027	11	0.002		
	Total	0.034	13			
Tardigrada	Intergroup	0.009	2	0.004	0.262	0.774
	Within a group	0.179	11	0.016		
	Total	0.188	13			
Ostracoda	Intergroup	0.027	2	0.013	1.189	0.341
	Within a group	0.123	11	0.011		
	Total	0.149	13			
Gastrotricha	Intergroup	0.083	2	0.042	2.659	0.114
	Within a group	0.173	11	0.016		

		Square sum	Degrees of freedom	Mean square	F	Significance
	Total	0.256	13			
Nauplius	Intergroup	1.198	2	0.599	5.502	0.022*
	Within a group	1.198	11	0.109		
	Total	2.396	13			
Other Copepod	Intergroup	0.047	2	0.024	1.916	0.193
	Within a group	0.136	11	0.012		
	Total	0.183	13			
Amphipoda	Intergroup	0.047	2	0.024	0.629	0.551
	Within a group	0.415	11	0.038		
	Total	0.462	13			
Acari	Intergroup	0.034	2	0.017	0.224	0.802
	Within a group	0.836	11	0.076		
	Total	0.870	13			
Bivalvia	Intergroup	0.001	2	0.000	0.157	0.856
	Within a group	0.033	11	0.003		
	Total	0.034	13			
Loricifera	Intergroup	0.135	2	0.067	2.625	0.117
	Within a group	0.282	11	0.026		
	Total	0.417	13			
Other	Intergroup	0.002	2	0.001	0.629	0.551
	Within a group	0.017	11	0.002		
	Total	0.018	13			
Total	Intergroup	1337.053	2	668.526	2.626	0.117
	Within a group	2800.475	11	254.589		
	Total	4137.528	13			

＊Significant difference at 0.05 level

5.2.3.4.6 Diversity of Nematoda

Nematodes is the most dominant group of meiofauna. Five stations (MC02, MC06, MC04A, MC05, MC07A) of nematoda samples were identified to the genus level, and a total of 37 genera were identified, belonging to two orders, six phyla, and 19 families (see Appendix table 2). More than half of these nematode individuals were juveniles, with males and females comprising a comparable 21% each of the adults (Figure 5-72), and common nematodes species in this area are shown in Figure 5-73.
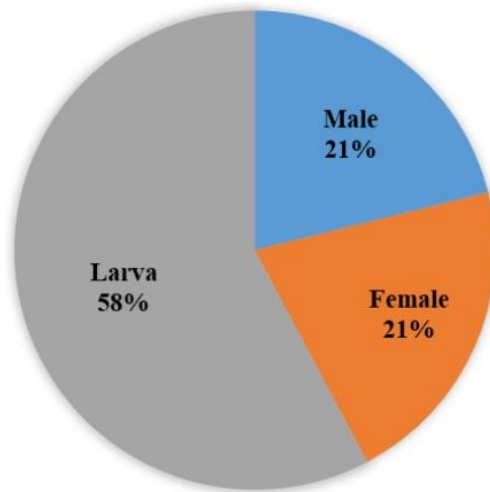
Figure 5-72 Sex composition of nematodes in Block M.
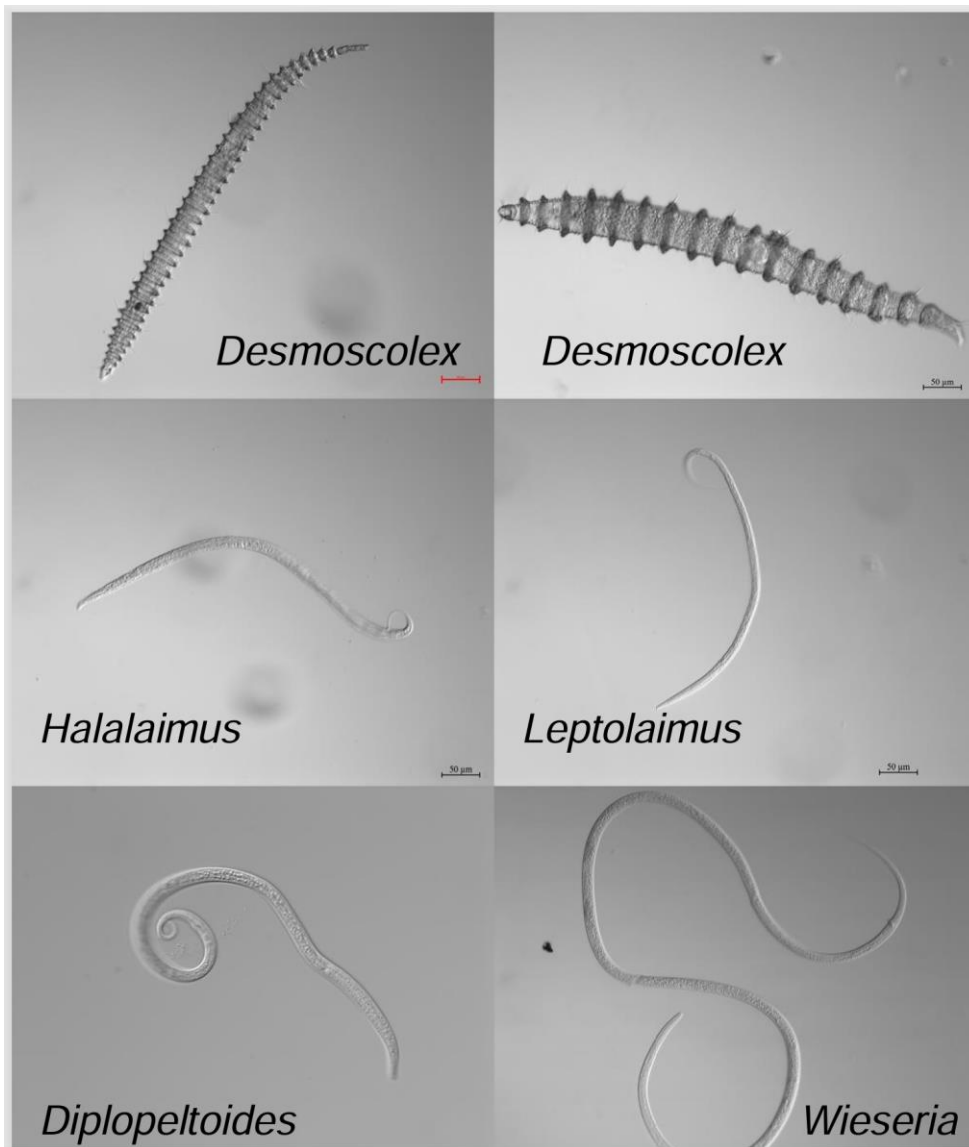
Figure 5-73 Common nematode species in Block M

5.2.3.4.7 Interannual Variation of Metazoan Meiofauna

Twelve stations of multicorer sampling for analyzing inter-annual variability of meiofauna were conducted during DY81 cruise (2023) in BPC's contract area, and 10 stations have been completed lab analysis. These 10 survey stations laid out within the three areas surveyed in 2022, as shown in Figure 5-74.
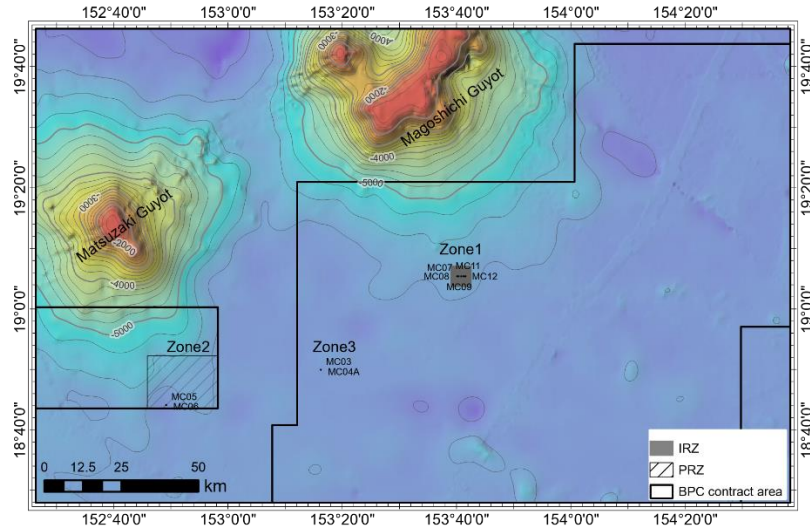
Figure 5-74 Schematic of 2023 Meiofauna survey stations.

Results showed that compared to the 15 groups of meiofauna founded in the 2022 survey, only 10 groups were found in 2023 survey sites, including Nematoda, Harpacticoida, Polychaeta, Ostracoda, Nauplius, Other Copepoda, Isopoda, Acari, Loricifera, and other, etc. Of the three zones, Zone 1 (IRZ) had found 10 groups, and Zone 3 had the fewest with only 6 groups (Figure 5-75).
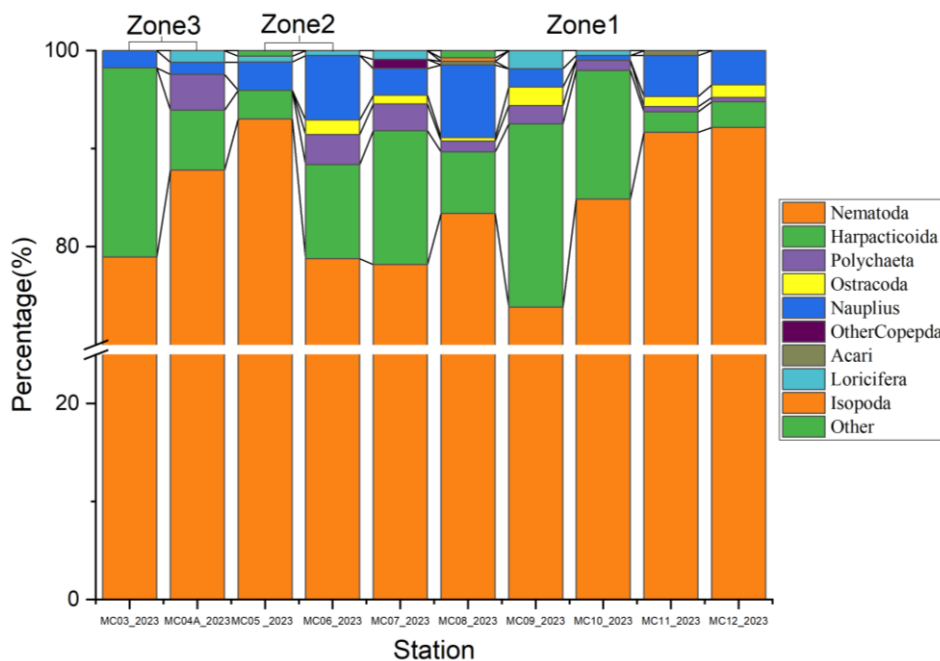
Figure 5-75 Meiofaunal community composition in 2023 survey stations

As shown in Figure 5-76, meiofauna were also dominated by the 63–125 μm size fraction at the 2023 survey stations, followed by the 125–250 μm size. Unlike the pattern of the 2022 survey, the size structure varied considerably from station to station, with a greater proportion of the 32–63 μm size fraction at Station MC07, which is located in Zone 1. While at Station MC09, 125–250 μm size fraction is higher than 63–125 μm size fraction. At Station MC04A (in Zone 3), size larger than 250 μm has a higher proportion than 63–125 μm fraction.
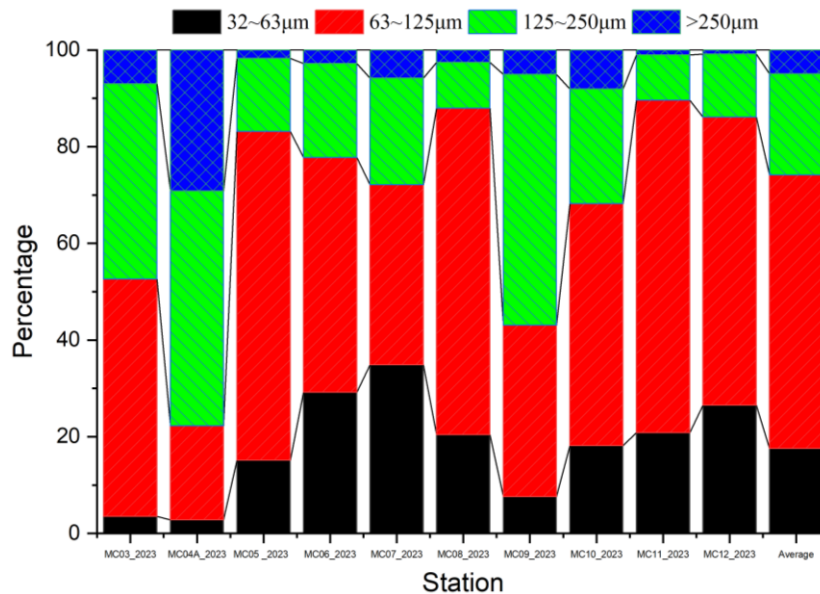
Figure 5-76 Size composition of meiofauna in 2023 survey stations

The vertical distribution characteristics of meiofauna in 2023 sites are shown in Figure 5-77, with the highest abundance in the 0–1 cm depth layer, but compared to 2022, its proportion decreased from 71% to 58%, and the lowest abundance was found in the 4–5 cm depth layer, with a proportion of about 2% in both years.
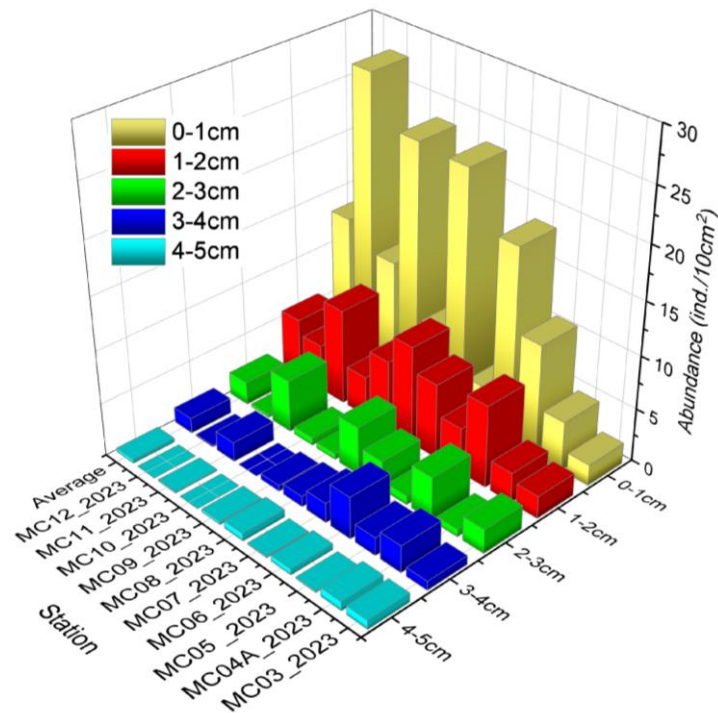
Figure 5-77 Vertical distribution of meiofaunal abundance in 2023

The meiofaunal abundance difference between 2022 and 2023 is shown in Table 5-37. The average abundance of meiofauna in 10 survey stations during the DY81 cruise (2023) was 22.86 ind./10cm^2, which was lower than the results of the survey in 2022. The highest value appeared in Zone1 and the lowest value was found in Zone3, which was consistent with the pattern of 2022. According to the results of one-way ANOVA analysis, meiofaunal abundance shows an obvious (P=0.048) difference between the IRZ (Zone1) and PRZ (Zone2). The abundance in these two zones was both obviously higher than that in Zone3 (P=0.016). Analysis shows that the year-to-year difference in meiofaunal abundance in Zone1 (IRZ) was not obvious (Table 5-38, P=0.167).

Table 5-37 Comparison of meiofaunal abundance in the contract area in 2022 and 2023

Area	Number of taxa		Meiofaunal abundance (ind./10cm)^2		Average abundance of nematode (ind./10cm)^2		Number of stations	
	2022	2023	2022	2023	2022	2023	2022	2023
Zone1	12	10	16.77	26.12	14.91	22.27	6	6
Zone2	13	7	38.64	26.10	35.79	22.29	6	2
Zone3	7	6	16.30	9.81	14.18	8.25	2	2
Average	15	10	26.21	22.86	23.75	19.47	14	10

Table 5-38 Results of analysis of variance (ANOVA) for meiofaunal abundance in 2022 and 2023 in the IRZ (Zone1)

	Square sum	Degrees of freedom	Mean square	F	Significance
Intergroup	262.754	1	262.754	2.218	0.167
Within a group	1184.696	10	118.470		
Total	1447.450	11			

Two station meiofauna surveys were conducted in Block M2 in 2020 (data unpublished), and combining the survey data from 2022 and 2023, we plot an interannual curve of meiofaunal abundance as shown in Figure 5-78. It indicates that the abundance of meiofauna in this area shows a slow increasing trend from 2020 to 2023.
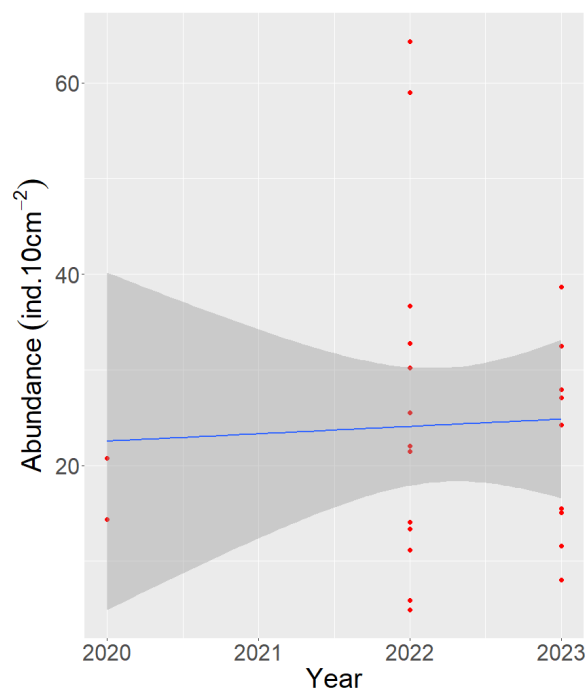
Figure 5-78 Interannual variation of meiofaunal abundance in Block M.

Based on the results of the statistical analysis of meiofaunal abundance from 24 stations (Figure 5-79), we assume the meiofaunal abundance baseline for the IRZ (Zone 1) to be ranged from 14.11 to 27.09 ind./10 cm^2 and from 25.54 to 45.00 ind./10 cm^2 for PRZ (Zone 2), respectively.
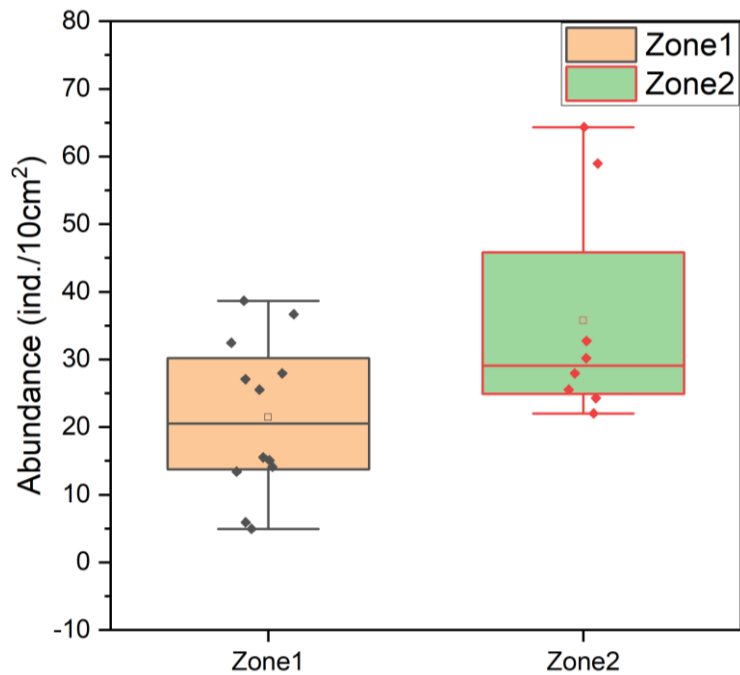
Figure 5-79 Comparison of Zone1 and Zone2 meiofaunal abundance

5.2.3.5 Macrofauna

5.2.3.5.1 Distribution Characteristics of Macrofaunal Abundance

DY75 cruise (2022) conducted a 39-station macrofauna survey in Block M using a box-corer. The results showed a low detection rate of macrofauna in Block M, with no specimens detected at 8 stations. A total of 69 macrofaunal specimens belonging to 38 species were detected in this survey.

Crustaceans were the most abundant with 47 specimens, followed by polychaetes with 20 specimens and mollusks and echinoderms with 1 specimen each. The most abundant crustaceans were isopods and benthic harpacticoids with 18 specimens each, followed by tanaidaceans with 8 specimens, and the most abundant polychaetes were the Cirratulidae (with 9 specimens).

DY81 cruise (2023) conducted a 14-station macrofauna survey in Block M utilizing a box-corer (7 stations were duplicated), with 4 stations failing due to box-corer leaks resulting in fail sampling. Sample analysis is currently completed for 4 stations (duplicate sampling at 2 stations). A total of 45 macrofaunal specimens were obtained. Of these, 25 are polychaete specimens, 17 are crustacean specimens, and 3 are other unidentified taxa. Polychaetes were the most abundant taxa, and the most abundant of the polychaetes were the families of Spionidae (6 specimens) and Cirratulidae (4 specimens). Crustaceans were dominated by isopods (8 specimens) and protopods (6 specimens). Species and specimen counts are shown in Table 5-39. The common macrofauna in the region are shown in Figure 5-80.

Table 5-39 Results of macrofaunal species identification in Block M.

Station	Layers (cm)	Taxon	Order	Family	Species	Number of specimens
DY75-I-M1-BC74	0~3	Crustacea	Isopoda	-	*Isopoda* sp.12	1
DY75-I-M2-BC05	0~3	Polychaete	-	Paraonidae	*Paraonidae* sp.1	1
DY75-I-M2-BC05	3~5	Crustacea	Pantopoda	-	*Pantopoda* sp.2	1
DY75-I-M2-BC06	0~3	Crustacea	Isopoda	Ischnomesidae	*Ischnomesidae* sp.1	1
DY75-I-M2-BC06	0~3	Crustacea	Tanaidacea	Anarthruridae	*Anarthrura* sp.	1
DY75-I-M2-BC06	0~3	Echinoderm	-	-	*Holothuroidea* sp.	1
DY75-I-M2-BC06	5~10	Crustacea	Harpacticoida	-	*Harpacticoida* sp.1	1
DY75-I-M2-BC06	5~10	Crustacea	Tanaidacea	-	*Tanaidacea* sp.8	1
DY75-I-M2-BC07	0~3	Crustacea	Isopoda	Mesosignidae	*Mesosignum* sp.1	1
DY75-I-M2-BC07	0~3	Crustacea	Harpacticoida	-	*Harpacticoida* sp.2	6
DY75-I-M2-BC07	0~3	Polychaete	Terebellida	Cirratulidae	*Chaetozone* sp.1	1
DY75-I-M2-BC08	3~5	Crustacea	Isopoda	-	*Isopoda* sp.8	1
DY75-I-M2-BC10	0~3	Crustacea	Isopoda	-	*Isopoda* sp.9	1
DY75-I-M2-BC11	0~3	Polychaete	Terebellida	Cirratulidae	*Chaetozone* sp.1	1
DY75-I-M2-BC11	0~3	Crustacea	Conchostraca	-	*Conchostraca* sp.2	1
DY75-I-M2-BC12	0~3	Crustacea	Harpacticoida	-	*Harpacticoida* sp.3	2
DY75-I-M2-BC13	0~3	Crustacea	Isopoda	-	*Isopoda* sp.10	1
DY75-I-M2-BC13	3~5	Crustacea	Isopoda	-	*Isopoda* sp.10	1
DY75-I-M2-BC15	0~3	Polychaete	-	Glyceridae	*Glycera* sp.	1
DY75-I-M2-BC15	0~3	Polychaete	-	Spionidae	*Spionidae* sp.1	1
DY75-I-M2-BC15	0~3	Crustacea	Harpacticoida	-	*Harpacticoida* sp.3	1
DY75-I-M2-BC16A	0~3	Crustacea	Isopoda	-	*Isopoda* sp.10	1
DY75-I-M2-BC17	0~3	Crustacea	Isopoda	-	*Isopoda* sp.4	1
DY75-I-M2-BC17	0~3	Crustacea	Isopoda	-	*Isopoda* sp.1	1
DY75-I-M2-BC17	0~3	Polychaete	Terebellida	Cirratulidae	*Cirratulidae* sp.4	1
DY75-I-M2-BC18	0~3	Polychaete	-	Opheliidae	*Opheliidae* sp.1	1

Station	Layers (cm)	Taxon	Order	Family	Species	Number of specimens
DY75-I-M2-BC18	0~3	Polychaete	Phyllodocida	Polynoidae	*Polynoidae* sp.1	1
DY75-I-M2-BC18	3~5	Polychaete	Terebellida	Cirratulidae	*Cirratulidae* sp.3	1
DY75-I-M2-BC18	3~5	Crustacea	Isopoda	-	*Isopoda* sp.11	1
DY75-I-M2-BC18	5~10	Crustacea	Harpacticoida	-	*Harpacticoida* sp.3	1
DY75-I-M2-BC19	0~3	Polychaete	Spionida	Spionidae	*Spionidae* sp.3	1
DY75-I-M2-BC20	0~3	Molluscs	Gastropoda	-	*Gastropoda* sp.1	1
DY75-I-M2-BC21	0~3	Polychaete	Terebellida	Cirratulidae	*Chaetozone* sp.2	1
DY75-I-M2-BC22	0~3	Polychaete	Polychaeta	-	*Polychaeta* sp. indet.1	1
DY75-I-M2-BC23	5~10	Crustacea	Tanaidacea	-	*Tanaidacea* sp.8	1
DY75-I-M2-BC24	0~3	Polychaete	Phyllodocida	Polynoidae	*Polynoidae* sp.1	1
DY75-I-M2-BC25	3~5	Polychaete	Terebellida	Cirratulidae	*Cirratulidae* sp.3	1
DY75-I-M2-BC28	0~3	Crustacea	Tanaidacea	-	*Tanaidacea* sp.8	1
DY75-I-M2-BC34	0~3	Crustacea	Isopoda	-	*Isopoda* sp.11	1
DY75-I-M2-BC36	0~3	Crustacea	Tanaidacea	Anarthruridae	*Anarthrura* sp.	2
DY75-I-M2-BC36	0~3	Crustacea	Isopoda	-	*Isopoda* sp.4	3
DY75-I-M2-BC42	0~3	Crustacea	Isopoda	-	*Isopoda* sp.9	1
DY75-I-M2-BC42	0~3	Crustacea	Harpacticoida	-	*Harpacticoida* sp.2	5
DY75-I-M2-BC42	0~3	Polychaete	-	-	*Polychaeta* sp. indet.2	1
DY75-I-M2-BC45	0~3	Crustacea	Isopoda	-	*Isopoda* sp.11	1
DY75-I-M2-BC45	0~3	Polychaete	Terebellida	Cirratulidae	*Chaetozone* sp.2	2
DY75-I-M2-BC45	0~3	Polychaete	Phyllodocida	-	*Phyllodocida* sp. indet.3	1
DY75-I-M2-BC46	0~3	Crustacea	Harpacticoida	-	*Harpacticoida* sp.5	2
DY75-I-M2-BC75	0~3	Polychaete	Terebellida	Cirratulidae	*Chaetozone* sp.1	1
DY75-I-M2-BC77	0~3	Crustacea	Isopoda	-	*Isopoda* sp. indet.1	1
DY75-I-M2-BC78	0~3	Crustacea	Tanaidacea	-	*Tanaidacea* sp. indet.1	1
DY75-I-M2-BC79	0~3	Crustacea	Tanaidacea	-	*Tanaidacea* sp.4	1

Station	Layers (cm)	Taxon	Order	Family	Species	Number of specimens
DY75-I-M2-BC80	0~3	Crustacea	-	-	*Crustacea* sp.indet.	1
DY75-I-M2-BC80	0~3	Polychaete	-	-	*Polychaeta* sp. indet.	1
DY81-BC41	0-3	Polychaeta	Terebellida	Cirratulidae	*Cirratulidae* indet.	1
DY81-BC41	0-3	Polychaete	-	-	*Polychaeta* indet.1	1
DY81-BC41	0-3	Crustacea	Tanaidacea	-	*Tanaidacea* sp.6	1
DY81-BC42	0-3	Crustacea	Tanaidacea		*Tanaidacea* sp.4	1
DY81-BC42	0-3	Crustacea	Isopoda		*Isopoda* sp.13	1
DY81-BC42	3-5	Crustacea	Isopoda	Ischnomesidae	*Ischnomesidae* indet.	1
DY81II-M1-ES08-BC43	0-3	Polychaete	Terebellida	Cirratulidae	*Cirratulidae* sp.3	1
DY81II-M1-ES08-BC43	0-3	Polychaete	Nereidida	Nephtyidae	*Aglaophamus* sp.	1
DY81II-M1-ES08-BC43	3-5	Polychaete			*Polychaeta* indet.2	1
DY81II-M1-ES08-BC43	5-10	Polychaete			*Polychaeta* indet.3	1
DY81II-M1-ES08-BC43	5-10	Crustacea	Tanaidacea		*Tanaidacea* sp.8	1
DY81II-M1-ES08-BC44	0~3	Polychaete	-	-	*Polychaeta* indet.4	1
DY81II-M1-ES08-BC44	3~5	Crustacea	Tanaidacea	-	*Tanaidacea* sp.8	1
DY81II-M1-ES08-BC44	3-5	Polychaete	-	-	*Polychaeta* indet.5	1
DY81II-M1-ES08-BC44	5~10	Polychaete	-	Spionidae	*Spionidae* sp.2	3
DY81-BC45	3-5	Crustacea			*Conchostraca* sp.6	1
DY81-BC46	0-3	Crustacea			*Isopoda* sp.4	1
DY81-BC46	3-5	Crustacea		Munnopsidae	*Munnopsidae* sp.	1
DY81-BC47	0-3	Polychaete		Spionidae	*Prionospio*? sp.	1
DY81-BC47	0-3	Polychaete		Cirratulidae	*Aphelochaeta*? sp.	1
DY81-BC47	0-3	Crustacea			Allodaposia sp.	1
DY81-BC47	5-10	Polychaete		Amphinomidae	*Amphinomidae* sp.	1
DY81-BC48	0-3	Polychaete		Lumbrineridae	*Lumbrineridae* sp.	1

Station	Layers (cm)	Taxon	Order	Family	Species	Number of specimens
DY81-BC48	0-3	Polychaete		Phyllodocidae	*Phyllodocidae* sp. 1	1
DY81-BC48	0-3	Polychaete		Hesionidae	*Hesionidae*	1
DY81II-M2-ES03-BC55	0~3	Crustacea	Amphipoda	-	*Amphipoda* sp.	1
DY81II-M2-ES03-BC55	0~3	Crustacea	Isopoda	-	*Isopoda* sp.4	2
DY81II-M2-ES03-BC55	0~3	Crustacea	Harpacticoida	-	*Harpacticoida* sp.	1
DY81II-M2-ES03-BC55	0~3	Polychaete	-	Spionidae	*Spionidae* sp.2	1
DY81II-M2-ES03-BC55	0~3	Polychaete	-	Polynoidae	*Polynoidae* sp.	1
DY81II-M2-ES03-BC55	0~3	Polychaete	-	Flabelligerida	*Flabelligerida* sp.	1
DY81II-M2-ES03-BC55	0~3	Unknown	-	-	-	3
DY81-BC59	0-3	Polychaete	-	Polynoidae	*Bathymoorea* indet.	1
DY81-BC59	0-3	Polychaete	-	Paralacydoniidae	*Paralacydonia* sp.	1
DY81-BC59	0-3	Polychaete	-	-	*polychaeta* indet.6	1
DY81-BC59	0-3	Polychaete	-	Spionidae	*Spionidae* sp.	1
DY81-BC59	0-3	Crustacea	Isopoda	Desmosomatidae	*Desmosomatidae* indet.	1
DY81-BC59	0-3	Crustacea	Isopoda	Munnopsidae	*Munnopsidae* sp.	1
DY81-BC59	0-3	Polychaete		Cirratulidae	*Cirratulidae* indet.	1
DY81-BC59	0-3	Crustacea	Tanaidacea	Tanaidacea	*Tanaidacea* indet.	1
DY81II-M2-ES03-BC56*	0~3	Polychaete	Terebellida	Cirratulidae	*Cirratulidae* sp.	1

"-" means this classification level could not be identified.

*Leakage of overlying water at tagged stations and severe disturbance of surface sediment samples.
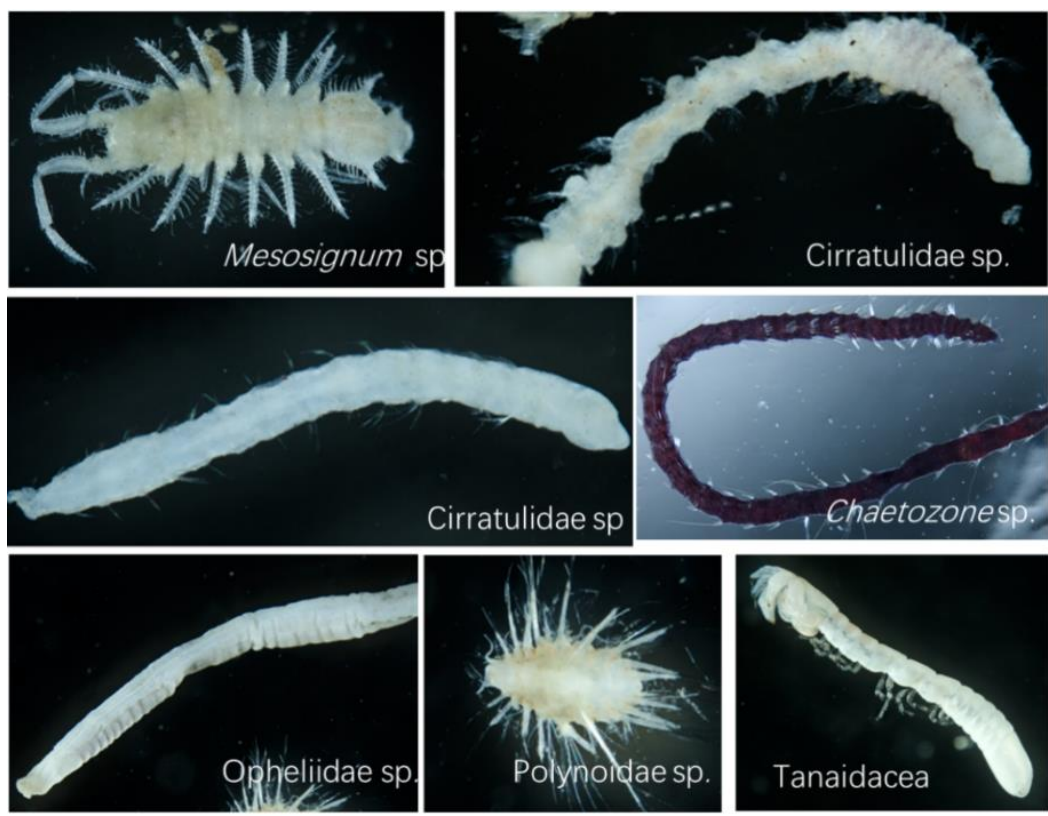
Figure 5-80 Photographs of common macrofauna in Block M.

The mean abundance of macrofauna at 39 survey stations in Block M during the DY75 cruise (2022) was 13.44 ± 15.69 ind/m^2. The maximum value was 64 ind/m^2. The spatial distribution of macrofauna was characterized by large abundance variations among different regions, and survey stations near seamounts had relatively low abundance (Figure 5-81).
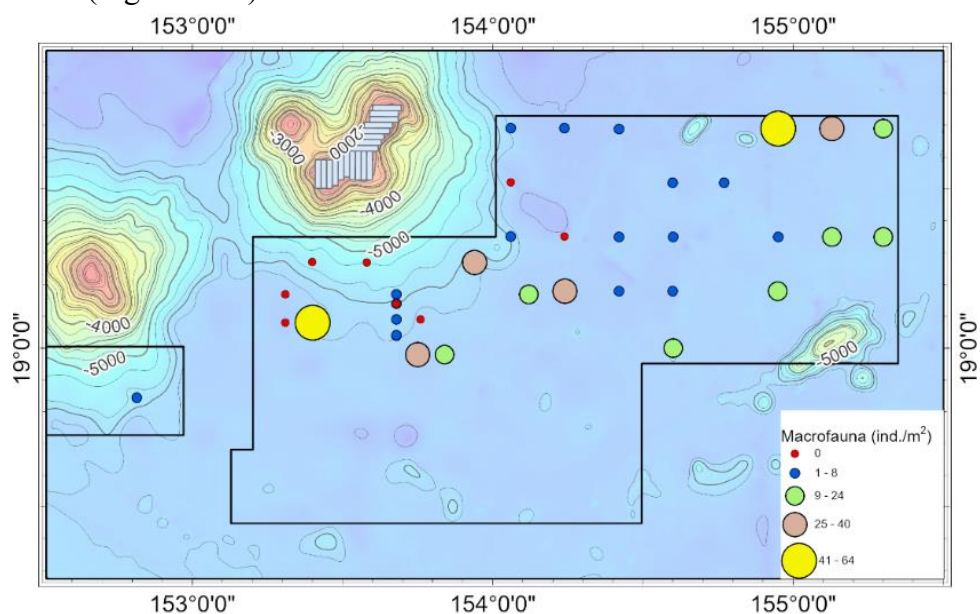
Figure 5-81 Distribution of macrofaunal abundance in Block M for the 2022 Survey

The average abundance of macrofauna at the 10 survey stations in Block M during the DY81 cruise (2023) was 18.0 ± 2.8 ind/m^2.

5.2.3.5.2 Vertical Distribution of Macrofauna

Macrofauna were predominantly found in the 0–3 cm layer. The number of specimens detected in sediment samples from the 0–3 cm, 3–5 cm, and 5–10 cm layers, 59, 6, and 4, respectively, in 2022. while, 33, 6, and 6 specimens were detected in sediment samples from the 0–3 cm, 3–5 cm, and 5–10 cm layers, respectively, in 2023 (Figure 5-82).
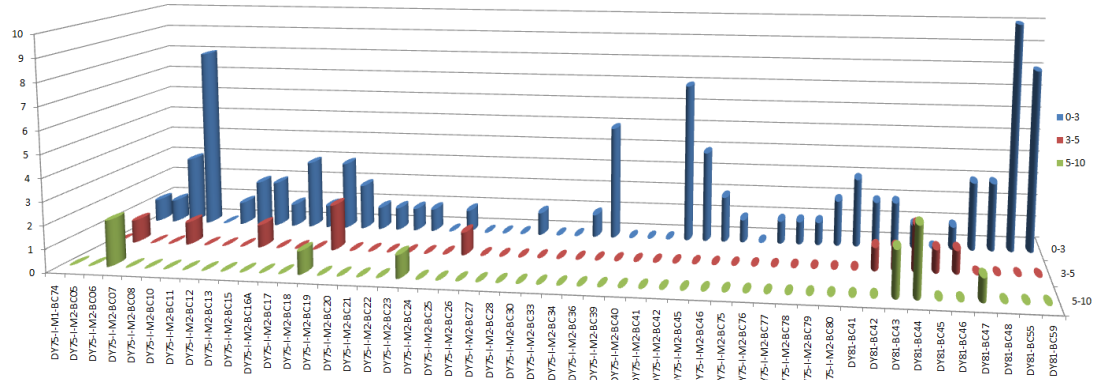
Figure 5-82 Vertical distribution of macrobenthic in Block M.

5.2.3.5.3 Analysis of Macrobenthic Diversity

The species richness of the 31 stations with detected specimens in Block M in 2022 is shown in Figure 5-83 (left), with the highest number of species at Stations BC06 and BC18, each with five species. The results of the Shannon Diversity Index analysis similarly showed higher diversity at Stations BC06 and BC18 (Figure 5-83).

The species richness of the 10 stations with detected specimens in Block M in 2023 is shown in Figure 5-83 (right), with the highest number of species at Stations BC59 and BC55, with 8 and 7 species, respectively.
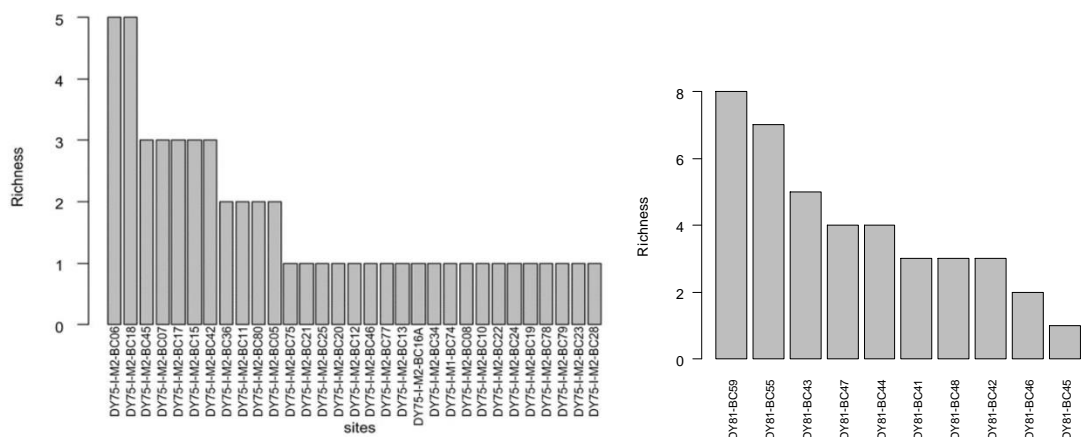
Figure 5-83 Comparison of Shannon's Index for macrofauna in Block M. (Left panel is survey in 2022, right panel is survey in 2023)

Species richness in the region is a fundamental component of biodiversity research, and although three cruises have been conducted in the region, the species accumulation

curve trend shows that the species richness is still rising rapidly, and more sampling is needed to accurately assess species richness in the region (Figure 5-84). Species richness in the region was predicted to be approximately 193 using the chao1 index.
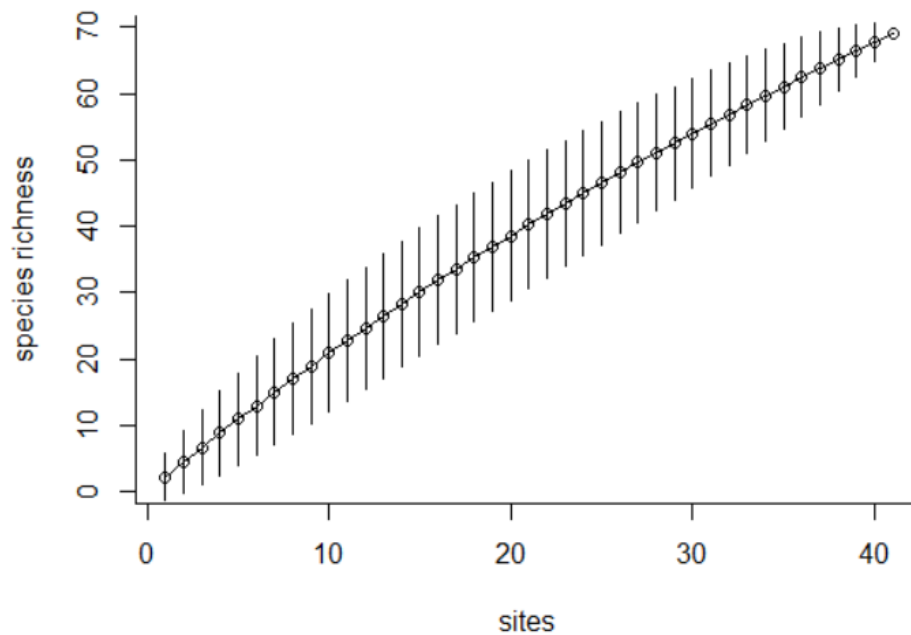
Figure 5-84 Cumulative macrobenthic species richness curves for Block M

The results of the cluster analysis showed that the survey stations in the neighboring seamounts and the stations in the basin area could be better distinguished (Figure 5-85), indicating that Seamounts in the region have a greater influence on the distribution of macrofauna.
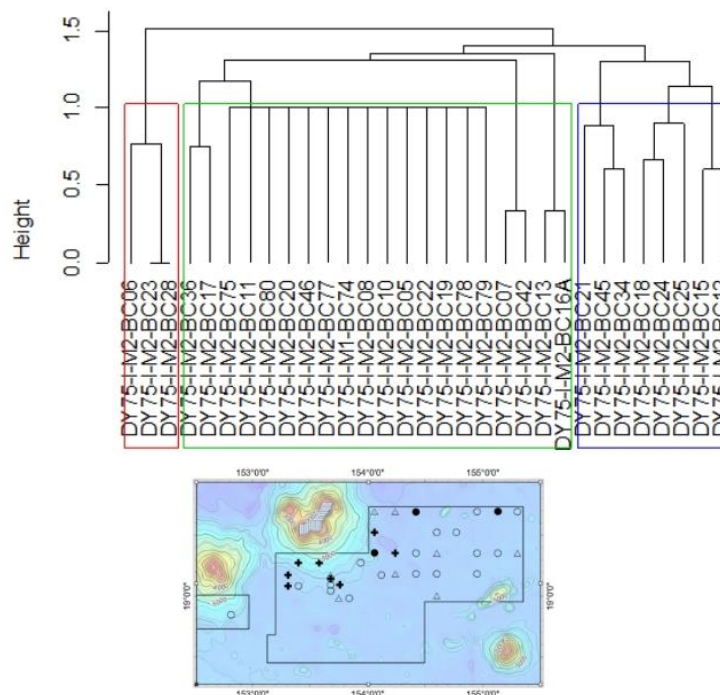
Figure 5-85 Results of cluster analysis of macrofaunal survey stations in Block M

5.2.3.5.4 Annual Changes

Stations BC43 and BC44 in 2023 are in close proximity to BC74 in 2022, and Stations BC55 and BC56 in 2023 are in close proximity to BC77 and BC78 in 2022.

Comparison of macrofaunal abundance between 2022 and 2023 indicated a more obvious difference (p=0.06 at 90% confidence level, Wilcoxon difference test).

Table 5-40 Comparison of macrofauna from DY75 and DY81 cruises

Year	Station	Abundance (ind/m^2)	Species richness	The most abundant taxa
2023	BC43	20	5	Polychaeta
	BC44	24	4	Polychaeta
	BC55	40	7	Crustaceans
	BC56*	4	1	Polychaeta
2022	BC74	4	1	Isopoda
	BC77	4	1	Isopoda
	BC78	4	1	Tanaidacea

*Leakage of overlying water is exposed at marked stations because surface sediment samples are heavily disturbed.

5.2.3.6 Megafauna

5.2.3.6.1 Megafauna Diversity

The seabed imagery data collected from three deep-towed camera transects (PL01, PL02, PL03, see Table 5-41 and Figure 5-86 for line information) in Block M2 during the DY69 cruise (2021) was analyzed, and one sampling area was taken at 10 km intervals quadrat for statistics to obtain a panoramic understanding of the biodiversity and community structure of the study area. The analysis of images data from deep-towed camera was based on the high-resolution photos taken. Megafauna were enumerated in the photos and classified to the most detailed taxonomic level possible. A total of 35 morphospecies belonging to 10 phylum was found in this area, including Porifera, Cnidaria, Annelida, Arthropoda, Mollusca, Echinodermata, Hemichordata, Chordata, Foraminifera, and Bryozoa (see Annex 4 for details), and organisms for which taxa could not be identified were recorded as unknown.

Table 5-41 Information on deep-towed camera transects and number of megafauna in Block M

Surveyor Line	PL01	PL02	PL03
Line length	65 km	56 km	106 km
Average water depth	5656 m	5535 m	5449 m
Number of photos taken	1127	1456	1547
Quadrat size (statistics)	7	6	11
Number of megafauna	1031	1129	1386
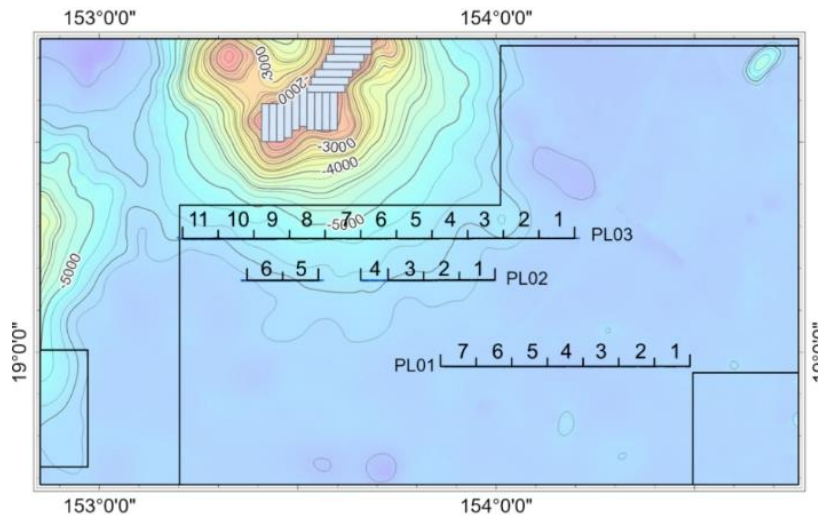
Figure 5-86 Schematic diagram of deep-towed camera transects and quadrats

Except for foraminifera (observed only in PL01) and Hemichordata (observed only in PL02 and PL03), all other taxa were found in all three transects. Echinodermata, Porifera, Arthropoda & Cnidaria were the dominant groups in all three lines, with Echinodermata being the most dominant group in PL02 and PL03 (42%, 44%, respectively), followed by Porifera (20%, 14%), while Porifera was the most dominant group in PL01(31%), followed by Echinodermata (30%). Arthropoda and Cnidaria accounted for 10–13% of the three transects (Figure 5-87).
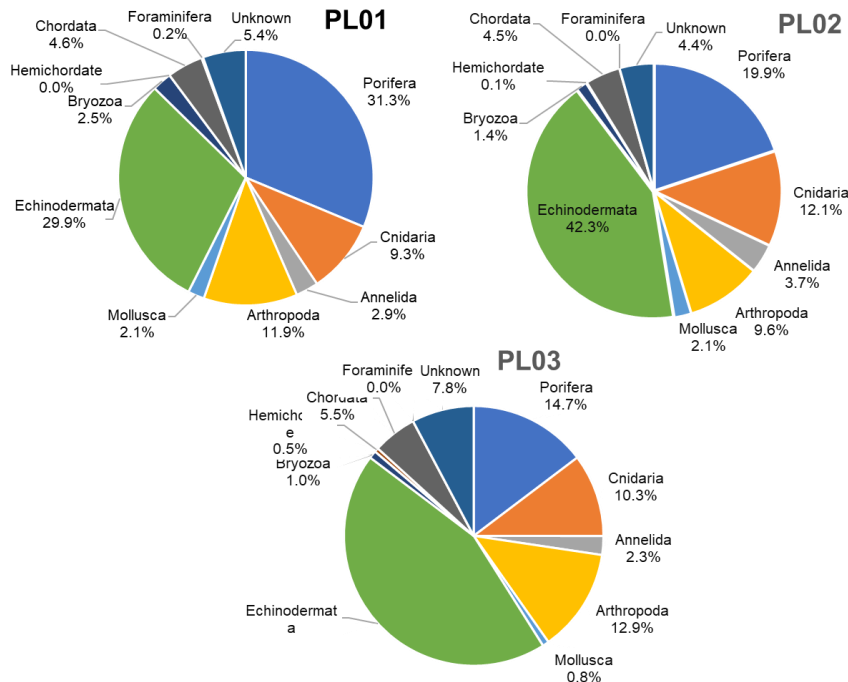
Figure 5-87 Composition of megafauna taxa for three survey lines in Block M2.

5.2.3.6.2 Spatial Variation in the Community Structure of Megafauna

Among the three transects, PL02 had the highest abundance of megafauna with an average value of 18.7 ind./km, and PL03 had the lowest abundance of 12.9 ind./km; the

highest abundance of megafauna among all quadrat was in PL02-4 (26.4 ind./km), and the lowest was in PL03-7 (6.7 ind./km) (Figure 5-88 to Figure 5-90).

Among the three survey transects, PL01 is far away from seamount and less affected by seamount topography. The average water depth of this transect is 5656 m, and the elevation difference of the transect is only about 100 m. The community structure of each quadrat is relatively consistent, and the most dominant group in this transect is Porifera (sessile filter-feeding), followed by Echinodermata. The abundance of megafauna showed an increasing trend from east to west of the Transect, with an average abundance of 15.5 ind./km (Figure 5-86). Foraminifera was detected only in quadrat PL01-1, which had a low abundance and different community structure, while quadrat PL01-6 had the highest abundance of Mollusca and Bryozoa, and PL01-5 had a high abundance of sponge.
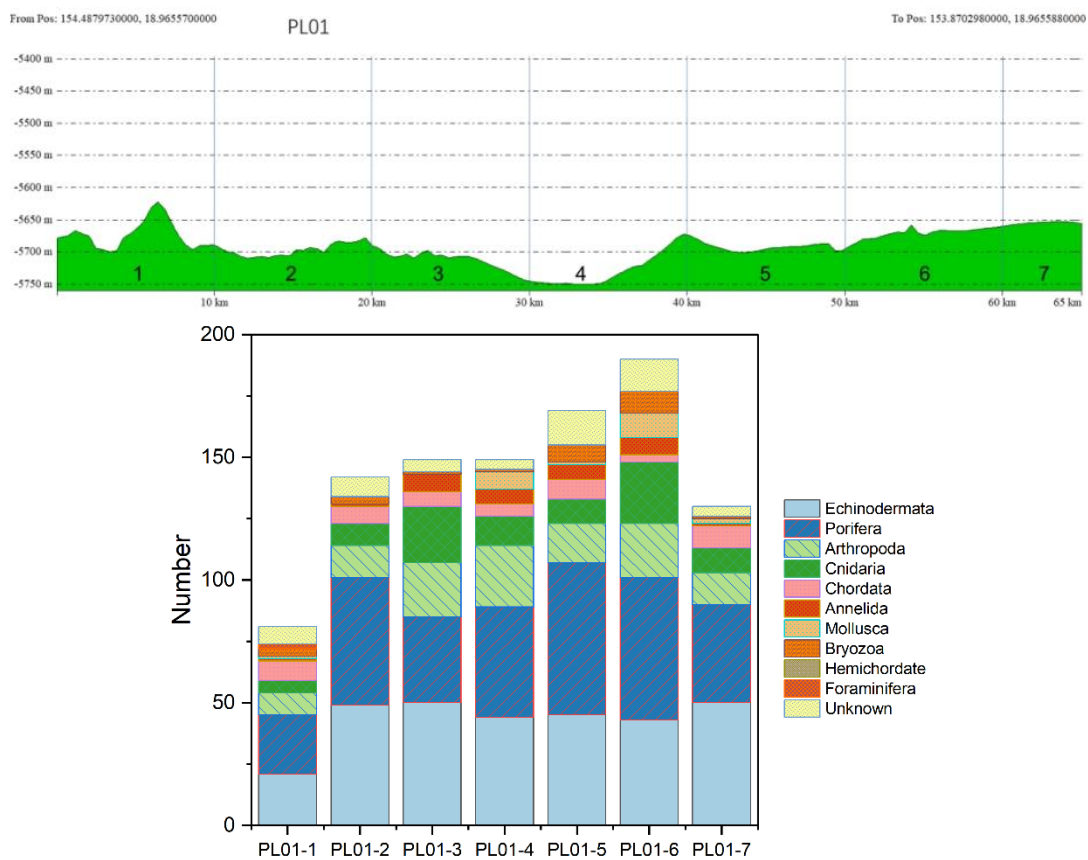
Figure 5-88 Topographic features of survey transect PL-01 (upper panel) and megafauna community structure (lower panel)
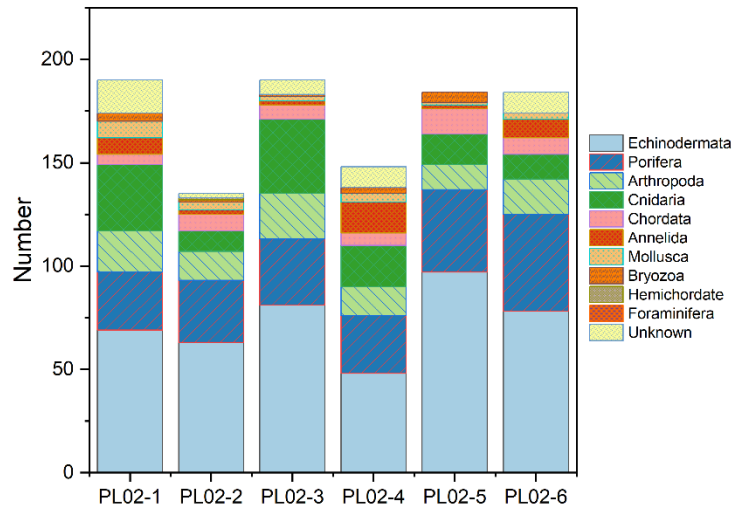
Figure 5-89 Topographic features of survey transect PL-02 (top panel) and megafauna community structure (bottom panel)
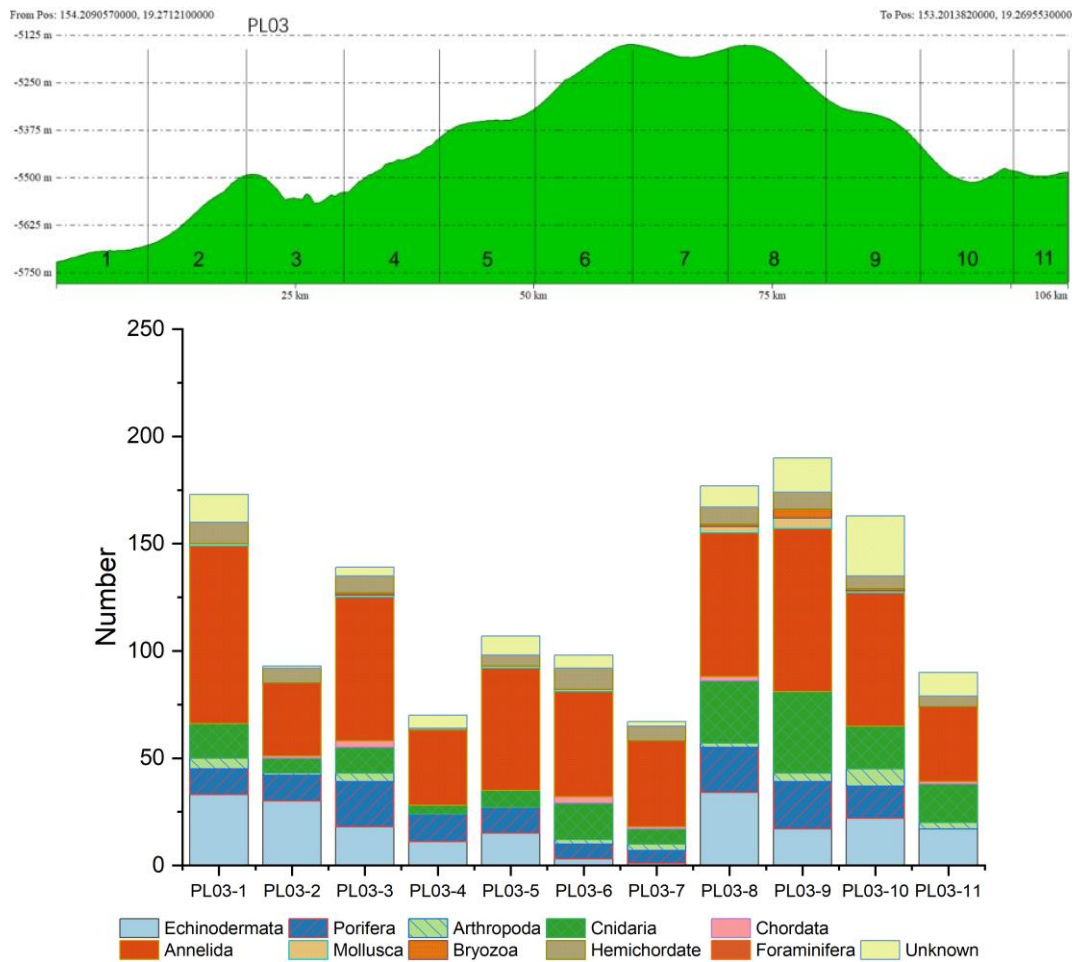
Figure 5-90 Topographic features of survey transect PL-03 (upper panel) and megafauna community structure (lower panel)

The PL02 survey line, with an average water depth of 5535 m and an elevation difference of about 300 m, had the highest abundance of megafauna among the three survey transects, with abundance ranging from 13.5 to 26.4 ind./km in each quadrat, and the average abundance in the transect was 18.7 ind./km. Among them, mollusks

were more abundant group in the PL02-1 quadrat, and chordates and echinoderms were more widely distributed in the PL02-5 quadrat.

PL03 transect was closer to Magoshichi Guyot, with an average water depth of 5449 m. Its Megafauna community was obviously different from the other two transects, and the clustering diagram showed that this transect could be distinguished from the other two transects (Figure 5-91). The abundance of annelids and hemichordates were obviously higher than the other two transects, whereas the abundance of sponges, arthropods, echinoderms, and chordates was relatively low.
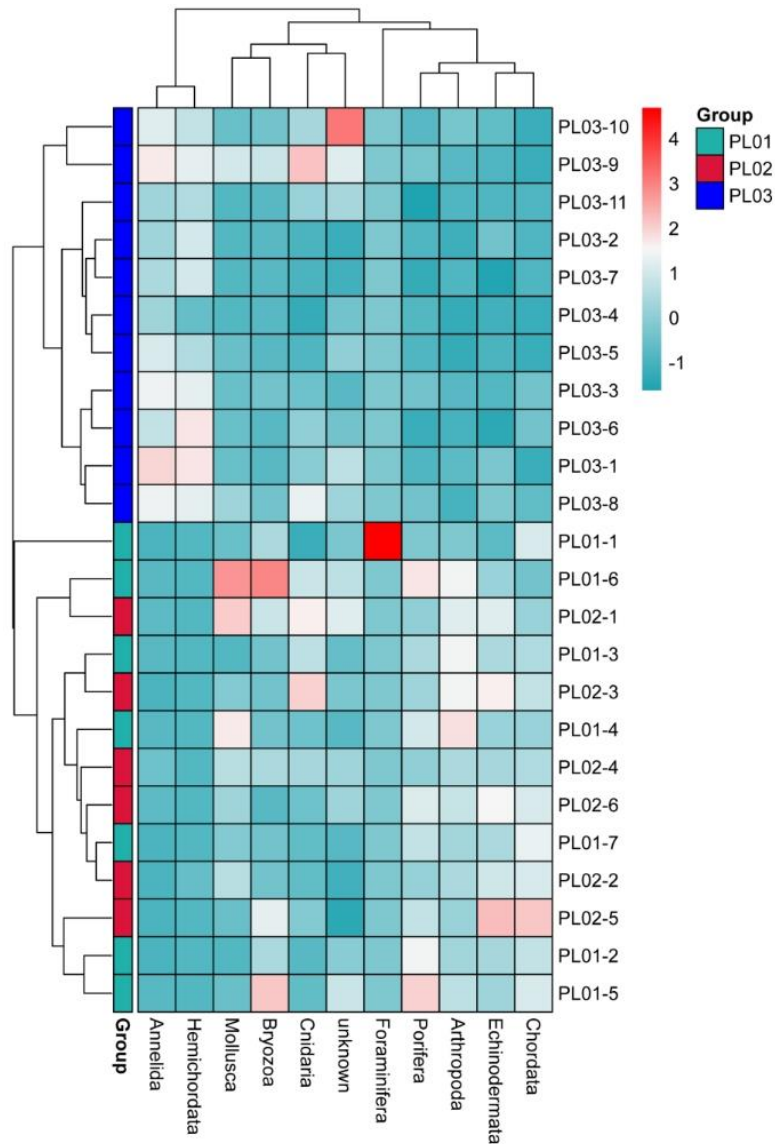
Figure 5-91 Heat map of clustering of megafauna survey quadrats

5.2.3.7 Scavenger

Scavenger surveys were conducted using Lander in 2021 and 2022, and four benthic scavengers species were collected, including *Eurythenes gryllus*, *Paralicella tenuipes*, *Hirondellea dubia*, and Macrouridae und. In addition, Lander-carried camera system was used to recorded observations of five additional groups of megafauna,

including two species of fish (Coryphaenoides sp. and Ophidiidae sp.), and three species of arthropods (Pycnogonida, Gammaridae, and Glyphocrangonidae). Figure 5-92 shows four of the most common megafauna found from the Lander survey in Block M. At Station Lander01 we recorded one Pycnogonida (Figure 5-92a, circled in red), which, from the imagery, appeared to be white in color, with a length of about 5 cm and thin, elongated tentacles that were about 10 cm long. In addition, a *Coryphaenoides* sp. was recorded, with a silvery gray body (Figure 5-92c), scaled all over, and about 30 cm long. Glyphocrangonidae (Figure 5-92b), a common species in the region, was found at all three Lander stations, with a reddish-brown body, well-developed appendages and caudal fins, and antennae that was about twice the length of the body. Demersal Ophidiidae sp. (Figure 5-92d), another demersal fish, was widely distributed in this survey area, and the largest individual observed was about 130 cm in body length.
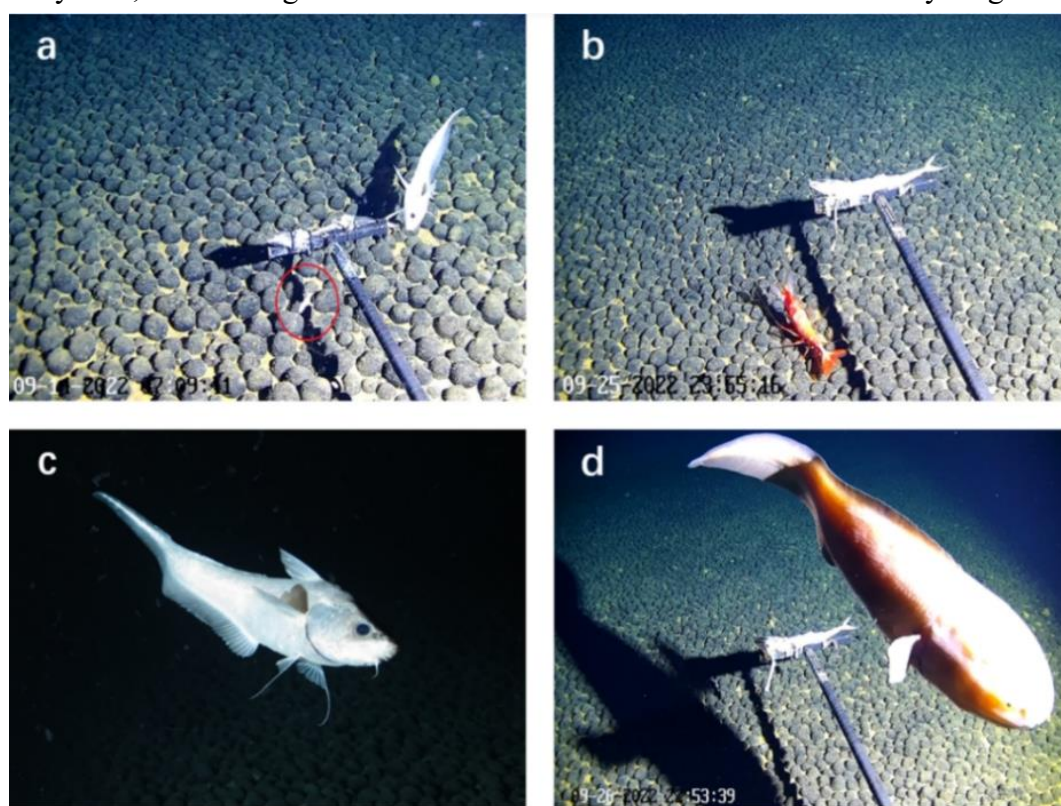
Figure 5-92 Major benthic scavengers recorded by Lander in Block M.

A total of 115 megafauna within three groups, Pycnogonida, crustaceans and demersal fish, were recorded by video at Station Lander01 (Figure 5-93). Crustacean was recorded within an hour of Lander reaching the sea floor, and six decapods and one demersal fish were observed in the third hour after landing. Subsequently, the number of decapods gradually declined while the number of demersal fish showed an increasing trend, reaching a maximum at hour 12, when six demersal fish were observed. Demersal fish continuously appeared near the bait between hour 3 and hour 27 (except for hour 6). After hour 28, the number of demersal fish fluctuated between 1 ~ 2 fish/hour and appeared discontinuously. At hour 22, the camera captured 1 Pycnogonida species.

Finally, a total of 34 crustacean decapods, 84 demersal fish, and 1 Pycnogonida appeared near the bait at this station.
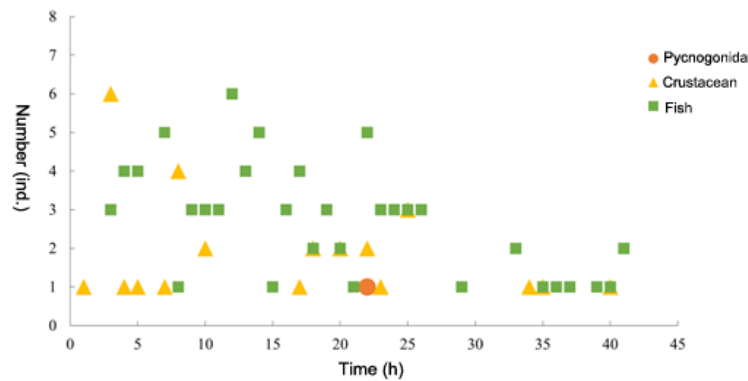
Figure 5-93 Observations of benthic scavengers at Station Lander01 during the DY75 cruise (2022)

Analysis of the video data from Station Lander02 (Figure 5-94) shows that a total of 76 benthos was recorded for crustaceans and benthos fishes. After Lander's arrival on the seafloor, as at Lander01, the crustacean first appeared in the 2nd hour and continued to appear for the next 7 h. After 10 h, the number of decapod numbers began to decline. Demersal fish did not appear near the bait until hour 14, and the camera recorded continuous demersal fish activity for the next 6 hours. The maximum number of demersal fish was recorded at hours 31 and 33, with 6 individuals each, after that demersal fish number declined rapidly, stabilizing at about 1 fish/hour until the end of the observation. In this survey, 26 crustaceans and 48 demersal fish were recorded, respectively.
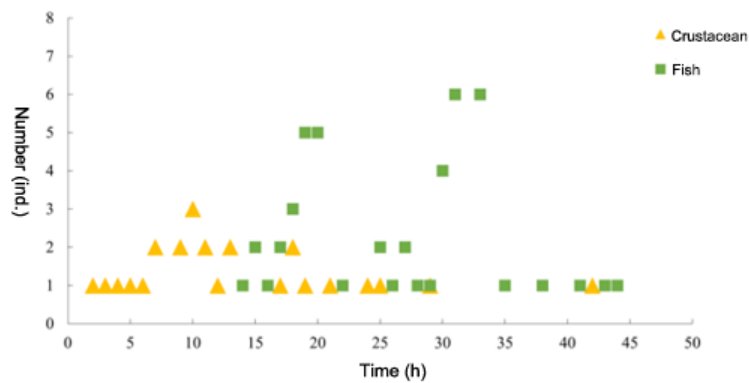
Figure 5-94 Observations of Lander02 benthic scavengers during the DY75 cruise (2022)

The Lander03 video record (Figure 5-95) shows that a total of 90 benthos was recorded for crustaceans and benthic fish at the Station Lander03. Unlike the previous 2 observations, not benthos was recorded until the 3rd hour after Lander landed. Thereafter, the number of decapods stabilized at 1/hour until the end of the observation, while the number of demersal fish fluctuated between 2~5 fishes/hour, with a maximum of 5 occurring at the 23rd, 25th, and 30th hour, respectively. In addition, the number of demersal fish (80) was much higher than the number of crustacean decapods (10).
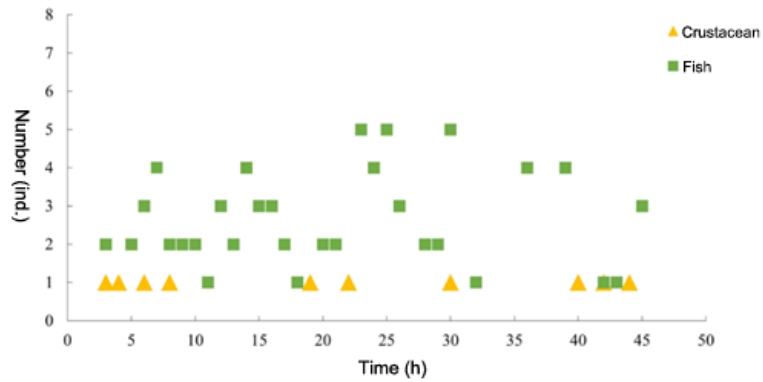
Figure 5-95 Observations of Lander03 benthic scavengers during the DY75 cruise (2022)

5.2.4 Seabirds, Sea Turtles, Large Marine Mammals

5.2.4.1 Underway Observation

During the 2021 and 2023 cruises, BPC carried out observations of marine mammals, seabirds, sea turtles and other large animals at 8:00, 12:00 and 18:00 (local time) everyday to observe the occurrence of these animals (colored markers in Figure 5-96). Due to the scarcity of observations in this area, this report synthesizes information from the OBIS and GBIF public databases and records a total of 4 species of mammals belong to 1 order, 3 families, 4 genera; 3 species of sea turtles in 1 order, 2 families, 3 genera; 24 species of seabirds in 11 families, 18 genera (Table 5-42).
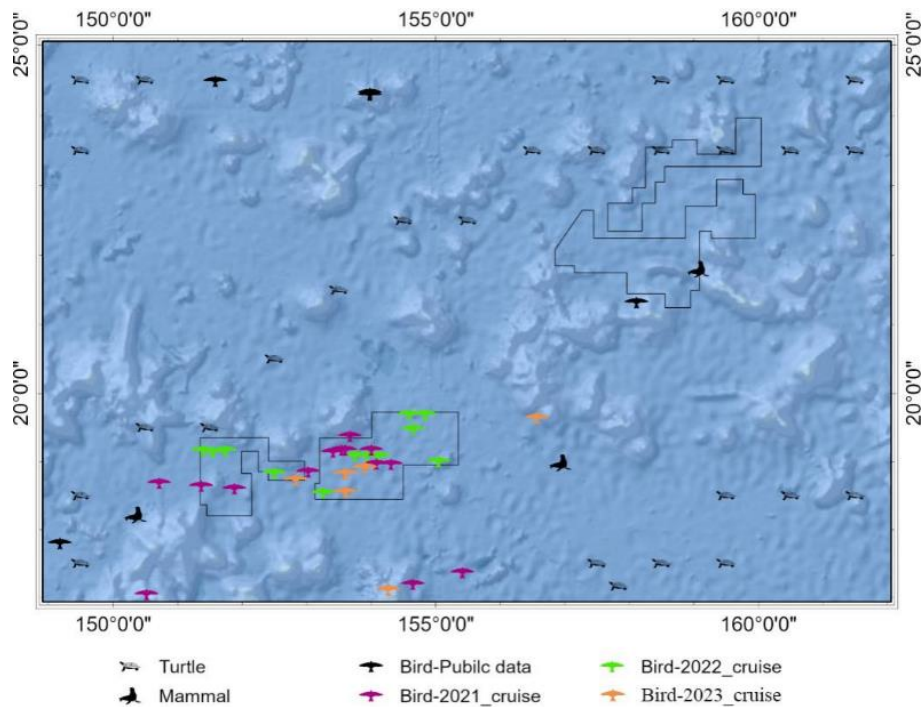
Figure 5-96 Record of observations of mammals, seabirds, and sea turtles in the contract area and adjacent area (Public database records are marked in black and gray in the figure)

According to the International Union for Conservation of Nature (IUCN) List of Threatened Species to be published in 2022, one globally endangered species (EN): *Numenius madagascariensis* (Open Data Base); Six Vulnerable species (VU): *Lepidochelys olivacea* (open database), *Caretta caretta* (open database), *Dermochelys coriacea*, *Physeter macrocephalus* (open database), *Calidris acuminata* (in 2022 cruise observation), and *Calidris acuminata* (in 2022 cruise observation), and *Oceanodroma leucorhoa* (in 2021 cruise observation); one Near-Threatened Species (NT): *Calonectris leucomelas* are recorded in the region (Table 5-42).

Table 5-42 List of mammals, seabirds, and sea turtles found in the contract area and adjacent area

Scientific Name	Class	Order	Family	Genus	Danger
Lepidochelys olivacea	Reptilia	Testudines	Cheloniidae	*Lepidochelys*	VU
Caretta caretta	Reptilia	Testudines	Cheloniidae	*Caretta*	VU
Dermochelys coriacea	Reptilia	Testudines	Dermochelyidae	*Dermochelys*	VU
Stenella coeruleoalba*	Mammalia	Cetartiodactyla	Delphinidae	*Stenella*	LC
Globicephala macrorhynchus*	Mammalia	Cetartiodactyla	Delphinidae	*Globicephala*	LC
Physeter macrocephalus	Mammalia	Cetartiodactyla	Physeteridae	*Physeter*	VU
Balaenoptera brydei	Mammalia	Cetartiodactyla	Balaenopteridae	*Balaenoptera*	LC
Sterna sumatrana	Aves	Charadriiformes	Laridae	*Sterna*	LC
Onychoprion anaethetus *	Aves	Charadriiformes	Laridae	*Onychoprion*	LC
Onychoprion fuscatus *	Aves	Charadriiformes	Laridae	*Onychoprion*	LC
Calidris canutus	Aves	Charadriiformes	Scolopacidae	*Calidris*	LC
Calidris acuminata *	Aves	Charadriiformes	Scolopacidae	*Calidris*	VU
Gallinago stenura	Aves	Charadriiformes	Scolopacidae	*Gallinago*	LC
Numenius madagascariensis	Aves	Charadriiformes	Scolopacidae	*Numenius*	EN
Pluvialis fulva *	Aves	Charadriiformes	Charadriidae	*Pluvialis*	LC
Stercorarius longicaudus *	Aves	Charadriiformes	Stercorariidae	*Stercorarius*	LC
Gvgis alba*	Aves	Charadriiformes	Laridae	*Gygis*	LC
Phaethon aethereu*	Aves	Pelecaniformes	Phaethontidae	*Phaethon*	LC
Phaethon rubricauda*	Aves	Pelecaniformes	Phaethontidae	*Phaethon*	LC
Sula dactylatra*	Aves	Pelecaniformes	Sulidae	*Sula*	LC
Sula leucogaster*	Aves	Pelecaniformes	Sulidae	*Sula*	LC
Sula sula*	Aves	Pelecaniformes	Sulidae	*Sula*	LC
Fregata minor*	Aves	Pelecaniformes	Fregatidae	*Fregata*	LC
Phaethon lepturus*	Aves	Pelecaniformes	Phaethontidae	*Phaethon*	LC
Oceanodroma tristrami*	Aves	Procellariiformes	Hydrobatidae	*Oceanodroma*	LC
Oceanodroma leucorhoa*	Aves	Procellariiformes	Hydrobatidae	*Oceanodroma*	VU
Pterodroma hypoleuca*	Aves	Procellariiformes	Procellariidae	*Pterodroma*	LC
Ardenna pacifica*	Aves	Procellariiformes	Procellariidae	*Ardenna*	LC
Bulweria bulwerii*	Aves	Procellariiformes	Procellariidae	*Bulweria*	LC
Calonectris leucomelas*	Aves	Procellariiformes	Procellariidae	*Calonectris*	NT
Pterodroma nigripennis*	Aves	Procellariiformes	Procellariidae	*Pterodroma*	LC

Note: "*" denotes from the 2021−2023 cruises; others are from publicly available databases.

Seabirds of the genus *Sula* are common in this area, with *Sula sula* being the most abundant species recorded in the contract area, followed by *Sula leucogaster*, *Sula dactylatra* with fewer observations. For the other species, fulmars were commonly seen, with *Ardenna pacifica* and *Calonectris leucomelas* being the most frequently recorded,

while other species occurring sporadically. Petrels were less recorded, because petrels maybe just finish breeding during the survey period and have not yet moved away from their breeding grounds. Phaethontidae birds were less frequently recorded during these cruises, which was also supposed to be related to the breeding season. The commonly seen seabird is shown in Figure 5-97.
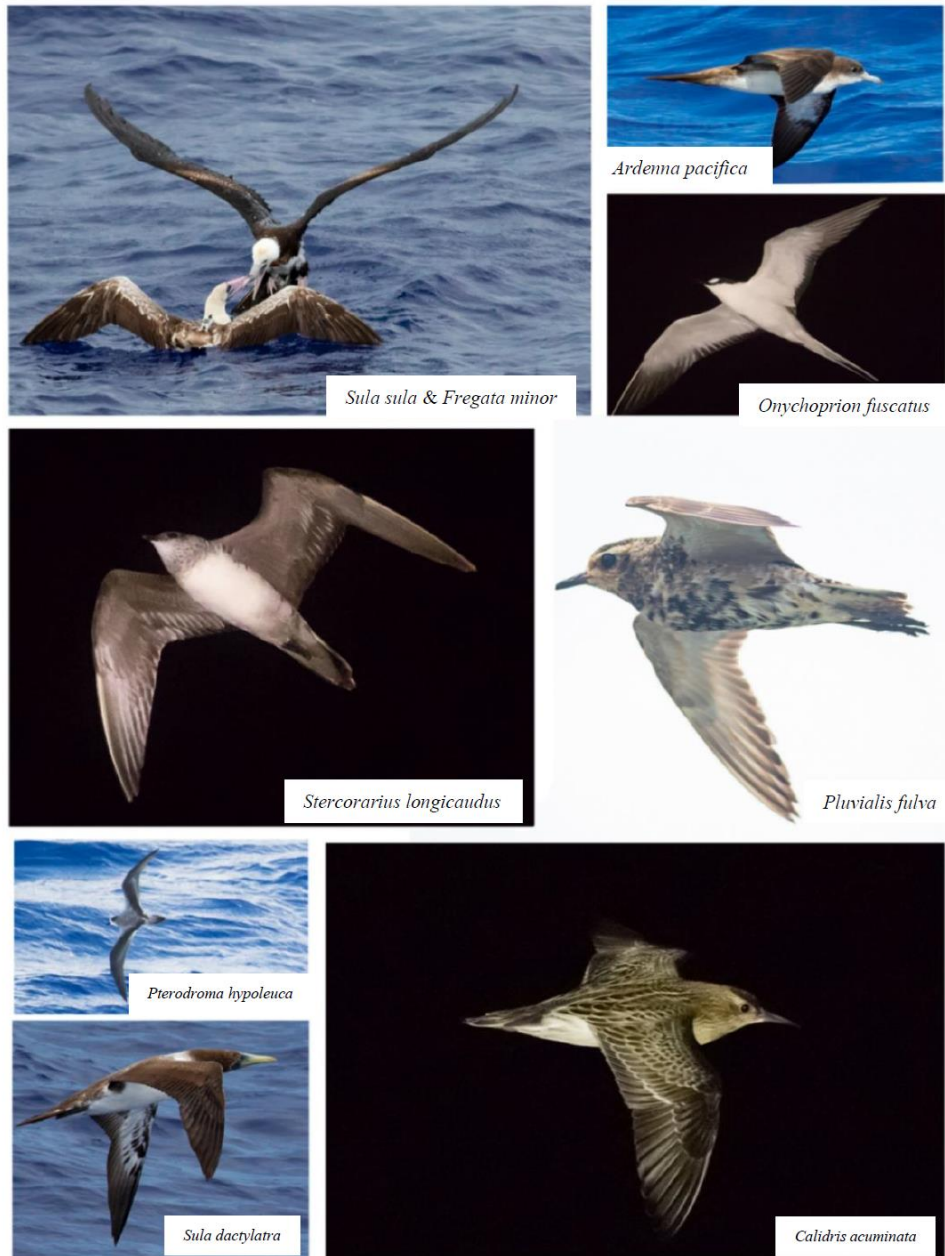
Figure 5-97 Common seabird observed during cruise from 2021 to 2023

5.2.4.2 Passive Acoustic Method

5.2.4.2.1 2021~2022 Results

The passive acoustic records described in section 4.3.6 shows a rich biodiversity of marine organisms, mainly baleen whales and toothed whales. The acoustic occurrences of cetaceans during the deployment are as follows,

(1) Baleen whales

During the one-year deployment, a total of six species of baleen whales were identified through passive acoustic data, namely *Balaenoptera physalus* (Figure 5-98), *Balaenoptera borealis* (Figure 5-99), *Megaptera novaeangliae* (Figure 5-100), *Balaenoptera acutorostrata* (Figure 5-101), *Balaenoptera brydei* (Figure 5-102) and *Balaenoptera musculus* (Figure 5-103), and an unknown baleen whale (Figure 5-104) was also recorded. Of these, *Balaenoptera acutorostrata*, *Balaenoptera brydei* and *Megaptera novaeangliae* occurred more frequently, while *Balaenoptera physalus* and *Balaenoptera musculus* occurred less frequently.

Within a year-long recording period, a total of six species of baleen whales were identified through passive acoustic data, namely the fin whale (*Balaenoptera physalus*, Figure 5-98), sei whale (*Balaenoptera borealis*, Figure 5-99), humpback whale (*Megaptera novaeangliae*, Figure 5-100), minke whale (*Balaenoptera acutorostrata*, Figure 5-101), Bryde's whale (*Balaenoptera brydei*, Figure 5-102) and blue whale(*Balaenoptera musculus*, Figure 5-103), alongside one unidentified baleen whale (Figure 5-104). Among these, the fin whale, blue whale, sei whale, and minke whale were detected more frequently, while spots of Bryde's whale and sei whale were less common.
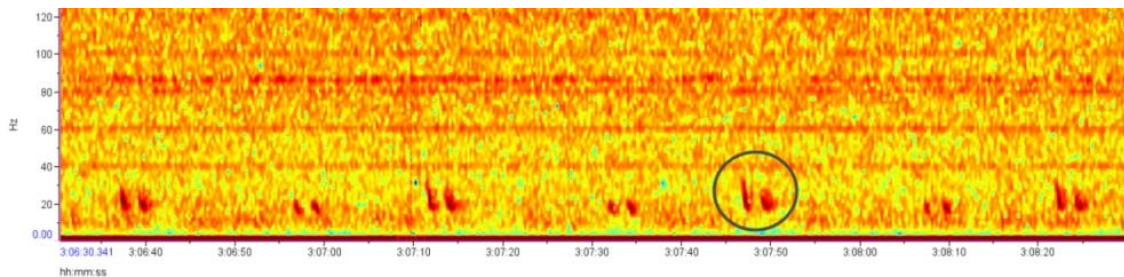
Figure 5-98 Spectrogram of fin whale.
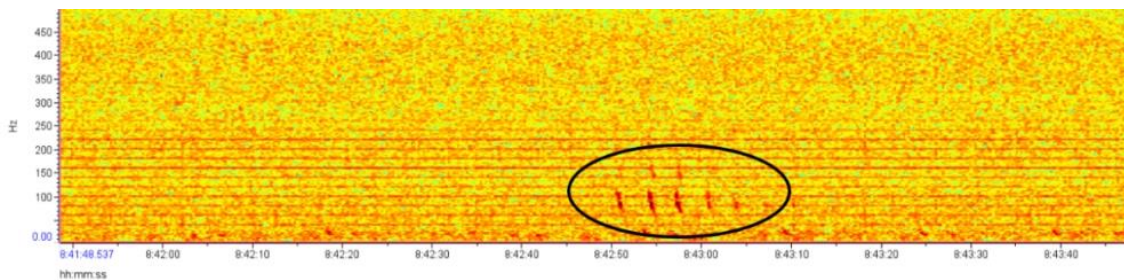
Figure 5-99 Spectrogram of Sei whale.
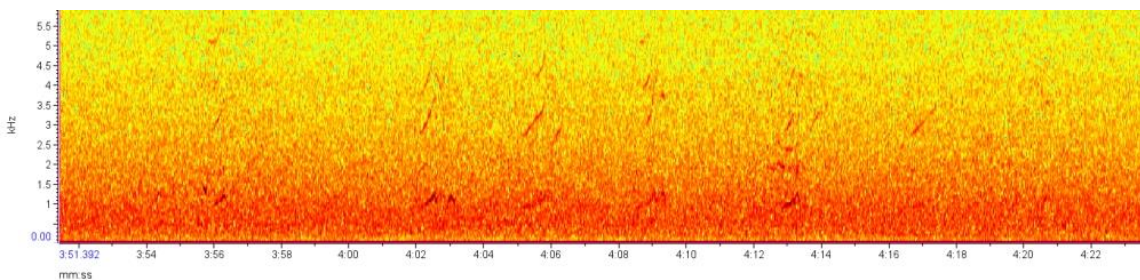
Figure 5-100 Spectrogram of humpback whale.
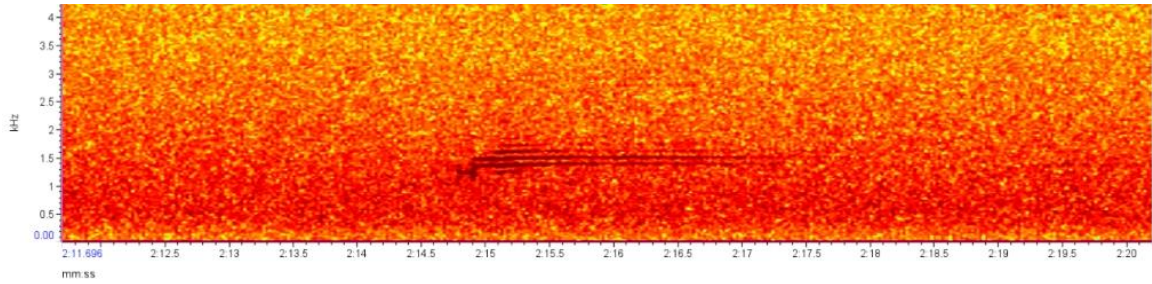
Figure 5-101 Spectrogram of minke whale.
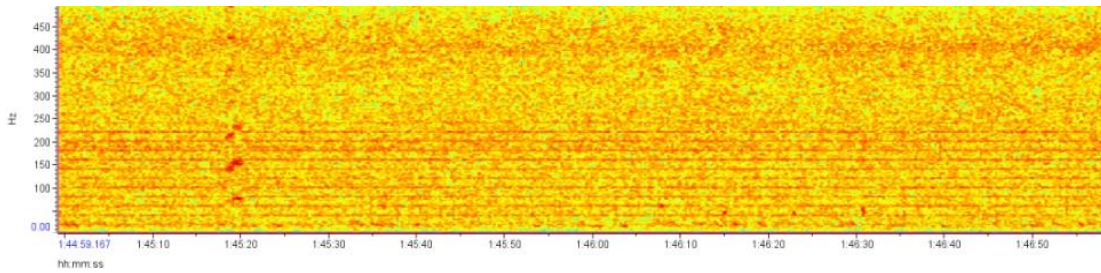
Figure 5-102 Spectrogram of Bryde's whale.
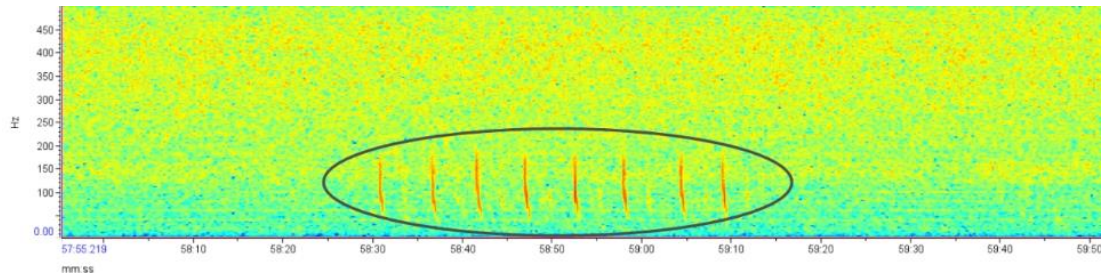
Figure 5-103 Spectrogram of blue whale.
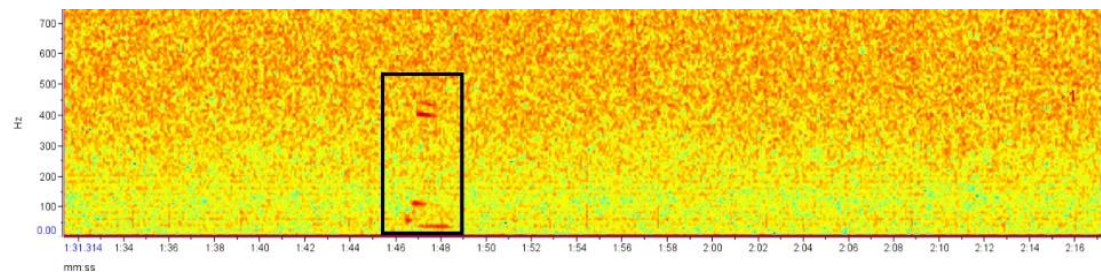
Figure 5-104 Spectrogram of an unknown Baleen Whale.

From the spectrogram of baleen whale vocalizations, we observe distinct patterns across species. Fin whales emit typical 20 Hz pulse signals (Figure 5-98), while sei whales produce segmented downswept signals ranging from 20 Hz to 170 Hz (Figure 5-99). Minke whale vocalizations feature complex wideband harmonic signals spanning from 500 Hz to 6 kHz (Figure 5-101), while Bryde's whales exhibit long-duration harmonic features in the 1 kHz to 2 kHz range (Figure 5-102). Blue whales are identified by their Type D downswept signals, ranging from 35 Hz to 150 Hz (Figure 5-103). Additionally, humpback whales demonstrate short-duration complex wideband characteristics (Figure 5-100). In Figure 5-104, a suspected minke whale is depicted, initially recorded by acoustic gliders during a University of Hawaii survey from 2014 to 2015 and subsequently detected in the western Pacific Ocean. China's surveys in the

Philippine Sea from 2020 to 2022 also recorded this species' vocalizations, indicating its widespread distribution in the region. However, due to the lack of synchronized visual observation data or relevant genetic testing information, further confirmation of its specific species name is required in future studies.

（2）Toothed whales

Compared to baleen whales, toothed whales exhibit wideband characteristics in their vocalizations, with more complex spectrogram features. Historical observations suggest that the western Pacific Ocean hosts a much larger variety of toothed whale species (including dolphins, beaked whales, and sperm whales) compared to baleen whales. During this survey period, toothed whales appeared with higher frequency, and their acoustic signals were recorded almost daily in substantial numbers. However, due to the similar characteristics of vocalizations among multiple toothed whale species, accurate identification and classification based solely on their spectrograms are challenging. For instance, the vocalizations of killer whales and pilot whales exhibit similar features, often requiring additional sightings or genetic testing analysis for effective differentiation.

Currently, within the surveyed area, the only toothed whale species identified through acoustic occurrences is the pilot whale (Figure 5-105). Additionally, a large number of mid- to high-frequency vocalizations produced by toothed whales were recorded (Figure 5-106). However, due to the lack of relevant sightings or other historical references, their species cannot be determined at present. These signals include various types such as whistles, clicks, and moans, associated with activities such as communication, navigation, foraging, and mating among toothed whales. Spectrograms reveal several signal types, including downsweeps, upsweeps, harmonics, and pulse trains. In addition to individual signal types, more complex combinations often occur, varying in bandwidth, inter-call intervals, and duration. Based on the spectrograms of these signals, we speculate that there are at least six different toothed whale species present in the surveyed area.
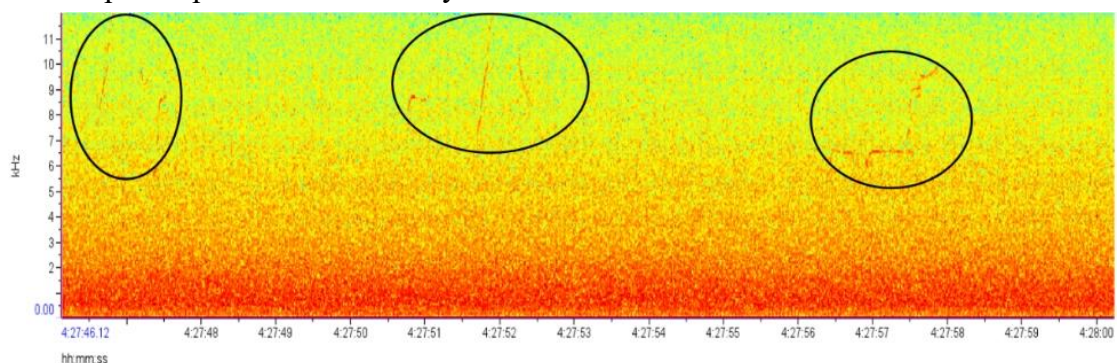
Figure 5-105 Spectrogram of pilot whale.
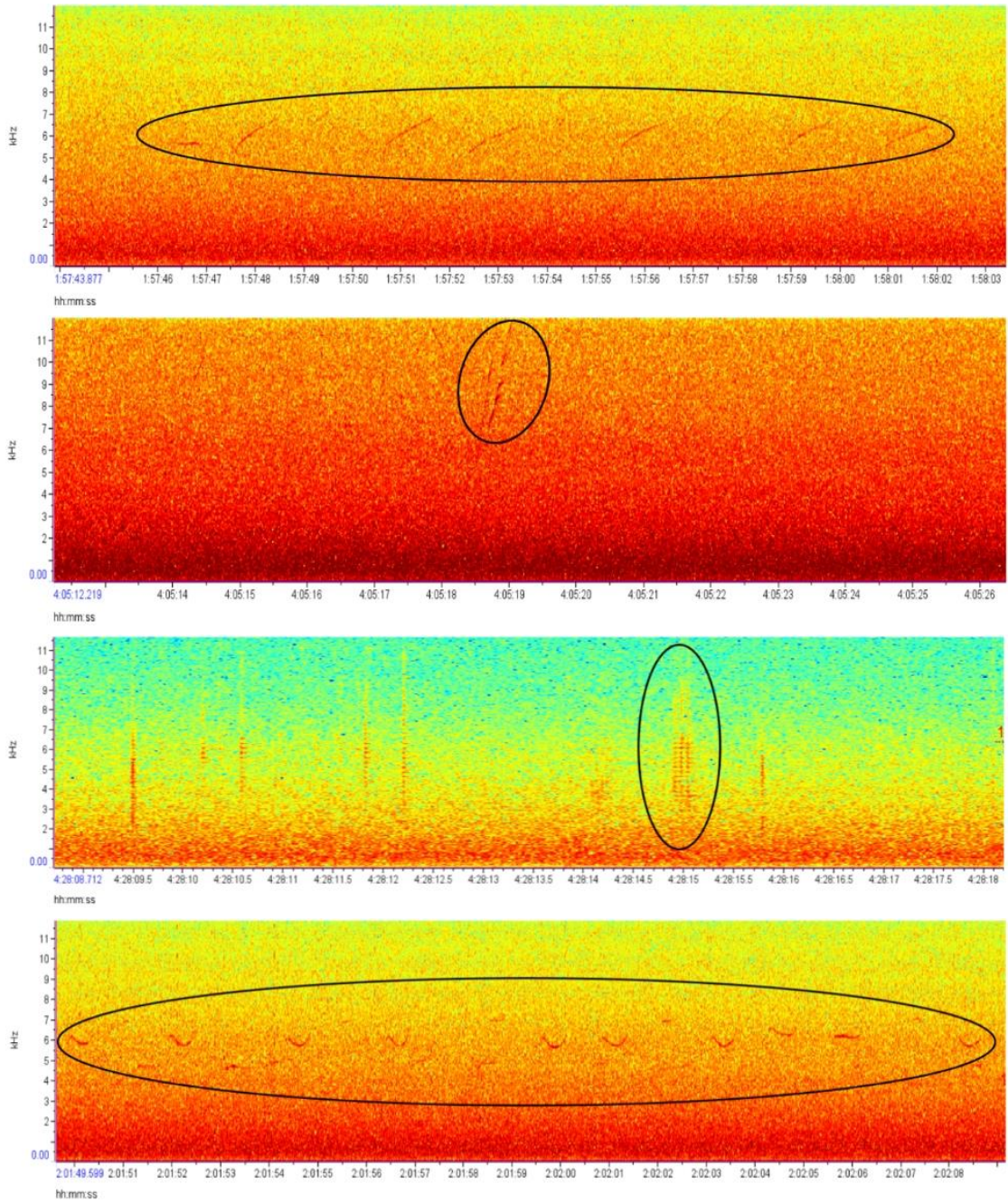
Figure 5-106 Spectrogram of other toothed whales.

5.2.4.2.2 2022~2023 Results

In 2022~2023, numerous of marine mammals were recorded by passive acoustic method, including baleen whales and toothed whales,

(1) Baleen whales

A total of five species of baleen whales, humpback whales, fin whales, Sei whales, minke whales, and blue whales, were recognized through passive acoustic data during the 2022–2023 deployment. In addition, one species of unidentified baleen whale was also recorded. No Bryde's whales were recorded and no new cetacean species were identified in the current year compared to the previous year. Humpback whales and fin

whales had the highest occurrence, while Sei whales, minke whales and blue whales occurred less frequently.

In data processing, the raw acoustic data were downsampled to 2 kHz for detection and identification of blue whales, fin whales and sei whales at low frequencies, whereas for minke whales and humpback whales, which have a higher vocal frequency, the raw data were downsampled to a sampling rate of 8 kHz for analysis.

In the processing of acoustic data for beaked whales, it's essential to downsample the original recordings to a 2 kHz sampling rate. This step enables the detection and identification of low-frequency vocalizations from blue whales, fin whales, and Sei whales. Conversely, for the higher-frequency vocalizations of smaller beaked whales and pilot whales, the original data with a sampling rate of 8 kHz is used for analysis.

To determine the occurrence of each cetacean species in the contract area over the past year, we counted the day number in each month for each cetacean species, calculated the percentage of days of occurrence in the month (days of occurrence in the month/total number of days in the month), and present the corresponding bar charts.

1) Humpback whale

The vocalization of humpback whales is the most complex and variable among all types of cetaceans, usually presenting a complex broadband harmonic signal of 500 Hz~6 kHz. The percentage of humpback whales (Figure 5-107) shows that this species occurs more frequently in the contract area and mainly in the winter and spring seasons (November~April), with no occurrence in June~August and a small number of occurrences in September~October. Humpback whales were recorded in 67 days during the deployment (330 days), with a percentage of occurrence of ~20.4%.
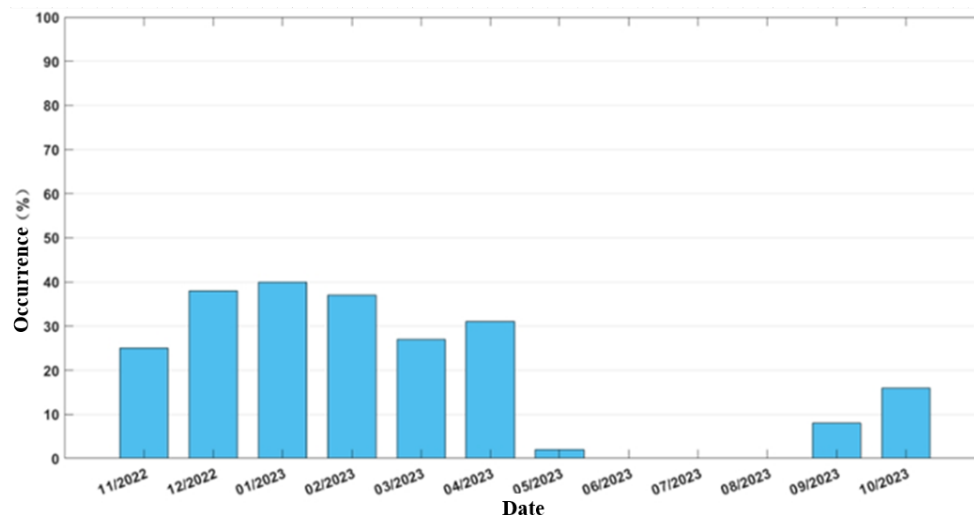
Figure 5-107 Percentage of humpback whale occurrences.

2) Fin whales

Fin whales vocalizations recorded in the contract area are typically characterized by 20 Hz downsweeps. In year 2022, fin whales occurred in all months except July to September (Figure 5-108), with the highest occurrence in April. Fin whales were recorded in 33 days during the deployment, with a percentage of occurrence of ~10%.
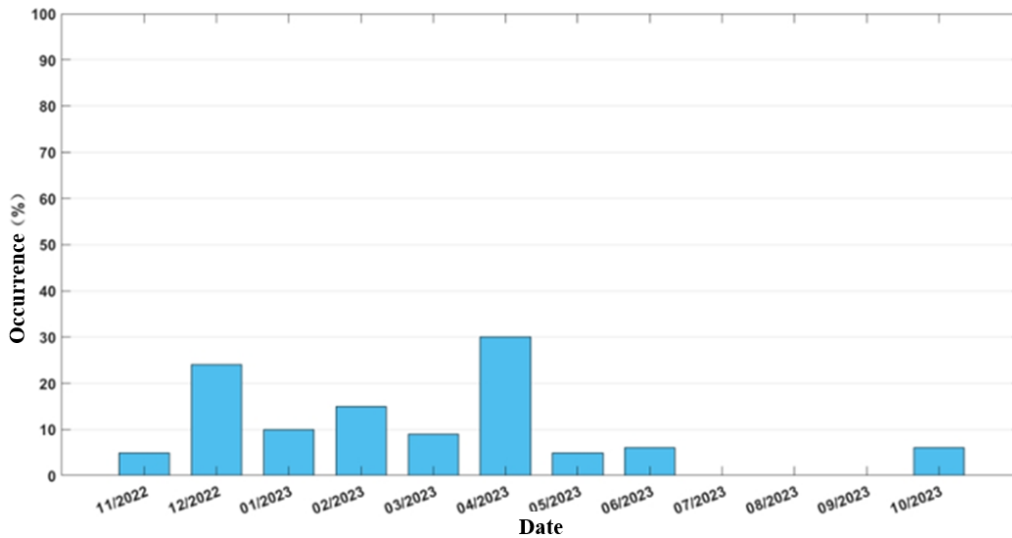
Figure 5-108 Percentage of fin whale occurrences.

3) Blue whales

Two types of blue whales acoustic signals were monitored, downswept D-calls from 35 Hz to 150 Hz and Central Pacific calls, occurring in the time periods of December to January and May to June, respectively, with no associated vocals recorded in the remaining months (Figure 5-109). Blue whales signals were recorded in 16 days during the deployment, with a percentage of occurrence ~5%.
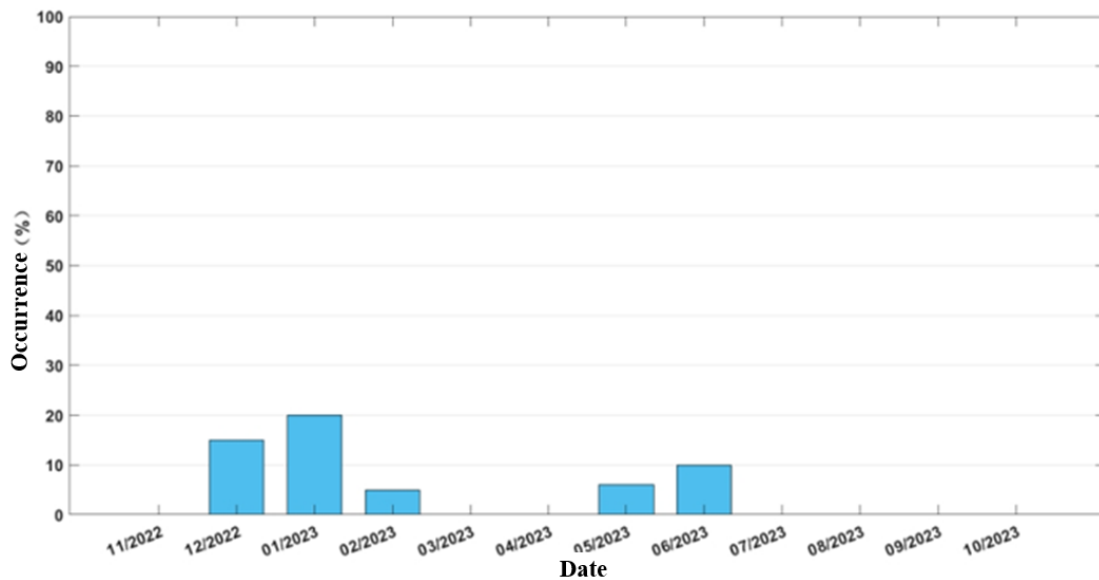
Figure 5-109 Percentage of blue whale occurrences.

4) Minke whales

Minke whales spotted in the contract area are Pacific minke whales, whose vocals are clearly characterized by boings. The spectrogram shows long duration harmonics from 1 kHz to 2 kHz. The occurrences of minke whales are concentrated in the period from January to March, and no relevant vocals were recorded in the remaining months (Figure 5-110). Minke whales vocalizations were recorded in 15 days during the deployment, with a percentage of occurrence of ~4.5%.
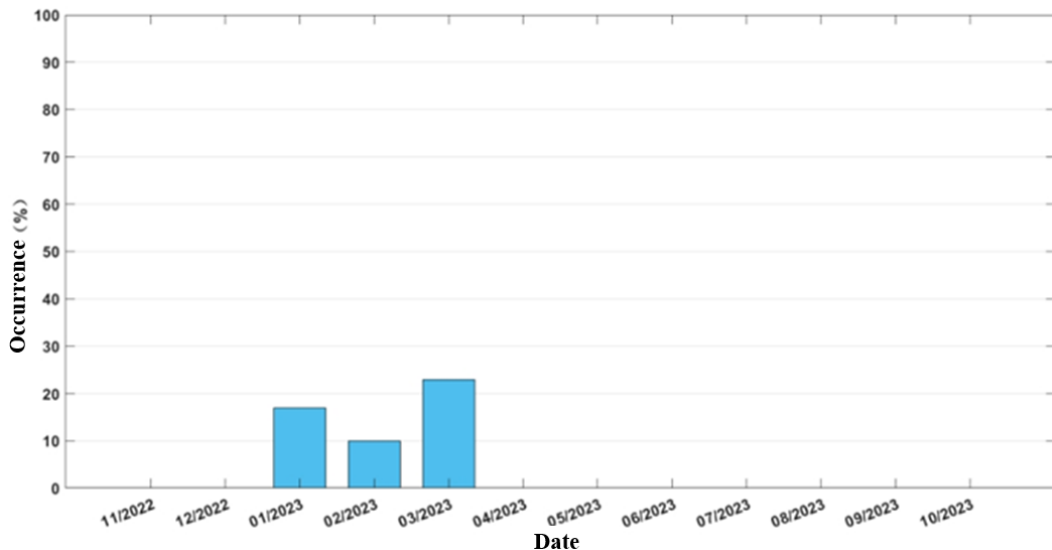
Figure 5-110 Percentage of minke whale occurrence

5) Sei whales

Sei whales vocalizations are downsweeps from 20 Hz to 180 Hz. The occurrence of Sei whales in the contract area is relatively low, concentrated in February and March, and no occurrence in the remaining months (Figure 5-111). Sei whales vocalizations were recorded in 8 days during the deployment, with a percentage of occurrence of ~2.5%.
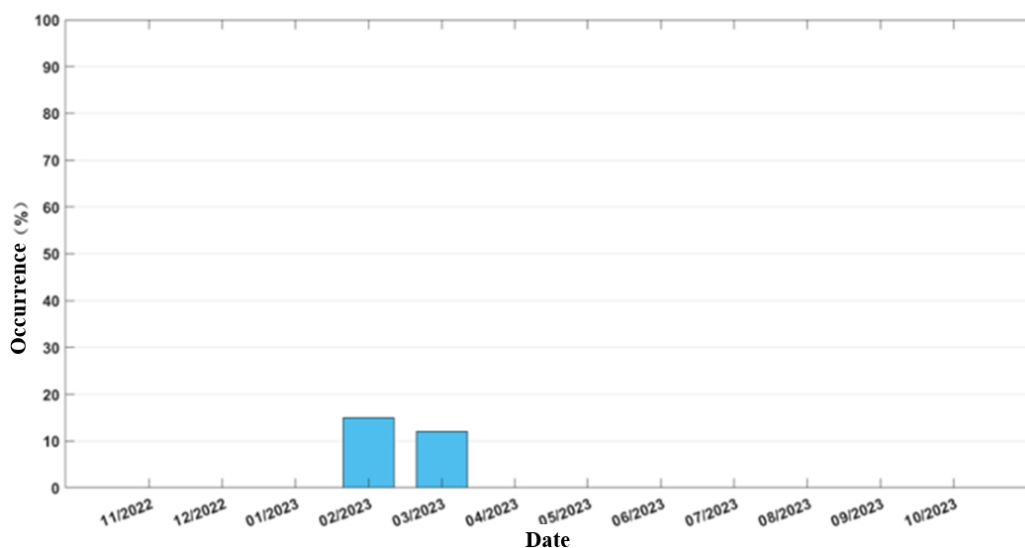
Figure 5-111 Percentage of Sei whale occurrences

6) Unidentified Baleen Whales

Various acoustic signatures of unidentified baleen whale species were recorded in the contract area, the most common of which was a suspected minke whale, a species that has been recorded during acoustic surveys of the contract area in 2022 and acoustic surveys in the Mariana Trench and Philippine Sea in recent years, and is a species that is widely distributed in the western Pacific Ocean waters, but remains unnamed. Numerous unidentified baleen whales were recorded in the contract area during the year

(Figure 5-112), except February and March. Unidentified baleen whale vocals were recorded in 38 days during the deployment, with a percentage of occurrence of ~11.5%.
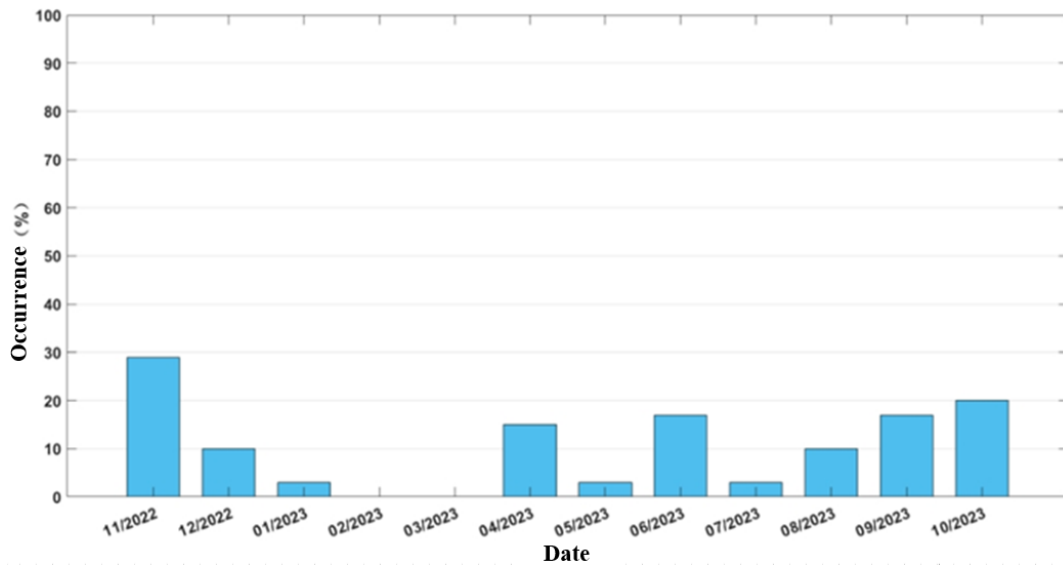
Figure 5-112 Percentage of Unknown Baleen Whale Occurrence

(2) Toothed whales

Compared with baleen whales, toothed whales have many species, and their vocals exhibit broadband characteristics and more complex spectrogram patterns. In year 2022, many more species of toothed whales than baleen whales were found in the contract area, and the percentage of occurrence was high. For simplicity, we only divide toothed whales into Sperm whales (*Physeter macrocephalus*) and other toothed whales.

The vocalizations produced by toothed whales in the contract area are mainly medium- to high-frequency acoustic signals, including whistles, clicks, and moans, and the spectrograms are downsweeps, upsweeps, harmonics, pulse trains, etc. We have found that toothed whales in the contract area produce more acoustic signals than baleen whales.

1) Sperm whales

The vocal of sperm whales in the contract area is a typical click, which occurs more frequently in this year. Sperm whale acoustic signals were detected in all months except November (which had only 8 days of passive acoustic data) (Figure 5-113), making it one of the most frequently occurring cetacean species in the contract area. Sperm whale vocalizations were recorded in 49 days during the deployment, with a percentage of occurrence of ~15.4%.
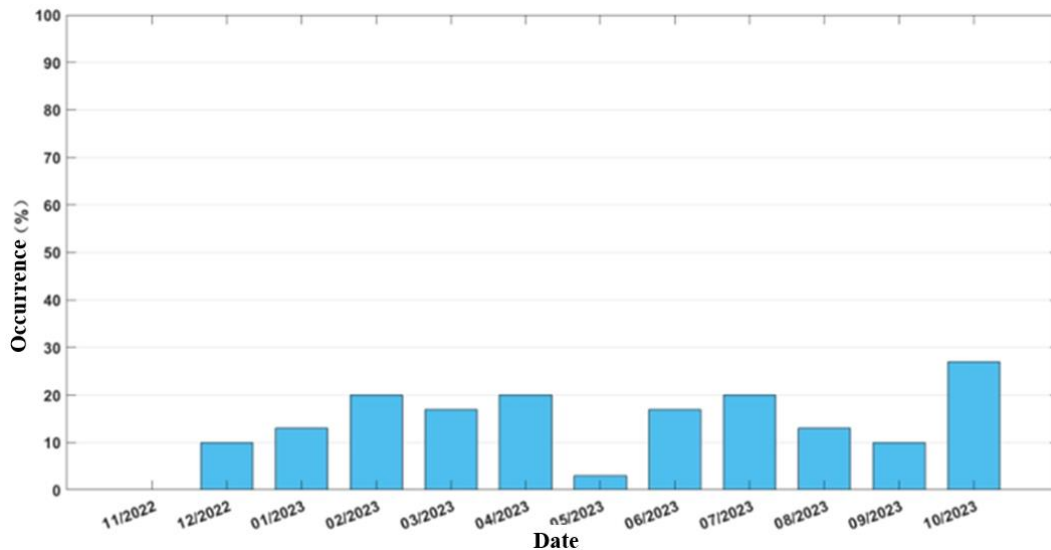
Figure 5-113 Percentage of sperm whale occurrences.

2) Other toothed whales

Other toothed whales in the contract area are more numerous and have high occurrence, with varying numbers of acoustic vocals recorded in all months of the year except May, when no other toothed whale acoustic signals were detected (Figure 5-114), with pilot whales being the highest percentage of occurrence among other toothed whale species in the contract area. Acoustic vocals of other toothed whales were recorded in 67 days during the deployment, with a percentage of occurrence of ~20.5%.
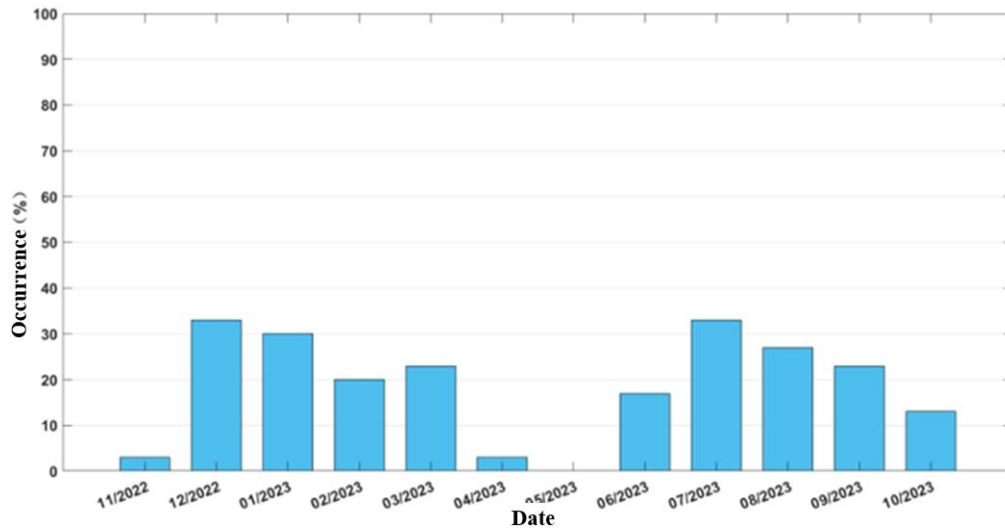
Figure 5-114 Percentage of beaked whales occurrence

Overall, the level of cetacean biodiversity in the contract area is high, with five identified baleen whales and one unidentified baleen whale and several species of toothed whales recorded during the November 2022 – October 2023 period. Temporally, although acoustic vocals of cetacean activity were recorded almost every day of the deployment, baleen whales occurred more frequently in the contract area during the winter and spring seasons from November to April, while toothed whales were relatively more evenly distributed across the seasons.

5.2.5 Fishery Resources

During 2021 cruise, ship-based Echo Sounder System was used to conduct fishery resource assessment in the contract area. The acoustic signal showed an obvious scattering layer in the contract area at night (Figure 5-115), and the Nautical Area Scattering Coefficient index (NASC) at night was obviously higher than daytime. During daytime, the mean NASC values ranged 4.02–14.90 m^2/n $mile^2$, with a mean of 9.78 m^2/n $mile^2$; the mean NASC during the nighttime ranged 46.96–90.68 m^2/n $mile^2$, with a mean of 65.69 m^2/n $mile^2$ (Figure 5-116). The nighttime NASC values are mainly affected by the scattering water layer above 200 m at night. The scattering layer is generally formed by the aggregation of Myctophidae and plankton. In the ocean, the scattering layer during the daytime is generally distributed in the deep layer at depth of 400 – 800 m, while at night, some Myctophidae/plankton could vertically migrate to the layer shallower than 100 m for feeding.
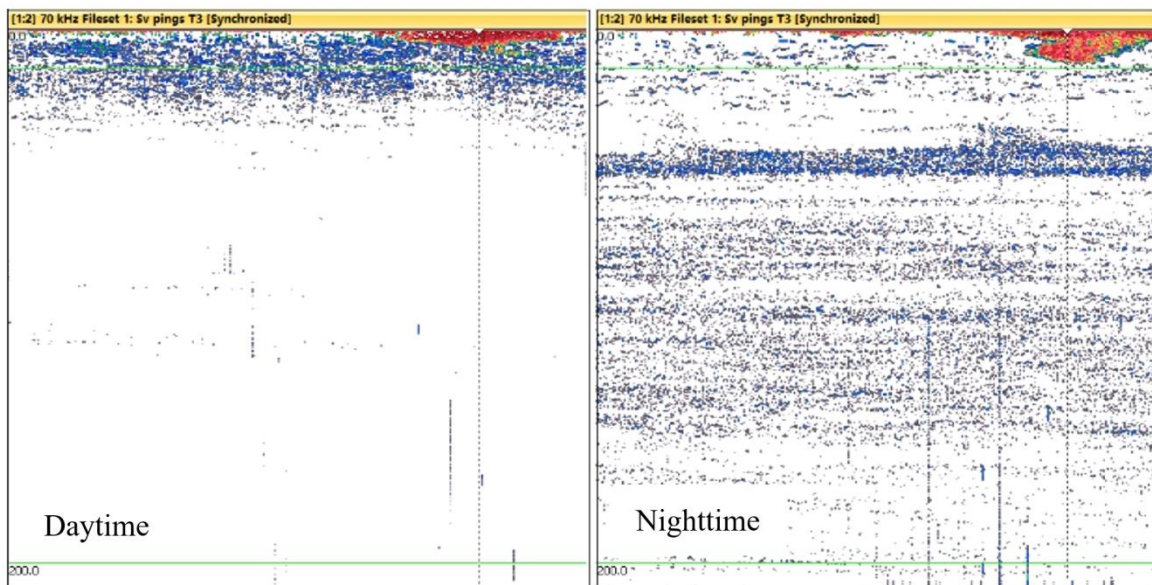
Figure 5-115 Characteristic of diurnal echo strength in the survey area
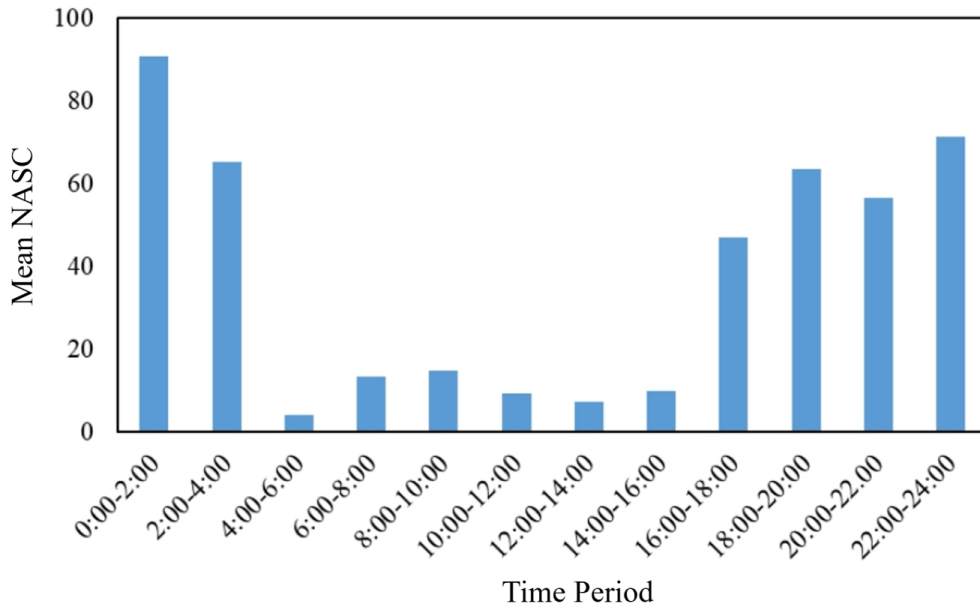
Figure 5-116 Mean NASC values for each time period in the surveyed area

Based on the underway acoustic signals analysis, the spatial distribution pattern of NASC in the contract area were obtained (Figure 5-117), which shows a higher NASC value in the northern part and a lower value in the southeastern part.
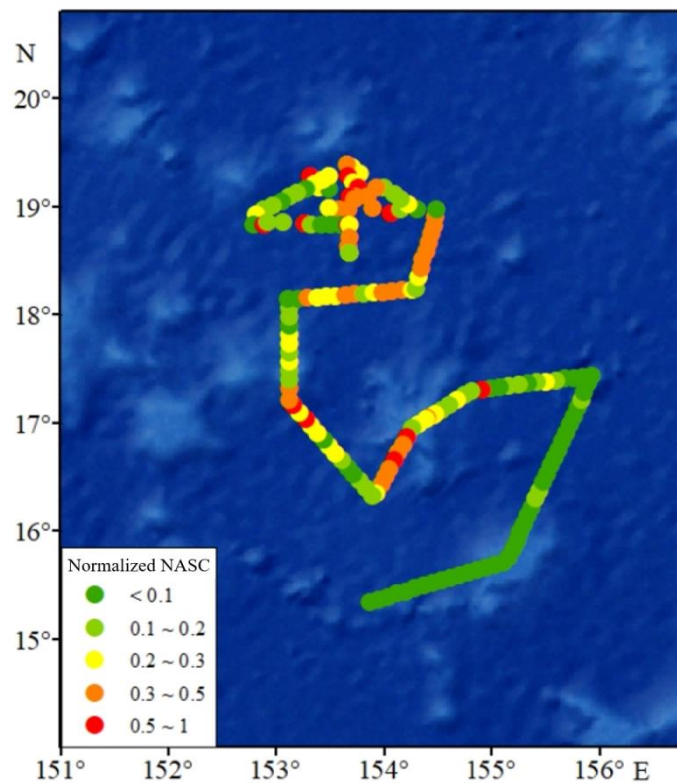
Figure 5-117 Distribution of normalized NASC values in the surveyed area

The main catch in the Western and Central Pacific Ocean is tuna (Shimei Zhang, 2004). The Western and Central Pacific Fisheries Commission (WCPFC) reported the major tuna species catches of the Western and Central Pacific Ocean in the Annual Report 2022 (WCPFC, 2022). As shown in Figure 5-118, the high value area of tuna

catch is mainly distributed in the tropical Pacific (20 °N – 20 °S), with a low yield in the contract area, and the main economic fish species are three species of tuna (albacore, yellowfin, and bigeye) and four species of sailfish (barred marlin, swordfish, striped marlin, and black marlin).
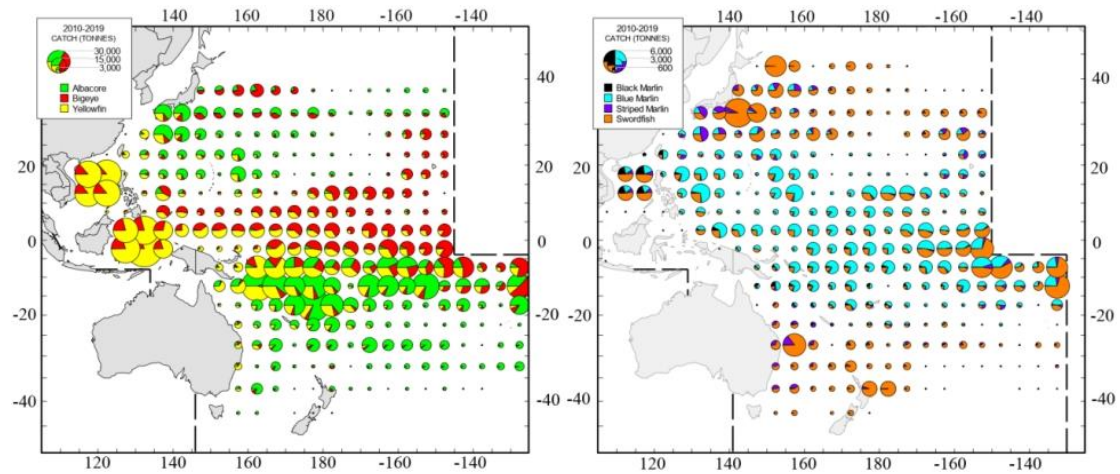
Figure 5-118 Catch of three species of tuna (left) and sailfish (right) by longlines fishing in the Western and Central Pacific from 2010 to 2019 (Source: WCPFC, 2022)

Existing studies show that the main type of fishing operation near the BPC's contract area is longline fishing (Figure 5-119), and the time spent by longline fishing vessels exceeds 50% of the total time for all operation types (Xing et al., 2023). However, location data of fishing vessel based on the AIS system show that from 2012 to 2020, the main fishing vessels in the Pacific are concentrated in the east of the Japanese islands and the equator and its southern region in the Northwest Pacific, and that the mining area is not the main fishing active area in the Pacific (Figure 5-120). According to the WCPFC report in 2022, there is a certain amount of longline fishing for tuna species in the BPC's contract area, but it is much lower than that in the Equator and its southern region. There is only little production from handline fishing and no production from purse seine in the BPC's contract area (Figure 5-121).
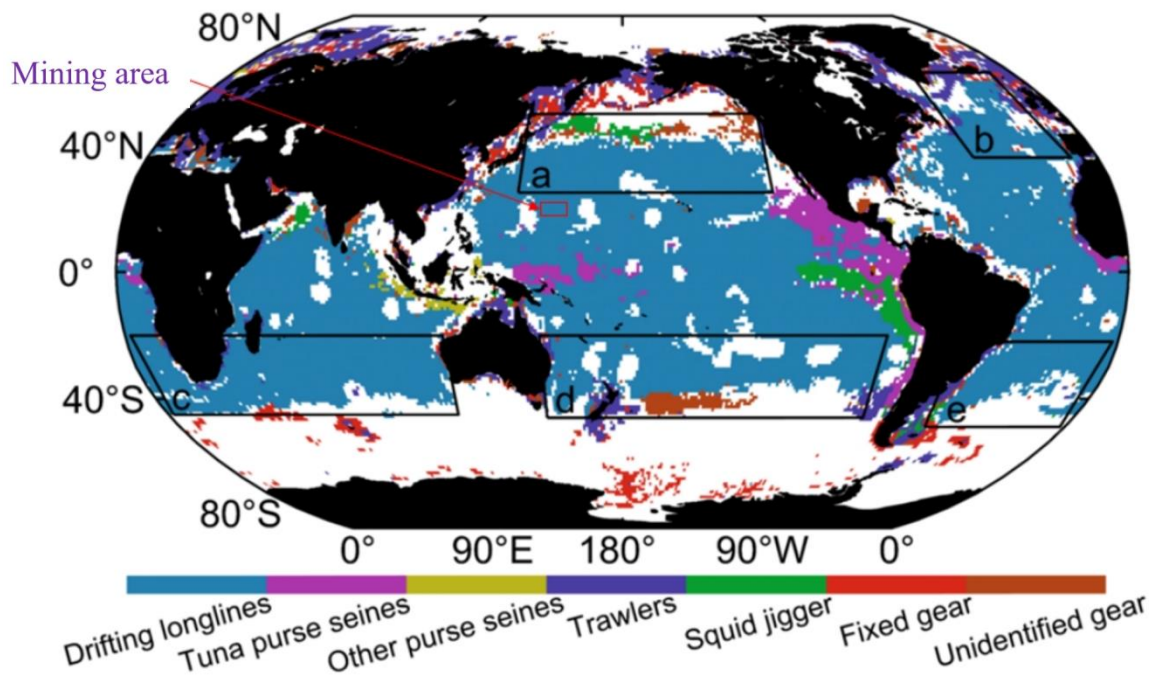
Figure 5-119 Distribution of the main types of fishing operation in the ocean (Source: Xing et al., 2023, fish and fisheries)
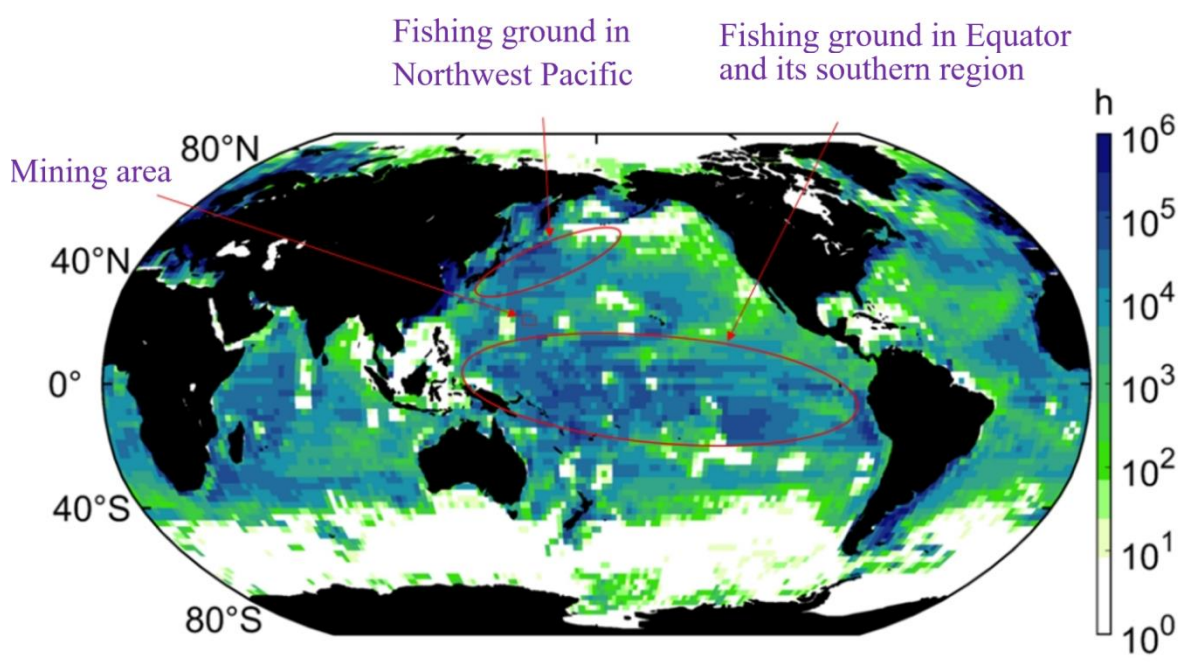
Figure 5-120 Distribution of average number of fishing vessels based on AIS for 2012 – 2020 (Source: Xing et al., 2023, fish and fisheries)
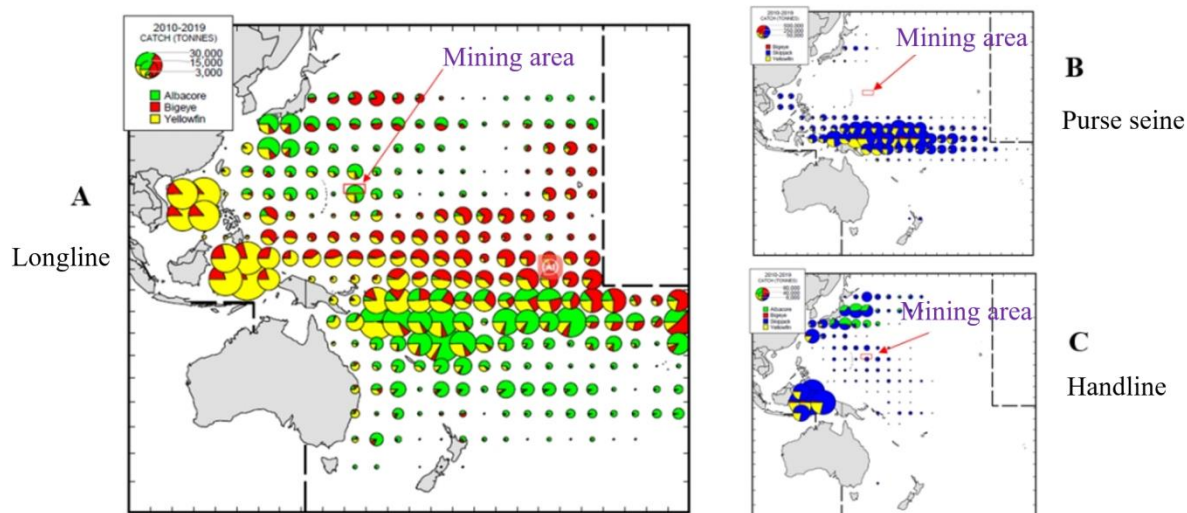
Figure 5-121 Distribution of tuna catches in the Western and Central Pacific Ocean with different types of operations, A: longline, B: purse seine, C: handline (Source: WCPFC, 2022)

5.3 Ecosystem Characteristics in Block M

5.3.1 Primary Productivity

5.3.1.1 Horizontal Distribution

The 2021 survey in Block M showed the mean primary productivity of the euphotic layer was 25.03 ± 10.43 mgC/m$^2 \cdot$h, which was about one-fifth higher than that in 2022 and basically the same as that in 2023 (Table 5-43). The horizontal distribution (Figure 5-122 to Figure 5-124) showed that the primary productivity content in 2021–2023 was generally high in west, low in east, and high in north, low in south.

Table 5-43 Annual variation in mean value and varying range of primary productivity in Block M (2021–2023)

Year	Sampling Time	Mean Value（mgC/m$^2 \cdot$h）	Varying Range (mgC/m$^2 \cdot$h)
2021	2021.10.21–2021.10.29	25.03±10.43	13.02–37.85
2022	2022.11.20–2022.11.29	20.95±9.09	8.95–29.16
2023	2023.08.26–2023.09.13	25.80±5.51	19.56–30.01
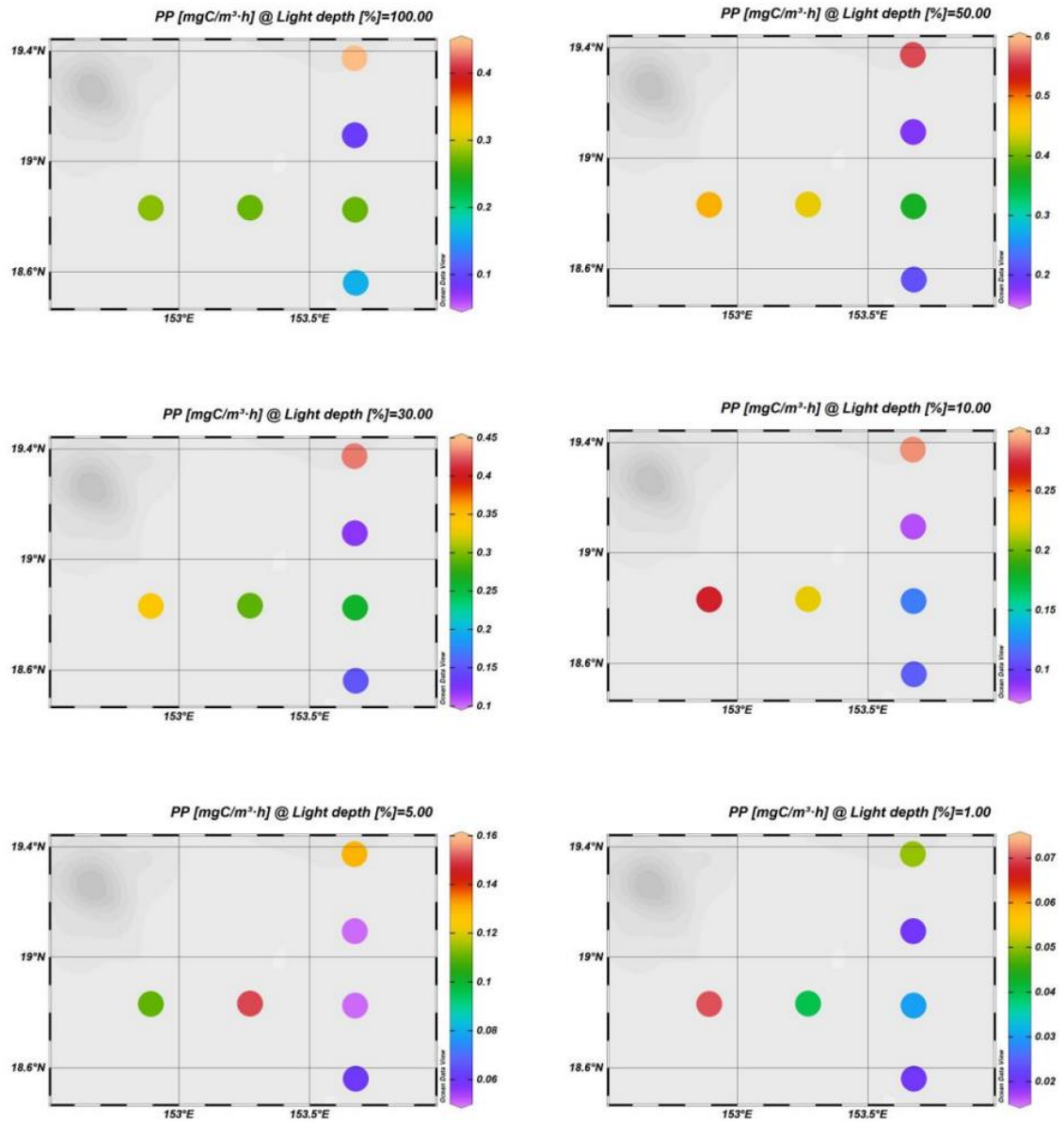
Figure 5-122 Horizontal distribution of water column primary productivity in the euphotic layer in contract area, 2021 (mg C/(m² · h))
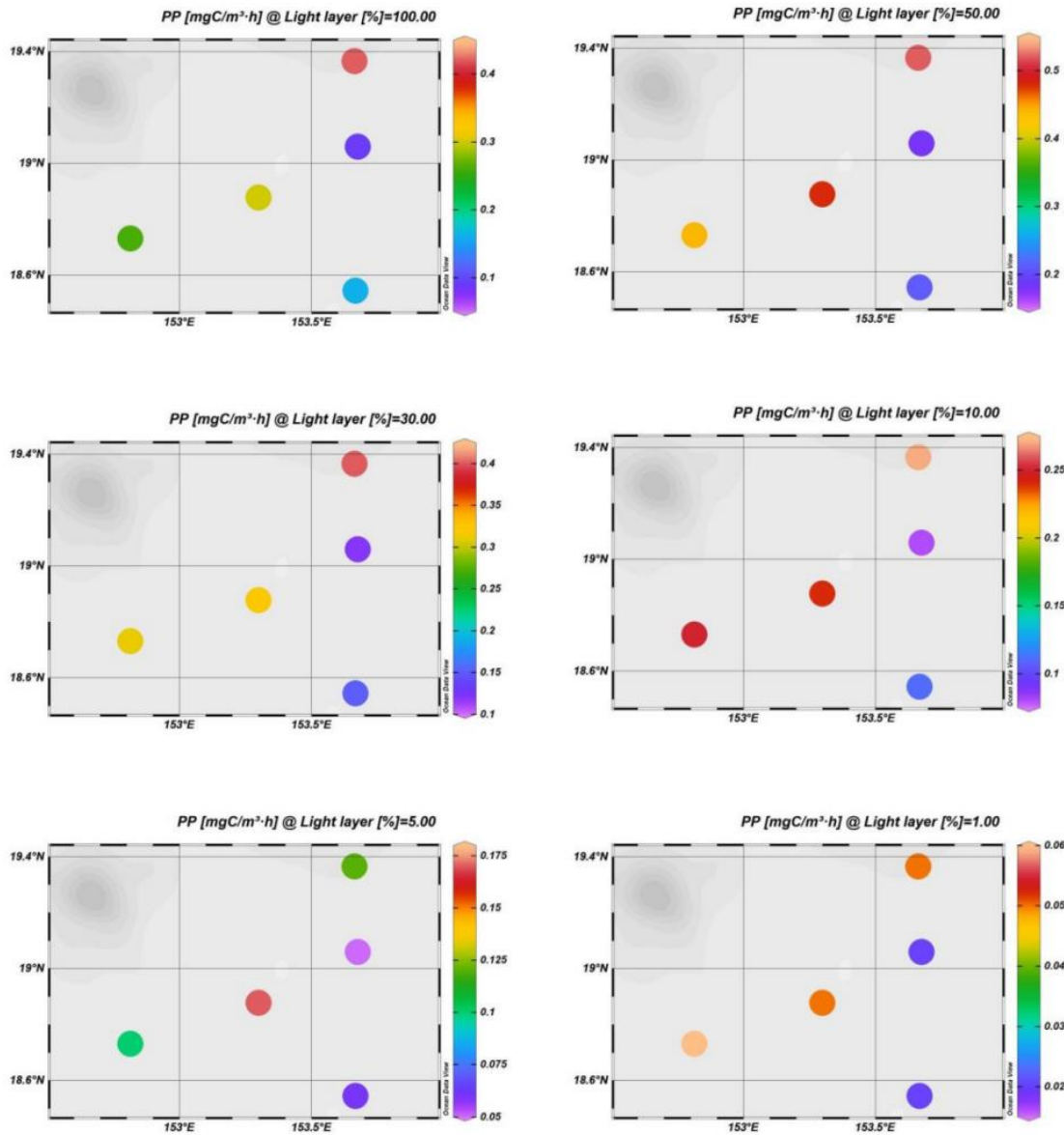
Figure 5-123 Horizontal distribution of water column primary productivity in the euphotic layer in contract area, 2022 (mg C/(m² · h))
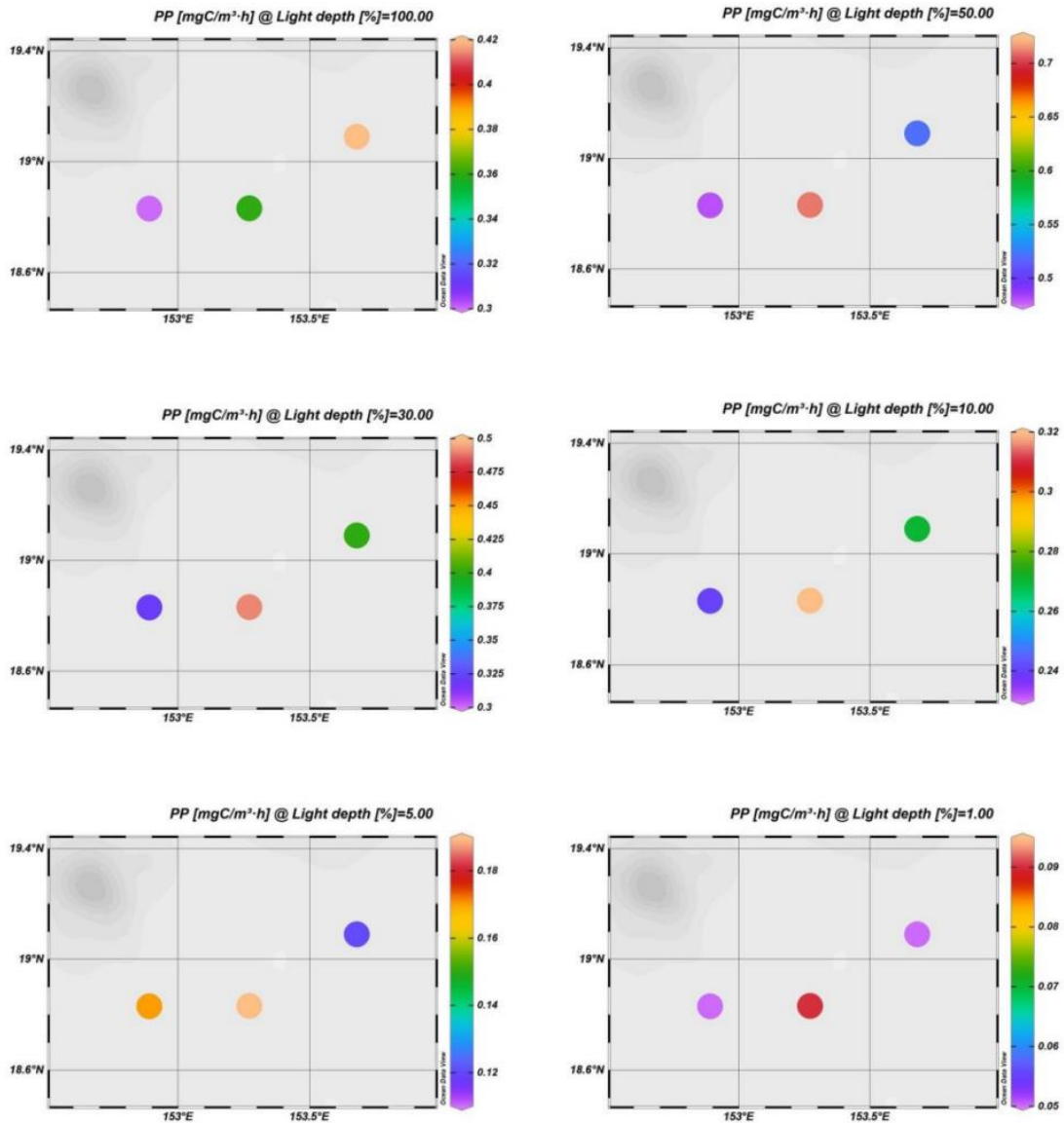
Figure 5-124 Horizontal distribution of water column primary productivity in the euphotic layer in contract area, 2023 (mg C/(m² · h))

5.3.1.2 Vertical Distribution

The 2021–2023 survey showed that the vertical distribution of primary productivity was a unimodal structure (Figure 5-125), and the maximum photosynthetic rate all appeared in the layer with 50% surface light intensity, which were 0.37 mgC/(m³·h), 0.37 mgC/(m³·h), and 0.57 mgC/(m³·h), respectively (Table 5-44). The depth of the layer with the maximum value was averagely 17 m, varying from 14 to 26 m. The lowest values often appeared in the bottom of euphotic layer which was with 1% surface light intensity, varying from 0.01 to 0.06 mgC/(m³·h). The depth of the euphotic layer was located between 82 m and 140 m, with an average of 118 m. This result showed the low biomass and productivity in Block M.

Table 5-44 Mean primary productivity in the layer with standard light intensity in Block M from 2021 to 2023 (mgC/(m^3·h))

Relative Surface Light Intensity Year	100%	50%	30%	10%	5%	1%
2021	0.25±0.12	0.37±0.15	0.27±0.12	0.18±0.09	0.09±0.04	0.04±0.02
2022	0.25±0.13	0.37±0.16	0.26±0.12	0.19±0.09	0.10±0.05	0.04±0.02
2023	0.36±0.06	0.57±0.12	0.40±0.08	0.28±0.04	0.16±0.04	0.06±0.03
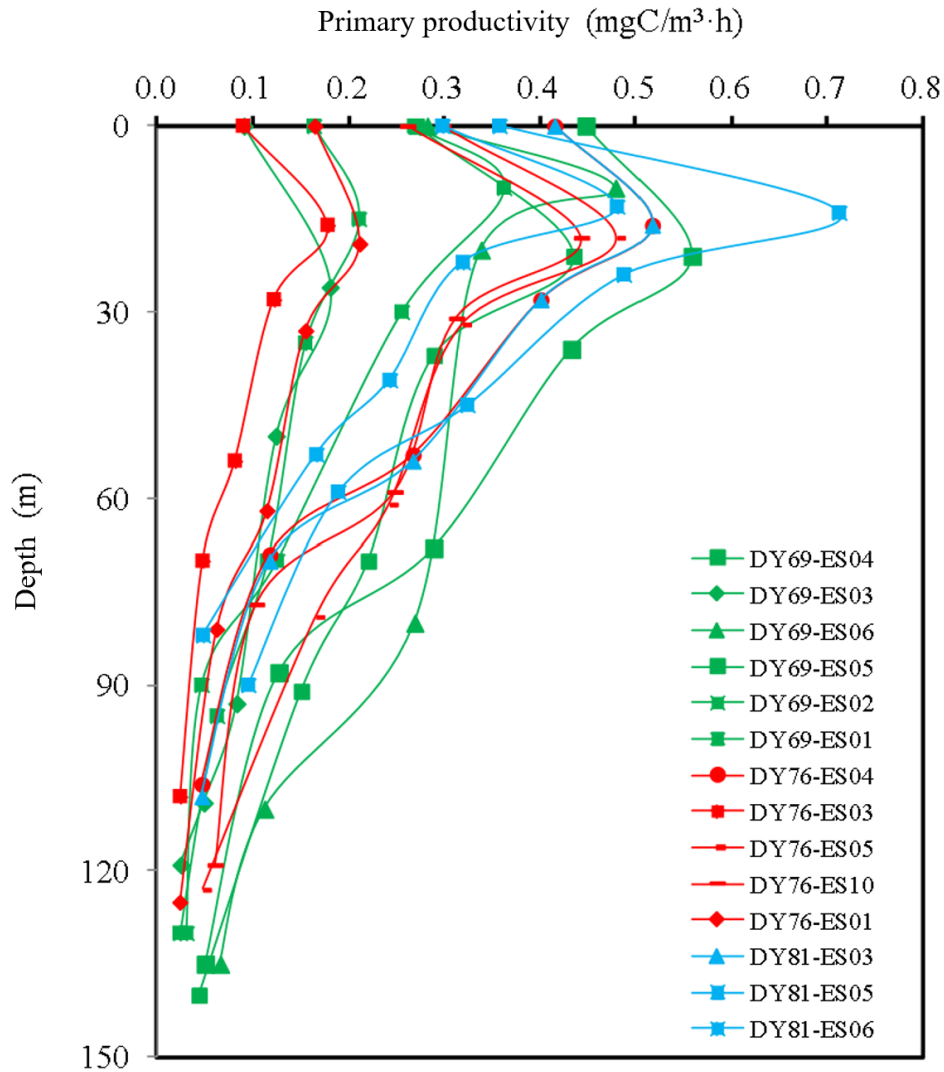
Figure 5-125 Vertical distribution of primary productivity in the layer with standard light intensity in the contract area (mg C/(m^3·h))

5.3.1.3 Control Mechanism

The correlations between primary productivity and environmental factors were shown in Table 5-45. The results showed that there was no obvious correlation between the environmental factors and primary productivity, except for the abundance of picoplankton, which had an obvious positive correlation with primary productivity in

the surface layer and the water column. It was suggested that the picoplankton was the main contributor to primary productivity. Since the Block M was located in a typical oligotrophic area, nutrients in the upper layer were depleted. The DCM layer was relatively rich in nutrients, but the primary productivity in this layer was limited by light. Therefore, the results of the above correlation analysis did not fully illustrate the real relationship between primary productivity and nutrients and light.

Table 5-45 Correlation between primary productivity and environmental factors in Block M in 2021

Layer	Correlation	Pico	Temper-ature	Salinity	Inorganic nitrogen	Phosphate	Silicate	SS	DO
100%I	Pearson	0.874*	−0.197	−0.32	−0.048	−0.438	0.267	−0.268	0.613
	Sig.	0.023	0.708	0.535	0.928	0.385	0.610	0.607	0.196
Water Column	Pearson	0.992**	0.147	−0.34	−0.258	−0.374	−0.076	−0.436	0.524
	Sig.	0.000	0.781	0.508	0.621	0.465	0.886	0.387	0.286

** means significantly correlated at the 0.01 level
* means significantly correlated at the 0.05 level

Block M was located in the North Pacific Subtropical Gyre zone, where the sea surface temperature (SST) was always higher than 15°C, and the distribution of primary productivity was mainly influenced by nutrients and light. In autumn, the SST in the North Pacific Subtropical Gyre was high, and the density difference between the upper and lower layer increased, which hindered the upward transport of nutrients and inhibited the increase of net primary productivity. In addition, the low phytoplankton and low light at the bottom of the euphotic layer caused low primary productivity. On the other hand, the deepening of the thermocline increased due to the elevation of the sea surface dynamical height accompanied by the deeper thermocline. The change in the thermocline reflected the change in the nitracline because of the temperature–nitrate relationship. In the subtropical oligotrophic zone, the nitracline was generally 100~150 m deeper than the thermocline, and the deepening of the nitracline was not beneficial to the vertical mixing to bring the nitrate-rich seawater below nitracline to the upper layer with low nitrate concentration, which resulted in the reduction of the net primary productivity due to the limitation of nutrient. This was reversed in spring and summer. When in the North Pacific Subtropical Gyre, strong westerly winds led to weaker upper ocean stratification, deeper mixed layer, more phytoplankton, and consequent increase in primary productivity (Figure 5-1).

5.3.2 Community Oxygen Consumption

Sediment community oxygen consumption was used as an indicator for overall community (mainly microbial) function. No baseline study had been conducted by BPC currently. The German and Belgium contractors applied the micro-profiling to measure

the total oxygen uptake (TOU) of the seafloor sediments by using the lander-carrying platform and the seafloor crawler robot, and they also used in-situ benthic incubator to determine the diffusive oxygen uptake (DOU). TOU consisted of the oxygen consumption rate by the sediment microbes and benthos. The traditional laboratory analysis was to carry out ex-situ measurements in the laboratory after collecting seafloor sediment samples, but the increase in temperature and decrease in pressure after sampling from the seafloor (especially in the deep sea) to the deck prompted certain sediment microbial cells to lyse and released reactive organic matter which was then utilized by the microbes with consuming additional oxygen. Zheng et al. (2023) studied the relationship between TOU, DOU and water depth in the abyssal Pacific and showed that the oxygen consumption of abyssal sediments in the abyssal Pacific had a good negative correlation with water depth (Figure 5-126). Since the respiratory oxygen consumption of benthos decreased with the water depth deepening, the difference between TOU and DOU decreased as well.
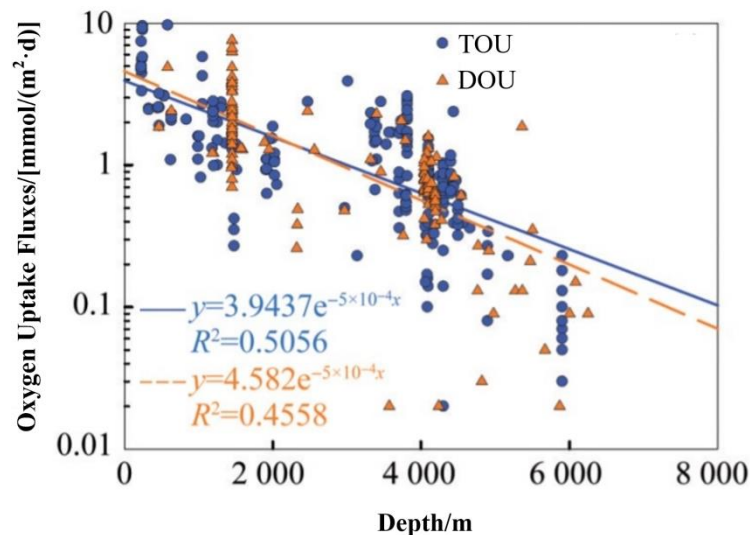
Figure 5-126 Correlation between oxygen uptake and water depth in the abyssal Pacific (Zheng et al., 2023)

5.3.3 Water Layer and Food Web Structure of Benthic Habitat

At present, BPC has not yet carried out food web structure research in its contract area. It plans to sample seawater, plankton, fish, benthic organisms and sediments during the 2024 cruise, and carry out food web research work using the stable isotope method to determine the trophic levels of different taxa of organisms and the contribution of major taxa to the food source.

5.3.4 Bioturbation

During the first voyage of the BPC, sediments were collected from 6 stations in blocks M1 and M2 for the measurement and analysis of ^{210}Pb and ^{226}Ra. Preliminary results show that the specific activity of ^{210}Pb in the investigated area ranges 37–1,922 Bq/kg with an average of 850±509 Bq/kg, the specific activity of ^{226}Ra ranges from 12–282 Bq/kg with an average of 161±83 Bq/kg, and the bioturbation rate and mixed depth in this area will be further studied based on the one-dimensional eddy-diffusion model. Meanwhile, the BPC has already sampled sediments in the 2023 cruise to continue studying the role of bioturbation in the sediments of the contract area by using the ^{210}Pb$_{ex}$ tracer.

Yang et al. (2011) showed that the bioturbation coefficients of sediments in the basin around the BPC contract area ranged 1.59–8.64 cm^2/a using the ^{210}Pb$_{ex}$ tracer. Yang et al. (2020) found that the bioturbation coefficients of the sediment in the seamount basket in the vicinity of the BPC contract area (Figure 5-127) ranged 1.79–27.10 cm^2/a, with a mean value of (10.8±9.2) cm^2/a, which is obviously higher than the values reported in the Northwest Pacific Basin (0.11–0.58 cm^2/a), the Equatorial Pacific (0.019–0.50 cm^2/a), and the Northeast Pacific (0.33–0.59 cm^2/a), and it is also obviously higher than the value estimated from the empirical relationship between the bioturbation rate and the linear deposition rate, indicating that deep-sea basin sediments are less bioturbated than the seamount basin.

Figure 5-127 Bioturbation survey stations around the BPC contract area

(Data source: Yang et al., 2011; Yang et al., 2020)

5.4 Summary

Based on the results of the environmental surveys in Block M1 and Block M2 during the 2021, 2022, and 2023 cruises, the key characteristics of the biological

community baseline in Block M are summarized in Table 5-46. A checklist of species in the BPC's contract area is provided in Annex 2.

Chlorophyll *a*: The contract area belonged to the global low biomass and low productivity zone in the fall. The mean values of chlorophyll *a* in the water column in 2021–2023 were 35.23 ± 4.91 mg/m^2, 35.45 ± 3.80 mg/m^2 and 40.97 ± 9.06 mg/m^2, respectively, and the annual changes were not obvious. From the above, the vertical distribution of chlorophyll *a* at all stations was characterized by an obvious single-peak structure, and the maximum chlorophyll *a* concentration of most stations was located between 120 and 150 m.

Primary productivity: Primary productivity was low in Block M. The mean values of primary productivity were 25.03 ± 10.43 mgC/(m^2·h), 20.95 ± 9.09 mgC/(m^2·h) and 25.80 ± 5.51 mgC/(m^2·h) from 2021 to 2023, respectively. The maximum photosynthetic rates were all found in the layer with 50% surface light intensity. The main reason for the low values of primary productivity was the high SST in the North Pacific Subtropical Gyre zone in the fall, which increased the difference between the density of the upper and the deeper layer, thus hindering the upward transport of nutrients and inhibiting the growth of net primary productivity.

Microbe: (1) Proteobacteria, Actinobacteria, Planctomycetes, Bacteroidetes, Cyanobacteria, Firmicutes, Candidatus, Saccharibacteria. Acidobacteria, Verrucomicrobia, and Chloroflexi were the dominant microbe taxa of water bodies in Block M. Among them, Planctomycetes had high abundance in almost all layers, and this taxon could maintain metabolism through nitrification and denitrification in low or anaerobic environments. Thus, this group might play an important role in the process of nitrogen cycling in the water body of Block M. (2) Sediment microbe in Block M: the results of β-diversity analysis showed that there was no obvious difference in the structure of microbe communities in Block M1 and Block M2. The top ten genera in terms of abundance included *Nitrosopumilus* from Crenarchaeota, *Sphingomonas*, *Woeseia* and *Ralstonia* from Pseudomonadota, and six uncultured taxa (Subgroup_21, JTB23, BD2-11_terrestrial_group, bacteriap25, S085, and NB1-j).

Picoplankton: The abundance of picoplankton, *Prochlorococcus*, *Synechococcus*, and picoeukaryotes in Block M was relatively stable in the fall, with unobvious annual changes. Pigment analysis showed that the abundance of *Prochlorococcus* was the highest in this area, followed by *Synechococcus* and Haptophyta, and the abundance of Bacillariophyta, Dinophyta and Cyanophyta were very low; the abundance of DCM layer varied obviously among the surveyed stations, but the differences in community structure were not obvious.

Micro- and nano-phytoplankton: In Block M, a total of 65 species nanoplankton belonged to 4 phyla and 37 genera, 155 species microphytoplankton belonged to 6 phyla and 56 genera were identified. Among them, Bacillariophyta were the most dominant group, followed by Dinophyta.

Zooplankton: (1) Species composition and abundance: A total of 406 species of zooplankton (including undetermined species) belonged to 6 phyla and 13 groups were recorded in the upper layer of Block M (200 m depth), with three-year average abundances of 79.02 ind/m^3, 46.37 ind/m^3 and 88.35 ind/m^3. The zooplankton community was generally characterized by low abundance and high biodiversity. In terms of vertical distribution, although the zooplankton abundance showed a decreasing trend with increasing depth, the diversity remained very high. Copepoda was the only dominant group, accounting for more than 90% of the total zooplankton abundance in all layers, and the percentage of Copepoda increased with the increasing depth. Copepoda accounted for more than 98% of the total abundance in the depth of 200 m. Therefore, Copepoda played a dominant role in zooplankton community. (2) Diurnal vertical migration: Diurnal vertical migration of zooplankton was shown in Block M. The species number and abundance of zooplankton sampled at night in was higher than those sampled during daytime. Copepoda dominated the vertical migration of zooplankton as the main group, and Ostracoda and Pteropoda did not show obvious vertical migration in euphotic layer.

Metazoan meiofauna: A total of 15 groups of metazoan meiofauna were found in Block M, among which nematodes were the main dominant group. For vertical distribution, meiofauna were mainly found in the surface sediments of 0~2 cm, with 63~125 μm in size. The abundance of meiofauna in the contract area ranged from 4.94 to 64.33 ind./10 cm^2, with a mean value of 26.21 ind./10 cm^2 and 22.86 ind./10 cm^2 in 2022 and 2023, respectivly. The mean abundance of meiofauna in the IRZ and PRZ was 23.2±10.3 ind./10 cm^2 and 35.7±16.4 ind./10 cm^2, respectively. For nematodes diversity, a total of 37 genera belonged to 19 families was found in this area.

Macrofauna: A total of 46 species of macrofauna were found in Block M. Crustaceans were the most abundant group, followed by polychaetes. The macrofauna average abundance in 2022 and 2023 changed obviously from 13.44±15.69 ind/m^2 to 18.0±2.8 ind/m^2, respectively. Macrofauna abundance in this area was obviously lower than that in the East Pacific CCZ area. Macrofauna mainly distributed in the upper 0–3 cm sediments. The species richness of macrofauna in this region is predicted to be about 193 using the chao1 index.

Megafauna: Preliminary analysis of the video images discovery 35 megafauna morphospecies belonging to 10 group in Block M. Among them, Echinodermata had the highest species number and the highest abundance, followed by Porifera. It reveals a different fauna community structure on seamount slope compared to that of the abyssal plains, with a high abundance of Annelida and Hemichordata in the Magoshichi guyot piedmonts area, and a relatively high abundance of Sponge, Annelida, Echinodermata and Chordata in the basin area.

Scavengers and demersal fishes: Lander trapping was used to obtain four species of benthic scavengers and fishes, including *Eurythenes gryllus*, *Paralicella tenuipes*,

Hirondellea dubia, and Macrouridae und. Video analysis also revealed five groups of benthos, including two species of fish (*Coryphaenoides* sp. and Ophidiidae sp.), and three species of Arthropods (Pycnogonida, Gammaridea and *Glyphocrangon* sp.).

Marine mammals, seabirds and sea turtles: Observations and publicly available information summuraized a total of 4 species of mammals belonging to 4 genera, 3 families, and 1 order recorded in Block M and adjacent sea areas; as well as 3 species of sea turtles in 1 order, 2 families, 3 genera; 24 species of seabirds in 3 orders, 11 families and 18 genera. Among them, there is one globally endangered species: *Numenius madagascariensis*, and six vulnerable species: *Lepidochelys olivacea*, *Caretta caretta*, *Dermochelys coriacea*, *Physeter macrocephalus*, and *Physeter macrocephalus*, *Calidris acuminata*, and *Oceanodroma leucorhoa*; and one near-threatened species: *Calonectris leucomelas*. Passive acoustic surveys indicate that there are six species of baleen whales in the region, including *Megaptera novaeangliae*, *Balaenoptera physalus*, etc. *Balaenoptera acutorostrata*, *Balaenoptera musculus*, *Balaenoptera borealis* were absent from August to October, and *Balaenoptera physalus* in October, *Megaptera novaeangliae* in September–October. *Balaenoptera brydei* in 2022–2023, and only in 2021 in small numbers.

Eukaryotic molecular biology characteristics: Using DNA high-throughput sequencing technology, the molecular diversity of eukaryotic organisms in the sediments of the contract area was investigated, and a total of 379,431 valid sequences were obtained, which could be classified into 10,944 OTUs at 98.65% similarity. A total of 652 species (excluding the unannotated species) were assigned in 30 phylums and 82 orders, 272 families, and the highest OTU number was the nematode (Figure 5-128).
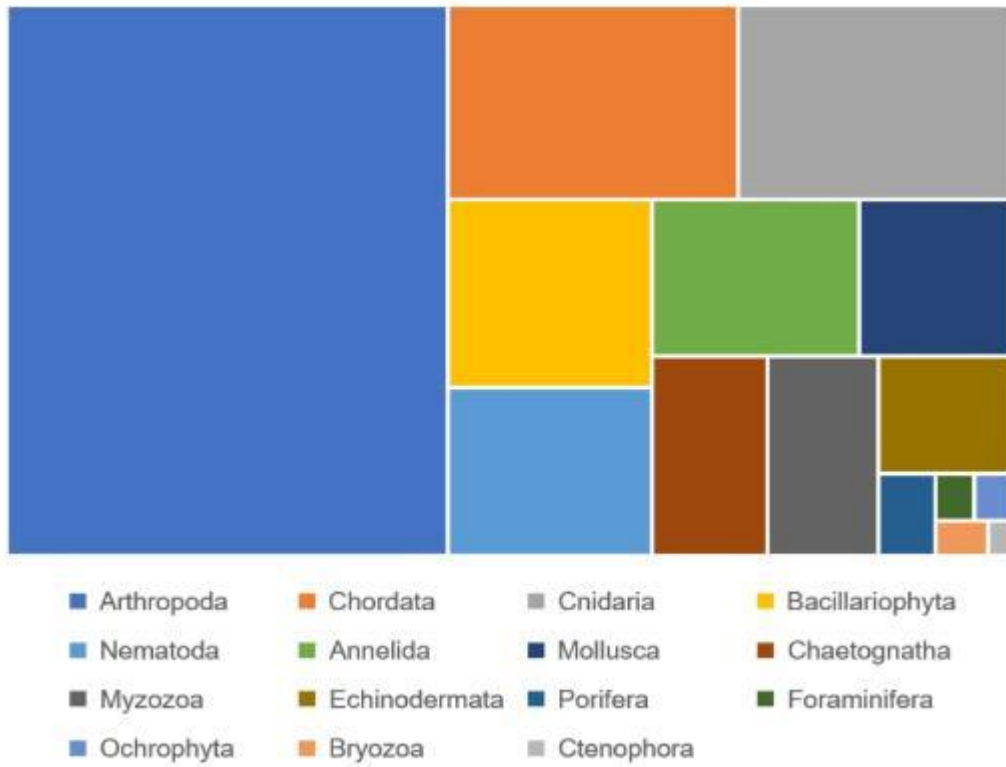
Figure 5-128 Characterization of eukaryotic diversity in Block M.

Table 5-46 Summary of biological communities baseline in Block M

Parameters	Survey Year	Average Value	Range of change	Number of Stations	Species
Chlorophyll *a* content in water column	2021	35.23±4.91 mg/m²	29.99~41.68 mg/m²	6	
	2022	35.45±3.80 mg/m²	30.47~40.13 mg/m²	5	
	2023	40.97±9.06 mg/m²	30.18~50.09 mg/m²	4	
Primary productivity	2021	25.03±10.43 mgC/(m²·h)	13.02~37.85 mgC/(m²·h)	6	
	2022	20.95±9.09 mgC/(m²·h)	8.95~29.16 mgC/(m²·h)	5	
	2023	25.80±5.51 mgC/(m²·h)	19.56~30.01 mgC/(m²·h)	4	
Picoplankton	2021	(50.38±7.31) ×10³ cells/ml	(41.29~59.38) ×10³ cells/ml	6	
	2022	(48.62±3.94) ×10³ cells/ml	(44.93~54.97) ×10³ cells/ml	5	
	2023	56.21 ± 8.05 × 10³ cells/ml		3	
Prochlorococcus	2021	(47.63±6.91) ×10³ cells/ml	(38.91~55.92) ×10³ cells/ml	6	
	2022	(45.79±3.88) ×10³ cells/ml	(42.18~52.05) ×10³ cells/ml	5	
	2023	(52.58 ± 8.12)×10³ cells/ml		3	
Polycoccus	2021	(2.14±0.32) ×10³ cells/ml	(1.87~2.68) ×10³ cells/ml	6	
	2022	(2.25±0.11) ×10³ cells/ml	(2.11~2.41) ×10³ cells/ml	5	
	2023	(2.85±0.24) × 10³ cells/ml		3	
Eukaryotic algae	2021	(0.61±0.13) ×10³ cells/ml	(0.44~0.78) ×10³ cells/ml	6	
	2022	(0.59±0.07) ×10³ cells/ml	(0.49~0.67) ×10³ cells/ml	5	
	2023	(0.78±0.20) × 10³ cells/ml		3	
Phytoplankton (Net harvesting)	2021	2.42 × 10³ cells/m³	(1.05~4.40) ×10³ cells/m³	6	3 phyla, 21 genera and 38 species
	2022	2.66×10³ cells/m³	(1.46~4.32) ×10³ cells/m³	7	5 phyla, 37 genera and 81 species
	2023	2.63 × 10³ cells/m³	(0.29~11.51) ×10³ cells/m³	5	4 phyla, 28 genera, 51 species
Zooplankton	2021	79.02±27.54 ind/m³	30.86~106.40 ind/m³	7	6 phyla, 11 categories and 200 species
	2022	46.37±27.45 ind/m³	28.68~105.62 ind/m³	7	220 species in 6 phyla and 12 categories
	2023	88.35 ± 51.66 ind/m³	32.20~167.42 ind/m³	5	213 types in 6 phyla and 13 categories
Foraminifera protozoa	-	-	-	-	3 families, 3 genera and 3 species
Metazoan meiofauna	2022	26.21±17.88 ind./10cm²	4.94~64.33 ind./10cm²	14	15 groups, nematodes species belong

Parameters	Survey Year	Average Value	Range of change	Number of Stations	Species
					to 37 genera, 19 families
	2023	22.86 ± 9.86 ind./10cm^2	8.04~38.66 ind./10cm^2	10	10 groups
Macrofauna	2022	13.44±15.69 ind/m^2	0~64 ind/m^2	39	46 species
	2023	18.0±2.8 ind/m^2	0~40 ind/m^2	14	37 species (one specie is undecided)
Megafauna	2021	-	12.7~18.7 ind./km	Length of survey line 227km	35 morphospecies, belong to 10 phyla
Demersal fish	2021-2022	-	-	5	2 families and 3 species
Scavenger	2021-2022	-	-	5	3 species
Marine mammals (visual)	2021-2023	-	-	-	1 order, 3 families, 4 genera and 4 species
Marine mammal (Acoustics)	2021-2022	-	-	2	6 baleen whales, 2 toothed whales
	2022-2023	-	-	2	5 species of baleen whales, many species of toothed whales
Seabird	2021-2023	-	-	-	3 order, 9 families, 16 genera and 23 species

6 ASSESSMENT OF PHYSICOCHEMICAL ENVIRONMENTAL IMPACTS AND PROPOSED MITIGATION MEASURES

This chapter focuses on the potential impacts of the mining component test on the marine environment, including the physical and chemical environment, as well as the potential risks and proposed mitigation measures. Based on the scale of this mining component test, an FVCOM sediment plume dispersion and redeposition model was constructed to provide a scientific basis for the impact prediction and the development of an on-site environmental monitoring program. At the same time, preliminary analyses of the substrate environment, marine traffic, air quality and transboundary impacts were conducted. Mitigation measures were developed to achieve control and mitigation of the potential environmental impacts of the tests.

6.1 Description of Potential Impact

This section analyzes the potential environmental impacts of deep-sea mining, mainly based on existing literature. It has been documented and recognized that the noise, light pollution and discharge of tailings and domestic wastewater generated by surface support vessels, mining systems during ore collection have potential impacts on the environment and organisms (Wang et al. 2001a, 2021b, Dooling et al. 2012, Hauton et al.,2017, Sharma, 2019), and that the potential environmental impacts of deep-sea mining include the following three depth zones:

6.1.1 Potential Impacts on the Deep Seabed Environment

Potential impacts on the deep seabed environment include:

(1) Sediment compaction effects caused by the travel of the collector (or collector head) on the seafloor;

(2) Changes in geological environment and habitat disturbance due to removal of polymetallic nodules and sediments;

(3) Sediment plume diffusion and redeposition resulting from ore-collecting processes;

(4) Plume spreading and redeposition from tailings discharge (if tailings are discharged in a bottom discharge);

(5) Potentially toxic heavy metals and/or substances released to bottom waters;

(6) Noise from ore collectors;

(7) Light pollution from mineral collectors.

6.1.2 Potential Impacts on the Mid-water Column Environment (below the euphotic zone to 100 m above the bottom)

Potential impacts to the mid-water column environment include:

(1) Impact of surface vessel and collector noise on the middle water column;

(2) Noise and vibration from riser systems, but not applicable to this project;

(3) Impacts to the water column environment from spilled tailings from unforeseen events such as rupture of the riser system, e.g.; elevated turbidity, nutrient and heavy metal concentrations, but not applicable to this project;

(4) Impacts to the column environment from plume dispersion from tailings discharge (if tailings are discharged in a mid-water column) such as; elevated turbidity, nutrient and heavy metal concentrations, but not applicable to this project;

(5) The release of potentially toxic heavy metals and other substances in the tailings into the water column may cause an increase in the concentration of heavy metals in the water column, which is not applicable to this project.

6.1.3 Potential Impacts on the Upper Environment (euphotic zone)

Potential impacts on the upper marine environment may include:

(1) Accidental discharges (hydrocarbon pollution, hydraulic fluids) or waste discharges from surface vessels into surface waters and their impact on the environment;

(2) Noise caused by the vessel itself or by acoustic systems installed in the ship's foundation or hull;

(3) Light pollution from ship lighting;

(4) Impacts on the environment of the euphotic zone from spilled tailings resulting from unforeseen events such as ruptures of riser systems. For example, changes in nutrient, particulate and heavy metal concentrations and temperature in the surface waters may be affected;

(5) Vessels emit gases such as carbon dioxide into the air.

For the polymetallic nodule collector test activity proposed by BPC Mining, the nodules are discharged directly in the CTA and are not lifted to the ship through risers, while the tailwater is also discharged near the bottom (4 m above the bottom height), so the impacts on the environment and organisms from this activity occur mainly in 2 depth zones, one is the seafloor environment near the collector mining trajectory, and the other is

the surface area where the ship activities take place. The only environmental and biological impacts on the mid-water column are potential impacts from noise, and none of the other 4 areas are applicable.

6.2 Plume Modeling and Impact Prediction

Since the 1970s, with the increasing frequency of deep-sea mineral resources exploration activities, the potential environmental problems of deep-sea mining have attracted extensive attention from the international community. The monitoring and modeling of the impacts of deep-sea Plumes is the focus and difficulty of the environmental impact assessment of deep-sea mining. Since the discharge of tailings at the surface obviously affects the productivity of the upper ocean, and the plume generated by the discharge in the lowest oxygen zone spreads farther, the discharge of tailings at the bottom is currently the dominant mode, especially in the polymetallic nodule mining areas of the inter-mountain basins of the Northwest Pacific Ocean. Coupled with the fact that mine-collecting operations generate large plumes at the bottom, bottom plumes are the focus of current mining environmental impact assessment studies.

In order to better assess and predict the spreading range and impact of the plume generated by deep-sea mining, the present study relies on the field observation data and uses the high-resolution regional ocean model FVCOM to simulate the spreading of the deep-sea near-bottom sediment plume during the mining test, and analyzes the horizontal and vertical distribution characteristics of the plume as well as the distribution characteristics of the thickness of the redeposition, so as to provide the scientific basis for the formulation of the monitoring plan of the mining plume.

6.2.1 Plume Model Configuration

Hydrodynamic model:

The FVCOM numerical model was used to construct a deep-sea mining Plume model centered on the CTA. The simulation range of the model is 50 km×50 km, with a grid resolution of 2000 m at the open boundary (Figure 6-1), a grid resolution of 100 m at the test center of 10 km×10 km (Figure 6-2), and a grid resolution of 50 m at the test center of 5 km×5 km (Figure 6-3). The number of model grid nodes is 28,775 and the number of triangular elements is 57,448. The vertical direction adopts the generalized bottom-following coordinate system, and the grid is encrypted in the near bottom, which is divided into 61 layers, of which the resolution above bottom 10 m is 1 m, the resolution above bottom 10–20 m is 2 m, the resolution above bottom 20–40 m is 5 m, the resolution above

bottom 40–80 m is 10 m, the resolution above bottom 80–100 m is 20 m, the resolution above bottom 100–200 m is 50 m, and the resolution above bottom 200–300 m is 100 m (Figure 6-5).
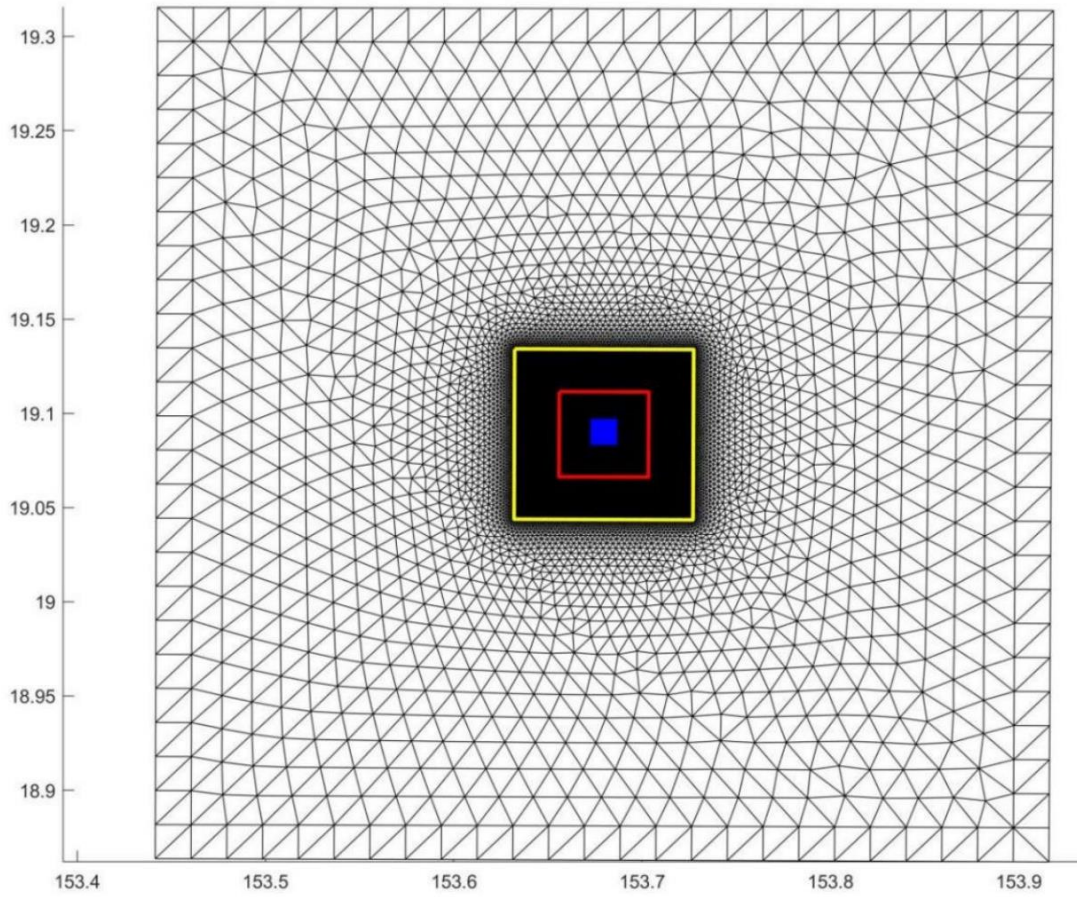
Figure 6-1 Grid of plume model
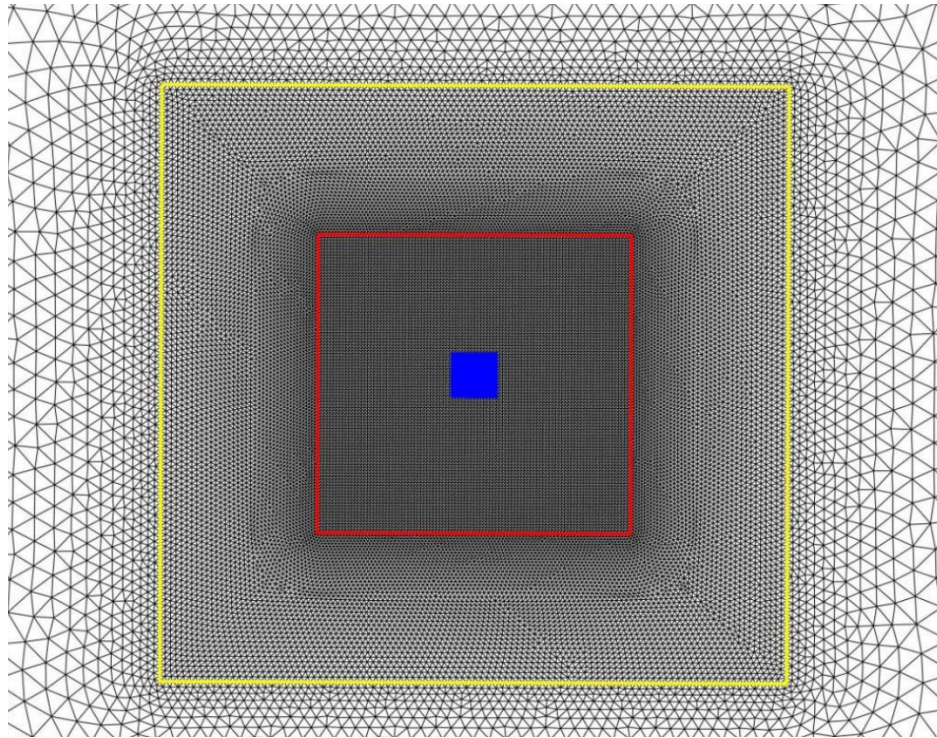
Figure 6-2 Grid of plume model mining test center (10 km×10 km)
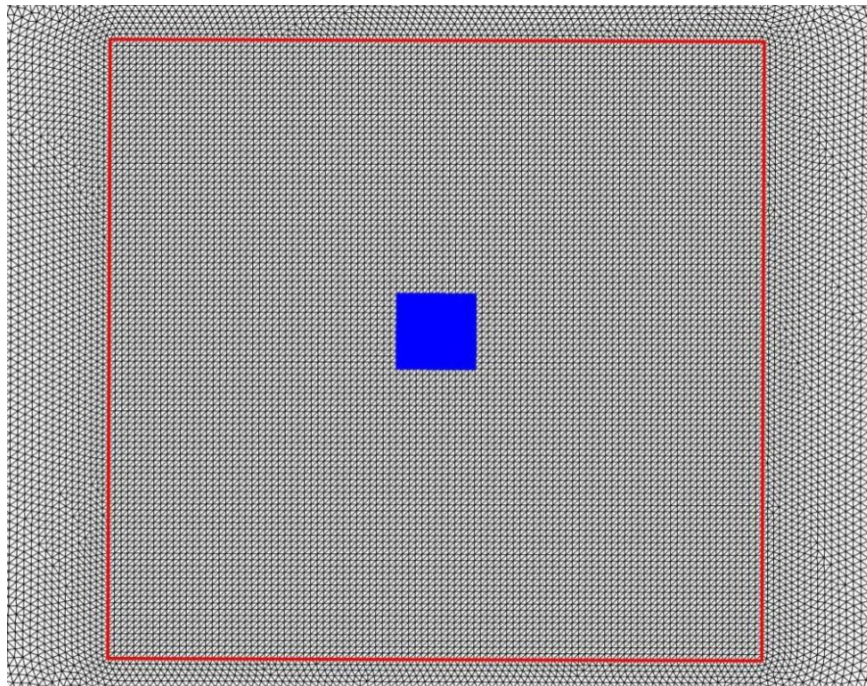
Figure 6-3 Grid of plume model mining test center (5 km × 5 km)
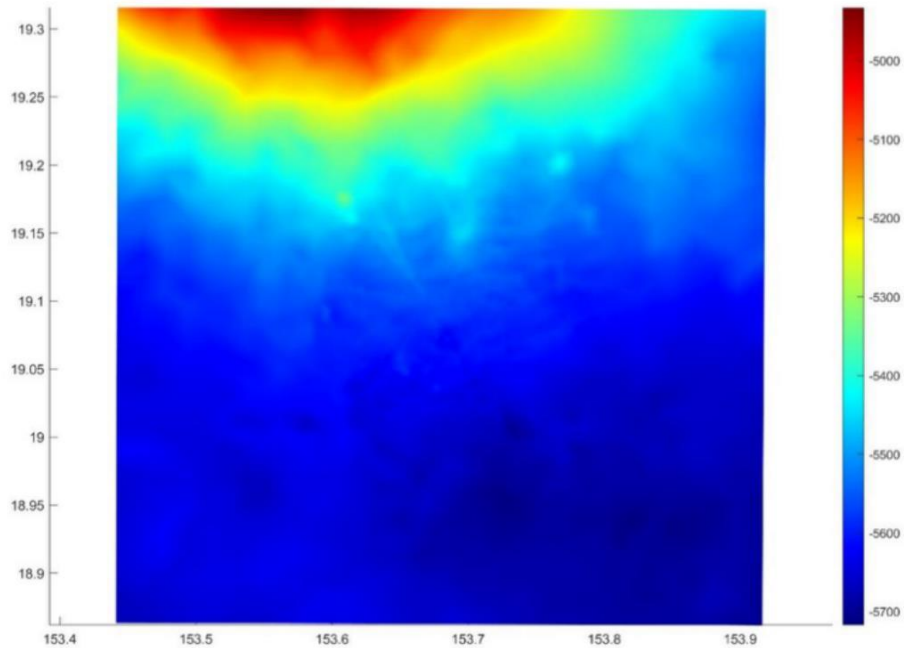
Figure 6-4 Detail of the plume model bathymetry
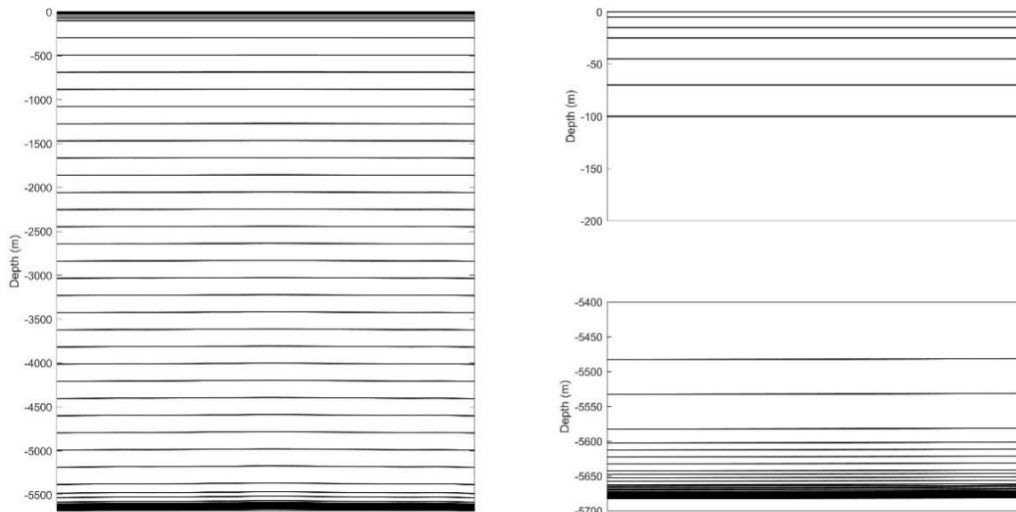
Figure 6-5 Vertical grid of plume model

The model bathymetry is based on multibeam measured data (50 m resolution). The structure of the temperature and salt profiles shows that there is no obvious change in temperature and salt in the near bottom layer. The CTA is located in the bottom layer, and there is no surface and middle layer discharge, etc., so the plume model is calculated as a barotropic model.

The open boundary tide level is derived from the global tidal model TPXO. Assuming a consistent background flow field in the simulation area, the residual flow field obtained

from the observed flow field after filtering out the tidal currents, is used as the open boundary condition for the model.

Plume model:

The plume model is simulated using the FVCOM sediment module, and the diffusion equation is as follows:

$$\frac{\partial C}{\partial t} + \frac{\partial (uC)}{\partial x} + \frac{\partial (vC)}{\partial y} + \frac{\partial \left[(w - w_s)C\right]}{\partial z} = \frac{\partial}{\partial x}\left(A_H \frac{\partial C}{\partial x}\right) + \frac{\partial}{\partial y}\left(A_H \frac{\partial C}{\partial y}\right) + \frac{\partial}{\partial z}\left(K_h \frac{\partial C}{\partial z}\right)$$

Where C and ws are the concentration of suspended sediment and the settle velocity, respectively, AH is the horizontal eddy coefficient, and Kh is the vertical eddy coefficient.

The concentration flux of suspended sediment on the bottom boundary is taken as follows:

$$K_h \frac{\partial C}{\partial z} = 0, \quad z = \zeta$$

$$K_h \frac{\partial C}{\partial z} = E - De, \quad z = -H$$

Where E denotes the bottom resuspension flux, De = Cbwb denotes the bottom settling flux, and Cb, wb denote the bottom suspended sediment concentration and settling velocity, respectively.

The disturbed sediment particle size and settling velocity in the plume model are categorized into the following 2 types:

1) Average case: referring to the flocculation and sedimentation test, the sediment particle size is 0.387 mm and the sedimentation velocity is 0.71 mm/s;

2) Extreme case: fine-grained sediments were selected to simulate plume diffusion in extreme cases, with a sediment particle size of 0.012 mm and a settling velocity of 0.10 mm/s. The sediment particle size and settling velocity were categorized as follows.

According to the design parameters of the collector, the bottom plume flow rate is 0.437 m³ /s, the sediment concentration is 60 g/L, and the discharge height is 4 m above the bottom.

6.2.2 Model Validation

A numerical model of deep-sea mining Plume is constructed based on FVCOM to compare the simulated flow field results with the observed flow field (observation results of the single-point current meter at 25 m above the bottom at station DY69-ES03-MX02). Considering that the expected operation time is from July to October, the numerical model is simulated from July to October. As shown in Figure 6-6, the simulated flow field is more consistent with the observed flow field.
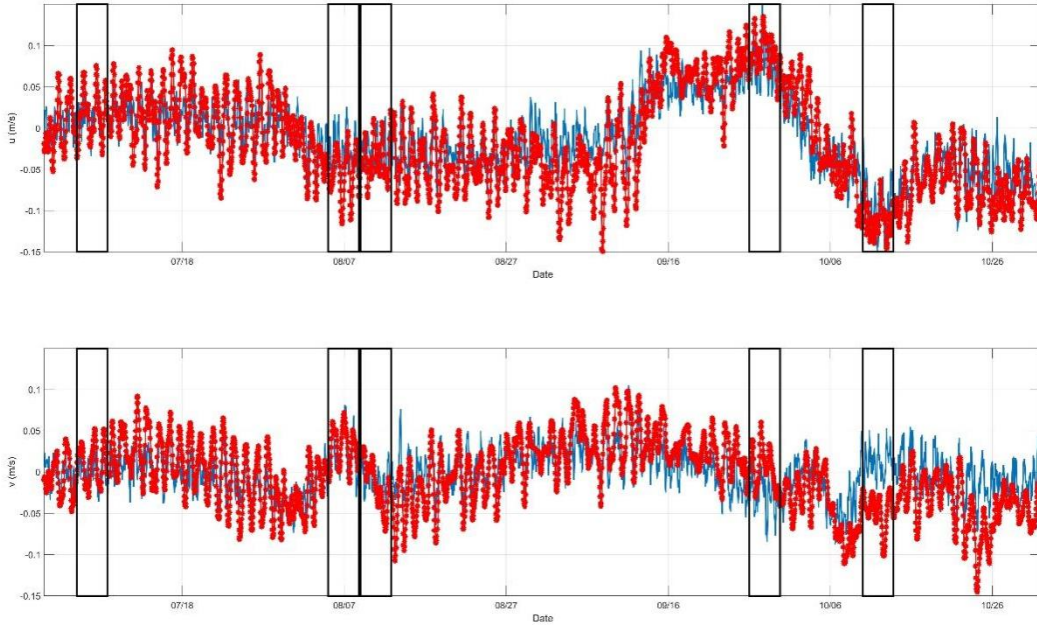
Figure 6-6 Comparison of simulated current (red) and observed current (blue)

(Upper panel: eastward component of current, lower panel: northward component of current, black boxes indicate operating time for each Case)

To quantify the accuracy of the model simulation, the method of Warner et al. is used with the following formula:

$$Skill = 1 - \frac{\sum\limits_{i=1}^{N}\left|X_{mod} - X_{obs}\right|^2}{\sum\limits_{i=1}^{N}(\left|X_{mod} - \bar{X}_{obs}\right| + \left|X_{obs} - \bar{X}_{obs}\right|)^2}$$

where: X denotes the parameter of comparison, and $\bar{X}$ denotes the average, and mod denotes the result of model simulation, and obs denotes the observation.

The result is calculated from 0– 1.0, where 1.0 indicates that the model calculation result is consistent with the actual measurements and 0 indicates that it is inconsistent, and the closer the value is to 1 indicates that the model simulation accuracy is higher.

Calculating the Skill value of the simulated velocity and the observed velocity, the magnitude and trend of the two are basically the same in the U component, with an average Skill value of 0.87; in the V component, the magnitude and trend of the two are also basically the same, with an average Skill value of 0.74. The average Skill of the velocity reaches 0.81, which indicates that the model simulation accuracy is very high, and the result of the numerical model of the hydrodynamics is credible.

6.2.3 Modeling Results and Impact Predictions

The plume model is utilized to study the spreading distribution of the deep-sea mining plume. From the observation results of the subsurface buoy at 20 m above the bottom, there are obvious changes in the magnitude and direction of the bottom current field from July to October, and here we especially select the weak northeastward, strong northwestward, weak southwestward, strong eastward, and strong southwestward currents in the mid-summer and fall of 2022 as examples, corresponding to the current fields on July 5th, August 5th, August 9th, September 26th, and October 12th, respectively. The main model parameters are shown in Table 6-1.

The trajectory of the operation with an area of 500 m×500 m is shown in Figure 6-7, which is set to collect from west to east following the north-south travel direction. Based on an average speed of 0.25 m/s, it takes 100.5 hours to complete the entire CTA.

Table 6-1 Setting of plume model

Case	Particle size (mm)	Settle velocity (mm/s)	Discharge height (above the bottom, m)	Simulated operating time	Remarks
Case 1	0.387	0.71	4	20220705-20220709	Weak northeastward current
Case 2	0.387	0.71	4	20220805-20220809	Strong northwestward current
Case 3	0.387	0.71	4	20220809-20220813	Weak southwestward current
Case 4	0.387	0.71	4	20220926-20220930	Strong eastward current
Case 5	0.387	0.71	4	20221012-20221016	Strong southwesterly current
Case 6	0.012	0.10	4	20220705-20220709	Weak northeastward current
Case 7	0.012	0.10	4	20220805-20220809	Strong northwestward current
Case 8	0.012	0.10	4	20220809-20220813	Weak southwestward current
Case 9	0.012	0.10	4	20220926-20220930	Strong eastward current
Case 10	0.012	0.10	4	20221012-20221016	Strong southwesterly current
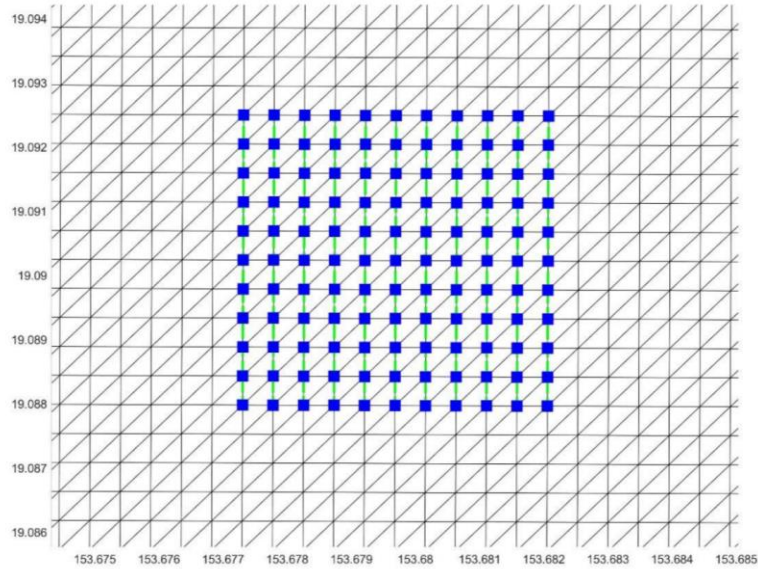
Figure 6-7 Simulation of mining collector trajectory (green line)

The lower limit of the effective monitoring concentration of the turbidity sensor is 0.1 mg/l (Munoz-Royo et al., 2022), and the plume dispersion assessment boundary taken with reference to the EIS report of NORI-D. Therefore, in the subsequent analysis of the characteristics of the horizontal and vertical distribution of the suspended sediment concentration, 0.1 mg/l was selected as the boundary value of the plume dispersion impact.

6.2.3.1 Horizontal Distribution of Plume

From the results of horizontal distribution of suspended sediment concentration in the near bottom layer at 1 m above the bottom (Figure 6-8), on average, the range of suspended sediment concentration greater than 1 g/l is only around the CTA, which disappears soon after the test ceases; the range of suspended sediment concentration of less than 10 mg/l is mainly located in the CTA, which disappears soon after the test ceases; the Plume disappears after 3–4 days of operation cessation (i.e., 8–9 days after the start of the test). The spreading direction of the Plume is related to the background current, with the Plume spreading in a northwest direction in the background of Case 2 northwestward flow, in a southwest direction in the background of Case 5 southwesterly current, and in an eastward direction in the background of Case 4 eastward current. The weak current scenarios (Case 1 and Case 3) have the smallest spreading range of the Plume. The maximum spreading distance (from the center of the CTA) of the deep-sea mining Plume is 5.42 km for Case 5 and the minimum is 2.93 km for Case 3 (Table 6-2). In extreme cases, the plume remained in the water longer than in the average case, and after 7-9 days of operation (i.e., 12-14 days after the start of the test), the plume disappeared. The maximum distance of the deep-

424

sea mining plume (from the center of the CTA) was 27.86 km in case 8 and the minimum was 14.51 km in case 9.

Table 6-2 Maximum diffusion distance, vertical maximum dispersion height and maximum redeposition thickness of the plume for each case

Case	Maximum Diffusion Distance 1 m above the bottom (km)	Maximum vertical spreading height (m)	Maximum redeposition thickness (cm)
Case 1	4.52	231	2.60
Case 2	5.13	210	2.31
Case 3	2.93	129	2.45
Case 4	4.91	123	2.14
Case 5	5.42	165	1.85
Case 6	21.23	346	0.99
Case 7	21.18	246	1.21
Case 8	27.86	189	1.48
Case 9	14.51	160	0.95
Case 10	22.67	178	0.85

Figure 6-8 Horizontal Distribution of suspended sediment concentration at 1m above the bottom for Each Case (4th Day of the test)

On average, the dispersal area of the plume 1 m above the bottom is not much different for each case with high suspended sediment concentration, and the area with suspended sediment concentration greater than 10 mg/l is the largest for Case 5, 0.39 km^2, Case 1 is the smallest, 0.27 km^2. The dispersal area for low suspended sediment concentration is related to the background flow field, and the dispersal area is obviously larger in strong flow than in weak flow. The area with a suspended sediment concentration greater than 0.1 mg/l is the largest in case 5, which is 8.12 km^2, and the smallest in case 3, which is 3.56 km^2 (Table 6-3). In extreme cases, the dispersal area is larger than the average state because the settling speed of small particles is slow. The maximum dispersal area for >10mg/l is the smallest in Case 6, 0.76 km^2, and the largest in Case 10, 1.61 km^2. The maximum dispersal area for >1mg/l is also the smallest in Case 6 and the largest in Case 10. The maximum area greater than 0.1mg/l was 67.13 km^2 for Case 7 and 36.55 km^2 for Case 6.

Table 6-3 Maximum dispersal area and impact time of plume concentration 1m from the bottom for each case

Case	Maximum dispersal area (km^2)			Impact time (hours)		
	≥10 mg/l	≥1 mg/l	≥0.1 mg/l	≥10 mg/l	≥1 mg/l	≥0.1 mg/l
Case 1	0.27	1.00	5.19	124	153	195
Case 2	0.32	1.44	7.40	121	150	185
Case 3	0.33	1.11	3.56	120	146	186
Case 4	0.33	1.83	6.40	125	148	196
Case 5	0.39	2.34	8.12	124	150	190
Case 6	0.76	4.52	36.55	162	238	337
Case 7	1.30	6.23	67.13	152	220	299
Case 8	1.42	6.35	50.44	157	244	308
Case 9	1.54	7.09	64.55	151	264	359
Case 10	1.61	7.47	64.54	141	208	264

Near-bottom suspended sediment concentration at 25 m above the bottom is less than 1 m above the bottom, and the plume dispersal distance is slightly greater than 1 m above the bottom. On average, the maximum plume spread distance (from the center of the CTA) at 25 m above the bottom was 5.03 km for Case 5 and 2.97 km for Case 3 (Figure 6-9); the maximum plume dispersal area was 8.07 km^2 for Case 5 and 3.36 km2 for Case 3. In extreme cases, the maximum plume dispersal distance (from the center of the CTA) at 25 m above the bottom was 27.90 km, and the minimum is 14.80 km for Case 9 (Figure 6-9); the maximum dispersal area is 69.75 km^2 for Case 10, and the minimum is 37.44 km^2 for Case 1.

Table 6-4 Maximum dispersal area and impact time of plume concentration 25 m from the bottom for each case

Case	Maximum dispersal area (km^2)			Impact time (hours)		
	≥10 mg/l	≥1 mg/l	≥0.1 mg/l	≥10 mg/l	≥1 mg/l	≥0.1 mg/l
Case 1	0.23	0.97	5.08	118	147	188
Case 2	0.27	1.45	7.32	111	141	178
Case 3	0.25	0.99	3.36	115	142	182
Case 4	0.32	1.81	6.50	118	144	190
Case 5	0.35	2.23	8.07	119	145	184
Case 6	0.72	4.52	37.44	154	233	332
Case 7	1.25	6.39	68.01	138	214	296
Case 8	1.37	6.37	52.91	152	241	303
Case 9	1.51	7.17	66.11	146	259	363
Case 10	1.57	7.45	69.75	137	204	268
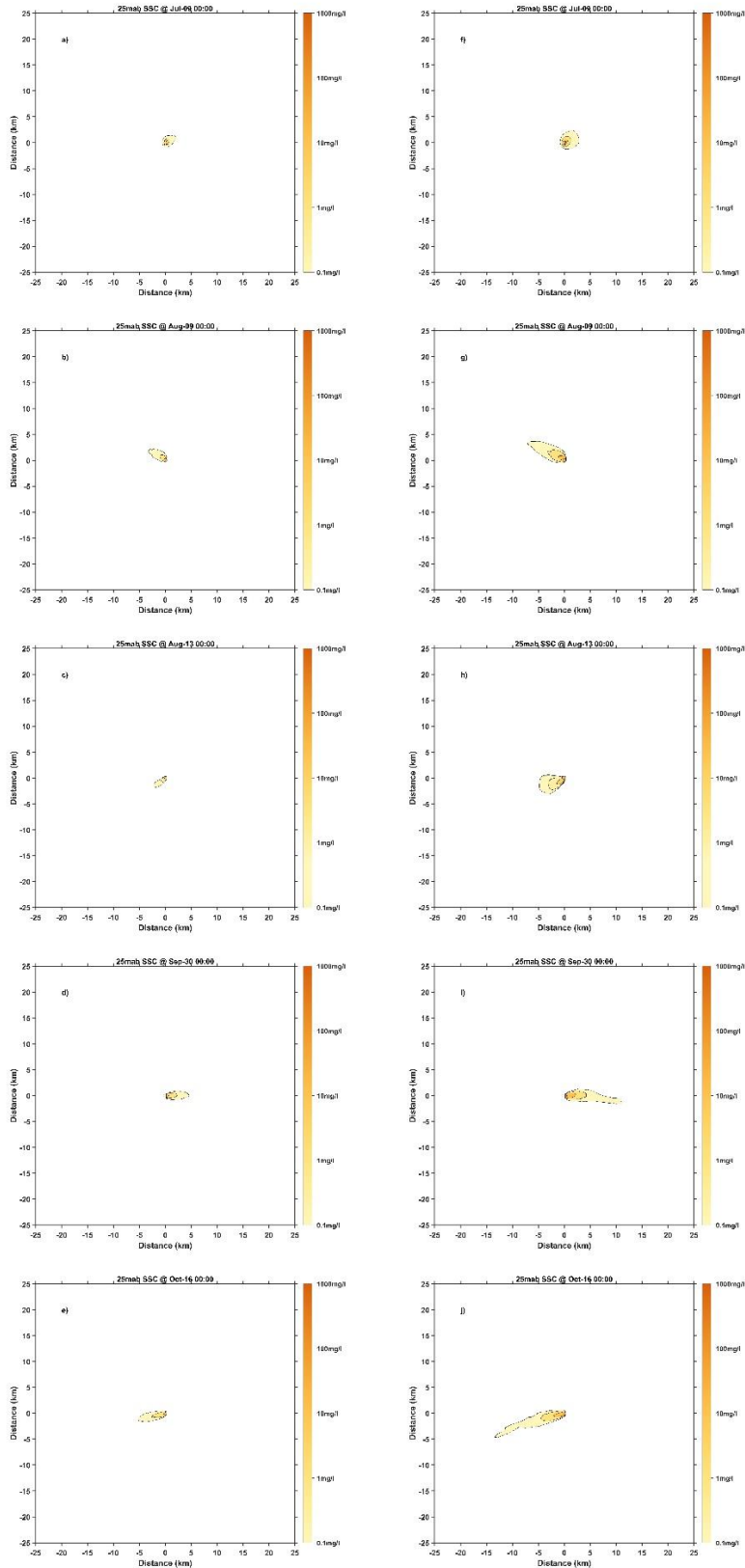
Figure 6-9 Horizontal Distribution of Suspended Sediment Concentration at 25 m above the bottom for Each Case (4th Day of the test)

6.2.3.2 Vertical Dispersion Distribution of the Plume

The point at 100 m from the boundary of the CTA is selected as the simulated monitoring point (Figure 6-10), and since the plume dispersal direction varies from month, the point at 100 m from the western boundary is selected for Case 2, Case 3, Case 5, Case 7, Case 8 and Case 10, and the point at 100 m from the eastern boundary is selected for Case 1, Case 4, Case 6 and Case 9, to analyze the characteristics of the vertical distribution of the deep-sea mining plume. As can be seen in Figure 6-11, on average, the maximum vertical dispersal height for a suspended sediment concentration of 10 mg/l is 64 m from the bottom (case 5), the maximum dispersal height for a concentration of 1 mg/l is 130 m (case 1), and the maximum vertical dispersal height for a suspended sediment concentration of 0.1 mg/l is 231 m from the bottom (case 1). In extreme cases, the maximum vertical dispersal height for a suspended sediment concentration of 10 mg/l is 113 m from the bottom (case 6), the maximum dispersal height for a concentration of 1 mg/l is 215 m (case 6), and the maximum vertical dispersal height for a concentration of 0.1 mg/l is 346 m from the bottom (case 6).
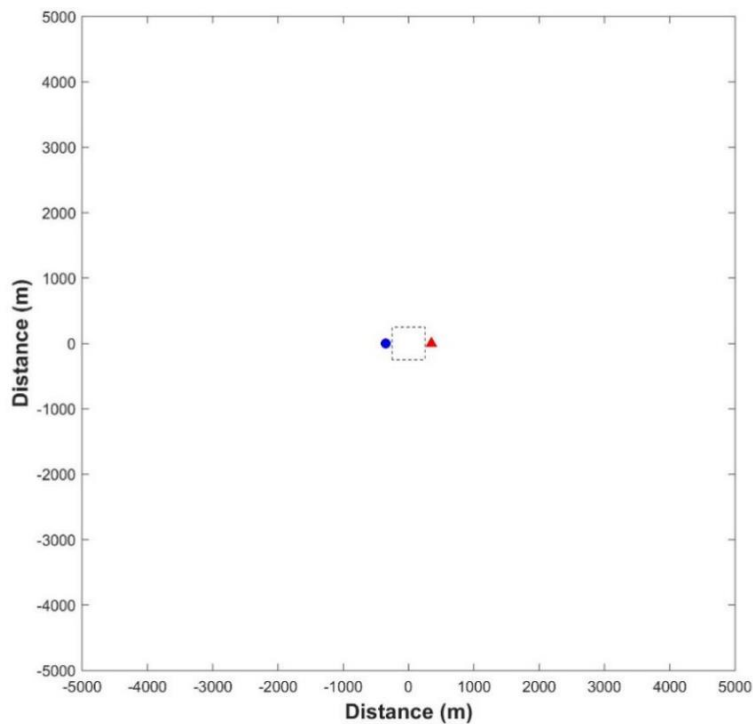
Figure 6-10 Location of points 100 m from the eastern (red, Case 1, Case 4, Case 6 and Case 9) and western (blue, Case 2, Case 3, Case 5, Case 7, Case 8 and Case 10) boundaries of the CTA.
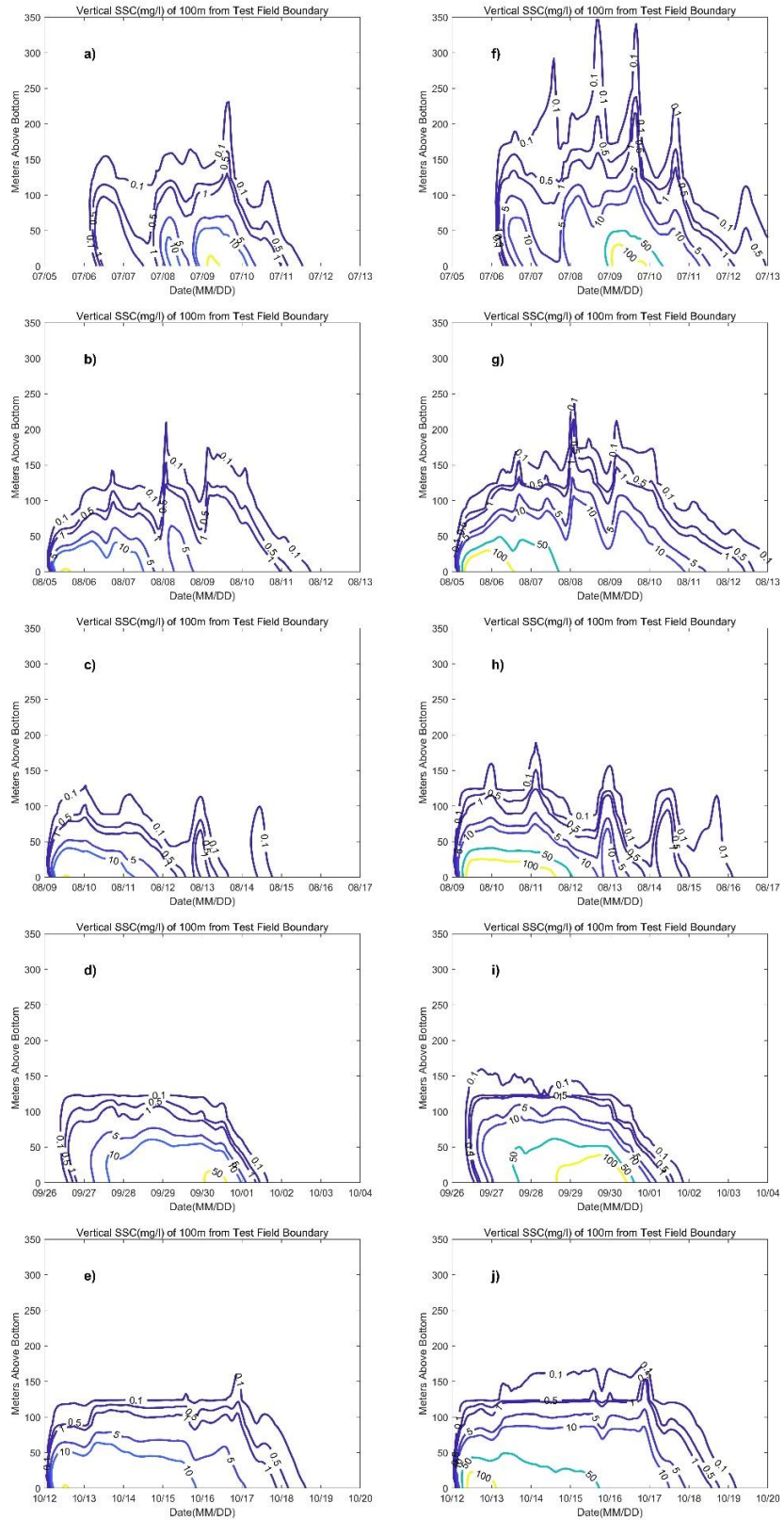
Figure 6-11 Vertical distribution of suspended sediment concentration at 100 m from the boundary of the CTA for each condition.

6.2.3.3 Distribution of Redeposition Thickness

Figure 6-12 shows the redeposition thickness 10 days after the end of discharge for each Case. As can be seen from the figure, the redeposition thickness of each case is greater than 1 cm in the CTA. On average, the maximum re-sedimentation thickness in each case is between 1.85 and 2.60 cm, with the maximum re-sedimentation thickness in case 1 being 2.60 cm and the minimum re-sedimentation thickness in case 5 being 1.85 cm. In extreme cases, the maximum re-sedimentation thickness of each case is between 0.85 and 1.48 cm, of which the maximum re-sedimentation thickness of case 8 is 1.48 cm; the maximum re-sedimentation thickness of case 10 is 0.85 cm (Table 6-2).

For the area distribution of redeposition thickness (Table 6-5), on average, the area of redeposition thickness greater than 1 cm does not differ much from one case to another, which is 0.28–0.31 km^2; the area of redeposition thickness greater than 1 mm is the largest in case 4, which is 0.76 km^2 , and the smallest in case 1, which is 0.55 km^2 (Table 6-5); and the area of redeposition thickness greater than 0.1 mm is the largest in case 5, which is 3.51 km^2 , and the smallest in case 1, which is 2.00 km^2. The area with redeposition thickness greater than 0.01 mm is largest in Case 4, 12.48 km^2, and smallest in Case 3, 7.74 km^2. In the extreme case, redeposition thickness greater than 1 cm occurs only in Case 7 (0.04 km^2) and Case 8 (0.17 km^2), which is smaller than the average; the area with redeposition thickness greater than 1 mm is largest in Case 9, 0.87 km^2, and Case 6 is the smallest with 0.56 km^2; the area with redeposition thickness greater than 0.1 mm is the largest with 5.90 km^2 in Case 9 and the smallest with 3.14 km^2 in Case 6; the area with redeposition thickness greater than 0.01 mm is the largest with 34.04 km^2 in Case 9 and the smallest with 17.75 km^2 in Case 10.
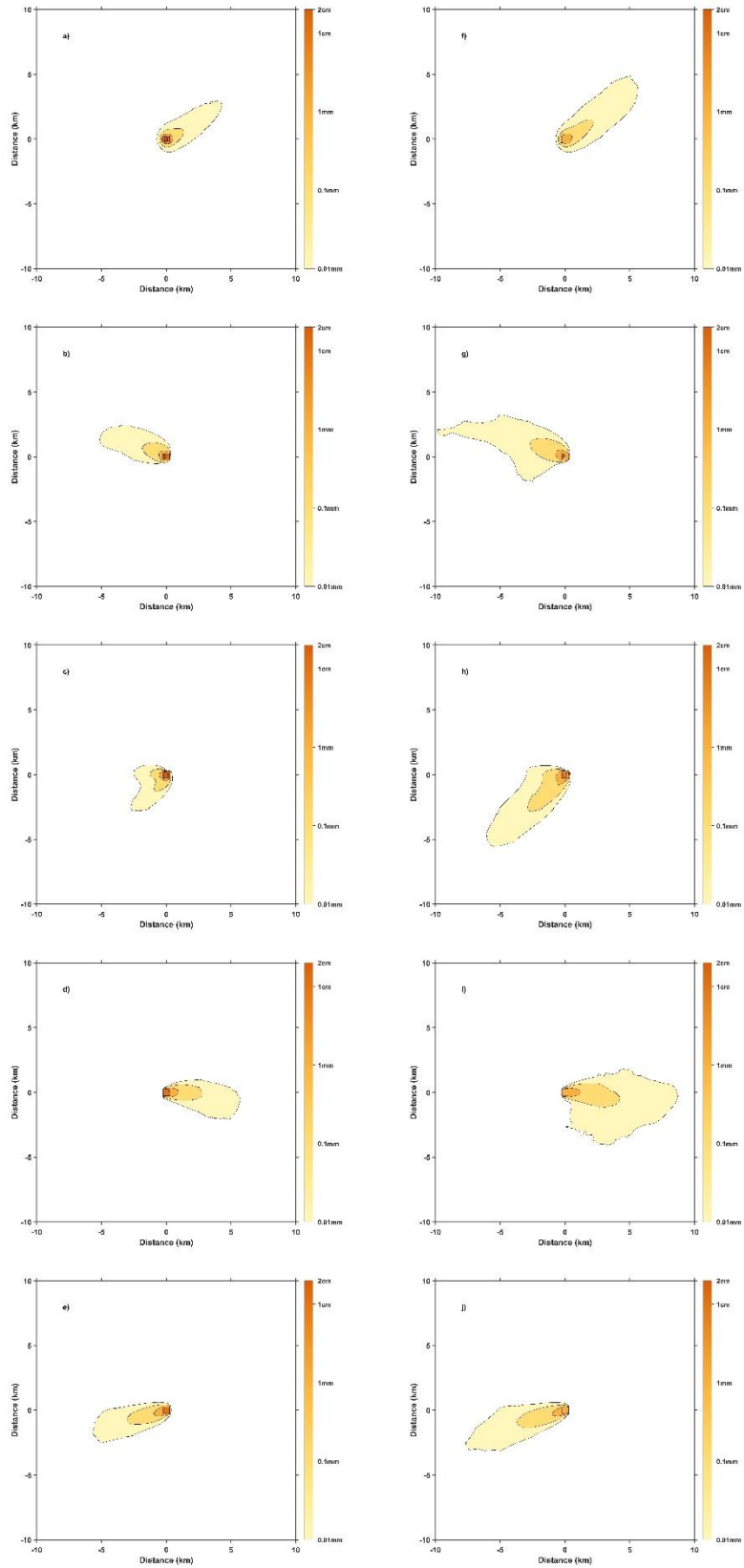
Figure 6-12 Distribution of redeposition thickness

433

Table 6-5 Plume redeposition thickness area

Case	Area with redeposition thickness greater than 1 cm (km²)	Area with redeposition thickness greater than 1 mm (km²)	Area with redeposition thickness greater than 0.1 mm (km²)	Area with redeposition thickness greater than 0.01 mm (km²)
Case 1	0.31	0.55	2.00	9.97
Case 2	0.28	0.60	2.43	11.10
Case 3	0.30	0.58	2.01	7.74
Case 4	0.28	0.76	3.14	12.48
Case 5	0.29	0.75	3.51	12.17
Case 6	0.00	0.56	3.14	17.87
Case 7	0.04	0.71	4.03	23.03
Case 8	0.17	0.84	5.68	21.10
Case 9	0.00	0.87	5.90	34.04
Case 10	0.00	0.73	4.48	17.75

6.2.3.4 Conclusions about Plume Dispersion and Redeposition Impact Prediction

A numerical model was used to simulate the diffusion and resedimentation of the deep-sea mining plume. Numerical simulation experiments were carried out on the average particle size and extreme particle size of the fine particles under the background of the current field of the weak northeast current, the strong northwest current, the weak southwest current, the strong east current, and the strong southwest current. The results show that, with a boundary of 0.1 mg/l, the maximum distance of the deep-sea mining plume is 5.43 km, and the area is 8.12 km². The mining plume disappears 3 to 4 days after the end of the test. At a distance of 100m from the boundary, the maximum vertical influence range of the plume is 231 m, and the high suspended sediment concentration (greater than 10 mg/l) was mainly located within 60 m from the bottom; the maximum re-sedimentation thickness was 2.60 cm, and the area with a resedimentation thickness greater than 1 cm was 0.28–0.31 km², slightly larger than the area of the CTA (0.25 km²), that is, a resedimentation thickness of 1 cm was basically confined to the vicinity of the CTA. In extreme cases, the maximum dispersal distance of the deep-sea mining plume was 27.86 km, covering an area of 69.75 km² (25m layer). The mining plume disappeared 7-9 days after the end of the experiment. 100m from the boundary, the maximum vertical influence of the plume was 346 m, and the high suspended sediment concentration (greater than 10 mg/l) was mainly within 110 m of the bottom; the maximum resedimentation thickness was 1.48 cm, and the area with a resedimentation thickness greater than 1 cm was 0.0~0.16 km². The horizontal dispersal distance of the plume depends on the bottom current, and the horizontal dispersal distance range depends on the bottom current velocity. In the case of

fine particles, the plume dispersal distance and dispersal area are both greater than the average for coarse particles.

6.3 Geological Environmental Impact

The mining test process involves in the removal of nodules and fine-grained sediments from the area. The removal of nodules and sediments not only leads to changes in the microtopography of the seafloor, but also generates a sediment plume in the water column near the seafloor, which affects seafloor bottom currents and sedimentation/redeposition processes. The target mining area in this test is only about 0.25 km^2. The active area is located in the center of a flat inter-mountain basin area without any critical habitat in it. Therefore, over a large scale, the removal of nodules and sediments had no obvious effect on the physico-chemical environment to this area.

Although mining collector may not have an obvious impact on the topography and physico-chemical environment of the test site, sediment plumes generated by collection activities can have some impact on the habitat of benthos in the vicinity of the test site. The extent of sediment plume deposition and dispersion is controlled by a variety of factors, such as the physical and chemical properties of the bottom sediments, geotechnical properties, hydrodynamic condition (near- and far-field), bottom topography, the type of mining equipment used, and the rate of mining, etc. Therefore, sediment disturbance tests and numerical modeling of plume dispersion are needed to assess the impact of mining activities on the surrounding environment.

Disturbance experiments by JET (Japan) and NOAA-BIE (USA) have shown that 90% of suspended particles by anthropogenic disturbance of the seafloor fall within a 2 km radius of the disturbed area. Experimental results from the MiningImpact 2 project carried out by the BGR in 2019 have shown that coarse-grained sediment re-settled soon after the release, but the settling of fine-grained sediments may take a period of several years. For example, models by Segschneider and Sündermann (1998) and Rolinski et al. (2001) suggest that 90 to 95% of the fine-grained sediment may take 3 to 14 years to redeposit, while 100% of the total mass may take 9 to 17 years to redeposit. In addition, the MiningImpact 1 project utilized a benthic sled (EBS) and remotely operated vehicle (ROV) to conduct sediment disturbance tests. The results show that the sediment plume does not rise more than 10 m above the seafloor, but the lateral spreading distance varies considerably and is mainly influenced by seafloor topography and bottom current.

6.4 Marine Traffic

The main shipping routes in the Pacific Ocean include (1) Far East-North America West Coast Route; (2) Far East-South America West Coast Route; (3) Far East-Southeast Asia Route; (4) Far East-Australia and New Zealand Route; (5) Australia and New Zealand -North America East and West Coast routes. According to the vessel position monitoring data of the Global Integrated Shipping Information System (GISIS) from 2015 to 2020, the BPC contract area is far away from the above major shipping routes (Figure 6-13).
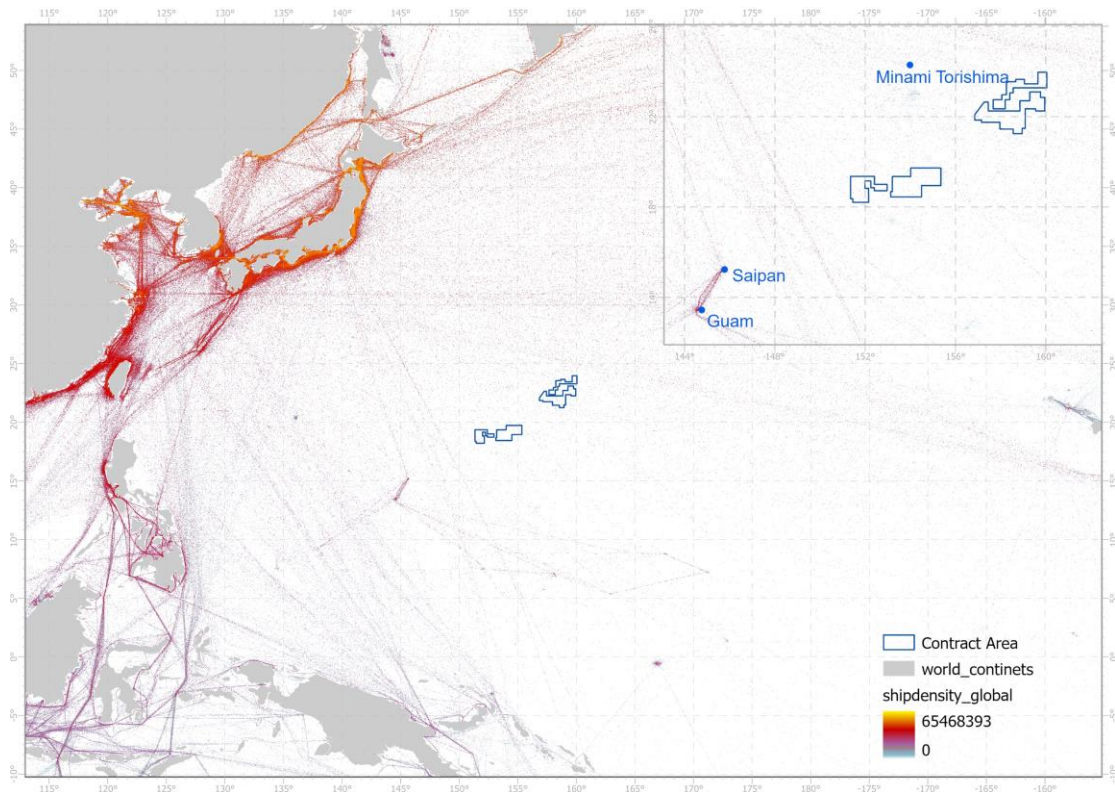
Figure 6-13 Density of vessel traffic in western Pacific

(Source: Cerdeiro et al., 2020)

The closest route to the BPC contract area is the eastern Far East-Australia route from Tokyo to Sydney via the Solomon Islands, and the closest distance from the CTA to this route is about 400 km, so the impact of the mining test activities to shipping is negligible.

6.5 Air Quality

The ships used in the project strictly comply to the obligations and standards of the International Maritime Organization (IMO) regarding environmental practices at sea, including the *International Convention for the Prevention of Pollution from Ships, 1973,*

as modified by the Protocol of 1978 (MARPOL 73/78), and the Protocol to the MARPOL Protocol of 1997 on the prevention of air pollution from ships. In this way, IMO regulates air emissions and develops the necessary anti-pollution measures aimed at minimizing all impacts of air and water pollution at sea.

Carbon emissions from this mining test activity were measured in accordance with the formula for calculating the carbon emission for marine diesel fuel in the *2019 Refinement to the 2006 IPCC Guidelines for National Greenhouse Gas Inventories*:

Default carbon dioxide emission factor (C) = default carbon content (A) ×default carbon oxide factor (B) × 44/12

That is, the default effective CO_2 emission factor for marine diesel is 74.1 g/MJ. Measured by the energy conversion efficiency of marine diesel generators, the CO_2 emissions from deep-sea mining range from 760 to 890 g/kWh. The green nature of the energy supply system needs to be taken into account in order to carry out offshore work, so clean energy should be introduced into the power supply of the deep-sea mining system, and the carbon dioxide emission of clean energy is 0. In order to ensure the continuity and safety of energy supply, the proportion of installed capacity of clean energy in the deep-sea mining energy supply system should not be less than 50 per cent. Based on the energy consumption of 100 kWh per ton of wet nodule mining, the carbon dioxide emission per ton of wet nodule mining is 38 to 44.5 kg when diesel power supply and clean energy power supply are each used at 50 per cent. It is therefore desirable to limit carbon dioxide emissions per ton of wet nodule mining to less than 45 kilograms.

During this test, diesel power supply and clean energy power supply were used 50% each, and deep-sea CO_2 emissions were taken as 450 g/kWh.

Before the test, the two vessels departed from the Qingdao port, China, and traveled to Block M2 in the western Pacific Ocean by the shortest route, with a route distance of 4,223 km and a round-trip distance of 8,446 km. The standard speed of the test vessel "Da Yang Yi Hao" and the environmental monitoring and protection vessel "Da Yang Hao" is 12 knots. Based on the standard speed, the round-trip ferrying time for both vessels is 15.8 days.

At standard speed, "Da Yang Yi Hao" needs to turn on one generator with a power of 2,940 KW and one with a power of 760 KW, and at the same time it needs to turn on one generator with a power of 3,060 KW and one with a power of 800 KW. In this process, "Da Yang Yi Hao" energy consumption would be 2940 + 760 + 3060 + 800 = 7560 KW, the carbon dioxide emissions are about 1290 tons. The "Da Yang Hao" needs to turn on one generator with a power of 2,900 KW at standard speed, and the carbon dioxide emission is 494.9 tons.

The total testing time in the work area is estimated to be 15 days, taking into account the necessary maneuvering and power positioning operations, both ships are calculated according to 50% of the converted speed, under this state of "Da Yang Yi Hao" carbon dioxide emissions of about 612.4 tons, the "Da Yang Hao" carbon dioxide emissions of about 234.9 tons. Emissions of "Da Yang Yi Hao" and "Da Yang Hao" are about 612.4 tons and 234.9 tons during the test, respectively.

During the underwater test of the collector, the test vessel "Da Yang Yi Hao" needs to turn on an additional set of generator system with a power of 1,400KW to ensure the power demand of the collector and other auxiliary equipment on board, and it needs to be turned on for 10 days in total, and the carbon dioxide emission in this process is 151.2 tons (Table 6-6).

Table 6-6 Greenhouse gas (GHG) emissions

Stage	Causes of GHG emissions (test phase)	Energy consumption (KW/h)	GHG emissions equivalent by component (tons)	Phase GHG emissions equivalent (tons)
Emissions outside Block M2 (non-test phase)	Round-trip cruise of "Da Yang Hao"	1099680	494.9	1784.9
	Round-trip cruise of "Da Yang Yi Hao"	2866752	1290	
Emissions in Block M2 (testing phase)	"Da Yang Hao" operating in Block M2	522060	234.9	998.4
	Auxiliary engine (to provide full power to the collector and surface support system)	336000	151.2	
	"Da Yang Yi Hao" operating in Block M2.	1360845	612.3	
Total				2783.3

6.6 Transboundary Impacts

The influence generated by some stressors may go beyond the boundary of the mining area, resulting in transboundary influence. According to the results of the plume simulation in section 6.2, the extreme value of the influence distance of the sediment plume spreading outward from the CTA is 3.48 km. This distance will not exceed the boundary of the contract area, so it will not cause transboundary impacts. As the test duration time is limited, there will be no serious light transboundary impacts. Noise is unavoidable stressor during the test period and may have a transboundary impact. There are fewer studies on the environmental impacts of noise on deep sea ecosystem, and a preliminary impact

assessment of noise impacts is provided in section 7.2.4. During this test we will advance the study of noise impacts on the deep sea. In the environmental monitoring plan, hydrophones will be used to monitor and evaluate the noise impact during the test (see Chapter 9). The duration of the seafloor test for this project is 100.5 hours and the collector is at a 1:5 ratio, so the potential noise impacts is small.

The likelihood of transboundary social or economic impacts is also extremely low, as the quantity of polymetallic nodules collected is small (7,500 tons) and most of them remain on the seafloor, with only a very small amount recovered with the collector on board the ship for metallurgy studies, which will not affect any existing metal producers.

6.7 Proposed Mitigation Measures

International conventions such as the *International Convention for the Prevention of Pollution from Ships* (MARPOL 73/78) will be strictly enforced by test ships and environmental monitoring ships during mining test, and the following mitigation measures will be taken:

(1) The Manta suspended collector is adopted in the design of this project, which can greatly reduce the milling and stirring intensity to the seabed. The previous test showed that the depth of the collector track is only 4–6 cm, and the disturbance to the seabed is obviously lighter than that of the tracked collector;

(2) Nodule collection by suction hydraulic collecting method to minimize disturbance of the seafloor sediments;

(3) Discharge of mining tailings near the bottom (4 m above the bottom) will reduce the spread of the plume;

(4) The majority of polymetallic nodules collected remain on the seafloor (Nodules are the attachment base for many attached organisms. Keeping nodules on the seabed provides an attachment base for organisms to attach to, which is conducive to accelerating the recovery process). The distance from the hose to the repeater is short, with lighter nodule fragmentation and differentiation, and not discharge to the surface or to the mid-layer.

Mitigation measures for environmental impacts during mining operations are detailed in Table 6-7.

Table 6-7 Mitigation Measures for Environmental Impacts from Mining Operations

Number	Work process	Target of an action	Impact results	Mitigation measure
1	Collector movement at seafloor	habitat disturbance	Changes in the structure of biological habitats	Limit the areas affected by the propulsion of collector operations and improve the technology of propulsion of mining collector
		Sediment compaction	Death of some benthos, biodiversity destruction	Adoption of suspended collector
2	Mineral collection process	habitat removal	Changing the structure of biological habitats	Instead of using the jet collection method, the nodules are drawn in by pump suction to minimize the disturbance of the surface sediments
		Hydraulic oil leakage	Estimated average 0.9 m^3 oil leakage	Use of pressure testing systems and biodegradable oils
		Loss or destruction of mining collector power	Result in equipment/tools being left on the seabed	Enhanced reliable technological development of mining equipment
		Seafloor plume generation	benthos asphyxiation /food chain alteration / affecting luminescent organisms communication between courtships etc.	Development mining technology to reduce the amount of sediment inhaled during mining operations
		Potential release of toxic substances such as heavy metals	Biological uptake of toxic substances such as heavy metals	No measured data available, monitored through testing
		Mining truck lights	Photosensitive organisms will be affected	Currently no measured data, monitored through testing and mining technology will be improved if found to be the case
		Mining truck noise	May interfere fish movement	Currently no measured data, monitored through testing and mining technology will be improved if found to be the case
		Vibrations from mining equipment	May interfere fish movement	Currently no measured data, monitored through testing and mining technology will be improved if found to be the case

6.8 Risk Assessment

The collection of deep-sea minerals would involve in the removal of seafloor sediments surrounding the minerals, which has an impact on the benthos habitat in the mining area. This obviously alters the seafloor habitat and leading to the generation of sediment plumes near the seafloor. Additionally, for the physical environment, the removal of minerals and sediments from the seafloor will also modify the topographic structure or roughness of the mining area, for example, by creating small seafloor gullies, which in turn will have an impact on the current dynamics near the seafloor, modulating the processes of deposition and redeposition of SS.

The redeposition of seafloor sediment plumes generated around mine sites can cover the seafloor bottom, causing burial of benthos and blocking the respiratory organs of filter feeders. Meanwhile, reactive components in sediment plume, such as unstable organic matter or reduction metals, can consume oxygen, causing oxygen depletion. Some deep-sea minerals contain potentially toxic metals, and the collection of these minerals results in the release and deposition of toxic metals, which can lead to the bioaccumulation of contaminants. These processes may change the structure and function of deep-sea ecosystems. To date, very few studies have focused on analyzing and modelling the magnitude of the impact of sediment plumes on the benthic environment during deep-sea mining at various environmentally relevant temporal and spatial scales. Impacts depend on the scale of the mining and local environmental condition, such as the physio-chemical feature of sediments, seafloor current, the topography of the bottom, the type of mining equipment used, and the rate of mineral collection, etc.

According to the simulation results of the numerical model for this test, with 0.1 mg/l SS as the background value,, the maximum dispersal distance of the deep-sea mining plume was 5.43 km and the area was 8.12 km^2 in average, and the mining plume disappeared 3–4 days after the end of the test; the maximum influence range of the plume in the vertical direction at the distance of 100 m from the boundary was 231 m, and the high concentration of SS (more than 10 mg/l) was mainly located within 60 m from the bottom; the maximum redeposition thickness was 2.60 cm, and the area with redeposition thickness greater than 1 cm was 0.28–0.31 km^2, which was slightly larger than the test area (0.25 cm^2).) was mainly located within 60 m from the bottom; the maximum redeposition thickness was 2.60 cm, and the area with redeposition thickness greater than 1 cm was 0.28–0.31 km^2, slightly larger than that of the CTA (0.25 km^2), i.e., the redeposition thickness of 1 cm was basically confined to the vicinity of the CTA. In the extreme case, the maximum spreading distance of the deep-sea mining Plume was 27.86 km, with an area of 69.75 km^2 (25 m layer), and the mining plume disappeared 7–9 days after the end of the test; 100 m from

the boundary, the maximum influence area of the plume was 346 m, and the high concentration of SS (more than 10 mg/l) was mainly located within 110 m from the bottom; the maximum thickness of redeposition was 1.48 cm. The area with redeposition thickness greater than 1 cm is 0.0–0.16 km^2.

Generally, considering the small spatiotemporal scale test, implementation of the environmental monitoring plan and proposed mitigation measures, as well as the rigorous reporting and regulatory procedures, it is reasonable to expect that all physicochemical, biological, and cumulative impacts can be sufficiently minimized to non-significant levels. In the absence of any significant unforeseen impacts, the risk of 'Serious Harm' to the marine environment on a regional scale from this testing of polymetallic nodule collector components is 'Low'.

7 ASSESSMENT OF IMPACTS ON THE BIOLOGICAL ENVIRONMENT AND PROPOSED MITIGATION MEASURES

7.1 Potential Impact Categories

According to the available literature, the potential impacts of deep-sea mining on the biological environment include the following three depth bands:

7.1.1 Potential Impacts on Deep-sea Benthic Organisms

Potential impacts on deep-sea benthic organisms include:

(1) Decrease in abundance of benthos and nodule fauna due to sediment compaction, removal of polymetallic nodules and sediment;

(2) Effects of sediment plume diffusion and redeposition from ore-collecting processes on the respiration and filter-feeding of benthos and benthopelagic animals;

(3) Impacts of plume dispersion and redeposition from tailings discharge (if tailings are discharged in a bottom-discharge manner) on the respiration and filter-feeding of benthos and bottom-dwelling organisms;

(4) Releases of potentially toxic heavy metals and/or substances to the bottom water column and their effects on benthos and benthopelagic animals;

(5) Noise generated by mineral collectors and its potential impact on benthos and benthopelagic animals.

(6) The collector test will impact even mobile benthopelagic species. (Stratmann et al.,2018).

7.1.2 Potential Impacts on Mesopelagic Organisms

The mesopelagic layer here refers to the layer below the euphotic zone to 100 meters above the bottom potential impacts on mesopelagic organisms include:

(1) Effects of vessel and collector noise on mid-water column swimmers;

(2) Impacts to water column nekton from noise and vibration generated by the mineral hoisting system (not applicable to this project);

(3) Impacts to water column nekton and zooplankton from spilled tailings from unforeseen events such as rupture of the mineral hoisting system (not applicable to this project);

(4) Impacts on respiration and feeding of nekton and zooplankton from plume diffusion from tailings discharge (if tailings are discharged in mesopelagic layer) (not applicable to this project);

(5) Impacts to nekton and plankton from the release of potentially toxic heavy metals and other substances from tailings into the water column (not applicable to this project).

7.1.3 Potential Impacts on Epipelagic Organisms

Potential impacts to epipelagic organisms may include:

(1) Accidental discharges (hydrocarbon pollution, hydraulic fluids) or waste discharges from surface vessels into surface waters and their effects on seabirds, mammals (whales, etc.) and plankton;

(2) Impacts on large nekton and seabirds on the surface of the water due to noise caused by the vessel itself or acoustic systems installed on the vessel;

(3) Effects of light pollution from ship lighting on nekton and plankton;

(4) Impact of spilled tailings from accidents such as rupture of mineral hoisting systems on primary production and biophysiological and biochemical processes in the euphotic zone.

The organisms that may be affected by the test activities of the polymetallic nodule collector to be carried out by BPC are mainly of two types: benthic and benthopelagic animals inhabiting the CTA and its adjacent areas. These organisms have a complex and diverse way of life as epifauna (including sessile, attached and encrusting organisms), infauna (including tubular, buried and burrowing organisms) and benthopelagic organisms. Different phases of collection test will affect benthic organisms with different life styles. Compared with the epifauna and infauna, the benthopelagic organisms are relatively more mobile, and it is expected that this collection test activity will have a relatively small impact on these organisms. The other types of organisms are those living on the sea surface, including seabirds, sea turtles, whales and other large mammals, as well as plankton and swimming organisms around the vessel. The Test is also expected to have a relatively small impact on these organisms.

BPC has not conducted collector test activities previously, and this assessment is based primarily on published literature on similar international test activities, and the potential biological impacts expected from this test activity are detailed in Table 7-1.

Table 7-1 Main impacts of deep-sea mining activities on the biological environment

Type of environment	Impact on the physical and chemical environment	Impact on the biological environment	Mitigation measure
Benthic environment	Removal of minerals	Loss of habitat for nodule-attaching organisms, causing a decrease in the abundance and diversity of these organisms	The use of suspended collectors to minimize compression and disturbance of the surface sediments on the seabed
	Sediment removal	Loss of habitat; partial removal of benthos, causing a declination in abundance and diversity	
	Compacted sediment	Compaction of surface sediments, degradation of habitats, loss of some benthos by crushing, decline in abundance and diversity	
	Increased concentration of suspended solid	Suspended solid deposited to a certain thickness will bury benthos and block the respiratory organs of benthos and benthopelagic organisms, causing some organisms to suffocate and die.	
	Changes in the hydrological environment	Altering the distribution of organisms and their juveniles	
	Altered biogeochemical cycles	Changing food sources	
	Electromagnetic radiation	Chronic effects	
	Light pollution	Behavior change	
	Noise pollution	Exceeding the threshold will interfere with the communication between animals and affect their behavior such as reproduction and feeding.	
Mid-water Layer (below the euphotic zone to 100 m above the bottom)	Ship Noise	Exceeding the threshold will interfere with the communication between nekton and affect the breeding, feeding and other behaviors of nekton.	
	Collector noise	Exceeding the threshold will interfere with the communication between nekton and affect the breeding, feeding and other behaviors of nekton.	
Epipelagic Environment (euphotic zone)	Ship Noise	Exceeding the threshold will interfere with the communication between animals and affect their behavior such as reproduction and feeding.	Prohibit surface discharges of tailings; turn off unnecessary lighting at night, to the
	Collector noise	Exceeding the threshold will interfere with the communication between animals and affect their	

Type of environment	Impact on the physical and chemical environment	Impact on the biological environment	Mitigation measure
		behavior such as reproduction and feeding.	extent possible, in addition to ensuring the safety of navigation and operations; in accordance with the sessile *Regulations on the Prevention and Control of Pollution from Ships to the Marine Environment* and the relevant provisions of the International Maritime Organization
	Light pollution	Behavioral changes in birds, cetaceans, fish, etc.	
	Release of carbon dioxide to surface waters and the atmosphere	Increases acidity and may inhibit biological growth	
	Domestic sewage	Phytoplankton uptake and utilization and transfer through trophic levels to higher trophic level organisms	
	Hazardous chemicals	Ecotoxicological effect	
	Trace metal release	Exceeding the threshold value can have an inhibitory or toxic effect on biological growth.	

7.2 Potential Biological Impacts

7.2.1 Direct Impact

7.2.1.1 Removal of Nodules and Its Impact on Benthos

Polymetallic nodules are the cemented substrate for epibenthic organisms such as sponges (Figure 7-1), cold-water corals, anemones, sea lilies, and protozoa (Figure 7-2) (Thiel et al., 1993; Cui et al., 2011; Wang et al., 2018). Vanreusel et al. (2016) analyzed the ROV imagery data collected in the CCZ. The results showed that the abundance of epibenthic organisms was more than twice as high in areas with high nodule coverage than in nodule-free areas, and that taxa such as soft corals and black corals were hardly found in the nodule-free areas (Figure 7-3). The test will remove most of the nodules from the collecting track, which will obviously destroy almost all

of the sessile Megafauna attached to the nodules, such as sponges, anemones, sea lilies, etc. The original benthic community with a mixture of soft-sediment and hard-substrate will be turned into a purely soft-sediment benthic community, thus reducing the diversity of Benthos in the test area (Bluhm et al., 1994; 1995). With the movement of the collecting vehicle, the less mobile organisms, such as starfish, sea urchins and sea cucumbers, will be crushed and killed or sucked into the vehicle and destroyed as they had no time to escape. In addition, the regeneration and recovery of epibenthic sessile communities that use nodules as a hard substrate for attachment will be affected by the removal of most of the nodules (Foell et al, 1992; Wang and Zhou, 2001b). Larvae of benthic organisms migrating in from outside the mining area will die soon afterward, as they cannot find the required hard substrate to attach to. Vanreusel et al (2016) returned to a track mined 37 years ago by the Nodule Test Mining experiment and found little redistribution of the aforementioned megabenthos on the nodule mining track, suggesting that mining permanently destroys nodule habitat, leading to extremely slow recovery of such organisms.

Nodule removal can also affect the Meiofauna community. Thiel et al. (1993) found Meiofauna distributed in nodule fissures. The structure of Meiofauna communities in nodule fissures differed significantly from those in the surrounding sediments. The former was characterized by smaller individuals and lower abundance in general, and higher abundance of the genera *Camacolaimus, Leptolaimus*, and *Acantholaimus* at the genus level, with *Camacolaimus* being the dominant genus of nematodes. Miljutina et al. (2010) found significant differences in nematode species composition between nodule-covering and nodule-free areas in the French contract area in the CCZ. The results of Singh et al. (2019) in the nodule area of the Central Indian Ocean basin revealed that the presence of nodules helps to increase Meiofauna species diversity. It can therefore be inferred that removal of nodules, loss of this habitat or disturbance activities will inevitably lead to a decrease in the diversity of Meiofauna living in nodule fissures, but quantitative studies are lacking.

Figure 7-1 *Chaunoplectella megapora attached* to a polymetallic nodule

（Wang et al., 2018）
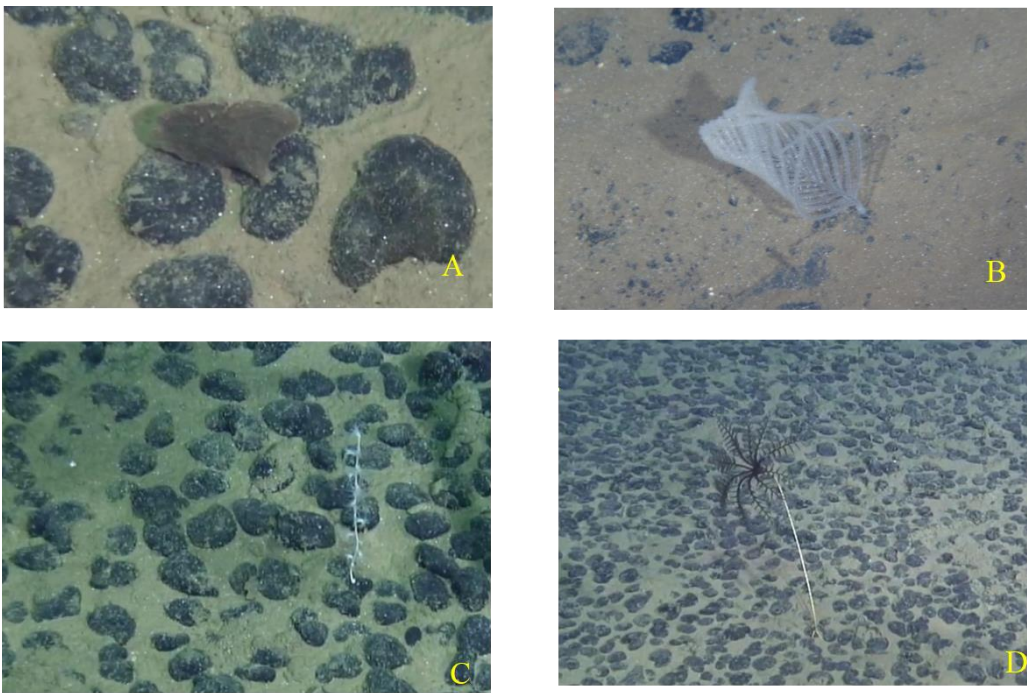
Figure 7-2 Nodule organisms (reported by Wang et al., DY31 cruise)

A．*Stannophyllum* sp. B. *Abyssopathes* sp. C. Isididae gen sp. D. Bathycrinidae gen sp.
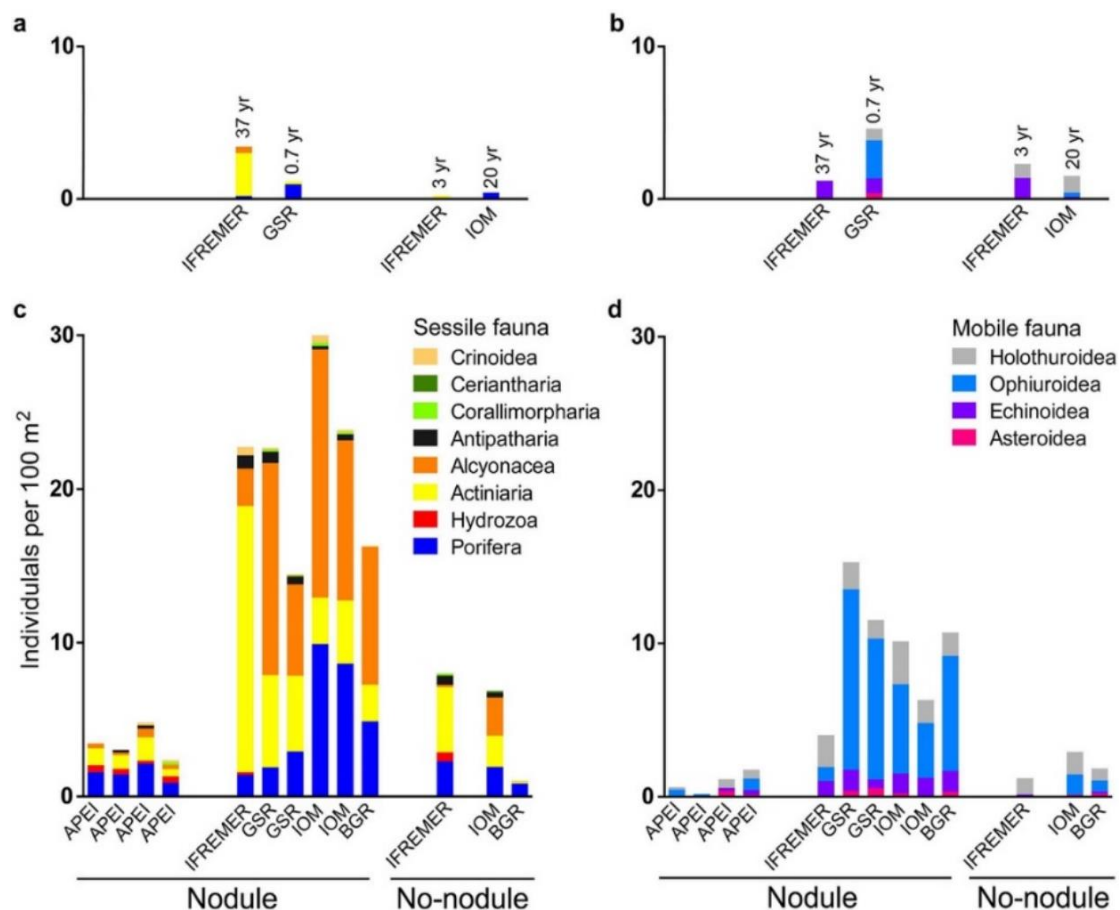
Figure 7-3 Differences in abundance of sessile benthos (a, c) and mobile benthos (b, d) in disturbed (a, b) and reference (c, d) areas (Vanreusel et al., 2016)

7.2.1.2 Sediment Removal and Its Impact on Benthos

In addition to the removal of nodules, the mining process removes a large amount of surface sediments from the seafloor. According to the assessment of Amos and Roels (1977), for every ton of polymetallic nodules mined, 2.5 to 5.5 tons of sediment are resuspended. Such a large amount of sediment resuspension and re-sedimentation processes are bound to have an impact on the bottom-dwelling Benthos living in the surface sediments. The results of the survey have shown that the benthic organisms in the nodule area are mainly distributed in the sediments shallower than 10 cm. After the sediment around the nodule being extracted by the collector, the organisms in the sediment will inevitably be caught up in the collector, and then drifted away with the current or re-settled. This process may cause some of the bottom-living organisms to die immediately, or to be preyed upon by the larger organisms, which will reduce the abundance of organisms. In the 1980s and 1990s, the DISCOL experiments and the BIE experiments revealed the long-term effects of the simulated disturbances on the infauna after the removal of the sediments. The DISCOL experiment was conducted in

Germany from 1988 to 1998, with time-series sampling before and after simulated disturbances (6 months, 3 years, and 7 years) in a circular area of 10.8 km². The results showed that the abundance of all macrofauna groups was obviously reduced after the disturbances (Figure 7-4), with the composition of polychaetes being obviously different from that before the disturbance (Schriever et al., 1997).
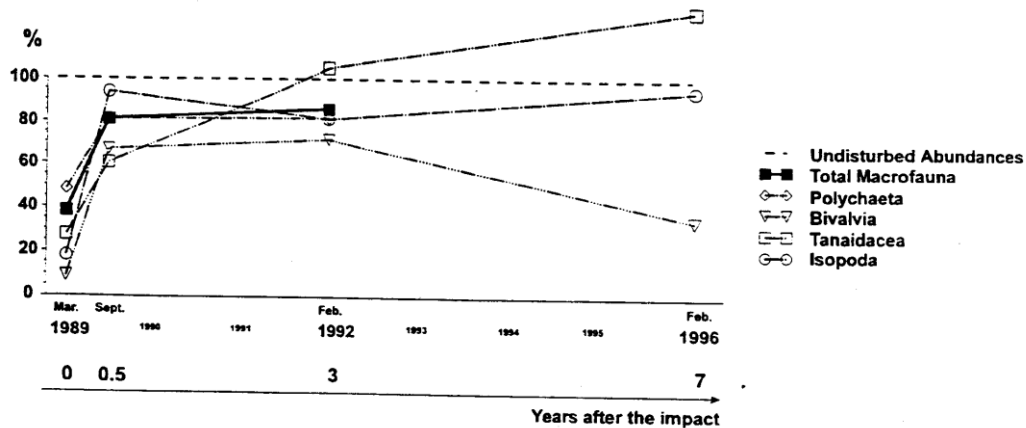
Figure 7-4 Changes in Macrofauna abundance following disturbance during the DISCOL experiment (Schriever et al., 1997)

The results of the DISCOL experiment (Figure 7-5) showed that the abundance of the three main taxa of Meiofauna, nematodes, harpacticoids, and foraminifera, declined to approximately 50% of their pre-disturbance abundance approximately 30 d after plowing and harrowing, and that nematodes and harpacticoids continued to decline in abundance while foraminifera abundance rebounded slightly after 0.5a. Nematode abundance increased to twice its pre-disturbance level after 3a, and harpacticoids abundance was above 60% of its pre-disturbance abundance. Unlike Megafauna, the abundance of Meiofauna had also increased at the reference site. Schriever et al. (1997) suggested that this could be due to additional food inputs from the euphotic layer.
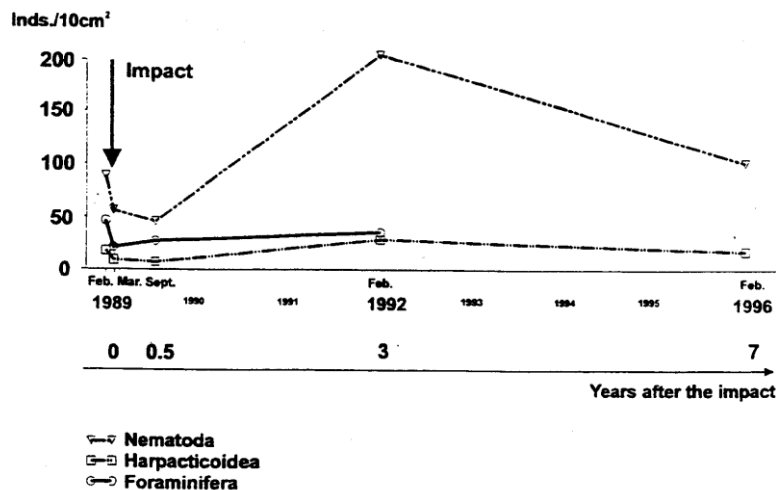
Figure 7-5 Changes in the abundance of each major group of Meiofauna during the DISCOL experiment (Schriever et al., 1997)

The results of a Japanese deep-sea impact experiment conducted by Nippon Metal Mining Corporation in 1994 using the DSSRS system showed that the abundance of Meiofauna in the sediment was greatly reduced by disturbance and returned to its original abundance only after two years, but with a different species composition, while the number of Macrofauna was still lower than that in the undisturbed area (Shirayama, 1999). BIE experiments in the SGL showed that feeding activity of motile demersal fish and shrimps increased after the disturbance and their abundance increased in the disturbed area compared to the pre-disturbance state (Tkatchenko et al., 1996). It is likely that the disturbance process exposed sediment organisms to the water column and increased their food supply.

7.2.1.3 Compaction of Sediments and Its Effects on Benthos

When surface sediments are disturbed and compacted, the abundance of Macrofauna and Meiofauna also decreases, but Microorganisms may increase. The results of the DISCOL experiment showed that extrusion resulted in a massive killing of bivalves at surface layer, with abundance dropping to 9.8% of their original abundance, and a lesser impact on polychaetes at deeper layer, with abundance dropping to 48.6% of their original abundance (Schriever et al., 1997). Meiofauna distributed in the sediment were similarly affected, with the abundance of nematodes, harpacticoids, and foraminifera decreasing to approximately 50% of their pre-disturbance abundance. At the same time, mining activities can bury much of the food

451

that settles from the upper layers to the bottom, leading to a decline in Benthos abundance.

The project utilizes a suspended collector, i.e. the collector body does not touch the seafloor and is equivalent to towing a bottom surface sled on the seafloor, similar to the bottom trawl used to collect nodule samples. This mode of operation greatly reduces the physical compression of the sediment by the collector and results in less disturbance and compaction of the surface sediment (less than 6 cm, Figure 7-6), whereas the operation of a conventional tracked collector would compress a loose sediment layer at least 10 cm thick. Moreover, the area of this collection test is very small (approximately 0.25 km²), and although it will locally reduce the abundance of benthos, it is not expected to affect the community structure, gene flow or species connectivity of the benthos or benthic ecosystem function in the contract area.
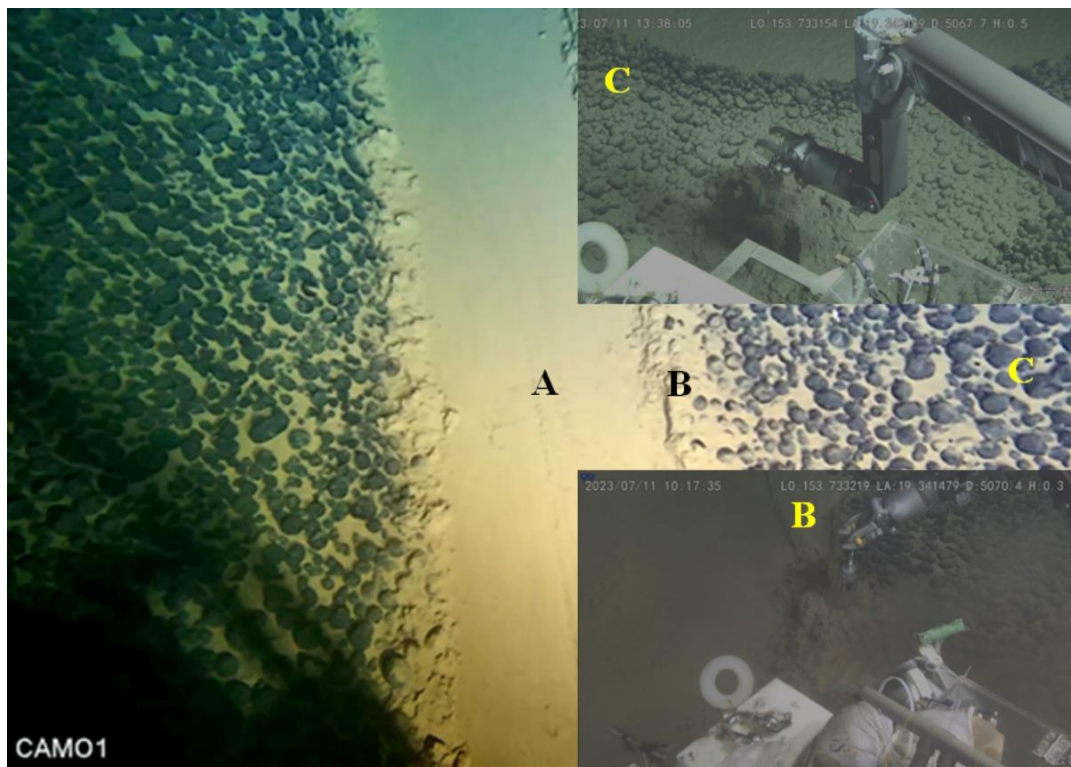
Figure 7-6 Pushcore sampling sites (A, B, C) in the Manta sampling test area revisited by the "Jiaolong" HOV in July 2023

In order to assess the impacts of the "Manta" sampling test, "Jiaolong" manned submersible revisited the sampling test area in July 2023, nine months after the Manta sampling test, and collected sediment pushcore samples from the inside of the Manta sampling track (Zone A), the sediment accumulation area outside the track (Zone B), the area 2–500 m outside the track that might be affected by the redeposition (Zone C), and the reference sites that were not affected by the plume (Figure 7.6 and Table 7.2)

Sediment samples from the Plume reference zones (Figure 7-6 and Table 7-2) were analyzed for Meiofauna abundance and diversity. Preliminary results showed that Meiofauna abundance in Zone A was very low and severely impacted, especially in the top 2 cm of the sediment, which was clearly disturbed and had a lower abundance than the 2–4 cm layer (Figure 7-7). Zone C also had obviously lower abundance of Meiofauna than the reference zones due to the IRZ by the plume and redeposition. The maximum value appears in zone B. Figure 7-7 shows that there is still a high abundance of Meiofauna in sediments deeper than 8 cm at Station JL240-99. The 8 cm layer here is supposed to be the original surface sediment, and the upper few centimeters of sediment is the overlaying sediment after the mining test. Therefore, the Meiofauna in the sediment in zone B is a mix of surface and deeper layer sediment.

Table 7-2 Meiofauna sampling stations and abundance at different locations of the Manta sampling track

Sampling location	Station	Latitude/ °N	Longitude / °E	Water depth (m)	Average abundance (ind/10cm^2)
Inside the track (A)	JL240-19	19.341828	153.732908	4962	1.3±0.0
Inside the track (A)	JL238-02	19.341162	153.733217	5070	
Area of sediment accumulation on the edge of the track (B)	JL240-09	19.341625	153.733515	5071	7.02±5.14
Area of sediment accumulation on the edge of the track (B)	JL240-99	19.341784	153.732759	4893	
2 m outside the track (C)	JL238-16	19.341172	153.733072	5070	3.9±0.97
2 m outside the track (C)	JL240-17	19.341733	153.732531	4686	
8 m outside the track (C)	JL238-13	19.341201	153.733747	5070	
500 m outside the trajectory (C)	JL238-09	19.341382	153.736934	5077	
Reference point	JL239-08	19.663410	152.951540	5776	6.24
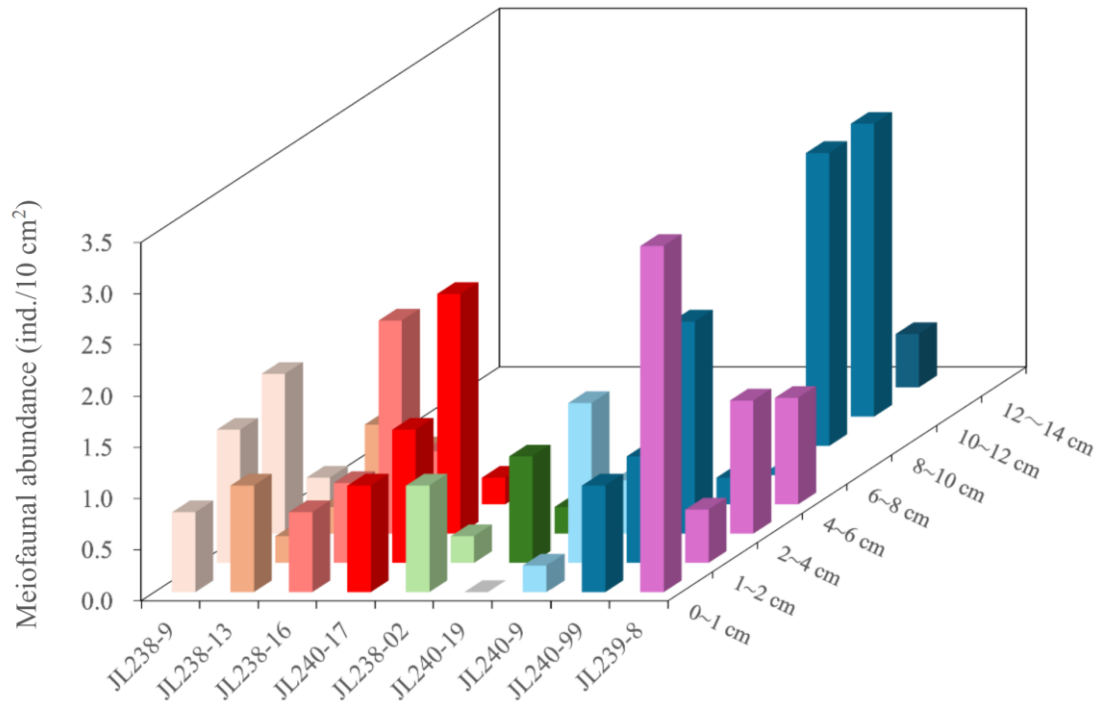
Figure 7-7 Abundance of meiofauna at different stations and depth layers

7.2.2 Plumes and Their Effects on Organisms

During test collector may intake large quantities of bottom sediments and nodules, as well as benthos and benthopelagic organisms living in and on the sediments, resulting in the death of some of the benthos and benthopelagic organisms. At the same time, the sediment is disturbed and spreads in all directions, especially downstream of the CTA, under the influence of the bottom current to form a sediment plume. Larger particles of sediment in the plume will quickly settle to the seafloor and cover the nodules, surface sediments and benthos in the spreading area. When it reaches a certain thickness, it will have a direct impact on the deep-sea benthos, burying and suffocating the organisms. The finer particles in the plume have a slower sedimentation rate and will remain in the water layer for a longer period of time and continue to spread under the influence of bottom currents, with redeposition occurring over a larger area of the seafloor, which can also have a chronic effect if the organisms in the spreading zones of these plumes are disturbed by low levels of sedimentation over a long period of time (Sharma, 2019).

There are several possible biological impacts of the plume:

(1) Burial/Asphyxiation Effects

During collection tests, the mobile organisms can move away from the plume dispersal zone to avoid such effects. These effects may occur for benthic fauna, such as sponges and corals, which are sessile or less motile in close proximity to the source of the disturbance.

Within the framework of the MIDAS (Managing the Impacts of Deep-Sea Resource Extraction) and Mining Impact 1 projects, the responses of deep-water corals and sponges exposed to different types of particulate matter were tested and observed: (a) *Lophelia pertusa* had a higher survival rate and less sublethal effects (Larsson et al., 2013); (b) *Dentomuricea meteor* showed reduced metabolic rate, deterioration of tissue condition, tissue necrosis and death; and (c) *Geodia baretti* increased their tolerance to the Plume through reduced metabolic activity (Kutti et al., 2015).

The test scale of this project is small, the collector will disturb about 6 cm of surface sediment, and the sediment produced by the disturbance is about 29,400 tons. According to the model prediction, the area in the plume diffusion zone with 1 cm thickness of redeposition is 0.278~0.298 km^2, i.e., basically all in the CTA (see Table 6-5 and Figure 6-13). That is to say, the area of redeposited area up to 1 cm thickness in the plume diffusion outside the test area is only 0.028 to 0.048 km^2. The results of the field mortality experiment conducted by the U.S. Underwater Remote Control in 1987 at a depth of 1,250 m in the Santa Gadelina Basin showed that a 1 cm thick sediment cover would not have a serious effect on macrofauna (Kukert et al., 1988).

(2) This experiment discharged tailwater near the bottom (at a height of 4 m above the bottom) such that a sediment plume was generated in the near-bottom water layer at a height of about 100 m above the seabed. Organic matter in deep-sea sediments is typically nearly two orders of magnitude lower than the organic matter content of particulate matter that settles to the seafloor in the upper layers (Kim, 2014; Jones, 2021), so it is unlikely that re-suspended solid would provide an additional food source for benthic organisms to have an impact, but rather that high concentrations of SS could clog gills or other filtration organs, impairing respiration and feeding ability (Anderson & Mackas, 1986). If affected for long periods of time, their growth and development may be affected.

(3) Passive ingestion of low-nutrient particulate matter by organisms will result in increased energy expenditure for feeding and may lead to starvation and reduced growth due to food scarcity, through trophic cascade effect, which affects organisms at higher trophic levels.

(4) Olfaction may be the primary mechanism that attracts and directs demersal scavengers to food. Sediment plumes generated by mining activities can interfere with odors released by food, reducing the probability to find food and leading to a general reduction in food availability for scavengers (Sainte-Marie, 1992).

(5) Many deep-sea creatures are bioluminescent. Bioluminescence can be used for communication to find mates (Widder et al. 2005). Enhanced turbidity in sediment plumes can reduce light transmission and therefore may obviously reduce the visibility of bioluminescence, thereby reducing the likelihood of finding mates and resulting in reduced reproductive rates.

7.2.3 Effect of Light

Light pollution is defined as the introduction of light into an environment where there is no natural (i.e., sunlight) source of light. Light pollution may have an impact on the surface environment, as light from vessels can attract insects, birds, fish, sharks, cephalopods and other invertebrates, as well as marine mammals (DNV.GL, 2016).

Currently, known and potential impacts of light pollution from artificial light sources on marine ecosystems include: (a) inhibiting or altering vertical migration of zooplankton; (b) attracting seabirds to collide with brightly lit vessels or offshore engineering platforms; (c) extending the reliance of birds on visual foraging behavior from normal daytime to nighttime hours; (d) impeding and altering the colonization of the larvae of a number of invertebrates; (e) triggering aggregations of fish resulting in increased predation; (f) causing disruption of reproductive behavior of corals, etc., which is controlled by moon phases; (g) interfering with the navigation of adult sea turtles, thereby affecting their reproduction, and interfering the navigation of sea turtle hatchlings, thereby affecting their survival (Davies et al. 2014).

Many deep-sea organisms are partially or completely devoid of eyes or light-sensing organs, but many fish and invertebrates can sense very weak bioluminescence. Bioluminescence occurs from bacteria to fish. Some fish chase bright lights, some escape them, and some do not respond to them. This undoubtedly increases the danger of seabed operations.

Polymetallic nodule collectors are equipped with light sources to illuminate the seafloor along the mining path in order to control operations using underwater television for risk avoidance. At the same time, remotely operated vehicles (ROVs), autonomous underwater vehicles (AUVs), Landers and monitoring nodes used for

survey, monitoring and maintenance also emit bright light depending on the monitoring requirements.

In this case, the ecological function of bioluminescence would be locally disrupted, and artificial light sources much stronger than bioluminescence could injure the eyes of some nearby organisms. Herring et al. (1998) found that the retinas of some deep-sea shrimps living in hydrothermal vents (e.g., *Rimicaris exoculata* and *Mirocaris (Chorocaris) fortuate)* were permanently damaged when illuminated by flash lights carried on board a manned submersible. Lights from ships operating at sea at night may also cause birds, especially young ones, to become disoriented or even fall out of the air, and these effects have not yet been adequately addressed.

Studies on the effects of two types of artificial light sources, LED lights and halogen lights, on the behavior of Amphipods have shown that both types of light sources attract Amphipod aggregations, and that the effects of LED lights are more dramatic (Navarro-Barranco and Hughes 2015). However, in deep-sea environments at depths of thousands of meters, there is currently no scientific evidence to confirm that anthropogenic light pollution causes direct adverse effects at the community or ecosystem level. And, in relation to this, an additional piece of evidence is that flash lights did not cause any identifiable disturbance to the behavior of scavenger fish and crustaceans during benthic scavenger surveys using the Lander trapping system (surveys conducted in the CCZ, unpublished data).

Due to the short duration and small scale of this experiment, the effects of light on organisms were only near the test area and were temporary in nature.

7.2.4 Effect of Noise

Ocean noise is the sound that transmits and spreads in the ocean caused by human activities. Starting in the 1960s, along with the process of globalization, the development of science and technology, the use of international trade and shipping, ocean engineering, seismic exploration and sonar technology, various types of human activities have led to a gradual increase in ocean noise (Figures 7-8), which have collectively raised the background noise to a potentially threatening level.

First, ocean noise poses a threat to the survival and reproduction of marine animals. Marine mammals and other aquatic animals have evolved over millions of years, and sound plays a critical role in key activities of marine species. Many marine species rely on sound for communication, migration, mate-hunting, locating prey, and avoiding predators. For example, cetaceans (whales, dolphins, and porpoises) send and receive

complex sounds to communicate with each other, navigate through the water and search for food. Noise disturbance may cause temporary or permanent hearing loss, interfere with feeding, reproduction/spawning, and affect their ability to survive. Particularly for migratory species, ocean noise may interfere with migratory paths and disrupt seasonal migratory habits, leading to disorientation and failure of migratory movements. Some impulsive noises may directly cause the death of affected organisms due to excessive transient volume (https://www.fisheries.noaa.gov/national/science-data/ocean-noise).
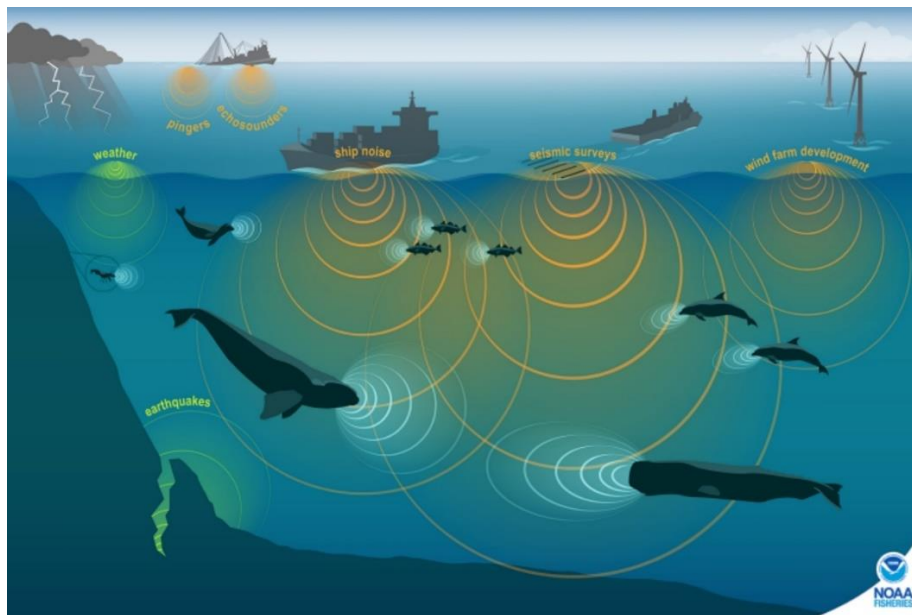
Figure 7-8 Marine animals live in noisy habitats with combined human, natural, and other species noise

(Quoted from NOAA Fisheries, https://www.fisheries.noaa.gov/national/science-data/ocean-noise)

Second, ocean noise can also impact the marine ecosystem as a whole. Fish and invertebrates also use sound to carry out essential life functions, so all levels of the ecosystem may be affected. Noise disturbances may affect the stability of the food chain, influence the predatory behavior of carnivores, and indirectly affect the structure of the benthic community. In addition, noise may cause some marine organisms to move away from their original habitats in search of quieter environments, thus profoundly altering the structure and function of localized ecosystems in some areas.

Ocean noise in the international seabed mining area arises mainly from surface ship navigation, marine resource exploration (seismic waves and sonar) and seabed mineral gathering systems.

7.2.4.1 Noise from Ships

(1) Impact on birds

Airborne noise generated by surface support vessels may prevent seabirds from locating mates or sharing foraging information by interfering with communication between seabirds (Dooling & Therrien, 2012). However, because the BPC contract area is thousands of kilometers away from the nearest major land mass, it is outside of the major migratory paths of migratory birds in the Northwest Pacific Ocean. Only the White-fronted Shearwater has a migrate branch that passes through the BPC contract area (Figures 7-9~Figure 7-12). The seabird species and abundance observed on the cruise paths from the East China Sea to the BPC contract area have been relatively low according to our on-site surveys since 2021, especially in the contract area, where seabirds have only been sporadically recorded. The BPC contract area is far from the main shipping lanes for commercial traffic thus is limitedly visited by vessels. Therefore, Project-related activities are not expected to obviously disrupt seabird mating or foraging behavior.
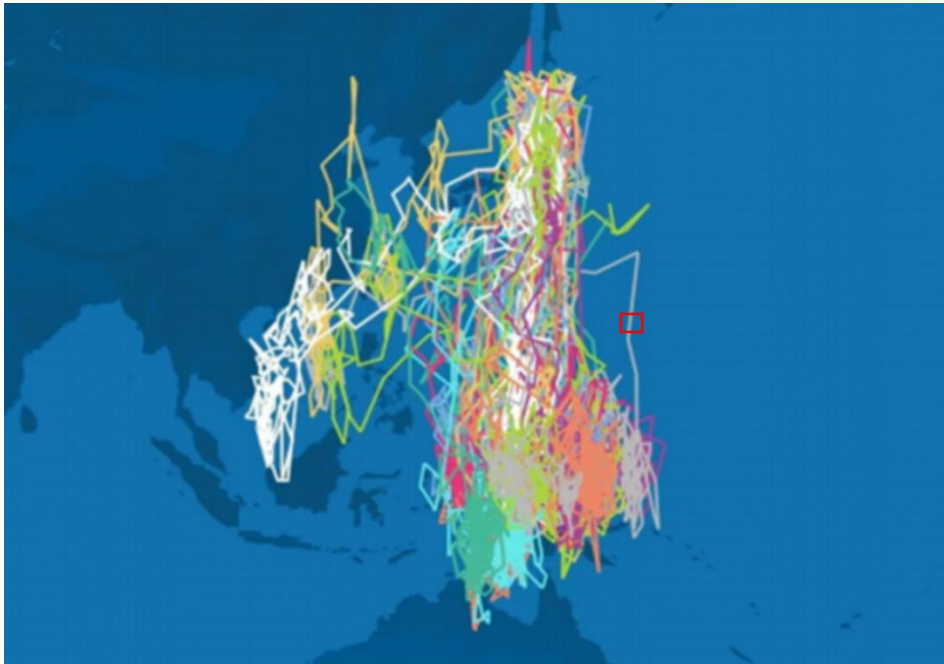
Figure 7-9 Migratory path of *Calonectris leucomelas* in the northwestern Pacific Ocean

(Data from seabird Tracking Database, red square boxes indicate BPC contract areas)

Figure 7-10 Black-footed albatross migration paths in the north Pacific Ocean

(Data from seabird Tracking Database, red square boxes indicate BPC contract areas)
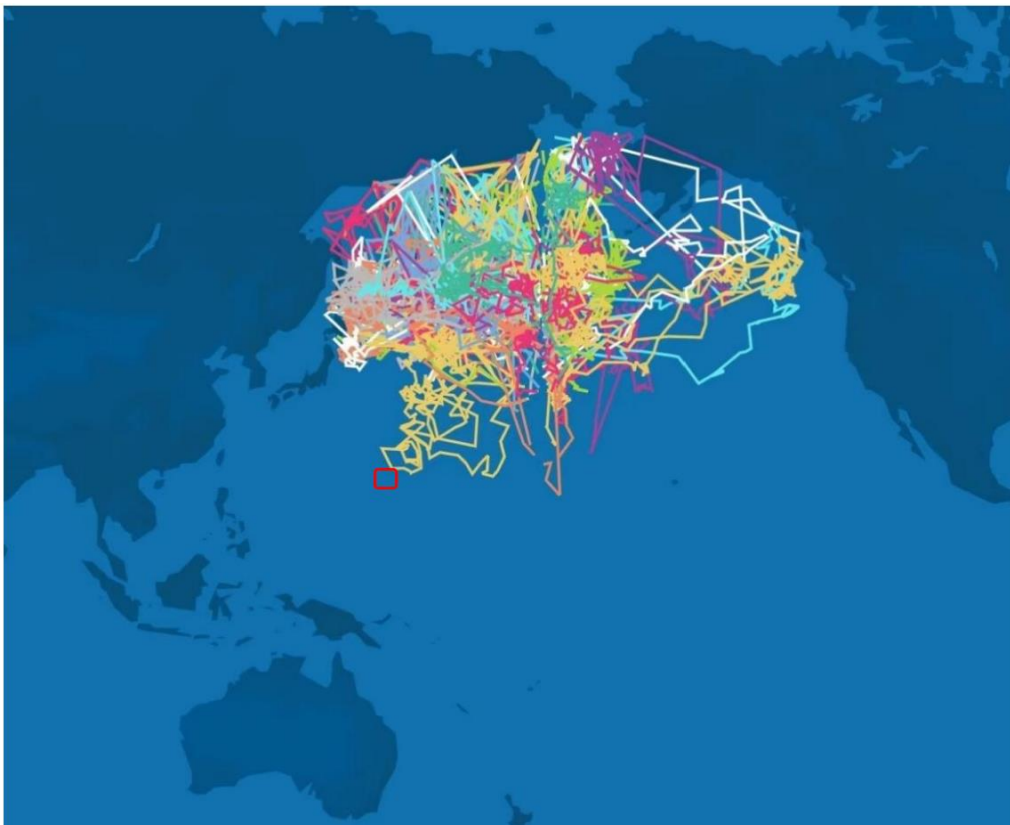
Figure 7-11 Black-backed albatross migration paths in the north Pacific Ocean

(Data from seabird Tracking Database, red square boxes indicate BPC contract areas)

Figure 7-12 Short-tailed albatross migration paths in the north Pacific Ocean

(Data from seabird Tracking Database, red square boxes indicate BPC contract areas)

(2) Impacts on whales and sea turtles

Six species of baleen whales, including *Megaptera novaeangliae*, *Balaenoptera physalus*, *Balaenoptera acutorostrata*, *Balaenoptera musculus*, *Balaenoptera borealis*, *Balaenoptera brydei* have been documented in the BPC contract area by hydrophones from October 2021 to October 2023, they occurred seasonally (Table 7-3), but they were not recorded from July to August.

Table 7-3 Months of occurrence for six species of baleen whales in the BPC contract area during 2021–2023

Species	Month of occurrence
Megapter a novaeangliae	1−5，9−12
Balaenoptera physalus	1−6，10−12
Balaenoptera acutorostrata	1−3
Balaenoptera musculus	1−2，5−6，12
Balaenoptera borealis	2−3
Balaenoptera brydei	1−5

This test is scheduled from July to August and is not expected to have an obvious impact on large cetaceans such as fin whales. Small and medium-sized cetaceans toothed whales have been recorded in some amount each season, with sperm whales

being one of the cetacean species with a high frequency of occurrence in the Contract Area, but the contract area is not a major distribution area for sperm whales nor is it located in their major migration paths, and the chances of occurrence are very low (Figure 7-13), and no obvious impacts on small and medium-sized cetaceans are expected.
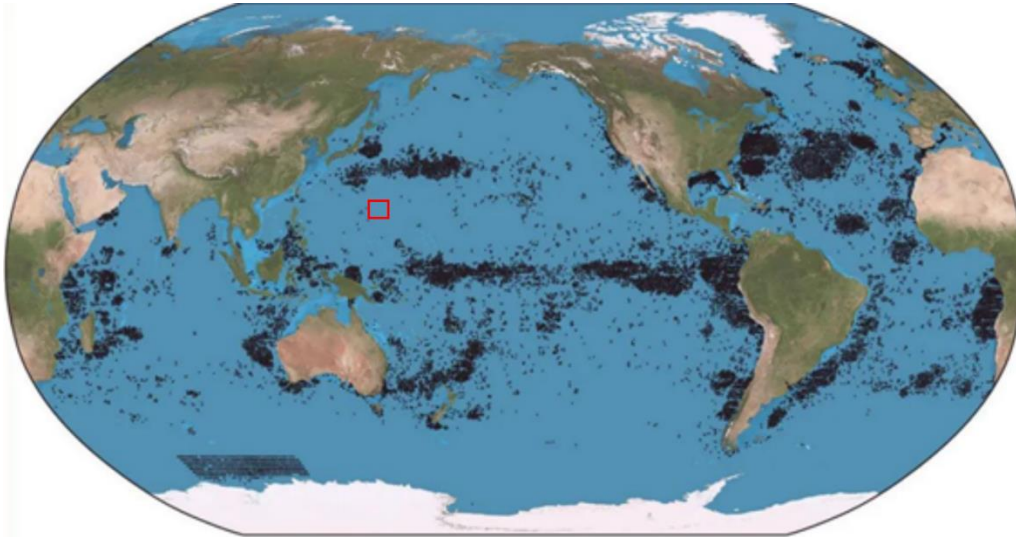
Figure 7-13 Global distribution of sperm whales (red box shows location of contract area)

This graph was created using GeoCart with data from

http://seamap.env.duke.edu/species/180488. by Kurzon. source: wikicommons, CC BY-SA 3.0

The Sea Turtle website (2024) indicates that sea turtles are predominantly found along the coast and in the EEZs of the SILs, with a migratory route in the vicinity of the BPC contract area (Figure 7-14), whereas no turtles were documented by BPC 's site surveys.

7.2.4.2 Noise from Marine Resource Exploration

Seismic Airgun Surveys are another major source of ocean noise. Such tools are commonly used to survey the seabed for oil and gas resources. However, this method of surveying can drive away *Balaenoptera physalus* and may result in mass mortalities of nekton within 1.2 km of the airgun.

BPC has never utilized such equipment during exploration for polymetallic nodule resources. However, a small number of seismic waves transmitted from a remote location were recorded during the environmental baseline survey of the polymetallic nodule contract area in 2022.
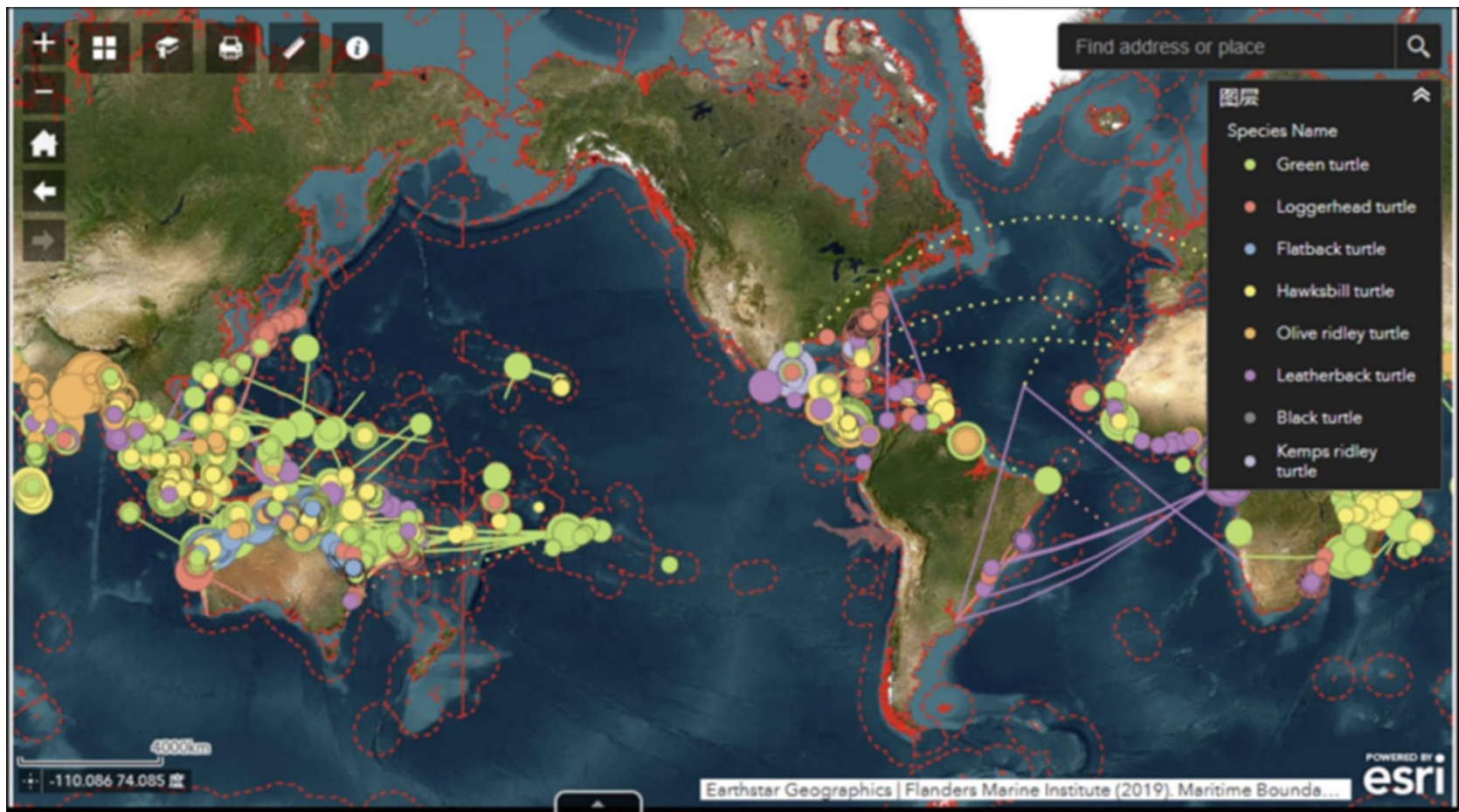
Figure 7-14 Sea Turtle nesting abundance and migration routes

(TurtleNet, accessed January 22, 2024) https://apps.information.qld.gov.au/TurtleDistribution)

7.2.4.3 Noise from Seafloor Collector

The operation of seafloor collector trucks inevitably generates a large amount of noise, which also has potential impacts on deep-sea bottom and water column organisms, but there are fewer studies in this area. Riccobene (2009) found that the background noise of deep-sea environments does not exceed 50 dB in the frequency range of 10–45 kHz, and does not exceed 60 dB in the even lower range of 2–10 kHz, which can be seen that most organisms live in low noise background environments. Groundfish typically communicate with low-frequency (<1.2 kHz) sounds (Rountree et al., 2012). Fish vocalize by a variety of mechanisms (Wahlberg, 2003), and in general, the percussive mechanism produces sounds with a predominant frequency of 1000 Hz or less (Wahlberg, 2003).

The friction articulation mechanism vocalizes at a dominant frequency of 3,000–5,000 Hz, and there is great variation in the duration, pulse interval, and other characteristics of these sounds, which may affect information exchange and produce species-specific responses. There is evidence that fish respond to mating calls, potential predator calls, prey calls, and sounds echoed back from other objects. Most fish can detect sounds below 800 Hz, and the predominant frequency of fish calls is below 1000 Hz. Studies of fish in some shallow water areas have found that noise can alter fish behavior and mask the communication sounds of these organisms, which can cause temporary or permanent hearing loss in fish (Nedelec et al., 2017, Gomez et al., 2016). Underwater sound transmission, especially in the lower frequency bands, can travel very far, and it is estimated that noise from mining systems can travel tens of kilometers and affect larger areas. Sound transmission is omnidirectional and can travel through the thermo-halocline to reach the surface layer, thus affecting not only deep-sea organisms but even the entire water column and surface organisms. The results of the baseline survey show that six species of baleen whales and no less than six species toothed whales are distributed in the BPC contract area and adjacent areas. The acoustic signals emitted by baleen whales are usually in the low-frequency range of 15 Hz–1000 Hz, mainly 20 Hz–250 Hz. Toothed whales, on the other hand, emit acoustic signals at relatively higher frequencies and in a wider frequency band, usually covering mid- and high-frequency components above 5 kHz (Figure 7-15).

Animals that utilize sound, whether actively or passively, for feeding, communication, navigation, etc., are affected in some way. In addition to directly harming sound sensors or misdirecting the behavior of marine organisms, anthropogenic noise may interfere with the natural application of sound, obscuring biological sound information or triggering false responses. Because there is no information on the generation and transmission of deep seabed mining noise and little is known about biological sound perception in the deep sea, deep-sea mining noise impacts are still difficult to predict.

Based on available information, existing noise threshold criteria are as follows (TMC 2022):

(1) Acoustic interference behavior threshold lower limit of 120 dB re 1μPa

The threshold for more subtle behavioral responses, such as an increase in the number of occurrences at the surface and a decrease in the number of dives, is not expected to be avoided. The application of the 120 dB re 1μParms threshold can sometimes cause problems because the threshold level may overlap with environmental background noise.
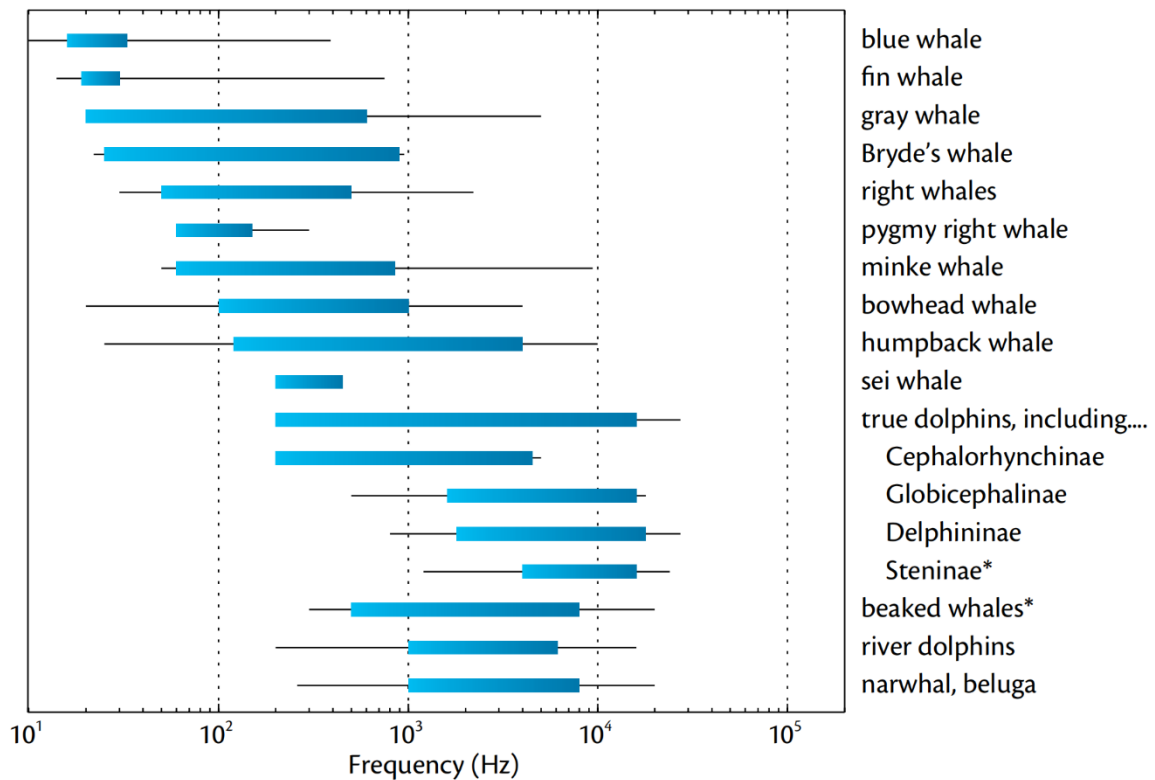
Figure 7-15 Distribution of cetacean vocalization frequencies （Mellinger et al., 2007）

(2) Acoustic interference behavior upper limit of 160 dB re 1μParms

Threshold for the onset of disruptive behavioral responses and obvious avoidance of nonimpulsive noise sources (NMFS, 2014).

(3) Threshold criteria for permanent and temporary hearing loss

Table 7-4 shows criteria for noise-induced permanent threshold shift (PTS) and noise-induced temporary threshold shift (TTS) thresholds for cetaceans with nonimpulsive sound based on information from NOAA (2016) and Finneran (2016).

Table 7-4 Threshold criteria for PTS and TTS for Non-Pulse sound in cetaceans

Cetacean functional hearing group (Southall et al., 2007)	Hearing range	Non-impulsive Sound Exposure Level (SEL$_{24-h}$) (dB re 1 µPa²·s)	
		PTS threshold	TTS threshold
Low-frequency (LF) cetaceans	7 Hz to 35 kHz	199	179
Mid-frequency (MF) cetaceans	150 Hz to 160 kHz	198	178
High-frequency (HF) cetaceans	227 Hz to 160 kHz	173	153

Source: NOAA (2016) and Finneran (2016). The SEL assumes that a cetacean would remain in the area for 24 hours, which is an unlikely scenario; therefore, threshold levels would be larger for shorter duration periods.

Threshold criteria for permanent PTS and TSS for cetacean impulse noise are given in Table 7-5.

Table 7-5 Threshold criteria for PTS and TSS for impulse noise in cetaceans

Hearing Group	NMFS (2014)	NMFS (2018)			
	Behaviour	PTS onset Thresholds*		TTS onset Thresholds*	
	SPL$_{rms}$	SEL$_{24h}$	SPL$_{pk}$	SEL	SPL$_{pk}$
	dB re 1 µPa	dB re 1 µPa²·s	dB re 1 µPa	dB re 1 µPa²·s	dB re 1 µPa
LF	160	183	219	168	213
MF		185	230	170	224
HF		155	202	140	196

Source: NMFS (2014, 2018). * Dual metric acoustic thresholds for impulsive sounds; whichever threshold results in the largest isopleth for calculating PTS onset is to be used. The threshold criteria are unweighted. LF, MF, and HF denotes low-frequency, mid-frequency and high-frequency cetacean functional hearing groups, respectively.

Since this collector test was conducted in July–August, when no mammals such as large cetaceans were present (Table 7-3), and no sea turtles were present in the test area (Figure 7-14), no permanent harm to aquatic organisms is expected.

At present, it is not possible to assess how much noise will be generated by the test and the extent of its impact, as BPC has not yet completed the construction of the MANTA II and has not yet obtained data on the underwater noise. However, according to field tests of the Blue Nodules company's mining vehicle prototype "Apollo II" (5.6 m x 2.5 m x 2.3 m) and the support vessel, underwater noise reached maximum levels at frequencies around 100 Hz and 1 kHz. Based on the concept of "research-oriented exploitation", in order to explore the impacts of collector noise on hydrobiota, multiple hydrophones were deployed to conduct noise monitoring during the test to accumulate data for the assessment of noise impacts from commercial mining. Due to the short duration of the test, no permanent harm to aquatic life is expected.

In addition, mining-induced sediment vibrations may also negatively affect benthic invertebrates (crustaceans and mollusks), causing behavioral and physiological changes and even physical damage.

7.2.5 Possible Release of Heavy Metal Toxicity

Mining plumes may release potentially toxic substances (e.g., heavy metals). Among these toxic substances may be taken up by predators and pose a toxicity risk to predators at higher trophic levels in the food chain, which may have impacts on ecosystem structure, ecological functioning, and ecosystem services as releases increase (Le et al, 2017).

Benthos have been experimentally shown to have avoidance responses, among other things, in environments with high heavy metal concentrations. For example, the freshwater clam *Corbicula fluminea* can close its bivalve shell in environments with high Cu concentrations and the time to respond decreases with increasing Cu concentrations, with the time to close the bivalve shell being 300 min and 30 min in environments with Cu concentrations of 5.6 and 19.5 μg L^{-1}, respectively (Jou et al., 2016). Brown et al. (2017a) observed that shallow sea cucumbers (*Holothuria forskali*) avoided being affected by sediment contaminated with a concentration of 5 mg L-1 Cu by climbing up the side of the experimental tank during a 96 h laboratory toxicology experiment at 4°C. Similar avoidance behavior was also observed in deep-sea sea cucumbers (*Amperima* sp.) in an *in situ* Cu-contaminated sediment exposure experiment conducted by Brown et al. in the Peru Basin at a depth of 4167 m (Brown et al., 2017a). Kwan et al. (2019) conducted an in-situ Cu exposure experiment in the polymetallic nodule zone of the South China Sea on the effects of scavenging amphipod in the deep-sea, using chicken meat as bait, and different concentrations (25, 50, and 100 μg/g) of CuCl$_2$ solution were added overnight at 4 °C to create a pollutant concentration gradient for the experiment. The experiments showed differences in protein expression of a common deep-sea amphipod (*Abyssorchomene distinctus*) under different copper ion concentration conditions. A total of 2,937 proteins were identified and annotated, and the proteins were screened based on differences in protein expression. Among the differentially expressed proteins, the abundance of some proteins (chitin synthesizing and metabolizing proteins, Na+/Ka+ ATPase, etc.) correlated with copper concentration, indicating that these proteins are highly sensitive to copper concentration (Kwan et al., 2019).

However, predicting the toxicity of heavy metals released from deep-sea mining is a great challenge (Hauton, 2017), and in the EU MIDAS project, where considerable research effort has been invested in assessing the lethal and sublethal susceptibility of different megafauna (shallow-water) species to the toxicity of a single metal such as copper, as well as to different combinations of metals and potential by-products of mining, it was found that the interactions are extremely complex and species-dependent (MIDAS, 2016). Firstly, the results of toxicological experiments on heavy metals in shallow water species conducted in the laboratory and offshore are not representative of the toxicity of heavy metals to deep-sea organisms, which may be biochemically and

physiologically different and will be subjected to these effects at low temperatures, high hydrostatic pressures, and potentially altered pH. Brown et al.'s (2017b) experiments showed that, for 96 h at low temperatures, the toxicity of both copper and cadmium was obviously reduced, but the effects of high hydrostatic pressure were more complex, with copper toxicity increasing obviously at high hydrostatic pressure but cadmium toxicity remaining unchanged. Similar results were found in an acute copper toxicity study of the experimental model organism *Halomonhystera disjuncta* (Mevenkamp et al., 2017), a close relative of the deep-sea nematode *Halomonhystera hermesi* that inhabits shallow-water mud volcanoes (Van Campenhout et al., 2014). In its isolated erythrocyte GD1, low temperatures (10 °C) reduced copper toxicity, while toxicity increased when the nematode was exposed to high hydrostatic pressure (10 MPa) (Mevenkamp et al., 2017). Secondly, the heavy metal concentrations used for the experiments are relatively high, but in the extensive oxidized environment that exists at the bottom of the deep-sea polymetallic nodule zone, it is unlikely that simple mechanical perturbations cause changes in the nature of the oxidized minerals that would result in large-scale heavy metal releases (BGR 2018), and the release of trace metals from nodule fragments into seawater is not obvious (Benjamin et al. 1981). Furthermore, Paul et al. (2021) showed that processes like deep-sea mining are unlikely to result in the release of toxic Cu^{2+} into seawater because > 99% of the Cu is organically complexed in pore water. Thirdly, the metal used in most current experiments is copper, and it is not actually copper that is the heavy metal that may be released in the polymetallic nodule zone. Simulated disturbance experiments on sediments from the BPC nodule contract area in the western Pacific Ocean have shown that there is obvious elemental specificity in the release of heavy metals (Shi et al., 2023), with only four heavy metals, vanadium, rubidium, molybdenum and cadmium, showing obvious and stable precipitation behaviors (Figure 7-16), and similar results have been found in studies by others (Koschinsky et al., 2001).

However, in the case of nekton such as fish, which are at the top of the marine food chain, there may be concern that toxic substances such as heavy metals from nodule debris, which are digested and absorbed by filter-feeding zooplankton, will gradually accumulate in organisms at higher trophic levels, such as fish, as they are passed along the food chain. However, studies have shown that the likelihood of zooplankton accumulating trace metals is low. On the one hand, the bioavailability of trace metals in nodule debris is low; on the other hand, these debris settle quickly, typically only in a few days, and once these zooplankton are not subjected to the effects of the tailings plume, these trace metals can be excreted from the body through normal biological processes (U.S. Department of Commerce, 1981). Heavy metal enrichment in animals at high trophic levels can only occur in closed ecosystems with short food chains. This is unlikely to occur in the open ocean, where most of the metals

accumulated in organisms at lower trophic levels of the food chain can be diluted in the complex food webs and open ecosystems of the ocean (Ellis, 1987).
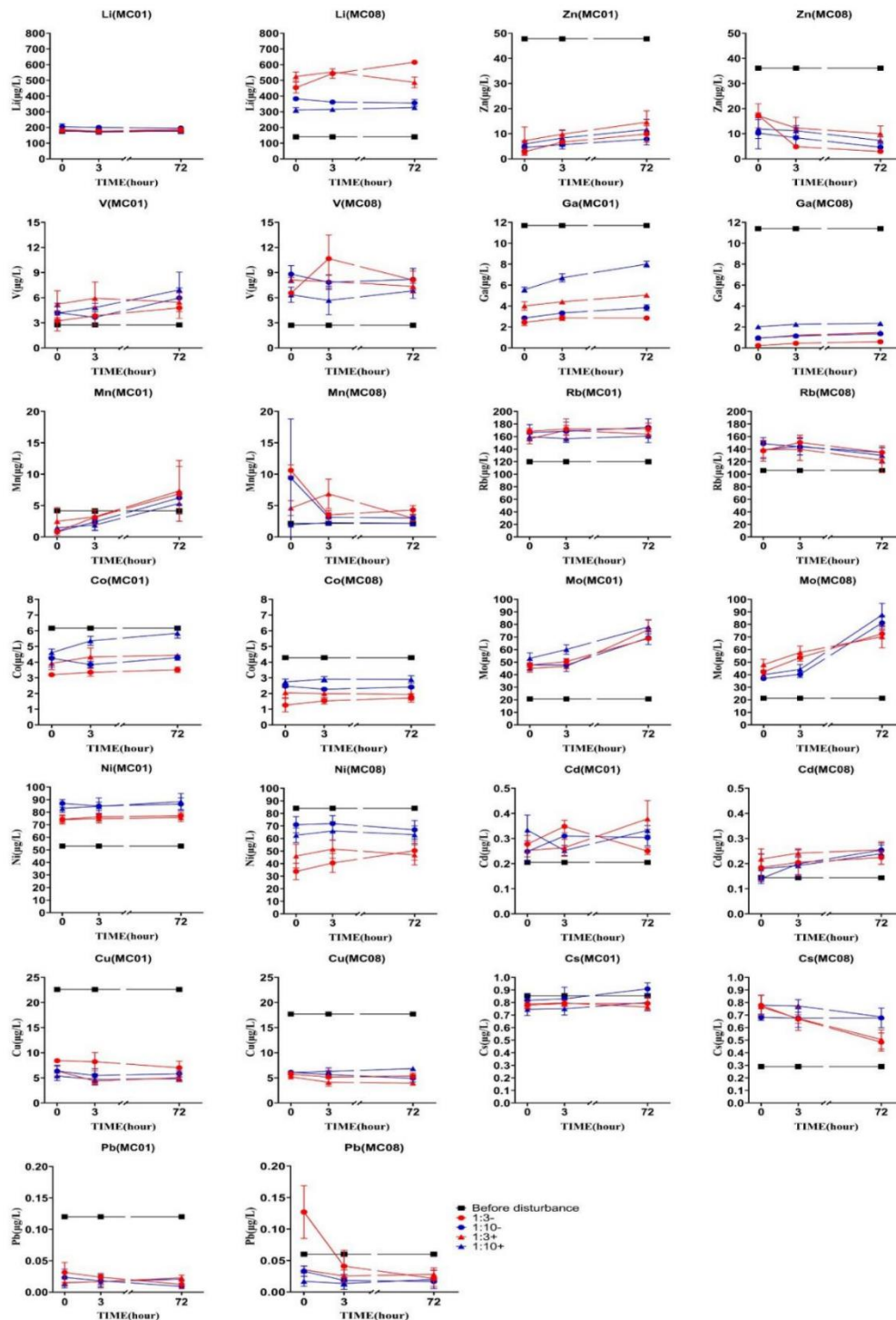
Figure 7-16 Results of the simulation test for the release of heavy metals from disturbed sediments in the nodule field (Shi et al. 2023).

In summary, the obvious shortcomings of the current toxicity tests on heavy metals are mainly reflected in the following 2 aspects: (1) most of the experiments have utilized a single metal rather than a combination of metals; and (2) the tests are mainly based on shallow-water species. Therefore, more research work is needed to determine

heavy metal concentration thresholds in the current toxicological risk assessment of potential polymetallic nodule mining.

7.2.6 Warming Effect

Mineral mining processes and transportation may release large amounts of heat, which can cause warming of seawater. There are not many studies in this field. Steiner (2009) estimated that these processes could lead to an increase in surrounding seawater temperatures of up to 11 °C when polymetallic sulphides are commercially mined. Nautilus has assessed that the sulphide mining process could lead to an increase in water temperatures of between 5.8 and 11.4 °C (Nautilus Minerals, 2008), but no warming due to polymetallic nodule mining has been reported. In the case of the present test, any thermal stresses generated by the plume during the collector test event were negligible owing to the small scale of the test. The location of the discharge was moving and the high degree of mixing and dilution of the discharge water with the surrounding seawater presumably did not cause localized warming.

However, the extent to which warming during commercial mining will affect the growth, reproduction, metabolism, and other processes of organisms in the mining area is unclear and requires further study.

7.2.7 Anaerobic Effect

In some basins such as the Peru Basin, where the depth of oxygenated sediments is shallow (Paul et al., 2018), nodule mining operations are likely to roll up hypoxic sediments resulting in lower ambient oxygen levels. However, the deeper marine sediments in the BPC mining area, as well as the near-bottom water layer, are highly oxygenated ($\sim$350 μmol/dm^3), and the increase in oxygen demand due to the release of anoxic sediments into the water column or microorganism decomposition of dead benthic fauna in the path of the mining is likely to have a negligible effect on dissolved oxygen concentrations (Christiansen et al., 2020).

Depletion of dissolved oxygen in the Near Bottom Layer water column may also result from depletion of active organic carbon in the plume by biological activity and further oxidation of metal ions (GSR, 2018). As the test area of this project is located in the oligotrophic zone of the Northwest Pacific Ocean, the organic carbon content of surface sediments is extremely low, and a large amount of total organic carbon in deep-sea sediments is inert organic carbon (Arndt et al., 2013), and considering the small total disturbance scale of this test and the mobility of bottom seawater, we expect that the change in bottom DO will be very slight, and the resultant ecological effect will not be obvious.

7.2.8 Biological Resilience

The impacts of deep-sea mining activities on deep-sea organisms vary depending on the scale and intensity of the mining activity. The potential for species to recover after disturbance also varies depending on the extent of their habitat destruction (Van Dover, 2011). Slow-growing deep-sea organisms are usually correspondingly less resilient to change (Rodrigues et al., 2001; Gollner et al., 2017). Recovery of benthic communities in the nodule area is difficult to estimate because colonization rates for most species are unknown, and there is a serious lack of research on population size, developmental biology characteristics, dispersal, and species connectivity (Hilário et al., 2015). In the absence of commercial operations, biological recovery studies rely on studies of the consequences of natural extinction events such as volcanic eruptions or simulated disturbance experiments, but at different spatial and temporal scales than commercial mining.

Long-term environmental monitoring of small-scale simulated mining tests was carried out in various countries from the 1970s onwards, and the results showed that the structure of biological communities was indeed obviously altered, with different impacts on different species, and that the abundance and diversity of some taxa recovered or even exceeded the pre-disturbance levels after disturbance, while many others did not recover after several centuries. Jones et al. used Meta analysis method to count the results of long-term environmental monitoring in 11 nodule test areas, and found that even in the face of small-scale simulated mining disturbances, most taxa organisms were difficult to recover to baseline levels of the undisturbed environment (Figure 7-17), and were still not fully recovered after 26 years (Jones et al., 2017).
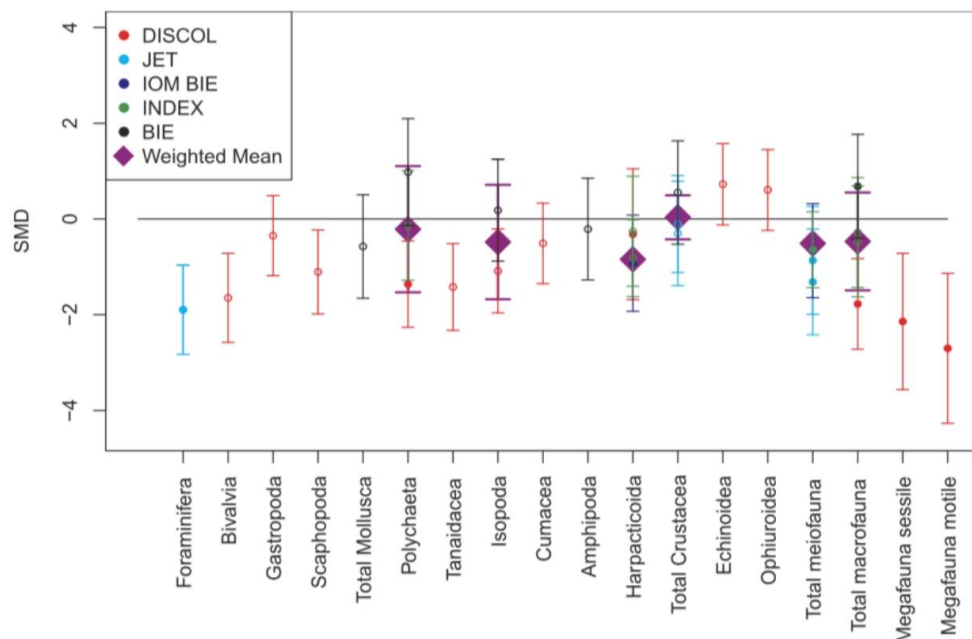
Figure 7-17 Long-term effects of mining activities on the abundance of different taxa (Jones et al., 2017)

For the resilience of benthic communities after anthropogenic disturbances, DISCOL observations showed that after 26 years of recovery, the present amount of biogenic carbon and food web activity in the disturbed area remained half as low as those outside the disturbed area (Stratmann et al., 2018), and filter feeders recovered obviously slower than organisms of other feeding strategies. A study of swimming organisms showed that the distributional abundance of the *Ipnops meadi* in the DISCOL disturbance test area was only 1/3 of that outside the disturbed area after 26 years, suggesting that the disturbance test has been consistently affecting the area. However, because most macrofauna and megafauna in the polymetallic nodule area are more widely distributed in the ocean (Foell et al., 1992), it is unlikely that localized seafloor mining will result in the complete extinction of a species from the ocean.

Overall, nodule collection will disturb the benthic habitat in the mining area, resulting in the loss of faunal habitat in both nodules and sediments. Disturbance of soft sediments (through extrusion or interstitial water discharge) may alter sediment biogeochemistry and structure. At least in the short- to medium-term, to some extent these sediments will be 'lost' to post-mining restoration as habitat (Simon-Lledó et al., 2019, Jones et al., 2017, GSR, 2018, BGR, 2018). Long-term studies have shown that the abundance of benthic and nodule-attached sessile animals (e.g., sponges), filter feeders, and mobile fauna (e.g., ophiuroids and crustaceans) on nodule hard substrates in the affected areas has declined obviously for at least several decades after nodule collection occurred (Vanreusel et al., 2016, Simon-Lledó et al., 2019, Jones et al., 2017). Few animal taxa have recovered to baseline levels or control condition levels after (at least) 20 years. Overall, despite some potential for recovery, the environmental impacts of polymetallic nodule mining are likely to be long-term (Jones et al., 2017; BGR, 2018; SPC, 2013). However, in the case of this test, due to the short duration (5d continuous working time) and small area of disturbance (0.25 km^2), no widespread impacts are expected and it is unlikely to lead to the extinction of some species in the area.

7.3 Impacts on Fishery Resources

Figure 5-121 shows that the BPC contract area is not a major fishery in the Pacific Ocean, and that the main type of fishery operation in the waters of the contract area is longline. According to the BPC survey in 2021–2023, no fishing vessels have been observed in the area. In this test, we will also strictly abide by the *Convention on the Conservation and Management of Highly Migratory Fish Stocks in the Western and Central Pacific* and *International Convention for the High seas Fisheries of the North Pacific Ocean, as amended*. Therefore, no adverse effects on fishing operations and fishery resources are expected during this test period.

7.4 Cumulative Impacts

Since this test is only a single activity, it is not expected that cumulative impacts from multiple operations will occur. Cumulative impacts from different pressures from a single activity can be expected, but at this stage, there is limited publicly available information on the cause-effect activity-pressure-effect relationships for the target ecosystems and their components (i.e., populations and communities, habitats, and ecosystem functions) and the cumulative pressures that mining activities may exert on ecosystems and their components (Tamis et al., 2016). In particular in the abyssal Northwest Pacific, more data are needed to quantify the impacts of mining activities and to identify specific pressures and their cumulative impacts on ecosystem vulnerability and resilience. Figure 7-18 illustrates the potential relationships between activities and pressures on different ecosystem components.

Although some studies have documented the individual impacts of different mining pressures on species and ecosystems (Auguste et al., 2016; Mevenkamp et al., 2017), there is still a complete lack of studies on the cumulative and interactive effects of multiple stressors from deep-sea nodule mining. One of the main objectives of the monitoring study presented here is to summarize and statistically analyze the possible scale and scope of cumulative impacts using the results of different individual impact studies before and after the "Manta II" experiment.
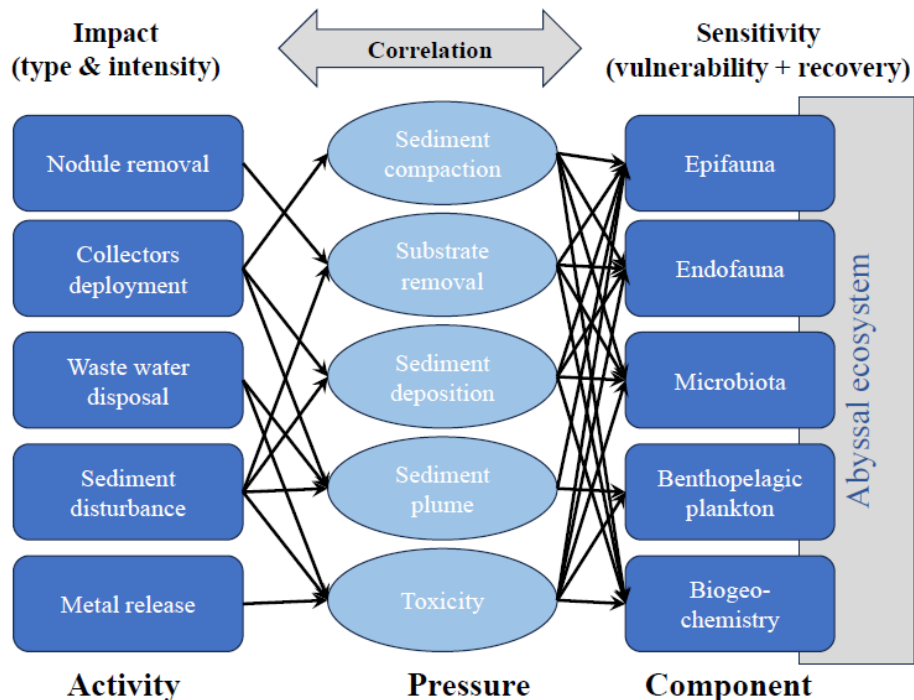
Figure 7-18 A general model for assessing the potential future cumulative effects of mining on the relationship between visual activity, stress and ecosystem components (based on GSR 2018 and Tamis et al. 2016).

7.5 Mitigation Measure

BPC will conduct this test with reference to the relevant environmental standards being prepared by the ISA and the principles of protection and preservation set out in the *Guidelines for Environmental Protection and Preservation in Deep Sea Mining Activities* (T/CAOE 41-2021) by adopting a precautionary approach, utilizing Best Available Techniques (BAT), and Good Environmental Practices (GEP), in order to avoid and Vendeuse mitigate the impacts of this test mining activity. Mitigation measures include avoidance/prevention measures, impact minimization measures, rehabilitation/restoration measures and compensation measures (see Tables 7-1 and Table 7-6).

During the operation of surface support vessels, specialized personnel will be equipped to monitor the activities of large mammals such as sea turtles and whales around the vessels and take active collision avoidance measures to avoid causing damage to these animals. During night operation, ship lighting will be reduced as much as possible under the premise of safeguarding operational safety, and upward irradiation of light will be avoided to reduce the impact on the activities of birds. In addition, BPC will strictly follow the Regulations on the Administration of Prevention and Control of Marine Pollution from Ships and the relevant provisions of the International Maritime Organization to ensure that pollutants such as garbage, domestic sewage, oily sewage, sewage containing poisonous and hazardous substances, and exhaust gases from ships during the event comply with the requirements of laws, administrative regulations, international treaties concluded by the People's Republic of China or to which it has acceded, as well as the relevant standards.

According to the environmental guideline ISBA/25/LTC/6/Rev.3 issued by the International Seabed Authority, BPC will carry out environmental monitoring during test activities, and will use multibeam, ROV, AUV, multi-tube, box, current meter, CTD, turbidimeter, deep-sea camera and other equipment to carry out investigations and monitoring. These activities fall under the list of activities listed in the guideline in Article 32 that will not cause serious environmental damage to the environment and do not require an environmental impact assessment.

During the test period, BPC will monitor environmental indicators in real time through the monitoring equipment carried by the mining truck itself, AUVs, and monitoring master stations and monitoring base stations deployed around the test area. Based on the results of tracking monitoring and follow-up evaluation, activities with actual impacts greater than the predicted impacts will be immediately stopped on-site and reported to the competent authorities.

Table 7-6 Impact levels and mitigation measures for proposed activities

Activity	Location of impact	Type of impact	Degree of impact	Mitigation measure
Surface Support Vessel Operations	Atmosphere, sea surface, water bodies	Tailpipe emissions, noise, light, temperature and drainage, oil, garbage (plastic, metal, glass, chemicals), human excreta	Few	Avoidance/prevention measures and impact minimization measures with reference to SOLAS and MARPOL guidelines
Research vessel data acquisition (radio communication and echo sounding)	Atmosphere, sea surface	Detection waves transmit through water and air with impacts on humans and marine life	Few	Referring to the SOLAS Guidelines (Chapter 4), impact minimization measures
Environmental Sample Collection	Water column, seabed	Mechanical disruption, chemical reactions, collection of biological samples, alteration of seafloor microtopography	Few	Impact minimization measures with reference to ISA environmental guidelines and MARPOL conventions
Underwater operation of mining trucks	Seafloor	Alteration of seafloor microgeomorphology, mechanical damage, changes in biological species diversity and abundance, plume dispersion and resedimentation	Small to medium	Minimum sediment disturbance, minimum working time, minimum area to be disturbed, avoidance of leaks or spills, impact minimization measures and conduct of remediation tests, e.g., artificial nodule deployment measures.

8 ACCIDENTS AND NATURAL DISASTERS

8.1 Extreme Weather and Natural Disasters

8.1.1 Natural Disasters

（1）Risk Analysis

The main natural environment risks in the CTA are adverse weather factors such as typhoons, storm surges, and cold waves, which can obviously, or even prohibitively, impact marine operations of the project.

The North Pacific, where the CTA is located, has two permanent atmospheric activity centers: the Aleutian Low and the North Pacific Subtropical High. In January, the North Pacific is under the control of the deep and strong Aleutian Low, while in July, it is entirely influenced by the North Pacific Subtropical High. During winter, the Eurasian continent is controlled by the strong Siberian High, with frequent cold air activity. Low pressure rapidly deepens over the sea, reaching its strongest near the Aleutian Islands. At this time, the North Pacific Subtropical High is located in the southeastern part of the ocean, weak and small in scope. After March, the Aleutian Low begins to weaken and contract to the northeast, while the North Pacific Subtropical High continuously strengthens and extends westward and northward. By around July, the Aleutian Low has weakened to its minimum and moved northward, while the North Pacific Subtropical High becomes the strongest. The high pressure connects with the Siberian High through a ridge extending along 25°N, so the tropical ocean surface south of 25°N is under the influence of the southern edge of the high pressure all year round, with prevailing northeast monsoons.

According to the effective wave height seasonality for global wind and swell waves in 2010 (Figure 8-1), near the survey area in the western Pacific, the effective wave height over the northeast Pacific gradually increases from autumn (September to November) and expands southwestward. It reaches its strongest in winter (December to February), with an average effective wave height between 2.60 and 3.60 m, and then gradually weakens. In summer (June to August), the average effective wave height in the survey area remains at a lower level, between 1 and 1.6 m. From the seasonal average distribution of sea surface 10 m wind speed and direction (Figure 8-2), it can be seen that the wind speed in the CTA reaches its maximum in winter, then gradually decreases, reaching its minimum in summer, and then gradually increases again.

Tropical storm path statistics (1949–2022) show (Figure 8-3) that there are relatively few tropical storms passing through the working area. Among the four contract areas of BPC, the southern contract areas (M1 and M2 blocks) experience fewer tropical storms than the northern areas (C1 and C2 blocks).
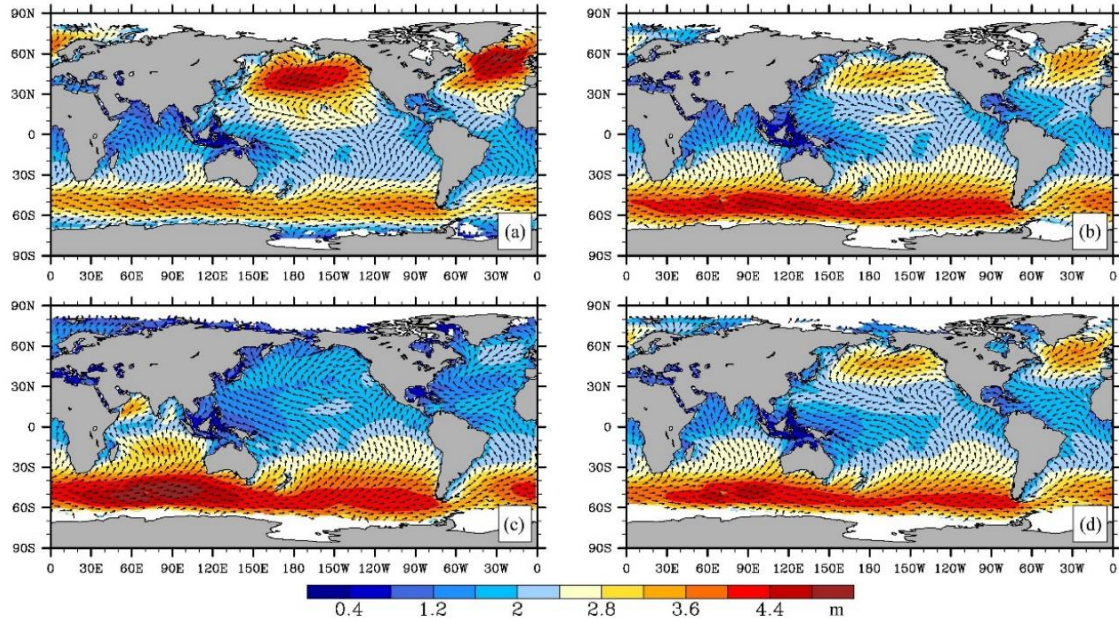
Figure 8-1 The average effective wave height Hs (m) and wave direction θ distribution of the global mixed wave during (a) Winter, (b) Spring, (c) Summer, (d) Autumn (Zhuang et al. 2014)
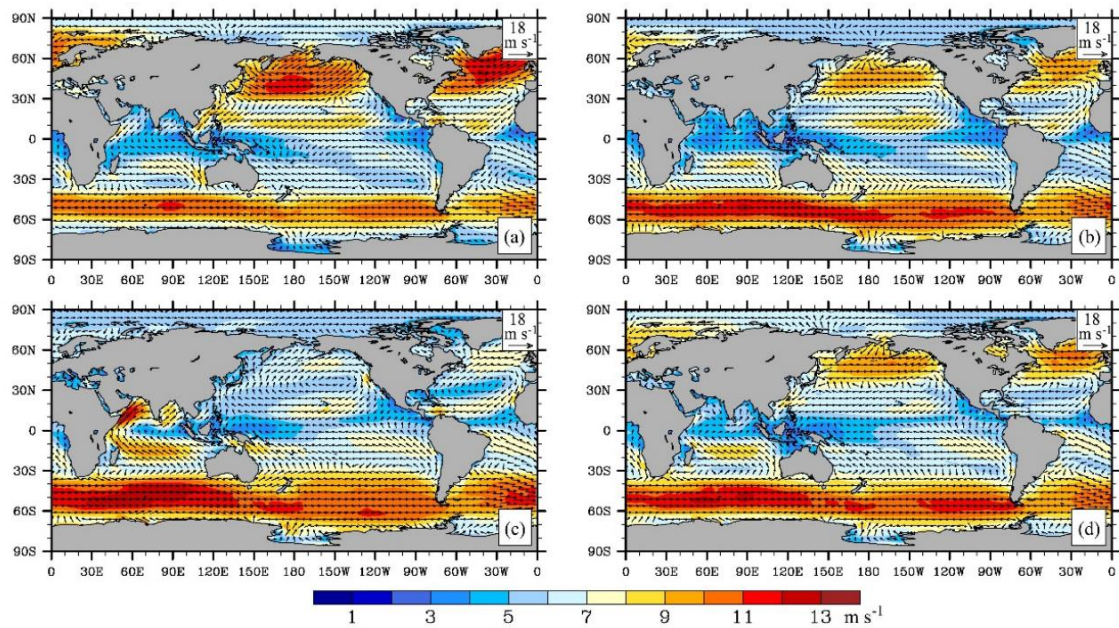
Figure 8-2 30-year average global sea surface 10 m wind speed U_{10} (m s^{-1}) and wind direction φ distribution

(Zhuang et al. 2014, where the shaded areas represent the magnitude of sea surface 10 m wind speed values, the length of the arrows represents the magnitude of the sea surface 10 m wind speed at that location, and the direction of the arrows represents the sea surface 10 m wind direction at that location)
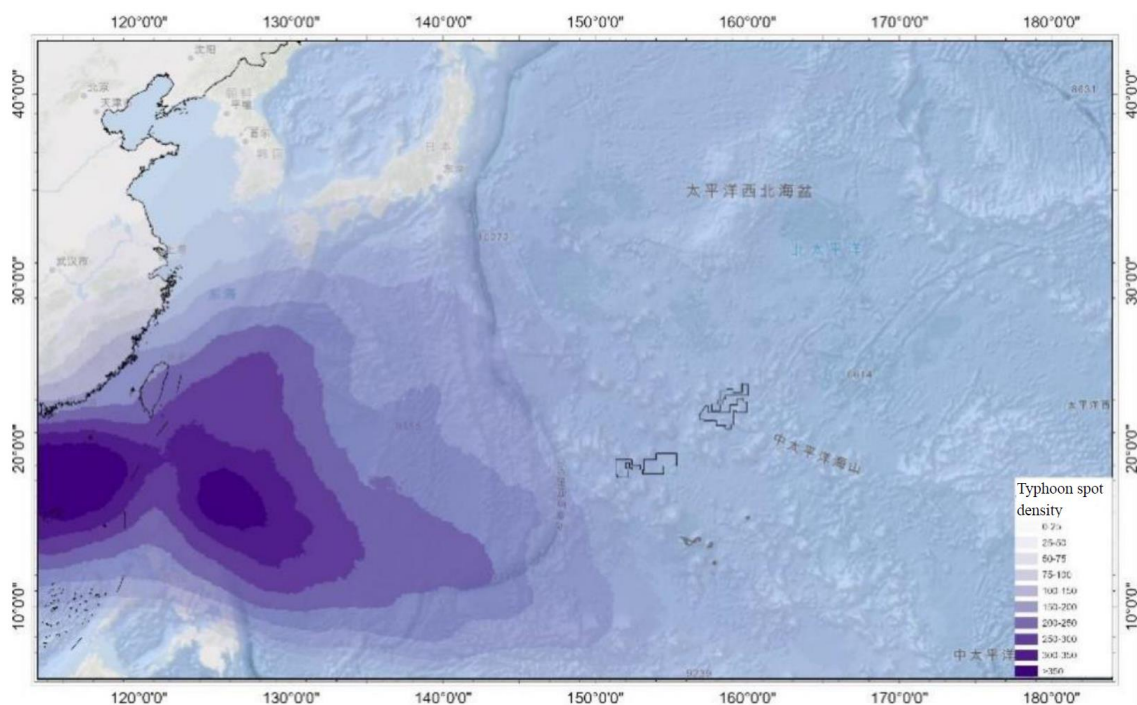
Figure 8-3 Northwest Pacific tropical storm path density distribution map (1949–2022, data source: China Meteorological Administration Tropical Cyclone Data Center)
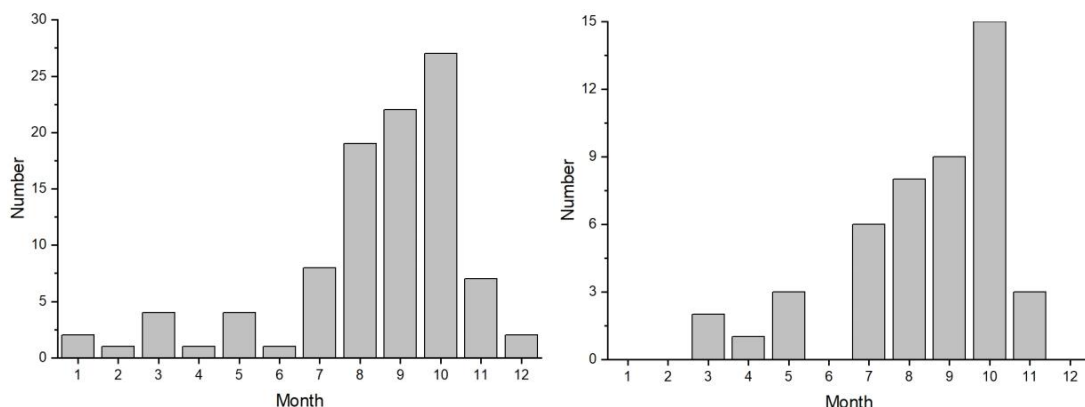
Figure 8-4 BPC polymetallic nodule mining area Block M2 tropical storm (left) and typhoon (right) monthly distribution map (1949–2022, data source: China Meteorological Administration Tropical Cyclone Data Center)

（2）Preventive Measures

a. Conduct meteorological forecasting work and reasonably schedule the test project. Based on historical data analysis of waves, wind speed, and typhoons (Figure 8-4), it is recommended to choose June and July as the best.

b. Within 24 hours of the start of the influence of the storm surge, immediately prepare for the evacuation of personnel, organize the evacuation, and complete the evacuation 12 hours before the start of the influence.

c. Collect on-site information, adjust action plans promptly, and organize the implementation of action plans.

d. Monitor the implementation process of emergency actions by the units in the CTA, and track the development of the situation to prepare for resuming work.

（3）Emergency Response Plan for Extreme Weather

a. It is the captain's responsibility to protect the ship from wind and typhoons and ensure the safety of the ship. Due to the great power and variable nature of typhoons, the captain should implement the policy of "safety first, prevention as the priority," and adhere to the principle of "focusing on prevention, combining prevention with resistance, evacuating early when necessary, and leaving room for maneuver" to achieve the goal of safely avoiding typhoons.

b. When a ship affected by a typhoon (tropical cyclone) is expected to encounter winds of force 6 within the next 24 hours, it should be considered to be in serious danger from the typhoon.

c. Collect weather reports on time daily. When affected by wind, increase the frequency of collection according to the captain's instructions, and make full use of shipboard meteorological instruments, radio meteorological forecast broadcasts along the route, meteorological fax charts, NAVTEX navigational warnings, and other means to obtain meteorological forecast information.

d. Establish a professional meteorological forecasting group composed of the captain, chief, team leader, chief assistant, first mate, second mate, etc., to make decisions for navigation operations based on weather reports.

e. Establish a "Typhoon Prevention Leadership Group" composed of the person in charge of the temporary party organization, captain, chief, chief assistant, team leader, department head, etc., to educate crew and scientific research personnel on typhoon prevention, improve knowledge and technical operation level of typhoon prevention, and implement specific measures for typhoon prevention.

f. Maintain close contact with ship management units and port departments.

g. Prepare for ship typhoon resistance and contingency deployment work.

8.1.2 Other Emergencies

According to Article 9 of Chapter 2 on "Exploration and Exploitation" in China's *Law of the People's Republic of China on Exploration and Exploitation of the Resources in Deep Seabed Area (Deep Seabed Law)*, contractors must ensure the safety of personnel and property, protect the marine environment, and consciously accept the supervision and inspection of maritime authorities, as well as fulfill other documents required by the UNCLOS and the ISA. Therefore, in the event of an emergency, as required by the "*Deep Seabed Law*", contractors should immediately activate the emergency plan and take the following measures:

(1) Immediately issue an alarm;

(2) Immediately report to the Oceanic Administration of the State Council;

(3) Take all practical and reasonable measures to prevent and control damage to persons, property, and the marine environment;

(4) Cooperate with other contractors to respond to emergencies as appropriate.

8.2 Potential Accidents

8.2.1 Ship Oil Spill

（1) Risk Analysis

a. The possibility of oil dripping or leaking accidents on the mining test support ship during the operation due to negligence in management or violation of operating procedures is relatively high. Such oil spill accidents have a relatively small environmental impact but can still cause oil pollution in the waters;

b. Damage to the ship's facilities, the influence of wind and waves at sea while sailing, or ship collisions, could all potentially cause oil to spill and pollute the environment.

The operational deck area on the ship will be equipped with directly accessible oil spill kits to prevent accidental discharge of liquids into the ocean. There will be emergency response procedures on the ship to help minimize the impact of any incidents that could lead to leaks and potentially affect the marine environment. In addition, a shipboard marine pollution emergency plan will be implemented to deal with any accidental leaks or unconventional pollutant discharges.

(2) Preventive Measures

a. The professional and technical skills of ship drivers should meet the requirements;

b. Implement a watch and lookout system;

c. Carry out orderly, with test operation ships operating within designated areas;

d. When it is necessary to demarcate a safety operation area related to the test operation, it should be approved by the maritime authorities; set up relevant signs, strictly prohibit unrelated ships from entering the operation area, and issue navigation announcements in advance and regularly;

e. Ships involved in the test operation must display prescribed signal lights and shapes at visible places around the clock according to relevant regulations; effective communication equipment should be equipped on the ship at the site;

f. Avoid operations during the foggy season and typhoon season; arrange for the operation ships to take shelter from the wind promptly when encountering adverse weather, and prohibit operations in poor visibility and winds greater than force 6;

g. Form a safety group on each ship, with the ship's captain (or project leader) as the team leader, responsible for safety publicity and education on the ship, formulating safety production measures, and carrying out daily safety supervision and inspection,

implementing decisions of the safety leadership group, and assigning safety responsibilities to individuals;

h. Establish a safety operation organization, appoint safety officers, and be responsible for daily safety production work, supervising all marine operation personnel to wear life jackets and safety helmets;

i. In the event of a ship traffic accident, all valves of the oil tank pipeline system should be closed as much as possible, and the ventilation holes of the oil tanks should be plugged to prevent oil spills.

8.2.2 Equipment Risk

（1）Risk Analysis

Deep-sea mining environmental surveys and monitoring work require large-scale deep-sea survey equipment, the normal operation of which is crucial for the environmental surveys and monitoring of deep-sea mining projects. The value and importance of this equipment are self-evident due to its specificity. Each task requires specific survey tools to be completed. The stability of various equipment functions and the safety of operations need to be considered. At the same time, since the main workload of the project is carried out at sea, and the CTA has complex and variable conditions, certain requirements are put forward for the instruments and equipment and the operating personnel.

（2）Response Measures

a. Strictly manage all instruments and equipment following various rules and regulations;

b. Assign a dedicated person responsible. Ensure that the equipment is assigned to individuals, with a clear division of labor and responsibility;

c. Strictly follow instrument operation procedures for marine operations and the use of instruments and equipment to prevent instrument loss;

d. Regular inspection and maintenance, timely correction, and exclusion of adverse factors to ensure stable performance of instruments and equipment;

e. Timely reporting system. In case of abnormal conditions of instruments and equipment, the person in charge should report promptly and work together to resolve the issue.

8.2.3 Chemical Leak Risk

All ship activities related to the implementation of the project will comply with the requirements of the *International Convention for the Prevention of Pollution from Ships* (MARPOL), which includes regulations aimed at preventing accidental pollution and routine ship operations pollution.

Chemicals or fuels may leak due to equipment leaks, accidental failures, or extreme accidents. Leaks can have harmful effects on water quality and adversely affect the marine ecosystem. Considering the results of the leak risk assessment, BPC will review and revise mitigation measures and operating procedures as needed. Proactive and reactive measures will be taken to minimize the risks and potential impacts of fuels and other hazardous materials. Proactive measures may include:

(1) Appropriate material selection for hoses, equipment, and tanks, and corrosion control.

(2) Monitoring pipeline/hose pressure to detect any leaks or spills early.

(3) Developing equipment maintenance and monitoring plans to ensure equipment integrity and detect losses of safety shells.

(4) System setup for emergency stop and safety protection shell systems.

(5) Purchasing and maintaining spill response and protection equipment suitable for any risk level and type, deployed in all areas where spills may occur.

(6) Implement personnel training and on-site drills in leak prevention, control, and response.

9 ENVIRONMENTAL MANAGEMENT MONITORING AND REPORTING

9.1 Organizational Structure and Responsibilities

9.1.1 BPC Environmental Management System

In accordance with the *Draft standard and guidelines on the development and application of environmental management systems* (ISBA/27/C/7), Pioneer has established an EMS. The management of this project is integrated into the company's Environmental Management System (please see the Appendix for the full version of BPC's EMS Philosophy, Objectives, and Policies). Guided by the company's leadership and policies, environmental work is organized around core processes that identify and utilize resources, awareness and capabilities, communication, and documentation that can provide a supportive role. The core processes include planning, operations management, and improvement, with each level providing support services in turn (see Figure 2-2).
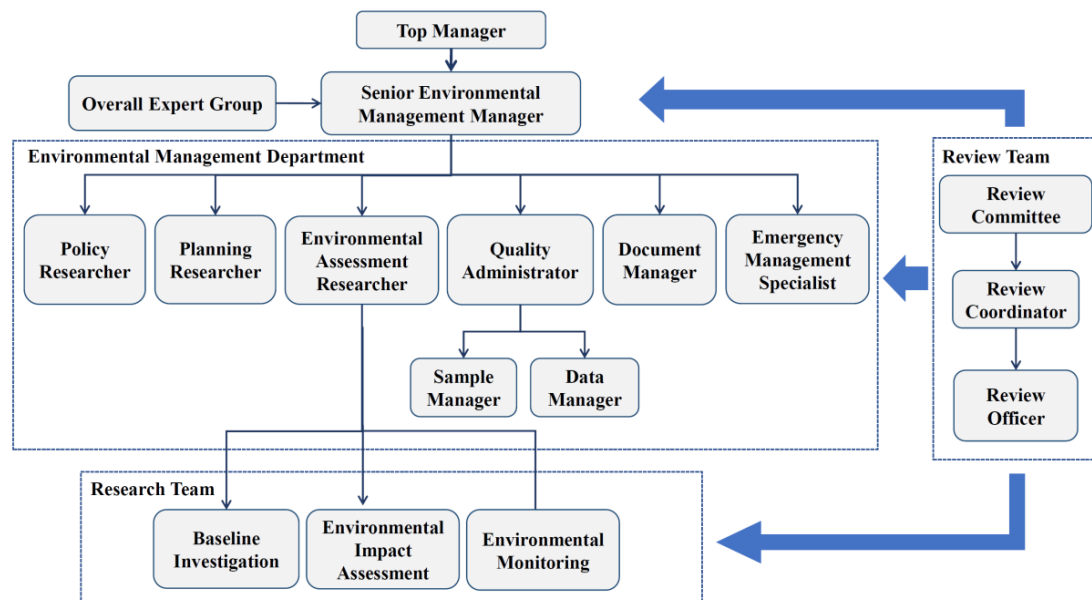
Figure 9-1 Personnel organization chart

The company's leadership attaches great importance to environmental work in mining areas and has made a commitment to responsive leadership. After signing the exploration contract with the ISA, we started to formulate guidelines related to the environment of deep-sea mining in 2021, we completed the *Technical Guidelines for*

Subsea Polymetallic Nodules Mining System, which proposed guidelines for mining systems to protect and preserve the marine environment. in 2021, we completed the *Guidelines for Environmental Protection and Preservation in Deep-Sea Mining Activities*, which set out the requirements of contractors' environmental work in the three phases of exploration, development and closure of the mine. The company will continue to gradually build an environmental management standard system based on the needs of environmental work.

The company places great emphasis on educating staff and subcontractors about the importance of environmental protection and implements scoring criteria for environmental protection measures in the bidding process for marine survey expeditions.

The company has a long-term plan and full-process management for the entire project and has formulated this document with the aim of implementing and enforcing the work of the EMS.

The company plans the establishment of environmental baselines, environmental impact assessments, development of environmental management and monitoring plans, and development of closure plans. It manages operations, including supervision, procurement, subcontractor management, development of emergency and contingency plans, performance evaluation, audits and reviews, reporting and notification, and plans for nonconformities and continuous improvement, providing support in the form of resources, awareness and competence, communication, and documentation of the EMS.

9.1.2 Project Organization

A project-level organizational and management framework has been established in the context of the project. China is the sponsoring State of the BPC polymetallic nodule contract area , the China Ocean Mineral Resources Research and Development Association (COMRA) is the competent authority for the Area in China, and the activities of BPC in the contract area are managed in accordance with the contractual agreements and the relevant regulations of the ISA and supervised by the COMRA in accordance with the *Deep Seabed Area Resource Exploration and Exploitation Law of the People's Republic of China* and other laws of China (Figure 9-2). This project is overseen by the Project Commander, who is fully responsible for the entire process and is guided by the Overall Expert Group. The positions of Chief Technical Engineer and Chief Environmental Scientist have been established, who are accountable for the project's technical and environmental aspects. The execution of the project is managed

by the General Manager of the Project. The project operations consist of the Offshore Execution Department and the Onshore Command Center. The Onshore Command Center includes the Security Management, the Operation Support, and the Emergency Coordination. The Offshore Execution Department, comprising the Captain, the Chief Scientist, and the Offshore Project Manager, coordinates the maritime implementation of the project. The Offshore Execution Department also establishes Contingency Planning, and designates roles for Data Managers, Sample Managers, and Key Equipment Managers.

Figure 9-2 Project Organization Chart

9.1.3 Overall Project Emergency Management

During the implementation of the project, it is essential to establish an emergency response system in advance to organize and respond to emergencies. The emergency response plan should employ a systematic approach to manage incidents and emergencies. This will be based on potential emergencies identified through the risk assessment process. The emergency plan system includes the following components:

(1) Emergency response team organization (structure, roles, responsibilities and decision makers).

(2) Manage flowcharts for various emergency response scenarios, as well as contact details of relevant personnel.

(3) The following description of response procedures (detailed information on response equipment and location, procedures, training requirements, and responsibilities):

- Ship-to-shore emergency response procedures

- Emergency deployment plan

- Command communications contingency plan

- Ship collision response measures and preparedness plans

- Fire and fire risk emergency measures and plans

- Emergency measures and plans for hazardous chemical spills

- Emergency measures and plans for shipboard personnel falling overboard

- Emergency measures and plans for injury to ships' personnel

- Emergency measures and plans for ships against storm and typhoon

BPC will execute the emergency plan following the six steps of Preparation, Detection, Suppression, Eradication, Recovery, and Review.

9.2 Environmental Monitoring Program

9.2.1 Purpose of Monitoring

In combination with the collection tests of nodule in the polymetallic nodule area of the western Pacific Ocean, a deep-sea mining environmental impact monitoring system will be deployed in the IRZ and PRZ to collect the environmental impact monitoring data during and after the test, in order to compensate for the lack of existing deep-sea mining knowledge and to enhance the scientific rigor of environmental impact assessments for such activities.

Furthermore, scientific research related to the potential impacts of deep-sea mining will be carried out to develop mitigation measures for future deep-sea mining programs and to provide a scientific basis for the development of environmentally friendly mining technologies in the deep sea.

9.2.2 Monitoring Areas and Phases

9.2.2.1 Monitoring Areas

The monitoring areas include the IRZ (including the CTA and the plume diffusion impact zone) and PRZ. The IRZ is in the northeastern part of the Block M2 of the BPC's contract area, specifically within the southern foothill of the Magoshichi Guyot. The core area of the IRZ is approximately 11.5 km x 11.5 km, but considering the extreme case of extremely fine particle dispersion (see Figure 3-3). The PRZ, located in Block M1, in the southern foothills of the Matsuzaki Guyot (Figure 3-4), with a total area of approximately 21 km × 16 km, about 78 km from the CTA.

Giving the special geographic location of the contract area in the inter-mountain basin in the western Pacific Ocean, and the concept of "research-oriented exploitation" and the precautionary principle, it is proposed to establish seamount monitoring areas in the foothill and slope of the Magoshichi Guyot (Figure 9-3). This initiative aims to investigate the potential impacts of mining on vulnerable organisms such as cold-water corals on seamount and to develop precautionary measures for potential future deep-sea mining plans. After deposition of sediments and nodule debris from mining plumes, these particles may be resuspended under the influence of physical oceanic processes such as mesoscale eddies in the ocean surface layer. The height of resuspension can reach hundreds of meters upward (Kim et al., 2021; Gardner et al., 2017; Kontar et al., 1994). During commercial mining, due to cumulative effects, there is a possibility that these resuspended particles may diffuse towards the foothills of the seamounts. Additionally, the presence of secondary circulation on seamount slopes (Figure 9-4, Xia et al., 2023) poses a risk of upward transport of these suspended particles along the seamount slopes, where large number of cold-water corals live on (from 3,000 m to the summits) (Figure 9-5; Miyamoto et al., 2017). Therefore, nodule mining has potential impacts on vulnerable biological community such as cold-water corals live on seamounts, especially Magoshichi Guyot, which is considered an Ecologically or Biologically Significant Marine Area (EBSA) and a vulnerable marine ecosystem (VME) (Du Preez et al., 2023). Although the current simulation results show that the plume from this test does not affect the seamount, there may be potential impacts during future commercial mining. Based on the precautionary principle, during the collection tests of collector components period of this project, the project team plans to carry out monitoring and research to determine whether or not polymetallic nodule mining in

basin has an impact on the nearby vulnerable ecosystems such as seamount, and the extent of such impact.
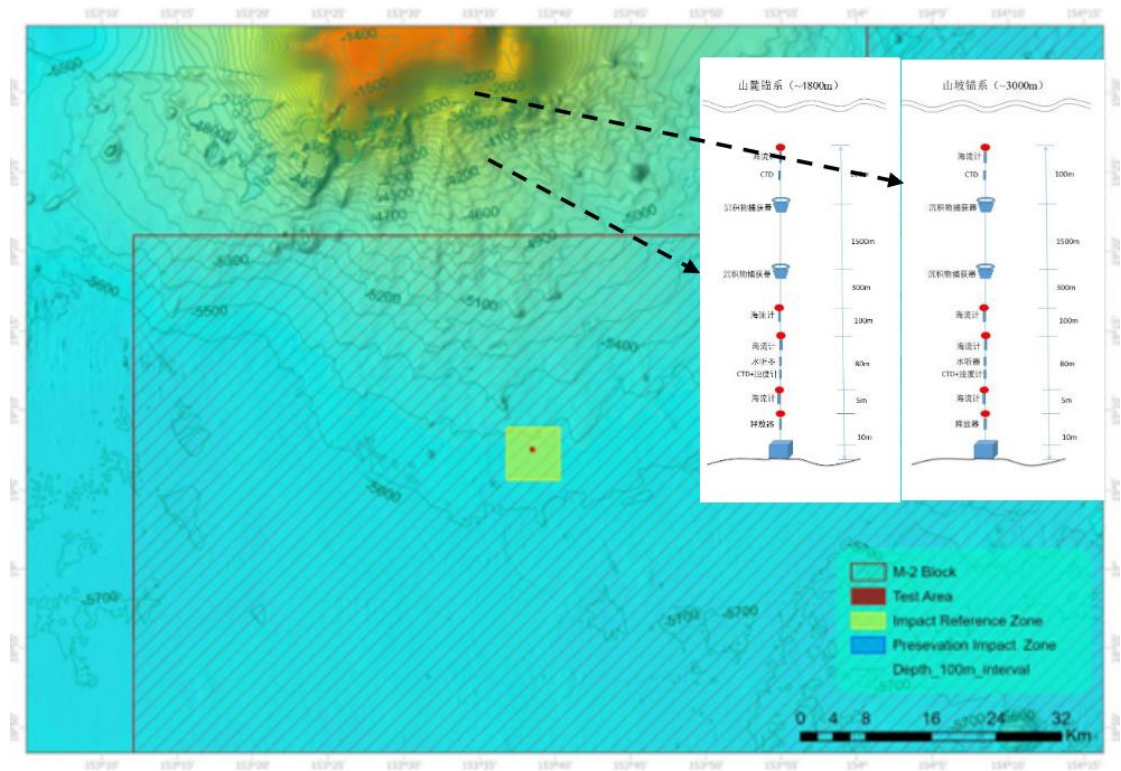
Figure 9-3 Schematic of seamount environmental monitoring areas and equipment
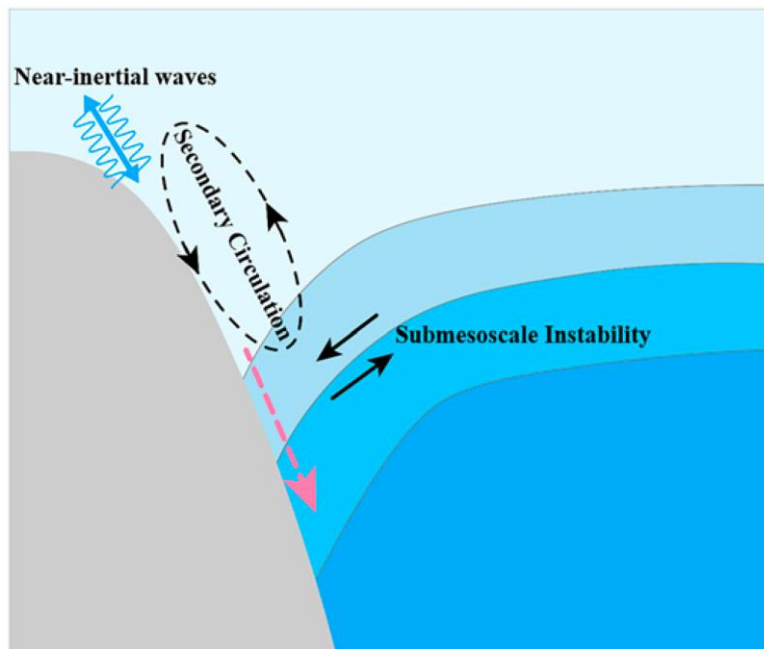
Figure 9-4 Secondary circulation on deep-water seamount slopes (Xie et al., 2023)
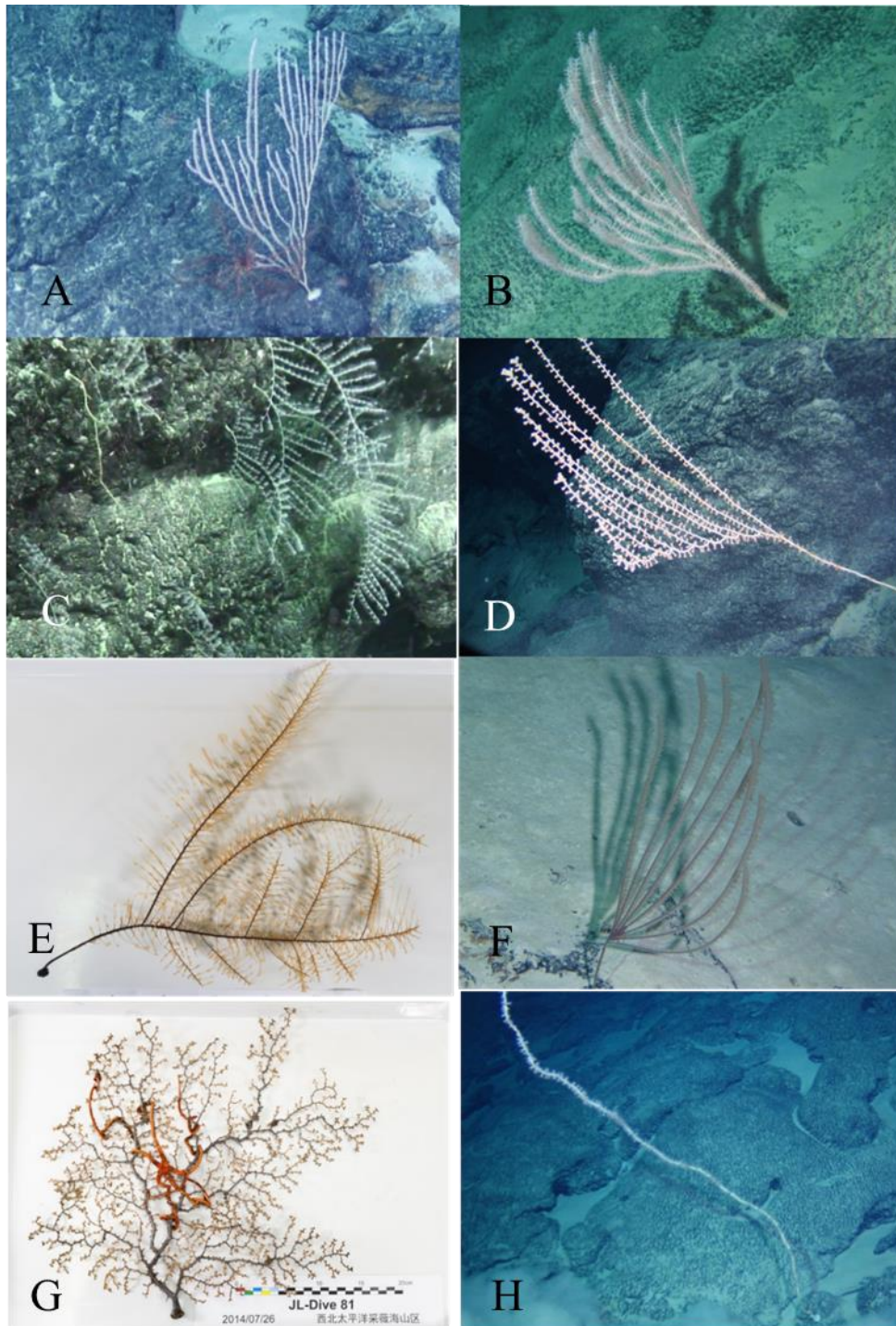
Figure 9-5 Cold-water corals on the seamounts in the western Pacifica Ocean (Wang et al. 2016, DY 35 cruise report)

A: *Narella* sp.; B: *Candidella* sp.; C: *Ramuligorgia militaris*；D: *Isidella* sp.；E: Cladopathidae gen. sp.；F: *Heteropathes* sp; G: Plexauridae gen. sp; H: *Lepidisis* sp.

9.2.2.2 Monitoring Phases

The environmental monitoring plan is divided into 4 phases. Phase I: environmental baseline survey before the test. It can be divided into 2 subphases.

Subphase I-1: to carry out the baseline survey in 2024 in the IRZ and PRZ. Subphase I-2: in 2025 (prior to the test), to deploy short-term subsurface buoys in the IRZ to collect bottom current data, which will provide a basis for determining or adjusting the environmental monitoring plan. Additionally, multicorer and box corer will be used to collect sediment samples. Phase II: environmental monitoring during the test in 2025. Phase III includes two subphases. Subphase III-1: after the test completed and the environmental monitoring equipment recovered in 2025, AUV or HOV will be used to conduct optical and acoustic surveys in the IRZ, and sediment and other samples will be collected from the IRZ and PRZ using multicorer and box corer, and one set of long-term observation Lander system will be deployed at the CTA. Subphase III-2: to revisit the IRZ and PRZ in 2026 (i.e. 1 year after the test) for post-test environmental monitoring. Phase IV: long-term environmental monitoring in the 3rd, 5th, and 7th year after the test (see Figure 9-6). Additionally, a set of subsurface buoys will be deployed at the southern foothills and slopes of Magoshichi-no-Hoshi Guyot before the test in 2025 to monitor the potential risk of upward transport of SS from the seabed along the seamount slope (Figure 9-3).
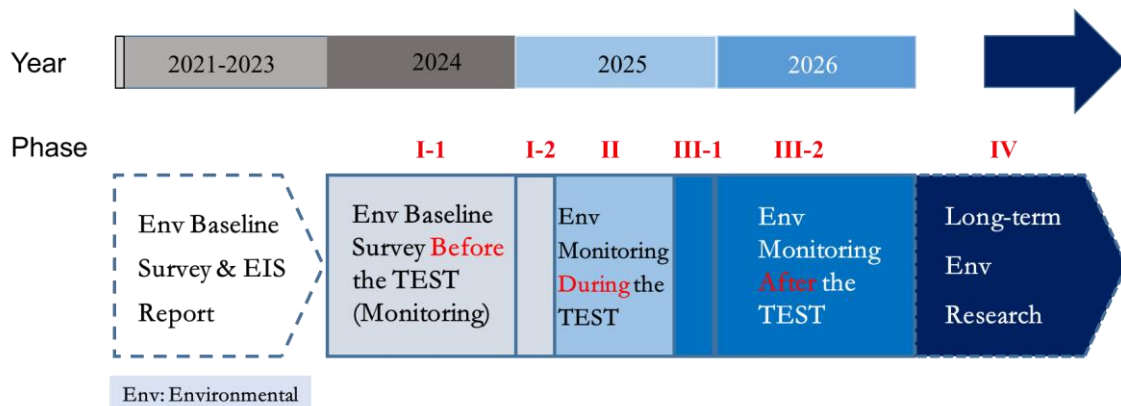
Figure 9-6 Environmental monitoring phases classification

9.2.3 Monitoring Index System

The environmental monitoring parameters are as follows, and are monitored throughout the entire test period to provide a basis for environmental impact assessment and threshold setting.

9.2.3.1 Physical Oceanography

The survey of the physical oceanographic data should include pressure, water temperature, salinity, currents, turbidity, optical and acoustic properties throughout the

water column and the near bottom layer, as well as sea surface meteorology, wave height and wave direction, etc.

9.2.3.2 Chemical Oceanography

The monitoring parameters of chemical oceanography is shown in Table 9-1. Concerning the fact that this project is small-scaled and not involve mineral hoisting or tailings discharge in the surface, the italicized parameters of Table 9-1 and Table 9-2 are not applicable to this project.

Table 9-1 Chemical oceanography monitoring parameters

Category	Elements	Parameters
Water chemistry	gas	Dissolved oxygen, *methane, carbon dioxide*
	carbonate system	alkalinity, pH, dissolved organic carbon
	nutrient	Nitrate, nitrite, ammonium, reactive phosphate, reactive silicate, total phosphorus, total nitrogen
	organic matter	Total organic carbon
	particulate matter	Particulate matter
	trace element	mercury, arsenic, copper, lead, cadmium, nickel, zinc, chromium, manganese, iron
Sediment chemistry	Sediment pore water	Total alkalinity, pH, total mercury, arsenic, copper, lead, cadmium, nickel, zinc, chromium, manganese, iron
	Redox system	Fe^{3+}/Fe^{2+} ratio, Eh
	Sediment trace elements	mercury, arsenic, copper, lead, cadmium, nickel, zinc, chromium
	other	Organic carbon
Organism	trace element	mercury, arsenic, copper, lead, cadmium, nickel, zinc, chromium, manganese, iron

9.2.3.3 Biological Communities

Biological communities monitoring parameters are shown in Table 9-2.

Table 9-2 Biological communities monitoring parameters

Category	Elements	Parameters
Benthic community	Megafauna	Abundance, diversity
	Macrofauna	Biomass, abundance, diversity
	Metazoan meiofauna	Biomass, abundance, diversity
	Foraminifera	Abundance, diversity
	Nodule biota	diversity
	Microbiota	Abundance, diversity, community respiration rate
	Demersal fish and scavengers	Species
Pelagic community	Microorganisms	*Abundance, diversity*
	Picoplankton	*Abundance, diversity*
	Nano- and Microplankton	*Abundance, diversity*
	Macroplankton	*Biomass, abundance, diversity, vertical migration*
	Ichthyoplankton	*Abundance, diversity*
	Nekton	*Biomass, abundance, diversity*
Other	Marine mammals and seabirds	*Species*
Ecosystem function	Primary productivity	*Primary productivity, chlorophyll a*
	Food-web	Biological and sediment δ^{13} C and δ^{15} N ratios, trophic levels and food source contributions of dominant taxa
	Sediment community	Oxygen demand

9.2.3.4 Geological Properties

The geological properties monitoring parameters are shown in Table 9-3.

Table 9-3 Monitoring parameters for geological properties

Category	Elements	Parameters
Mining-induced sediment disturbance	Mining track	Depth
	Sediment plume redeposition	Thickness, grain size, mineral composition
Sediment geological Properties	geological property	Composition, moisture content, bulk density, specific gravity of solid particles, specific gravity, critical moisture content
	Mechanical property	Compressive strength, penetration strength, shear strength
Bioturbation	Biological activity	Depth of biological trace
	Rate of bioturbation	Excess ^{210}Pb activity
Fluxes to the sediment	Particulate deposition rate	Total particulate fluxes and fluxes of total carbon, total nitrogen, organic carbon, inorganic carbon

9.2.4 Monitoring Techniques and Equipment

9.2.4.1 Physical Oceanography

(1) Temperature, salinity, pressure

CTD profilers is used for monitoring.

(2) Bottom currents

Monitoring is conducted by using deployment of the LADCP and current meter nodes (Figure 9-7), by subsurface buoy and by observation nodes.
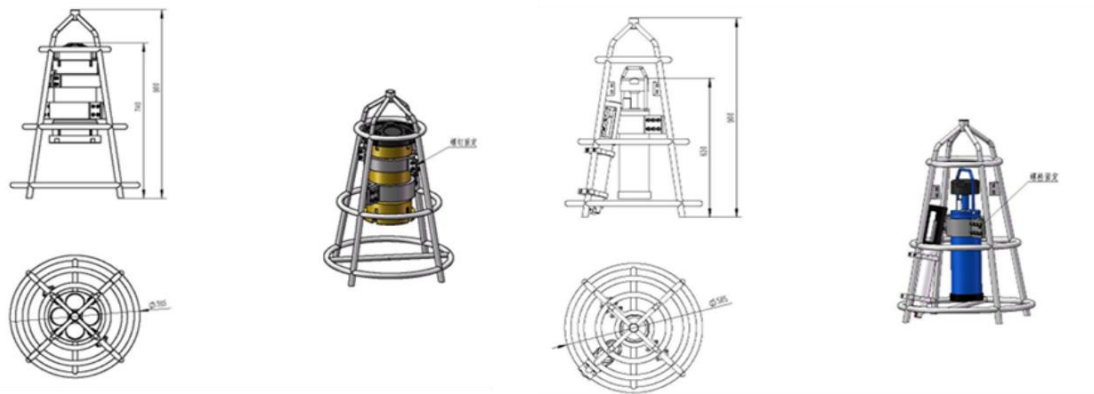
Figure 9-7 LADCP nodes (left) and current meter (right) nodes

(3) Turbidity (plume) monitoring

Turbidity data can be obtained from the turbidity sensor array, subsurface buoy, the observation nodes, and the turbidity sensor mounted on the AUV which cruises at different altitudes of 5 m, 10 m, 25 m and 50 m above the bottom (Figure 9-8). In addition, the deep-sea particle observation camera (Figure 9-9) at the seafloor plume redeposition and biological observation node can obtain data such as plume particle size spectra and plume velocity.
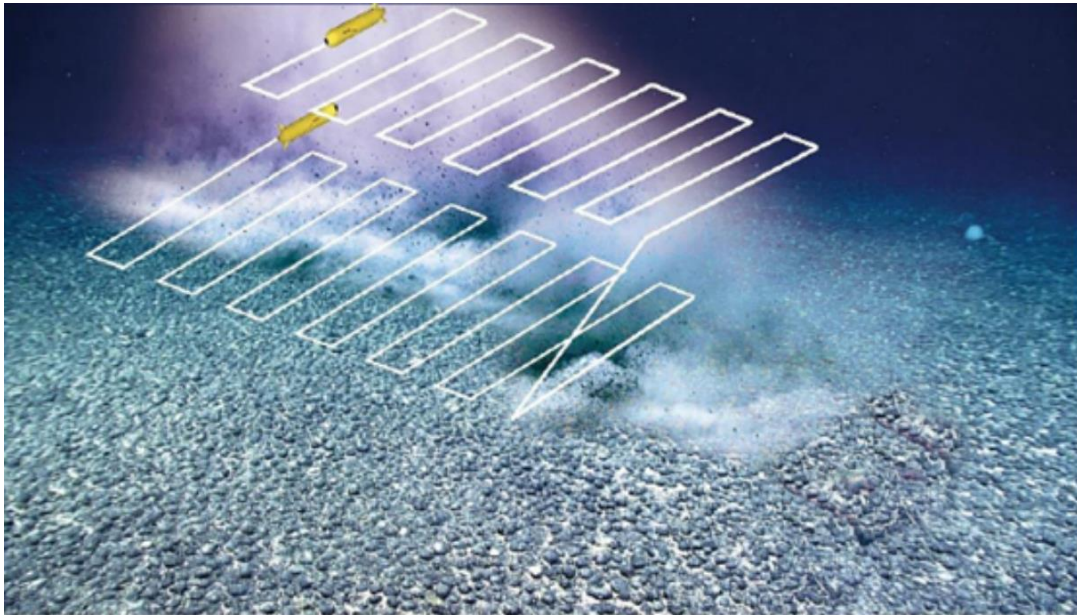
Figure 9-8 AUVs with turbidity sensors cruise at different heights

Stereoscopic camera

Particle Observation Camera

Sediment profile camera
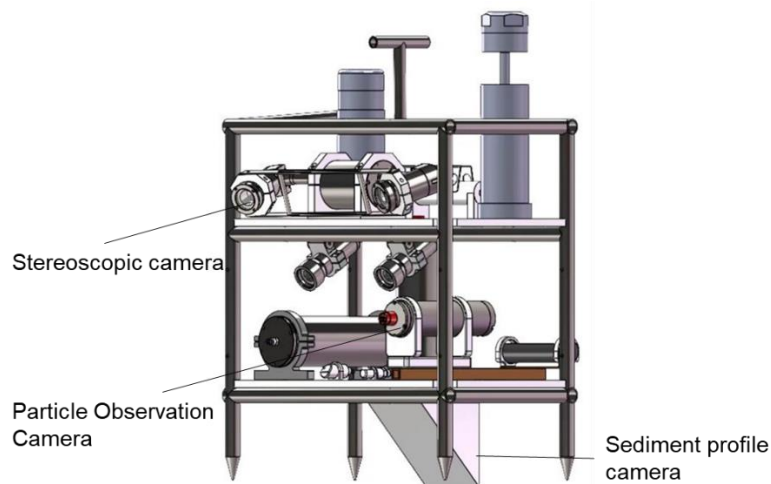
Figure 9-9 Nodes for redeposition and biological observations of the seafloor plume

(4) Noise

Noise data during the test can be obtained by using hydrophones mounted on subsurface buoy and on the seafloor plume redeposition and biological observation nodes.

9.2.4.2 Chemical Oceanography

(1) Seawater chemistry

Samples for nutrients, dissolved oxygen, pH, total alkalinity, and dissolved inorganic carbon are collected using a CTD profilers.

Water samples for trace metal analysis are collected using an autonomous clean environmental (ACE) sampler.

Suspended solid samples are collected by water sampler mounted on the collector and CTD.

(2) Deposition chemistry

Samples for sediment pore water nutrient, trace metal, and organic carbon analyses are collected using a multicorer (Figure 9-10).
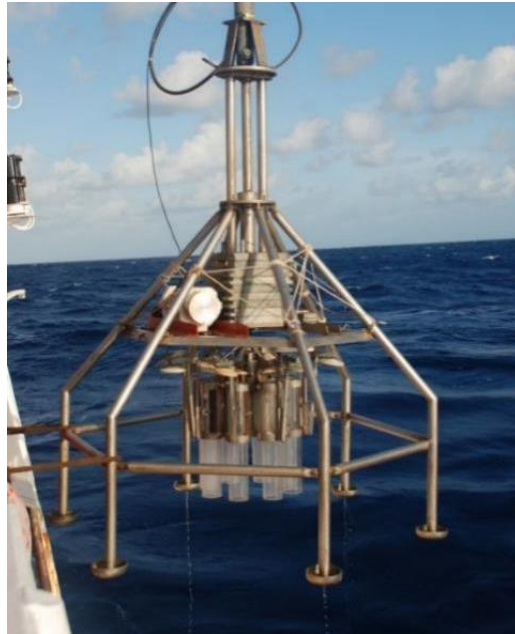
Figure 9-10 TV multicorer

Redox system is monitored using sensors mounted at observation nodes and sediment profile cameras (Figure 9-11).
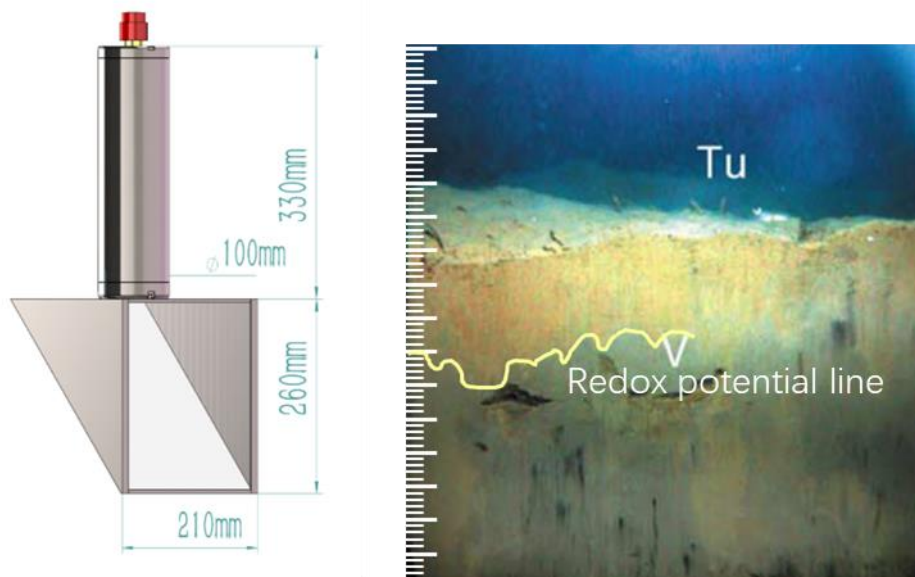
Figure 9-11 Schematic of sediment profile camera and photographed sediment profile

(3) Organism

The lander system (Figure 9-12) is used to collect biological samples, such as fish, before and after the test to analyze the heavy metal content in the organisms.
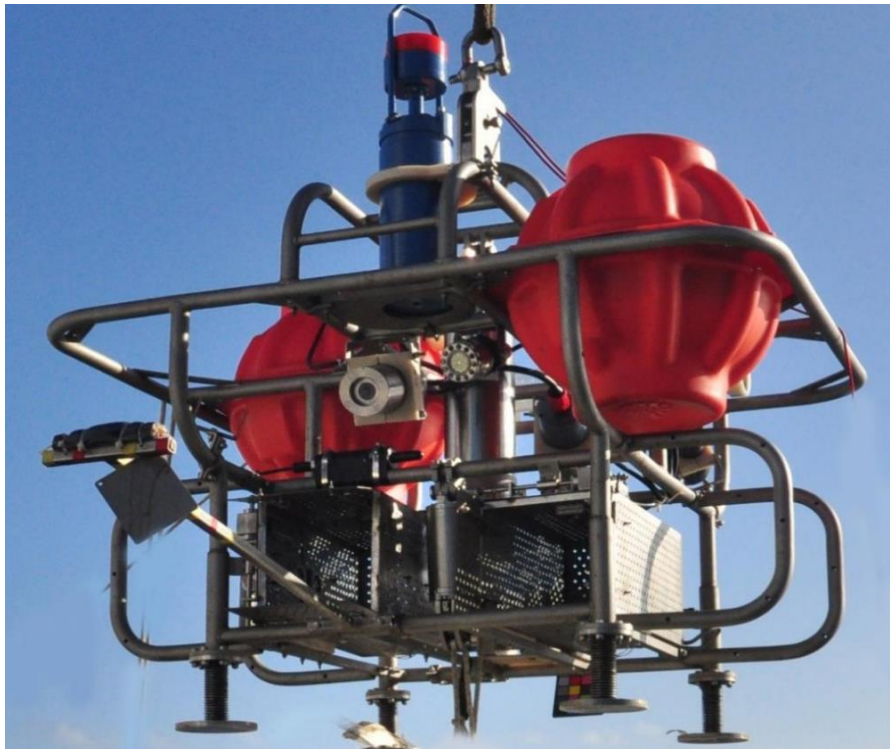
Figure 9-12 Lander system

9.2.4.3 Geological Properties

(1) Characterization of depositional properties

Samples are collected by multicorer and a sediment sampler on a self-developed deep-sea in situ time-series sampling station.

(2) Redeposition thickness

The AUV carries a high-resolution sub-bottom profiler (Table 9-4), which is navigated at a fixed altitude of 5 m above the bottom to obtain surface redeposition thickness data and can be calibrated with the redeposition thickness data obtained from the sediment profiling camera (Figure 9-11) and the sediment collection box.

(3) Mining track depth

A laser scanner and laser range finder are used to measure the depth of the mining track.

Table 9-4 Main technical specifications of high-resolution sub-bottom profiler

Index	parameters
Working depth	6000 m
Resolution	0.5 cm
working height above the floor	≤6 m
Penetration depth	≥30 cm (silt substrate)
Beam angel	1° x 1°
Electricity supply	24V DC

9.2.4.4 Biodiversity and Ecosystem Functioning

(1) Megafauna

Species identification was conducted using samples collected by the "Jiaolong" HOV (Figure 9-13) and videos and photos obtained by AUV navigation (Figure 9-14), and combined with eDNA analysis to investigate the species composition and community structure of megafauna. Megafauna abundance is estimated using video footage of line surveys obtained from AUVs.
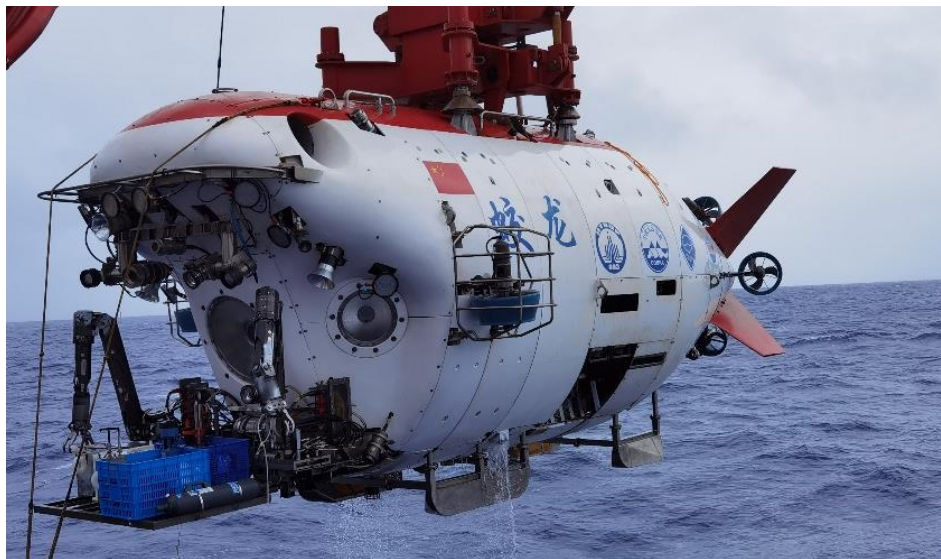
Figure 9-13 "Jiaolong" HOV

Figure 9-14 Photographs of deep-sea sea cucumbers taken by "Qianlong I" AUV

(2) Scavengers

Observations and sampling using lander system (Figure 9-15).

Figure 9-15 Deep-sea scavengers observed by lander system (*Coryphaenoides* sp. and

Ophidiiformes)

(3) Macrofauna

Sediment samples collected for macrofauna analysis using a box corer with an opening area of 0.25 m^2.

(4) Meiofauna

Samples collected with a (TV) multicorer and a sediment sampler on a self-developed deep-sea in situ time-series sampling station.

(5) Microorganisms and Eukaryotes

Samples collected with a (TV) multicorer and a sediment sampler on a self-developed deep-sea in situ time-series sampling station and a water collector mounted on the test collector.

(6) Nodule fauna

Samples collected by box corers and HOVs, and videos and pictures obtained by HOVs and AUVs (Figure 9-16).

Figure 9-16 Nodule fauna (crinoid)

(7) Ecosystem function (food web)

Megafauna, macrofauna, meiofauna, demersal fish and scavengers, sediment and seawater samples will be collected according to the relevant methods mentioned above. By using the stable isotope tracer method (Yang et al., 2020), the characteristics of the changes in the benthic food web structure before and after the test will be assessed.

9.2.4.5 Noise

Noise is monitored by hydrophones mounted on the collector and on the subsurface buoy.

9.2.4.6 Real-time/quasi-real-time Data Transmission

The data/images acquired by the observation nodes will be transmitted in real time/quasi-real time to the shipboard or shore-based laboratory via a high-bandwidth, multilevel link, bi-directional communication monitoring main station (Figure 9-17), through which commands for adjusting the monitoring frequency will be sent to the observation nodes, if necessary.
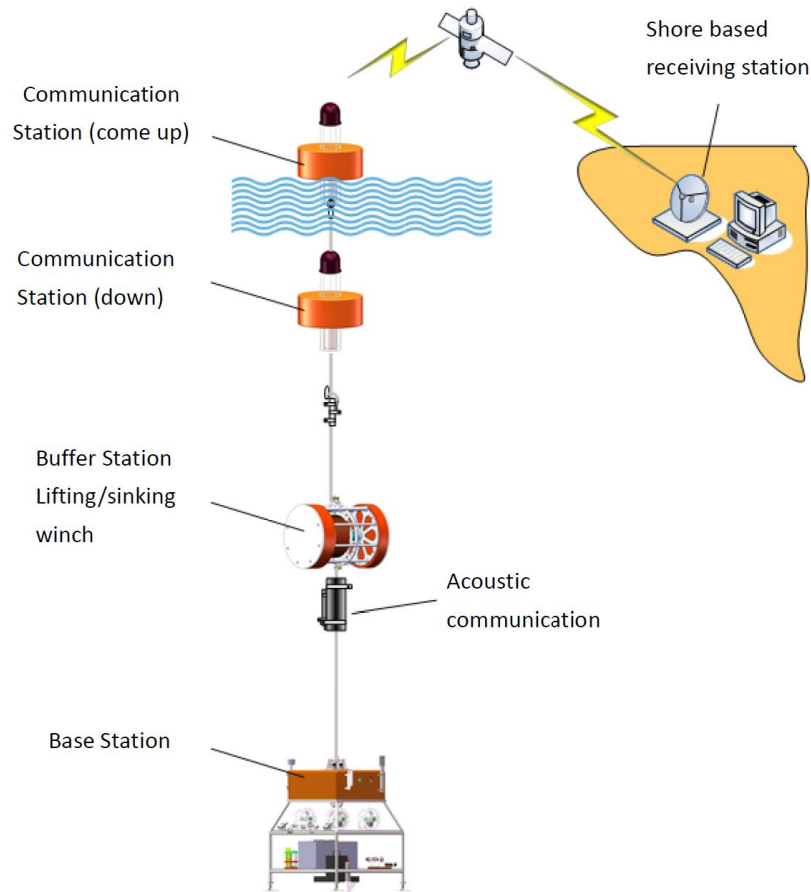
Figure 9-17 Monitoring master station with high bandwidth, multi-level link and bidirectional communication function

9.2.4.7 Auxiliary Operating Platforms

(1) AUV

"Dongcha Hao" AUV

BPC and the Shenyang Institute of Automation of the Chinese Academy of Sciences (SIA) jointly developed a 6,000-meter-class AUV for seafloor mining surveys that has the ability to conduct long-term operations independently from its mother ship (Figure 9-19). The "Dongcha Hao" AUV has the capability to navigate and perform photography tasks at a fixed-height close to seabed for a long period of time. With the assistance of the acoustic ultra-short baseline of the mother-ship, it can achieve long-term near-bottom continuous autonomous observation. Its main technical specifications are as follows:

Maximum working depth: 6000 m;

Maximum range ≥ 1300 km;

Weight ≤ 600 kg;

Maximum speed: 2knots;

Basic configuration: CTD and underwater camera system;

Wireless, satellite and hydroacoustic communications capability;

Possesses positioning and navigation capability based on the combination of USBL + electronic compass + DVL.

In this project it is proposed to use near-bottom optical surveys in the pre- and post-test period in the CTA and plume-affected areas. The underwater video data obtained are used to analyze changes in the diversity and abundance of megafauna and changes in the substrate before and after the test.
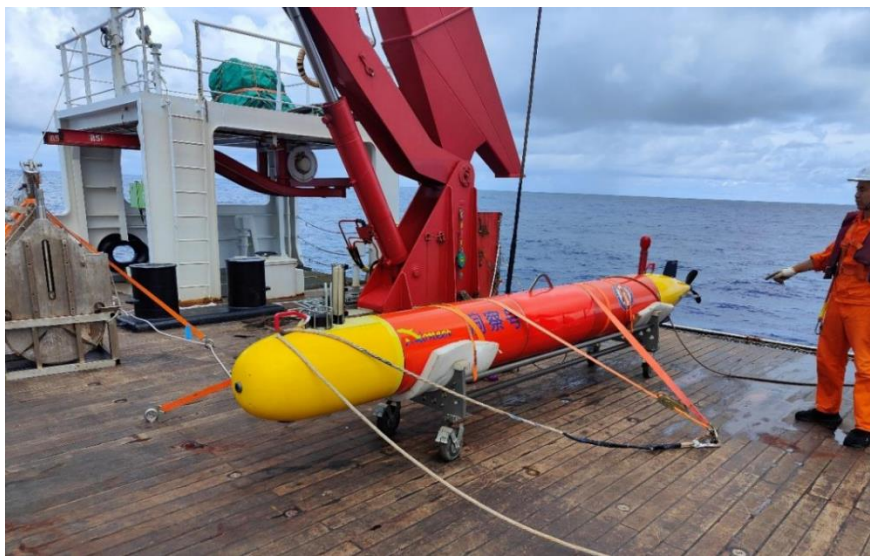
Figure 9-18 6000-meter-class "Dongcha Hao" AUV

"Qianlong IV Hao" AUV

The "Qianlong IV Hao" AUV is a 6,000-meter-class AUV (Figure 9-19) developed by the Shenyang Institute of Automation of the Chinese Academy of Sciences, and is mainly applied to the exploration of polymetallic nodule areas and to monitor environmental impact of polymetallic nodule mining. The "Qianlong IV Hao" AUV has the ability to navigate at a fixed depth and a fixed height. It is integrated with a high-resolution sub-bottom profiler, a CTD sensor and a multi-parameter CTD (turbidity, oxidation-reduction potential and dissolved oxygen), which can be used for conducting high-precision topography survey, detecting redeposition thickness and plume spatial distribution, as well as optical photographing. Its main technical specifications are as follows:
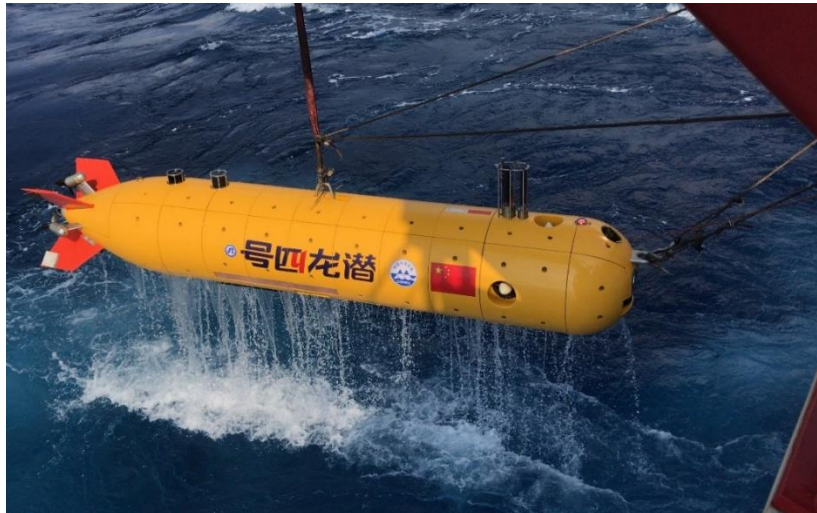
Figure 9-19 6,000-meter-class "Qianlong IV Hao" AUV

Weight (in air): 1400 kg;

Maximum working depth: 6000 m;

Maximum speed: 3kn, optical and redeposition thickness detection at speed 1kn;

Maximum endurance ≥24h;

Basic configuration: high-resolution sub-bottom profiler, CTD, RBR maestro3 CTD and underwater camera system;

Wireless, satellite and hydroacoustic communications capability;

Possesses positioning and navigation capability based on the combination of USBL + electronic compass + DVL.

In this project it is used for three-dimensional monitoring of turbidity and dissolved oxygen in the near bottom layer during test and post-test period and conduct a high-resolution sedimentary profiling measurement (mining plume re-sedimentation thickness detection).

(2) "Jiaolong" manned submersible (HOV)

The main technical specifications of the manned submersible "Jiaolong" (Figure 9-20) are as follows:

Maximum working depth: 7000 meters

Main scale: 8.6 meters long; 3.9 meters wide; 3.4 meters high

Manned pressure-resistant spherical shell: 2.1 m internal diameter; 1 viewing window 200 mm diameter, 2 viewing windows 120 mm diameter

Weight in air: 22.3 tons

Payload: 220 kg

Speed: 2.5 knots maximum; 1 knot cruise speed

Crew: 3 persons

Length of stay underwater: 12 hours

Propulsion system: 4 main push conduit propellers; 2 vertical push rotatable conduit propellers; 1 side push channel propeller.

Operating system: one seven-function master-slave robot; one seven-function switching robot

Observation system: Imaging sonar (range 100 meters); bathymetric side-scan sonar (coverage width: bathymetry 2×250 meters, side-scan 2×300 meters); 6 underwater camera (2 high-resolution, 3 standard-resolution, 1 Monochrome); 1 underwater camera.

Communication system: 2 hydroacoustic communicators; 1 hydrophone; VHF radio communication.

Positioning systems: USBL positioning sonar (maximum range 8,000 m); motion sensors; Side scan sonar (range 100 m); range-finding sonar (range 60 m); GPS positioning.

Sensors: 1 altimeter, 1 pressure gauge, 1 CTD sensors.

Emergency safety system: emergency battery (1.2 kWh energy)

Contingency loading: two manipulators, main battery box, sampling basket, working tools, longitudinal inclination adjustment medium can be discarded, and emergency buoys can be released.

In this project it is proposed to use the "Jiaolong" HOV to carry out sediment cover experiments and revisit the CTA for precise sampling.

Figure 9-20 7,000-meter class "Jiaolong" HOV

（3）ROV-based precision Deployment/ Recovery system for near-bottom equipment

BPC has developed a precise Deployment/Recovery system for monitoring nodes based on a ROV system (Figure 9-21), which is mainly equipped with deep-water manipulator, deployment and recovery device, camera and lighting, drive control device, deep-water sensors, etc. It has the ability to navigate at fixed depth and fixed height, and it can carry multiple monitoring nodes at one time, and achieve precise deployment and recovery operations in the seabed. Its main technical specifications are as follows:

Working depth: 6000m

Carrying capacity: 1200kg

Controllable movement range: ≥100m

Navigation system: equipped with IMU+ DVL combined navigation system, the accuracy can reach 0.3% of the range.

Deployment and recovery: can simultaneously complete the deployment and recovery of more than 2 sets of monitoring nodes.

Figure 9-21 ROV-based precision deployment/retrieval system

In this project, it is planned to be used for the precise deployment and recovery of the seafloor monitoring nodes in the IRZ. The deployment of multiple sets of monitoring nodes will be completed prior to the test, and the environmental monitoring nodes and stations will be recovered after the test.

9.2.5 Monitoring Framework

9.2.5.1 Pre-test Monitoring

Environmental baseline survey has been conducted in the past three years and will continue survey in IRZ and PRZ in 2024 (Subphase I-1). The survey items and workplan for 2024 are shown in Table 9-5 and Figure 9-22. The survey items and workload are shown in Table 9-5 and Figure 9-22. One multi-corer and one box corer sampling station will be set up in the CTA and PRZ, respectively, and three samples will be taken at each station. Four multi corer and box corer stations will be deployed in the plume impact zone on the east and west sides of the CTA, and three samples will be taken at each station. Three AUV or deep-towed optical survey lines will be deployed, including one east-west and one north-south survey line in the IRZ, and one east-west survey line in the PRZ. The two sets of recovered subsurface buoys were equipped with current meters, turbidity meters, hydrophones and sediment traps. The data obtained from the above surveys will be submitted to the ISA in the annual report of 2024 by the end of March, 2025 to improve the environmental baseline.

Table 9-5 Environmental baseline survey workload in 2024

Area	PRZ (No. of stations)	IRZ (No. of stations)		Total
		CTA	Plume impact zone	
Subsurface buoy recovery	1	1		2
Subsurface buoy deployment	1	1		2
Box corer	3	3	9	15
Multicorer	3	3	9	15
CTD + water sampling	2	2	2	6
Vertical plankton net	1	1	1	3
Multinet	1	1	1	3
Lander system	1	1	2	4
AUV or deep towed camera system	1	2		3
HOV		Twice dive		2

Before the test in 2025 (Subphase I-2), short-term (3-7 days) bottom current observation will be carried out, to obtain immediate bottom current data. If the current direction and size of the bottom current are similar to the settings of the numerical model, the monitoring equipment will be deployed according to the established program. If the results are different from the settings of the numerical model, the deployment program of the monitoring equipment will need to be adjusted. Meanwhile, prior to the 2025 test, sediment samples will be collected at two stations in the CTA, plume impact zone, and PRZ using box-corers and multi-corers, respectively. CTD collected water samples at two stations in the CTA and the PRZ (the station locations are shown in Figure 9-22) to analyze trace nutrients.
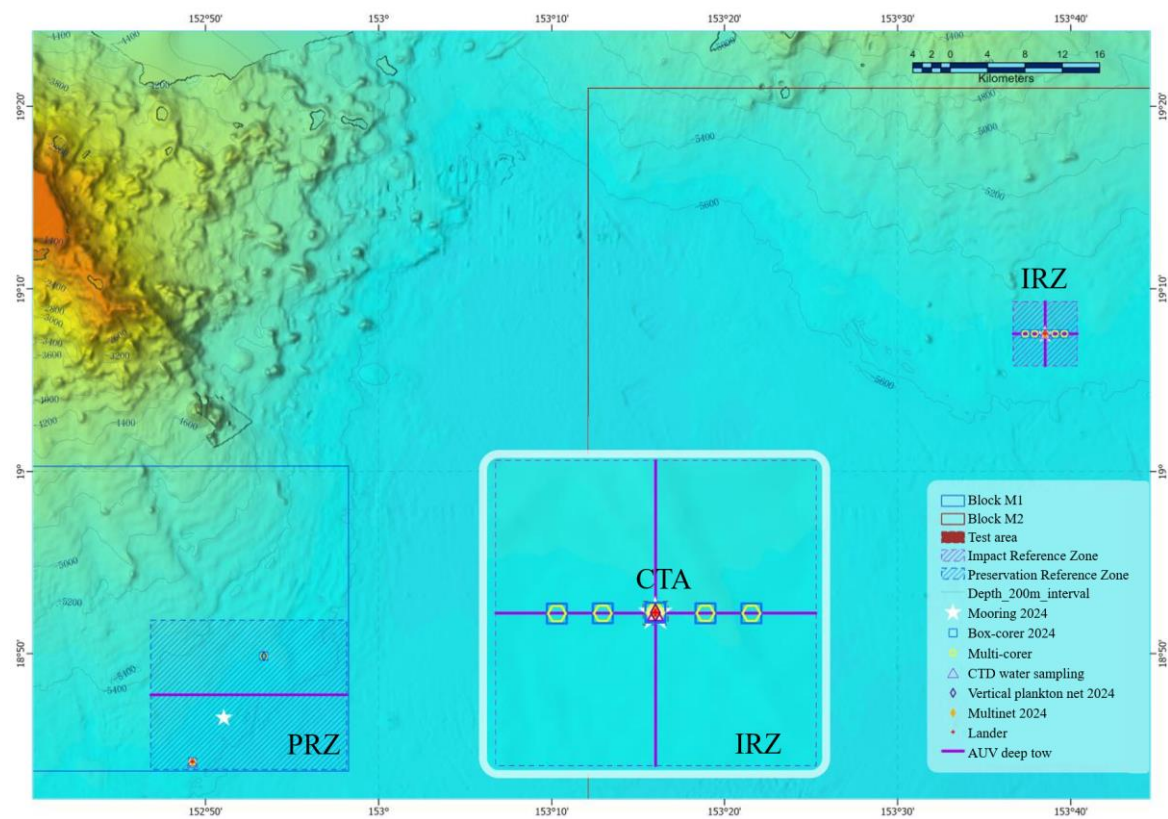
Figure 9-22 Environmental baseline survey stations in 2024

9.2.5.2 Monitoring during the Test

9.2.5.2.1 Spatial Layout of Monitoring Equipment

As an example, the spatial layout of monitoring equipment for the strong northwesterly flow in August is as follows:

Upstream of the CTA: A portable turbidity meter, a current meter node and a set of observation nodes will be deployed 200 m from the edge of the CTA, and an subsurface buoy will be deployed 300 m away.

Both sides and downstream of the CTA: A portable turbidity meter, a current meter and an ADCP node will be deployed 50 m from the border of the CTA. Most of the other equipment will be mainly placed in the plume dispersal area downstream of the CTA, with three observation nodes placed at 100, 300 and 600 m downstream of the CTA. Two sampling nodes will be placed at 100 and 300 m. The six subsurface buoys downstream will be arranged in a fan shape, with the first one 200 m downstream of the CTA, the second and third 500 m downstream of the CTA, and the fourth to sixth 800 m downstream of the CTA. The main communication station will be located 1 km downstream of the CTA (Figure 9-23 and Figure 9-24). An AUV survey line will be designed for the area 1000 m downstream of the CTA, cruising at different heights from the bottom to obtain turbidity data (Figure 9-8).

However, the spatial layout of the equipment on the top, bottom and both sides of the CTA is adjusted accordingly due to the flow direction, and the relative distance between the equipment remains unchanged, and only the orientation of the fan-shaped monitoring system needs to be adjusted. Monitoring such as bottom flow will also be carried out before the test in 2025, and the bottom flow data will be transmitted from the communication two-way real-time communication master station to the shipboard laboratory to determine the immediate flow direction and flow rate, and then the monitoring equipment layout plan will be determined according to the current velocity and current direction.

PRZ: 1 set of subsurface buoys and 1 set of observation nodes will be deployed respectively.

Southern foothills and slopes of Magoshichi Guyot: 1 set of subsurface buoys will be deployed respectively (Figure 9-3).

On the collector: turbidity, hydrophone and water sampler will be installed.
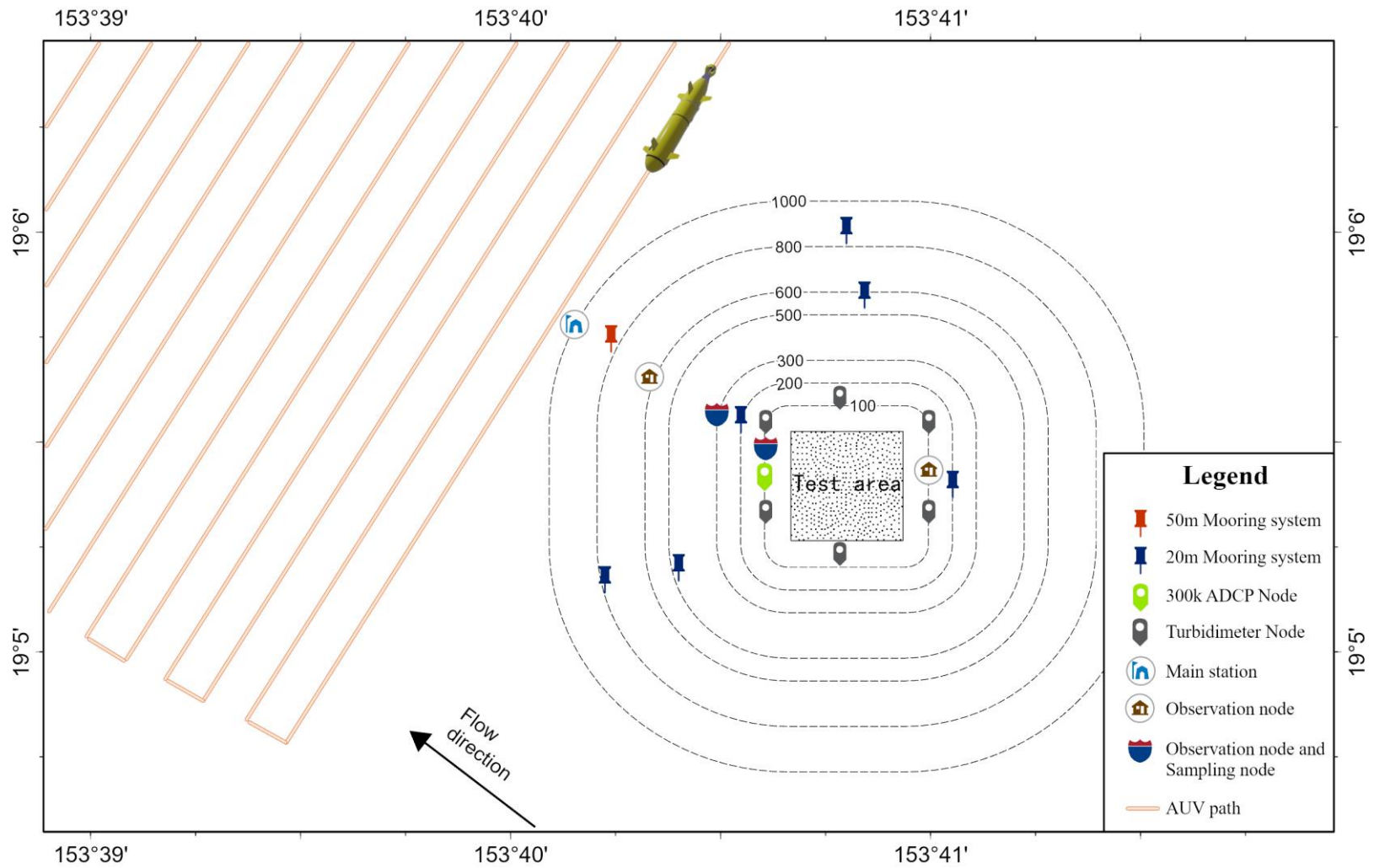
Figure 9-23 Spatial layout of monitoring equipment
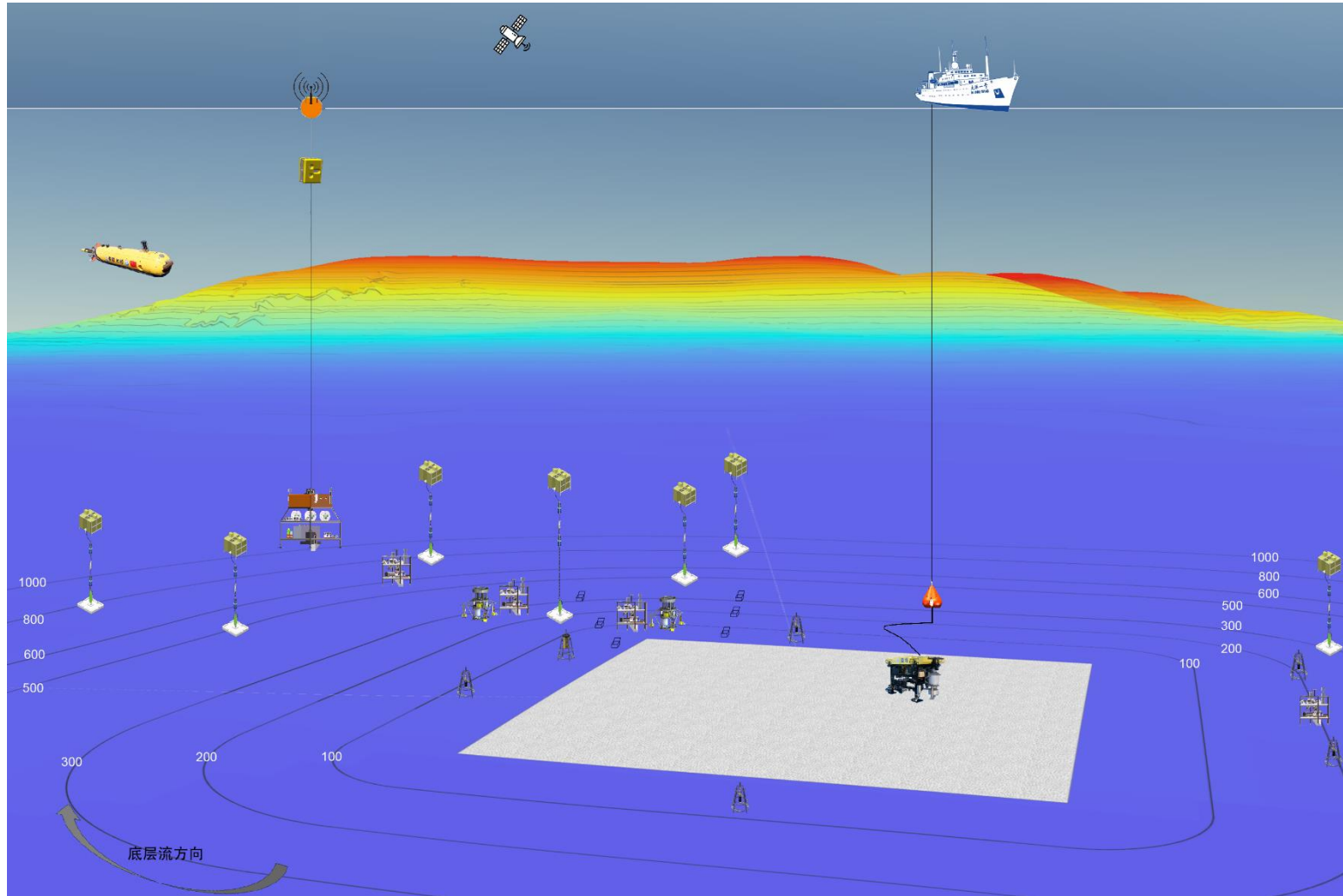
Figure 9-24 Three-dimensional deployment scenario for monitoring equipment

9.2.5.2.2 Three-Dimensional Plume Monitoring during Test

AUV-based technology was used to obtain turbidity, dissolved oxygen, Eh, temperature and salinity data from seawater at different heights off the bottom around the collector during the test, to identify the test plume anomalies and to define the three-dimensional spatial distribution range of the plume.

Operational survey line: Based on the current data and plume modeling result, the potential plume impact area will be determined and an AUV operational survey lines will be designed in the area up to 1,000 m downstream of the CTA (Figure 9-8).

9.2.5.2.3 Duration and Frequency of Monitoring

Sediment plumes and their redeposition processes will be monitored for a minimum of 3 months, and may be extended to 1 year if necessary.

The observation elements of the subsurface buoys are temperature, salinity, current speed, current direction, turbidity, dissolved oxygen, etc. Temperature, salinity, and dissolved oxygen are observed by probes carried by CTD, current speed and direction are observed by single-point current meter and ADCP, and sediment flux is observed by sediment trap.

Frequency: 1 time/min during the test. 1 time/5 minutes after the test and up to the first 3 months. 3 months to 1 year: for the hydrological element, the frequency of observation of current velocity, direction of flow, temperature, salinity, and seawater turbidity is 1 time/hour; for the chemical element, the sediment flux is set to 1 bottle/month.

9.2.5.2.4 Equipment Deployment/Recovery Program

Except for the master station, which was released from the surface, the rest of the monitoring equipment will be deployed on the seafloor by the Efficient Precision Deployment and Recovery System (EPDRS), an ROV-based system. Portable nodes, observation nodes and sampling base stations will be recovered by the EPDRS. Subsurface buoy and the master station will be released by the acoustic releaser and then floated up to the surface for recovery.

9.2.5.3 Post-test Monitoring

Phase III-1 is the period after the test when the environmental monitoring equipment is recovered. In this phase, an AUV will be used to navigate at a fixed altitude of 5 m above the bottom to obtain sediment thickness data for redeposition and seafloor video and photographs (Figure 9-25). Sediment samples will be collected using multicorer and box corer, and near bottom water samples will be collected by CTD.

In 2026 (Subphase III-2), a one-year post-test environmental monitoring will be conducted in the CTA, plume impact area and PRZ.
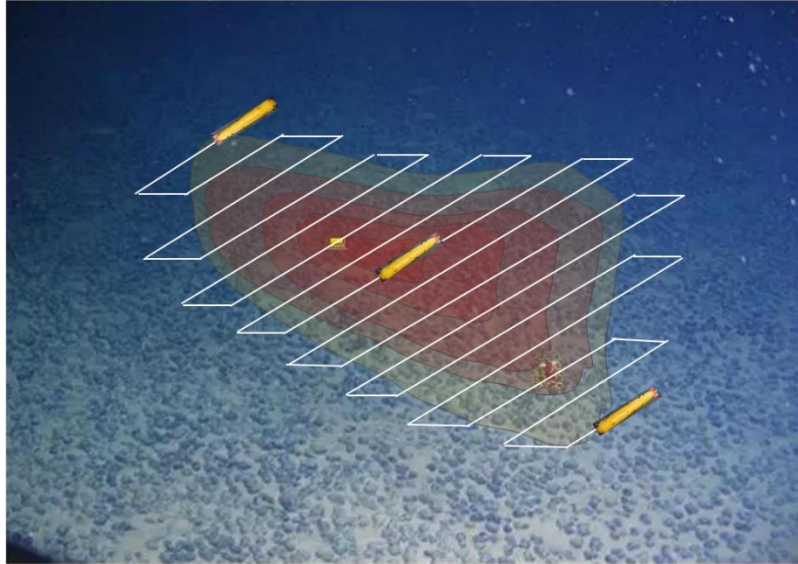
Figure 9-25 Path planning for thickness detection of redeposited sediment based on AUV

9.2.5.4 Long-term Monitoring

Long-term environmental impact monitoring will start in 2027, with impact monitoring at least at the 3rd, 5th and 7th years after the test, and if necessary, even monitoring for longer time periods.

9.2.5.5 Monitoring Parameters and Methods

9.2.5.5.1 Monitoring Parameters and Methods in the CTA

The monitoring parameters and methods at the different phases in the CTA are shown in Table 9-6.

Table 9-6 Parameters and methods of monitoring at different phases in the CTA

Monitoring parameters	Potential monitoring methods	Monitoring phases					
		I-1	I-2	II	III-1	III-2	IV
Physical and chemical parameters							
Depth of sediment disturbance by mining trucks	Mechanical measurement /Acoustic Detection/AUV				√		
Traces of lateral disturbance by mining trucks (microtopographic changes)	Mechanical measurement /Acoustic Detection/AUV				√		
Traces of mining truck operations (width, length)	Mechanical measurement /Acoustic Detection/AUV				√		
Volume and particle size of waste discharged from the	Collector mounted Sensors			√			

Monitoring parameters	Potential monitoring methods	Monitoring phases					
		I-1	I-2	II	III-1	III-2	IV
collector							
Plume particulate emissions and particle size (source strength)	In-situ pump filtration/turbidimeter/water collection			√			
Physical oceanography (turbidity, temperature, salinity, current velocity , current direction)	Lander system/Subsurface buoy	√	√		√		
Noise pollution	Hydrophones mounted on mining collector			√			
Near bottom layer seawater chemistry (DO, pH, nutrients, TOC, total alkalinity, heavy metals)	CTD sampling	√	√		√	√	√
Pore water chemistry (DO, pH, Eh, nutrients, TOC, heavy metals)	Multicorer sampling	√	√		√	√	√
Biological community							
redox system	Sediment Profile Camera	√		√	√	√	
Microorganisms	CTD/multicorer/pushcore sampling, eDNA analysis	√	√		√	√	√
Meiofauna	Multicorer/pushcore sampling, eDNA analysis, species identification	√	√		√	√	√
Macrofauna	Box-corer sampling, eDNA analysis, species identification	√	√		√	√	√
Megafauna	AUV/HOV/Deep-tow video and still photography system	√			√		√
Trace metal in organisms	Biological sampling, trace metal mesurement	√			√	√	√
Food web	Sampling, stable isotope method	√			√	√	√
Sessile/Mobile filter feeders	AUV/HOV/Deep-tow video and still photography system	√			√	√	√

9.2.5.5.2 Monitoring Parameters and Methods in the Plume Impact Area

The monitoring parameters and methods for the different phases in the plume impact area are shown in Table 9-7.

Table 9-7 Monitoring parameters and methods at different phases in the plume impact area

Monitoring parameters	Potential monitoring methods	Monitoring phases					
		I-1	I-2	II	III-1	III-2	IV
Physical and chemical parameters							
Particle flux and size	Sediment traps/in-situ pump filtration/water sampling	√		√	√	√	
Spatial extent of plume dispersion	AUV turbidimeter measurements/turbidimeters at subsurface buoys and observation nodes, ADCP observations/CTD turbidimeter measurements and profile water extraction analysis			√	√		
Thickness of redeposition sediment	Sediment Trap Box/Sediment Profile Camera Image Analysis/High Resolution Acoustic Detection			√	√		
Physical oceanography (turbidity, temperature, salinity, current velocity, current direction)	Subsurface buoy	√		√	√		
Noise pollution	Hydrophone	√		√			
Near Bottom Layer seawater chemistry (DO, pH, nutrients, TOC, total alkalinity, heavy metals)	CTD sampling	√			√	√	
	Sampling node			√			
Pore water chemistry (DO, pH, Eh, nutrients, TOC, heavy metals)	Multicorer sampling	√			√	√	√
	Sampling node			√			
Biological community							
Redox system	Multicorer/sediment profile camera	√		√	√	√	
Microorganisms	Multi-corer/sampling node	√		√	√	√	
Meiofauna	Multicorer /pushcore sampling, eDNA analysis and species identification	√			√	√	√
Macrofauna	Box corer sampling, eDNA analysis and species identification	√			√	√	√
Megafauna	AUV/HOV/Deep-tow video and still photography system	√			√	√	√
Scavenger	Lander trapping	√		√		√	√

Monitoring parameters	Potential monitoring methods	Monitoring phases					
		I-1	I-2	II	III-1	III-2	IV
Trace metal in Organisms	Biological sampling, trace metal Determination	√		√		√	√
Food web	Sampling, stable isotope method	√			√	√	√
Sediment community oxygen consumption	In-situ profiler or cabin measurement			√	√	√	
Sessile/Mobile filter feeders	AUV/HOV/Deep-tow video and still photography system	√			√	√	

9.2.5.5.3 Monitoring Parameters and Methods in the PRZ

The monitoring parameters and methods at the different phases in the PRZ are shown in Table 9-8.

Table 9-8 Monitoring parameters and methods at different phases in the PRZ

Monitoring parameters	Potential monitoring methods	Monitoring phases					
		I-1	I-2	II	III-1	III-2	IV
Physical and chemical parameters							
particulate matter flux	Sediment traps	√		√		√	
Physical oceanography (turbidity, temperature, salinity, current velocity, current direction)	Subsurface buoy	√		√		√	
Noise pollution	Hydrophone	√		√			
Near bottom layer seawater chemistry (DO, pH, nutrients, TOC, total alkalinity, heavy metals)	CTD sampling	√	√		√	√	√
Pore water chemistry (DO, pH, Eh, nutrients, TOC, heavy metals)	Multicorer sampling	√	√		√	√	√
Biological community							
Microorganisms	CTD/multicorer sampling, eDNA analysis	√	√		√	√	√
Meiofauna	Multi-corer sampling, eDNA and	√	√		√	√	√

	analysis/species identification					
Macrofauna	Box corer sampling, eDNA analysis/species identification	√	√	√	√	√
Megafauna	AUV/HOV/Deep-tow video and still photography system	√		√		√
Scavenger	Lander trapping	√			√	√
Trace metal in organisms	Biological sampling, trace metal determination	√		√	√	√
Food web	Sampling, stable isotope method	√		√	√	√

9.2.5.6 In-situ Experiments and Monitoring Programs

9.2.5.6.1 Sediment Coverage Experiment

Sediment coverage experiments will be conducted using the "Jiaolong" HOV or ROV with reference to experimental methods such as Mevenkamp et al. (2019). Follow these steps: (a) insert three stainless steel rings with a diameter of 25 cm and a height of 10 cm (Figure 9-26) into the undisturbed sediment on the seafloor for 5 cm depth to set the experimental areas. (b) rotate the handle of the releaser (Figure 9-27) to release the pre-treated sediments into the experimental areas, covering the seabed with about 2 cm, 5 cm, and 10 cm thick of sediment, respectively, (c) remove the releaser. (d) record the location and operation information. (e) A few days later, revisit the experimental areas, and use pushcores to take sediment samples in the experimental areas and the sediment in the nearby areas. (f) analyze and compare the abundance and species composition of meiofauna in the experimental areas and nearby sediments.
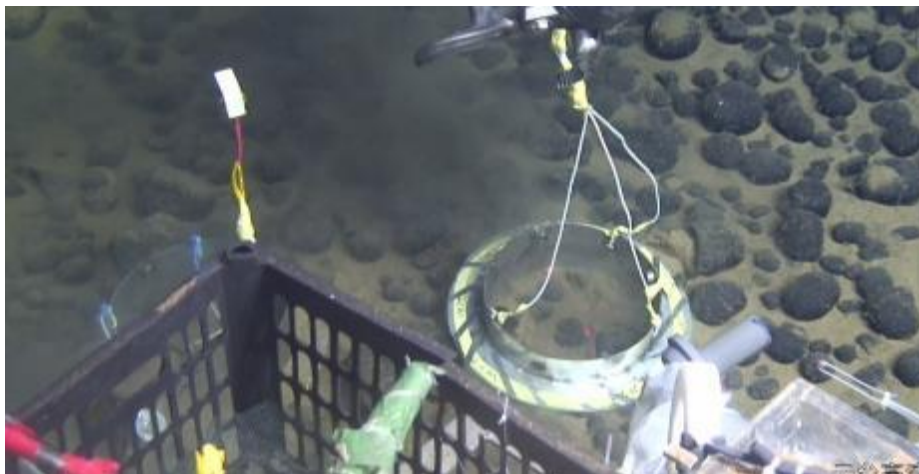
Figure 9-26 In situ sediment coverage experiment
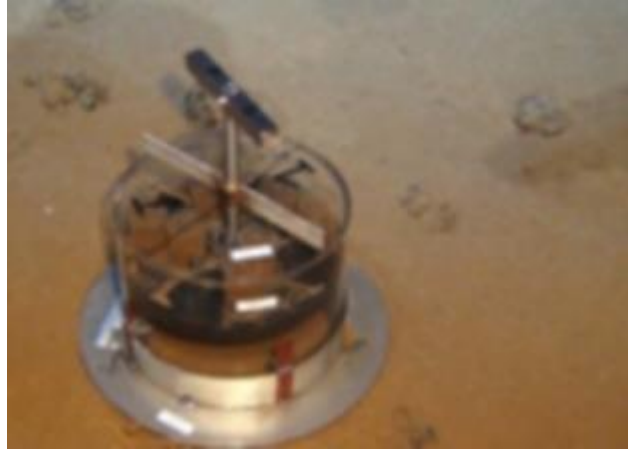
Figure 9-27 Sediment releaser device (Mevenkamp et al., 2019)

9.2.5.6.2 Heavy Metal Exposure Test

Referring to the method used by Kwan et al. (2019), heavy metal-treated food will be used as bait to trap benthic scavengers by Lander system, and the response of benthic scavengers to heavy metal exposure will be investigated by analyzing the genomes of the trapped animals.

9.2.6 Environmental Impact Assessment Follow-up (EIA follow-up)

Based on the baseline investigation before the test, monitoring data during and after the test, the EIA follow-up will be conducted by the following research:

- To monitor changes of the benthic community before and after the test and to assess the rate of recovery of the benthic community;

- To conduct in situ sediment coverage experiments to study the relationship between sediment plume re-sedimentation thickness and benthos mortality;

- To study the collector noise and biological response;

- To reveal bottom plume diffusion mechanisms by modeling high-resolution bottom plumes;

- To study the impacts of mining component tests on marine ecosystem functions, including the bottom food chain, and to assess the resilience and recovery of deep-sea ecosystem;

- To evaluate the effects of plumes and redeposition on benthos;

- To study the kinetic mechanisms of upward transport of suspended solid along seamount slope;

- To assess the potential environmental impacts of suspended ore collector and provide a scientific basis for the development of environment-friendly mining technologies.

9.3 Reporting

9.3.1 Supervision

To implement the relevant regulatory requirements, BPC will invite observers from the sponsoring State (China) and the ISA to board the experimental vessel to conduct supervisory activities.

9.3.2 Transparency

BPC has consulted with the ISA observer, the China Biodiversity Conservation and Green Development Foundation, and invited it to participate in relevant environmental monitoring and assessment activities. The company will also regularly disclose the progress of the experimental mining activities and related data to the public through its website or other media.

9.3.3 Research and Test Reports

The *Regulations on Prospecting and Exploration for Polymetallic Nodules in the Area* (ISBA/19/C/17) stipulates in Article 32 that contractors are required to report to the International Seabed Authority (ISA) on an annual basis. Specifically, it states:

"The contractor shall report annually in writing to the Secretary-General on the implementation and results of the monitoring programme referred to in paragraph 1 and shall submit data and information, taking into account any recommendations issued by the Commission pursuant to regulation 39. The Secretary-General shall transmit such reports to the Commission for its consideration pursuant to article 165 of the Convention."

In compliance with this provision, BPC is expected to submit an annual report to the ISA, detailing the execution and findings of the environmental monitoring and mitigation program (EMMP) related to the mining test activities. The report will assess the environmental impact based on the monitoring results and describe the compliance of the EMMP, addressing any recommendations made by the Legal and Technical Commission.

Additionally, BPC plans to regularly disclose the environmental monitoring outcomes and assessment results of the mining test activities on its website.

Furthermore, BPC intends to publish the findings of environmental impact monitoring research in scholarly articles within relevant journals and share the environmental monitoring results at contractor meetings or other international symposiums. This approach aligns with the ISA's commitment to transparency and the dissemination of knowledge for the benefit of the international community.

9.3.4 Incident Report

In accordance with regulation 33 of ISBA/19/C/17, the contractor shall promptly report in writing to the Secretary-General by the most effective means, any incident arising from activities which have caused, are causing or pose a threat of serious harm to the marine environment.

Incident reports to the ISA will include the following:
- Details of the incident
- Incident-cause analysis
- Actions taken at the incident site to avoid or mitigate any adverse environmental impacts
- Any corrective measures taken or likely to be taken
- Next steps to prevent the recurrence of similar incidents.

10 CONSULTATION

10.1 Public Consultation

From May 1, 2024, to June 6, 2024, the bilingual version of the *Environmental Impact Statement-Joint Test of Deep-sea Miner and Buffer Station in Beijing Pioneer Polymetallic Nodule Contract Area, Western Pacific* has been simultaneously released to the public on the ISA website and BPC's official website to solicit feedback from all relevant stakeholders.

10.1.1 Background

BPC plans to conduct a 1:5 scale polymetallic nodule joint test of deep-sea miner and buffer station in the southern piedmont of Magoshichi Guyot within the Block M2 of the contract area in the latter half of 2025. The aim is to verify the reliability of the suspended collection method and the buffer station joint test. Based on the environmental baseline data collected in advance and the environmental monitoring data during and after the test, an environmental impact assessment of the test activities will be carried out.

Moreover, following the concept of "Research-oriented exploitation", this test will be utilized as a significant opportunity to enhance understanding of the deep-sea and ecosystems. It will facilitate open research on relevant scientific issues in the deep-sea domain, providing a basis for the formulation of regulations for future deep-sea mining activities and the development of green mining technologies. BPC has prepared an environmental impact statement in accordance with the recommendations of the ISA - *Recommendations for the Guidance of Contractors for the Assessment of the Possible Environmental Impacts arising from Exploration for Marine Mineral in the Area* (ISBA/25/LTC/6/Rev.3). From May 1, 2024, to June 6, 2024, the bilingual version of the *Environmental Impact Statement-Joint Test of Deep-sea Miner and Buffer Station in Beijing Pioneer Polymetallic Nodule Contract Area, Western Pacific* has been simultaneously released to the public on the ISA website and BPC's official website to solicit feedback from all relevant stakeholders. BPC has updated this report according to stakeholders' comments and suggestions, and has supplemented it with relevant explanatory information.
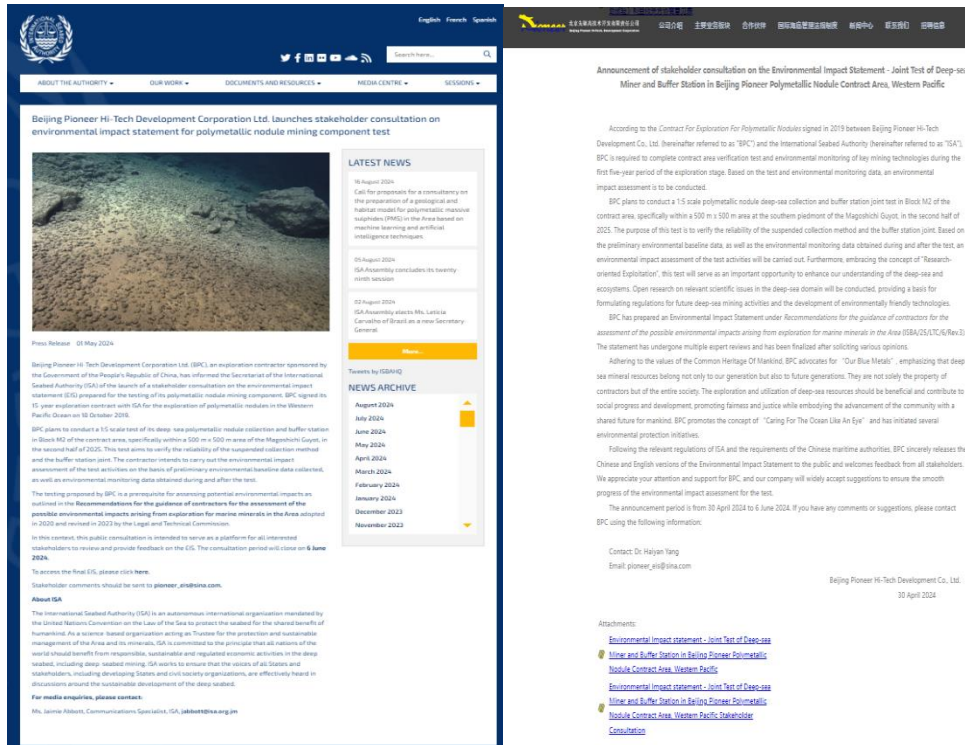
Figure 10-1 Public Stakeholder Consultation Statement (Left: News on the Official Website of the ISA; Right: News on the Official Website of the BPC)

10.1.2 Submitter

During the stakeholder consultation period, a total of 10 emails were received from international organizations/national governments including the UK government, Canada government, U.S. Observer Delegation to the International Seabed Authority, Deep Sea Conservation Coalition, etc. See Table 10-1 for the list of submitters.

Table 10-1 Submitter of Stakeholder Consultation

NO.	Government/Organization
1	China Biodiversity Conservation and Green Development Foundation
2	Deep Sea Conservation Coalition
3	World Wildlife Fund
4	UK government
5	Pew Charitable Trusts
6	Ocean Foundation
7	Deep-Ocean Stewardship Initiative
8	Oceans North
9	Canada government
10	U.S. Observer Delegation to the International Seabed Authority

10.1.3 Comments Content

BPC received a total of 308 comments, of which 12 were positive or appreciative comments. For example, the UK government mentioned that "The fully suspended nature of the Manta II sampling equipment reduces the impact on the seabed when compared to equipment that would be affixed to or deposited onto the seabed…This constitutes good practice, in our view, to reduce environmental impacts as far as possible", "It's valuable that, beyond monitoring of natural variability and impacts, in situ experiments are being developed to explore specific knowledge gaps concerning the effects of identified impacts", "The inclusion of a summarizing table of which environmental parameters have been collected, and whether they cover spatial, temporal, and depth variability, is highly valued and provides welcome transparency for parameters which were difficult to obtain".

There were 270 specific and relevant comments, covering the following 16 topics (see Figure 10-2 for the number distribution):

1） Baseline data

2） Collector test

3） Cumulative impacts

4） Ecotoxicology

5） Ecosystem function

6） Light impacts

7） Mitigation measures

8） Monitoring plan

9） Noise impacts

10） Plume

11） Reasonable identification of PRZ/IRZ

12） Policy and law

13） Stakeholder engagement

14） EIS text/figure update

15） Survey methods

16） Flocculation experiment
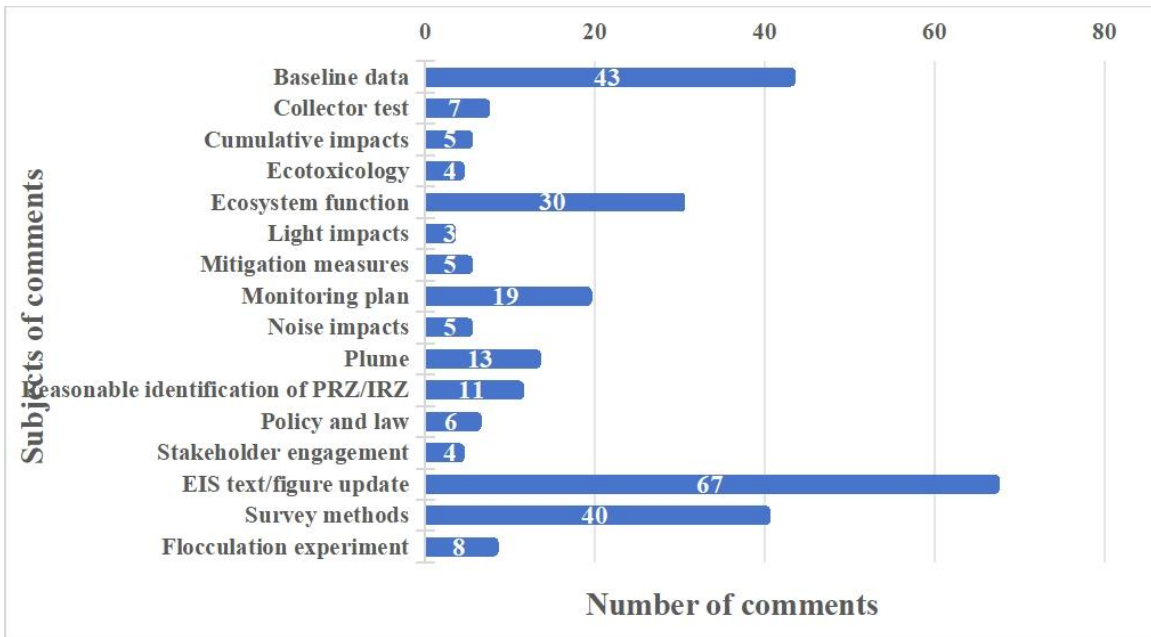
Figure 10-2 Chart of stakeholder consultation comments

10.1.4 Summary of Responses

In accordance with the relevant provisions of the Exploration Contract between the ISA and BPC, in order to fulfill our obligations under the contract, we intend to carry out the relevant test work in accordance with the agreed procedures to ensure that the objectives of the contract are successfully achieved and that the performance requirements under the contract are met. BPC has made appropriate changes to the EIS after careful consideration of the valid and relevant comments received from the stakeholder consultations. The following is a detailed response to the 16 key stakeholder topics of concern and describes the modifications made to the corresponding sections to ensure that the content of the EIS comprehensively covers the concerns of all parties.

1）Baseline data

The stakeholders including the UK government, Oceans North, Deep Sea Conservation Coalition and World Wildlife Fund have made suggestions for the missing baseline data, and part of the results of the 2023 cruise have been added to the report. However, the data on the subsurface buoys of the current meters and sediment traps deployed in the 2023 cruise will be added after the recovery of the 2024 cruise in the second half of 2024. BPC will continue to conduct environmental baseline surveys in 2024 (survey items and workloads are shown in Table 9-5), and the analysis results of the 2024 cruise and the results of the current meters and sediment trap subsurface buoys deployed in the 2023 cruise will be supplemented in the report.

a. Baseline content supplemented in the report

(1) Sediment parameters: BPC deployed 2 time-series sediment traps in Block M from October 2021 to September 2022, completed sample analysis in 2024, and obtained parameters including total mass of sinking particulates, flux of sinking particulates, percentage contents of total carbon and nitrogen, percentage contents of particulate organic carbon and calcium carbonate, and stable isotope values of particulate carbon and nitrogen. This report has supplemented relevant content (see "Section 4.3.5.8 Sediment Flux").

(2) Nanoplankton: Identification results of nanoplankton in 2022 have been added to "Section 5.2.1.4.2".

b. Environmental parameters planned to be surveyed in the 2024-2025 cruise

(1) Suspended Solid (SS): BPC has conducted a survey of SS concentrations in the water column during the cruise surveys of 2021-2023. Considering that the turbidimeter, an important monitoring probe for plume monitoring, is based on optical principles rather than the SS weighing method, it needs to be calibrated. Therefore, CTD water sampling in the 2024 cruise will prioritize meeting the measurement needs for deep-sea SS concentrations, increasing the sampling volume of deep-sea water to address issues with CTD turbidity and particle concentration ratio measurements.

(2) Nodule organisms: Analyze samples collected in 2023 and collect all nodule organisms found in box cores (including resource survey box cores) during the 2024 cruise.

(3) Total Organic Carbon in Water: Collect and analyze in the 2024 cruise.

(4) Trace nutrients: The extremely low levels of marine nutrients (nM level) in the upper ocean waters exceed the measuring limits of existing commercial instruments, but there are scientific instruments that can measure low concentrations of nutrients. This technology is extremely demanding for on-site analysts, and only a small number of professionals can operate it. The BPC team plans to organize professionals to participate in the cruise and analyze trace nutrients in the 2025 cruise.

(5) Sediment community oxygen consumption: It is planned to use the seabed experiment module or in situ profiler for measurements during the before-test baseline survey in 2025.

c. Explanation of baseline data

(1) Temporal variation: Several comments mentioned that baseline surveys were conducted in the same season, so there is no data on seasonal variation. BPC believes that the main purpose of the first three years was to study the annual changes in the environmental baseline, so the surveys were basically conducted in the same season. However, BPC also attempts to collect annual data to study the seasonal changes in environmental baselines. For example, chlorophyll a concentration is inferred from remote sensing of water color, the species and occurrence of mammals are analyzed based on hydrophone data, and data on currents, temperature, salinity, and material fluxes are obtained from subsurface buoys of current meters and sediment traps.

(2) The influence of La Niña and El Niño on the environmental baseline: Some comments also mentioned that the baseline survey should include La Niña and El Niño years. The BPC also believes that La Niña and El Niño events are the two most important factors affecting the inter-annual variation of the environmental baseline in the Pacific Ocean. It would be preferable to include La Niña and El Niño years in the environmental baseline survey. However, survey plans of BPC are determined one year in advance, and due to the difficulty in early forecasting of ENSO events, it is uncertain whether the survey period for the next year's cruise schedule will coincide with a La Niña or El Niño year. The last three years have been La Niña years, but we will still be conducting baseline surveys in the next few years, and there is still a chance that we will encounter El Niño events.

(3) Many environmental parameters only have a 1-year data: BPC has met the 3-year (2021-2023) requirement for most environmental parameters, as detailed in Chapters 4 and 5. Some samples collected in 2023 are still being analyzed, and two environmental baseline surveys will be conducted before collector test in 2024 and 2025 (see Section 9.2). The requirement for at least 3 years of baseline data can be met.

(4) Low species identification resolution: The identification results of the benthos are listed in the benthos species list in Block M of Annex 2-3, and most of them are identified to the genus level, not the phylum/order level. The main reasons for the low identification resolution of deep-sea organisms are as follows: firstly, the proportion of juveniles in deep-sea benthos is very high. For example, the juveniles of Nematoda, the most dominant group of deep-sea benthos, account for as high as 57.7% of the total number of Nematoda in the BPC's contract area. Due to the incomplete growth of juveniles, it is difficult to identify to the species level. The best level of biological identification may currently be to the genus/family. On the other hand, the deep sea has a high level of biodiversity, including

many new species, and the identification and publication of new species takes at least 2-3 years. Our identification of benthic species is still ongoing.

(5) Inaccurate identification of species: There are two errors in the English version of the EIS report. We checked the Chinese version and found that the errors were caused by the translation from Chinese to English. In Table 3-5, " *Daphnia magna* " should be " harpacticoides"; in Appendix I, the deep-sea mascot of the company, the genus *Rossia* of the family Sepiolidae, should be *Cirroteuthis* sp. of the family Cirroteuthidae.

(6) eDNA sampling method: Since the deep-sea species-level DNA sequence database is currently very weak, the number of species identified by the eDNA sampling is far less than that of traditional morphological identification. Therefore, the eDNA sampling method is only supplementary to the identification of deep-sea benthic species. However, we recognize that this method is an efficient and promising method. We have begun collecting eDNA samples since 2023, and plan to continue to expand the amount of eDNA samples collected in 2024. We plan to collect eDNA samples from all benthos sampling stations and establish a local DNA sequence database to provide a foundation for the future application of this method. This is also the direction in which the company is working.

2）Collector test

Stakeholders such as the UK Government, Deep Sea Conservation Coalition, Deep-Ocean Stewardship Initiative and others suggested that details of the test be provided.

According to the contract signed in 2019 between BPC and the ISA for the exploration of polymetallic nodules in the Northwest Pacific, BPC is required to complete contract area verification test and environmental monitoring of key mining technologies during the first five-year period of the exploration stage, and assess the environmental impact based on the test and environmental monitoring data. Since the signing of the contract, BPC has gradually advanced the research of deep-sea mining technology based on the GERIS (Green, Economy, Reliability and Robustness, Intelligence, and Safe) mining concept. By developing the "Manta" series of polymetallic nodule sampling test machines and collection test prototypes, it has eventually evolved into a green deep-sea mining system suitable for commercial use.

According to the concept of "research-oriented exploitation", this project plans to conduct a polymetallic nodule deep-sea collection and buffer station joint test to verify the reliability of the suspended collection method and the buffer station joint, while carrying out long-term environmental impact monitoring and assessment. Based on the environmental baseline data collected previously and the environmental monitoring data collected before, during, and after the test, the environmental impact assessment of the test is carried out. At the same time, research will be conducted on scientific issues related to the potential impacts of deep-sea mining, in order to develop environmental impact

mitigation measures for future deep-sea commercial mining plans and provide design basis for the development of deep-sea green mining technologies.

BPC plans to conduct a 1:5 scale polymetallic nodule deep-sea collection and buffer station joint test in a 500 m × 500 m area in the southern foothills of Magoshichi-no-Hoshi Seamount in Block M2 of the Northwest Pacific polymetallic nodule contract area in the second half of 2025. In the report, additional details have been included regarding the detailed diagram of collector component sampling test nodule discharges (refer to "Section 3.4.1.2 Test Area and Operation Path Design"), the calculation formula for sediment disturbance (refer to the "Executive Summary"), and plans are in place to collect more samples for geotechnical testing of surface sediments in the IRZ in future work. Based on the acquired data, research related to slope stability and foundation bearing capacity will be conducted to further assess the potential impact of collectors on sediment stability.

3）Cumulative impacts

Stakeholders such as the UK Government, Deep Sea Conservation Coalition, Oceans North, World Wildlife Fund and others suggested that the cumulative impacts need to be considered.

Since this test is only a single activity, it is not expected that cumulative impacts from multiple operations will occur. Cumulative impacts from different pressures from a single activity can be expected, but at this stage, there is limited publicly available information on the cause-effect activity-pressure-effect relationships for the target ecosystems and their components (i.e., populations and communities, habitats, and ecosystem functions) and the cumulative pressures that mining activities may exert on ecosystems and their components (Tamis et al., 2016). In particular in the abyssal Northwest Pacific, more data are needed to quantify the impacts of mining activities and to identify specific pressures and their cumulative impacts on ecosystem vulnerability and resilience.

Although some studies have documented the individual impacts of different mining pressures on species and ecosystems (Auguste et al., 2016; Mevenkamp et al., 2017), there is still a complete lack of studies on the cumulative and interactive effects of multiple stressors from deep-sea nodule mining. One of the main objectives of the monitoring study presented here is to summarize and statistically analyze the possible scale and scope of cumulative impacts using the results of different individual impact studies before and after the "Manta II" experiment.

In the report, cumulative impact-related model diagrams were added. Please refer to "Section 7.4 Cumulative Impact". The potential relationship between the activities and pressures of different ecosystem components is illustrated.

4）Ecotoxicology

Stakeholders such as the UK Government, Deep Sea Conservation Coalition, Deep-Ocean Stewardship Initiative and others suggested that the ecotoxicology needs to be considered.

Although there are many ecotoxicological studies, the limitations of these studies are also obvious, mainly in the following two aspects: (1) the studies are mainly based on shallow water species, because deep sea benthos are difficult to cultivate in the laboratory (except for some hydrothermal and cold seep organisms), so there is little possibility ofcarrying out toxicological experiments using living deep sea organisms; (2) most of the experiments used a single metal. Therefore, more research on the threshold of heavy metal concentration is needed to assess the potential toxicological risk of polymetallic nodule mining. BPC pays close attention to the progress of the ISA threshold establishment and MIDAS project, etc.

This project plans to collect muscles and seawater samples of benthic fish and invertebrate populations before, during, and after collector test using Landers and sampling stations for trace metal element analysis to monitor potential changes resulting from collector test activities (refer to "Section 9.2 Environmental Monitoring Program"). In addition, attempts are being made to use deep-sea organisms that can be cultured in the laboratory, such as hydrothermal and cold seep mussels, to begin trace metal toxicology experiments.

5）Ecosystem function

Stakeholders such as the China Biodiversity Conservation and Green Development Foundation, UK Government, Deep-Ocean Stewardship Initiative and others suggested that the impact of ecosystem function needs to be considered. In BPC's opinions:

(1) Food web analysis: Other components of the ecosystem have been sampled, except for megafauna and scavengers, as some reviews have pointed out that it is difficult and time-consuming to capture samples of megafauna. However, BPC has planned to deploy four sets of Lander traps for Megafauna and scavengers in 2024. At the same time, the "Jiaolong" HOV will conduct two dives in the BPC CTA and adjacent waters during the Western Pacific habitat survey cruise in August and September 2024 to collect some benthic samples to provide sample support for food web analysis (see Table 9-5)..

(2) Sediment community oxygen consumption: It is planned to use the seabed experiment module or in situ profiler for measurements during the before-test baseline survey in 2025.

(3) Ecosystem: Characteristics of basic ecosystem functions such as POC degradation and microbial activity will be added to the monitoring in subsequent work.

6）Light impacts

Stakeholders such as the Deep Sea Conservation Coalition, Deep-Ocean Stewardship Initiative and others suggested that the light impact needs to be considered.

Light pollution is defined as the introduction of light into an environment where there is no natural (i.e., sunlight) source of light. Light pollution may have an impact on the surface environment, as light from vessels can attract insects, birds, fish, sharks, cephalopods and other invertebrates, as well as marine mammals (DNV.GL, 2016).

Currently, known and potential impacts of light pollution from artificial light sources on marine ecosystems include: (a) inhibiting or altering vertical migration of zooplankton; (b) attracting seabirds to collide with brightly lit vessels or offshore engineering platforms; (c) extending the reliance of birds on visual foraging behavior from normal daytime to nighttime hours; (d) impeding and altering the colonization of the larvae of a number of invertebrates; (e) triggering aggregations of fish resulting in increased predation; (f) causing disruption of reproductive behavior of corals, etc., which is controlled by moon phases; (g) interfering with the navigation of adult sea turtles, thereby affecting their reproduction, and interfering the navigation of sea turtle hatchlings, thereby affecting their survival (Davies et al. 2014).

Due to the short duration and small scale of this experiment, the effects of light on organisms were only near the test area and were temporary in nature. During nighttime operations, the ship's lighting will be minimized as much as possible while ensuring operational safety, and upward light will be avoided to reduce the impact on bird activity. During the collector test period, light is primarily for the safety of the collector, with limited forward and downward light control and the use of cool light sources to minimize potential impacts on organisms. And BPC will observe the behaviors of benthos and scavengers in response to light through the video monitoring equipment on the collector main body and the AUV.

7）Mitigation measures

Stakeholders such as the China Biodiversity Conservation and Green Development Foundation, UK government, Oceans North, Deep Sea Conservation Coalition and others commented on the mitigation measures. In BPC's opinions:

(1) Collection test mitigation measures: Measures for recovery or restoration related to the collector test are not listed in the report mainly on the basis of the following reasons: Firstly, due to the small scale of the CTA and the plume impact area in this collector test, and the short duration of the test, it will not cause the extinction of benthos and changes in benthic ecosystem function in the contract area and adjacent waters. Secondly, after this test, long-term environmental impact monitoring will be conducted in the CTA and the plume impact area to study the natural recovery rate of benthos, community resilience, and the resilience of the benthic ecosystem. This aims to enhance the understanding of the self-

recovery/restoration potential of deep-sea ecosystems, providing a scientific support for designing mining path rules and restoration/recovery plans during future commercial exploitation. Thirdly, it is not appropriate to add anthropogenic substances and restoration measures to deep-sea ecosystems without clarifying whether these measures are effective or not, avoiding causing secondary pollution.

(2) Assessment of Physical and Chemical Environmental Impacts and Proposed Mitigation Measures: Enhance the explanation and description of the assessment of physical and chemical environmental impacts and proposed mitigation measures, including seabed nodule retention, in "Section 6.7 Proposed Mitigation Measures".

8）Monitoring plan

Stakeholders such as the UK government, Canada government, U.S. Observer Delegation to the International Seabed Authority, Pew Charitable Trusts, Oceans North, Deep-Ocean Stewardship Initiative and others commented on the monitoring plans. In BPC's opinions:

(1) Deployment of plume monitoring equipment and whether it can fully capture the plume: Based on the bottom current data obtained from the baseline survey, the plume dispersion under 10 operating conditions from July to October 2025 was simulated (see Chapter 6), providing a scientific basis for the deployment of monitoring equipment. Figure 9-23 in Chapter 9 only shows the plan for the horizontal deployment of monitoring equipment under the strong northwestward current in August. There are corresponding deployment plans for different currents, and the relative distance between the equipment remains the same. Only the direction of the fan-shaped monitoring system needs to be adjusted. Before the 2025 collector test, bottom current monitoring needs to be carried out. The bottom current data is transmitted from the two-way real-time communication master station to the ship's laboratory to determine the real-time current direction and velocity, and then the monitoring equipment deployment plan is determined based on the flow speed and direction. Please see the details at section 9.2.5.2.1.

(2) Why is seamount environmental monitoring being carried out: The joint test mentioned in this report took place in the Magoshichi Guyot foothill area. Although the plume from this test is unlikely to affect the seamount based on the current simulation results (Figure 9-3), there may be potential impacts during future commercial mining. Based on the precautionary principle, a seamount monitoring area is proposed to be established in the southern foothills and slopes of the Magoshichi Guyot (Figure 9-3). Magoshichi Guyot is considered an Ecologically or Biologically Significant Marine Area (EBSA) and a vulnerable marine ecosystem (VME) (Du Preez et al., 2023), after the sediment and nodule debris in the mining plume settle, physical oceanographic processes such as mesoscale eddies in the ocean surface can cause sediment resuspension, which can

reach heights of hundreds of meters (Kim et al., 2021; Gardner et al., 2017; Kontar et al., 1994). During commercial mining, due to cumulative effects, there is a possibility that these resuspended particles may diffuse towards the foothills of the seamounts. Additionally, the presence of secondary circulation on seamount slopes (Figure 9-4, Xie et al., 2023) poses a risk of upward transport of these suspended particles along the seamount slopes. Therefore, the project team plans to carry out monitoring and research to determine whether or not polymetallic nodule mining in basin has an impact on the adjacent vulnerable ecosystems such as seamount, and the extent of such impact. These efforts will provide a basis for environmental impact assessment of larger-scale mining tests or commercial mining activities in the future.

(3) IRZ/PRZ monitoring parameters and methods: See Tables 9-6 to 9-8 for details. In addition to monitoring the plume, BPC scheduled AUV (optical) and box-corer and multicorer sampling in the IRZ/PRZ both before and after the test to monitor the effects on benthic organisms.

9）Noise impacts

Stakeholders such as the UK government, World Wildlife Fund, Oceans North, Deep Sea Conservation Coalition, Deep-Ocean Stewardship Initiative and others commented on the noise impacts.

Section 4.3.6 has added descriptions of the locations and frequency bands for noise collection, along with an explanation for the "missing data in November in the figures". A comparative noise analysis of the Manta II and the small tracked mining vehicle prototype of the Dutch company IHC has been added to section 7.2.4. In 2023, one hydrophone was deployed in both the IRZ and the PRZ, and will be recovered in September 2024. It is expected that one-year passive acoustic data will be obtained for comparison. In 2024 and 2025, hydrophones will continue to be deployed to collect noise data before and during collector test to assess the impact of noise generated by the collector test on the deep-sea environment.

10）Plume

Stakeholders such as the UK government, Canada government, Pew Charitable Trusts, Oceans North, Deep-Ocean Stewardship Initiative and others commented on the plume. In BPC's opinions:

(1) FVCOM (Finite Volume Community Ocean Model) is a three-dimensional unstructured grid primitive equation numerical model. It uses triangular grids in the horizontal direction and a generalized terrain-following coordinate system in the vertical direction. It includes a sediment transport module for sediment dynamic processes and has been proven effective for simulating sediment dynamics (Chen et al. 2003, 2006, Ge et al. 2015, 2020, Li et al. 2023). In the EIS report, we have added an introduction to the sediment

transport module and parameter settings in "Section 6.2". There were no surface discharges in this test, thus no surface plumes were generated.

(2) Based on the suspended sediment background concentration and the effective monitoring range of the monitoring equipment, the boundary values of suspended sediment concentration and the boundary values of re-deposition thickness were modified and figures and statistics were updated. An introduction of the sediment transport module and parameter settings was added. Model input settings were further clarified. Descriptions of the sediment plume model were added. In 2025, data (including near-field and far-field data) will be collected during collector test to establish and validate a near-field turbidity model, which will also provide a good basis for future deep-sea mining plume model.

(3) Base on stakeholders' suggestions, plume dispersion simulation experiments with a fine-grained particle size of 0.012mm were added. The simulation results have been appended to "Section 6.2.3" and "Appendix III".

11）Reasonable identification of PRZ/IRZ

Stakeholders such as the UK government, Pew Charitable Trusts, Deep-Ocean Stewardship Initiative and others commented on the reasonable identification of PRZ/IRZ.

The IRZ and PRZ selection are primarily based on the principle of similarity (see Table 3-1 for details).

(1) Geological environment similarity: both are located in the foothills of seamounts, with similar water depths, and the sediment types are deep-sea clays, with siliceous debris dominating the material composition.
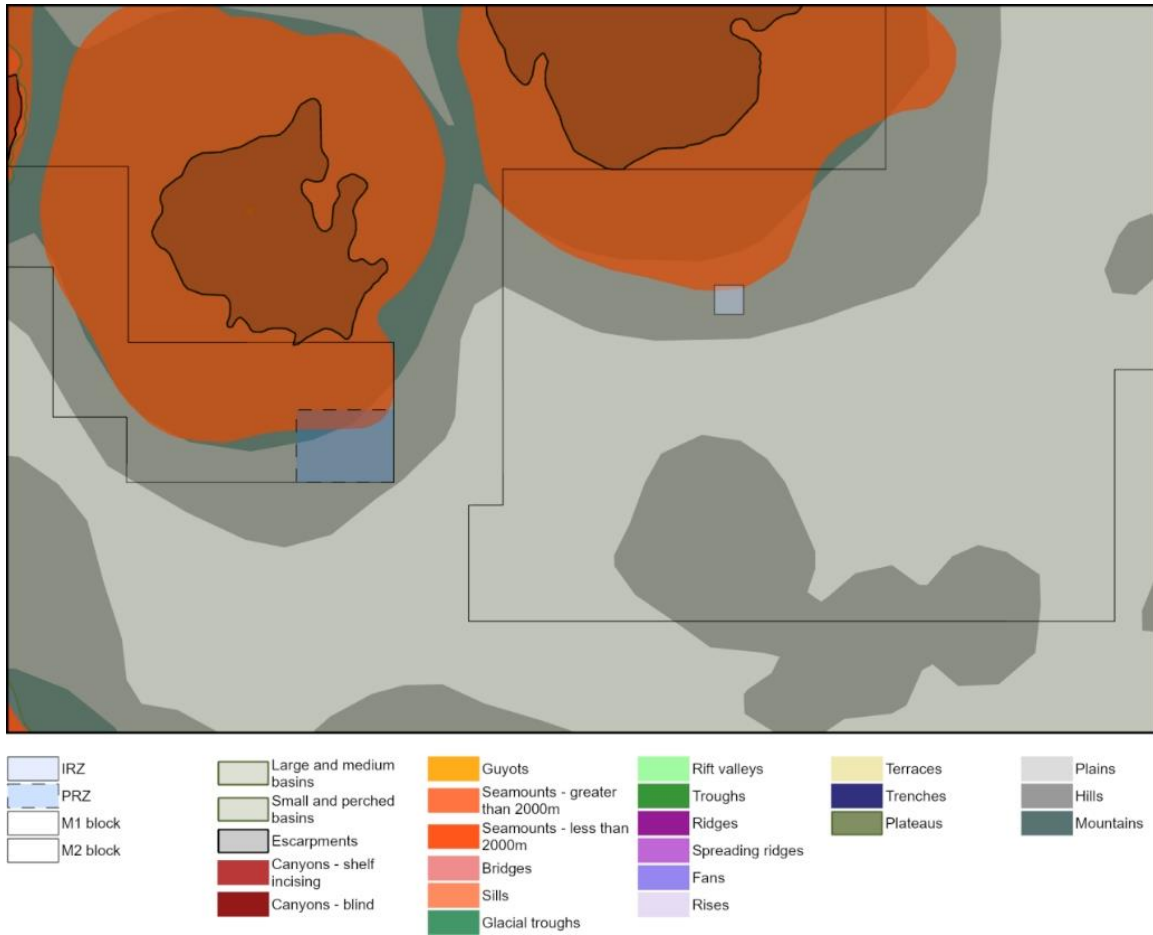
Figure 10-3 Seafloor geomorphic features map of Block M(Harris et al. 2014)

The fan-shaped area on the southern side of the Matsuzaki Guyot covers approximately 2900 km², with a slope of about 3°, echo intensity around −30 dB, features symmetrical cross-sections and sinuous-shaped to straight wave peaks (Wang et al., 2024). The predominant nodule types in the region are large to medium-sized ellipsoidal and spherical nodules. The fan-shaped area on the southern side of the Magoshichi Guyot covers about 2800 km², with a slope of around 3°, scatter intensity approximately -26 dB, and characterized by asymmetrical cross-sections and sinuous-shaped wave peak (Wang et al., 2024). The main nodule types in the area are large to medium-sized ellipsoidal and spherical nodules.

The PRZ is situated in the southwest part of the fan-shaped area, approximately 50 km from the klint of the Matsuzaki Guyot summit; while the IRZ is located in the southern part of the fan-shaped area, about 50 km from the klint of the Magoshichi Guyot summit. The two zones have similar geological settings, nodule types and distribution characteristics (Yao et al., 2024), but there are obvious differences in nodule abundance and coverage.

(2) Physico-chemical environmental similarities: Bottom flows, sediment geochemical characteristics and total mass fluxes of sinking particulate matter are all similar.

(3) Biological community similarities: chlorophyll *a*, primary productivity, pico-, micro-, nanoplankton, and zooplankton abundance were all relatively similar; Meiofaunal and Macrofaunal abundance were similar, species composition was comparable, and the dominant taxa were essentially the same; and Megafaunal species composition was similar, and most of the dominant species were also the same (Please find the details at Table 3-1).

12）Policy and law

Stakeholders such as the China Biodiversity Conservation and Green Development Foundation, Canada government and others commented on the policy and law.

Many thanks to the stakeholders for adding to the 2024 REMP workshop. BPC has collated Section 2.1.1, including relevant regulations, recommendations and standard guidelines developed by the ISA and other international and regional agreements relevant to deep sea activities. Following the received suggestions, we have further supplemented the Chinese domestic laws, regulations, and normative documents as outlined in section 2.2 including specific guidance on domestic legal obligations under the Deep Seabed Law in respect of the management system for exploration activities, the environmental protection system, and the management of scientific research and information, and adds references to the "Marine Environmental Protection Law of the People's Republic of China", "Regulation on the Prevention and Control of Vessel-induced Pollution to the Marine Environment", "Maritime Traffic Safety Law of the People's Republic of China", and other relevant domestic laws, regulations and standards, and A series of national standards for international seabed area surveys are also introduced and cited. We also added sections 2.3, 2.4, and 2.6. Regarding the "Environmental Impact Assessment (EIA) considerations for the missing Western Pacific REMP", we believe that the ISA currently only requires the development of a REMP before commercial exploitation. This joint test is only a small-scale collector test, part of the exploration phase of mining component trials, and not a commercial mining activity. Therefore, it does not relate to the REMP.

13）Stakeholder engagement

Stakeholders such as the World Wildlife Fund, Deep Sea Conservation Coalition, Pew Charitable Trusts, Ocean Foundation and others commented on the stakeholder engagement.

In accordance with the relevant provisions of the Exploration Contract signed between the ISA and BPC, in order to fulfill our obligations under the contract, we will carry out the relevant test work in accordance with the agreed procedures to ensure the successful achievement of the contractual objectives and to comply with the performance

requirements stipulated in the contract. BPC has made appropriate revisions to the EIS after giving careful consideration to the valid and relevant comments received from the stakeholder consultation.

Currently, BPC has made general comments on the stakeholder consultation and divided the stakeholder comments into different topics for summary responses, which are supplemented in Chapters 2 and 10, and plans to organize an international workshop in the second half of 2024 to invite stakeholders (organizations/individuals) to discuss and respond to the contents of this EIS and the consultation comments.

14）EIS text/figure update

Stakeholders such as the UK government, Canada government, Deep-Ocean Stewardship Initiative and others commented on the text/figure update.

In response to suggestions from stakeholders, we have made revisions and additional descriptions to the EIS executive summary, chapters 1, 2, 3, 4, 5, 6, 7, 9 and 10, as well as annexes I-III, and have also updated some of the images.

15）Survey methods

Stakeholders such as the UK government, U.S. Observer Delegation to the International Seabed Authority, World Wildlife Fund, Pew Charitable Trusts, Deep Sea Conservation Coalition, Deep-Ocean Stewardship Initiative and others commented on the survey methods.

As requested by stakeholders, we have added the methods for sampling, processing, and analysis of geology, physical oceanography, chemistry, biological environmental baseline parameters. For more details, please refer to Appendix IV. The geological baseline includes topographic and geomorphological data such as multibeam bathymetry, sediment parameters such as surface sediment type, surface sediment Eh and pH, elemental geochemistry, mineralogical characteristics, sediment pore water, and mechanical characteristics of the sediment, as well as methods of collection of data on polymetallic nodule parameters, such as abundance, coverage, physical properties, nodule type, and nodule elemental content, and means of assessing their quality, and the physical oceanic baseline includes data on the subsurface buoys, temperature and salt structure, surface currents, meteorology, and noise. Physical marine baselines include subsurface buoys, temperature and salt structure, surface currents, meteorology, noise and other data survey equipment, analysis methods and quality assessment tools. The chemical baseline mainly includes: pH, dissolved oxygen (DO), total alkalinity (TA), nitrate (NO_3^--N), nitrite (NO_2^--N), ammonium (NH_4^+-N), phosphate (PO_4^{3-}-P), silicate (SiO_3^{2-}-Si), suspended particulate matter (SS), particulate organic carbon (POC), and other investigative parameter analysis methods, quality assurance and control means. The baseline of the biological community includes the survey techniques, data processing methods and quality assessment means for

the elements of chlorophyll *a* and photosynthetic pigment microorganisms, microphytoplankton, phytoplankton, zooplankton, post-habitat meiofauna, benthic protozoa, macrofauna, megafauna, scavengers, fishery resources, seabirds, sea turtles and mammals, and primary productivity.

Regarding the size of the macrofauna sieve: All previous environmental guidelines, including ISBA/25/LTC/6/Rev.1, recommended using a 250 μm sieve, and the macrofauna sieve size was subsequently adjusted to 300 μm. However, ISBA/25/LTC/6/Rev.3 also states: "Contractors can continue to use the sieve size they previously used to ensure that the data are compatible... If contractors decide to continue to use a 250 μm sieve, then interpretation of the results will require some intercalibration between the two sieve sizes." According to Gage et al. (2002), a study of box-corer samples collected at a water depth of 1900 m, using a 300 μm sieve would result in the loss of some macrofauna, with a 3.5% decrease in abundance and a decrease in the number of species (see Table 10-2), and the deeper the water, the higher the oligotrophy, the smaller the benthos, and the higher the proportion of macrofauna that will be missed when using a 300 μm sieve, Therefore, the ISO 22787 standard issued by ISO in 2023 also recommends a 250 μm sieve for macrofauna. Therefore, we use a 250 μm sieve for macrofauna.

Table 10-2 Diversity statistics applied to pooled data from box-core samples (total biomass, no, of individuals, no. of species) by sieve size

Diversity index	Sieve size (mesh, mm)				
	1.0	0.5	0.425	0.3	0.25
Shannon's H' (log base 2)	5.71	5.83	5.85	5.85	5.89
Pielou's J'	0.87	0.81	0.79	0.79	0.79
Simpson's diversity index $(1/D)$	31.88	22.04	21.66	23.20	24.27
Berger-Parker $1/d$	7.82	5.69	5.79	6.32	6.52
$E(S_{258})$	93	87.23	87.39	84.47	85.01
Total biomass (g 0.5 m^{-2})	0.940	0.987	0.998	1.002	1.003
Total N (0.5 m^{-2})	258	820	1094	1334	1383
Total S (0.5 m^{-2})	93	149	165	169	173

16）Flocculation experiment

Stakeholders such as the Canada government, Deep-Ocean Stewardship Initiative and others commented on the flocculation experiment.

While the flocculation experiments and their data are not required by the "*Recommendations for the Guidance of Contractors for the Assessment of the Possible Environmental Impacts arising from Exploration for Marine Mineral in the Area*" (ISBA/25/LTC/6/Rev.3), considering the re-suspension and re-deposition of plumes and

sediments and their potential impact on benthos and seafloor sediment characteristics, we conducted sediment flocculation experiments.

In situ observations of flocculent particle settling are challenging tasks. In the regional environmental impact analysis of mining activities, we have not seen any experimental reports regarding in situ observations of flocculent particle settling. Currently, we believe that in situ observations of flocculation and settlement of resuspended solid from deep-sea mining are technically challenging. Therefore, we can only refer to the previous methods to generate flocculation in the laboratory and observe the settling rate to provide parameters for following numerical simulations. The flocculation experiments in this report were on the basis of laboratory studies of flocculent particle settling rates by Manning et al. (2010), Manning et al. (2011), MacDonald et al. (2013), etc. These experiments were conducted by camera-recording the flocculating particles inside a transparent settling tube to obtain their settling rate. Our experiments, similar to those of Manning et al. (2010), Manning et al. (2011), and MacDonald et al. (2013), encountered the issue of wall effects as suggested by experts. However, in our flocculent particle settling rate experiments, we specifically focused on particles located in the central region of the settling tube to minimize wall effects.

As acknowledged by experts, our experiments were limited. Experts noted that we only measured settling rates for 35 flocculent particles, which is a relatively small dataset but still statistically obvious (greater than 30). Our experiments served as preliminary observational studies. Through these experiments, we confirmed that (1) flocculent particles are indeed generated during sediment re-suspension in polymetallic nodule areas, (2) settling rates of larger flocculent particles were recorded (limited to flocculent particles with diameters greater than 150 μm observable by our experimental setup), and (3) the settling rates of flocculent particles we obtained were similar to those reported by Oebius et al. (2001).

Factors such as the size and concentration of re-suspended particles generated during actual deep-sea mining (related to sieving and stirring in experiments) require further experimental observations and research. We are committed to collaborating with scientists to gain a deeper understanding of the flocculation settling characteristics of resuspended particles in deep-sea mining activities.

References

Chen, C., Beardsley, R., & Cowles, G. (2006). An Unstructured Grid, Finite-Volume Coastal Ocean Model (FVCOM) System. *Oceanography*, *19*(1), 78–89.

Chen, C., Zhu, J., Beardsley, R. C., & Franks, P. J. S. (2003). Physical-biological sources for dense algal blooms near the Changjiang River. *Geophysical Research Letters*, *30*(10), 2002GL016391.

Davies T.W., Duffy J.P., Bennie J., Gaston K.J., The nature, extent, and ecological implications of marine light pollution. Front Ecol Environ. 2014,12(6):347–355. https://doi.org/10.1890/130281.

DNV GL . Recommended Practice. Managing environmental aspects and impacts of seabed mining. DNV GL-RP-O601 Edition September, 2016.

Du Preez, C., Amon, D. J., Baco, A. R., Best, M., Clyde, G., Colaço, A., ... & Tunnicliffe, V. (2023). *Identification of Ecologically or Biologically Significant Marine Areas (EBSAs) in Areas Beyond National Jurisdiction (ABNJ): the Northwest Pacific Seamounts*. Fisheries and Oceans Canada, Science Branch, Pacific Region, Institute of Ocean Sciences.

Gage J.D., Hughes D.J. and Vecino J.L.G. Sieve size influence in estimating biomass, abundance and diversity in samples of deep-sea macrobenthos. Marine ecology. Progress series, 2002-01, Vol.225, p.97-107.

Ge, J., Chen, C., Wang, Z. B., Ke, K., Yi, J., & Ding, P. (2020). Dynamic Response of the Fluid Mud to a Tropical Storm. *Journal of Geophysical Research: Oceans*, *125*(3), e2019JC015419.

Ge, J., Shen, F., Guo, W., Chen, C., & Ding, P. (2015). Estimation of critical shear stress for erosion in the C hangjiang E stuary: A synergy research of observation, GOCI sensing and modeling. *Journal of Geophysical Research: Oceans*, *120*(12), 8439–8465.

Harris, P. T., Macmillan-Lawler, M., Rupp, J., & Baker, E. K. (2014). Geomorphology of the oceans. *Marine Geology*, *352*, 4-24.

ISO 22787:2023(E). Marine environmental impact assessment (MEIA) — Technical specifications for marine biotic surveys in the international seabed area — General principles. ISO, Published in Switzerland, July 10, 2023.

Li, L., Wang, J., Zheng, Y., Yao, Y., & Guan, W. (2023). Fluid Mud Dynamics and Its Correlation to Hydrodynamics in Jiaojiang River Estuary, China. *Ocean Science Journal*, *58*(1), 8.

MacDonald, I. T., Vincent, C. E., Thorne, P. D., & Moate, B. D. (2013). Acoustic scattering from a suspension of flocculated sediments. *Journal of Geophysical Research: Oceans*, *118*(5), 2581-2594.

Manning, A. J., Baugh, J. V., Soulsby, R. L., Spearman, J. R., & Whitehouse, R. J. S. (2011). Cohesive sediment flocculation and the application to settling flux modelling. *Sediment Transport*, 91-116.

Manning, A. J., Langston, W. J., & Jonas, P. J. C. (2010). A review of sediment dynamics in the Severn Estuary: influence of flocculation. *Marine Pollution Bulletin*, *61*(1-3), 37-51.

Oebius, H. U., Becker, H. J., Rolinski, S., & Jankowski, J. A. (2001). Parametrization and evaluation of marine environmental impacts produced by deep-sea manganese nodule mining. *Deep Sea Research Part II: Topical Studies in Oceanography*, *48*(17-18), 3453-3467.

Tamis, J. E., de Vries, P., Jongbloed, R. H., Lagerveld, S., Jak, R. G., Karman, C. C., Van der Wal, J. T., Slijkerman, D. M., & Klok, C. Toward a harmonized approach for environmental assessment of human activities in the marine environment. *Integrated Environmental Assessment and Management*, 2016, *12*(4), 632–642. https://doi.org/10.1002/ieam.1736.

Wang, X., Li, H., Cheng, Y., Yao, P., Chu, F., Ma, W., Wang, H., Lv, S., Li, X., Li, Z., Zhang, W., & Dong, Y. (2024). Submarine Morphological Description of the Ancient Archipelagic Aprons in the Marcus–Wake Seamount Group, Northwestern Pacific Ocean. *Journal of Marine Science and Engineering*, *12*(4), 670.

Yao P., Li H., Wang X., et al. (2024). Geological and oceanographic constrains on the deposit of ferromanganese nodules on the archipelagic aprons of seamounts, Manuscript submitted for publication.

Xie, X., Liu, X., Chen, Z., Wang, Y., Chen, D., Li, W., & Zhang, D. (2023). Pure Inertial Waves Radiating from Low-Frequency Flows Over Large-Scale Topography. *Geophysical Research Letters*, *50*(4), e2022GL099889.

10.2 Public Activities

Initiative of Blue Eye Actions

To all who love the blue sea,

The sky is vast and the seas are grand,
Blue, a color simultaneously eyed across the land.

Born on land, yet we're drawn to the waves,
Sharing joys with them as the tide timely behaves.

Exploring the secrets of oceans in the eyes of the beholder,
From azure to navy, I assumed the deeper would be blueishly bolder.

Alas, descending to the seabed, I found a solemn plight,

Corals strangled with plastic bags -- which may be caused by one of your careless blight.

Action, let's take actions now, 'tis a deep sea fight,
Let's end the pollution, with all our might.

Let's return the blue hope to the ocean's deep,
And restore its original beauty, for all to keep.

Note: "DONGCHA" AUV is an autonomous underwater vehicle (AUV) with near-bottom optical fine survey and measurement system developed by the BPC in collaboration with the Shenyang Institute of Automation, Chinese Academy of Sciences. "Manta" is a new deep-sea polymetallic nodule in-situ collecting technology verification platform developed by the BPC. "Shenhaibaobao" is the deep-sea mascot chosen by the BPC with the scientific name of the ear-shaped *Cirroteuthis* sp..

10.2.1 Live Linking Activities for "Manta" track visits

As mentioned in Chapter 3 in report, "Manta", the polymetallic nodule sample-collecting device, which was completed in October 2022, has provided a new technological idea for the development of a sustainable green collecting system for polymetallic nodules. The Manta test conducted by the BPC in 2022 has also attracted a wide range of attention.

In July 2023, the "Manta" sampling track was revisited by the DY80 cruise using the "Jiaolong". In order to improve the understanding of the Manta experiment and the stakeholder consultation process, on July 14, 2023, the BPC organized media organizations such as China.org.cn, China Natural Resources News, BlueRibbon Ocean Conservation Association, and WeChat Official Account "Creek's Life in the Ocean", and teachers and students from Beijing No. 5 Middle School to link up with the research team in DY80 cruise. They communicated about the revisit of the "Manta" sampling track which took place in October 2022. During the meeting, the chief of the cruise, Dr. Zhang Dongsheng, said, "The track is clear and there is almost no nodule remained, which shows the high sampling efficiency of the 'Manta'. Besides that, the track of 'Manta' formed a special picture on the seafloor and purple sea cucumbers were found near the track." There was basically no plume left on the surface of the nodules near the sampling area, which fully reflects its technical advantages of excellent sampling performance and low disturbance to the seafloor environment, and its adoption of the suspended marching sampling technology

provides a new technological idea for the future development of a green collecting system for polymetallic nodules.

Figure 10-4 Revisiting one of the "Manta I" track

Figure 10-5 Revisiting one of the "Manta I" track

10.2.2 Activities of "Blue Eyes in Action"

On August 9th, 2023, the BPC, the contractor of the polymetallic nodule mining area in the ISA, in collaboration with the China Natural Resources News and the Second Institute of Oceanography of the Ministry of Natural Resources (SIO), organized a public nonprofit environmental protection activity entitled "Blue Eyes in Action" at the dock of Zhoushan in Zhejiang Province where base of the SIO is located.

Leaders and representatives of the Department of Treaty and Law in the Ministry of Foreign Affairs of the People's Republic of China, China Ocean Mineral Resource R&D

Association, the BPC, the Second Institute of Oceanography, the Third Institute of Oceanography, China Natural Resources News, the China Biodiversity Conservation and Green Development Foundation (CBCGDF), Shenyang Institute of Automation of Chinese Academy of Sciences, Zhejiang University, Zhejiang Ocean University, the first cruise of the research team in DY81 cruise, international trainees from Kenya JOHN TROON OMONDI, LAWRENCE TARAKWA KOTEENE, and Malaysia SUSIE CAHYANTI BINTI TASMAN for offshore exploration training, and the public such as "Ningbo Sunshine Teenager" participated in this activity. Dr. Zhou Jinfeng, Vice President and Secretary General of the CBCGDF, delivered the opening remark.

The theme of the event was "To know the deep-sea ecosystem". The event invited the public, including participating leaders, oceanographic researchers on "Da Yang Hao", local Zhoushan residents and primary and middle school students, to do coloring on pictures of marine animals in order to improve the public's understanding of the oceans, in particular deep-sea creatures, and to achieve the purpose of publicizing the marine environment protection to the public and deepening the public's awareness of the marine environment conservation.

Figure 10-6 "Blue Eyes in Action" site

Figure 10-7 Teenagers in "Blue Eyes in Action"

Figure 10-8 International trainees in "Blue Eyes in Action"

It is reported that this activity is the third-time "Blue Eyes in Action" public environmental protection activities initiated by the BPC. In the activity, the representative of the organizer read out the initiative of "Blue Eyes in Action", and the Marine Division of CBCGDF responded to the "Blue Eyes in Action", calling on everyone to "love the ocean as much as we love our eyes". "Ningbo Sunshine Teenager" actively participated in the activity and presented the "Wave Treading Dance" and "Military Song Ceremonial Movement".

Figure 10-9 "Blue Eyes in Action" initiative for the protection of the marine environment

Figure 10-10 Teenager dance in "Blue Eyes in Action"

11 GLOSSARY, ABBREVIATIONS & ACRONYMS

Glossary

TERM	DEFINITION
Autonomous underwater vehicle	Unpiloted and cableless submersible that can operate according to predetermined procedures or adapt to environmental changes
Benthic boundary layer	Pertaining to the layer of water immediately above the ocean bottom water layer/sediment interface that is influenced by the bottom.
Box-corer	Sediment sampler that has a detachable, square, open-ended steel sample box attached to a weighted column with a removable spade closure for the bottom of the box
Chlorophyll *a*	Pigment in the cells of autotrophic plants, the main substance that absorbs and transmits light energy during photosynthesis in plants
CTD	Pertaining to a system for measuring conductivity (indicator of salinity), temperature and depth (defined from pressure measurements).
Cumulative impacts	Impacts resulting from incremental changes caused by past, present or foreseeable actions. It means any material consequences in the marine environment arising over time from the conduct of exploitation activities or in combination with other stressors and activities in the same area, including those not regulated by the Authority.
Demersal scavenger	Animals that eat waste products and dead remains of other animals and plants that they did not kill themselves.
Ecosystem	A community of living organisms in conjunction with the non-living components of their environment interacting as a system
Environmental baseline	Sufficient information collected from the exploration area to describe the natural values of environmental factors and biocompetence succession without being directly affected by intense human activities, such as exploration and exploitation of deep-sea resources
environmental DNA	DNA molecule in the environment, including water and sediment, or exfoliated tissues and excreta released from organisms into the environment, that can reflect their current and past biological activities and existence in the environment
Protection and Preservation of the Marine Environment	Based on the best available scientific evidence, a precautionary approach and best practices are adopted to preserve biodiversity and stabilize ecosystem structure and function.
Euphotic zone	The upper section of the ocean which receives sufficient light for photosynthesis. In clear oceanic waters, the euphotic zone can extend to a maximum water depth of 150 m.

TERM	DEFINITION
Foraminifera	The main protistan component of abyssal benthic communities across the meiofaunal, macrofaunal and megafaunal size categories.
Halocline	A layer of water in which there is a steep gradient in salinity.
Human-occupied vehicle	Self-propelled submersible with its own energy, life support and accessory system
Impact reference zones	Areas used to assess the effect of test-mining in the Area on the marine environment. The impact reference zone must be in the contractor's area.
Lander system	System equipped with camera and trap deployed to the seafloor to observe animals in situ or recover specimens to the surface
Macrofauna	Animals retained on a 250-μm mesh, typically sorted and identified with a microscope, that include taxa such as polychaetes, bivalves, isopods and tanaids.
Marine mammals	Viviparous vertebrates, with characters of lactation, pulmonary respiration, constant body temperature, streamline, and forelimbs specialized as fins.
Megafauna	Animals large enough (larger than 2 cm) to be determined in photographs, proposed as key taxon (see taxonomy) for environmental impact assessment in deep-sea mining.
Metazoan meiofauna	Small invertebrate retained on a 32-μm sieve (except foraminifera), typically sorted and identified with a microscope, includes taxa such as nematodes, harpacticoid copepods, ostracods and kinorhynchs.
Microbiota	Organisms invisible to the naked eye, smaller than meiofauna. Operationally defined as <32 μm.
Microorganisms	A group of tiny unicellular or multicellular primary organisms with simple structure and a variety of physiological characters, including: the prokaryotes, such as bacteria, actinomycetes, mycoplasma, rickettsia, chlamydia and cyanobacteria; the eukaryotes, such as fungi (yeasts and molds), protozoa and microscopic algae; non-cellular organisms, such as viruses, viroids and prions.
Multicorer	Sediment sampler that consists of an outer framework and weighted collecting head of plastic core tubes hanging from a water-filled hydraulic damper
Multinet	Sampler equipped with multiple nets for sampling planktons from multiple water layers by opening and closing the nets in succession
Nekton	Fish, squids, crustaceans and marine mammals that are active swimmers in the open ocean environment.
Nodule fauna	Fauna attached to the surface and crevices of polymetallic nodules

TERM	DEFINITION
Oxygen minimum	A water layer present in all oceans at depths between 100–1,000 m, caused by the sinking and degradation by bacteria of organic matter produced in the surface ocean. The oxygen scarcity can cause particulate metals to dissolve. An oxygen minimum is distinct from an oxygen minimum zone, which is defined as having very low oxygen content (<0.5 ml/L O_2), and is found in distinct geographic regions of the ocean
pH	A measure of acidity based on the concentration of hydrogen ions.
Phytoplankton	Microscopic plants that are primary producers in the oceans.
plankton	group of organisms lacking advanced locomotive organs, with no or weak mobility, floating in the water layer and often moving with the flow, including phytoplankton and zooplankton
Plume	A dispersion of seawater that contains dense sediment particles. Seabed-disturbance plume is a stream of water containing suspended particles of seafloor sediment, abraded minerals and macerated benthic biota that emanates from the mining collector as a result of collector disturbance of the sea floor and spreads in a zone close to the sea floor. The far-field component of the seabed-disturbance plume is termed the "rain of fines". Discharge plume is a stream of water containing suspended particles of sea floor sediment, abraded minerals and macerated benthic biota resulting from the separation, on board the mining ship, of the nodules from the water carrier, and spreads in a zone closer than seabed-disturbance plume to the ocean surface.
Porewater	The water present within the spaces between sediment particles; also called "interstitial water".
Preservation reference zone	For exploration, a preservation reference zone is identified as part of test-mining. The zone selected should be comparable to the test-mining area. The preservation reference zone should be carefully located and large enough not to be affected by testing activities, including the effects from seabed-disturbance and discharge plumes. For test-mining, a preservation reference zone should be within the contractor's area, if possible. The aim of this zone is to act as a control area.
Primary productivity	Ability of autotrophic organisms to produce organic matter through photosynthesis. Primary productivity is usually calculated as the mass of the organic matter (usually expressed in organic carbon) per unit area (or volume) per unit time (year or day), corresponding to the primary production in the same area (or volume) over that time.

TERM	DEFINITION
Remote operated vehicle	Underwater vehicle that is remotely controlled by the connected cable transmitting signals and power from the support vehicle
Seabirds	Birds that are fully adapted to the marine environment in morphology and behavior and can forage in salt water.
Serious harm	Any effect from activities in the Area on the marine environment that represents a significant adverse change in the marine environment, determined according to the rules, regulations and procedures adopted by the International Seabed Authority on the basis of internationally recognized standards and practices informed by the best available scientific evidence.
Spatial scale	Scales characteristic of dimensions in space, as of oceanic phenomena, for example, the diameter of an eddy or the length phenomena, for example, the diameter of an eddy or the length sampling stations.
Synoptic scales	Scales of hydrodynamic variability or events encompassing temporal scales ranging from one to two weeks to one to two months and spatial scales of one to several hundred kilometers. A typical feature is synoptic eddies 100–200 km in diameter passing through the north-east tropical Pacific from east to west and often penetrating to the sea floor.
Testing of mining components	The use and testing of recovery systems and equipment and the component parts of a mining system, including seafloor collectors, riser systems and equipment and discharge systems and equipment. This project only refers to the test of seabed nodule collector components.
Thermocline	A layer of water in which there is a rapid change of temperature with depth.
Transect	The vertical plane (reference for all the measures and sampling taken during the survey), from surface to the sea bottom, of the route of a survey oceanographic vessel, from point A to point B.
Zooplankton	Unlike phytoplankton, these organisms cannot produce organic matter on their own and thus feed on other organisms.

Note. Referring to ISBA/25/LTC/6/Rev.3 and ISO 22787:2023(E)

Abbreviations & Acronyms

ABBREVIATION/ ACRONYM	DEFINITION
ADCP	Acoustic Doppler Current Profilers
AUV	Autonomous Underwater Vehicle
AVISO	Archiving, Validation and Interpretation of Satellite Oceanographic
BBL	Benthic Boundary Layer
BIE	Benthic Impact Experiment
BPC	Beijing Pioneer High tech Development Co., Ltd
CCHDO	CLIVAR and Carbon Hydrographic Data Office
CCFZ	Clarion-Clipperton Fracture Zone
COMRA	China Ocean Mineral Resources Research and Development Association
CTA	Collector Test Area
CTD	Conductivity, Temperature, Depth
DCM	Deep Chlorophyll Maximum
DIC	Dissolved Inorganic Carbon
DISCOL	DIS-turbance and re-COL-onization experiment
DO	Dissolved Oxygen
DOC	Dissolved Organic Carbon
DSSRS	Deep Sea Sediment Resuspention System
eDNA	Environmental Deoxyribonucleic Acid
EEZ	Exclusive Economic Zone
EIA	Environmental impact assessment
EIS	Environmental impact statement
EN	Endangered
FVCOM	Finite Volume Coast and Ocean Model
GBIF	Global Biodiversity Information Facility
GSR	Global Sea Mineral Resources
HOV	Human Occupied Vehicle
IMO	International Maritime Organization
ind./m^2	Number of individuals per square meter
ind./m^3	Number of individuals per cubic meter
IOM	Interoceanmetal Joint Organization
ISA	International Seabed Authority
IRZ	Impact Reference Zones

kg	Kilogram
kHz	Kilohertz
km	Kilometre
kW	Kilowatt
kyr	kiloyear
L (l)	Litre
LC	least concern
LCPW	Lower Circumpolar Water
MARPOL	International Convention for the Prevention Pollution from Ships
META	Mesoscale Eddy Trajectory Atlas
mg/l	Milligrams Per Litre
NEC	North Equatorial Current
NECC	North Equatorial Counter Current
NO_2^-	Nitrite
NO_3^-	Nitrate
NPSG	North Pacific Subtropical Gyre
NT	Near Threatened;
OBIS	Ocean Biogeographic Information System
PAAS	Post-Archaean Average Australian Sedimentary Rock
pH	potential of hydrogen
PO_4^{3-}	Phosphate
PRZ	Preservation reference zone
REMP	Regional environmental management plans
REY	Rare earth elements and yttrium
ROV	remotely operated vehicle
SLA	Sea Level Anomaly
sp.	Species
TIC	Total Inorganic Carbon
TMC	The Metals Company
TMF	Total mass of settling particulate matter flux
TOC	Total Organic Carbon
TSS	Total Suspended Solids
SiO_3^{2-}	Silicate
SS	Suspended Solid
SPM	Sinking Particulate Matter

SST	Sea Surface Temperature
mg/l	Micrograms Per Litre
mmol/l	Micromolar Per Litre
USBL	Ultrashort Baseline Acoustic Position System
VU	Vulnerable
WOA 23	World Ocean Atlas 2023

12 STUDY TEAM

The study team of this report consists of a writing team, a professional consulting team and a review team, covering a wide range of fields such as physical oceanography, meteorology, marine chemistry, marine biology, marine geology, ship and ocean engineering, machinery, remote sensing, acoustics and other specialties.

Table 12-1 Information of study team

Name	Affiliation	Expertise
Bo Li	China Ocean Mineral Resource R&D Association /BPC	Marine Sciences
Chunsheng Wang	Second Institute of Oceanography, Ministry of Natural Resources (SIO)	Marine Biology
Huaiming Li	SIO	Marine Geology
Xuebao He	TIO	Marine Biology
Shiquan Lin	SIO	Marine Biology
Dongfeng Xu	SIO	Physical Oceanography
Guangjiao Zhuang	Shanghai Jiao Tong University	Mechanical Engineering
Yuntian Pang	BPC Head of Digital Ocean Department	Geography Information System
Lina Xiao	BPC Head of Deep-sea Mining Equipment Department	Naval Architecture and Ocean Engineering
Haiyan Yang	BPC Environmental Assessment Project Manager	Physical Oceanography
Lin Zhu	BPC Environmental Assessment Project Manager	Physical Oceanography
Luwei Han	BPC Environmental Assessment Project Manager	Marine Sciences
Dan Zhang	China Institute for Marine Affairs, Ministry of Natural Resources	International law
Jun Wang	SIO	Physical Oceanography
Xuetian Wang	BPC Data Center Project Manager	Geology
Hongyi Wang	BPC Data Center Project Manager	Geography Information System
Jiangtao Guo	BPC Data Center Project Manager	Mineralogy, Petrology, Mineral Deposit Geology
Yang Wang	BPC Resource Evaluation Project Manager	Geological Engineering
Dong Sun	SIO	Marine Biology

Name	Affiliation	Expertise
Chengcheng Shen	SIO	Marine Ecology
Xiaogu Wang	SIO	Marine Biology
Lei Qiu	SIO	Geophysics
Jiang Huang	Third Institute of Oceanography, Ministry of Natural Resources (TIO)	Physical Oceanography
Hangyu Chen	TIO	Physical Oceanography
Xiwu Zhou	TIO	Physical Oceanography
Huiquan Lu	TIO	Geophysics
Xudong Fang	TIO	Geophysics
Cai Lin	TIO	Marine Chemistry
Weiming Kuang	TIO	Marine Chemistry
Feng Lin	TIO	Marine Chemistry
Yueyun Wang	SIO	Marine Biology
Lei Wang	TIO	Marine Ecology
Jianhua Kang	TIO	Marine Ecology
Rimei Ou	TIO	Marine Ecology
Yaqin Huang	TIO	Marine Biology
Kun Liu	TIO	Marine Biology
Sujing Fu	TIO	Marine Biology
Peng Xiang	TIO	Marine Biology
Yu Wang	TIO	Marine Biology
Yanghang Chen	TIO	Marine Biology
Hao You	SIO	Marine Biology
Ruiyan Zhang	SIO	Marine Biology
Yingbao Gai	TIO	Microbiology
Guizhen Li	TIO	Microbiology
Hongchang Zhai	SIO	Marine Biology
Nan Jin	TIO	Marine Biology
Yuan Li	TIO	Marine Biology
Shigang Liu	TIO	Marine Biology
Yongshou Cheng	National Marine Data and Information Service (NMDIS)	Geological Engineering
Dandan Zhuang	NMDIS	Geological Engineering
Weiguo Wang	TIO	Marine Geology
Sitian Huang	TIO	Marine Geology
Yang Liu	TIO	Marine Geology
Min Jiang	TIO	Marine Geology
Shihui Lv	China University of Geosciences Beijing	Geological Engineering
Weiyan Zhang	SIO	Marine Geology
Xiao Wang	SIO	Marine Geology
Yong Yang	Guangzhou Marine Geological Survey (GMGS)	Marine Geology
Miao Yu	GMGS	Marine Geology

* In no particular order

13 REFERENCES

Amos, A. F., & Roels, O. A. (1977). Environment aspects of manganese nodule mining. *Marine Policy*, *1*(2), 156-163.

Anderson, E. P., & Mackas, D. L. (1986). Lethal and sublethal effects of a molybdenum mine tailing on marine zooplankton: mortality, respiration, feeding and swimming behavior in Calanus marshallae, Metridia pacifica and Euphausia pacifica. *Marine environmental research*, *19*(2), 131-155.

Arndt, S., Jørgensen, B. B., LaRowe, D. E., Middelburg, J. J., Pancost, R. D., & Regnier, P. (2013). Quantifying the degradation of organic matter in marine sediments: A review and synthesis. *Earth-science reviews*, *123*, 53-86.

Arnold, E., Merrill, J., Leinen, M., & King, J. (1998). The effect of source area and atmospheric transport on mineral aerosol collected over the North Pacific Ocean. *Global and Planetary Change*, *18*(3-4), 137-159.

Auguste, M., Mestre, N. C., Rocha, T. L., Cardoso, C., Cueff-Gauchard, V., Le Bloa, S., Cambon-Bonavita, M. A., Shillito, B., Zbinden, M., Ravaux, J., & Bebianno, M. J. (2016). Development of an ecotoxicological protocol for the deep-sea fauna using the hydrothermal vent shrimp Rimicaris exoculata. *Aquatic Toxicology*, *175*, 277–285. https://doi.org/10.1016/j.aquatox.2016.03.024

Baker, E. T., Feely, R. A., & Takahashi, K. (1979). Chemical composition, size distribution and particle morphology of suspended particulate matter at DOMES sites A, B, and C: Relationships with local sediment composition. *Marine geology and oceanography of the Pacific Manganese Nodule Province*, 163-201.

Bau, M., & Koschinsky, A. (2006). Hafnium and neodymium isotopes in seawater and in ferromanganese crusts: the "element perspective". *Earth and Planetary Science Letters*, *241*(3-4), 952-961.

Bau, M., & Koschinsky, A. (2009). Oxidative scavenging of cerium on hydrous Fe oxide: evidence from the distribution of rare earth elements and yttrium between Fe oxides and Mn oxides in hydrogenetic ferromanganese crusts. *Geochemical Journal*, *43*(1), 37-47.

Benjamin, M. M., & Felmy, A. (1981). Trace metal exchange between ferromanganese nodules and artificial seawater. *Mar. Min*, *3*, 151-183.

BGR. (2018). Submission of an Environmental Impact Assessment for the testing of collector components in the German license area. Berlin: Bundesanstalt für Geowissenschaften und Rohstoffe.

Bischoff, J. L., Heath, G. R., & Leinen, M. (1979). Geochemistry of deep-sea sediments from the Pacific manganese nodule province: DOMES Sites A, B, and C. *Marine geology and oceanography of the Pacific manganese nodule province*, 397-436.

Bluhm, H. (1994). Monitoring megabenthic communities in abyssal manganese nodule sites of the East Pacific Ocean in association with commercial deep-sea mining. *Aquatic Conservation: Marine and Freshwater Ecosystems*, *4*(3), 187-201.

Bluhm, H., Schriever, G., & Thiel, H. (1995). Megabenthic recolonization in an experimentally disturbed abyssal manganese nodule area. *Marine georesources & geotechnology*, *13*(4), 393-416.

Brandhorst, W. (1959). Nitrification and Denitrification in the Eastern Tropical North Pacific. *ICES Journal of Marine Science*, *25*(1), 3–20.

Brown, A., Wright, R., Mevenkamp, L., & Hauton, C. (2017). A comparative experimental approach to ecotoxicology in shallow-water and deep-sea holothurians suggests similar behavioural responses. *Aquatic Toxicology*, *191*, 10-16.

Brown, A., Thatje, S., & Hauton, C. (2017). The effects of temperature and hydrostatic pressure on metal toxicity: insights into toxicity in the deep sea. *Environmental Science & Technology*, *51*(17), 10222-10231.

Bussau, C., Schriever, G., & Thiel, H. (1995). Evaluation of abyssal metazoan meiofauna from a manganese nodule area of the eastern South Pacific. *Vie et Milieu/Life & Environment*, 39-48.

Cao, X., Cai, Y., Cao, W., Wang, J. (2011). Analysis on deep-sea sediments' bearing capacity controlled by subsidence depth, Journal of Hunan University, 38(5):13-18. (in Chinese with English abstract)

Cerdeiro, D. A., Cerdeiro, M. D. A., Komaromi, A., Liu, Y., & Saeed, M. (2020). *World seaborne trade in real time: A proof of concept for building AIS-based nowcasts from scratch* (No. 20-57). International Monetary Fund.

Chamley, H., & Chamley, H. (1989). Clay formation through weathering. *Clay sedimentology*, 21-50.

Chassignet, E. P., Hurlburt, H. E., Smedstad, O. M., Halliwell, G. R., Hogan, P. J., Wallcraft, A. J., ... & Bleck, R. (2007). The HYCOM (hybrid coordinate ocean model) data assimilative system. *Journal of Marine Systems*, *65*(1-4), 60-83.

Chelton, D. B., Schlax, M. G., Samelson, R. M., & de Szoeke, R. A. (2007). Global observations of large oceanic eddies. *Geophysical Research Letters*, *34*(15).

Chelton, D. B., Schlax, M. G., & Samelson, R. M. (2011). Global observations of nonlinear mesoscale eddies. *Progress in oceanography*, *91*(2), 167-216.

Christiansen, B., Denda, A., & Christiansen, S. (2020). Potential effects of deep seabed mining on pelagic and benthopelagic biota. *Marine Policy*, *114*, 103442.

Crain, C. M., Kroeker, K., & Halpern, B. S. (2008). Interactive and cumulative effects of multiple human stressors in marine systems. *Ecology letters*, *11*(12), 1304-1315.

Cui, W. C., Liu, F., Hu, Z., Zhu, M., Guo, W., & Liu, C. G. (2012). 7 000 m sea trials test of the deep manned submersible "Jiaolong". *Journal of Ship Mechanics*, *16*(10), 1131-1143.

Davranche, M., Pourret, O., Gruau, G., Dia, A., & Le Coz-Bouhnik, M. (2005). Adsorption of REE (III)-humate complexes onto MnO2: Experimental evidence for cerium anomaly and lanthanide tetrad effect suppression. *Geochimica et Cosmochimica Acta*, *69*(20), 4825-4835.

Davies, T. W., Duffy, J. P., Bennie, J., & Gaston, K. J. (2014). The nature, extent, and ecological implications of marine light pollution. *Frontiers in Ecology and the Environment*, *12*(6), 347-355.

DNV GL. (2016). Recommended Practice. Managing environmental aspects and impacts of seabed mining. DNV GL-RP-O601 Edition 2019-09 - Amended 2021-10.

Dooling, R. J., & Therrien, S. C. (2012). Hearing in birds: what changes from air to water. *The effects of noise on aquatic life*, 77-82.

Du Preez, C., Amon, D. J., Baco, A. R., Best, M., Clyde, G., Colaço, A., ... & Tunnicliffe, V. (2023). *Identification of Ecologically or Biologically Significant Marine Areas (EBSAs) in Areas Beyond National Jurisdiction (ABNJ): the Northwest Pacific Seamounts*. Fisheries and Oceans Canada, Science Branch, Pacific Region, Institute of Ocean Sciences.

Egbert, G. D., & Erofeeva, S. Y. (2002). Efficient inverse modeling of barotropic ocean tides. *Journal of Atmospheric and Oceanic technology*, *19*(2), 183-204.

Ellis, D. V. (1987). A decade of environmental impact assessment at marine and coastal mines. *Mar. Min.*, *6*(4), 385-417.

Feng, J., Zhang, W. (1997). Physical and mechanical characterization of modern sediments in estuaries along the silty coast of northwest Bohai Bay. Journal of Sediment Research, 22(1):55-61. (in Chinese)

Flierdt, T. V. D., Frank, M., Lee, D.-C., Halliday, A. N., Reynolds, B. C., & Hein, J. R. (2004). New constraints on the sources and behavior of neodymium and hafnium in seawater from Pacific Ocean ferromanganese crusts. *Geochimica et Cosmochimica Acta*, *68*(19), 3827–3843.

Foell, E. J., Schriever, G., Bluhm, H., Borowski, C., Bussau, C., & Thiel, H. (1992, May). Disturbance and recolonization experiment in the abyssal South Pacific Ocean (diseol): an update. In *Offshore Technology Conference* (pp. OTC-6805). OTC, 25-34.

Garcia, H.E., Z. Wang, C. Bouchard, S.L. Cross, C.R. Paver, J.R. Reagan, T.P. Boyer, R.A. Locarnini, A.V. Mishonov, O. Baranova, D. Seidov, and D. Dukhovskoy. World Ocean

Atlas 2023, Volume 3: Dissolved Oxygen, Apparent Oxygen Utilization, and Oxygen Saturation. A. Mishonov, Tech. Ed. NOAA Atlas NESDIS 91

Gardner, W. D., Tucholke, B. E., Richardson, M. J., & Biscaye, P. E. (2017). Benthic storms, nepheloid layers, and linkage with upper ocean dynamics in the western North Atlantic. *Marine Geology*, *385*, 304-327.

Gao C, Chen M, Zhou L, Feng L, Zhang R H. (2022). The 2020–2021 prolonged La Niña evolution in the tropical Pacific. Science China Earth Sciences, 65(12): 2248–2266.

Gao, Y., Gao, Y., Ibarra, D. E., Du, X., Dong, T., Liu, Z., & Wang, C. (2021). Clay mineralogical evidence for mid-latitude terrestrial climate change from the latest Cretaceous through the earliest Paleogene in the Songliao Basin, NE China. *Cretaceous Research*, *124*, 104827.

GBIF. 2023.Accessed at https://www.gbif.org/ on May 1st

GB/T 24001-2016/ISO14001:2015. (2015). Environmental management systems–Requirements with guidance for use. Beijing: Standards Press of China.

GB/T 42629.1-2023. (2023). Code of practice for international seabed and high seas environmental survey—Part 1: General. Beijing: Standards Press of China.

GB/T 42629.1-2023. (2023). Code of practice for international seabed and high seas environmental survey—Part 2: Marine chemical survey. Beijing: Standards Press of China.

GB/T 42629.1-2023. (2023). Code of practice for international seabed and high seas environmental survey—Part 3: Marine biological survey. Beijing: Standards Press of China.

GB/T 42629.1-2023. (2023). Code of practice for international seabed and high seas environmental survey—Part 4: Physical features survey of marine sediments. Beijing: Standards Press of China.

Gingele, F. X., De Deckker, P., & Hillenbrand, C. D. (2001). Clay mineral distribution in surface sediments between Indonesia and NW Australia—source and transport by ocean currents. *Marine Geology*, *179*(3-4), 135-146.

Gjerde, K. M., Weaver, P., Billett, D., Paterson, G., Colaco, A., Dale, A., ... & Sweetman, A. (2016). Report on the implications of MIDAS results for policy makers with recommendations for future regulations to be adopted by the EU and the ISA. *no. December*, 61.

Gollner, S., Kaiser, S., Menzel, L., Jones, D. O., Brown, A., Mestre, N. C., ... & Arbizu, P. M. (2017). Resilience of benthic deep-sea fauna to mining activities. *Marine Environmental Research*, *129*, 76-101.

Gomez, C., Lawson, J. W., Wright, A. J., Buren, A. D., Tollit, D., & Lesage, V. (2016). A systematic review on the behavioural responses of wild marine mammals to noise: the disparity between science and policy. *Canadian Journal of Zoology*, *94*(12), 801-819.

GSR (2018).Environmental Impact Statement - Small-scale testing of nodule collector components on the seafloor of the Clarion-Clipperton Fracture Zone and its environmental impact.

Han, J., Li, X., Cui, J., et al. (1997). Relationship between the paleoceanographic environment and the formation of polymetallic nodules. China University of Geosciences Press, 43-50. (in Chinese)

Harris, P. T., Macmillan-Lawler, M., Rupp, J., & Baker, E. K. (2014). Geomorphology of the oceans. *Marine Geology*, *352*, 4-24.

Hauton, C., Brown, A., Thatje, S., Mestre, N. C., Bebianno, M. J., Martins, I., ... & Weaver, P. (2017). Identifying toxic impacts of metals potentially released during deep-sea mining—a synthesis of the challenges to quantifying risk. *Frontiers in Marine Science*, *4*, 368.

Hein, J. R., Conrad, T. A., Frank, M., Christl, M., & Sager, W. W. (2012). Copper-nickel-rich, amalgamated ferromanganese crust-nodule deposits from Shatsky Rise, NW Pacific. *Geochemistry, Geophysics, Geosystems*, *13*(10).

Hein, J. R., Konstantinova, N., Mikesell, M., Mizell, K., Fitzsimmons, J. N., Lam, P. J., ... & Till, C. P. (2017). Arctic deep water ferromanganese-oxide deposits reflect the unique characteristics of the Arctic Ocean. *Geochemistry, Geophysics, Geosystems*, *18*(11), 3771-3800.

Hein, J. R., Spinardi, F., Okamoto, N., Mizell, K., Thorburn, D., & Tawake, A. (2015). Critical metals in manganese nodules from the Cook Islands EEZ, abundances and distributions. *Ore Geology Reviews*, *68*, 97-116.

Hein, J. R., Mizell, K., Koschinsky, A., & Conrad, T. A. (2013). Deep-ocean mineral deposits as a source of critical metals for high-and green-technology applications: Comparison with land-based resources. *Ore Geology Reviews*, *51*, 1-14.

Herring, P. J., Gaten, E., & Shelton, P. M. (1999). Are vent shrimps blinded by science?. *Nature*, *398*(6723), 116-116.

Hilário, A., Metaxas, A., Gaudron, S. M., Howell, K. L., Mercier, A., Mestre, N. C., ... & Young, C. (2015). Estimating dispersal distance in the deep sea: challenges and applications to marine reserves. *Frontiers in Marine Science*, *2*, 6.

Hu, D., Wu, L., Cai, W., Gupta, A. S., Ganachaud, A., Qiu, B., ... & Kessler, W. S. (2015). Pacific western boundary currents and their roles in climate. *Nature*, *522*(7556), 299-308.

Huang, J., Wan, S., Zhang, G., Xu, Z., Liu, H., Dong, J., ... & Li, T. (2017). Impact of seafloor topography on distribution of clay minerals in the east Philippines Sea. *Marine Geology & Quaternary Geology*, *37*(1), 77-85. (in Chinese with English abstract)

International Seabed Authority. (2022). Draft standard and guidelines on the development and application of environmental management systems. Report No. ISBA/27/C/7. Kingston, Jamaica.

International Seabed Authority. (2023). Recommendations for the guidance of contractors for the assessment of the possible environmental impacts arising from exploration for marine minerals in the Area. Report No. ISBA/25/LTC/6/Rev. 3. Kingston, Jamaica.

International Seabed Authority. (2019). Draft regulations on exploitation of mineral resources in the Area. Report No. ISBA/25/C/WP.1. Kingston, Jamaica.

International Seabed Authority. (2013). Regulations on Prospecting and Exploration for Polymetallic Nodules in the Area. Report No. ISBA /19/C/WP.1. Kingston, Jamaica.

ISO 22787:2023(E). Marine environment impact assessment (MEIA) — Technical specifications for marine biotic surveys in the international seabed area — General principles. Switzerland, International Organization for Standardization, 2023.

Jin, N., Li, A., Liu, H., Meng, Q., Wan, S., & Xu, Z. (2007). Clay minerals in surface sediment of the northwest Parece Vela Basin: distribution and provenance. *Oceanologia et Limnologia Sinica*, *38*(6), 504-511. (in Chinese with English abstract)

Jones, D. O., Durden, J. M., Murphy, K., Gjerde, K. M., Gebicka, A., Colaço, A., ... & Billett, D. S. (2019). Existing environmental management approaches relevant to deep-sea mining. *Marine Policy*, *103*, 172-181.

Jones, D. O., Simon-Lledó, E., Amon, D. J., Bett, B. J., Caulle, C., Clement, L., ... & Huvenne, V. A. (2021). Environment, ecology, and potential effectiveness of an area protected from deep-sea mining (Clarion Clipperton Zone, abyssal Pacific). *Progress in Oceanography*, *197*, 102653.

Jou, L. J., Chen, B. C., Chen, W. Y., & Liao, C. M. (2016). Sensory determinants of valve rhythm dynamics provide in situ biodetection of copper in aquatic environments. *Environmental Science and Pollution Research*, *23*, 5374-5389.

Karl, D. M., & Church, M. J. (2017). Ecosystem structure and dynamics in the North Pacific Subtropical Gyre: new views of an old ocean. *Ecosystems*, *20*, 433-457.

Karl, D., Letelier, R., Tupas, L., Dore, J., Christian, J., & Hebel, D. (1997). The role of nitrogen fixation in biogeochemical cycling in the subtropical North Pacific Ocean. *Nature*, *388*(6642), 533-538.

Kato, F., & Kawabe, M. (2009). Volume transport and distribution of deep circulation at 165 W in the North Pacific. *Deep Sea Research Part I: Oceanographic Research Papers*, *56*(12), 2077-2087.

Kawabe, M., Fujio, S., & Yanagimoto, D. (2003). Deep-water circulation at low latitudes in the western North Pacific. *Deep Sea Research Part I: Oceanographic Research Papers*, *50*(5), 631-656.

Kawabe, M., Yanagimoto, D., Kitagawa, S., & Kuroda, Y. (2005). Variations of the deep western boundary current in Wake Island Passage. *Deep Sea Research Part I: Oceanographic Research Papers*, *52*(7), 1121-1137.

Kawabe, M., Yanagimoto, D., & Kitagawa, S. (2006). Variations of deep western boundary currents in the Melanesian Basin in the western North Pacific. *Deep Sea Research Part I: Oceanographic Research Papers*, *53*(6), 942-959.

Kawabe, M., Fujio, S., Yanagimoto, D., & Tanaka, K. (2009). Water masses and currents of deep circulation southwest of the Shatsky Rise in the western North Pacific. *Deep Sea Research Part I: Oceanographic Research Papers*, *56*(10), 1675-1687.

Kawabe, M., & Fujio, S. (2010). Pacific Ocean circulation based on observation. *Journal of oceanography*, *66*, 389-403.

Kim, H. J., Kim, D., Hyeong, K., Hwang, J., Yoo, C. M., Ham, D. J., & Seo, I. (2015). Evaluation of resuspended sediments to sinking particles by benthic disturbance in the Clarion-Clipperton nodule fields. *Marine Georesources & Geotechnology*, *33*(2), 160-166.

Kim, M., Kim, H. J., Ko, A., Yoo, C. M., Ju, S. J., & Hwang, J. (2021). Characteristics of sediment resuspension on a deep abyssal plain in the Eastern Tropical Pacific Ocean. *Journal of Sea Research*, *175*, 102085.

Kontar, E. A., & Sokov, A. V. (1994). A benthic storm in the northeastern tropical Pacific over the fields of manganese nodules. *Deep Sea Research Part I: Oceanographic Research Papers*, *41*(7), 1069-1089.

Koschinsky, A. (2001). Heavy metal distributions in Peru Basin surface sediments in relation to historic, present and disturbed redox environments. *Deep Sea Research Part II: Topical Studies in Oceanography*, *48*(17-18), 3757-3777.

Koschinsky, A., & Hein, J. R. (2003). Uptake of elements from seawater by ferromanganese crusts: solid-phase associations and seawater speciation. *Marine Geology*, *198*(3-4), 331-351.

Korschinek, G., Bergmaier, A., Faestermann, T., Gerstmann, U. C., Knie, K., Rugel, G., ... & Remmert, A. (2010). A new value for the half-life of 10Be by heavy-ion elastic recoil detection and liquid scintillation counting. *Nuclear Instruments and Methods in*

Physics Research Section B: Beam Interactions with Materials and Atoms, *268*(2), 187-191.

Kukert, H. (1988). Burial resistance and modes of recolonization in deep-sea macrofauna (abstr.). In *Fifth International Deep-sea Biological Symposium, Brest, France, 1988*.

Kutti, T., Bannister, R. J., Fosså, J. H., Krogness, C. M., Tjensvoll, I., & Søvik, G. (2015). Metabolic responses of the deep-water sponge Geodia barretti to suspended bottom sediment, simulated mine tailings and drill cuttings. *Journal of experimental marine biology and ecology*, *473*, 64-72.

Kwan, Y. H., Zhang, D., Mestre, N. C., Wong, W. C., Wang, X., Lu, B., Wang, C., Qian, P.-Y., & Sun, J. (2019). Comparative Proteomics on Deep-Sea Amphipods after in Situ Copper Exposure. *Environmental Science & Technology*, *53*(23), 13981–13991.

Larsson, A. I., van Oevelen, D., Purser, A., & Thomsen, L. (2013). Tolerance to long-term exposure of suspended benthic sediments and drill cuttings in the cold-water coral Lophelia pertusa. *Marine pollution bulletin*, *70*(1-2), 176-188.

Le, J. T., Levin, L. A., & Carson, R. T. (2017). Incorporating ecosystem services into environmental management of deep-seabed mining. *Deep Sea Research Part II: Topical Studies in Oceanography*, *137*, 486-503.

Lee, S. H., & Chang, Y. S. (2019). Classification of the global tidal types based on auto-correlation analysis. *Ocean Science Journal*, *54*, 279-286.

Leinen, M., Prospero, J. M., Arnold, E., & Blank, M. (1994). Mineralogy of aeolian dust reaching the North Pacific Ocean: 1. Sampling and analysis. *Journal of Geophysical Research: Atmospheres*, *99*(D10), 21017-21023.

Li, Z., Li, H., Hein, J. R., Dong, Y., Wang, M., Ren, X., ... & Chu, F. (2021). A possible link between seamount sector collapse and manganese nodule occurrence in the abyssal plains, NW Pacific Ocean. *Ore Geology Reviews*, *138*, 104378.

Ling, H. F., Jiang, S. Y., Frank, M., Zhou, H. Y., Zhou, F., Lu, Z. L., ... & Ge, C. D. (2005). Differing controls over the Cenozoic Pb and Nd isotope evolution of deepwater in the central North Pacific Ocean. *Earth and Planetary Science Letters*, *232*(3-4), 345-361.

Lipschultz, F. (1995). Nitrogen-specific uptake rates of marine phytoplankton isolated from natural populations of particles by flow cytometry. *Marine Ecology Progress Series*, *123*, 245-258.

Locarnini, R.A., A.V. Mishonov, O.K. Baranova, J.R. Reagan, T.P. Boyer, D. Seidov, Z. Wang, H.E. Garcia, C. Bouchard, S.L. Cross, C.R. Paver, and D. Dukhovskoy. World Ocean Atlas 2023, Volume 1: Temperature. A. Mishonov Technical Ed. NOAA Atlas NESDIS 89.

Lovell, J. M., Findlay, M. M., Moate, R. M., & Yan, H. Y. (2005). The hearing abilities of the prawn Palaemon serratus. *Comparative Biochemistry and Physiology Part A: Molecular & Integrative Physiology*, *140*(1), 89-100.

Machida, S., Fujinaga, K., Ishii, T., Nakamura, K., Hirano, N., & Kato, Y. (2016). Geology and geochemistry of ferromanganese nodules in the Japanese Exclusive Economic Zone around Minamitorishima Island. *Geochemical Journal*, *50*(6), 539-555.

Ma, J., Song, J., Li, X., Yuan, H., Li, N., Duan, L., & Wang, Q. (2020). Geochemical Characteristics of Particulate Organic Carbon in the Kocebu Seamount Waters of the Western Pacific Ocean in Spring 2018. *Advances in Earth Science*, *35*(7), 731-741. (in Chinese with English abstract)

Ma, W., Rhee, C. van, & Schott, D. (2018). A numerical calculation method of environmental impacts for the deep sea mining industry – a review. *Environmental Science: Processes & Impacts*, *20*(3), 454–468.

Ma, W. B., Rao, Q. H., Wu, H. Y., Guo, S. C., & Li, P. (2014). Macroscopic properties and microstructure analyses of deep-sea sediment. *Rock and Soil Mechanics*, *35*(6), 1641-1646. (in Chinese with English abstract)

Ma Xiao. (2015). Hydrographic diagnostic analysis in the western Tropical Pacific based on a streamfunction projection method. University of Chinese Academy of Sciences. (in Chinese with English abstract)

McGuire, W. J. (1996). Volcano instability: a review of contemporary themes. *Geological Society, London, Special Publications*, *110*(1), 1-23.

Mellinger, D. K., Stafford, K. M., Moore, S. E., Dziak, R. P., & Matsumoto, H. (2007). An Overview of Fixed Passive Acoustic Observation Methods for Cetaceans. *Oceanography*, *20*(4), 36–45.

Mestre, N. C., Calado, R., & Soares, A. M. (2014). Exploitation of deep-sea resources: the urgent need to understand the role of high pressure in the toxicity of chemical pollutants to deep-sea organisms. *Environmental pollution*, *185*, 369-371.

Mestre, N. C., Rocha, T. L., Canals, M., Cardoso, C., Danovaro, R., Dell'Anno, A., ... & Bebianno, M. J. (2017). Environmental hazard assessment of a marine mine tailings deposit site and potential implications for deep-sea mining. *Environmental Pollution*, *228*, 169-178.

Mevenkamp, L., Brown, A., Hauton, C., Kordas, A., Thatje, S., & Vanreusel, A. (2017). Hydrostatic pressure and temperature affect the tolerance of the free-living marine nematode Halomonhystera disjuncta to acute copper exposure. *Aquatic toxicology*, *192*, 178-183.

Mevenkamp, L., Guilini, K., Boetius, A., De Grave, J., Laforce, B., Vandenberghe, D., ... & Vanreusel, A. (2019). Responses of an abyssal meiobenthic community to short-

term burial with crushed nodule particles in the south-east Pacific. *Biogeosciences*, *16*(11), 2329-2341.

Mevenkamp, L., Stratmann, T., Guilini, K., Moodley, L., van Oevelen, D., Vanreusel, A., Westerlund, S., & Sweetman, A. K. (2017). Impaired Short-Term Functioning of a Benthic Community from a Deep Norwegian Fjord Following Deposition of Mine Tailings and Sediments. *Frontiers in Marine Science*, *4*. https://doi.org/10.3389/fmars.2017.00169.

Miljutina, M. A., Miljutin, D. M., Mahatma, R., & Galéron, J. (2010). Deep-sea nematode assemblages of the Clarion-Clipperton Nodule Province (tropical north-eastern Pacific). *Marine Biodiversity*, *40*, 1-15.

Miyamoto, M., Kiyota, M., Hayashibara, T., Nonaka, M., Imahara, Y., & Tachikawa, H. (2017). Megafaunal composition of cold-water corals and other deep-sea benthos in the southern Emperor Seamounts area, North Pacific Ocean. *Galaxea, Journal of Coral Reef Studies*, *19*(1), 19–30.

Nautilus, Minerals Environmental Impact Statement. 2008, http://www.cares.nautilusminerals. com.

Navarro-Barranco, C., & Hughes, L. E. (2015). Effects of light pollution on the emergent fauna of shallow marine ecosystems: Amphipods as a case study. *Marine pollution bulletin*, *94*(1-2), 235-240.

Nayak, B., Das, S. K., & Munda, P. (2013). Biogenic signature and ultra microfossils in ferromanganese nodules of the Central Indian Ocean Basin. *Journal of Asian Earth Sciences*, *73*, 296-305.

Nedelec, S. L., Radford, A. N., Pearl, L., Nedelec, B., McCormick, M. I., Meekan, M. G., & Simpson, S. D. (2017). Motorboat noise impacts parental behaviour and offspring survival in a reef fish. *Proceedings of the Royal Society B: Biological Sciences*, *284*(1856), 20170143.

Nishi, K., Usui, A., Nakasato, Y., & Yasuda, H. (2017). Formation age of the dual structure and environmental change recorded in hydrogenetic ferromanganese crusts from Northwest and Central Pacific seamounts. *Ore Geology Reviews*, *87*, 62-70.

OBIS. 2023, Accessed at https://obis.org/ on May 1st.

Paul, S. A., Gaye, B., Haeckel, M., Kasten, S., & Koschinsky, A. (2018). Biogeochemical regeneration of a nodule mining disturbance site: trace metals, DOC and amino acids in deep-sea sediments and pore waters. *Frontiers in Marine Science*, *5*, 117.

Paul, S. A., Zitoun, R., Noowong, A., Manirajah, M., & Koschinsky, A. (2021). Copper-binding ligands in deep-sea pore waters of the Pacific Ocean and potential impacts of polymetallic nodule mining on the copper cycle. *Scientific reports*, *11*(1), 18425.

Pelleter, E., Fouquet, Y., Etoubleau, J., Cheron, S., Labanieh, S., Josso, P., ... & Langlade,

J. (2017). Ni-Cu-Co-rich hydrothermal manganese mineralization in the Wallis and Futuna back-arc environment (SW Pacific). *Ore Geology Reviews*, *87*, 126-146.

Qian, W., Zhang, X., Wang, J. (2006), Relationship between the annual number of tropical storms generated in the northwestern Pacific Ocean and early basin-scale SST anomalies. Progress in Natural Science, 16(12):1657-1661. (in Chinese)

Quartau, R., Ramalho, R. S., Madeira, J., Santos, R., Rodrigues, A., Roque, C., ... & Da Silveira, A. B. (2018). Gravitational, erosional and depositional processes on volcanic ocean islands: Insights from the submarine morphology of Madeira Archipelago. *Earth and Planetary Science Letters*, *482*, 288-299.

Radziejewska, T. (2002). Responses of deep-sea meiobenthic communities to sediment disturbance simulating effects of polymetallic nodule mining. *International Review of Hydrobiology: A Journal Covering all Aspects of Limnology and Marine Biology*, *87*(4), 457-477.

Reagan, James R.; Boyer, Tim P.; García, Hernán E.; Locarnini, Ricardo A.; Baranova, Olga K.; Bouchard, Courtney; Cross, Scott L.; Mishonov, Alexey V.; Paver, Christopher R.; Seidov, Dan; Wang, Zhankun; Dukhovskoy, Dmitry (2023). World Ocean Atlas 2023 (NCEI Accession 0270533). NOAA National Centers for Environmental Information. Dataset.

Reagan, J.R., D. Seidov, Z. Wang, D. Dukhovskoy, T.P. Boyer, R.A. Locarnini, O.K. Baranova, A.V. Mishonov, H.E. Garcia, C. Bouchard, S.L. Cross, and C.R. Paver. World Ocean Atlas 2023, Volume 2: Salinity. A. Mishonov, Technical Editor, NOAA Atlas NESDIS 90.

Riccobene, G., & Nemo Collaboration. (2009). Long-term measurements of acoustic background noise in very deep sea. *Nuclear Instruments and Methods in Physics Research Section A: Accelerators, Spectrometers, Detectors and Associated Equipment*, *604*(1-2), S149-S157.

Rodrigues, N., Sharma, R., & Nath, B. N. (2001). Impact of benthic disturbance on megafauna in Central Indian Basin. *Deep Sea Research Part II: Topical Studies in Oceanography*, *48*(16), 3411-3426.

Rountree, R. A., Juanes, F., Goudey, C. A., & Ekstrom, K. E. (2012). Is Biological Sound Production Important in the Deep Sea? In A. N. Popper & A. Hawkins (Eds.), *The Effects of Noise on Aquatic Life* (pp. 181–183). Springer.

Roy, A., Field, M. J., Adam, V., & Bourgeois, D. (2011). The nature of transient dark states in a photoactivatable fluorescent protein. *Journal of the American Chemical Society*, *133*(46), 18586-18589.

Sainte-Marie, B. (1992). Foraging of Scavenging Deep-Sea Lysianassoid Amphipods. In G. T. Rowe & V. Pariente (Eds.), *Deep-Sea Food Chains and the Global Carbon Cycle* (pp. 105–124). Springer Netherlands.

Santos, R., Quartau, R., da Silveira, A. B., Ramalho, R., & Rodrigues, A. (2019). Gravitational, erosional, sedimentary and volcanic processes on the submarine environment of Selvagens Islands (Madeira Archipelago, Portugal). *Marine Geology*, *415*, 105945.

Schriever, C., Ahnert, A., Bluhm, H., Borowski, C., & Thiel, H. (1997, May). Results of the large scale deep-sea environmental impact study DISCOL during eight years of investigation. In *ISOPE International Ocean and Polar Engineering Conference* (pp. ISOPE-I). ISOPE.

Sharma, R. (2015). Environmental issues of deep-sea mining. *Procedia Earth and Planetary Science*, *11*, 204-211.

Shirayama, Y. (1999, November). Biological results of the JET project: an overview. In *ISOPE Ocean Mining and Gas Hydrates Symposium* (pp. ISOPE-M). ISOPE.

Shiraishi, F., Mitsunobu, S., Suzuki, K., Hoshino, T., Morono, Y., & Inagaki, F. (2016). Dense microbial community on a ferromanganese nodule from the ultra-oligotrophic South Pacific Gyre: Implications for biogeochemical cycles. *Earth and Planetary Science Letters*, *447*, 10-20.

Siedler, G., Holfort, J., Zenk, W., Müller, T. J., & Csernok, T. (2004). Deep-water flow in the Mariana and Caroline Basins. *Journal of Physical Oceanography*, *34*(3), 566-581.

Simon-Lledó, E., Bett, B. J., Huvenne, V. A., Köser, K., Schoening, T., Greinert, J., & Jones, D. O. (2019). Biological effects 26 years after simulated deep-sea mining. *Scientific reports*, *9*(1), 8040.

Singh, R., Sautya, S., & Ingole, B. S. (2019). The community structure of the deep-sea nematode community associated with polymetallic nodules in the Central Indian Ocean Basin. *Deep Sea Research Part II: Topical Studies in Oceanography*, *161*, 16-28.

Song L. (1999). Geotechnical properties of oceanic polymetallic nodule sediments. Acta Oceanologica Sinica, 21(6), 47-54. (in Chinese with English abstract)

SPC (2013).Deep Sea Minerals: Cobalt-rich Ferromanganese Crusts, a physical, biological, environmental, and technical review.

Steiner, R. (2009). independent review of the environmental impact statement for the proposed nautilus minerals solwara 1 seabed mining project, Papua New Guinea. *Bismarck-Solomon Indigenous Peoples Council. Available online at: http://www.deepseaminingoutofourdepth.org/wp-content/uploads/Steiner-Independent-review-DSM1.pdf (Accessed January 18, 2013)*.

Stratmann, T., Lins, L., Purser, A., Marcon, Y., Rodrigues, C. F., Ravara, A., ... & Van Oevelen, D. (2018). Abyssal plain faunal carbon flows remain depressed 26 years after a simulated deep-sea mining disturbance. *Biogeosciences*, *15*(13), 4131-4145.

Sun, Y., Xiao, W., Wang, R., Wu, L., & Wu, Y. (2021). Changes in sediment provenance and ocean circulation on the northern slope of the Bering Sea since the last deglaciation. *Marine Geology*, *436*, 106492.

Symons, W. O., Sumner, E. J., Talling, P. J., Cartigny, M. J., & Clare, M. A. (2016). Large-scale sediment waves and scours on the modern seafloor and their implications for the prevalence of supercritical flows. *Marine Geology*, *371*, 130-148.

Tamis, J. E., de Vries, P., Jongbloed, R. H., Lagerveld, S., Jak, R. G., Karman, C. C., Van der Wal, J. T., Slijkerman, D. M., & Klok, C. (2016). Toward a harmonized approach for environmental assessment of human activities in the marine environment. *Integrated Environmental Assessment and Management*, *12*(4), 632–642. https://doi.org/10.1002/ieam.1736.

Tao, Z., Zhou, X., Xie, F., Lv, T., Wang, J. (2019). Time Series of Monthly Global Marine NPP Dataset Based on MODIS and SABPM Model (Since 2003). Digital Journal of Global Change Data Repository, 2019. https://doi.org/10.3974/geodb.2019.05.01.V1.

Tang, B., Hou, Y., Yin, Y., Hu, P. (2019). Statistical characteristics of mesoscale eddies and the distribution in the north pacific subtropical countercurrent. Oceanologia et Limnologia Sinica, 50(5):937-947. (in Chinese with English abstract)

T/CAOE 41-2021. The Guidelines for Protection and Preservation of the Marine Environment in Deep-sea Mining. (2021). China Association of Oceanic Engineering. Beijing.

The Standing Committee of National People's Congress. (2016). The Law of the People's Republic of China on Exploration for and Exploitation of Resources in the Deep Seabed Area. Beijing, China. (in Chinese)

The Standing Committee of National People's Congress. (2017). Marine Environment Protection Law of the People's Republic of China. Beijing, China. (in Chinese)

Thiel, H., Schriever, G., Bussau, C., & Borowski, C. (1993). Manganese nodule crevice fauna. *Deep Sea Research Part I: Oceanographic Research Papers*, *40*(2), 419-423.

Tkatchenko, G., Radziejewska, T., Stoyanova, V., Modlitba, I., & Parizek, A. (1996, October). Benthic impact experiment in the IOM pioneer area: testing for effects of deep-sea disturbance. In *Int Seminar on Deep Sea-bed Mining Tech, China Ocean Mineral Resources R&D Assoc, Beijing, C55-C68*.

Turcheniuk, K., Bondarev, D., Singhal, V., & Yushin, G. (2018). Ten years left to redesign lithium-ion batteries. *Nature*, *559*(7715), 467–470.

U.S. (1981). Department of Commerce. Deep seabed mining final programmatic environmental impact statement. National Oceanic and Atmospheric Administration, Office of Ocean Minerals and Energy, pp295.

Van Campenhout, J., Derycke, S., Tchesunov, A. V., Portnova, D., & Vanreusel, A. (2014). The dominant Håkon Mosby mud volcano nematode is genetically differentiated from its shallow–water relatives and shows genetic structure within the mud volcano. *Journal of Zoological Systematics and Evolutionary Research*, *52*, 203-216.

Van Dover, C. L. (2011). Tighten regulations on deep-sea mining. *Nature*, *470*(7332), 31-33.

Vanreusel, A., Hilario, A., Ribeiro, P. A., Menot, L., & Arbizu, P. M. (2016). Threatened by mining, polymetallic nodules are required to preserve abyssal epifauna. *Scientific reports*, *6*(1), 26808.

Wahlberg, M., & Westerberg, H. (2003). Sounds produced by herring (Clupea harengus) bubble release. *Aquatic Living Resources*, *16*(3), 271-275.

Wang, C. and Lu, D. (2002). Application of deep-towed photographic and video systems to the study of deep-sea megafauna. Oceanography in China 14, China Ocean Press. 75-82. (in Chinese)

Wang, C., Zhang, Y., Lu, B., & Wang, D. (2018). New Hexactinellid Sponge Chaunoplectella megapora sp. nov. (Lyssacinosida: Leucopsacidae) from Clarion-Clipperton Fracture Zone, Eastern Pacific Ocean. *Zootaxa*, *4375*(1), 136-142.

Wang, C., & Zhou, H. (2001). Assessment of potential impacts of deep-sea mining on marine ecosystem II. Benthic ecosystem. Marine Environmental Science, 20(2), 32-37. (in Chinese with English abstract)

Wang, C., Zhou, H., & Ni, J (2003). Studies on the environmental effects of deep-sea mining: progress, problems and prospects. *Donghai Marine Science*, *21*(1), 55-64. (in Chinese with English abstract)

Wang, F., Hu, D., Mu, M., Wang, Q., He, J., Zhu, J., & Liu, Z. (2012). Structure, Variations and Climatic Impacts of Ocean Circulation and the Warm Pool in the Tropical Pacific Ocean. Advances in Earth Science, 27(6), 595. (in Chinese with English abstract)

Wang F., Zhuang D. (2018). The Researches on Geotechnical Mechanics Characteristics of Sediments in Pacific Polymetallic Nodules/Crusts Area. Proceedings of the 6th Academic Conference of Geology Resource Management and Sustainable Development.

Wang, K., Wu, J., & An, Y. (2011). Physico-mechanic properties of surface sediments in the north of Bohai Sea. Marine Geology Frontiers, 27(1), 14-18. (in Chinese with English abstract)

Wang, L., Zhu, W., Xie, J., Li, L., & Zhang, C. (2015). Study of the shear strength of sediments in main sedimentation stages. *Marine Georesources & Geotechnology*, *33*(6), 556-566.

Wang, X., Li, H., Cheng, Y., Yao, P., Chu, F., Ma, W., ... & Dong, Y. (2024). Submarine Morphological Description of the Ancient Archipelagic Aprons in the Marcus–Wake Seamount Group, Northwestern Pacific Ocean. Journal of Marine Science and Engineering, 12(4), 670.

Wang, X., Zhou, Y., Zhang, D., Hong, L., & Wang, C. (2013). A study of meiofauna in the COMRA's contracted area during the summer of 2005. Acta Ecologica Sinica, 33, 492-500. (in Chinese with English abstract)

Wang, Y., Lv, S., Su, X., Li, J., Li, H., Ren, X. (2021). Assemblage of clay minerals at polymetallic nodules contract area in Northwest Pacific Ocean. The Chinese Journal of Nonferrous Metals, 31(10): 2696−2712. (in Chinese with English abstract)

Watling, L., Guinotte, J., Clark, M. R., & Smith, C. R. (2013). A proposed biogeography of the deep ocean floor. *Progress in Oceanography*, *111*, 91-112.

Weaver, P. P. E., Aguzzi, J., Boschen-Rose, R. E., Colaço, A., de Stigter, H., Gollner, S., ... & Thomsen, L. (2022). Assessing plume impacts caused by polymetallic nodule mining vehicles. *Marine Policy*, *139*, 105011.

Weber, M. E., Von Stackelberg, U., Marchig, V., Wiedicke, M., & Grupe, B. (2000). Variability of surface sediments in the Peru basin: dependence on water depth, productivity, bottom water flow, and seafloor topography. *Marine Geology*, *163*(1-4), 169-184.

Wei, L., Pant, R., & Tumay, M. (2010). A case study of undrained shear strength evaluation from in situ tests in soft Louisiana soils. In *Soil Behavior and Geo-Micromechanics* (pp. 35-42).

Widder, E. A., Robison, B. H., Reisenbichler, K. R., & Haddock, S. H. D. (2005). Using red light for in situ observations of deep-sea fishes. *Deep Sea Research Part I: Oceanographic Research Papers*, *52*(11), 2077-2085.

Williams, R., Wright, A. J., Ashe, E., Blight, L. K., Bruintjes, R., Canessa, R., ... & Wale, M. A. (2015). Impacts of anthropogenic noise on marine life: Publication patterns, new discoveries, and future directions in research and management. *Ocean & Coastal Management*, *115*, 17-24.

Winterer, E. L., Natland, J. H., Van Waasbergen, R. J., Duncan, R. A., McNutt, M. K., Wolfe, C. J., Silva, I. P., Sager, W. W., & Sliter, W. V. (1993). Cretaceous guyots in the northwest Pacific: An overview of their geology and geophysics. In M. S. Pringle, W. W. Sager, W. V. Sliter, & S. Stein (Eds.), *Geophysical Monograph Series* (Vol. 77, pp. 307–334). American Geophysical Union.

Wooster, W., Chow, T., & Barrett, I. (1965). Nitrite distribution in Peru current waters. *Journal of Marine Research*, *23*(3).

Wu, L., Liu, Q., Hu, D., Li, C., Zuo, J., & Yu, Y., Variability of the subtropical gyre in North Pacific and its impacts on dynamic environment of China marginal seas. Advances in Earth Science, 2007, 22(12): 1224-1230. (in Chinese with English abstract)

Xie, X., Liu, X., Chen, Z., Wang, Y., Chen, D., Li, W., & Zhang, D. (2023). Pure Inertial Waves Radiating from Low-Frequency Flows Over Large-Scale Topography. *Geophysical Research Letters*, *50*(4), e2022GL099889.

Xie, X., Wang, Y., Liu, Z., Liu, X., Chen, D., Zhang, D., & Wang, J. (2023). Observation of Near-Inertial Waves in the Bottom Boundary Layer of an Abyssal Seamount. *Journal of Physical Oceanography*, *53*(2), 635-645.

Xiong, Z., Li, T., Chang, F., Algeo, T. J., Clift, P. D., Bretschneider, L., ... & Huang, J. (2018). Rapid precipitation changes in the tropical West Pacific linked to North Atlantic climate forcing during the last deglaciation. *Quaternary Science Reviews*, *197*, 288-306.

Xiong, Z., Li, T., Jiang, F., Chang, F., & Chen, S. (2019). Millennial-scale evolution of elemental ratios in bulk sediments from the western Philippine Sea and implications for chemical weathering in Luzon since the Last Glacial Maximum. *Journal of Asian Earth Sciences*, *179*, 127-137.

Xu, Z., Wan, S., Colin, C., Li, T., Clift, P. D., Chang, F., ... & Lim, D. (2020). Enhanced terrigenous organic matter input and productivity on the western margin of the Western Pacific Warm Pool during the Quaternary sea-level lowstands: Forcing mechanisms and implications for the global carbon cycle. *Quaternary Science Reviews*, *232*, 106211.

Yanagimoto, D., Kawabe, M., & Fujio, S. (2010). Direct velocity measurements of deep circulation southwest of the Shatsky Rise in the western North Pacific. *Deep Sea Research Part I: Oceanographic Research Papers*, *57*(3), 328-337.

Yang, H., Mao, X., Guo, X. (2018). A preliminary study on nutrients concentration within the mixed layer in the northwest pacific based on WOD data. Periodical of Ocean University of China, 48(8), 1-9. (in Chinese with English abstract)

Yang, S., & Sheng, L. (2004). The characteristic and property of physical-mechanics about deposit of sea beach area of the Bohai bay west coast. *Hydrogeology & Engineering Geology*, *31*(3), 93-95. (in Chinese with English abstract)

Yang, W., Zhang, X., Chen, M., et al. (2011). Bioturbation and its 210 Pb tracing of organic carbon transport in western Pacific sediments. Journal of Central South University (Science and Technology), 42(z2):189-195. (in Chinese)

Yang, Z., Qian, Q., Chen, M., Zhang, R., Yang, W., Zheng, M., & Qiu, Y. (2020). Enhanced but highly variable bioturbation around seamounts in the northwest Pacific. *Deep Sea Research Part I: Oceanographic Research Papers*, *156*, 103190.

Yao, P., Li, H., Wang, X., Zhu, F., Zhu, J., Lv, S., Dong, Y., Zhang, W., Pang, Y., Chu, F. (2024). Geological and oceanographic constrains on the deposit of ferromanganese nodules on the archipelagic aprons of seamounts. Manuscript submitted for publication.

Yu, X., Jiang, C. (1984). A study of modern marine sedimentary minerals and their X-ray diffraction. Science Press. Beijing. (in Chinese)

Zeng, Q., Huang, D., Lin, R., & Wang, J. (2018). Deep-sea metazoan meiofauna from a polymetallic nodule area in the Central Indian Ocean Basin. *Marine Biodiversity*, *48*, 395-405.

Zhang, L., Yao, D., Liang, H. (1994). Geochemistry of interstitial water in sediments from eastern Pacific Basin. Geochimica, 23,201-209. (in Chinese with English abstract)

Zhang, W., Wang, B., & Wei, Q. (2016). Spatial distribution of primary nitrite maximum and its influencing factors in the east Indian Ocean in spring. Advances in Marine Science, 343, 403-410. (in Chinese with English abstract)

Zhao, M., Liu, Q., Zhang, D., Liu, Z., Wang, C., & Liu, X. (2020). Deep-sea meiofauna assemblages with special reference to marine nematodes in the Caiwei Guyot and a Polymetallic Nodule Field in the Pacific Ocean. *Marine Pollution Bulletin*, *160*, 111564.

Zheng, M., Luo, M., Pan, B. (2023). Research progress of oxygen consumption in marine sediments. Advances in Earth Science, 38(3):236-255. (in Chinese with English abstract)

Zhu, K. (2015). Study on physical and mechanical properties of sediment from central-western Pacific basin. Soil Engineering and Foundation, 29(3), 149-152. (in Chinese with English abstract)

Zhu, K. (2002). Petrology of the substrate in seamounts MA, MC, MD, ME and MF from Magellan Seamounts. Marine Geology and Quaternary Geology, 22(1), 49-50. (in Chinese with English abstract)

14 APPENDICES

Appendix I BPC's Environmental Management System Philosophy, Objectives, and Policies

Preface

According to the 1982 United Nations Convention on the Law of the Sea (hereinafter referred to as the "UNCLOS"), the Area means "the sea–bed and ocean floor and subsoil thereof, beyond the limits of national jurisdiction" (UNCLOS, Article 1), "the Area and its resources are the common heritage of mankind" (UNCLOS, Article 136), and the International Seabed Authority (UNCLOS, Article 156) was established to carry out its functions. In October 2019, Beijing Pioneer High-tech Development Co., Ltd. (hereinafter referred to as "BPC") entered into a fifteen-year exploration contract with the International Seabed Authority (ISA), becoming a contractor for the polymetallic nodule mining area within the Area.

With the rapid increase in demand for large-capacity batteries driven by the utilization of new energy sources, the demand for metals such as cobalt and nickel has also surged. It is projected that by 2050, the annual production of 50 to 80 million electric vehicles will require between 500,000 to 800,000 tons of cobalt, which will far exceed current mining capabilities starting from the year 2030. Similarly, the demand for nickel is expected to increase by two to three times by 2050. A shortage of nickel will become apparent by the mid-2030s. Exploration results indicate that polymetallic nodules are rich in metals such as manganese, nickel, and cobalt.

At the same time, there is a growing demand for the protection and conservation of the marine environment. On July 13, 2022, the Secretariat of the United Nations Convention on Biological Diversity released the first official draft of the *Global Biodiversity Framework* (GBF), which includes a key target to protect 30% of the global land and marine areas by 2030, surpassing the current protection levels of 16.64% for land and 7.74% for oceans. On March 4, 2023, the draft agreement of the conservation and sustainable use of marine Biodiversity Beyond National Jurisdiction (referred to as the BBNJ Agreement) was adopted. To further strengthen the management within the Area, the Exploration Regulations approved by the ISA require contractors to collect environmental baseline data and establish environmental baselines for the purpose of assessing the potential impacts of the activities outlined in their exploration work plans on the marine environment, and to develop monitoring and reporting schemes for these impacts. The ISA has also been continuously updating its *Recommendations for the Guidance of Contractors*

for the Assessment of the Possible Environmental Impacts arising from Exploration for Marine Mineral in the Area (hereinafter referred to as the 'Environmental Guidelines'), adding new parameters for environmental baseline surveys and setting more stringent and specific requirements for the technical methods and data quality of environmental parameter surveys.

In line with the United Nations Decade of Ocean Science for Sustainable Development goals. To promote the implementation of the related objectives of the UN's "2030 Agenda for Sustainable Development," resolutions were passed by the 72nd and 75th sessions of the United Nations General Assembly, designating the years 2021 to 2030 as the "United Nations Decade of Ocean Science for Sustainable Development" (referred to as the "Ocean Decade") and adopting an implementation plan. The aim is to take a series of actions to build "an ocean that is clean, healthy and resilient, productive, predictable, safe, accessible and inspiring, and attractive".

In the operation of enterprises, to prevent adverse environmental impacts, the ISO 14001 Environmental Management System standard implements environmental management in business operations through planned and coordinated management activities, with a clear organizational structure of responsibilities and obligations. Subsequently, China introduced the ISO standard into its national standards, forming the *Environmental Management Systems—Requirements with guidance for use* (GB/T24001-2016). When formulating development regulations and their supporting standards and guidelines, the ISA, with reference to ISO 14001, has developed a *Draft standard and guidelines on the development and application of environmental management systems* (ISBA/27/C/7) to accompany the draft development regulations. Pioneer companies, as contractors of polymetallic nodule mining areas in the Area, have formulated this document with a responsible attitude towards the environment, aiming to protect and preserve the marine environment. As the project progresses, scientific understanding develops, and technology advances, this document will be updated and reviewed in a timely manner.
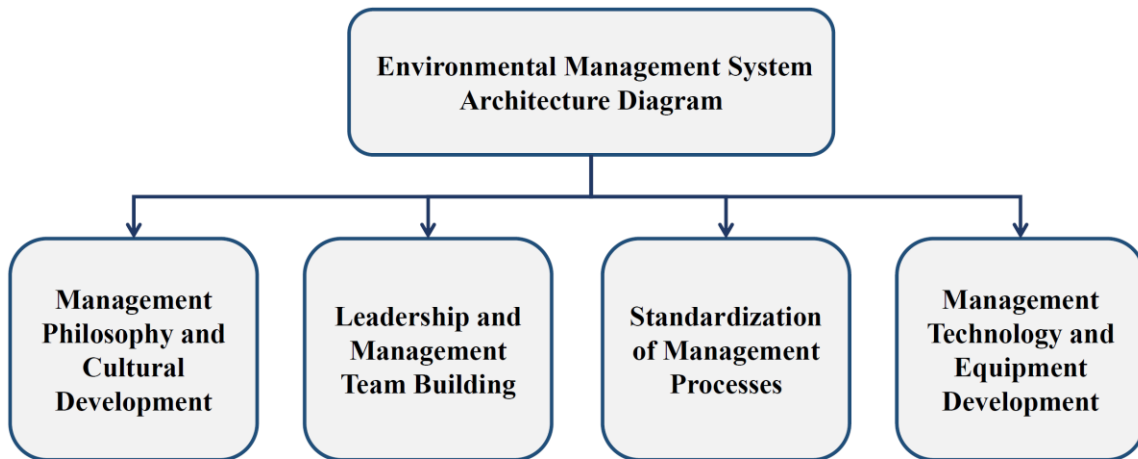
Figure 1 Environmental management system framework

1 Working Basis

In terms of marine surveys and laboratory studies, the Company completed BPC Cruise 1 in 2021, BPC Cruise 2 and BPC Cruise 3 in 2022, and carried out baseline studies of the environment in the mining area in conjunction with part of the results of DY36 cruise, DY41B cruise, DY48 cruise, DY61 cruise, and DY66 cruise, as well as with the publicly available environmental data of the Authority and publicly available data from other sources.

With regard to the construction of standards and specifications, in 2021, the Company organized the relevant units to formulate the *Technical Guidelines for Subsea Polymetallic Nodules Mining System*, which guides the Company to do a good job of environmental protection and preservation in accordance with the relevant principles and procedures when carrying out deep-sea mining activities. In 2022, the Company organized the relevant units to formulate the *Specification for Bottom-setting Environmental Baseline Long-term Observation in Polymetallic Nodule Mining Areas*, which is aimed at guiding the Company in the deployment of near-bottom observation platforms during the exploration phase in polymetallic nodule mining areas, and obtaining partially comparable environmental baseline data that meets the exploration needs of contractors. It also promotes the harmonization of China's environmental survey techniques and methods in the international seabed area with international standards.

In terms of environmental protection and conservation awareness, the company has established an eco-friendly brand, selected a deep-sea mascot, and held public welfare activities for the protection of the marine environment called "Blue Eyes in Action." The company places great emphasis on advancing research in deep-sea scientific cognition,

identifying and establishing a roster of deep-sea benthic organisms. In February 2021, after consultation and expert opinions, the company selected the Octopoda of the family Cirroteuthidae, genus *Cirroteuthis* sp. (Figure 2), from the class Cephalopoda, order Octopoda, as the company's deep-sea mascot. This initiative aims to forge an eco-friendly philosophy and reflect the company's commitment to the protection and preservation of deep-sea biodiversity. In August 2022, during the mobilization event of the 75th cruise of the "Da Yang Hao" (BPC Cruise 2), a public welfare environmental protection activity titled "Blue Eyes in Action," initiated by BPC and participated in by the Second Institute of Oceanography, the North China Sea Technology Center, and other units, was specially held. The joint initiative called for the collective advocacy of "caring for the ocean as we care for our eyes" (Figure 3 and Figure 4).

Figure 2 Company's deep-sea mascot

Figure 3 Signing Ceremony for the "Blue Eyes in Action"
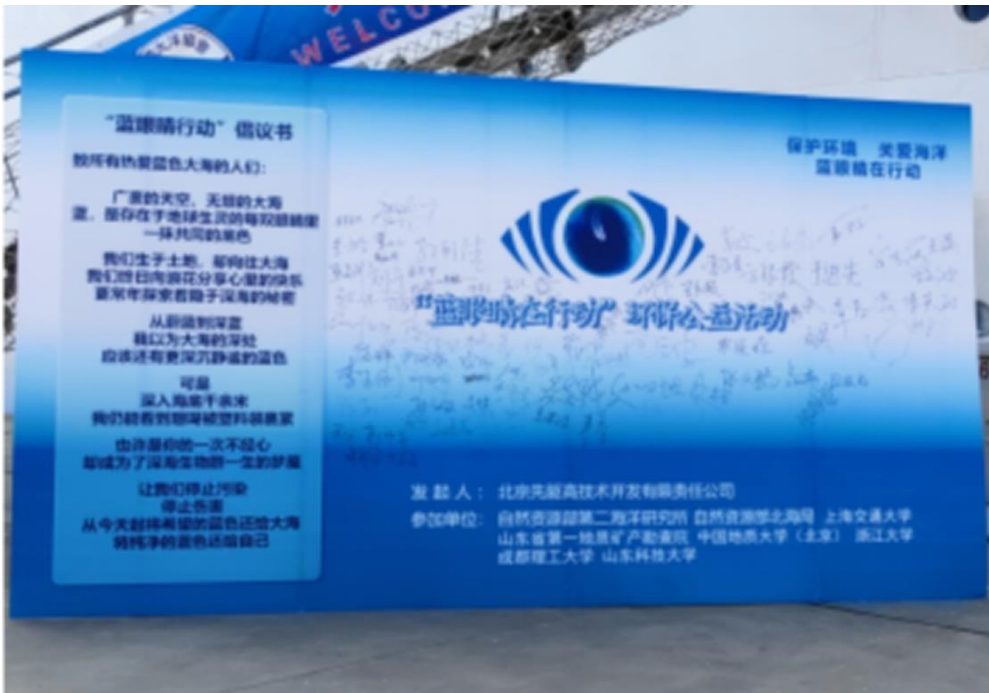
Figure 4 "Blue eyes in action" activity site

2 Objectives, Strategies and Policies

2.1 Environmental Objective

2.1.1 Long-term objectives

The company integrates the "Sustainable Development" into its business strategy, managing various economic, environmental, social, and governance issues related to the exploration and development of mining areas in a responsible manner. The company's long-term environmental objectives are as follows: With the objective of protecting and preserving the environment and biodiversity of the deep-sea polymetallic nodule area, promote the rational utilization of the common heritage of mankind for the benefit of social development. To establish a strategy of "research-oriented exploitation", incorporate deep-sea scientific research throughout the entire process of deep-sea activities, continuously improve knowledge of deep-sea ecosystems, and develop environmental monitoring and restoration technologies by applying precautionary approaches in a timely manner. Apply the highest environmental management standards, conduct environmental impact assessments in advance and adopt the best environmental management measures and tools. With green standards, develop technical and equipment systems for deep-sea mining and achieve sustainable utilization of deep-sea mineral resources.

2.1.2 Medium-term objectives

Formulate the main standards for deep-sea environmental protection and preservation; initially construct the company's environmental protection and preservation standard system for deep-sea mining activities. Enrich and increase the collection of data related to deep-sea mining environmental assessments; establish an environmental baseline data index system and standardization system. Establish an environmental impact assessment model; determine the PRZ and IRZ; and comprehensively monitor the biological communities potentially affected by mining activities in the contract area. Formulate and implement a complete set of internal environmental control systems to manage and reduce the impact of the company's activities on the environment.

2.1.3 Short-term objectives

Establish a company environmental management system to provide a systematic and structured operational mechanism for the company's environmental management. Through the implementation of the environmental management system, strengthen the environmental management of the mining area and the company's operations; make more effective use of energy and resources; reduce energy consumption; save operating costs; and continuously improve the company's environmental performance, achieving minimal impact on the environment from the activities conducted by the company. Establish a mining area environmental management system; clarify the research and development tasks of green key technology and equipment; and propose technical requirements for green mining equipment.

2.2 Strategy

- Establish the concept of "research-oriented exploitation", strengthen cooperation with domestic and international scientific communities; continuously improve the understanding of deep-sea ecosystems; and provide scientific basis for the development of green mining processes and technologies, commercial development scale determination, regional environmental management plan establishment, cumulative impact model and environmental threshold research, and the formulation of environmental impact mitigation measures.

- Adhere to the implementation of sustainable development and responsible environmental management strategies. Prioritize responsible and sustainable management of the environment in all company operations, incorporating it into every aspect of business and exploration and development activities. Persist in using an integrated approach to optimize production and operational energy efficiency; establish company environmental performance objectives; and regularly review these goals to achieve optimal environmental management.

- Explore responsible deep-sea mining operations that are considerate of the environment. Undertake technological and equipment innovation, improve work methods; enhance the efficiency of natural resources, equipment, and energy usage, and develop green deep-sea mining systems. Advance comprehensive digital ocean technologies that enhance human understanding, deep-sea clean energy technologies, and environmental protection planning and ecological restoration technologies for deep-sea spaces.

- Implement environmental risk management strategies and preventive measures. Conduct environmental risk management to identify risks and potential consequences; establish a corporate ethic of environmental responsibility, and develop and implement environmental education and training programs. Ensure that company employees, contractors, and suppliers of equipment, materials, and services understand and comply with the company's environmental policies and specific requirements. Develop strategies for stakeholder participation and environmental public welfare promotion to maintain and enhance the company's reputation.

2.3 Environmental Policy

BPC is a promoter of deep-sea environmental protection, insisting on the development concept of green and low carbon, the business principle of "Exploration, Innovation, Cooperation and Sharing", exploring sustainable ways of deep-sea mineral exploitation, implementing environmentally sustainable development policies. The company will enhance the value of its sustainable development by integrating good environmental practices into all aspects of its business, develop the resources of the international seabed area for the benefit of all mankind, and support the realization of the United Nations Sustainable Development Goals (SDGs). The Company's environmental policy contains the following aspects.

- In compliance with all applicable laws, regulations, and environmental protection guidelines for deep-sea resource exploration, development, and conservation, the company is committed to developing and refining its internal environmental policy framework. The Company undertakes to effectively comply with the "Deep Seabed Area Resource Exploration and Exploitation Law of the People's Republic of China", the United Nations Convention on the Law of the Sea , and the "Regulations on Prospecting and Exploration for Polymetallic Nodules in the Area" established by the ISA. Operating in accordance with the company's environmental regulations, the company will establish a baseline environmental monitoring system for the mining area, an environmental impact assessment system, and environmental management and monitoring protocols. It will also develop and regularly update contingency plans and closure plans.

- To explore sustainable approaches to deep-sea mineral development and to integrate environmental protection requirements and awareness throughout the mining process. The Company is committed to considering environmental impacts and implementing a precautionary approach at all phases of a mining project. The Company adopts best industry practices to protect the environment

and resources in the exploration and development activities. It will utilize available advanced technology and take the necessary measures to prevent, reduce and control pollution and other hazards to the marine environment caused by deep-sea exploration and development activities. Efforts are made to protect and preserve rare or fragile ecosystems, as well as the living environment of depleted, threatened or endangered species and other marine organisms, conserve marine biodiversity, and safeguard the sustainable use of marine resources.

- In the company's strategic planning, procurement, and operational decision-making, environmental impacts are taken into account to minimize the effects on the environment and the consumption of resources. The Company is committed to considering reducing environmental impact and operational carbon emissions in all phases of deep-sea exploration and development, as well as in its daily business. By advancing resource conservation, energy efficiency, waste reduction, and recycling initiatives, the company is actively committed to the sustainable reuse of resources and strives to preserve biodiversity and the environment. The company educates, trains, and encourages employees to carry out their daily tasks with an environmentally friendly way, and support our suppliers and subcontractors to work together to protect the environment.

- Establish reasonable and appropriate long-term environmental objectives and specific environmental targets, and regularly review these goals. Promote continuous improvement in environmental performance by regularly reviewing the company's operations and service processes to make sure that reasonable environmental objectives are established and their implementation is monitored to help the company evaluate and continually improve its environmental performance. Collaborate with stakeholders and take their opinions and suggestions into account when developing environmental objectives and improving environmental actions.

3 Organizational Structure

3.1 Regulatory Framework

Under the guidance of the company's leadership and policies, environmental work is conducted around core processes, identifying and leveraging supportive resources, knowledge and capabilities, communications, and documentation. The core processes

include planning, operations management, and improvement, with each level providing support services in turn (Figure 5).
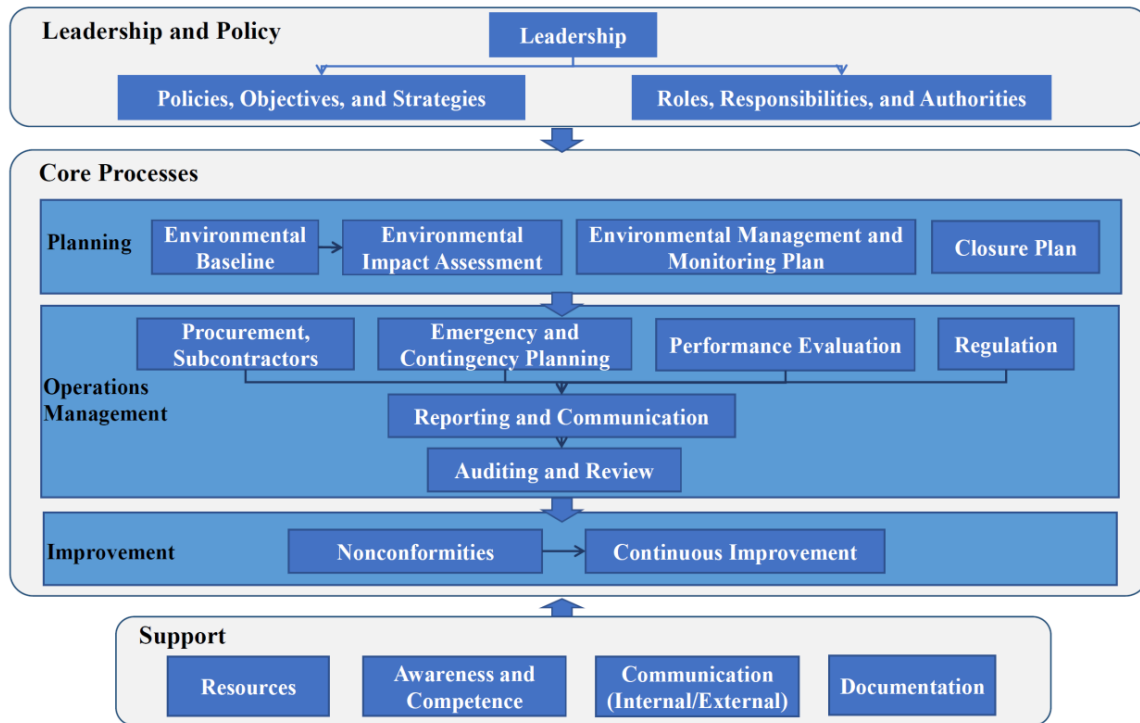
Figure 5 Organizational chart of environmental measures

●Leadership and policy: The leadership role of the company in ensuring that the EMS is established and operated.

(1) Leadership: Positions, deployments and commitments made by the company in the EMS.

(2) Policies, Objectives and Strategies: The policies followed by the company's EMS, the objectives set, and the strategies for achieving these objectives.

(3) Roles, Responsibilities, and Authorities: the responsibilities and authorities of the relevant roles in the EMS, and the work done to establish and implement it.

●Core Processes: Under the leadership of the company, operate the core processes of the environmental management system, including planning, operations management, and improvement.

(1) Planning: Clarify the environmental work requirements in the company's business activities, and carry out environmental work that is appropriate for different business stages.

a. Environmental Baseline: Collect environmental baseline data during the exploration phase, establish an environmental baseline, and provide baseline data for environmental impact assessments.

b. Environmental Impact Assessment (EIA): An EIA is conducted prior to testing mining components, test mining and development applications to control potential environmental impacts within thresholds.

c. Environmental Management and Monitoring: Based on the scale and equipment of the activities (testing of mining components, test mining, or application development), as well as the results of the environmental impact assessment, develop an environmental management and monitoring plan.

d. Closure plan: Develop a closure plan based on the results of the EIA and the plan of work.

(2) Operational Management: Operational management is carried out during the execution of planned operations, including management of procurement, subcontractors, emergency and contingency plans, performance evaluation, supervision, reporting and notification, and auditing and review.

a. Procurement, Subcontractors: Procurement includes purchase of equipment and other physical assets as well as services. Subcontracting refers to the company assigning a part of its business activities to subcontractors.

b. Emergency and Contingency Plan: Aims to establish, implement, maintain, and improve the processes required to prepare for and respond to potential emergencies.

c. Performance Evaluation: Evaluate the performance of the requirements of the EMS through established standards, methods, and frequencies, including environmental performance evaluation.

d. Supervision: Define the positions, responsibilities and authorities for supervision.

e. Reporting and Notification: Report and notify as required by domestic management agencies and the ISA.

f. Audit and Review: Audit and review the planning, operation, inspection and improvement of the EMS.

●Improvement: Identify nonconformities through implementation and propose improvement measures.

a. Nonconformities: Items that do not meet the requirements.

b. Continuous Improvement: Continuously improve the suitability, adequacy and effectiveness of the EMS.

●Support: Resources, awareness and competence, communication and documentation that support the establishment and implementation of the EMS.

a. Resources: Resources used in the EMS, including personnel, equipment, funds and time with relevant capabilities.

b. Awareness and Competence: Knowledge and capabilities for scientific understanding of the deep sea, environmental management, protection and conservation of the deep-sea environment.

c. Communication (Internal and External): Internal and external communication on the concept, establishment and implementation of the EMS.

d. Documentation: Documents in the process of establishing and implementing the EMS.

3.2 Personnel Organization Structure

The personnel organizational structure is shown in Figure 6.
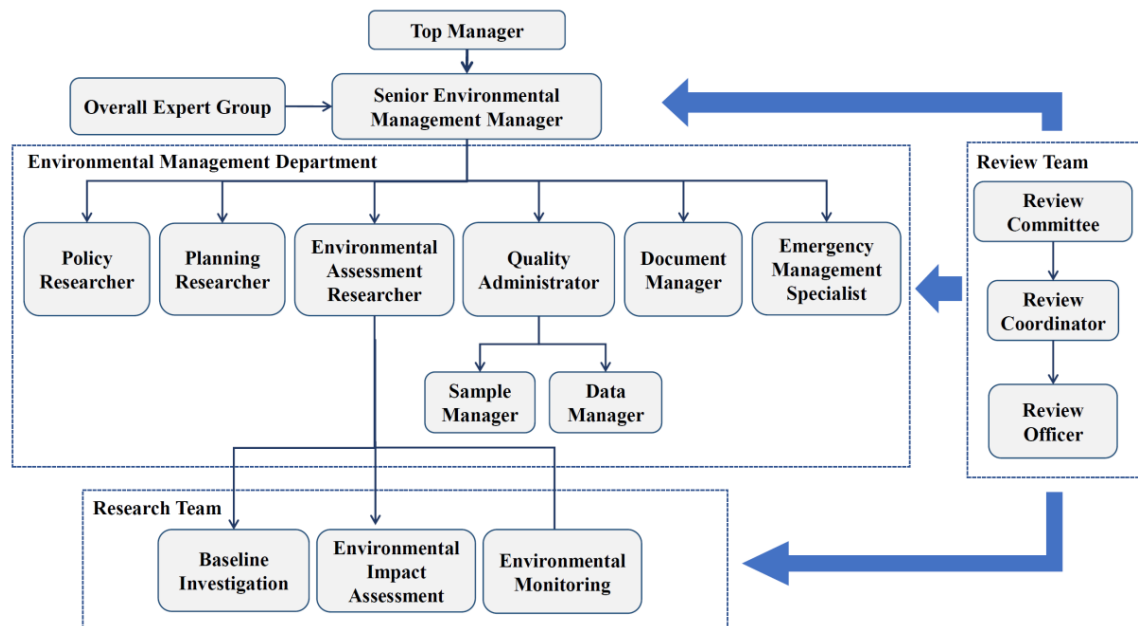
Figure 6 Personnel organization chart

Top management

●Top Manager: The top manager of the company, responsible for the overall planning and top leadership of the EMS.

●Overall Expert Group: Responsible for providing expert advice and guidance on the establishment and implementation of the EMS.

●Senior Environmental Management Manager: Responsible for leading the establishment and implementation of the EMS.

Ministry of Environmental Management

●Policy Researcher: Responsible for conducting research on domestic and international environmental policies, including international law, relevant requirements of the International Seabed Authority, domestic deep-sea law,

environmental law, etc., and formulating policies and environmental systems that are in line with the development objectives of the company's EMS.

●Planning Researcher: Responsible for the planning of environmental work in the EMS, including planning of environmental baseline surveys, planning of environmental impact assessment work, environmental management and monitoring plans, closure plans, and other related operations.

●Environmental Assessment Researcher: Responsible for environmental assessment, including baseline assessment, environmental impact assessment, and monitoring.

●Quality Administrator: Responsible for the overall quality of samples and data obtained in the company's environmental operations.

●Sample Manager: Responsible for the management of samples obtained in the company's environmental business, including the collection, warehousing and use of samples.

●Data Manager: Responsible for the management of data acquired in the company's environmental business, including the collection, entry and use of data.

●Documentation Manager: Responsible for organizing and compiling documents in the EMS.

Research Team

●Baseline Survey: Responsible for environmental baseline survey and analysis.

●EIA: Responsible for assisting environmental assessment researchers with environmental impact assessments, etc.

●Environmental Monitoring: Responsible for assisting the Environmental Assessment Fellow with environmental monitoring.

Review Team

●Review Committee: The EMS Audit Committee is elected by the company's management to supervise and manage the audit work, and to elect an audit coordinator before each audit.

●Review Coordinator: Responsible for conducting regular internal audits of the EMS, and is elected by the Audit Committee before each audit.

●Review Officer: Responsible for assisting the Audit Coordinator in conducting internal audits of the EMS. Audit Officers are temporarily assigned from various departments, and in principle, there should be no fewer than three Audit Officers.

3.3 Leadership and Commitment

The BPC's leadership places a high priority on environmental work in the mining area and has begun to formulate guidelines related to the environmental aspects of deep-sea

mining after signing an exploration contract with the ISA. In 2021, it completed the *Technical Guidelines for Subsea Polymetallic Nodules Mining System*, which propose green criteria for mining systems to protect and preserve the marine environment. In 2021, it completed the *Guidelines for Environmental Protection and Preservation in Deep-Sea Mining Activities* as a group standard, setting requirements for environmental work during the exploration, development, and mine closure phases for contractors. The company will continue to build a system of environmental management standards based on the needs of environmental work.

The company places great emphasis on educating staff and subcontractors about the importance of environmental protection and implements scoring criteria for environmental protection measures in the bidding process for marine survey expeditions.

The company has a long-term plan and full-process management for the entire project and has formulated this document with the aim of implementing and enforcing the work of the EMS.

4 Planning (Work Program)

4.1 Establishment of Environmental Baselines

4.1.1 Spatial Planning and Initialization of the Work Plan

The analysis and study of historical data provided a preliminary understanding of the resource and environmental characteristics of the mining area. Based on the environmental baseline survey items listed in the ISA's *Draft Guidelines for the Establishment of Baseline Environmental Data* (ISBA/27/C/11) and the actual situation of the mining area, spatial planning for the environmental baseline survey is conducted, and preliminary short-, medium-, and long-term work plans are designed. Key attention is given to environmental elements such as hydrodynamic intensity, biological productivity, composition and physicochemical properties of the substrate material, as well as natural processes such as particle diffusion and sedimentation near the seabed, acoustic and optical propagation, and benthic biological succession, to accurately predict environmental impacts and preliminarily establish an environmental baseline and impact indicator system. A combination of large-scale surveys and local regional surveys is used to know the large-scale and local spatial variation of environmental elements. Data are collected on a long-term to understand the temporal variation of environmental elements. Considering the scope of environmental impact, the scope of the environmental survey should be expanded

relative to the mining area itself. The findings are disclosed to stakeholders, subject to inquiry, and third-party certification is obtained as appropriate.

4.1.2 Acquisition and Analysis of Data

Following the methods stipulated in the ISA's *Draft Guidelines for the Establishment of Baseline Environmental Data* (ISBA/27/C/11), and in conjunction with the actual situation of the mining area and the best available technology, environmental baseline data is collected according to spatial planning and work plans. Combining Geographic Information Systems, digital twin technology, and other best available technologies, along with robust numerical analysis and mathematical statistical methods, a standardized system for environmental baseline data is gradually established. Based on this, the collected data is analyzed to preliminarily determine the environmental baseline conditions of the mining area and its adjacent areas, the delineation plan for the reference areas, and the REMP.

4.1.3 Adjustment of Spatial Planning and Program of Work

Adjustments to the initial spatial planning and work plan based on continuously updated survey data and analysis. Further investigation and research are conducted on environmental elements with obvious spatiotemporal variations, while the investigation and research on elements with less obvious spatiotemporal changes will be relatively reduced. Additional regional investigations will be carried out based on the delineation plan for the reference area and the REMP. According to the adjusted spatial planning and work plan, further environmental baseline data is acquired.

4.1.4 Assessment and Confirmation of Baseline

The obtained baseline data is subject to error analysis and standardization verification, and is cross-validated by published data. The spatiotemporal distribution and natural variation of the environmental elements are interpreted and evaluated using marine science theories to check its reliability. Self-checks and internal and external audits are conducted on the test data. Based on the established environmental baseline indicator system, the environmental baseline data is systematically organized, and the environmental baseline is established. Depending on the situation, a digital and visual model of the spatiotemporal distribution and natural variation of the environmental baseline may be created.

4.2 Environmental Impact Assessment (EIA)

4.2.1 Establishment of Environmental Impact Elements and Thresholds

In accordance with the content and requirements listed in the ISA's Recommendations for the *Guidance of Contractors for the Assessment of the Possible Environmental Impacts arising from Exploration for Marine Mineral in the Area* (ISBA/25/LTC/6/Rev.3), and based on the established environmental baseline, further screen the environmental elements and corresponding threshold systems that may require assessment. Clarify key organisms, critical control elements, and their interrelationships to establish an environmental impact assessment model, which requires a theoretical foundation in marine science and ecological mechanism studies. These environmental elements can be graded according to the likelihood and severity of their impact by mining activities, including elements that are highly likely, likely, or essentially unlikely to be affected by mining activities, to carry out a focused and targeted assessment. These environmental elements should address the main impact processes of mining activities, including, for example, luminescence, acoustics, substrate stripping and disturbance, plume dispersion and redeposition. Thresholds are graded based on the tolerance (or recoverability) of biological habitats to changes in certain environmental elements, which requires theoretical research and simulation experiments. The establishment of environmental impact elements and thresholds should consider both instantaneous and short-term impacts, as well as medium and long-term impacts. It should take into account the impact of single elements as well as the combined cumulative impact of multiple elements, and also consider the differences in impacts and thresholds for different organisms and habitats. Research mitigation, restoration, and compensation measures for potential impacts.

4.2.2 Pre-evaluation

Prior to mining activities at different scales, a pre-assessment of the potential environmental impacts and their extent is required, which relies on written studies and model simulation. Simulation of deep-sea mining activities based on the spatial and temporal distribution and natural variability characteristics of environmental baselines. Algorithmic analyses are carried out through oceanographic and ecological theories to simulate the degree and extent of impacts of pollutants on organisms and habitats in the reference area at different spatial and temporal scales, in conjunction with defined thresholds, so that the extent of impacts of mining activities on biological habitats can be

assessed. The expected effects of mitigation, restoration and compensation measures are modeled. An environmental impact pre-assessment report is prepared to describe the results of the above assessment and to confirm the feasibility of the mining activity in terms of environmental protection and preservation. If the mining plan is feasible, it may be approved after consultation with stakeholders; if it is not feasible, the mining plan will need to be optimized to reduce environmental impacts.

4.2.3 Assessment of the Test

Collect data on the instantaneous, short-term, medium-term and long-term environmental impacts of the surveyed area and adjacent areas after the test, compare and verify them with the baseline and pre-assessment data to optimize the model, and evaluate the environmental impacts in conjunction with the determined thresholds to form an environmental impact assessment report on the test. Trial mitigation, restoration and compensation measures are attempted and their effectiveness is verified using measured data. If the test-mining scheme is feasible, it can be approved for commercial mining in accordance with the mining scheme after consulting with stakeholders and obtaining third-party certification, as appropriate, and a pre-assessment of the environmental impacts of commercial mining will be conducted using the digital model, resulting in a pre-assessment report on the environmental impacts of commercial mining; if it is not feasible, the test-mining scheme will need to be optimized in order to reduce the environmental impacts.

4.3 Development of an Environmental Management and Monitoring Plan

Commercial mining requires frequent monitoring and assessment of the environmental impacts of the activity. Based on the predicted extent and scope of environmental impact, an environmental monitoring plan should be developed. This plan should include the rational and effective deployment of environmental monitoring equipment and the acquisition of monitoring data at appropriate times and frequencies. The collected data should be compared and validated against baseline and pre-assessment data to improve the model. In conjunction with digital and visual systems, high-frequency (real-time or near-real-time) assessments of environmental impacts should be conducted, with timely warnings for situations that exceed habitat thresholds and prompt adjustments to operational plans. Combine digital and visualization systems to assess environmental impacts at high frequency (real-time or quasi-real-time), provide early warning of

exceeding biohabitat thresholds, and adjust the plan of work in time. Mitigation, restoration, and compensation measures should be taken to reduce environmental impacts, and the effectiveness of these measures should be evaluated. After an annual commercial mining operation, data on the instantaneous, short-term, medium-term and long-term environmental impacts of the operation and adjacent areas need to be collected in order to assess the environmental impacts of the mining activities during the year, and an annual environmental impact assessment report needs to be prepared, made available to stakeholders and subject to questions. Given the long-term nature of commercial mining projects and the accompanying technological developments, the monitoring and assessment program may be updated in phases as necessary.

4.4 Developing a Closure Plan

After the completion of a multi-year commercial mining project and prior to mining closure, the contractor should develop a closure plan, including post-closure monitoring of residual and natural environmental impacts. Predictions of residual impacts and recovery of biological habitats from mining are made through algorithmic analyses based on oceanographic and ecological theories through researches or model simulations. Undertake regular on-site environmental monitoring and assessment, calibration and optimization of models and results in the longer term after mining closure. Mitigation, restoration and compensation measures are taken to reduce environmental impacts and the effectiveness of these measures is assessed, and a post-mining environmental assessment report is prepared and published for consultation with stakeholders, and third-party certification is obtained as appropriate. Any temporary suspension of production should also have an interruption plan in place, as necessary. Establish a post-mining monitoring and assessment program and an acceptable system of indicators, so that when the environment has been restored to an acceptable level, subsequent monitoring and assessment can be discontinued.

5 Operations Management

5.1 Regulation

The core processes of the EMS are divided into four parts, the establishment of an environmental baseline, environmental impact assessment, environmental management and monitoring, and closure plans, with leadership at all levels overseeing daily supervision and management tasks.

5.2 Procurement, Subcontractors

The Company attaches great importance to the potential environmental impacts during the procurement and subcontracting process. Currently, for the expeditions completed during the exploration phase, there are requirements for evaluating and scoring environmental protection measures during the bidding process. During the execution of the expeditions, the winning bidders also carry out environmental protection propaganda for the crew on board and activities such as sorting of domestic waste. At present, the company mainly conducts environmental baseline surveys during the exploration phase. Procurement and subcontracting mainly occur in the purchase of equipment and expedition surveys. In the next phase, for activities such as environmental impact assessments, collection tests, environmental management and monitoring, and closure planning, it is necessary to identify procurement and subcontracting needs, set environmental management requirements for procurement and subcontracting, and supervise their implementation.

5.3 Establishing Emergency and Contingency Plans

The emergency response team should work in conjunction with the core activities to identify potential risks and incidents, develop emergency response plans, and establish emergency and contingency mechanisms.

Currently, during the exploration phase, the company primarily carries out environmental baseline surveys. In the expedition surveys, an implementation support group, an emergency coordination group, and a safety assurance group are established. The emergency coordination group is jointly established by the competent department, the company, the unit responsible for organizing the expedition, and the ship security unit. It is responsible for responding to major emergencies during the expedition, making decisions on emergency plans for expedition adjustments, and commanding and coordinating the handling of emergencies by relevant units and personnel.

The safety assurance group is composed of the ship security unit, the cruise organization and implementation unit as well as the personnel of the relevant navigation units, and is fully responsible for the ship security work during the cruise. The implementation support group is led by the cruise organization and implementation unit, and is composed of personnel from the competent unit, the company, and the ship security unit, etc. It coordinates and promotes the implementation of the security work of each unit responsible for the implementation of the cruise during the cruise, as well as strengthening

the communication and collaboration of the participating cruise units and establishing ship communication, reporting system, roadbed protection and meteorological protection.

5.4 Evaluation of Implementation and Environmental Performance

Environmental performance is evaluated by scoring environmental performance according to the environmental performance scoring sheets (Annex I and Annex II in Appendix I).

5.5 Audits and Reviews

5.5.1 Internal and External Reviews

The company conducts internal audits in accordance with the audit system within the environmental management system and also cooperates with the ISA for external audits. An Audit Committee is established within the internal audit system, which is elected by the company's management. Before each audit, the Audit Committee elects an Audit Team Leader, and the Audit Officers are temporarily assigned from various departments. In principle, there should be no fewer than three Audit Officers.

5.5.2 Management Review

The Audit Committee is responsible for the supervision and management of the audit process. Once the audit documentation has been reviewed and approved by the Audit Committee, it is then handed over to the Document Manager to be incorporated into the EMS's documentation.

5.6 Reporting and Notification

Submission of annual reports and notifiable events as required by domestic administrations and the ISA.

6 Improvement

6.1 Nonconformity

The company shall check the EMS requirements by internal and external reviews, identify nonconformities, and the company shall develop an audit process and corrective actions for nonconformities. The company should also report these as required by the ISA.

6.2 Continuous Improvement

Continuously improve the applicability, adequacy and effectiveness of the EMS to enhance environmental performance, and update and review this document as appropriate.

7 Support

7.1 Resources

The company provides the resources necessary for the establishment, implementation, maintenance and continuous improvement of the EMS, including funds, technology, personnel, equipment, infrastructure and so on. The leadership of the company makes clear provisions for the roles, responsibilities and authority of key employees in environmental work, determines the requirements for each job position and environmental responsibility in the EMS, document these and transmits them. The Company provides software and hardware equipment for the EMS, supports the construction of environmental monitoring facilities, provides digital technology, information and communication technology, and encourages scientific research in the field of environmental protection.

7.2 Awareness and Competence

The company implements an environmental protection responsibility system, clarifies everyone's environmental protection responsibility, and formulates and implements relevant training programs. Regular environmental protection training is provided to employees to help them better understand the company's environmental policies, objectives and common actions, to ensure that they have knowledge and skills of environmental protection and environmental management, good awareness and behavior of the EMS, and to share environmental protection knowledge and information with stakeholders, such as

purchasers and subcontractors. Develop a regular evaluation system to assess and improve the effectiveness of the measures taken.

7.3 Communication

The Company develops, implements, and maintains the processes for internal and external communications related to the EMS. It ensures that all inquiries, consultations, complaints, and information exchanges are discussed and addressed at relevant company meetings, enhancing environmental transparency. Stakeholder engagement measures are developed, and the company regularly conducts public welfare activities to popularize and promote environmental knowledge.

Internally, the company ensures that its environmental management policies, objectives, plans, and performance are communicated to all employees through notice boards, internal networks, or company newsletters. Mechanisms and channels are established to ensure that any inquiries from employees regarding the company's EMS and environmental matters are relayed to the responsible department heads.

Externally, the company regularly participates in meetings of international organizations such as the International Seabed Authority to stay informed about the latest developments and trends in deep-sea environmental protection, and to update the company's environmental work requirements accordingly. The company's environmental policies and guidelines are made available through administrative departments and on its website, with environmental plans and reports published on the company's website.

Stakeholder engagement measures are formulated, specifying the methods of stakeholder participation, channels for information disclosure, timelines for participation, and methods for handling feedback. Relevant information is promptly disclosed on the company's website, and the opinions received from stakeholder consultations, as well as the company's responses, are made public on the website.

7.4 Environmental Management System Documentation

Maintain and manage documents by categories and develop an EMS document number.
(1) Environmental policy and standards documents (BPC/EMS/P/XX)
(2) Documentation of environmental management system records (BPC/EMS/R/XX)
(3) Stakeholder consultation documents (BPC/EMS/SC/XX)
(4) Environmental baseline related documents (BPC/EMS/BL/XX)
(5) Environmental Impact Assessment Report (BPC/EMS/EIS/XX)

(6) Environmental management and monitoring plan documents (BPC/EMS/EMMP/XX)

(7) Closure plan documents (BPC/EMS/CP/XX)

(8) Other documents (BPC/EMS/O/XX)

References

[1] Turcheniuk, K., Bondarev, D., Singhal, V., & Yushin, G. (2018). Ten years left to redesign lithium-ion batteries. *Nature*, *559*(7715), 467–470.

[2] Draft standard and guidelines on the development and application of environmental management systems (ISBA/27/C/7), International Seabed Authority, 2022.

[3] Technical Guidelines for Subsea Polymetallic Nodules Mining System (T/CAOE 40-2021), 2021.

[4] Draft guidelines for the establishment of baseline environmental data (ISBA/27/C/11), International Seabed Authority, 2022.

[5] Guidance of Contractors for the Assessment of the Possible Environmental Impacts arising from Exploration for Marine Mineral in the Area (ISBA/25/LTC/6/Rev.3), International Seabed Authority, 2023.

[6] Draft standard and guidelines for the environmental impact assessment process (ISBA/27/C/4), International Seabed Authority, 2022.

[7] Environmental management systems–Requirements with guidance for use (National Standard GB/T24001-2016/ISO14001:2015), 2015.

[8] Deep Seabed Area Resource Exploration and Exploitation Law of the People's Republic of China, the National People's Congress Standing Committee, 2016.

[9] Marine Environment Protection Law of the People's Republic of China, the National People's Congress Standing Committee, 2017.

[10] Draft regulations on exploitation of mineral resources in the Area, International Seabed Authority, 2019.

[11] Regulations for Prospecting and Exploration for Resources in the International Seabed Area, China Ocean Mineral Resources R & D Association, Ocean Press 2015.

[12] Regulations on prospecting and exploration for polymetallic nodules in the Area, International Seabed Authority, 2013.

[13] Regulations on prospecting and exploration for polymetallic sulphides in the Area, International Seabed Authority, 2010.

[14] Regulations on prospecting and exploration for cobalt-rich ferromanganese crusts in the Area, International Seabed Authority, 2012.

BPC Environmental Management System Philosophy, Objectives and Policies

Annex I

Internal Review of the Environmental Performance Scoring Sheet

Scorer：   Time：

Evaluation items and scoring criteria	Scoring criteria	Full score	Score	Note
Construction of environmental management system	● Whether documents related to the environmental management system are developed/updated. ● No environmental management system documentation has been developed/updated.	20 points		
Environmental management system operation	● Actively implement environmental management system requirements. ● Failure to implement environmental management system requirements.	20 points		
Regulatory aspects of environmental management systems	● Regulated in accordance with the requirements of the environmental management system. ● Failure to regulate in accordance with the requirements of the environmental management system.	20 points		
Environmental management system improvement aspects	● Identify deficiencies in the operation of the environmental management system and make improvements. ● unimproved	20 points		
Environmental management system support aspects	Availability of resources, awareness and capacity to communicate internally and externally, and relevant documentation to manage.	20 points		
Total score				

BPC Environmental Management System Philosophy, Objectives and Policies

Annex II

Subcontracting or Procurement Environmental Performance Scoring Sheet

Subcontracting or Purchasing Program：

Head of Subcontracting or Purchasing Party:

Scorer：　　　　　　　　　　　Time：

Evaluation items and scoring criteria	Scoring criteria	Full score	Score	Note
Is there an environmental management organization and measures for environmental management?	• Clear organization and high level of awareness. • Cooperate with requests and solicitations for investigations from investigating organizations, but have not established an environmental management organization of their own. • Low environmental awareness.	20 points		
Implementation of environmental measures?	• Full implementation of environmental measures. • Implementation of the environmental measures component. • Environmental measures are not enforced.	20 points		
Is there any publicity and education on environmental protection?	• Actively conducting numerous awareness and education campaigns on environmental protection, both for internal staff and for the outside public. • Less movement • No awareness-raising and educational activities on environmental protection have been carried out.	30 points		
Have there been incidents of environmental damage in the course of the project?	• There have been incidents of environmental damage in the course of the project. • There were no incidents of environmental damage.	30 points		
Total score				

Appendix II Flocculation and Sedimentation Experiments

1 Methods

Sedimentation experiments were conducted on ships during cruise and in land laboratories. During the BPC Cruise 1, 500 ml of filtered seawater was loaded into two beakers on survey vessel "Xiangyanghong 03", 1 ml and 2 ml of seabed sediments were added to the beaker, and stirred with glass rods, so that the sediment was fully dispersed in the seawater. The dispersed turbid fluid was then quickly poured into two graduated 550 mL syringes to photograph the syringe every 5min to observe the sediment deposition.

Considering that the shaking of the scientific research vessel during the cruise execution affects the accuracy of the settlement experiment results, the flocculation and settlement experiment was carried out again in the laboratory after the cruise. The seawater used for the experiment was collected in the Block M during the BPC Cruise 1. The tested sediment was collected from the upper 20 cm of seabed in Station DY69-M2B1-ES 02-BC22. Both seawater and sediment samples were kept 4℃ refrigerated.

In the laboratory, the *Millipore* acetate fiber filter with a pore diameter of 0.45 μm was used to remove impurities in seawater that used for sedimentation experiment. Since flocculation deposition occurs only in fine particles, a 20 μm sediment sample was wet-sieved to remove siliceous biological debris and coarse minerals from the sediment. The smear slides showed that the wet-sieved sediment was composed of clay and fine silty minerals, and no siliceous biogenic skeleton or coarse volcanic grains (Figure 1)
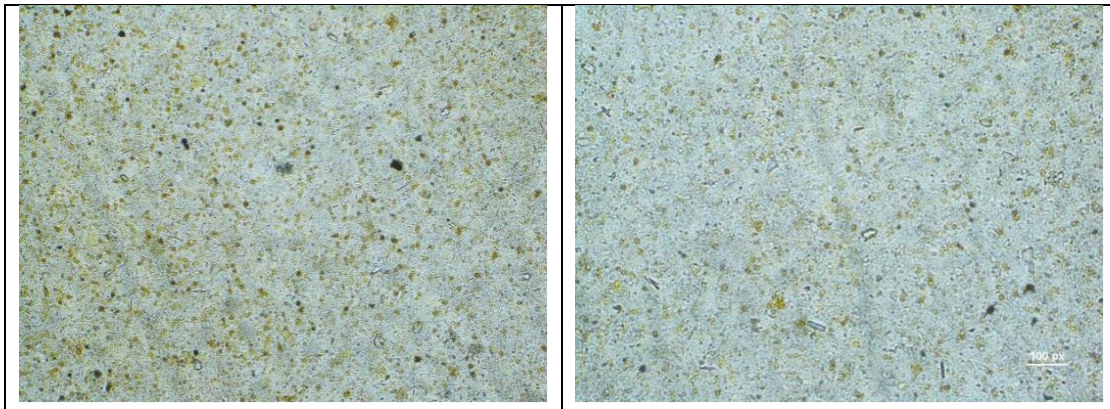
Figure 1 Sediment smears used for sedimentation experiments after wet screening

For flocculation settlement experiment, 2000 mL of filtered seawater was poured into a beaker, adding 2 mL, 4 mL and 6 mL of filtered sediment respectively, stirring for 5 min, 10 min and 15 min. After stirring for 3 min, absorb a small amount of upper 3 cm water with pipette, make a smear slide and filter with 0.45 μm *Millipore* acetate fiber filter, and

observe whether flocculation particles were produced under electron microscope scanning electron microscope respectively (SEM). The smear slides observation results showed that the stirring time is not strongly correlated with the number of flocculation particles, that is, stirring for 5 min can produce flocculation particles. However, the concentration of sediment affects the flocculation particles. When 2 mL of sediment particles are added, there are less flocculation particles in the sample; a large number of flocculation particles are produced when 4 mL of sediment is added. Also, when the sediment concentration is above 6 mL, the particles are mainly dispersed in the smear slides and electron microscope, while the flocculation particles are reduced. Figure 2 shows the flocculation particles in the smear and Figure 3 shows the flocculation particles in SEM.
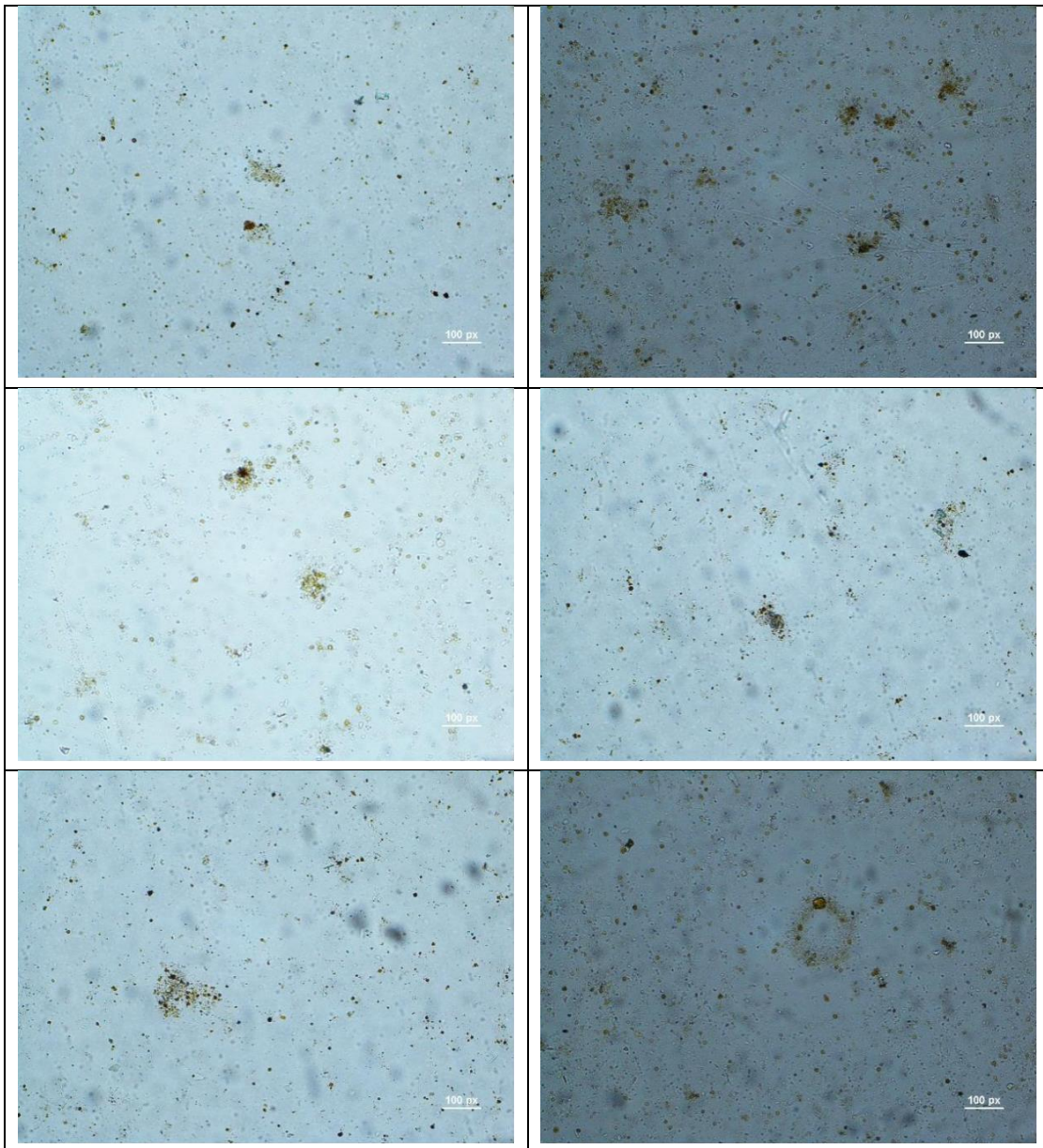
Figure 2 Flocculation particles in the smear

After determining the sediment resuspension and that a large number of flocs could be produced in the environment of turbulent disturbance, the researchers conducted the observation of the flocs sedimentation rate. The experimental observation device is as described in (Mhashhash et al., 2018). For flocculation sedimentation observation, the microscope was placed horizontally and the settled flocculation was captured using the CCD camera. The flocculation particles were then selected and the distance of flocculation particles settlement per unit time was calculated to calculate the settlement rate.
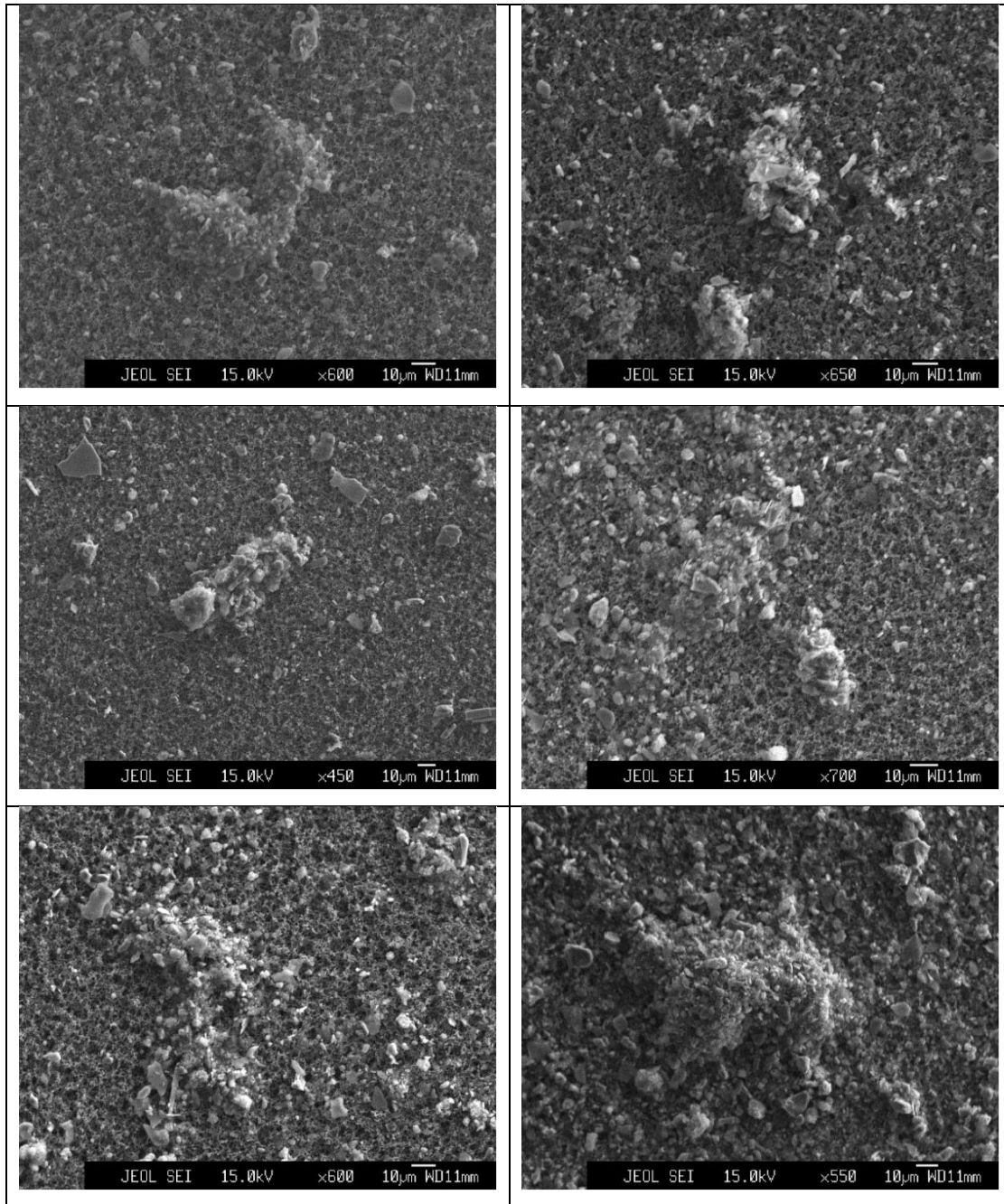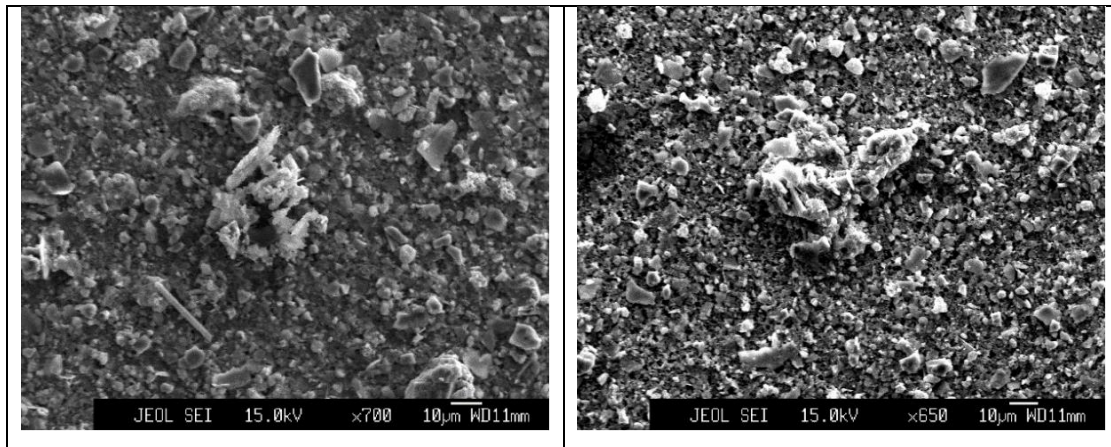
Figure 3 Flocculation particles in SEM
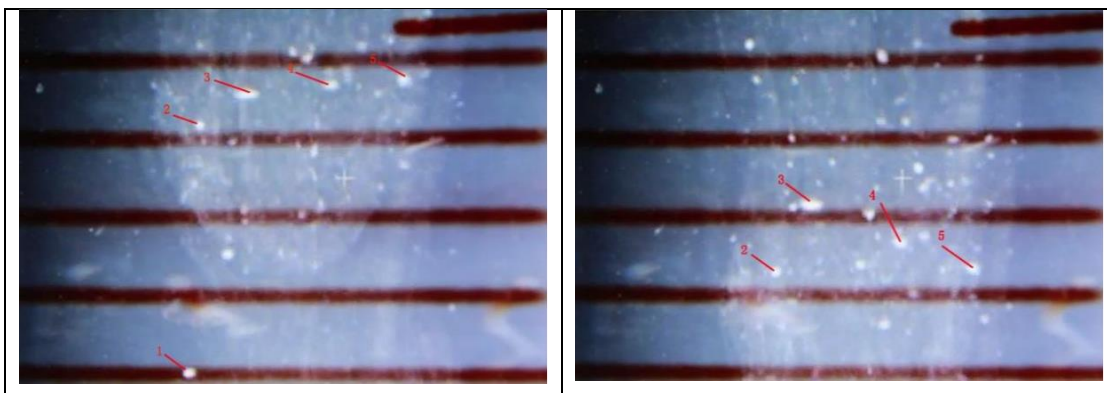
Figure 4 Flocculated particle tracking and settling rate tests (left panel after 0 seconds, right panel after 5 seconds)

2 Results

2.1 Field Experimental Observations

In the field sediment resuspension sedimentation experiment, it was found that when the sediment concentration was 0.2%, because the concentration was too low, the sedimentation process of resuspension sediment could not be seen by the equipment. When the sediment concentration is 0.4%, it can be shown by photography. As can be seen from Figure 5, the deposition of the resuspended sediment in the first 20 min is obvious, the suspended sediment in seawater gradually decreased, and the light transmittance of seawater gradually increased. At this time, it should be non-flocculation settlement, sediment according to Stokes's law, large particles settle firstly, then the deposition of small particles. After 28 min, the light transmittance of the middle and lower part of the settlement tube no longer changes, indicating that the non-flocculation settlement ends and the flocculation in the seawater begins to settle. When the flocs are slowly settling, the

uppermost sea water becomes clear and more transparent. After 1 h, the flocs settlement was not obvious, and there were always turbid flocs in the lower part of the settlement tube. This may be related to the suboptimal experimental conditions on board. The shaking of the ship leads to the flocculation in the settlement tube cannot settle, and even rising phenomenon. According to the obvious flocculation and settlement between 23 min and 28 min, and the position change of the interface between clear seawater and turbid seawater, the rate of flocculation and settlement is about 1.68 mm / min.
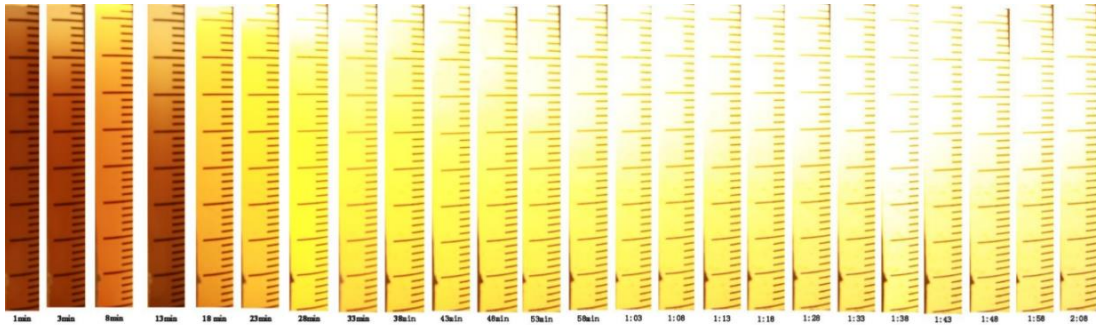
Figure 5 Field experiment resuspended sediment settling process

2.2 Results of the Laboratory Experiments

By tracking 35 flocculation particles (Table 1), the sedimentation rate of each flocculation particle was calculated, and the average sedimentation rate of the flocculation particles was 0.7 mm/s. There is a weak positive correlation between flocculation particle size and deposition rate (Figure 6).

Table 1 Flocculation deposition rate test results

NO.	Size of flocculating particles (μm)	Time (s)	Settling height (mm)	Settling rate; (mm/s)
1	383.63	12.82	6.93	0.54
2	255.75	11.30	6.93	0.61
3	639.39	13.38	6.93	0.52
4	426.26	10.86	6.93	0.64
5	554.13	7.98	6.93	0.87
6	554.13	7.43	6.93	0.93
7	724.64	6.76	6.93	1.03
8	596.76	10.00	6.93	0.69
9	298.38	11.32	6.93	0.61
10	255.75	15.15	6.93	0.46
11	341.01	6.92	6.93	1.00
12	383.63	8.08	6.93	0.86
13	255.75	18.78	6.93	0.37

NO.	Size of flocculating particles (μm)	Time (s)	Settling height (mm)	Settling rate; (mm/s)
14	213.13	10.82	6.93	0.64
15	511.51	10.33	6.93	0.67
16	285.59	7.50	6.93	0.92
17	289.86	8.10	6.93	0.86
18	383.63	8.53	6.93	0.81
19	511.51	6.60	6.93	1.05
20	234.44	13.30	6.93	0.52
21	153.45	9.95	6.93	0.70
22	468.88	18.40	6.93	0.38
23	217.39	8.38	6.93	0.83
24	306.91	8.68	6.93	0.80
25	426.26	7.36	6.93	0.94
26	221.65	8.12	6.93	0.85
27	404.94	6.05	6.93	1.15
28	426.26	7.95	6.93	0.87
29	383.63	17.75	6.93	0.39
30	298.38	17.70	6.93	0.39
31	409.21	10.20	6.93	0.68
32	639.39	10.28	6.93	0.67
33	387.89	14.50	6.93	0.48
34	255.75	18.76	6.93	0.37
35	468.88	16.92	6.93	0.41
Average	387.65			0.70
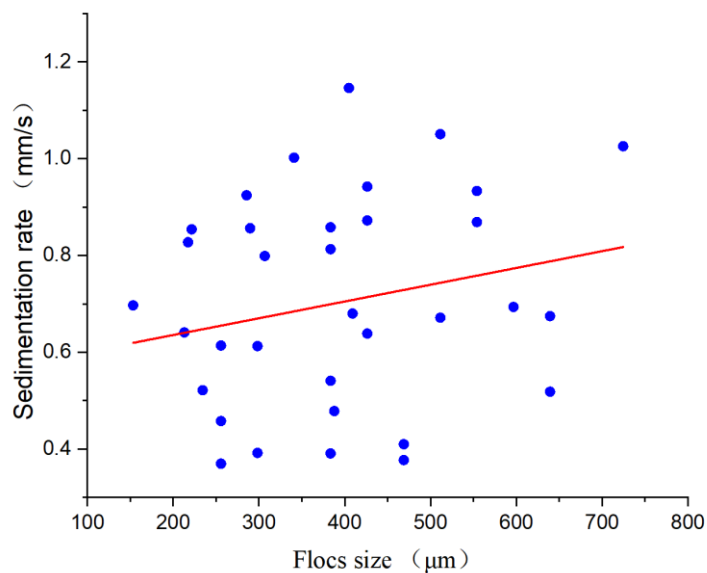
Figure 6 Scatter plot of the particle size and sedimentation rate of the flocculation particles

Flocculation particles can be divided into large flocculation (macroflocs) and small flocculation (microflocs), which are divided by 160 μm (Manning et al., 2010). The flocculation particles observed in this experiment belong to large flocculation, and their sedimentation rate is basically consistent with the results of Manning et al (2010) and Oebius et al. (2001), that is, the sedimentation rate of large flocculation particles is about 1 mm/s.

Appendix III Plume Dispersion Model Results

1 Characteristics of Plume Horizontal Dispersion

1.1 Dispersion Characteristics of Near-bottom Suspended Sediment at 1 m Above the Bottom

The results of the horizontal distribution of suspended sediment concentration (SSC) at a depth of 1 m from the bottom (Figure 1 to Figure 54) show that, on average, the range of suspended sediment concentration greater than 1 g/l is only around the CTA, and it disappears quickly after the test stops; the range of suspended sediment concentration at 10 mg/l is mainly in the CTA, and it also disappears quickly after the test stops; the plume disappears 3-4 days after the operation stops (i.e., 8-9 days after the test starts). The direction of the plume spread is related to the background flow field. Under the background flow field of northwest flow in Case 2, the direction of the plume spread is northwest. Under the background flow field of southwest flow in Case 5, the direction of the plume spread is southwest. Under the background flow field of east flow in Case 4, the direction of the plume spread is east. The plume spread is the smallest in the weak current cases (Case 1 and Case 3). The maximum plume spread distance (from the center of the CTA) of deep-sea mining plumes is 5.42 km in Case 5, and the minimum is 2.93 km in Case 3 (Table 6-2). In extreme cases, the plume time in the water increases compared to the average case, and the plume disappears after 7 to 9 days of operation (i.e., 12 to 14 days after the start of the test). The maximum distance of the plume (from the center of the CTA) was 27.86 km in Case 8 and 14.51 km in Case 9.

Figure 1 Horizontal distribution of SSC at 1 mab for Case 1 (1 day later)

Figure 2 Horizontal distribution of SSC at 1 mab for Case 1 (3 days later)

Figure 3 Horizontal distribution of SSC at 1 mab for Case 1 (5 days later)

Figure 4 Horizontal distribution of SSC at 1 mab for Case 1 (7 days later)

Figure 5 Horizontal distribution of SSC at 1 mab for Case 2 (1 day later)

Figure 6 Horizontal distribution of SSC at 1 mab for Case 2 (3 days later)

Figure 7 Horizontal distribution of SSC at 1 mab for Case 2 (5 days later)

Figure 8 Horizontal distribution of SSC at 1 mab for Case 2 (7 days later)

Figure 9 Horizontal distribution of SSC at 1 mab for Case 3 (1 day later)

Figure 10 Horizontal distribution of SSC at 1 mab for Case 3 (3 days later)

609

Figure 11 Horizontal distribution of SSC at 1 mab for Case 3 (5 days later)

Figure 12 Horizontal distribution of SSC at 1 mab for Case 3 (7 days later)
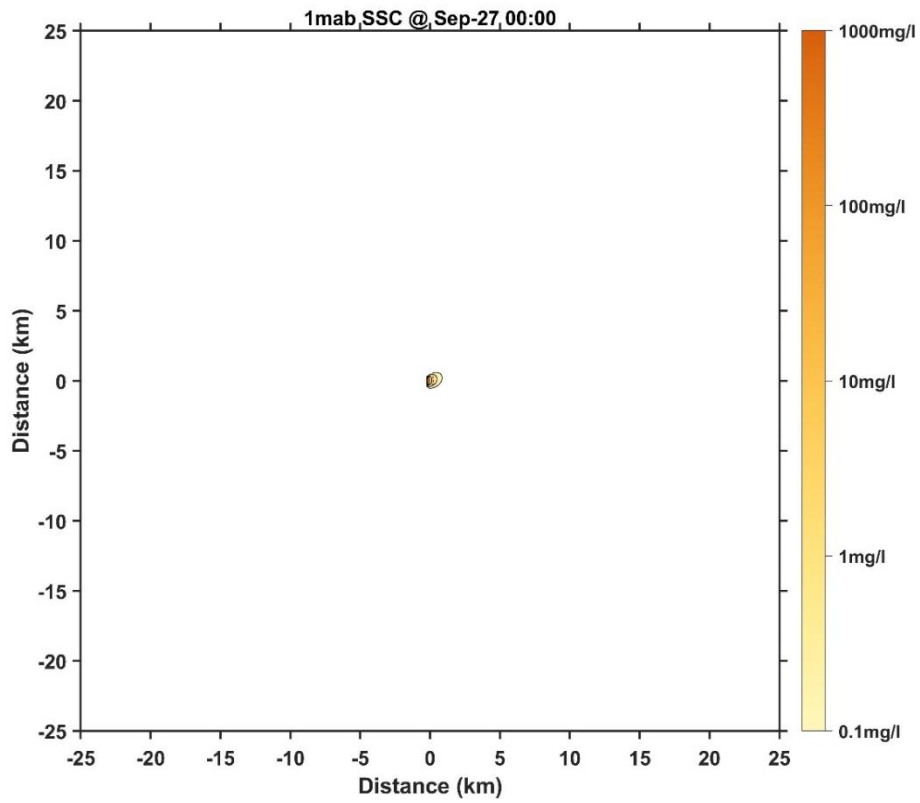
Figure 13 Horizontal distribution of SSC at 1 mab for Case 4 (1 day later)
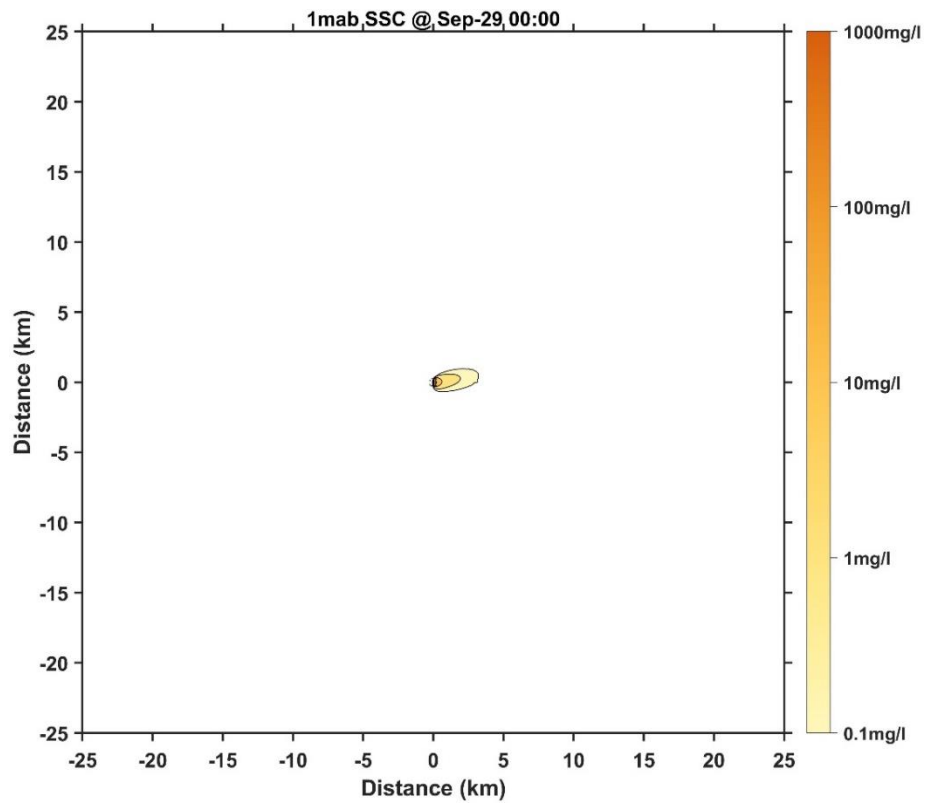
Figure 14 Horizontal distribution of SSC at 1 mab for Case 4 (3 days later)
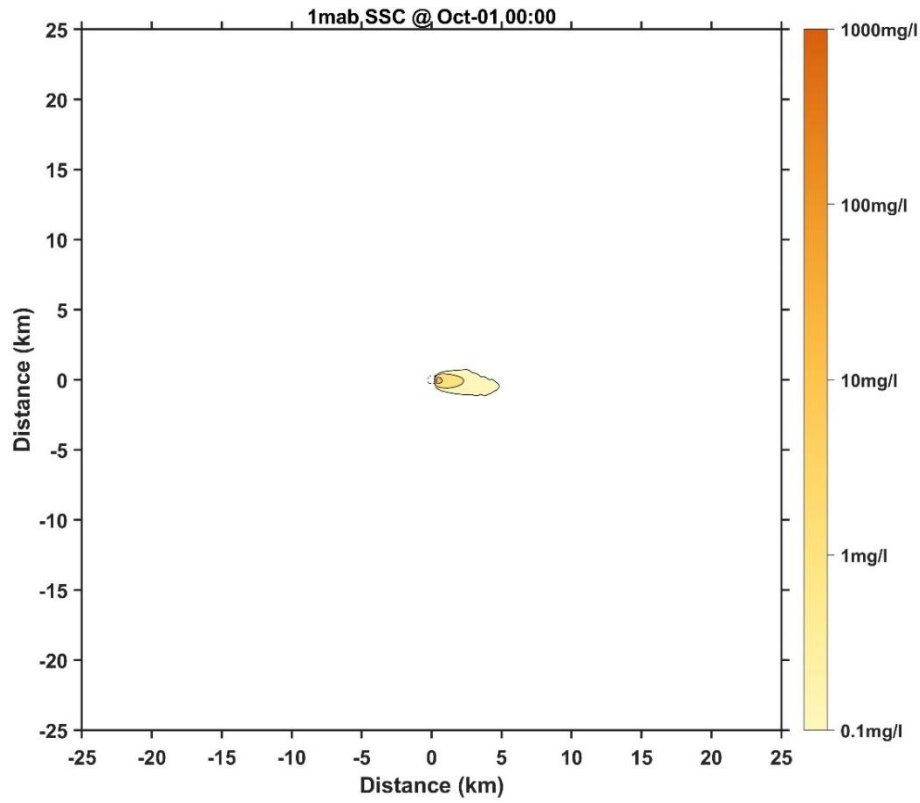
Figure 15 Horizontal distribution of SSC at 1 mab for Case 4 (5 days later)
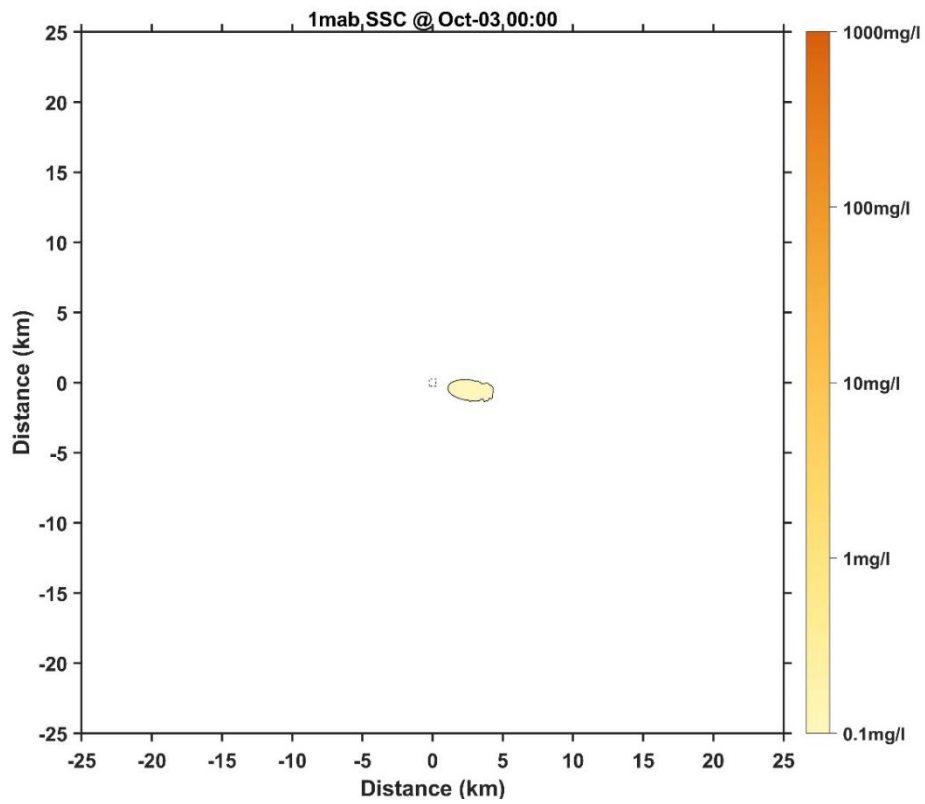
Figure 16 Horizontal distribution of SSC at 1 mab for Case 4 (7 days later)
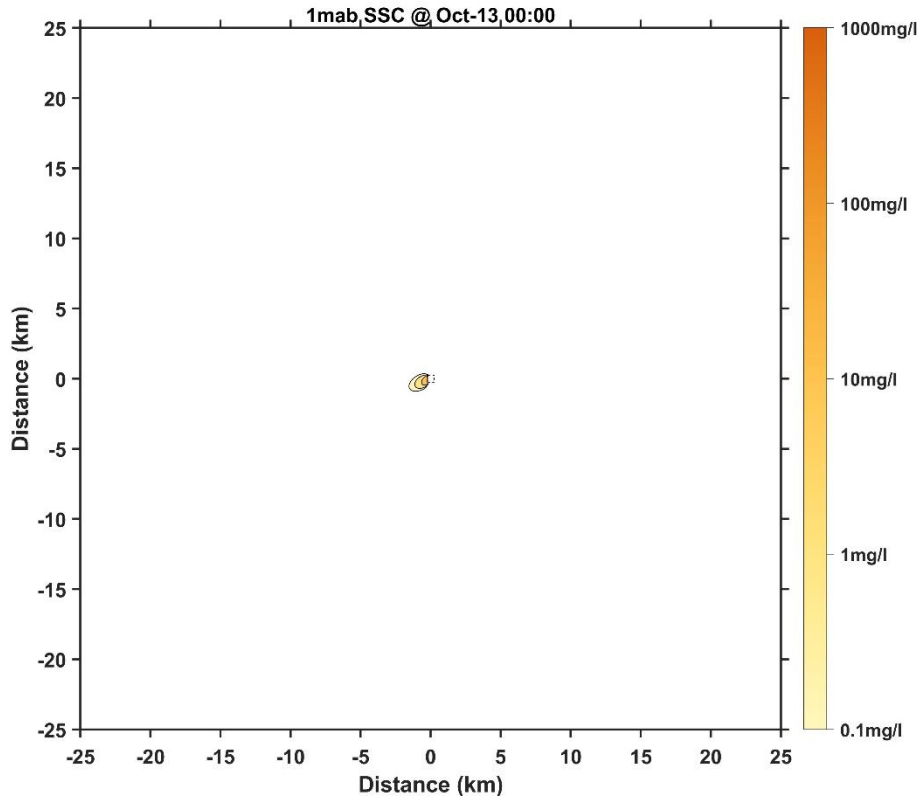
Figure 17 Horizontal distribution of SSC at 1 mab for Case 5 (1 day later)
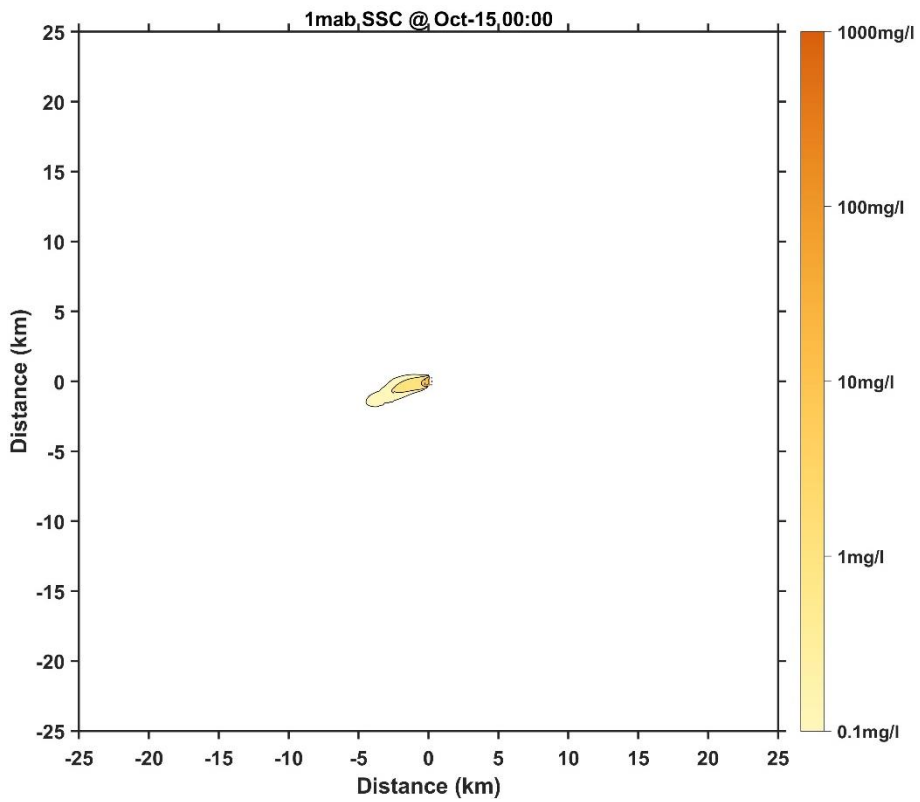
Figure 18 Horizontal distribution of SSC at 1 mab for Case 5 (3 days later)
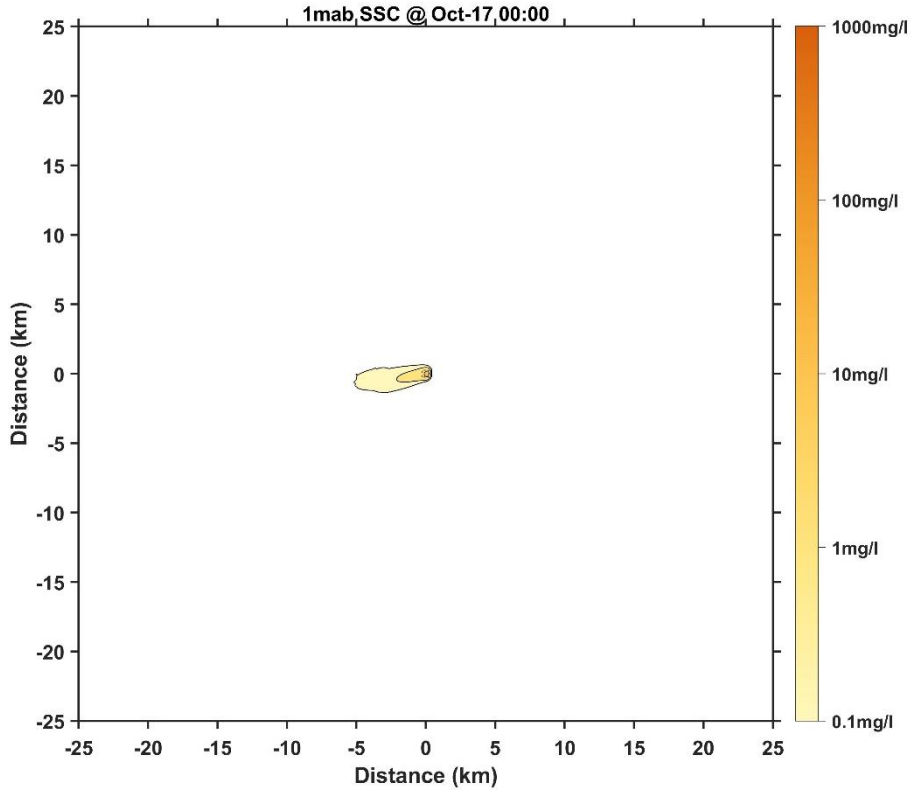
Figure 19 Horizontal distribution of SSC at 1 mab for Case 5 (5 days later)
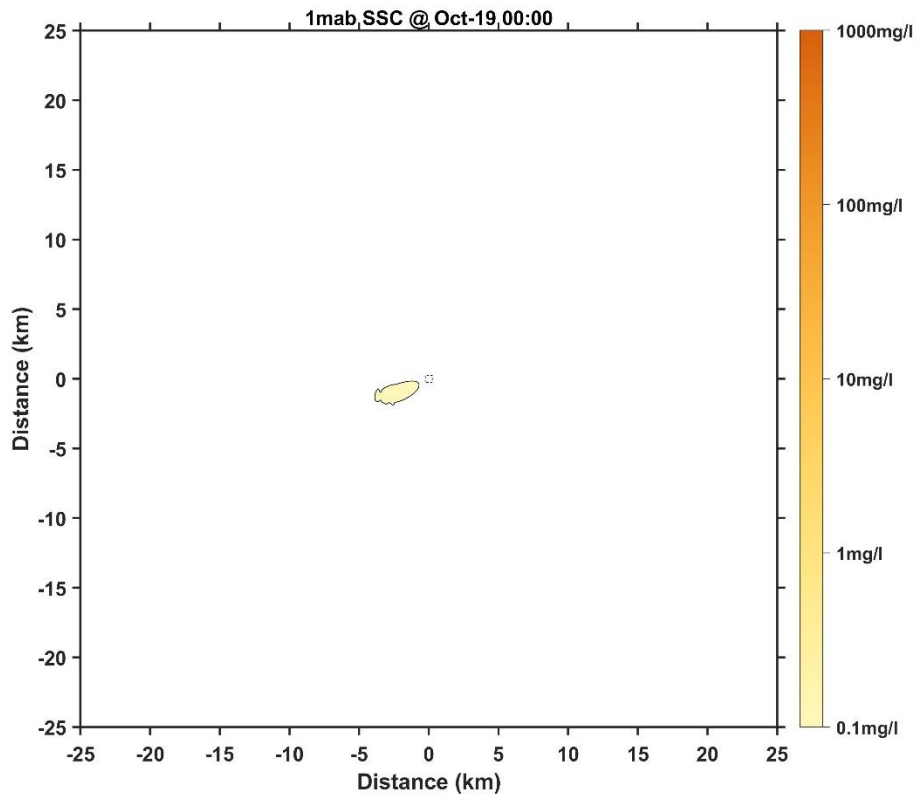
Figure 20 Horizontal distribution of SSC at 1 mab for Case 5 (7 days later)
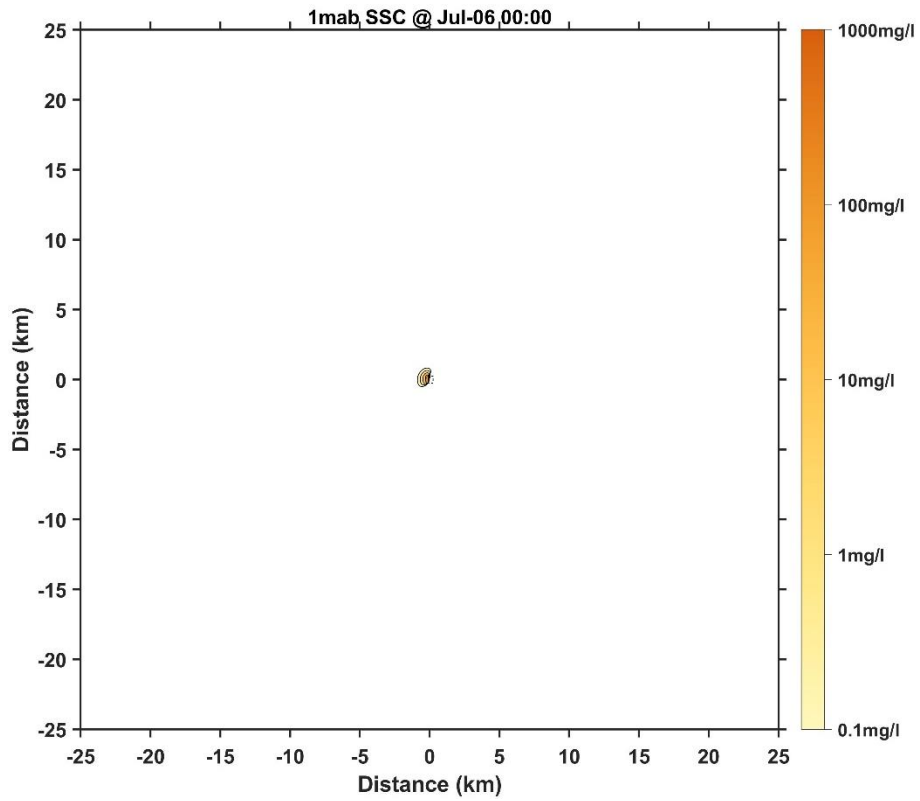
Figure 21 Horizontal distribution of SSC at 1 mab for Case 6 (1 day later)
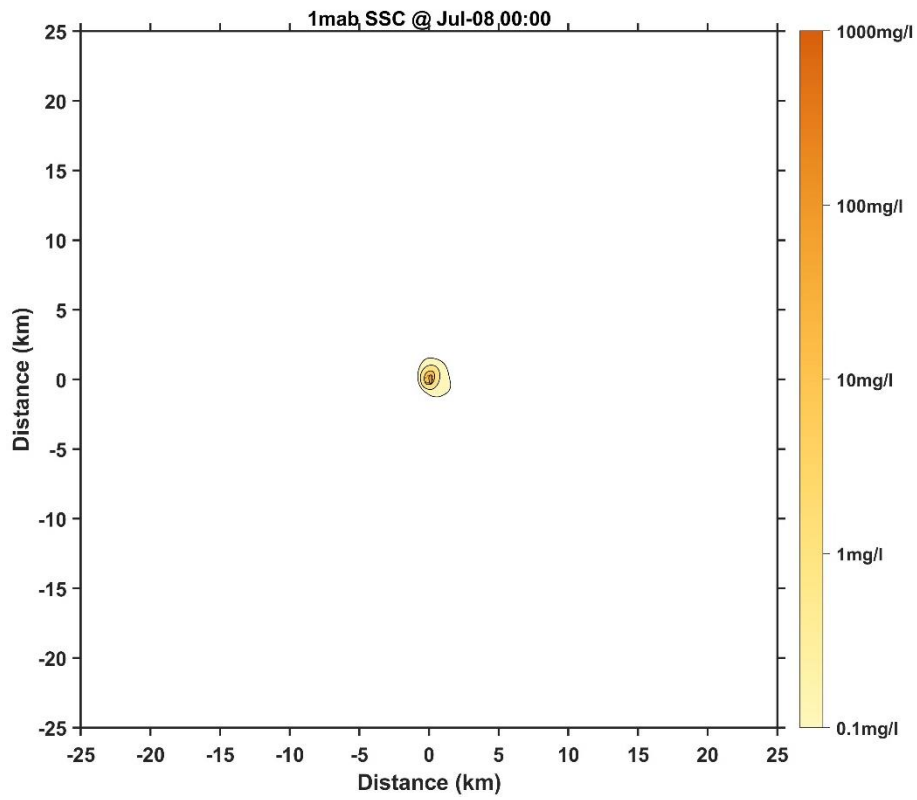
Figure 22 Horizontal distribution of SSC at 1 mab for Case 6 (3 days later)
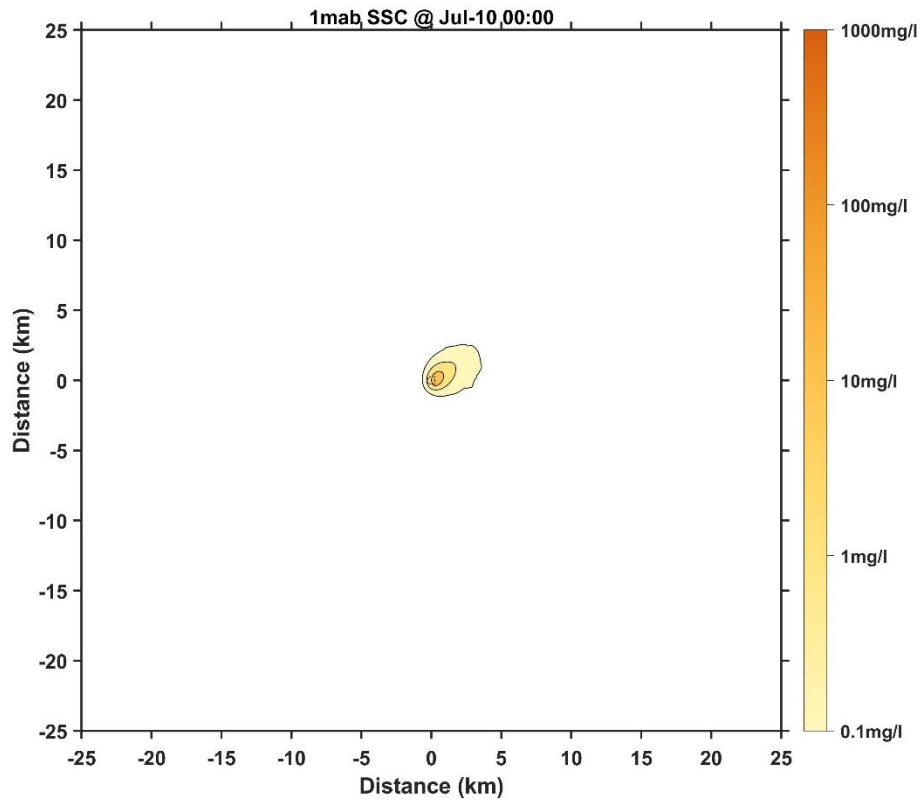
Figure 23 Horizontal distribution of SSC at 1 mab for Case 6 (5 days later)
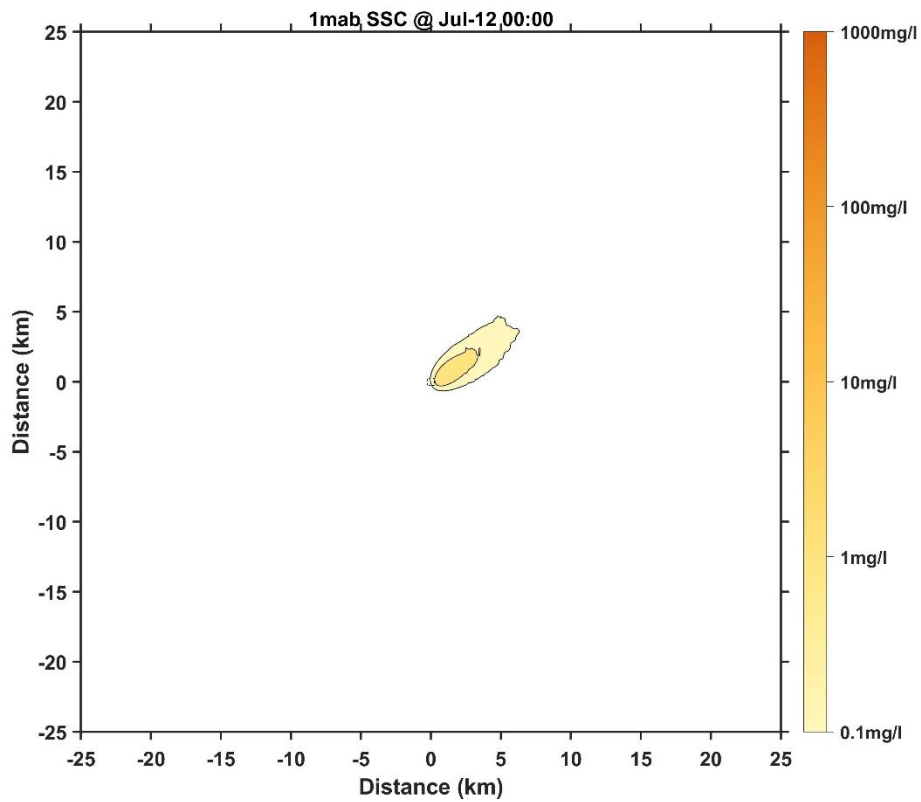
Figure 24 Horizontal distribution of SSC at 1 mab for Case 6 (7 days later)
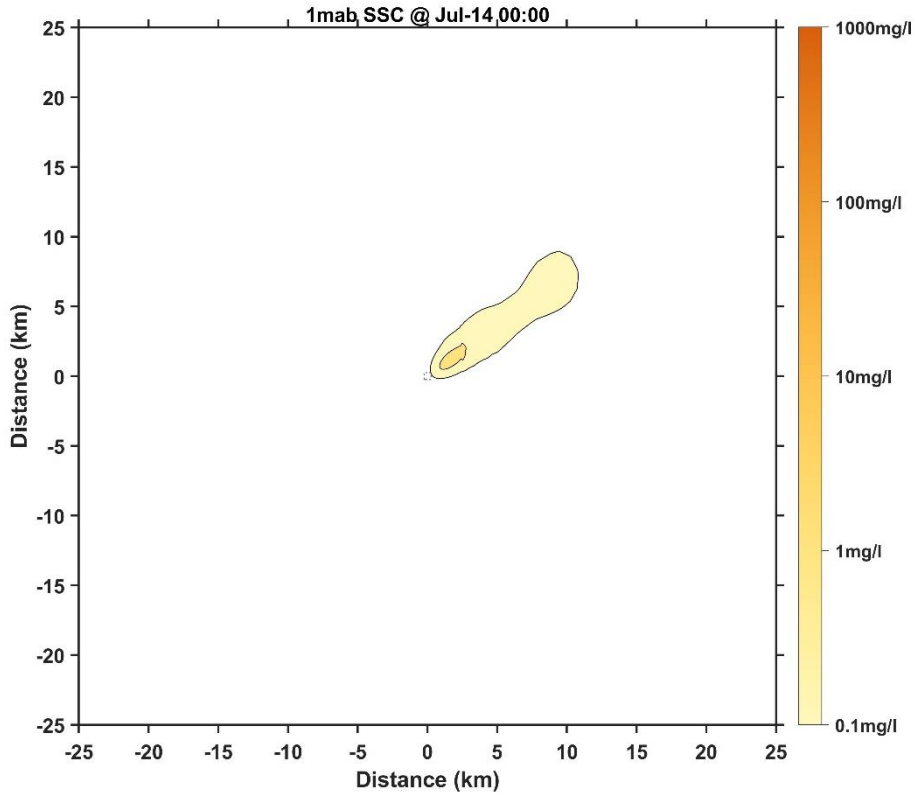
Figure 25 Horizontal distribution of SSC at 1 mab for Case 6 (9 days later)
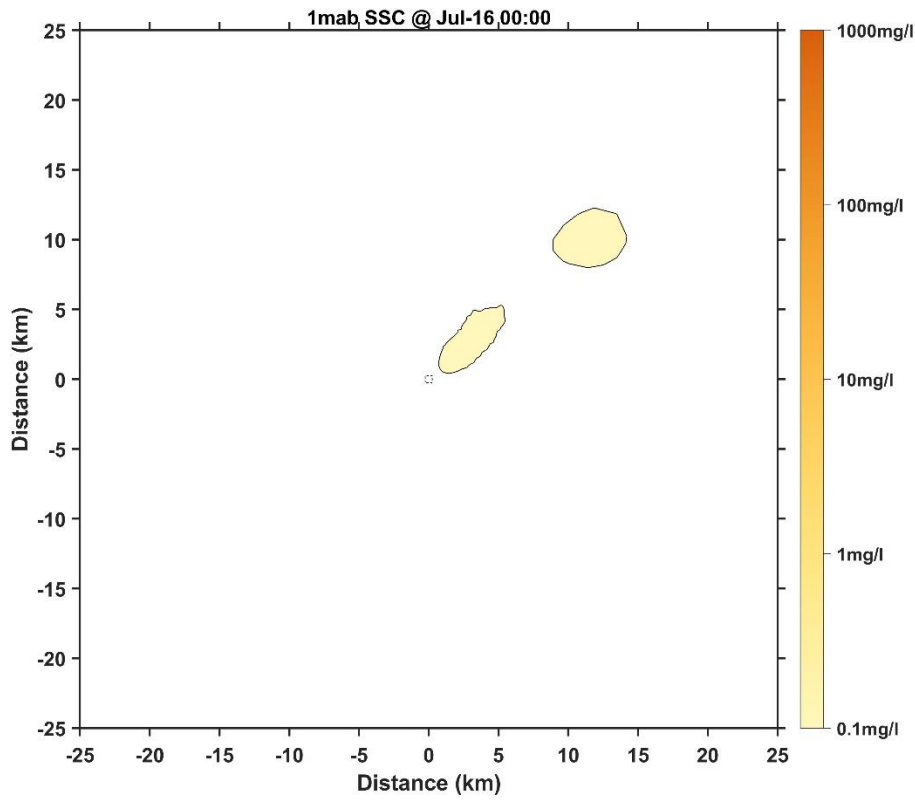
Figure 26 Horizontal distribution of SSC at 1 mab for Case 6 (11 days later)
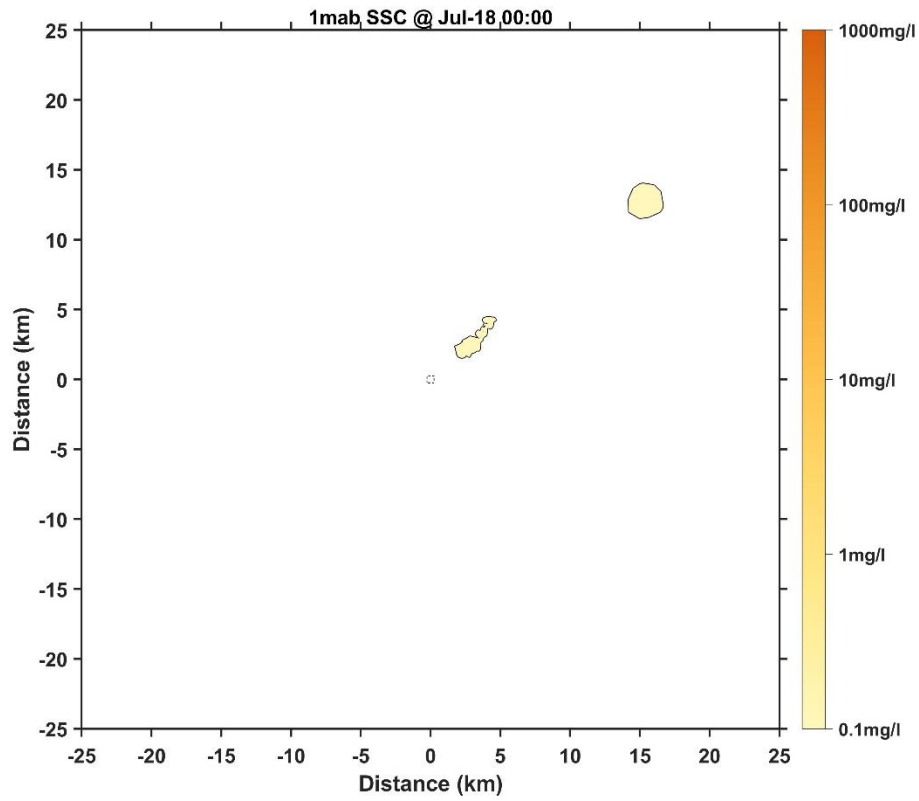
Figure 27 Horizontal distribution of SSC at 1 mab for Case 6 (13 days later)
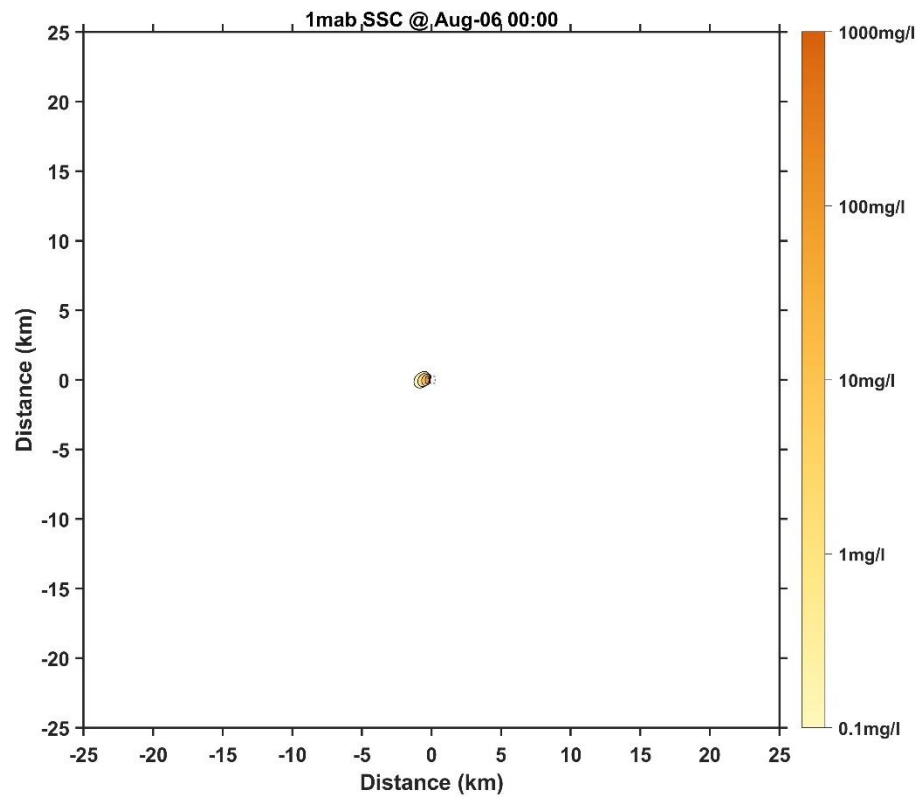
Figure 28 Horizontal distribution of SSC at 1 mab for Case 7 (1 day later)

618
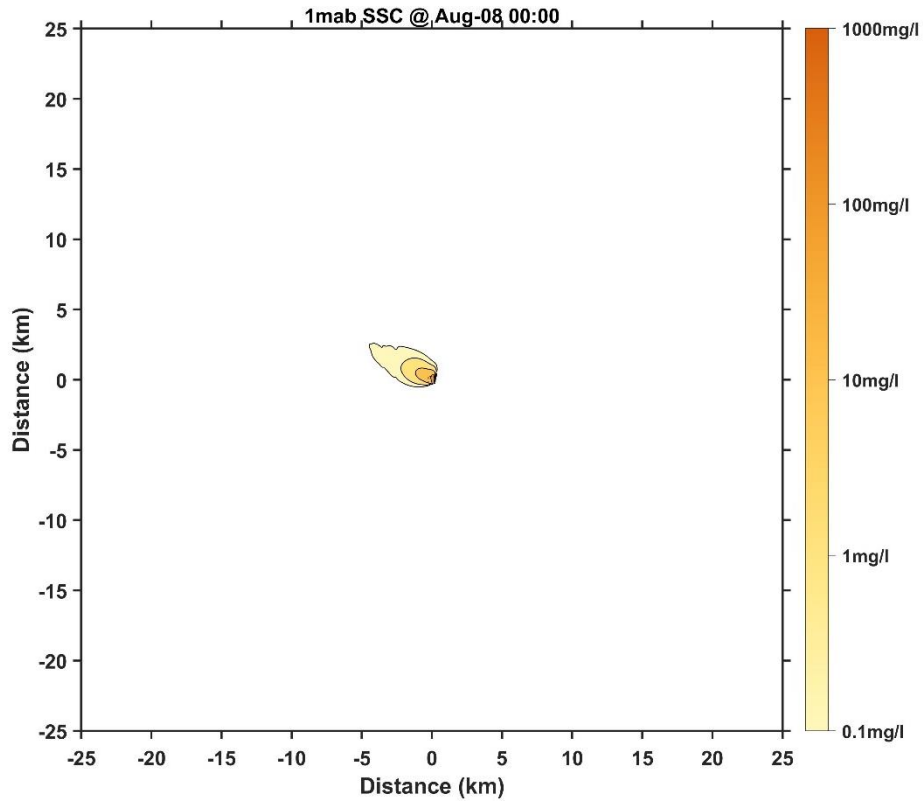
Figure 29 Horizontal distribution of SSC at 1 mab for Case 7 (3 days later)
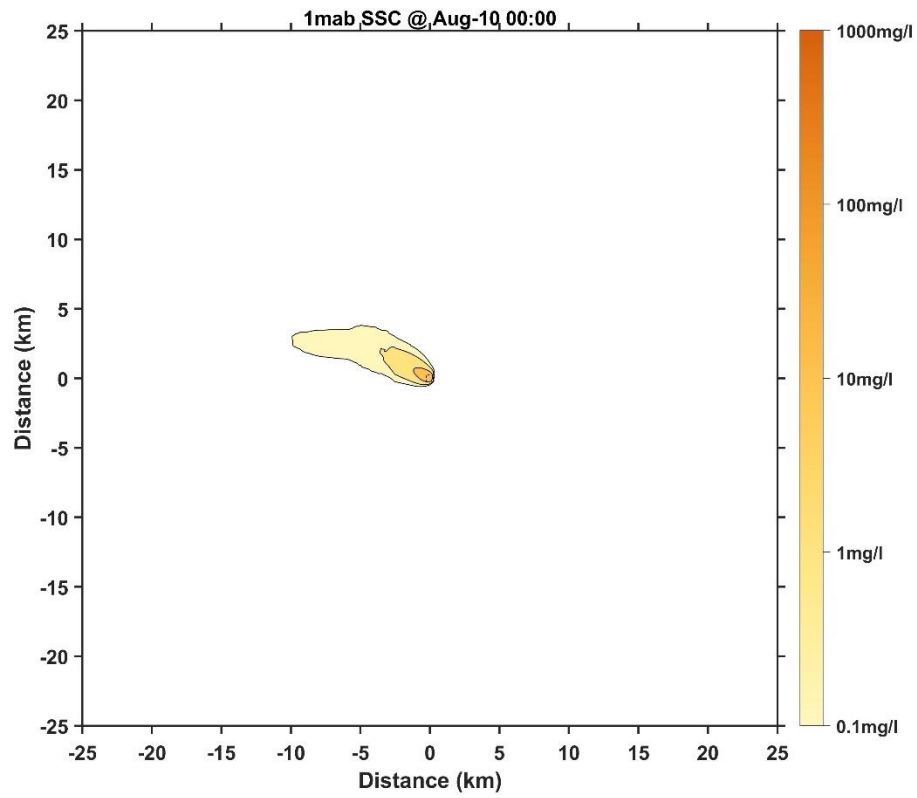
Figure 30 Horizontal distribution of SSC at 1 mab for Case 7 (5 days later)
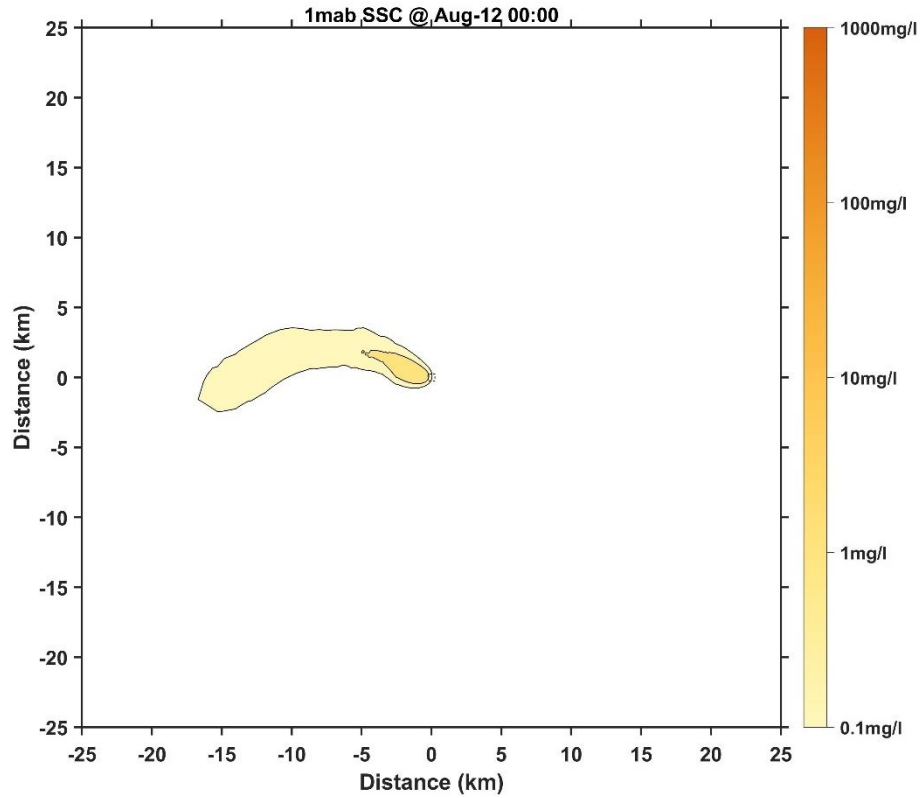
Figure 31 Horizontal distribution of SSC at 1 mab for Case 7 (7 days later)
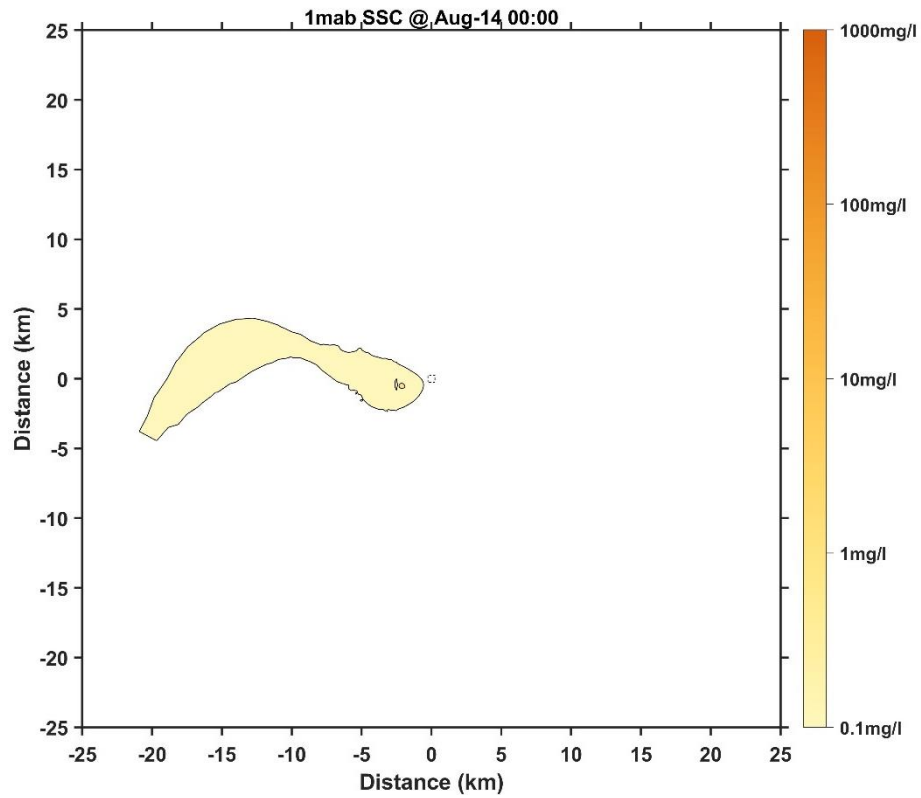
Figure 32 Horizontal distribution of SSC at 1 mab for Case 7 (9 days later)
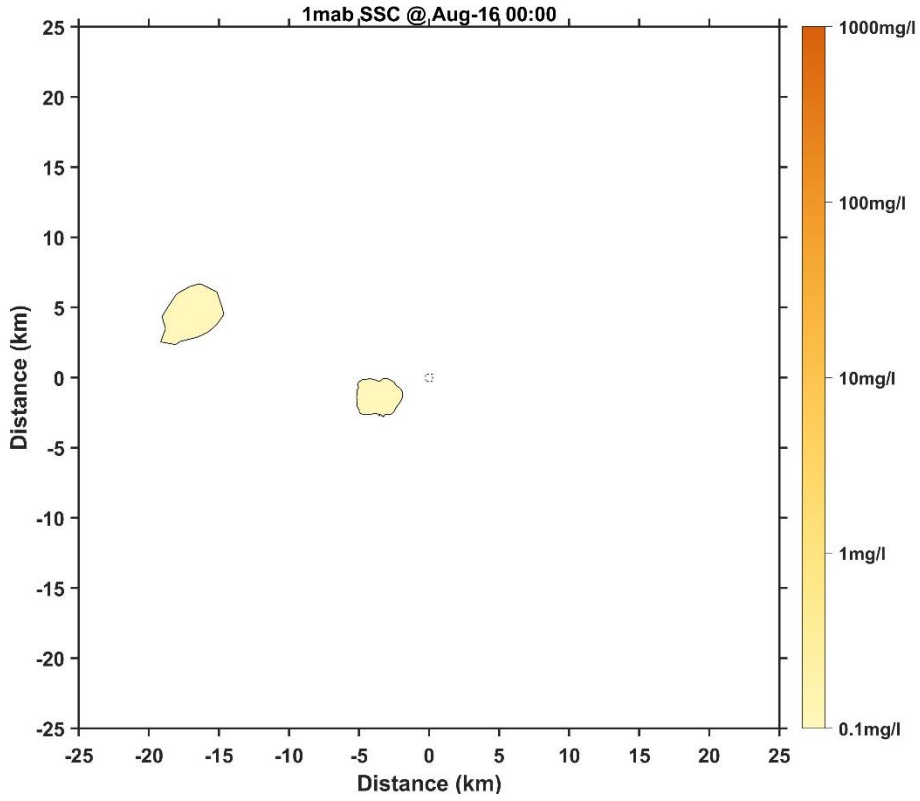
Figure 33 Horizontal distribution of SSC at 1 mab for Case 7 (11 days later)
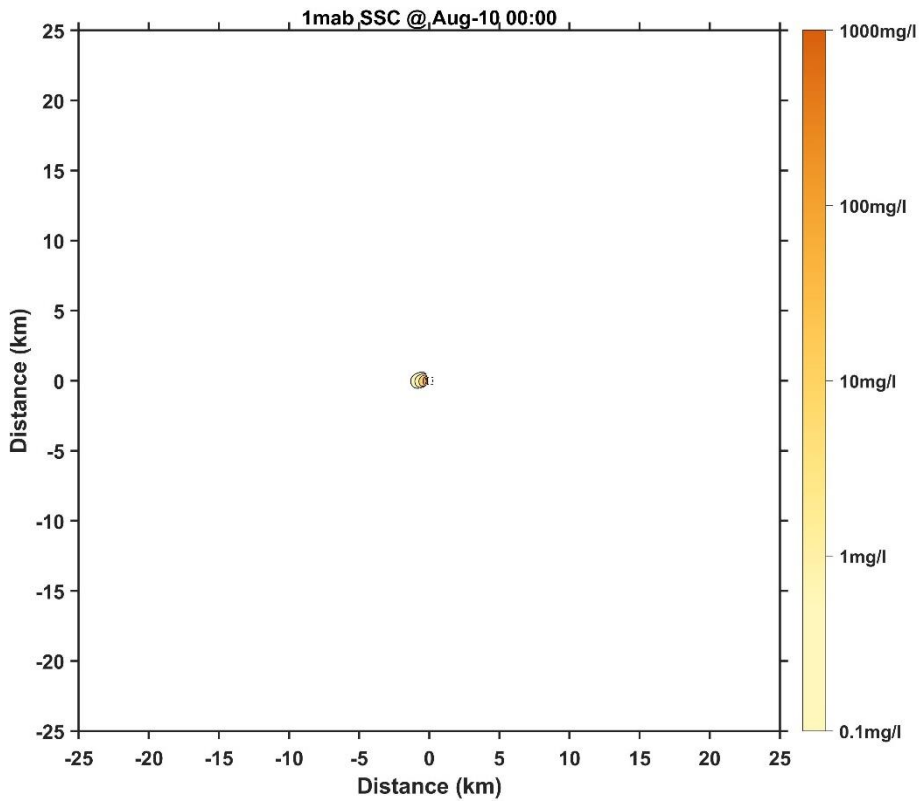
Figure 34 Horizontal distribution of SSC at 1 mab for Case 8 (1 day later)

621
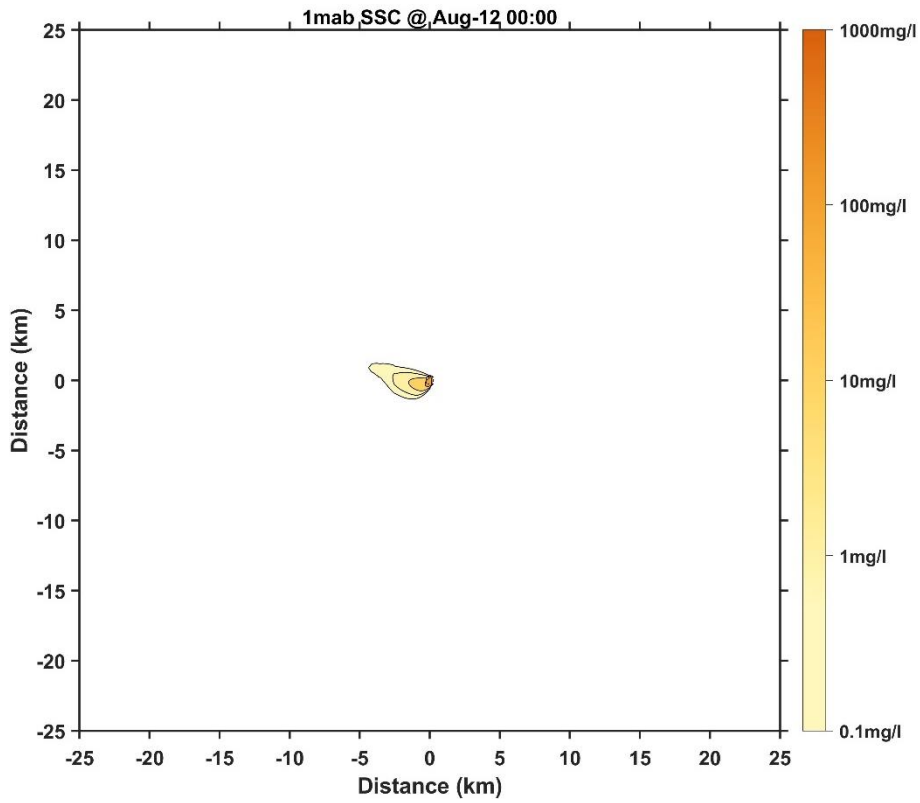
Figure 35 Horizontal distribution of SSC at 1 mab for Case 8 (3 days later)
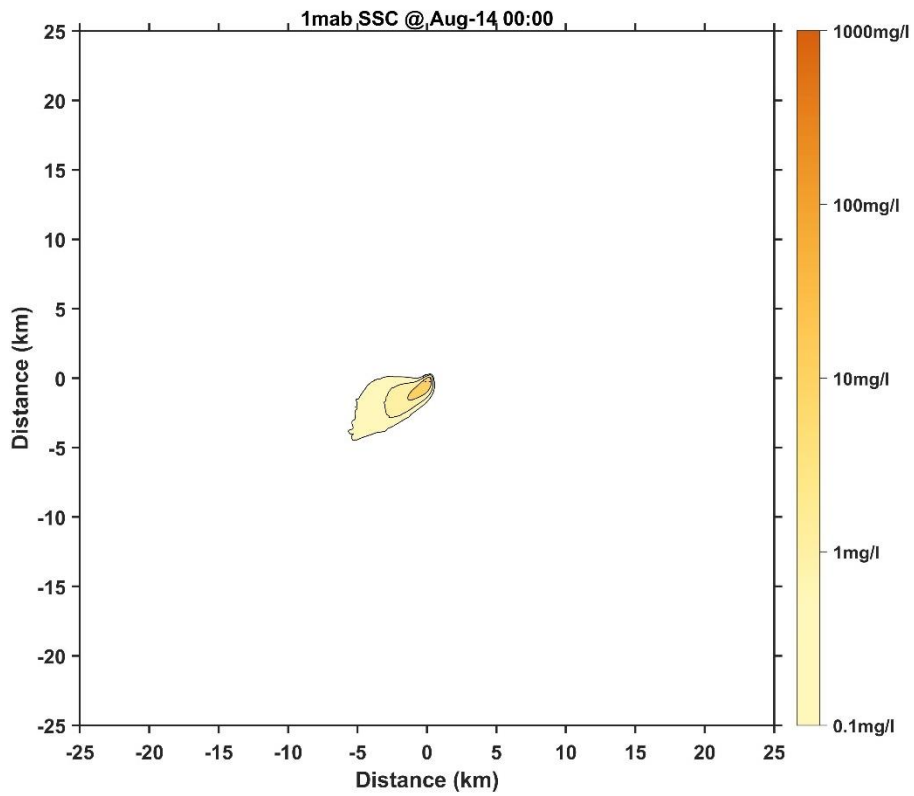
Figure 36 Horizontal distribution of SSC at 1 mab for Case 8 (5 days later)
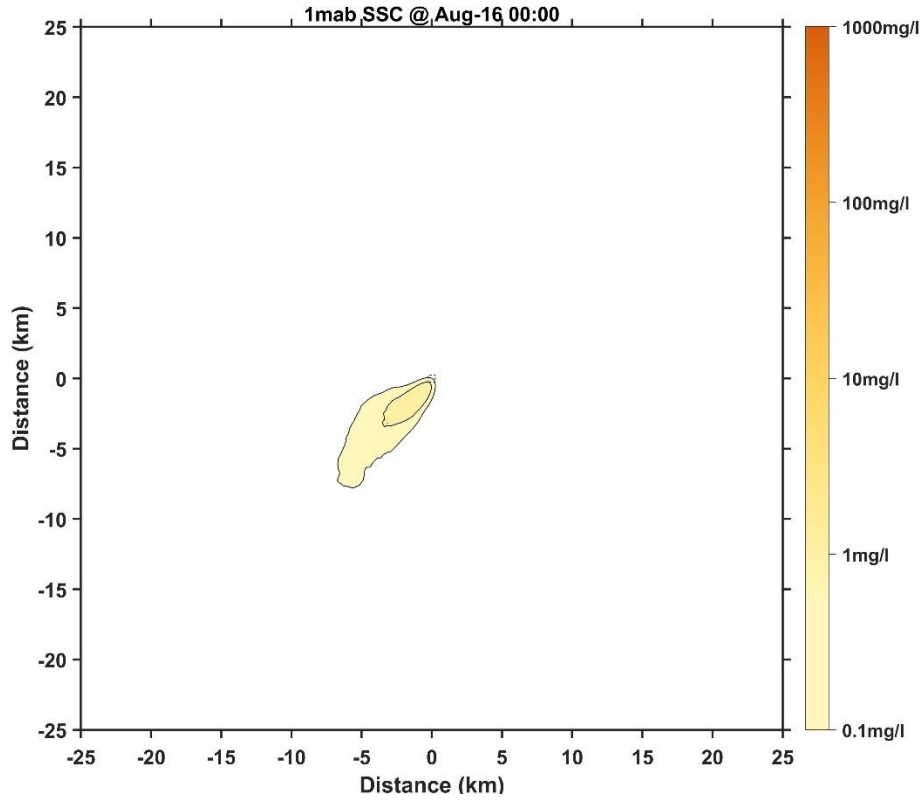
Figure 37 Horizontal distribution of SSC at 1 mab for Case 8 (7 days later)
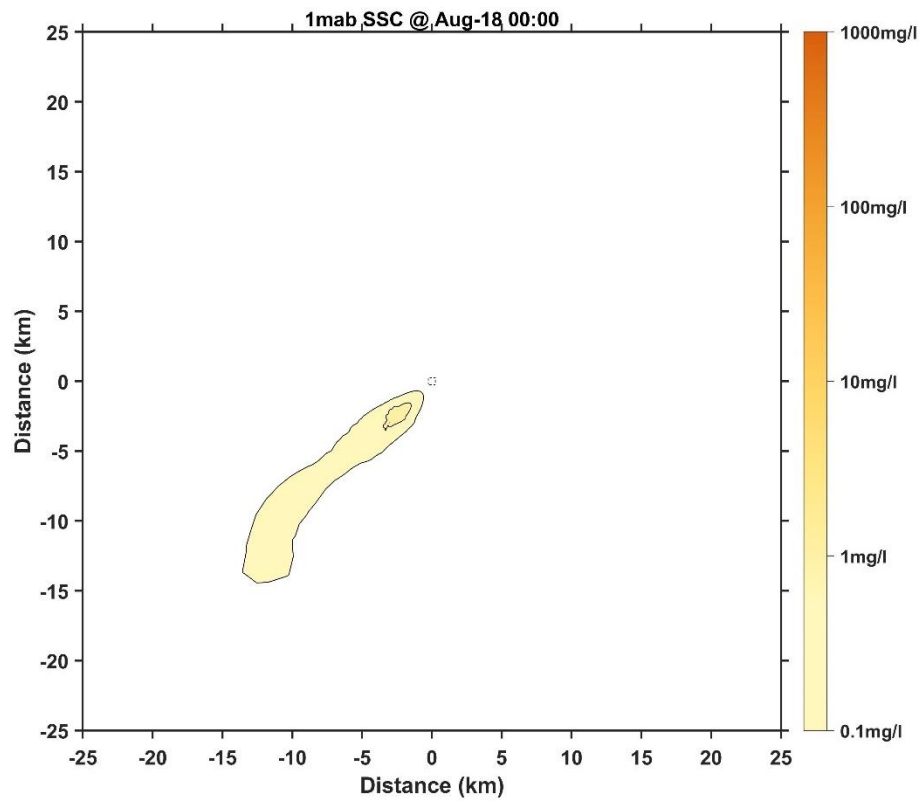
Figure 38 Horizontal distribution of SSC at 1 mab for Case 8 (9 days later)
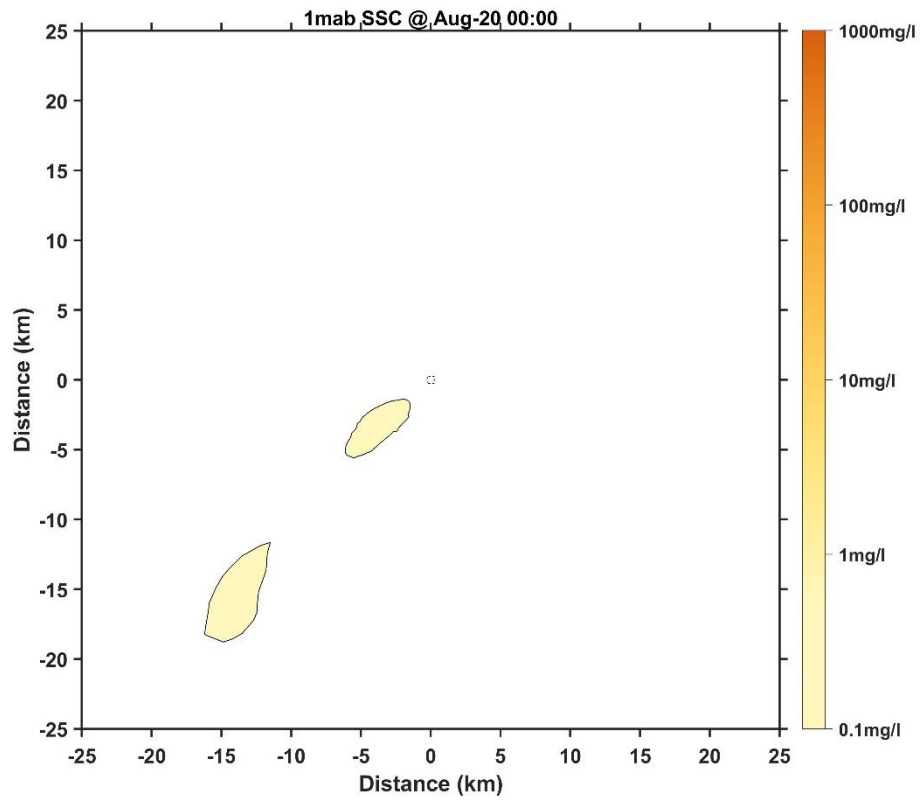
Figure 39 Horizontal distribution of SSC at 1 mab for Case 8 (11 days later)
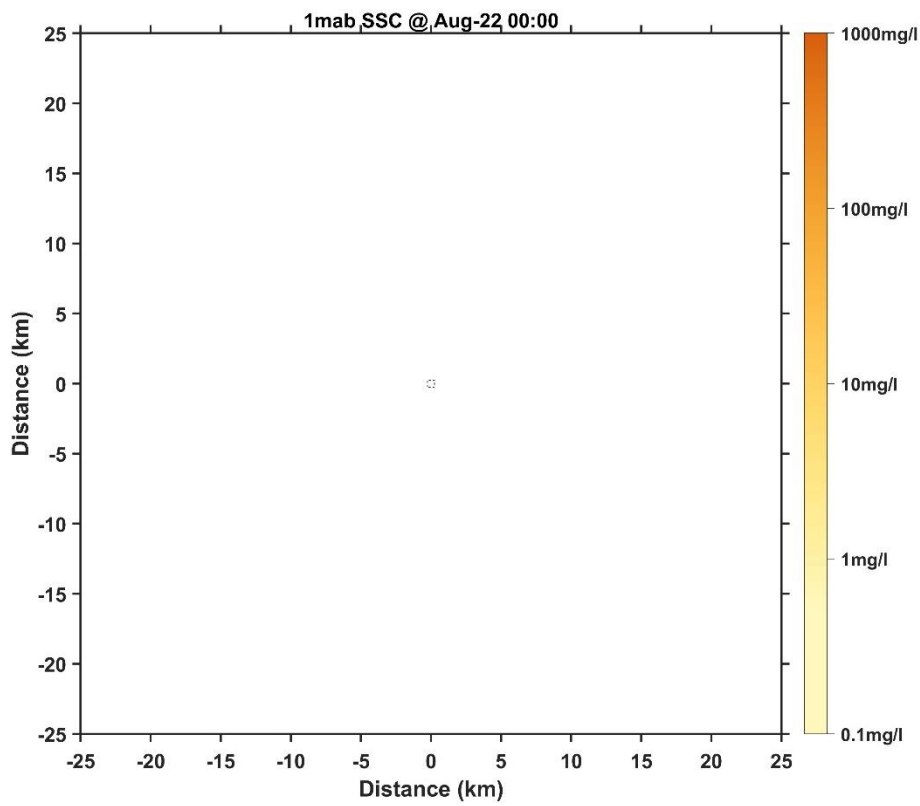
Figure 40 Horizontal distribution of SSC at 1 mab for Case 8 (13 days later)
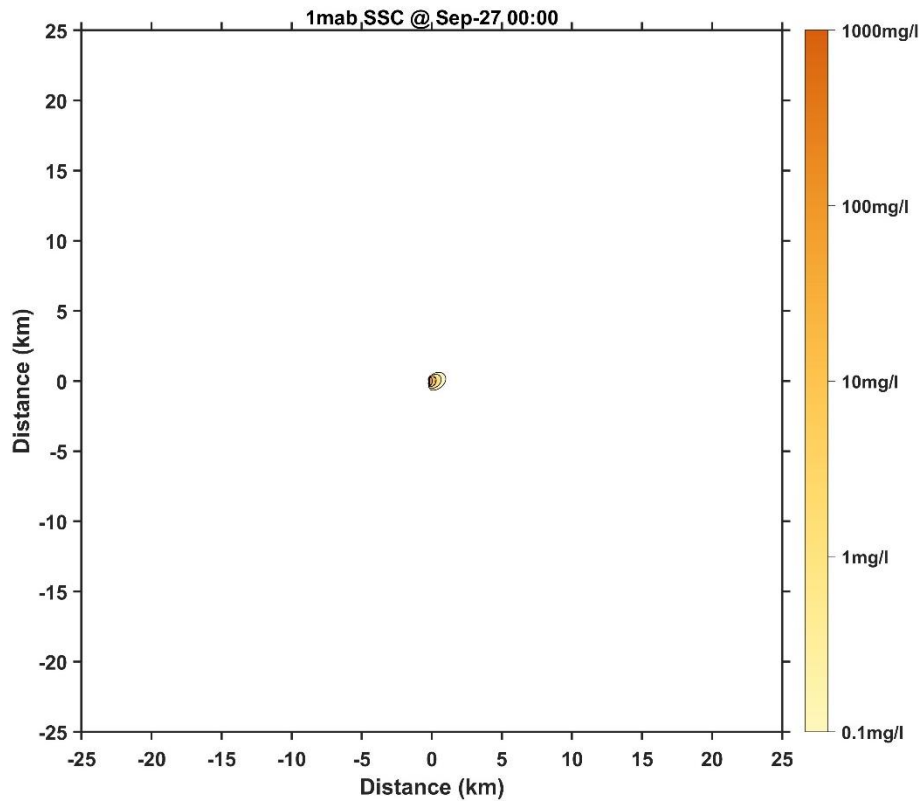
Figure 41 Horizontal distribution of SSC at 1 mab for Case 9 (1 day later)
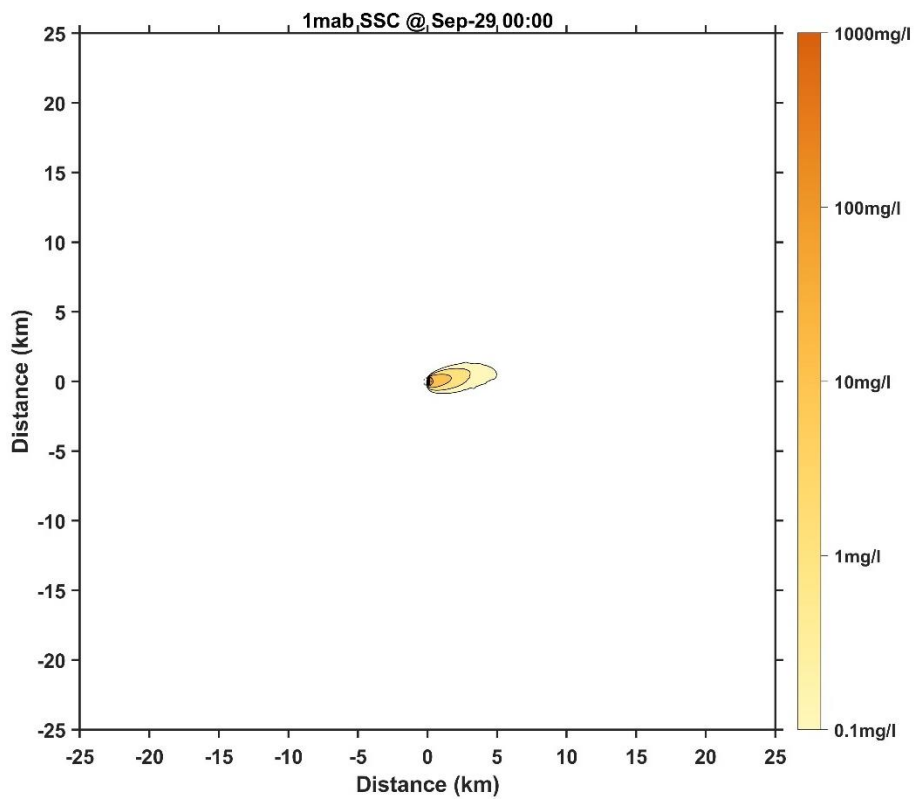
Figure 42 Horizontal distribution of SSC at 1 mab for Case 9 (3 days later)
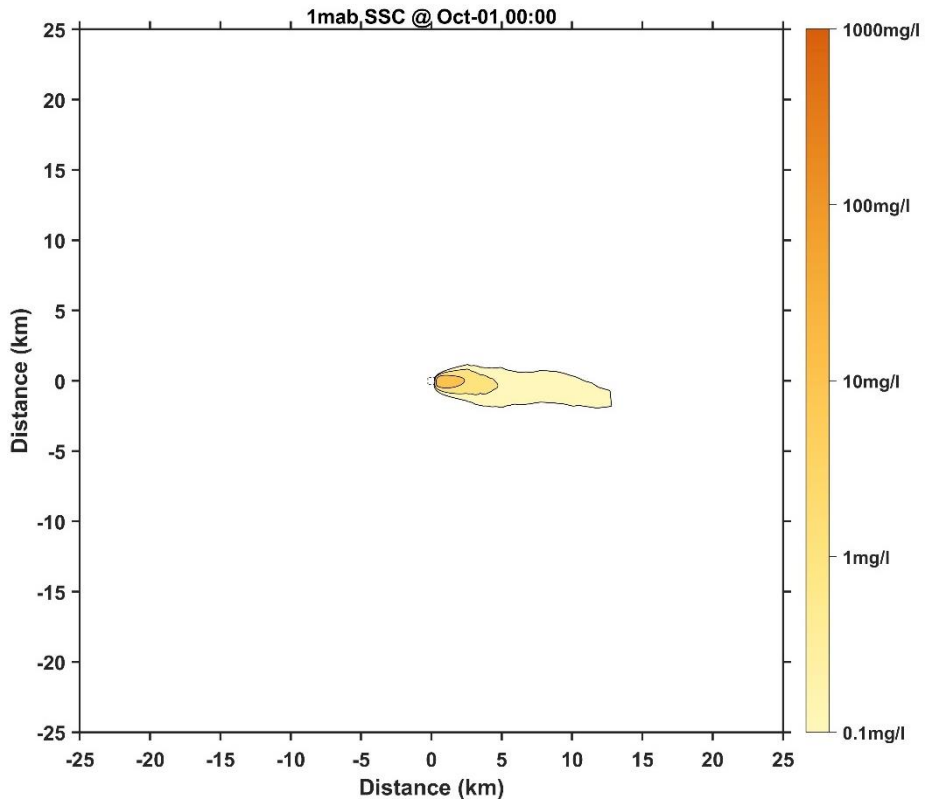
Figure 43 Horizontal distribution of SSC at 1 mab for Case 9 (5 days later)
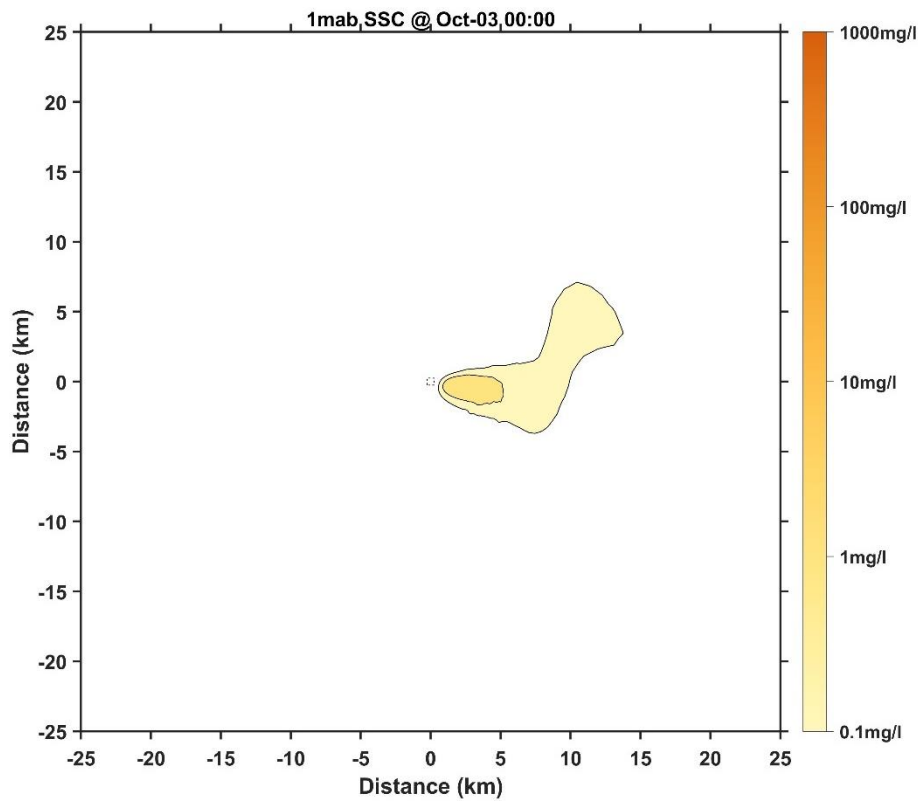
Figure 44 Horizontal distribution of SSC at 1 mab for Case 9 (7 days later)
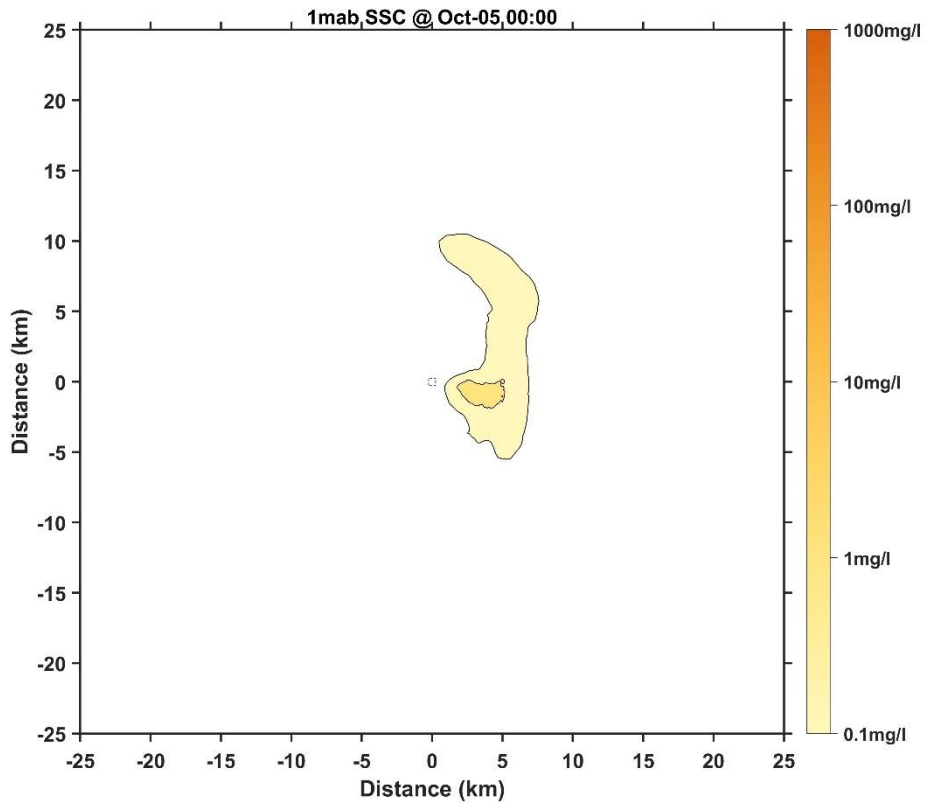
Figure 45 Horizontal distribution of SSC at 1 mab for Case 9 (9 days later)
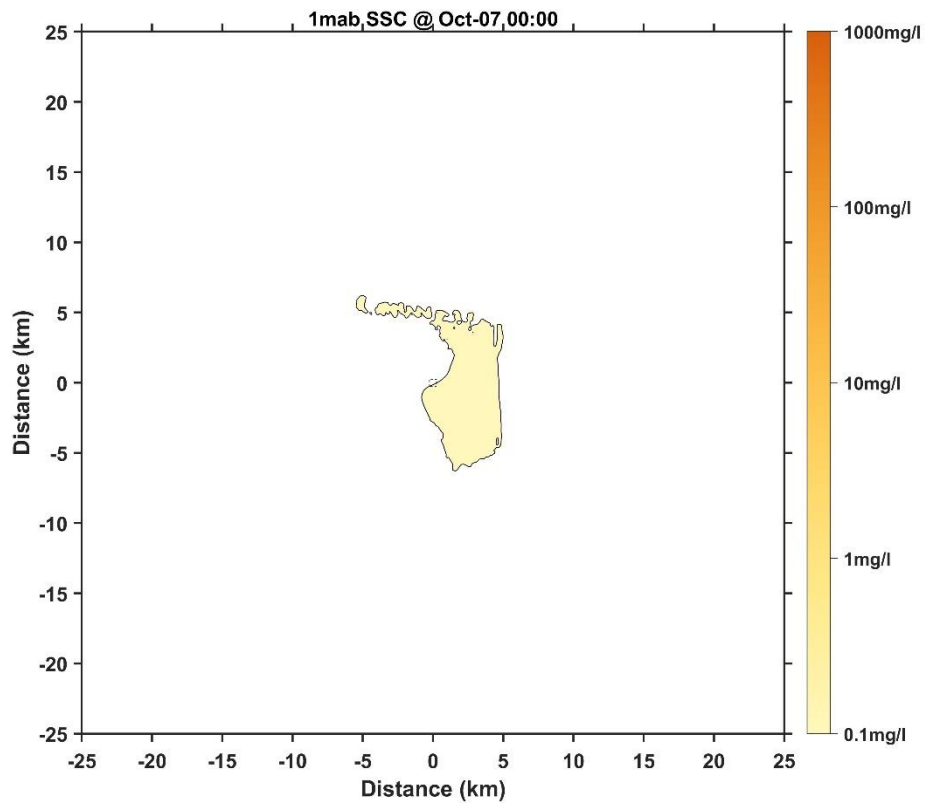
Figure 46 Horizontal distribution of SSC at 1 mab for Case 9 (11 days later)
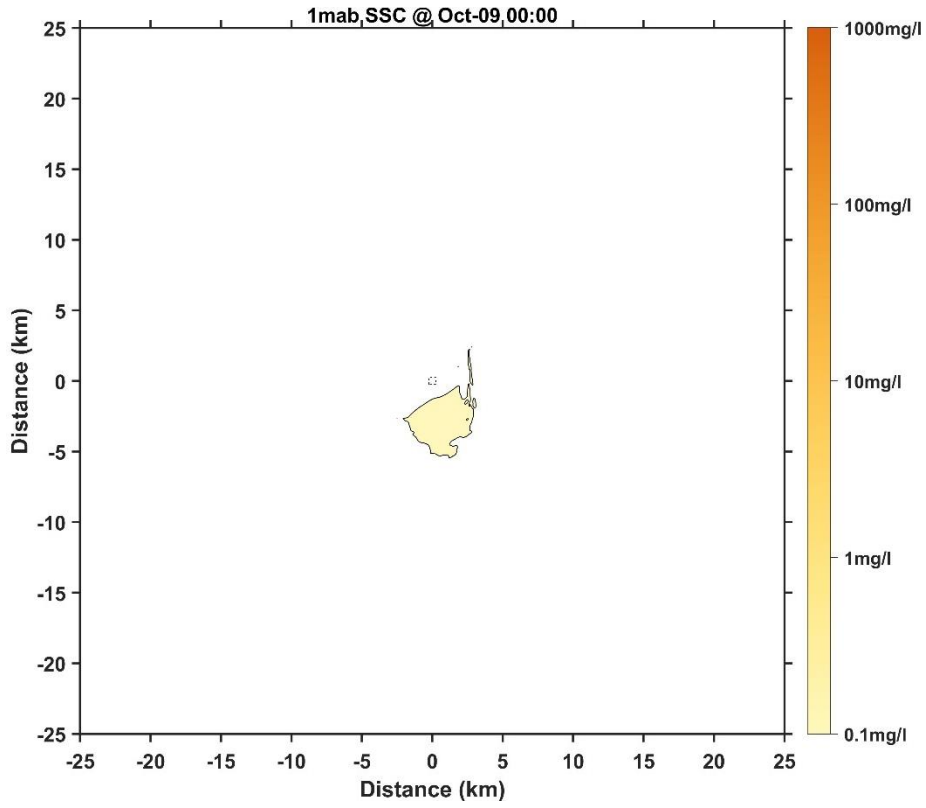
Figure 47 Horizontal distribution of SSC at 1 mab for Case 9 (13 days later)
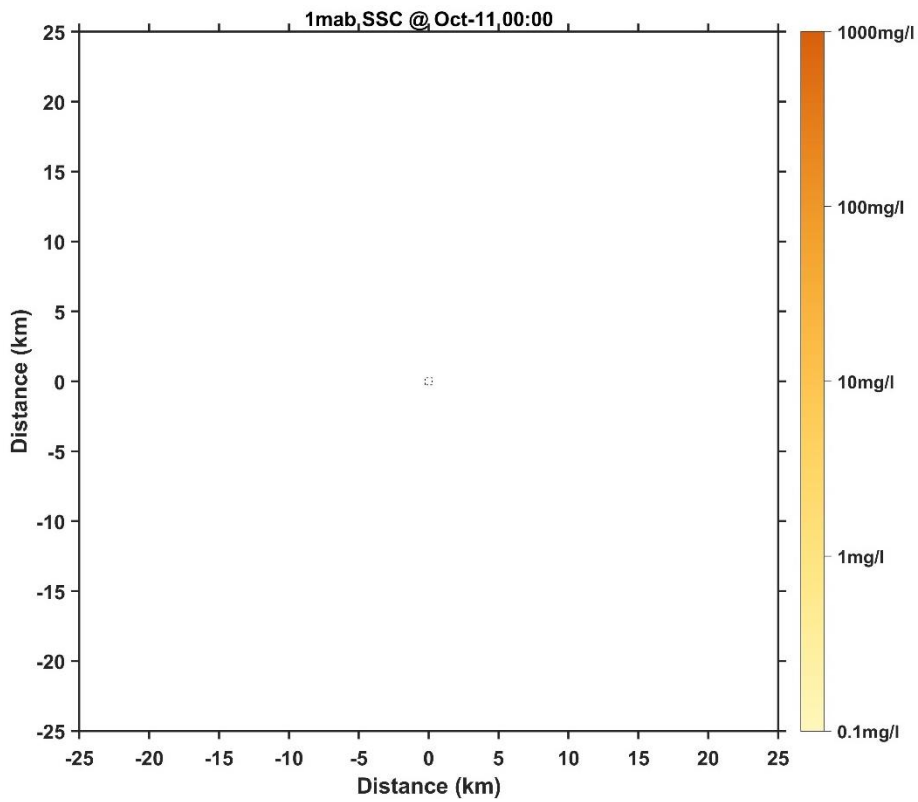
Figure 48 Horizontal distribution of SSC at 1 mab for Case 9 (15 days later)
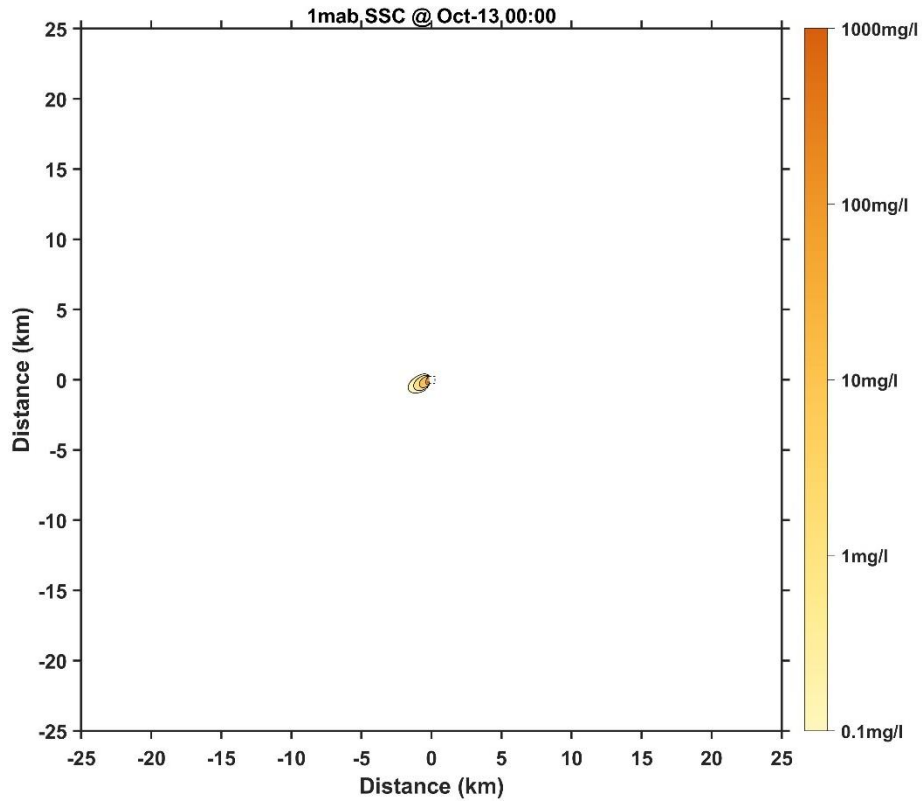
Figure 49 Horizontal distribution of SSC at 1 mab for Case 10 (1 day later)
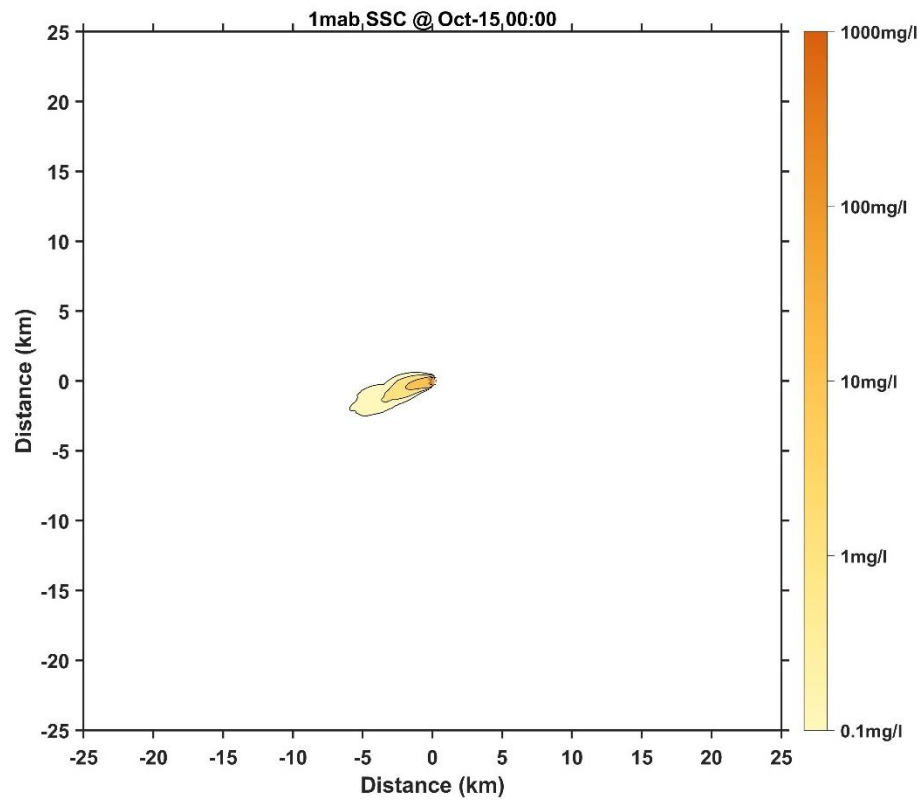
Figure 50 Horizontal distribution of SSC at 1 mab for Case 10 (3 days later)
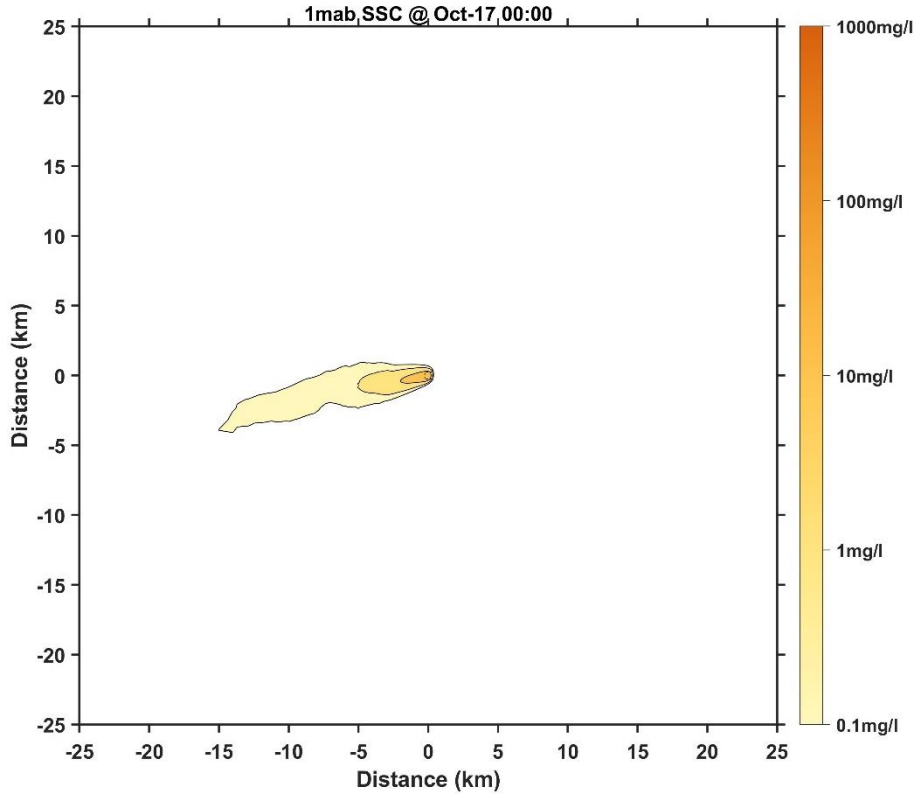
Figure 51 Horizontal distribution of SSC at 1 mab for Case 10 (5 days later)
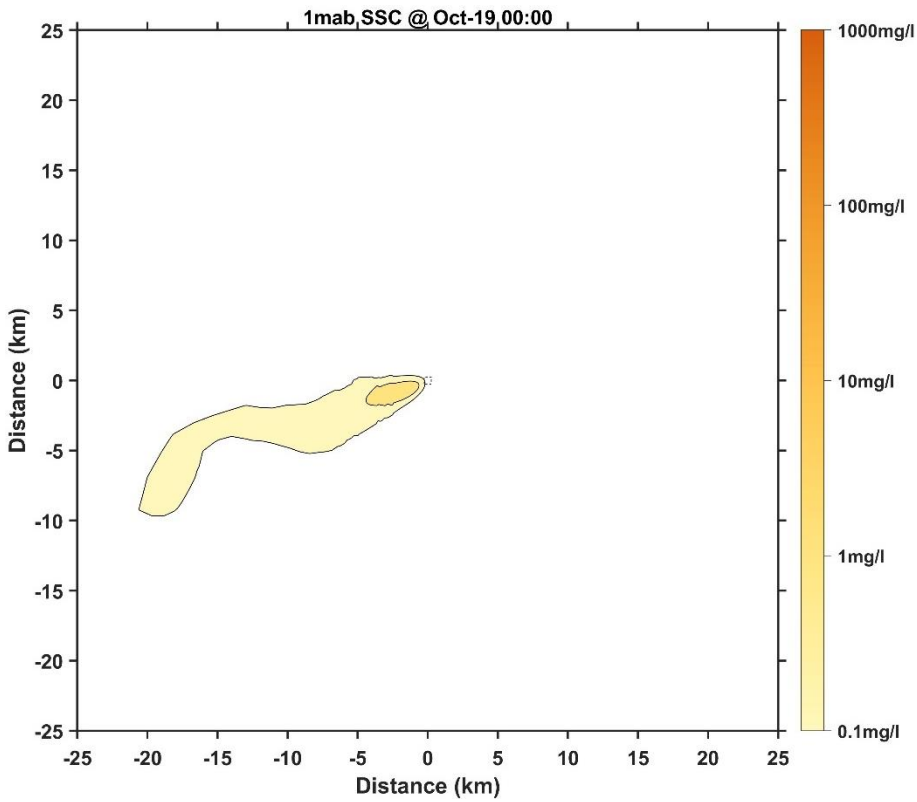
Figure 52 Horizontal distribution of SSC at 1 mab for Case 10 (7 days later)
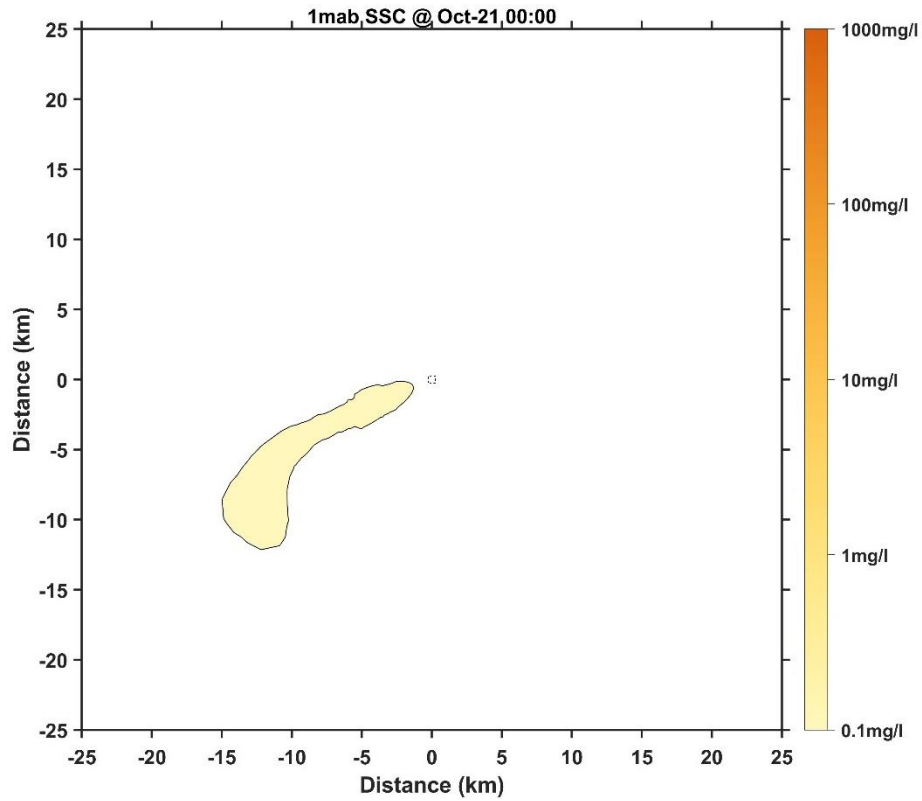
Figure 53 Horizontal distribution of SSC at 1 mab for Case 10 (9 days later)
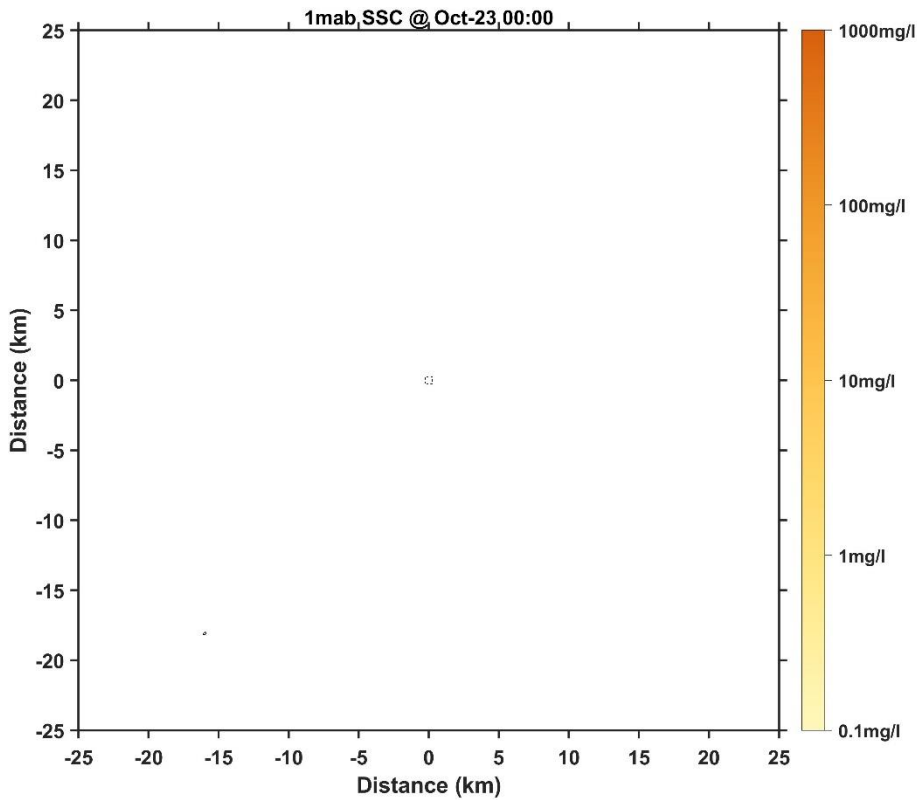
Figure 54 Horizontal distribution of SSC at 1 mab for Case 10 (11 days later)

1.2 Dispersion Characteristics of Near-bottom Suspended Sediment at 5 mab

The horizontal distribution of suspended sediment concentration at a depth of 5 m (Figure 55 to Figure 108) is similar to that at a depth of 1 m, with high suspended sediment concentration mainly in the working area. On average, the maximum distance of the plume (from the center of the CTA) at 5 m above the bottom was 5.41 km for Case 5 and 3.04 km for Case 3. In extreme cases, the maximum distance of the plume (from the center of the CTA) at 5 m above the bottom was 27.80 km for Case 8 and 14.55 km for Case 9.
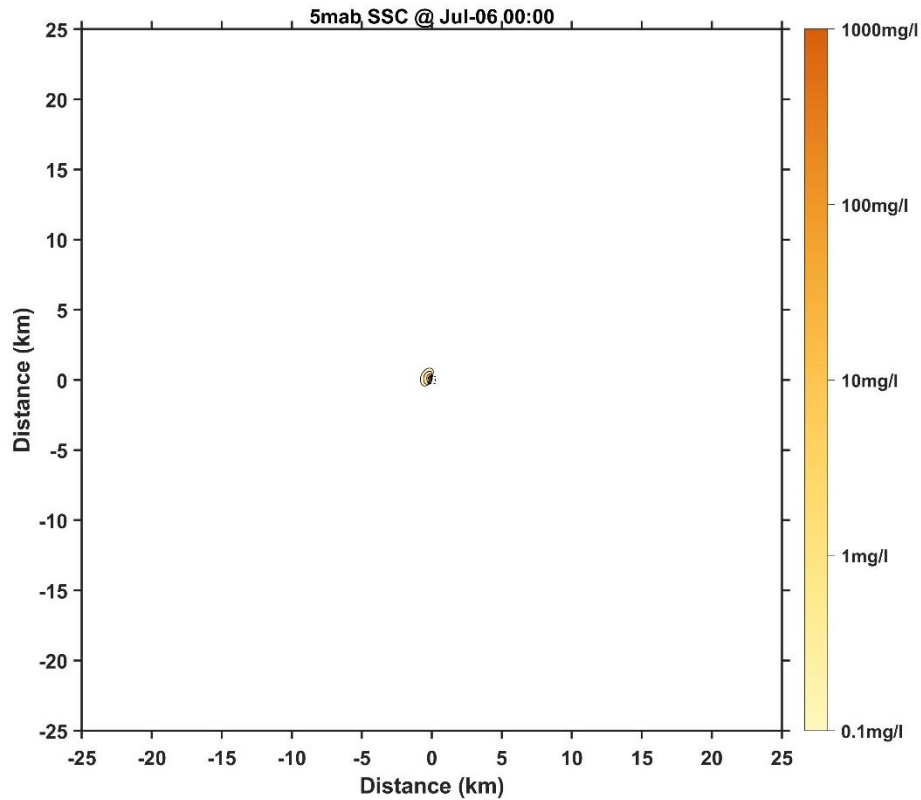
Figure 55 Horizontal distribution of SSC at 5 mab for Case 1 (1 day later)
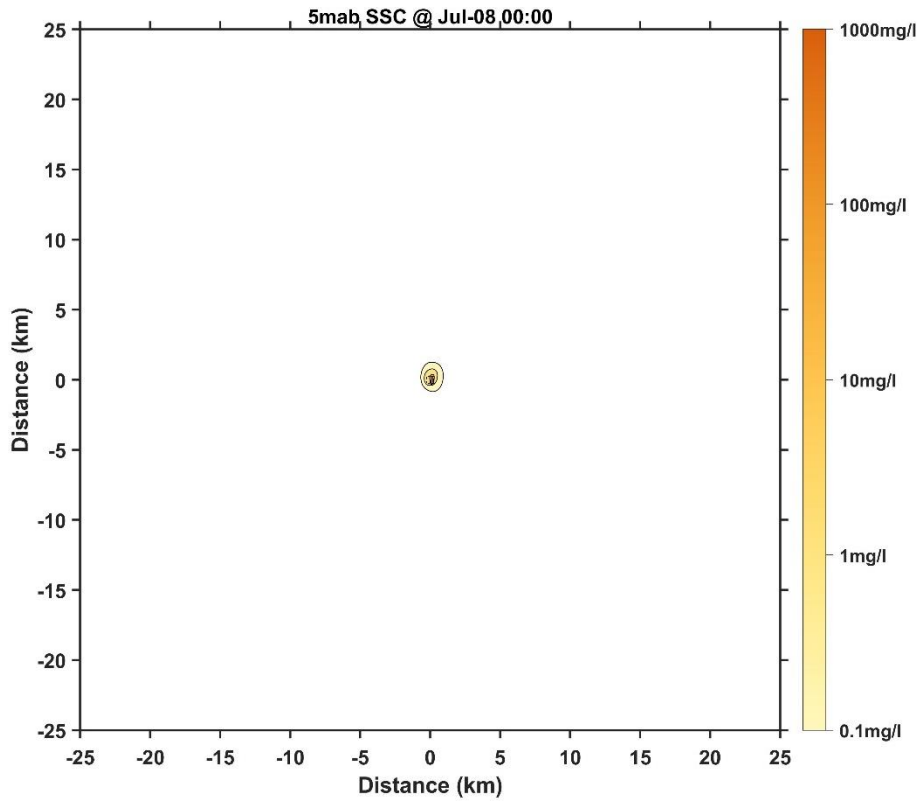
Figure 56 Horizontal distribution of SSC at 5 mab for Case 1 (3 days later)
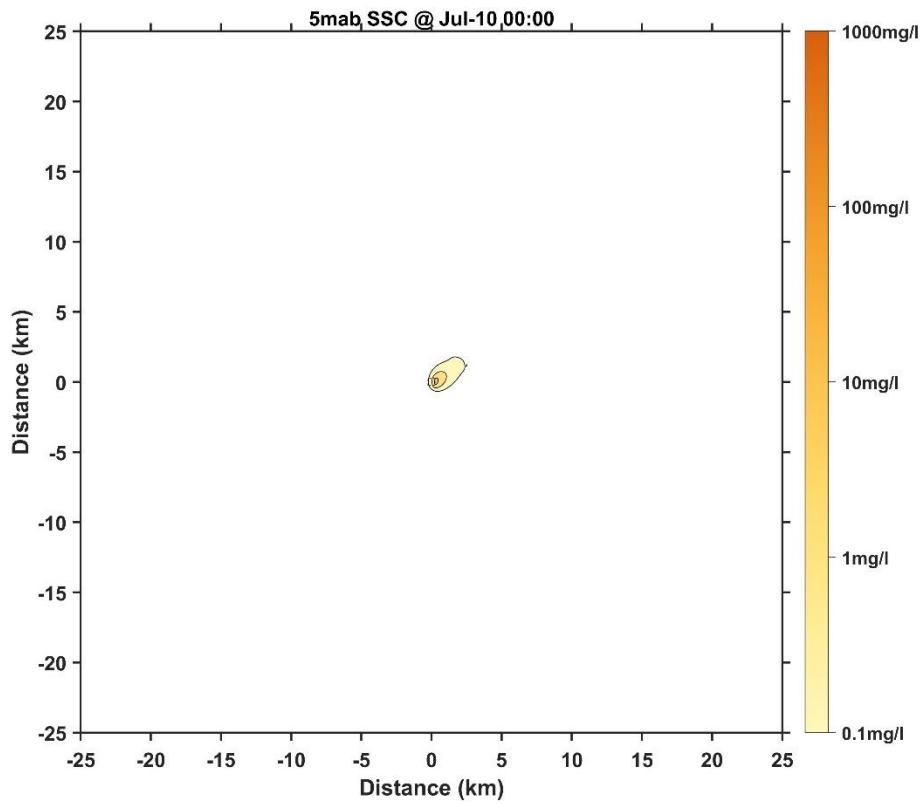
Figure 57 Horizontal distribution of SSC at 5 mab for Case 1 (5 days later)
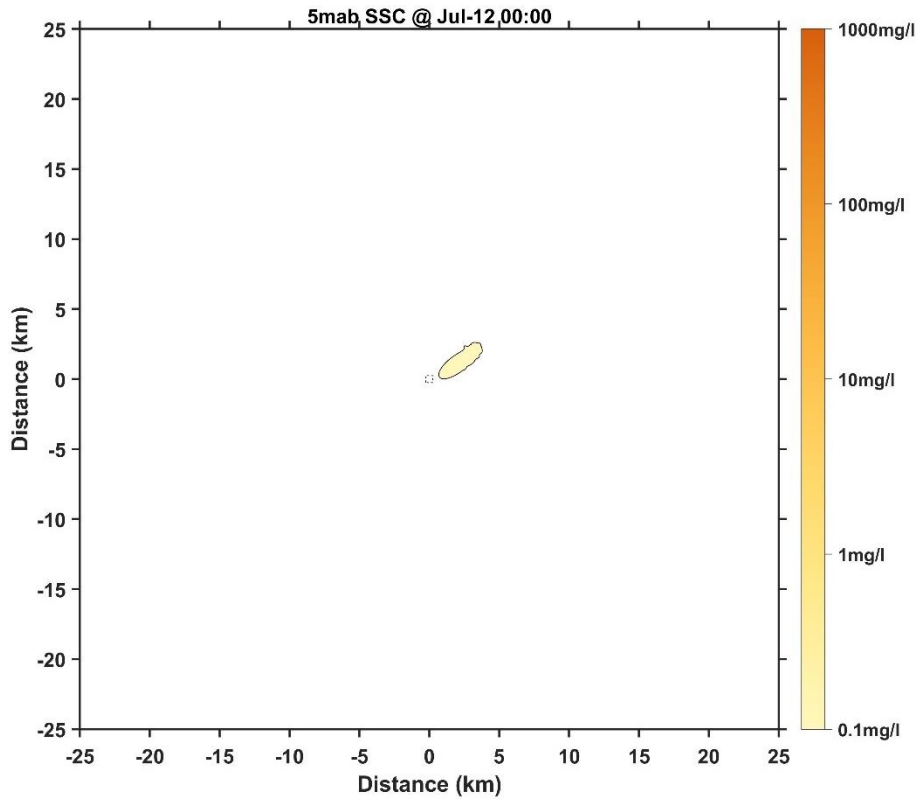
Figure 58 Horizontal distribution of SSC at 5 mab for Case 1 (7 days later)
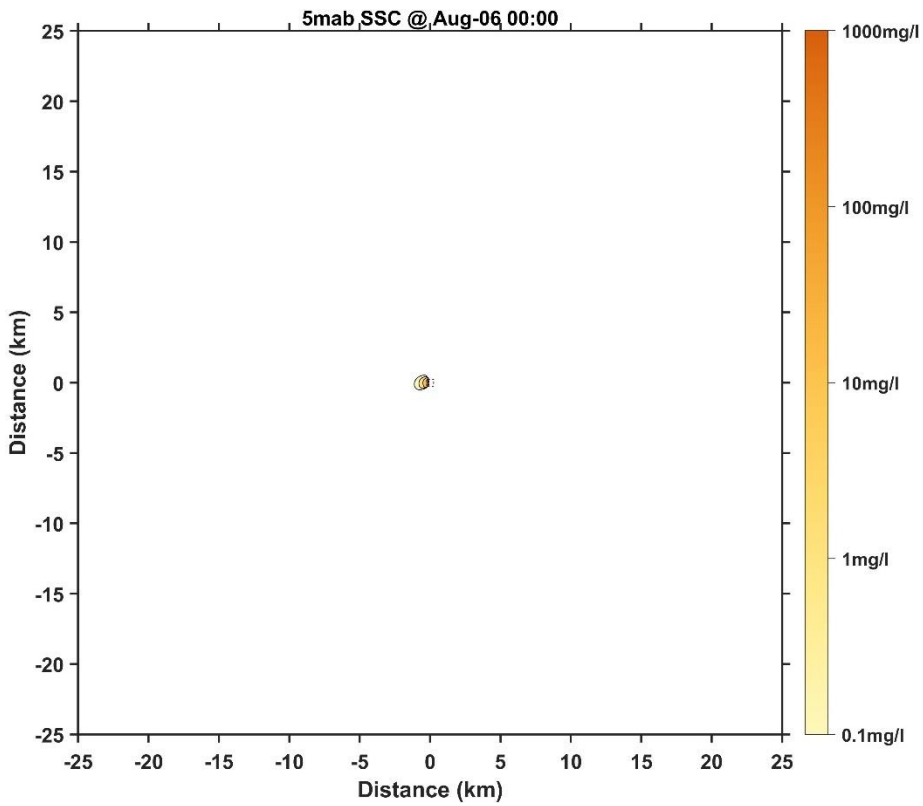
Figure 59 Horizontal distribution of SSC at 5 mab for Case 2 (1 day later)
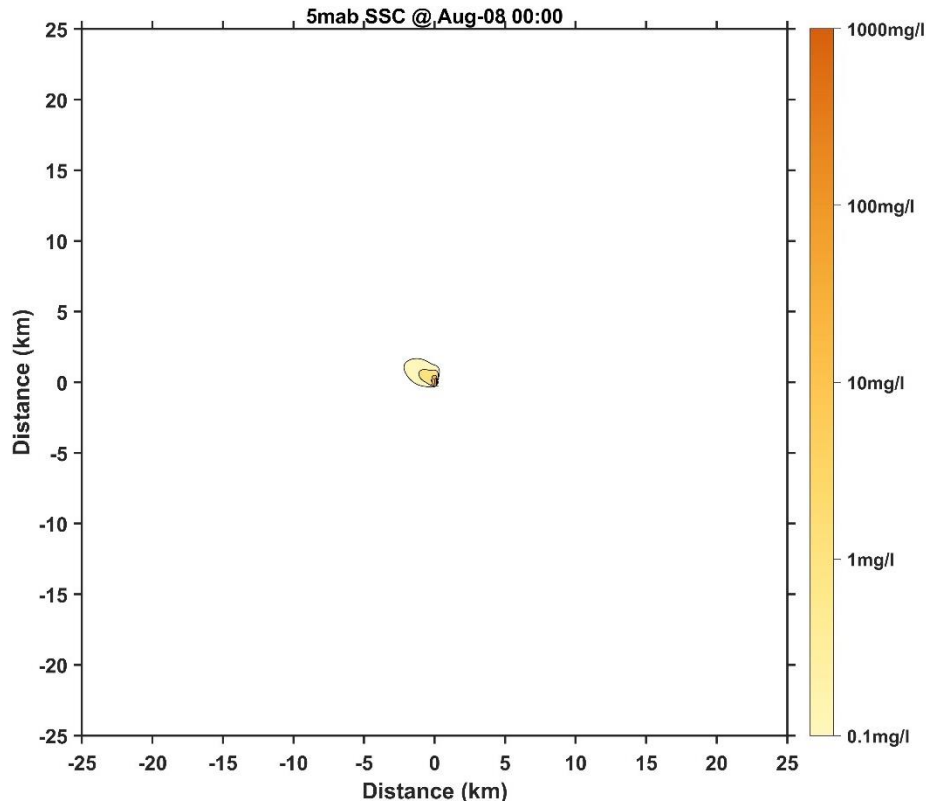
Figure 60 Horizontal distribution of SSC at 5 mab for Case 2 (3 days later)
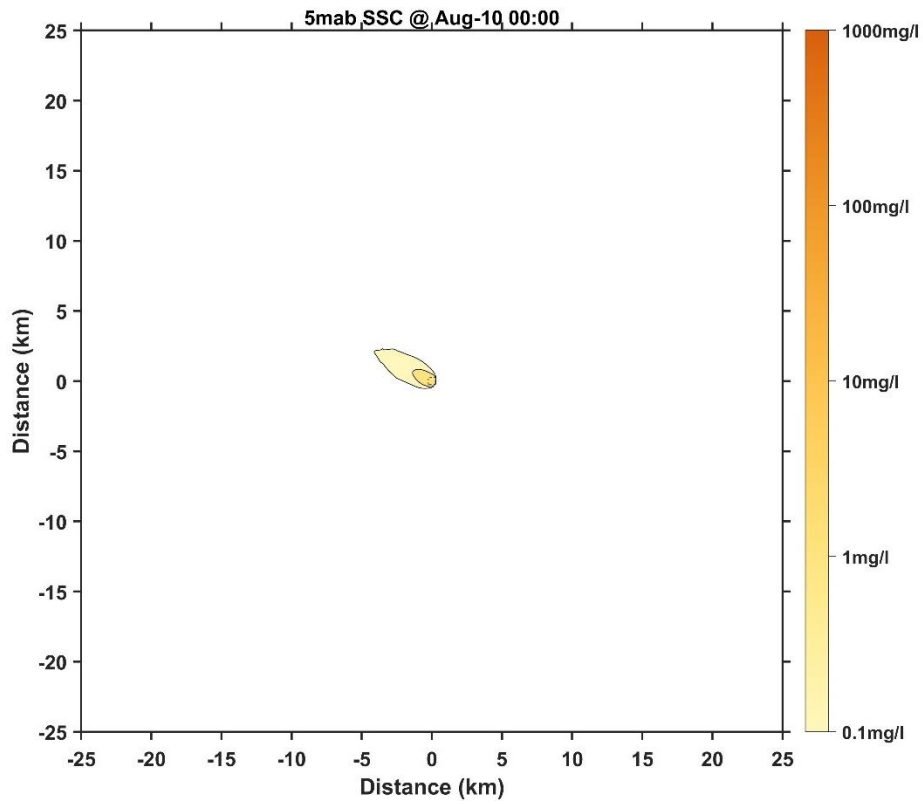
Figure 61 Horizontal distribution of SSC at 5 mab for Case 2 (5 days later)
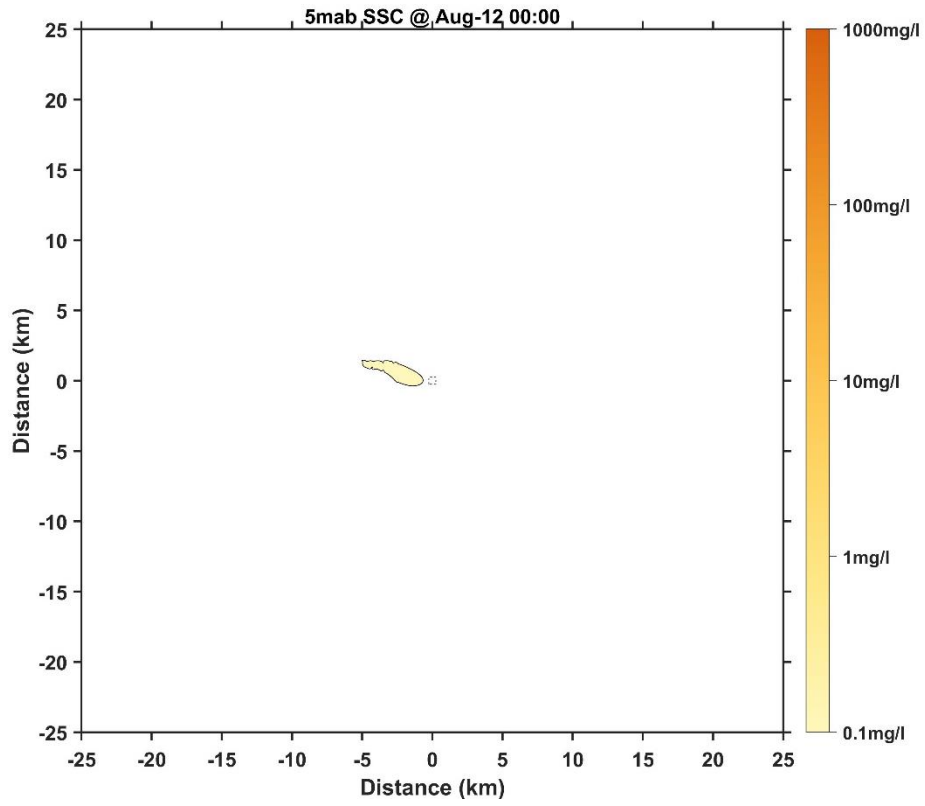
Figure 62 Horizontal distribution of SSC at 5 mab for Case 2 (7 days later)
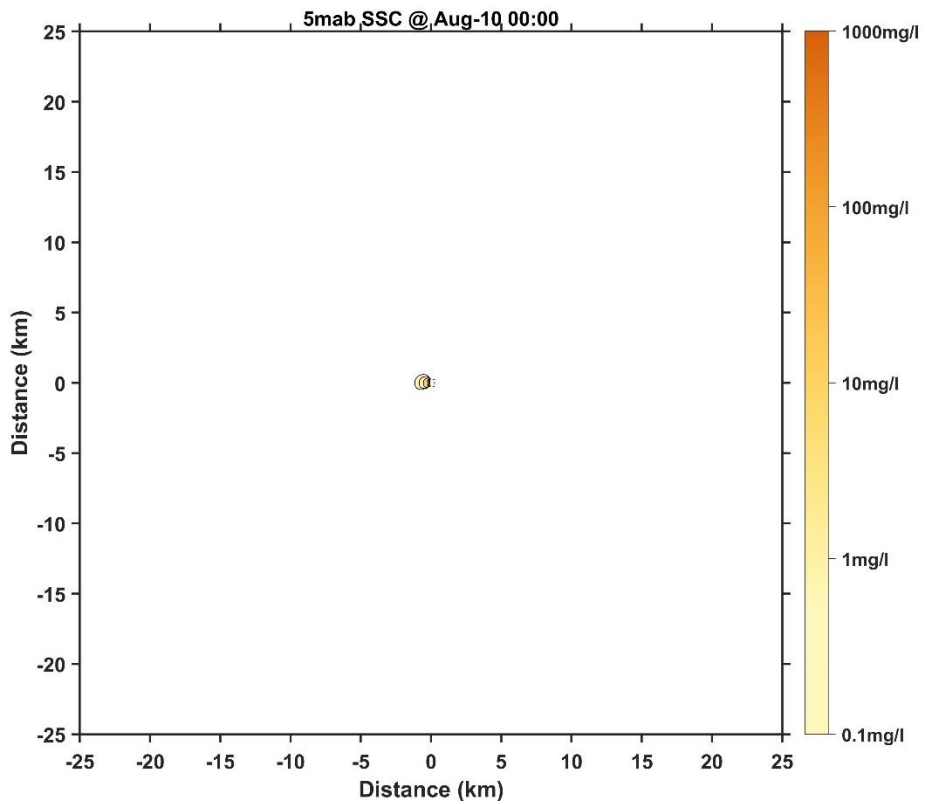
Figure 63 Horizontal distribution of SSC at 5 mab for Case 3 (1 day later)
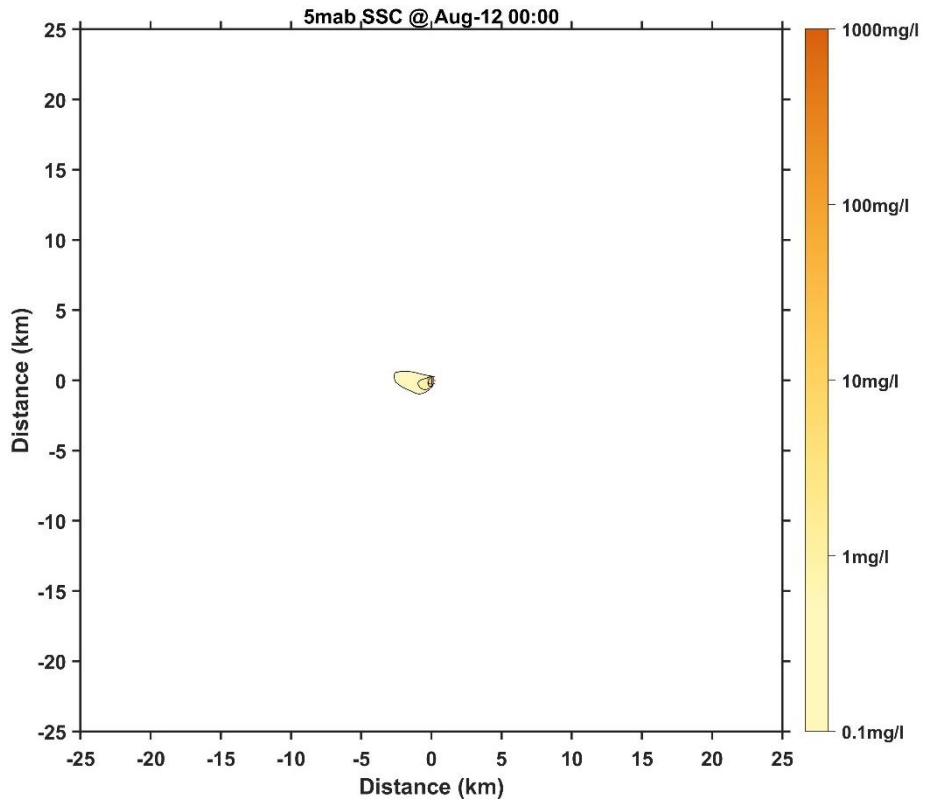
Figure 64 Horizontal distribution of SSC at 5 mab for Case 3 (3 days later)
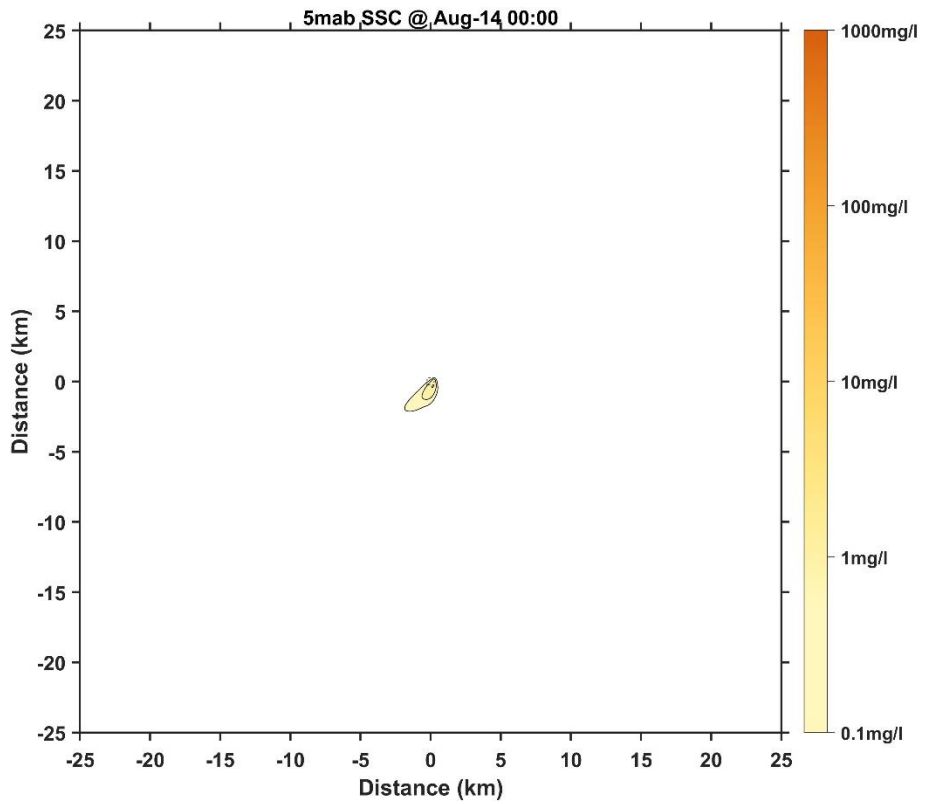
Figure 65 Horizontal distribution of SSC at 5 mab for Case 3 (5 days later)

637
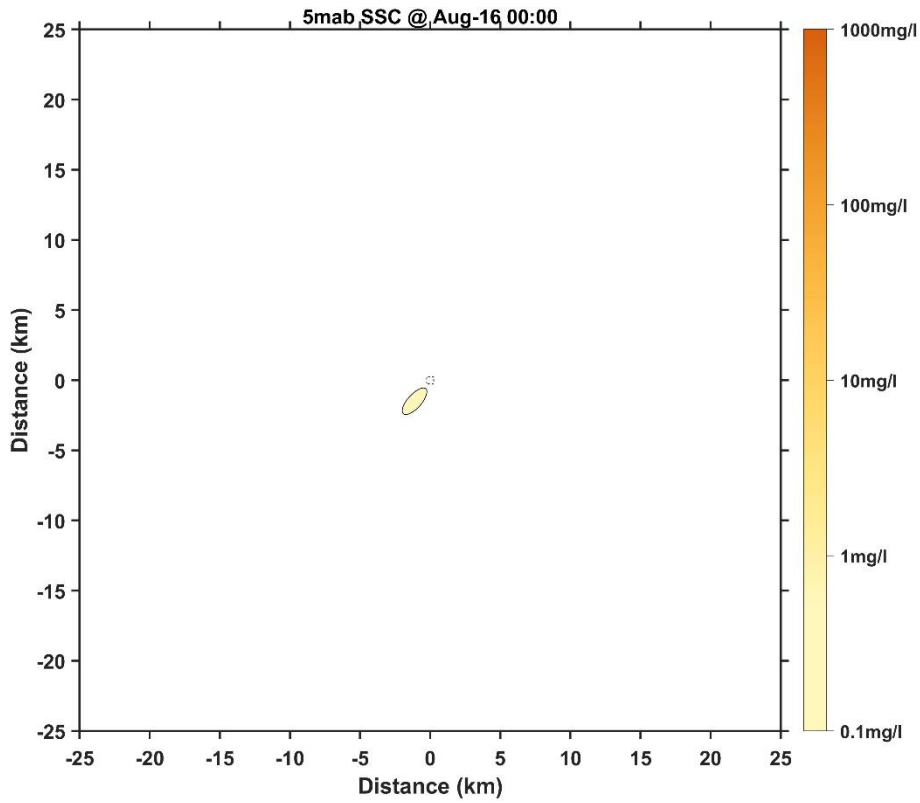
Figure 66 Horizontal distribution of SSC at 5 mab for Case 3 (7 days later)
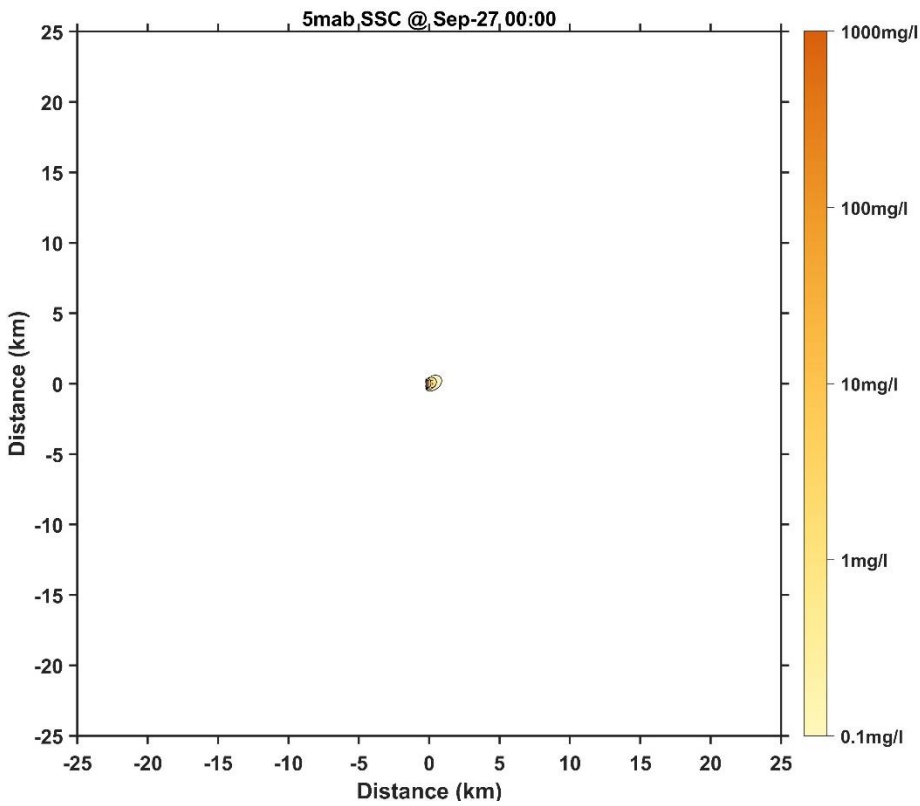
Figure 67 Horizontal distribution of SSC at 5 mab for Case 4 (1 day later)
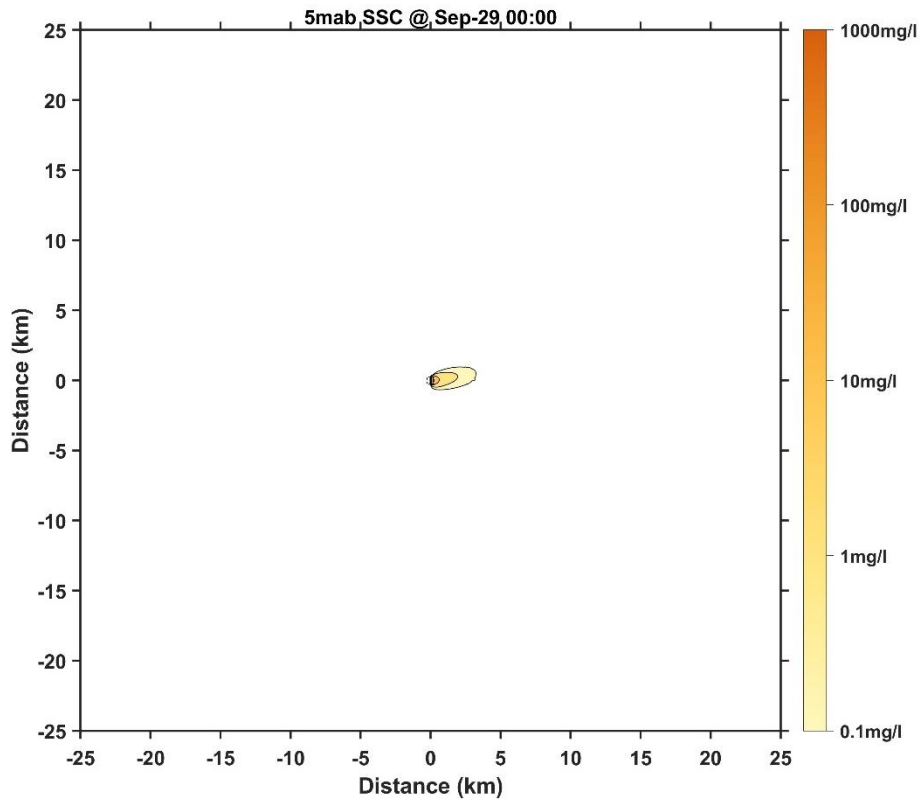
Figure 68 Horizontal distribution of SSC at 5 mab for Case 4 (3 days later)
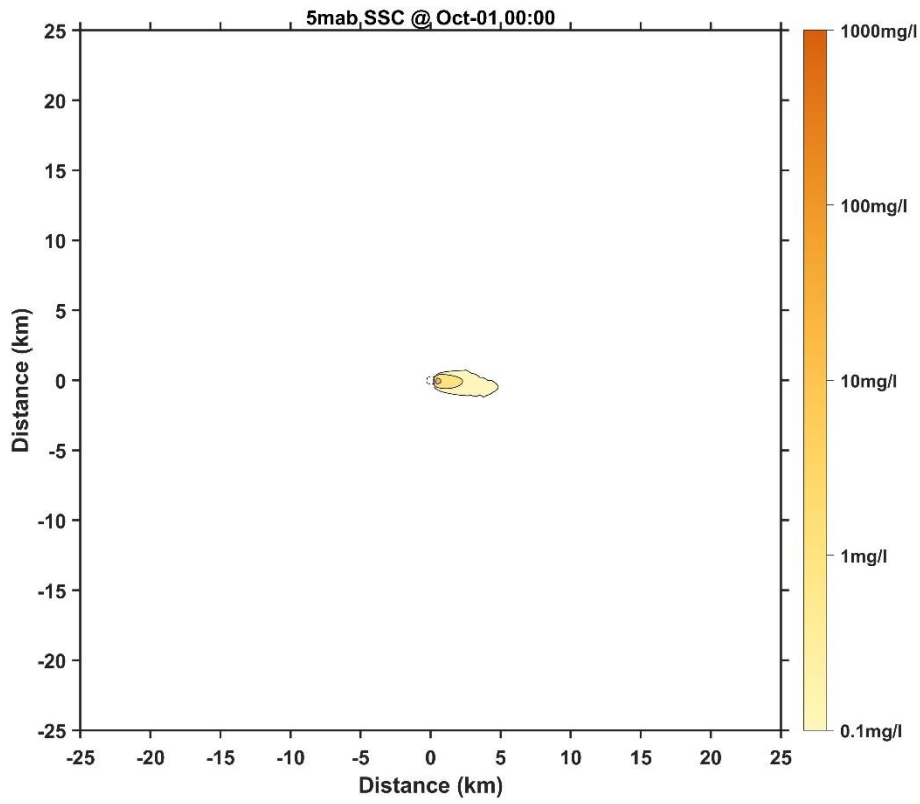
Figure 69 Horizontal distribution of SSC at 5 mab for Case 4 (5 days later)
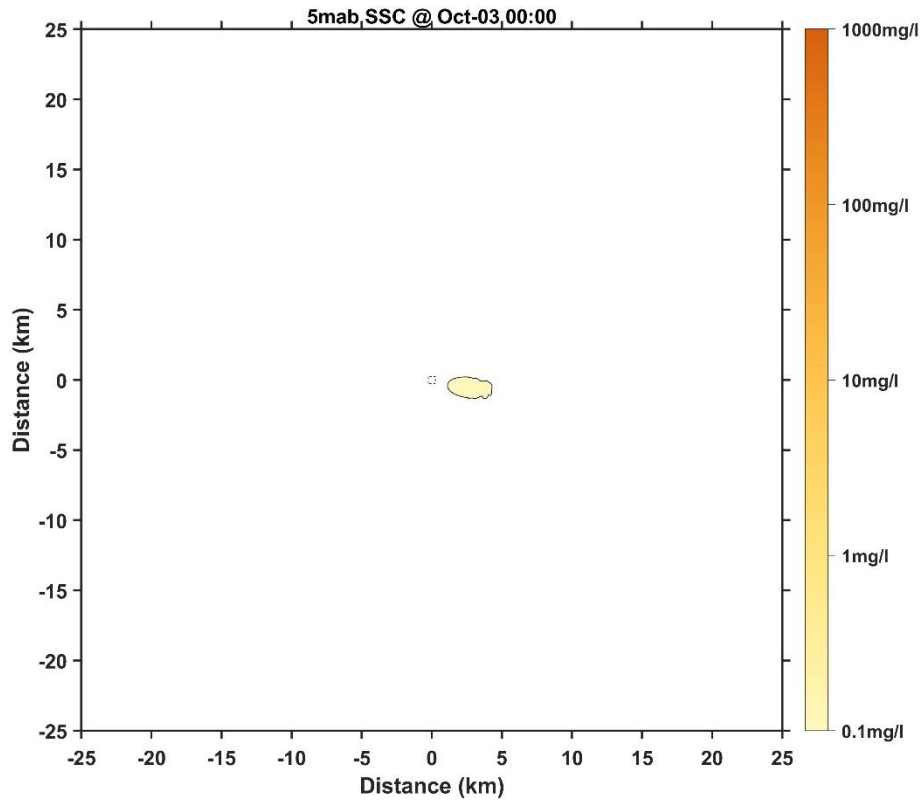
Figure 70 Horizontal distribution of SSC at 5 mab for Case 4 (7 days later)
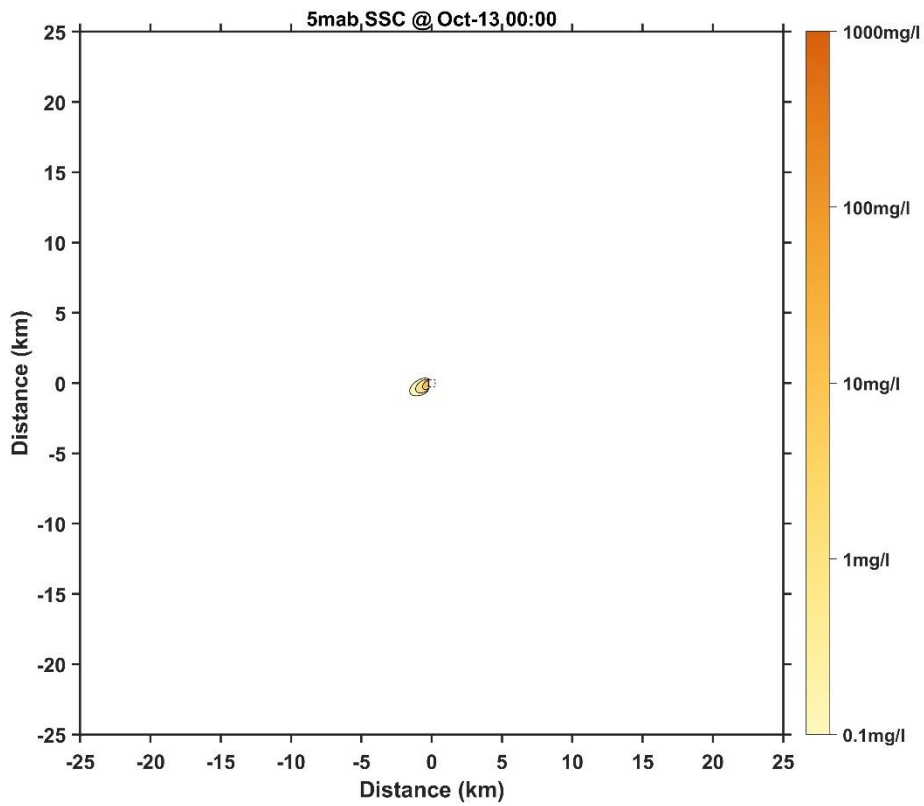
Figure 71 Horizontal distribution of SSC at 5 mab for Case 5 (1 day later)
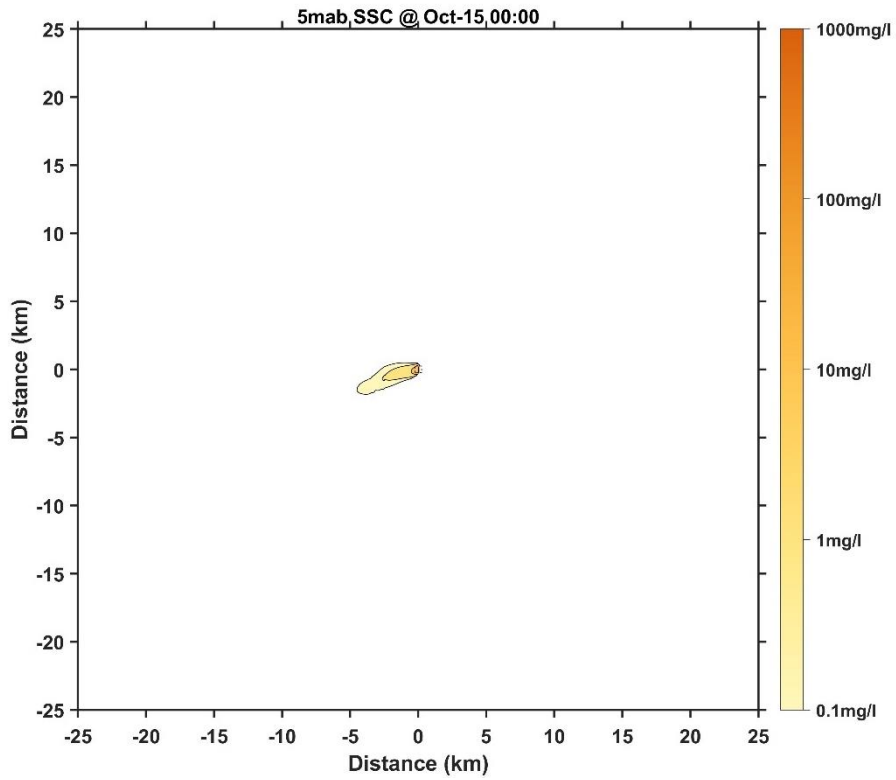
Figure 72 Horizontal distribution of SSC at 5 mab for Case 5 (3 days later)
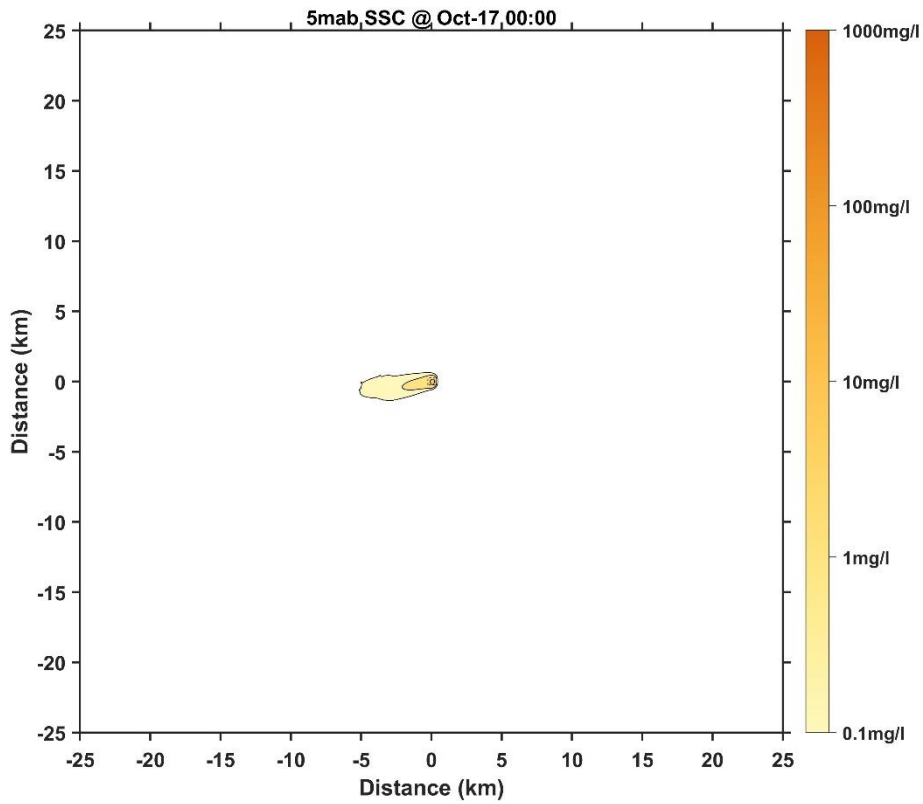
Figure 73 Horizontal distribution of SSC at 5 mab for Case 5 (5 days later)
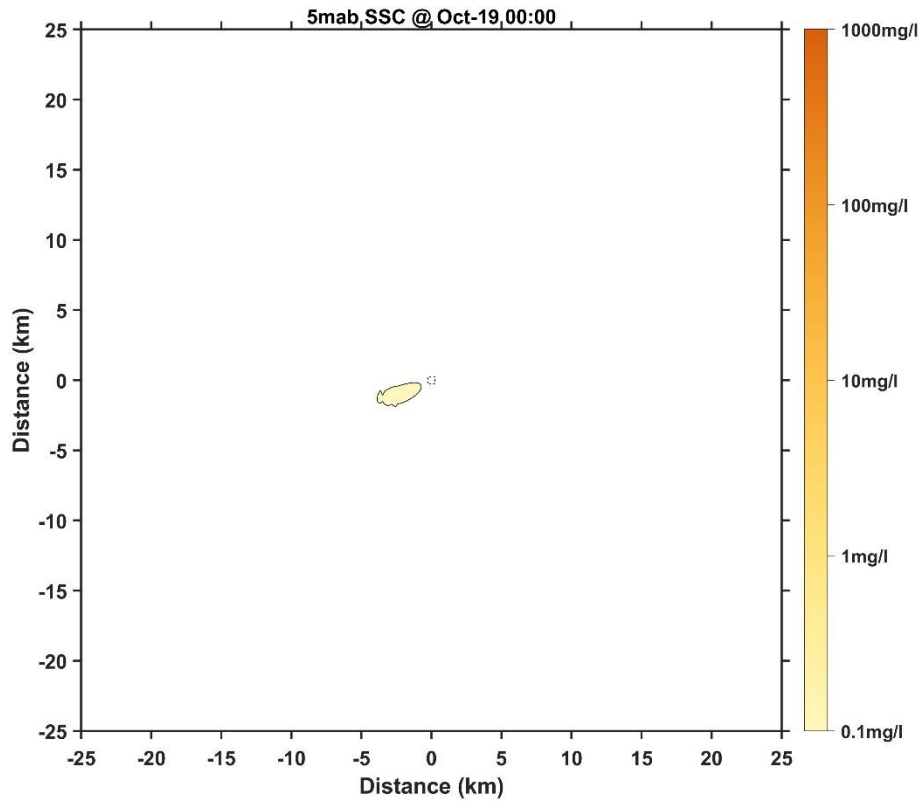
Figure 74 Horizontal distribution of SSC at 5 mab for Case 5 (7 days later)
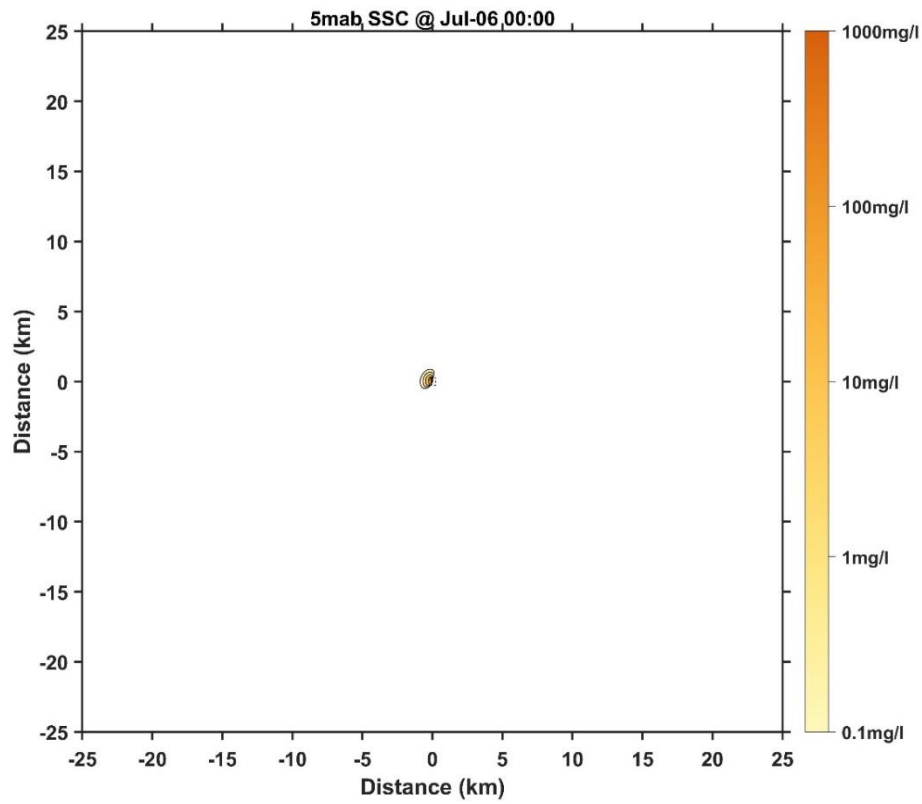
Figure 75 Horizontal distribution of SSC at 5 mab for Case 6 (1 day later)
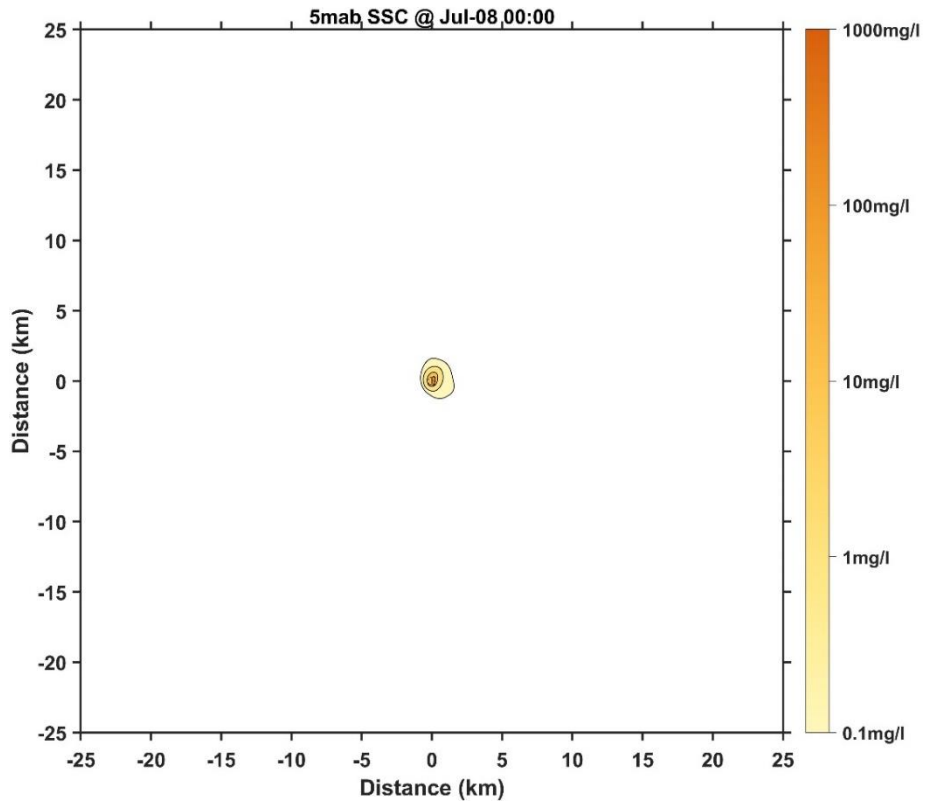
Figure 76 Horizontal distribution of SSC at 5 mab for Case 6 (3 days later)
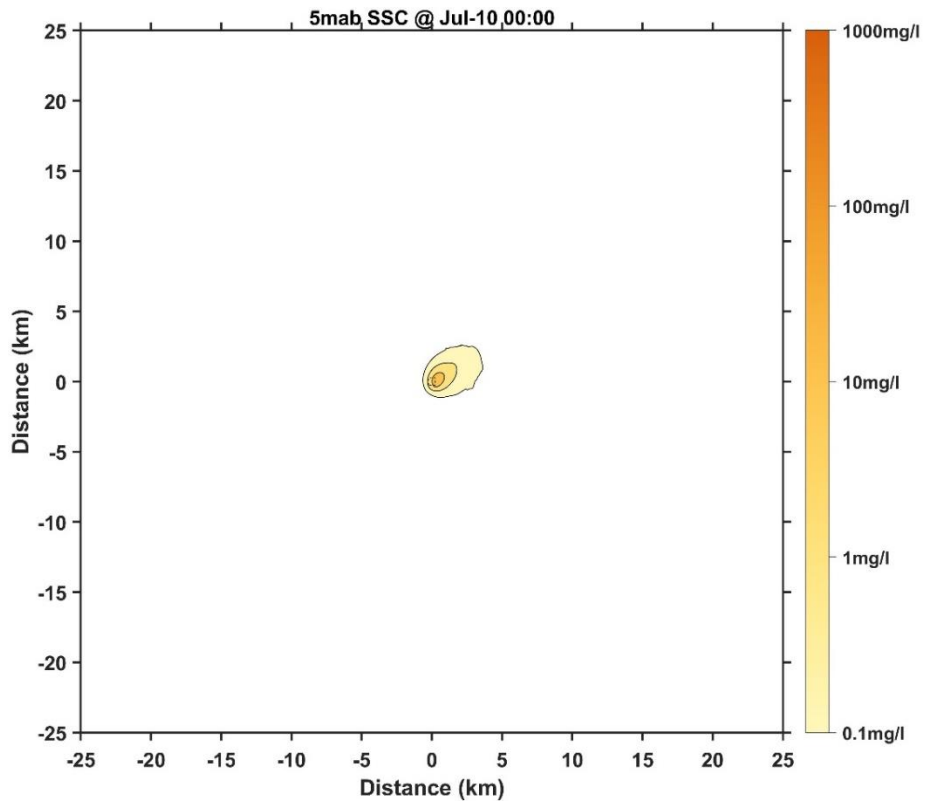
Figure 77 Horizontal distribution of SSC at 5 mab for Case 6 (5 days later)
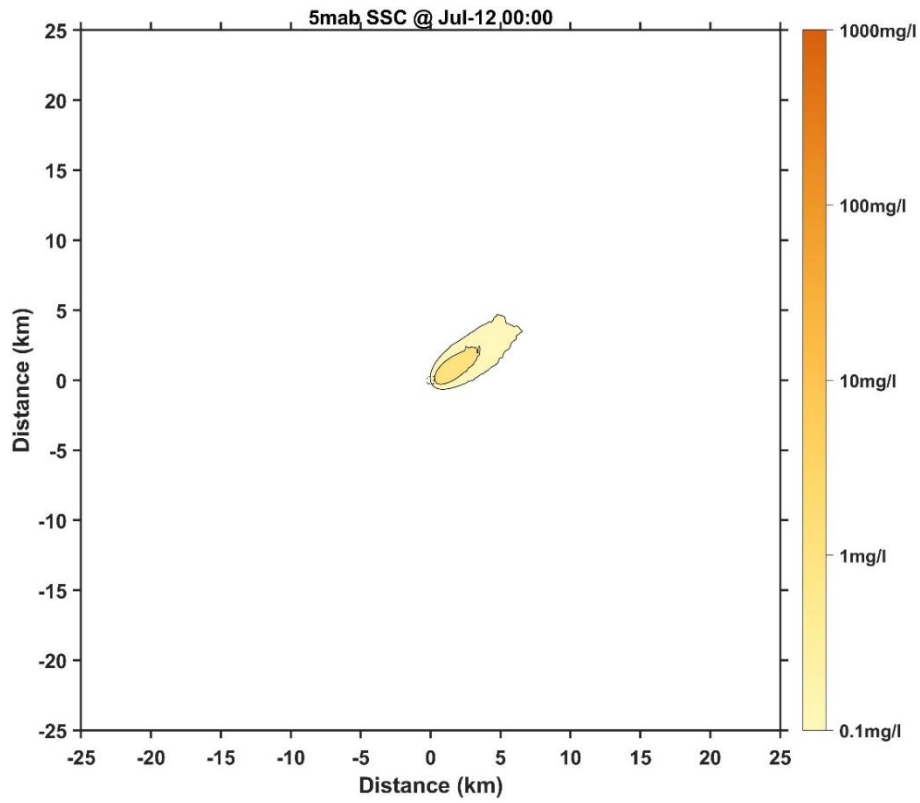
Figure 78 Horizontal distribution of SSC at 5 mab for Case 6 (7 days later)
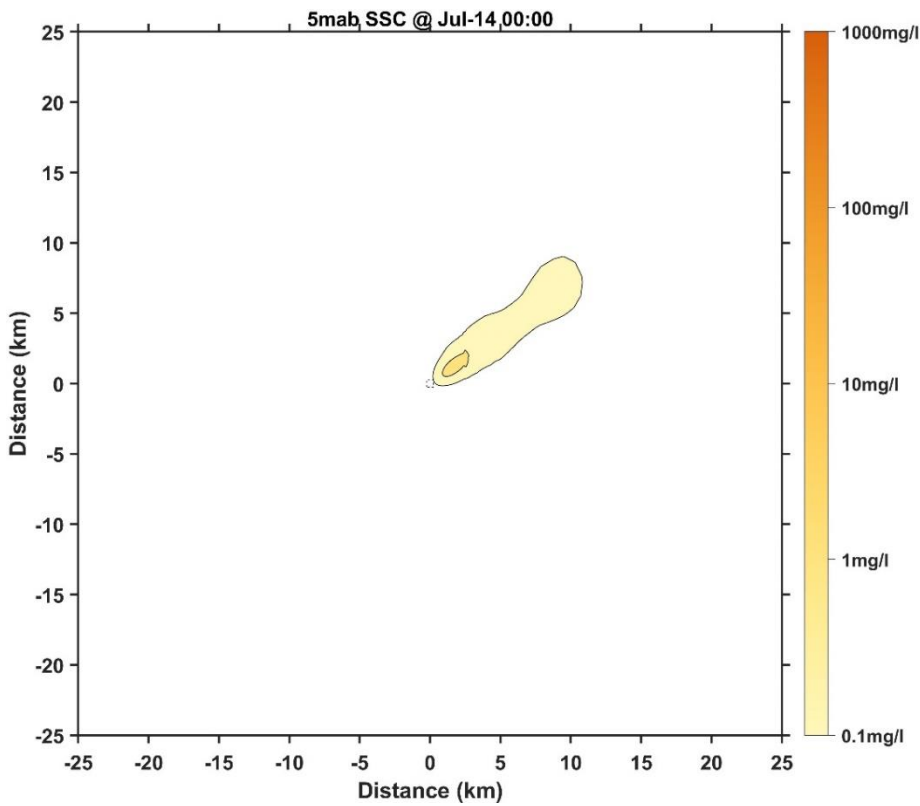
Figure 79 Horizontal distribution of SSC at 5 mab for Case 6 (9 days later)

644
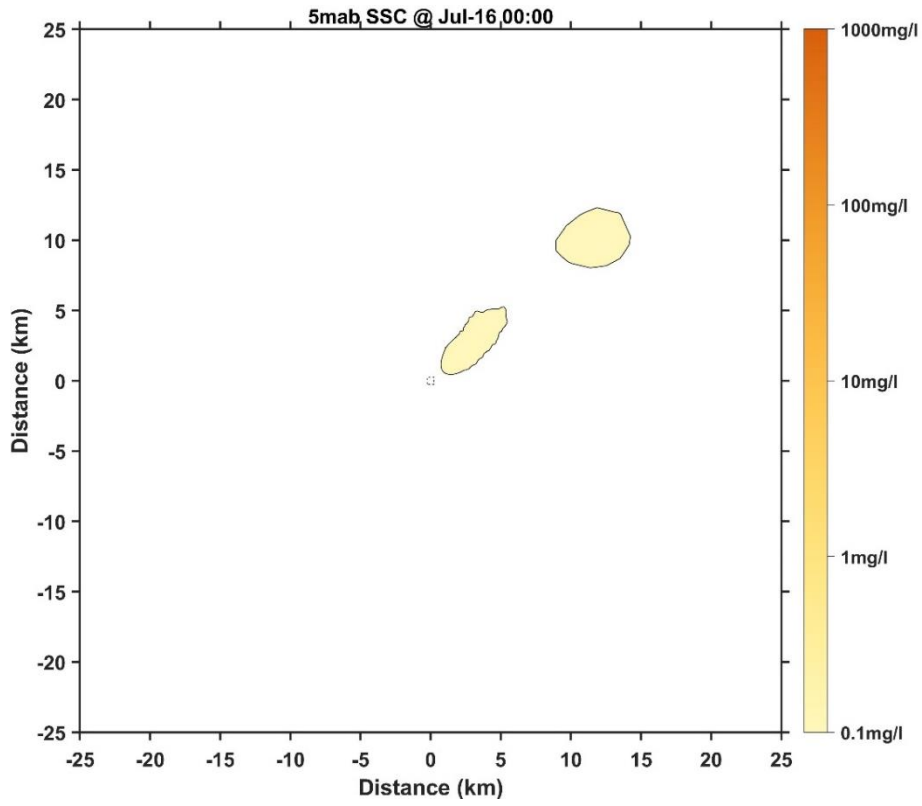
Figure 80 Horizontal distribution of SSC at 5 mab for Case 6 (11 days later)
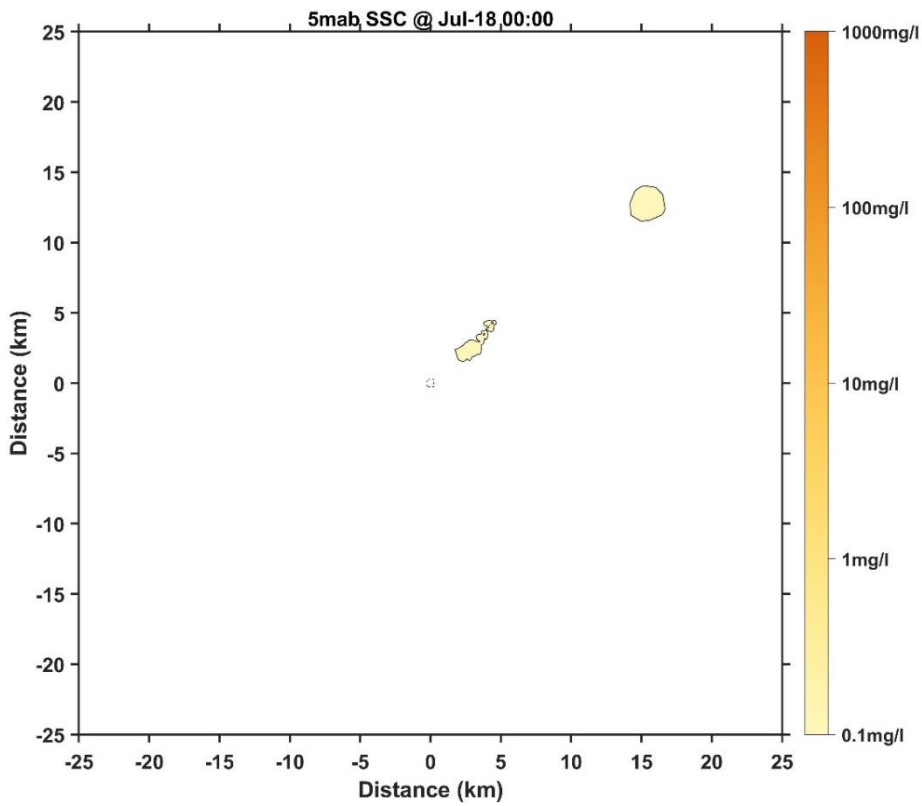
Figure 81 Horizontal distribution of SSC at 5 mab for Case 6 (13 days later)
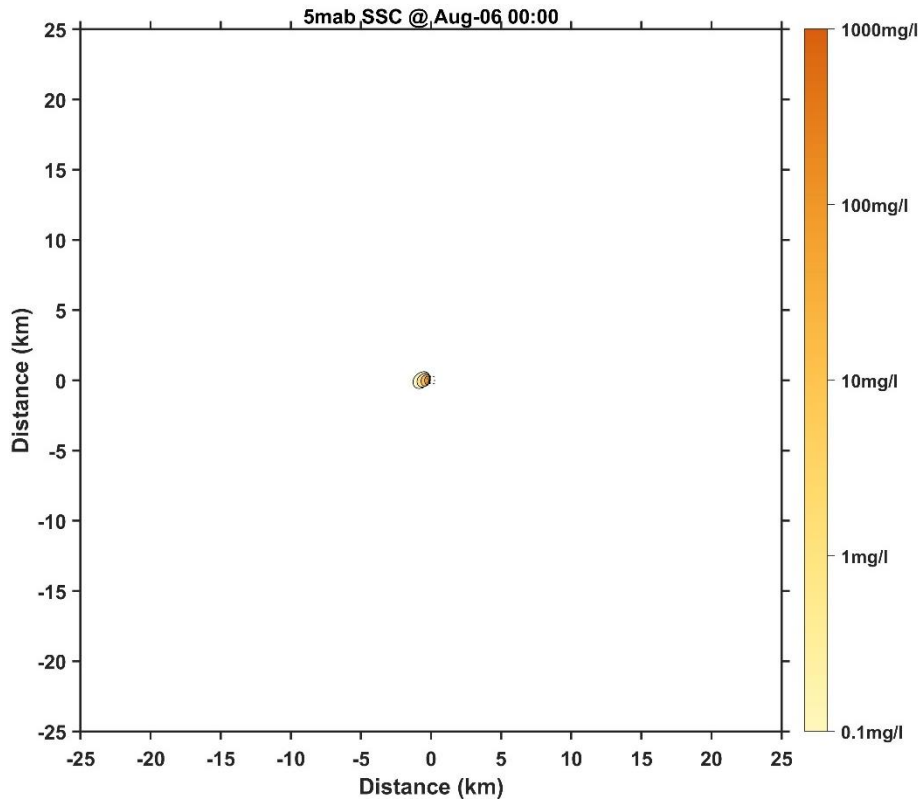
Figure 82 Horizontal distribution of SSC at 5 mab for Case 7 (1 day later)
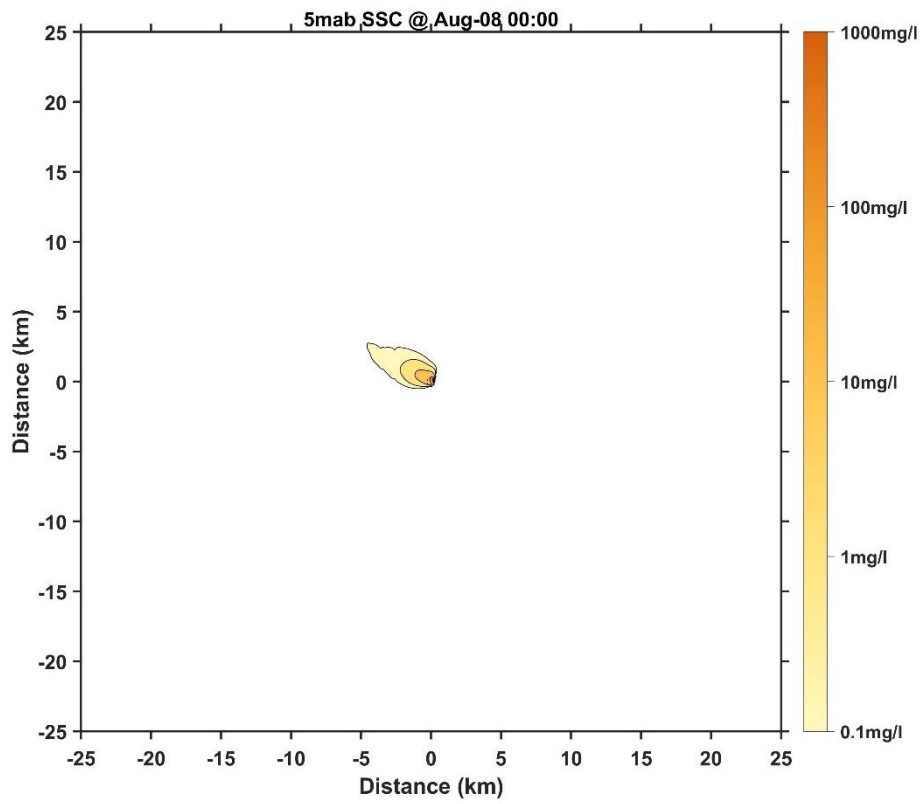
Figure 83 Horizontal distribution of SSC at 5 mab for Case 7 (3 days later)
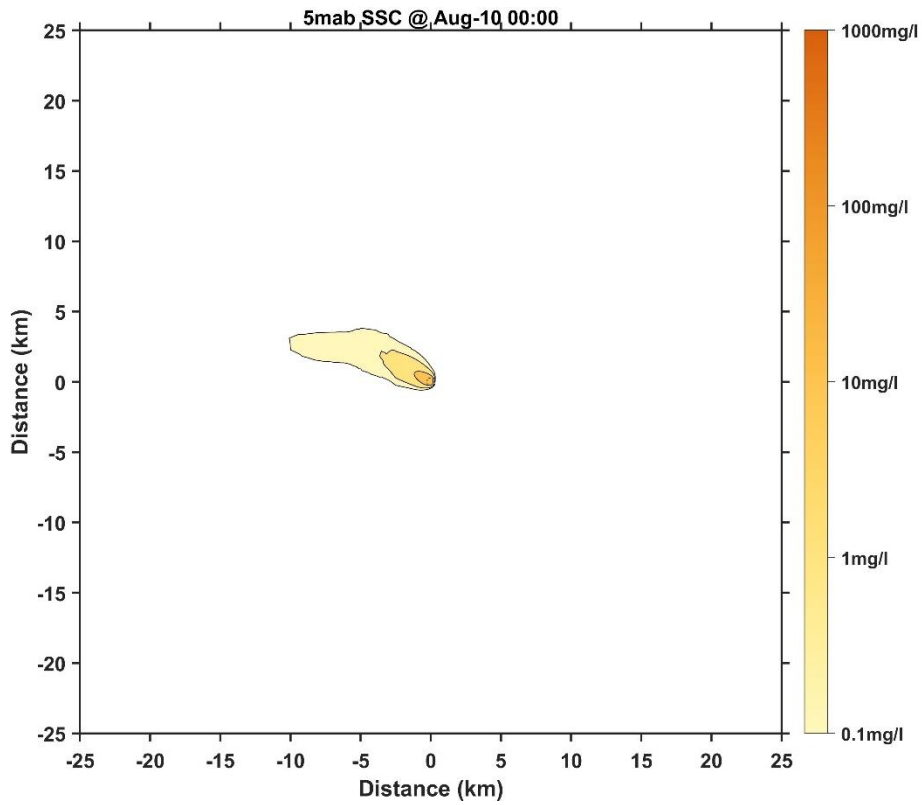
Figure 84 Horizontal distribution of SSC at 5 mab for Case 7 (5 days later)
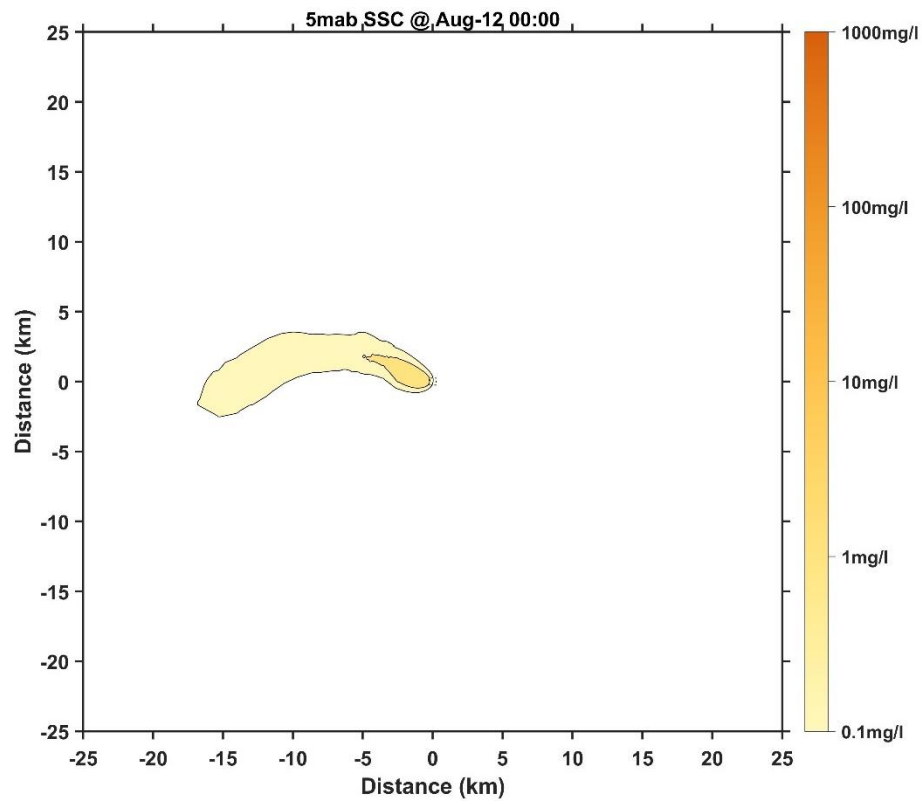
Figure 85 Horizontal distribution of SSC at 5 mab for Case 7 (7 days later)

647
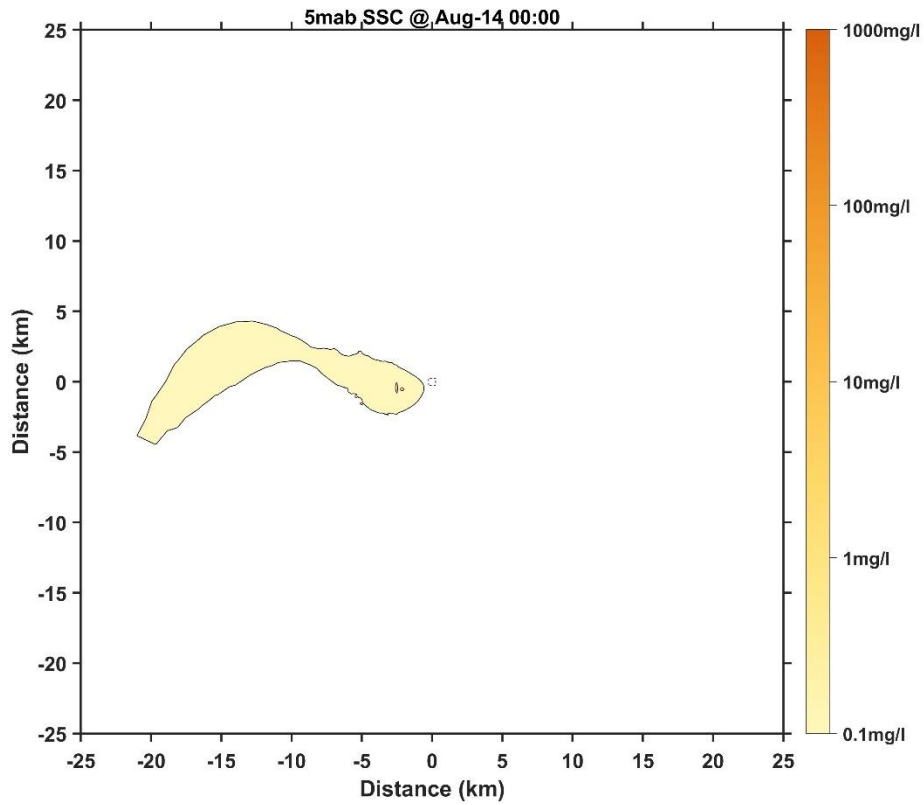
Figure 86 Horizontal distribution of SSC at 5 mab for Case 7 (9 days later)
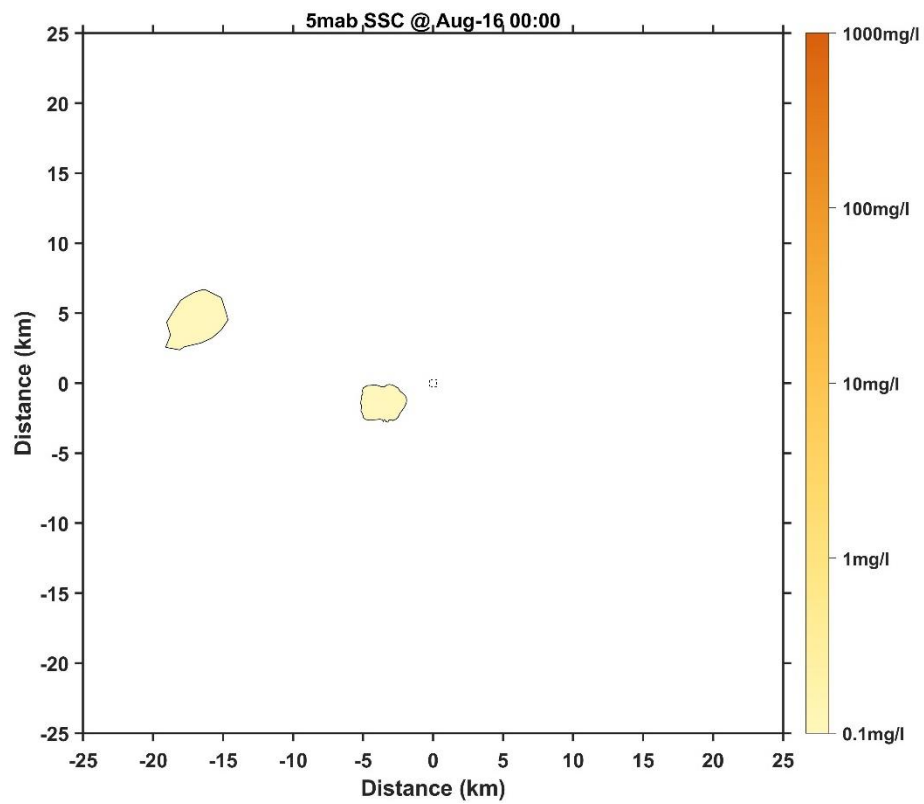
Figure 87 Horizontal distribution of SSC at 5 mab for Case 7 (11 days later)
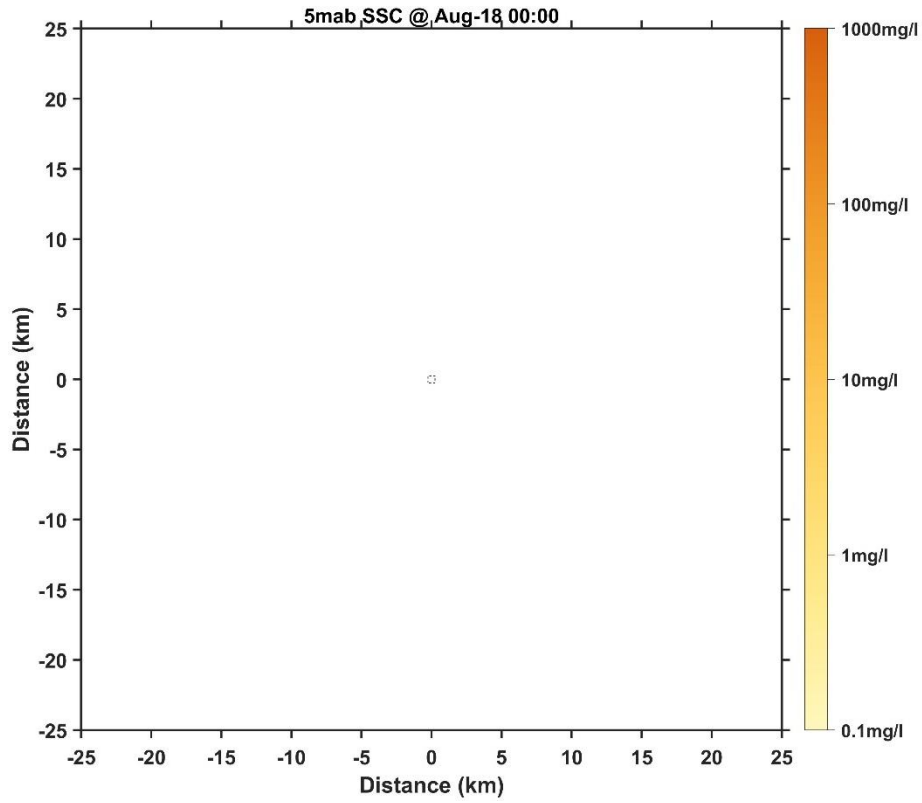
Figure 88 Horizontal distribution of SSC at 5 mab for Case 7 (13 days later)
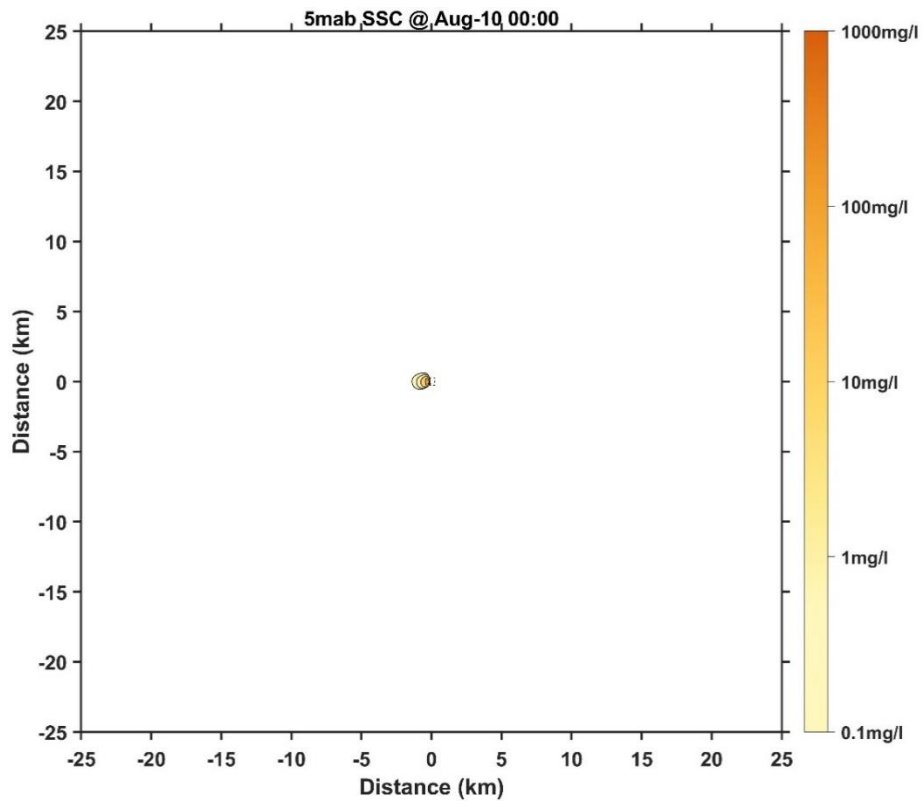
Figure 89 Horizontal distribution of SSC at 5 mab for Case 8 (1 day later)
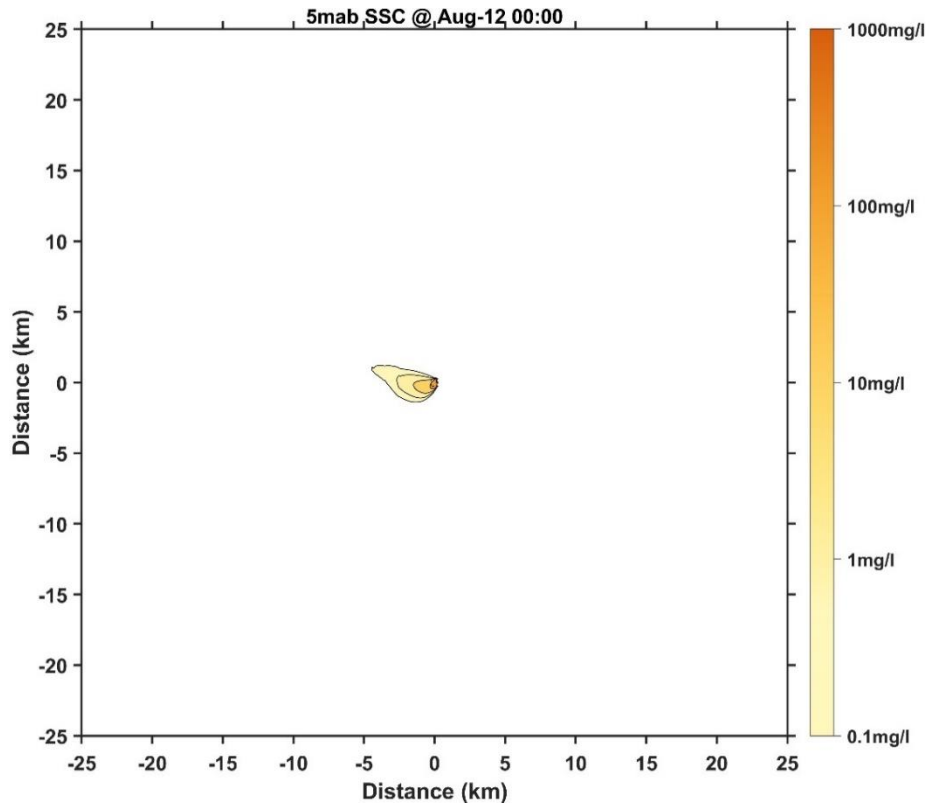
Figure 90 Horizontal distribution of SSC at 5 mab for Case 8 (3 days later)
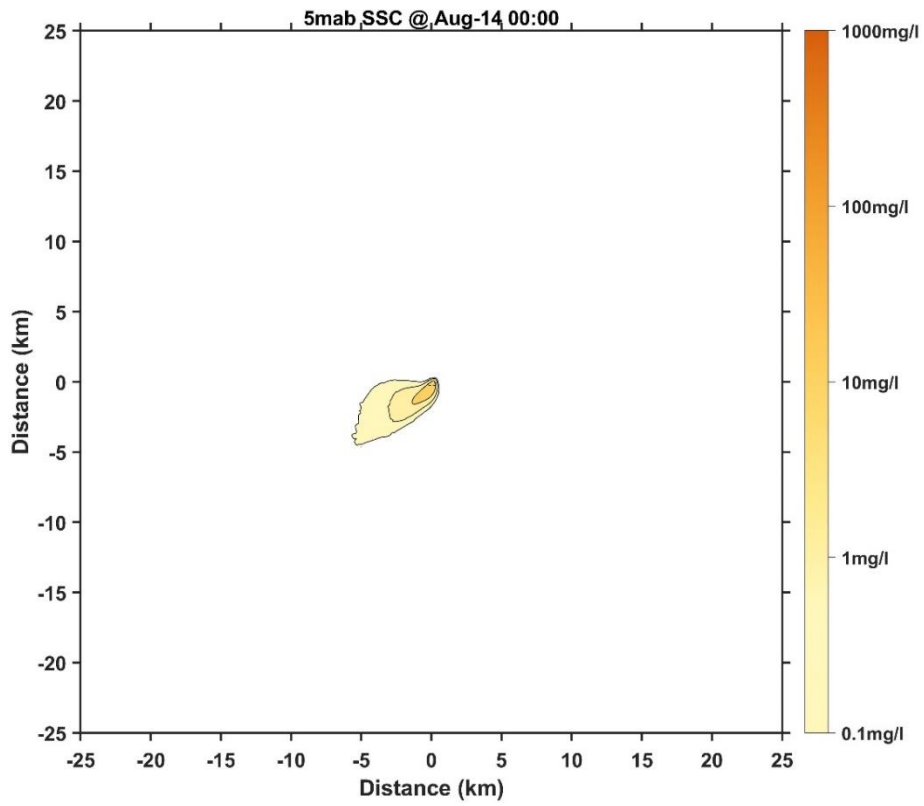
Figure 91 Horizontal distribution of SSC at 5 mab for Case 8 (5 days later)
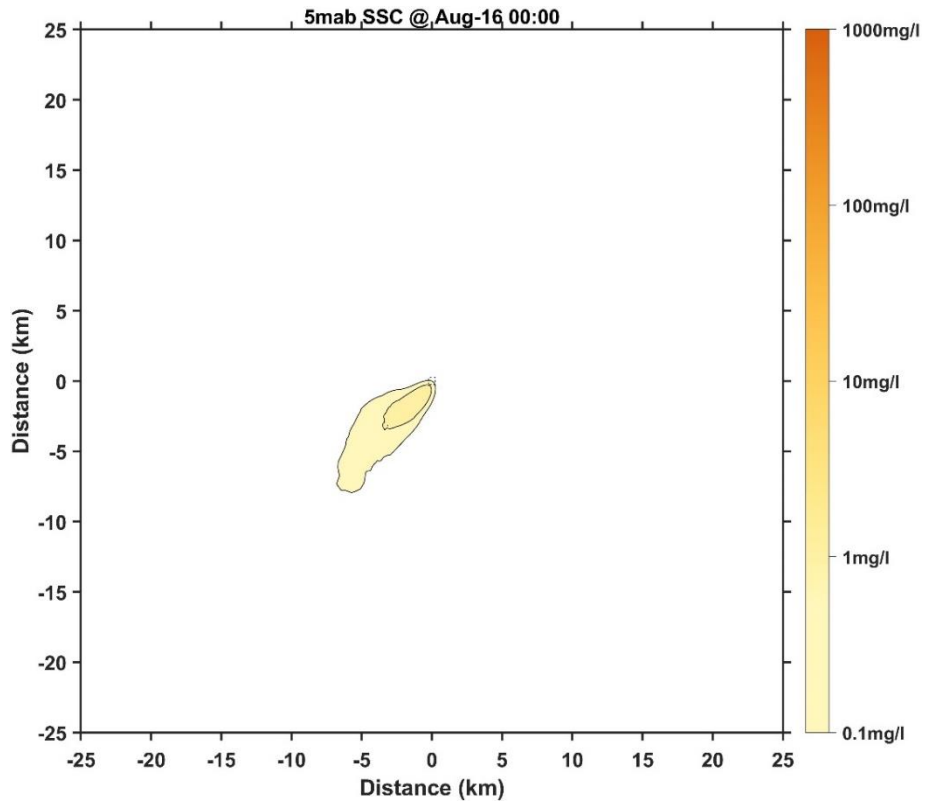
Figure 92 Horizontal distribution of SSC at 5 mab for Case 8 (7 days later)
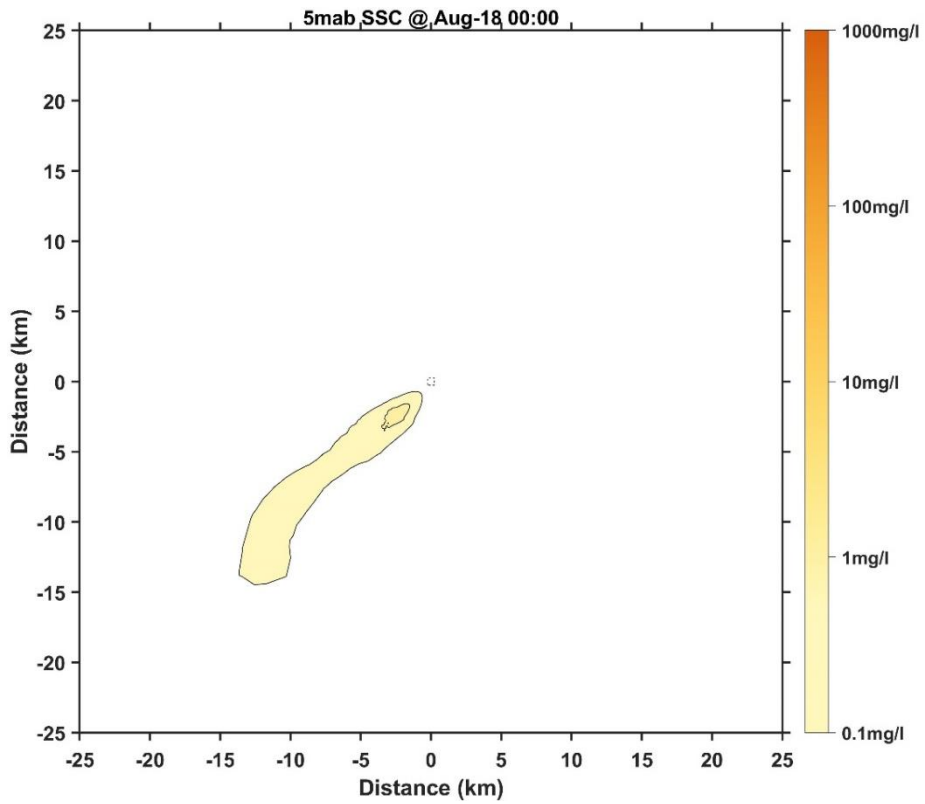
Figure 93 Horizontal distribution of SSC at 5 mab for Case 8 (9 days later)
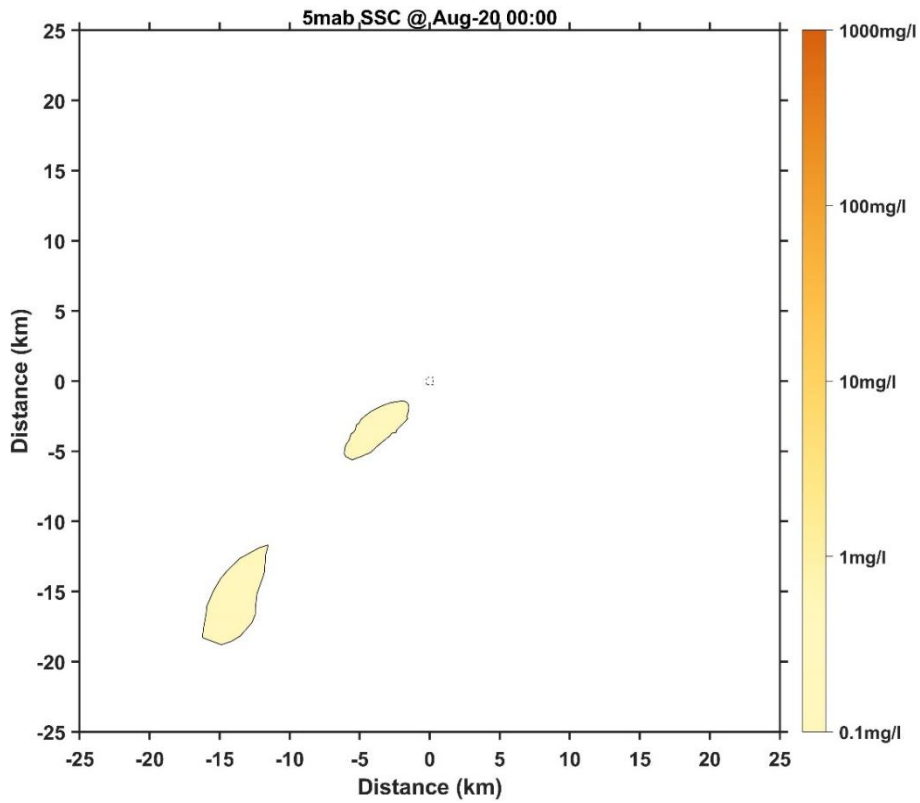
Figure 94 Horizontal distribution of SSC at 5 mab for Case 8 (11 days later)
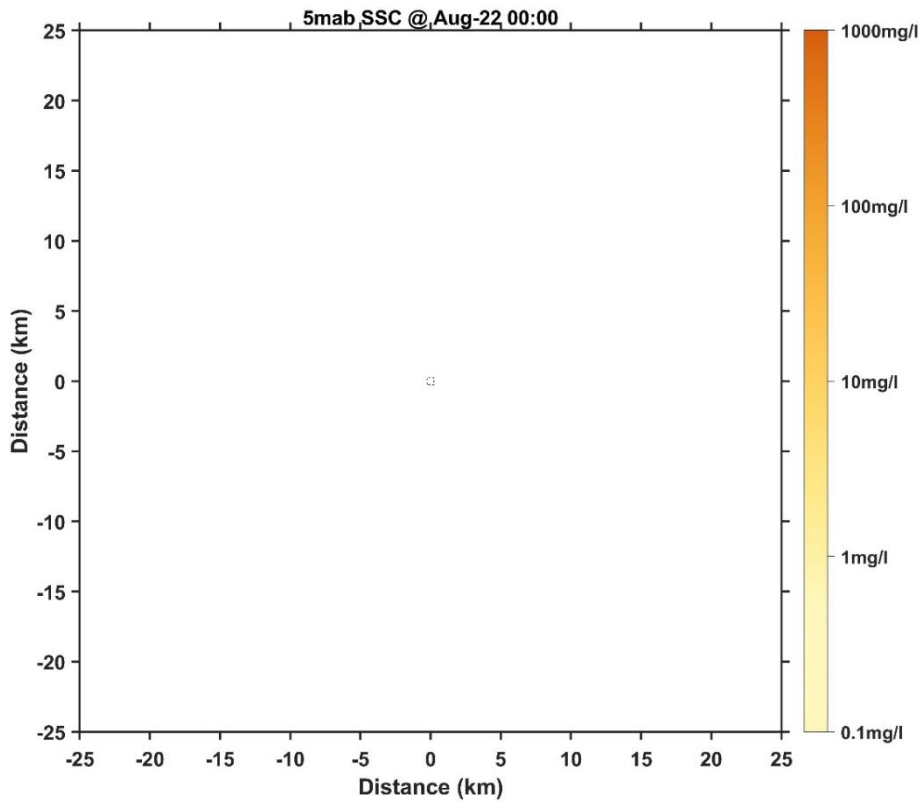
Figure 95 Horizontal distribution of SSC at 5 mab for Case 8 (13 days later)
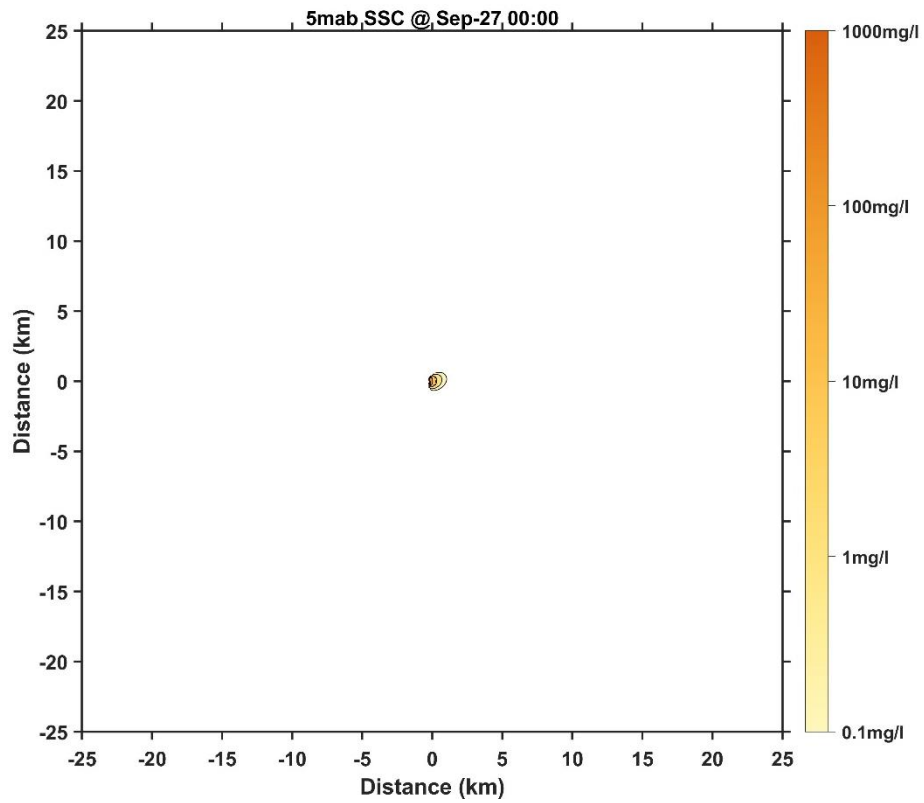
Figure 96 Horizontal distribution of SSC at 5 mab for Case 9 (1 day later)
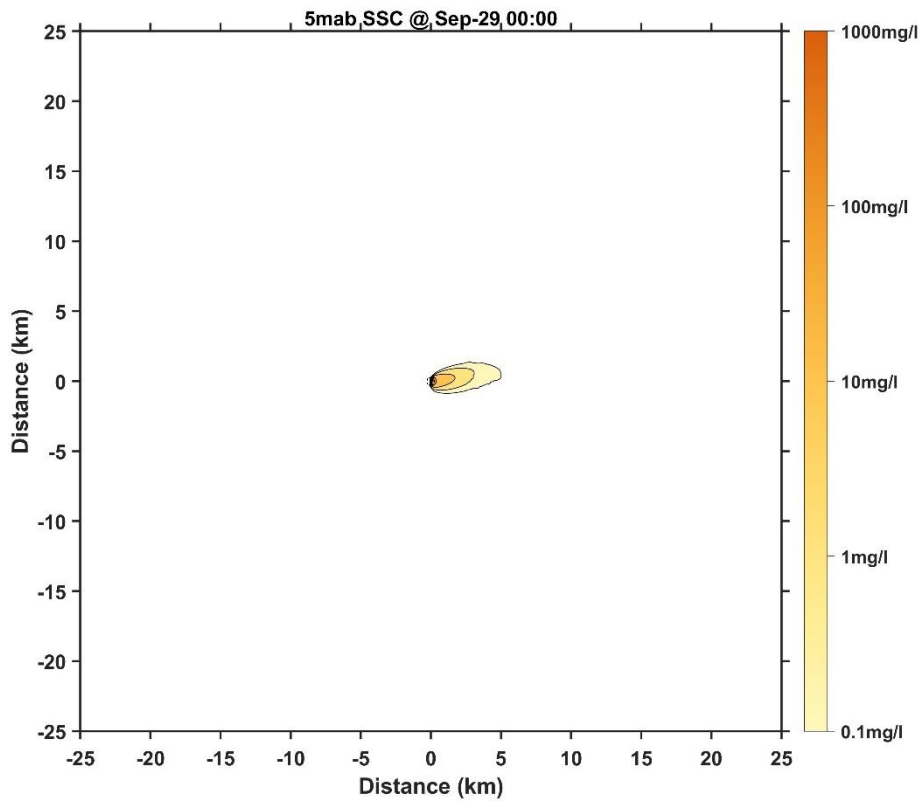
Figure 97 Horizontal distribution of SSC at 5 mab for Case 9 (3 days later)

653
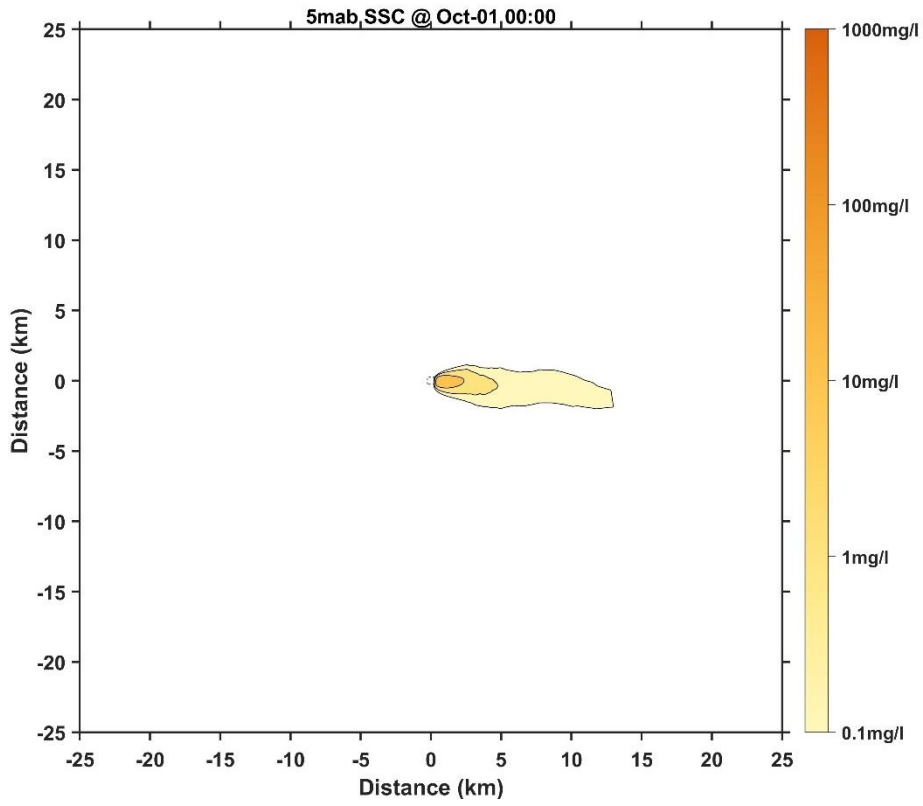
Figure 98 Horizontal distribution of SSC at 5 mab for Case 9 (5 days later)
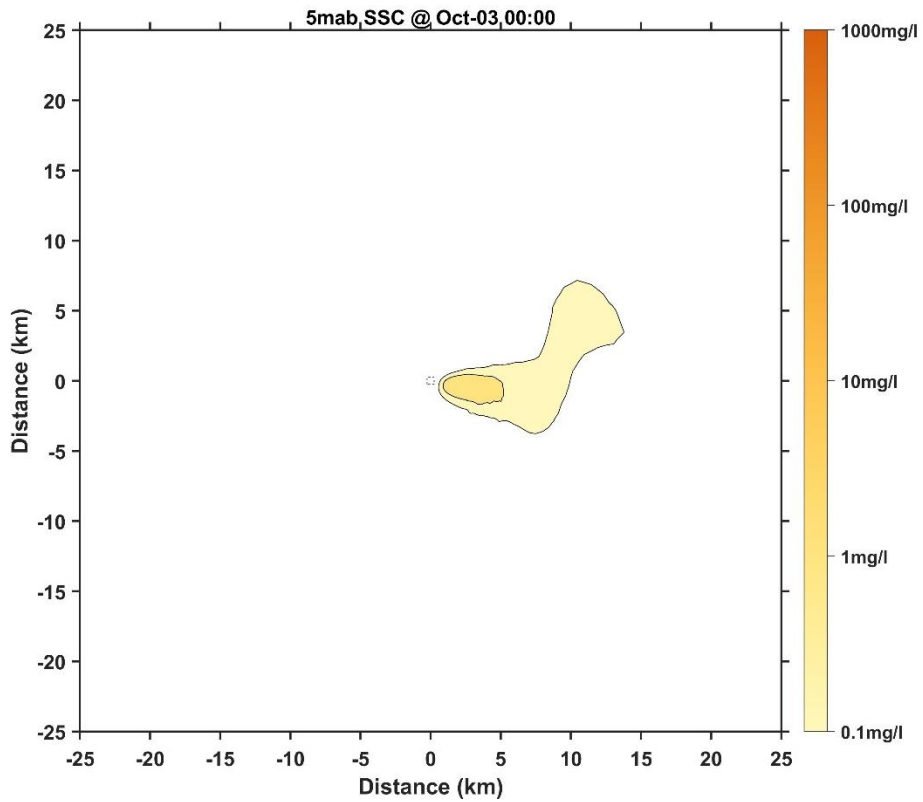
Figure 99 Horizontal distribution of SSC at 5 mab for Case 9 (7 days later)

654
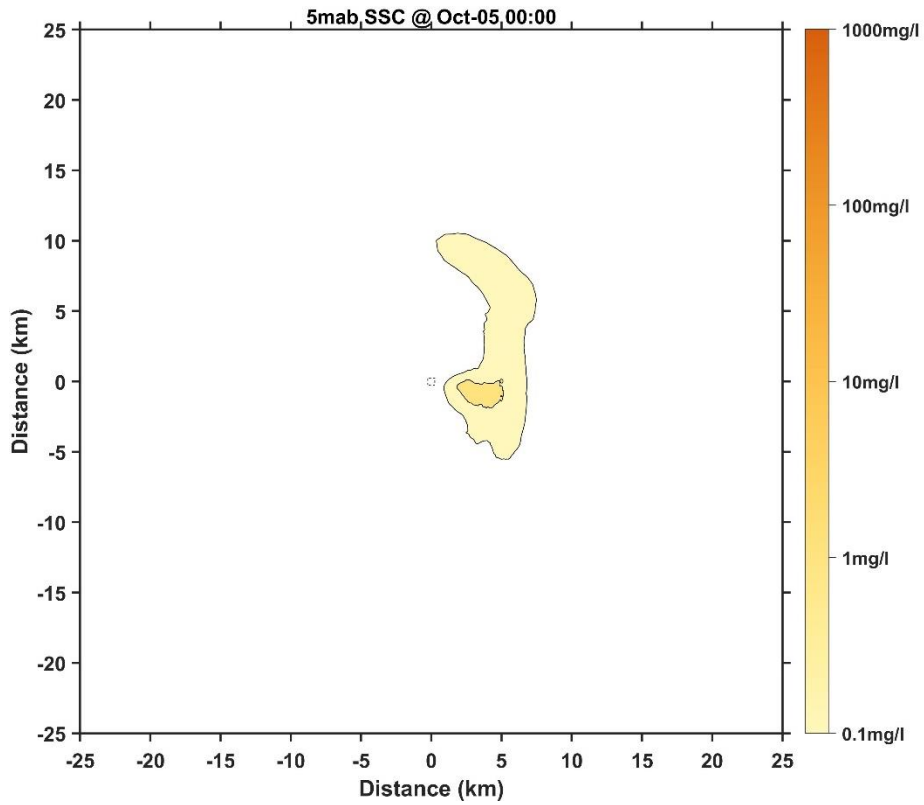
Figure 100 Horizontal distribution of SSC at 5 mab for Case 9 (9 days later)
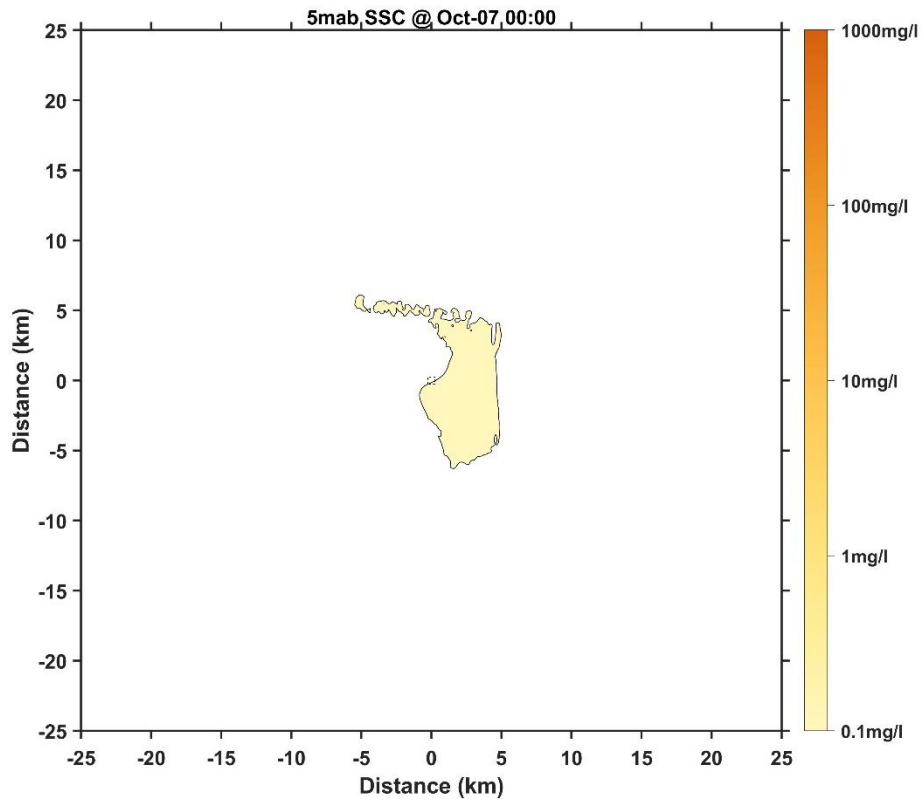
Figure 101 Horizontal distribution of SSC at 5 mab for Case 9 (11 days later)
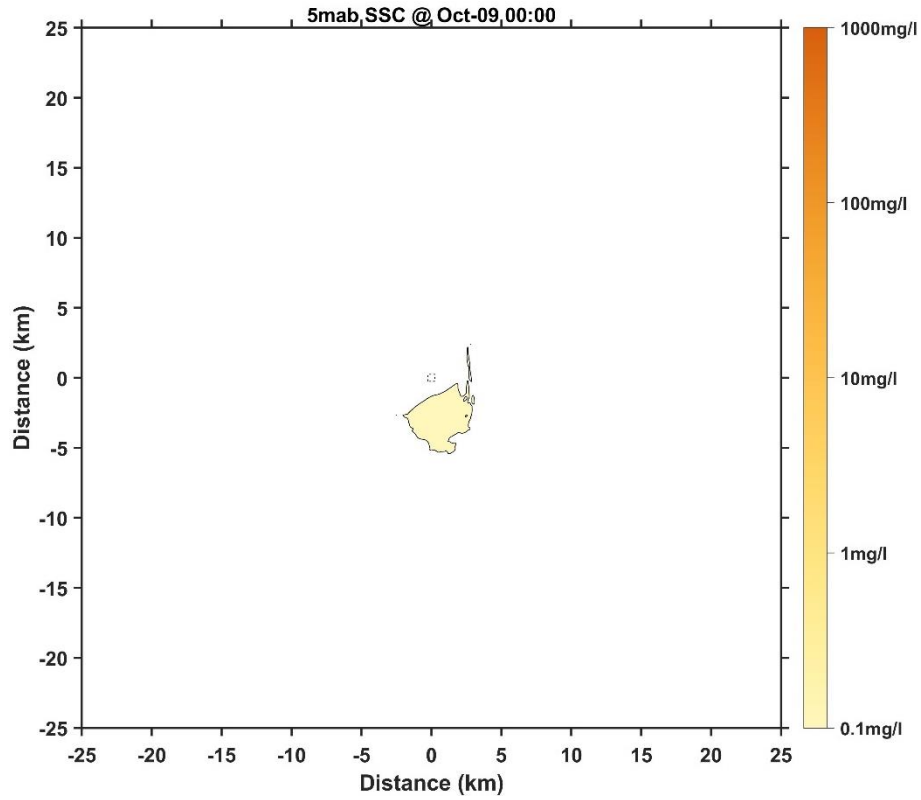
Figure 102 Horizontal distribution of SSC at 5 mab for Case 9 (13 days later)
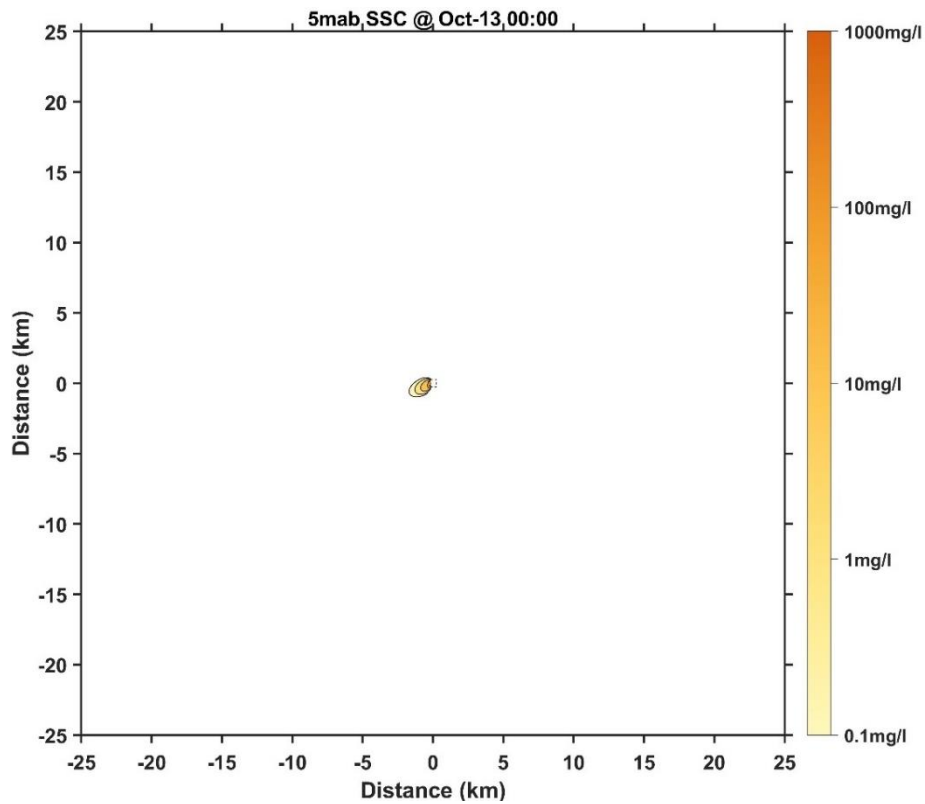
Figure 103 Horizontal distribution of SSC at 5 mab for Case 10 (1 day later)
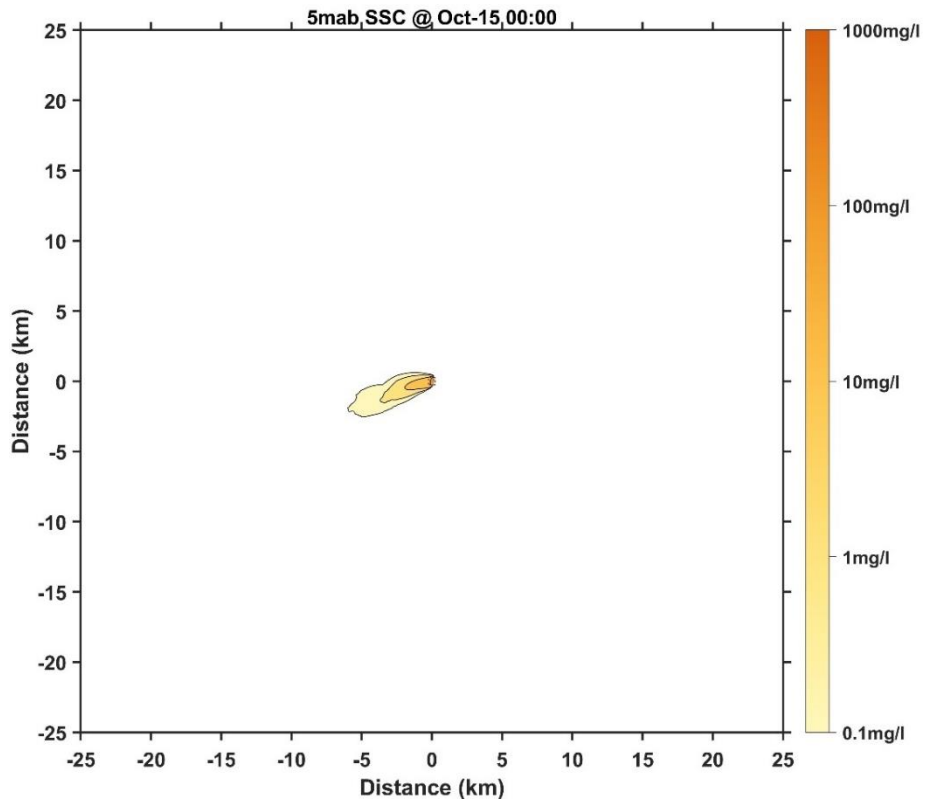
Figure 104 Horizontal distribution of SSC at 5 mab for Case 10 (3 days later)
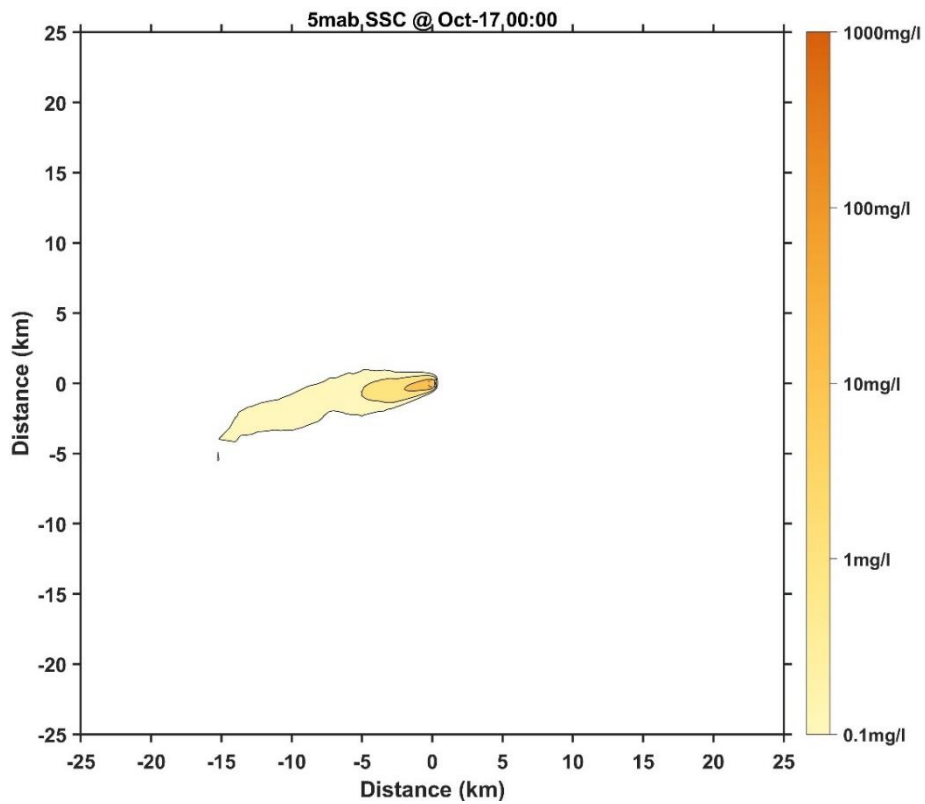
Figure 105 Horizontal distribution of SSC at 5 mab for Case 10 (5 days later)
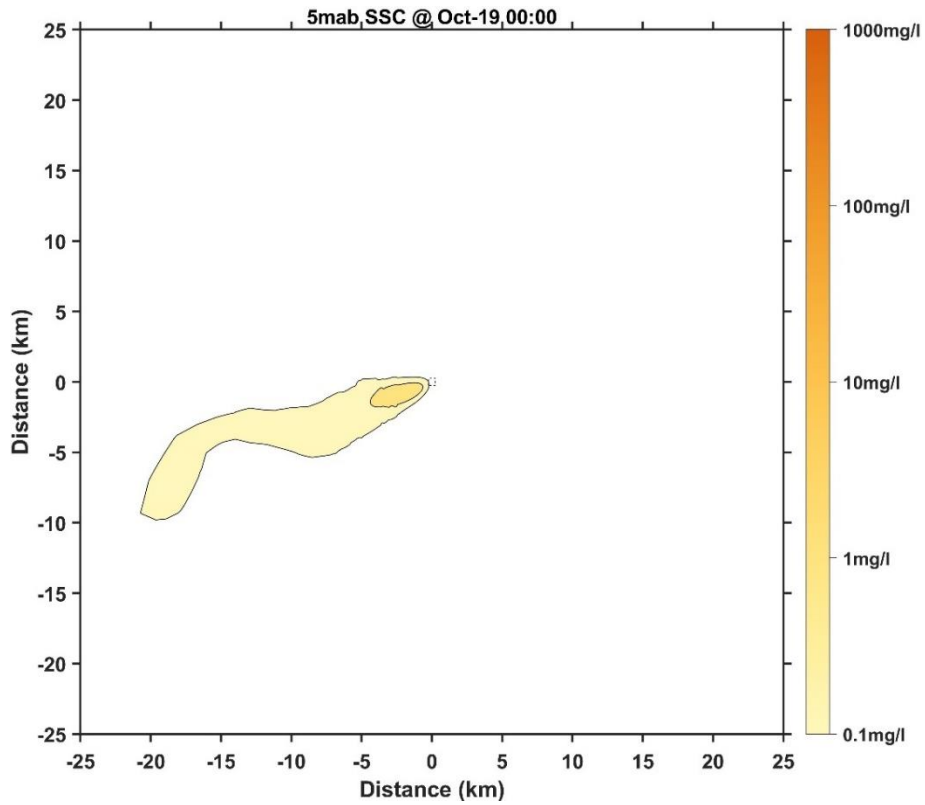
Figure 106 Horizontal distribution of SSC at 5 mab for Case 10 (7 days later)
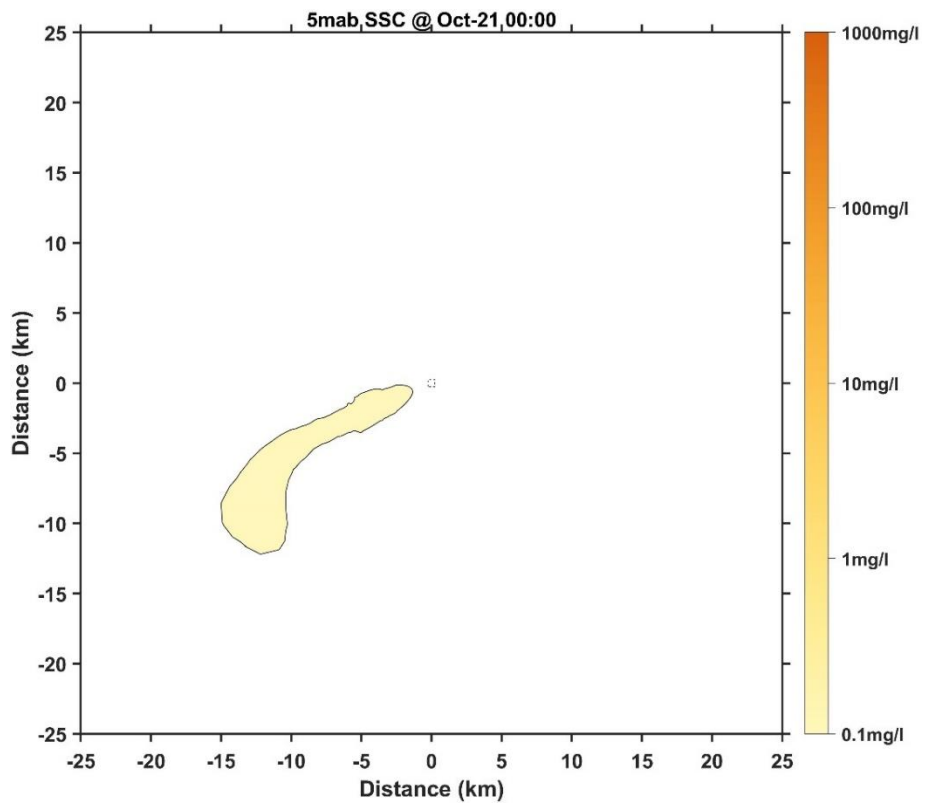
Figure 107 Horizontal distribution of SSC at 5 mab for Case 10 (9 days later)
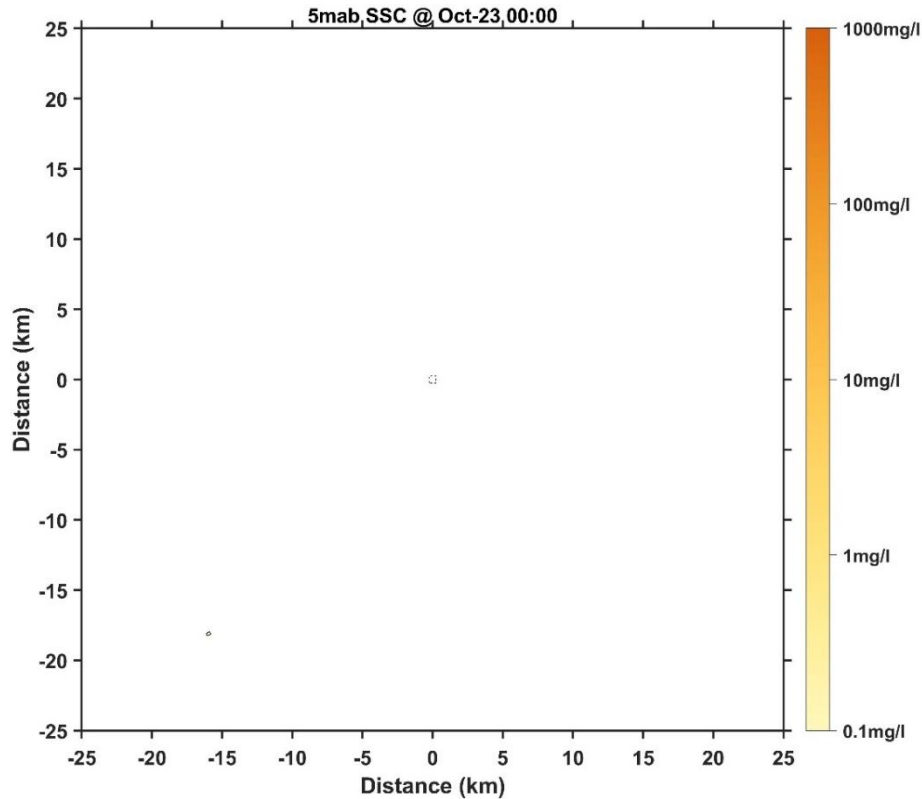
Figure 108 Horizontal distribution of SSC at 5 mab for Case 10 (11 days later)

1.3 Dispersion Characteristics of Near-bottom Suspended Sediment at 25 mab

The horizontal distribution of suspended sediment concentration in the near-bottom layer 25 m from the bottom (Figure 109 to Figure 160) shows that the concentration of suspended sediment in the near-bottom layer 25 m from the bottom is less than that in the near-bottom layer 1 m from the bottom, and the concentration of suspended sediment in the near-bottom layer 25 m from the bottom is less than that in the near-bottom layer 1 m from the bottom, and the plume diffusion distance is slightly greater than 1 m from the bottom. On average, the maximum plume spread distance (from the center of the CTA) at 25 m from the bottom was 5.03 km for Case 5 and 2.97 km for Case 3; the maximum plume spread area was 8.07 km^2 for Case 5 and 3.36 km^2 for Case 3. In extreme cases, the maximum distance of the plume from the bottom (from the center of the CTA) is 27.90 km for Case 8 and 14.80 km for Case 9; the maximum area of dispersion is 69.75 km^2 for Case 10 and 37.44 km^2 for Case 6.
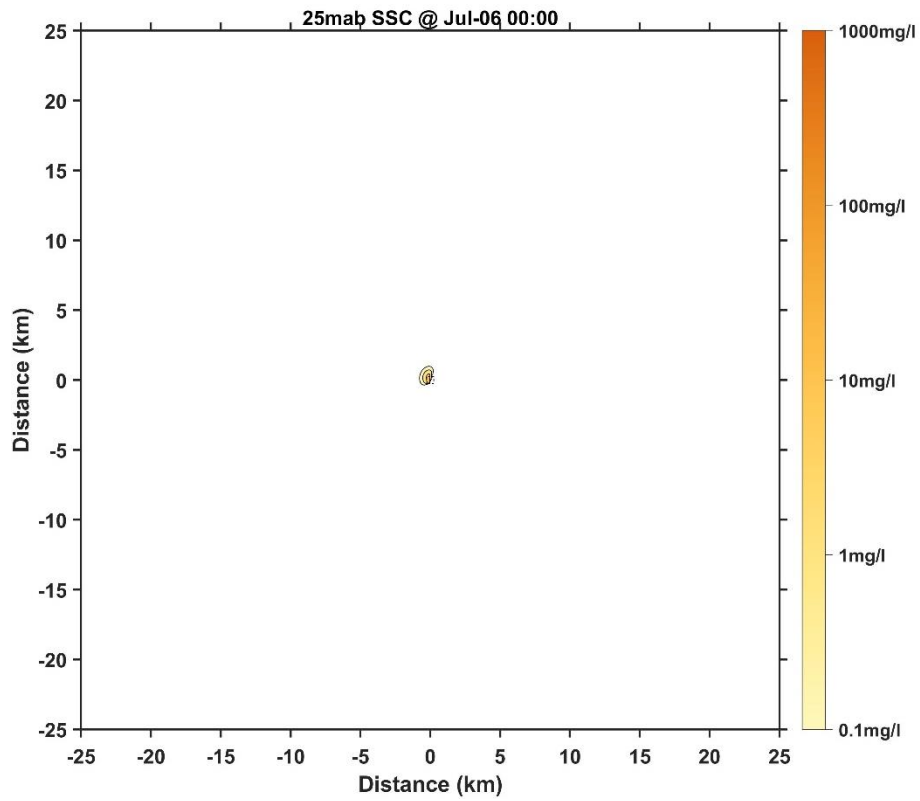
Figure 109 Horizontal distribution of SSC at 25 mab for Case 1 (1 day later)
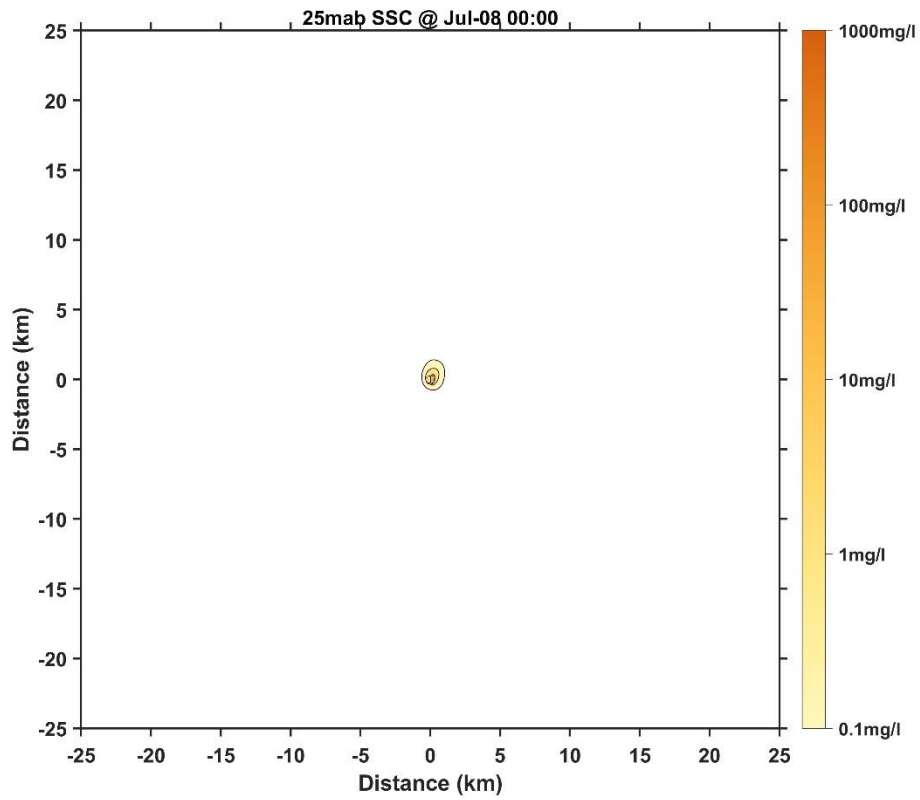
Figure 110 Horizontal distribution of SSC at 25 mab for Case 1 (3 days later)
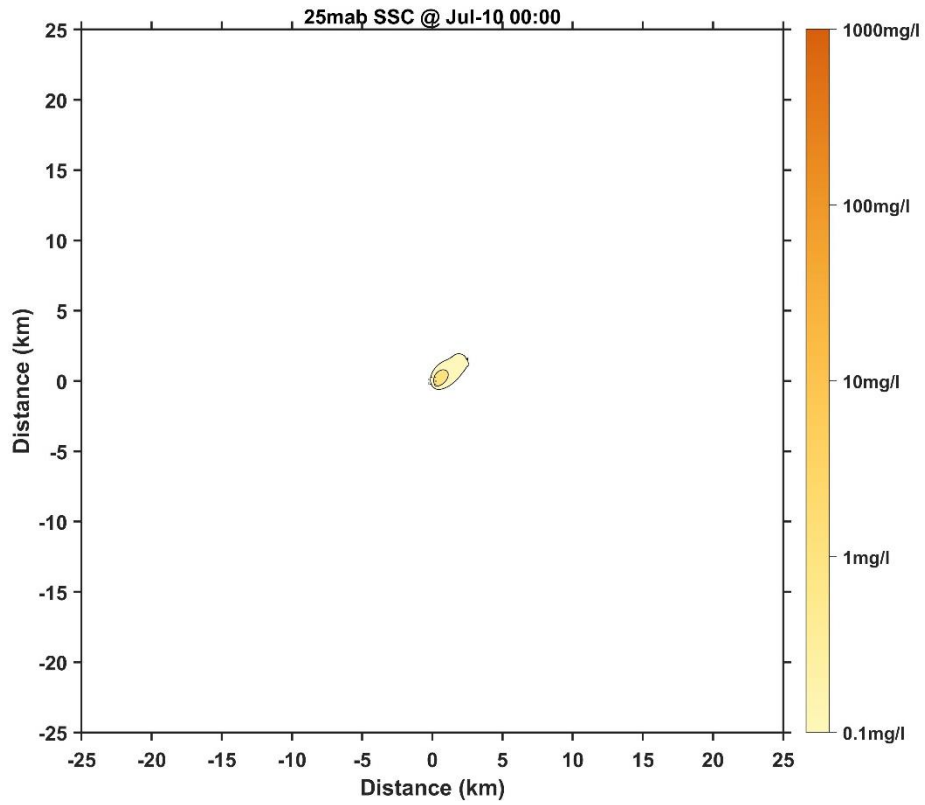
Figure 111 Horizontal distribution of SSC at 25 mab for Case 1 (5 days later)
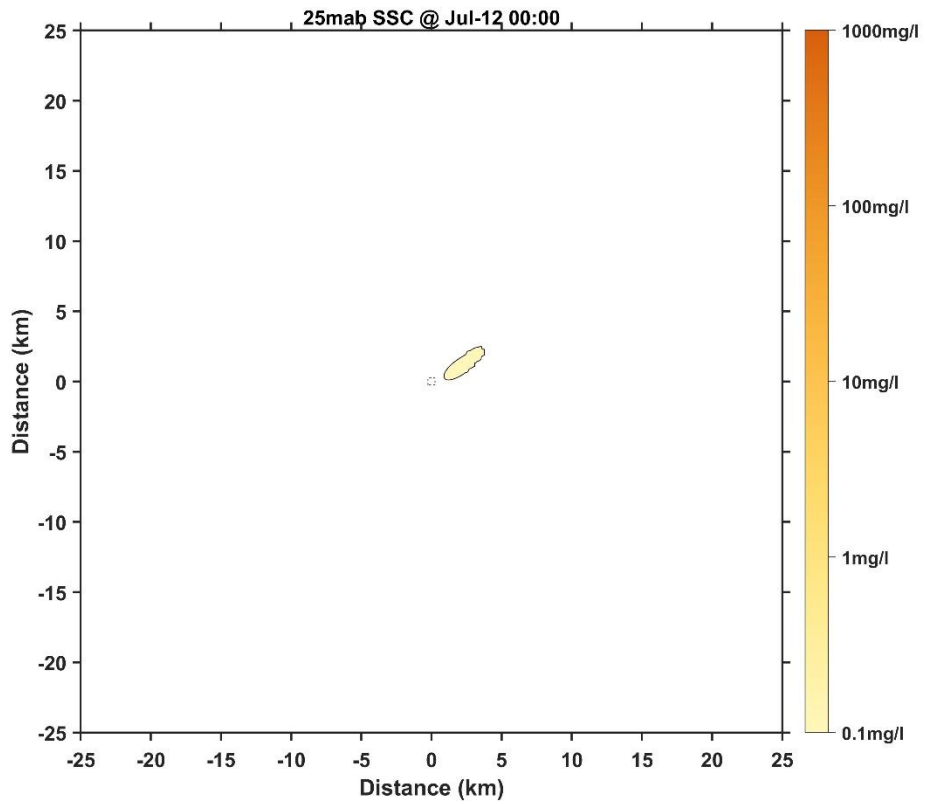
Figure 112 Horizontal distribution of SSC at 25 mab for Case 1 (7 days later)
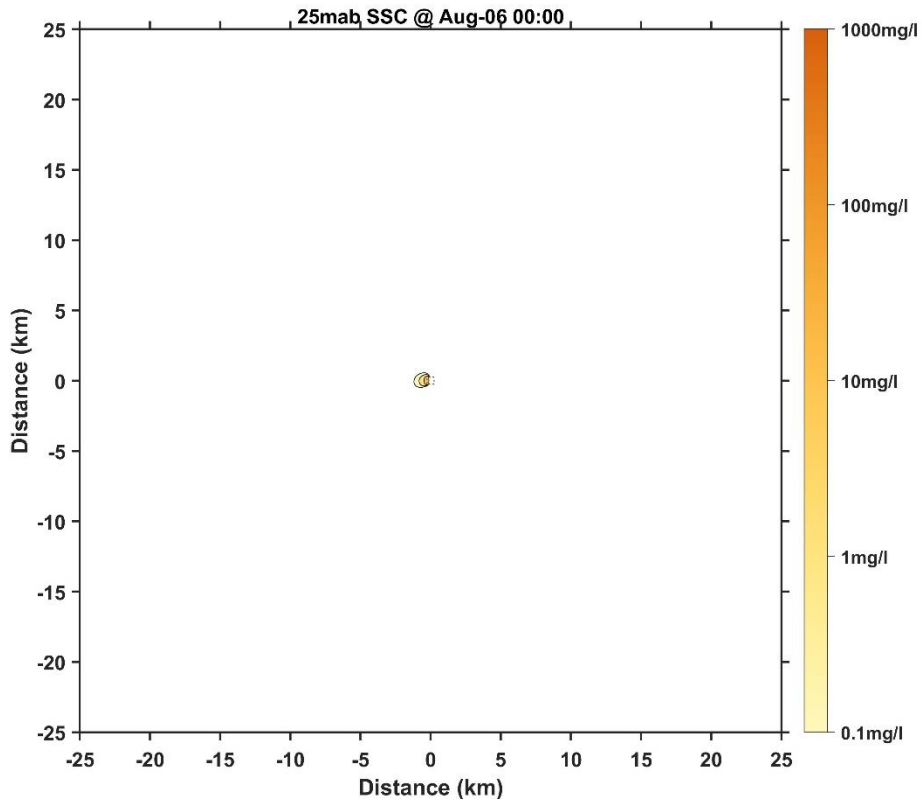
Figure 113 Horizontal distribution of SSC at 25 mab for Case 2 (1 day later)
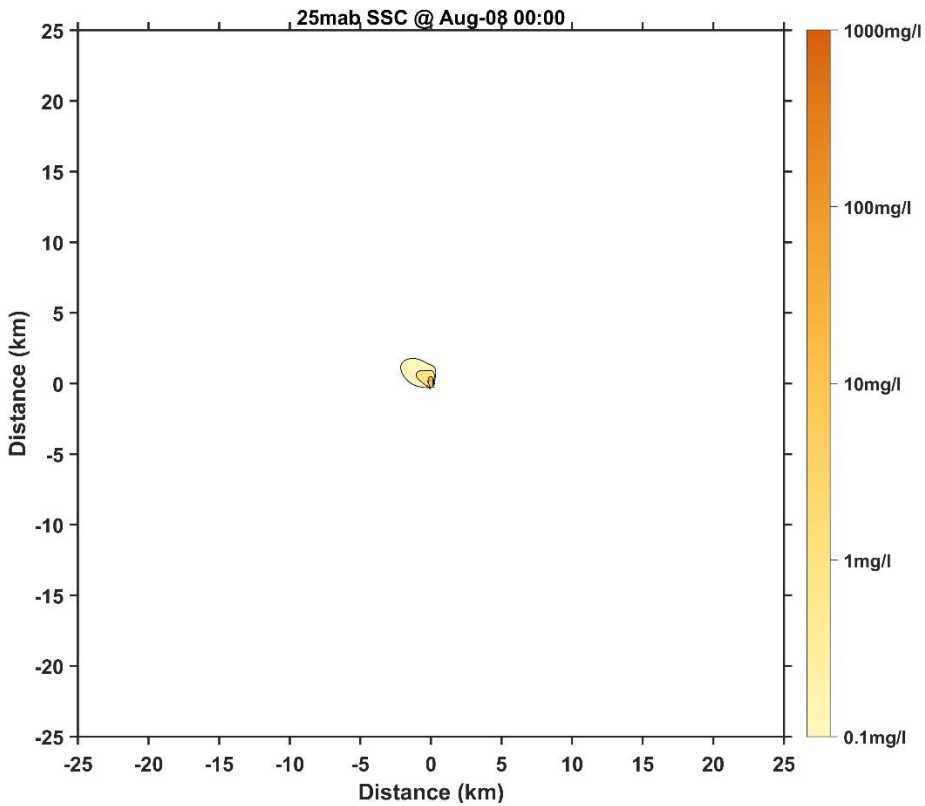
Figure 114 Horizontal distribution of SSC at 25 mab for Case 2 (3 days later)
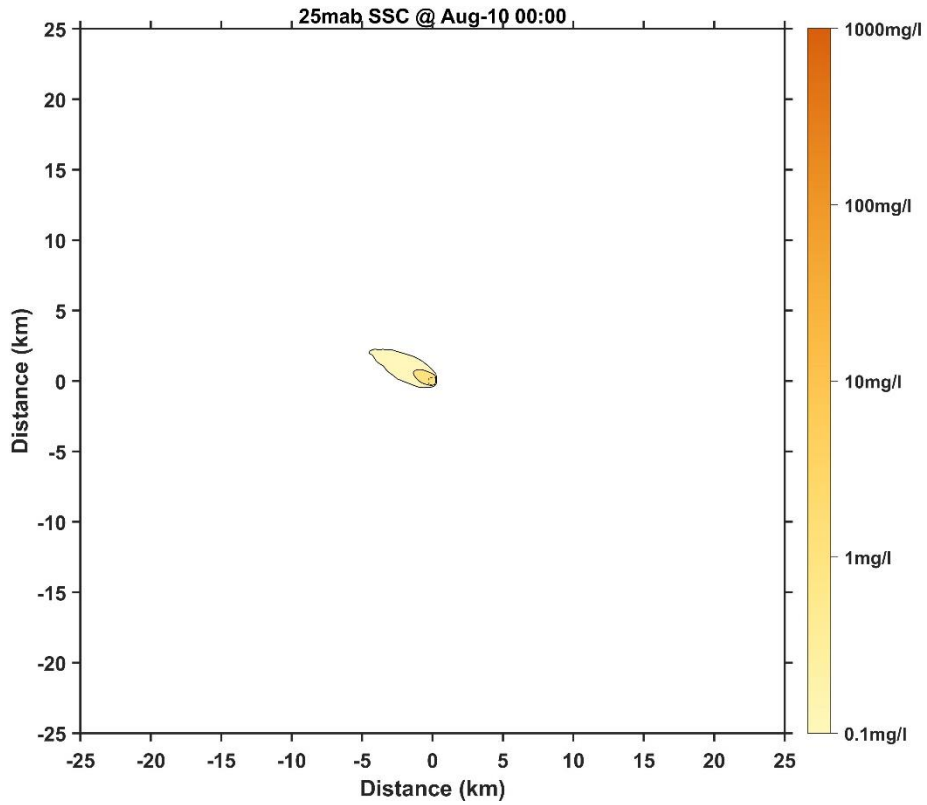
Figure 115 Horizontal distribution of SSC at 25 mab for Case 2 (5 days later)
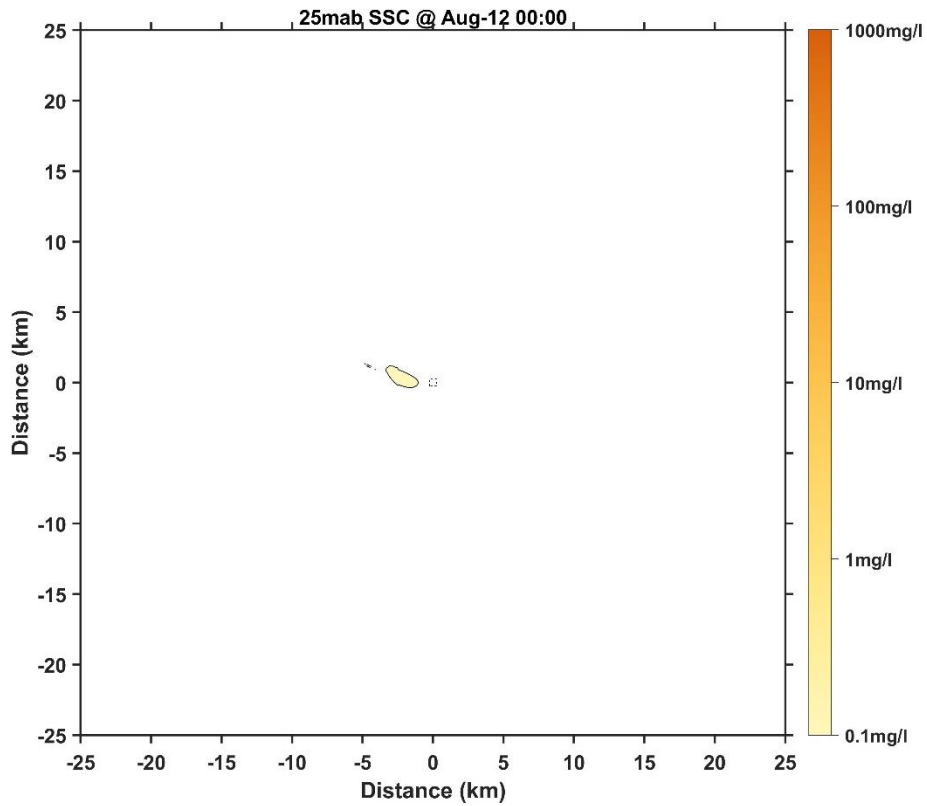
Figure 116 Horizontal distribution of SSC at 25 mab for Case 2 (7 days later)
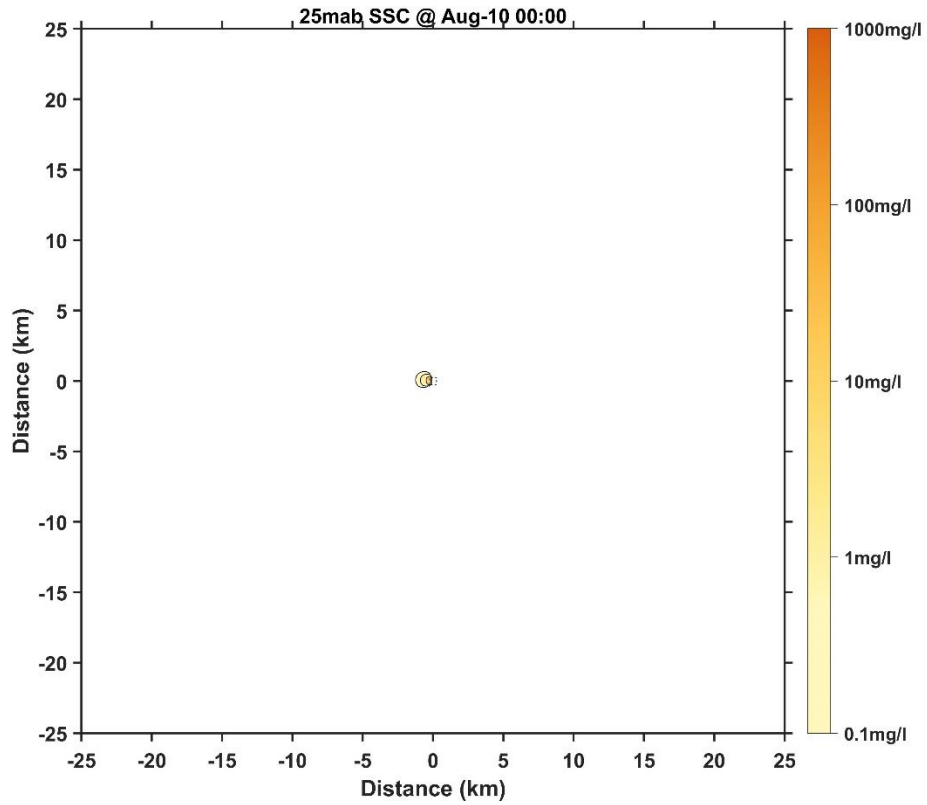
Figure 117 Horizontal distribution of SSC at 25 mab for Case 3 (1 day later)
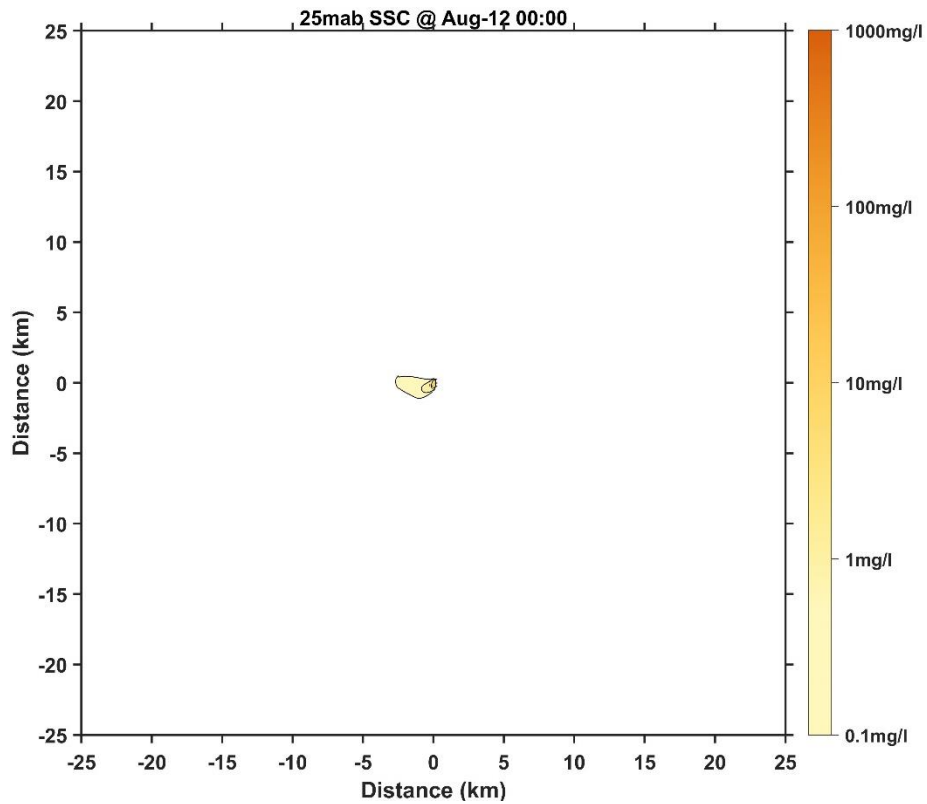
Figure 118 Horizontal distribution of SSC at 25 mab for Case 3 (3 days later)
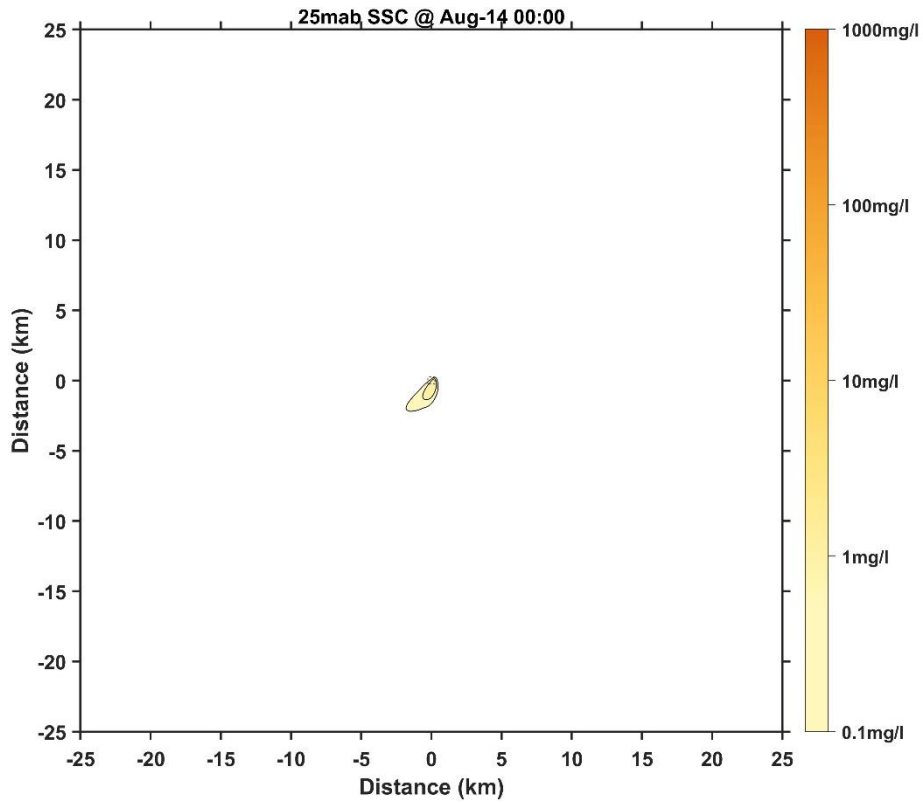
Figure 119 Horizontal distribution of SSC at 25 mab for Case 3 (5 days later)
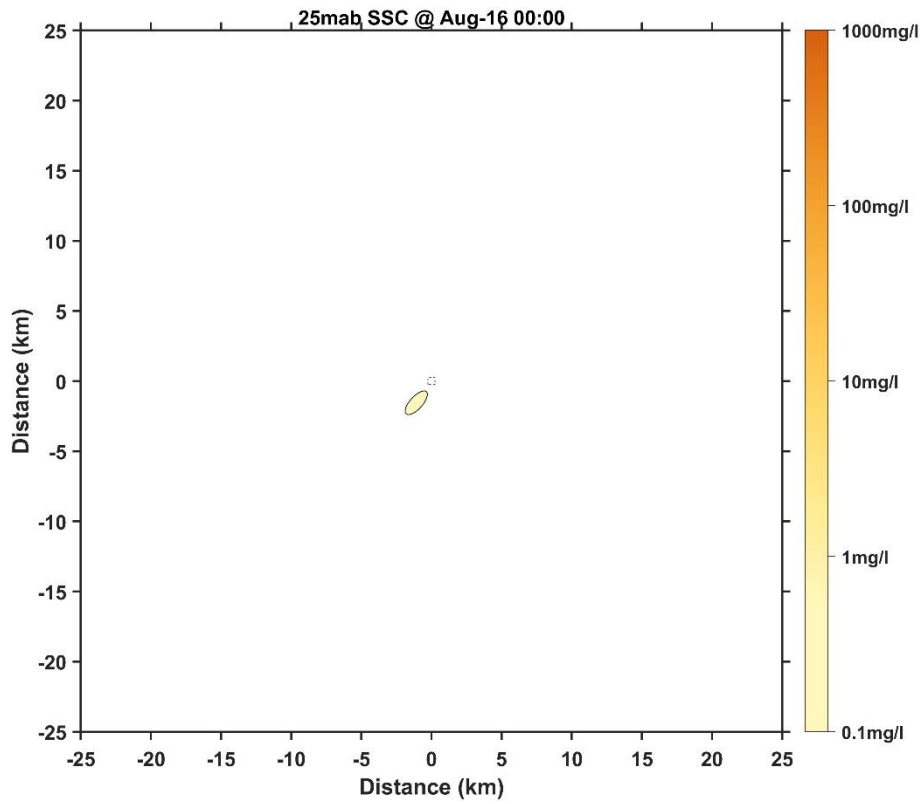
Figure 120 Horizontal distribution of SSC at 25 mab for Case 3 (7 days later)
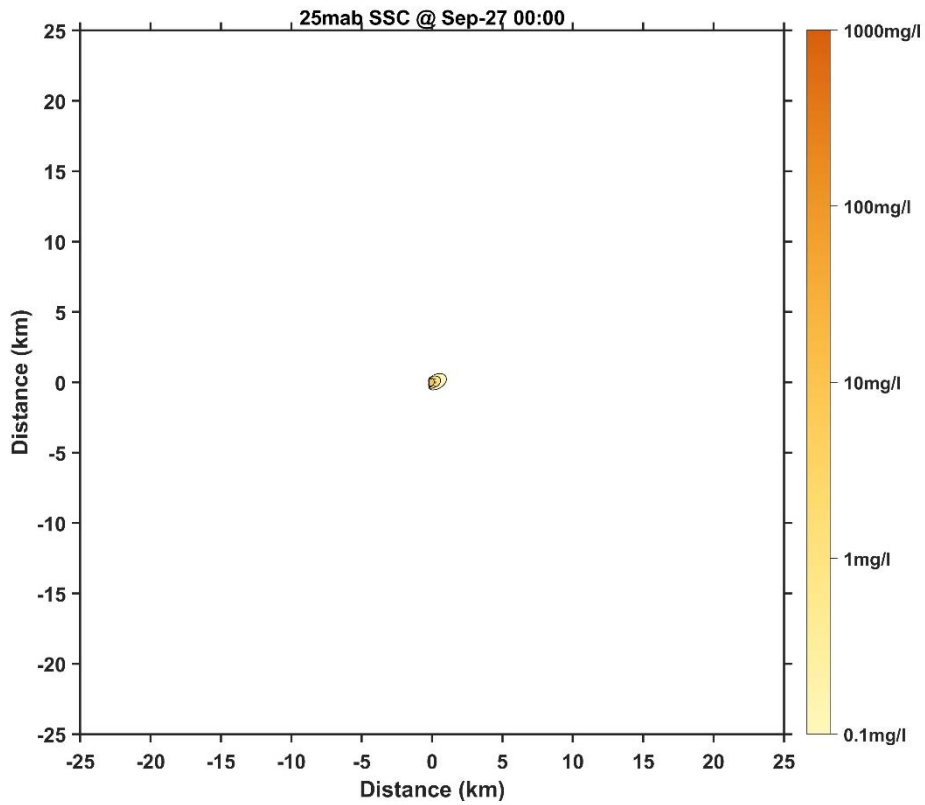
Figure 121 Horizontal distribution of SSC at 25 mab for Case 4 (1 day later)
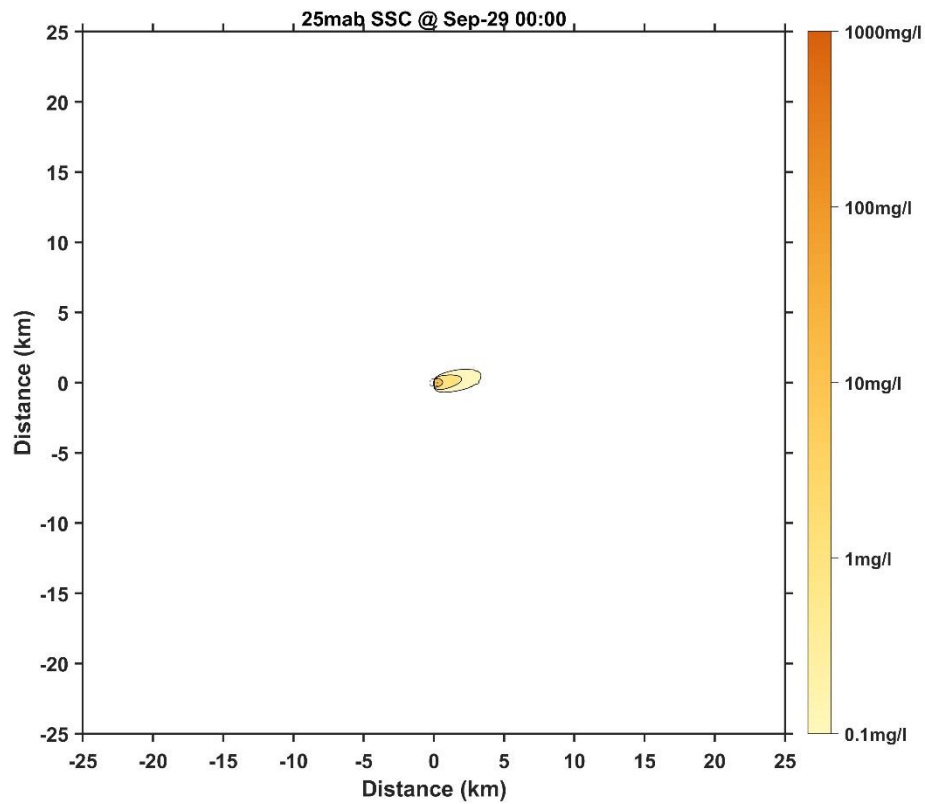
Figure 122 Horizontal distribution of SSC at 25 mab for Case 4 (3 days later)
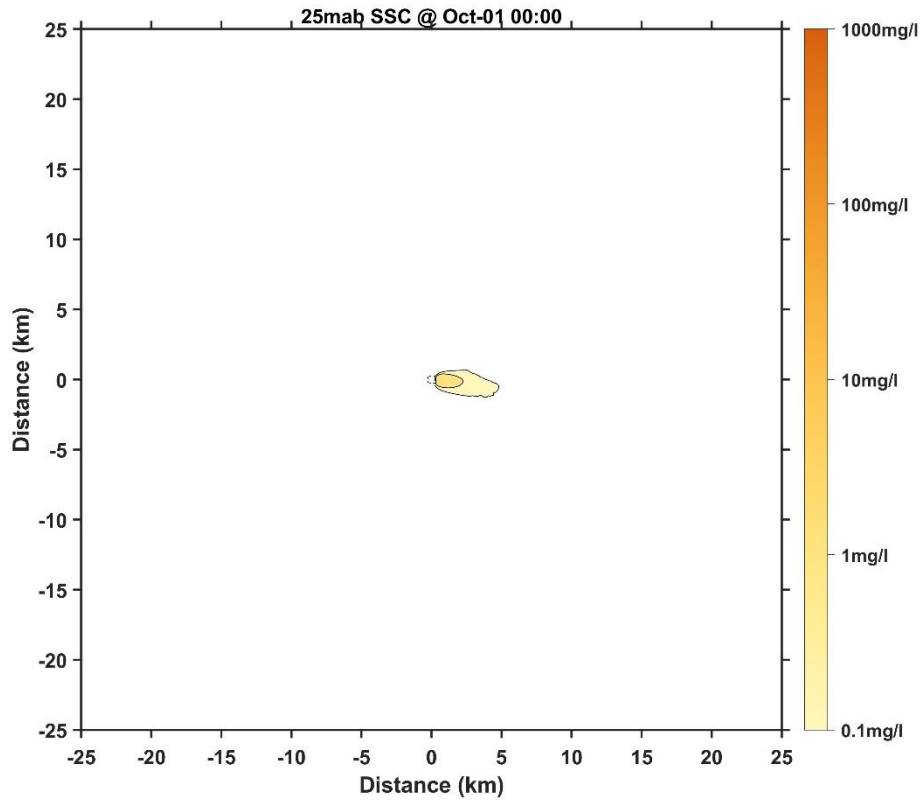
Figure 123 Horizontal distribution of SSC at 25 mab for Case 4 (5 days later)
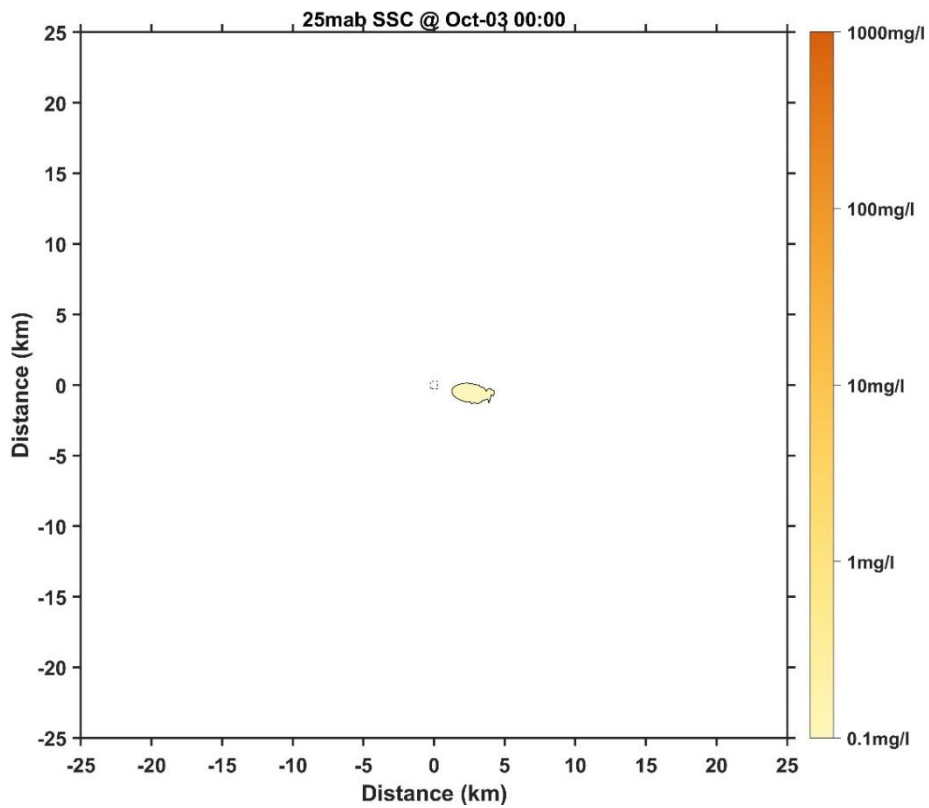
Figure 124 Horizontal distribution of SSC at 25 mab for Case 4 (7 days later)
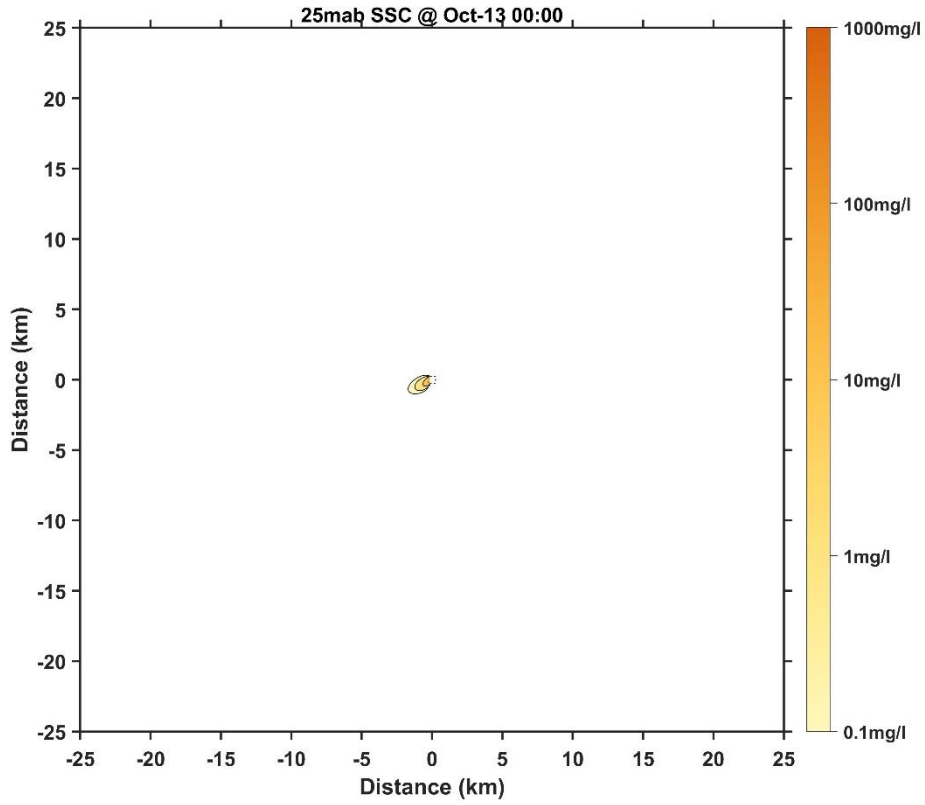
Figure 125 Horizontal distribution of SSC at 25 mab for Case 5 (1 day later)
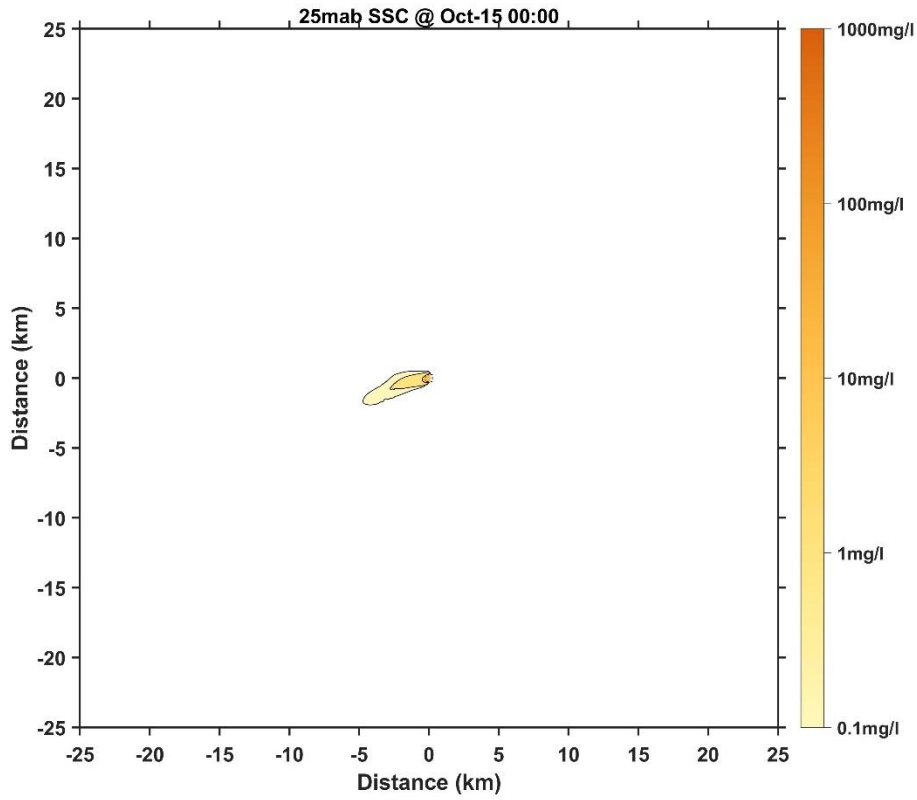
Figure 126 Horizontal distribution of SSC at 25 mab for Case 5 (3 days later)
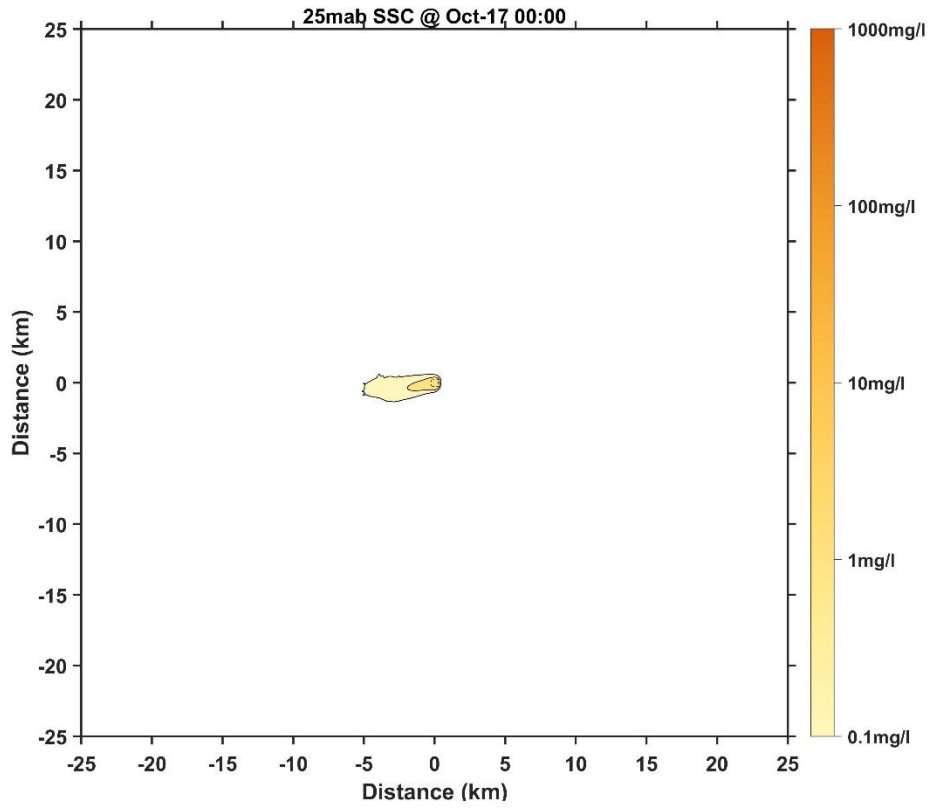
Figure 127 Horizontal distribution of SSC at 25 mab for Case 5 (5 days later)
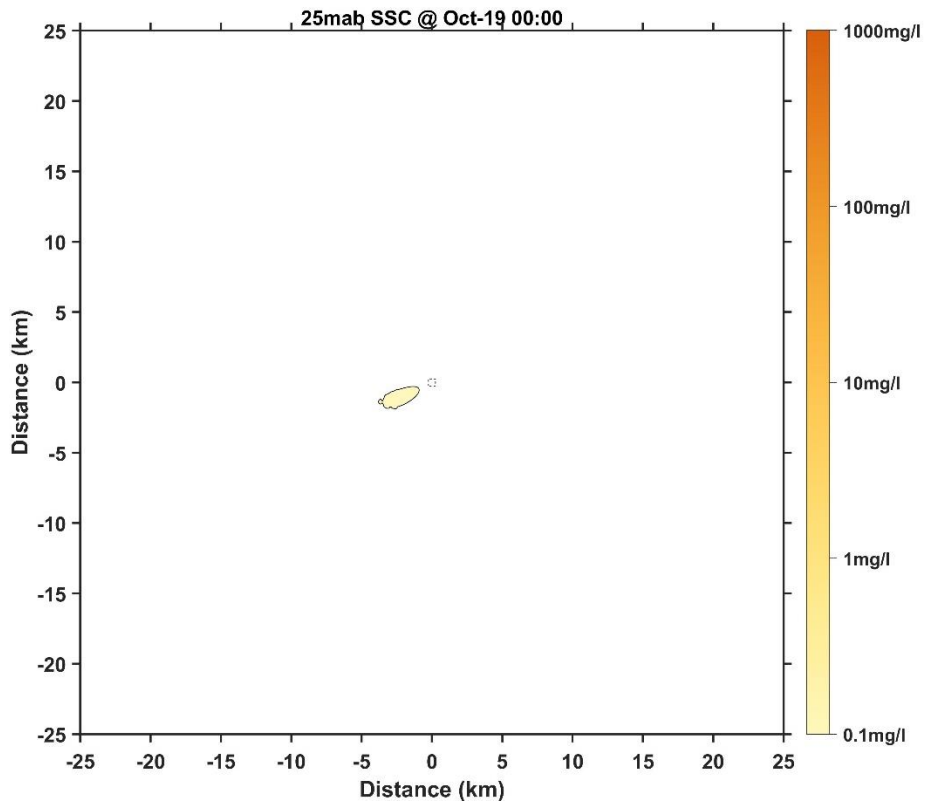
Figure 128 Horizontal distribution of SSC at 25 mab for Case 5 (7 days later)
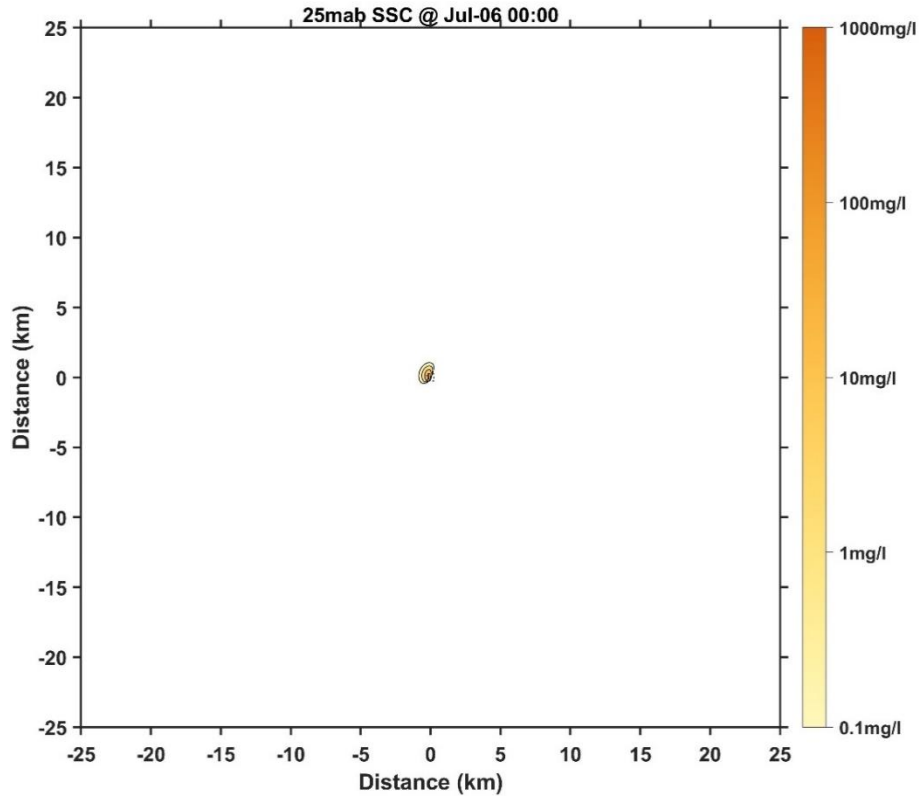
Figure 129 Horizontal distribution of SSC at 25 mab for Case 6 (1 day later)
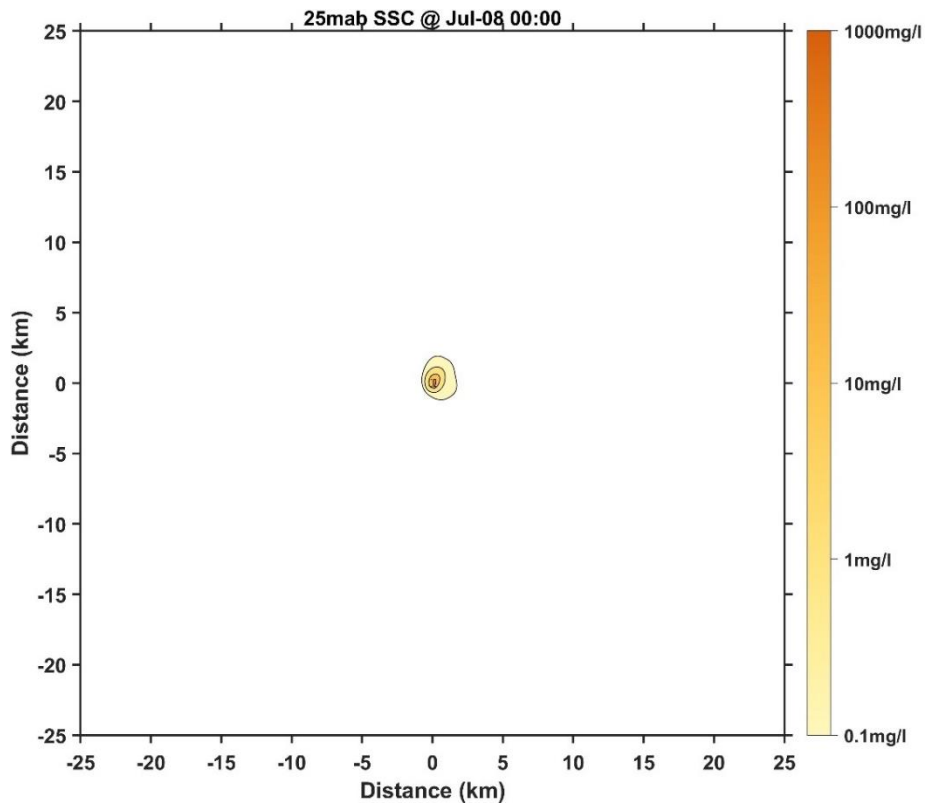
Figure 130 Horizontal distribution of SSC at 25 mab for Case 6 (3 days later)
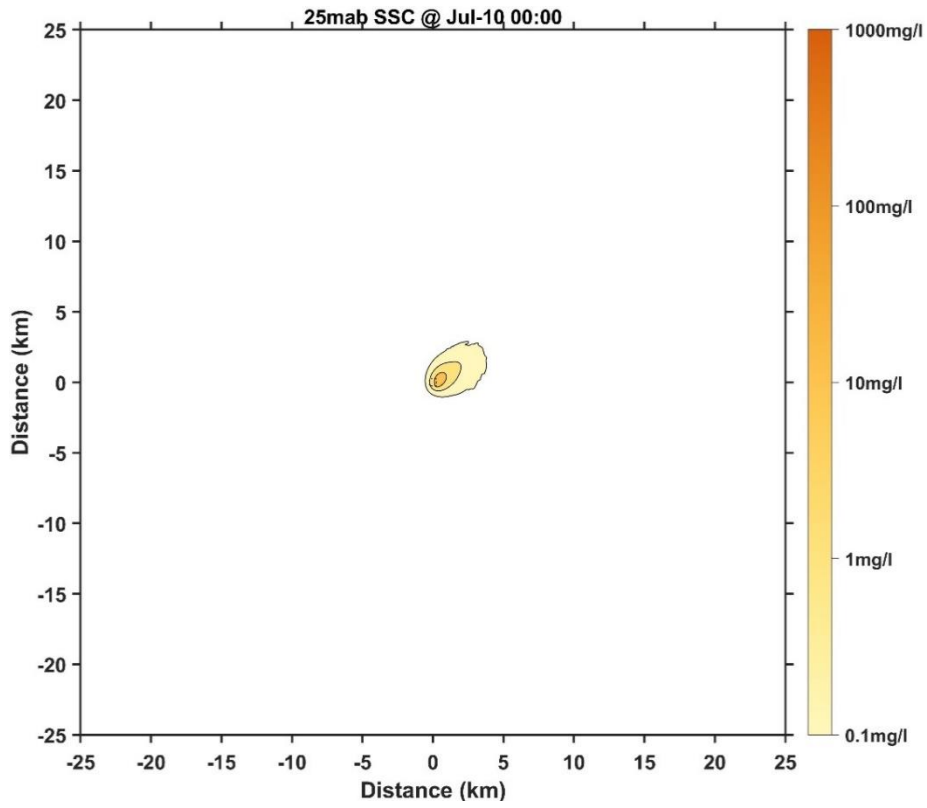
Figure 131 Horizontal distribution of SSC at 25 mab for Case 6 (5 days later)
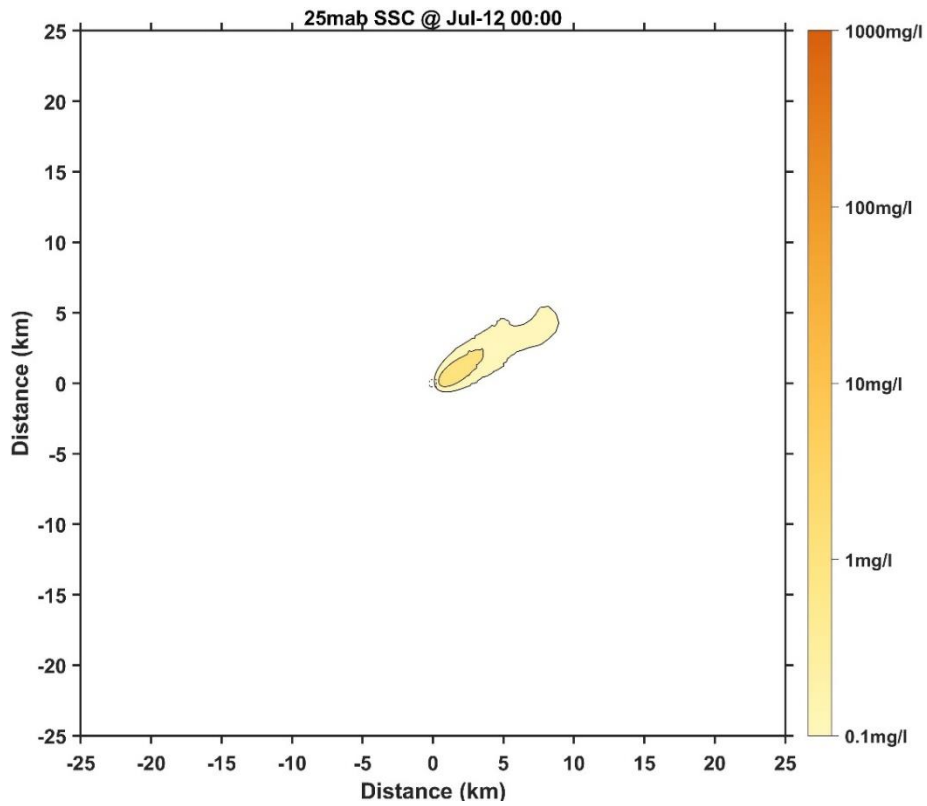
Figure 132 Horizontal distribution of SSC at 25 mab for Case 6 (7 days later)
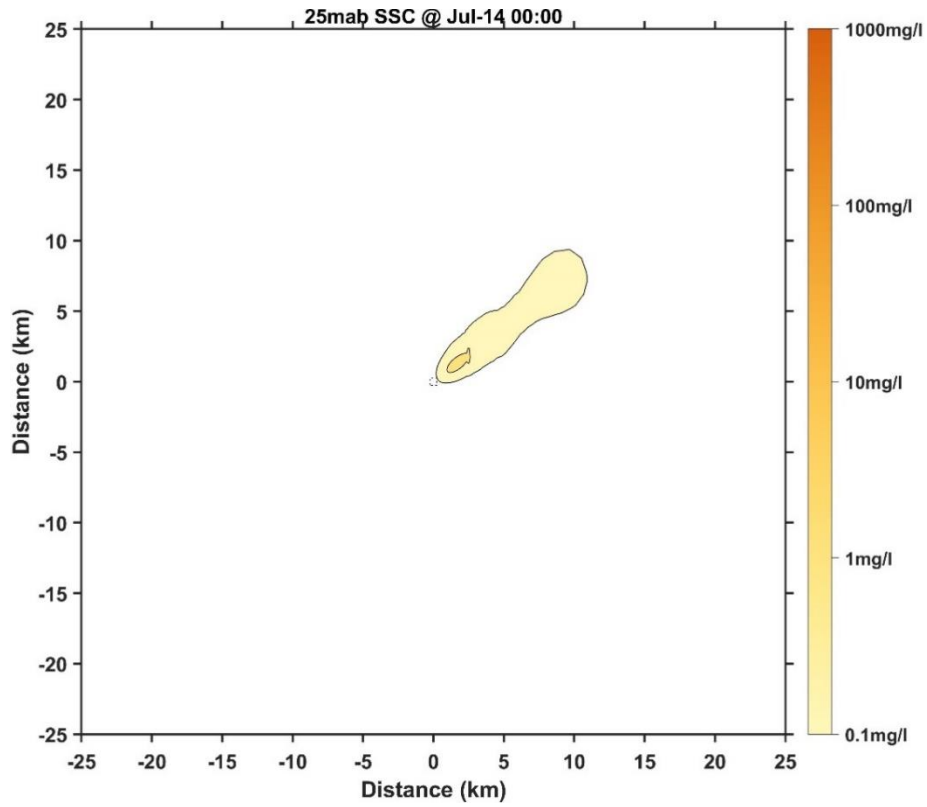
Figure 133 Horizontal distribution of SSC at 25 mab for Case 6 (9 days later)
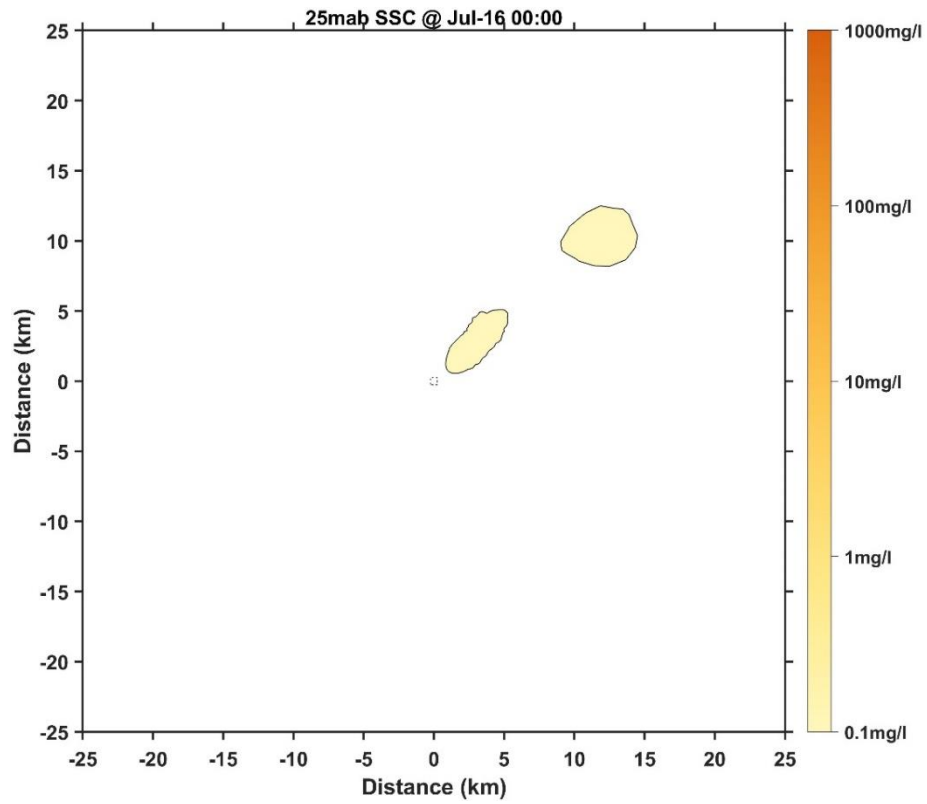
Figure 134 Horizontal distribution of SSC at 25 mab for Case 6 (11 days later)
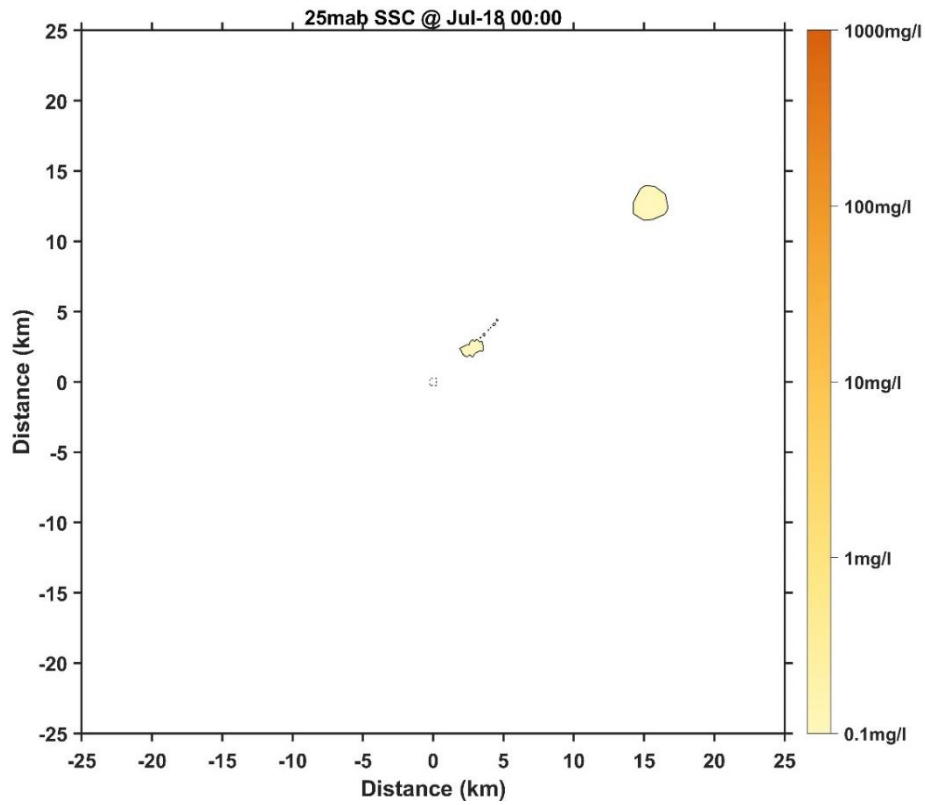
Figure 135 Horizontal distribution of SSC at 25 mab for Case 6 (13 days later)
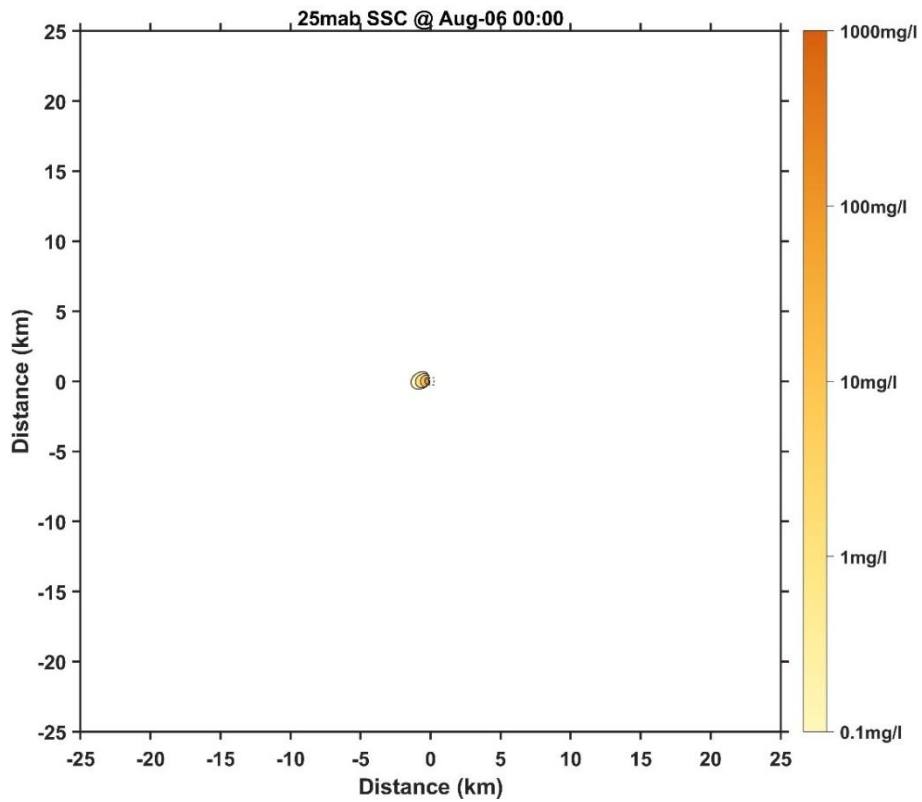
Figure 136 Horizontal distribution of SSC at 25 mab for Case 7 (1 day later)
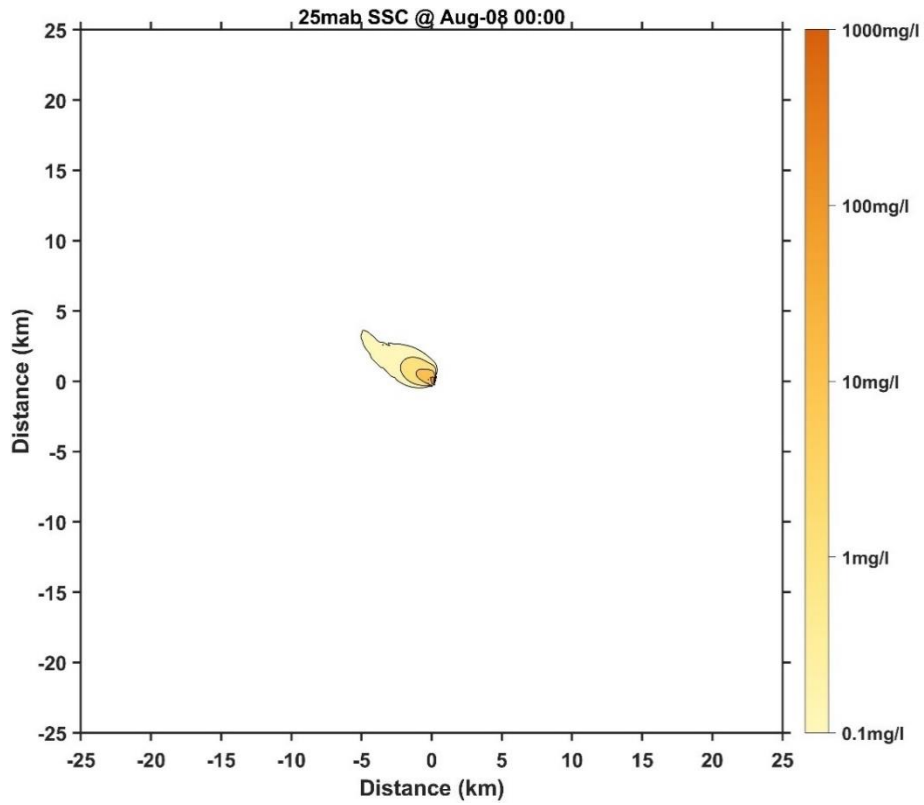
Figure 137 Horizontal distribution of SSC at 25 mab for Case 7 (3 days later)
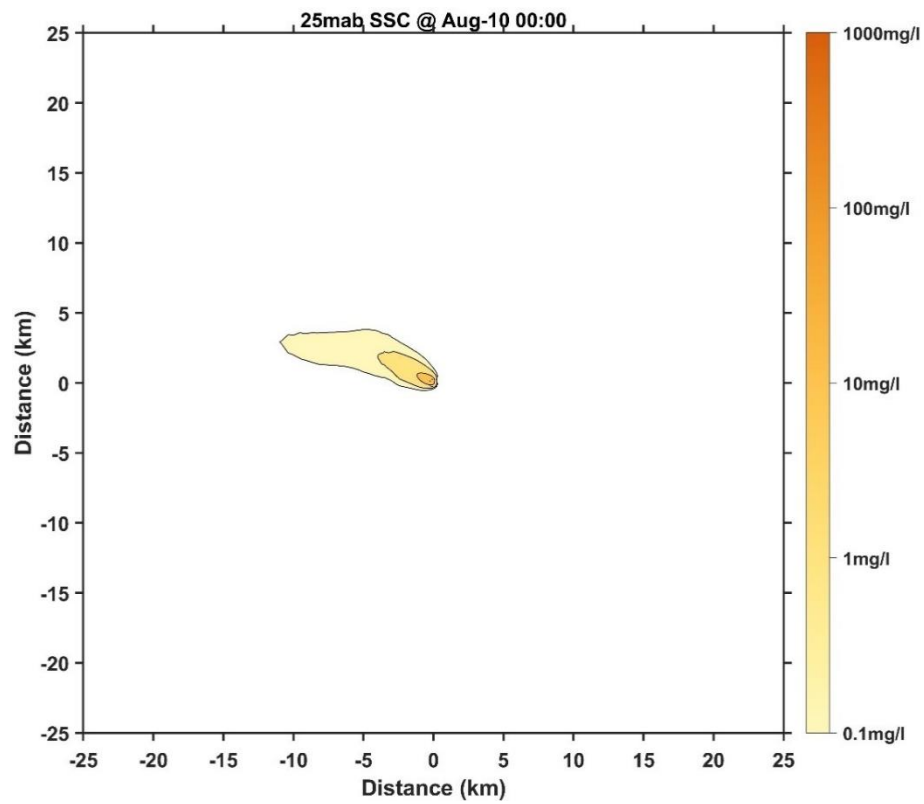
Figure 138 Horizontal distribution of SSC at 25 mab for Case 7 (5 days later)

674
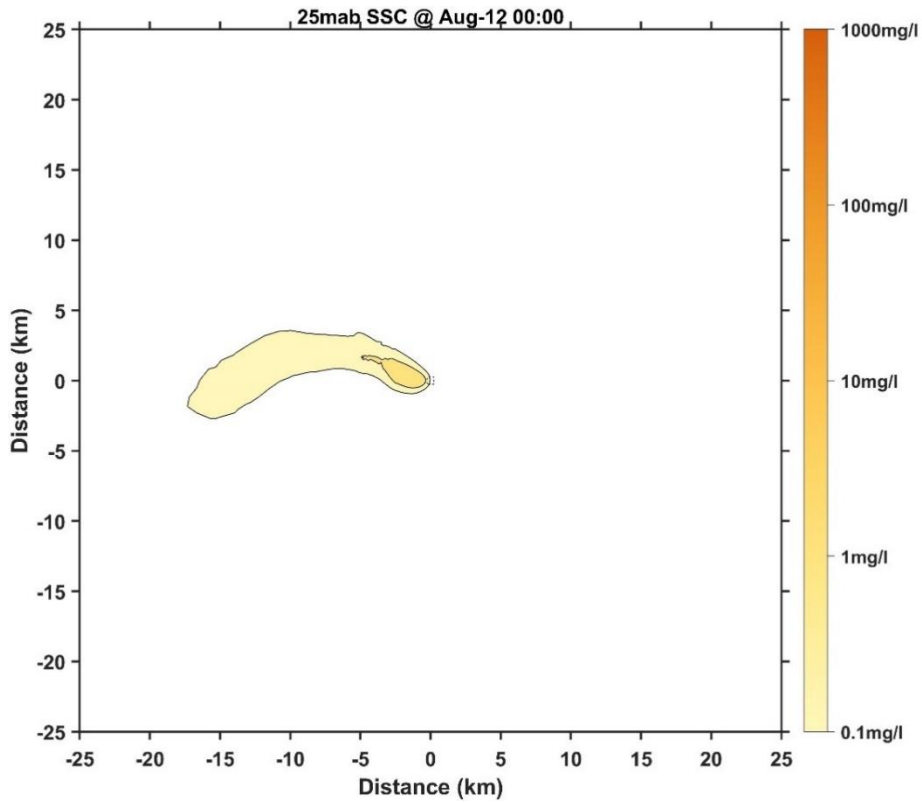
Figure 139 Horizontal distribution of SSC at 25 mab for Case 7 (7 days later)
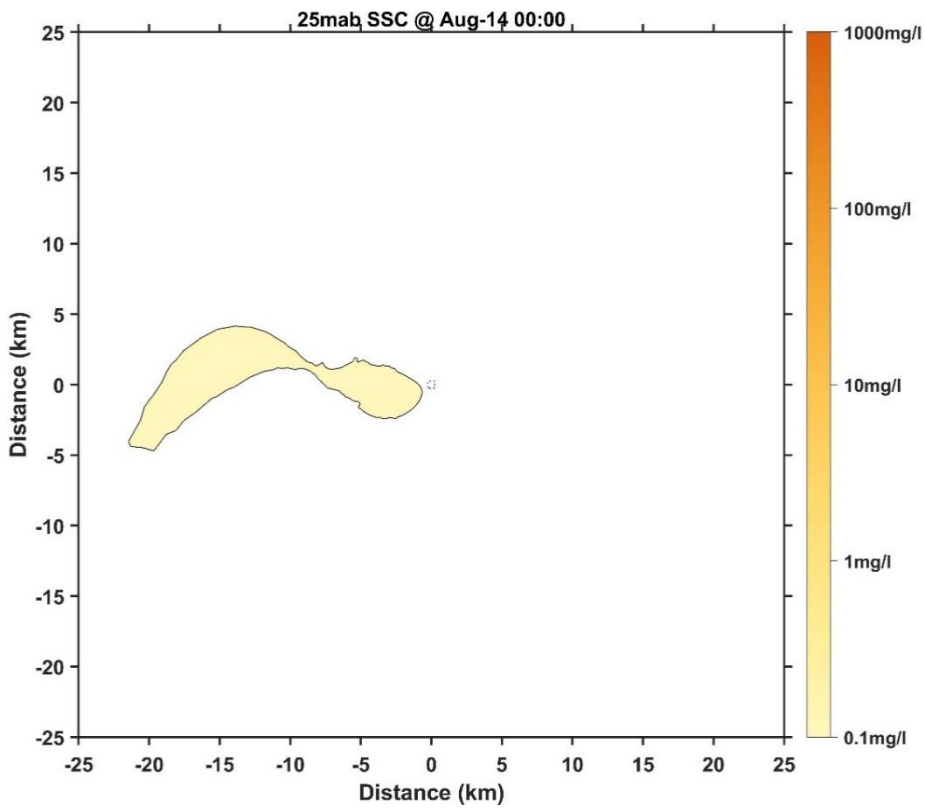
Figure 140 Horizontal distribution of SSC at 25 mab for Case 7 (9 days later)

675
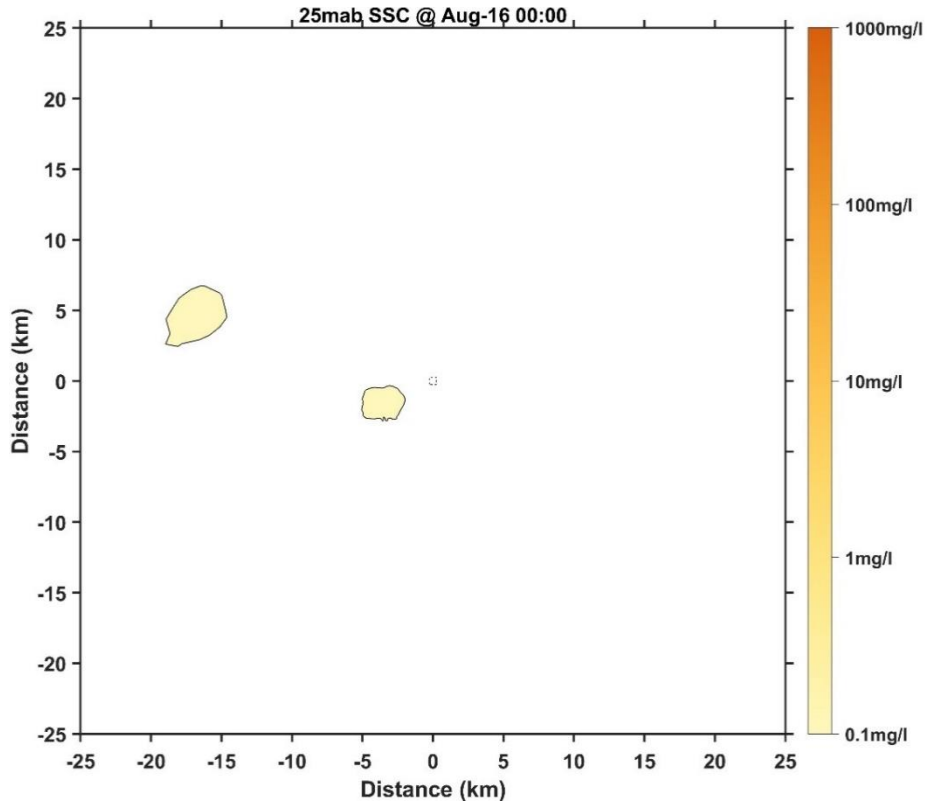
Figure 141 Horizontal distribution of SSC at 25 mab for Case 7 (11 days later)
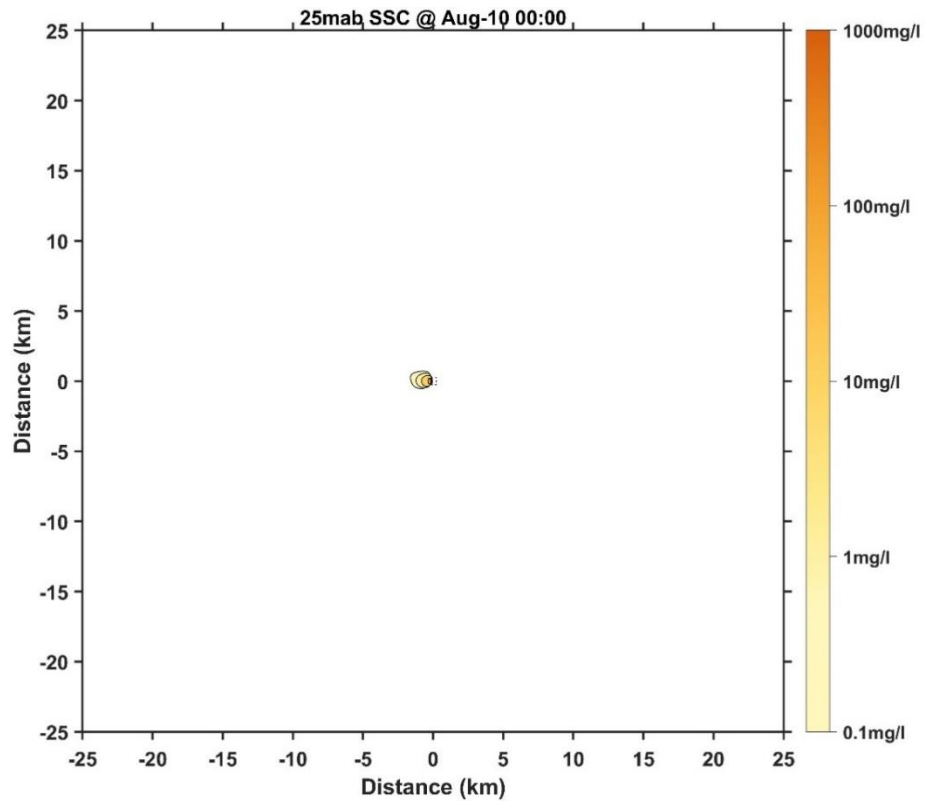
Figure 142 Horizontal distribution of SSC at 25 mab for Case 8 (1 day later)
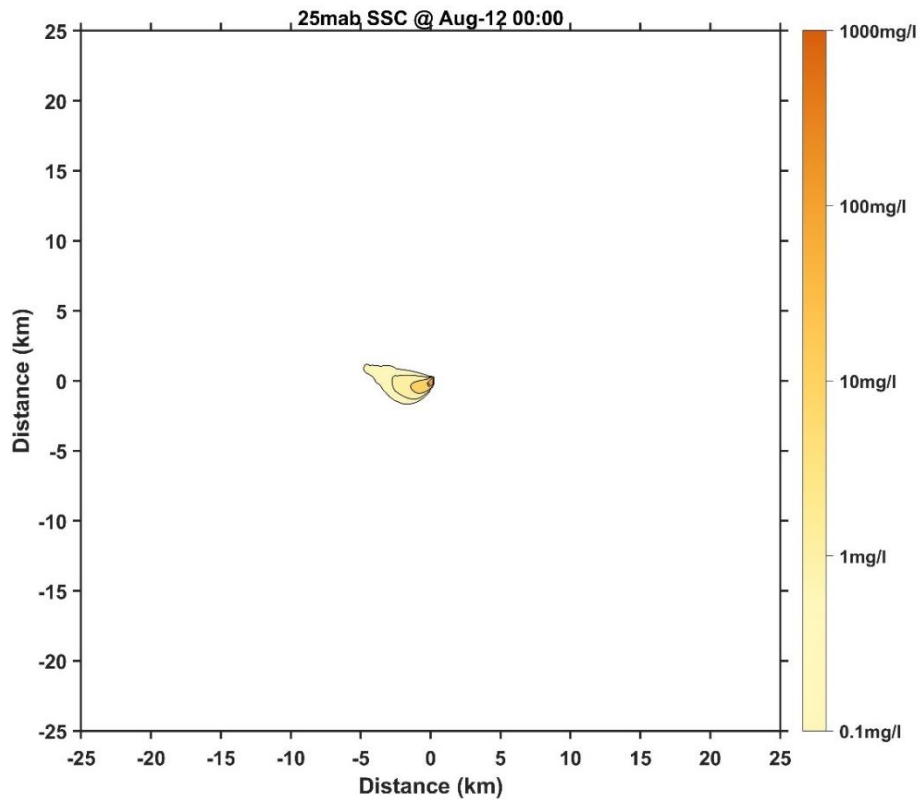
Figure 143 Horizontal distribution of SSC at 25 mab for Case 8 (3 days later)
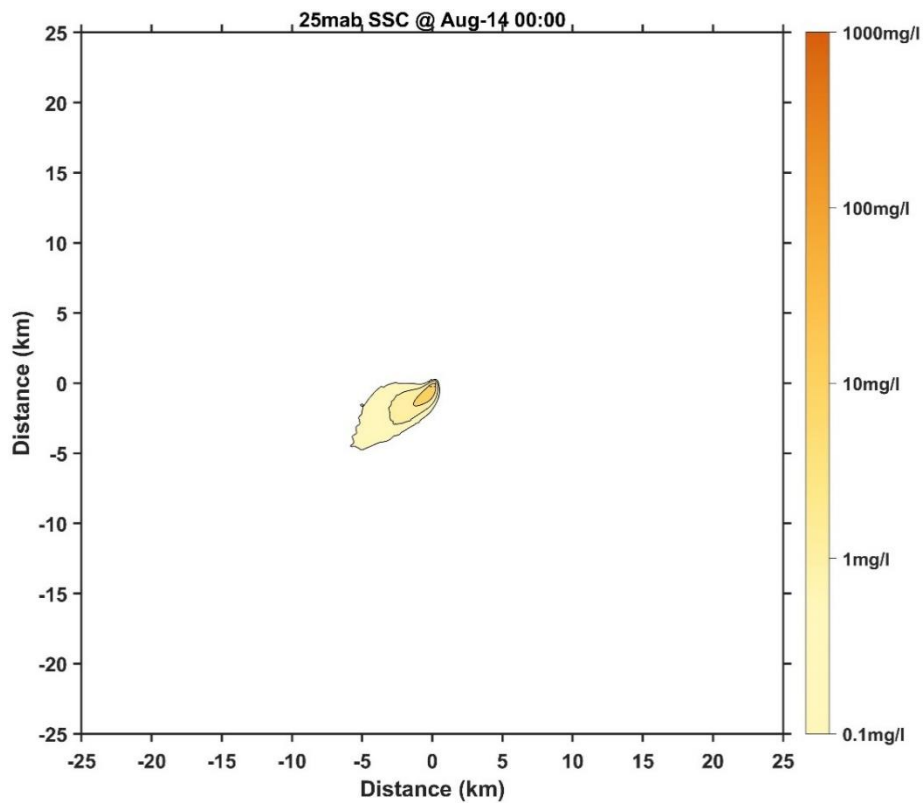
Figure 144 Horizontal distribution of SSC at 25 mab for Case 8 (5 days later)
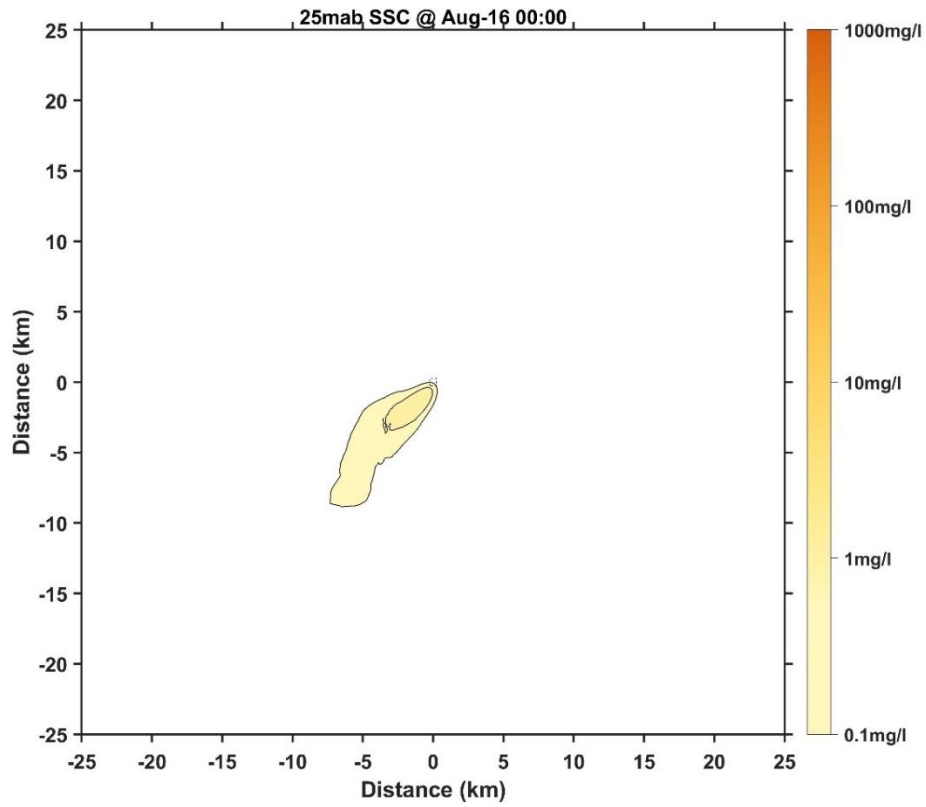
Figure 145 Horizontal distribution of SSC at 25 mab for Case 8 (7 days later)
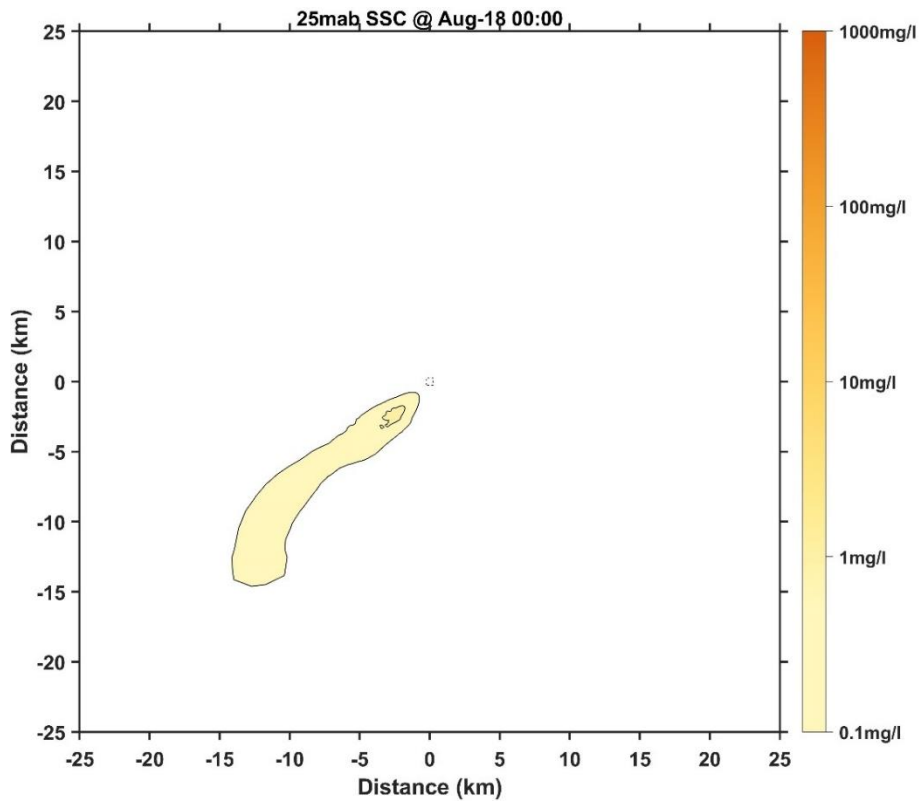
Figure 146 Horizontal distribution of SSC at 25 mab for Case 8 (9 days later)
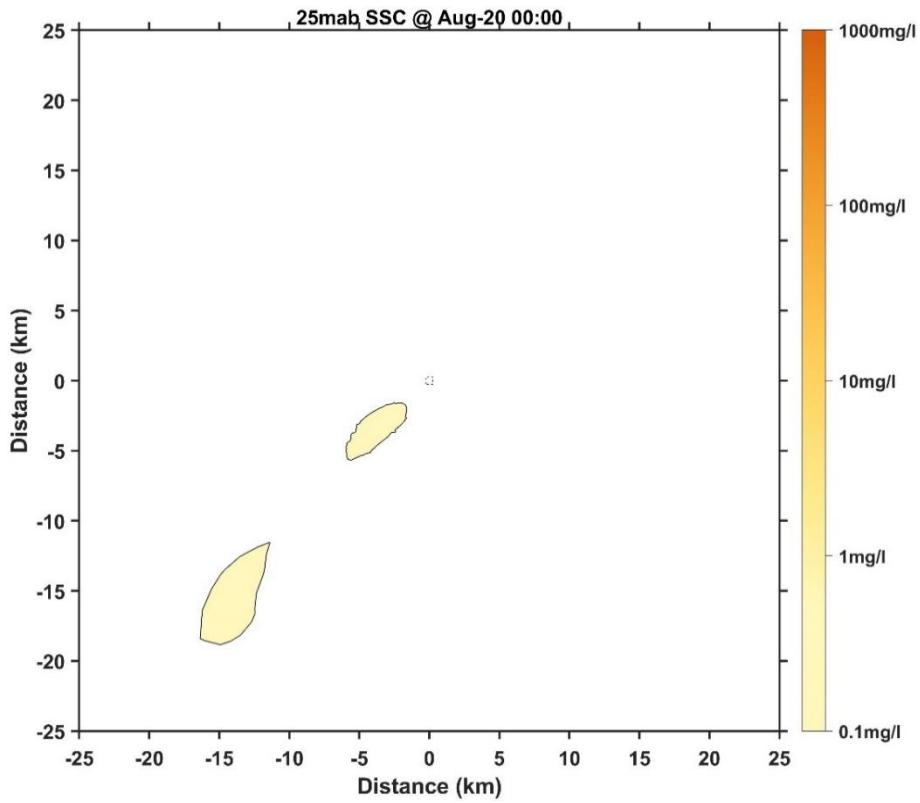
Figure 147 Horizontal distribution of SSC at 25 mab for Case 8 (11 days later)
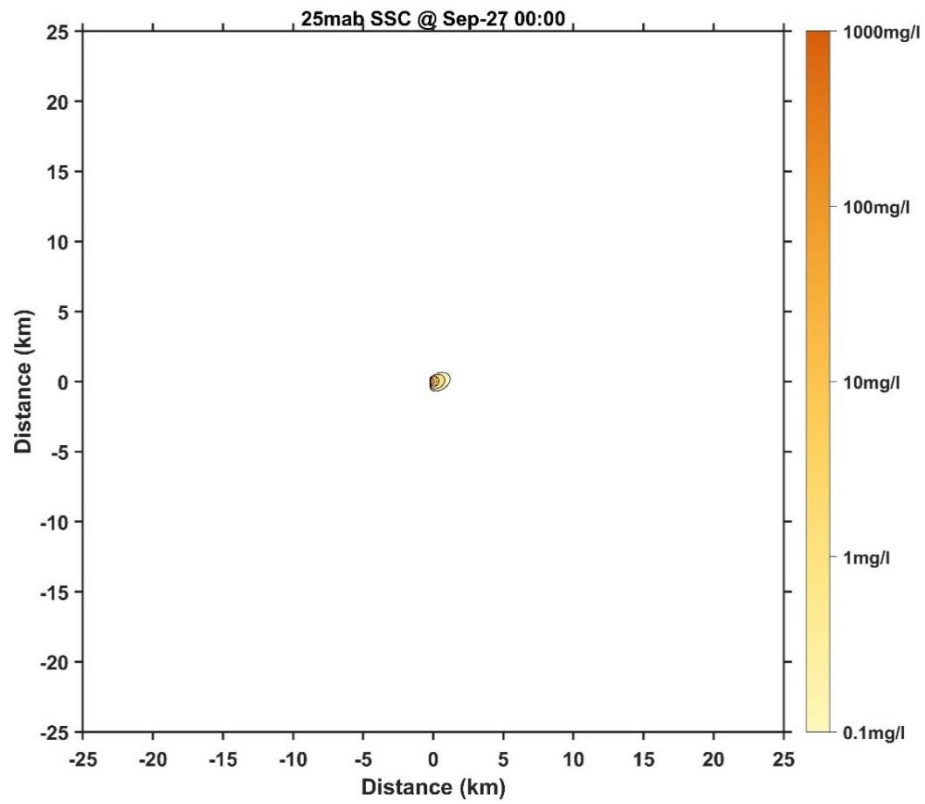
Figure 148 Horizontal distribution of SSC at 25 mab for Case 9 (1 day later)
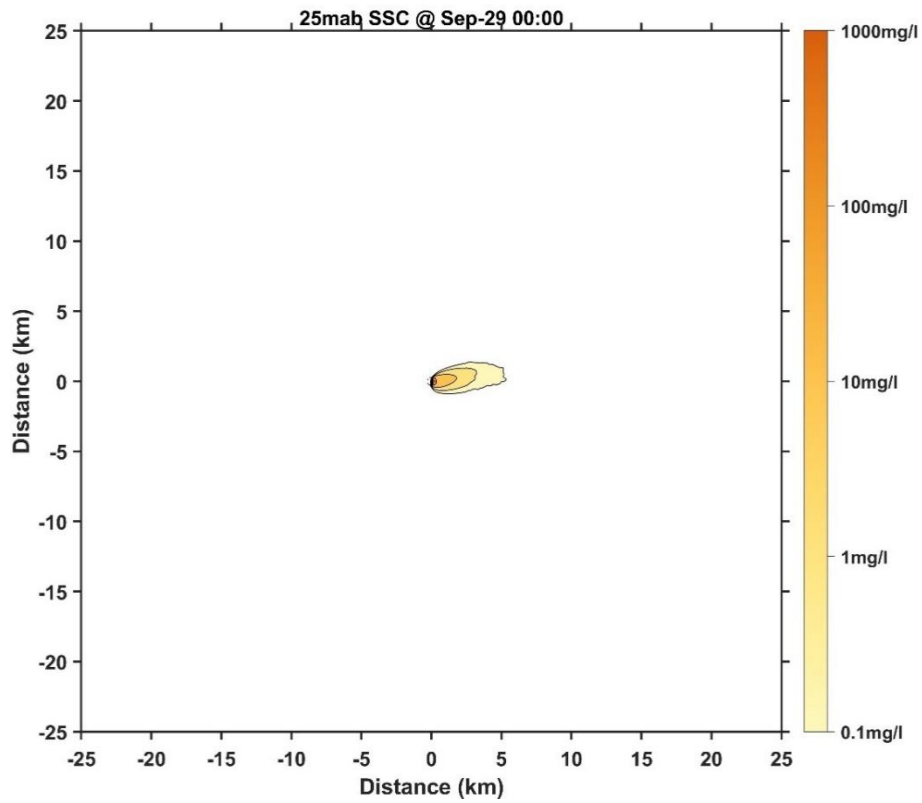
Figure 149 Horizontal distribution of SSC at 25 mab for Case 9 (3 days later)
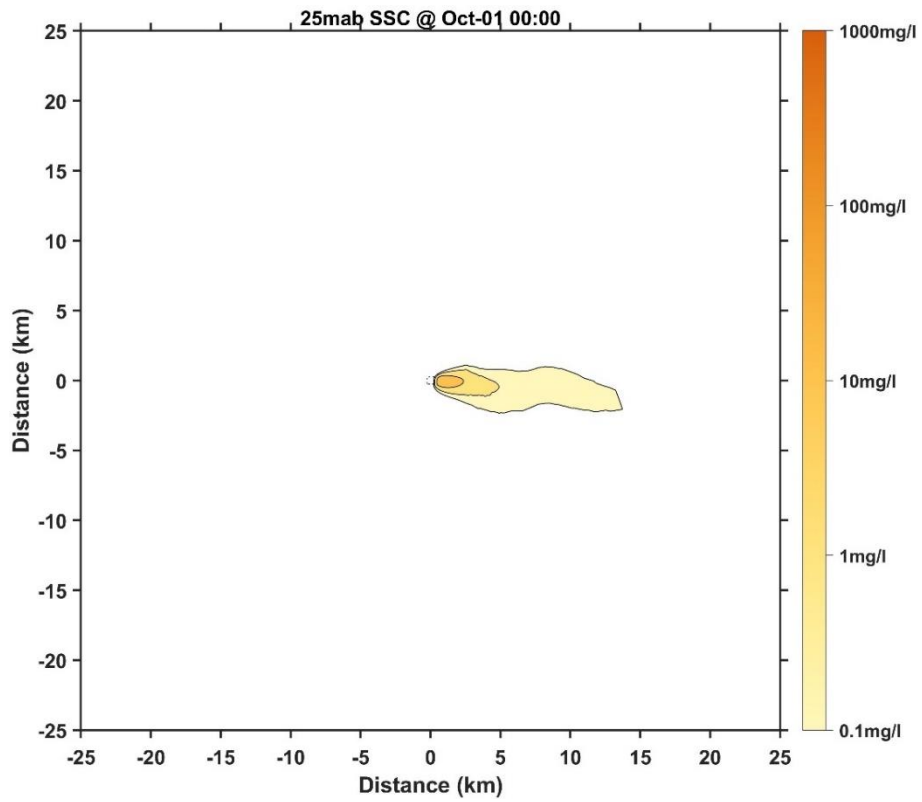
Figure 150 Horizontal distribution of SSC at 25 mab for Case 9 (5 days later)

680
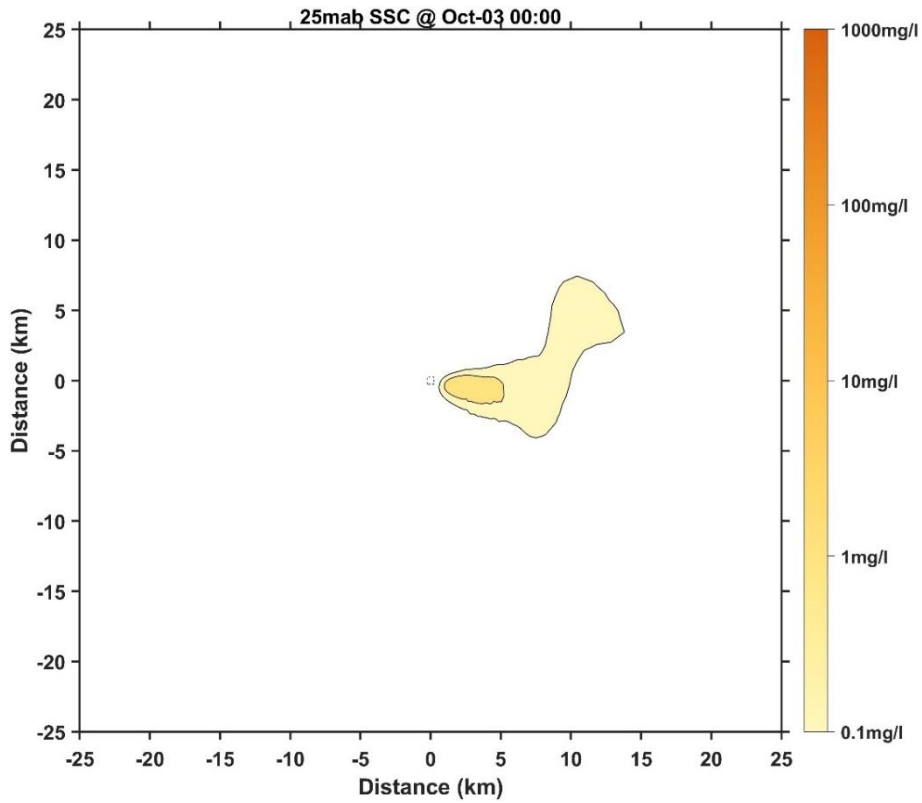
Figure 151 Horizontal distribution of SSC at 25 mab for Case 9 (7 days later)
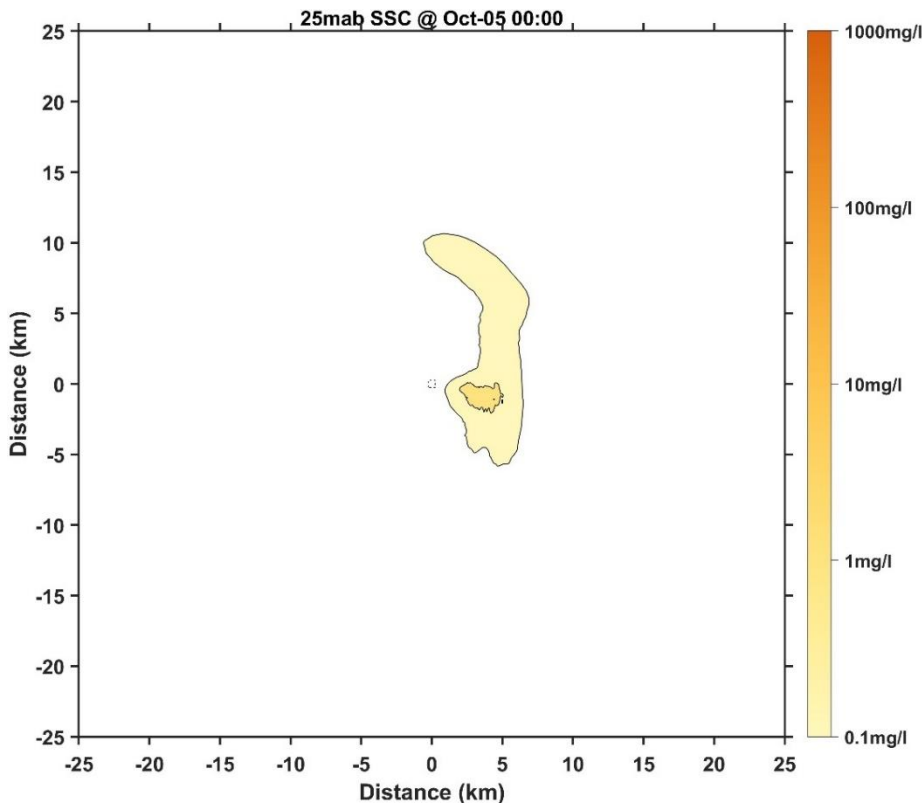
Figure 152 Horizontal distribution of SSC at 25 mab for Case 9 (9 days later)
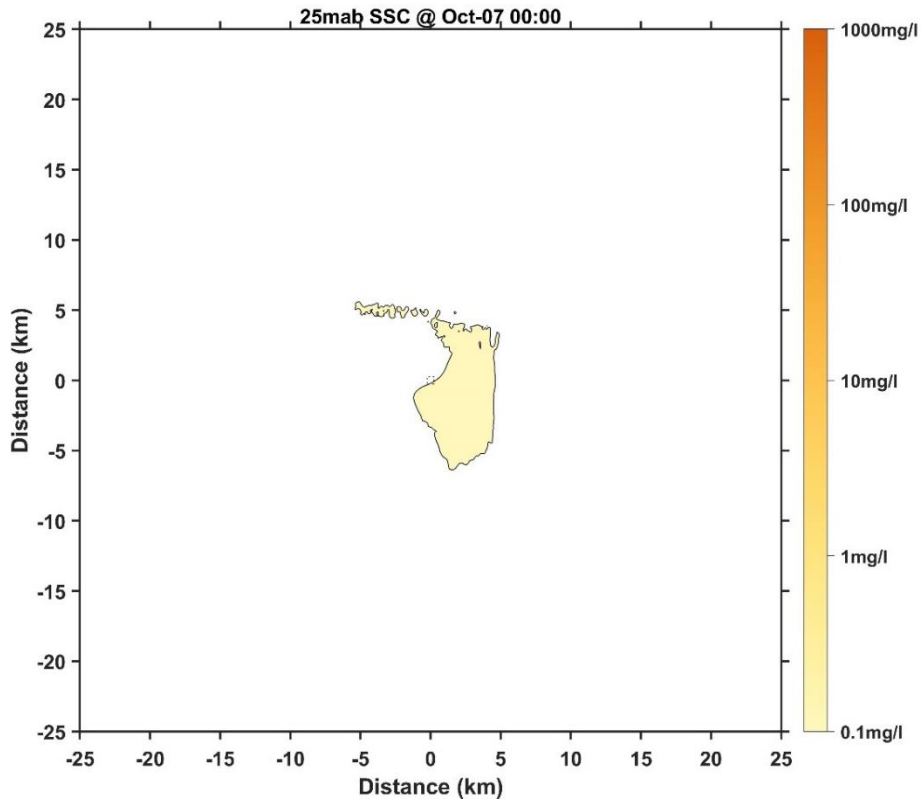
Figure 153 Horizontal distribution of SSC at 25 mab for Case 9 (11 days later)
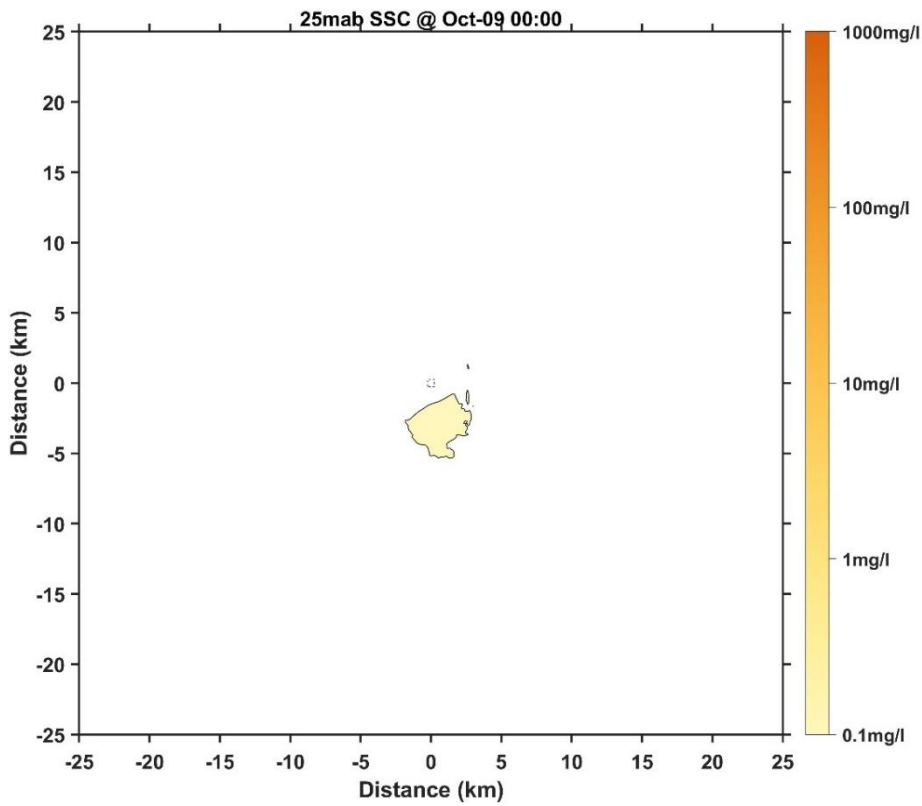
Figure 154 Horizontal distribution of SSC at 25 mab for Case 9 (13 days later)
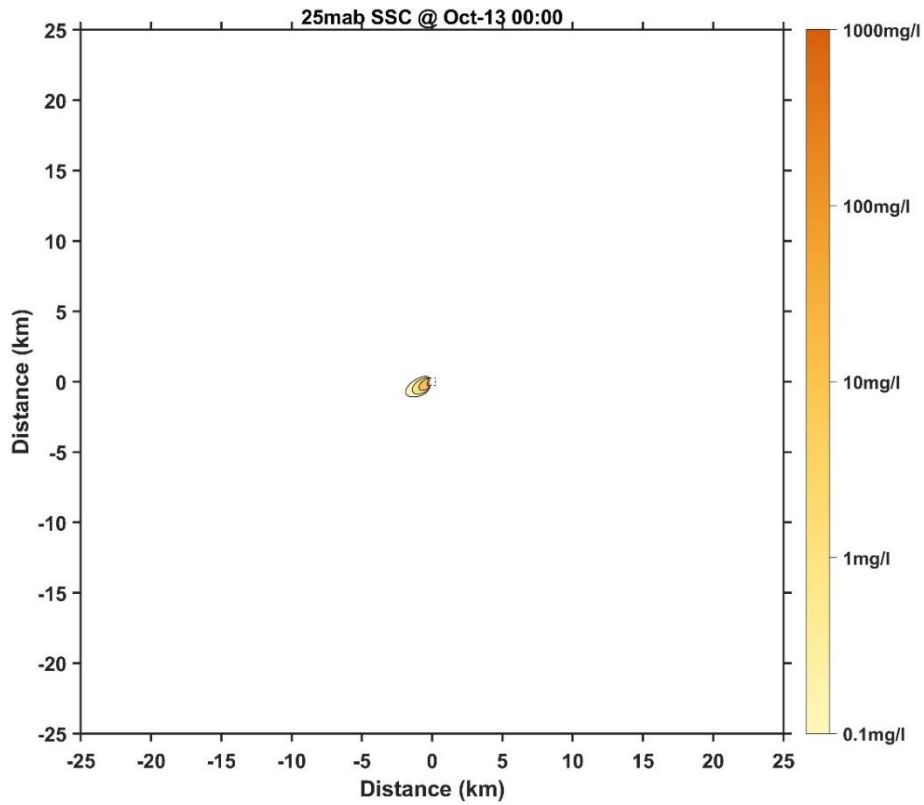
Figure 155 Horizontal distribution of SSC at 25 mab for Case 10 (1 day later)
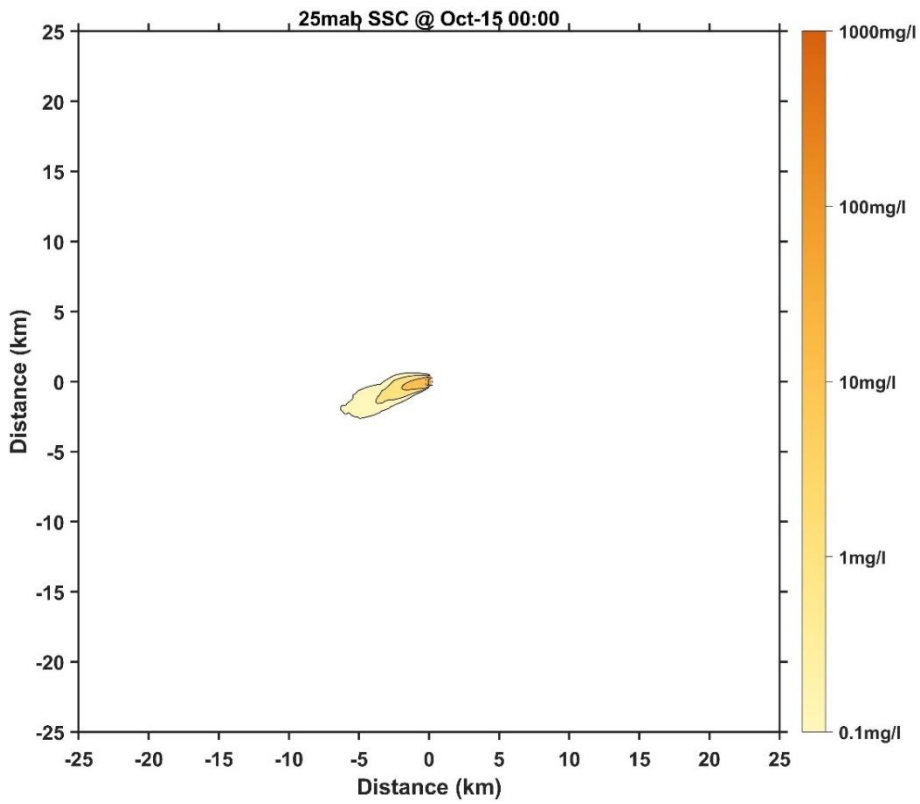
Figure 156 Horizontal distribution of SSC at 25 mab for Case 10 (3 days later)
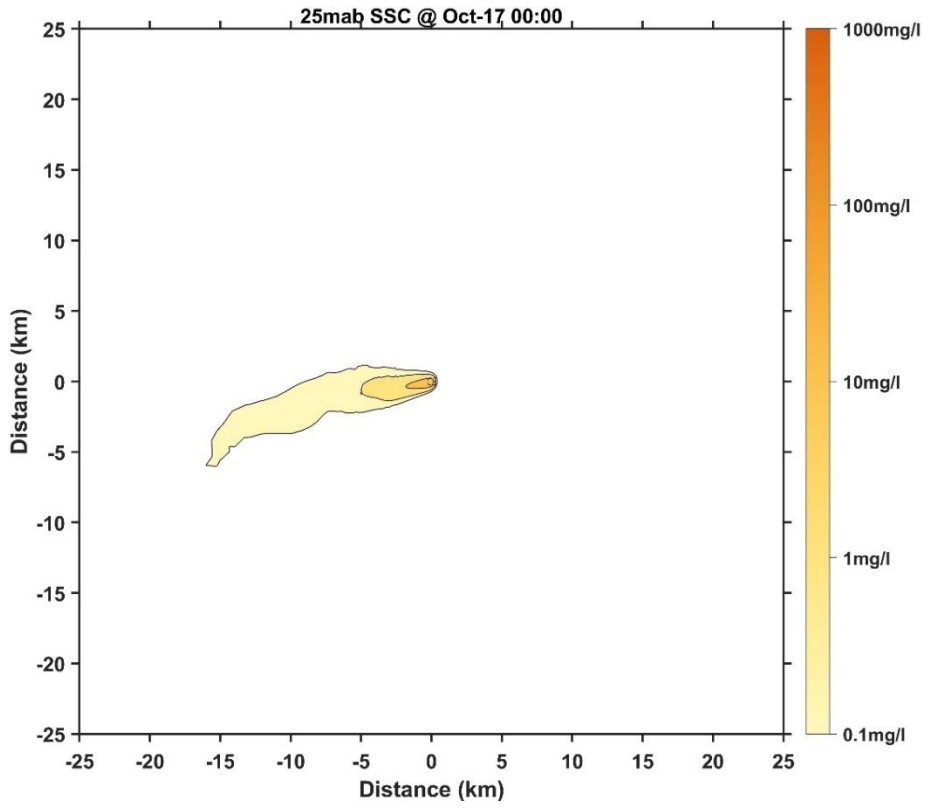
Figure 157 Horizontal distribution of SSC at 25 mab for Case 10 (5 days later)
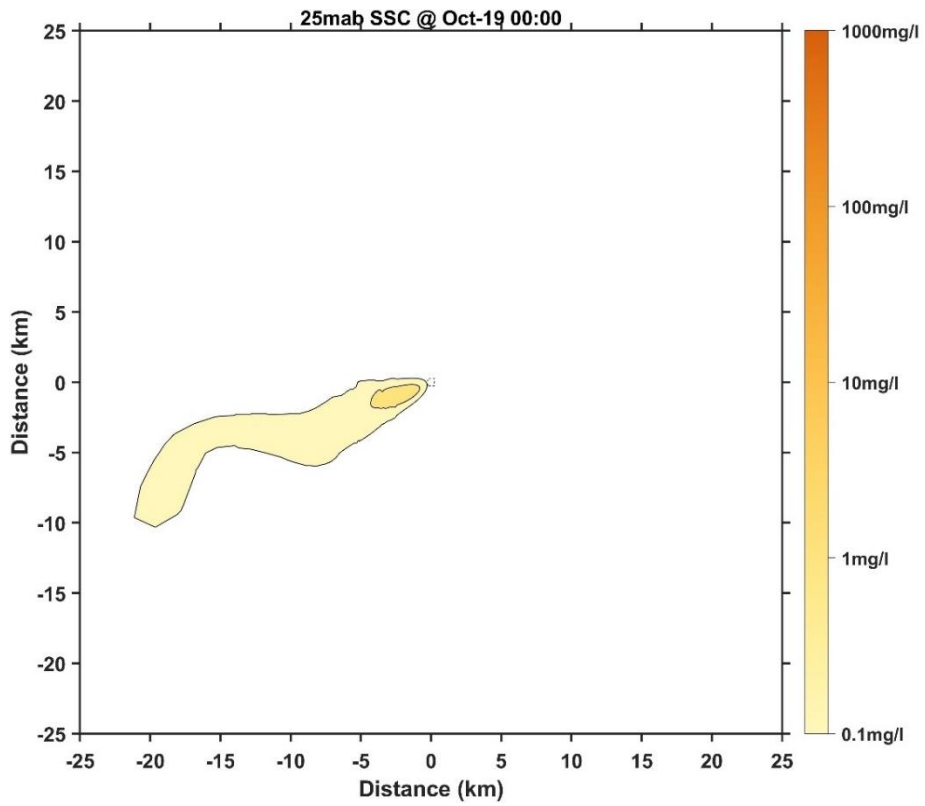
Figure 158 Horizontal distribution of SSC at 25 mab for Case 10 (7 days later)
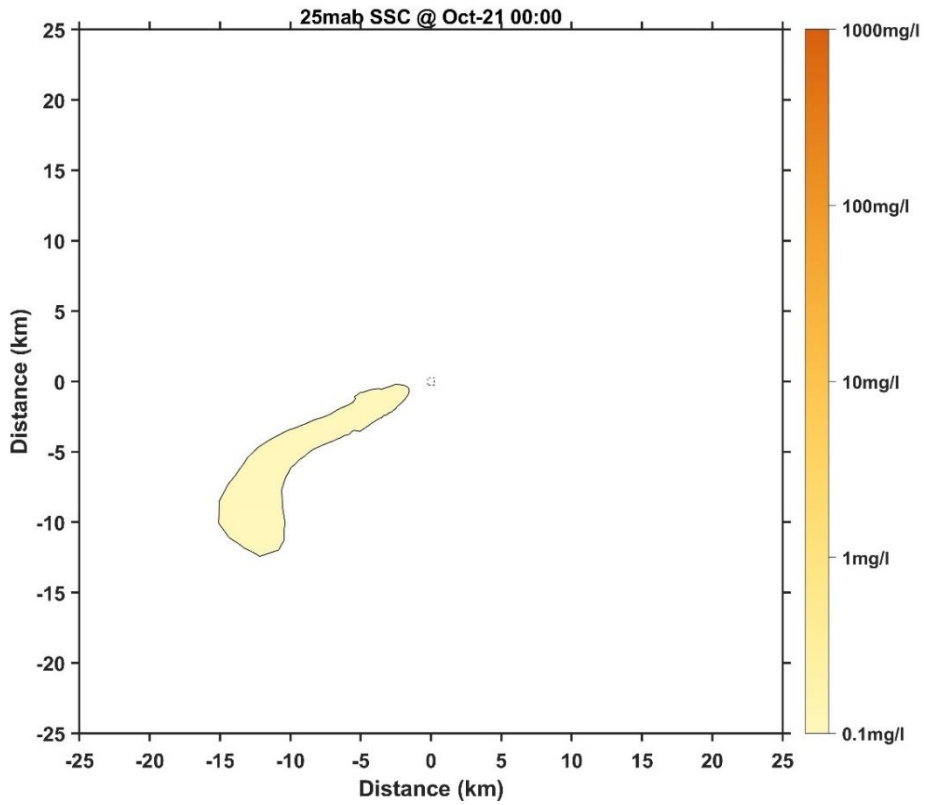
Figure 159 Horizontal distribution of SSC at 25 mab for Case 10 (9 days later)
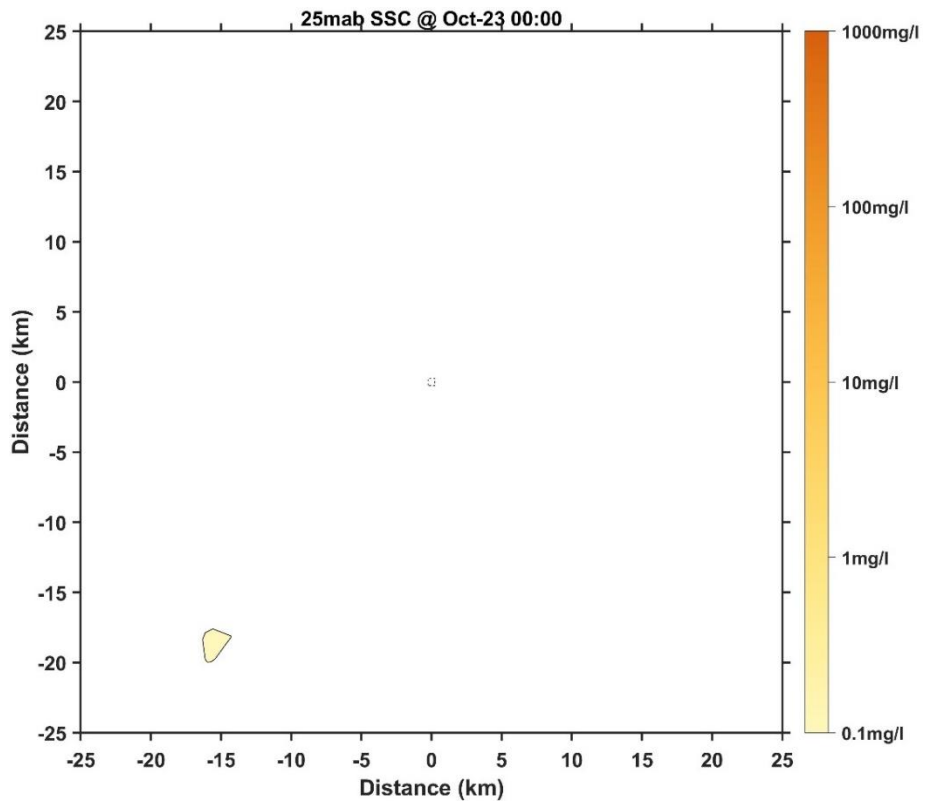
Figure 160 Horizontal distribution of SSC at 25 mab for Case 10 (11 days later)

685

1.4 Dispersion Characteristics of Near-bottom Suspended Sediment at 50 mab

The results of the horizontal distribution of suspended sediment concentration at the near-bottom layer 50 m from the bottom (Figure 161 to 212) show that, on average, the maximum distance of the plume (from the center of the CTA) is 5.55 km for Case 5 and 3.17 km for Case 3. In extreme cases, the maximum distance of the plume (from the center of the CTA) is 27.88 km for Case 8 and 15.05 km for Case 9.
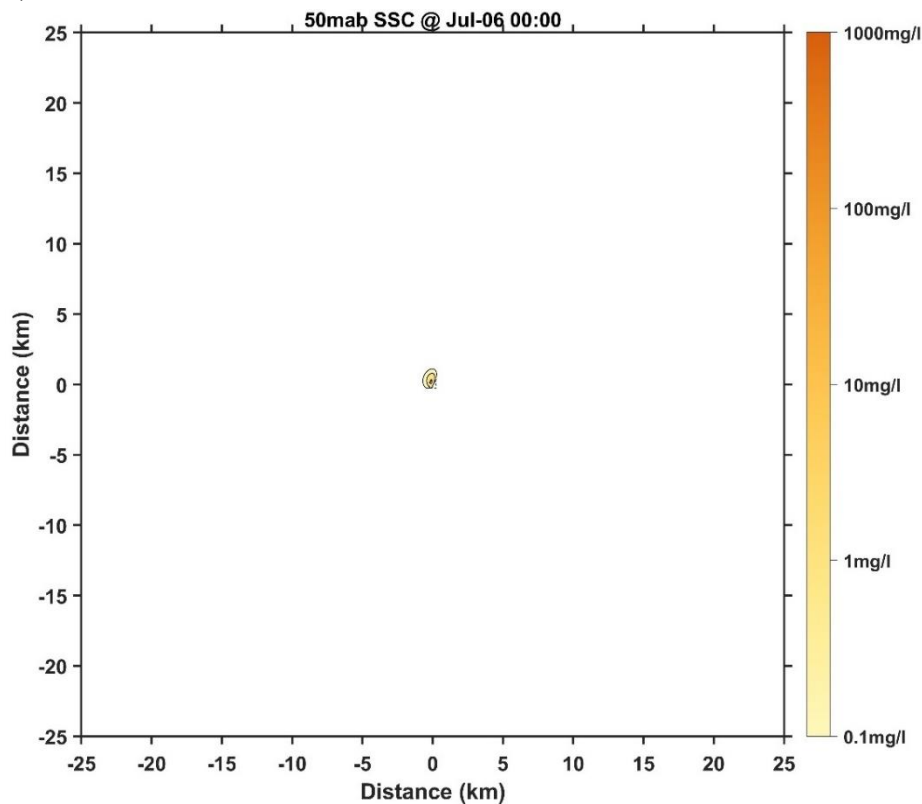
Figure 161 Horizontal distribution of SSC at 50 mab for Case 1 (1 day later)
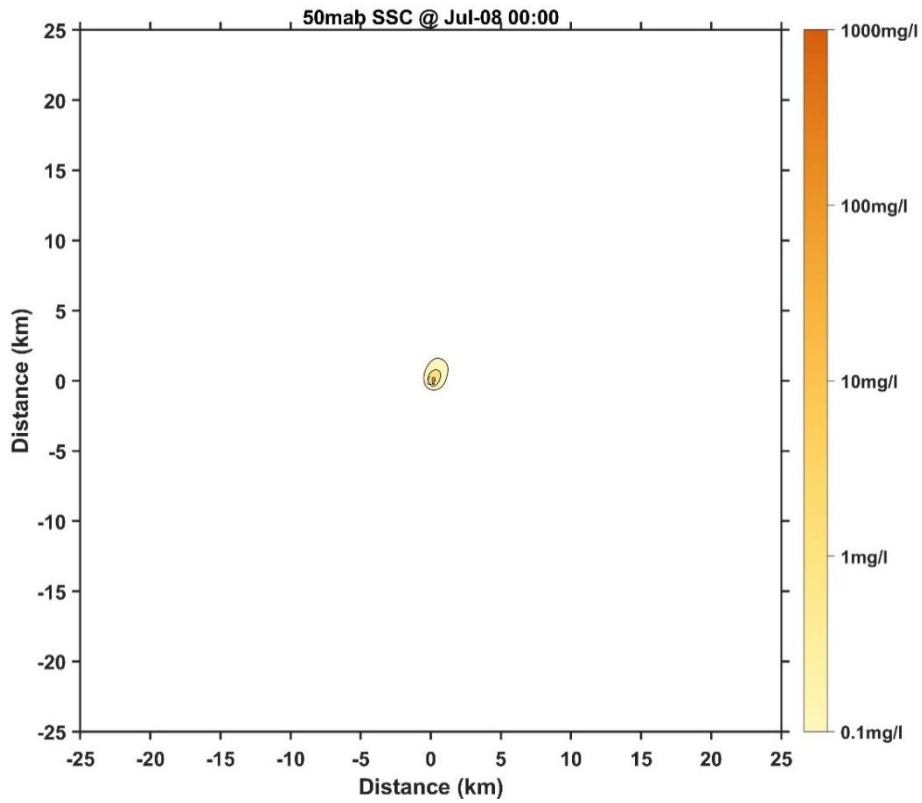
Figure 162 Horizontal distribution of SSC at 50 mab for Case 1 (3 days later)
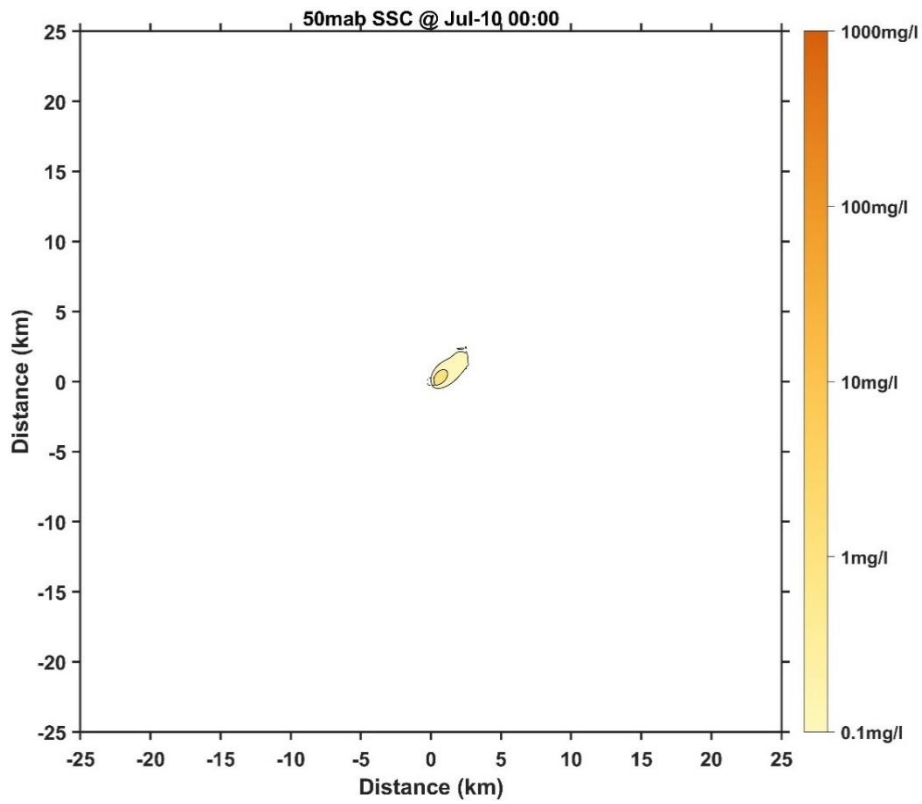
Figure 163 Horizontal distribution of SSC at 50 mab for Case 1 (5 days later)
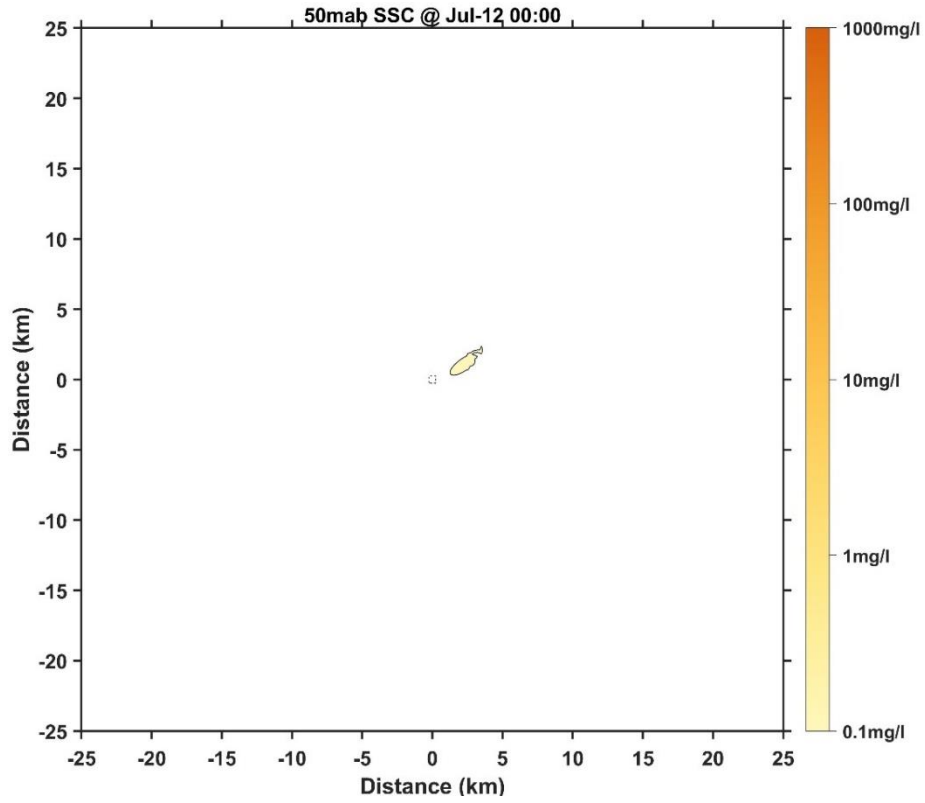
Figure 164 Horizontal distribution of SSC at 50 mab for Case 1 (7 days later)
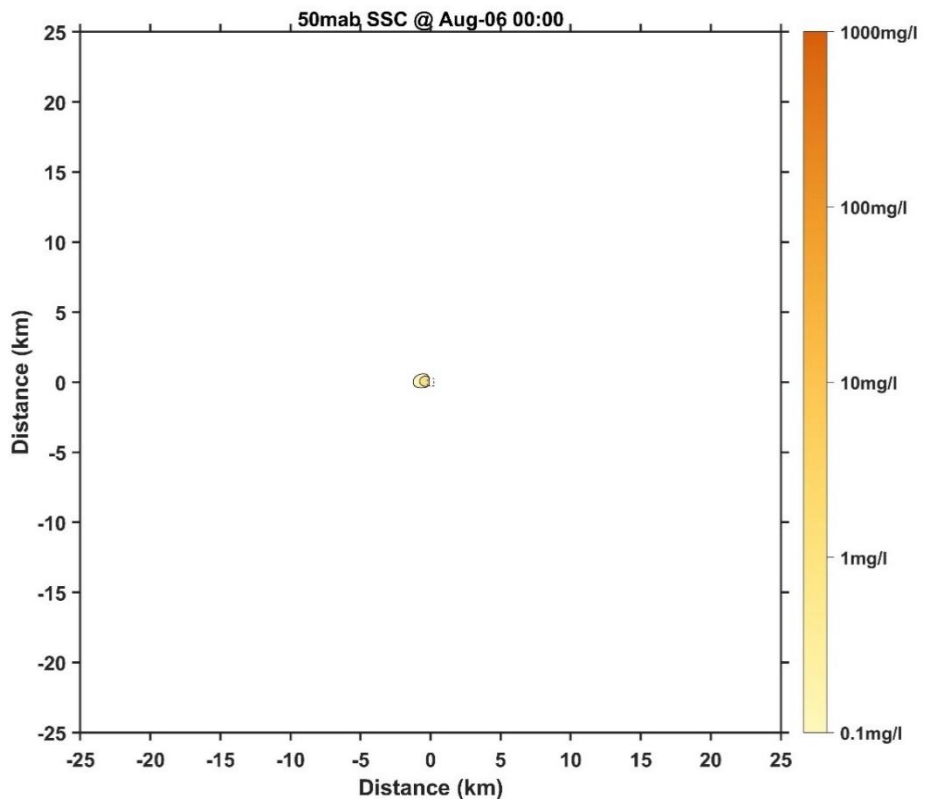
Figure 165 Horizontal distribution of SSC at 50 mab for Case 2 (1 day later)
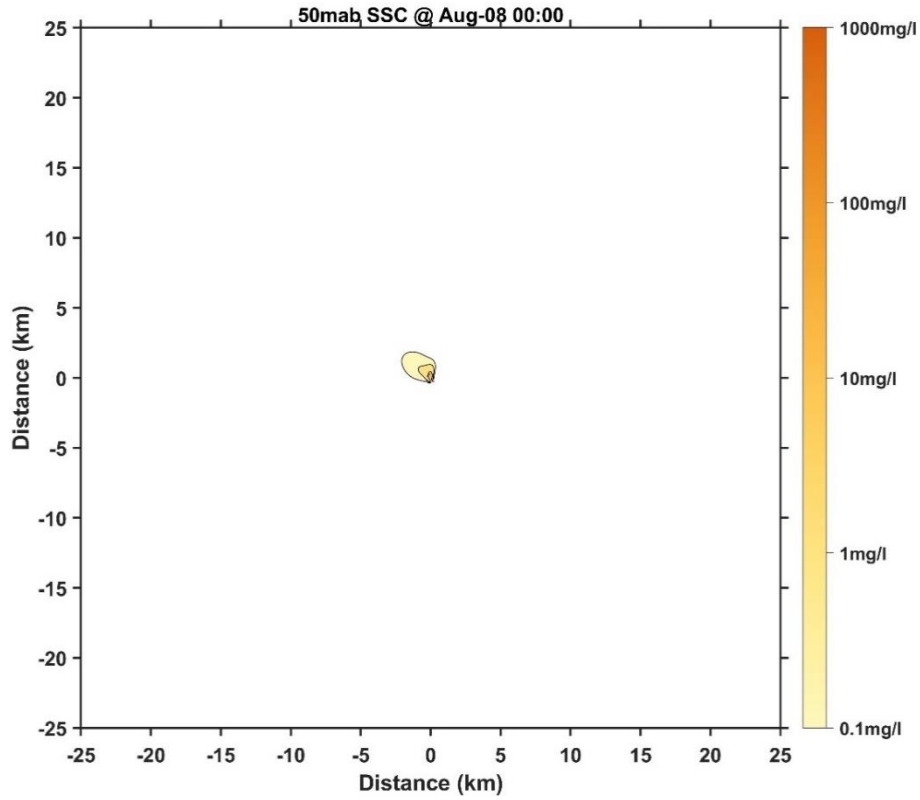
Figure 166 Horizontal distribution of SSC at 50 mab for Case 2 (3 days later)
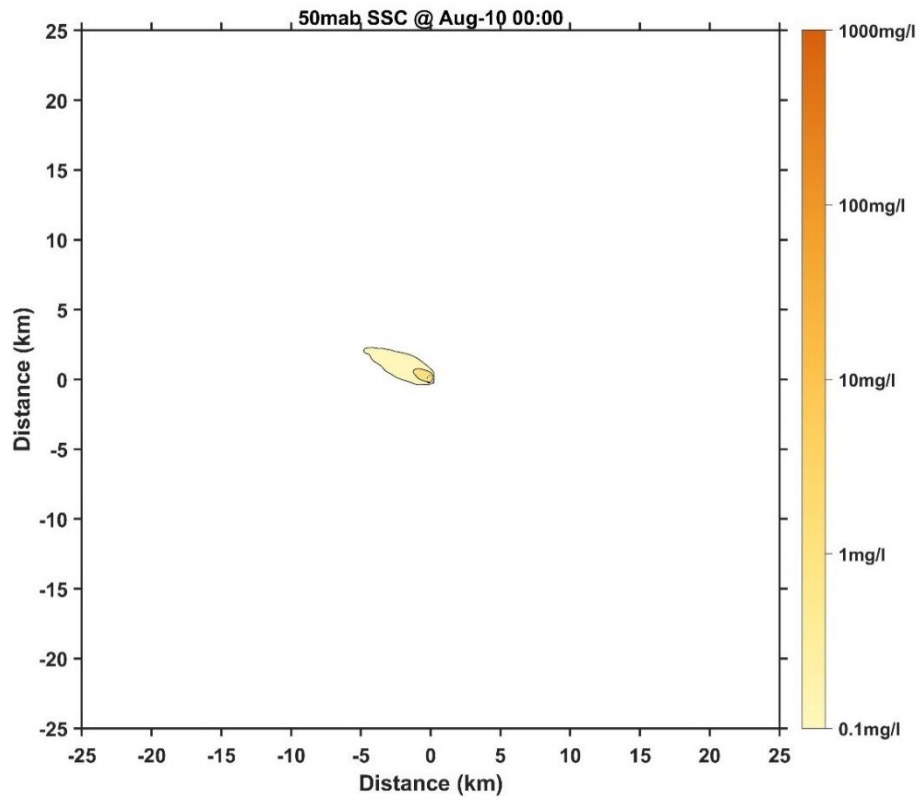
Figure 167 Horizontal distribution of SSC at 50 mab for Case 2 (5 days later)
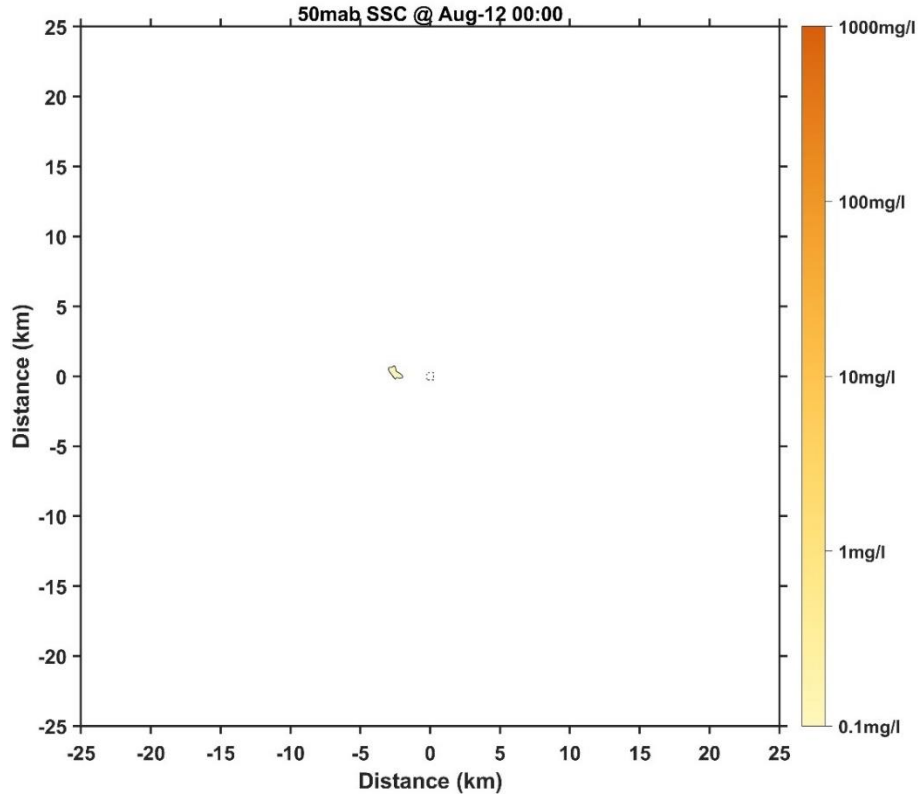
Figure 168 Horizontal distribution of SSC at 50 mab for Case 2 (7 days later)
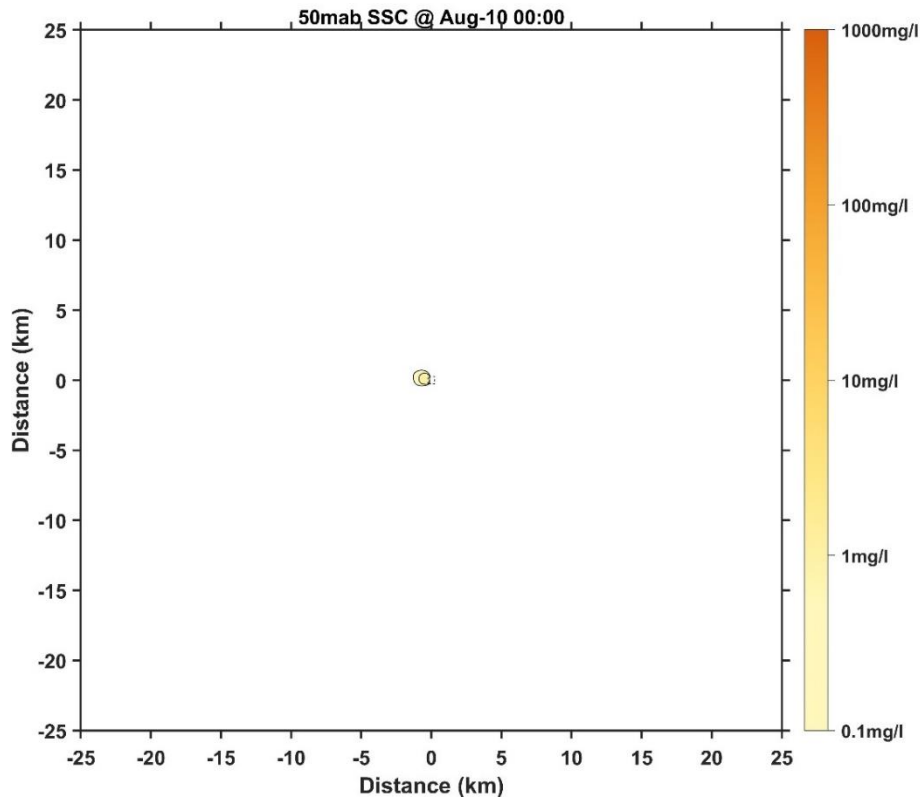
Figure 169 Horizontal distribution of SSC at 50 mab for Case 3 (1 day later)
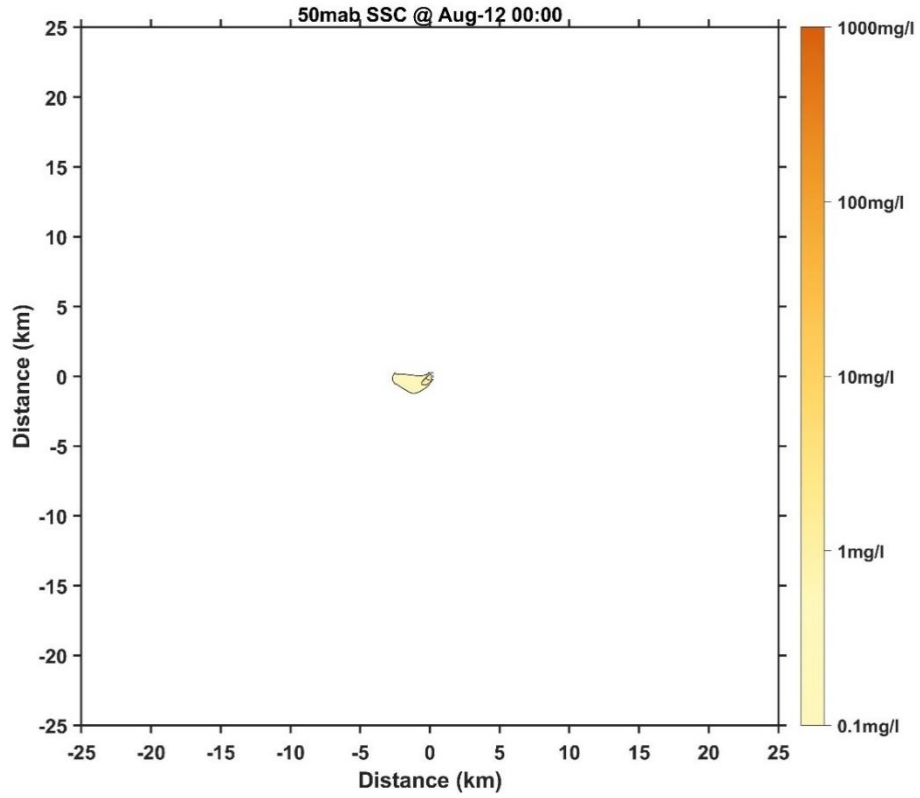
Figure 170 Horizontal distribution of SSC at 50 mab for Case 3 (3 days later)
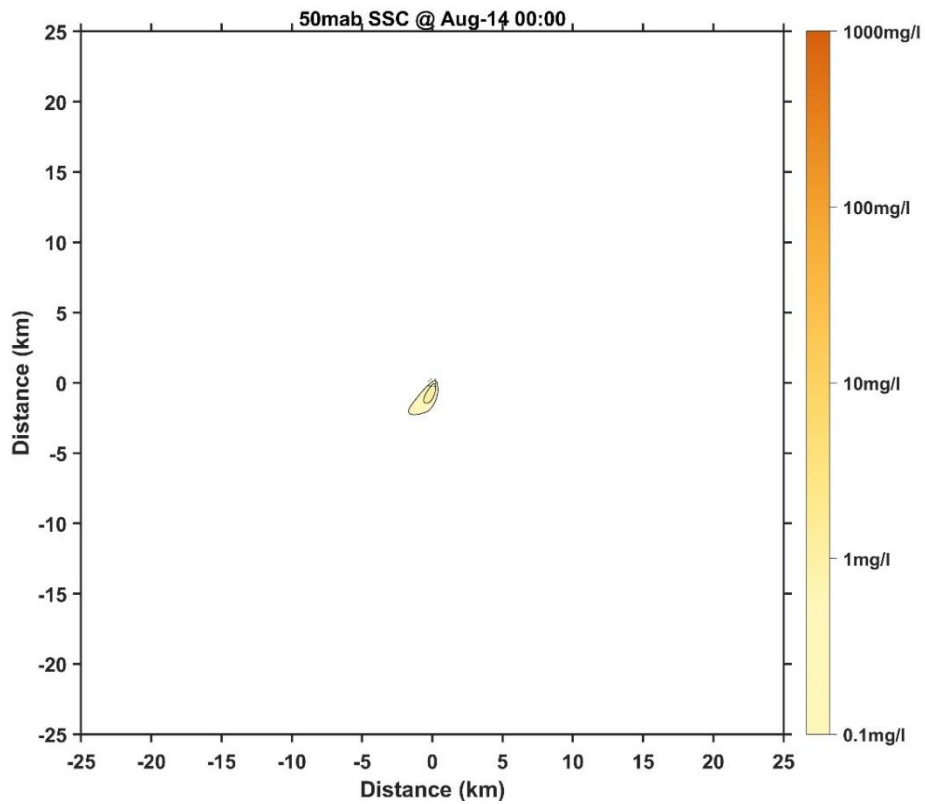
Figure 171 Horizontal distribution of SSC at 50 mab for Case 3 (5 days later)
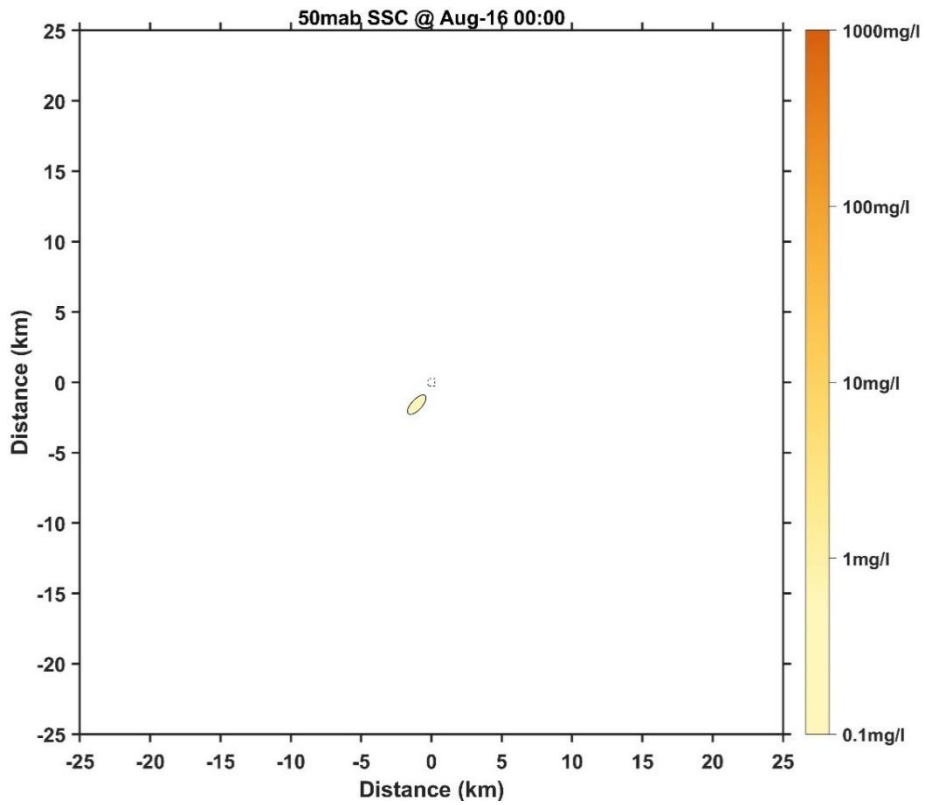
Figure 172 Horizontal distribution of SSC at 50 mab for Case 3 (7 days later)
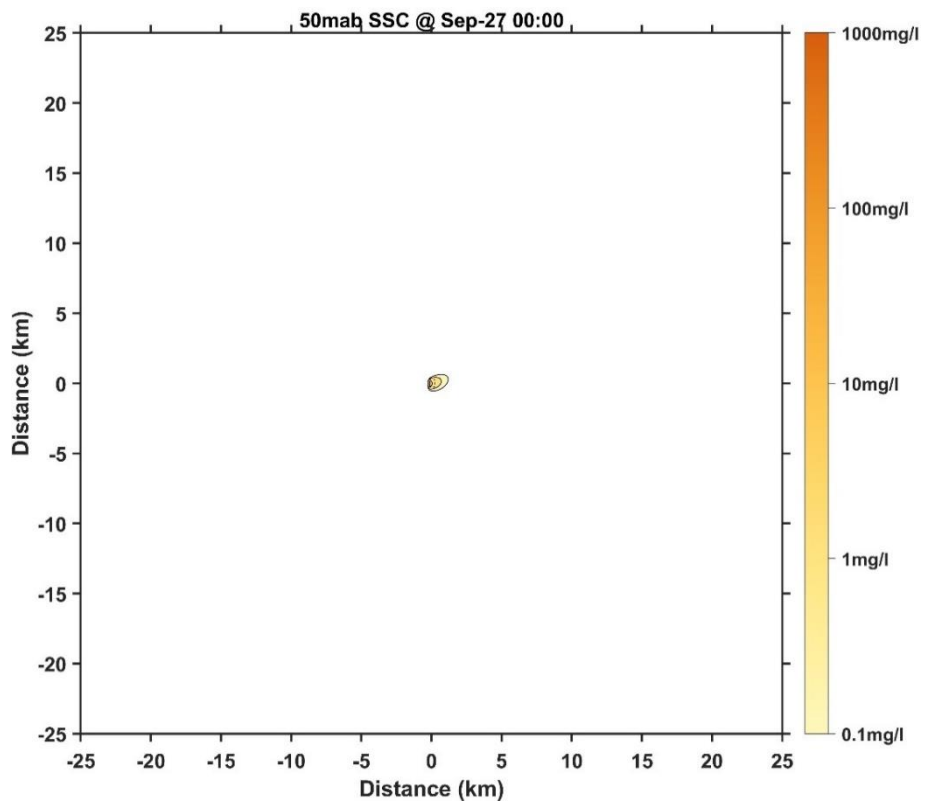
Figure 173 Horizontal distribution of SSC at 50 mab for Case 4 (1 day later)
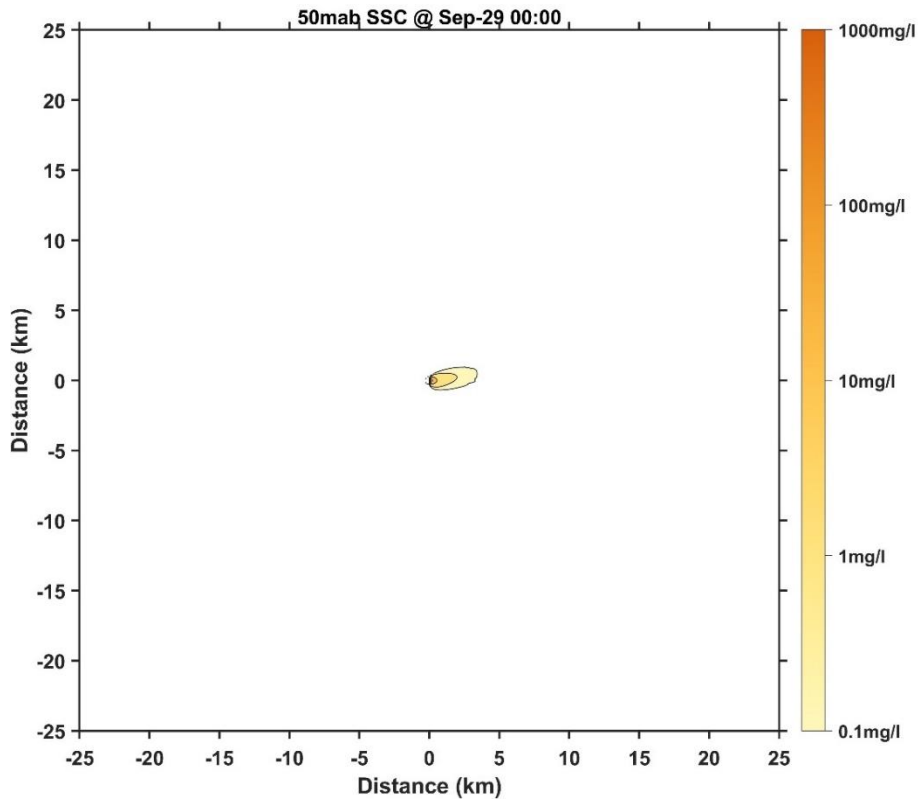
Figure 174 Horizontal distribution of SSC at 50 mab for Case 4 (3 days later)
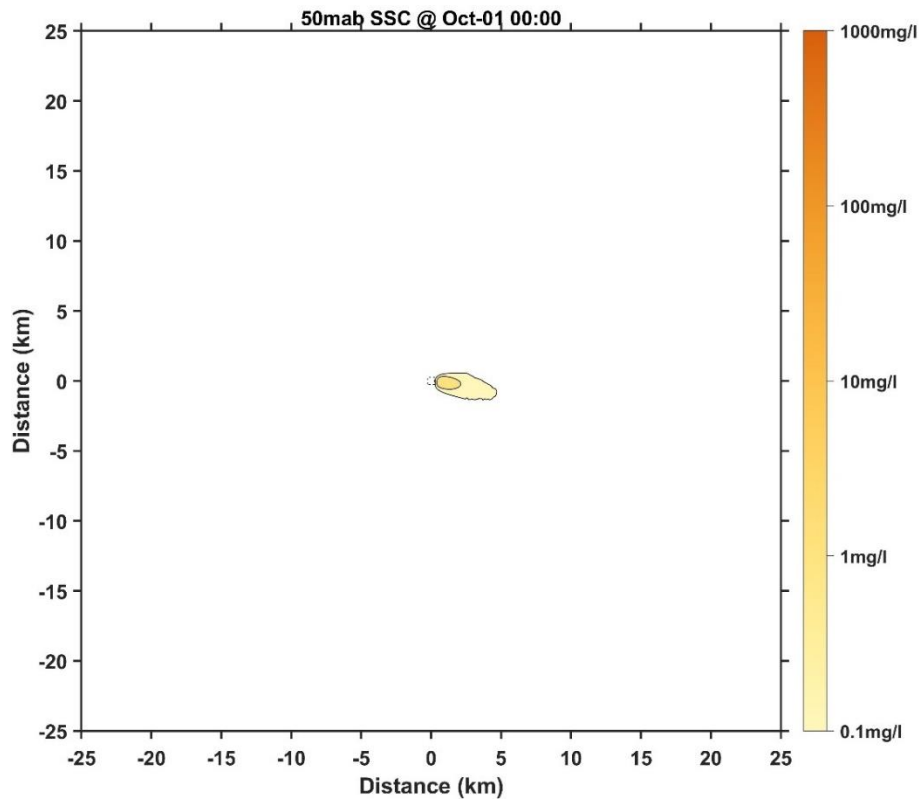
Figure 175 Horizontal distribution of SSC at 50 mab for Case 4 (5 days later)
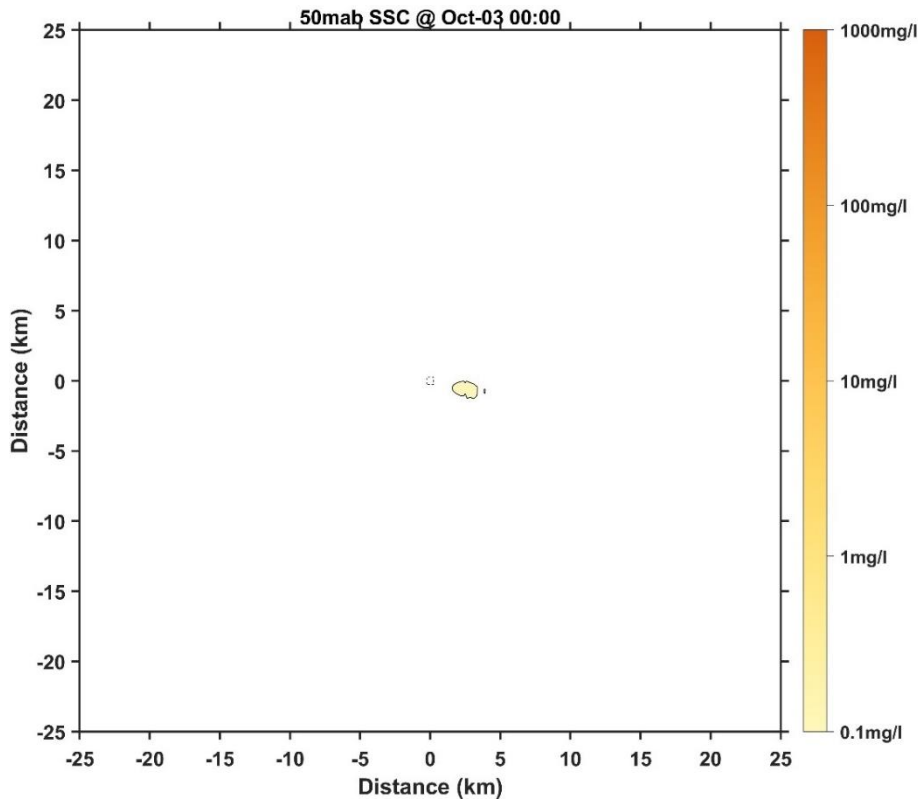
Figure 176 Horizontal distribution of SSC at 50 mab for Case 4 (7 days later)
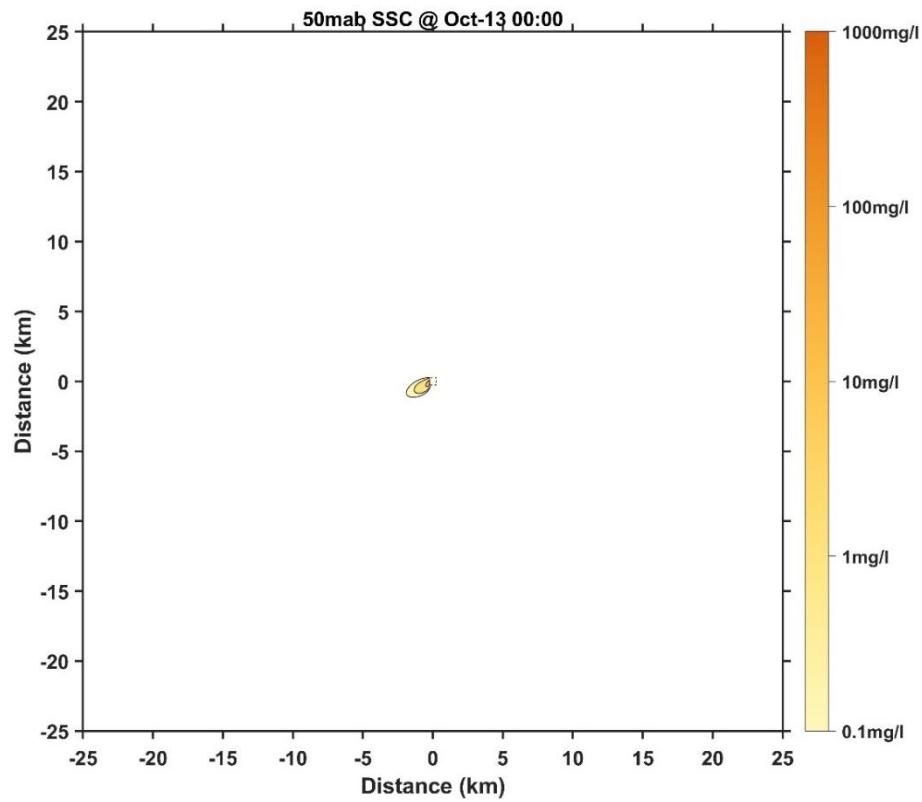
Figure 177 Horizontal distribution of SSC at 50 mab for Case 5 (1 day later)
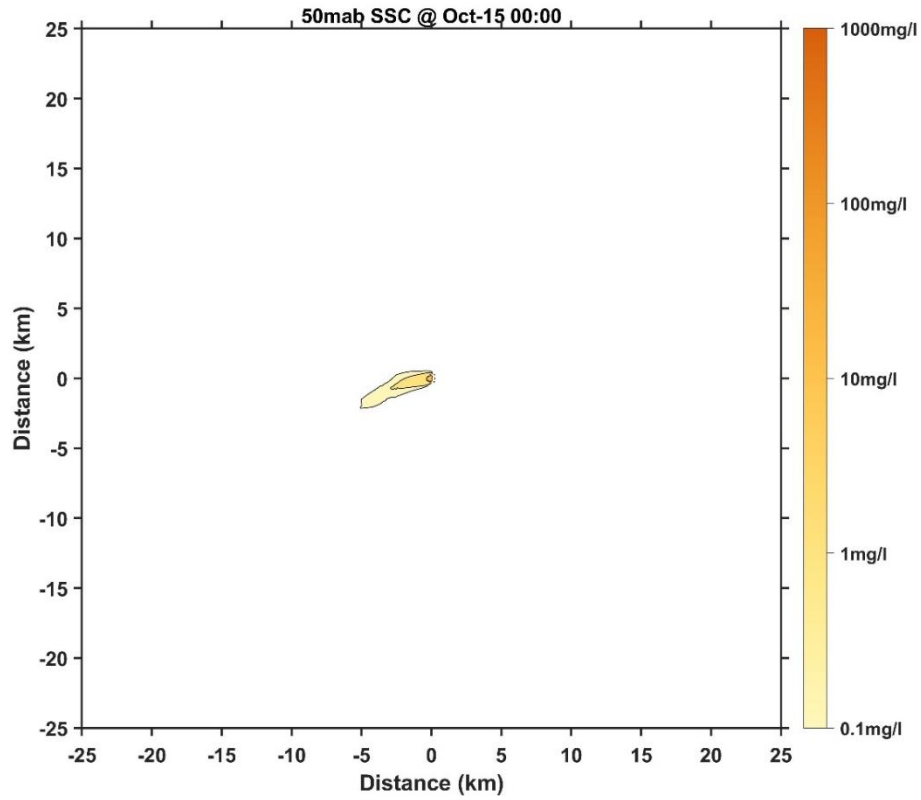
Figure 178 Horizontal distribution of SSC at 50 mab for Case 5 (3 days later)
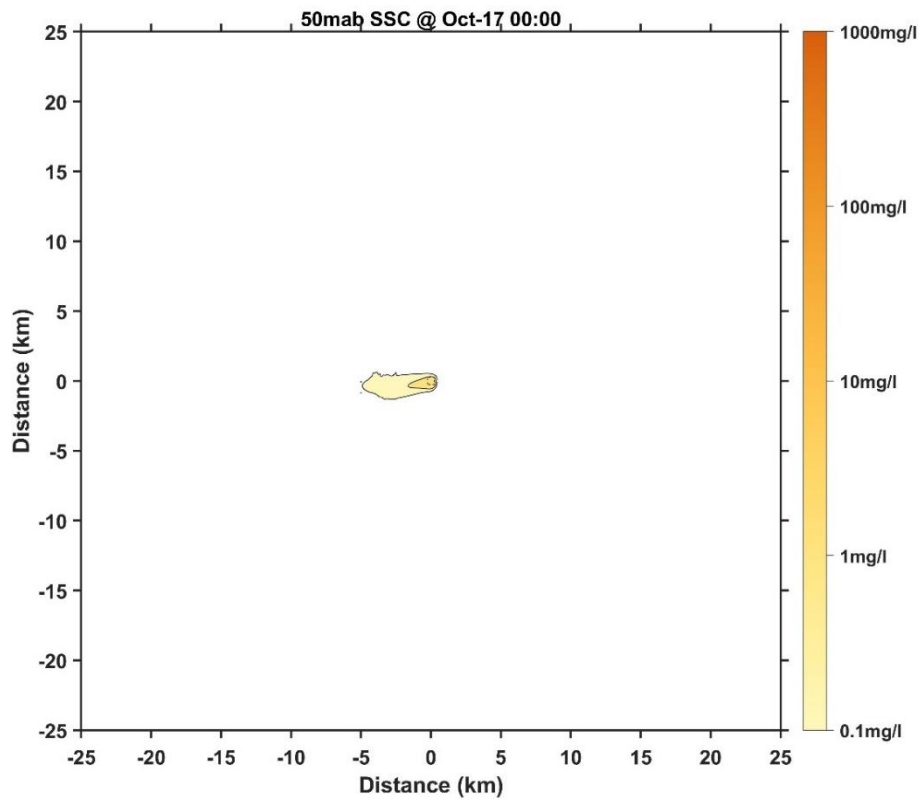
Figure 179 Horizontal distribution of SSC at 50 mab for Case 5 (5 days later)
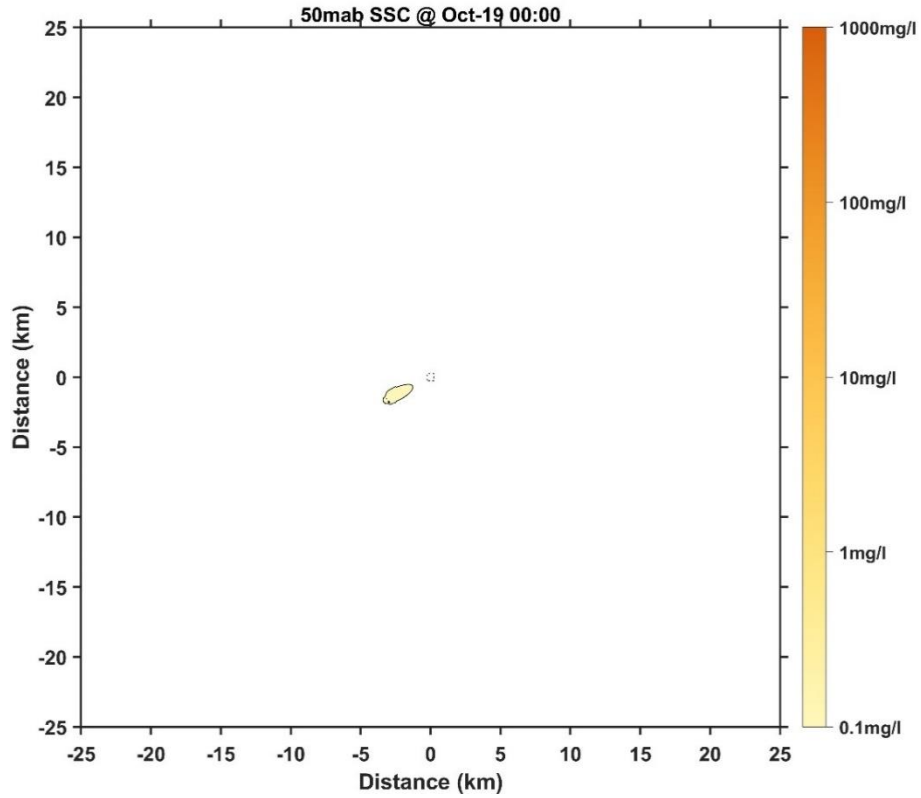
Figure 180 Horizontal distribution of SSC at 50 mab for Case 5 (7 days later)
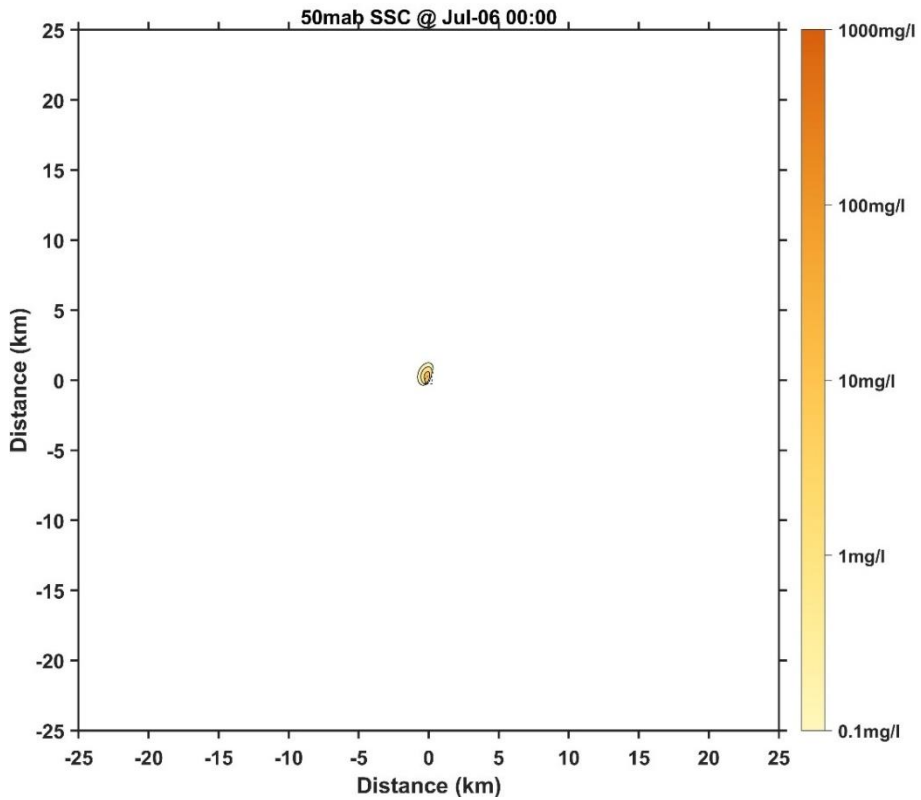
Figure 181 Horizontal distribution of SSC at 50 mab for Case 6 (1 day later)
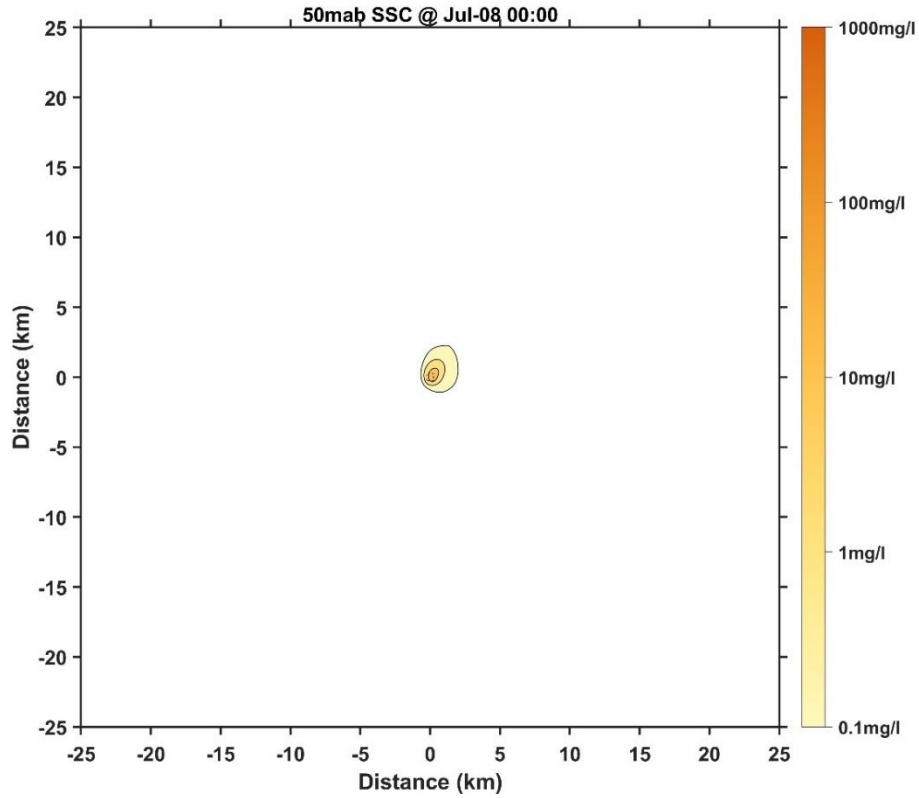
Figure 182 Horizontal distribution of SSC at 50 mab for Case 6 (3 days later)
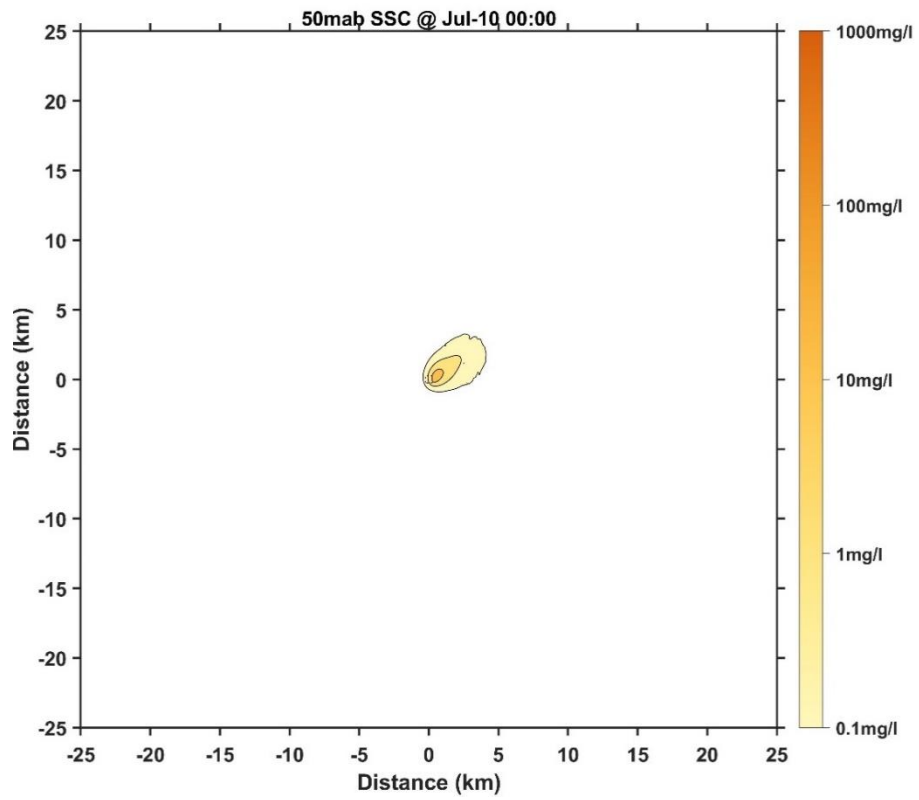
Figure 183 Horizontal distribution of SSC at 50 mab for Case 6 (5 days later)
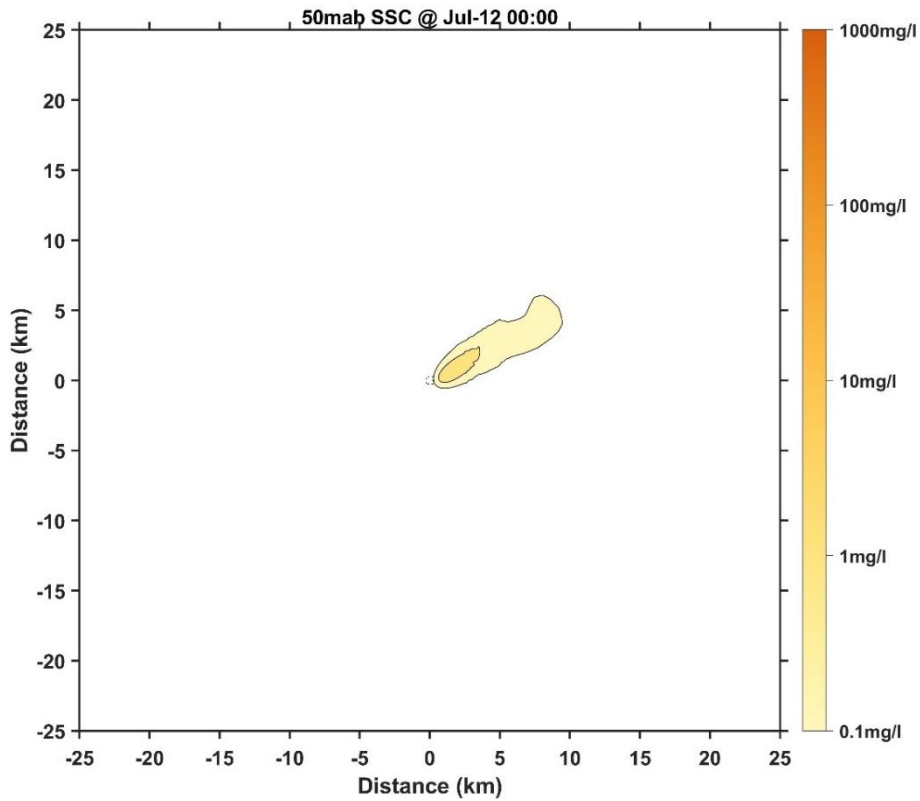
Figure 184 Horizontal distribution of SSC at 50 mab for Case 6 (7 days later)
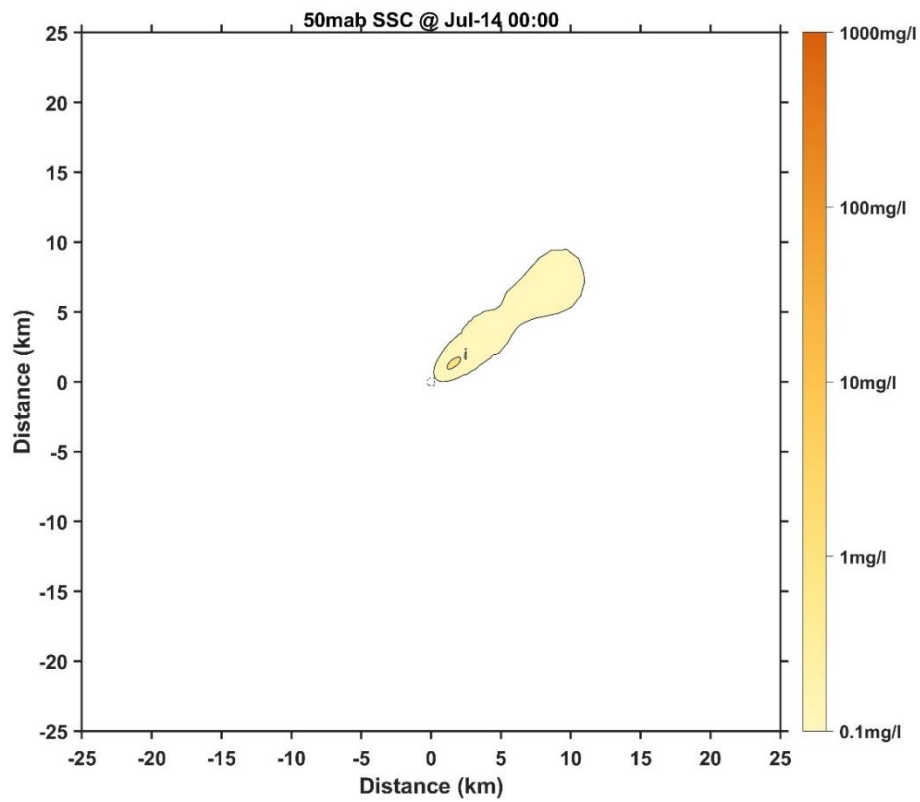
Figure 185 Horizontal distribution of SSC at 50 mab for Case 6 (9 days later)
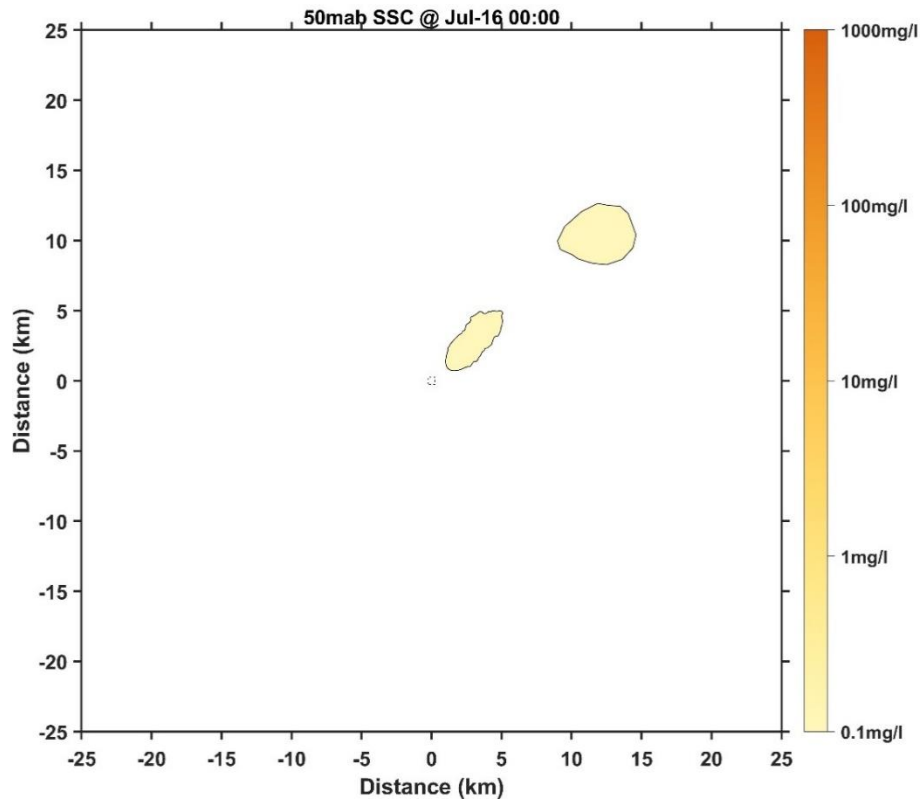
Figure 186 Horizontal distribution of SSC at 50 mab for Case 6 (11 days later)
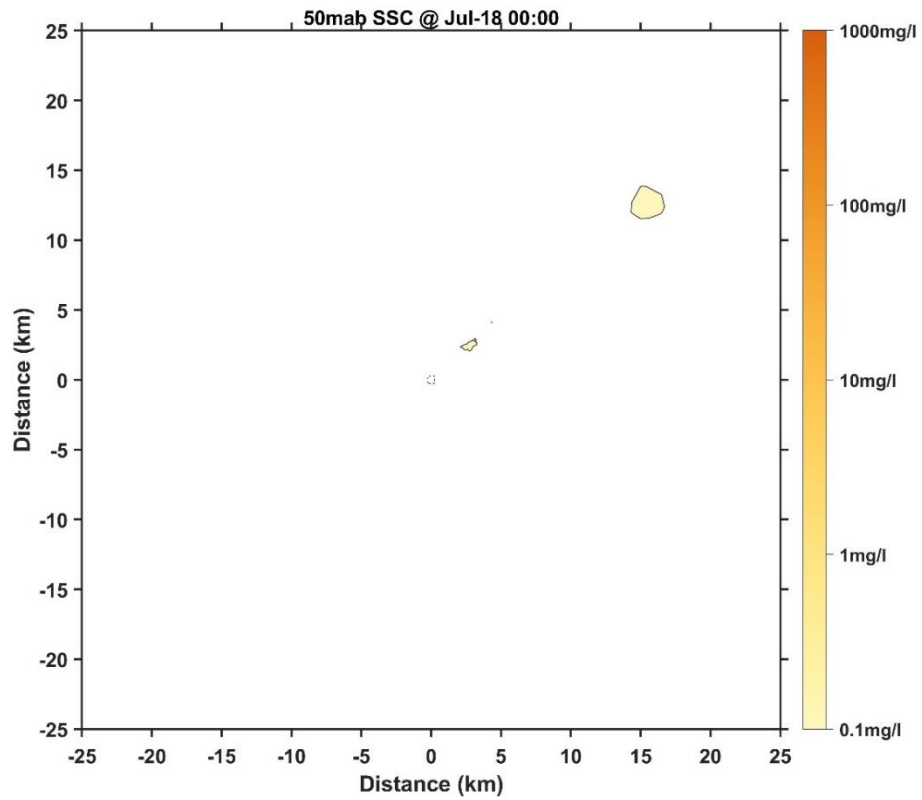
Figure 187 Horizontal distribution of SSC at 50 mab for Case 6 (13 days later)
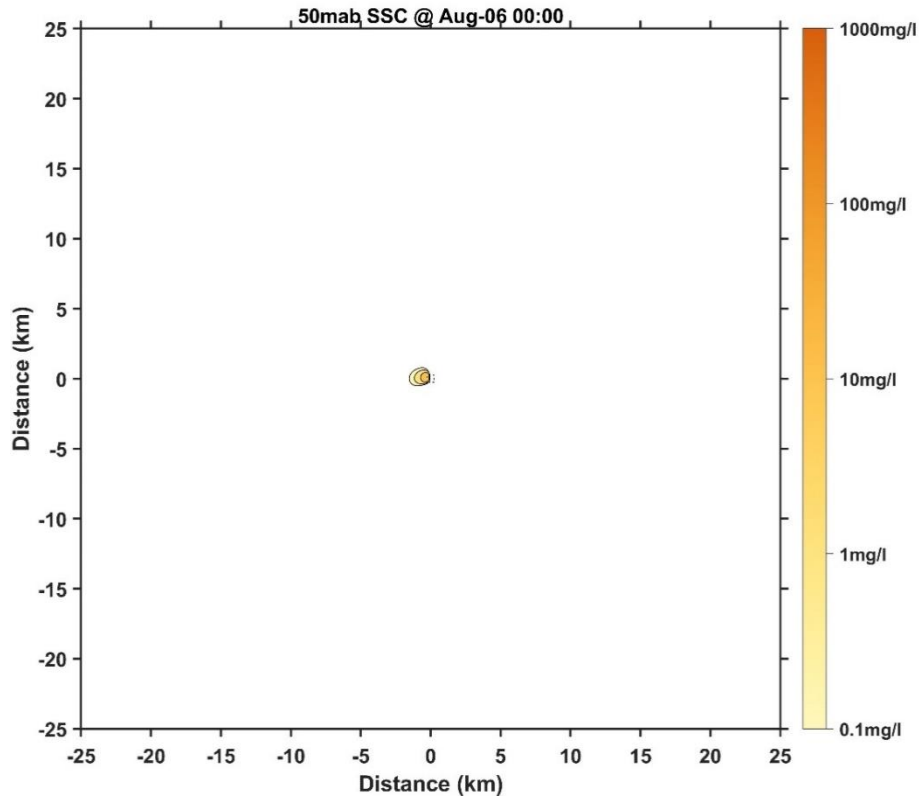
Figure 188 Horizontal distribution of SSC at 50 mab for Case 7 (1 day later)
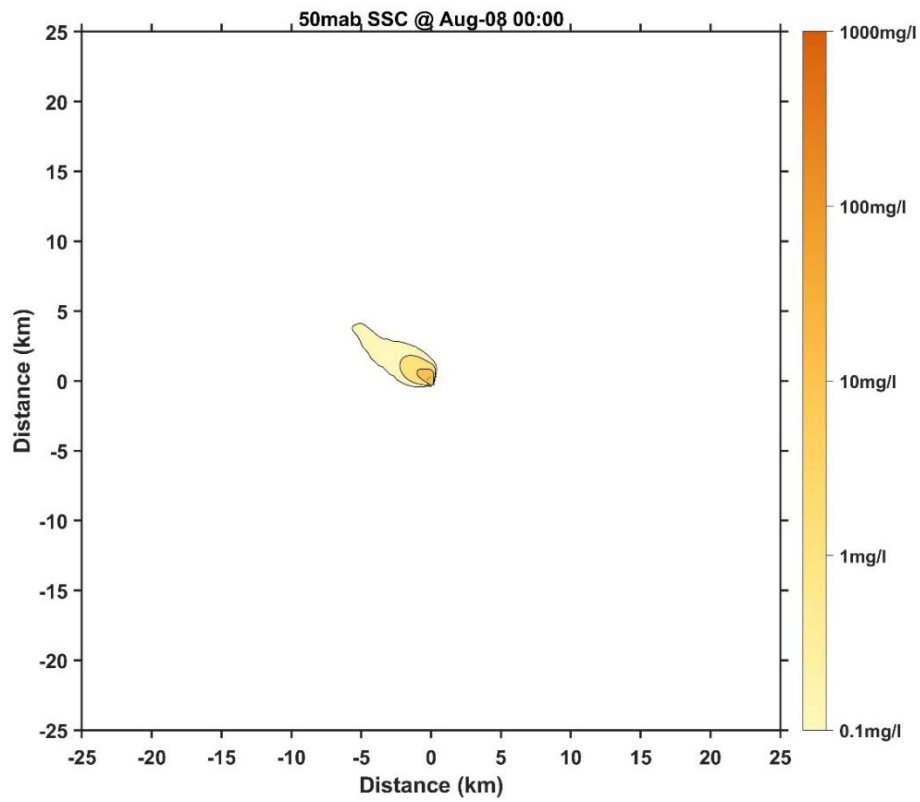
Figure 189 Horizontal distribution of SSC at 50 mab for Case 7 (3 days later)
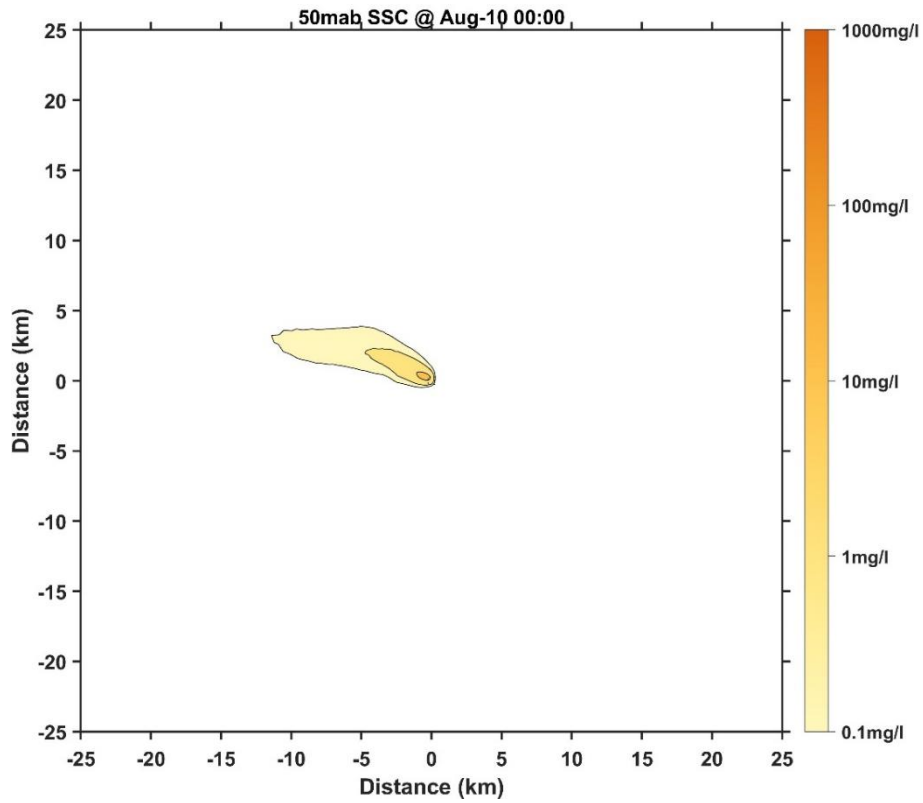
Figure 190 Horizontal distribution of SSC at 50 mab for Case 7 (5 days later)
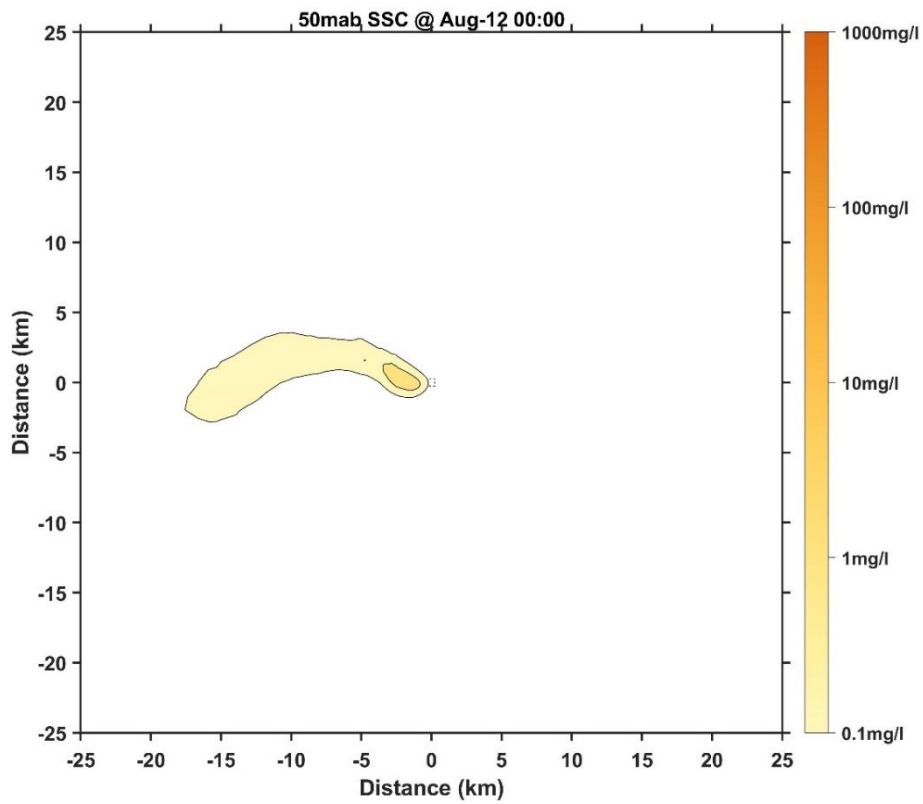
Figure 191 Horizontal distribution of SSC at 50 mab for Case 7 (7 days later)
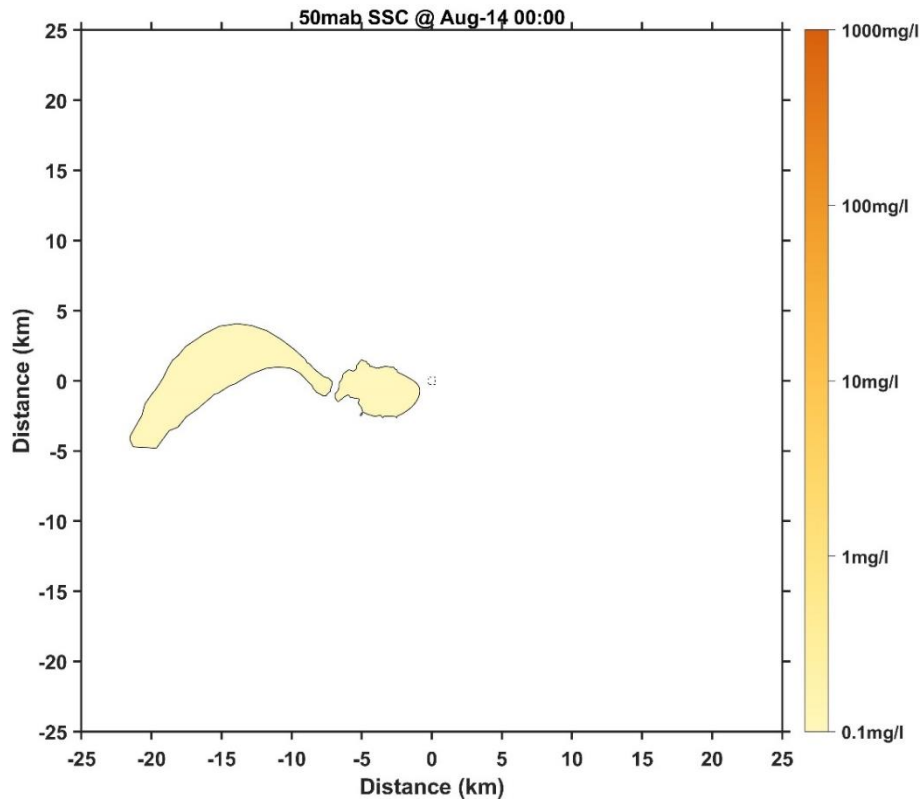
Figure 192 Horizontal distribution of SSC at 50 mab for Case 7 (9 days later)
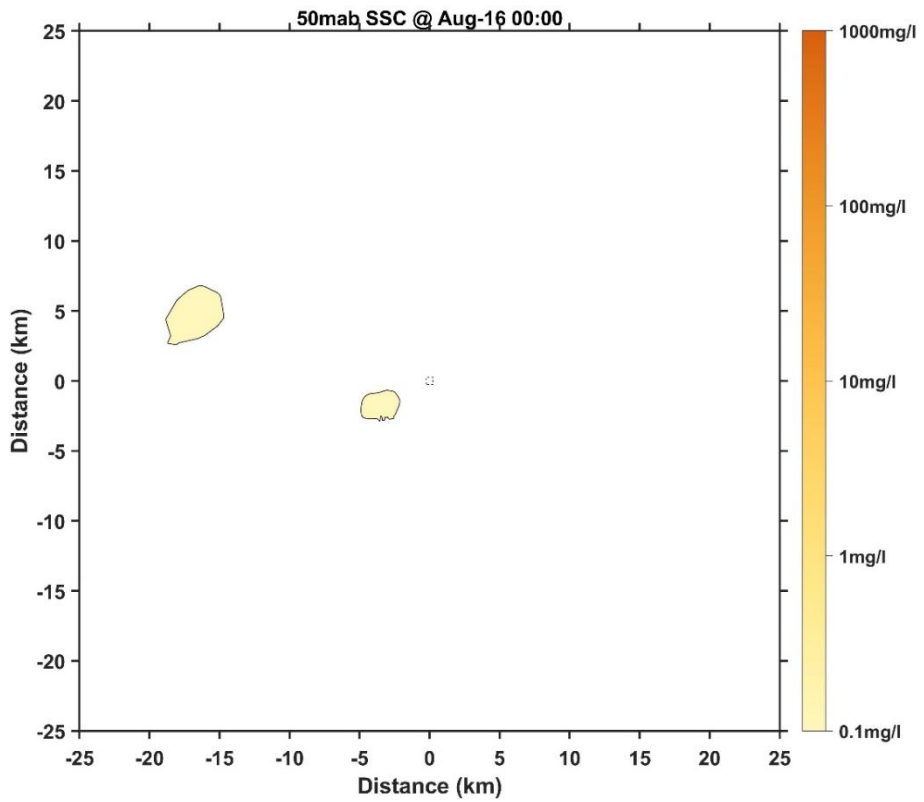
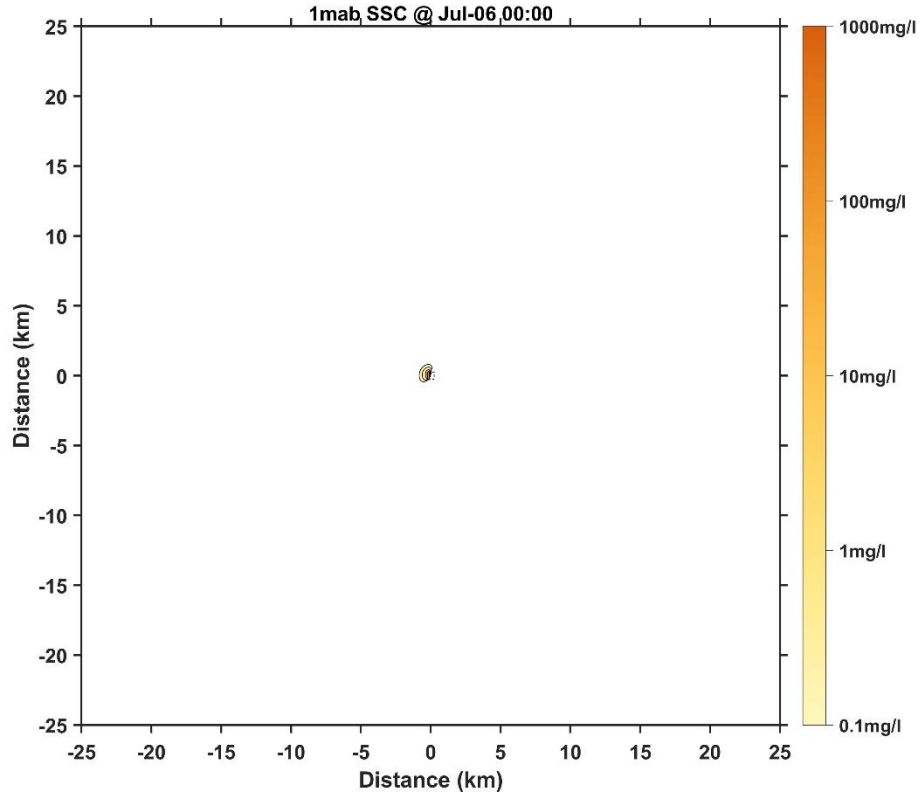Figure 193 Horizontal distribution of SSC at 50 mab for Case 7 (11 days later)
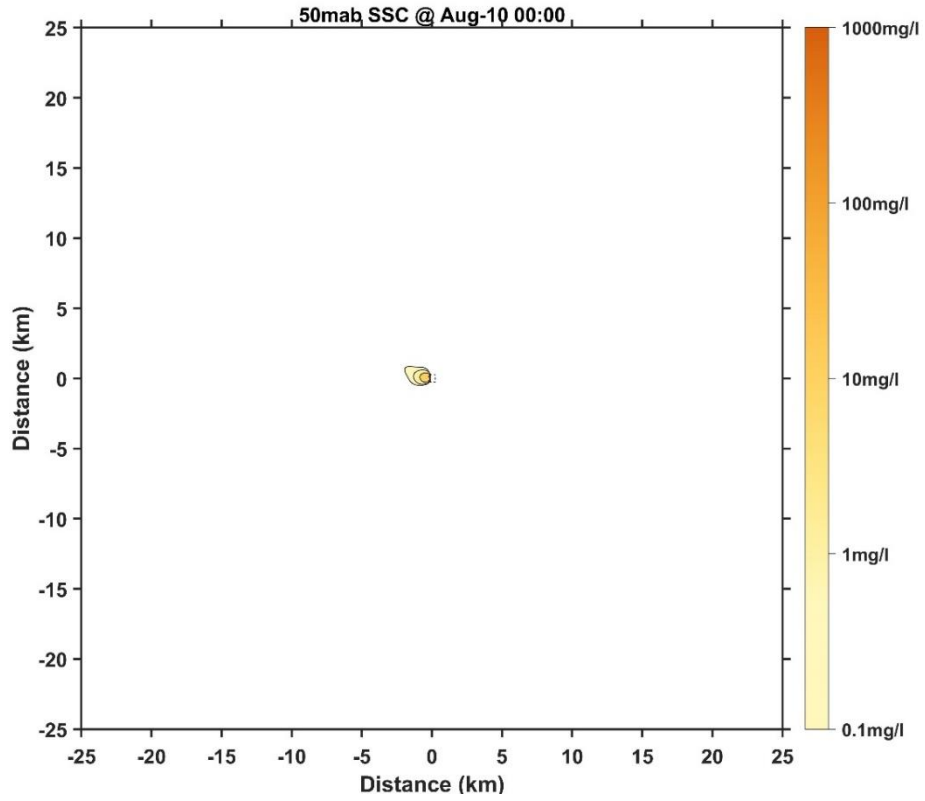
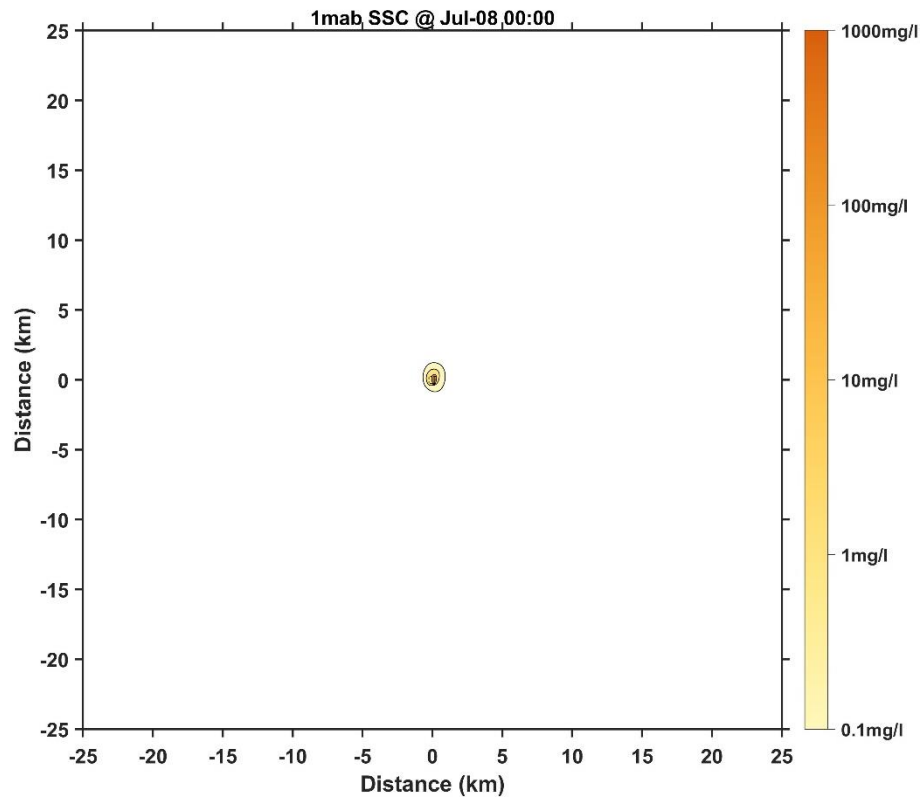Figure 194 Horizontal distribution of SSC at 50 mab for Case 8 (1 day later)
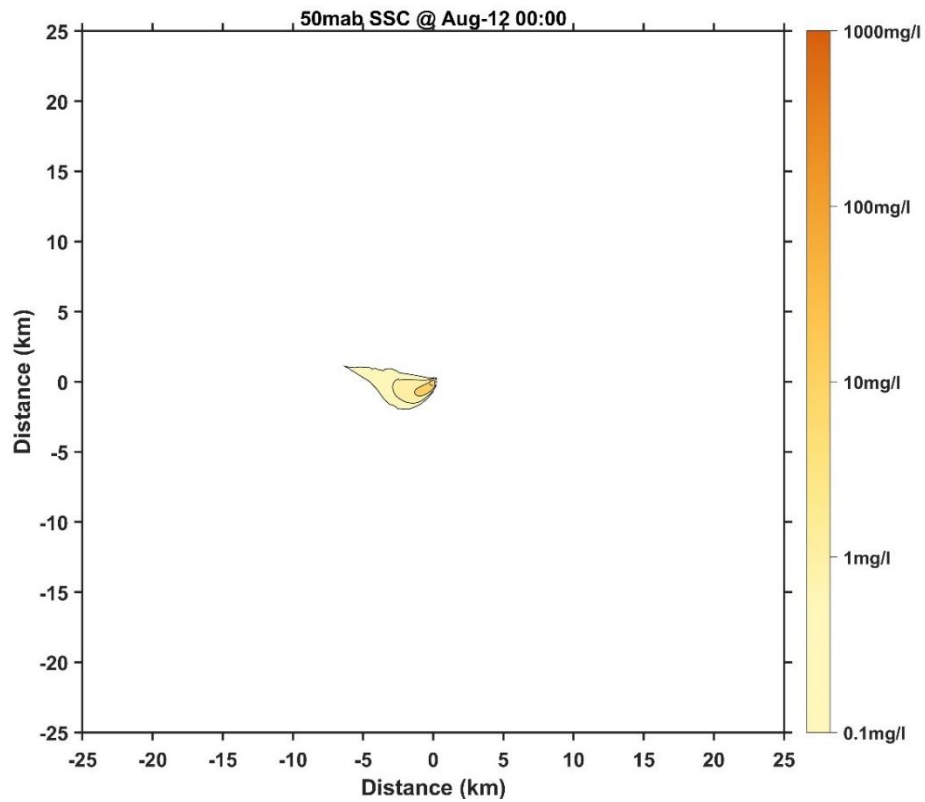
Figure 195 Horizontal distribution of SSC at 50 mab for Case 8 (3 days later)
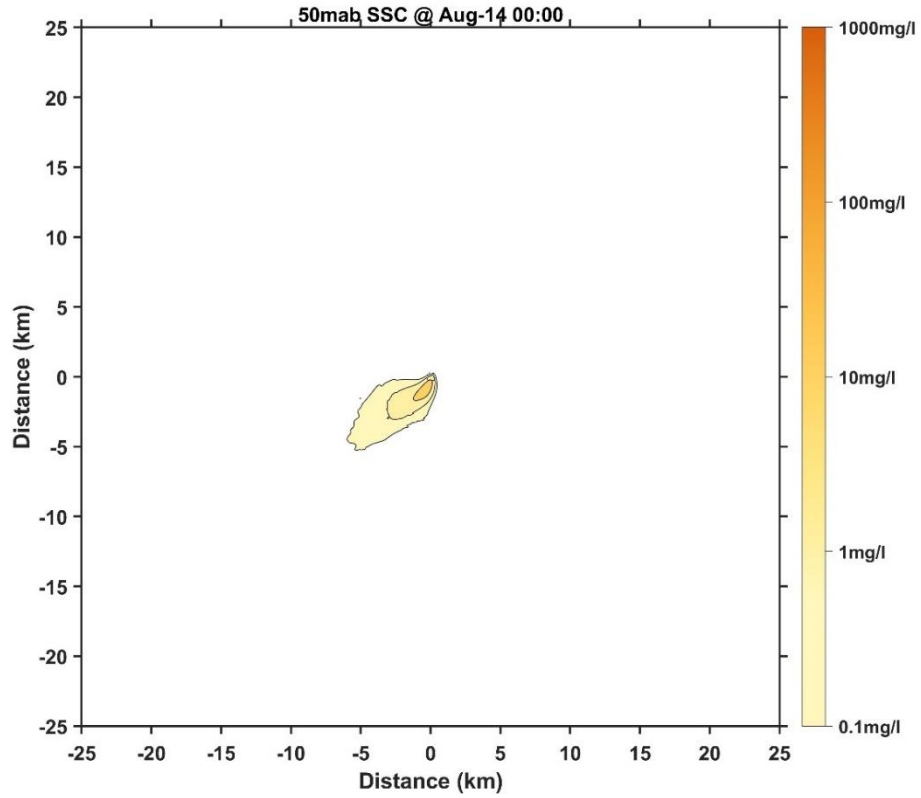
Figure 196 Horizontal distribution of SSC at 50 mab for Case 8 (5 days later)
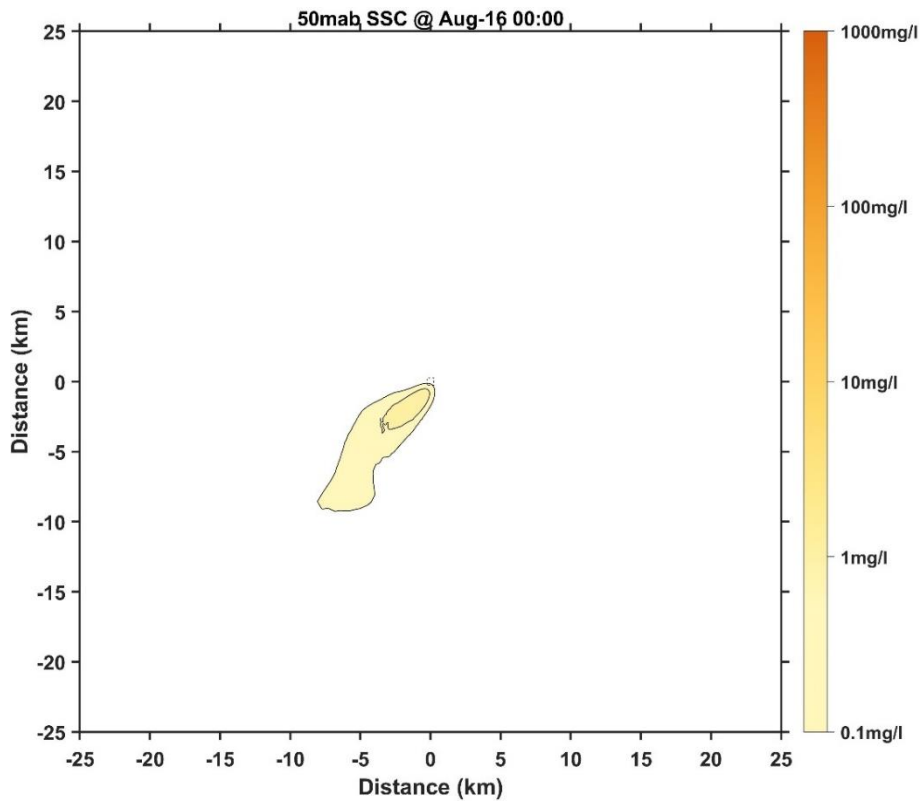
Figure 197 Horizontal distribution of SSC at 50 mab for Case 8 (7 days later)

704
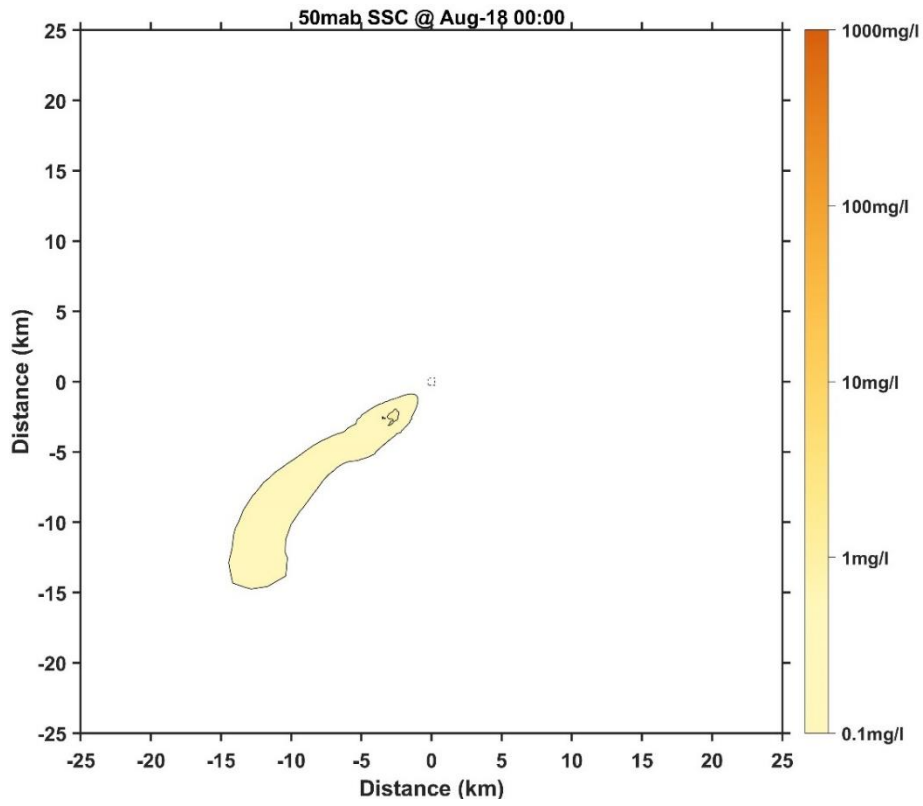
Figure 198 Horizontal distribution of SSC at 50 mab for Case 8 (9 days later)
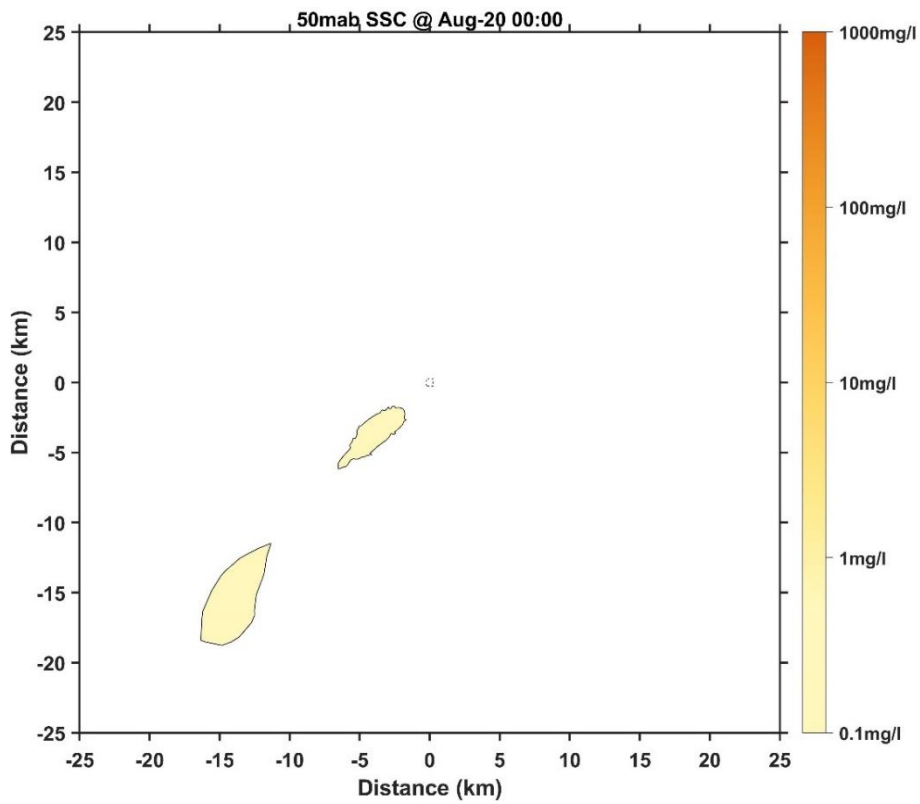
Figure 199 Horizontal distribution of SSC at 50 mab for Case 8 (11 days later)
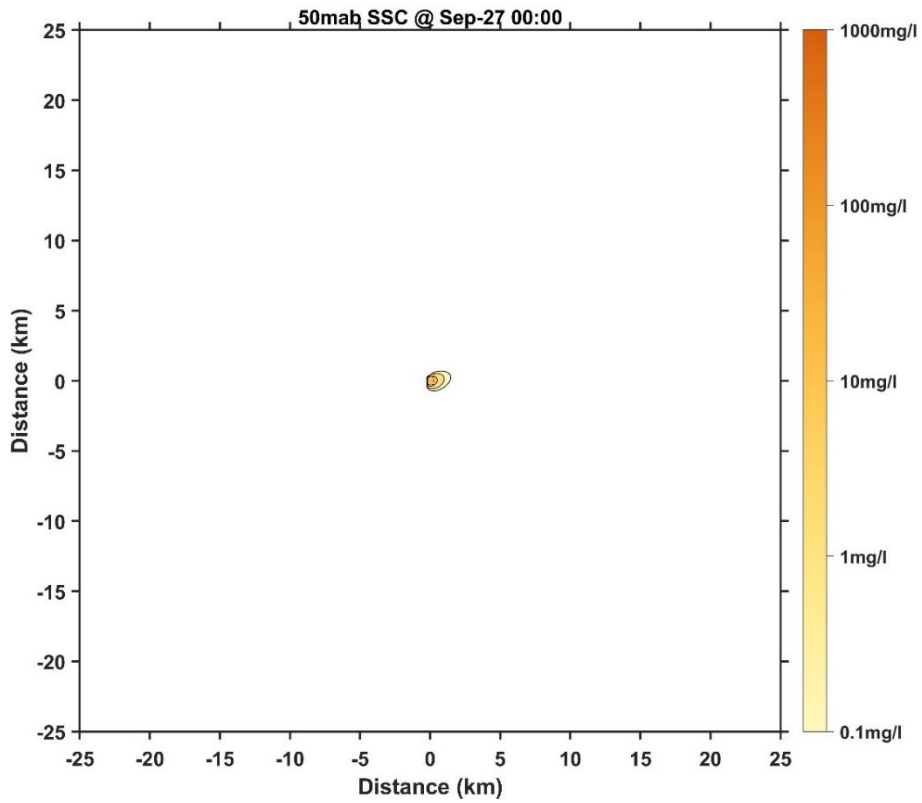
Figure 200 Horizontal distribution of SSC at 50 mab for Case 9 (1 day later)
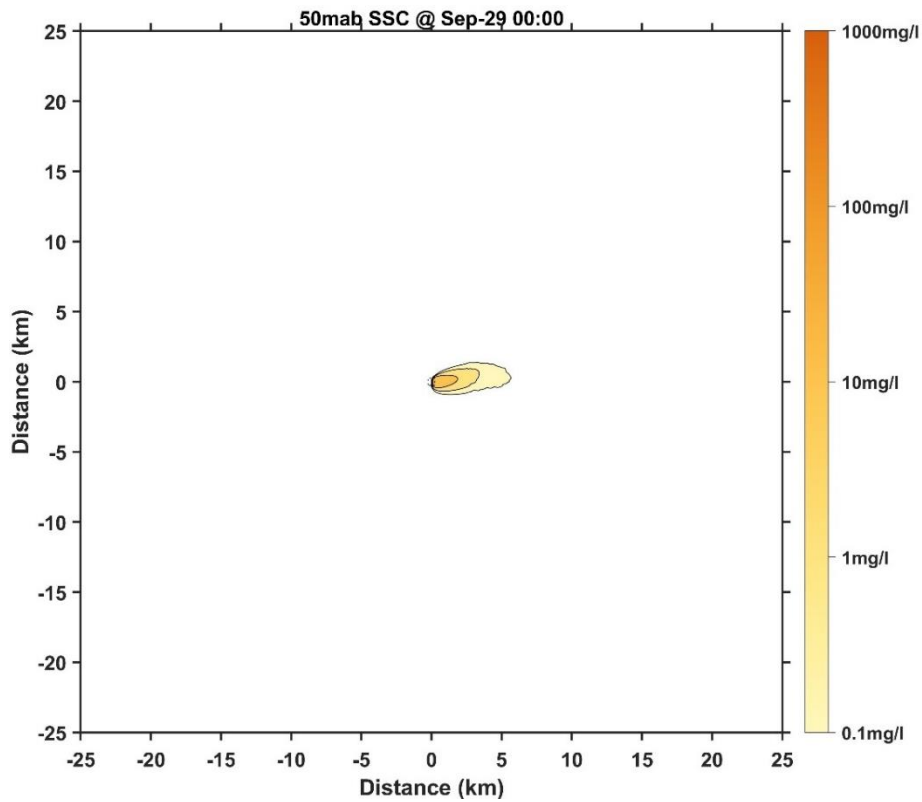
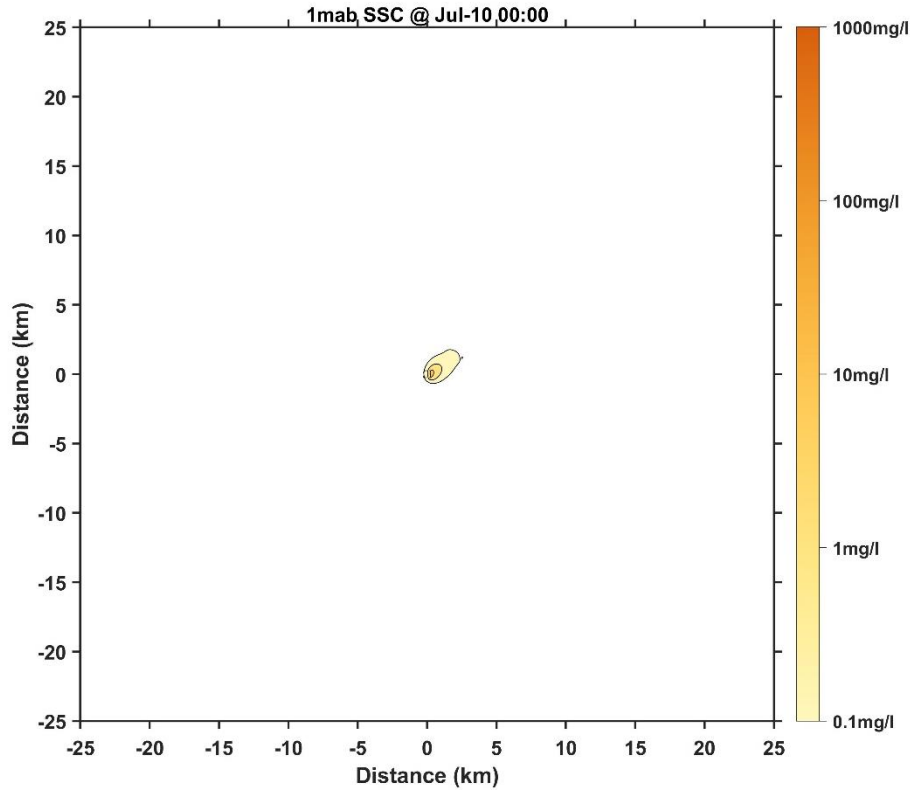Figure 201 Horizontal distribution of SSC at 50 mab for Case 9 (3 days later)
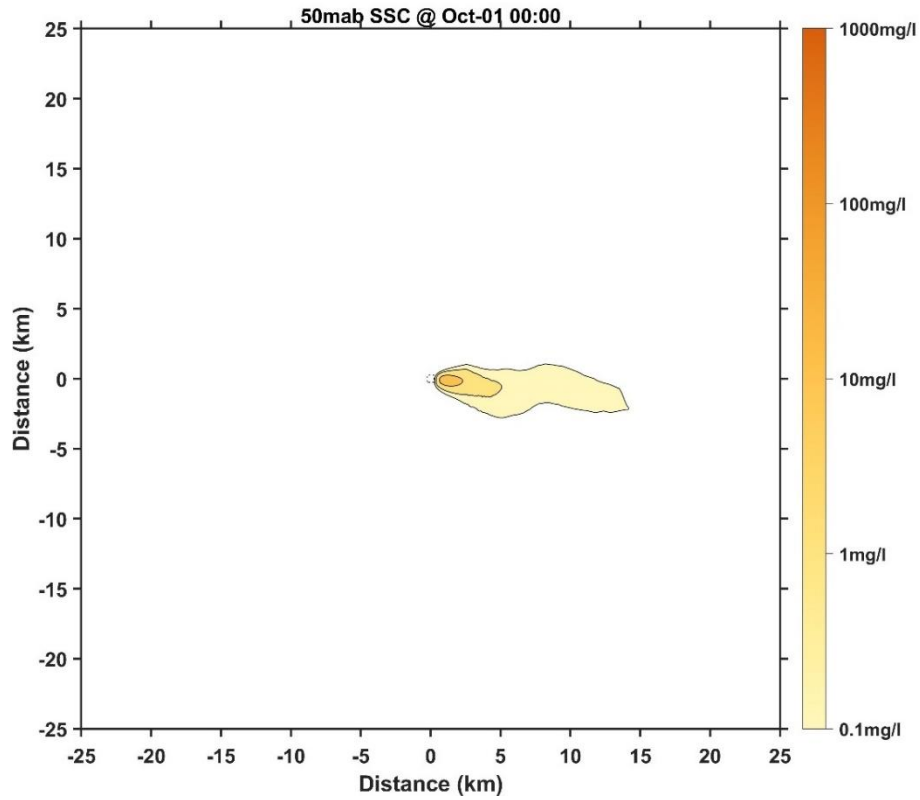
Figure 202 Horizontal distribution of SSC at 50 mab for Case 9 (5 days later)
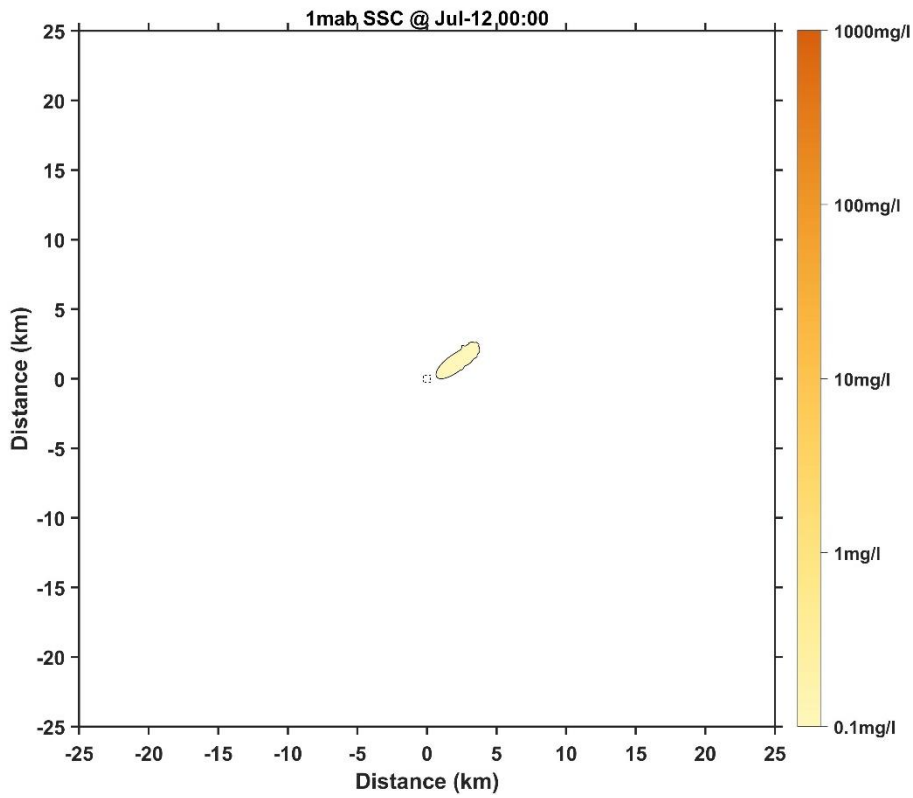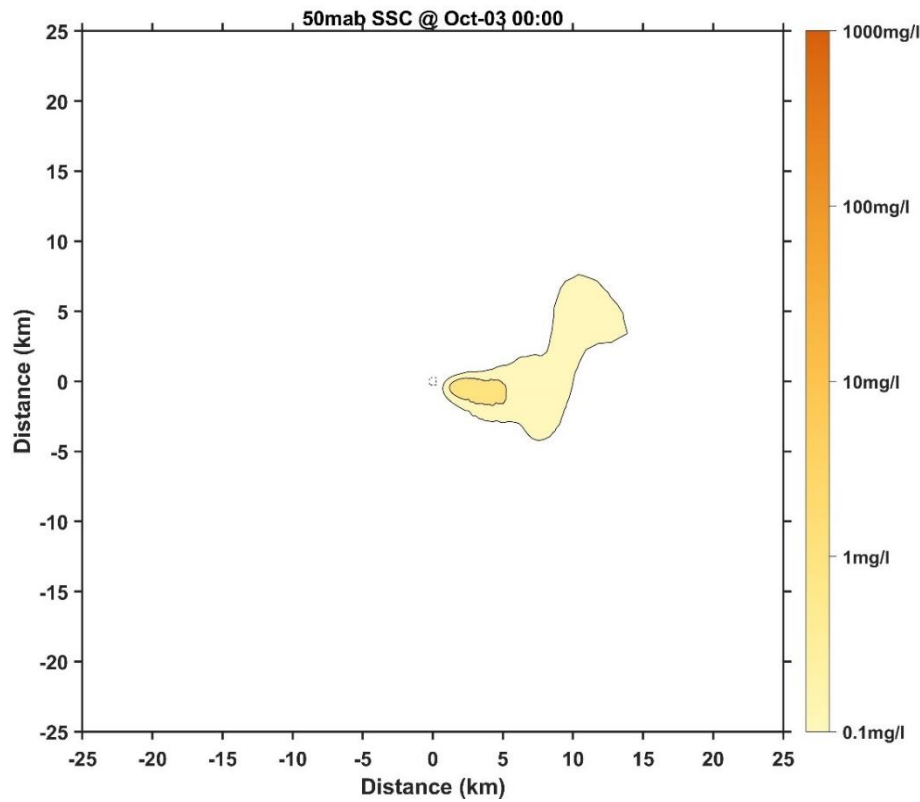

Figure 203 Horizontal distribution of SSC at 50 mab for Case 9 (7 days later)
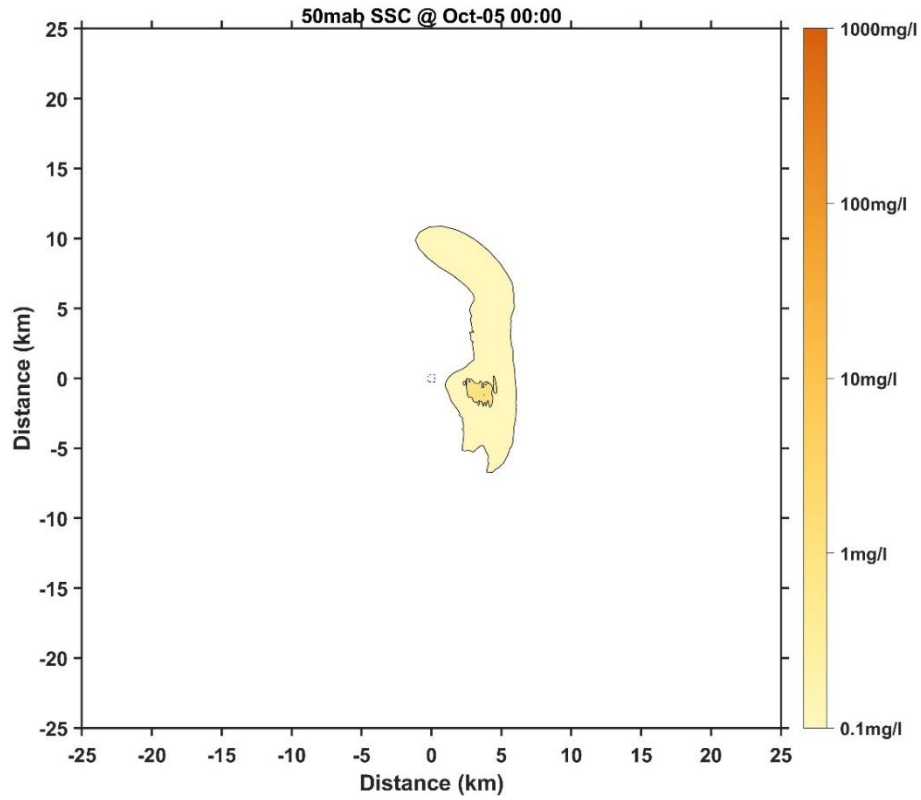
Figure 204 Horizontal distribution of SSC at 50 mab for Case 9 (9 days later)
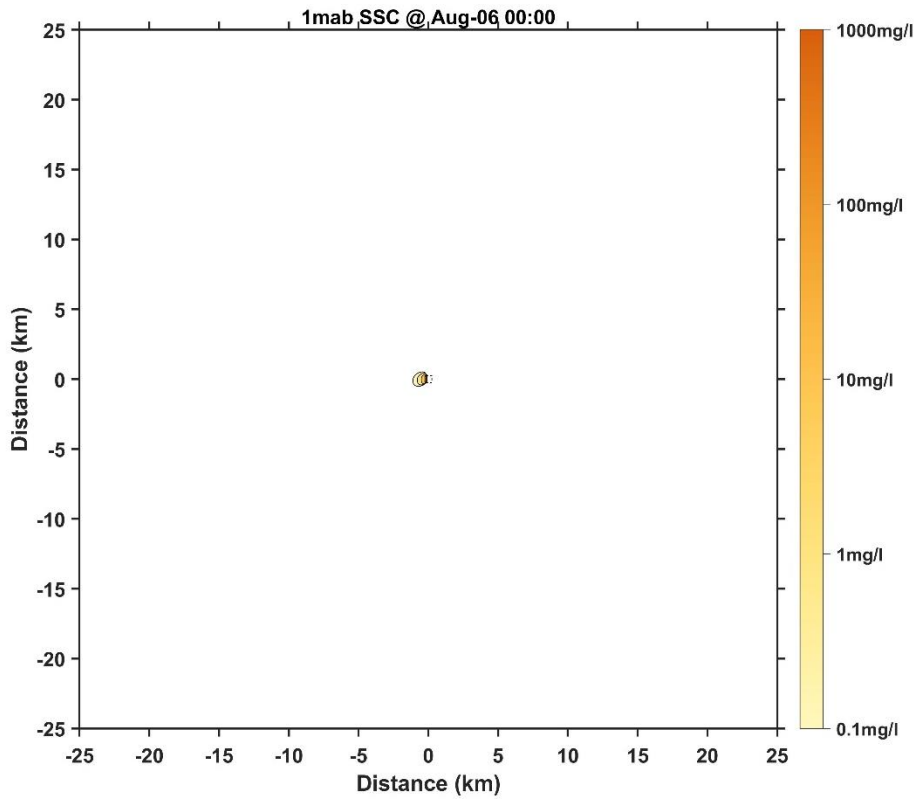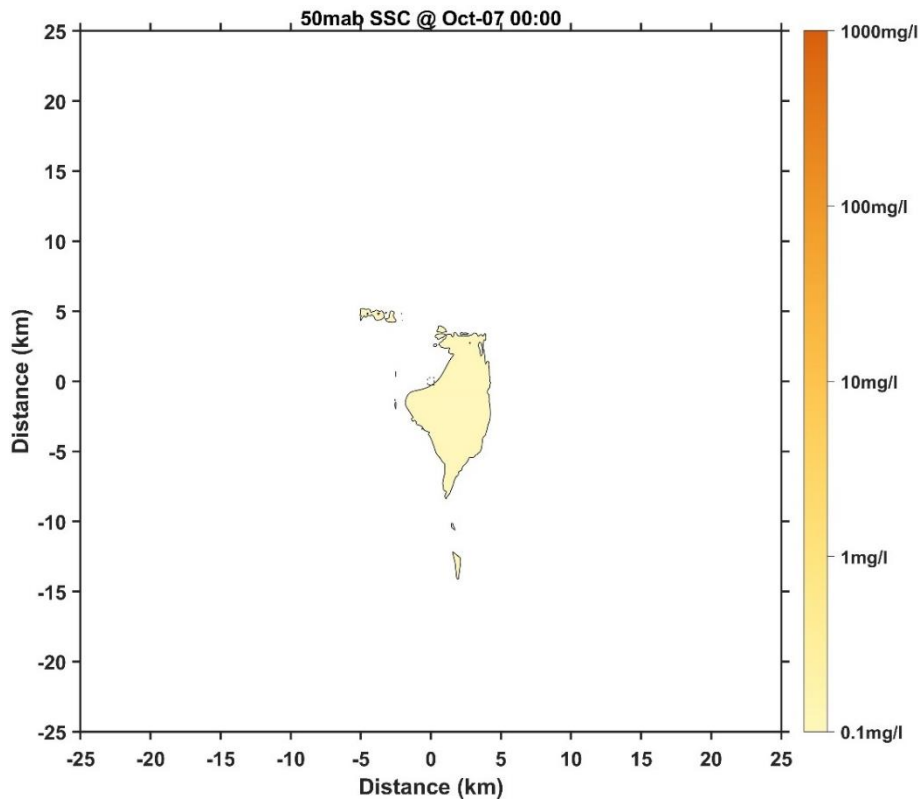

Figure 205 Horizontal distribution of SSC at 50 mab for Case 9 (11 days later)
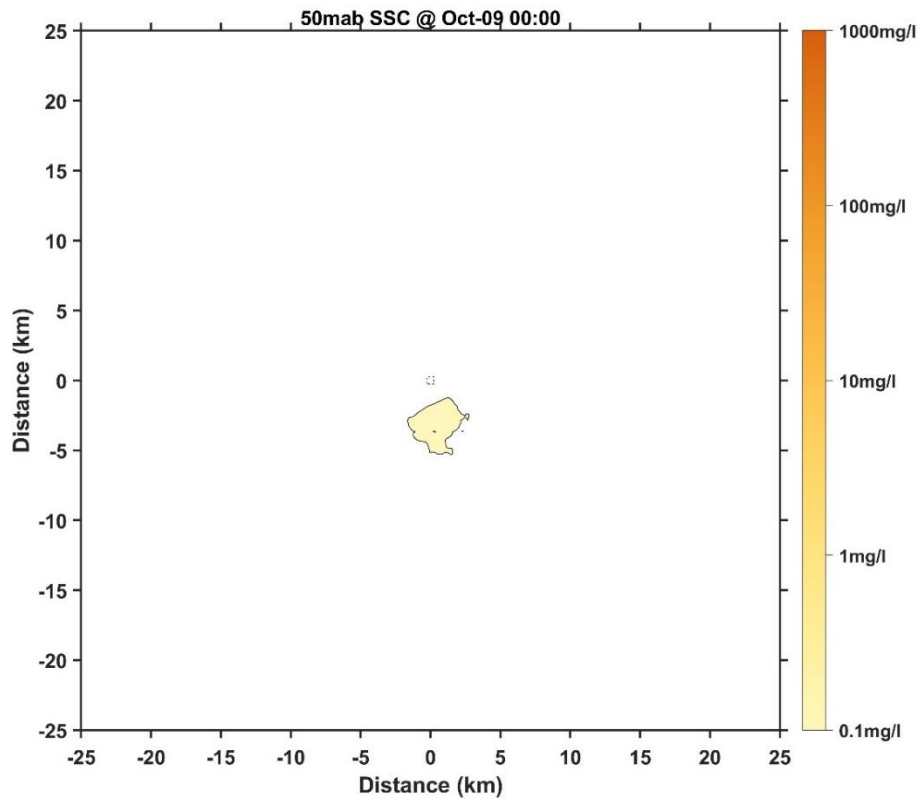
Figure 206 Horizontal distribution of SSC at 50 mab for Case 9 (13 days later)
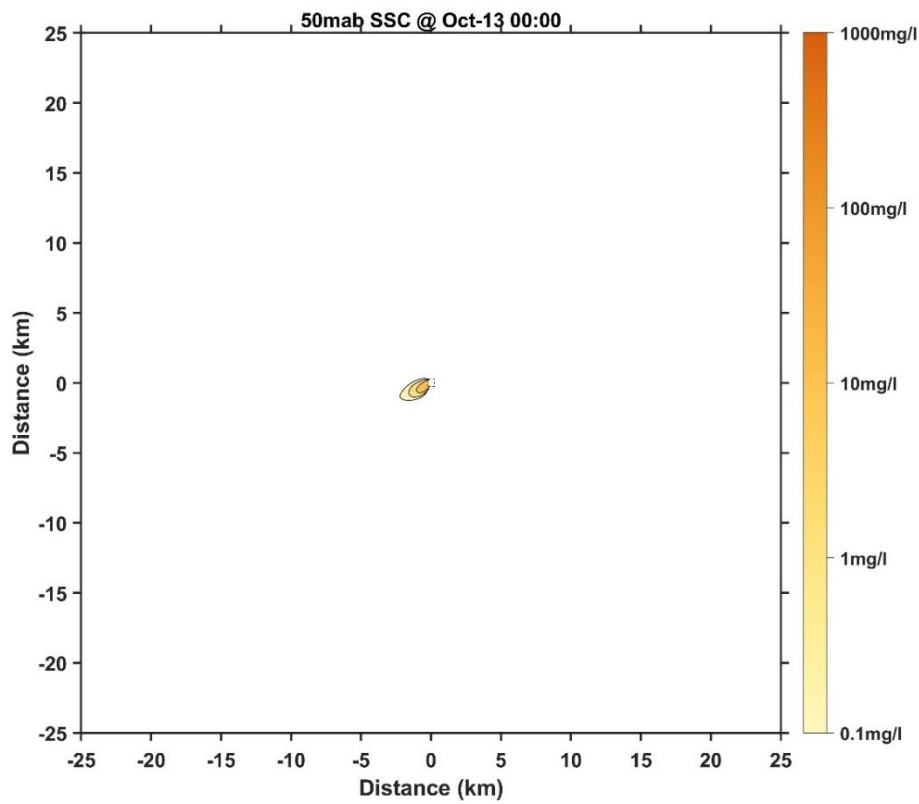
Figure 207 Horizontal distribution of SSC at 50 mab for Case 10 (1 day later)
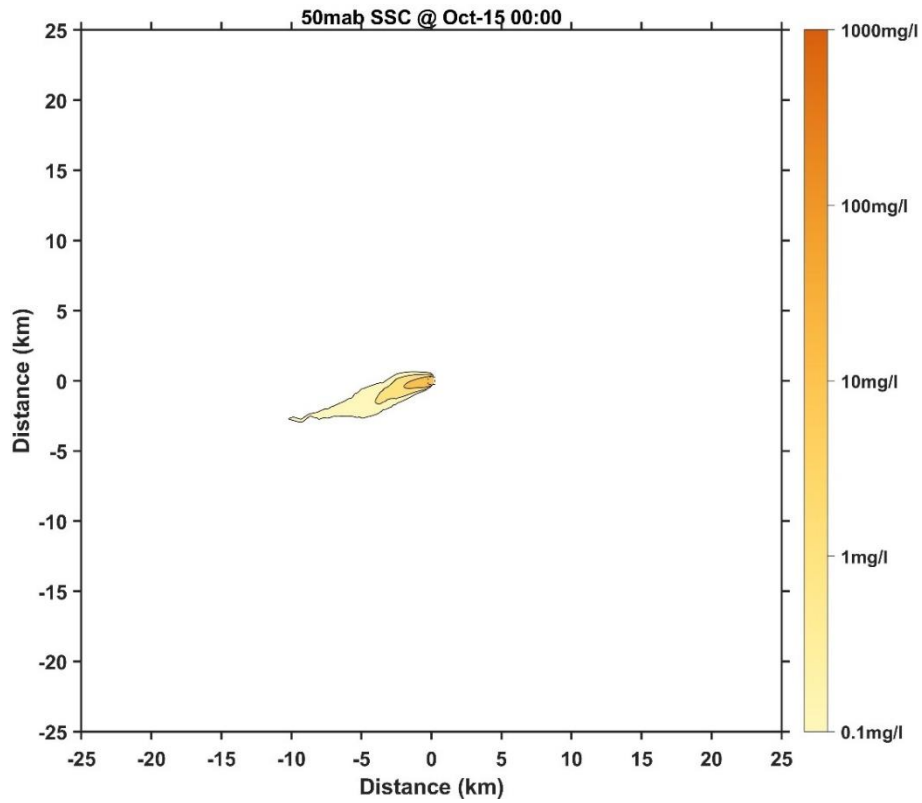
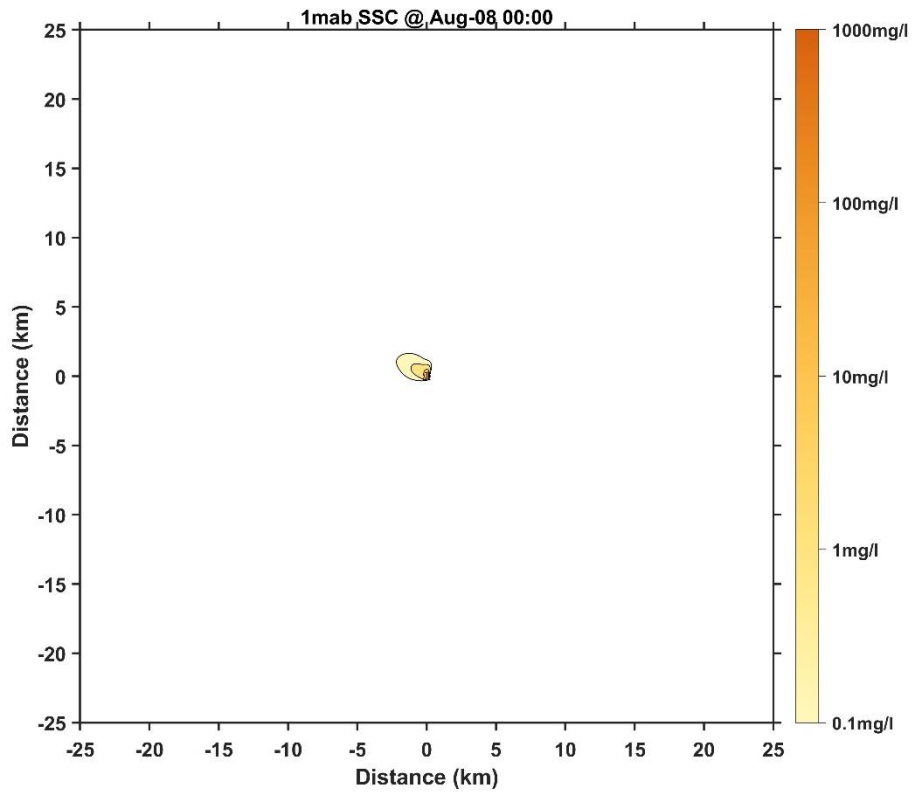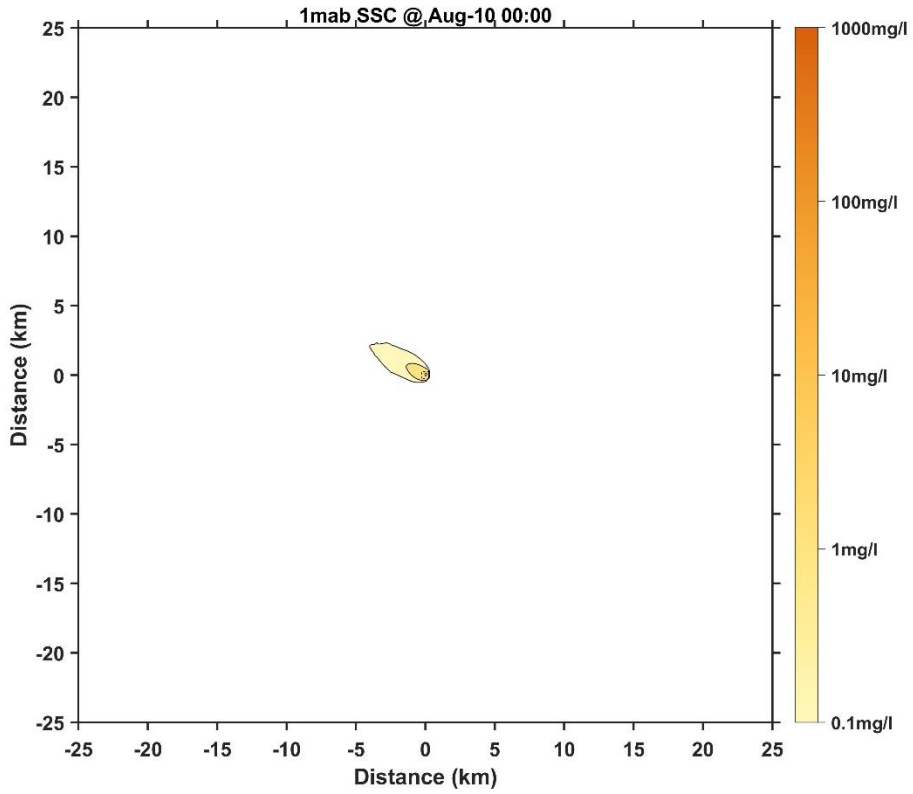Figure 208 Horizontal distribution of SSC at 50 mab for Case 10 (3 days later)
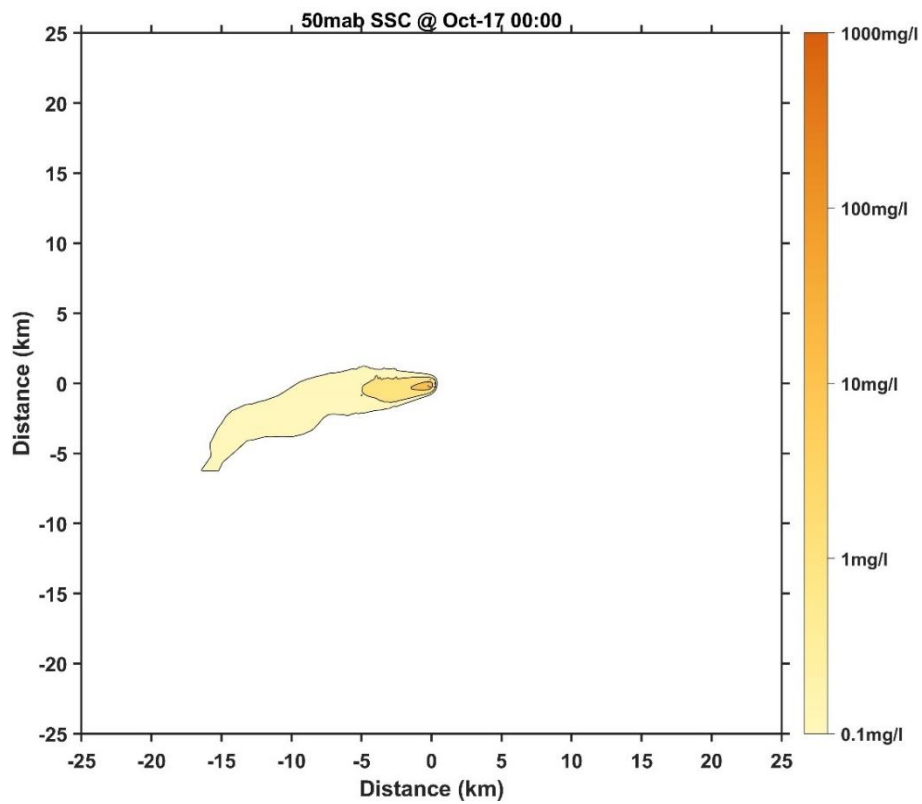
Figure 209 Horizontal distribution of SSC at 50 mab for Case 10 (5 days later)
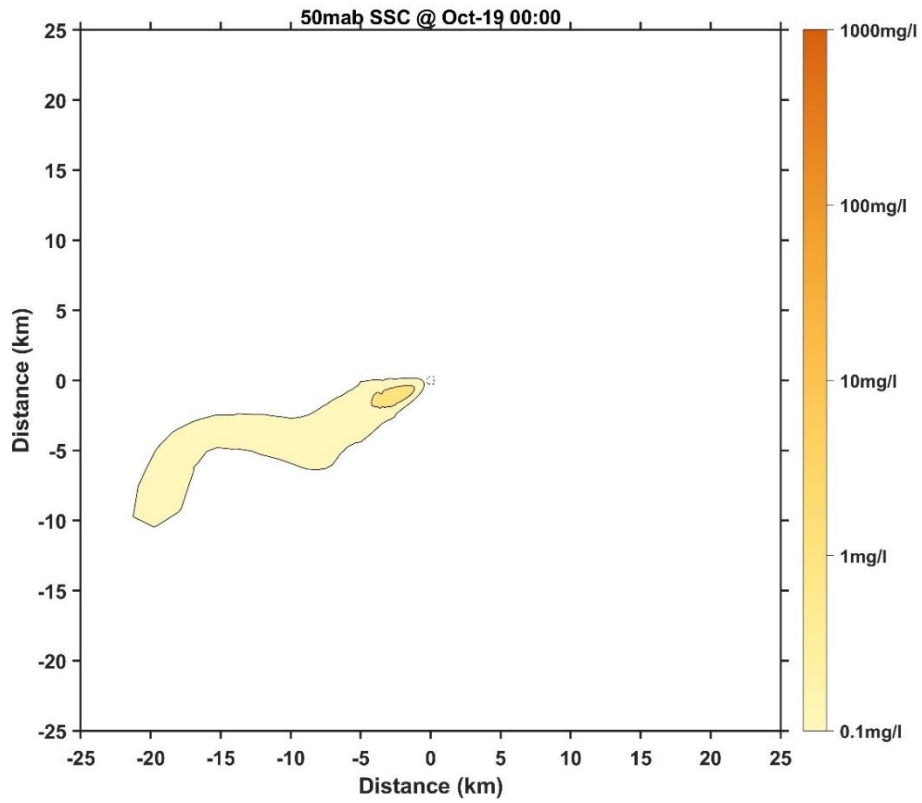
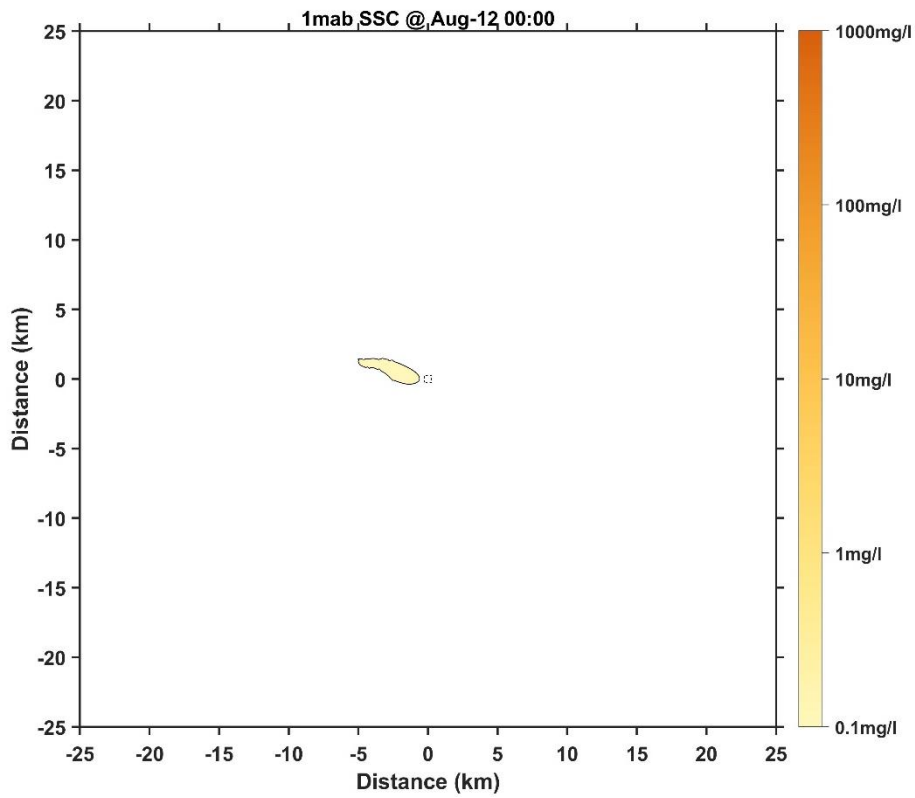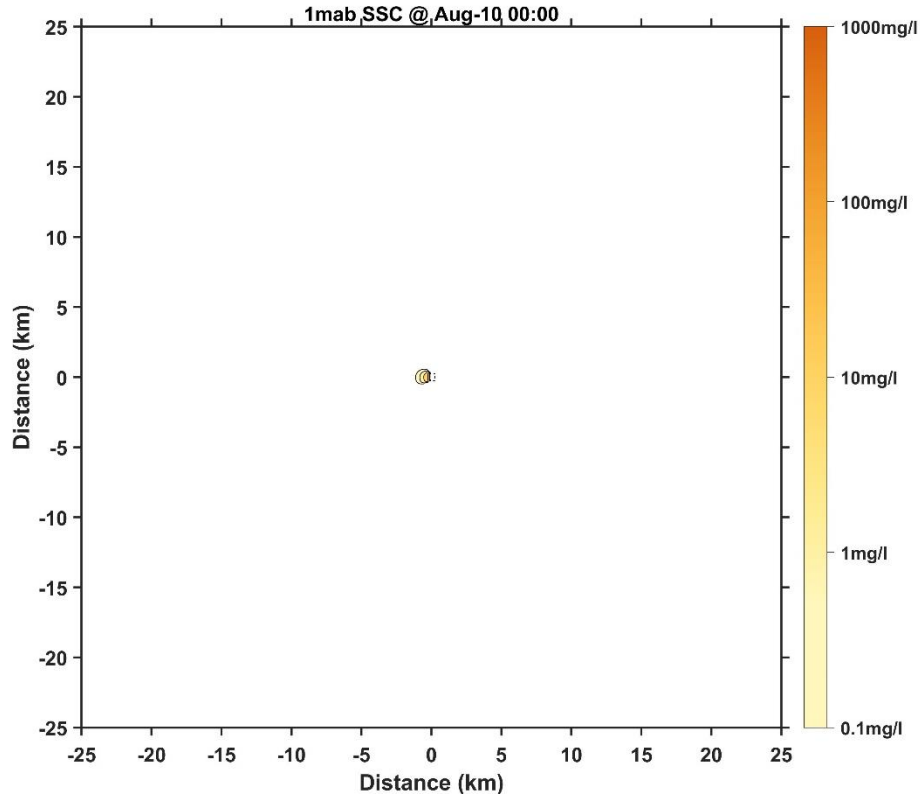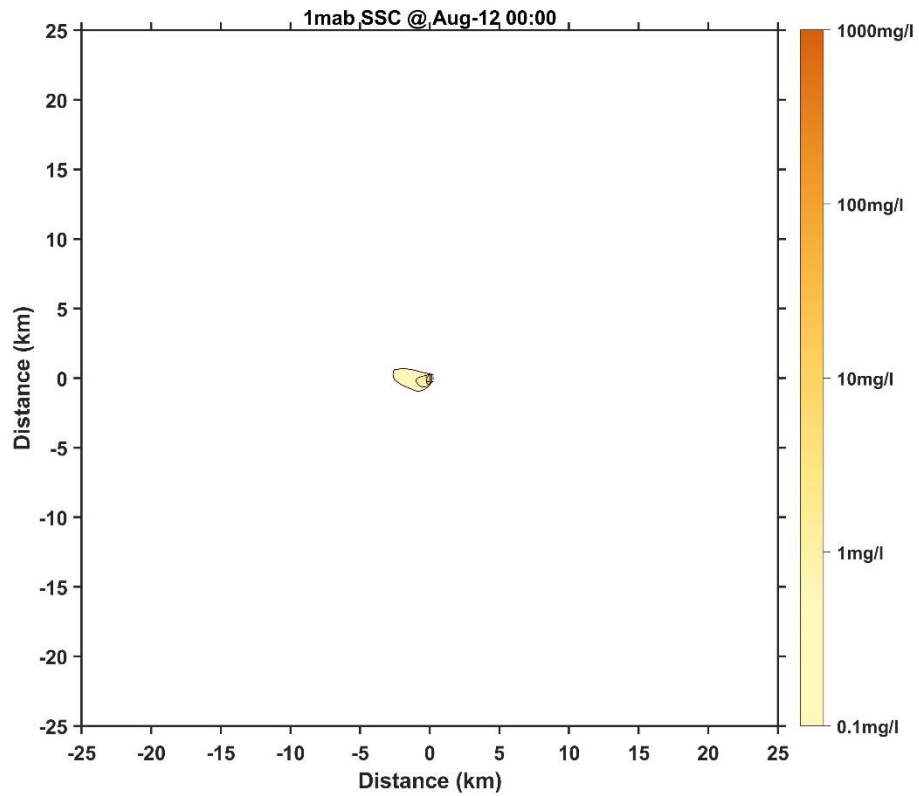Figure 210 Horizontal distribution of SSC at 50 mab for Case 10 (7 days later)

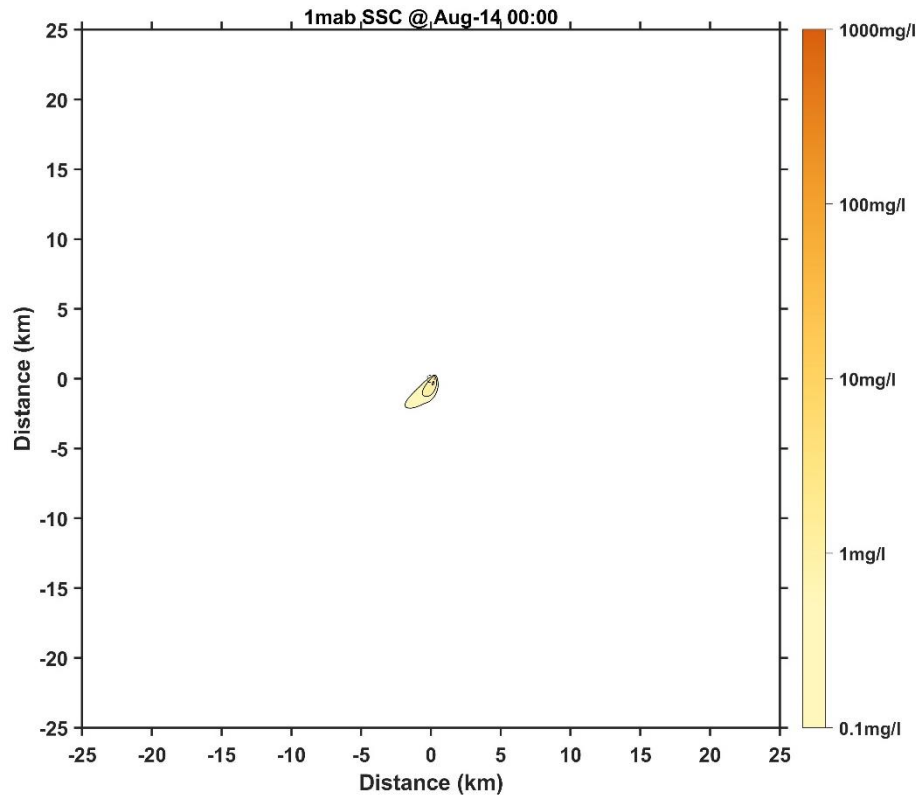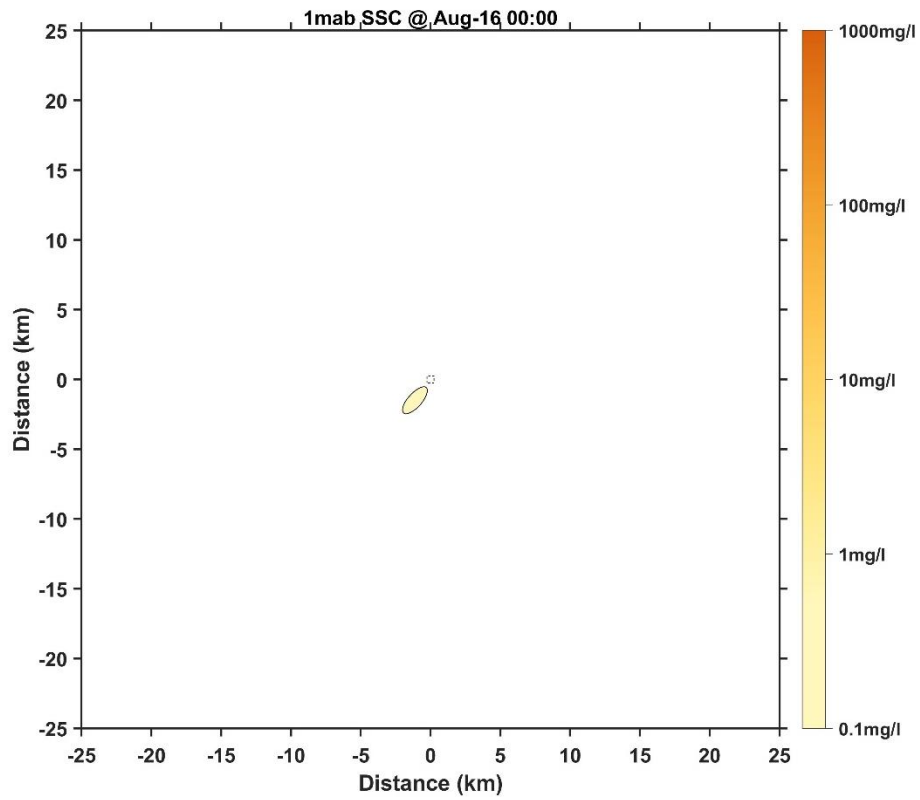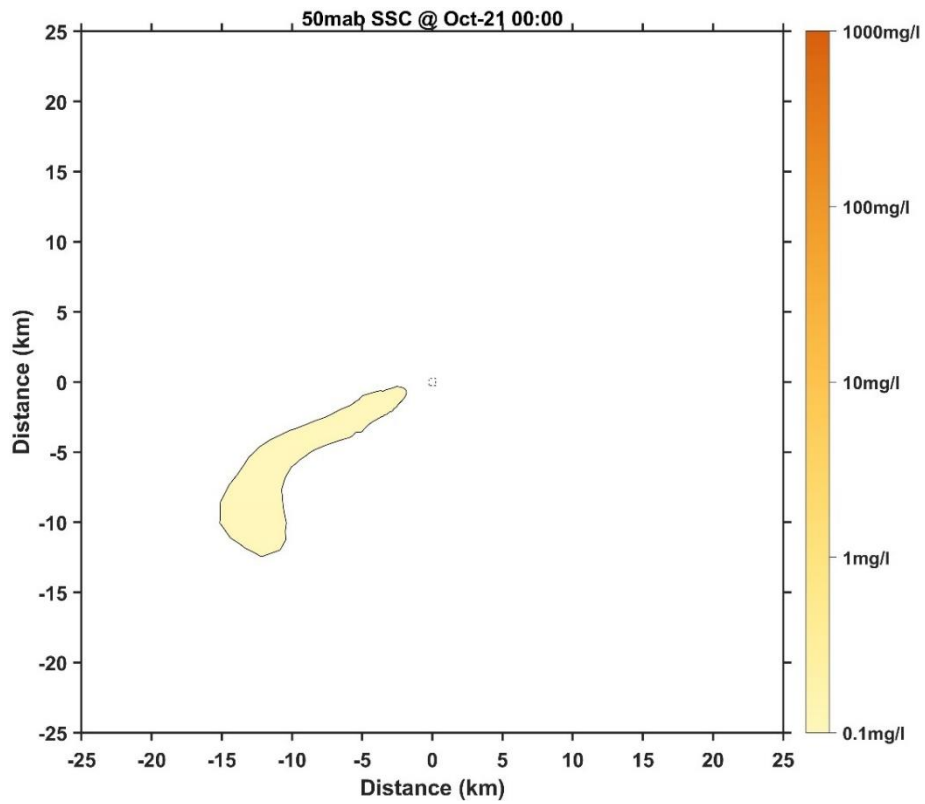Figure 211 Horizontal distribution of SSC at 50 mab for Case 10 (9 days later)
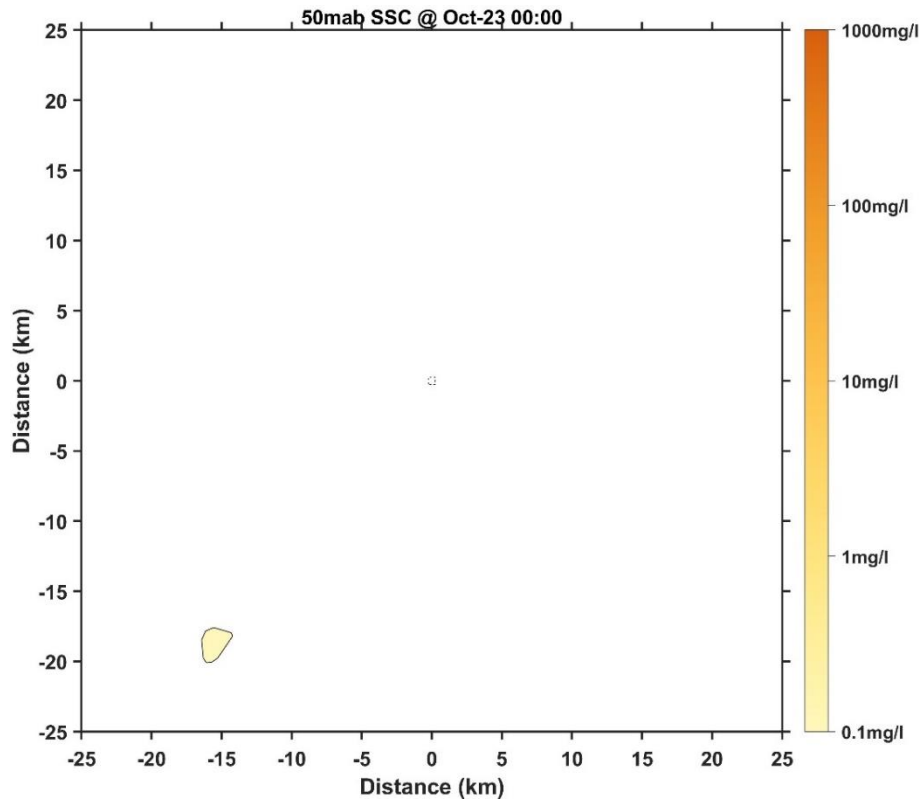
Figure 212 Horizontal distribution of SSC at 50 mab for Case 10 (11 days later)

2 Characteristics of Plume Vertical Dispersion

The monitoring points were selected 100 m from the boundary of the CTA (Fig. 213). Due to the different directions of plume dispersion in each month, the monitoring points were selected 100 m from the western boundary in Cases 2, 3, 5, 7, 8 and 10, and 100 m from the eastern boundary in Cases 1, 4, 6 and 9 to analyze the vertical distribution characteristics of deep-sea mining plume dispersion. Figure 214 to Figure 223 show that, on average, the maximum vertical diffusion height of 10 mg/l suspended sediment concentration is 64 m from the bottom (Case 5), the maximum diffusion height of 1 mg/l is 130 m (Case 1), and the maximum vertical diffusion height of 0.1 mg/l suspended sediment concentration is 231 m from the bottom (Case 1). In extreme cases, the maximum vertical diffusion height for a suspended sediment concentration of 10 mg/l is 113 m from the bottom (Case 6), the maximum diffusion height for 1 mg/l is 215 m (Case 6), and the maximum vertical diffusion height for a suspended sediment concentration of 0.1 mg/l is 346 m from the bottom (Case 6).
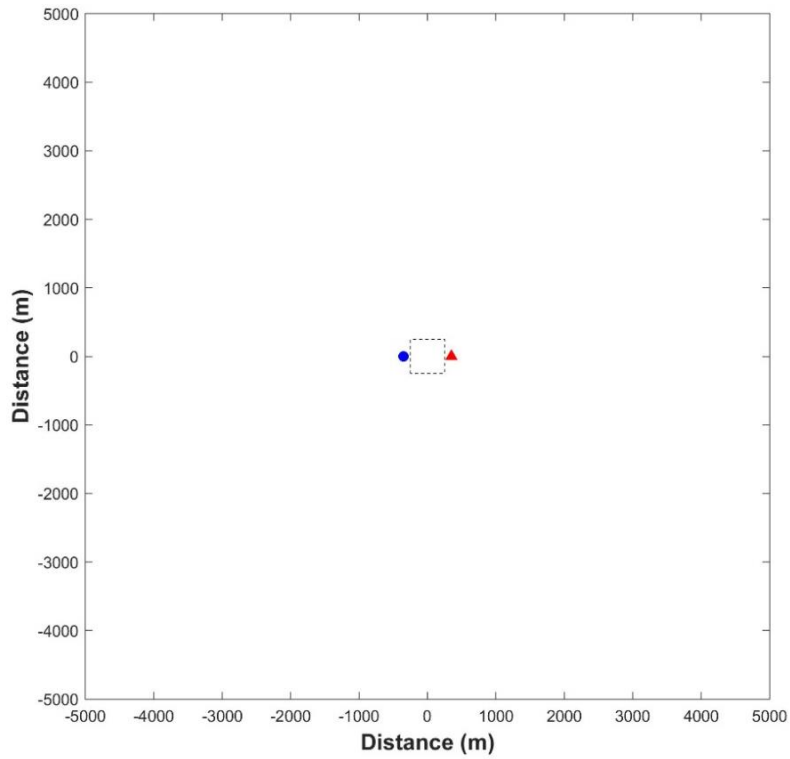
Figure 213 Location map of selected sites 100m away from the eastern (red) and western (blue) boundaries of the CTA
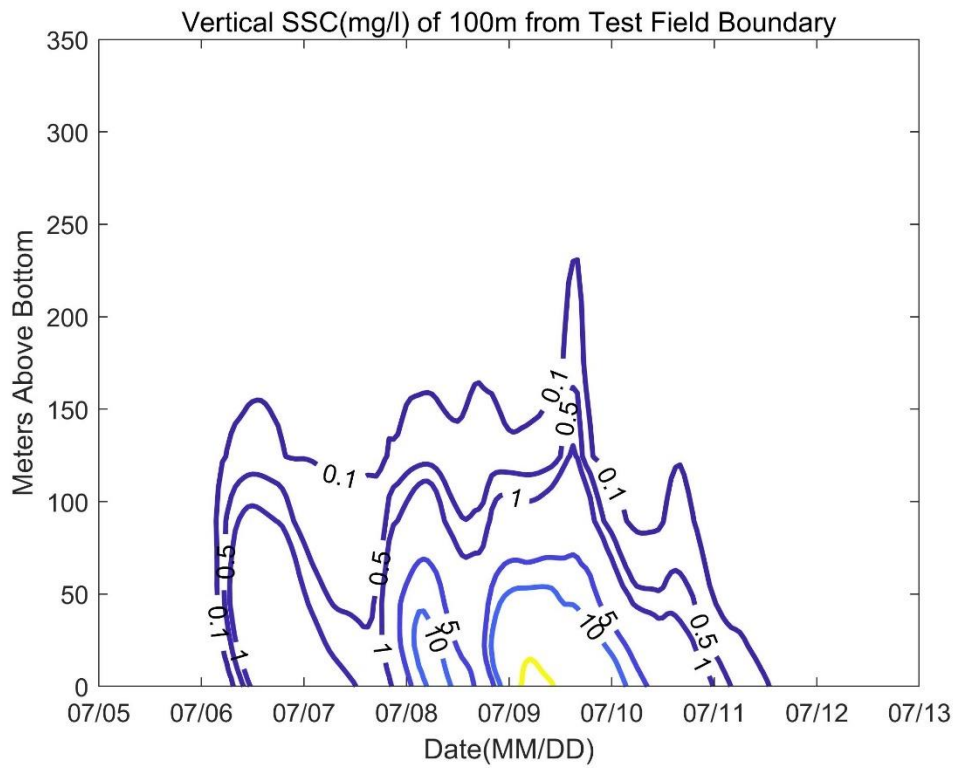
Figure 214 Vertical distribution of SSC at 100 m from the eastern boundary for Case 1
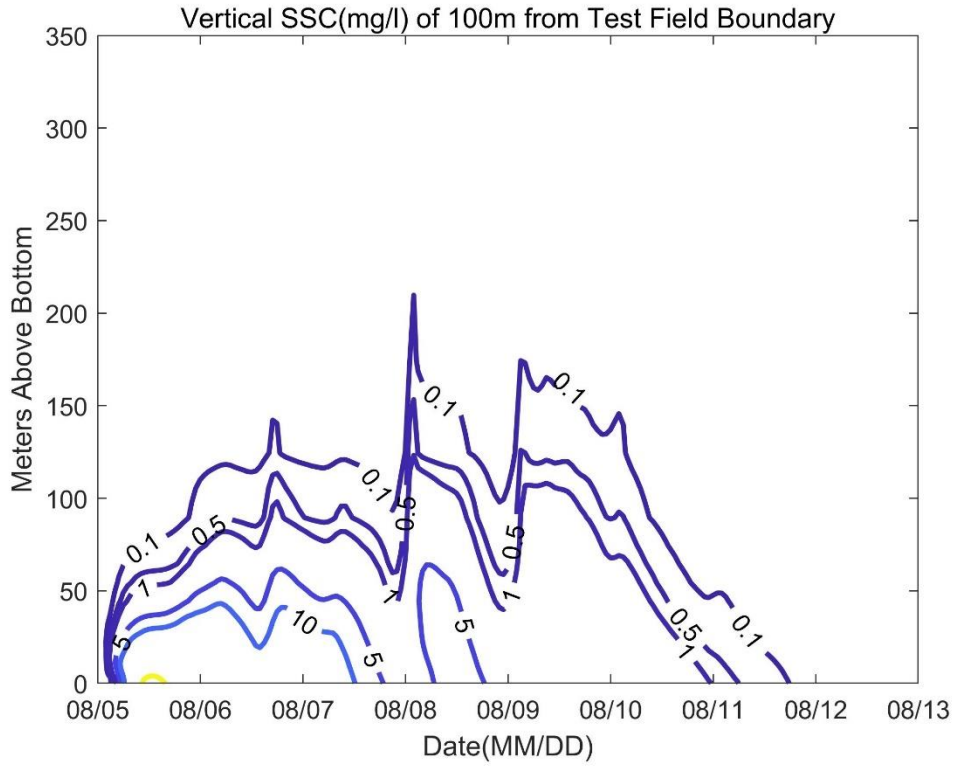
Figure 215 Vertical distribution of SSC at 100 m from the western boundary for Case 2
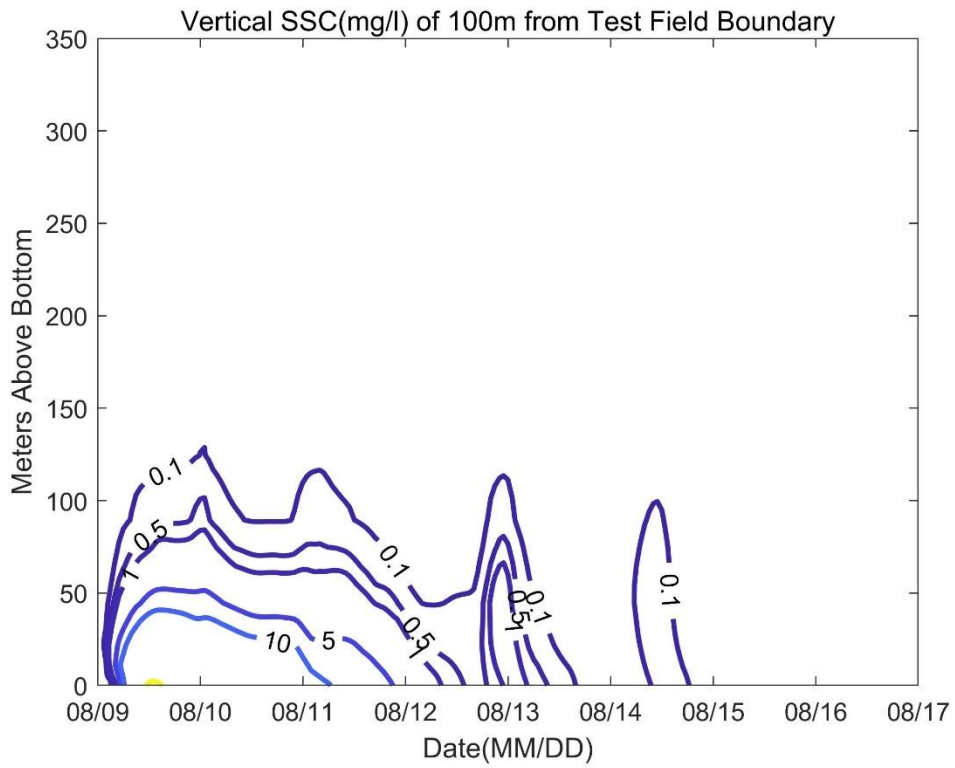
Figure 216 Vertical distribution of SSC at 100 m from the western boundary for Case 3
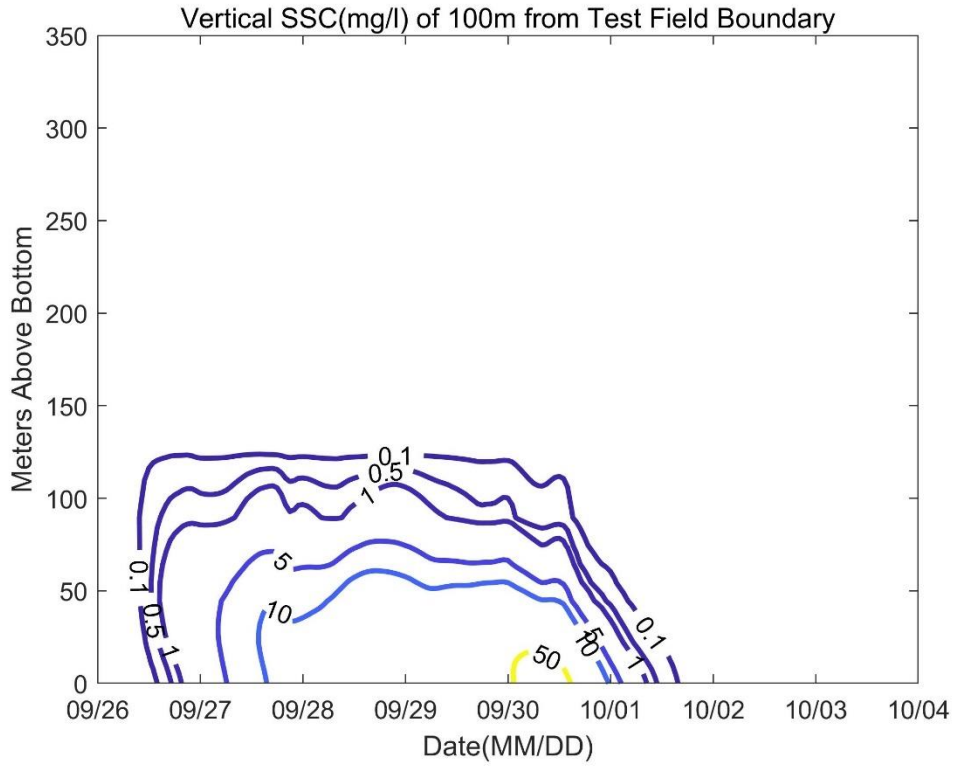
Figure 217 Vertical distribution of SSC at 100 m from the eastern boundary for Case 4
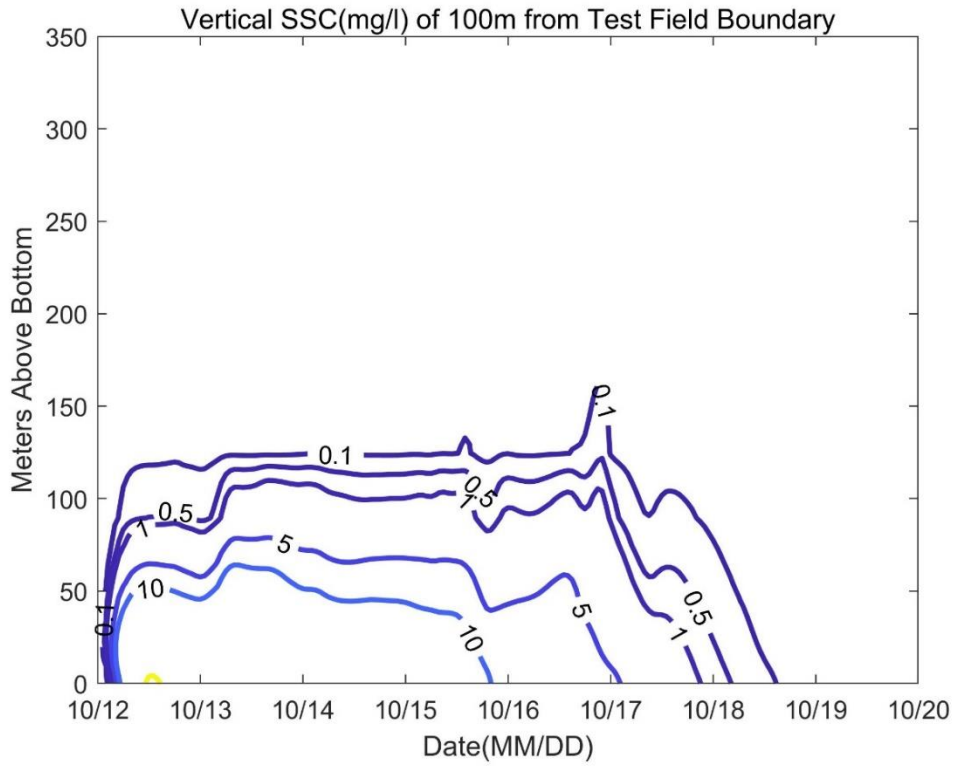
Figure 218 Vertical distribution of SSC at 100 m from the western boundary for Case 5
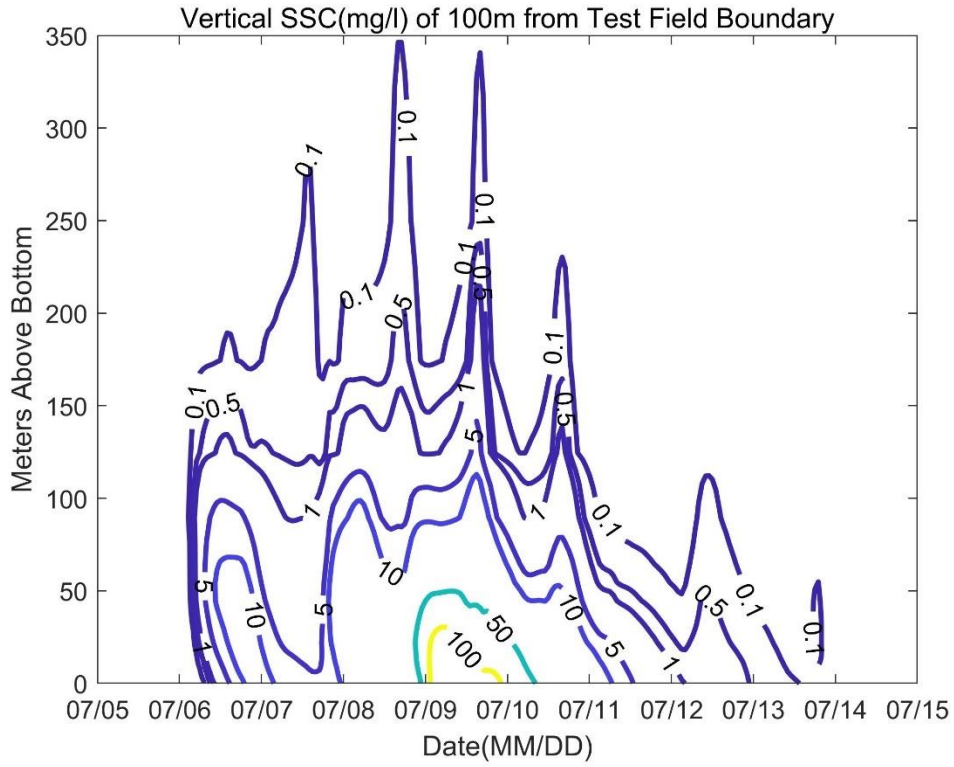
Figure 219 Vertical distribution of SSC at 100 m from the eastern boundary for Case 6
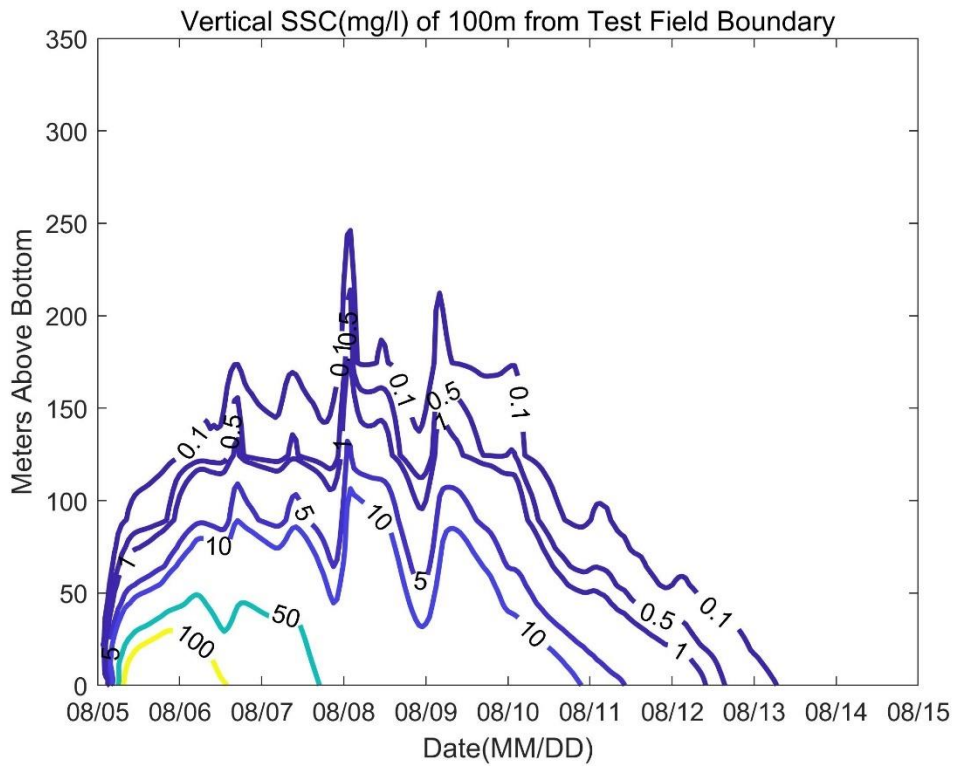
Figure 220 Vertical distribution of SSC at 100 m from the western boundary for Case 7
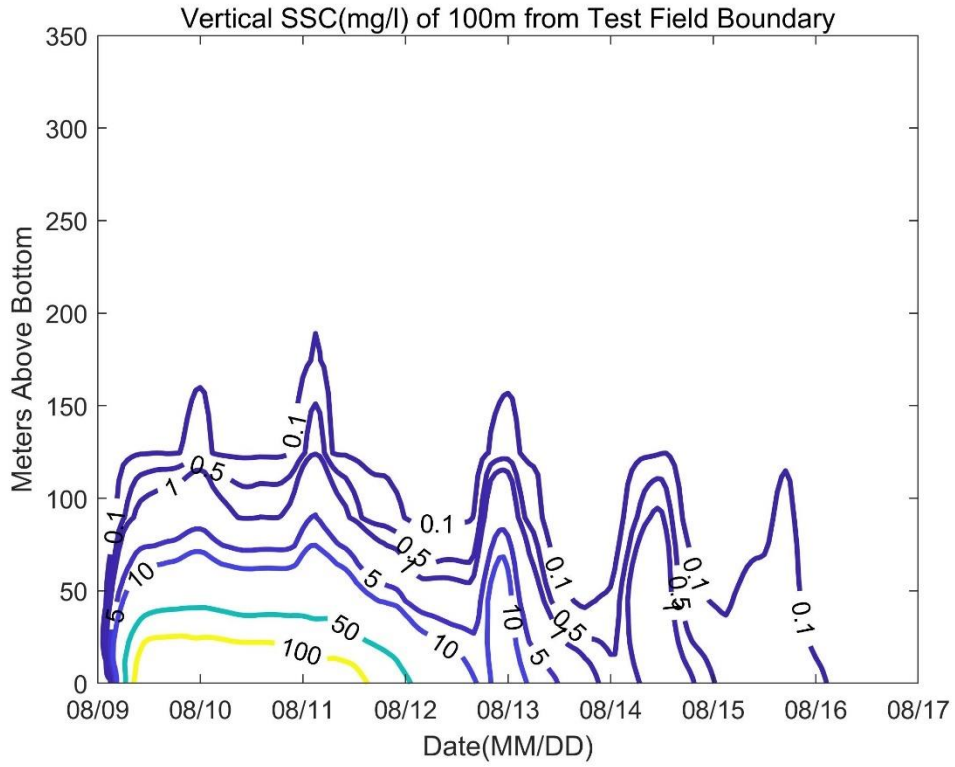
Figure 221 Vertical distribution of SSC at 100 m from the western boundary for Case 8
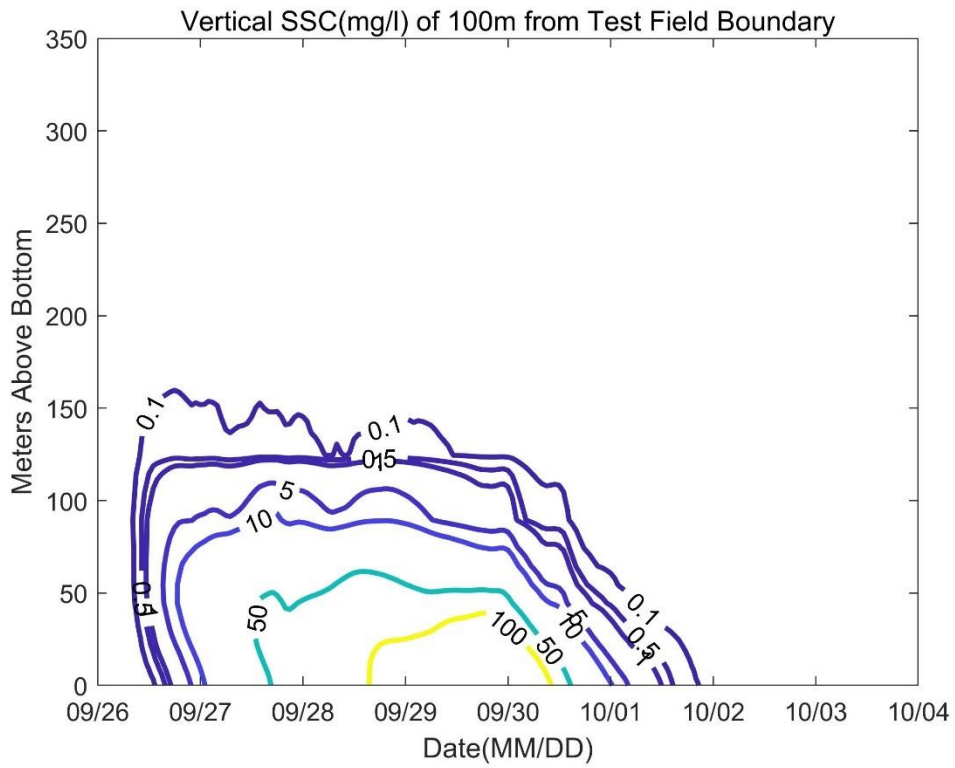
Figure 222 Vertical distribution of SSC at 100 m from the eastern boundary for Case 9
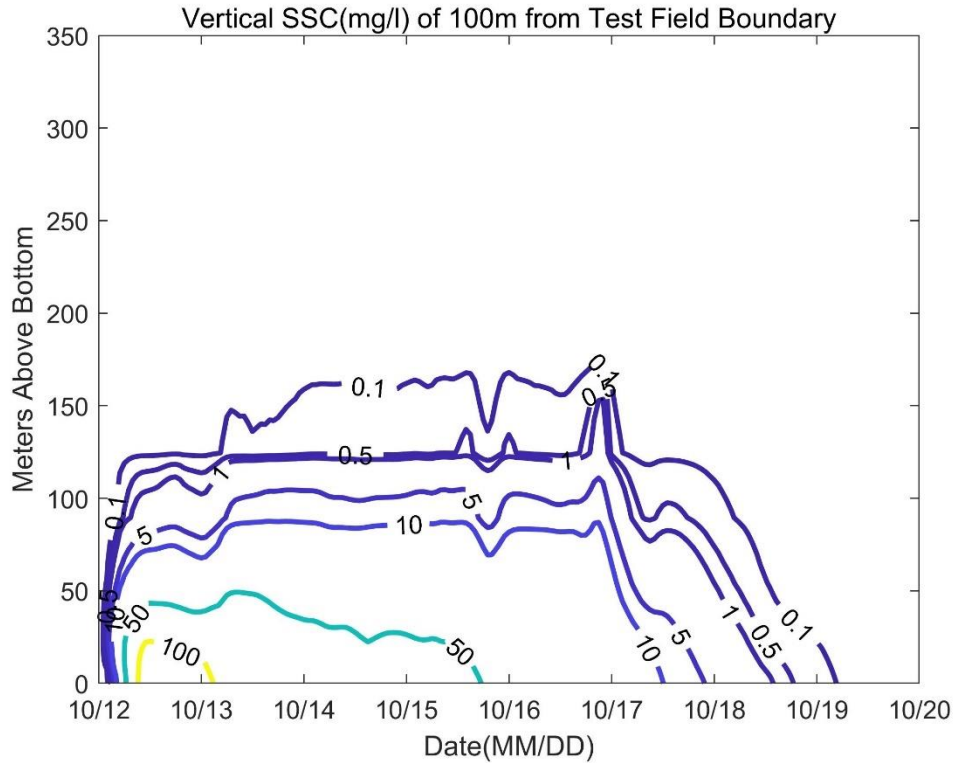
Figure 223 Vertical distribution of SSC at 100 m from the western boundary for Case 10

3 Characteristics of Redeposition Thickness Distribution

Figure 224 to Figure 233 show the thickness of re-sedimentation 10 days after the end of each working condition. It can be seen from the figures that the re-sedimentation thickness of each working condition is greater than 1 cm and is located in the test area. On average, the maximum re-sedimentation thickness of each working condition is between 1.85 and 2.60 cm, of which the maximum re-sedimentation thickness of working condition 1 is the largest, reaching 2.60 cm; the maximum re-sedimentation thickness of working condition 5 is the smallest, at 1.85 cm. In extreme cases, the maximum re-sedimentation thickness of each working condition is between 0.85 and 1.48 cm, of which the maximum re-sedimentation thickness of working condition 8 is 1.48 cm; the maximum re-sedimentation thickness of working condition 10 is 0.85 cm.

In terms of the area distribution of re-deposited thickness, the area with a re-deposited thickness greater than 1 cm is not obviously different for each working condition, ranging from 0.28 to 0.31 km². The area with a re-deposited thickness greater than 1 mm is the largest in working Case 4, at 0.76 km², and the smallest in working Case 1, at 0.55 km². The area with a re-deposited thickness greater than 0.1 mm is the largest in working Case

5, at 3.51 km², Case 1 is the smallest, at 2.00 km²; the area with a re-sedimentation thickness greater than 0.01 mm is the largest in Case 4, at 12.48 km², and the smallest in Case 3, at 7.74 km². In extreme cases, the re-sedimentation thickness greater than 1 cm only occurs in Case 7 (0.04 km²) and 8 (0.17 km²), which is smaller than the average; the area with a re-sedimentation thickness greater than 1 mm Case 9 is the largest, with 0.87 km², and Case 6 is the smallest, with 0.56 km²; the area with a re-deposited thickness greater than 0.1 mm is Case 9, with 5.90 km², and Case 6 is the smallest, with 3.14 km²; the area with a re-deposited thickness greater than 0.01 mm is Case 9, with 34.04 km², and Case 10 is the smallest, with 17.75 km².
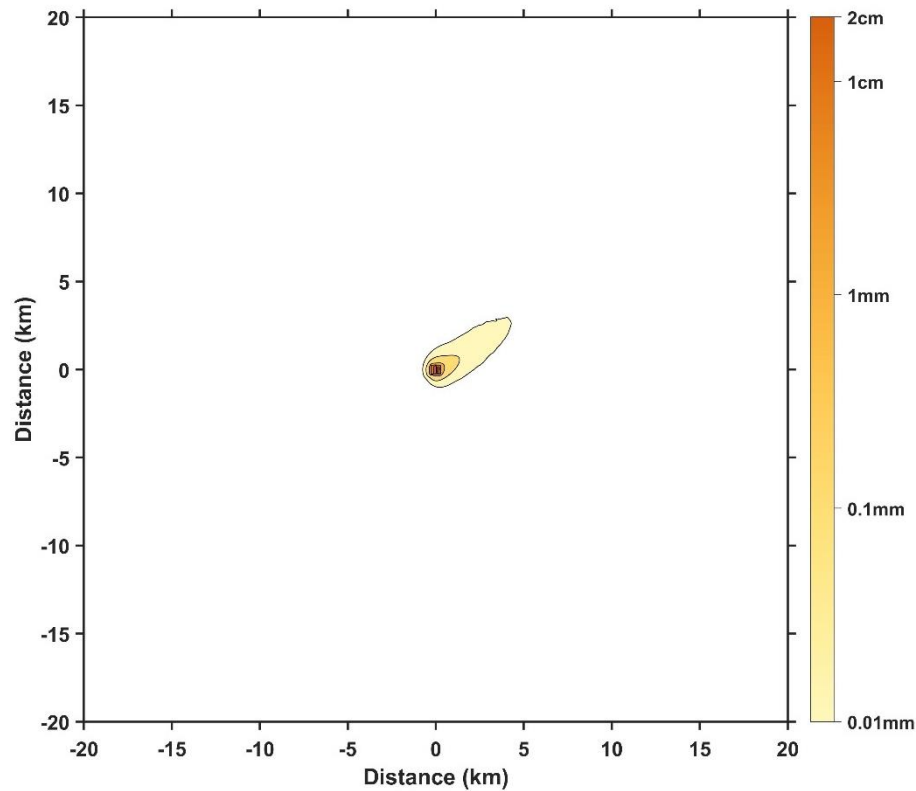
Figure 224 Redeposition thickness for Case 1
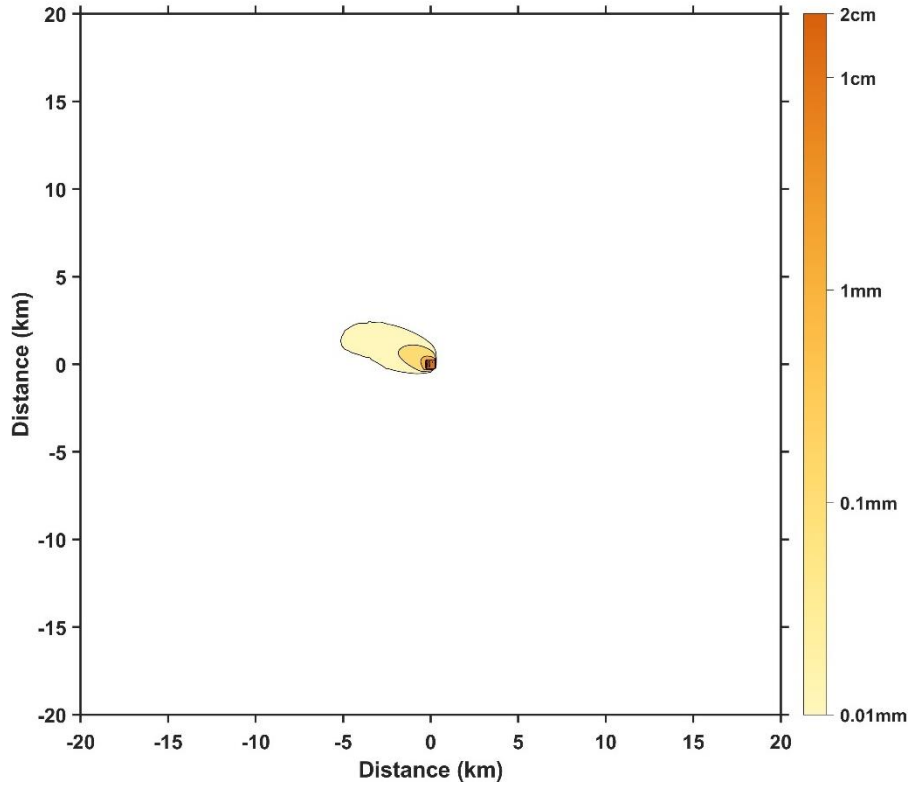
Figure 225 Redeposition thickness for Case 2
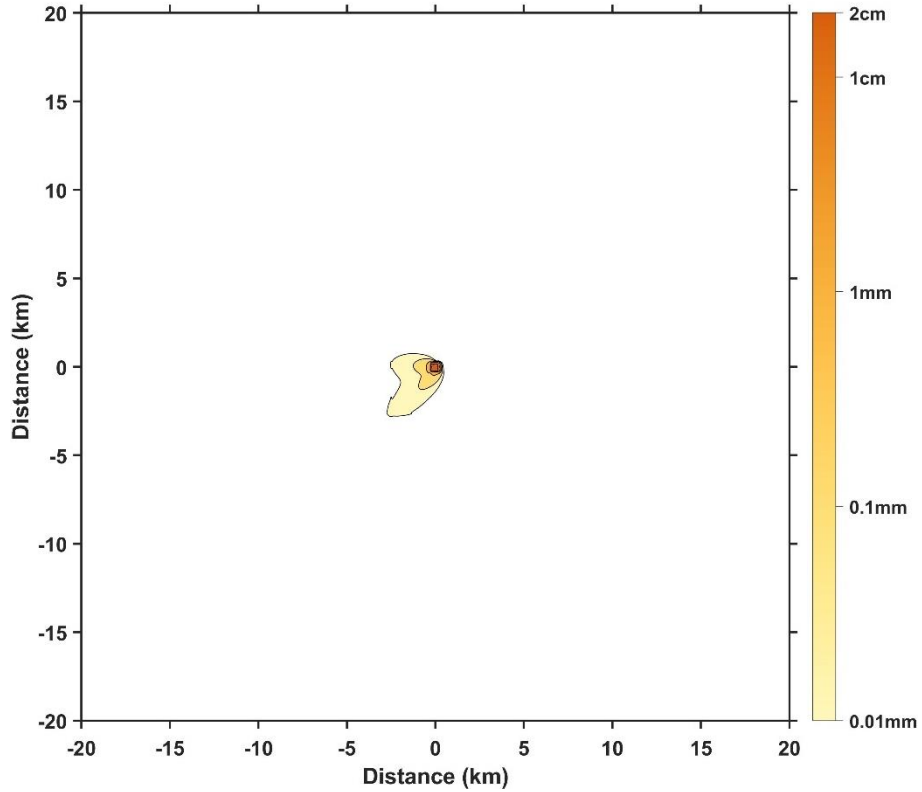
Figure 226 Redeposition thickness for Case 3
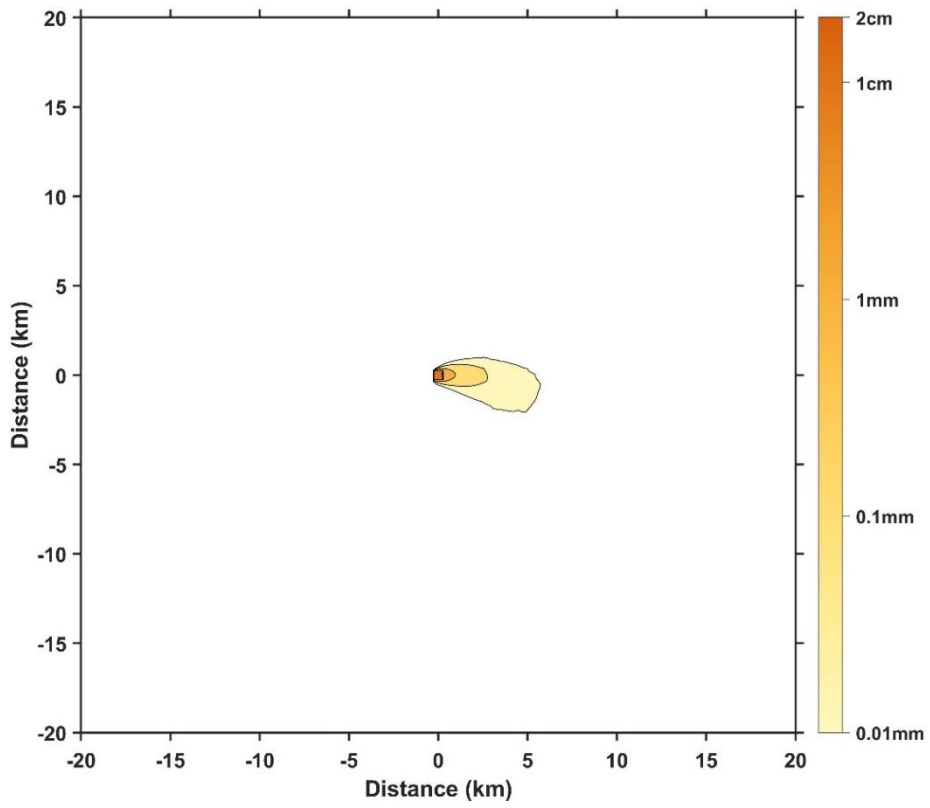
Figure 227 Redeposition thickness for Case 4
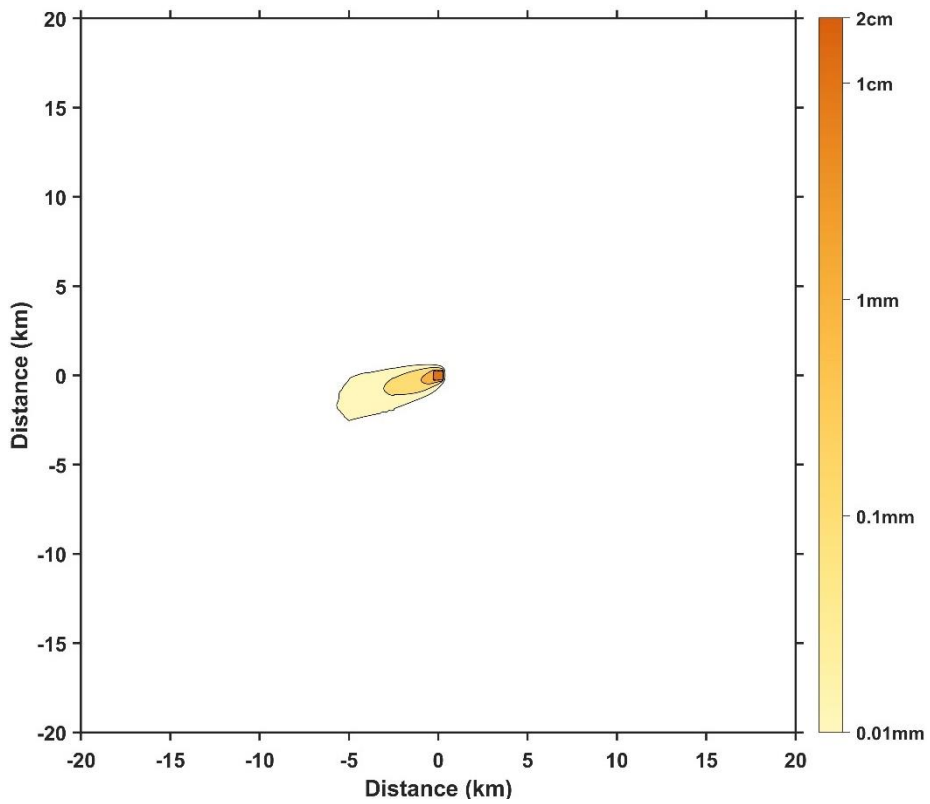
Figure 228 Redeposition thickness for Case 5
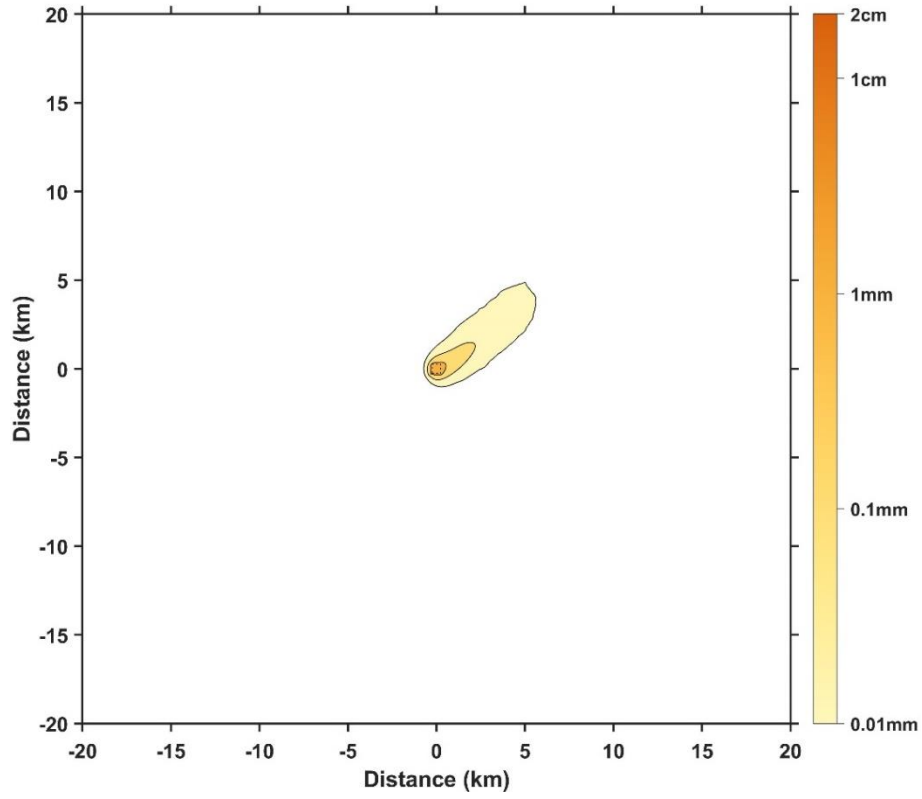
Figure 229 Redeposition thickness for Case 6
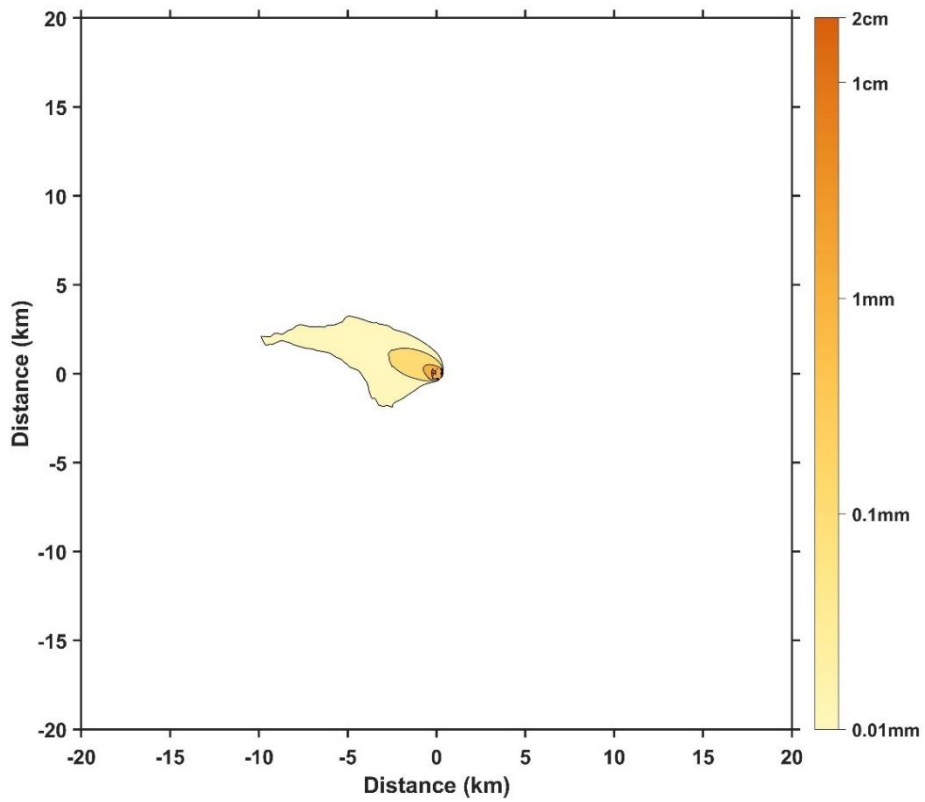
Figure 230 Redeposition thickness for Case 7
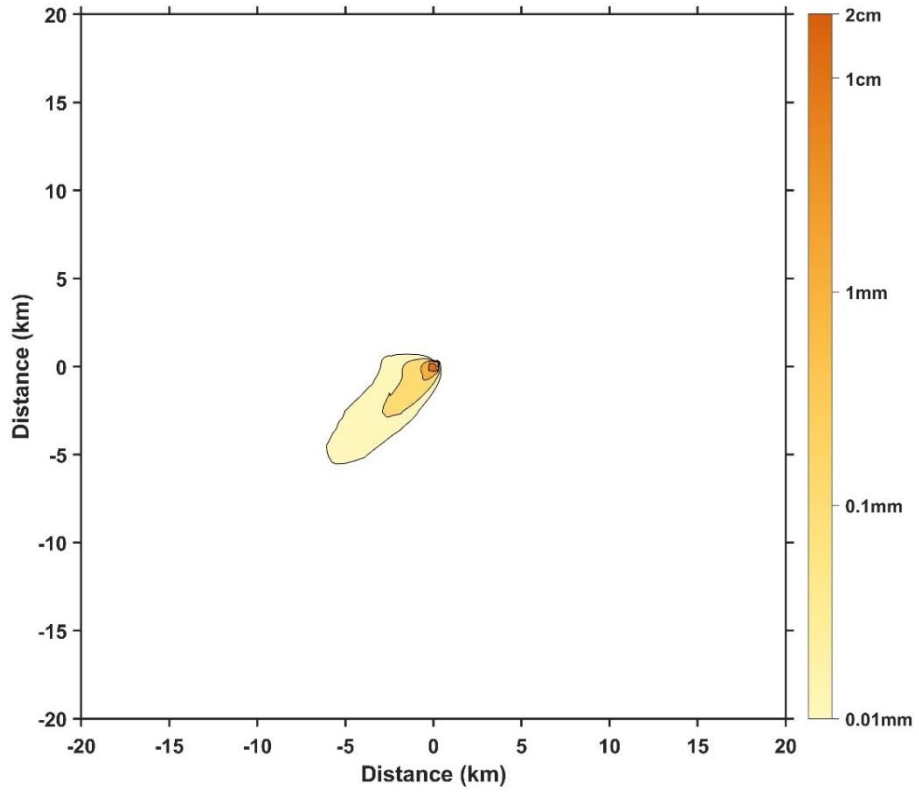
Figure 231 Redeposition thickness for Case 8
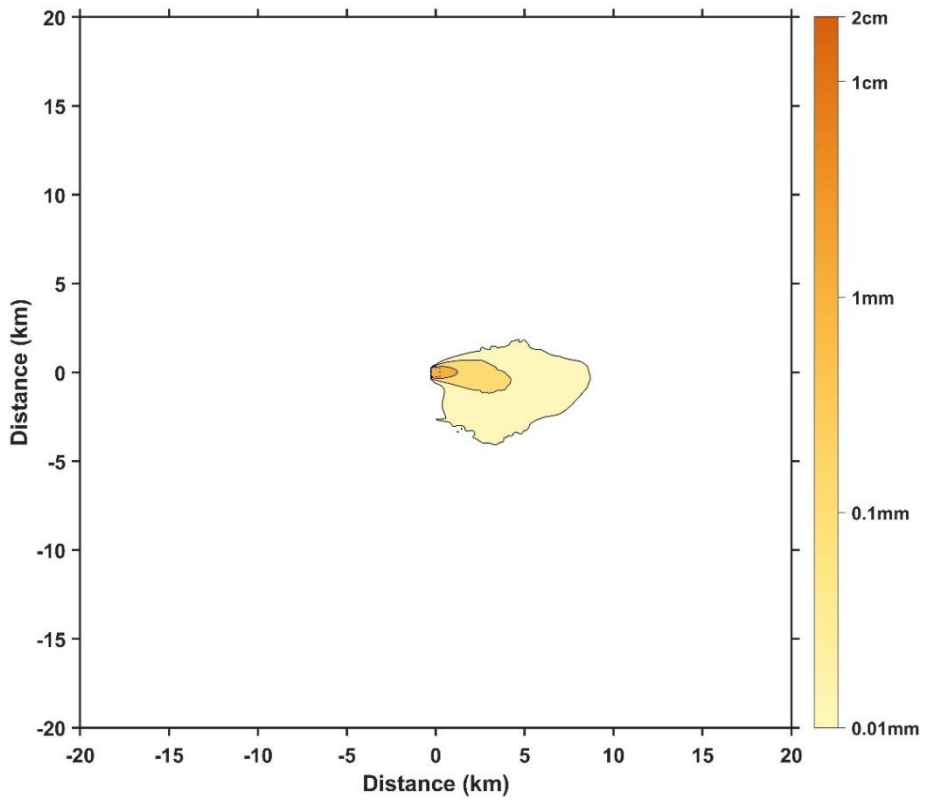
Figure 232 Redeposition thickness for Case 9
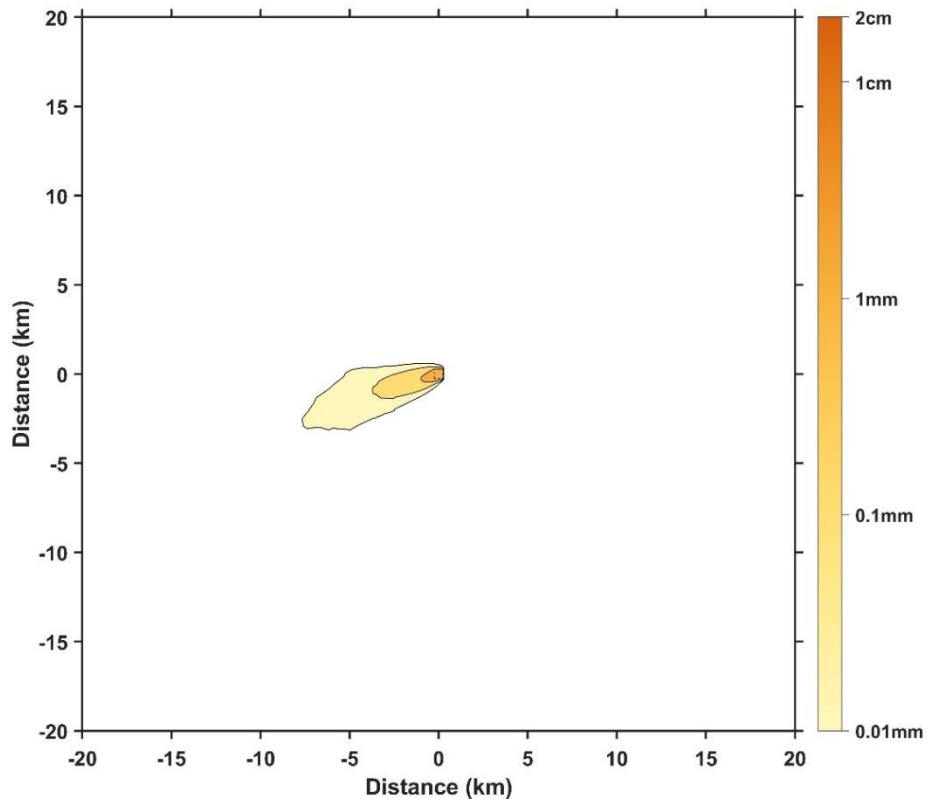
Figure 233 Redeposition thickness for Case 10

Table 1 The plume's maximum spreading distance and maximum redeposition thickness for each case

Case	Maximum horizontal dispersion distance 1 mab (km)	Maximum vertical dispersion height (m)	Maximum redeposition thickness (cm)
Case 1	4.52	231	2.60
Case 2	5.13	210	2.31
Case 3	2.93	129	2.45
Case 4	4.91	123	2.14
Case 5	5.42	165	1.85
Case 6	21.23	346	0.99
Case 7	21.18	246	1.21
Case 8	27.86	189	1.48
Case 9	14.51	160	0.95
Case 10	22.67	178	0.85

Table 2 Plume redeposition thickness area statistics for each case

Case	Area with redeposition thickness greater than 1cm (km2)	Area with redeposition thickness greater than 1mm (km2)	Area with redeposition thickness greater than 0.1mm (km2)	Case
Case 1	0.31	0.55	2.00	9.97
Case 2	0.28	0.60	2.43	11.10
Case 3	0.30	0.58	2.01	7.74
Case 4	0.28	0.76	3.14	12.48
Case 5	0.29	0.75	3.51	12.17
Case 6	0.00	0.56	3.14	17.87
Case 7	0.04	0.71	4.03	23.03
Case 8	0.17	0.84	5.68	21.10
Case 9	0.00	0.87	5.90	34.04
Case 10	0.00	0.73	4.48	17.75

Appendix IV Environmental Baseline Survey Methodology and Data Quality Assessment

1 Geological Baseline

1.1 Topography

The topographic data and backscatter intensity data in the contract area mainly come from the surveyed data of eight cruises by the Chinese vessels "Hai Yang Di Zhi Liu Hao", "Xiangyanghong 10", "Da Yang Yi Hao", and " Xiangyanghong 03 " from 2014 to 2018 and 2021 to 2022., respectively, a total of eight survey cruises of multibeam bathymetric survey data, of which the BPC Cruise 1 (DY69), BPC Cruise 2 (DY75) and BPC Cruise 3 (DY76) are new cruises added after the application of the mine site, and the others use historical topographic data. The multibeam bathymetric systems used in the field survey include EM122 multibeam system and SeaBeam3012 deep-water multibeam system.

1.1.1 Multibeam Bathymetric Data

1.1.1.1 Shipboard multibeam bathymetric data processing

The multibeam bathymetric data collected by the two systems, EM122 and Seabeam3012, were processed using CARIS Hips/Sips (version 11.0) developed in Canada. The data processing methods and processes follow the national standard, *DZ/T 0292-2016 Marine Multibeam Bathymetry Regulations of the Geological and Mineral Standards of the People's Republic of China*. The results of bathymetric data accuracy evaluation are shown in Table 1-1. The processed result data all meet the requirements of the *DZ/T 0292-2016 Marine Multibeam Bathymetry Regulations* (95% confidence level).

Table 1-1 Evaluation of bathymetric data accuracy

Relative error range	Percentage of intersection inconsistencies	Summary
relative err< –2.0%:	0.01%	Summary: total number of intersections 105036; relative error = <1.0% total 98.161%, which meets the IHO standard of 99.9873 %; mean error of absolute value is 0.3731 %
relative err= –2.0–1.0%:	1.82%	
relative err= –1.0–0.0%:	53.99%	
relative err= 0.0–1.0%:	44.17%	
relative err= 1.0–2.0%:	0.00%	
relative err> 2.0%:	0.00%	

1.1.1.2 Fusion of Multibeam Survey Bathymetry and Historical Terrain Data

Existing seabed topographic data are categorized into multibeam bathymetric data, satellite altimetry inversion data and so on according to their sources. The principle of selecting bathymetric data in the same region is to select them in accordance with the principle of priority, with multibeam bathymetric data in the order of priority, followed by full-coverage satellite altimetry inversion data (GEBCO2022 is generally selected); for the same type of survey data, the latest survey results are generally selected. The basic process of data fusion is as follows:

Bathymetric data processing, fusion, and evaluation were performed to solve the problems of different sources. (Independent grid files, such as Gridmb 1 (I, J) and Gridmb 2(I, J), were maintained using the Gauss weighted average method for the multibeam data from different cruises. The grid files of Gridmb (I, J) with the same resolution were merged. The GEBCO grid file, which is referred to as Gridgebco (I, J), was maintained through Gaussian spline interpolation or the Gauss weighted average method. The GEBCO grid file, which is referred to as Gridgebco (I, J), was maintained through Gaussian spline interpolation or the Gauss weighted average method. Finally, data fusion, cutting, and splitting of the bathymetric data were performed. The error (Δd) in the overlapping area data was chosen as the criterion used for correcting the errors in the nonoverlapping data. The error (Δd) in the overlapping area data was chosen as the criterion used for correcting the errors in the nonoverlapping area. As discreet data, Δd (I, J) was calculated using Gridmb (I, J) subducting Gridgebco (I, J). The corrected Gridgebco_corrent (I, J) data was obtained using Gridmb (I, J) subducting Gridgebco (I, J). $\triangle d$ (I, J) was gridded into the Griderror based on the grid spacing of Gridmb through the trend surface analysis method. The corrected Gridgebco_corrent (I, J) data was obtained using Gridgebco (I, J) plus Griderror (I, J). Finally, Gridgebco_corrent (I, J) was cut and merged with Gridmb (I, J).

1.1.2 Multibeam Backscatter Intensity Data

For EM122 system collecting backscatter intensity data, Caris software is applied to process, the specific flow is shown in Figure 1-1. For the Seabeam3012 system, the self-developed algorithm is used to correct the angle filter correction, topographic correction, center beam correction, and band mosaic to obtain the results of multibeam backscatter intensity data. The main process is shown in Figure 1-2.
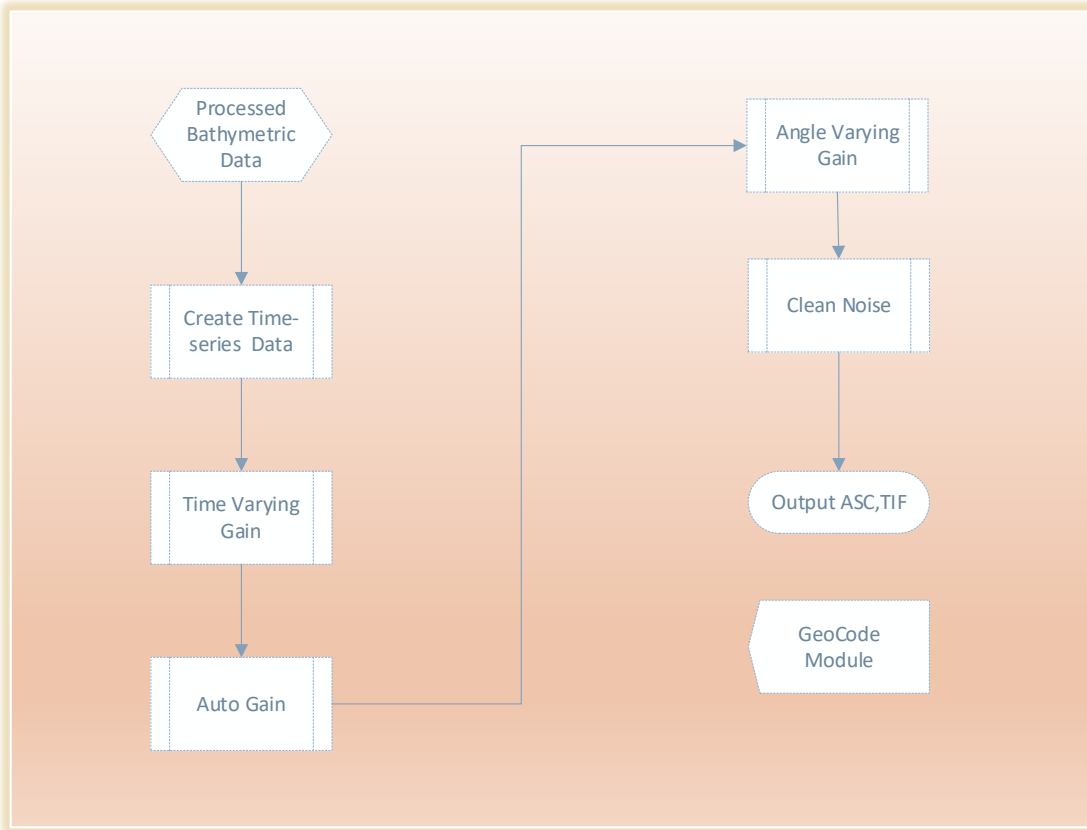
Figure 1-1 Flow chart for data processing echo intensity from EM122 multibeam bathymetric system
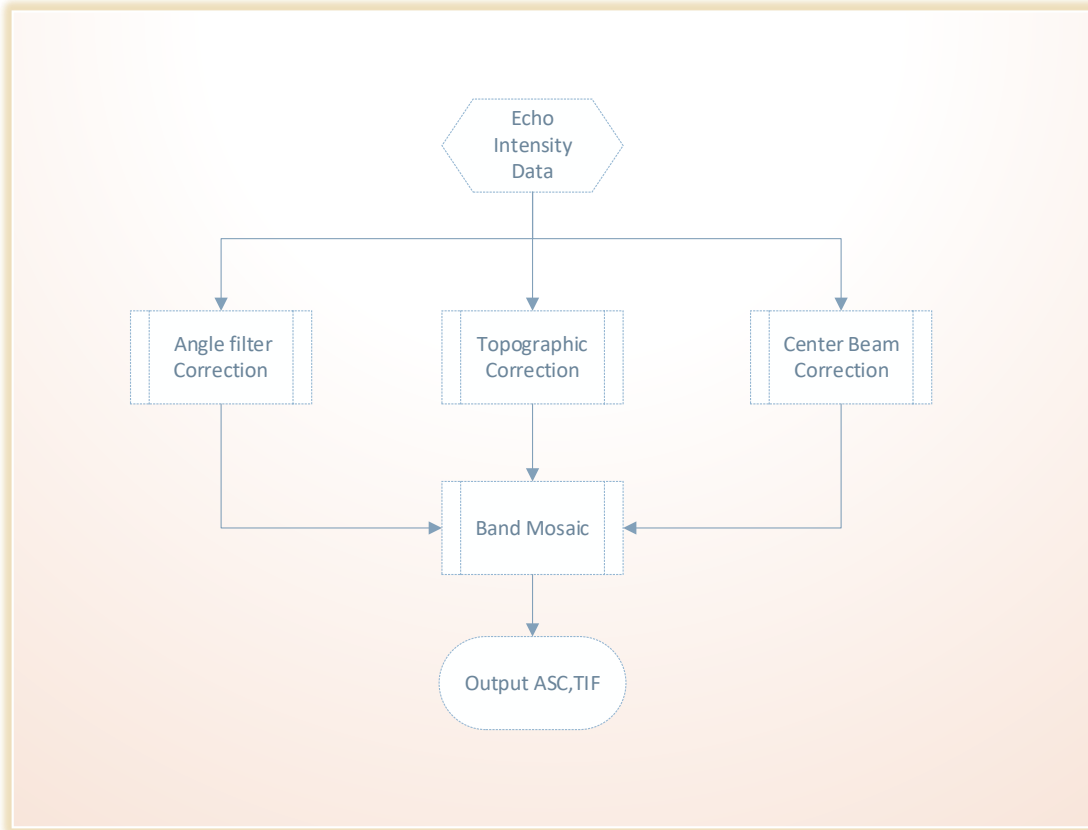
Figure 1-2 Flow chart for data processing echo intensity from seabeam multibeam bathymetric system

For sections with overlapping areas, relative errors were calculated for the echo intensity surface. The overlapping work area data is divided into two parts, each of which generates a separate DTM surface, and the two overlapping parts are combined with the topography operation. Combined terrain is a combination of two grid layers with different elevation characteristics at the same location, averaged and filtered to produce a grid layer that represents the difference in bathymetry between the overlapping work areas. The average value of the two is regarded as the true value of the measurement, (D1-D2)/2 is the deviation of the measurement value relative to the true value, and the absolute value of the relative error of the intersection is given by the formula:

$$\text{Relative error} = \frac{0.5 \times (D_1 - D_2)}{\overline{D}} \times 100\% = \frac{D_1 - D_2}{D_1 + D_2} \times 100\%$$

Standard Deviation (Standard Deviation, mean squared error), different from the mean squared error (mean squared error), the mean squared error is the mean of the data deviation from the true value of the distance squared, that is, the average of the sum of squares of the error, which opens up for the root mean squared error, the standard deviation is away from the mean squared sum of squares averaged after the square root of the error, expressed in δ, the formula is as follows:

$$\delta = \sqrt{\frac{n \sum x^2 - (\sum x)^2}{n(n-1)}}$$

The standard deviation is a measure of the dispersion of the mean of a set of data. A large standard deviation represents a large difference between most of the values and their mean; a smaller standard deviation represents that the data are closer to the mean. For example, two sets of numbers {0, 5, 9, 14} and {5, 6, 8, 9} both have a mean of 7, but the second set has a smaller standard deviation.

There are overlapping areas of work zones to carry out statistical results are shown in Table 1-2. As can be seen from the data in the table, there is a tenfold difference in the number of intersection points in the work area, but the average difference and standard deviation of the echo intensity data are flat. It is believed that the echo intensity of the multibeam system is well stabilized and the data quality is reliable.

Table 1-2 Statistics of Backscatter intensity Differences

Survey area	Number of intersections	Average difference	Standard deviation
Blocks M1 and M2	1193315	3.263%	3.7345

1.2 Sediment Parameters

1.2.1 Surface Sediment Type

1.2.1.1 Particle size analysis

Before sampling, the sample to be tested is first mixed well. Then the number of samples was determined according to the particle size of the sample, and 0.1g ~ 0.2g of wet sample of sediment was taken into a beaker, and the organic matter in the sediment was removed by adding with an excess of hydrogen peroxide (H_2O_2) solution. Then a few drops of 0.5 N sodium metaphosphate were added to the beaker and soaked for 24 h. The samples were stirred with a glass rod or ultrasonically shaken to fully disperse the samples. Particle size analysis was performed using a MasterSizer 2000 laser particle sizer, with the optical parameters of the dispersant (i.e., distilled water) set to default (i.e., universal mode) and 1.33 (refractive index of distilled water); the sample concentration (shading) was usually controlled at 10% to 20%. The particle size of the MasterSizer 2000 was tested in the range of 0.02–2000 μm, with a relative error of <3% for each component for repeated measurements. The measurement results were used to derive the volume percentage of a total of 100 groups of particle sizes within the test range for particle fraction analysis using

the random software of this laser particle sizer at 0.166φ intervals (φ = –log2(D), where D is the particle size in mm).

Particle size grading was divided into four classes using the Uden-Windward Wahl isobaric grading standard:

a) >2mm (<–1φ) is gravelly.

b) 2～0.063mm (–1φ～4φ) for sand grade

c) 0.063～0.004mm (4φ～8φ) for chalk grade

d) <0.004mm (>8φ) for clay grade

All analytical tests are carried out in accordance with ISO9001 quality management system. The sediment particle size analysis project has obtained the certificate of qualification accreditation for inspection and testing organizations, and the analytical testing instruments have been self-tested in accordance with the relevant management regulations and are within the validity period.

1.2.1.2 Smear identification

Sediment smear preparation was carried out on surface sediment samples from 20 stations in the M2 work area, and the identification of the material composition of surface sediments was completed under a polarized light microscope, and the type classification and naming of surface sediments was carried out (specific reference is made to GBT 12763.8-2007 *Specifications for Oceanographic Survey - Part 8: Marine Geology and Geophysics Survey*).

1.2.2 Surface Sediment Eh and pH

Immediately after the recovery of the box corer, the pH and Eh of surface sediments and temperature were tested by "INESA-PHB-J-260 Portable Tester" on deck, details are as follows: (1) Before and after conducting tests with the meter, rinse the meter probe thoroughly with distilled water and store it in a protective sleeve filled with saturated potassium chloride solution. (2) Perform an initial calibration of the tester using calibration solution before the first test, and recalibrate after every 20 samples. (3) Upon completion of box corer sampling and retrieval to the deck, and after removal of overlying seawater, insert the tester probe into the surface sediment at a depth of 3–5 cm. Activate the test by switching on the device and record relevant data once readings stabilize (typically within 2–3 minutes).

1.2.3 Elemental Geochemistry

(1) Surface sediments

Sample pretreatment: The sediment samples to be analyzed were first dried in an oven at 100°C, and then the samples were ground to 200 mesh or more using an agate mortar and pestle.

1) macronutrients and Zr analyzed by fluorescence spectrometry (XRF)

Weigh a 4.00 g specimen (accuracy to 0.01 g) and pour it into a mold, ensuring a boric acid powder rim around the specimen to prevent overflow during pressing. Use a press to apply 20 MPa pressure and compact the specimen. After pressing, label the non-measured surface with a sample number using a marker pen. Place the labeled specimen in a desiccator to prevent moisture absorption, preparing it for testing. The testing will be conducted using a PW4400/40 X-ray fluorescence spectrometer manufactured by Panacor, NetherlandsLoss on ignition (LOI) analysis:

Weigh the dried and grounded sediment sample 0.5 g of the sample in a porcelain dry pan, dry again at 100°C to a constant weight and then place the dry pan in a muffle furnace and scorch at 950–1000°C for 1 hour. Removed and placed in a desiccator, cooled to room temperature and weighed. The amount of burn loss was calculated:

Loss on Burning % = (Gt/G) × 100

Where Gt is the weight after cauterization and G is the weight of the sample before cauterization.

2) As, Sb, Hg by Atomic Fluorescence Spectrometry

Weigh 0.2 to 0.5 grams of sample (accurate to 0.1 milligrams) into a 25 mL colorimeter tube. Add 10 mL of aqua regia solution (1 part nitric acid to 3 parts hydrochloric acid), and place the tube in a boiling water bath for 2 hours to dissolve, shaking 2 to 3 times during this period. Remove the tube and allow it to cool to room temperature, then dilute with water to the mark on the tube. Shake well, allow to settle, and clarify if necessary; this solution is referred to as the sample solution. For simultaneous determination of arsenic and antimony: Take 5.00 mL of the sample solution and transfer it to a 10 mL colorimeter tube. Add 2.50 mL of 1 g/L ferric oxide solution and 2.50 mL of a thiourea-ascorbic acid mixed solution (thiourea: 50 g/L, ascorbic acid: 50 g/L). Shake the mixture well and let it stand for 30 minutes; this solution is used for arsenic and antimony determination. The atomic fluorescence spectrometer (AFS) was set to specified working conditions. The fluorescence intensity of antimony in both the mixed calibration solution of arsenic and antimony and the sample determination solution was measured, using a 20 g/L potassium borohydride solution as the reducing agent. The mass concentration of arsenic and antimony was determined from the calibration curve, and their mass fractions

were calculated accordingly. For determination of mercury: Use a 2 g/L potassium borohydride solution as the reducing agent. Set the AFS working conditions and measure the fluorescence intensity of mercury in both the mercury calibration solution and the sample solution. The mass concentration of mercury was found from the calibration curve, and its mass fraction was calculated. Arsenic and antimony were measured using the AFS-3100 atomic fluorescence photometer from Beijing Haiguang Instrument Co., Ltd., while mercury was measured using the AFS-2100 atomic fluorescence photometer from the same manufacturer.

3) Plasma mass spectrometry testing of trace elements and rare earth elements sampling

Sediment trace elements and rare earth elements were tested on an X-SERIES2 inductively coupled plasma mass spectrometer manufactured by Thermo Fisher Scientific.

The geochemical analysis of sediments was completed in the School of Geological Sciences and Mineral Resources of Lanzhou University, and national standard substances such as GSS17, GSS23, GSS27, and GSS28 were added during the analysis of the project to check the testing accuracy and quality control, in which the standard deviation of the data of macronutrients was ≤5%, and that of the data of trace elements was ≤10%, which is shown in Attachment 1.

(2) Short columnar deposits

SiO_2 , Al_2O_3 , Fe_2O_3 , MgO, CaO, Na_2O, K_2O, MnO, TiO_2, P_2O_5, and Cr, Zr test based on the *Methods for Chemical Analysis of Silicate Rocks - Part 28: Determination of 16 Major and Minor Elements Content* （GB/T 14506.28-2010）; trace elements Co, Ni, Cu, Zn, V, Ba test based on the *Chemical analysis methods for marine sediment* (GB/T 20260-2006) *"Chapter 8 primary and secondary component analysis, inductively coupled plasma atomic emission spectrometry"*; trace elements Sc, Ga, Pb, Sr, Li, Rb, Nb, Cs, Ta, W, Th, U, Mo, and rare earth elements based on the *Chemical analysis methods for marine sediment (GB/T 20260-2006)* "Chapter 9 trace and micro-constituents, inductively coupled plasma mass spectrometry"; trace elements Co, Ni, Cu, Zn, V, Ba based on the *Chemical analysis methods for marine sediment* (GB/T 20260-2006) "Chapter 9 primary and secondary components analysis, inductively coupled plasma atomic emission spectrometry Inductively coupled plasma mass spectrometry".

1.2.4 Mineral Characteristics

The clay mineral content was calculated according to the Biscaye (1965) method, which is also the calculation method prescribed in the *Code of Practice for International Seabed Area and High Seas Environmental Survey—Part 4: Physical Features Survey of*

Marine Sediments (GB/T 42629.4-2023). The weighting factors during the calculation of the sampled MDI Jada 6.5 software were determined as follows: the weighting factors used in the calculation with MDI Jada 6.5 software for sediment analysis were determined as follows: monazite has a weighting factor of 1, illite is weighted by a factor of 4, and chlorite plus kaolinite by a factor of 2. The proportion of kaolinite to chlorite content was determined by fitting the ratio of diffraction peak heights at 3.58 Å (K (002)) to 3.54 Å (CH (004)) near 25° (2θ).

1.2.5 Sediment Pore Water

1.2.5.1 Pore Water Metal elements

Determination of metallic elements (Mn, Fe, Co, Cu, Zn, Cd, Pb) in sediment pore water was primarily conducted using Inductively Coupled Plasma Mass Spectrometer (ICP-MS 7700x). The instrument is equipped with a high-salt sample inlet system (HMI) and a He gas collision cell. It features a dynamic linear concentration range spanning 9 orders of magnitude, with detection limits of 0.5 ppt for low-mass Be (9), 0.1 ppt for medium-mass In (115), and high-mass Bi (209). Oxide interferences CeO^+/Ce^+ and double-charge interferences Ce^{2+}/Ce^+ were controlled to within 1.5% and 3.0%, respectively. The mass spectral range covers from 2 amu to 260 amu.

Quality control of the analytical process of sediment pore water analysis was carried out using laboratory parallel sample analysis and insertion of standard samples.

1.2.5.2 Pore Water Nutrients

According to the "GBT 12763.4-2007 Marine Investigation Specifications Part 4: Seawater Chemical Element Survey" regulations, pore water samples for NH_4^+, NO_2^-, PO_4^{3-}, and SiO_2 are determined using a Hach DR890 spectrophotometer. The testing methods are as follows: NH_4^+ using the salicylate method, NO_2^- using the diazotization method, reactive phosphorus using the ascorbic acid method, and silicon using the silicomolybdic acid method. Select the corresponding test program, prepare the appropriate solutions according to the procedure, wipe the outer wall of the cuvette or reagent bottle clean with dust-free paper, place it into the spectrophotometer, cover with a light shield, and record the reading.

For NO_3^-, it is determined using a NO502-US ion electrode. Rinse the NO_3^- ion electrode with ultrapure water and dry it with dust-free paper before immersing it into the solution to be tested. Agitate the electrode rod for a moment, then let it stand still for about 30-60 seconds, and record the data after the reading stabilizes.

During the analysis of nutrients in pore water, national first-class standard materials such as GBW08633, GBW08623, GBW08641, and GBW08649 are used to test the accuracy and quality control of the test.

1.2.6 Geomechanical Characterization

The first and second cruises of BPC (DY69 & DY75) completed in-situ geotechnical testing, at-sea field analytical testing and laboratory analytical testing of sediments in the study area.

1.2.6.1 Geotechnical Testing of Sediments on board

The geotechnical testing of sediments on board mainly includes penetration strength and shear strength testing and analysis. The penetration strength test is completed by miniature penetrometer (TT-MP1 and WGII miniature penetrometer), and the shear strength test is completed by miniature cross plate shear instrument (TT-MVS1 and SJL miniature cross plate shear instrument). During the geotechnical testing on board, the equipment is in good condition, the instruments are used correctly, and the test operation is in line with the requirements of the *Code of Practice for International Seabed Area and High Seas Environmental Survey—Part 4: Physical Features Survey of Marine Sediments* (GB/T 42629.4-2023) , the *Standard for Geotechnical Testing Method* (GB/T 50123-2019) and the *Rules of Pocket Penetrometer Test* (CECS 54:93) of the China Construction Engineering Standardization Association. The test data are accurate and reliable, and the self-inspection is qualified. The measurement levels meet the requirements of the *Recommendations for the guidance of contractors for the assessment of the possible environmental impacts arising from exploration for marine minerals in the Area* (ISBA/19/LTC/8), the *Standardization of Environmental Data and Information: development of guidelines* (ISA/19/LTC/8), and the *Development of guidelines* (ISA/02/02), Chapter 23.

1.2.6.2 Laboratory Geotechnical Testing of Sediments

Laboratory geotechnical testing and analysis of sediment samples were conducted to assess various physical properties, including natural moisture content, specific gravity, natural density, natural porosity ratio, plastic limit, liquid limit, plasticity index, and liquidity index. Additionally, mechanical properties such as compression coefficient, compression modulus, cohesion, and internal friction coefficient were thoroughly evaluated.

Natural Moisture Content: Determined using the drying method, the soil samples from the ring knife specimen production are heated in an electric constant temperature drying

oven at 100–105°C until reaching constant weight. The ratio of water mass lost during drying to the mass of the dried soil, expressed as a percentage, gives the natural moisture content.

Natural Density: Assessed using the ring knife method, columnar samples are sectioned at 5 cm intervals and compacted into ring knife samples with a height of 2 cm and cross-sectional area of 30 cm². After weighing the soil samples, the natural wet density of the sediment is calculated in g/cm³. Equipment includes a ring knife and electronic balance.

Specific Gravity: Determined via the specific gravity bottle method, where dried and ground soil samples are tested using a 50 ml specific gravity bottle. Equipment used includes a 50 ml specific gravity bottle, electronic balance, and vacuum pump.

Plastic Limit and Liquid Limit: Evaluated using the combined method, where the liquid limit denotes the boundary between soft plastic and flowing states of cohesive soil, while the plastic limit marks the moisture content boundary between plastic and hard plastic (semi-consolidated) states, expressed as percentages. Testing equipment includes an LP-100D combined tester, electric air blower, and electronic balance.

Compression Coefficient and Compression Modulus: Determined using the rapid consolidation test method. In-situ soil samples, prepared according to *Standard for Geotechnical Testing Method* (GB/T 50123-2019) Section 3.1.4, are sectioned and tested using ring knife samples every 5 cm vertically. Samples undergo compression testing to assess deformation under different loads and lateral confinement conditions. Testing equipment consists of a KTG fully automatic consolidation test system and ring knife.

Cohesion and Internal Friction Coefficient: Assessed using the rapid shear test method. In-situ soil samples, prepared as *Standard for Geotechnical Testing Method* (GB/T 50123-2019) Section 3.1.4, are vertically sectioned and tested using ring knife samples. Multiple parallel sample tests are conducted to determine cohesion and internal friction coefficient. Equipment includes an SDJ-1 strain-type direct shear instrument, data collector, and processing system.

1.3 Polymetallic Nodule

The data on polymetallic nodule characteristics in the contract area was obtained from geological sampling surveys. The geological sampling was mainly box corers. The external data include longitude, latitude, depth, quality and proportion of nodule size types, quality and proportion of nodule morphology types, abundance, and coverage, while the internal data include nodule element content.

Whether the mechanical part of the geological box corer is in normal working condition and how many samples are collected are the main factors affecting the quality of geological sampling. According to the design requirements of the cruise, the quality evaluation standards of various sampling equipment and the quality evaluation of the sampling results are as follows:

- Box Corer Sampling: A station is deemed successful if geological samples are successfully obtained using the box corer. A qualified station is one where there is no noticeable leakage of overlying water and sediments from the box.

- Geologic Trawling: Stations are considered successful if geological samples are obtained through geologic trawling. A qualified station is one where there is no breakage of the net coat and no obvious leakage of nodule samples.

1.3.1 Polymetallic Nodule Abundance

According to the relevant specifications outlined in the *Specification for Oceanic Polymetallic Nodules Exploration* (GB/T 35571-2017) and *The Expertise for Oceanic Polymetallic Nodules Survey* (GB/T 17229-1998), the determination of polymetallic nodule abundance during the cruise primarily employed the direct method of assessment. This involved using a box corer to collect samples of polymetallic nodules, weighing them with a balance, and calculating nodule abundance by dividing the mass of nodules by the sampling area of the box. During cruises DY40B, DY48, and DY75, the mass of polymetallic nodules at each station was measured using a balance with a precision of 1 gram. In other cruises, an electronic scale was used for measuring the nodules' mass at each station.

1.3.2 Polymetallic Nodule Coverage

According to the relevant specifications and requirements outlined in the *Specification for Oceanic Polymetallic Nodules Exploration* (GB/T 35571-2017) and *The Expertise for Oceanic Polymetallic Nodules Survey* (GB/T 17229-1998), the estimation of polymetallic nodule coverage at each station during geological sampling in the operational area is conducted using an on-site box-sampling simulation method:

A white plastic box measuring 50 cm × 50 cm is prepared, divided into a grid of 1 cm × 1 cm cells (totaling 625 cells).

After collecting polymetallic nodule samples using the box corer, the nodule samples are evenly distributed within the white box without overlap or obvious gaps. The area occupied by the nodule samples in the box is then measured and divided by the total area

of the box (0.25 m²) to determine the percentage coverage of polymetallic nodules on the station's deck.

1.3.3 Physical Characterization of Polymetallic Nodules

The physical characterization of polymetallic nodules includes their wet density and water content, which are measured as follows:

To measure the wet density, the wet mass of the nodules is first obtained by weighing with a balance, and then the volume of the nodules is measured using the drainage method, which in turn calculates the wet density of the nodules. After weighing the wet weight and volume of the nodules, the nodules were carefully removed and placed in a beaker, and then the weighed nodules were dried in an oven at 105°C for 10 hours, and then cooled down and their dry weight was measured again in a dry environment to calculate their moisture content. The formulae for calculating the wet density and water content of nodules are given below:

Equation for wet density of nodules: wet density (g/cm³) = wet weight (g) / volume (cm³)

Nodule moisture content formula: moisture content (%) = (wet weight (g) - dry weight (g)) / wet weight (g)

1.3.4 Polymetallic Nodule Type

The size of polymetallic nodules is typically assessed using vernier calipers or a straightedge to measure the triaxial dimensions: the long-axis, short-axis, and thickness of nodule samples. According to the Regulations for *The Expertise for Oceanic Polymetallic Nodules Survey* (GB/T 17229-1998), nodule samples are classified based on grain size into large-sized (>6 cm), medium-sized (3–6 cm), and small-sized (<3 cm) categories. During the second cruise conducted by Beijing Pioneer Company (DY75), three-dimensional laser scanning was employed to scan each polymetallic nodule sample. Post-processing of the scanning data yielded three-axis measurements and volume data of hand specimens. This data, combined with visual identification, enabled classification based on particle size and morphology, resulting in the following categories: huge-sized (>=7 cm), large-sized (5–7 cm), medium-sized (3–5 cm), and small-sized (<3 cm) nodule samples.

Additionally, the morphology of polymetallic nodule samples was visually categorized into shapes such as spherical, ellipsoidal, conidial, mushroom, crumbly, and discoidal. The upper and lower surface roughness of the samples was assessed and categorized as smooth (s) or rough (r). Detailed descriptions of morphological types and

surface structures observed at each station during cruises were recorded in sample registration forms.

1.3.5 Elemental Content of Polymetallic Nodules

Internal and external tests and analyses are carried out in accordance with relevant national specifications such as *The Expertise for Oceanic Polymetallic Nodules Survey* (GB/T 17229-1998) and the provisions of relevant management specifications for geological experiments, such as *Geology and Mineral Resources Laboratory Testing Quality Management Specification Part 3: Chemical Analysis and Composition Analysis of Rock and Mineral Samples* (DZ/T 0130.3-2006).

. The key parameters of the instruments were debugged and calibrated before analysis, and standard samples were used for monitoring during the testing process, and duplicate samples were randomly selected for parallel sample analysis. The content of the main mineralizing elements (Mn, Fe, Cu, Co, Ni) was tested on-site in the field of DY36, DY41-1, and DY41B, using X-ray fluorescence spectrometry. Samples from DY40B were analyzed at the Institute of Geology of Nuclear Industry (IGNI). Samples from DY48 and DY75 were analyzed at the Second Institute of Oceanography, Ministry of Natural Resources of China. The analytical method employed was X-ray fluorescence analysis, with sample preparation conducted using the melting flake method. The PANalytical Axios wavelength dispersive X-ray fluorescence spectrometer was utilized to analyze key metallic elements such as Mn, Fe, Co, Ni, Cu, etc. The samples were tested at the Second Institute of Oceanography, Ministry of Natural Resources. In-house analysis of samples from the BPC Cuise 1 (DY69) was conducted by the Guangzhou Marine Resources Monitoring Center, Ministry of Natural Resources, using an Axios X-ray fluorescence spectrometer. Elements analyzed included Mn, Fe, Cu, Co, Ni, among others.

During sample measurement, drift-corrected samples were utilized for standardization to correct for long-term instrument drift. National standards including GBW07249, GBW07295, GBW07296, Nod-A-1, Nod-P-1, GBW07339, and GBW07337 were inserted into the batch sample tests for validation and analysis to monitor the accuracy of the analytical methods. Parallel samples were employed for quality control and evaluation of the analysis. The quality control results from internal tests of each cruise are detailed in Tables 1-3. Analysis of the test results demonstrates the reliability of the analytical methods, controlled testing conditions, long-term stability of the instruments, accuracy of the monitoring standards, and compliance with error-checking pass rates for parallel samples as per specifications. Consequently, the test data is deemed accurate and dependable.

Table 1-3 Statistics of National Standard Substance Test Results by Cruise for Laboratory Tests

Standard substance name	TFe$_2$O$_3$	MnO	Co	Ni	Cu	Note
GBW07249	26.75	27.01	0.35	0.36	0.28	Reference value
measured value	26.99	26.97	0.35	0.37	0.28	Cruise DY75
sd (%)	0.90	0.14	0.41	2.38	0.45	
GBW07295	15.54	31.89	0.29	1.02	0.69	Reference value
measured value	15.77	31.61	0.29	1.02	0.70	Cruise DY29
sd (%)	1.48	0.88	0.00	0.00	1.45	
measured value	15.27	31.21	0.30	0.99	0.66	Cruise DY48
sd (%)	1.74	2.13	3.45	2.94	4.35	
measured value	15.61	31.84	0.29	1.04	0.69	Cruise DY75
sd (%)	0.46	0.16	1.02	1.75	0.44	
GBW07296	6.72	41.58	0.17	1.55	1.36	Reference value
measured value	6.71	40.75	0.17	1.56	1.27	Cruise DY40B
sd (%)	0.15	2.00	0.00	0.65	6.62	
measured value	6.66	40.31	0.17	1.52	1.33	Cruise DY48
sd (%)	0.89	3.05	0.00	1.94	2.21	
measured value	6.68	41.47	0.18	1.55	1.36	Cruise DY75
sd (%)	0.54	0.26	7.04	0.14	0.03	
GBW07337	24.45	29.96	1.30	0.44	0.14	Reference value
measured value	24.49	29.13	1.30	0.48	0.14	Cruise DY48
sd (%)	0.16	2.77	0.00	9.09	0.00	
measured value	24.49	30.18	1.31	0.45	0.14	Cruise DY75
sd (%)	0.14	0.73	0.77	1.60	0.36	
GBW07339	21.30	26.47	0.56	0.40	0.15	Reference value
measured value	21.29	26.05	0.51	0.40	0.12	Cruise DY40B
sd (%)	0.05	1.59	8.93	0.00	20.00	
measured value	20.93	25.72	0.57	0.42	0.16	Cruise DY48
sd (%)	1.74	2.83	1.79	5.00	6.67	
measured value	21.21	26.36	0.56	0.42	0.16	Cruise DY75
sd (%)	0.41	0.43	0.17	4.65	5.41	
Nod-A-1	15.60	23.90	0.31	0.64	0.11	Reference value
measured value	15.73	23.73	0.34	0.60	0.11	Cruise DY48
sd (%)	0.83	0.71	9.32	5.66	0.00	
measured value	15.94	24.35	0.32	0.64	0.11	Cruise DY75
sd (%)	2.19	1.89	2.21	0.22	1.74	
Nod-P-1	8.30	37.60	0.22	1.34	1.15	Reference value
measured value	8.48	36.87	0.23	1.33	1.15	Cruise DY48
sd (%)	2.17	1.94	2.68	0.75	0.00	
measured value	8.49	38.04	0.24	1.34	1.15	Cruise DY75
sd (%)	2.25	1.17	5.07	0.08	0.28	

2 Physical Oceanographic Baselines

2.1 Subsurface buoy

2.1.1 Survey Equipment and Parameters

The subsurface buoy observation equipment deployed and recovered mainly consists of CTDs, ADCPs, single-point current meters, sediment traps, acoustic releases and floats, and other major equipment. The main technical index requirements for each type of equipment are as follows:

The CTD uses the SBE16plus and SBE37 from Seabird USA to observe elements such as pressure, temperature, and conductivity, which can be synchronized to obtain several of these parameters. Their technical requirements are shown in Table 2-1.

The ADCP utilizes the WHLR75 (referred to as the 75K ADCP) from TRDI, USA. The ADCP has four convex transducers arranged at an angle of 20° to the vertical direction, and utilizes its acoustic Doppler effect to measure the flow velocity distribution in the water column profile, with built-in sensors for pressure, temperature, inclination, and longitude. The flow velocity measurement range is ±500 cm/s and the maximum depth of the profile is 650 m. The technical specifications are shown in Table 2-2.

The single-point current meter utilizes Andra's single-point current meter, the Seaguard RCM (RCM). It utilizes the acoustic Doppler effect to measure the flow velocity distribution around the device, with built-in tilt and compass sensors. It can also be extended as a platform to add other measurement parameters such as temperature, conductivity, depth, and dissolved oxygen. Its technical requirements are shown in Table 2-2.

Sediment traps are primarily used to collect sediment particles at fixed depths in the ocean, and can be set to sample for as long as needed, from a few days to a few weeks or up to a year and a half underwater, with sample bottles automatically collecting sediment samples at least every 1 month, and a minimum of 12 bottles set to sample a 1-year anniversary.

The releases use Oceano 2500s from IXSEA, France, which utilize an integrated transducer to receive and actuate commands from the deck unit. The safe working load is 2,500 kg and the pressure resistance is 6,000 m. The release is designed to be used in a wide range of applications.

Some of the subsurface buoy structures are shown in Figure 2-1, with the addition of a near-bottom current meter observation level for the subsurface buoys in 2023 and 2024.

Table 2-1 Temperature, conductivity and pressure specifications

Parameters	Resolution	Accuracy	Stability
Temperature	0.0001 °C	±0.002 °C	0.0002 °C/month
Conductivity (salinity)	0.00001 S/m	±0.0003 S/m	0.0003 S/m/month
Pressure	0.002% x full range	±0.1%×full range	0.1% of full range/year

Table 2-2 Technical indicators for monitoring of current elements

Current meter	Current speed resolution	Current speed accuracy	Current direction resolution	Current direction Accuracy
RCM	0.1 mm/s	±0.15 cm/s	0.01°	±2°
75K ADCP	0.1 cm/s	±1% x full scale ±0.5 cm/s	0.01°	±2°

Figure 2-1 Structure of the subsurface buoy

2.1.2 Analytical Methods and Quality Control

2.1.2.1 Temperature and Salinity

Data preprocessing: The moored CTD data were processed using the SBEDataProcessing-Win32 software of SeaBird to convert the raw observation data (hexadecimal) from the temperature-depth and temperature-salt sensors into data in ASCII format.

Data quality control:

Remove the subsurface buoy T,S,D data during the deployed, picked up and exposed in the air process.

Remove airborne data and reject data from decentralization and recycling processes.

- Range check: The data are checked against the extremes of the historical information on the temperature and salinity elements of the sea area where the system is deployed. Data exceeded the extreme value interval are eliminated and supplied with adjacent normal data by linear interpolation.

- Trend check: Observed data should not exceed the corresponding magnitude within a certain period of time. Segmented tests are performed, with each segment being 15 days, and data that change by more than 2.5 times the standard deviation are considered as abnormal data. Abnormal data are eliminated and then supplied with neighboring normal data by linear interpolation.

- Time series plot inspection: manual judgmental checking by plotting time series plots of water temperature and salinity.

2.1.2.2 Current Data

1) Data preprocessing:

The current data ADCP acquired by the subsurface buoy were converted from the original hexadecimal data of ADCP to ASCII code data by WINADCP software, and elements such as flow velocity, flow direction, and intactness were extracted from the data according to the 1 h interval. The single-layer current data obtained by the Andra current meter were exported using the Seaguard Studio software, and elements such as current speed and direction were extracted from the data at 1 h intervals.

2) Data quality control

- Data processing starts with data inspection to understand the basic information of the data acquired from observation, such as: instrument model, installation depth, blind zone of the instrument, stratum thickness setting, layer number

setting, sampling interval and other basic information, as well as the sea state during the observation process, in order to prepare for further data processing.

- According to the relevant parameters of the observation instruments, preliminary control is carried out to delete missing data, signal interruption data and data that do not satisfy the requirements of important parameters, so as to form the basic time-series-ordered subsurface buoy observation data.

- The data after the above initial quality control were subjected to a reasonableness check and instrumental error correction. Reasonability check includes the appearance of garbled codes and unreasonable characters in the data file, the observed data such as overflowed velocity and flow direction, and the data of two neighboring layers are too large in sudden change. Instrument error correction includes the value of compass, correction of instrument inclination, correction of instrument position change, etc., to check whether these data are reasonable and to correct the error.

- Range tests, dispersion checks, statistical analyses and other methods are used to filter out the obvious anomalies in the data. Finally, time-series plots and other relevant graphs of the subsurface buoy data are plotted, and the reasonableness of the subsurface buoy data is manually judged in the light of historical experience in the observing area, and then necessary corrections are made to the problematic data.

2.2 Thermohaline Structure

2.2.1 Sampling Equipment

The real-time temperature salt and depth measurement system utilizes the SBE911plus CTD meter from SeaBird, USA. The system consists of SBE9plus underwater CTD equipment and SBE11plus deck equipment and armored cable and acquisition computer. The armored cable 911plus system allows for real-time data acquisition and storage. When releasing the 911plus CTD system, the power supply for the underwater unit is provided by the deck unit via the armored cable. The armored cable is also used to transfer data into the SBE11plus deck unit. The deck unit decodes the 911plus CTD data and then transmits them to the data acquisition computer, which displays the data in real time and records the data to disk. The system can observe pressure, temperature, conductivity and other hydrological elements, and is also equipped with water collection bottles controlled by the underwater unit with automatic stimulated function, which can

obtain water samples for seawater chemical and biological analyses. The main technical parameters of the 911plus CTD system are shown in Table 2-3.

Table 2-3 Key Technical Parameters of the SBE911plus CTD System

Technical Parameters	Measurement range	Precision	Stability (per month)	Response time (s)
Conductivity (s/m)	0 to 7	0.0003	0.0003	0.065
Temperature (°C)	–5 to +35	0.001	0.0002	0.065
Pressure (psia)	10000	0.015%FS	0.0015%FS	0.015

2.2.2 Data Processing

The SBE Data Processing software provided by Seabird USA was applied to process the CTD data, and the data processing steps were as follows:

1) Data conversion

Converts raw observation data (hexadecimal) into ASCII form data, specific data elements include pressure, water temperature, conductivity, pump status, etc.

2) Pressure revision and deletion of records in the air

Pressure data before water entry and after water exit from the CTD were taken and averaged, and then the observed pressure values were subtracted from this average. The data before water entry, after water exit, and during the temperature sensing phase of the CTD were manually eliminated based on pressure, conductivity, and pump status.

3) Filtering (filter)

A low-pass filter provided by Seabird USA was used to filter one or more items of data for the purpose of smoothing out high-frequency (rapidly changing) data noise. The pressure filtering time constant was taken as 0.15s and the others as 0.0s.

4) Hysteresis calibration (Align CTD)

In order for the elements standardized by pressure to be consistent in time and to ensure that the calculations of other elements such as conductivity in the data processing are for the same water sample, a lag calibration was performed using Align CTD. The Align CTD program was applied for lag calibration of conductivity, where the conductivity parameter was taken as +0.073.

5) Heat Flux Revision (Cell Thermal Mass)

To eliminate the conductivity measurement error caused by large temperature gradients, the Cell Thermal Mass program was run for heat flux revision. The heat flux revision parameters Amplitude Alpha and Lag time Tau were taken as 0.03 and 7, respectively.

6) Loop Edit

In order to eliminate the water depth inverse jitter caused by the ship's oscillation, the Loop Edit program is applied to eliminate the inverspressure of the data, in which the minimum lowering speed of the CTD is taken as 0.25 m/s.

7) Calculation of water depth (derive)

The water depth can be calculated by the Derive program.

8) Data average (bin average)

Averaged at a depth of 1 meter.

9) Calculation of salinity (derive)

The Derive program was applied to calculate salinity.

10) Data quality checks and corrections

Vertical distribution maps of each element were plotted, and necessary manual corrections were made based on the vertical distribution maps and combined with empirical analysis. The quality of full water column and 1500m CTD observation data of this cruise is good without correction.

11) Separation of uplink and downlink data (Split)

Separate CTD releasing and ascending data.

12) Output data (ASCII Out)

Remove the table header information, leaving only the data.

2.2.3 Data Quality Evaluation

1) Instrument calibration

The SBE911plus CTD used was calibrated and the time of the survey was within the validity period of the calibration.

2) T-S dot plot property test

The T-S characterization of the observed temperature and salt data is shown in Figure 2-3. It can be seen that the T-S point clustering plot has good consistency among the stations, indicating that the stability of SBE 911 plus CTD instrument is good.
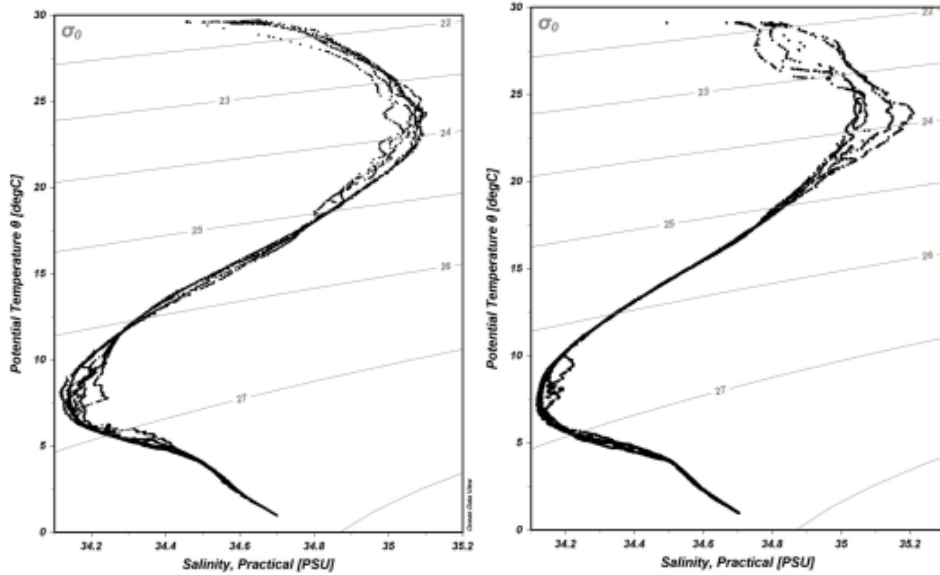
Figure 2-3 T-S point clusters of CTD stations from BPC Cruise 1 (left panel) and BPC Cruise 3 (DY76) (right panel)

2.3 Surface Current

2.3.1 Equipment

The OS38K ADCP is an acoustic doppler ocean current measurement system manufactured by RD Instruments, U.S.A. The ADCP consists of a hull-mounted transducer, a deck unit, an external compass, a GPS, and an operating computer. The main technical specifications are shown inTable .

Table 2-4 OS38K ADCP Key Technical Specifications

Model Name	OS38K	
Center frequency	38 K Hz	
Beam number (of a radio signal)	4 beams generated by beamformer	
Beam angle	Angle of 30° to the vertical line	
Long-term accuracy	1% V $\pm$ 0.5 cm/s (V is the value of flow velocity)	
Maximum profile depth	Broadband mode:	730–780m
	Narrowband mode:	800–1000m
Blind spot	16m	
Number of depth units	1–128	
Depth cell length	16, 24m or your choice	
Maximum Pulse Emission Rate	0.4HZ	
Accurate	<2cm/s	
Speed range	10m/s	

According to the technical parameters of the instrument, the actual observation water depth of OS38K ADCP is about 38m to 800m. The parameter settings used in the walk-around ADCP survey are as followsTable is shown in Table 2-5.

Table 2-5 Walking ADCP Operational Parameter Setting Table

Parameters	OS38K
Layer thickness (BINSIZE)	8m
Number of layers (NUMBER OF BINS)	128
Blind spot (BLANK)	16m
Transducer Depth (TRANDUCER DEPTH)	5m
Transducer declination	45°
Short-term average time	60s
Long-term average time	300s

2.3.2 Methods of Analysis

With the water depth not exceeding the bottom tracking depth of the ADCP, WINADCP, a software program provided by RDI, was used to convert the raw data in hexadecimal from the shipboard ADCP to ASCII code data, and to extract the horizontal flow velocity, horizontal flow direction, vertical flow velocity, flow velocity error, data intactness, GPS, and water depth for each observation layer corrected by the bottom tracking ship speed from the 5-min averaged data, boat speed, boat direction, and water temperature data at the transducer. In the case where the water depth exceeds the ADCP bottom tracking depth, various data corrected by GPS ship speed are extracted and processed.

Shipboard ADCPs operate on the acoustic Doppler principle, and the multiple environmental conditions present in the ocean can affect their measurements, resulting in observation errors. According to the data processing requirements of the water column survey, quality control of the current data is required in data processing.

(1) Data processing is first carried out to check the data and understand the basic information of the data, such as: instrument model, installation depth, instrument blind zone, layer thickness setting, layer number setting, sampling interval and other basic information, in order to prepare for further data processing.

(2) The stability of the ADCP current direction is determined by whether the current direction at the corners of the route in the plan view changes with the heading of the survey vessel, and it can be seen that the current direction does not change with the heading, which

proves that the shipborne ADCP instrument is working stably without any anomalies (Figure 2-4 and Figure 2-5).
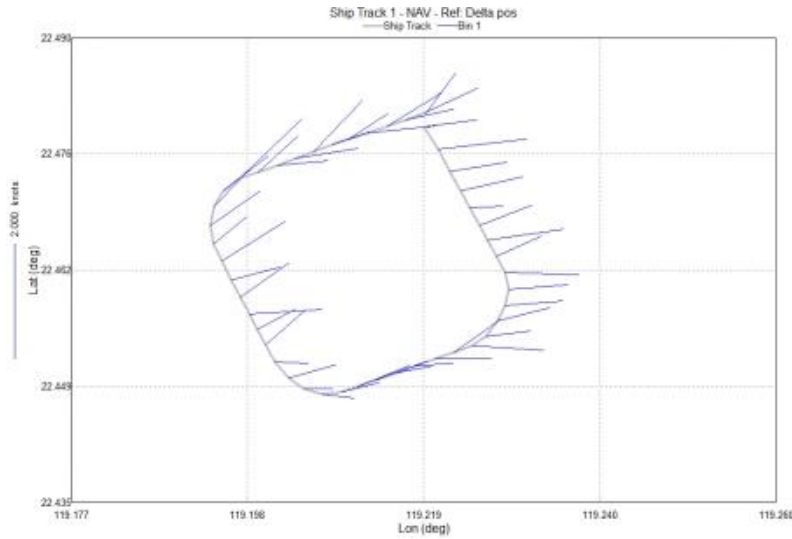
Figure 2-4 BPC Cruise 1 Shipboard ADCP Stability Test Plot
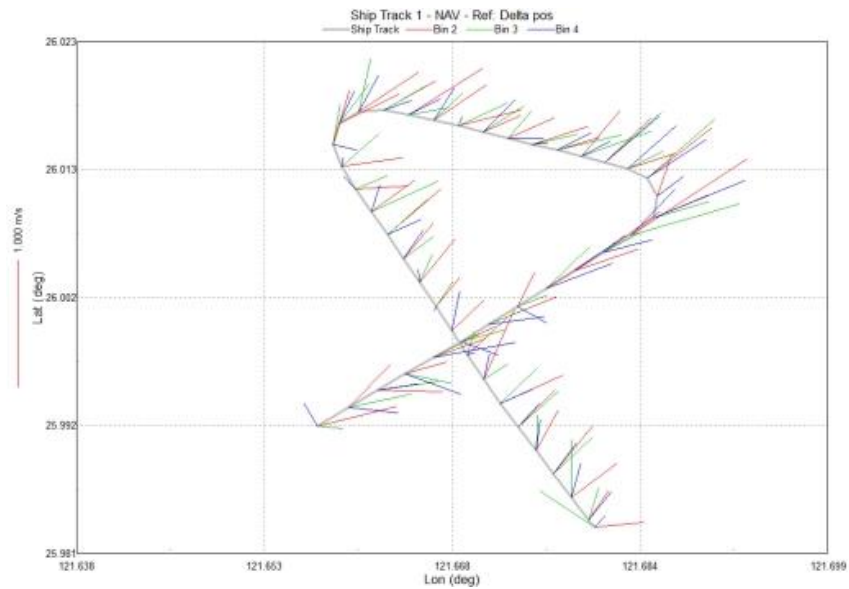
Figure 2-5 BPC Cruise 3 Shipboard ADCP Stability Test Plot

3) Based on the intactness rate (greater than 50%) and the correlation coefficient (greater than 0.8), an initial control was performed to remove data of poor quality.

4) Delete the information when the GPS signal is interrupted.

5) Delete missing data when boat speed or boat direction missing.

6) Delete the abnormal data in the surface layer. Instrument surface data are prone to poor data quality due to the disturbance of the ship's hull, and it is necessary to judge and analyze the surface data to delete the abnormal values.

7) Deletion of bottom anomaly data. For the measurement of layer depth is greater than the water depth of the data to be deleted. The reflection of the seabed on the acoustic beam affects the quality of the data in the bottom layer of several bin, to analyze and determine the anomalies to be deleted, usually the two adjacent layers of the flow velocity mutation is greater than 50cm / s considered anomalous.

8) Due to weather, sea state, ship's swaying, and other unknown reasons, the data obtained by ADCP in individual observation periods are obviously large (greater than 250 cm/s) and the change of flow direction is obviously not in line with the actual change rule of tidal currents in the sea area, and will be deleted as appropriate according to the actual situation in the processing.

2.4 Meteorology

2.4.1 Equipment

The meteorological data in the work area mainly come from the meteorological data observed in the western Pacific Ocean by the BPC cruises 1 and 2 during the period from 2021 to 2022. The on-board meteorological observation system is XZC6-1 ship automatic meteorological measurement system produced by Tianjin Haihua Technology Development Center, which is developed and produced by National Marine Technology Center. The full cruise implementation of wind speed, wind direction, air temperature, air pressure, relative humidity were conducted. Shipboard automatic weather station consists of wind speed and direction measurement system, display panel and operation computer and other units, the main technical indicators are shown in Table 2-6.

Table 2-6 Table of technical parameters of shipborne automatic weather stations

Key constituent	Range of measuring equipment	Accuracy
Wind direction	0~360°	±5°
Wind velocity	0 ~ 95m/s	±1m (wind speed≤20m), ±5% (wind speed>20m)
Air temperature	–40 ~ +60°C	±0.5°C
Air pressure	800–1100hPa	±1hPa
Relative humidity	0~100%	±2% (RH ≤ 90%), ±3% (RH > 90%)

2.4.2 Data Processing Methods and Quality Control

Recording of field observations is done as described below:

1) Strict use of UTC for observation time;

2) Each observation begins 30 minutes prior to the hour and ends on the hour;

3) Observations of meteorological items are concluded no later than 15 minutes before the main hour, and barometric pressure observations are made close to the main hour;

4) Missing measurements were clearly noted in the log sheet;

5) Daily calibration of the observation clock, the error is controlled within 1 minute;

6) When observing at night, stay in a dark place for 10 minutes and wait for your eyes to adjust before observing.

It should receives daily meteorological facsimile charts and atmospheric and oceanic data, and refers to the results of forecasting models to study the changes in weather systems along the route in a timely manner and to forecast future weather and meteorological conditions. The forecasts are based on 0.125°*0.125° high-resolution numerical prediction results, with region-wide coverage of 240-hour forecasts of barometric pressure and 240-hour forecasts of wind speed and direction; the waves are based on 0.25°×0.25° high-resolution region-wide coverage of 240-hour effective wave height forecasts.

Meteorological observation in this section is carried out regularly every day in strict accordance with the provisions of the *Specifications for Oceanographic Survey - Part 2: Marine Hydrographic Observation* (GB 12763.2-2007) and the (GB/T 17838-2017) *Specification for the Ships' Auxiliary Marine Hydrology and Meteorological Observations*. The instruments used have been certified by the National Marine Measurement Station without manual intervention, and the observers are marine meteorological professionals who have received rigorous training and have been working in forecasting and observation positions for many years with rich experience, so the quality of the observation data on wind speed, wind direction, barometric pressure, relative humidity, etc., is credible.

2.5 Noises

2.5.1 Equipment

In 2021, an ambient noise survey was conducted in Block M2 using a self-capacitating underwater sound recorder (USR) on a subsurface buoy. The USR was mounted on the bottom of the submersible, with a receiving depth of 4820 m ~ 25 m above the seafloor. The instrument was produced by the Institute of Acoustics, Chinese Academy of Sciences (CAS), and the sensitivity of the hydrophone was –170.3±1 dB re 1V/μPa in the frequency band of 20 Hz~5 kHz. In order to record higher frequency noises, the sampling rate was set to 24k Hz. Due to limitations in battery capacity and data storage space, an interval sampling mode was employed, recording 5 minutes of data every 3 hours, resulting in a

duty cycle of 2.8%. The recorded time span extends from October 2021 to October 2022, covering a total of 362 days, with a relatively high signal-to-noise ratio in the data.

2.5.2 Analytical Methods and Quality Control

Given the high sampling rate and large volume of acoustic data in this study, methods such as downsampling, filtering, and time-frequency transformation were applied for comprehensive processing and analysis to improve data analysis efficiency.

1）Downsampling

To identify low-frequency acoustic signals of large whales (typically baleen whales), the raw data was resampled into three different frequency bands. The original data, sampled at 24 kHz, was downsampled to 500 Hz and 4 kHz, while retaining the original 24 kHz sampling rate, thus obtaining low, mid, and high-frequency acoustic data. The Nyquist frequencies of the downsampled data were 250 Hz, 2 kHz, and 12 kHz, respectively. The 500 Hz low-frequency signal is suitable for identifying most baleen whales, whereas the mid- and high-frequency signals at 4 kHz and 24 kHz are appropriate for the identification and classification of toothed whales and some baleen whales.

2）Filtering

The time series of the acoustic data was subjected to frequency-domain filtering to enhance the signal-to-noise ratio and selectively retain characteristic frequency bands. In the data processing, a 20 Hz Butterworth high-pass filter was employed to eliminate common low-frequency background noise in the ocean while preserving most frequency bands associated with marine biological and anthropogenic noise signals.

3）Time-spectrum analysis

The Short-Time Fourier Transform (STFT) method was used to compute the time-frequency spectrum. Specifically, the Hann window function was applied as the sliding window. For a sampling rate of 2 kHz, the sliding window size was set to 512 samples (corresponding to a window length of 0.256 seconds), with a window overlap of 75%, resulting in a frequency resolution of approximately 4 Hz. For acoustic signals sampled at 24 kHz, the FFT window size was also set to 512 samples (with a window length of 0.021 seconds), and the window overlap was 75%, yielding a frequency resolution of approximately 47 Hz. During data analysis, the FFT window size was adjusted as needed.

3 Chemical Oceanographic Baseline

3.1 Methods of Survey Parameters

Seawater chemistry baseline field survey parameters mainly include: pH, dissolved oxygen (DO), total alkalinity (TA), nitrate (NO_3^--N), nitrite (NO_2^--N), ammonium (NH_4^+-N), phosphate (PO_4^{3-}-P), silicate (SiO_3^{2-}-Si), suspended solid (SS), particulate organic carbon (POC), and so on. The collection, storage, transportation, pretreatment and determination process of water samples are all in accordance with *Code of practice for international seabed area and high seas environmental survey- Part 2: Marine chemical survey* (GB/T 42629.2-2023), *The specification for marine monitoring- Part 4: Seawater analysis* (GB 17378.4-2007), *Specification for oceanographic survey- Part 4: Survey of chemical parameters in sea water* (GB/T 12763.4-2007), and *Determination of organic carbon in sea water by nondispersive infrared absorption spectrometry* (HY/T 150-2013), and other relevant provisions of standard documents. The analytical methods used for each survey parameter are shown in Table 3-1.

Table 3-1 Methods for survey parameters of seawater chemistry

Survey parameters	Analytical methods	Methodological basis
pH	pH meter method	*Code of practice for international seabed area and high seas environmental survey- Part 2: Marine chemical survey* (GB/T 42629.2-2023) *The specification for marine monitoring- Part 4: Seawater analysis* (GB 17378.4-2007)
Dissolved oxygen	Iodometry	*Code of practice for international seabed area and high seas environmental survey- Part 2: Marine chemical survey* (GB/T 42629.2-2023) *The specification for marine monitoring- Part 4: Seawater analysis* (GB 17378.4-2007)
Nitrate	Cadmium column reduction method	*Code of practice for international seabed area and high seas environmental survey- Part 2: Marine chemical survey* (GB/T 42629.2-2023) *The specification for marine monitoring- Part 4: Seawater analysis* (GB 17378.4-2007)
Nitrite	Diazotization-azotization	*Code of practice for international seabed area and high seas environmental survey- Part 2: Marine chemical survey* (GB/T 42629.2-2023) *The specification for marine monitoring- Part 4: Seawater analysis* (GB 17378.4-2007)

Survey parameters	Analytical methods	Methodological basis
Phosphates	Phosphomolybden um blue method	*Code of practice for international seabed area and high seas environmental survey- Part 2: Marine chemical survey* (GB/T 42629.2-2023) *The specification for marine monitoring- Part 4: Seawater analysis* (GB 17378.4-2007)
Silicate	Silicon molybdenum blue method	*Code of practice for international seabed area and high seas environmental survey- Part 2: Marine chemical survey* (GB/T 42629.2-2023) *The specification for marine monitoring- Part 4: Seawater analysis* (GB 17378.4-2007)
Ammonium	Indophenol blue method	*Code of practice for international seabed area and high seas environmental survey- Part 2: Marine chemical survey* (GB/T 42629.2-2023) *Specification for oceanographic survey- Part 4: Survey of chemical parameters in sea water* (GB/T 12763.4-2007)
Suspended solid	Gravimetric method	*Code of practice for international seabed area and high seas environmental survey- Part 2: Marine chemical survey* (GB/T 42629.2-2023) *The specification for marine monitoring- Part 4: Seawater analysis analysis* (GB 17378.4-2007)
Total alkalinity	pH meter method	*Code of practice for international seabed area and high seas environmental survey- Part 2: Marine chemical survey* (GB/T 42629.2-2023) *Specification for oceanographic survey- Part 4: Survey of chemical parameters in sea water* (GB/T 12763.4-2007)
Particulate organic carbon	Nondispersive infrared absorption spectrometry	*Code of practice for international seabed area and high seas environmental survey- Part 2: Marine chemical survey* (GB/T 42629.2-2023) *Determination of organic carbon in sea water by nondispersive infrared absorption spectrometry* (HY/T 150-2013)

3.2 Quality Assurance and Quality Control (QA&QC)

Sampling, storage, transportation, pretreatment, analysis, measurement, and data processing of water samples at the survey site strictly adhere to methods and techniques specified in the relevant national standards and marine industry standards. Seawater samples are collected at designated stations and depths according to the cruise plan, using CTD systems for stratified sampling. Sampling sequence is rigorously controlled; some parameters are measured directly on-site after sampling, while others are preserved and transported back to the shore-based laboratory for analysis. Sampling locations and times are carefully selected to avoid potential contamination. Prior to use, sample bottles undergo two or more soaking in high-purity acid, each soaking lasting over 24 h, with a final rinse

using RO water and Milli-Q ultrapure water three times or more. Laboratory conditions and quality control meet metrological certification system requirements, with corresponding quality control measures implemented. Specific aspects include:

(1) Clearly defining detection content, detection cycles, detection precision, accuracy, and other technical indicators as required by the project. Ensuring proper preparation and pre-cruise inspection of instruments, equipment, reagents, standards, and various experimental tools;

(2) Preparing appropriate standards and chemical reagents, with designated personnel for custody. National certified reference materials within their validity period must be used, while prepared chemical reagents are stored under specified conditions and used within specified time limits;

(3) Sampling locations should be far from ship sewage outlets. Strict measures must be taken to prevent contamination during sampling. Samples should be collected systematically according to relevant parameters, with priority given to gas samples. Sample pretreatment and preservation should follow national or industry standards;

(4) Laboratory environments should address condition such as noise, vibration, and dust to ensure c meets the requirement for instrument use and sample analysis. If environmental conditions are abnormal or cannot support analytical work, appropriate measures should be taken to resolve them before proceeding with analysis;

(5) Check the performance of inspection instruments, equipment, and various measuring instruments to ensure they meet testing requirements. All instruments used should be within their valid calibration period. Upon arrival at the site, instruments should undergo performance and stability checks, with necessary on-site calibration conducted. Instruments can only be used for analysis and testing once their performance is conformed to be good, with stable and reproducible data;

(6) Prior to analysis, laboratories must verify and carefully check whether the samples meet the testing requirements and whether the analysis scope is clearly defined;

(7) Ultrapure water used in the experiments should be properly stored and brought to the site as needed to ensure it meets the requirements for analytical testing;

(8) Laboratory personnel must hold professional qualifications and strictly adhere to safety regulations during testing. Smoking, eating snacks, drinking water, and storing food are strictly prohibited in the laboratory. Non-laboratory personnel are not permitted to enter without permission.

(9) Testing must strictly adhere to technical specifications as stipulated in the national standard or industry standards. After testing concludes, personnel should inspect and record the technical status of the testing instruments and equipment, as well as the environmental conditions.

(10) Quality control samples should be inserted at regular intervals during parameters analysis to ensure analysis quality. Necessary on-site blank and parallel sample testing should also be conducted;

(11) The original records of analysis testing must truthfully reflect the test results and are not allowed to be altered at will. Quality assurance personnel have the right to inspect the original records and provide feedback;

(12) Original records should be standardized in format, filled out completely, and signed by both the testing personnel and the verifier. Verifiers must carefully check testing data and promptly correct any issues;

(13) Assigned personnel are responsible for safeguarding original records and testing data to prevent loss.

4 Biological Community Baseline

The methods of biological community investigation are mainly based on the *Code of Practice for International Seabed Area and High Seas Environmental Survey—Part 3: Marine Biological Survey* (GB/T 42629.3-2023) and *The Technology Specification for the Pre-treatment of Deep-Sea Microorganism Samples* (GB/T 30744-2014) and the related technical regulations and specifications. The biological community elements analyzed in this report mainly include chlorophyll *a*, photosynthetic pigments, microorganisms, microphytoplankton, phytoplankton, zooplankton, small benthic organisms, macro benthic organisms, scavengers, fish, seabirds and mammal.

In addition, information on the spatial and temporal distribution of chlorophyll *a* and primary productivity was downloaded from the EU Copernicus Marine Services Data Center (https://www.copernicus.eu/). Information on the biogeographic distribution of the study area was collected from databases such as the World Bird Database (WBD), the Ocean Biogeographic Information System (OBIS), the Global Biodiversity Information Facility (GBIF), the Japan Marine Biodiversity Database (BISMaL), and the International Union for Conservation of Nature (IUCN).

4.1 Chlorophyll *a* and Photosynthetic Pigments

4.1.1 Survey Method

Water samples for chlorophyll *a* analysis were collected by a SBE911 plus CTD, according to the settled sampling levels, and the samples (0.6 L) collected from each level were filtered through 25 mm-diameter Whatman GF/F membrane. The collected samples

were wrapped in aluminum foil tape and stored in ultra-low temperature refrigerator for analysis when brought back to the laboratory. The extraction of chlorophyll *a* was carried out at 4°C. After stored at room temperature in dark for 0.5 h and acidated for 30 s, the extract was determined by TURNER-10-AU-005-CE fluorometer.

Water samples for photosynthetic pigment analysis were collected on membranes by a multiple inverted filtration. The samples were filtered through Millipore Swinnex® membrane filters with 25 mm diameter Merck GF/D membranes. The collected samples were stored in ultra-low temperature refrigerator (–80°C) for analysis in the laboratory. 3 mL of N, N-dimethylformamide (DMF) was added for the extraction of photosynthetic pigments, and the sample was extracted at –20 °C for one hour in dark (Furuya, et al., 1998). The extract was shaken for tens of seconds in dark. The supernatant was filtered through a 13 mm diameter Whatman® GF/F filter membrane (Swinnex Filter Holder). 0.6 mL of the filtered supernatant was mixed with 0.6 mL of ammonium acetate (1 mol L^{-1}), and then stored in a refrigerator at –20°C in dark. In this study, DMF was used as the organic extraction solvent for photosynthetic pigments.

The analytical system for photosynthetic pigments was an Agilent 1100 Series liquid chromatography workstation with a diode array detector (DAD) for the detection of elution peaks, and the scanning band was from 300 to 700 nm, and the peak spectral characteristics were recorded at fixed wavelengths of 440 nm and 663 nm. The separation was carried out on an Eclipse XDB C8 column (100×4.6 mm; Agilent Technologies, Germany) with a particle size of 3.5 μm. The mobile phase A was methanol: ammonium acetate buffer solution (1 mol L^{-1}) in the ratio of 4:1, and the mobile phase B was methanol. The gradient elution program was shown in Table 4-1, and the mobile phase flow rate was 1 mL min^{-1}. The interval time between every twice sample injection and program initiation was ~10 min (Mendes, et al., 2007).

Table 4-1 Gradient elution procedure for HPLC separation and analysis of photosynthetic pigments

Time (min)	Mobile phase A (%)	Mobile phase B (%)	gradient system
0	100	0	injection
2	100	0	linear gradient
16	55	45	linear gradient
27	0	100	linear gradient
32	0	100	linear gradient
36	100	0	equilibrium

4.1.2 Data Processing and Quality Control

The collection, pretreatment, storage and transportation of chlorophyll *a* and photosynthetic pigment samples were operated in accordance with the *Specifications for Oceanographic Survey* (GB12763.6-2007). The quality control of chlorophyll *a* was mainly the determination of duplicate samples in the laboratory to test the relative error of sample reproducibility in the process of chlorophyll *a* determination. Specific measures were to select a certain proportion of stations that could cover the entire surveyed sea area to a certain extent, and then to carry out duplicate sample determination. The quality control results of the duplicate sample determination of chlorophyll *a* should be in line with the *Code of Practice for International Seabed Area and High Seas Environmental Survey— Part 3: Marine Biological Survey* (GB/T 42629.3-2023).

The quality control and evaluation program for photosynthetic pigment was conducted according to Roy et al. (2011). It included: daily injection of standards to determine the resolution and retention time of the chromatographic peaks; daily determination of the change in absorption values and retention time of the chromatographic peaks based on the peak spectra of the standards; daily calibration of the Chl *a* concentration; daily test and analysis of the extraction efficiency of the samples; daily analysis of the HPLC spectra of the standard samples to confirm the change in the absorption wavelengths; confirmation of the working curve of the Chl *a* when changing the chromatographic column; analysis and control of the detector noise values; analysis and control of the noise level of the detector.

4.2 Microbe

4.2.1 Techniques

Microbial diversity analysis of seawater and sediments and surveys of culturable micro-organisms were carried out in accordance with the *Specifications for Oceanographic Survey - Part 6: Marine Biological Survey* (GB12763.6-2007).

Microbial samples were collected and processed in accordance with the *Technology Specification for the Pre-treatment of Deep-Sea Microorganism Samples* (GB/T 30744-2014). On-site sediment samples were preserved using three preservation methods: 4°C refrigerated, –20° frozen and –80°C frozen.

Microbial analysis data were obtained by extracting DNA from seawater and sediment samples and specifically amplifying one or two consecutive hypervariable regions, and sequencing the sequences of the hypervariable regions using a high-throughput sequencing platform. Subsequently, the sequencing data were processed and analyzed by bioinformatics analysis methods to obtain the composition of microbial communities and species annotation information in the samples.

The Deep-sea sediment DNA Extraction Kit was FastDNA® SPIN Kit for Soil, and the Water Filter Membrane DNA Extraction Kit was the PowerWater DNA Isolation Kit. 16S rRNA gene amplification primers:

27F: 5'-AGAGTTTGATCCTGGCTCAG-3'
1492R: 5'-ACGGCTACCTTGTTACGACT-3'

PCR amplification and product electrophoresis assay were performed using genomic DNA as a template, primers with barcode and PremixTaq (TaKaRa). After comparing the concentration of PCR products by Gene Tools Analysis Software (Version 4.03.05.0, SynGene), the required volume of each sample was calculated according to the principle of equal mass, and each PCR product was mixed. The mixed PCR products were recovered during analysis using the E.Z.N.A.® GelExtractionKit Gel Recovery Kit, and the target DNA fragments were recovered by elution using TE buffer. Subsequently, the recovered DNA samples were subjected to library construction operation, which was performed according to the NEBNext® Ultra™DNALibraryPrepKitforIllumina® standard procedure to ensure the accuracy and reliability of sequencing. After the library construction was completed, the samples were sequenced on-line using the high-throughput sequencing platforms Hiseq or Miseq.

The raw image data files obtained from sequencing are analyzed by BaseCalling to convert them into raw sequencing sequences (RawReads). The sequencing results are stored in FASTQ (abbreviated as fq) file format, which contains sequence information of

the sequenced sequences (Reads) and their corresponding sequencing quality information. These data can be further analyzed for bioinformatics, such as sequence alignment, species annotation, SNP detection, etc., to understand the genomic composition of the samples and genetic variation and other characteristics.

4.2.2 Data Processing Methods and Quality Control

The microbial diversity data analysis process is shown inFigure shows the process of microbial diversity data analysis.
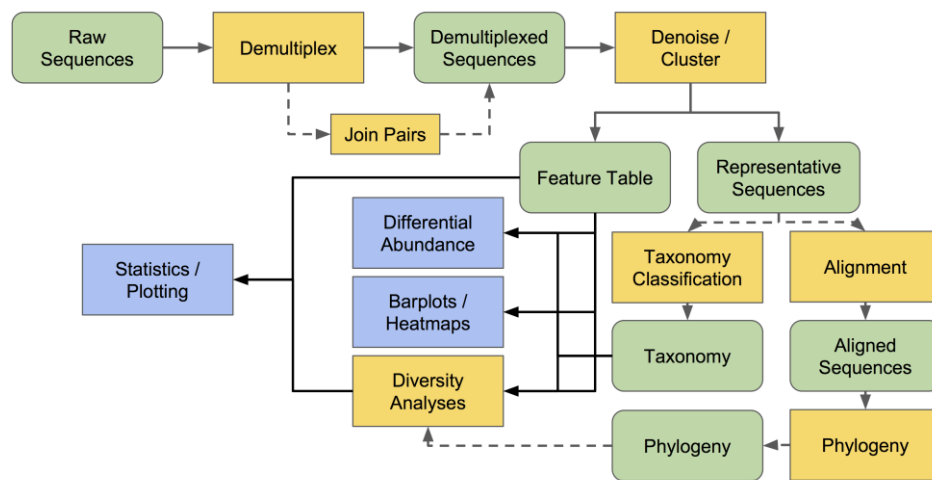
Figure 4-1 Microbial diversity analysis process

(1) Raw data Quality Control (QC) operation: Data QC is a crucial part of bioinformatics research. This step usually involves checking the sequencing quality of raw data, removing low-quality reads, and removing contamination to ensure the accuracy and reliability of the analysis results in the next step.

(2) Demultiplexing: Qiime software is a software used to process high-throughput sequencing data, which helps to remove chimeras (chimeras) from sequencing data and to cluster the reads. In the clustering process, the reads are sorted according to their abundance from largest to smallest and clustered using the criterion of 97% similarity to obtain OTUs. Each OTU is considered to represent a species.

(3) Random draw leveling operation: the tags of each sample are randomly leveled and the corresponding OTU sequences are extracted. This step aims to reduce the differences between samples, making the comparison between samples more accurate and reliable.

(4) Dilution curves for diversity indices: Dilution curves of α and β diversity indices were plotted using the Qiime software to help select appropriate pumping leveling parameters.

(5) OTU classification: in this step, representative sequences are utilized to compare with the 16S database, thus classifying each OTU into species.

(6) Obtain the OTU abundance table: Based on the number of sequences in each OTU, the OTU abundance table will be obtained. This table will be used for subsequent analyses, such as species diversity analysis, community structure analysis, functional analysis, and so on.

Due to the large difference in the number of reads corresponding to different samples, in order to ensure that the results of the later analysis are reasonable, the data of each sample is processed by random draw leveling. This method can eliminate the influence of the difference in the number of reads in different samples on the analysis results, making the analysis results more reliable and comparable. The selection of the leveling parameters is very important, and we determine the leveling parameters according to the dilution curve of the alpha diversity index.

The methodology for analyzing the microbial population structure of enriched colonies and environmental samples focused on the use of PacBio raw reads processed using SMRT Link Analysis software version 6.0 to obtain circular coherence sequence (CCS) reads: parameters were set to a minimum number of passes = 3, and minimum prediction accuracy = 0.99. Raw reads were processed through SMRT Portal processing to screen for sequence length (1300–1500 bp) and quality. Further filtering was performed by removing barcode, primer sequences, chimeras and sequences containing 10 consecutive identical bases. OTUs were clustered according to a similarity threshold of 98.65% using UPARSE (version 7.1, http://drive5.com/uparse/), and chimeric sequences were identified and removed using UCHIME.RDPClassifier (http://rdp.cme.msu.edu/) was used against Silva (SSU132) 16S rRNA database and analyzed the phylogenetic relationships of each 16S rRNA gene sequence using a 70% confidence threshold.

4.3 Picoplankton

4.3.1 Survey Method

Picophytoplankton species and abundance were determined by flow cytometry (Olson et al., 1993). Water samples were collected using a SBE 911 plus CTD, fixed with 500 μL of 20% paraformaldehyde and stored in liquid nitrogen. When arrived at the laboratory, flow cytometers (BD FACSCalibur) were used to identify picophytoplankton species and

determine abundance. The sensitivity and accuracy of the flow cytometer were checked according to the method provided by the instrument manufacturer (the CV value generally should be less than 2.0) to ensure that the instrument was in good condition.

4.3.2 Data Processing and Quality Control

The quality control of picophytoplankton was mainly the determination of laboratory duplicate samples to test the relative error of sample repeatability. The number of duplicate samples was 26, which represented 33.3% of the total number of samples. The quality control results of the determination of the duplicate picophytoplankton samples showed that the sample repeatability error was 0.20% ~ 9.50%, less than ±10%, and the determination accuracy was in accordance with the *Code of practice for International Seabed Area and High Seas environmental survey—Part 3: Marine biological survey* (GB/T 42629.3-2023).

4.4 Phytoplankton

4.4.1 Survey Method

Phytoplankton samples were collected by CTD and phytoplankton vertical trawl. The layers of water samples included 0m, 25m/30m, 50m, 75m, 100m, 125m, 150m, 200m, as well as the chlorophyll a maximum layer (DCM). 2L of seawater samples were collected, fixed with 5% formaldehyde solution and preserved at room temperature. Phytoplankton net with a mesh of 20 μm was vertically towed from 200 m underwater to the surface, then rinsed and collected in sample bottles, fixed with 5% formaldehyde solution, and stored at room temperature. The water filtration was measured by a flowmeter of Hydro-Bios No. 438115.

For laboratory analyses, phytoplankton samples were first subjected to stationary settling for >48h, then the supernatant was siphoned off. The samples were concentrated, and then observed under a microscope for species identification and enumeration.

4.4.2 Data Processing and Quality Control

Plankton sampling net, procedure, samples treatment and preservation, and laboratory analysis method were carried out in accordance with the Specification of Oceanographic Investigation to ensure the quality of the samples.

The diversity index was calculated using a logarithmic formula as follows:

$$H' = -\sum (p_i \log_2 p_i)$$

The evenness was calculated by the formula:

$$J' = H'/\log_2 S$$

The data obtained from the identification analysis were statistically processed by SPSS software.

4.5 Zooplankton

4.5.1 Survey Method

The macro- and meso- plankton samples were collected by plankton WP2 nets with a mesh size of 200 μm, which were vertically towed from 200 m underwater to the surface, then rinsed and collected in sample bottles, fixed with 5% formaldehyde solution, and stored at room temperature. Water filtration was measured by a Hydro-Bios mesh flowmeter.

The investigation of plankton stratified distribution was carried out by using a plankton stratified trawl (HydroBios Multinet System Maxi) After layer vertical towed for 0~50m, 50~100m, 100~200m, 200~500m, 500~1000m, 1000~2000m, 2000~3000m, 3000m~4000, 4000~4500m, samples were rinsed and collected in sample bottles, fixed with 5% formaldehyde solution and stored at room temperature. Water filtration and other environmental parameters were collected by the instrument sensors.

4.5.2 Data Processing and Quality Control

Zooplankton diversity analysis calculation and quality control were shown in 4.4.2.

4.6 Metazoan meiofauna

Metazoan meiofaunal samples were collected using a multi-corer from which undisturbed core samples were taken. At least three sediment samples were taken at each station, with one of the three samples used for metazoan meiofaunal abundance calculations and species identification, one sample for molecular biological analyses, and one for determination of sediment environmental parameters.

The steps for processing core samples in situ are as follows:

a) The 2 tubes of sediment core samples were sliced into 5 layers according to 0 cm–1 cm, 1 cm–2 cm, 2 cm–3 cm, 3 cm–4 cm and 4 cm–5 cm (additional layers may be added as appropriate). The organisms in the overlying water of each core were intercepted by a 32 μm mesh sieve and loaded together with sediment samples of the layer of 0–1 cm while the sediment samples from the remaining layers were bottled separately. Samples for morphological identification were fixed by 5% formaldehyde and samples for molecular biology analysis were fixed and preserved by 95% alcohol.

b) The upper 10-cm sediment layer for sediment environmental parameter analysis is sliced into 10 layers at 1-cm intervals. It at least includes sediment grain size, total organic carbon (%), chlorophyll *a* and phaeophytin *a* samples. The organic carbon and chlorophyll samples should be stored at –20 ℃. The sediment sample mass for analysis of grain size and organic carbon should not be less than 50 g, and the sample mass for chlorophyll analysis should not be less than 5 g.

4.7 Benthic protozoa

One tube of undisturbed multi-core samples was taken, and 0–5 cm of sediment was sliced by 1-cm thickness, and preserved in the same way as the samples analyzed for the metazoan meiofaunal morphology. In addition, a handful of 0–2cm sediments were taken from the core samples used for the analysis of sediment environmental parameters to collect molecular data on benthic protozoa.

4.8 Macrofauna

Macrofauna were sampled using a box-corer (0.25m^2), and sample pre-treatment was carried out in accordance with the *Code of Practice for International Seabed Area and High Seas Environmental Survey* (GB/T 42629.3-2023) and the *Recommendations for the guidance of contractors for the assessment of the possible environmental impacts arising from exploration for marine minerals in the Area* (ISBA/25/LTC/6). Top water was removed from the box through a 0.25-millimetre screen and the residue was later added to the 0–1 cm layer sample. The sediment was collected from each depth according to the spacing of 0–1 cm, 1–5 cm, and 5–10 cm, and the sediment samples were eluted with a 250 μm mesh sieve on site in order to obtain the macrofauna samples, which were fixed and preserved by adding 95% ethanol. The macrofauna was sorted into taxa in the laboratory and then submitted to taxonomic experts for morphological identification and counting. The samples were weighed using an analytical balance with a sensitivity of 0.0001g.

For quality control, duplicated sampling at the same station was conducted and only un-disturbed box-corer sample was chosen to macrofauna research. Sampling and sample pre-processing were carried out in accordance with the GB/T 42629.3-2023, and the sample analysis and identification were completed by personnel with relevant professional qualifications for oceanographic investigation and checked by a second person.

① Regarding the size of the macrofauna sieve: All previous environmental guidelines, including ISBA/25/LTC/6/Rev.1, recommended using a 250 μm sieve, and the macrofauna sieve size was subsequently adjusted to 300 μm. However, ISBA/25/LTC/6/Rev.3 also states: "Contractors can continue to use the sieve size they previously used to ensure that the data are compatible... If contractors decide to continue to use a 250 μm sieve, then interpretation of the results will require some intercalibration between the two sieve sizes." According to Gage et al. (2002), a study of box-corer samples collected at a water depth of 1900 m, using a 300 mm sieve would result in the loss of some macrofauna, with a 3.5% decrease in abundance and a decrease in the number of species (see Table 4-2), and the deeper the water, the higher the oligotrophy, the smaller the benthos, and the higher the proportion of macrofauna that will be missed when using a 300 μm sieve, Therefore, the ISO 22787 standard issued by ISO in 2023 also recommends a 250 μm sieve for macrofauna. Therefore, we use a 250 μm sieve for macrofauna.

Table 4-2 Diversity statistics applied to pooled data from box-core samples (total biomass, no, of individuals, no. of species) by sieve size

Diversity index	Sieve size (mesh, mm)				
	1.0	0.5	0.425	0.3	0.25
Shannon's H' (log base 2)	5.71	5.83	5.85	5.85	5.89
Pielou's J'	0.87	0.81	0.79	0.79	0.79
Simpson's diversity index ($1/D$)	31.88	22.04	21.66	23.20	24.27
Berger-Parker $1/d$	7.82	5.69	5.79	6.32	6.52
$E(S_{258})$	93	87.23	87.39	84.47	85.01
Total biomass (g 0.5 m^{-2})	0.940	0.987	0.998	1.002	1.003
Total N (0.5 m^{-2})	258	820	1094	1334	1383
Total S (0.5 m^{-2})	93	149	165	169	173

4.9 Megafauna

Currently, analytical research on megafauna is conducted using survey methods such as deep-towed camera system.

Deep-towed camera system: Using a deep-towed camera system for near-bottom photography, estimate the nodule coverage in the images obtained by the deep-towed

camera system, manually observe real-time high-definition images of the seabed, identify and count the types and number of megafauna, and take high-definition photos of megafauna. Study the relationship between megafauna distribution and nodule coverage by comparing the nodule coverage and the distribution characteristics of the number and types of megafauna with a gradient of every 5%.

In the current report, the analysis of megafauna is primarily based on photos obtained from a deep-towed camera system. The number of photos listed refers to the manually selected photos containing megafauna, not the total number captured by the camera system. The resolution is not high enough for distinguishing megafauna of 2–3 cm in size, and there are difficulties in species identification.

Photographs and high-resolution video of megafauna using AUV and HOV altimetry are planned for 2024 cruise for megafauna abundance estimation, combined with species identification of biological specimens collected by HOV.

4.10 Scavenger

The deep-sea bio-trapping & observation system (Lander) was utilized to conduct deep-sea scavenger sampling and video survey. The survey method was as follows: after the Lander arrived at the seafloor, the image recording system was set to start at regular intervals, the camera was set to take pictures at a rate of 1 picture/minute, and the camera was dormant for 30 minutes after each 30-minute period of continuous recording. After landing on the seafloor for approximately 48 h, the equipment was recovered. Immediately after the equipment returned to the deck, biological samples were collected from the trapping cage into 4°C seawater, photographed on-site, selected samples were stored at –80°C, and the remaining samples were stored in 100% alcohol.

Based on the morphology of the organisms, swimming trajectories and other characteristics to determine whether the similar individuals appearing continuously in a short period of time are the same body, observe and record the type of all benthos and the number of individuals at the station, and summarize and analyze the data in a graphical form.

4.11 Fisheries Resources

4.11.1 Techniques

Fishery acoustic survey using fish detector Simrad EK80, comprehensive consideration of the depth of detection of a transducer, the quality of data and noise

interference to choose the 70 kHz frequency data for analysis, acoustic data using a special data display and recording software ER80 for preservation, the main technical parameters as shown in Table 4-3.

Table 4-3 Main Technical Parameters and Setting Parameters of Fish Finder

Transducer parameters	Value	Transducer parameters	Value
Transducer Model	ES70-7C	Frequency	70 kHz
Beam Type	Split	Equivalent beam Stereo angle	−21.00°
Beam Transverse Angle	7.00°	Firing power	250 W
Longitudinal beam angle	7.00°	Beam Type	split
Transducer Installation Water Depth	6 m	Absorption coefficient	Adjusted for temperature and salinity data
Pulse width	1.024 ms	Velocity	Adjusted for temperature and salinity data

4.11.2 Data Processing Methods and Quality Control

Figure 4-2 shows a schematic of the process for analyzing fisheries acoustic survey data.
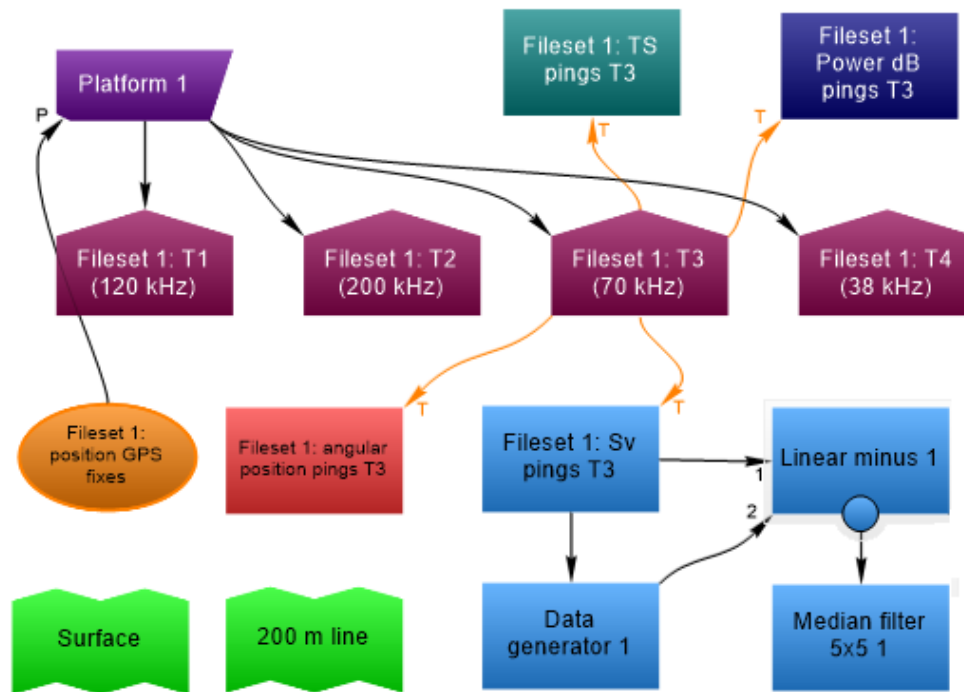
Figure 4-2 Schematic diagram of the acoustic data analysis process

In order to reduce the ambient noise interference, the noise was eliminated by using set thresholds, simulated background noise elimination method, 5×5 mean filtering and manual method. The minimum threshold was set to –78 dB for this analysis.

For two fish with the same target intensity, the fish farther away from the transducer reflects less sound intensity due to the propagation loss, so distance compensation (TVG) is needed for the echo signal intensity. In this project, the background noise is set to –126 dB, which can better reject the noise without affecting the valid data. On the basis of the above processing, the 5×5 mean filter module in Echoview is used to continue the image processing to remove the traveling vessel noise. Finally, the noise that cannot be removed by any of the above methods is manually removed (Figure 4-3).
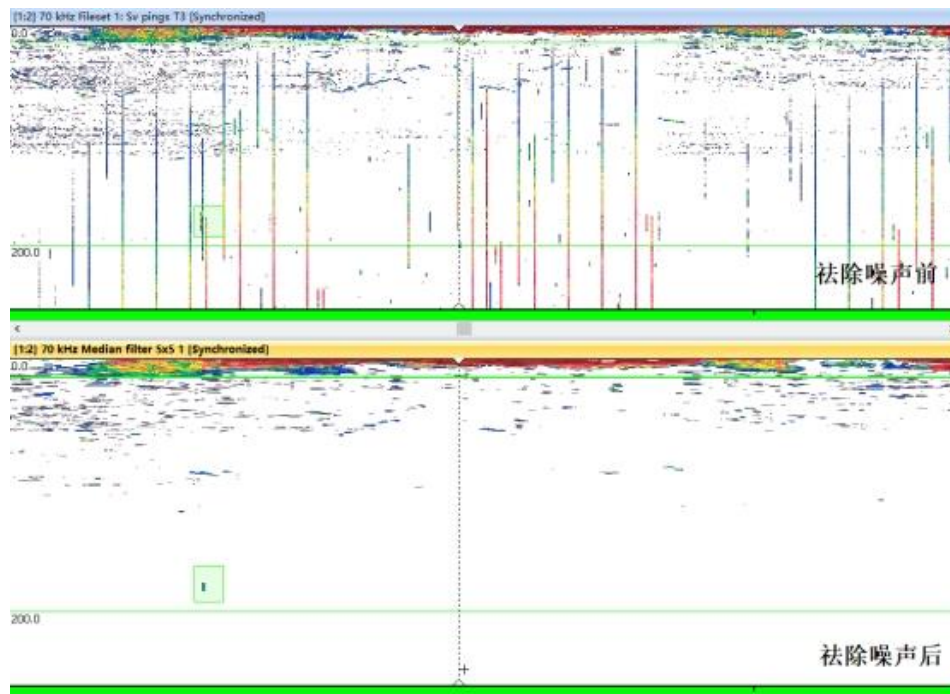
Figure 4-3 Comparison of acoustic data noise rejection effects

Since swimming animals were not sampled in this survey, an accurate assessment of the resources could not be made. Therefore, the Nautical Area Scattering Coefficient (NASC) of the surveyed sea area was analyzed using the echo integration method, and because of the linear relationship followed between the NASC value and the fishery resources, the amount of the NASC value can represent the relatively high and low fishery resources.

Considering the surface noise, the detection capability of the transducer, and the noise situation, the depth of the water layer analyzed in this study is between 15 and 200 m. The basic integration cruise unit of the data used to analyze the distribution of NASC values is set to be 5 n mile, and the basic analysis unit of 2 h is used to analyze the diurnal variation of NASC.

4.12 Seabirds, Turtles and Mammals

Sea turtle, marine mammal and seabird diversity surveys were conducted with walkover observations combined with open data, mainly investigating the species composition of marine mammals such as pinnipeds and cetaceans and seabirds.

Seabird surveys are based primarily on the *Technical Guidelines for Biodiversity Monitoring: Birds* (HJ710.42014) and *Draft guidelines for the establishment of baseline environmental data*（ISBA/27/C/11）. Observation surveys are usually conducted in weather conditions with good visibility (≥ 500 m) and low wind and wave conditions. Observations were carried out on the observation platform using binoculars in combination with naked eye observations. The left and right observation ranges were 100° on their respective sides, i.e., the waters from 90° on their respective sides to 10° beyond the centerline with the course direction as 0°. A survey consists of a series of 5 min observation periods, which are exclusively dedicated to detecting birds. Information was recorded after sighting the animal including the exact time of sighting and location of the locus.

After the field observation data were collated, the list of sea turtles, marine mammals and seabird species in the surveyed sea area was listed, and the endangered class was listed according to the IUCN list.

4.13 Primary Productivity

4.13.1 Survey Method

Primary productivity was determined using the ^{14}C black and white bottle method. The transparency of seawater was first determined using a transparency disk. After determined the optical depth of sampling, the seawater from each layer was collected using the SBE 911 plus CTD and dispensed into 175mL narrow-mouth square bottles, with two white bottles and one black bottle at each depth. Then ^{14}C markers were added to the samples. The sample bottles of different water layers were dispensed into the corresponding light attenuating membrane sleeves for six gradients of 100%, 50%, 30%, 10%, 5% and 1% of the surface layer light intensity, respectively. The membrane sleeves box was cultured in the surface water flow temperature-controlled deck culture tank for 4~6 h. After cultured the samples would be collected back to the isotope container laboratory, and filtered in the isotope of the 6-connected negative pressure filtration. After filtered through 25 mm diameter 0.22 μm pore size polycarbonate filter membrane, the membrane would be put into the scintillation, treated with concentrated hydrochloric acid

and stored in a refrigerator at –20°C. After the samples were brought back to the laboratory, the scintillation liquid was added to the scintillation bottle which contained the filter membrane. The bottle was placed in the liquid scintillation counter Tricarb-3110TR after oscillation, and the measurement was carried out after the samples were dark adapted completely.

In addition, monthly spatial distribution data of global ocean primary productivity at 9 km resolution were downloaded since 2003 from the Electronic Journal of *Global Change Data Repository*. This data was calculated using the SABPM model for global ocean primary productivity remote sensing monitoring data by six types of MODIS product data, namely phytoplankton absorption coefficient, chlorophyll concentration, true photosphere depth, 490 nm diffuse attenuation coefficient, photosynthetically active radiation and sea surface temperature. This dataset was time-series data (with monthly frequency) and stored in.hdf format (Tao et al., 2019).

4.13.2 Data Processing and Quality Control

The quality control of primary productivity was mainly the determination of duplicate samples of white and black bottles in the laboratory to test the relative error of sample repeatability. The specific quality control measure was the determination of duplicate samples for all black and white bottle samples. The number of duplicate samples was 108, representing 100% of the total number of samples. The quality control results of the primary productivity determination of duplicate samples showed that the sample repeatability error was 0.12%~7.50%, less than ±10%, and the determination accuracy was in accordance with the requirements of the *Code of Practice for International Seabed Area and High Seas Environmental Survey—Part 3: Marine Biological Survey* (GB/T 42629.3-2023).

References

Biscaye, P. E. (1965). Mineralogy and Sedimentation of Recent Deep-Sea Clay in the Atlantic Ocean and Adjacent Seas and Oceans. *Geological Society of America Bulletin*, *76*(7), 803. https://doi.org/10.1130/0016-7606(1965)76[803:MASORD]2.0.CO;2

Gage, J. D., Hughes, D. J., & Vecino, J. L. G. (2002). Sieve size influence in estimating biomass, abundance and diversity in samples of deep-sea macrobenthos. *Marine Ecology Progress Series*, *225*, 97–107.

ISO 22787:2023(E). Marine environmental impact assessment (MEIA) — Technical specifications for marine biotic surveys in the international seabed area — General principles. ISO, Published in Switzerland, July 10, 2023.

Olson, R. J., Zettler, E. R., & DuRand, M. D. (1993). Phytoplankton Analysis Using Flow Cytometry. In *Handbook of Methods in Aquatic Microbial Ecology*. CRC Press.

Tao, Z., Zhou, X., Xie, F., Lv, T., & Wang, J. (2019). *Time Series of Monthly Global Marine NPP Dataset Based on MODIS and SABPM Model (Since 2003).* Digital Journal of Global Change Data Repository. https://doi.org/10.3974/geodb.2019.05.01.V1

Schedule 1 Standard Deviation of Trace Element Data

Testing items	Results	GSS-17	GSS-23	GSS-27	GSS-28
SiO$_2$	Recommended value（%）	78.30	59.80	58.87	61.10
	Measured value（%）	77.43	60.78	61.63	63.21
	Relative deviation（%）	1.11	1.64	4.69	3.45
Al$_2$O$_3$	Recommended value（%）	9.65	13.92	13.15	18.10
	Measured value（%）	9.57	13.99	12.49	17.48
	Relative deviation（%）	0.83	0.50	5.02	3.43
CaO	Recommended value（%）	1.83	4.21	4.91	0.40
	Measured value（%）	1.79	4.16	4.87	0.42
	Relative deviation（%）	2.19	1.19	0.81	5.00
Fe$_2$O$_3$	Recommended value（%）	2.07	5.54	6.12	6.50
	Measured value（%）	2.01	5.61	6.39	6.52
	Relative deviation（%）	2.90	1.26	4.41	0.31
MgO	Recommended value（%）	0.78	2.61	2.75	1.18
	Measured value（%）	0.81	2.52	2.65	1.15
	Relative deviation（%）	3.85	3.45	3.64	2.54
K$_2$O	Recommended value（%）	2.56	2.64	2.37	2.83
	Measured value（%）	2.52	2.68	2.35	2.76
	Relative deviation（%）	1.56	1.52	0.84	2.47
Na$_2$O	Recommended value（%）	2.31	1.91	1.22	0.29
	Measured value（%）	2.40	1.85	1.28	0.30
	Relative deviation（%）	3.90	3.14	4.92	3.45
MnO	Recommended value（%）	0.04	0.11	0.12	0.15
	Measured value（%）	0.04	0.11	0.12	0.15
	Relative deviation（%）	0.00	3.51	2.44	3.45
P$_2$O$_5$	Recommended value（%）	0.05	0.16	0.18	0.11
	Measured value（%）	0.05	0.16	0.17	0.11
	Relative deviation（%）	3.85	3.23	4.49	2.65
TiO$_2$	Recommended value（%）	0.30	0.83	1.07	0.85
	Measured value（%）	0.30	0.85	1.09	0.85
	Relative deviation（%）	0.00	1.92	1.87	0.00
Zr	Recommended value(mg/kg)	134.00	210.00	262.00	225.00
	Measured value(mg/kg)	138.00	195.00	246.00	231.00
	Relative deviation（%）	2.99	7.14	6.11	2.67
As	Recommended value（mg/kg）	6.20	11.80	13.30	28.50
	Measured value（mg/kg）	6.26	11.90	14.00	27.60
	Relative deviation（%）	0.97	0.85	5.26	3.16
Sb	Recommended value（mg/kg）	0.56	0.77	1.21	3.60
	Measured value（mg/kg）	0.53	0.81	1.22	3.70
	Relative deviation（%）	5.36	5.19	0.83	2.78
Hg	Recommended value（mg/kg）	0.01	0.06	0.12	0.14
	Measured value（mg/kg）	0.01	0.06	0.12	0.14

Testing items	Results	GSS-17	GSS-23	GSS-27	GSS-28
	Relative deviation（%）	0.00	6.90	5.17	2.10
Li	Recommended value（mg/kg）	14.20	50.00	41.00	66.00
	Measured value（mg/kg）	14.20	49.20	41.40	67.70
	Relative deviation（%）	0.00	1.60	0.98	2.58
Be	Recommended value（mg/kg）	1.30	2.30	2.30	3.60
	Measured value（mg/kg）	1.24	2.29	2.37	3.67
	Relative deviation（%）	4.62	0.43	3.04	1.94
Sc	Recommended value（mg/kg）	5.10	13.80	14.20	16.30
	Measured value（mg/kg）	4.83	14.10	14.10	17.20
	Relative deviation（%）	5.29	2.17	0.70	5.52
Co	Recommended value（mg/kg）	5.00	16.00	19.00	18.20
	Measured value（mg/kg）	4.90	15.80	18.80	18.70
	Relative deviation（%）	2.00	1.25	1.05	2.75
Ni	Recommended value（mg/kg）	9.60	38.00	43.00	43.00
	Measured value（mg/kg）	10.00	38.10	42.50	41.50
	Relative deviation（%）	4.17	0.26	1.16	3.49
Cu	Recommended value（mg/kg）	12.60	32.00	54.00	38.00
	Measured value（mg/kg）	13.00	32.90	54.50	37.60
	Relative deviation（%）	3.17	2.81	0.93	1.05
Zn	Recommended value（mg/kg）	29.00	97.00	127.00	134.00
	Measured value（mg/kg）	28.80	95.10	130.00	134.00
	Relative deviation（%）	0.69	1.96	2.36	0.00
Ga	Recommended value（mg/kg）	10.80	18.50	17.90	25.00
	Measured value（mg/kg）	10.30	18.50	18.50	24.90
	Relative deviation（%）	4.63	0.00	3.35	0.40
Rb	Recommended value（mg/kg）	80.00	123.00	105.00	182.00
	Measured value（mg/kg）	77.90	121.00	106.00	185.00
	Relative deviation（%）	2.62	1.63	0.95	1.65
Sr	Recommended value（mg/kg）	209.00	154.00	146.00	51.00
	Measured value（mg/kg）	211.00	156.00	148.00	50.40
	Relative deviation（%）	0.96	1.30	1.37	1.18
Nb	Recommended value（mg/kg）	6.30	17.40	20.00	19.60
	Measured value（mg/kg）	5.98	16.50	21.30	21.40
	Relative deviation（%）	5.08	5.17	6.50	9.18
Cd	Recommended value（mg/kg）	0.06	0.15	0.59	0.52
	Measured value（mg/kg）	0.05	0.16	0.57	0.54
	Relative deviation（%）	6.90	8.00	2.88	3.85
In	Recommended value（mg/kg）	0.02	0.07	0.09	0.12
	Measured value（mg/kg）	0.02	0.07	0.09	0.12
	Relative deviation（%）	4.17	1.52	0.00	0.82
Cs	Recommended value（mg/kg）	3.00	9.30	7.70	19.60
	Measured value（mg/kg）	2.88	9.00	7.54	20.20

Testing items	Results	GSS-17	GSS-23	GSS-27	GSS-28
	Relative deviation（%）	4.00	3.23	2.08	3.06
Ba	Recommended value（mg/kg）	606.00	441.00	496.00	532.00
	Measured value（mg/kg）	601.00	438.00	496.00	546.00
	Relative deviation（%）	0.83	0.68	0.00	2.63
Hf	Recommended value（mg/kg）	3.80	6.10	7.10	6.40
	Measured value（mg/kg）	3.84	5.98	6.57	6.69
	Relative deviation（%）	1.05	1.97	7.46	4.53
Ta	Recommended value（mg/kg）	0.42	1.30	1.49	1.80
	Measured value（mg/kg）	0.40	1.25	1.39	1.70
	Relative deviation（%）	4.76	3.85	6.71	5.56
Pb	Recommended value（mg/kg）	17.40	28.00	41.00	61.00
	Measured value（mg/kg）	16.60	28.20	41.40	61.00
	Relative deviation（%）	4.60	0.71	0.98	0.00
Bi	Recommended value（mg/kg）	0.15	0.44	0.79	1.53
	Measured value（mg/kg）	0.16	0.43	0.78	1.49
	Relative deviation（%）	6.67	2.27	1.27	2.61
Th	Recommended value（mg/kg）	4.30	13.50	13.20	21.00
	Measured value（mg/kg）	3.99	13.40	11.90	22.50
	Relative deviation（%）	7.21	0.74	9.85	7.14
U	Recommended value（mg/kg）	1.20	2.60	2.90	5.20
	Measured value（mg/kg）	1.11	2.51	2.76	5.41
	Relative deviation（%）	7.50	3.46	4.83	4.04
Mo	Recommended value（mg/kg）	0.51	0.65	0.84	1.18
	Measured value（mg/kg）	0.52	0.62	0.80	1.19
	Relative deviation（%）	1.96	4.62	4.76	0.85
W	Recommended value（mg/kg）	0.70	2.10	45.00	23.00
	Measured value（mg/kg）	0.77	2.05	42.80	24.90
	Relative deviation（%）	10.00	2.38	4.89	8.26
Tl	Recommended value（mg/kg）	0.51	0.71	0.67	1.20
	Measured value（mg/kg）	0.47	0.69	0.65	1.26
	Relative deviation（%）	7.84	2.82	2.99	5.00
V	Recommended value（mg/kg）	40.00	104.00	120.00	124.00
	Measured value（mg/kg）	41.90	109.00	123.00	122.00
	Relative deviation（%）	4.75	4.81	2.50	1.61
Cr	Recommended value（mg/kg）	25.00	82.00	92.00	94.00
	Measured value（mg/kg）	23.40	81.80	92.10	96.60
	Relative deviation（%）	6.40	0.24	0.11	2.77
Ge	Recommended value（mg/kg）	1.11	1.40	1.47	1.83
	Measured value（mg/kg）	1.06	1.44	1.47	1.80
	Relative deviation（%）	4.50	2.86	0.00	1.64
Y	Recommended value（mg/kg）	12.70	29.00	31.00	34.00
	Measured value（mg/kg）	12.60	29.10	31.10	34.40

Testing items	Results	GSS-17	GSS-23	GSS-27	GSS-28
	Relative deviation（%）	0.79	0.34	0.32	1.18
La	Recommended value（mg/kg）	14.00	42.00	43.00	50.00
	Measured value（mg/kg）	14.80	40.40	43.60	54.50
	Relative deviation（%）	5.71	3.81	1.40	9.00
Ce	Recommended value（mg/kg）	25.00	78.00	82.00	107.00
	Measured value（mg/kg）	25.50	71.00	78.60	111.00
	Relative deviation（%）	2.00	8.97	4.15	3.74
Pr	Recommended value（mg/kg）	3.20	9.30	9.80	11.00
	Measured value（mg/kg）	3.01	8.99	10.40	12.00
	Relative deviation（%）	5.94	3.33	6.12	9.09
Nd	Recommended value（mg/kg）	12.40	36.00	44.00	43.00
	Measured value（mg/kg）	12.20	35.20	44.00	43.60
	Relative deviation（%）	1.61	2.22	0.00	1.40
Sm	Recommended value（mg/kg）	2.40	6.60	6.90	7.40
	Measured value（mg/kg）	2.45	6.32	6.94	7.60
	Relative deviation（%）	2.08	4.24	0.58	2.70
Eu	Recommended value（mg/kg）	0.66	1.40	1.50	1.38
	Measured value（mg/kg）	0.71	1.34	1.50	1.42
	Relative deviation（%）	7.58	4.29	0.00	2.90
Gd	Recommended value（mg/kg）	2.20	5.80	6.20	6.60
	Measured value（mg/kg）	2.20	5.61	6.15	6.77
	Relative deviation（%）	0.00	3.28	0.81	2.58
Tb	Recommended value（mg/kg）	0.37	0.93	1.00	1.11
	Measured value（mg/kg）	0.39	0.98	1.04	1.05
	Relative deviation（%）	5.41	5.38	4.00	5.41
Dy	Recommended value（mg/kg）	2.30	5.40	5.70	6.30
	Measured value（mg/kg）	2.21	4.90	5.26	5.84
	Relative deviation（%）	3.91	9.26	7.72	7.30
Ho	Recommended value（mg/kg）	0.46	1.08	1.13	1.27
	Measured value（mg/kg）	0.47	0.98	1.10	1.16
	Relative deviation（%）	2.17	9.26	2.65	8.66
Er	Recommended value（mg/kg）	1.30	3.00	3.20	3.70
	Measured value（mg/kg）	1.33	2.71	2.95	3.40
	Relative deviation（%）	2.31	9.67	7.81	8.11
Tm	Recommended value（mg/kg）	0.23	0.49	0.51	0.60
	Measured value（mg/kg）	0.25	0.45	0.50	0.56
	Relative deviation（%）	8.70	8.16	2.94	6.67
Lu	Recommended value（mg/kg）	0.24	0.48	0.50	0.59
	Measured value（mg/kg）	0.23	0.46	0.47	0.55
	Relative deviation（%）	4.17	4.17	6.00	6.78

Schedule 2 List of Species in the Contract Area

Schedule 2-1 Inventory of seabirds, sea turtles and large mammal species in the contract area and adjacent areas

Scientific Name	Kingdom	Phylum	Class	Order	Family	Genus	Danger	Source
Caretta caretta	Animalia	Chordata	Reptilia	Testudines	Cheloniidae	*Caretta*	VU	③
Lepidochelys olivacea	Animalia	Chordata	Reptilia	Testudines	Cheloniidae	*Lepidochelys*	VU	③
Dermochelys coriacea	Animalia	Chordata	Reptilia	Testudines	Dermochelyidae	*Dermochelys*	VU	③
Pluvialis fulva	Animalia	Chordata	Aves	Charadriiformes	Charadriidae	*Pluvialis*	LC	④
Gvgis alba	Animalia	Chordata	Aves	Charadriiformes	Laridae	*Gygis*	LC	④
Onychoprion anaethetus	Animalia	Chordata	Aves	Charadriiformes	Laridae	*Onychoprion*	LC	④
Onychoprion fuscatus	Animalia	Chordata	Aves	Charadriiformes	Laridae	*Onychoprion*	LC	④
Sterna sumatrana	Animalia	Chordata	Aves	Charadriiformes	Laridae	*Sterna*	LC	③
Calidris acuminata	Animalia	Chordata	Aves	Charadriiformes	Scolopacidae	*Calidris*	VU	④
Calidris canutus	Animalia	Chordata	Aves	Charadriiformes	Scolopacidae	*Calidris*	LC	③
Gallinago stenura	Animalia	Chordata	Aves	Charadriiformes	Scolopacidae	*Gallinago*	LC	③
Numenius madagascariensis	Animalia	Chordata	Aves	Charadriiformes	Scolopacidae	*Numenius*	EN	③
Stercorarius longicaudus	Animalia	Chordata	Aves	Charadriiformes	Stercorariidae	*Stercorarius*	LC	④
Phaethon aethereu	Animalia	Chordata	Aves	Pelecaniformes	Phaethontidae	*Phaethon*	LC	④
Phaethon lepturus	Animalia	Chordata	Aves	Pelecaniformes	Phaethontidae	*Phaethon*	LC	④
Phaethon rubricauda	Animalia	Chordata	Aves	Pelecaniformes	Phaethontidae	*Phaethon*	LC	④
Sula dactylatra	Animalia	Chordata	Aves	Pelecaniformes	Sulidae	*Sula*	LC	④
Sula leucogaster	Animalia	Chordata	Aves	Pelecaniformes	Sulidae	*Sula*	LC	④
Sula sula	Animalia	Chordata	Aves	Pelecaniformes	Sulidae	*Sula*	LC	④
Fregata minor	Animalia	Chordata	Aves	Pelecaniformes	Fregatidae	*Fregata*	LC	④
Oceanodroma leucorhoa	Animalia	Chordata	Aves	Procellariiformes	Hydrobatidae	*Oceanodroma*	VU	④
Oceanodroma tristrami	Animalia	Chordata	Aves	Procellariiformes	Hydrobatidae	*Oceanodroma*	LC	④
Ardenna pacifica	Animalia	Chordata	Aves	Procellariiformes	Procellariidae	*Ardenna*	LC	④
Bulweria bulwerii	Animalia	Chordata	Aves	Procellariiformes	Procellariidae	*Bulweria*	LC	④
Calonectris leucomelas	Animalia	Chordata	Aves	Procellariiformes	Procellariidae	*Calonectris*	NT	④

Scientific Name	Kingdom	Phylum	Class	Order	Family	Genus	Danger	Source
Pterodroma hypoleuca	Animalia	Chordata	Aves	Procellariiformes	Procellariidae	*Pterodroma*	LC	④
Pterodroma nigripennis	Animalia	Chordata	Aves	Procellariiformes	Procellariidae	*Pterodroma*	LC	④
Balaenoptera physalus	Animalia	Chordata	Mammalia	Cetartiodactyla	Balaenopteridae	*Balaenoptera*	VU	①
Balaenoptera acutorostrata	Animalia	Chordata	Mammalia	Cetartiodactyla	Balaenopteridae	*Balaenoptera*	LC	①
Balaenoptera borealis	Animalia	Chordata	Mammalia	Cetartiodactyla	Balaenopteridae	*Balaenoptera*	EN	①
Balaenoptera brydei	Animalia	Chordata	Mammalia	Cetartiodactyla	Balaenopteridae	*Balaenoptera*	LC	②
Balaenoptera musculus	Animalia	Chordata	Mammalia	Cetartiodactyla	Balaenopteridae	*Balaenoptera*	EN	①
Megaptera novaeangliae	Animalia	Chordata	Mammalia	Cetartiodactyla	Balaenopteridae	*Megaptera*	LC	①
Globicephala macrorhynchus	Animalia	Chordata	Mammalia	Cetartiodactyla	Delphinidae	*Globicephala*	LC	④
Stenella coeruleoalba	Animalia	Chordata	Mammalia	Cetartiodactyla	Delphinidae	*Stenella*	LC	④
Physeter macrocephalus	Animalia	Chordata	Mammalia	Cetartiodactyla	Physeteridae	*Physeter*	VU	③

Note：① Record of hydrophone survey； ② Hydrophone surveys and public database records； ③ Public database records； ④ Visual records

Schedule 2-2 List of zooplankton species in Block M

Scientific Name	Kingdom	Phylum	Class	Order	Family	Genus
Eunotogramma debile	Chromista	Bacillariophyta	Bacillariophyceae	Anaulales	Anaulaceae	*Eunotogramma*
Asteromphalus elegans	Chromista	Bacillariophyta	Bacillariophyceae	Asterolamprales	Asterolampraceae	*Asteromphalus*
Asteromphalus rubustus	Chromista	Bacillariophyta	Bacillariophyceae	Asterolamprales	Asterolampraceae	*Asteromphalus*
Asterolampra vanheurckii	Chromista	Bacillariophyta	Bacillariophyceae	Asterolamprales	Asterolampraceae	*Asterolampra*
Bacteriastrum comosum	Chromista	Bacillariophyta	Bacillariophyceae	Biddulphiales	Bacteriastraceae	*Bacteriastrum*
Fragilariopsis doliolus	Chromista	Bacillariophyta	Bacillariophyceae	Bacillariales	Bacillariaceae	*Fragilariopsis*
Psammodictyon constrictum f. parvum	Chromista	Bacillariophyta	Bacillariophyceae	Bacillariales	Bacillariaceae	*Psammodictyon*
Nitzschia distantoides	Chromista	Bacillariophyta	Bacillariophyceae	Bacillariales	Bacillariaceae	*Nitzschia*
Nitzschia frustulum	Chromista	Bacillariophyta	Bacillariophyceae	Bacillariales	Bacillariaceae	*Nitzschia*
Nitzschia longissima	Chromista	Bacillariophyta	Bacillariophyceae	Bacillariales	Bacillariaceae	*Nitzschia*
Surirella navicularis	Chromista	Bacillariophyta	Bacillariophyceae	Surirellales	Surirellaceae	*Surirella*
Nitzschia paleacea	Chromista	Bacillariophyta	Bacillariophyceae	Bacillariales	Bacillariaceae	*Nitzschia*
Cerataulina pelagica	Chromista	Bacillariophyta	Bacillariophyceae	Biddulphiales	Bacteriastraceae	*Cerataulina*
Chaetoceros affinis	Chromista	Bacillariophyta	Bacillariophyceae	Chaetocerotanae incertae sedis	Chaetocerotaceae	*Chaetoceros*
Chaetoceros brevis	Chromista	Bacillariophyta	Bacillariophyceae	Chaetocerotanae incertae sedis	Chaetocerotaceae	*Chaetoceros*
Chaetoceros decipiens f. singularis	Chromista	Bacillariophyta	Bacillariophyceae	Chaetocerotanae incertae sedis	Chaetocerotaceae	*Chaetoceros*
Chaetoceros denticulatus	Chromista	Bacillariophyta	Bacillariophyceae	Chaetocerotanae incertae sedis	Chaetocerotaceae	*Chaetoceros*
Chaetoceros peruvianus	Chromista	Bacillariophyta	Bacillariophyceae	Chaetocerotanae incertae sedis	Chaetocerotaceae	*Chaetoceros*
Chaetoceros tortissimus	Chromista	Bacillariophyta	Bacillariophyceae	Chaetocerotanae incertae sedis	Chaetocerotaceae	*Chaetoceros*

Scientific Name	Kingdom	Phylum	Class	Order	Family	Genus
Climacodium frauenfeldianum	Chromista	Bacillariophyta	Bacillariophyceae	Biddulphiales	Eucampiaceae	*Climacodium*
Coscinodiscus bipartitus	Chromista	Bacillariophyta	Bacillariophyceae	Coscinodiscales	Coscinodiscaceae	*Coscinodiscus*
Coscinodiscus gigas	Chromista	Bacillariophyta	Bacillariophyceae	Coscinodiscales	Coscinodiscaceae	*Coscinodiscus*
Coscinodiscus granii	Chromista	Bacillariophyta	Bacillariophyceae	Coscinodiscales	Coscinodiscaceae	*Coscinodiscus*
Coscinodiscus jonesianus	Chromista	Bacillariophyta	Bacillariophyceae	Coscinodiscales	Coscinodiscaceae	*Coscinodiscus*
Coscinodiscus marginatus	Chromista	Bacillariophyta	Bacillariophyceae	Coscinodiscales	Coscinodiscaceae	*Coscinodiscus*
Coscinodiscus radiatus	Chromista	Bacillariophyta	Bacillariophyceae	Coscinodiscales	Coscinodiscaceae	*Coscinodiscus*
Coscinodiscus subtilis	Chromista	Bacillariophyta	Bacillariophyceae	Coscinodiscales	Coscinodiscaceae	*Coscinodiscus*
Gossleriella tropica	Chromista	Bacillariophyta	Bacillariophyceae	Discoidales	Coscinodiscaeae	*Gossleriella*
Guinardia flaccida	Chromista	Bacillariophyta	Bacillariophyceae	Discoidales	Leptocylindraceae	*Guinardia*
Hemiaulua membranaceus	Chromista	Bacillariophyta	Bacillariophyceae	Hemiaulales	Hemiaulaceae	*Hemiaulus*
Hemiaulus sinensis	Chromista	Bacillariophyta	Bacillariophyceae	Hemiaulales	Hemiaulaceae	*Hemiaulus*
Leptocylindrus danicus	Chromista	Bacillariophyta	Bacillariophyceae	Leptocylindrales	Leptocylindraceae	*Leptocylindrus*
Ditylum brightwellii	Chromista	Bacillariophyta	Bacillariophyceae	Lithodesmiales	Lithodesmiaceae	*Ditylum*
Mastogloia braunii	Chromista	Bacillariophyta	Bacillariophyceae	Mastogloiales	Mastogloiaceae	*Mastogloia*
Melosira moniliformis	Chromista	Bacillariophyta	Bacillariophyceae	Melosirales	Melosiraceae	*Melosira*
Navicula directa	Chromista	Bacillariophyta	Bacillariophyceae	Naviculales	Naviculaceae	*Navicula*
Navicula gaillonii	Chromista	Bacillariophyta	Bacillariophyceae	Naviculales	Naviculaceae	*Navicula*
Nitzschia frustulum	Chromista	Bacillariophyta	Bacillariophyceae	Surirellales	Nitzschiaceae	*Nitzschia*
Nitzschia paleacea	Chromista	Bacillariophyta	Bacillariophyceae	Surirellales	Nitzschiaceae	*Nitzschia*
Pinnularia borealis	Chromista	Bacillariophyta	Bacillariophyceae	Naviculales	Pinnulariaceae	*Pinnularia*
Pinnularia directa var. directa	Chromista	Bacillariophyta	Bacillariophyceae	Naviculales	Pinnulariaceae	*Pinnularia*
Halamphora coffeaeformis	Chromista	Bacillariophyta	Bacillariophyceae	Naviculales	Amphipleuraceae	*Halamphora*

Scientific Name	Kingdom	Phylum	Class	Order	Family	Genus
Proboscia alata	Chromista	Bacillariophyta	Bacillariophyceae	Rhizosoleniales	Rhizosoleniaceae	*Proboscia*
Rhizosolenia gracillima	Chromista	Bacillariophyta	Bacillariophyceae	Rhizosoleniales	Rhizosoleniaceae	*Rhizosolenia*
Rhizosolenia imbricata	Chromista	Bacillariophyta	Bacillariophyceae	Rhizosoleniales	Rhizosoleniaceae	*Rhizosolenia*
Rhizosolenia robusta	Chromista	Bacillariophyta	Bacillariophyceae	Rhizosoleniales	Rhizosoleniaceae	*Rhizosolenia*
Rhizosolenia stolterfothii	Chromista	Bacillariophyta	Bacillariophyceae	Rhizosoleniales	Rhizosoleniaceae	*Rhizosolenia*
Rhizosolenia styliformis	Chromista	Bacillariophyta	Bacillariophyceae	Rhizosoleniales	Rhizosoleniaceae	*Rhizosolenia*
Rhizosolenia truncata	Chromista	Bacillariophyta	Bacillariophyceae	Rhizosoleniales	Rhizosoleniaceae	*Rhizosolenia*
Schröederella delicatula	Chromista	Bacillariophyta	Bacillariophyceae	Discoidales	Thalassiosiraceae	*Schröederella*
Streptothece tamesis	Chromista	Bacillariophyta	Bacillariophyceae	Biddulphiales	Eucampiaceae	*Streptothece*
Synedra gaillonii	Chromista	Bacillariophyta	Bacillariophyceae	Diatomales	Diatomaceae	*Synedra*
Sundstroemia setigera	Chromista	Bacillariophyta	Bacillariophyceae	Rhizosoleniales	Rhizosoleniaceae	*Sundstroemia*
Surirella collare	Chromista	Bacillariophyta	Bacillariophyceae	Surirellales	Surirellaceae	*Surirella*
Thalassionema nitzschioides	Chromista	Bacillariophyta	Bacillariophyceae	Thalassionematales	Thalassionemataceae	*Thalassionema*
Thalassiothrix longissima	Chromista	Bacillariophyta	Bacillariophyceae	Thalassionematales	Thalassionemataceae	*Thalassiothrix*
Cyclotella striata	Chromista	Bacillariophyta	Bacillariophyceae	Thalassiosirales	Stephanodiscaceae	*Cyclotella*
Skeletonema costatum	Chromista	Bacillariophyta	Bacillariophyceae	Thalassiosirales	Skeletonemaceae	*Skeletonema*
Eupodiscus jonesianus	Chromista	Bacillariophyta	Bacillariophyceae	Triceratiales	Triceratiaceae	*Eupodiscus*
Gaillonella sulcata	Chromista	Bacillariophyta	Bacillariophyceae	Discoidales	Melosiraceae	*Gaillonella*
Neomoelleria cornuta	Chromista	Bacillariophyta	Bacillariophyceae			*Neomoelleria*
Vibrio paxillifer	Chromista	Bacillariophyta	Bacillariophyceae			Vibrio
Ceratium contortum var. saltans	Chromista	Pyrrophyta	Pyrrophyceae	Goneaulacales	Ceratiaceae	*Ceratium*
Ceratium fusus	Chromista	Pyrrophyta	Pyrrophyceae	Goneaulacales	Ceratiaceae	*Ceratium*

Scientific Name	Kingdom	Phylum	Class	Order	Family	Genus
Ceratium hexacanthum var. contortum	Chromista	Pyrrophyta	Pyrrophyceae	Goneaulacales	Ceratiaceae	*Ceratium*
Ceratium horridum	Chromista	Pyrrophyta	Pyrrophyceae	Goneaulacales	Ceratiaceae	*Ceratium*
Ceratium horridum var. molle	Chromista	Pyrrophyta	Pyrrophyceae	Goneaulacales	Ceratiaceae	*Ceratium*
Ceratium horridum var. tenue	Chromista	Pyrrophyta	Pyrrophyceae	Goneaulacales	Ceratiaceae	*Ceratium*
Ceratium macroceros	Chromista	Pyrrophyta	Pyrrophyceae	Goneaulacales	Ceratiaceae	*Ceratium*
Ceratium macroceros var. gallicum	Chromista	Pyrrophyta	Pyrrophyceae	Goneaulacales	Ceratiaceae	*Ceratium*
Ceratium massiliense	Chromista	Pyrrophyta	Pyrrophyceae	Goneaulacales	Ceratiaceae	*Ceratium*
Ceratium massiliense var. armatum	Chromista	Pyrrophyta	Pyrrophyceae	Goneaulacales	Ceratiaceae	*Ceratium*
Ceratium trichoceors	Chromista	Pyrrophyta	Pyrrophyceae	Goneaulacales	Ceratiaceae	*Ceratium*
Dinophysis miles	Chromista	Pyrrophyta	Pyrrophyceae	Dinophysiales	Dinophysiaceae	*Dinophysis*
Noctiluca scintillans	Chromista	Pyrrophyta	Pyrrophyceae	Noctilucales	Noctilucaceae	*Noctiluca*
Prorocentrum micans	Chromista	Pyrrophyta	Pyrrophyceae	Prorocentrates	Prorocentraceae	*Prorocentrum*
Scrippsiella trochoidea	Chromista	Pyrrophyta	Pyrrophyceae	Peridiniales	Peridiniaceae	*Scrippsiella*
Trichodesmium thiebautii	Chromista	Cyanophyta	Cyanophyceae	Nostocales	Oscillatoriaceae	*Trichodesmium*
Phaeocystis globosa	Chromista	Prymnesiophyta	Prymnesiophyceae	Prymnesiales	Phaeocystaceae	*Phaeocystis*
Lopadorrhynchus brevis	Animalia	Annelida	Polychaeta	Phyllodocida	Lopadorrhynchidae	*Lopadorrhynchus*
Lopadorrhynchus krohnii	Animalia	Annelida	Polychaeta	Phyllodocida	Lopadorrhynchidae	*Lopadorrhynchus*
Lopadorrhynchus uncinatus	Animalia	Annelida	Polychaeta	Phyllodocida	Lopadorrhynchidae	*Lopadorrhynchus*

Scientific Name	Kingdom	Phylum	Class	Order	Family	Genus
Pedinosoma curtum	Animalia	Annelida	Polychaeta	Phyllodocida	Lopadorrhynchidae	*Pedinosoma*
Pelagobia longicirrata	Animalia	Annelida	Polychaeta	Phyllodocida	Lopadorrhynchidae	*Pelagobia*
Alciopina parasitica	Animalia	Annelida	Polychaeta	Phyllodocida	Phyllodocidae	*Alciopina*
Krohnia lepidota	Animalia	Annelida	Polychaeta	Phyllodocida	Phyllodocidae	*Krohnia*
Plotohelmis capitata	Animalia	Annelida	Polychaeta	Phyllodocida	Phyllodocidae	*Plotohelmis*
Rhynchonereella gracilis	Animalia	Annelida	Polychaeta	Phyllodocida	Phyllodocidae	*Rhynchonereella*
Rhynchonereella petersii	Animalia	Annelida	Polychaeta	Phyllodocida	Phyllodocidae	*Rhynchonereella*
Vanadis formosa	Animalia	Annelida	Polychaeta	Phyllodocida	Phyllodocidae	*Vanadis*
Vanadis minuta	Animalia	Annelida	Polychaeta	Phyllodocida	Phyllodocidae	*Vanadis*
Tomopteris cavallii	Animalia	Annelida	Polychaeta	Phyllodocida	Tomopteridae	*Tomopteris*
Tomopteris (Johnstonella) pacifica	Animalia	Annelida	Polychaeta	Phyllodocida	Tomopteridae	*Tomopteris*
Tomopteris krampi	Animalia	Annelida	Polychaeta	Phyllodocida	Tomopteridae	*Tomopteris*
Tomopteris ligulata	Animalia	Annelida	Polychaeta	Phyllodocida	Tomopteridae	*Tomopteris*
Tomopteris planktonis	Animalia	Annelida	Polychaeta	Phyllodocida	Tomopteridae	*Tomopteris*
Tomopteris rolasi	Animalia	Annelida	Polychaeta	Phyllodocida	Tomopteridae	*Tomopteris*
Sagitella kowalewskii	Animalia	Annelida	Polychaeta	Phyllodocida	Typhloscolecidae	*Sagitella*
Travisiopsis dubia	Animalia	Annelida	Polychaeta	Phyllodocida	Typhloscolecidae	*Travisiopsis*
Travisiopsis levinseni	Animalia	Annelida	Polychaeta	Phyllodocida	Typhloscolecidae	*Travisiopsis*
Travisiopsis sp.	Animalia	Annelida	Polychaeta	Phyllodocida	Typhloscolecidae	*Travisiopsis*
Typhloscolex muelleri	Animalia	Annelida	Polychaeta	Phyllodocida	Typhloscolecidae	*Typhloscolex*
Acartia (Acartia) danae	Animalia	Arthropoda	Copepoda	Calanoida	Acartiidae	*Acartia*
Acartia (Acartia) negligens	Animalia	Arthropoda	Copepoda	Calanoida	Acartiidae	*Acartia*

Scientific Name	Kingdom	Phylum	Class	Order	Family	Genus
Acartia (Odontacartia) erythraea erythraea	Animalia	Arthropoda	Copepoda	Calanoida	Acartiidae	*Acartia*
Acartia (Odontacartia) pacifica	Animalia	Arthropoda	Copepoda	Calanoida	Acartiidae	*Acartia*
Aetideus acutus	Animalia	Arthropoda	Copepoda	Calanoida	Aetideidae	*Aetideus*
Chiridiella macrodactyla	Animalia	Arthropoda	Copepoda	Calanoida	Aetideidae	*Chiridiella*
Chiridius gracilis	Animalia	Arthropoda	Copepoda	Calanoida	Aetideidae	*Chiridius*
Euchirella amoena	Animalia	Arthropoda	Copepoda	Calanoida	Aetideidae	*Euchirella*
Euchirella bella	Animalia	Arthropoda	Copepoda	Calanoida	Aetideidae	*Euchirella*
Euchirella curticauda	Animalia	Arthropoda	Copepoda	Calanoida	Aetideidae	*Euchirella*
Euchirella galeata	Animalia	Arthropoda	Copepoda	Calanoida	Aetideidae	*Euchirella*
Euchirella orientalis	Animalia	Arthropoda	Copepoda	Calanoida	Aetideidae	*Euchirella*
Euchirella sp.	Animalia	Arthropoda	Copepoda	Calanoida	Aetideidae	*Euchirella*
Gaetanus minispinus	Animalia	Arthropoda	Copepoda	Calanoida	Aetideidae	*Gaetanus*
Gaetanus minor	Animalia	Arthropoda	Copepoda	Calanoida	Aetideidae	*Gaetanus*
Gaetanus armiger	Animalia	Arthropoda	Copepoda	Calanoida	Aetideidae	*Gaetanus*
Gaetanus kruppii	Animalia	Arthropoda	Copepoda	Calanoida	Aetideidae	*Gaetanus*
Undeuchaeta plumosa	Animalia	Arthropoda	Copepoda	Calanoida	Aetideidae	*Undeuchaeta*
Valdiviella brevicornis	Animalia	Arthropoda	Copepoda	Calanoida	Aetideidae	*Valdiviella*
Valdiviella insignis	Animalia	Arthropoda	Copepoda	Calanoida	Aetideidae	*Valdiviella*
Augaptilus longicaudatus	Animalia	Arthropoda	Copepoda	Calanoida	Augaptilidae	*Augaptilus*
Centraugaptilus rattrayi	Animalia	Arthropoda	Copepoda	Calanoida	Augaptilidae	*Centraugaptilus*
Euaugaptilus bullifer	Animalia	Arthropoda	Copepoda	Calanoida	Augaptilidae	*Euaugaptilus*
Euaugaptilus elongatus	Animalia	Arthropoda	Copepoda	Calanoida	Augaptilidae	*Euaugaptilus*

Scientific Name	Kingdom	Phylum	Class	Order	Family	Genus
Euaugaptilus hecticus	Animalia	Arthropoda	Copepoda	Calanoida	Augaptilidae	*Euaugaptilus*
Euaugaptilus laticeps	Animalia	Arthropoda	Copepoda	Calanoida	Augaptilidae	*Euaugaptilus*
Euaugaptilus longimanus	Animalia	Arthropoda	Copepoda	Calanoida	Augaptilidae	*Euaugaptilus*
Euaugaptilus nodifrons	Animalia	Arthropoda	Copepoda	Calanoida	Augaptilidae	*Euaugaptilus*
Euaugaptilus sp.	Animalia	Arthropoda	Copepoda	Calanoida	Augaptilidae	*Euaugaptilus*
Haloptilus austini	Animalia	Arthropoda	Copepoda	Calanoida	Augaptilidae	*Haloptilus*
Haloptilus bulliceps	Animalia	Arthropoda	Copepoda	Calanoida	Augaptilidae	*Haloptilus*
Haloptilus longicornis	Animalia	Arthropoda	Copepoda	Calanoida	Augaptilidae	*Haloptilus*
Haloptilus mucronatus	Animalia	Arthropoda	Copepoda	Calanoida	Augaptilidae	*Haloptilus*
Haloptilus sp.	Animalia	Arthropoda	Copepoda	Calanoida	Augaptilidae	*Haloptilus*
Haloptilus fons	Animalia	Arthropoda	Copepoda	Calanoida	Augaptilidae	*Haloptilus*
Haloptilus longicirrus	Animalia	Arthropoda	Copepoda	Calanoida	Augaptilidae	*Haloptilus*
Haloptilus ornatus	Animalia	Arthropoda	Copepoda	Calanoida	Augaptilidae	*Haloptilus*
Haloptilus paralongicirrus	Animalia	Arthropoda	Copepoda	Calanoida	Augaptilidae	*Haloptilus*
Haloptilus spiniceps	Animalia	Arthropoda	Copepoda	Calanoida	Augaptilidae	*Haloptilus*
Pseudaugaptilus orientalis	Animalia	Arthropoda	Copepoda	Calanoida	Augaptilidae	*Pseudaugaptilus*
Temorites brevis	Animalia	Arthropoda	Copepoda	Calanoida	Bathypontiidae	*Temorites*
Temorites spinifera	Animalia	Arthropoda	Copepoda	Calanoida	Bathypontiidae	*Temorites*
Canthocalanus pauper	Animalia	Arthropoda	Copepoda	Calanoida	Calanidae	*Canthocalanus*
Cosmocalanus darwinii darwinii	Animalia	Arthropoda	Copepoda	Calanoida	Calanidae	*Cosmocalanus*
Mesocalanus tenuicornis	Animalia	Arthropoda	Copepoda	Calanoida	Calanidae	*Mesocalanus*
Nannocalanus minor	Animalia	Arthropoda	Copepoda	Calanoida	Calanidae	*Nannocalanus*

Scientific Name	Kingdom	Phylum	Class	Order	Family	Genus
Neocalanus gracilis	Animalia	Arthropoda	Copepoda	Calanoida	Calanidae	*Neocalanus*
Neocalanus robustior	Animalia	Arthropoda	Copepoda	Calanoida	Calanidae	*Neocalanus*
Candacia bispinosa	Animalia	Arthropoda	Copepoda	Calanoida	Candaciidae	*Candacia*
Candacia catula	Animalia	Arthropoda	Copepoda	Calanoida	Candaciidae	*Candacia*
Candacia ethiopica	Animalia	Arthropoda	Copepoda	Calanoida	Candaciidae	*Candacia*
Candacia longimana	Animalia	Arthropoda	Copepoda	Calanoida	Candaciidae	*Candacia*
Candacia truncata	Animalia	Arthropoda	Copepoda	Calanoida	Candaciidae	*Candacia*
Centropages calaninus	Animalia	Arthropoda	Copepoda	Calanoida	Centropagidae	*Centropages*
Centropages elongatus	Animalia	Arthropoda	Copepoda	Calanoida	Centropagidae	*Centropages*
Centropages gracilis	Animalia	Arthropoda	Copepoda	Calanoida	Centropagidae	*Centropages*
Centropages tenuiremis	Animalia	Arthropoda	Copepoda	Calanoida	Centropagidae	*Centropages*
Clausocalanus arcuicornis arcuicornis	Animalia	Arthropoda	Copepoda	Calanoida	Clausocalanidae	*Clausocalanus*
Clausocalanus farrani	Animalia	Arthropoda	Copepoda	Calanoida	Clausocalanidae	*Clausocalanus*
Clausocalanus furcatus	Animalia	Arthropoda	Copepoda	Calanoida	Clausocalanidae	*Clausocalanus*
Clausocalanus ingens	Animalia	Arthropoda	Copepoda	Calanoida	Clausocalanidae	*Clausocalanus*
Clausocalanus jobei	Animalia	Arthropoda	Copepoda	Calanoida	Clausocalanidae	*Clausocalanus*
Clausocalanus lividus	Animalia	Arthropoda	Copepoda	Calanoida	Clausocalanidae	*Clausocalanus*
Clausocalanus mastigophorus	Animalia	Arthropoda	Copepoda	Calanoida	Clausocalanidae	*Clausocalanus*
Clausocalanus minor	Animalia	Arthropoda	Copepoda	Calanoida	Clausocalanidae	*Clausocalanus*
Clausocalanus parapergens	Animalia	Arthropoda	Copepoda	Calanoida	Clausocalanidae	*Clausocalanus*
Clausocalanus paululus	Animalia	Arthropoda	Copepoda	Calanoida	Clausocalanidae	*Clausocalanus*
Clausocalanus pergens	Animalia	Arthropoda	Copepoda	Calanoida	Clausocalanidae	*Clausocalanus*

Scientific Name	Kingdom	Phylum	Class	Order	Family	Genus
Microcalanus pusillus	Animalia	Arthropoda	Copepoda	Calanoida	Clausocalanidae	*Microcalanus*
Pseudocalanus minutus	Animalia	Arthropoda	Copepoda	Calanoida	Clausocalanidae	*Pseudocalanus*
Pareucalanus attenuatus	Animalia	Arthropoda	Copepoda	Calanoida	Eucalanidae	*Pareucalanus*
Euchaeta indica	Animalia	Arthropoda	Copepoda	Calanoida	Euchaetidae	*Euchaeta*
Euchaeta media	Animalia	Arthropoda	Copepoda	Calanoida	Euchaetidae	*Euchaeta*
Euchaeta rimana	Animalia	Arthropoda	Copepoda	Calanoida	Euchaetidae	*Euchaeta*
Euchaeta tenuis	Animalia	Arthropoda	Copepoda	Calanoida	Euchaetidae	*Euchaeta*
Paraeuchaeta confusa	Animalia	Arthropoda	Copepoda	Calanoida	Euchaetidae	*Paraeuchaeta*
Temoropia mayumbaensis	Animalia	Arthropoda	Copepoda	Calanoida	Fosshageniidae	*Temoropia*
Temoropia minor	Animalia	Arthropoda	Copepoda	Calanoida	Fosshageniidae	*Temoropia*
Disseta palumbii	Animalia	Arthropoda	Copepoda	Calanoida	Heterorhabdidae	*Disseta*
Heterorhabdus pacificus	Animalia	Arthropoda	Copepoda	Calanoida	Heterorhabdidae	*Heterorhabdus*
Heterorhabdus papilliger	Animalia	Arthropoda	Copepoda	Calanoida	Heterorhabdidae	*Heterorhabdus*
Heterorhabdus spinifrons	Animalia	Arthropoda	Copepoda	Calanoida	Heterorhabdidae	*Heterorhabdus*
Heterorhabdus subspinifrons	Animalia	Arthropoda	Copepoda	Calanoida	Heterorhabdidae	*Heterorhabdus*
Mesorhabdus gracilis	Animalia	Arthropoda	Copepoda	Calanoida	Heterorhabdidae	*Mesorhabdus*
Paraheterorhabdus compactus	Animalia	Arthropoda	Copepoda	Calanoida	Heterorhabdidae	*Paraheterorhabdus*
Paraheterorhabdus robustus	Animalia	Arthropoda	Copepoda	Calanoida	Heterorhabdidae	*Paraheterorhabdus*
Paraheterorhabdus vipera	Animalia	Arthropoda	Copepoda	Calanoida	Heterorhabdidae	*Paraheterorhabdus*
Lucicutia aurita	Animalia	Arthropoda	Copepoda	Calanoida	Lucicutiidae	*Lucicutia*
Lucicutia curta	Animalia	Arthropoda	Copepoda	Calanoida	Lucicutiidae	*Lucicutia*
Lucicutia sp.	Animalia	Arthropoda	Copepoda	Calanoida	Lucicutiidae	*Lucicutia*

Scientific Name	Kingdom	Phylum	Class	Order	Family	Genus
Lucicutia flavicornis	Animalia	Arthropoda	Copepoda	Calanoida	Lucicutiidae	*Lucicutia*
Lucicutia gaussae	Animalia	Arthropoda	Copepoda	Calanoida	Lucicutiidae	*Lucicutia*
Lucicutia gemina	Animalia	Arthropoda	Copepoda	Calanoida	Lucicutiidae	*Lucicutia*
Lucicutia intermedia	Animalia	Arthropoda	Copepoda	Calanoida	Lucicutiidae	*Lucicutia*
Lucicutia longicornis	Animalia	Arthropoda	Copepoda	Calanoida	Lucicutiidae	*Lucicutia*
Lucicutia magna	Animalia	Arthropoda	Copepoda	Calanoida	Lucicutiidae	*Lucicutia*
Lucicutia ovalis	Animalia	Arthropoda	Copepoda	Calanoida	Lucicutiidae	*Lucicutia*
Lucicutia polaris	Animalia	Arthropoda	Copepoda	Calanoida	Lucicutiidae	*Lucicutia*
Lucicutia wolfendeni	Animalia	Arthropoda	Copepoda	Calanoida	Lucicutiidae	*Lucicutia*
Metridia brevicauda	Animalia	Arthropoda	Copepoda	Calanoida	Metridinidae	*Metridia*
Metridia macrura	Animalia	Arthropoda	Copepoda	Calanoida	Metridinidae	*Metridia*
Metridia venusta	Animalia	Arthropoda	Copepoda	Calanoida	Metridinidae	*Metridia*
Pleuromamma abdominalis abdominalis	Animalia	Arthropoda	Copepoda	Calanoida	Metridinidae	*Pleuromamma*
Pleuromamma gracilis gracilis	Animalia	Arthropoda	Copepoda	Calanoida	Metridinidae	*Pleuromamma*
Pleuromamma piseki	Animalia	Arthropoda	Copepoda	Calanoida	Metridinidae	*Pleuromamma*
Pleuromamma robusta robusta	Animalia	Arthropoda	Copepoda	Calanoida	Metridinidae	*Pleuromamma*
Pleuromamma xiphias	Animalia	Arthropoda	Copepoda	Calanoida	Metridinidae	*Pleuromamma*
Nullosetigera auctiseta	Animalia	Arthropoda	Copepoda	Calanoida	Nullosetigeridae	*Nullosetigera*
Nullosetigera helgae	Animalia	Arthropoda	Copepoda	Calanoida	Nullosetigeridae	*Nullosetigera*
Acrocalanus monachus	Animalia	Arthropoda	Copepoda	Calanoida	Paracalanidae	*Acrocalanus*
Acrocalanus gibber	Animalia	Arthropoda	Copepoda	Calanoida	Paracalanidae	*Acrocalanus*
Acrocalanus gracilis	Animalia	Arthropoda	Copepoda	Calanoida	Paracalanidae	*Acrocalanus*

Scientific Name	Kingdom	Phylum	Class	Order	Family	Genus
Acrocalanus longicornis	Animalia	Arthropoda	Copepoda	Calanoida	Paracalanidae	*Acrocalanus*
Bestiolina zeylonica	Animalia	Arthropoda	Copepoda	Calanoida	Paracalanidae	*Bestiolina*
Calocalanus pavo	Animalia	Arthropoda	Copepoda	Calanoida	Paracalanidae	*Calocalanus*
Calocalanus plumulosus	Animalia	Arthropoda	Copepoda	Calanoida	Paracalanidae	*Calocalanus*
Calocalanus contractus	Animalia	Arthropoda	Copepoda	Calanoida	Paracalanidae	*Calocalanus*
Calocalanus styliremis	Animalia	Arthropoda	Copepoda	Calanoida	Paracalanidae	*Calocalanus*
Mecynocera clausi	Animalia	Arthropoda	Copepoda	Calanoida	Paracalanidae	*Mecynocera*
Mecynocera gracilis	Animalia	Arthropoda	Copepoda	Calanoida	Paracalanidae	*Mecynocera*
Paracalanus aculeatus aculeatus	Animalia	Arthropoda	Copepoda	Calanoida	Paracalanidae	*Paracalanus*
Paracalanus nanus	Animalia	Arthropoda	Copepoda	Calanoida	Paracalanidae	*Paracalanus*
Paracalanus gracilis	Animalia	Arthropoda	Copepoda	Calanoida	Paracalanidae	*Paracalanus*
Paracalanus parvus parvus	Animalia	Arthropoda	Copepoda	Calanoida	Paracalanidae	*Paracalanus*
Calanopia minor	Animalia	Arthropoda	Copepoda	Calanoida	Pontellidae	*Calanopia*
Pontellina morii	Animalia	Arthropoda	Copepoda	Calanoida	Pontellidae	*Pontellina*
Pontellina plumata	Animalia	Arthropoda	Copepoda	Calanoida	Pontellidae	*Pontellina*
Rhincalanus nasutus	Animalia	Arthropoda	Copepoda	Calanoida	Rhincalanidae	*Rhincalanus*
Amallothrix valens	Animalia	Arthropoda	Copepoda	Calanoida	Scolecitrichidae	*Amallothrix*
Landrumius gigas	Animalia	Arthropoda	Copepoda	Calanoida	Scolecitrichidae	*Landrumius*
Lophothrix latipes	Animalia	Arthropoda	Copepoda	Calanoida	Scolecitrichidae	*Lophothrix*
Pseudoamallothrix emarginata	Animalia	Arthropoda	Copepoda	Calanoida	Scolecitrichidae	*Pseudoamallothrix*
Pseudoamallothrix ovata	Animalia	Arthropoda	Copepoda	Calanoida	Scolecitrichidae	*Pseudoamallothrix*
Scaphocalanus brevicornis	Animalia	Arthropoda	Copepoda	Calanoida	Scolecitrichidae	*Scaphocalanus*

Scientific Name	Kingdom	Phylum	Class	Order	Family	Genus
Scaphocalanus echinatus	Animalia	Arthropoda	Copepoda	Calanoida	Scolecitrichidae	*Scaphocalanus*
Scaphocalanus elongatus	Animalia	Arthropoda	Copepoda	Calanoida	Scolecitrichidae	*Scaphocalanus*
Scaphocalanus magnus	Animalia	Arthropoda	Copepoda	Calanoida	Scolecitrichidae	*Scaphocalanus*
Scaphocalanus sp.	Animalia	Arthropoda	Copepoda	Calanoida	Scolecitrichidae	*Scaphocalanus*
Scolecithricella abyssalis	Animalia	Arthropoda	Copepoda	Calanoida	Scolecitrichidae	*Scolecithricella*
Scolecithricella dentata	Animalia	Arthropoda	Copepoda	Calanoida	Scolecitrichidae	*Scolecithricella*
Scolecithricella marginata	Animalia	Arthropoda	Copepoda	Calanoida	Scolecitrichidae	*Scolecithricella*
Scolecithricella nicobarica	Animalia	Arthropoda	Copepoda	Calanoida	Scolecitrichidae	*Scolecithricella*
Scolecitrichopsis ctenopus	Animalia	Arthropoda	Copepoda	Calanoida	Scolecitrichidae	*Scolecitrichopsis*
Scolecithricella tenuipes	Animalia	Arthropoda	Copepoda	Calanoida	Scolecitrichidae	*Scolecitrichopsis*
Scolecithrix bradyi	Animalia	Arthropoda	Copepoda	Calanoida	Scolecitrichidae	*Scolecithrix*
Scolecithrix danae	Animalia	Arthropoda	Copepoda	Calanoida	Scolecitrichidae	*Scolecithrix*
Spinocalanus horridus	Animalia	Arthropoda	Copepoda	Calanoida	Spinocalanidae	*Spinocalanus*
Spinocalanus longicornis	Animalia	Arthropoda	Copepoda	Calanoida	Spinocalanidae	*Spinocalanus*
Spinocalanus magnus	Animalia	Arthropoda	Copepoda	Calanoida	Spinocalanidae	*Spinocalanus*
Spinocalanus oligospinosus	Animalia	Arthropoda	Copepoda	Calanoida	Spinocalanidae	*Spinocalanus*
Spinocalanus spinosus	Animalia	Arthropoda	Copepoda	Calanoida	Spinocalanidae	*Spinocalanus*
Subeucalanus pileatus	Animalia	Arthropoda	Copepoda	Calanoida	Eucalanidae	*Subeucalanus*
Subeucalanus subtenuis	Animalia	Arthropoda	Copepoda	Calanoida	Eucalanidae	*Subeucalanus*
Calanoida sp.1	Animalia	Arthropoda	Copepoda	Calanoida		
Calanoida sp.2	Animalia	Arthropoda	Copepoda	Calanoida		
Calanoida sp.3	Animalia	Arthropoda	Copepoda	Calanoida		

Scientific Name	Kingdom	Phylum	Class	Order	Family	Genus
Calanoida sp.4	Animalia	Arthropoda	Copepoda	Calanoida		
Calanoida sp.5	Animalia	Arthropoda	Copepoda	Calanoida		
Calanoida sp.6	Animalia	Arthropoda	Copepoda	Calanoida		
Calanoida sp.7	Animalia	Arthropoda	Copepoda	Calanoida		
Calanoida sp.8	Animalia	Arthropoda	Copepoda	Calanoida		
Calanoida sp.9	Animalia	Arthropoda	Copepoda	Calanoida		
Calanoida sp.10	Animalia	Arthropoda	Copepoda	Calanoida		
Calanoida sp.11	Animalia	Arthropoda	Copepoda	Calanoida		
Calanoida sp.12	Animalia	Arthropoda	Copepoda	Calanoida		
Calanoida sp.13	Animalia	Arthropoda	Copepoda	Calanoida		
Calanoida sp.14	Animalia	Arthropoda	Copepoda	Calanoida		
Calanoida sp.15	Animalia	Arthropoda	Copepoda	Calanoida		
Calanoida sp.16	Animalia	Arthropoda	Copepoda	Calanoida		
Calanoida sp.17	Animalia	Arthropoda	Copepoda	Calanoida		
Calanoida sp.18	Animalia	Arthropoda	Copepoda	Calanoida		
Calanoida sp.19	Animalia	Arthropoda	Copepoda	Calanoida		
Calanoida sp.20	Animalia	Arthropoda	Copepoda	Calanoida		
Agetus flaccus	Animalia	Arthropoda	Copepoda	Cyclopoida	Corycaeidae	*Agetus*
Agetus limbatus	Animalia	Arthropoda	Copepoda	Cyclopoida	Corycaeidae	*Agetus*
Agetus typicus	Animalia	Arthropoda	Copepoda	Cyclopoida	Corycaeidae	*Agetus*
Corycaeus crassiusculus	Animalia	Arthropoda	Copepoda	Cyclopoida	Corycaeidae	*Corycaeus*
Corycaeus speciosus	Animalia	Arthropoda	Copepoda	Cyclopoida	Corycaeidae	*Corycaeus*

Scientific Name	Kingdom	Phylum	Class	Order	Family	Genus
Corycaeus sp.	Animalia	Arthropoda	Copepoda	Cyclopoida	Corycaeidae	*Corycaeus*
Ditrichocorycaeus asiaticus	Animalia	Arthropoda	Copepoda	Cyclopoida	Corycaeidae	*Ditrichocorycaeus*
Farranula carinata	Animalia	Arthropoda	Copepoda	Cyclopoida	Corycaeidae	*Farranula*
Farranula concinna	Animalia	Arthropoda	Copepoda	Cyclopoida	Corycaeidae	*Farranula*
Farranula gibbula	Animalia	Arthropoda	Copepoda	Cyclopoida	Corycaeidae	*Farranula*
Farranula longicaudis	Animalia	Arthropoda	Copepoda	Cyclopoida	Corycaeidae	*Farranula*
Onychocorycaeus agilis	Animalia	Arthropoda	Copepoda	Cyclopoida	Corycaeidae	*Onychocorycaeus*
Onychocorycaeus pacificus	Animalia	Arthropoda	Copepoda	Cyclopoida	Corycaeidae	*Onychocorycaeus*
Onychocorycaeus pumilus	Animalia	Arthropoda	Copepoda	Cyclopoida	Corycaeidae	*Onychocorycaeus*
Urocorycaeus lautus	Animalia	Arthropoda	Copepoda	Cyclopoida	Corycaeidae	*Urocorycaeus*
Urocorycaeus furcifer	Animalia	Arthropoda	Copepoda	Cyclopoida	Corycaeidae	*Urocorycaeus*
Lubbockia marukawai	Animalia	Arthropoda	Copepoda	Cyclopoida	Lubbockiidae	*Lubbockia*
Lubbockia aculeata	Animalia	Arthropoda	Copepoda	Cyclopoida	Lubbockiidae	*Lubbockia*
Lubbockia sp.	Animalia	Arthropoda	Copepoda	Cyclopoida	Lubbockiidae	*Lubbockia*
Lubbockia squillimana	Animalia	Arthropoda	Copepoda	Cyclopoida	Lubbockiidae	*Lubbockia*
Oithona decipiens	Animalia	Arthropoda	Copepoda	Cyclopoida	Oithonidae	*Oithona*
Oithona fallax	Animalia	Arthropoda	Copepoda	Cyclopoida	Oithonidae	*Oithona*
Oithona fragilis	Animalia	Arthropoda	Copepoda	Cyclopoida	Oithonidae	*Oithona*
Oithona linearis	Animalia	Arthropoda	Copepoda	Cyclopoida	Oithonidae	*Oithona*
Oithona longispina	Animalia	Arthropoda	Copepoda	Cyclopoida	Oithonidae	*Oithona*
Oithona plumifera	Animalia	Arthropoda	Copepoda	Cyclopoida	Oithonidae	*Oithona*
Oithona rigida	Animalia	Arthropoda	Copepoda	Cyclopoida	Oithonidae	*Oithona*

Scientific Name	Kingdom	Phylum	Class	Order	Family	Genus
Oithona robusta	Animalia	Arthropoda	Copepoda	Cyclopoida	Oithonidae	*Oithona*
Oithona tenuis	Animalia	Arthropoda	Copepoda	Cyclopoida	Oithonidae	*Oithona*
Oithona setigera setigera	Animalia	Arthropoda	Copepoda	Cyclopoida	Oithonidae	*Oithona*
Oithona sp.	Animalia	Arthropoda	Copepoda	Cyclopoida	Oithonidae	*Oithona*
Dioithona oculata	Animalia	Arthropoda	Copepoda	Cyclopoida	Oithonidae	*Dioithona*
Dioithona rigida	Animalia	Arthropoda	Copepoda	Cyclopoida	Oithonidae	*Dioithona*
Oncaea clevei	Animalia	Arthropoda	Copepoda	Cyclopoida	Oncaeidae	*Oncaea*
Oncaea gracilis	Animalia	Arthropoda	Copepoda	Cyclopoida	Oncaeidae	*Oncaea*
Oncaea media	Animalia	Arthropoda	Copepoda	Cyclopoida	Oncaeidae	*Oncaea*
Oncaea mediterranea	Animalia	Arthropoda	Copepoda	Cyclopoida	Oncaeidae	*Oncaea*
Oncaea ornata	Animalia	Arthropoda	Copepoda	Cyclopoida	Oncaeidae	*Oncaea*
Oncaea venusta	Animalia	Arthropoda	Copepoda	Cyclopoida	Oncaeidae	*Oncaea*
Oncaea sp.	Animalia	Arthropoda	Copepoda	Cyclopoida	Oncaeidae	*Oncaea*
Triconia minuta	Animalia	Arthropoda	Copepoda	Cyclopoida	Oncaeidae	*Triconia*
Triconia conifera	Animalia	Arthropoda	Copepoda	Cyclopoida	Oncaeidae	*Triconia*
Copilia lata	Animalia	Arthropoda	Copepoda	Cyclopoida	Sapphirinidae	*Copilia*
Copilia mirabilis	Animalia	Arthropoda	Copepoda	Cyclopoida	Sapphirinidae	*Copilia*
Copilia longistylis	Animalia	Arthropoda	Copepoda	Cyclopoida	Sapphirinidae	*Copilia*
Copilia quadrata	Animalia	Arthropoda	Copepoda	Cyclopoida	Sapphirinidae	*Copilia*
Sapphirina darwinii	Animalia	Arthropoda	Copepoda	Cyclopoida	Sapphirinidae	*Copilia*
Sapphirina nigromaculata	Animalia	Arthropoda	Copepoda	Cyclopoida	Sapphirinidae	*Sapphirina*
Sapphirina stellata	Animalia	Arthropoda	Copepoda	Cyclopoida	Sapphirinidae	*Sapphirina*

Scientific Name	Kingdom	Phylum	Class	Order	Family	Genus
Sapphirina scarlata	Animalia	Arthropoda	Copepoda	Cyclopoida	Sapphirinidae	*Sapphirina*
Vettoria granulosa	Animalia	Arthropoda	Copepoda	Cyclopoida	Sapphirinidae	*Vettoria*
Aegisthus aculeatus	Animalia	Arthropoda	Copepoda	Harpacticoida	Aegisthidae	*Aegisthus*
Aegisthus mucronatus	Animalia	Arthropoda	Copepoda	Harpacticoida	Aegisthidae	*Aegisthus*
Aegisthus sp.	Animalia	Arthropoda	Copepoda	Harpacticoida	Aegisthidae	*Aegisthus*
Clytemnestra scutellata	Animalia	Arthropoda	Copepoda	Harpacticoida	Peltidiidae	*Clytemnestra*
Goniopsyllus rostratus	Animalia	Arthropoda	Copepoda	Harpacticoida	Peltidiidae	*Goniopsyllus*
Macrosetella gracilis	Animalia	Arthropoda	Copepoda	Harpacticoida	Miraciidae	*Macrosetella*
Microsetella norvegica	Animalia	Arthropoda	Copepoda	Harpacticoida	Ectinosomatidae	*Microsetella*
Microsetella rosea	Animalia	Arthropoda	Copepoda	Harpacticoida	Ectinosomatidae	*Microsetella*
Mormonilla phasma	Animalia	Arthropoda	Copepoda	Mormonilloida	Mormonillidae	*Mormonilla*
Neomormonilla minor	Animalia	Arthropoda	Copepoda	Mormonilloida	Mormonillidae	*Neomormonilla*
Caligus longicaudus	Animalia	Arthropoda	Copepoda	Siphonostomatoida	Caligidae	*Caligus*
Pontoeciella abyssicola	Animalia	Arthropoda	Copepoda	Siphonostomatoida	Pontoeciellidae	*Pontoeciella*
Pontoeciella sp.	Animalia	Arthropoda	Copepoda	Siphonostomatoida	Pontoeciellidae	*Pontoeciella*
Lanceola sayana	Animalia	Arthropoda	Malacostraca	Amphipoda	Lanceolidae	*Lanceola*
Hyperietta vosseleri	Animalia	Arthropoda	Malacostraca	Amphipoda	Lestrigonidae	*Hyperietta*
Hyperioides longipes	Animalia	Arthropoda	Malacostraca	Amphipoda	Lestrigonidae	*Hyperioides*
Lestrigonus bengalensis	Animalia	Arthropoda	Malacostraca	Amphipoda	Lestrigonidae	*Lestrigonus*
Themistella fusca	Animalia	Arthropoda	Malacostraca	Amphipoda	Lestrigonidae	*Themistella*
Simorhynchotus antennarius	Animalia	Arthropoda	Malacostraca	Amphipoda	Lycaeidae	*Simorhynchotus*
Lycaeopsis zamboangae	Animalia	Arthropoda	Malacostraca	Amphipoda	Lycaeopsidae	*Lycaeopsis*

Scientific Name	Kingdom	Phylum	Class	Order	Family	Genus
Streetsia mindanaonis	Animalia	Arthropoda	Malacostraca	Amphipoda	Oxycephalidae	*Streetsia*
Phronimella elongata	Animalia	Arthropoda	Malacostraca	Amphipoda	Phronimidae	*Phronimella*
Phronima pacifica	Animalia	Arthropoda	Malacostraca	Amphipoda	Phronimidae	*Phronima*
Phrosina semilunata	Animalia	Arthropoda	Malacostraca	Amphipoda	Phrosinidae	*Phrosina*
Primno latreillei	Animalia	Arthropoda	Malacostraca	Amphipoda	Phrosinidae	*Primno*
Primno brevidens	Animalia	Arthropoda	Malacostraca	Amphipoda	Phrosinidae	*Primno*
Paratyphis maculatus	Animalia	Arthropoda	Malacostraca	Amphipoda	Platyscelidae	*Paratyphis*
Scina borealis	Animalia	Arthropoda	Malacostraca	Amphipoda	Scinidae	*Scina*
Scina nana	Animalia	Arthropoda	Malacostraca	Amphipoda	Scinidae	*Scina*
Vibilia stebbingi	Animalia	Arthropoda	Malacostraca	Amphipoda	Vibiliidae	*Vibilia*
Lucifer typus	Animalia	Arthropoda	Malacostraca	Decapoda	Luciferidae	*Lucifer*
Euphausia brevis	Animalia	Arthropoda	Malacostraca	Euphausiacea	Euphausiidae	*Euphausia*
Euphausia diomedeae	Animalia	Arthropoda	Malacostraca	Euphausiacea	Euphausiidae	*Euphausia*
Euphausia mutica	Animalia	Arthropoda	Malacostraca	Euphausiacea	Euphausiidae	*Euphausia*
Euphausia pacifica	Animalia	Arthropoda	Malacostraca	Euphausiacea	Euphausiidae	*Euphausia*
Euphausia pseudogibba	Animalia	Arthropoda	Malacostraca	Euphausiacea	Euphausiidae	*Euphausia*
Euphausia tenera	Animalia	Arthropoda	Malacostraca	Euphausiacea	Euphausiidae	*Euphausia*
Stylocheiron carinatum	Animalia	Arthropoda	Malacostraca	Euphausiacea	Euphausiidae	*Stylocheiron*
Stylocheron longicorne	Animalia	Arthropoda	Malacostraca	Euphausiacea	Euphausiidae	*Stylocheiron*
Stylocheron suhmii	Animalia	Arthropoda	Malacostraca	Euphausiacea	Euphausiidae	*Stylocheiron*
Subeucalanus mucronatus	Animalia	Arthropoda	Malacostraca	Euphausiacea	Euphausiidae	*Subeucalanus*
Thysanopoda aequalis	Animalia	Arthropoda	Malacostraca	Euphausiacea	Euphausiidae	*Thysanopoda*

Scientific Name	Kingdom	Phylum	Class	Order	Family	Genus
Alacia minor	Animalia	Arthropoda	Ostracoda	Halocyprida	Halocyprididae	*Alacia*
Alacia valdiviae	Animalia	Arthropoda	Ostracoda	Halocyprida	Halocyprididae	*Alacia*
Archiconchoecia striata	Animalia	Arthropoda	Ostracoda	Halocyprida	Halocyprididae	*Archiconchoecia*
Conchoecetta acuminata	Animalia	Arthropoda	Ostracoda	Halocyprida	Halocyprididae	*Conchoecetta*
Conchoecia magna	Animalia	Arthropoda	Ostracoda	Halocyprida	Halocyprididae	*Conchoecia*
Conchoecia subarcuata	Animalia	Arthropoda	Ostracoda	Halocyprida	Halocyprididae	*Conchoecia*
Conchoecilla daphnoides	Animalia	Arthropoda	Ostracoda	Halocyprida	Halocyprididae	*Conchoecilla*
Conchoecissa imbricata	Animalia	Arthropoda	Ostracoda	Halocyprida	Halocyprididae	*Conchoecissa*
Conchoecissa symmetrica	Animalia	Arthropoda	Ostracoda	Halocyprida	Halocyprididae	*Conchoecissa*
Discoconchoecia tamensis	Animalia	Arthropoda	Ostracoda	Halocyprida	Halocyprididae	*Discoconchoecia*
Discoconchoecia elegans	Animalia	Arthropoda	Ostracoda	Halocyprida	Halocyprididae	*Discoconchoecia*
Euconchoecia aculeata	Animalia	Arthropoda	Ostracoda	Halocyprida	Halocyprididae	*Euconchoecia*
Euconchoecia bifurcata	Animalia	Arthropoda	Ostracoda	Halocyprida	Halocyprididae	*Euconchoecia*
Fellia bicornis	Animalia	Arthropoda	Ostracoda	Halocyprida	Halocyprididae	*Fellia*
Fellia cornuta	Animalia	Arthropoda	Ostracoda	Halocyprida	Halocyprididae	*Fellia*
Halocypria globosa	Animalia	Arthropoda	Ostracoda	Halocyprida	Halocyprididae	*Halocypria*
Halocypris inflata	Animalia	Arthropoda	Ostracoda	Halocyprida	Halocyprididae	*Halocypris*
Loricoecia loricata	Animalia	Arthropoda	Ostracoda	Halocyprida	Halocyprididae	*Loricoecia*
Macrochoecilla macrocheira	Animalia	Arthropoda	Ostracoda	Halocyprida	Halocyprididae	*Macrochoecilla*
Metaconchoecia rotundata	Animalia	Arthropoda	Ostracoda	Halocyprida	Halocyprididae	*Metaconchoecia*
Mikroconchoecia curta	Animalia	Arthropoda	Ostracoda	Halocyprida	Halocyprididae	*Mikroconchoecia*

Scientific Name	Kingdom	Phylum	Class	Order	Family	Genus
Mikroconchoecia stigmatica	Animalia	Arthropoda	Ostracoda	Halocyprida	Halocyprididae	*Mikroconchoecia*
Orthoconchoecia atlantica	Animalia	Arthropoda	Ostracoda	Halocyprida	Halocyprididae	*Orthoconchoecia*
Orthoconchoecia bispinosa	Animalia	Arthropoda	Ostracoda	Halocyprida	Halocyprididae	*Orthoconchoecia*
Paraconchoecia dentata	Animalia	Arthropoda	Ostracoda	Halocyprida	Halocyprididae	*Paraconchoecia*
Paraconchoecia echinata	Animalia	Arthropoda	Ostracoda	Halocyprida	Halocyprididae	*Paraconchoecia*
Proceroecia macroprocera	Animalia	Arthropoda	Ostracoda	Halocyprida	Halocyprididae	*Proceroecia*
Paraconchoecia mamillata	Animalia	Arthropoda	Ostracoda	Halocyprida	Halocyprididae	*Paraconchoecia*
Paraconchoecia oblonga	Animalia	Arthropoda	Ostracoda	Halocyprida	Halocyprididae	*Paraconchoecia*
Paramollicia dichotoma	Animalia	Arthropoda	Ostracoda	Halocyprida	Halocyprididae	*Paramollicia*
Parthenoecia parthenoda	Animalia	Arthropoda	Ostracoda	Halocyprida	Halocyprididae	*Parthenoecia*
Porroecia porrecta	Animalia	Arthropoda	Ostracoda	Halocyprida	Halocyprididae	*Porroecia*
Porroecia spinirostris	Animalia	Arthropoda	Ostracoda	Halocyprida	Halocyprididae	*Porroecia*
Porroecia porrecta pacifica	Animalia	Arthropoda	Ostracoda	Halocyprida	Halocyprididae	*Porroecia*
Proceroecia procera	Animalia	Arthropoda	Ostracoda	Halocyprida	Halocyprididae	*Proceroecia*
Pseudoconchoecia concentrica	Animalia	Arthropoda	Ostracoda	Halocyprida	Halocyprididae	*Pseudoconchoecia*
Cypridina dentata	Animalia	Arthropoda	Ostracoda	Myodocopida	Cypridinidae	*Cypridina*
Krohnitta subtilis	Animalia	Chaetognatha	Sagittoidea	Aphragmophora	Krohnittidae	*Krohnitta*
Pterosagitta draco	Animalia	Chaetognatha	Sagittoidea	Aphragmophora	Pterosagittidae	*Pterosagitta*
Aidanosagitta delicata	Animalia	Chaetognatha	Sagittoidea	Aphragmophora	Sagittidae	*Aidanosagitta*
Aidanosagitta johorensis	Animalia	Chaetognatha	Sagittoidea	Aphragmophora	Sagittidae	*Aidanosagitta*
Aidanosagitta neglecta	Animalia	Chaetognatha	Sagittoidea	Aphragmophora	Sagittidae	*Aidanosagitta*
Aidanosagitta regularis	Animalia	Chaetognatha	Sagittoidea	Aphragmophora	Sagittidae	*Aidanosagitta*

Scientific Name	Kingdom	Phylum	Class	Order	Family	Genus
Aidanosagitta septata	Animalia	Chaetognatha	Sagittoidea	Aphragmophora	Sagittidae	*Aidanosagitta*
Caecosagitta macrocephala	Animalia	Chaetognatha	Sagittoidea	Aphragmophora	Sagittidae	*Caecosagitta*
Decipisagitta decipiens	Animalia	Chaetognatha	Sagittoidea	Aphragmophora	Sagittidae	*Decipisagitta*
Ferosagitta ferox	Animalia	Chaetognatha	Sagittoidea	Aphragmophora	Sagittidae	*Ferosagitta*
Ferosagitta robusta	Animalia	Chaetognatha	Sagittoidea	Aphragmophora	Sagittidae	*Ferosagitta*
Flaccisagitta enflata	Animalia	Chaetognatha	Sagittoidea	Aphragmophora	Sagittidae	*Flaccisagitta*
Flaccisagitta hexaptera	Animalia	Chaetognatha	Sagittoidea	Aphragmophora	Sagittidae	*Flaccisagitta*
Mesosagitta minima	Animalia	Chaetognatha	Sagittoidea	Aphragmophora	Sagittidae	*Mesosagitta*
Parasagitta tenuis	Animalia	Chaetognatha	Sagittoidea	Aphragmophora	Sagittidae	*Parasagitta*
Pseudosagitta lyra	Animalia	Chaetognatha	Sagittoidea	Aphragmophora	Sagittidae	*Pseudosagitta*
Sagitta bipunctata	Animalia	Chaetognatha	Sagittoidea	Aphragmophora	Sagittidae	*Sagitta*
Serratosagitta pacifica	Animalia	Chaetognatha	Sagittoidea	Aphragmophora	Sagittidae	*Serratosagitta*
Serratosagitta pseudoserratodentata	Animalia	Chaetognatha	Sagittoidea	Aphragmophora	Sagittidae	*Serratosagitta*
Zonosagitta bedoti	Animalia	Chaetognatha	Sagittoidea	Aphragmophora	Sagittidae	*Zonosagitta*
Zonosagitta littoralis	Animalia	Chaetognatha	Sagittoidea	Aphragmophora	Sagittidae	*Zonosagitta*
Zonosagitta nagae	Animalia	Chaetognatha	Sagittoidea	Aphragmophora	Sagittidae	*Zonosagitta*
Zonosagitta pulchra	Animalia	Chaetognatha	Sagittoidea	Aphragmophora	Sagittidae	*Zonosagitta*
Eukrohnia bathypelagica	Animalia	Chaetognatha	Sagittoidea	Phragmophora	Eukrohniidae	*Eukrohnia*
Eukrohnia fowleri	Animalia	Chaetognatha	Sagittoidea	Phragmophora	Eukrohniidae	*Eukrohnia*
Eukrohnia sp.	Animalia	Chaetognatha	Sagittoidea	Phragmophora	Eukrohniidae	*Eukrohnia*
Appendicularia sicula	Animalia	Chordata	Appendicularia	Copelata	Fritillariidae	*Appendicularia*
Fritillaria abjornseni	Animalia	Chordata	Appendicularia	Copelata	Fritillariidae	*Fritillaria*

Scientific Name	Kingdom	Phylum	Class	Order	Family	Genus
Fritillaria borealis	Animalia	Chordata	Appendicularia	Copelata	Fritillariidae	*Fritillaria*
Fritillaria formica	Animalia	Chordata	Appendicularia	Copelata	Fritillariidae	*Fritillaria*
Fritillaria fraudax	Animalia	Chordata	Appendicularia	Copelata	Fritillariidae	*Fritillaria*
Fritillaria gracilis	Animalia	Chordata	Appendicularia	Copelata	Fritillariidae	*Fritillaria*
Fritillaria haplostoma	Animalia	Chordata	Appendicularia	Copelata	Fritillariidae	*Fritillaria*
Fritillaria pellucida	Animalia	Chordata	Appendicularia	Copelata	Fritillariidae	*Fritillaria*
Fritillaria venusta	Animalia	Chordata	Appendicularia	Copelata	Fritillariidae	*Fritillaria*
Fritillaria sp.	Animalia	Chordata	Appendicularia	Copelata	Fritillariidae	*Fritillaria*
Megalocercus huxleyi	Animalia	Chordata	Appendicularia	Copelata	Oikopleuridae	*Megalocercus*
Oikopleura (Coecaria) fusiformis	Animalia	Chordata	Appendicularia	Copelata	Oikopleuridae	*Oikopleura*
Oikopleura (Coecaria) gracilis	Animalia	Chordata	Appendicularia	Copelata	Oikopleuridae	*Oikopleura*
Oikopleura (Coecaria) intermedia	Animalia	Chordata	Appendicularia	Copelata	Oikopleuridae	*Oikopleura*
Oikopleura (Coecaria) longicauda	Animalia	Chordata	Appendicularia	Copelata	Oikopleuridae	*Oikopleura*
Oikopleura (Vexillaria) albicans	Animalia	Chordata	Appendicularia	Copelata	Oikopleuridae	*Oikopleura*
Oikopleura (Vexillaria) cophocerca	Animalia	Chordata	Appendicularia	Copelata	Oikopleuridae	*Oikopleura*
Oikopleura (Vexillaria) gaussica	Animalia	Chordata	Appendicularia	Copelata	Oikopleuridae	*Oikopleura*
Oikopleura (Vexillaria) labradoriensis	Animalia	Chordata	Appendicularia	Copelata	Oikopleuridae	*Oikopleura*
Oikopleura (Vexillaria) parva	Animalia	Chordata	Appendicularia	Copelata	Oikopleuridae	*Oikopleura*
Oikopleura (Vexillaria) rufescens	Animalia	Chordata	Appendicularia	Copelata	Oikopleuridae	*Oikopleura*
Stegosoma magnum	Animalia	Chordata	Appendicularia	Copelata	Oikopleuridae	*Stegosoma*

Scientific Name	Kingdom	Phylum	Class	Order	Family	Genus
Doliolum nationalis	Animalia	Chordata	Thaliacea	Doliolida	Doliolidae	*Doliolum*
Pyrosoma atlanticum	Animalia	Chordata	Thaliacea	Pyrosomatida	Pyrosomatidae	*Pyrosoma*
Cyclosalpa pinnata	Animalia	Chordata	Thaliacea	Salpida	Salpidae	*Cyclosalpa*
Salpa fusiformis	Animalia	Chordata	Thaliacea	Salpida	Salpidae	*Salpa*
Salpa sp.	Chromista	Bacillariophyta	Bacillariophyceae			*Salpa*
Thalia cicar	Animalia	Chordata	Thaliacea	Salpida	Salpidae	*Thalia*
Thalia rhomboides	Animalia	Chordata	Thaliacea	Salpida	Salpidae	*Thalia*
Thalia democratica	Animalia	Chordata	Thaliacea	Salpida	Salpidae	*Thalia*
Traustedtia multitentaculata	Animalia	Chordata	Thaliacea	Salpida	Salpidae	*Traustedtia*
Nubiella tubularia	Animalia	Cnidaria	Hydrozoa	Anthoathecata	Bougainvilliidae	*Nubiella*
Bougainvillia niobe	Animalia	Cnidaria	Hydrozoa	Anthoathecata	Bougainvilliidae	*Bougainvillia*
Bythotiara apicigastera	Animalia	Cnidaria	Hydrozoa	Anthoathecata	Bythotiaridae	*Bythotiara*
Bythotiara depressa	Animalia	Cnidaria	Hydrozoa	Anthoathecata	Bythotiaridae	*Bythotiara*
Corymorpha knides	Animalia	Cnidaria	Hydrozoa	Anthoathecata	Corymorphidae	*Corymorpha*
Euphysilla pyramidata	Animalia	Cnidaria	Hydrozoa	Anthoathecata	Sphaerocorynidae	*Euphysilla*
Zanclea apicata	Animalia	Cnidaria	Hydrozoa	Anthoathecata	Zancleidae	*Zanclea*
Malagazzia carolinae	Animalia	Cnidaria	Hydrozoa	Leptothecata	Malagazziidae	*Malagazzia*
Liriope tetraphylla	Animalia	Cnidaria	Hydrozoa	Limnomedusae	Geryoniidae	*Liriope*
Solmundella bitentaculata	Animalia	Cnidaria	Hydrozoa	Narcomedusae	Solmundaeginidae	*Solmundella*
Abylopsis eschscholtzii	Animalia	Cnidaria	Hydrozoa	Siphonophorae	Abylidae	*Abylopsis*
Abylopsis tetragona	Animalia	Cnidaria	Hydrozoa	Siphonophorae	Abylidae	*Abylopsis*
Bassia bassensis	Animalia	Cnidaria	Hydrozoa	Siphonophorae	Abylidae	*Bassia*

Scientific Name	Kingdom	Phylum	Class	Order	Family	Genus
Agalma elegans	Animalia	Cnidaria	Hydrozoa	Siphonophorae	Agalmatidae	*Agalma*
Agalma okenii	Animalia	Cnidaria	Hydrozoa	Siphonophorae	Agalmatidae	*Agalma*
Halistemma rubrum	Animalia	Cnidaria	Hydrozoa	Siphonophorae	Agalmatidae	*Halistemma*
Nanomia bijuga	Animalia	Cnidaria	Hydrozoa	Siphonophorae	Agalmatidae	*Nanomia*
Nanomia cara	Animalia	Cnidaria	Hydrozoa	Siphonophorae	Agalmatidae	*Nanomia*
Chuniphyes multidentata	Animalia	Cnidaria	Hydrozoa	Siphonophorae	Clausophyidae	*Chuniphyes*
Clausophyes moserae	Animalia	Cnidaria	Hydrozoa	Siphonophorae	Clausophyidae	*Clausophyes*
Chelophyes appendiculata	Animalia	Cnidaria	Hydrozoa	Siphonophorae	Diphyidae	*Chelophyes*
Chelophyes contorta	Animalia	Cnidaria	Hydrozoa	Siphonophorae	Diphyidae	*Chelophyes*
Dimophyes arctica	Animalia	Cnidaria	Hydrozoa	Siphonophorae	Diphyidae	*Dimophyes*
Diphyes bojani	Animalia	Cnidaria	Hydrozoa	Siphonophorae	Diphyidae	*Diphyes*
Diphyes chamissonis	Animalia	Cnidaria	Hydrozoa	Siphonophorae	Diphyidae	*Diphyes*
Eudoxoides mitra	Animalia	Cnidaria	Hydrozoa	Siphonophorae	Diphyidae	*Eudoxoides*
Eudoxoides spiralis	Animalia	Cnidaria	Hydrozoa	Siphonophorae	Diphyidae	*Eudoxoides*
Lensia campanella	Animalia	Cnidaria	Hydrozoa	Siphonophorae	Diphyidae	*Lensia*
Lensia challengeri	Animalia	Cnidaria	Hydrozoa	Siphonophorae	Diphyidae	*Lensia*
Lensia conoidea	Animalia	Cnidaria	Hydrozoa	Siphonophorae	Diphyidae	*Lensia*
Lensia cordata	Animalia	Cnidaria	Hydrozoa	Siphonophorae	Diphyidae	*Lensia*
Lensia cossack	Animalia	Cnidaria	Hydrozoa	Siphonophorae	Diphyidae	*Lensia*
Lensia fowleri	Animalia	Cnidaria	Hydrozoa	Siphonophorae	Diphyidae	*Lensia*
Lensia grimaldii	Animalia	Cnidaria	Hydrozoa	Siphonophorae	Diphyidae	*Lensia*
Lensia hotspur	Animalia	Cnidaria	Hydrozoa	Siphonophorae	Diphyidae	*Lensia*

Scientific Name	Kingdom	Phylum	Class	Order	Family	Genus
Lensia leloupi	Animalia	Cnidaria	Hydrozoa	Siphonophorae	Diphyidae	*Lensia*
Lensia lelouveteau	Animalia	Cnidaria	Hydrozoa	Siphonophorae	Diphyidae	*Lensia*
Lensia meteori	Animalia	Cnidaria	Hydrozoa	Siphonophorae	Diphyidae	*Lensia*
Lensia multicristata	Animalia	Cnidaria	Hydrozoa	Siphonophorae	Diphyidae	*Lensia*
Lensia subtilis	Animalia	Cnidaria	Hydrozoa	Siphonophorae	Diphyidae	*Lensia*
Lensia subtiloides	Animalia	Cnidaria	Hydrozoa	Siphonophorae	Diphyidae	*Lensia*
Sulculeolaria chuni	Animalia	Cnidaria	Hydrozoa	Siphonophorae	Diphyidae	*Sulculeolaria*
Forskalia edwardsii	Animalia	Cnidaria	Hydrozoa	Siphonophorae	Forskaliidae	*Forskalia*
Hippopodius hippopus	Animalia	Cnidaria	Hydrozoa	Siphonophorae	Hippopodiidae	*Hippopodius*
Vogtia glabra	Animalia	Cnidaria	Hydrozoa	Siphonophorae	Hippopodiidae	*Vogtia*
Amphicaryon peltifera	Animalia	Cnidaria	Hydrozoa	Siphonophorae	Prayidae	*Amphicaryon*
Desmophyes annectens	Animalia	Cnidaria	Hydrozoa	Siphonophorae	Prayidae	*Desmophyes*
Rosacea cymbiformis	Animalia	Cnidaria	Hydrozoa	Siphonophorae	Prayidae	*Rosacea*
Rosacea plicata	Animalia	Cnidaria	Hydrozoa	Siphonophorae	Prayidae	*Rosacea*
Sphaeronectes bougisi	Animalia	Cnidaria	Hydrozoa	Siphonophorae	Sphaeronectidae	*Sphaeronectes*
Sphaeronectes koellikeri	Animalia	Cnidaria	Hydrozoa	Siphonophorae	Sphaeronectidae	*Sphaeronectes*
Aglaura hemistoma	Animalia	Cnidaria	Hydrozoa	Trachymedusae	Rhopalonematidae	*Aglaura*
Amphogona apsteini	Animalia	Cnidaria	Hydrozoa	Trachymedusae	Rhopalonematidae	*Amphogona*
Amphogona pusilla	Animalia	Cnidaria	Hydrozoa	Trachymedusae	Rhopalonematidae	*Amphogona*
Rhopalonema funerarium	Animalia	Cnidaria	Hydrozoa	Trachymedusae	Rhopalonematidae	*Rhopalonema*
Rhopalonema velatum	Animalia	Cnidaria	Hydrozoa	Trachymedusae	Rhopalonematidae	*Rhopalonema*
Hormiphora palmata	Animalia	Ctenophora	Tentaculata	Cydippida	Cydippidae	*Hormiphora*

Scientific Name	Kingdom	Phylum	Class	Order	Family	Genus
Atlanta brunnea	Animalia	Mollusca	Gastropoda	Littorinimorpha	Atlantidae	*Atlanta*
Atlanta helicinoidea	Animalia	Mollusca	Gastropoda	Littorinimorpha	Atlantidae	*Atlanta*
Atlanta lesueurii	Animalia	Mollusca	Gastropoda	Littorinimorpha	Atlantidae	*Atlanta*
Protatlanta souleyeti	Animalia	Mollusca	Gastropoda	Littorinimorpha	Atlantidae	*Protatlanta*
Pterotrachea coronata	Animalia	Mollusca	Gastropoda	Littorinimorpha	Pterotracheidae	*Pterotrachea*
Pterotrachea hippocampus	Animalia	Mollusca	Gastropoda	Littorinimorpha	Pterotracheidae	*Pterotrachea*
Diacria trispinosa	Animalia	Mollusca	Gastropoda	Pteropoda	Cavoliniidae	*Diacria*
Telodiacria quadridentata	Animalia	Mollusca	Gastropoda	Pteropoda	Cavoliniidae	*Telodiacria*
Clio chaptalii	Animalia	Mollusca	Gastropoda	Pteropoda	Cliidae	*Clio*
Clio pyramidata	Animalia	Mollusca	Gastropoda	Pteropoda	Cliidae	*Clio*
Paraclione longicaudata	Animalia	Mollusca	Gastropoda	Pteropoda	Clionidae	*Paraclione*
Creseis virgula	Animalia	Mollusca	Gastropoda	Pteropoda	Creseidae	*Creseis*
Creseis acicula	Animalia	Mollusca	Gastropoda	Pteropoda	Creseidae	*Creseis*
Styliola subula	Animalia	Mollusca	Gastropoda	Pteropoda	Creseidae	*Styliola*
Corolla ovata	Animalia	Mollusca	Gastropoda	Pteropoda	Cymbuliidae	*Corolla*
Cymbulia peronii	Animalia	Mollusca	Gastropoda	Pteropoda	Cymbuliidae	*Cymbulia*
Desmopterus papilio	Animalia	Mollusca	Gastropoda	Pteropoda	Desmopteridae	*Desmopterus*
Heliconoides inflatus	Animalia	Mollusca	Gastropoda	Pteropoda	Heliconoididae	*Heliconoides*
Hyalocylis striata	Animalia	Mollusca	Gastropoda	Pteropoda	Hyalocylidae	*Hyalocylis*
Agadina stimpsoni	Animalia	Mollusca	Gastropoda	Pteropoda	Limacinidae	*Agadina*
Limacina bulimoides	Animalia	Mollusca	Gastropoda	Pteropoda	Limacinidae	*Limacina*
Limacina helicina	Animalia	Mollusca	Gastropoda	Pteropoda	Limacinidae	*Limacina*

Scientific Name	Kingdom	Phylum	Class	Order	Family	Genus
Limacina trochiformis	Animalia	Mollusca	Gastropoda	Pteropoda	Limacinidae	*Limacina*
Peracle reticulata	Animalia	Mollusca	Gastropoda	Pteropoda	Peraclidae	*Peracle*
Pneumoderma violaceum	Animalia	Mollusca	Gastropoda	Pteropoda	Pneumodermatidae	*Pneumoderma*

Schedule 2-3 List of Benthos Species in Block M

Scientific Name	Kingdom	Phylum	Class	Order	Family	Genus
Paraphysomonas foraminifera	Chromista	Ochrophyta	Chrysophyceae	Chromulinales	Paraphysomonadaceae	*Paraphysomonas*
Ammonia beccarii	Chromista	Foraminifera	Globothalamea	Rotaliida	Ammoniidae	*Ammonia*
Syringammina corbicula	Chromista	Foraminifera	Monothalamea		Psamminidae	*Syringammina*
Hyalonema sp.	Animalia	Porifera	Hexactinellida	Amphidiscosida	Hyalonematidae	*Hyalonema*
Raspailiidae indet.	Animalia	Porifera	Demospongiae	Axinellida	Raspailiidae	
Darwinellidae indet.	Animalia	Porifera	Demospongiae	Dendroceratida	Darwinellidae	
Poecilosclerida indet.	Animalia	Porifera	Demospongiae	Poecilosclerida		
Polymastiidae indet.	Animalia	Porifera	Demospongiae	Polymastiida	Polymastiidae	
Demospongiae indet.	Animalia	Porifera	Demospongiae			
Abyssopathes sp.	Animalia	Cnidaria	Anthozoa	Antipatharia	Cladopathidae	*Abyssopathes*
Bodonema sp.	Animalia	Nematoda	Chromadorea	Araeolaimida	Bodonematidae	*Bodonema*
Dorylaimopsis sp.	Animalia	Nematoda	Chromadorea	Araeolaimida	Comesomatidae	*Dorylaimopsis*
Coninckia sp.	Animalia	Nematoda	Chromadorea	Araeolaimida	Coninckiidae	*Coninckia*
Hopperia sp.	Animalia	Nematoda	Chromadorea	Araeolaimida	Comesomatidae	*Hopperia*
Laimella sp.	Animalia	Nematoda	Chromadorea	Araeolaimida	Comesomatidae	*Laimella*
Minolaimus sp.	Animalia	Nematoda	Chromadorea	Araeolaimida	Comesomatidae	*Minolaimus*
Pierrickia sp.	Animalia	Nematoda	Chromadorea	Araeolaimida	Comesomatidae	*Pierrickia*
Southerniella sp.	Animalia	Nematoda	Chromadorea	Araeolaimida	Diplopeltidae	*Southerniella*
Paralongicyatholaimus sp.	Animalia	Nematoda	Chromadorea	Chromadorida	Cyatholaimidae	*Paralongicyatholaimus*
Paramarylynnia sp.	Animalia	Nematoda	Chromadorea	Chromadorida	Cyatholaimidae	*Paramarylynnia*
Desmoscolex sp.	Animalia	Nematoda	Chromadorea	Desmoscolecida	Desmoscolecidae	*Desmoscolex*

Scientific Name	Kingdom	Phylum	Class	Order	Family	Genus
Hapalomus sp.	Animalia	Nematoda	Chromadorea	Desmoscolecida	Desmoscolecidae	*Hapalomus*
Terschellingia sp.	Animalia	Nematoda	Chromadorea	Monhysterida	Linhomoeidae	*Terschellingia*
Diplolaimella sp.	Animalia	Nematoda	Chromadorea	Monhysterida	Monhysteridae	*Diplolaimella*
Amphimonhystera sp.	Animalia	Nematoda	Chromadorea	Monhysterida	Xyalidae	*Amphimonhystera*
Daptonema sp.	Animalia	Nematoda	Chromadorea	Monhysterida	Xyalidae	*Daptonema*
Elzalia sp.	Animalia	Nematoda	Chromadorea	Monhysterida	Xyalidae	*Elzalia*
Gnomoxyala sp.	Animalia	Nematoda	Chromadorea	Monhysterida	Xyalidae	*Gnomoxyala*
Linhystera sp.	Animalia	Nematoda	Chromadorea	Monhysterida	Xyalidae	*Linhystera*
Manganonema sp.	Animalia	Nematoda	Chromadorea	Monhysterida	Xyalidae	*Manganonema*
Rhynchonema sp.	Animalia	Nematoda	Chromadorea	Monhysterida	Xyalidae	*Rhynchonema*
Theristus sp.	Animalia	Nematoda	Chromadorea	Monhysterida	Xyalidae	*Theristus*
Aegialoalaimus sp.	Animalia	Nematoda	Chromadorea	Plectida	Aegialoalaimidae	*Aegialoalaimus*
Ceramonema sp.	Animalia	Nematoda	Chromadorea	Plectida	Ceramonematidae	*Ceramonema*
Pselionema sp.	Animalia	Nematoda	Chromadorea	Plectida	Ceramonematidae	*Pselionema*
Diplopeltoides sp.	Animalia	Nematoda	Chromadorea	Plectida	Diplopeltoididae	*Diplopeltoides*
Leptolaimus sp.	Animalia	Nematoda	Chromadorea	Plectida	Leptolaimidae	*Leptolaimus*
Tubolaimoides sp.	Animalia	Nematoda	Chromadorea	Plectida	Tubolaimoididae	*Tubolaimoides*
Symplocostoma sp.	Animalia	Nematoda	Enoplea	Enoplida	Enchelidiidae	*Symplocostoma*
Thalassironus sp.	Animalia	Nematoda	Enoplea	Enoplida	Ironidae	*Thalassironus*
Halalaimus sp.	Animalia	Nematoda	Enoplea	Enoplida	Oxystominidae	*Halalaimus*
Litinium sp.	Animalia	Nematoda	Enoplea	Enoplida	Oxystominidae	*Litinium*
Wieseria sp.	Animalia	Nematoda	Enoplea	Enoplida	Oxystominidae	*Wieseria*

Scientific Name	Kingdom	Phylum	Class	Order	Family	Genus
Thalassoalaimus sp.	Animalia	Nematoda	Enoplea	Enoplida	Oxystominidae	*Thalassoalaimus*
Oxystomina sp.	Animalia	Nematoda	Enoplea	Enoplida	Oxystominidae	*Oxystomina*
Syringolaimus sp.	Animalia	Nematoda	Enoplea	Enoplida	Rhabdolaimidae	*Syringolaimus*
Bathylaimus sp.	Animalia	Nematoda	Enoplea	Enoplida	Tripyloididae	*Bathylaimus*
Chaetozone sp.1	Animalia	Annelida	Polychaeta	Terebellida	Cirratulidae	*Chaetozone*
Chaetozone sp.2	Animalia	Annelida	Polychaeta	Terebellida	Cirratulidae	*Chaetozone*
Cirratulidae sp.3	Animalia	Annelida	Polychaeta	Terebellida	Cirratulidae	
Cirratulidae sp.4	Animalia	Annelida	Polychaeta	Terebellida	Cirratulidae	
Glycera sp.	Animalia	Annelida	Polychaeta	Phyllodocida	Glyceridae	*Glycera*
Hemipodia sp.	Animalia	Annelida	Polychaeta	Phyllodocida	Glyceridae	*Hemipodia*
Phyllodocida sp. indet.3	Animalia	Annelida	Polychaeta	Phyllodocida		
Polynoidae sp.1	Animalia	Annelida	Polychaeta	Phyllodocida	Polynoidae	
Magelona sp.	Animalia	Annelida	Polychaeta		Magelonidae	*Magelona*
Opheliidae sp.1	Animalia	Annelida	Polychaeta		Opheliidae	
Paraonidae sp.1	Animalia	Annelida	Polychaeta		Paraonidae	
Spionidae sp.1	Animalia	Annelida	Polychaeta	Spionida	Spionidae	
Spionidae sp.3	Animalia	Annelida	Polychaeta	Spionida	Spionidae	
Polychaeta sp. indet.	Animalia	Annelida	Polychaeta			
Polychaeta sp. indet.1	Animalia	Annelida	Polychaeta			
Polychaeta sp. indet.2	Animalia	Annelida	Polychaeta			
Gastropoda sp.1	Animalia	Mollusca	Gastropoda			
Scintilla sp.	Animalia	Mollusca	Bivalvia	Galeommatida	Galeommatidae	*Scintilla*

Scientific Name	Kingdom	Phylum	Class	Order	Family	Genus
Conchostraca sp.1	Animalia	Arthropoda	Branchiopoda			
Conchostraca sp.2	Animalia	Arthropoda	Branchiopoda			
Harpacticoida sp.1	Animalia	Arthropoda	Copepoda	Harpacticoida		
Harpacticoida sp.2	Animalia	Arthropoda	Copepoda	Harpacticoida		
Harpacticoida sp.3	Animalia	Arthropoda	Copepoda	Harpacticoida		
Harpacticoida sp.5	Animalia	Arthropoda	Copepoda	Harpacticoida		
Harpacticoida indet.	Animalia	Arthropoda	Copepoda	Harpacticoida		
Eurythenes gryllus	Animalia	Arthropoda	Malacostraca	Amphipoda	Eurytheneidae	*Eurythenes*
Gammarus sp.	Animalia	Arthropoda	Malacostraca	Amphipoda	Gammaridae	*Gammarus*
Hirondellea dubia	Animalia	Arthropoda	Malacostraca	Amphipoda	Hirondelleidae	*Hirondellea*
Paralicella tenuipes	Animalia	Arthropoda	Malacostraca	Amphipoda	Alicellidae	*Paralicella*
Anthuridae indet.	Animalia	Arthropoda	Malacostraca	Isopoda	Anthuridae	
Asellidae indet.	Animalia	Arthropoda	Malacostraca	Isopoda	Asellidae	
Ischnomesidae sp.1	Animalia	Arthropoda	Malacostraca	Isopoda	Ischnomesidae	
Isopoda sp. indet.1	Animalia	Arthropoda	Malacostraca	Isopoda		
Isopoda sp.1	Animalia	Arthropoda	Malacostraca	Isopoda		
Isopoda sp.4	Animalia	Arthropoda	Malacostraca	Isopoda		
Isopoda sp.8	Animalia	Arthropoda	Malacostraca	Isopoda		
Isopoda sp.9	Animalia	Arthropoda	Malacostraca	Isopoda		
Isopoda sp.10	Animalia	Arthropoda	Malacostraca	Isopoda		
Isopoda sp.11	Animalia	Arthropoda	Malacostraca	Isopoda		
Isopoda sp.12	Animalia	Arthropoda	Malacostraca	Isopoda		

Scientific Name	Kingdom	Phylum	Class	Order	Family	Genus
Mesosignum sp.1	Animalia	Arthropoda	Malacostraca	Isopoda	Mesosignidae	*Mesosignum*
Leptognathiidae indet.	Animalia	Arthropoda	Malacostraca	Tanaidacea	Leptognathiidae	
Anarthrura sp.	Animalia	Arthropoda	Malacostraca	Tanaidacea	Anarthruridae	*Anarthrura*
Apseudidae indet.	Animalia	Arthropoda	Malacostraca	Tanaidacea	Apseudidae	
Tanaidacea sp. indet.1	Animalia	Arthropoda	Malacostraca	Tanaidacea		
Tanaidacea sp.4	Animalia	Arthropoda	Malacostraca	Tanaidacea		
Tanaidacea sp.8	Animalia	Arthropoda	Malacostraca	Tanaidacea		
Glyphocrangon sp.	Animalia	Arthropoda	Malacostraca	Decapoda	Glyphocrangonidae	*Glyphocrangon*
Hymenopenaeus sp.	Animalia	Arthropoda	Malacostraca	Decapoda	Solenoceridae	*Hymenopenaeus*
Nematocarcinus sp.	Animalia	Arthropoda	Malacostraca	Decapoda	Nematocarcinidae	*Nematocarcinus*
Cerataspis sp.	Animalia	Arthropoda	Malacostraca	Decapoda	Aristeidae	*Cerataspis*
Pantopoda sp.1	Animalia	Arthropoda	Pycnogonida	Pantopoda		
Pycnogonida sp.2	Animalia	Arthropoda	Pycnogonida			
Smithsonius sp.	Animalia	Bryozoa	Gymnolaemata	Cheilostomatida	Tessaradomidae	*Smithsonius*
Notoplites sp.	Animalia	Bryozoa	Gymnolaemata	Cheilostomatida	Candidae	*Notoplites*
Bathycrinus sp.	Animalia	Echinodermata	Crinoidea	Comatulida	Bathycrinidae	*Bathycrinus*
Freyastera sp.	Animalia	Echinodermata	Asteroidea	Brisingida	Freyellidae	*Freyastera*
Freyella sp.	Animalia	Echinodermata	Asteroidea	Brisingida	Freyellidae	*Freyella*
Hymenaster sp.	Animalia	Echinodermata	Asteroidea	Velatida	Pterasteridae	*Hymenaster*
Amphioplus sp.	Animalia	Echinodermata	Ophiuroidea	Amphilepidida	Amphiuridae	*Amphioplus*
Ophiotypa sp.	Animalia	Echinodermata	Ophiuroidea	Amphilepidida	Ophiolepididae	*Ophiotypa*
Ophiacantha sp.	Animalia	Echinodermata	Ophiuroidea	Ophiacanthida	Ophiacanthidae	*Ophiacantha*

Scientific Name	Kingdom	Phylum	Class	Order	Family	Genus
Amperima sp.	Animalia	Echinodermata	Holothuroidea	Elasipodida	Elpidiidae	*Amperima*
Peniagone sp.	Animalia	Echinodermata	Holothuroidea	Elasipodida	Elpidiidae	*Peniagone*
Benthodytes sp.	Animalia	Echinodermata	Holothuroidea	Elasipodida	Psychropotidae	*Benthodytes*
Psychropotes sp.	Animalia	Echinodermata	Holothuroidea	Elasipodida	Psychropotidae	*Psychropotes*
Mesothuria sp.	Animalia	Echinodermata	Holothuroidea	Holothuriida	Mesothuriidae	*Mesothuria*
Synallactes sp.	Animalia	Echinodermata	Holothuroidea	Synallactida	Synallactidae	*Synallactes*
Holothuroidea sp.1	Animalia	Echinodermata	Holothuroidea			
Coryphaena hippurus	Animalia	Chordata	Teleostei	Carangiformes	Coryphaenidae	*Coryphaena*
Microphysogobio amurensis	Animalia	Chordata	Teleostei	Cypriniformes	Cyprinidae	*Microphysogobio*
Macrouridae indet.	Animalia	Chordata	Teleostei	Gadiformes	Macrouridae	
Coryphaenoides sp	Animalia	Chordata	Teleostei	Gadiformes	Macrouridae	*Coryphaenoides*
Ophidiidae gen. sp.	Animalia	Chordata	Teleostei	Ophidiiformes	Ophidiidae	

Schedule 3-1 List of Data Obtained at Stations (Sediment)

Station	Longitude/°E	Latitude/°N	Water Depth /m	Block	Smear Identification	Particle Size Analysis	Major Trace Element	Clay Mineral	Pore Water Major Metallic Elements	Penetration	Shear Strength	Natural Moisture Content	Wet Density	Porosity	Proportion	Liquid Limit	Plastic Limit	Plasticity Index	Liquidity Index	Compressibility	Compression Modulus	Cohesive Force	Internal Friction
DY69-M2B1-PS13-BC01	153.94402	18.88123	5702	M2	√	√	√																
DY69-M2B1-PS01-BC02	154.12474	18.97067	5718	M2	√	√	√			√	√												
DY69-M2B1-PS02-BC03	154.30565	18.96199	5675	M2	√	√	√			√	√												
DY69-M2B1-PS05-BC04	153.58545	19.17258	5434	M2	√	√	√																
DY69-M2B1-PS04-BC05	153.40173	19.16932	5589	M2	√	√	√			√	√												
DY69-M2B1-PS08-BC06	153.31253	19.27086	5520	M2	√	√	√			√	√												
DY69-M2B1-PS07-BC07	153.94103	19.16952	5576	M2	√	√	√			√	√												
DY69-M2B1-PS11-BC08	153.85039	19.27061	5443	M2	√	√	√			√	√												
DY69-M2-ES04-BC09	153.67167	19.37304	4842	M2	√	√	√	√	√	√	√												
DY69-M2B1-PS10-BC10	153.67034	19.27093	5193	M2	√	√	√			√	√												
DY69-M2B1-PS06-BC11	153.75938	19.37272	5508	M2	√	√	√			√	√												
DY69-M2B1-PS03-BC12	153.85101	19.08253	5621	M2	√	√	√			√	√												
DY69-M2B1-ESO3-BC13	153.67292	19.09477	5569	M2	√																		
DY69-M2B1-PS14-BC14	153.49430	18.97486	5632	M2	√	√	√			√	√												
DY69-M2B1-PS15-BC15	153.49288	19.07620	5593	M2	√	√	√			√	√												
DY69-M2B1-PS09-BC16	153.49258	19.27211	5248	M2	√	√	√			√	√												
DY69-M1-ES06-BC17	152.88986	18.83053	5528	M1	√	√	√	√	√	√	√												
DY69-M2B1-ES06-BC20	153.27106	18.83172	5668	M2	√	√	√		√														
DY69-M2B1-ES02-BC22	153.67486	18.82680	5650	M2	√	√	√	√	√	√	√												
DY69-M2B1-ES01-BC25	153.67626	18.56169	5645	M2	√	√	√	√	√	√	√												
DY69-M2B1-ES05-BC20	153.27110	18.83172	5668	M2						√	√												
DY69-M2B1-ES03-MC02	153.67183	19.09644	5576	M2		√	√	√	√	√	√												
DY75I-M2-BC03A	155.12989	19.51949	5685	M2	√		√			√	√												
DY75I-M2-BC04	155.30042	19.52016	5651	M2	√		√			√	√												
DY75I-M2-BC05	155.30001	19.68959	5625	M2	√		√			√	√												
DY75I-M2-BC06	155.12997	19.68962	5675	M2	√		√					√	√	√	√	√	√	√	√	√	√	√	√
DY75I-M2-BC07	154.94993	19.68953	5716	M2	√		√			√	√												
DY75I-M2-BC08	154.77000	19.51955	5616	M2	√		√			√	√												
DY75I-M2-BC09	154.95602	19.51950	5675	M2	√		√			√	√												
DY75I-M2-BC10	154.94997	19.34958	5684	M2	√		√																
DY75I-M2-BC11	155.13003	19.34954	5658	M2	√		√			√	√	√	√	√	√	√	√	√	√	√	√	√	√
DY75I-M2-BC12	155.29983	19.34958	5678	M2	√		√			√	√												
DY75I-M2-BC13	154.94974	19.17960	5629	M2	√		√			√	√	√	√	√	√	√	√	√	√	√	√	√	√
DY75I-M2-BC14	154.76992	19.17951	5671	M2	√		√			√	√												
DY75I-M2-BC15	154.60012	18.99956	5659	M2	√		√			√	√												
DY75I-M2-BC16A	154.59997	19.17950	5690	M2	√		√			√	√	√	√	√	√	√	√	√	√	√	√	√	√

Station	Longitude/°E	Latitude/°N	Water Depth /m	Block	Smear Identification	Particle Size Analysis	Major Trace Element	Clay Mineral	Pore Water Major Metallic Elements	Penetration	Shear Strength	Natural Moisture Content	Wet Density	Porosity	Proportion	Liquid Limit	Plastic Limit	Plasticity Index	Liquidity Index	Compressibility	Compression Modulus	Cohesive Force	Internal Friction
DY75I-M2-BC17	154.12020	19.16957	5719	M2	√		√			√	√												
DY75I-M2-BC18	154.24032	19.17967	5725	M2						√	√	√	√	√	√	√	√	√	√	√	√	√	√
DY75I-M2-BC19	154.41992	19.17952	5704	M2	√		√			√	√												
DY75I-M2-BC20	154.41992	19.34954	5669	M2	√		√			√	√	√	√	√	√	√	√	√	√	√	√	√	√
DY75I-M2-BC21	154.60017	19.34961	5673	M2	√		√			√	√												
DY75I-M2-BC22	154.59965	19.51962	5659	M2	√		√			√	√												
DY75I-M2-BC23	154.42067	19.68705	5737	M2	√		√			√	√												
DY75I-M2-BC24	154.23958	19.68996	5770	M2	√		√			√	√												
DY75I-M2-BC25	154.05982	19.69040	5585	M2	√		√			√	√												
DY75I-M2-BC26	154.05952	19.52010	5636	M2	√		√			√	√												
DY75I-M2-BC27	154.23950	19.35019	5695	M2	√		√			√	√												
DY75I-M2-BC28	154.05954	19.35023	5500	M2	√		√			√	√	√	√	√	√	√	√	√	√	√	√	√	√
DY75I-M2-BC29	154.02978	19.16972	5664	M2	√		√			√	√												
DY75I-M2-BC30	153.75955	19.08981	5587	M2	√		√			√	√												
DY75I-M2-BC31	153.57951	19.08003	5571	M2	√		√			√	√	√	√	√	√	√	√	√	√	√	√	√	√
DY75I-M2-BC32	153.49042	19.16985	5507	M2	√		√			√	√												
DY75I-M2-BC33	153.58030	19.26962	5148	M2	√		√			√	√	√	√	√	√	√	√	√	√	√	√	√	√
DY75I-M2-BC34	153.67982	19.16954	5478	M2	√		√			√	√												
DY75I-M2-BC35	153.52467	19.16963	5471	M2	√		√			√	√	√	√	√	√	√	√	√	√	√	√	√	√
DY75I-M2-BC36	153.93995	19.26952	5539	M2	√		√			√	√												
DY75I-M2-BC37A	153.84962	19.16960	5520	M2						√	√												
DY75I-M2-BC38A	153.75955	19.27021	5302	M2	√		√			√	√												
DY75I-M2-BC39A	153.39987	19.26999	5428	M2	√		√			√	√												
DY75I-M2-BC40	153.31028	19.16958	5647	M2	√		√			√	√												
DY75I-M2-BC41A	153.30992	19.07990	5654	M2	√		√			√	√												
DY75I-M2-BC42	153.40049	19.08014	5618	M2	√		√			√	√												
DY75I-M2-BC43	153.39026	18.98961	5655	M2	√		√			√	√												
DY75I-M2-BC44	153.57990	18.96957	5632	M2	√		√			√	√	√	√	√	√	√	√	√	√	√	√	√	√
DY75I-M2-BC45	153.74964	18.97966	5680	M2	√		√			√	√												
DY75I-M2-BC46	153.83989	18.97954	5673	M2	√		√			√	√												
DY75I-M2-BC47	153.93996	19.07953	5626	M2	√		√			√	√												
DY75II-M2-BC48A	154.03022	19.08005	5660	M2	√		√			√	√												
DY75I-M2-BC49	154.03005	18.96953	5702	M2	√		√			√	√												
DY75I-M2-BC50	154.12001	19.07953	5695	M2	√		√			√	√												
DY75I-M2-BC51	154.21041	19.07973	5698	M2	√		√			√	√												
DY75I-M2-BC52A	154.21032	18.96865	5683	M2	√		√			√	√												
DY75I-M2-BC53	154.39041	18.96990	5660	M2	√		√			√	√												
DY75I-M2-BC54	154.33999	18.87999	5696	M2	√		√			√	√												

Station	Longitude/°E	Latitude/°N	Water Depth /m	Block	Smear Identification	Particle Size Analysis	Major Trace Element	Clay Mineral	Pore Water Major Metallic Elements	Penetration	Shear Strenth	Natural Moisture Content	Wet Density	Porosity	Proportion	Liquid Limit	Plastic Limit	Plasticity Index	Liquidity Index	Compressibility	Compression Modulus	Cohesive Force	Internal Friction
DY75I-M2-BC55	154.15999	18.87994	5706	M2	√		√			√	√												
DY75I-M2-BC56	153.98005	18.71001	5657	M2	√		√			√	√	√	√	√	√	√	√	√	√	√	√	√	√
DY75I-M2-BC57	154.15999	18.70995	5665	M2	√		√			√	√												
DY75I-M2-BC58	154.33990	18.70992	5659	M2	√		√			√	√												
DY75I-M2-BC59	154.33978	18.53978	5654	M2	√		√			√	√												
DY75I-M2-BC60A	154.16004	18.53995	5667	M2	√		√			√	√												
DY75I-M2-BC61	153.25986	18.54024	5664	M2	√		√			√	√												
DY75I-M2-BC62	153.43969	18.54008	5660	M2																			
DY75I-M2-BC63	153.98000	18.54004	5678	M2	√		√			√	√	√	√	√	√	√	√	√	√	√	√	√	√
DY75I-M2-BC64	153.61994	18.70992	5731	M2	√		√			√	√	√	√	√	√	√	√	√	√	√	√	√	√
DY75I-M2-BC65	153.43925	18.70984	5706	M2	√		√			√	√												
DY75I-M2-BC66	153.25000	18.70994	5690	M2	√		√			√	√												
DY75I-M1-BC73	152.88999	18.73496	5625	M2	√		√			√	√												
DY75I-M2-BC75	153.67958	19.13998	5496	M2	√		√			√	√												
DY75I-M2-BC76	153.67961	19.13961	5510	M2																			
DY75I-M2-BC77	153.67992	19.08982	5543	M2	√		√																
DY75I-M2-BC78	153.68008	19.08992	5562	M2	√		√			√	√												
DY75I-M2-BC79	153.67987	19.04005	5611	M2	√		√			√	√												
DY75I-M2-BC80	153.68001	19.03994	5618	M2	√		√																
DY75I-M1-BC68	152.89007	18.82997	5525	M1	√		√																
DY75I-M1-BC69	152.89002	18.82992	5529	M1	√		√																
DY75I-M1-BC70	152.81999	18.73493	5566	M1																			
DY75I-M1-BC71	152.82003	18.73492	5554	M1	√		√																
DY75I-M1-BC72	152.88996	18.73491	5623	M1	√		√																
DY75I-M1-BC74	152.81553	18.84369	5393	M1	√		√																
DY75II-M2-BC81	153.26007	18.99278	5681	M2	√		√			√	√												
DY75II-M2-BC82	153.29610	18.87647	5669	M2	√		√			√	√												
DY75II-M1-BC83	152.66583	19.23978	1287	M1	√		√																
DY75II-M1-BC84	152.64593	18.73478	5483	M1	√		√			√	√												
DY75II-M1-BC85	152.65295	18.86710	5157	M1	√		√																
DY75II-M1-BC86	152.65293	18.99994	4398	M1	√		√			√	√												
DY75II-M1-BC87	152.71968	19.00946	4526	M1	√		√			√	√												
DY75II-M1-BC88	152.68973	18.99977	4567	M1	√		√			√	√												
DY75II-M1-BC89	152.70503	18.99849	4570	M1	√		√			√	√												
DY75II-M2-BC90	154.03224	19.27791	5490	M2	√		√			√	√												
DY75II-M2-BC91	153.73165	19.34160	5078	M2	√		√			√	√												
DY75II-M2-BC92	153.93600	18.97003	5687	M2	√		√			√	√												
DY75II-M2-BC93	154.30307	19.07983	5656	M2	√		√			√	√												

Station	Longitude/°E	Latitude/°N	Water Depth /m	Block	Smear Identification	Particle Size Analysis	Major Trace Element	Clay Mineral	Pore Water Major Metallic Elements	Penetration	Shear Strength	Natural Moisture Content	Wet Density	Porosity	Proportion	Liquid Limit	Plastic Limit	Plasticity Index	Liquidity Index	Compressibility	Compression Modulus	Cohesive Force	Internal Friction
DY75II-M2-BC94	154.39805	19.07999	5711	M2	√		√			√	√												
DY75II-M2-BC95	154.33021	19.17998	5712	M2	√		√			√	√												
DY75I-M2-MC02	153.67988	19.13992	5519	M2	√		√			√	√												
DY75II-M2-MC03C	153.67984	19.14002	5516	M2																			
DY75I-M2-MC04a	153.67999	19.03982	5608	M2																			
DY75I-M2-MC05	153.67989	19.04001	5619	M2	√		√			√	√												
DY75I-M2-MC06	153.67995	19.08987	5561	M2	√		√																
DY75I-M2-MC07a	153.68001	19.08995	5566	M2																			
DY75II-M1-MC10	152.89000	18.82992	5526	M1						√	√												
DY75II-M1-MC11	152.82000	18.77990	5539	M1						√	√												
DY75II-M1-MC12	152.82006	18.77985	5521	M1																			
DY75II-M1-MC13	152.82007	18.73496	5576	M1																			
DY75II-M1-MC14	152.82015	18.73498	5572	M1						√	√												
DY75II-M2-MC15	153.29584	18.87621	5659	M2						√	√												
DY75II-M2-MC16	153.29557	18.87628	5675	M2																			
DY61-1-M2-S109CTD30	154.48810	18.95610	5656	M2																			
DY61-I-M2-S110CTD31	154.38100	18.94440	5683	M2																			
DY69-M1-ES07-CTD01	151.87980	18.60220	5434	M1																			
DY69-M2-ES04-CTD02	153.67212	19.37340	4840	M2																			
DY69-M2-ES04-CTD03	153.67140	19.37300	4842	M2																			
DY69-M1-ES03-CTD06	153.67287	19.09472	5565	M1																			
DY69-M2B1-ES03-CTD05	153.67230	19.09410	5565	M2																			
DY69-M1-ES06-CTD07	152.89480	18.83110	5563	M1																			
DY69-M1-ES06-CTD08	152.89259	18.83184	5528	M1																			
DY69-M2B1-ES05-CTD09	153.27090	18.83200	5669	M2																			
DY69-M2B1-ES05-CTD10	153.27182	18.83288	5669	M2																			
DY69-M2B1-ES02-CTD11	153.67445	18.82577	5650	M2																			
DY69-M2B1-ES02-CTD12	153.67450	18.82610	5650	M2																			
DY69-M2B1-ES01-CTD13	153.67600	18.56180	5644	M2																			
DY69-M2B1-ES01-CTD14	153.67605	18.56193	5643	M2																			
DY76-I-M2-S055CTD13	153.66260	19.36520	5673	M2																			
DY76-I-M2-S057CTD13	153.66820	19.35310	4841	M2																			
DY76-I-M2-S062CTD14	153.67660	19.07510	5632	M2																			
DY76-I-M2-S065CTD14	153.65190	19.02070	5615	M2																			
DY76-I-M2-S071CTD15	154.43550	19.04600	5698	M2																			
DY76-I-M2-S075CTD16	153.60480	18.54770	5669	M2																			
DY76-I-M2-S076CTD16	153.56910	18.54430	5673	M2																			
DY76-I-M1-S080CTD17	152.81390	18.73190	5571	M1																			

Station	Longitude/°E	Latitude/°N	Water Depth /m	Block	Smear Identification	Particle Size Analysis	Major Trace Element	Clay Mineral	Pore Water	Major Metallic Elements	Penetration	Shear Strength	Natural Moisture Content	Wet Density	Porosity	Proportion	Liquid Limit	Plastic Limit	Plasticity Index	Liquidity Index	Compressibility	Compression Modulus	Cohesive Force	Internal Friction
DY76-I-M1-S083CTD17	152.80210	18.70690	5576	M2																				
DY76-I-M2-S085CTD18	153.29910	18.87750	5669	M2																				
DY69-M1-ES06-BC18	152.89043	18.83025	5529	M1																				
DY69-M2B1-ES02-BC24	153.67745	18.82594	5650	M2																				
DY69-M2B1-ES03-MC04	153.67276	19.09467	5565	M2																				
DY76-I-M1-S088BC04	151.74670	18.45990	5285	M1																				
DY76-I-M1-S090BC06	151.92980	18.45520	5403	M1																				
DY76-I-M1-S091BC07	151.92820	18.29070	5250	M1																				
DY76-I-M1-S092BC08	151.75140	18.29340	5306	M1																				
DY61-M2-MX2006	154.49850	19.05030	5676	M2																				
DY66-M2-MX2101	154.48680	19.04840	5680	M2																				
DY69-ES04-MX01	153.67210	19.37340	4840	M2																				
DY69-ES03-MX02	153.67750	19.08690	5571	M2																				
DY69-ES06-MX03	152.81800	18.77500	5638	M1																				
DY69-M2-ES04-NET03	153.67201	19.37347	4842	M2																				
DY69-M2B1-ES03-NET04	153.67199	19.09655	5569	M2																				
DY69-M1-ES06-NET05	152.89252	18.83181	5523	M1																				
DY69-M2B1-ES05-NET06	153.27184	18.83223	5668	M2																				
DY69-M2B1-ES02-NET07	153.67452	18.82600	5650	M2																				
DY69-M2B1-ES01-NET08	153.67606	18.56178	5645	M2																				
DY76-I-M2-S059VN13	153.65380	19.35840	4828	M2																				
DY76-I-M2-S063VN14-1	153.67360	19.05700	5608	M2																				
DY76-I-M2-S063VN14-2	153.67360	19.05700	5608	M2																				
DY76-I-M2-S074VN15-1	153.65200	18.56240	5661	M2																				
DY76-I-M2-S074VN15-2	153.65200	18.56240	5661	M2																				
DY76-I-M1-S079VN16-1	152.81890	18.73620	5567	M1																				
DY76-I-M1-S079VN16-2	152.81890	18.73620	5567	M1																				
DY69-M1-ES07-NET02	151.88222	18.59799	5424	M1																				
DY69-M2-ES04-BIO01	153.64919	19.37932	4736	M2																				
DY69-M2B1-ES03-BIO02	153.67420	19.09850	5557	M2																				
DY69-M2B1-ES03-BIO03	153.67270	19.09466	5566	M2																				
DY69-M1-ES06-BIO04	152.91129	18.83703	5531	M1																				
DY69-M1-ES06-BIO05	152.89257	18.83212	5522	M1																				
DY69-M2B1-ES05-BIO06	153.27181	18.83312	5669	M2																				
DY69-M2B1-ES01-BIO07	153.67624	18.56137	5647	M2																				
DY76-I-M2-S058MN09	153.65660	19.36130	4809	M2																				
DY76-I-M2-S064MN10	153.66940	19.04430	5606	M2																				
DY76-I-M2-S077MN11a	153.54000	18.53970	5669	M2																				

Station	Longitude/°E	Latitude/°N	Water Depth /m	Block	Smear Identification	Particle Size Analysis	Major Trace Element	Clay Mineral	Pore Water	Major Metallic Elements	Penetration	Shear Strength	Natural Moisture Content	Wet Density	Porosity	Proportion	Liquid Limit	Plastic Limit	Plasticity Index	Liquidity Index	Compressibility	Compression Modulus	Cohesive Force	Internal Friction
DY76-I-M1-S078MN12	152.81800	18.73480	5572	M1																				
DY61-I-M2-S106MC04	154.51250	18.99900	5697	M2																				
DY61-I-M2-S108MC04R	154.52220	18.98590	5677	M2																				
DY61-I-M2-S114MC05	154.49730	19.49980	5704	M2																				
DY69-M2B1-ES03-BC13	153.67292	19.09477	5569	M2																				
DY69-M2B1-ES05-BC21	153.27153	18.83274	5669	M2																				
DY69-M2B1-ES03-L01	153.67575	19.11203	5555	M1																				
DY69-M1-ES06-L02	152.92630	18.85197	5557	M1																				
DY75I-M2-Lander01	153.68991	19.09002	5561	M2																				
DY75I-M2-Lander02	153.67537	18.56210	5635	M2																				
DY75I-M1-Lander03	152.82119	18.78086	5535	M1																				
DY81I-M2-ES03-CTD01	153.6799	19.0898	5562	M2																				
DY81I-M2-ES03-CTD03	153.6799	19.0899	5535	M2																				
DY81I-M2-ES05-CTD02	153.2711	18.8319	5676	M2																				
DY81I-M2-ES05-CTD02-200	153.2711	18.8319	5675	M2																				
DY81I-M1-ES06-CTD04	152.8901	18.8300	5535	M1																				
DY81I-M1-ES06-CTD04-200	152.8901	18.8300	5535	M1																				
DY81II-M1-ES08-MX04	152.8549	18.7708	5605	M1																				
DY81II-M2-ES03-MX05	153.6710	19.1155	5555	M2																				
DY81I-M2-ES05-DX01	153.2710	152.8901	5676	M2																				
DY81I-M2-ES03-DX02	153.6799	19.0899	5574	M2																				
DY81I-M2-ES03-DX03	153.6799	19.0899	5575	M2																				
DY81I-M2-DX04	154.7174	19.0899	5575	M2																				
DY81I-M1-ES06-DX05	152.8901	18.8300	5534	M1																				
DY81I-M2-ES05-F01	153.2710	18.8319	5676	M2																				
DY81I-M2-ES03-F02	153.6799	19.0899	5574	M2																				
DY81I-M2-F03	154.7174	19.3819	5673	M2																				
DY81I-M2-ES03-F04	153.6800	19.0899	5574	M2																				
DY81I-M2-ES03-F05	153.6800	19.0899	5573	M2																				
DY81I-M1-ES06-F06	152.8901	18.8300	5536	M1																				
DY81I-M1-ES06-F07	152.8901	18.8300	5535	M1																				
DY81II-M2-ES05-MC04	153.2709	18.8319	5684	M2																				
DY81II-M1-ES08-MC05	152.8201	18.7352	5581	M1																				
DY81II-M2-ES03-MC07	153.6682	19.0900	5577	M2																				
DY81II-M2-ES03-MC08	153.6730	19.0900	5572	M2																				
DY81II-M2-ES03-MC09	153.6799	19.0899	5572	M2																				

Station	Longitude/°E	Latitude/°N	Water Depth /m	Block	Smear Identification	Particle Size Analysis	Major Trace Element	Clay Mineral	Pore Water Major Metallic Elements	Penetration	Shear Strenrth	Natural Moisture Content	Wet Density	Porosity	Proportion	Liquid Limit	Plastic Limit	Plasticity Index	Liquidity Index	Compressibility	Compression Modulus	Cohesive Force	Internal Friction
DY81II-M2-ES03-MC11	153.6870	19.0899	5574	M2																			

Station	Lon/ °E	Lat/ °N	Water Depth/m	Block	Nodule abundance	Nodule Coverage	Wet density of nodule	Water content of nodule	Nodule type (mass and percentage of large, medium and small)	Temperature	Salinity	Current speed	Current direction	Turbidity
DY69-M2B1-PS13-BC01	153.94402	18.88123	5702	M2	√	√	√	√	√					
DY69-M2B1-PS01-BC02	154.12474	18.97067	5718	M2	√	√	√	√	√					
DY69-M2B1-PS02-BC03	154.30565	18.96199	5675	M2	√	√	√	√	√					
DY69-M2B1-PS05-BC04	153.58545	19.17258	5434	M2	√	√	√	√	√					
DY69-M2B1-PS04-BC05	153.40173	19.16932	5589	M2	√	√	√	√	√					
DY69-M2B1-PS08-BC06	153.31253	19.27086	5520	M2	√	√	√	√	√					
DY69-M2B1-PS07-BC07	153.94103	19.16952	5576	M2	√	√	√	√	√					
DY69-M2B1-PS11-BC08	153.85039	19.27061	5443	M2	√	√	√	√	√					
DY69-M2-ES04-BC09	153.67167	19.37304	4842	M2	√	√	√	√	√					
DY69-M2B1-PS10-BC10	153.67034	19.27093	5193	M2	√	√	√	√	√					
DY69-M2B1-PS06-BC11	153.75938	19.37272	5508	M2	√	√	√	√	√					
DY69-M2B1-PS03-BC12	153.85101	19.08253	5621	M2	√	√	√	√	√					
DY69-M2B1-ESO3-BC13	153.67292	19.09477	5569	M2	√	√	√	√	√					
DY69-M2B1-PS14-BC14	153.49430	18.97486	5632	M2	√	√	√	√	√					
DY69-M2B1-PS15-BC15	153.49288	19.07620	5593	M2	√	√	√	√	√					
DY69-M2B1-PS09-BC16	153.49258	19.27211	5248	M2	√	√	√	√	√					
DY69-M1-ES06-BC17	152.88986	18.83053	5528	M1										
DY69-M2B1-ES06-BC20	153.27106	18.83172	5668	M2	√	√	√	√	√					
DY69-M2B1-ES02-BC22	153.67486	18.82680	5650	M2	√	√	√	√	√					
DY69-M2B1-ES01-BC25	153.67626	18.56169	5645	M2	√	√	√	√	√					
DY69-M2B1-ES05-BC20	153.27110	18.83172	5668	M2										
DY69-M2B1-ES03-MC02	153.67183	19.09644	5576	M2										
DY75I-M2-BC03A	155.12989	19.51949	5685	M2	√	√	√	√	√					
DY75I-M2-BC04	155.30042	19.52016	5651	M2	√	√	√	√	√					
DY75I-M2-BC05	155.30001	19.68959	5625	M2	√	√	√	√	√					
DY75I-M2-BC06	155.12997	19.68962	5675	M2	√	√	√	√	√					
DY75I-M2-BC07	154.94993	19.68953	5716	M2	√	√	√	√	√					
DY75I-M2-BC08	154.77000	19.51955	5616	M2	√	√	√	√	√					
DY75I-M2-BC09	154.95602	19.51950	5675	M2	√	√	√	√	√					
DY75I-M2-BC10	154.94997	19.34958	5684	M2	√	√	√	√	√					
DY75I-M2-BC11	155.13003	19.34954	5658	M2	√	√	√	√	√					
DY75I-M2-BC12	155.29983	19.34958	5678	M2	√	√	√	√	√					
DY75I-M2-BC13	154.94974	19.17960	5629	M2	√	√	√	√	√					
DY75I-M2-BC14	154.76992	19.17951	5671	M2	√	√	√	√	√					

Station	Lon/°E	Lat/°N	Water Depth/m	Block	Nodule abundance	Nodule Coverage	Wet density of nodule	Water content of nodule	Nodule type (mass and percentage of large, medium and small)	Tempe rature	Salinity	Current speed	Current direction	Turbidity
DY75I-M2-BC15	154.60012	18.99956	5659	M2	√	√	√	√	√					
DY75I-M2-BC16A	154.59997	19.17950	5690	M2	√	√	√	√	√					
DY75I-M2-BC17	154.12020	19.16957	5719	M2	√	√	√	√	√					
DY75I-M2-BC18	154.24032	19.17967	5725	M2	√	√	√	√	√					
DY75I-M2-BC19	154.41992	19.17952	5704	M2	√	√	√	√	√					
DY75I-M2-BC20	154.41992	19.34954	5669	M2	√	√	√	√	√					
DY75I-M2-BC21	154.60017	19.34961	5673	M2	√	√	√	√	√					
DY75I-M2-BC22	154.59965	19.51962	5659	M2	√	√	√	√	√					
DY75I-M2-BC23	154.42067	19.68705	5737	M2	√	√	√	√	√					
DY75I-M2-BC24	154.23958	19.68996	5770	M2	√	√	√	√	√					
DY75I-M2-BC25	154.05982	19.69040	5585	M2	√	√	√	√	√					
DY75I-M2-BC26	154.05952	19.52010	5636	M2	√	√	√	√	√					
DY75I-M2-BC27	154.23950	19.35019	5695	M2	√	√	√	√	√					
DY75I-M2-BC28	154.05954	19.35023	5500	M2	√	√	√	√	√					
DY75I-M2-BC29	154.02978	19.16972	5664	M2	√	√	√	√	√					
DY75I-M2-BC30	153.75955	19.08981	5587	M2	√	√	√	√	√					
DY75I-M2-BC31	153.57951	19.08003	5571	M2	√	√	√	√	√					
DY75I-M2-BC32	153.49042	19.16985	5507	M2	√	√	√	√	√					
DY75I-M2-BC33	153.58030	19.26962	5148	M2	√	√	√	√	√					
DY75I-M2-BC34	153.67982	19.16954	5478	M2	√	√	√	√	√					
DY75I-M2-BC35	153.52467	19.16963	5471	M2	√	√	√	√	√					
DY75I-M2-BC36	153.93995	19.26952	5539	M2	√	√	√	√	√					
DY75I-M2-BC37A	153.84962	19.16960	5520	M2	√	√	√	√	√					
DY75I-M2-BC38A	153.75955	19.27021	5302	M2	√	√	√	√	√					
DY75I-M2-BC39A	153.39987	19.26999	5428	M2	√	√	√	√	√					
DY75I-M2-BC40	153.31028	19.16958	5647	M2	√	√	√	√	√					
DY75I-M2-BC41A	153.30992	19.07990	5654	M2	√	√	√	√	√					
DY75I-M2-BC42	153.40049	19.08014	5618	M2	√	√	√	√	√					
DY75I-M2-BC43	153.39026	18.98961	5655	M2	√	√	√	√	√					
DY75I-M2-BC44	153.57990	18.96957	5632	M2	√	√	√	√	√					
DY75I-M2-BC45	153.74964	18.97966	5680	M2	√	√	√	√	√					
DY75I-M2-BC46	153.83989	18.97954	5673	M2	√	√	√	√	√					
DY75I-M2-BC47	153.93996	19.07953	5626	M2	√	√	√	√	√					
DY75II-M2-BC48A	154.03022	19.08005	5660	M2	√	√	√	√	√					
DY75I-M2-BC49	154.03005	18.96953	5702	M2	√	√	√	√	√					
DY75I-M2-BC50	154.12001	19.07953	5695	M2	√	√	√	√	√					

Station	Lon/°E	Lat/°N	Water Depth/m	Block	Nodule abundance	Nodule Coverage	Wet density of nodule	Water content of nodule	Nodule type (mass and percentage of large, medium and small)	Temperature	Salinity	Current speed	Current direction	Turbidity
DY75I-M2-BC51	154.21041	19.07973	5698	M2	√	√	√	√	√					
DY75I-M2-BC52A	154.21032	18.96865	5683	M2	√	√	√	√	√					
DY75I-M2-BC53	154.39041	18.96990	5660	M2	√	√	√	√	√					
DY75I-M2-BC54	154.33999	18.87999	5696	M2	√	√	√	√	√					
DY75I-M2-BC55	154.15999	18.87994	5706	M2	√	√	√	√	√					
DY75I-M2-BC56	153.98005	18.71001	5657	M2	√	√	√	√	√					
DY75I-M2-BC57	154.15999	18.70995	5665	M2	√	√	√	√	√					
DY75I-M2-BC58	154.33990	18.70992	5659	M2	√	√	√	√	√					
DY75I-M2-BC59	154.33978	18.53978	5654	M2	√	√	√	√	√					
DY75I-M2-BC60A	154.16004	18.53995	5667	M2	√	√	√	√	√					
DY75I-M2-BC61	153.25986	18.54024	5664	M2	√	√	√	√	√					
DY75I-M2-BC62	153.43969	18.54008	5660	M2	√	√	√	√	√					
DY75I-M2-BC63	153.98000	18.54004	5678	M2	√	√	√	√	√					
DY75I-M2-BC64	153.61994	18.70992	5731	M2	√	√	√	√	√					
DY75I-M2-BC65	153.43925	18.70984	5706	M2	√	√	√	√	√					
DY75I-M2-BC66	153.25000	18.70994	5690	M2	√	√	√	√	√					
DY75I-M1-BC73	152.88999	18.73496	5625	M2										
DY75I-M2-BC75	153.67958	19.13998	5496	M2	√ (+76)	√ (+76)	√ (+76)	√ (+76)	√ (+76)					
DY75I-M2-BC76	153.67961	19.13961	5510	M2	√ (+75)	√ (+75)	√ (+75)	√ (+75)	√ (+75)					
DY75I-M2-BC77	153.67992	19.08982	5543	M2	√ (+78)	√ (+78)	√ (+78)	√ (+78)	√ (+78)					
DY75I-M2-BC78	153.68008	19.08992	5562	M2	√ (+77)	√ (+77)	√ (+77)	√ (+77)	√ (+77)					
DY75I-M2-BC79	153.67987	19.04005	5611	M2	√ (+80)	√ (+80)	√ (+80)	√ (+80)	√ (+80)					
DY75I-M2-BC80	153.68001	19.03994	5618	M2	√ (+79)	√ (+79)	√ (+79)	√ (+79)	√ (+79)					
DY75I-M1-BC68	152.89007	18.82997	5525	M1										
DY75I-M1-BC69	152.89002	18.82992	5529	M1										
DY75I-M1-BC70	152.81999	18.73493	5566	M1										
DY75I-M1-BC71	152.82003	18.73492	5554	M1										
DY75I-M1-BC72	152.88996	18.73491	5623	M1										
DY75I-M1-BC74	152.81553	18.84369	5393	M1										
DY75II-M2-BC81	153.26007	18.99278	5681	M2	√	√	√	√	√					

Station	Lon/°E	Lat/°N	Water Depth/m	Block	Nodule abundance	Nodule Coverage	Wet density of nodule	Water content of nodule	Nodule type (mass and percentage of large, medium and small)	Temperature	Salinity	Current speed	Current direction	Turbidity
DY75II-M2-BC82	153.29610	18.87647	5669	M2	√	√	√	√	√					
DY75II-M1-BC83	152.66583	19.23978	1287	M1										
DY75II-M1-BC84	152.64593	18.73478	5483	M1										
DY75II-M1-BC85	152.65295	18.86710	5157	M1										
DY75II-M1-BC86	152.65293	18.99994	4398	M1										
DY75II-M1-BC87	152.71968	19.00946	4526	M1										
DY75II-M1-BC88	152.68973	18.99977	4567	M1										
DY75II-M1-BC89	152.70503	18.99849	4570	M1										
DY75II-M2-BC90	154.03224	19.27791	5490	M2	√	√	√	√	√					
DY75II-M2-BC91	153.73165	19.34160	5078	M2	√	√	√	√	√					
DY75II-M2-BC92	153.93600	18.97003	5687	M2	√	√	√	√	√					
DY75II-M2-BC93	154.30307	19.07983	5656	M2	√	√	√	√	√					
DY75II-M2-BC94	154.39805	19.07999	5711	M2	√	√	√	√	√					
DY75II-M2-BC95	154.33021	19.17998	5712	M2	√	√	√	√	√					
DY75I-M2-MC02	153.67988	19.13992	5519	M2										
DY75II-M2-MC03C	153.67984	19.14002	5516	M2										
DY75I-M2-MC04a	153.67999	19.03982	5608	M2										
DY75I-M2-MC05	153.67989	19.04001	5619	M2										
DY75I-M2-MC06	153.67995	19.08987	5561	M2										
DY75I-M2-MC07a	153.68001	19.08995	5566	M2										
DY75II-M1-MC10	152.89000	18.82992	5526	M1										
DY75II-M1-MC11	152.82000	18.77990	5539	M1										
DY75II-M1-MC12	152.82006	18.77985	5521	M1										
DY75II-M1-MC13	152.82007	18.73496	5576	M1										
DY75II-M1-MC14	152.82015	18.73498	5572	M1										
DY75II-M2-MC15	153.29584	18.87621	5659	M2										
DY75II-M2-MC16	153.29557	18.87628	5675	M2										
DY61-1-M2-S109CTD30	154.48810	18.95610	5656	M2						√	√			
DY61-I-M2-S110CTD31	154.38100	18.94440	5683	M2										
DY69-M1-ES07-CTD01	151.87980	18.60220	5434	M1						√	√			
DY69-M2-ES04-CTD02	153.67212	19.37340	4840	M2										
DY69-M2-ES04-CTD03	153.67140	19.37300	4842	M2						√	√			
DY69-M1-ES03-CTD06	153.67287	19.09472	5565	M1										
DY69-M2B1-ES03-CTD05	153.67230	19.09410	5565	M2						√	√			
DY69-M1-ES06-CTD07	152.89480	18.83110	5563	M1						√	√			
DY69-M1-ES06-CTD08	152.89259	18.83184	5528	M1										

Station	Lon/°E	Lat/°N	Water Depth/m	Block	Nodule abundance	Nodule Coverage	Wet density of nodule	Water content of nodule	Nodule type (mass and percentage of large, medium and small)	Temperature	Salinity	Current speed	Current direction	Turbidity
DY69-M2B1-ES05-CTD09	153.27090	18.83200	5669	M2						√	√			
DY69-M2B1-ES05-CTD10	153.27182	18.83288	5669	M2										
DY69-M2B1-ES02-CTD11	153.67445	18.82577	5650	M2										
DY69-M2B1-ES02-CTD12	153.67450	18.82610	5650	M2						√	√			
DY69-M2B1-ES01-CTD13	153.67600	18.56180	5644	M2						√	√			
DY69-M2B1-ES01-CTD14	153.67605	18.56193	5643	M2										
DY76-I-M2-S055CTD13	153.66260	19.36520	5673	M2										
DY76-I-M2-S057CTD13	153.66820	19.35310	4841	M2						√	√			
DY76-I-M2-S062CTD14	153.67660	19.07510	5632	M2						√	√			
DY76-I-M2-S065CTD14	153.65190	19.02070	5615	M2										
DY76-I-M2-S071CTD15	154.43550	19.04600	5698	M2						√	√			
DY76-I-M2-S075CTD16	153.60480	18.54770	5669	M2						√	√			
DY76-I-M2-S076CTD16	153.56910	18.54430	5673	M2										
DY76-I-M1-S080CTD17	152.81390	18.73190	5571	M1										
DY76-I-M1-S083CTD17	152.80210	18.70690	5576	M2						√	√			
DY76-I-M2-S085CTD18	153.29910	18.87750	5669	M2										
DY69-M1-ES06-BC18	152.89043	18.83025	5529	M1										
DY69-M2B1-ES02-BC24	153.67745	18.82594	5650	M2										
DY69-M2B1-ES03-MC04	153.67276	19.09467	5565	M2										
DY76-I-M1-S088BC04	151.74670	18.45990	5285	M1										
DY76-I-M1-S090BC06	151.92980	18.45520	5403	M1										
DY76-I-M1-S091BC07	151.92820	18.29070	5250	M1										
DY76-I-M1-S092BC08	151.75140	18.29340	5306	M1										
DY61-M2-MX2006	154.49850	19.05030	5676	M2						√	√	√	√	
DY66-M2-MX2101	154.48680	19.04840	5680	M2						√	√	√	√	√
DY69-ES04-MX01	153.67210	19.37340	4840	M2						√	√	√	√	
DY69-ES03-MX02	153.67750	19.08690	5571	M2						√	√	√	√	
DY69-ES06-MX03	152.81800	18.77500	5638	M1						√	√	√	√	
DY69-M2-ES04-NET03	153.67201	19.37347	4842	M2										
DY69-M2B1-ES03-NET04	153.67199	19.09655	5569	M2										
DY69-M1-ES06-NET05	152.89252	18.83181	5523	M1										
DY69-M2B1-ES05-NET06	153.27184	18.83223	5668	M2										
DY69-M2B1-ES02-NET07	153.67452	18.82600	5650	M2										
DY69-M2B1-ES01-NET08	153.67606	18.56178	5645	M2										
DY76-I-M2-S059VN13	153.65380	19.35840	4828	M2										
DY76-I-M2-S063VN14-1	153.67360	19.05700	5608	M2										

Station	Lon/°E	Lat/°N	Water Depth/m	Block	Nodule abundance	Nodule Coverage	Wet density of nodule	Water content of nodule	Nodule type (mass and percentage of large, medium and small)	Temperature	Salinity	Current speed	Current direction	Turbidity
DY76-I-M2-S063VN14-2	153.67360	19.05700	5608	M2										
DY76-I-M2-S074VN15-1	153.65200	18.56240	5661	M2										
DY76-I-M2-S074VN15-2	153.65200	18.56240	5661	M2										
DY76-I-M1-S079VN16-1	152.81890	18.73620	5567	M1										
DY76-I-M1-S079VN16-2	152.81890	18.73620	5567	M1										
DY69-M1-ES07-NET02	151.88222	18.59799	5424	M1										
DY69-M2-ES04-BIO01	153.64919	19.37932	4736	M2										
DY69-M2B1-ES03-BIO02	153.67420	19.09850	5557	M2										
DY69-M2B1-ES03-BIO03	153.67270	19.09466	5566	M2										
DY69-M1-ES06-BIO04	152.91129	18.83703	5531	M1										
DY69-M1-ES06-BIO05	152.89257	18.83212	5522	M1										
DY69-M2B1-ES05-BIO06	153.27181	18.83312	5669	M2										
DY69-M2B1-ES01-BIO07	153.67624	18.56137	5647	M2										
DY76-I-M2-S058MN09	153.65660	19.36130	4809	M2										
DY76-I-M2-S064MN10	153.66940	19.04430	5606	M2										
DY76-I-M2-S077MN11a	153.54000	18.53970	5669	M2										
DY76-I-M1-S078MN12	152.81800	18.73480	5572	M1										
DY61-I-M2-S106MC04	154.51250	18.99900	5697	M2										
DY61-I-M2-S108MC04R	154.52220	18.98590	5677	M2										
DY61-I-M2-S114MC05	154.49730	19.49980	5704	M2										
DY69-M2B1-ES03-BC13	153.67292	19.09477	5569	M2										
DY69-M2B1-ES05-BC21	153.27153	18.83274	5669	M2										
DY69-M2B1-ES03-L01	153.67575	19.11203	5555	M1										
DY69-M1-ES06-L02	152.92630	18.85197	5557	M1										
DY75I-M2-Lander01	153.68991	19.09002	5561	M2										
DY81I-M2-ES03-CTD01	153.6799	19.0898	5562	M2						√	√			
DY81I-M2-ES03-CTD03	153.6799	19.0899	5535	M2						√	√			
DY81I-M2-ES05-CTD02	153.2711	18.8319	5676	M2						√	√			
DY81I-M2-ES05-CTD02-200	153.2711	18.8319	5675	M2						√	√			
DY81I-M1-ES06-CTD04	152.8901	18.8300	5535	M1						√	√			
DY81I-M1-ES06-CTD04-200	152.8901	18.8300	5535	M1						√	√			
DY81II-M1-ES08-MX04	152.8549	18.7708	5605	M1						√	√	√	√	√
DY81II-M2-ES03-MX05	153.6710	19.1155	5555	M2						√	√	√	√	√
DY81I-M2-ES05-DX01	153.2710	152.8901	5676	M2										

Station	Lon/ °E	Lat/ °N	Water Depth/m	Block	Nodule abundance	Nodule Coverage	Wet density of nodule	Water content of nodule	Nodule type (mass and percentage of large, medium and small)	Temperature	Salinity	Current speed	Current direction	Turbidity
DY81I-M2-ES03-DX02	153.6799	19.0899	5574	M2										
DY81I-M2-ES03-DX03	153.6799	19.0899	5575	M2										
DY81I-M2-DX04	154.7174	19.0899	5575	M2										
DY81I-M1-ES06-DX05	152.8901	18.8300	5534	M1										
DY81I-M2-ES05-F01	153.2710	18.8319	5676	M2										
DY81I-M2-ES03-F02	153.6799	19.0899	5574	M2										
DY81I-M2-F03	154.7174	19.3819	5673	M2										
DY81I-M2-ES03-F04	153.6800	19.0899	5574	M2										
DY81I-M2-ES03-F05	153.6800	19.0899	5573	M2										
DY81I-M1-ES06-F06	152.8901	18.8300	5536	M1										
DY81I-M1-ES06-F07	152.8901	18.8300	5535	M1										
DY81II-M2-ES05-MC04	153.2709	18.8319	5684	M2										
DY81II-M1-ES08-MC05	152.8201	18.7352	5581	M1										
DY81II-M2-ES03-MC07	153.6682	19.0900	5577	M2										
DY81II-M2-ES03-MC08	153.6730	19.0900	5572	M2										
DY81II-M2-ES03-MC09	153.6799	19.0899	5572	M2										
DY81II-M2-ES03-MC11	153.6870	19.0899	5574	M2										

Schedule 3-3 List of Data Obtained at Stations (Marine Chemistry)

Station	Lon/ °E	Lat/ °N	Water Depth/ m	Block	pH	DO	Nitrate	Nitrite	Nitrogen and Phosphorus	Ammonium Salt	Silicate	Suspended Solid (SS)	Total alkalinity	Dissolved Inorganic Carbon
DY69-M2B1-PS13-BC01	153.94402	18.88123	5702	M2										
DY69-M2B1-PS01-BC02	154.12474	18.97067	5718	M2										
DY69-M2B1-PS02-BC03	154.30565	18.96199	5675	M2										
DY69-M2B1-PS05-BC04	153.58545	19.17258	5434	M2										
DY69-M2B1-PS04-BC05	153.40173	19.16932	5589	M2										
DY69-M2B1-PS08-BC06	153.31253	19.27086	5520	M2										
DY69-M2B1-PS07-BC07	153.94103	19.16952	5576	M2										
DY69-M2B1-PS11-BC08	153.85039	19.27061	5443	M2										
DY69-M2-ES04-BC09	153.67167	19.37304	4842	M2										
DY69-M2B1-PS10-BC10	153.67034	19.27093	5193	M2										
DY69-M2B1-PS06-BC11	153.75938	19.37272	5508	M2										
DY69-M2B1-PS03-BC12	153.85101	19.08253	5621	M2										
DY69-M2B1-ESO3-BC13	153.67292	19.09477	5569	M2										
DY69-M2B1-PS14-BC14	153.49430	18.97486	5632	M2										
DY69-M2B1-PS15-BC15	153.49288	19.07620	5593	M2										
DY69-M2B1-PS09-BC16	153.49258	19.27211	5248	M2										
DY69-M1-ES06-BC17	152.88986	18.83053	5528	M1										
DY69-M2B1-ES06-BC20	153.27106	18.83172	5668	M2										
DY69-M2B1-ES02-BC22	153.67486	18.82680	5650	M2										
DY69-M2B1-ES01-BC25	153.67626	18.56169	5645	M2										
DY69-M2B1-ES05-BC20	153.27110	18.83172	5668	M2										
DY69-M2B1-ES03-MC02	153.67183	19.09644	5576	M2										
DY75I-M2-BC03A	155.12989	19.51949	5685	M2										
DY75I-M2-BC04	155.30042	19.52016	5651	M2										
DY75I-M2-BC05	155.30001	19.68959	5625	M2										
DY75I-M2-BC06	155.12997	19.68962	5675	M2										
DY75I-M2-BC07	154.94993	19.68953	5716	M2										
DY75I-M2-BC08	154.77000	19.51955	5616	M2										
DY75I-M2-BC09	154.95602	19.51950	5675	M2										
DY75I-M2-BC10	154.94997	19.34958	5684	M2										
DY75I-M2-BC11	155.13003	19.34954	5658	M2										
DY75I-M2-BC12	155.29983	19.34958	5678	M2										
DY75I-M2-BC13	154.94974	19.17960	5629	M2										
DY75I-M2-BC14	154.76992	19.17951	5671	M2										
DY75I-M2-BC15	154.60012	18.99956	5659	M2										
DY75I-M2-BC16A	154.59997	19.17950	5690	M2										
DY75I-M2-BC17	154.12020	19.16957	5719	M2										
DY75I-M2-BC18	154.24032	19.17967	5725	M2										

Station	Lon/ °E	Lat/ °N	Water Depth/ m	Block	pH	DO	Nitrate	Nitrite	Nitrogen and Phosphorus	Ammonium Salt	Silicate	Suspended Solid (SS)	Total alkalinity	Dissolved Inorganic Carbon
DY75I-M2-BC19	154.41992	19.17952	5704	M2										
DY75I-M2-BC20	154.41992	19.34954	5669	M2										
DY75I-M2-BC21	154.60017	19.34961	5673	M2										
DY75I-M2-BC22	154.59965	19.51962	5659	M2										
DY75I-M2-BC23	154.42067	19.68705	5737	M2										
DY75I-M2-BC24	154.23958	19.68996	5770	M2										
DY75I-M2-BC25	154.05982	19.69040	5585	M2										
DY75I-M2-BC26	154.05952	19.52010	5636	M2										
DY75I-M2-BC27	154.23950	19.35019	5695	M2										
DY75I-M2-BC28	154.05954	19.35023	5500	M2										
DY75I-M2-BC29	154.02978	19.16972	5664	M2										
DY75I-M2-BC30	153.75955	19.08981	5587	M2										
DY75I-M2-BC31	153.57951	19.08003	5571	M2										
DY75I-M2-BC32	153.49042	19.16985	5507	M2										
DY75I-M2-BC33	153.58030	19.26962	5148	M2										
DY75I-M2-BC34	153.67982	19.16954	5478	M2										
DY75I-M2-BC35	153.52467	19.16963	5471	M2										
DY75I-M2-BC36	153.93995	19.26952	5539	M2										
DY75I-M2-BC37A	153.84962	19.16960	5520	M2										
DY75I-M2-BC38A	153.75955	19.27021	5302	M2										
DY75I-M2-BC39A	153.39987	19.26999	5428	M2										
DY75I-M2-BC40	153.31028	19.16958	5647	M2										
DY75I-M2-BC41A	153.30992	19.07990	5654	M2										
DY75I-M2-BC42	153.40049	19.08014	5618	M2										
DY75I-M2-BC43	153.39026	18.98961	5655	M2										
DY75I-M2-BC44	153.57990	18.96957	5632	M2										
DY75I-M2-BC45	153.74964	18.97966	5680	M2										
DY75I-M2-BC46	153.83989	18.97954	5673	M2										
DY75I-M2-BC47	153.93996	19.07953	5626	M2										
DY75II-M2-BC48A	154.03022	19.08005	5660	M2										
DY75I-M2-BC49	154.03005	18.96953	5702	M2										
DY75I-M2-BC50	154.12001	19.07953	5695	M2										
DY75I-M2-BC51	154.21041	19.07973	5698	M2										
DY75I-M2-BC52A	154.21032	18.96865	5683	M2										
DY75I-M2-BC53	154.39041	18.96990	5660	M2										
DY75I-M2-BC54	154.33999	18.87999	5696	M2										
DY75I-M2-BC55	154.15999	18.87994	5706	M2										
DY75I-M2-BC56	153.98005	18.71001	5657	M2										
DY75I-M2-BC57	154.15999	18.70995	5665	M2										
DY75I-M2-BC58	154.33990	18.70992	5659	M2										
DY75I-M2-BC59	154.33978	18.53978	5654	M2										

Station	Lon/°E	Lat/°N	Water Depth/m	Block	pH	DO	Nitrate	Nitrite	Nitrogen and Phosphorus	Ammonium Salt	Silicate	Suspended Solid (SS)	Total alkalinity	Dissolved Inorganic Carbon
DY75I-M2-BC60A	154.16004	18.53995	5667	M2										
DY75I-M2-BC61	153.25986	18.54024	5664	M2										
DY75I-M2-BC62	153.43969	18.54008	5660	M2										
DY75I-M2-BC63	153.98000	18.54004	5678	M2										
DY75I-M2-BC64	153.61994	18.70992	5731	M2										
DY75I-M2-BC65	153.43925	18.70984	5706	M2										
DY75I-M2-BC66	153.25000	18.70994	5690	M2										
DY75I-M1-BC73	152.88999	18.73496	5625	M2										
DY75I-M2-BC75	153.67958	19.13998	5496	M2										
DY75I-M2-BC76	153.67961	19.13961	5510	M2										
DY75I-M2-BC77	153.67992	19.08982	5543	M2										
DY75I-M2-BC78	153.68008	19.08992	5562	M2										
DY75I-M2-BC79	153.67987	19.04005	5611	M2										
DY75I-M2-BC80	153.68001	19.03994	5618	M2										
DY75I-M1-BC68	152.89007	18.82997	5525	M1										
DY75I-M1-BC69	152.89002	18.82992	5529	M1										
DY75I-M1-BC70	152.81999	18.73493	5566	M1										
DY75I-M1-BC71	152.82003	18.73492	5554	M1										
DY75I-M1-BC72	152.88996	18.73491	5623	M1										
DY75I-M1-BC74	152.81553	18.84369	5393	M1										
DY75II-M2-BC81	153.26007	18.99278	5681	M2										
DY75II-M2-BC82	153.29610	18.87647	5669	M2										
DY75II-M1-BC83	152.66583	19.23978	1287	M1										
DY75II-M1-BC84	152.64593	18.73478	5483	M1										
DY75II-M1-BC85	152.65295	18.86710	5157	M1										
DY75II-M1-BC86	152.65293	18.99994	4398	M1										
DY75II-M1-BC87	152.71968	19.00946	4526	M1										
DY75II-M1-BC88	152.68973	18.99977	4567	M1										
DY75II-M1-BC89	152.70503	18.99849	4570	M1										
DY75II-M2-BC90	154.03224	19.27791	5490	M2										
DY75II-M2-BC91	153.73165	19.34160	5078	M2										
DY75II-M2-BC92	153.93600	18.97003	5687	M2										
DY75II-M2-BC93	154.30307	19.07983	5656	M2										
DY75II-M2-BC94	154.39805	19.07999	5711	M2										
DY75II-M2-BC95	154.33021	19.17998	5712	M2										
DY75I-M2-MC02	153.67988	19.13992	5519	M2										
DY75II-M2-MC03C	153.67984	19.14002	5516	M2										
DY75I-M2-MC04a	153.67999	19.03982	5608	M2										
DY75I-M2-MC05	153.67989	19.04001	5619	M2										
DY75I-M2-MC06	153.67995	19.08987	5561	M2										
DY75I-M2-MC07a	153.68001	19.08995	5566	M2										

Station	Lon/°E	Lat/°N	Water Depth/m	Block	pH	DO	Nitrate	Nitrite	Nitrogen and Phosphorus	Ammonium Salt	Silicate	Suspended Solid (SS)	Total alkalinity	Dissolved Inorganic Carbon
DY75II-M1-MC10	152.89000	18.82992	5526	M1										
DY75II-M1-MC11	152.82000	18.77990	5539	M1										
DY75II-M1-MC12	152.82006	18.77985	5521	M1										
DY75II-M1-MC13	152.82007	18.73496	5576	M1										
DY75II-M1-MC14	152.82015	18.73498	5572	M1										
DY75II-M2-MC15	153.29584	18.87621	5659	M2										
DY75II-M2-MC16	153.29557	18.87628	5675	M2										
DY61-1-M2-S109CTD30	154.48810	18.95610	5656	M2										
DY61-I-M2-S110CTD31	154.38100	18.94440	5683	M2	√	√	√	√	√	√	√			
DY69-M1-ES07-CTD01	151.87980	18.60220	5434	M1										
DY69-M2-ES04-CTD02	153.67212	19.37340	4840	M2										
DY69-M2-ES04-CTD03	153.67140	19.37300	4842	M2	√	√	√	√	√	√	√	√	√	√
DY69-M1-ES03-CTD06	153.67287	19.09472	5565	M1										
DY69-M2B1-ES03-CTD05	153.67230	19.09410	5565	M2	√	√	√	√	√	√	√	√	√	√
DY69-M1-ES06-CTD07	152.89480	18.83110	5563	M1	√	√	√	√	√	√	√	√	√	√
DY69-M1-ES06-CTD08	152.89259	18.83184	5528	M1										
DY69-M2B1-ES05-CTD09	153.27090	18.83200	5669	M2	√	√	√	√	√	√	√	√	√	√
DY69-M2B1-ES05-CTD10	153.27182	18.83288	5669	M2										
DY69-M2B1-ES02-CTD11	153.67445	18.82577	5650	M2										
DY69-M2B1-ES02-CTD12	153.67450	18.82610	5650	M2	√	√	√	√	√	√	√	√	√	√
DY69-M2B1-ES01-CTD13	153.67600	18.56180	5644	M2	√	√	√	√	√	√	√	√	√	√
DY69-M2B1-ES01-CTD14	153.67605	18.56193	5643	M2										
DY76-I-M2-S055CTD13	153.66260	19.36520	5673	M2	√	√	√	√	√	√	√			
DY76-I-M2-S057CTD13	153.66820	19.35310	4841	M2										
DY76-I-M2-S062CTD14	153.67660	19.07510	5632	M2	√	√	√	√	√	√	√			
DY76-I-M2-S065CTD14	153.65190	19.02070	5615	M2										
DY76-I-M2-S071CTD15	154.43550	19.04600	5698	M2										
DY76-I-M2-S075CTD16	153.60480	18.54770	5669	M2	√	√	√	√	√	√	√			
DY76-I-M2-S076CTD16	153.56910	18.54430	5673	M2										
DY76-I-M1-S080CTD17	152.81390	18.73190	5571	M1	√	√	√	√	√	√	√			
DY76-I-M1-S083CTD17	152.80210	18.70690	5576	M2										
DY76-I-M2-S085CTD18	153.29910	18.87750	5669	M2	√	√	√	√	√	√	√			
DY69-M1-ES06-BC18	152.89043	18.83025	5529	M1										
DY69-M2B1-ES02-BC24	153.67745	18.82594	5650	M2										
DY69-M2B1-ES03-MC04	153.67276	19.09467	5565	M2										
DY76-I-M1-S088BC04	151.74670	18.45990	5285	M1										
DY76-I-M1-S090BC06	151.92980	18.45520	5403	M1										
DY76-I-M1-S091BC07	151.92820	18.29070	5250	M1										
DY76-I-M1-S092BC08	151.75140	18.29340	5306	M1										
DY61-M2-MX2006	154.49850	19.05030	5676	M2										
DY66-M2-MX2101	154.48680	19.04840	5680	M2										

Station	Lon/°E	Lat/°N	Water Depth/m	Block	pH	DO	Nitrate	Nitrite	Nitrogen and Phosphorus	Ammonium Salt	Silicate	Suspended Solid (SS)	Total alkalinity	Dissolved Inorganic Carbon
DY69-ES04-MX01	153.67210	19.37340	4840	M2										
DY69-ES03-MX02	153.67750	19.08690	5571	M2										
DY69-ES06-MX03	152.81800	18.77500	5638	M1										
DY69-M2-ES04-NET03	153.67201	19.37347	4842	M2										
DY69-M2B1-ES03-NET04	153.67199	19.09655	5569	M2										
DY69-M1-ES06-NET05	152.89252	18.83181	5523	M1										
DY69-M2B1-ES05-NET06	153.27184	18.83223	5668	M2										
DY69-M2B1-ES02-NET07	153.67452	18.82600	5650	M2										
DY69-M2B1-ES01-NET08	153.67606	18.56178	5645	M2										
DY76-I-M2-S059VN13	153.65380	19.35840	4828	M2										
DY76-I-M2-S063VN14-1	153.67360	19.05700	5608	M2										
DY76-I-M2-S063VN14-2	153.67360	19.05700	5608	M2										
DY76-I-M2-S074VN15-1	153.65200	18.56240	5661	M2										
DY76-I-M2-S074VN15-2	153.65200	18.56240	5661	M2										
DY76-I-M1-S079VN16-1	152.81890	18.73620	5567	M1										
DY76-I-M1-S079VN16-2	152.81890	18.73620	5567	M1										
DY69-M1-ES07-NET02	151.88222	18.59799	5424	M1										
DY69-M2-ES04-BIO01	153.64919	19.37932	4736	M2										
DY69-M2B1-ES03-BIO02	153.67420	19.09850	5557	M2										
DY69-M2B1-ES03-BIO03	153.67270	19.09466	5566	M2										
DY69-M1-ES06-BIO04	152.91129	18.83703	5531	M1										
DY69-M1-ES06-BIO05	152.89257	18.83212	5522	M1										
DY69-M2B1-ES05-BIO06	153.27181	18.83312	5669	M2										
DY69-M2B1-ES01-BIO07	153.67624	18.56137	5647	M2										
DY76-I-M2-S058MN09	153.65660	19.36130	4809	M2										
DY76-I-M2-S064MN10	153.66940	19.04430	5606	M2										
DY76-I-M2-S077MN11a	153.54000	18.53970	5669	M2										
DY76-I-M1-S078MN12	152.81800	18.73480	5572	M1										
DY61-I-M2-S106MC04	154.51250	18.99900	5697	M2										
DY61-I-M2-S108MC04R	154.52220	18.98590	5677	M2										
DY61-I-M2-S114MC05	154.49730	19.49980	5704	M2										
DY69-M2B1-ES03-BC13	153.67292	19.09477	5569	M2										
DY69-M2B1-ES05-BC21	153.27153	18.83274	5669	M2										
DY69-M2B1-ES03-L01	153.67575	19.11203	5555	M1										
DY69-M1-ES06-L02	152.92630	18.85197	5557	M1										
DY75I-M2-Lander01	153.68991	19.09002	5561	M2										
DY75I-M2-Lander02	153.67537	18.56210	5635	M2										
DY75I-M1-Lander03	152.82119	18.78086	5535	M1										
DY81I-M2-ES03-CTD01	153.6799	19.0898	5562	M2	√	√	√	√	√	√	√	√	√	√
DY81I-M2-ES03-CTD03	153.6799	19.0899	5535	M2	√	√	√	√	√	√	√	√		√
DY81I-M2-ES05-CTD02	153.2711	18.8319	5676	M2	√	√	√	√	√	√	√	√		√

Station	Lon/ °E	Lat/ °N	Water Depth/ m	Block	pH	DO	Nitrate	Nitrite	Nitrogen and Phosphorus	Ammonium Salt	Silicate	Suspended Solid (SS)	Total alkalinity	Dissolved Inorganic Carbon
DY81I-M2-ES05-CTD02-200	153.2711	18.8319	5675	M2										
DY81I-M1-ES06-CTD04	152.8901	18.8300	5535	M1	√	√	√	√	√	√	√	√		√
DY81I-M1-ES06-CTD04-200	152.8901	18.8300	5535	M1										
DY81II-M1-ES08-MX04	152.8549	18.7708	5605	M1										
DY81II-M2-ES03-MX05	153.6710	19.1155	5555	M2										
DY81I-M2-ES05-DX01	153.2710	152.8901	5676	M2										
DY81I-M2-ES03-DX02	153.6799	19.0899	5574	M2										
DY81I-M2-ES03-DX03	153.6799	19.0899	5575	M2										
DY81I-M2-DX04	154.7174	19.0899	5575	M2										
DY81I-M1-ES06-DX05	152.8901	18.8300	5534	M1										
DY81I-M2-ES05-F01	153.2710	18.8319	5676	M2										
DY81I-M2-ES03-F02	153.6799	19.0899	5574	M2										
DY81I-M2-F03	154.7174	19.3819	5673	M2										
DY81I-M2-ES03-F04	153.6800	19.0899	5574	M2										
DY81I-M2-ES03-F05	153.6800	19.0899	5573	M2										
DY81I-M1-ES06-F06	152.8901	18.8300	5536	M1										
DY81I-M1-ES06-F07	152.8901	18.8300	5535	M1										
DY81II-M2-ES05-MC04	153.2709	18.8319	5684	M2										
DY81II-M1-ES08-MC05	152.8201	18.7352	5581	M1										
DY81II-M2-ES03-MC07	153.6682	19.0900	5577	M2										
DY81II-M2-ES03-MC08	153.6730	19.0900	5572	M2										
DY81II-M2-ES03-MC09	153.6799	19.0899	5572	M2										
DY81II-M2-ES03-MC11	153.6870	19.0899	5574	M2										

Schedule 3-4 List of Data Obtained at Stations (Biology)

Station	Longitude/°E	Latitude/°N	Water Depth/m	Block	Chlorophyll*a*	Photosynthetic Pigments	Microbe	Picoplankton	Phytoplankton	Plankton	Meiofauna	Macrofauna	Nodule-attached Organism	Scavenger	Primary Productivity	Bioturbation
DY69-M2B1-PS13-BC01	153.94402	18.88123	5702	M2			√									
DY69-M2B1-PS01-BC02	154.12474	18.97067	5718	M2			√									
DY69-M2B1-PS02-BC03	154.30565	18.96199	5675	M2			√									
DY69-M2B1-PS05-BC04	153.58545	19.17258	5434	M2												
DY69-M2B1-PS04-BC05	153.40173	19.16932	5589	M2			√									
DY69-M2B1-PS08-BC06	153.31253	19.27086	5520	M2			√									
DY69-M2B1-PS07-BC07	153.94103	19.16952	5576	M2			√									
DY69-M2B1-PS11-BC08	153.85039	19.27061	5443	M2			√									
DY69-M2-ES04-BC09	153.67167	19.37304	4842	M2			√					√				√
DY69-M2B1-PS10-BC10	153.67034	19.27093	5193	M2			√									
DY69-M2B1-PS06-BC11	153.75938	19.37272	5508	M2			√									
DY69-M2B1-PS03-BC12	153.85101	19.08253	5621	M2			√									
DY69-M2B1-ESO3-BC13	153.67292	19.09477	5569	M2												
DY69-M2B1-PS14-BC14	153.49430	18.97486	5632	M2			√									
DY69-M2B1-PS15-BC15	153.49288	19.07620	5593	M2			√									
DY69-M2B1-PS09-BC16	153.49258	19.27211	5248	M2			√									
DY69-M1-ES06-BC17	152.88986	18.83053	5528	M1								√				√
DY69-M2B1-ES06-BC20	153.27106	18.83172	5668	M2												
DY69-M2B1-ES02-BC22	153.67486	18.82680	5650	M2								√				√
DY69-M2B1-ES01-BC25	153.67626	18.56169	5645	M2			√					√				√
DY69-M2B1-ES05-BC20	153.27110	18.83172	5668	M2			√					√				√
DY69-M2B1-ES03-MC02	153.67183	19.09644	5576	M2			√									√
DY75I-M2-BC03A	155.12989	19.51949	5685	M2			√									
DY75I-M2-BC04	155.30042	19.52016	5651	M2			√									
DY75I-M2-BC05	155.30001	19.68959	5625	M2			√					√	√			
DY75I-M2-BC06	155.12997	19.68962	5675	M2			√					√	√			
DY75I-M2-BC07	154.94993	19.68953	5716	M2			√					√				
DY75I-M2-BC08	154.77000	19.51955	5616	M2			√					√				
DY75I-M2-BC09	154.95602	19.51950	5675	M2			√									
DY75I-M2-BC10	154.94997	19.34958	5684	M2			√					√				
DY75I-M2-BC11	155.13003	19.34954	5658	M2			√					√	√			
DY75I-M2-BC12	155.29983	19.34958	5678	M2			√					√				
DY75I-M2-BC13	154.94974	19.17960	5629	M2			√					√	√			
DY75I-M2-BC14	154.76992	19.17951	5671	M2			√									
DY75I-M2-BC15	154.60012	18.99956	5659	M2			√					√				

Station	Longitude/°E	Latitude/°N	Water Depth/m	Block	Chlorophyll*a*	Photosynthetic Pigments	Microbe	Picoplankton	Phytoplankton	Plankton	Meiofauna	Macrofauna	Nodule-attached Organism	Scavenger	Primary Productivity	Bioturbation
DY75I-M2-BC16A	154.59997	19.17950	5690	M2			√					√				
DY75I-M2-BC17	154.12020	19.16957	5719	M2			√					√	√			
DY75I-M2-BC18	154.24032	19.17967	5725	M2			√					√				
DY75I-M2-BC19	154.41992	19.17952	5704	M2			√					√				
DY75I-M2-BC20	154.41992	19.34954	5669	M2			√					√	√			
DY75I-M2-BC21	154.60017	19.34961	5673	M2			√					√				
DY75I-M2-BC22	154.59965	19.51962	5659	M2			√					√	√			
DY75I-M2-BC23	154.42067	19.68705	5737	M2			√					√	√			
DY75I-M2-BC24	154.23958	19.68996	5770	M2			√					√				
DY75I-M2-BC25	154.05982	19.69040	5585	M2			√					√				
DY75I-M2-BC26	154.05952	19.52010	5636	M2			√					√				
DY75I-M2-BC27	154.23950	19.35019	5695	M2			√					√	√			
DY75I-M2-BC28	154.05954	19.35023	5500	M2			√					√	√			
DY75I-M2-BC29	154.02978	19.16972	5664	M2			√									
DY75I-M2-BC30	153.75955	19.08981	5587	M2			√					√				
DY75I-M2-BC31	153.57951	19.08003	5571	M2			√									
DY75I-M2-BC32	153.49042	19.16985	5507	M2			√									
DY75I-M2-BC33	153.58030	19.26962	5148	M2			√					√				
DY75I-M2-BC34	153.67982	19.16954	5478	M2			√					√				
DY75I-M2-BC35	153.52467	19.16963	5471	M2			√									
DY75I-M2-BC36	153.93995	19.26952	5539	M2			√					√				
DY75I-M2-BC37A	153.84962	19.16960	5520	M2			√									
DY75I-M2-BC38A	153.75955	19.27021	5302	M2			√									
DY75I-M2-BC39A	153.39987	19.26999	5428	M2			√									
DY75I-M2-BC40	153.31028	19.16958	5647	M2			√					√				
DY75I-M2-BC41A	153.30992	19.07990	5654	M2			√									
DY75I-M2-BC42	153.40049	19.08014	5618	M2			√					√				
DY75I-M2-BC43	153.39026	18.98961	5655	M2			√									
DY75I-M2-BC44	153.57990	18.96957	5632	M2			√									
DY75I-M2-BC45	153.74964	18.97966	5680	M2			√					√				
DY75I-M2-BC46	153.83989	18.97954	5673	M2			√					√				
DY75I-M2-BC47	153.93996	19.07953	5626	M2			√									
DY75II-M2-BC48A	154.03022	19.08005	5660	M2												
DY75I-M2-BC49	154.03005	18.96953	5702	M2			√									
DY75I-M2-BC50	154.12001	19.07953	5695	M2			√									
DY75I-M2-BC51	154.21041	19.07973	5698	M2			√						√			
DY75I-M2-BC52A	154.21032	18.96865	5683	M2			√						√			

Station	Longitude/°E	Latitude/°N	Water Depth/m	Block	Chlorophyll*a*	Photosynthetic Pigments	Microbe	Picoplankton	Phytoplankton	Plankton	Meiofauna	Macrofauna	Nodule-attached Organism	Scavenger	Primary Productivity	Bioturbation
DY75I-M2-BC53	154.39041	18.96990	5660	M2			√									
DY75I-M2-BC54	154.33999	18.87999	5696	M2			√									
DY75I-M2-BC55	154.15999	18.87994	5706	M2			√									
DY75I-M2-BC56	153.98005	18.71001	5657	M2			√						√			
DY75I-M2-BC57	154.15999	18.70995	5665	M2			√									
DY75I-M2-BC58	154.33990	18.70992	5659	M2			√									
DY75I-M2-BC59	154.33978	18.53978	5654	M2			√									
DY75I-M2-BC60A	154.16004	18.53995	5667	M2			√									
DY75I-M2-BC61	153.25986	18.54024	5664	M2			√									
DY75I-M2-BC62	153.43969	18.54008	5660	M2			√									
DY75I-M2-BC63	153.98000	18.54004	5678	M2			√						√			
DY75I-M2-BC64	153.61994	18.70992	5731	M2			√						√			
DY75I-M2-BC65	153.43925	18.70984	5706	M2												
DY75I-M2-BC66	153.25000	18.70994	5690	M2			√									
DY75I-M1-BC73	152.88999	18.73496	5625	M2			√					√				
DY75I-M2-BC75	153.67958	19.13998	5496	M2			√					√				
DY75I-M2-BC76	153.67961	19.13961	5510	M2			√					√				
DY75I-M2-BC77	153.67992	19.08982	5543	M2			√					√	√			
DY75I-M2-BC78	153.68008	19.08992	5562	M2			√					√				
DY75I-M2-BC79	153.67987	19.04005	5611	M2			√					√				
DY75I-M2-BC80	153.68001	19.03994	5618	M2			√					√	√			
DY75I-M1-BC68	152.89007	18.82997	5525	M1								√				
DY75I-M1-BC69	152.89002	18.82992	5529	M1			√					√	√			
DY75I-M1-BC70	152.81999	18.73493	5566	M1			√					√				
DY75I-M1-BC71	152.82003	18.73492	5554	M1			√					√				
DY75I-M1-BC72	152.88996	18.73491	5623	M1			√					√				
DY75I-M1-BC74	152.81553	18.84369	5393	M1			√					√				
DY75II-M2-BC81	153.26007	18.99278	5681	M2												
DY75II-M2-BC82	153.29610	18.87647	5669	M2												
DY75II-M1-BC83	152.66583	19.23978	1287	M1												
DY75II-M1-BC84	152.64593	18.73478	5483	M1												
DY75II-M1-BC85	152.65295	18.86710	5157	M1												
DY75II-M1-BC86	152.65293	18.99994	4398	M1												
DY75II-M1-BC87	152.71968	19.00946	4526	M1												
DY75II-M1-BC88	152.68973	18.99977	4567	M1												
DY75II-M1-BC89	152.70503	18.99849	4570	M1												
DY75II-M2-BC90	154.03224	19.27791	5490	M2												

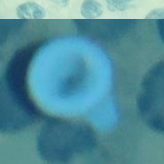| Station	Longitude/°E	Latitude/°N	Water Depth/m	Block	Chlorophyll*a*	Photosynthetic Pigments	Microbe	Picoplankton	Phytoplankton	Plankton	Meiofauna	Macrofauna	Nodule-attached Organism	Scavenger	Primary Productivity	Bioturbation
DY75II-M2-BC91	153.73165	19.34160	5078	M2												
DY75II-M2-BC92	153.93600	18.97003	5687	M2												
DY75II-M2-BC93	154.30307	19.07983	5656	M2												
DY75II-M2-BC94	154.39805	19.07999	5711	M2												
DY75II-M2-BC95	154.33021	19.17998	5712	M2												
DY75I-M2-MC02	153.67988	19.13992	5519	M2												
DY75I-M2-MC03C	153.67984	19.14002	5516	M2			√									
DY75I-M2-MC04a	153.67999	19.03982	5608	M2												
DY75I-M2-MC05	153.67989	19.04001	5619	M2												
DY75I-M2-MC06	153.67995	19.08987	5561	M2												
DY75I-M2-MC07a	153.68001	19.08995	5566	M2			√				√					
DY75II-M1-MC10	152.89000	18.82992	5526	M1												
DY75II-M1-MC11	152.82000	18.77990	5539	M1												
DY75II-M1-MC12	152.82006	18.77985	5521	M1			√				√					
DY75II-M1-MC13	152.82007	18.73496	5576	M1			√				√					
DY75II-M1-MC14	152.82015	18.73498	5572	M1			√				√					
DY75II-M2-MC15	153.29584	18.87621	5659	M2			√									
DY75II-M2-MC16	153.29557	18.87628	5675	M2			√				√					
DY61-1-M2-S109CTD30	154.48810	18.95610	5656	M2												
DY61-I-M2-S110CTD31	154.38100	18.94440	5683	M2	√											
DY69-M1-ES07-CTD01	151.87980	18.60220	5434	M1		√										
DY69-M2-ES04-CTD02	153.67212	19.37340	4840	M2	√	√	√	√	√						√	
DY69-M2-ES04-CTD03	153.67140	19.37300	4842	M2												
DY69-M1-ES03-CTD06	153.67287	19.09472	5565	M1	√	√	√	√	√						√	
DY69-M2B1-ES03-CTD05	153.67230	19.09410	5565	M2												
DY69-M1-ES06-CTD07	152.89480	18.83110	5563	M1												
DY69-M1-ES06-CTD08	152.89259	18.83184	5528	M1	√	√	√	√	√						√	
DY69-M2B1-ES05-CTD09	153.27090	18.83200	5669	M2												
DY69-M2B1-ES05-CTD10	153.27182	18.83288	5669	M2	√	√	√	√	√							
DY69-M2B1-ES02-CTD11	153.67445	18.82577	5650	M2	√	√	√	√	√						√	
DY69-M2B1-ES02-CTD12	153.67450	18.82610	5650	M2												
DY69-M2B1-ES01-CTD13	153.67600	18.56180	5644	M2												
DY69-M2B1-ES01-CTD14	153.67605	18.56193	5643	M2	√	√	√	√	√						√	
DY76-I-M2-S055CTD13	153.66260	19.36520	5673	M2	√	√		√	√						√	
DY76-I-M2-S057CTD13	153.66820	19.35310	4841	M2			√									
DY76-I-M2-S062CTD14	153.67660	19.07510	5632	M2	√	√	√	√							√	
DY76-I-M2-S065CTD14	153.65190	19.02070	5615	M2					√							

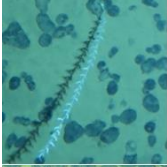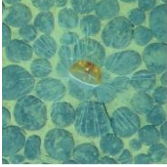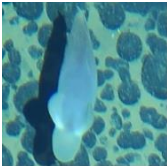| Station	Longitude/°E	Latitude/°N	Water Depth/m	Block	Chlorophyll a	Photosynthetic Pigments	Microbe	Picoplankton	Phytoplankton	Plankton	Meiofauna	Macrofauna	Nodule-attached Organism	Scavenger	Primary Productivity	Bioturbation
DY76-I-M2-S071CTD15	154.43550	19.04600	5698	M2												
DY76-I-M2-S075CTD16	153.60480	18.54770	5669	M2	√	√	√	√							√	
DY76-I-M2-S076CTD16	153.56910	18.54430	5673	M2					√							
DY76-I-M1-S080CTD17	152.81390	18.73190	5571	M1	√	√		√	√						√	
DY76-I-M1-S083CTD17	152.80210	18.70690	5576	M2			√									
DY76-I-M2-S085CTD18	153.29910	18.87750	5669	M2	√			√	√						√	
DY69-M1-ES06-BC18	152.89043	18.83025	5529	M1			√									
DY69-M2B1-ES02-BC24	153.67745	18.82594	5650	M2			√					√				
DY69-M2B1-ES03-MC04	153.67276	19.09467	5565	M2			√									
DY76-I-M1-S088BC04	151.74670	18.45990	5285	M1			√					√				
DY76-I-M1-S090BC06	151.92980	18.45520	5403	M1								√				
DY76-I-M1-S091BC07	151.92820	18.29070	5250	M1			√					√				
DY76-I-M1-S092BC08	151.75140	18.29340	5306	M1								√				
DY61-M2-MX2006	154.49850	19.05030	5676	M2												
DY66-M2-MX2101	154.48680	19.04840	5680	M2												
DY69-ES04-MX01	153.67210	19.37340	4840	M2												
DY69-ES03-MX02	153.67750	19.08690	5571	M2												
DY69-ES06-MX03	152.81800	18.77500	5638	M1												
DY69-M2-ES04-NET03	153.67201	19.37347	4842	M2					√	√						
DY69-M2B1-ES03-NET04	153.67199	19.09655	5569	M2					√	√						
DY69-M1-ES06-NET05	152.89252	18.83181	5523	M1					√	√						
DY69-M2B1-ES05-NET06	153.27184	18.83223	5668	M2					√	√						
DY69-M2B1-ES02-NET07	153.67452	18.82600	5650	M2					√	√						
DY69-M2B1-ES01-NET08	153.67606	18.56178	5645	M2					√	√						
DY76-I-M2-S059VN13	153.65380	19.35840	4828	M2					√	√						
DY76-I-M2-S063VN14-1	153.67360	19.05700	5608	M2					√	√						
DY76-I-M2-S063VN14-2	153.67360	19.05700	5608	M2					√	√						
DY76-I-M2-S074VN15-1	153.65200	18.56240	5661	M2					√	√						
DY76-I-M2-S074VN15-2	153.65200	18.56240	5661	M2					√	√						
DY76-I-M1-S079VN16-1	152.81890	18.73620	5567	M1					√	√						
DY76-I-M1-S079VN16-2	152.81890	18.73620	5567	M1				√	√	√						
DY69-M1-ES07-NET02	151.88222	18.59799	5424	M1						√						
DY69-M2-ES04-BIO01	153.64919	19.37932	4736	M2						√						
DY69-M2B1-ES03-BIO02	153.67420	19.09850	5557	M2						√						
DY69-M2B1-ES03-BIO03	153.67270	19.09466	5566	M2						√						
DY69-M1-ES06-BIO04	152.91129	18.83703	5531	M1						√						
DY69-M1-ES06-BIO05	152.89257	18.83212	5522	M1						√						

Station	Longitude/°E	Latitude/°N	Water Depth/m	Block	Chlorophyll*a*	Photosynthetic Pigments	Microbe	Picoplankton	Phytoplankton	Plankton	Meiofauna	Macrofauna	Nodule-attached Organism	Scavenger	Primary Productivity	Bioturbation
DY69-M2B1-ES05-BIO06	153.27181	18.83312	5669	M2						√						
DY69-M2B1-ES01-BIO07	153.67624	18.56137	5647	M2						√						
DY76-I-M2-S058MN09	153.65660	19.36130	4809	M2						√						
DY76-I-M2-S064MN10	153.66940	19.04430	5606	M2						√						
DY76-I-M2-S077MN11a	153.54000	18.53970	5669	M2						√						
DY76-I-M1-S078MN12	152.81800	18.73480	5572	M1						√						
DY61-I-M2-S106MC04	154.51250	18.99900	5697	M2							√					
DY61-I-M2-S108MC04R	154.52220	18.98590	5677	M2							√					
DY61-I-M2-S114MC05	154.49730	19.49980	5704	M2							√					
DY69-M2B1-ES03-BC13	153.67292	19.09477	5569	M2								√				
DY69-M2B1-ES05-BC21	153.27153	18.83274	5669	M2								√				
DY69-M2B1-ES03-L01	153.67575	19.11203	5555	M1										√		
DY69-M1-ES06-L02	152.92630	18.85197	5557	M1										√		
DY75I-M2-Lander01	153.68991	19.09002	5561	M2										√		
DY75I-M2-Lander02	153.67537	18.56210	5635	M2										√		
DY75I-M1-Lander03	152.82119	18.78086	5535	M1										√		
DY81I-M2-ES03-CTD01	153.6799	19.0898	5562	M2	√	√		√							√	
DY81I-M2-ES03-CTD03	153.6799	19.0899	5535	M2	√			√								
DY81I-M2-ES05-CTD02	153.2711	18.8319	5676	M2		√										
DY81I-M2-ES05-CTD02-200	153.2711	18.8319	5675	M2	√			√							√	
DY81I-M1-ES06-CTD04	152.8901	18.8300	5535	M1												
DY81I-M1-ES06-CTD04-200	152.8901	18.8300	5535	M1	√	√		√							√	
DY81II-M1-ES08-MX04	152.8549	18.7708	5605	M1												
DY81II-M2-ES03-MX05	153.6710	19.1155	5555	M2												
DY81I-M2-ES05-DX01	153.2710	152.8901	5676	M2					√	√						
DY81I-M2-ES03-DX02	153.6799	19.0899	5574	M2					√	√						
DY81I-M2-ES03-DX03	153.6799	19.0899	5575	M2					√	√						
DY81I-M2-DX04	154.7174	19.0899	5575	M2					√	√						
DY81I-M1-ES06-DX05	152.8901	18.8300	5534	M1					√	√						
DY81I-M2-ES05-F01	153.2710	18.8319	5676	M2					√	√						
DY81I-M2-ES03-F02	153.6799	19.0899	5574	M2					√	√						
DY81I-M2-F03	154.7174	19.3819	5673	M2					√	√						
DY81I-M2-ES03-F04	153.6800	19.0899	5574	M2					√	√						
DY81I-M2-ES03-F05	153.6800	19.0899	5573	M2					√	√						
DY81I-M1-ES06-F06	152.8901	18.8300	5536	M1					√	√						
DY81I-M1-ES06-F07	152.8901	18.8300	5535	M1					√	√						
DY81II-M2-ES05-MC04	153.2709	18.8319	5684	M2												

Station	Longitude/°E	Latitude/°N	Water Depth/m	Block	Chlorophyll*a*	Photosynthetic Pigments	Microbe	Picoplankton	Phytoplankton	Plankton	Meiofauna	Macrofauna	Nodule-attached Organism	Scavenger	Primary Productivity	Bioturbation
DY81II-M1-ES08-MC05	152.8201	18.7352	5581	M1												
DY81II-M2-ES03-MC07	153.6682	19.0900	5577	M2												
DY81II-M2-ES03-MC08	153.6730	19.0900	5572	M2												
DY81II-M2-ES03-MC09	153.6799	19.0899	5572	M2												
DY81II-M2-ES03-MC11	153.6870	19.0899	5574	M2												

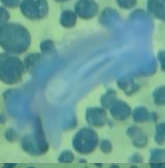## Schedule 4 List of Megafauna Occurring in BPC's Blocks M1 and M2 Respectively
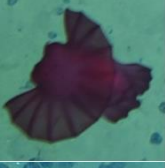
Taxonomy	Morphospecies names	Example images	Block M2	Block M1
PHYLUM: PORIFERA **Class: Hexactinellida**				
(Subclass: Amphidiscophora) Order: Amphidiscosida Family: Hyalonematidae	*Hyalonema* sp.		+	+
(Subclass: Amphidiscophora) Order: Amphidiscosida	Amphidiscosida fam. indet.			+
(Subclass: Hexasterophora) Order: Lyssacinosida Family: Rossellidae	*Caulophacus* sp.1		+	+
(Subclass: Hexasterophora) Order: Lyssacinosida Family: Rossellidae	Rossellidae gen. indet.			+
(Subclass: Hexasterophora) Order: Lyssacinosida Family: Euplectellidae Subfamily: Euplectellinae	*Holascus spinosus* sp. inc.			+
(Subclass: Hexasterophora) Order: Lyssacinosida Family: Euplectellidae Subfamily: Euplectellinae	*Holascus taraxacum* sp. inc.			+
(Subclass: Hexasterophora) Order: Lyssacinosida Family: Euplectellidae Subfamily: Euplectellinae	*Docosaccus nidulus* sp. inc.		+	+
(Subclass: Hexasterophora) Order: Lyssacinosida Family: Euplectellidae Subfamily:Corbitellinae	*Corbitella discasterosa* sp. inc.		+	
Class: Demospongiae				

Taxonomy	Morphospecies names	Example images	Block M2	Block M1
(Subclass: Heteroscleromorpha) Order: Poecilosclerida Family: Cladorhizidae	Cladorhizidae gen. indet.			+
(Subclass: Heteroscleromorpha) Order: Poecilosclerida Family: Cladorhizidae	Cladorhizidae gen. indet.		+	
PHYLUM: CNIDARIA Class: Anthozoa				
(Subclass: Hexacorallia) Order: Antipatharia Family: Cladopathidae	*Abyssopathes* sp.		+	+
(Subclass: Hexacorallia) Order: Actiniaria Family: Actinostolidae	Actinostolidae gen. indet.		+	
(Subclass: Octocorallia) Order: Scleralcyonacea Family: Mopseidae	Mopseidae gen. indet.		+	+
Class: Hydrozoa Order: Anthoathecata Suborder: Aplanulata Family: Rhopalonematidae	Rhopalonematidae gen. indet.		+	+
PHYLUM: ANNELIDA Class: Polychaeta				
Family: Acrocirridae	Acrocirridae gen. indet.		+	+
PHYLUM MOLLUSCA Class: Cephalopoda				
Order: Octopoda Suborder: Cirrata Family: Cirroteuthidae	*Cirroteuthis muelleri* sp. inc.		+	+
Superorder：Decapodiformes				

Taxonomy	Morphospecies names	Example images	Block M2	Block M1
Family: Magnapinnidae	*Magnapinna* sp.indet		+	
PHYLUM ARTHROPODA (SUBPHYLUM CRUSTACEA) **Class: Malacostraca** Order: Decapoda				
(Infraorder: Caridea) Family: Aristeidae	*Cerataspis monstrosus* sp. inc.		+	+
PHYLUM BRYOZOA				
Class: Gymnolaemata Order: Cheilostomatida	Cheilostomatida fam. indet.		+	+
PHYLUM ECHINODERMATA				
Class: Crinoidea Order: Comatulida Family: Bathycrinidae	Bathycrinidae gen. indet.			+
Class: Asteroidea Order: Brisingida Family: Freyellidae	*Freyastera* sp. indet.		+	
Class: Ophiuroidea Order: Ophiacanthida (Suborder: Ophiacanthina) Family: Ophiacanthidae	*Ophiacanth*a sp.indet.		+	+
Class: Echinoidea Order:Holasteroida	Holasteroida order inc.		+	
Class: Holothuroidea Order: Elasipodida Family: Elpidiidae	*Amperima* sp. indet.		+	+

Taxonomy	Morphospecies names	Example images	Block M2	Block M1
Class: Holothuroidea Order: Elasipodida Family: Elpidiidae	*Peniagone* sp. indet.		+	+
Class: Holothuroidea Order: Elasipodida Family: Psychropotidae	*Benthodytes* sp. indet.		+	
Class: Holothuroidea Order: Elasipodida Family: Psychropotidae	*Benthodytes sanguinolenta* sp. inc.		+	+
Class: Holothuroidea Order: Elasipodida Family: Psychropotidae	*Psychropotes verrucicaudatus* sp. inc.		+	+
Class: Holothuroidea Order: Synallactida Family: Synallactidae	*Synallactes* sp. indet.		+	+
Class: Holothuroidea Order: Elasipodida Family: Pelagothuriidae	*Enypniastes eximia*		+	
Class: Holothuroidea Order: Synallactida Family: Deimatidae	Deimatidae gen. indet		+	+
PHYLUM HEMICHORDATA	Hemichordata sp. indet.		+	+
PHYLUM UROCHORDATA **SubPhylum Tunicata**				
Class: Ascidiacea Order: Phlebobranchia Family: Octacnemidae	*Megalodicopia* sp. indet.		+	

Taxonomy	Morphospecies names	Example images	Block M2	Block M1
PHYLUM CHORDATA **Superclass: Pices**				
Class: Actinopterygii Order: Gadiformes Family: Macrouridae	Macrouridae sp. indet.		+	+
Order: Ophidiiformes Family: Ophidiidae	*Leucicorus* sp. indet.		+	+